OAK RIDGE
NATIONAL LABORATORY
MANAGED BY UT-BATTELLE
FOR THE DEPARTMENT OF ENERGY

ORNL/TM-13720

Source Terms for HFIR Beam Tube Shielding Analyses, and a Complete Shielding Analysis of the HB-3 Tube

J. A. Bucholz

UT-BATTELLE
ORNL-27 (4-00)

DOCUMENT AVAILABILITY

Reports produced after January 1, 1996, are generally available free via the U.S. Department of Energy (DOE) Information Bridge.

Web site http://www.osti.gov/bridge

Reports produced before January 1, 1996, may be purchased by members of the public from the following source.

National Technical Information Service
5285 Port Royal Road
Springfield, VA 22161
Telephone 703-605-6000 (1-800-553-6847)
TDD 703-487-4639
Fax 703-605-6900
E-mail info@ntis.fedworld.gov
Web site http://www.ntis.gov/support/ordernowabout.htm

Reports are available to DOE employees, DOE contractors, Energy Technology Data Exchange (ETDE) representatives, and International Nuclear Information System (INIS) representatives from the following source.

Office of Scientific and Technical Information
P.O. Box 62
Oak Ridge, TN 37831
Telephone 865-576-8401
Fax 865-576-5728
E-mail reports@adonis.osti.gov
Web site http://www.osti.gov/contact.html

This report was prepared as an account of work sponsored by an agency of the United States Government. Neither the United States Government nor any agency thereof, nor any of their employees, makes any warranty, express or implied, or assumes any legal liability or responsibility for the accuracy, completeness, or usefulness of any information, apparatus, product, or process disclosed, or represents that its use would not infringe privately owned rights. Reference herein to any specific commercial product, process, or service by trade name, trademark, manufacturer, or otherwise, does not necessarily constitute or imply its endorsement, recommendation, or favoring by the United States Government or any agency thereof. The views and opinions of authors expressed herein do not necessarily state or reflect those of the United States Government or any agency thereof.

ORNL/TM-13720

Source Terms for HFIR Beam Tube Shielding Analyses, and a Complete Shielding Analysis of the HB-3 Tube

J. A. Bucholz

Date published: July 2000

Work performed for the Research Reactors Division,
in support of the HFIR Upgrade Project (1998)

Prepared by the
OAK RIDGE NATIONAL LABORATORY
Oak Ridge, TN 37831-6363
Managed by
UT-BATTELLE, LLC,
for the
U.S. DEPARTMENT OF ENERGY
under contract DE-AC05-00OR22725

TABLE OF CONTENTS

LIST OF FIGURES ix

LIST OF TABLES xiii

ABSTRACT xix

1.0 INTRODUCTION AND EXECUTIVE SUMMARY 1

1.1 Background 1

1.2 Objectives 2

1.3 Executive Summary 2

2.0 SOURCE TERMS FOR BEAM TUBE SHIELDING ANALYSES 7

2.1 Methodology 7

2.2 Selection of Detector Locations 7

2.3 Pedigree of MCNP Run GF211 for HB-1 and HB-4 7

2.4 Pedigree of MCNP Runs GF209, GF214, and GF215 for HB-2 and HB-3 10

2.5 Recommended Equivalent Point Sources for Shielding Calculations 11

2.6 Verification of Point Sources in All Beam Tubes 11

2.7 Intended Use of Point Sources in Beam Tubes 11

2.8 Validation of Point Sources in HB-3 14

2.9 Validation of Point Sources in HB-2 18

3.0 DESCRIPTION OF THE 3-D MCNP MODEL(S) AND THEIR ORIGIN 21

3.1 Pictorial Orientation (Overview) 26

3.2 Figures Showing Components Affecting the Dosimetry Analysis 43

3.3 Older Engineering Drawings Used in Formulating This Model 44

3.4 Newer Engineering Drawings Used in Formulating This Model 46

4.0 DOSIMETRY ANALYSIS 49

4.1 Geometric Model Used in the Final Analysis 49

4.2 Other MCNP Modeling Parameters Used in the Final Analysis 49

4.3 Theoretical Basis for Laterally Offsetting Sources from the Centerline in the Final Analysis 51

4.4 Final Results and Conclusions 53

4.5 Historical Evolution of the Model to Its Final State, Lessons Learned, and Sensitivities 54

5.0 TREATMENT OF NEUTRONS AND SECONDARY GAMMAS IN THE WATER-TUBE SHIELDING ANALYSIS 61

5.1 Initial (Since Abandoned) Approach Using MCNP 61

5.2 Some Engineering Insights on Neutron and Gamma Dose Rates 63

5.3 Use of ANISN to Confirm that the Direct Neutron Dose Rate is Negligible 67

5.4 Determination of Secondary Gamma Source Terms Using ANISN 71

5.5 Primary and Secondary Gamma Dose Rates Based on a QAD-like Procedure 72

5.6 Conclusions Regarding Neutron and Secondary Gamma Dose Rates 80

6.0 TREATMENT OF PRIMARY GAMMAS IN THE WATER-TUBE SHIELDING ANALYSIS 81

6.1 Discussion of the 1-D ANISN Model Used in the Adjoint Analysis 82

6.2 Obtaining Properly Normalized 1-D Broad-Group Weight Windows from the Adjoint Information 84

6.3 Other Factors Affecting Proper Normalization 85

6.4 Obtaining 3-D Broad-Group Weight Windows for Use in MCNP 91

6.5 Magnet Points and On-The-Fly Directional Biasing 98

6.6 Role of the Broad Group Weight Windows in Accelerating the Final MCNP Calculation 102

6.7 General Review of the 3-D MCNP Model Used in the Final Gamma-Only Shielding Analysis (Run HB308G) 104

6.8 Other Aspects of the 3-D MCNP Model Used in the Final Gamma-Only Shielding Analysis (Run HB308G) 109

6.8.1 Use of the Weight Window File and Importance Specifications 109

6.8.2 Creating, Saving, and Using and Internal Boundary Source Downstream of the Collimator 110

6.8.3 Source Terms Included, and Values Used on the "fm" Multiplier Cards 111

6.8.4 Source Direction Biasing and Starting Weights 112

6.8.5 The Importance Cutoff Plane 112

6.8.6 List of the Flux, Leakage, and Dose Rate Tallies in Run HB308G 113

6.8.7 Comments in the Header Records of Run HB308G Shown in Appendix D.4 114

6.9 Results from the final gamma-only shielding analysis (MCNP4B Run HB308G5) 115

6.9.1 Point Detector Results Along the Centerline 115

6.9.1.1 Confirmation of Dose Rate Upstream of Shutter 115

6.9.1.2 Confirmation of Dose Rate Downstream of Shutter 115

6.9.2 Boundary Crossing Data Just Downstream of Collimator 118

6.9.2.1 Binary Particle History File Available for Future Use 118

6.9.2.2 Boundary Crossing Estimate of Dose Rate Confirms Point Detector 118

6.9.2.3 Brief Discussion of Supplemental Tabulated Data Available in Appendix D.5 118

6.9.3 Axial Variation of Dose Rates in Water, Based on Segmented Volume Tallies 119

6.9.3.1 Volumetric Track Length Estimate of Dose Rate Confirms Point Detector 119

6.9.3.2 Why These Dose Rates Must Be Regarded as Approximate 121

6.9.3.3 Significance of this Approximate Data 121

6.9.4 Summary of Independent Checks on the Dose Rate Just Upstream of the Shutter ... 122

6.9.5 Boundary Crossing Data Downstream of Entire Shield Configuration 124

6.9.5.1 Boundary Crossing Estimate of Dose Rate Confirms Point Detector 127

6.9.5.2 Significance of This Confirmation 127

6.9.5.3 Asymmetric Variations Indicative of Streaming Through and Around the Shutter 127

6.9.5.3.1 Clear Right-to-Left Variations Indicative of Streaming in the Shutter Beam Hole 129

6.9.5.3.2 Slight Top-to-Bottom Variations Indicative of Streaming in the Gap Above the Shutter 129

6.10 Simple Checks for Reasonableness 129

6.10.1 External Dose Rate at the Centerline Due to Direct Transmission 129

6.10.2 Equivalent Point Source 131

6.10.3 Angular Flux Intensity Ratio 133

6.10.4 More General Method of Estimating External Dose Rate at the Centerline Due to Transmission 134

6.10.5 Direct External Dose at the Midplane, in Front of a Tall Thin Clearance Gap .. 135

6.10.6 Methodology for Treating Scattering: The Strength of Scattering Source(s) ... 137

6.10.7 Contributions from "The First Bounce" Scattered Sources Streaming Through the Gap 140

6.10.8 Concluding Remarks on Scattered Radiation and Streaming 141

6.11 Concluding Remarks on the Final Gamma-Only Shielding Analysis 144

7.0 ACTIVATION ANALYSIS AND RESULTING DOSE RATES 149

7.1 Key Radioactive Nuclides and Nuclear Reaction Processes By Which They Are Formed 150

7.2 Determination of the Spatially-Dependent Reaction Rates Using MCNP Run HB309 152

7.3 Activation Program Used to Determine the Gamma Source Terms 7 Days After Shutdown 153

7.4 Gamma Shielding Analysis Based on Activation Sources in the Shutter (Run HB310) 160

7.4.1 Overview of Model, Including Source Term Specifications 160

7.4.2 Final Results: Activation Dose Rates Downstream of the Rotary Shutter 161

7.4.2.1 Point Detector Results Along the Centerline 161

7.4.2.2 Boundary Crossing Data Downstream of Entire Shield Configuration 164

7.4.3 Simple Checks for Reasonableness 164

7.4.3.1 Estimate of Total Gamma Source Within the Shutter 169

7.4.3.2 Estimate of the Activation Gamma Dose Rate Downstream of the Shutter . 171

7.5 Comparison of Calculated Activation Dose Rate Against Recent Experimental Measurements 171

7.6 Parametric Variations as a Function of Initial Cobalt Content 176

7.7 Conclusions Regarding the Activation Analysis and All Other Shielding Calculations in This Report 178

REFERENCES (for Main Text and Appendices) 181

Appendices Related to Sect 2

A.1 Neutron and Gamma Source Terms in MCNP Format for Each Beam Tube 183

A.2 Comparison of the Approximate Fluxes and Dose Rates Resulting from Use of the Equivalent Point Sources, Against the Original Fluxes and Dose Rates Calculated Directly by MCNP 189

Appendices Related to Sect 4

B.1 Input Listing for the Final (Reference) HB-3 Dosimetry Analysis, MCNP Run HB304M4 201

B.2 FADIST7.FOR: A simple Fortran program to determine the "relative" outward-directed current impingent on the inner wall of the HB-3 beam tube in the vicinity of the two dosimeters, and to determine a lateral offset that will allow a line of isotropic point sources "near" the centerline to reproduce that asymmetric effect based on the logic described in Sect 4 227

Appendices Related to Sect 5

C.1 Initial (Since Abandoned) Attempt to Use MCNP for the Neutron and Secondary Gammas in the Shielding Analysis of the 1998 Water-Tube Problem 233

C.1.1 Overview; Lessons Learned; Ultimate Success from Initial Failures 234

C.1.2 Basic Model of the Flooded HB-3 Tube Used in the HB305 Series of Runs 235

C.1.3 Additional Changes Required to Add Importance Cells Needed for Geometric Splitting . 235

C.1.4 Initial Results, Other Variations, and the Necessary Conclusion 237

C.2 MCNP4B Solution of an Academic 3-D Problem Involving the Transmission of a Narrow Collimated Beam of Neutrons Impingent on the Bottom of a Large Cylindrical Tank of Water, Using Geometry-Independent Space-Energy-Direction-Dependent Weight Windows Based on a Simple 1-D Deterministic Adjoint Flux Calculation 243

C.2.1 General Comments on Biasing Techniques 244

C.2.2 Difficulties With Traditional Biasing Techniques 244

C.2.3 Recent Developments: Geometry-Independent Weight Windows 245

C.2.4 Definition on an Academic Problem for Testing Purposes 246

C.2.5 Use of a 1-D Adjoint Calculation to Generate a 3-D Broad-Group Weight Window File 248

C.2.6 Results Obtained from MCNP4B When Using a Geometry-Independent Weight Window File 252

C.2.7 Verification of The MCNP Results 255

C.2.8 Conclusion 257

C.3 Informal notes on the format of the "geometry-independent weight window" file to be used with MCNP4B 259

C.4 GETWIN8.SCR: A fully self-contained script file for automatically generating the broad-group weight window file used by MCNP4B in the solution of the academic water tank problem described in Appendix C.2 267

C.5 Listing of the MCNP4B input file (WWT08) used in the solution of the academic water tank problem described in Appendix C.2 291

C.6 Preliminary, highly simplified, MCNP models once used for exploratory gamma-only analyses of the HB-3 beam tube using the newly proposed 1998 water tube design concept, as well as the original 1960 design concept 297

C.6.1 Reason for Including These Calculations in This Appendix 298

C.6.2 Reason for Looking at These Highly Simplified Models 299

C.6.3 Description of the Highly Simplified Model(s) 299

C.6.4 Discussion of Importance Zones in This Model 305

C.6.5 Key Results 311

C.6.6 Conclusions and Possible Improvements 313

C.6.7 Listing of the input file for MCNP Run HB307C, which was a preliminary (highly simplified) MCNP model once used for an exploratory analysis of the HB-3 beam tube using the newly proposed 1998 water tube design concept 321

C.6.8 Listing of the input file for MCNP Run HB307D, which was a preliminary (highly simplified) MCNP model once used for an exploratory analysis of the HB-3 beam tube using the original 1960 water tube design concept 331

C.7 GBA.SCR: A script file used for submitting and running a series of "forward mode" Group-Banded ANISN calculations involving a 1-D infinite slab model of the HB-3 beam tube including the 1998 water tube, the water-filled collimator, and the rotary shutter shield plug, as described in Sect 5.3 and Table 5.2 337

C.8 QADD3: A QAD-like point kernel shielding code used to estimate the gamma dose rate at Z=400 cm, just downstream of the collimator section, when the HB-3 water tube and collimator sections are both flooded 347

Appendices Related to Sect 6

D.1 GETWING3.SCR: A script file for performing a 1-D adjoint shielding analysis (of the HB-3 water tube, collimator, and rotary shutter) and generating properly normalized broad-group weight window information that is later used in the 3-D weight window generator (WW308G.F) which then produces the actual weight window file used in the MCNP4B Run HB308G gamma-only shielding analysis where the 1998 water tube and collimator sections are both flooded, the shutter is closed, and the HFIR is operating at 100 MW (cf Sect 6) 359

D.2 Listing of the 3-D broad-group weight window generator code (WW308G.F), described in Sect 6, that was actually used to create and write the weight window file used in MCNP Run HB308G for the gamma-only shielding analysis of the HB-3 beam tube and rotary shutter when the 1998 water tube and collimator sections are both flooded, the shutter is closed, and the HFIR is operating at 100 MW 383

D.3 Low-Order Justification for the Assumed Mesh-to-Mesh Weight Reduction Factor in Barytes Concrete 395

D.4 Listing of the input file for MCNP Run HB308G, used in the gamma-only shielding analysis of the HB-3 beam tube and rotary shutter when the 1998 water tube and collimator sections are both flooded, the shutter is closed, and the HFIR is operating at 100 MW 399

D.5 Additional Supplemental Results from the Final Gamma-Only Shielding Analysis, Run HB308G .. 451

D.5.1 Results 2.4945 cm Downstream of Collimator Exit 452

D.5.2 Dose Rates and Leakage Rates Downstream of the Entire Configuration 456

D.5.2.1 Clear Right-to-Left Asymmetry in External Dose and Leakage Rates Due to Steaming in Shutter 459

D.5.2.2 Slight Top-to-Bottom Asymmetry in External Dose and Leakage Rates Due to Steaming Around Shutter 459

D.5.2.3 Boundary Crossing Confirmation of Point Detector Dose Rate Downstream of Shield 459

Appendices Related to Sect 7

E.1 Description of the input for MCNP Run HB309, a neutron-only beam tube calculation to determine the fluxes, and 12 different nuclear reaction rates, in each of 39 1-cm-thick cylindrical shells around the large beam hole in the rotary shutter when the water tube and collimator sections are both void and the shutter is in the open position 465

E.2 ACTSRC.FOR: An ad hoc activation program to obtain the (activation) decay gamma source terms (p/s/cc) and (p/s) in each of the 39 1-cm-thick cylindrical shells concentrically centered around the 3.5-inch-diam beam hole through the HB-3 rotary shutter 475

E.3 SI.FOR: A utility program to take the "spatially-dependent (activation) decay gamma source terms per unit volume (p/s/cc) in each of the 39 1-cm-thick cylindrical shells concentrically centered around the 3.5-inch-diam beam hole through the HB-3 rotary shutter, 7 days after shutdown (as calculated by the ACTSRC.FOR program)" and produce the si2 and sp2 (source information and source probability) distributions needed for use with the SDEF card in the subsequent MCNP gamma-only shielding analysis (Run HB310) based on these activation source terms 491

E.4 Input listing for MCNP Run HB310, a gamma-only shielding calculation used to determine the dose rate downstream of the closed rotary shutter, seven days after shutdown, due to prior activation of the carbon steel rotary shutter itself 495

LIST OF FIGURES

2.1. Location of the point detectors used to obtain the reference fluxes in each of the four beam tubes 9

3.1. Overview of the original 1960 HB-4 beam tube before the cold source or any of the recently proposed upgrades 22

3.2. Basic MCNP model used in the HB-3 dosimetry analysis, shown with the 1960 beam tube void and the rotary shutter's large-diameter aperture open 23

3.3. Basic MCNP model used in the final HB-3 gamma shielding analysis, shown with the 1998 water tube and collimator sections both flooded and the shutter closed 24

3.4. Variation of the basic MCNP model, shown with the HB-3 water tube void and the rotary shutter's small-diameter aperture open 27

3.5. Variation of the basic MCNP model, showing the axial extent of the water in the original (simplified model of the) 1960 water tube 28

3.6. Variation of the basic MCNP model, showing the axial extent of the water in newly proposed 1998 water tube 29

3.7. Variation of the basic MCNP model, showing the 1998 water tube and collimator sections both flooded 30

3.8. Close-up view of the HB-3 beam tube (and the 1960 internal water tube), the surrounding stainless steel sleeve, the dosimeter holder ring, the coolant collector assembly, all located in the vicinity of the pressure vessel's HB-3 nozzle 31

3.9. Close-up view the 1998 HB-3 beam tube design in the vicinity of the first aluminum window defining the start of the 1998 water tube 32

3.10. Top view of a horizontal slice through the 1998 collimator design and the attendant radial and eccentric shields, as well as the pool seals, with the water tube flooded but the collimator section dry 33

3.11. Vertical slice through the MCNP model near the middle of the collimator, showing the rectangular hole down the center of the collimator, the collimator itself, the surrounding beam tube, the radial shield, the eccentric shield, a thin steel liner, and the surrounding biological shield 34

3.12. Top view of a horizontal (YZ) slice through the rotary shutter, including the downstream end of the collimator, the steel-line stepped concrete box holding the rotary shutter, and surrounding portions of the biological shield 35

3.13. Axial view of a vertical (XY) slice through the rotary shutter assembly and surrounding materials including the biological shield (with the shutter in the open position) 36

3.14. Close-up view of a horizontal (YZ) slice through the HB-3 beam tube (and the 1960 internal water tube), the surrounding stainless steel sleeve, the dosimeter holder ring, and the coolant collector assembly, as modeled in the dosimetry analysis for Key 3, positions 3 and 8 37

3.15. Close-up view of a vertical (XZ) slice through the HB-3 beam tube (and the 1960 internal water tube), the surrounding stainless steel sleeve, the dosimeter holder ring, and the coolant collector assembly, as modeled in the dosimetry analysis for Key 3, positions 3 and 8 38

3.16. Vertical (XY) slice through the coolant collector assembly mounted near the end of the stainless steel sleeve surrounding the HB-3 beam tube 39

3.17. Vertical slice through the rear section of the dosimeter holder ring (in the rotated plane of the holder ring), showing the Charpy V-notch specimens at Key 3, positions 3 and 8 40

3.18. Vertical slice just upstream of the dosimeter holder ring (in a plane rotated parallel to holder ring), showing the bolts and mounting lugs holding the dosimeter ring together, close to the dosimeters of interest 41

6.1. Magnet points for the regions in and around the rotary shutter 101

6.2. Values of WTAVG for each of the four broad gamma weight-window groups along the centerline of the flooded HB-3 beam tube and shutter 105

6.3. Values of WTLOW for each of the four broad gamma weight-window groups along the centerline of the flooded HB-3 beam tube and shutter 106

6.4. Values of WTLOW, WTAVG, and WTHIGH for each of the four broad gamma weight-window groups along the centerline of the flooded HB-3 beam tube and shutter 107

6.5. Centerline dose rates upstream and downstream of the rotary shutter in HB-3 when the 1998 water tube and collimator sections are both flooded, the shutter is closed, and the HFIR is operating at 100 MW 116

6.6. External dose rates averaged over different portions of the downstream surface of the entire shield configuration (at Z=478.79 cm), including the central 6.5-inch-diam hole downstream of the shutter, the main face of the concrete block assembly holding the rotary shutter, and each of the four 1.74625-cm-wide clearance gaps between the biological shield and the concrete block assembly, when the 1998 water tube and collimator sections are both flooded, the shutter is closed, and the HFIR is operating at 100 MW 125

6.7. Top view of the rotary shutter showing the amount of steel along the centerline, as used in the simple analytic determination of the dose rate downstream of the shutter 132

6.8. Three different paths by which gammas emerging from the collimator exit may contribute to the dose rate downstream of the void clearance gap between the biological shield and the concrete block assembly holding the rotary shutter 136

6.9. Two large spherical shells (in a bulk shielding material, centered about a point source) which bound a small spherically-shaped volume element in which the scattering rate is to be determined 138

6.10. One possible path by which scattered radiation might conceivably increase the dose rate along the centerline, directly downstream of the rotary shutter 145

6.11. Two of many possible paths showing how radiation that has passed through only a minimal amount of shielding material and scattered just once may preferentially tend to increase the dose rate downstream of the shield on one side of the shutter more than on the other side 146

7.1. Nuclear processes leading to the production of four key radioactive nuclides (Fe-59, Co-60, Mn-56, and Mn-54) in Type 1020 carbon steel 151

7.2 Centerline dose rates downstream of the HB-3 rotary shutter due to activation sources in the shutter itself, 7 days after shutdown, subsequent to operating at 100 MW for 30 years 162

7.3 External dose rates averaged over different portions of the downstream surface of the entire shield configuration at Z=478.79 cm due to activation sources in the rotary shutter, 7 days after shutdown, subsequent to operating at 100 MW for 30 years 165

7.4. Portion of the rotary shutter, beyond the 3.5-inch-diam beam hole, that is directly exposed to the highly collimated neutron beam coming from the 2.75-inch x 5.5-inch rectangular hole in the collimator under normal operating conditions 172

7.5. An elementary point source representation of the activation sources in the rotary shutter that proved woefully inadequate for representing the actual spatial distribution of the decay gamma sources, and could lead to very misleading estimates of the activation dose rate downstream of the shutter 173

7.6. Location of experimentally measured activation dose rates after shutdown 175

C2.1. Simple "academic" model used for testing the use of geometry-independent weight windows 247

C6.1 Isometric view of the highly-simplified model of the HB-3 water tube and collimator sections used in the preliminary gamma-only shielding analyses corresponding to MCNP Runs HB307C and HB307D 300

C6.2 Highly-simplified preliminary model of the 1998 HB-3 water tube and collimator sections used in MCNP Run HB307C 306

C6.3 Highly-simplified preliminary model of the 1960 HB-3 water tube and collimator sections used in MCNP Run HB307D 307

C6.4 Segmented areas used to tally the total gamma leakage (by energy group) at Z=399.48 cm in Tables C6.8 and C6.9 316

D5.1 Sketch of the 130-cm-diam internal boundary surface at Z=401.9645 cm, looking back towards the collimator from the rotary shutter 453

D5.2 Sketch of the 130-cm-diam external downstream surface of the entire shield configuration at Z=478.79 cm, looking back from outside the system (ie, from where the monochrometer drum would normally be located) 460

LIST OF TABLES

2.1. Location in the various beam tubes where point detector estimates of the neutron and gamma fluxes from global MCNP analyses were tallied and binned into the VELM 61n/23g group structures 8

2.2a. Equivalent point sources (n/s) in each beam tube for each of the 61 neutron groups in the VELM 61n/23g library structure 12

2.2b. Equivalent point sources (p/s) in each beam tube for each of the 23 gamma groups in the VELM 61n/23g library structure 13

2.3. Comparison of calculated neutron fluxes 6.55 meters from the tip of the HB-3 beam tube with the measured values reported by Blosser and Thomas in June 1968 15

2.4. Comparison of calculated and measured neutron reaction rates in the Ni-58 and Fe-54 dosimeters at HFIR Key 3, positions 3 and 8, around the HB-3 beam tube, just inside the pressure vessel 17

2.5. Comparison of calculated neutron fluxes 6.45 meters from the tip of the HB-2 beam tube with the measured values reported by Blosser and Thomas in June 1968 19

4.1. Comparison of calculated and measured neutron reaction rates in the Ni-58 and Fe-54 dosimeters at HFIR Key 3, positions 3 and 8, around the HB-3 beam tube, just inside the pressure vessel 55

4.2. Evolution of the dosimetry model which subsequently became the base MCNP model 56

5.1. Relaxation lengths for different particles in water and iron 66

5.2. ANISN 1-D slab model of the HB-3 water tube and collimator that was used to get a rough feel for what was important and what was not 68

5.3. Number of secondary gammas produced in each gamma energy group in zones 4 through 14 of the 1-D slab model given that the 61-group neutron source impingent on the first aluminum window here (zone 4) has the same intensities (n/s/cm2) as the 61-group neutron source impingent on the first aluminum window of the 1998 water tube at Z=174.27 cm 73

5.4. QADD3 point kernel results showing the total gamma dose rate downstream of the flooded collimator section (for the 1998 and 1960 HB-3 water tubes), and estimates of the relative dose rates there due to the original primary (impingent) gammas, secondary gammas in the first aluminum window, and secondary gammas in the first 32.8 cm of water, in eight 4.1-cm increments 76

5.5. Gamma dose rates impingent on the rotary shutter as given by the 3-group formula (which did not include secondary gammas, the 23-group point kernel method that did include secondary gammas, and the preliminary MCNP runs (HB307C and HB307D) which did not include secondary gammas 77

5.6. Cumulative fractional gamma dose rates at Z=400 cm as given by the QADD3 point kernel code for the "Top 25" contributors, in terms of source location and source energy group, ranked in order of importance, for the 1998 and 1960 HB-3 water tube shielding problem 78

6.1. ANISN 1-D buckled slab model (of the flooded 1998 HB-3 water tube, flooded collimator, and rotary shutter) used in the adjoint analysis of the gamma-only shielding problem to generate broad-group weight window information that could then be used in subsequent 3-D MCNP analyses 83

6.2a. Spatially-averaged broad-group neutron and gamma adjoint fluxes for the HB-3 gamma-only problem as summarized by GETWING3.SCR 86

6.2b. Space- and energy-dependent weight window lower limits (WTLOW) along the centerline of the flooded HB-3 system [for the six broad neutron weight-window groups and four broad gamma weight-window groups] in the gamma-only shielding analysis of the flooded HB-3 system, as calculated by GETWING3.SCR based on the associated 1-D adjoint analysis and the source-weight renormalization procedures in GETWING3.SCR 88

6.2c. Original MCNP4B source intensities and the new recommended (biased) source intensities that are consistent with the recommended weight windows for the HB-3 gamma-only problem (when 1998 water tube and collimator sections are both flooded) as determined by GETWING3.SCR 90

6.3. Space- and energy-dependent weight window lower limits (WTLOW) along the centerline of the system [for the gamma groups in the gamma-only problem], as well as the ratio of those values from one importance mesh to the next (calculated by GETWING3.F based on the associated 1-D adjoint analysis) 93

6.4. Key parameters used by the WW308G program to generate the 3-D broad group weight window file finally used by MCNP4B in the gamma-only shielding analysis of the flooded 1998 water tube, collimator, and rotary shutter assembly 95

6.5. Spatial definition of the 3-D lower weight window limits, and the location of the magnet points, as a function of importance mesh location (x,y,z) for the gamma-only MCNP4B analysis of the 1998 water tube problem 96

6.6. Gamma fluxes and dose rates at key axial locations along the HB-3 centerline, with the 1998 water tube and collimator sections both flooded, the shutter closed, and HFIR at 100 MW 117

6.7. Approximate gamma dose rates and fractional standard deviations, up through the 1998 HB3 water tube and the flooded rectangular hole in the collimator with the HFIR operating at 100 MW 120

6.8. Various estimates of the gamma dose rate (Rem/hr) between the end of the water-filled collimator and the rotary shutter 123

6.9. Integrated gamma leakage rates (p/s) and area-averaged gamma dose rates (mrem/hr) for various portions of a plane surface immediately downstream of the entire shield configuration (ie, at Z=478.79 cm, corresponding to the downstream surface of the stainless steel liner on the concrete block assembly holding the rotary shutter) 126

6.10. Integrated gamma leakage rates (p/s) and area-averaged gamma dose rates (mrem/hr) by energy group, at Z=478.29 cm, immediately downstream of the 6.5-inch-diam hole and the remainder of the square (83.5 cm x 83.5 cm) face of the concrete block assembly holding the rotary shutter 128

6.11a. Asymmetric right-to-left variations in external dose rates and leakage rates 130

6.11b. Asymmetric top-to-bottom variations in external dose rates and leakage rates 130

6.12. Simplistic program to calculate the local dose rate up and down on the external (downstream) face of the HB-3 shield configuration, directly in front of the void clearance gap between the biological shield and the concrete block assembly holding the rotary shutter, as well as the average dose rate over the long narrow gap 142

6.13. Scattered dose rate, direct dose rate, and total dose rate (mrem/hr) at nine different vertical locations directly in front of one of the tall thin clearance gaps between the biological shield and the concrete block assembly holding the rotary shutter 143

7.1. Broad-group neutron fluxes (n/s/cm2) in each segment of the rotary shutter under nominal conditions, and the actual volume of each of the 39 1-cm-thick cylindrical segments going outward from the 3.5-inch beam hole 154

7.2. Key reaction rates (per unit atom density) in each segment of the rotary shutter under nominal conditions 155

7.3. Buildup/depletion equations used during irradiation 156

7.4. Time-dependent results from the (ACTSRC) activation program for the first (innermost) 1-cm-thick shell next to the shutter's large beam hole, assuming the steel initially contained 0.45 wt% Mn-55 and 0.015 wt% Co-59 158

7.5. Disintegration rates for the four key radioactive nuclides, and the equivalent gamma source (p/s/cc) at 1.25 MeV, for the steel portion of each of the 39 1-cm-thick cylindrical shells around the shutter's large beam hole, 7 days after shutdown (subsequent to 30 years of irradiation), assuming the steel initially contained 0.45 wt% Mn-55 and 0.015 wt% Co-59 159

7.6. Gamma fluxes and dose rates at key axial locations along the HB-3 centerline (with the shutter closed), due to activation sources in the rotary shutter, 7 days after shutdown, subsequent to operating at 100 MW for 30 years 163

7.7. Integrated gamma leakage rates (p/s) and area-averaged gamma dose rates (mrem/hr) for various portions of a plane surface immediately downstream of the entire shield configuration (at Z=478.79 cm) due to activation sources in the rotary shutter, 7 days after shutdown, subsequent to operating at 100 MW for 30 years 166

7.8. Integrated gamma leakage rates (p/s) and area-averaged gamma dose rates (mrem/hr) by energy group at Z=478.29 cm [immediately downstream of the 6.5-inch-diam hole and the remainder of the square (83.5 cm x 83.5 cm) face of the concrete block assembly holding the rotary shutter], due to activation sources in the rotary shutter, 7 days after shutdown, subsequent to operating at 100 MW for 30 years 167

7.9a. Clear asymmetric right-to-left variations in external dose rates and leakage rates for Run HB310, based on the decay gamma activation sources in the rotary shutter, 7 days after shutdown 168

7.9b. Non-existence of asymmetric top-to-bottom variations in external dose rates and leakage rates for Run HB310, based on the decay gamma activation sources in the rotary shutter, 7 days after shutdown 168

7.10. Results of radiological survey HFIR-98-1712 in the region downstream of the HB-3 rotary shutter after shutdown (Feb 1998) 174

7.11. Total volume-integrated equivalent gamma source (p/s at 1.25 MeV) in each of the 39 cylindrical shells around the 3.5-inch hole in the rotary shutter, 7 days after shutdown, as a function of the initial Co-59 concentration (wt%) in the steel 177

A.2.1. Comparison of the approximate and original MCNP fluxes at each detector location in HB-1 shown in Table 2.1 190

A.2.2. Comparison of the approximate and original MCNP fluxes at each detector location in HB-2 shown in Table 2.1 192

A.2.3. Comparison of the approximate and original MCNP fluxes at each detector location in HB-3 shown in Table 2.1 194

A.2.4. Comparison of the approximate and original MCNP fluxes at each detector location in HB-4 shown in Table 2.1 196

A.2.5. Comparison of the approximate and original MCNP dose rates (mrem/hr) at each detector location shown in Table 2.1 198

C1.1 List of 307 additional new "importance" cells needed to replace just six or seven of the simple "material" cells near the centerline in the flooded HB-3 water-tube shielding analysis, as taken from the MCNP input for Run HB305B 239

C2.1a. Spatially-averaged broad-group neutron and adjoint fluxes for the academic problem as summarized by GETWIN8.SCR 249

C2.1b. Space- and energy-dependent weight window lower limits (based on adjoint fluxes for the academic problem) as summarized by GETWIN8.SCR 250

C2.1c. Original MCNP source intensities and the new recommended (biased) source intensities that are consistent with the recommended weight windows for the academic problem as determined by GETWIN8.SCR 251

C2.2. Total neutron and secondary gamma flux up through the central 20-cm-diam region of the academic problem, from MCNP Run WWT08 with 96 million histories 254

C6.1. Simplest possible geometry description (with no special importance zones) for the highly simplified, preliminary, gamma-only MCNP model for the HB-3 beam tube using the 1998 water tube design 301

C6.2. Simplest possible geometry description (with no special importance zones) for the highly simplified, preliminary, gamma-only MCNP model for the HB-3 beam tube using the 1960 water tube design 302

C6.3. Axially-dependent photon importance zones used in MCNP Run HB307C with the new (shorter) 1998 water tube starting at Z=174.27 cm, and in MCNP Run HB307D with the original (longer) 1960 water tube starting at 116.7841 cm 308

C6.4. Population of "numerical particles" (ever increasingly lower-weight particles) representing the gammas in each water-filled cell along the centerline in various MCNP runs 310

C6.5. Gamma fluxes and dose rates at a point midway between the collimator and rotary shutter when the water tube and collimator sections are both flooded and the HFIR is operating at 100 MW 312

C6.6. Gamma leakage (p/s) and corresponding fsd's, in various energy and angular ranges, on the downstream (exit) side of the 2.75-inch x 5.5-inch rectangular hole through the collimator when the 1998 water tube and collimator sections are both flooded and the HFIR is operating at 100 MW 314

C6.7. Gamma leakage (p/s) and corresponding fsd's, in various energy and angular ranges, on the downstream (exit) side of the 2.75-inch x 5.5-inch rectangular hole through the collimator when the 1960 water tube and collimator sections are both flooded and the HFIR is operating at 100 MW 315

C6.8. Total integrated gamma leakage (p/s) across the entire downstream surface of the collimator at Z=399.48 cm, including the water-filled rectangular hole (segment 5), when the 1998 water tube and collimator sections are both flooded and the HFIR is operating at 100 MW 317

C6.9. Total integrated gamma leakage (p/s) across the entire downstream surface of the collimator at Z=399.48 cm, including the water-filled rectangular hole (segment 5), when the 1960 water tube and collimator sections are both flooded and the HFIR is operating at 100 MW 318

D5.1. Gamma leakage (p/s) across the various segments of a plane surface at Z=401.9745 cm, located 2.4945 cm downstream of the collimator exit 454

D5.2. Gamma dose rates (mrem/hr) averaged across the various segments of a plane surface at Z=401.9745 cm, located 2.4945 cm downstream of the collimator exit 455

D5.3. Gamma leakage (p/s) and corresponding fsd's, in various energy and angular ranges, on the downstream (exit) side of the 2.75-inch x 5.5-inch rectangular hole through the collimator when the 1998 water tube and collimator sections are both flooded and the HFIR is operating at 100 MW (based on Run HB308G) 457

D5.4. Gamma leakage (p/s) and corresponding fsd's, in various energy and angular ranges, on the downstream (exit) side of the 2.75-inch x 5.5-inch rectangular hole through the collimator when the 1998 water tube and collimator sections are both flooded and the HFIR is operating at 100 MW (based on a composite of Runs HB308G and HB307C) 458

D5.5. Gamma leakage (p/s) across the various segments of a plane surface at Z=478.79 cm, corresponding to the downstream surface of the stainless steel liner on the concrete block assembly holding the rotary shutter 461

D5.6. Gamma dose rates (mrem/hr) averaged across the various segments of a plane surface at Z=478.79 cm, corresponding to the downstream surface of the stainless steel liner on the concrete block assembly holding the rotary shutter 462

E1.1. Key reaction rates (per unit atom density), and associated fsd's, in each segment of the rotary shutter under nominal conditions 472

ABSTRACT

The High Flux Isotope Reactor (HFIR) at the Oak Ridge National Laboratory is in the midst of a massive upgrade program to enhance experimental facilities. The reactor presently has four horizontal experimental beam tubes, all of which will be replaced or redesigned. The HB-2 beam tube will be enlarged to support more guide tubes, while the HB-4 beam tube will soon include a cold neutron source. To perform maintenance work on some experimental equipment while the reactor is still operating at 100 MW requires that the 2-ft-diam carbon steel rotary shutter at the end of a given beam tube be closed while an internal water tube (within the beam tube) is flooded. With the newly proposed designs, the internal water tubes needed for shielding will necessarily be as much as 1.89 feet shorter than those presently in use. This report examines the effect of that change on the downstream dose rates for a typical beam tube (HB-3), and establishes useful shielding methodologies and beam-tube-dependent source terms that may be used for all four beam tubes.

Section 2 describes a set of equivalent point sources that may be used in stand-alone shielding analyses for each beam tube. These are reported in terms of 61 neutron energy groups and 23 gamma energy groups. These were based on a series of large global analyses for the entire HFIR system using a detailed 3-D MCNP model. Results using these simplified source terms are compared against early experimental measurements made in HB-2 and HB-3 in 1968.

Section 3 describes the detailed 3-D MCNP model of the HB-3 beam tube used in all the remaining analyses.

Section 4 describes the neutron dosimetry analysis performed for HB-3 using the above source terms. The objective was partially to validate the source terms in HB-3 prior to their use in a detailed shielding analysis, and partially to determine if a Monte Carlo code like MCNP could really be used for good and reliable neutron dosimetry analyses. Ni58(n,p)Co58 reaction rates (primarily for neutrons above 1.0 MeV), and Fe54(n,p)Mn54 reaction rates (primarily for neutrons above 0.1 MeV) were calculated directly by MCNP at Key 3, Positions 3 and 8 and compared with experimental measurements. The C/E ratios for both reaction rates at both locations were all relatively small and fell in a narrow band between 1.17 and 1.25.

Sections 5 and 6 begin to focus on the HB-3 shielding problem with the water tube and collimator sections both flooded, the rotary shutter closed, and the HFIR operating at 100 MW. (With these sections void and the shutter open, the neutron and gamma dose rates in the main beam just downstream of the shutter would normally be 5.89e+8 mrem/hr and 8.44e+7 mrem/hr, respectively.)

Section 5 focuses on the determination of the dose rates impingent on the rotary shutter, and explores a diverse set of calculational techniques used to determine which transport phenomena are important and which are not. These techniques include the use of 1- and 3-group handbook equations, 1-D ANISN analyses using 61 neutron groups and 23 gamma groups, a 23-group point kernel approach (for gammas), and some preliminary 3-D MCNP analyses. The main conclusion is that, when flooded, the dose rates due to neutrons and secondary gammas impingent on the shutter are both totally negligible when compared to the 104.0 Rem/hr due to the original gamma sources. Remarkably, the point kernel calculations were within 1% of the final MCNP results.

Section 6 focuses on calculating the dose rate downstream of the rotary shutter due to the transmission of source gammas through the water tube, collimator, and rotary shutter when the shutter is closed and the 1998 water tube and collimator sections are both flooded. This particular deep penetration problem with its complex streaming paths was one of the more difficult shielding analyses performed at ORNL in recent years, and required advanced analytic techniques that two or three months earlier were simply unavailable. Rigorous solution of this particular problem required a host of biasing techniques including: use of only the most energetic source groups (a form of source-energy biasing); directional biasing of the source; on-the-fly directional biasing that was location dependent; and the extensive use of 3-D broad-group weight windows based on a preliminary 1-D adjoint analysis. The last was, by far, the most important. This analysis represents the bulk of the report. Sects 6.1 through 6.6 describe the use of a fine-group adjoint analysis to determine optimal 3-D broad-group weight windows for use in MCNP4B, and the role of those broad-group weight windows in accelerating the MCNP calculation. These were supplied to MCNP4B in a new "geometry independent" format that greatly simplified the analysis. Sections 6.7-6.9 describe other aspects of the final calculation while Sect 6.10 describes a number of simple independent checks for reasonableness, including one or two simple traditional checks on direct transmission, as well as a new technique for estimating the dose rate due to gamma radiation from a highly anisotropic source which scatters once or twice before streaming through clearance gaps near the end of the shield configuration. The final conclusion was that the transmitted component of the dose rate on the centerline, immediately downstream of the rotary shutter, was 0.89 mrem/hr under the above conditions.

Section 7 describes a detailed 3-D activation analysis of the rotary shutter, and a subsequent 3-D gamma-only shielding analysis based on decay gamma source terms in the rotary shutter at 7 days after shutdown, following an irradiation period of 30 years. While numerous components may become activated, the main problem will be activation gammas coming from those regions of the shutter within the first few centimeters of the large beam hole, the inner surface of which is normally in immediate (albeit tangential) contact with the neutron beam. The calculated dose rate 1.43 cm downstream of the rotary shutter, due to activation of the shutter itself, was 43.16 mrem/hr. This is in good to excellent agreement with the experimentally measured contact dose rate of 50 mrem/hr, as measured during the Feb 1998 shutdown.

1.0 INTRODUCTION AND EXECUTIVE SUMMARY

1.1 Background

The High Flux Isotope Reactor#1 (HFIR) at the Oak Ridge National Laboratory was designed in the early 1960's and began operation in 1968. In addition to its many irradiation facilities, the reactor has four horizontal beam tubes (HB-1, HB-2, HB-3, and HB-4) to accommodate a wide variety of neutron scattering experiments. The HB-2 beam tube is a radial beam tube which looks straight at the reactor core. The other three are tangential beam tubes whose centerlines are offset with respect to the core centerline so as to minimize radiation from high-energy neutrons and gammas. The HFIR Upgrade Project, now in the planning stage and soon to be implemented, encompasses a number of improvements that will enable the reactor to continue as a world class research facility well into the next century. In addition to replacing the beryllium reflector, each of the four horizontal beam tubes will be upgraded in one fashion or another. The most notable change will be in the HB-4 beam tube which will be redesigned and retrofitted with a cold neutron source#2 using liquid hydrogen at 20 deg.K. This will allow a whole new class of neutron scattering experiments to be performed involving very low-energy neutrons (well below 10 millivolts) which interact with matter in a wave-like fashion, with wavelengths in the 5 to 15 angstrom range. The next most dramatic change will involve the radial HB-2 beam tube#3. Now 4.0 inches in diameter, it will be replaced with a larger beam tube, having an inside diameter of 7.052 inches, which can accommodate up to five new guide tubes, each leading to separate experimental facilities outside the biological shield. To enhance the thermal neutron flux in these guide tubes, two large beryllium inserts will be placed inside the end of the beam tube closest to the core. The smaller 4-inch-diam HB-1 and HB-3 (tangential) beam tubes will also be replaced with new tubes, but their design will be left basically unchanged.

Each of the horizontal beam tubes in the existing HFIR reactor terminate at a shutter located just upstream of the respective monochrometer drums. Each rotary shutter (shield plug) has a large-diameter and small-diameter beam hole which may be selected for use in different experiments as needed. Alternately, each rotary shutter may also be rotated to the closed position to shut off the beam when on-line maintenance work is required on the monochrometer drum or other components downstream of the shutter. By themselves, the 2-ft-diam Type 1020 carbon steel rotary shutters do no provide sufficient shielding for such maintenance work while the reactor is on-line and operating. So that on-line maintenance work may be performed under such conditions, the existing beam tubes are each fitted with an internal water tube that may be flooded when on-line maintenance is required. Together, the flooded water tube and closed shutter provide adequate shielding for such work while the reactor is operating at full power.

The present beam tube/water tube design utilizes a "tube within a tube" concept insofar as, within each beam tube, there now exists a separate inner tube which may be flooded with water. Because a water tube is a physically separate tube that resides inside each beam tube, the present water tubes can and do extend inward through most of the biological shield, the reactor pool, past the pressure vessel nozzles, all the way to the inner surface of the pressure vessel, thus maximizing the amount of water available for shielding. Closing the 2-ft-diam Type 1020 carbon steel rotary shutter downstream of a given beam tube after flooding the internal water tube then provides the shielding necessary to isolate a given beam tube for maintenance work on the monochrometer drum (or other components) downstream of the shutter while the reactor is still operating at full power. Note that neither the closed shutter or the flooded water tube alone would provide adequate shielding; both are required. Unfortunately, having a physically separate water tube inside a beam tube reduces the effective diameter of the beam available for experiments.

As part of the HFIR Upgrade Project, the newly proposed designs for all four beam tubes would no longer use the former "tube within a tube" concept, but similar functionality would be provided by making a widely separated pair of internal aluminum windows an integral part of the main body of each beam tube, such that the region between the aluminum windows may be flooded as before. [Likewise, the collimator section of the beam tube (between the water tube section and the rotary shutter) would also be flooded separately, as before, whenever the water tube is flooded.] Because of various mechanical design considerations, however, the first aluminum window closest to the core would now be located near the beam tube expansion, downstream of the seal flange on the outside of the reactor vessel nozzle, thus reducing (by as much as two feet) the amount of water that is available for temporary shielding in the "water tube" portion of each beam tube. In the case of HB-3, for example, the effective water tube would be 1.89 feet shorter than the existing configuration where the inner water tube had extended all the way in to the inner wall of the pressure vessel. This shortening of the water tube region will raise the neutron and gamma loading impingent on the rotary shutter. The effect of this on dose rates downstream of the rotary shutter during maintenance operations is one of the key concerns addressed in this study. At the request of HFIR staff, the HB-3 beam tube was specifically chosen as a pilot case for more intensive analytic study. Methodologies developed for the HB-3 analysis may later be used in shielding analyses for other beam tubes.

1.2 Objectives

The key objective of this study was to conduct a detailed shielding analysis of a typical beam tube (HB-3) under these new conditions and to determine if any additional changes to the rotary shutter design would be necessitated by the new water tube concept. That study comprises the bulk of this report.

A secondary but prerequisite objective of this study (addressed in Sect 2) was to determine a set of simplified neutron and gamma source terms that could be used in the shielding analysis of all four beam tubes, including HB-4 with the proposed cold source, and the newly enlarged HB-2 radial beam tube with the beryllium pieces near the hot end of the beam tube. Eventually, shielding analyses like those performed here for HB-3 may have to be performed for HB-1 and HB-4. If so, those results will be reported separately at a later date. The primary objective of this study was to develop and demonstrate a reliable methodology, and the necessary source terms, that could be used in those analyses if necessary.

In the case of HB-2, the source terms developed here will eventually be needed for two different purposes. First, the initial source terms for HB-2 with the water tube voided (as in normal operation) will be needed for the design of the HB-2 guide tubes -- to determine the heating rates at the hot end of the guide tubes, to determine the shielding requirements for the backstop downstream of the guide tubes and all experimental equipment, and to determine scattering densities in the walls of the guide tubes downstream of the biological shield and the resulting radial shielding requirements in that region. Secondly, the source terms developed here will have to be used to generate an auxiliary set of simplified source terms that will accurately represent radiation entering the guide tubes (downstream of the actual HB-2 beam tube) when the beam tube is flooded. This auxiliary set of radiation source terms will be used by external vendors in the design of the new shutter mechanism that will be needed to accommodate the multiple rectangular guide tubes now planned. Both of these additional studies will be reported separately at some later time and are outside the scope of the present report.

1.3 Executive Summary

Section 2 describes a set of equivalent point sources that may be used in future stand-alone shielding analyses for each of the four horizontal beam tubes (HB-1, HB-2, HB-3, and HB-4). Tables 2.2a and 2.2b explicitly lists the 61-group neutron sources and 23-group gamma sources to be used for each beam tube. These were based on large global analyses of the entire HFIR system using a detailed 3-D MCNP#4 model. The model(s) used included the July 1996 conceptual cold source design#2 in HB-4, as well as the beryllium inserts inside the new 7.052-inch-ID HB-2 beam tube#3. These equivalent point sources are intended for use in shielding calculations where the region(s) of interest may be several meters from the tip of the beam tube(s). Testing shows these simplified source terms to generally reproduce the original MCNP results to within about 10%, one to three meters from the tip of the beam tube(s). Comparisons with earlier energy-dependent neutron measurements made by Blosser and Thomas#5 6.5 meters from the tip of HB-2 and HB-3 were made. In the case of HB-2, a simple ad hoc adjustment had to be made to account for the fact that the new beam tube has a larger diameter than that which existed at the time of the measurements. After this simple adjustment, the average C/E ratio was 0.89; except for one or two energy ranges, the bulk of the C/E ratios were between 0.91 and 1.09. Similar comparisons in HB-3 required no such correction since the HB-3 design had not changed. While the C/E ratios for thermal neutrons at 6.5 meters were a bit high (1.69), the results for faster neutrons were much better, with the average C/E ratio for the entire energy range being 1.44. Part of this discrepancy is believed to be due to modeling uncertainties stemming from insufficient documentation of the experimental configuration in 1968. (Nevertheless, these source terms are wholly acceptable for most types of shielding work where the uncertainty in the calculated shield effectiveness would normally be much higher than this.) More rigorously controlled dosimetry measurements on the inner surface of the vessel near HB-3 provide a second (more credible) basis for comparison. Based on directly measured Ni58(n,p)Co58 reaction rates#6 for neutrons above 1.0 MeV, and Fe54(n,p)Mn54 reaction rates#6 for neutrons above 0.1 MeV, the C/E ratios at this location are relatively small and lay in a narrow band between 1.17 and 1.25.

Section 3 describes the 3-D MCNP model(s) used in all (or most) of the analyses described in this report. The approach taken was to use the same (very complete) basic model for all calculations, with only minor variations, as necessary. It included everything within 65 cm of the beam tube centerline, from the tip of the beam tube, out past the downstream surface of the rotary shutter. Figs 3.2 through 3.18 show a number of different views of the basic model, each highlighting a different aspect of the model or showing it from a different perspective. Figs. 3.2 through 3.13 are of greatest interest for most of the shielding analyses, whereas Figs 3.14 through 3.18 focus on things important to the vessel dosimetry analysis. Sects 3.1 and 3.2 contain descriptive text pertaining to each figure. Note that these figures were made from the actual MCNP model. Sects 3.3 and 3.4 list and describe the nine older engineering drawings used in formulating this model, as well as the four recent conceptual drawings used in formulating this model. Separate paragraphs describe specifically what information was taken and used from each drawing.

Section 4 describes the neutron dosimetry analysis performed for HB-3. This effort was undertaken for two reasons: (1) to help validate the equivalent point sources for this beam tube before their anticipated use in the water tube shielding analysis, and (2) to determine if a Monte Carlo method like MCNP could really be used for good and reliable neutron dosimetry analyses. The final model used here (MCNP Run HB304M4) is the most detailed geometry model ever developed, representing the dosimeters and other materials in the neighborhood with the greatest fidelity ever. Based on the geometry alone, it is clearly a benchmark calculation. Moreover, it also gives the best C/E ratios ever obtained by any DORT#7, TORT#8, or MCNP#4 model. Ni58(n,p)Co58 reaction rates (primarily for neutrons above 1.0 MeV), and Fe54(n,p)Mn54 reaction rates (primarily for neutrons above 0.1 MeV) were directly calculated by MCNP at Key 3, Positions 3 and 8 using 120 million neutron histories. Here the pointwise energy-dependent fluxes were folded directly with the pointwise energy-dependent cross sections to obtain the integrated reaction rates at both locations, thus circumventing the need to collapse the fluxes or use group-averaged cross sections which might introduce uncertainties of their own. These integral reaction rates were then compared directly against the experimentally measured reaction rates. The C/E ratios for both reaction rates at both locations were relatively small and laid in a narrow band between 1.17 and 1.25. Moreover, both the calculated results and the measured results showed the Ni58 and Fe54 reaction rates at Key 3 Position 8 to be 2.29 to 2.37 times higher than at Position 3, thus increasing our confidence in the model and the source terms still more. By comparison, the best prior 3-D TORT analysis#6 gave an average C/E ratio of 0.69 and showed the flux tilt between these two dosimeters to be between 1.95 and 1.99 (rather than 2.29 or 2.37, as actually measured). Lastly, Sect 4.5 describes the historical evolution of the model, the lessons learned, and the sensitivity of the model to many different things. Because they are not directly related to the shielding analysis, those findings will not be repeated here, but anyone planning to perform future dosimetry work should certainly review this section first. The importance of accurately modeling seemingly small geometric details in the neutron dosimetry analysis cannot be overstated.

Section 5 begins to focus on the HB-3 water tube shielding problem. With the water tube and collimator sections both void and the rotary shutter in the open position, the neutron and gamma dose rates in the beam, immediately downstream of the shutter, would be 5.89e+8 mrem/hr and 8.44e+7 mrem/hr, respectively. In the ultimate case of interest, the water tube and collimator sections would both be flooded and the shutter would be closed. Sections 6 and 7 describe the calculation of the dose rates downstream of the shutter under those conditions. As an intermediate step, Sect 5 focuses on the determination of the dose rates impingent on the rotary shutter (just downstream of the flooded water tube and collimator sections), and explores a diverse set of calculational techniques used to determine which transport phenomena are important and which are not. These techniques include the use of 1- and 3-group handbook equations, 1-D ANISN#9 analyses using the 61 neutron groups and 23 gamma groups in the VELM library#10, a 23-group point kernel approach (for gammas), and some preliminary 3-D MCNP analyses. Several key conclusions may be drawn from these studies:

(1) The main conclusion is that, when flooded, the dose rate(s) due to neutrons and secondary gammas are both totally negligible when compared to that due to the original gamma sources.

(2) With the 1960 water tube design, the dose rate impingent on the shutter under these conditions is about 25 Rem/hr, 98.9% of which is due to source gammas above 3 MeV; With the 1998 water tube design, the dose rate is about 103 Rem/hr, 98.1% of which is due to source gammas above 3 MeV.

(3) For the 1998 water tube, the gamma dose rate impingent on the shutter is well known and was calculated several different ways: a simple 3-group handbook formula gave 90.2 Rem/hr, the 23-group point kernel method gave 103.0 Rem/hr, a preliminary (highly simplified) MCNP model gave 109.3 Rem/hr, and the final MCNP reference run (see Sect 6) gave 104.0 Rem/hr. From this, it is safe to conclude that the simple 23-group point kernel method is satisfactory for many gamma-only problems that do not involve highly localized streaming effects, and may well be the tool of choice in many preliminary design calculations.

Other supplemental observations are as follows:

(4) The use of importance regions and simple geometric splitting as variance reduction techniques in MCNP can be prohibitively impractical for deep penetration problems involving complex geometries. Except for its use in a couple of highly simplified models, that approach had to be abandoned here. A new technique making use of "geometry independent" broad group weight windows appears to be far more promising. This approach has since allowed similar problems to run 10,000 times faster than they otherwise would have run (cf Appendix C.2), and has since made it possible to solve problems that three months earlier would have been literally impossible (cf Sect 6).

(5) With the water tube and collimator sections flooded, handbook formulae indicate that the direct neutron dose rate impingent on the shutter may be totally unimportant; 1-D ANISN calculations confirm that conclusion.

(6) The 1-D ANISN calculations can be used to obtain secondary gamma productions rates "per unit volume" which can then be used in point kernel codes where one can then account for the actual secondary sources based on more realistic volume elements.

(7) Results of those point kernel calculations agree remarkably well with more elaborate 3-D Monte Carlo results (within 1%).

(8) The number of secondary gammas born in the water tube is comparable in magnitude with those entering the water tube but, because the secondary gammas are born isotropically whereas source gammas streaming down the beam tube and entering the water tube are already very forward-directed, the secondary gammas are completely negligible relative to the latter by the time they reach the rotary shutter. The point kernel method provides a convenient vehicle for studying their relative effectiveness, by source type and location, and by energy group.

Section 6 focuses on calculating the dose rate downstream of the rotary shutter due to the transmission of source gammas through the water tube, collimator, and rotary shutter when the shutter is closed and the 1998 water tube and collimator sections are both flooded. This is a complex gamma-only analysis involving only the original gamma sources (cf Table 2.2b) above 3 MeV. [Based on findings in Sect 5, the total dose rate even upstream of the shutter was totally insensitive to the neutron source and the resulting secondary gammas. Likewise, the original source gammas below 3 MeV contributed less than 2% of the total dose at this location. Downstream of the shutter, these low-energy gammas will contribute even less, and can be safely neglected as well.] Clearly this was one of the most difficult shielding analyses ever performed at ORNL (if not the most difficult), and required advanced analytic techniques that two or three months earlier were simply unavailable. Because of that, and the importance of this particular deep penetration problem with its complex streaming paths, Sect 6 and the supporting appendices represent the bulk of this report. Sects 6.1 through 6.6 describe the use of a fine-group adjoint analysis to determine optimal 3-D broad-group weight windows for use in MCNP4B#4, and the role of those broad-group weight windows in accelerating the MCNP calculation. (Apart from the documentation in this report, the all-important ability to supply those 3-D broad group weight windows to MCNP4B in a "geometry independent" format via a separate auxiliary input file remains an undocumented feature of the code that will not be publicly announced until its next official release in the year 2000.) Sects 6.7 and 6.8 then present a general review of the physical model used in this final 3-D gamma-only shielding analysis, as well as a detailed discussion of all other aspects of this particular calculation. Sect 6.9 describes the final results obtained (summarized below), while Sect 6.10 describes a number of simple independent checks for reasonableness. This last section, which is divided into 10 parts, describes one or two simple (traditional) checks on the direct transmission of gammas through the rotary shutter shield plug, but then goes on to develop a whole new (elementary) technique for estimating the dose due to gamma radiation from a highly anisotropic source that has scattered once or twice before finally streaming out of the shield configuration through the large 1.75-cm-wide clearance gaps between the biological shield and the concrete block assembly holding the rotary shield plug. Surprisingly (and perhaps fortuitously), these latter results were within 11% (less than half a standard deviation) of the more rigorously obtained MCNP results. The worth of this report lies partly in the final MCNP results (described below), but largely in new and extremely powerful biasing techniques described in Sects 6.1 through 6.6, and in the description of the independent (simplistic) checks for reasonableness. Key results from this 3-D MCNP analysis are as follows:

(1) The dose rate on the centerline, immediately downstream of the shutter (at Z=479.29 cm) was found to be 0.8934 mrem/hr +/- 3.4%. At 1.5 feet from the surface of the rotary shutter housing (at Z=524.51 cm), the centerline dose rate was found to be 0.3033 mrem/hr +/- 1.1%, while at 3.0 feet from this surface (at Z=570.23 cm) the centerline dose rate was found to be 0.2088 mrem/hr +/- 0.6%. The dose rate at the closest point was calculated using a point detector estimate, but verified using a much more rigorous boundary crossing tally which exhibited exceptionally good statistics in every energy range of interest. The dose rate at the closest point was also verified using simple analytic approximations.

(2) Streaming effects associated with the 1.74625-cm clearance gaps between the biological shield and the concrete block assembly holding the shutter caused the dose rates in front of those locations to be two orders of magnitude higher than they otherwise would have been without any clearance gaps. MCNP and a simple analytic method used to check those results both saw this effect, and both yield essentially the same result. Fortunately, the dose rates obtained by both methods (even with streaming) were totally negligible (less than 0.05 mrem/hr). In the case of MCNP, the average dose rate for the gap on the right side of the configuration (0.0477 mrem/hr) was found to be 2.13 times higher than on the left (0.0217 mrem/hr) due to streaming through the large beam hole in the rotary shutter which is rotated 66.75 degrees from the beam tube centerline when the shutter is in the closed position. In addition, the average dose rate for the clearance gap above the concrete block assembly holding the rotary shutter (0.0222 mrem/hr) was found to be marginally higher that for the clearance gap on the bottom (0.0150 mrem/hr) due to a small amount of streaming in the 5/16-inch clearance gap above the carbon steel shield plug inside the rotary shutter assembly. While not of any programmatic significance because of their low values, these small, physically justifiable, asymmetric variations are indicative of the small details that can be seen with this detailed 3-D model when used in combination with the 3-D broad-group weight window file which was developed for this analysis using a fine-group 1-D adjoint analysis.

(3) A useful by-product of this analysis was a very detailed boundary source file for a surface perpendicular to the centerline, just upstream of the rotary shutter assembly. This binary file is an MCNP boundary crossing history file (at Z=401.9645 cm) which contains the coordinates, direction cosines, energies and weights of the 5,688,819 photons crossing this surface in Run HB308G5. This particular file, which requires 542 MB of disk space, can then be used as an internal boundary source file in subsequent

follow-up shielding analyses of this rotary shutter (or any similar shutter design in the future) by using the procedures outlined in Sect 6.8.2.

(4) Rigorous solution of this particular problem required a host of biasing techniques including: use of only the most energetic source groups (a form of source-energy biasing); directional biasing of the source; on-the-fly directional biasing that was location dependent; and the extensive use of 3-D broad-group weight windows based on a preliminary 1-D adjoint analysis. The last was, by far, the most important. Without it, the rigorous solution of this problem would have been totally impossible.

Given prior expectations based on health physics measurements, the calculated centerline dose rate immediately downstream of the shutter (0.89 mrem/hr) was surprisingly low. However, given that this point detector estimate was verified using a much more rigorous boundary crossing tally which exhibited exceptionally good statistics in every energy range of interest, and that the dose rate at this point was also verified using simple analytic approximations, it must be accepted at face value. It should be noted, however, that this calculated dose rate downstream of the rotary shutter is only that portion of the dose rate "due to the transmission of source gammas" through the water tube, collimator, and rotary shutter when the shutter is closed and the 1998 water tube and collimator sections are both flooded. Notably, by intent, it did not include contributions from activation gammas in the rotary shutter or any other components in the vicinity. As later discovered, and shown in Sect 7, the actual dose rate here (43-50 mrem/hr) is almost entirely due to such activation sources.

Section 7 describes a detailed 3-D activation analysis of the rotary shutter, and a subsequent 3-D gamma-only shielding analysis based on decay gamma source terms in the rotary shutter at 7 days after shutdown, following an irradiation period of 30 years. While numerous components may become activated to one degree or another, the main problem will be activation gammas coming from those regions of the shutter within the first few centimeters of the large beam hole, the inner surface of which is normally in immediate (albeit tangential) contact with the neutron beam. Even when the shutter is in the closed position, these activated regions are never far away from the external surface of the shield configuration, and the amount of steel available for self-attenuation is minimal.

This study involved three or four key steps: (1) identification of the key radioactive nuclides (Co-60, Fe-59, Mn-54, and Mn-56) responsible for the activation dose, and the twelve nuclear reaction processes by which these are created, (2) running a 3-D MCNP neutron-only beam tube analysis to determine all twelve of the necessary reaction rates in each of 39 1-cm-thick cylindrical shells around rotary shutter beam hole under normal conditions with the shutter open; (3) performing a detailed activation analysis for each of these 39 regions so as to determine the concentration levels after 30 years of exposure and at various times (0-60 days) after a subsequent shutdown; and (4) putting the resulting gamma source terms for each region back into the 3-D MCNP model, rotating the shutter to the closed position with the sources in place, and performing the attendant 3-D gamma shielding analysis.

The basic activation analysis assumed that the Type 1020 carbon steel rotary shutter initially contained 0.45 wt% Mn-55 and 0.015 wt% Co-59 (the same as the HFIR pressure vessel#6), although several variations were later considered with initial Co-59 concentrations of 0.000 and 0.001 wt%, as well as 0.005 to 0.030 wt%, in increments of 0.005 wt%. Decay gamma source terms for the base case, seven days after shutdown, were used in the subsequent 3-D shielding analysis. (Note that one or two days after shutdown, the shortlived sources from the decay of Mn-56 are essentially gone. With halflives of 312.2 days, 44.51 days, and 5.271 years, for Mn-54, Fe-59, and Co-60, respectively, the remaining decay gamma source terms and resulting dose rates change very slowly over the next few weeks. Of the radioactive sources, Co-60 is by far the most important. During the first few weeks or months, Fe-59 is the next most important, with the Mn-54 being a distant third.) The key conclusions from this activation study and subsequent shielding analysis are as follows:

(1) The calculated dose rate 1.43 cm downstream of the rotary shutter, due to activation of the shutter alone, was 43.16 mrem/hr. This is in good to excellent agreement with the experimentally measured contact dose rate of 50 mrem/hr, as measured#11 during the Feb 1998 shutdown.

(2) This dose due to activation would be present whenever the shutter is closed, whether the HFIR is operating or not. Because this inherent activation of the shutter is the result of neutrons streaming down the beam tube during years of normal operation when the water tube is normally void, the intensity of this activation source and the resulting dose rate (43 mrem/hr) will be independent of water tube design (ie, it will be essentially the same whether one switches to the new 1998 design or continues to use the original 1960 design).

(3) More importantly, this dose rate due to activation alone (43-50 mrem/hr) is far greater than the 0.8934 mrem/hr (cf Sect 6) that results from direct transmission of radiation down the beam tube and through the shutter when the new (shorter) 1998 water tube and collimator sections are both flooded, the shutter is closed, and the HFIR is operating at 100 MW.

For these reasons, one is forced to conclude that the total dose rate downstream of the shutter, under these conditions, will remain in the 43-50 mrem/hr range and will be independent of water tube design (ie, it will be essentially the same whether one switches to the new 1998 design or continues to use the original 1960 design). Indeed, that is the main conclusion of this entire report.

Other miscellaneous observations related to the activation study are as follows:

(4) For most initial cobalt concentrations of interest (between 0.005 wt% and 0.030 wt%), the gamma sources vary almost linearly with the amount of Co-59 initially present. If the amount of Co-59 initially present were 2.0 times higher (ie, 0.030 wt%), the total gamma source would be 1.8 to 1.9 times higher; while if the amount of Co-59 initially present were 3.0 times lower (ie, 0.005 wt%), the total gamma source would be 2.2 to 2.4 times lower. For very low initial Co-59 concentrations (0.000 wt% and 0.001 wt%), the relationship is no longer linear. If the initial amount of Co-59 is reduced by a factor of 15 (from 0.015 wt%, down to 0.001 wt%), the total gamma source would only be 4 to 5 times lower, while if the initial Co-59 is reduced to zero, the total gamma source would be about 5 to 8 times lower than for the case with 0.015 wt% Co-59.

(5) Switching to a new rotary shutter design which only has one beam hole and could therefore be turned 90 degrees when closed (rather than 66.75 degrees as in the present design) will, in fact, reduce the dose rate somewhat, although the extent of that decrease has not been evaluated.

2.0 SOURCE TERMS FOR BEAM TUBE SHIELDING ANALYSES

Shielding analyses for the individual beam tubes will generally require modeling materials and components located several meters from the core. A typical model will, for example, include the hot tip of the given beam tube, the entire length of the beam tube and surrounding media (as is passes out of the beryllium reflector, through the water in the vessel, through the wall of the pressure vessel, through the pool, and through the concrete forming the biological shield), the internal water tube and beam collimator, and the rotary shutter (shield plug) assembly further downstream. As such, it would be totally impractical to incorporate such analyses directly into the large global analysis for the HFIR core and reflector. So that shielding analyses may be performed separately for each of the individual beam tubes, it was necessary to have a separate set of source terms which accurately characterized the neutron and gamma sources entering each beam tube.

2.1 Methodology

It was ultimately found that a series of point sources (in each beam tube) was wholly adequate for this purpose. This section describes how those equivalent point sources were determined, while this and subsequent sections document their validity. Simply stated, the equivalent point sources were determined as follows: (1) Several large global 3-D MCNP analyses were performed for the HFIR core and reflector with the beam tubes extending out through the biological shield. (2) In each calculation, point detectors were used to obtain highly converged estimates of the neutron and gamma fluxes at various points down a given beam tube. These detectors were located at: 4 separate points down HB-1, 4 separate points down HB-3, 4 separate points down HB-4, and 7 separate points down HB-2. While MCNP tracks particles as a continuous function of energy, the results at the point detectors were tallied and "binned" into the 61 neutron groups and/or 23 gamma groups used in the VELM shielding library#10. This was done in recognition of the fact that future shielding calculations may use the DORT (2-D) or TORT (3-D) shielding codes and the VELM 61n/23g cross section library. (3) For a given beam tube, and a given neutron or gamma energy group, the equivalent point source was found by: picking an assumed source location (x0) near the hot tip of the beam tube, assuming the flux varies as F(x,g)=S(g)/[4*pi*(x-x0)^2], and finding the source term S(g) that best fits the MCNP fluxes at the 4 (or 7) points corresponding to the point detectors in that beam tube. Having done that, increment the assumed source location (x0) by 0.1 cm, and repeat the process every 0.1 cm down the entire length of the beam tube. Having done that, there will be one source location [x0(g)] and one source intensity [S(x0,g)] that provides the "best" fit for the MCNP fluxes in this energy group at all 4 (or 7) points.

2.2 Selection of Detector Locations

Table 2.1 and Fig 2.1 show the location of the point detectors used to obtain the reference fluxes in each beam tube, while Table 2.1 also shows the selection criteria used for these points. Anticipating the need for future beam tube shielding calculations with the (newly proposed 1998) water tubes flooded and dry, it was predicated that the equivalent point sources to be determined here should be able to reproduce the known (MCNP) fluxes in the dry water tube. Detector locations were therefore chosen at the start, end, and midpoint of each water tube, as well as one equidistant point upstream of the water tube. In the case of HB-2, results from an earlier calculation (MCNP Run GF209) were also included. These included earlier results at the start of the guide tubes (so that Runs GF209 and GF215 would have a common point where the results could be cross checked), as well as a more distant point where the guide tubes emerge from the biological shield.

2.3 Pedigree of MCNP Run GF211 for HB-1 and HB-4

Results in HB-1 and HB-4 will be affected by the recently proposed changes in this region, including the elimination of the through tube (thereby making HB-1 and HB-4 separate tubes), as well as the presence of the newly proposed cold source. [These results will be unaffected by the recently proposed changes to the HB-2 beam tube on the other side of the system.] Results for HB-1 and HB-4 are based on MCNP Run GF211 which is identical to cold source reference calculation GF130 except that: (1) the old tallies have been stripped out and replaced by those for the point detectors described in Table 2.1, and (2) Cells 8903, 8904, and 8905 (representing the two aluminum windows in HB-4) have been replaced by a void for the purposes of the present flux determination. More details of GF130 are given below.

Table 2.1. Location in the various beam tubes where point detector estimates of the neutron and gamma fluxes from global MCNP analyses were tallied and binned into the VELM 61n/23g group structures. The Run ID's identify the respective MCNP calculational runs, while the Tally ID's identify the reference tallies used in each run.

Loc ID	MCNP RunID	N-Flx Tally	G-Flx Tally	Beam Tube	Distances & Global Coordinates (X,Y) in cm Q(*)	P(*)	X	Y	Selection Criteria: Why given point was chosen
A	GF211	115	215	HB-1	98.1835	103.6825	-18.62571	108.96868	<-- A,B,C,D are equidistant
B	GF211	125	225	HB-1	163.4800	168.9790	-51.27396	165.51711	<-- water tube begins here
C	GF211	135	235	HB-1	228.7765	234.2755	-83.92221	222.06553	<-- water tube midpoint
D	GF211	145	245	HB-1	294.0730	299.5720	-116.57046	278.61396	<-- water tube ends here
U'	GF209	735	765	HB-2	------	117.4750	-117.4750	0.0	<-- arb pt where DORT results were available
U	GF215	515	615	HB-2	------	126.0890	-126.0890	0.0	<-- U,V,W,Z are equidistant
V	GF215	525	625	HB-2	------	199.8410	-199.8410	0.0	<-- water tube begins here
W	GF215	535	635	HB-2	------	273.5930	-273.5930	0.0	<-- W=(V+Z)/2
Z	GF215	545	645	HB-2	------	347.3450	-347.3450	0.0	<-- individual guides start here
Z'	GF209	745	775	HB-2	------	347.3450	-347.3450	0.0	<-- individual guides start here
Z''	GF209	755	785	HB-2	------	635.6350	-635.6350	0.0	<-- guides emerge from bio shield
K	GF214	115	215	HB-3	98.1835	120.6879	-37.24705	-117.85379	<-- K,L,M,N are equidistant
L	GF214	125	225	HB-3	163.4800	185.9844	-69.89530	-174.40222	<-- water tube begins here
M	GF214	135	235	HB-3	228.7765	251.2809	-102.54355	-230.95064	<-- water tube midpoint
N	GF214	145	245	HB-3	294.0730	316.5774	-135.19180	-287.49907	<-- water tube ends here
E	GF211	515	615	HB-4	------	134.6719	100.55149	-97.45229	<-- E,F,G,H are equidistant
F	GF211	525	625	HB-4	------	214.3364	140.38374	-166.44377	<-- water tube begins here
G	GF211	535	635	HB-4	------	294.0009	180.21599	-235.43525	<-- water tube midpoint
H	GF211	545	645	HB-4	------	373.6654	220.04824	-304.42673	<-- water tube ends here

P = distance (cm) from "the (core) radial plane perpendicular to centerline of the beam tube" to the point of interest; for example, the distance from center of the HB-1/HB-4 thru tube to point of interest.
Q = distance (cm) from outer spherical tip of HB-1 or HB-3 to point of interest
(X,Y) = absolute coordinates (cm) for the detector of interest, where (0,0)=core centerline

Note: Run GF211 is identical to Ref Calc GF130 except that (1) all the old tallies have been stripped out and replaced with those shown above, and (2) Cells 8903, 8904, and 8905 (representing the two aluminum windows in HB-4) have been replaced by a void. Run GF130, which uses a boundary source around the HB-1/HB-4 thru tube, is still the best ref calc for the cold source, even though it uses the original 4-inch-diam HB-2 beam tube. This particular boundary source (used in Runs GF130 and GF211) is based on Run GF123 which used 12.24 million neutron histories.

Note: Runs GF214 and GF215 are identical to GF209 except that all the old detector tallies have been stripped out and replaced with those shown above. Like Run GF209: these are coupled n/g k-eff calculations using the new (larger) 7.052-inch-ID HB-2 with the two Be pieces inside HB-2; EF-3 and EF-4 have been removed; and the control rods are in their normal end of cycle position. This basic configuration was first modeled in Run GF202 in Sept 1997 (for Dick Rothrock's neutron-only keff calc), and later retained in Run GF209 (a coupled n/g keff calculation) to get the original point sources for the HB-2 backstop analyses. Runs GF209, GF214, and GF215 are all based on 2.88 million histories.

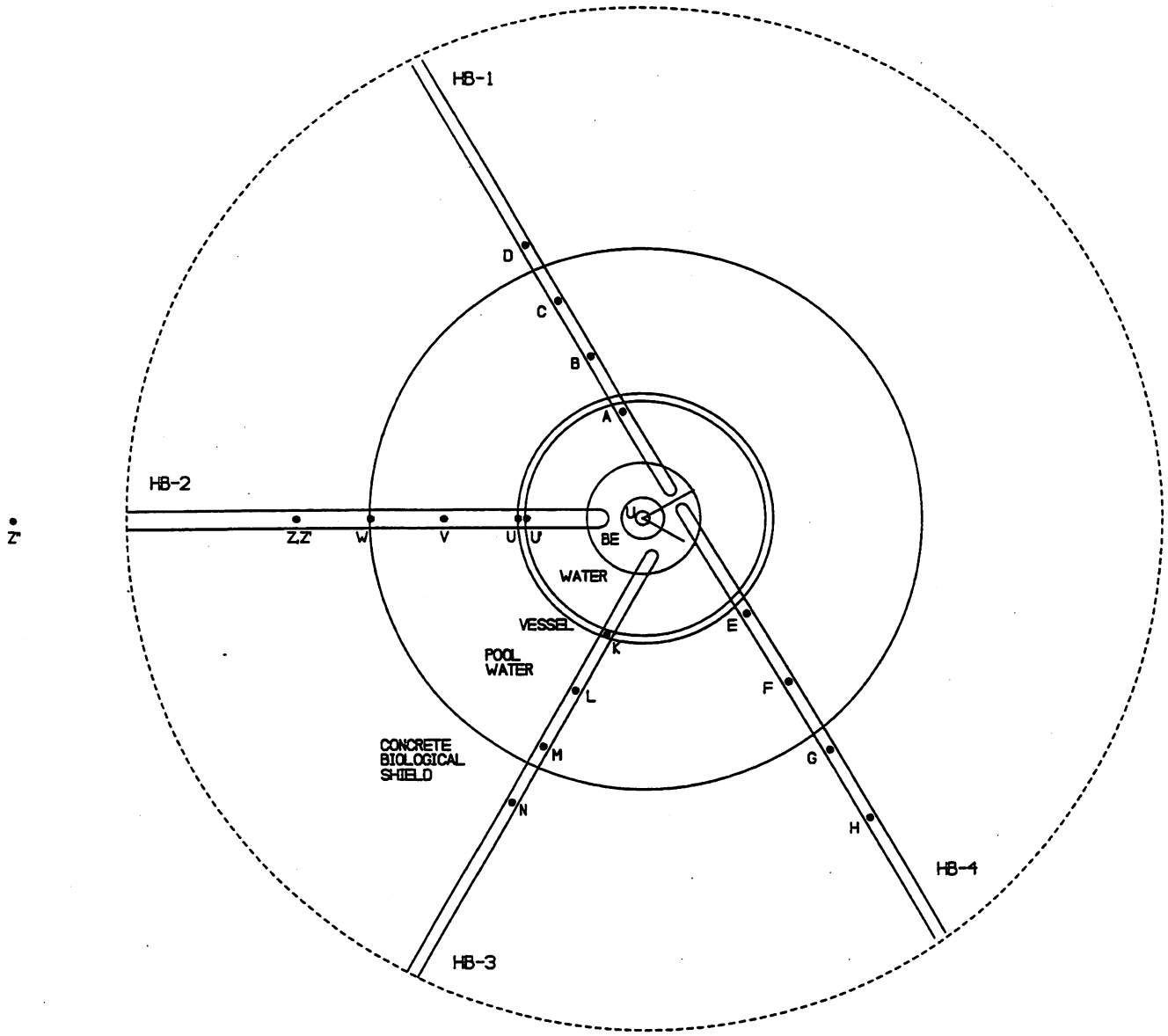


Fig. 2.1. Locations of the point detectors used to obtain the reference fluxes in each of the four beam tubes. For exact locations, see Table 2.1.

The best reference calculations for the cold source at the time of this study, were reference calculations GF123 and GF130 from April 25-30, 1997. These are based on the conceptual design for the 505 cc cold source as frozen in July 1996. With only extremely minor exceptions, which are believed to have essentially no neutronic effects of consequence, this corresponds to the final design which is yet to be analyzed. A good description of the cold source as modeled in GF123 and GF130 may be found in the "HFIR Cold Source Project Review#12,13, May 29-30, 1997". This document also describes the fluxes and heating rates in and around the cold source. Summary level information may also be found in the "HFIR Cold Neutron Source Reference Design Concept" document#2.

Cold source Run GF123 was a large global analysis of the entire HFIR, including the core, the beryllium reflector (with all the VXF positions plugged with beryllium plugs), the EF-3 slant tube (with empty positions for the other slant tubes which were physically not present), the surrounding water, the pressure vessel, the pool, and the concrete biological shield, with all four horizontal beam tubes extending out through the biological shield. The through tube had been removed, and HB-1 and HB-4 were modeled as separate tubes in accordance with the new design. All of the necessary modifications to HB-4 had been made, including the presence of the cold source and the vacuum vessel, the enlargement of the HB-4 beam tube just outside the beryllium reflector, and a further enlargement in the pool outside the reactor vessel. In this particular model, HB-2 had not yet been modified, and corresponded to the original HB-2 design from 1960. Trace amounts of Li-6 (corresponding to equilibrium conditions) and trace amounts of He-3 (corresponding to the reactor after 50 cycles of operation) had been distributed in a graded fashion throughout 3 discrete radial regions in the removable beryllium reflector and 5 discrete radial regions in the permanent beryllium reflector. So as to obtain the maximum flux levels (and heating rates) in the cold source and the rest of the system, this coupled n/g keff calculation was performed with the reactor at end-of-cycle -- meaning that fuel in each of 7 axial regions and 17 radial regions (119 regions altogether) had been irradiated in a 3-D VENTURE burnup analysis#14,15 so as to represent EOC conditions, and the control rods were modeled in their EOC positions (wide open). The final calculated keff, after 12.24 million neutron histories was 1.00759 +/- 0.00024. This coupled n/g keff calculation (GF123) included all prompt gammas from the core, all the delayed fission product gammas from the core (by using a special U-235 cross section dataset developed especially for this project), and all secondary gammas from all materials in the system. By using a special Al-27 cross section, developed especially for this project, it also accounted for all of the Al-28 decay gammas resulting from neutron capture in Al-27. Moreover, these Al-28 decay gammas were tracked through the entire calculational model just as if they were instantaneous secondary gammas.

While the cold source brightness and local heating rates were calculated in Run GF123, the main purpose was to develop a very good boundary source in the region around the HB-1 and HB-4 beam tubes that could be used in subsequent parametric analyses. (That is why GF123 was run for 12.24 million neutron histories when 2-4 million would have sufficed if one were only interested in the immediate results inside the cold source.) In the course of this calculation, therefore, an imaginary cylinder was drawn 15 cm from the HB-1/HB-4 centerline. All neutron and gamma particle tracks crossing this imaginary surface were recorded for future use. This boundary source, which requires 592 MB of disk space, has been used in numerous parametric calculations since May 1997. In particular, Run GF130 represents such a calculation. It, however, is regarded as the cold source "reference calculation" insofar as it uses this boundary source (from Run GF123) but is otherwise unperturbed such that the geometry and materials correspond exactly to Run GF123. Run GF130 was run as a base reference case simply to verify that, within small statistical limits, it completely reproduced the known results from global analysis in Run GF123. The advantage of Run GF130, and all similar runs using this boundary source, is that one does not need to track neutrons and gammas outside the 30-cm-diam boundary source region, that it reproduces the results of the full global analysis based on 12.24 million histories, and that it can run in a small fraction of the time required for the large global analysis. Moreover, use of this boundary source is the best and fastest way to produce highly accurate results down the HB-1 or HB-4 beam tubes with the cold source present.

Except for the removal of the two thin aluminum windows in HB-4, Run GF211 is essentially identical with Run GF130. These two thin aluminum windows in HB-4 were removed in GF211 so that we could get the unperturbed fluxes in the HB-4 beam tube, upon which the equivalent point sources could be based. Future shielding calculations for HB-4 using these point sources would, of course, include these aluminum windows defining the beginning and end of the water tube, as well as a more detailed description of the collimator and rotary shutter several meters downstream from the cold source.

2.4 Pedigree of MCNP Runs GF209, GF214, and GF215 for HB-2 and HB-3

In Sept 1997, we were asked to assess the impact of the new (larger) 7.052-inch-ID HB-2 beam tube (with the two Be pieces located inside the beam tube near the tip of the tube) on the worth of the control rods#3. Because of the new larger-diameter beam tube, the EF-3 slant tube would be removed, and the new beryllium reflector design would no longer have provisions for accommodating

either the EF-3 or EF-4 slant tubes. Starting with the model used in GF123, the modifications described above were made to create Run GF202, a neutron-only calculation to determine the keff of the system with these modifications. Here the enlarged HB-2 beam tube, with this new inside diameter, was modeled as a straight tube with no further modifications beyond the beryllium reflector (i.e., no further enlargements past the beryllium or the pressure vessel, and no guide tubes or shutter mechanism in the biological shield). This was documented#3 as RRD Calculation C-HFIR-97-25, dated Sept 30, 1997. Basically it showed that the new (larger) beam tube with the two beryllium pieces inside would have no effect of the keff of the system. Run GF202 gave a keff of 1.00758 +/- 0.00054 after 2.88 million histories. This same model, with a few additional point detectors added, was later run in Nov 1997 as a coupled n/g keff calculation to obtain neutron and gamma fluxes at several points down along the centerline of the HB-2 beam tube. This was denoted as Run GF209. Its purpose, at that time, was to facilitate comparisons with several DORT analyses that had been performed for the vessel dosimetry project, and to provide a basis for some simplified sources that could be used in further dosimetry work (and potentially for the preliminary HB-2 backstop analyses that were underway at that time). Runs GF214 and GF215 in the present study are identical to Run GF209 except that all the old detector tallies have been stripped out and replaced with those shown in Table 2.1. Like Run GF209: these are coupled n/g k-eff calculations using the new (larger) 7.052-inch-ID HB-2 with the two Be pieces inside HB-2; EF-3 and EF-4 have been removed; and the control rods are in their normal end-of-cycle position. Runs GF209, GF214, and GF215 are all based on 2.88 million neutron histories.

2.5 Recommended Equivalent Point Sources for Shielding Calculations

The methodology for determining the equivalent point sources for each neutron and gamma energy group based on the calculated MCNP fluxes at several points down a beam tube is described above. The recommended equivalent point sources for each of the 61 neutron energy groups and 23 gamma energy groups (in the VELM 61n/23g group structure) in each of the four beam tubes (HB-1,2,3,4) are shown in Tables 2.2a and 2.2b. While the point sources are located along the centerline of the given beam tube, the effective point source for each energy group may be at a different axial location. The variable "x0" shows the distance (in cm) from the point source for a given group back to core radial plane perpendicular to the beam tube.

2.6 Verification of Point Sources in All Beam Tubes

The methodology for determining the equivalent point sources for each neutron and gamma energy group based on the calculated MCNP fluxes at several points down a beam tube is described above. That methodology is embodied in a small Fortran utility program called "MULT-ISO.FOR". It also provides a comparison of the resulting approximate fluxes in each energy group (resulting from use of the equivalent point sources), and the resulting overall dose rates, against the original fluxes and dose rates calculated directly by MCNP. These comparisons at each point in each beam tube are described at some length in Appendix A.2. As shown by the flux ratios there, the approximate fluxes are generally within 10% of the original MCNP fluxes and seldom differ by more than 2 FSD's (fractional standard deviations). In those few cases where the fluxes do differ by more than this amount, it is generally because of stochastic noise in the fine-group MCNP fluxes -- ie, if the flux ratio is high in one fine-group, it is generally low by a similar offsetting amount in the adjacent energy group(s). In general, the agreement shown here is considered to be good to excellent. Generally the dose rates based on the approximate flux values (using the equivalent point sources) are within 5 to 10% of those calculated directly by MCNP. For shielding calculations where other uncertainties may be between 50% and a factor or 2, the approximate fluxes and dose rates resulting from use of these equivalent point source terms are considered wholly adequate.

2.7 Intended Use of Point Sources in Beam Tubes

Obviously the equivalent point sources described above are intended for use in the shielding analyses of the internal water tubes and other shield configurations further downstream, such as the beam tube collimator and/or rotary shutter. As with all "point sources", the calculated fluxes will blow up if one gets too close. Thus, they should only be used to calculate fluxes some distance away. Moreover, as shown in the initial verification (Appendix A.2), they are wholly adequate for calculating fluxes just upstream of the start of the water tube and beyond. In the course of the HB-3 dosimetry analysis described in Sect 4, it has also been demonstrated that these source terms are wholly adequate for calculating vessel fluences. Less obvious, however, might be the way these localized MCNP models for the beam tubes should be constructed. While it is fine to include the hot tip of the beam tube and the surrounding beryllium in the local model for illustrative purposes, that portion of the aluminum beam tube within a foot or two of any point

Table 2.2a. Equivalent point sources (n/s) in each beam tube for each of the 61 neutron groups in the VELM 61n/23g library structure. Table also shows the effective location (X0) of the neutron source in each neutron energy group(*).

IGN	Emin(MeV)	Emax(MeV)	NSRC (HB-1)	XON1	NSRC (HB-2)	XON2	NSRC (HB-3)	XON3	NSRC (HB-4)	XON4
1	1.2214E+01	1.4918E+01	3.08026E+09	79.2	1.09787E+13	34.5	2.74800E+09	99.9	3.25386E+10	10.0
2	1.0000E+01	1.2214E+01	3.99094E+11	39.7	7.93888E+13	50.3	6.92602E+12	31.1	5.13981E+12	51.4
3	8.1873E+00	1.0000E+01	1.08706E+12	58.3	2.48357E+14	37.2	8.64293E+12	68.7	1.11369E+12	50.0
4	6.7032E+00	8.1873E+00	3.53515E+12	52.9	5.63371E+14	37.5	3.05242E+13	42.9	4.80519E+12	63.6
5	5.4881E+00	6.7032E+00	9.85249E+12	56.0	9.82537E+14	54.3	7.32282E+13	59.5	1.97320E+13	59.2
6	4.4933E+00	5.4881E+00	2.62833E+13	64.4	1.55944E+15	53.4	1.36477E+14	62.6	4.06939E+13	73.9
7	3.6788E+00	4.4933E+00	4.48929E+13	45.3	2.01809E+15	56.4	2.06360E+14	47.9	4.25672E+13	68.7
8	3.0119E+00	3.6788E+00	5.41415E+13	55.1	1.79911E+15	56.4	1.61947E+14	56.9	6.39971E+13	62.3
9	2.4660E+00	3.0119E+00	6.93878E+13	48.9	1.84949E+15	56.4	2.41078E+14	65.3	7.37185E+13	71.1
10	2.3457E+00	2.4660E+00	2.69013E+13	46.1	7.86217E+14	54.6	1.35333E+14	43.5	2.56186E+13	52.9
11	2.2313E+00	2.3457E+00	2.95862E+13	44.0	8.22294E+14	61.6	2.00073E+14	33.3	2.86747E+13	48.2
12	2.0190E+00	2.2313E+00	7.75874E+13	44.1	1.67723E+15	58.8	3.12945E+14	52.1	7.15232E+13	59.8
13	1.6530E+00	2.0190E+00	1.96210E+14	48.7	3.79686E+15	62.2	8.54720E+14	50.2	2.01888E+14	52.8
14	1.3534E+00	1.6530E+00	2.62407E+14	50.8	3.11387E+15	68.9	8.07055E+14	59.7	2.15642E+14	54.9
15	1.1080E+00	1.3534E+00	2.46072E+14	51.4	2.02508E+15	69.8	7.09512E+14	46.8	2.56365E+14	43.5
16	9.0718E-01	1.1080E+00	3.00075E+14	42.6	2.01784E+15	64.9	5.40055E+14	70.1	2.40525E+14	42.6
17	7.4274E-01	9.0718E-01	2.17359E+14	60.0	1.70706E+15	72.1	6.65098E+14	44.1	2.12911E+14	49.6
18	6.0810E-01	7.4274E-01	2.16209E+14	52.1	1.59906E+15	70.6	5.35177E+14	56.8	2.04653E+14	54.4
19	5.2340E-01	6.0810E-01	1.69143E+14	49.6	1.07362E+15	75.6	3.61470E+14	50.3	1.53089E+14	53.7
20	4.9787E-01	5.2340E-01	6.25375E+13	39.2	4.24300E+14	64.7	1.49367E+14	52.9	5.15963E+13	42.5
21	3.8774E-01	4.9787E-01	2.71588E+14	52.4	1.52963E+15	68.4	5.85513E+14	58.8	2.34828E+14	45.6
22	3.0197E-01	3.8774E-01	2.83441E+14	45.3	1.80933E+15	64.6	6.29256E+14	49.6	2.52780E+14	45.3
23	2.9849E-01	3.0197E-01	9.72508E+12	43.2	5.38008E+13	77.1	3.65651E+13	42.3	8.16811E+12	45.4
24	2.9721E-01	2.9849E-01	4.33179E+12	38.2	2.08255E+13	52.3	7.68584E+12	53.7	2.48863E+12	46.2
25	2.9452E-01	2.9721E-01	7.91646E+12	52.3	4.40442E+13	80.0	1.38494E+13	63.8	8.20767E+12	21.1
26	2.7324E-01	2.9452E-01	9.40518E+13	41.3	4.36229E+14	70.1	2.12840E+14	42.4	6.34254E+13	63.7
27	2.2371E-01	2.7324E-01	2.47877E+14	48.7	1.19915E+15	73.8	7.35199E+14	34.2	2.03836E+14	42.1
28	1.8316E-01	2.2371E-01	1.79164E+14	55.0	1.06795E+15	66.1	4.33245E+14	48.9	1.69151E+14	41.2
29	1.4996E-01	1.8316E-01	1.86655E+14	35.6	8.76802E+14	67.6	3.63241E+14	42.5	1.26213E+14	51.2
30	1.2277E-01	1.4996E-01	2.56507E+14	45.5	9.30940E+14	76.3	4.29193E+14	45.6	1.59338E+14	51.8
31	8.6517E-02	1.2277E-01	2.42117E+14	47.7	1.13709E+15	73.2	5.59006E+14	45.7	2.16102E+14	47.3
32	5.6562E-02	8.6517E-02	4.18163E+14	45.1	1.70292E+15	67.0	8.89397E+14	47.4	3.09633E+14	49.6
33	5.2475E-02	5.6562E-02	5.36186E+13	50.6	2.45790E+14	69.3	1.29680E+14	56.7	5.45132E+13	29.3
34	3.4307E-02	5.2475E-02	2.32623E+14	39.0	1.13406E+15	65.8	4.96958E+14	52.9	1.83967E+14	49.1
35	2.8501E-02	3.4307E-02	2.18288E+14	41.4	6.93489E+14	67.0	3.03507E+14	79.8	1.35653E+14	48.6
36	2.7000E-02	2.8501E-02	7.80191E+13	36.0	2.74072E+14	63.7	1.21873E+14	67.5	4.67136E+13	23.0
37	2.6058E-02	2.7000E-02	4.22279E+13	42.4	1.22345E+14	75.0	5.24714E+13	62.6	2.60682E+13	51.5
38	2.4788E-02	2.6058E-02	5.39204E+13	48.1	1.93557E+14	73.3	1.12860E+14	46.7	3.81986E+13	40.0
39	2.3579E-02	2.4788E-02	5.62891E+13	36.6	1.61758E+14	62.9	6.69650E+13	69.0	6.36810E+13	10.0
40	1.5034E-02	2.3579E-02	3.67329E+14	50.5	1.62195E+15	61.6	7.42049E+14	54.0	2.97379E+14	43.9
41	9.1188E-03	1.5034E-02	4.57210E+14	42.4	1.76510E+15	66.5	9.84217E+14	50.7	3.03564E+14	44.2
42	5.5308E-03	9.1188E-03	3.59507E+14	57.5	1.74494E+15	71.9	8.76077E+14	52.7	3.16192E+14	44.9
43	3.7074E-03	5.5308E-03	3.29352E+14	45.9	1.48446E+15	70.0	7.55438E+14	53.3	2.72559E+14	47.3
44	3.0354E-03	3.7074E-03	1.68435E+14	46.0	6.79285E+14	68.4	3.36538E+14	65.1	1.17327E+14	51.5
45	2.6126E-03	3.0354E-03	1.08823E+14	64.4	5.09912E+14	68.6	2.54975E+14	55.0	1.00723E+14	40.2
46	2.2487E-03	2.6126E-03	1.60061E+14	44.7	4.86574E+14	78.3	2.76622E+14	49.5	8.59309E+13	59.1
47	2.0347E-03	2.2487E-03	6.66316E+13	56.6	3.38748E+14	77.8	2.04908E+14	43.0	6.72898E+13	53.9
48	1.2341E-03	2.0347E-03	4.33392E+14	52.2	1.83135E+15	66.1	8.87245E+14	60.5	3.27352E+14	46.5
49	7.4852E-04	1.2341E-03	4.80954E+14	46.9	1.77021E+15	67.6	8.53691E+14	61.2	3.56115E+14	46.6
50	4.5400E-04	7.4852E-04	5.17013E+14	44.9	1.75804E+15	71.4	8.74122E+14	52.6	3.70852E+14	46.4
51	2.7536E-04	4.5400E-04	5.07730E+14	49.8	1.84391E+15	67.6	9.50610E+14	53.8	3.81395E+14	50.9
52	1.6702E-04	2.7536E-04	4.87720E+14	49.7	1.73245E+15	75.9	9.69821E+14	51.1	3.61966E+14	49.7
53	1.0130E-04	1.6702E-04	5.20223E+14	47.5	1.88854E+15	76.5	9.03837E+14	56.0	4.03643E+14	45.3
54	4.7851E-05	1.0130E-04	7.57662E+14	51.5	2.82080E+15	76.9	1.45876E+15	55.4	6.46494E+14	49.5
55	2.2603E-05	4.7851E-05	7.62547E+14	51.6	2.95904E+15	71.9	1.54759E+15	56.5	6.53783E+14	46.9
56	1.0677E-05	2.2603E-05	8.06771E+14	50.1	2.91875E+15	73.9	1.58981E+15	48.2	6.52905E+14	58.6
57	5.0435E-06	1.0677E-05	7.81961E+14	54.8	3.12475E+15	73.6	1.55274E+15	54.5	6.71028E+14	48.5
58	2.3824E-06	5.0435E-06	8.45061E+14	52.3	2.82574E+15	76.1	1.30212E+15	76.1	6.83147E+14	49.9
59	1.1253E-06	2.3824E-06	8.60077E+14	54.8	3.25137E+15	79.0	1.52979E+15	65.2	7.22306E+14	61.0
60	4.1399E-07	1.1253E-06	1.32866E+15	54.0	4.56223E+15	80.1	2.25679E+15	57.3	9.92916E+14	64.8
61	1.0000E-11	4.1399E-07	5.31877E+16	72.3	1.27996E+17	93.7	6.30365E+16	80.2	4.52747E+16	86.8
			----------		----------		----------		----------	
	total source (n/s):		6.92450E+16		2.11702E+17		9.64595E+16		5.82768E+16	

(*) x0 is the effective location (cm) of the point source along the centerline of the beam tube relative to the radial plane (extending from the core) perpendicular to the tube centerline, such that if x is the location (ie, distance from this same plane) where the flux is desired, it would be given by: Flux(x,g)=S(x0,g)/[4*pi*(x-x0)^2].

Table 2.2b. Equivalent point sources (p/s) in each beam tube for each of the 23 gamma groups in the VELM 61n/23g library structure. Table also shows the effective location (XO) of the photon source in each gamma energy group(*).

IGG	Emin(MeV)	Emax(MeV)	GSRC (HB-1)	XOG1	GSRC (HB-2)	XOG2	GSRC (HB-3)	XOG3	GSRC (HB-4)	XOG4
1	1.0000E+01	1.4000E+01	6.73779E+09	87.2	4.72146E+12	41.1	1.23250E+11	97.4	4.55814E+09	99.9
2	8.0000E+00	1.0000E+01	3.04858E+13	90.2	4.75524E+14	87.0	6.19421E+13	99.9	4.71480E+13	99.9
3	7.5000E+00	8.0000E+00	2.26137E+15	68.0	7.67819E+15	84.9	1.51983E+15	94.4	2.38110E+15	76.1
4	7.0000E+00	7.5000E+00	1.02398E+14	82.6	8.92992E+14	81.1	1.60183E+14	96.0	1.98826E+14	89.5
5	6.0000E+00	7.0000E+00	7.05919E+14	81.0	5.21478E+15	79.5	1.23378E+15	93.9	1.00541E+15	85.8
6	5.0000E+00	6.0000E+00	7.06655E+14	79.3	7.53651E+15	72.4	6.75453E+14	96.4	9.17647E+14	84.7
7	4.0000E+00	5.0000E+00	1.80302E+15	72.9	1.57178E+16	75.2	1.98361E+15	93.2	2.64709E+15	78.1
8	3.0000E+00	4.0000E+00	1.90084E+15	78.3	3.03766E+16	67.2	2.34929E+15	92.6	2.70895E+15	83.3
9	2.5000E+00	3.0000E+00	1.17847E+15	79.9	2.56328E+16	67.5	1.42777E+15	96.6	1.57823E+15	86.0
10	2.0000E+00	2.5000E+00	3.59955E+15	80.3	4.92481E+16	73.6	2.66951E+15	99.2	7.78940E+15	80.1
11	1.5000E+00	2.0000E+00	4.40082E+15	78.4	7.21632E+16	70.2	4.23989E+15	96.9	6.18428E+15	86.1
12	1.0000E+00	1.5000E+00	2.27631E+15	87.0	1.19189E+17	61.0	5.27935E+15	93.6	3.46054E+15	97.9
13	7.0000E-01	1.0000E+00	2.07064E+15	88.0	1.05252E+17	64.0	7.31636E+15	86.8	3.37424E+15	97.6
14	6.0000E-01	7.0000E-01	1.16662E+15	86.0	4.06972E+16	68.6	4.03975E+15	83.2	1.69776E+15	94.7
15	5.1000E-01	6.0000E-01	2.01818E+15	86.0	4.22019E+16	74.2	4.80101E+15	88.8	2.84838E+15	92.7
16	4.0000E-01	5.1000E-01	3.74129E+15	81.6	6.00657E+16	71.0	7.17665E+15	84.7	4.47890E+15	89.1
17	3.0000E-01	4.0000E-01	4.76182E+15	83.0	6.18177E+16	73.3	1.03805E+16	81.6	6.62631E+15	82.8
18	1.5000E-01	3.0000E-01	1.50947E+16	82.5	1.31735E+17	78.1	2.56708E+16	84.5	1.77459E+16	88.3
19	1.0000E-01	1.5000E-01	1.18909E+16	82.5	8.95231E+16	79.4	1.82855E+16	83.9	1.35354E+16	90.4
20	7.0000E-02	1.0000E-01	1.11793E+16	82.7	6.39484E+16	83.8	1.67705E+16	82.1	1.23622E+16	88.1
21	4.5000E-02	7.0000E-02	8.84390E+15	82.9	4.73267E+16	80.7	1.65029E+16	68.1	9.00884E+15	85.9
22	2.0000E-02	4.5000E-02	1.19589E+15	77.5	8.70290E+15	69.9	2.84514E+15	61.9	1.10320E+15	77.0
23	1.0000E-02	2.0000E-02	2.41702E+12	91.7	4.95649E+14	69.3	8.72837E+12	10.0	3.54722E+13	93.1
			---		---		---		---	
	total source (p/s):		8.09315E+16		9.85896E+17		1.35399E+17		1.01735E+17	

(*) x0 is the effective location (cm) of the point source along the centerline of the beam tube relative to the radial plane (extending from the core) perpendicular to the tube centerline, such that if x is the location (ie, distance from this same plane) where the flux is desired, it would be given by: Flux(x,g)=S(x0,g)/[4*pi*(x-x0)^2].

source should be assigned an importance of zero so that as particles pass from the internal void into the body of the beam tube in this imp=0 region, they vanish immediately. If this were not the case, they would scatter in the adjacent materials and contribute further to the fluxes and dose rates further downstream when, in fact, the effects of such scattering events near the hot end of the beam tube have already been represented in the global analyses and incorporated in the determination of the equivalent point sources. To not use a zero importance zone in this region would cause the subsequent calculations to effectively count many scattering events two or more times. As a practical matter, this zero importance region should extend down to the start of the internal water tube (points B, V, L, and F in Table 2.1), or at least down to or past points A, U, K, and E in Table 2.1. Beyond that location, one should use an importance of 1.0 or greater so that physical tracking will not be interrupted. In addition to having this "zero importance region" near the hot end of the beam tube, it is also recommended that the MCNP sdef card be modified so as to allow strong angular biasing of the source. As a practical matter, it generally makes little or no sense to sample neutrons (or gammas) whose initial starting directions lay outside the solid angle defined by the inner diameter of the beam tube at the start of the water tube, and starting source particles should be constrained to this limited solid angle. (Note that the starting weights will also have to be reduced accordingly.) This strong angular source biasing will improve the efficiency of these beam tube calculations by more than a factor of a hundred.

2.8 Validation of Point Sources in HB-3

Verification requires that one compare new results against those obtained using other methods or codes. Validation, on the other hand, requires that one compare the new results against some measured reality. The latter is always more desirable, but is not always possible. In June 1968, during preliminary low power testing of the HFIR, Blosser and Thomas#5 made a number of energy-dependent spectral measurements of the neutron beam intensity approximately 6.5 meters from the tips of the HB-2 and HB-3 beam tubes (cf Tables 3, 5 and 6 of Ref 5). Except for a few minor changes in the location of the aluminum windows in the voided beam tube, and in the design of the collimator (which would not effect the uncollided flux), the new HB-3 beam tube is virtually identical to the original HB-3 beam tube from 1968, such that the original Blosser and Thomas measurements can be used to provide an excellent benchmark against which the approximate fluxes based on the new equivalent point sources may be judged. Moreover, because the HB-3 beam tube design inside the pressure vessel has not changed at all, earlier dosimetry measurements from 1988 (cf Ref 6) can also be used as rigorous benchmarks. Unfortunately, because the new HB-2 beam tube (for which the equivalent point sources have been developed) has been enlarged and now has two beryllium pieces located inside the hot tip of the beam tube, the earlier Blosser and Thomas measurements (and/or earlier dosimetry measurements) are no longer directly applicable. Nevertheless, with minor adjustments to account for the differences in beam tube diameter, the original Blosser and Thomas measurements can still be used to validate the equivalent point sources for HB-2 as well.

The bulk of this report focuses on analyses performed for the HB-3 beam tube. Section 3 describes the MCNP model for that beam tube in great detail, while Sect 4 gives additional information related to the dosimetry analysis for Key 3, positions 3 and 8, around the HB-3 beam tube. The basic model described in Sect 3 is generalized, complete, and very flexible, such that by making very few changes to the input file, one can (1) look at neutron or gamma sources, (2) look at the flooded or voided water tube, (3) swap back and forth between the original 1960 water tube design and the newly proposed 1998 water tube design, and (4) run the model with the rotary shutter either closed or open using the large beam hole or the small beam hole.

MCNP Run HB302 is a variant that was used to model the HB-3 beam tube as it existed during the Blosser and Thomas experiment. As such: (a) the aluminum windows inside the beam tube were placed in their 1960 axial locations, (b) the water tube was void, and (c) the small beam hole in the rotary shutter was placed in the open position as was the case for HB-3. [Note that Blosser and Thomas used the small aperture in the HB-3 rotary shutter, and the large aperture in the HB-2 shutter.] Table 2.3 shows a comparison of calculated neutron fluxes 6.55 meters from the tip of the HB-3 beam tube with the measured values reported by Blosser and Thomas at a point 655.6629 cm from the tip of the HB-3 (i.e., at a point 678.1673 cm from the core radial plane perpendicular to the HB-3 beam tube). Calculated results are based on a point detector at this distant location. More than 98% of the calculated flux in each energy group is due to neutrons streaming uncollided from the equivalent point sources described above. While the C/E ratios are a bit high for thermal neutrons and for neutrons in the 1.0-1.9 eV energy range (1.69 and 1.87, respectively), the results for the faster neutrons are much better, such that the average C/E ratio for the entire energy range is 1.44. While such ratios would clearly be too high for most reactor physics work, they are generally acceptable for shielding work where the uncertainty in the calculated shield effectiveness would normally be much higher than this relatively small uncertainty due to the use of these equivalent point sources. Moreover, this degree of agreement is really considered quite good, given that the point of interest is so distant (6.5 m) from the tip of the beam tube.

Table 2.3. Comparison of calculated neutron fluxes 6.55 meters from the tip of the HB-3 beam tube with the measured values reported by Blosser and Thomas in June 1968 (cf. Tables 3, 5 and 6 in ORNL-TM-2221). Calculated results here are based on MCNP4B Run HB302 (Tally 15), where this particular point detector was located at X=-302.194553 cm, Y=-576.756319 cm, Z=0 cm in the global HFIR geometry, which is 655.6629 cm from the tip of the actual HB-3 beam tube (where Blosser and Thomas made their measurements). In the HB302 model geometry, this corresponds to x=0, y=0, z=678.1673 cm, which is 678.1673 cm from the radial plane perpendicular to the HB-3 beam tube. This particular calculation (HB302) was based on 1,000,000 neutron histories.

MCNP Fluxes from Run HB302, Tally 15

Emin	Emax	MCNP FLUX at 100 MW (n/s/cm2)	fsd	MCNP FLUXES in same units as exp report	C/E Ratio	Measured Fluxes	How experimental measurements were made
0.0	0.40 eV	1.14245E+10	.0008	==> 11.42E+7 n/s/cm2/MW	(1.69)	6.75E+7 <==	Avg Measured Th Flux based on Au, Cu, In, Co & Na foils, bare & Cd covered; values ranged from 6.5E+7 to 7.0E+7
0.40 eV	1.00 eV	7.27224E+08	.0048				
1.00 eV	1.90 eV	2.39121E+08	.0084	==> 2.657E+6 n/s/cm2/eV/MW	(1.87)	1.42E+6 <==	Measured flux using In-115 foil with Res at 1.46 eV half-width of resonance appx: 1.386 to 1.530 eV
1.90 eV	4.00 eV	2.54174E+08	.0083				
4.00 eV	6.00 eV	1.42901E+08	.0111	==> 7.145E+5 n/s/cm2/eV/MW	(1.55)	4.61E+5 <==	Measured flux using Au-197 foil with Res at 4.9 eV half-width of resonance appx: 4.7593 to 5.0527 eV
6.00 eV	25.0 eV	5.30868E+08	.0055				
25.0 eV	100 eV	4.93134E+08	.0058				
100 eV	170 eV	1.74100E+08	.0098	==> 2.487E+4 n/s/cm2/eV/MW	(1.49)	1.67E+4 <==	Measured flux using Co-59 foil with Res at 132 eV half-width of resonance appx: 127.1 to 136.9 eV
170 eV	640 eV	4.18765E+08	.0062				
640 eV	2.4 keV	4.21620E+08	.0063				
2.4 keV	3.8 keV	1.41414E+08	.0109	==> 10.10E+2 n/s/cm2/eV/MW	(1.40)	7.19E+2 <==	Measured flux using Na-23 with Res at 2850 eV half-width of resonance appx: 2660 to 3140 eV
3.8 keV	20. keV	5.26767E+08	.0056				
20. keV	100 keV	3.74901E+08	.0063				
100 keV	1.0 MeV	7.65511E+08	.0040				
1.0 MeV	2.9 MeV	5.07778E+08	.0052				
2.9 MeV	6.3 MeV	9.54237E+07	.0127				
2.9 MeV	20. MeV	1.07056E+08	.0120	(b) =====> 10.71E+5 n/s/cm2/MW	(1.35)	7.93E+5 <==	Measured flux, E > 2.9 MeV, based on S32-(n,p)-P32 reaction
6.3 MeV	8.1 MeV	8.36489E+06	.0436				
6.3 MeV	20. MeV	1.16320E+07	.0371	(a) =====> 1.163E+5 n/s/cm2/MW	(0.95)	1.23E+5 <==	Measured flux, E > 6.3 MeV, based on Mg24-(n,p)-Na24 reaction
8.1 MeV	20. MeV	3.26715E+06	.0708	=====> 3.267E+4 n/s/cm2/MW	(1.25)	2.62E+4 <==	Measured flux, E > 8.1 MeV, based on Al27-(n,a)-Na24 reaction
	total:	1.72499E+10	.0001	Avg C/E ratio:	(1.44) +/- 0.28		

Note: (a) and (b) were obtained by summing over the last 2 or 3 MCNP energy groups.

In the Spring of 1998, a concerted effort was made to calculate dosimeter responses at HFIR key 3, positions 3 and 8, around the HB-3 beam tube, just inside the pressure vessel. This effort was undertaken partially to help validate the "equivalent point sources" that had been developed for that beam tube (prior to their anticipated use in the HB-3 "water tube" shielding analysis) and partially to see if MCNP could be used for good and reliable neutron dosimetry analysis. The 3-D geometric model of the HB-3 beam tube used in the final dosimetry reference run (MCNP Run HB304M4) is the same as that described in Sect 3 below, with the water tube void and the rotary shutter in the full open position so as to simulate normal operations. The importance of different aspects of this model, especially the fine details in and around the dosimeters, is discussed more fully in Sect 4, as are other aspects of the analysis which were invoked so as to make this reference calculation as efficient as possible. Basically, these involved minor things such as having a neutron cutoff energy of 27 keV, and increasing the importance (used for neutron splitting) in the geometry zones representing the water and steel around the vessel nozzle and in the vicinity of the dosimeters. Because the dosimeters are closer to the point sources than other points of interest down the water tube, it was also necessary to sample a wider range of angular directions than might be used in the water tube analysis, and to move the location of the importance cutoff plane back a little closer to the source locations. In the dosimetry analyses, for example, we sampled all source neutrons whose direction cosines with respect to the tube centerline were between 0.71 and 1.0 (while making the necessary adjustment in the starting weight), so as to allow neutrons from even the most forward equivalent point source (at Z=68.7 cm) to hit the beam tube at Z=75.473 cm, which is well (31.654 cm) upstream of the first dosimeter which is located at Z=107.1276 cm. Likewise, the location of the importance cutoff plane, normally at Z=118.6879 cm and used to increase efficiency of the water tube shielding calculations, had to be moved back to Z=75.473 cm, which is 31.6546 cm upstream of first dosimeter. (The normal location used in the water tube shielding calculations would have precluded any neutrons from ever reaching the dosimeter locations.) Lastly, instead of locating the point sources along the actual centerline of the beam tube, they were all shifted 1.6986 cm horizontally off the centerline in the dosimetry analysis, but were otherwise left unaltered. This shift was necessary to simulate the fact that neutrons really do enter this tangential beam tube in an asymmetric fashion that cannot be represented by isotropic point sources along the centerline. It is marginally important if one is interested in small spatial variations in the flux close to the core (like the dosimeter locations) but is totally inconsequential for shielding calculations where one is interested in the flux at great distances down the beam tube. [Moreover, the size of the horizontal shift needed to simulate this asymmetric effect was determined a priori using a straightforward theoretical model which accounted for spatial variations in the fast neutron scattering density (at 84,400 points) over the hemispherical tip of the beam tube due to the natural spatial gradient of the fast flux in this region of the beryllium reflector as determined by 1-D calculations performed by Cheverton in 1970 (see Fig 5.1 of Ref 1). Note that from one side of the hemispherical tip to the other, the magnitude of the fast flux is known to change by a factor of 4, thus causing the asymmetric affect alluded to above.] Because consideration was limited to only neutrons above 27 keV, and because of the other efficiencies described above, it was possible to run a great many neutron histories in a relatively short amount of computer time. MCNP Run HB304M4, for example, used 120 million neutron histories and required only 11 hours of wallclock time on each of eight nodes on the ORNL SP2 computer running in parallel. Additional details of this dosimetry analysis may be found in Sect 4.

Table 2.4 shows the calculated and measured neutron reaction rates for the Ni-58 and Fe-54 dosimeters at HFIR Key 3, positions 3 and 8, around the HB-3 beam tube, just inside the pressure vessel, with the HFIR operating at 100 MW. The measured reference reaction rates were taken directly from Table E.12 of Ref 6. While that document also reports inferred fluxes based on activation analyses and one-group activation cross sections, as well as inferred fluxes based on detailed 3-D TORT analyses with experimentally determined E/C ratios, it was judged far more appropriate to make comparisons based on the most fundamental data available -- the actual measured reaction rates in the dosimeters themselves. To that end, the MCNP flux and reaction rate tallies were defined such that the continuous (pointwise) energy-dependent MCNP fluxes at the two dosimeter locations were folded on-line with the continuous (pointwise) energy-dependent Ni58(n,p)Co58 and Fe54(n,p)Mn54 reaction cross sections to get the corresponding integral reaction rates. Those integral reaction rates could then be compared directly with the measured reaction rates, as shown in Table 2.4. The most striking aspect of these results is that all of the C/E ratios are relatively small and lay in a narrow band between 1.17 and 1.25. (By comparison, the less detailed and far more expensive 1988 TORT analyses#6 yielded an average C/E ratio of 0.69 at these same locations.) Moreover, these C/E ratios (1.17 to 1.25) are also consistent with the C/E ratios at 6.55 meters down the beam tube based on calculated results from MCNP Run HB302 as well as the 1968 measurements of Blosser and Thomas in this energy range (see Table 2.3). Together, MCNP Runs HB302 and HB304M4 clearly show that the equivalent point sources defined above are wholly adequate for the HB-3 shielding calculations that were to follow.

Table 2.4. Comparison of calculated and measured neutron reaction rates for Ni-58 and Fe-54 dosimeters at HFIR Key 3, positions 3 and 8, around the HB-3 beam tube, just inside the pressure vessel. Calculated reaction rates (based on MCNP Run HB304M4) and measured reaction rates from Table E.12 of ORNL/TM-10444 are all for the HFIR operating at 100 MW.

Tally 35 (Key 3, Pos 8) just on the HB4 side of HB3			Tally 25 (Key 3, Pos 3) just on the HB2 side of HB3		
Ni58(n,p)Co58 reactions/sec/atom			Ni58(n,p)Co58 reactions/sec/atom		
Calculated MCNP Value	Measured Ref Value	C/E ratio	Calculated MCNP Value	Measured Ref Value	C/E ratio
3.838E-16	3.17E-16	1.21	1.674E-16	1.34E-16	1.25
fsd=3%			fsd=4%		
Fe54(n,p)Mn54 reactions/sec/atom			Fe54(n,p)Mn54 reactions/sec/atom		
Calculated MCNP Value	Measured Ref Value	C/E ratio	Calculated MCNP Value	Measured Ref Value	C/E ratio
2.839E-16	2.36E-16	1.20	1.202E-16	1.03E-16	1.17
fsd=3%			fsd=4%		

(a) Ni58(n,p)Co58 reactions are typically used to measure neutron fluxes above 1.0 MeV; Fe54(n,p)Mn54 reactions are typically used to measure neutron fluxes above 0.1 MeV.
(b) Calculated Ni58(n,p)Co58 reactions based on tally multiplier bin 2 for material 71.
(c) Calculated Fe54(n,p)Mn54 reactions based on tally multiplier bin 3 for material 72.
(d) Measured reference values shown are taken from Table E.12 on pp 208 of "Evaluation of HFIR Pressure-Vessel Integrity Considering Radiation Embrittlement" (ORNL/TM-10444) by R.D.Cheverton, J.G.Merkle, and R.K.Nanstad.

2.9 Validation of Point Sources in HB-2

The original Blosser and Thomas measurements#5 provided an excellent benchmark against which the equivalent point sources in HB-3 (and the resulting fluxes) could be judged. Moreover, experience with other simplified source terms based on the type of approach described above (but for the original HB-2 design) has shown that such source terms can and have been used to calculationally reproduce the measured 1988 dosimetric dpa values (displacements per atom) around the original HB-2 beam tube near the pressure vessel to within 1% (see Ref 16). Unfortunately, because the new HB-2 beam tube (for which the equivalent point sources in Tables 2.2a and 2.2b were developed) has been enlarged and now has two beryllium pieces located inside the hot tip of the beam tube, the earlier Blosser and Thomas measurements from 1968 (and/or earlier dosimetry measurements) are no longer directly applicable. Nevertheless, with a simple ad hoc adjustment in the MCNP fluxes to account for the differences in beam the tube diameters, comparisons with the original Blosser and Thomas measurements can still be used to partially validate the equivalent point sources for HB-2 as well.

MCNP Run HB202 was used for this purpose. Since calculations show that 98% of the neutrons "that reach the distant location where Blosser and Thomas made their measurements" remained uncollided after entering the beam tube, modeling the beam tube with great fidelity was not a major concern, and not nearly as important as using the proper source terms. Thus, Run HB202 does not pretend to model HB-2 with any fidelity, but was constructed by simply taking the existing geometric model for HB-3 (from Run HB302) and making the following changes: (1) The point sources were changed to correspond to those for HB-2 in Table 2.2a (based on the enlarged beam tube); (2) The f15 tally was moved out slightly to the Blosser-Thomas point of interest for HB-2, and the fm15 card was modified to account for the real source intensity in HB-2 (ie, the sum of the multigroup source terms in Table 2.2a); (3) The orientation of the rotary shutter was altered so as to open the large beam hole in the shutter, as actually used (for HB-2) at the time Blosser and Thomas made their measurements. [Note that they used the small beam hole in the HB-3 shutter, but the large beam hole in the HB-2 shutter.] Since the original HB-2 beam tube was the same diameter as HB-3, and since the flux at the Blosser-Thomas point is basically the uncollided flux anyway, the expedient use of this model (ie, a slightly modified form of Run HB302) is wholly justified for the purpose of this particular comparison even though the model used in Run HB202 would have to be modified considerably if one really wanted to perform a rigorous shielding analysis of HB-2 beam tube, water tube, or guide tubes.

Table 2.5 shows a comparison of the calculated neutron fluxes 6.45 meters from the tip of the HB-2 beam tube with the measured values reported by Blosser and Thomas at a point 645.0584 cm from the tip of the HB-2 beam tube (i.e., at a point 679.10964 cm from the core centerline). Calculated results are based on a point detector at this distant location. As before, more than 98% of the calculated flux in each energy group is due to neutrons streaming uncollided from the equivalent point sources described above. Here, however, it must be recognized that the original HB-2 beam tube at the time of the Blosser-Thomas measurements had an inside diameter of 4.0 inches while the equivalent point sources in Table 2.2a are based on the new enlarged HB-2 beam tube design with an inside diameter of 7.052 inches near the core. Thus, before making any comparisons of the MCNP fluxes with the old Blosser-Thomas measurements, an ad hoc (approximate) correction is necessary, in which the actual MCNP fluxes are multiplied by the ratio of the diameters squared [=(4.0/7.052)^2] to obtain the diameter-adjusted MCNP fluxes. Having done that, the comparisons between the newly calculated values and the old measured values look surprisingly good, with an average C/E ratio of 0.89. Except for one or two energy ranges, the bulk of the C/E ratios are between 0.91 and 1.09. The fact that the calculated fluxes above 2.9 MeV and above 8.1 MeV are both in good agreement with the measured fluxes in those ranges while the calculated and measured fluxes above 6.3 MeV are not in good agreement, simply indicates that, with source terms based on having the Be pieces in the enlarged HB-2 beam tube, more of the source neutrons formerly in the 6.3-8.1 MeV range have shifted to the 2.9-6.3 MeV range. Because of differences in the former and present beam tube designs, and the ad hoc correction that was necessary to partially account for these differences, it would be incorrect to view these comparisons of HB-2 fluxes as a rigorous validation of the new HB-2 source terms. Nevertheless, they do provide a high degree of reassurance that these new source terms are at least reasonably correct and wholly adequate for any beam tube shielding analyses that might follow.

Table 2.5. Comparison of calculated neutron fluxes 6.45 meters from the tip of the HB-2 beam tube with the measured values reported by Blosser and Thomas in June 1968 (cf. Tables 3, 5 and 6 in ORNL-TM-2221). Calculated results here are based on MCNP4B Run HB202 (Tally 15), where this particular point detector was located at X=-679.10964 cm, Y=0 cm, Z=0 cm in the global HFIR geometry, which is 645.0584 cm from the tip of the actual HB-2 beam tube (where Blosser and Thomas made their measurements). In the HB202 model geometry, this corresponds to x=0, y=0, z=679.10964 cm, which is 679.10964 cm from the radial plane perpendicular to the HB-2 beam tube. This particular calculation (HB202) was based on 1,000,000 neutron histories.

MCNP Fluxes from Run HB202, Tally 15

Emin	Emax	MCNP FLUX at 100 MW (n/s/cm2)	fsd	Diameter Adjusted(a) MCNP FLUXES in same units as exp report	C/E Ratio	Measured Fluxes	How experimental measurements were made
0.0	0.40 eV	2.43160E+10	.0008	==> 7.823E+7 n/s/cm2/MW	(1.02)	7.65E+7 <==	Avg Measured Th Flux based on Au, Cu, In, Co & Na foils, bare & Cd covered; values ranged from 6.5E+7 to 7.0E+7
0.40 eV	1.00 eV	1.56979E+09	.0050				
1.00 eV	1.90 eV	5.28714E+08	.0086	==> 1.890E+6 n/s/cm2/eV/MW	(1.09)	1.74E+6 <==	Measured flux using In-115 foil with Res at 1.46 eV half-width of resonance appx: 1.386 to 1.530 eV
1.90 eV	4.00 eV	5.56624E+08	.0084				
4.00 eV	6.00 eV	2.99048E+08	.0115	==> 4.811E+5 n/s/cm2/eV/MW	(0.95)	5.07E+5 <==	Measured flux using Au-197 foil with Res at 4.9 eV half-width of resonance appx: 4.7593 to 5.0527 eV
6.00 eV	25.0 eV	1.07714E+09	.0060				
25.0 eV	100 eV	1.01709E+09	.0061				
100 eV	170 eV	3.80898E+08	.0102	==> 1.751E+4 n/s/cm2/eV/MW	(0.91)	1.92E+4 <==	Measured flux using Co-59 foil with Res at 132 eV half-width of resonance appx: 127.1 to 136.9 eV
170 eV	640 eV	8.56784E+08	.0067				
640 eV	2.4 keV	8.70949E+08	.0066				
2.4 keV	3.8 keV	2.79900E+08	.0117	==> 6.432E+2 n/s/cm2/eV/MW	(0.62)	1.04E+3 <==	Measured flux using Na-23 with Res at 2850 eV half-width of resonance appx: 2660 to 3140 eV
3.8 keV	20. keV	1.07988E+09	.0059				
20. keV	100 keV	8.12876E+08	.0065				
100 keV	1.0 MeV	2.06420E+09	.0037				
1.0 MeV	2.9 MeV	2.24203E+09	.0037				
2.9 MeV	6.3 MeV	1.02050E+09	.0057				
2.9 MeV	20. MeV	1.21581E+09	.0052	(b) =====> 3.912E+6 n/s/cm2/MW	(1.05)	3.72E+6 <==	Measured flux, E > 2.9 MeV, based on S32-(n,p)-P32 reaction
6.3 MeV	8.1 MeV	1.35740E+08	.0158				
6.3 MeV	20. MeV	1.95305E+08	.0132	(c,d) =====> 6.284E+5 n/s/cm2/MW	(0.50)	1.25E+6 <==	Measured flux, E > 6.3 MeV, based on Mg24-(n,p)-Na24 reaction
8.1 MeV	20. MeV	5.95654E+07	.0241	=====> 1.916E+5 n/s/cm2/MW	(0.94)	2.04E+5 <==	Measured flux, E > 8.1 MeV, based on Al27-(n,a)-Na24 reaction
	total:	3.91677E+10	.0001	Avg C/E ratio:	(0.89) +/- 0.21		

(a) The old HB2 beam tube had an inner radius of 5.08 cm while the new (enlarged) HB2 beam tube has an inner radius of 8.956 cm. So as to provide a rough basis for comparing calculated fluxes in the new beam tube (left column) with measured fluxes in the old beam tube, the "diameter adjusted fluxes" have all been multiplied by (5.08/8.956)^2.
(b) and (c) were obtained by summing over the last 2 or 3 MCNP energy groups.
(d) The fact that the calculated and measured fluxes above 8.1 MeV and above 2.9 MeV are in both good agreement while the calculated and measured fluxes above 6.3 MeV are not, simply indicates that, with the Be pieces in the enlarged HB-2 beam tube, more of the neutrons formerly in the 6.3-8.1 MeV range have shifted to the 2.9-6.3 MeV range.

3.0 DESCRIPTION OF THE 3-D MCNP MODEL(S) AND THEIR ORIGIN

Shielding analyses for the individual beam tubes will generally require modeling materials and components located several meters from the core. Fig 3.1, for example, shows the overview layout drawing for the original (1960) HB-4 beam tube before the cold source or any of the recently proposed upgrades. HB-3 is similar. A typical model used in the beam tube shielding analysis will, for example, include the hot tip of the given beam tube, the entire length of the beam tube and surrounding media (as is passes out of the beryllium reflector, through the water in the vessel, through the wall of the pressure vessel, through the pool, and through the concrete forming the biological shield), the internal water tube and beam collimator, and the rotary shutter (shield plug) assembly further downstream. As such, it would be totally impractical to incorporate such analyses directly into the large "global" analysis for the entire HFIR core and reflector.

The base model used in the HB-3 shielding analysis is shown in Figs. 3.2 and 3.3. The first shows the original 1960 water tube when void, as in normal operation, with the large aperture of the rotary shutter in the open position, while the second shows the newly designed 1998 water tube and collimator sections both flooded, and the shutter in the closed position. (Many small variations of this base "local" model are described below and in subsequent sections.) Basically this local model of the HB-3 beam tube includes everything within a radius of 65 cm of the beam tube centerline, starting (axially) at the core radial plane perpendicular to the beam tube (Z=0) and extending 700 cm along its centerline, out past the point where Blosser and Thomas made their measurements, although everything past the downstream surface (Z=478.79 cm) of the steel-clad concrete housing assembly holding the rotary shutter is considered void, and therefore not shown in Figs. 3.2 and 3.3. Likewise, a vacuum boundary condition was applied on the outer radial surface of the base model, as well as at the two axial ends. All neutron and gamma source terms were represented by the equivalent point sources within the beam tube, as listed in Tables 2.2a and 2.2b.

Use of the point sources within the beam tube precludes the necessity of modeling the HFIR core itself. Moreover, in this case, the hot tip of the beam tube and the surrounding beryllium have been included in the geometric model for illustrative purposes only. The reality is that the portion of the aluminum beam tube within a foot or so of any point source should be assigned an importance of zero so that as particles pass from the central void region into the aluminum body of the beam tube in this imp=0 region, they vanish immediately. (If this were not the case, they would scatter in the adjacent materials and contribute further to the fluxes and dose rates downstream when, in fact, the effects of such scattering events near the hot end of the beam tube have already been represented in the global analyses and have already been incorporated in the determination of the equivalent point sources. To not use a zero importance zone in this region would cause the subsequent calculations to effectively count many scattering events two or more times. See additional discussion in Sects 2.7 and 2.8.) The exact location of this "importance cutoff plane" (below which the geometric details for everything outside the beam tube become irrelevant) depends on the problem being solved. In the water tube shielding analyses, one is concerned primarily with radiation (neutrons or gammas) impinging directly on the water tube or on nearby regions. In the 1998 design, the water tube begins at Z=174.27 cm, and the "importance cutoff plane" (surface 1007) was located at Z=118.6879 cm (close to the inner surface of the pressure vessel) so that scattering events in and around the vessel nozzle would be included in the analysis. In the analysis of the 1960 water tube (mentioned only briefly in Sect 5.5), the hemispherical tip of the internal water tube is located at approximately Z=117 cm. Nevertheless, because it was inside the beam tube and the importance cutoff plane affects only those things outside the beam tube, the location of the importance cutoff plane was left unchanged. In both cases, efficiency demanded that we track only those particles that had a reasonable chance of contributing to the dose rate at locations much further downstream. In the dosimetry analysis mentioned in Sect 2.8 and described more fully in Sect 4, the importance cutoff plane (surface 1007) had to be relocated since the dosimeters at Key 3, positions 3 and 8, are located outside the beam tube but inside the pressure vessel. In this case, the importance cutoff plane was located at Z=75.473 cm, a full 35.85638 cm upstream of the first dosimeter which is located at Z=111.32938 cm. Likewise, in the name of efficiency, the isotropic point sources were only sampled over a very narrow range forward directions which were likely to contribute to the result of interest in the particular problem being solved. In the water tube shielding calculations, for example, these sources were only sampled over a narrow cone of directions within 15.13 degrees of the centerline, where cos(theta) was greater than 0.965335056. This was deemed adequate on the basis that source particles at the most forward source location (Z=99.9 cm), starting in this angular range, would diverge to fill the entire inner diameter of the beam tube (diam=10.16 cm) before getting to the importance cutoff plane at Z=118.6879 cm, which itself is well upstream of the start of the 1998 water tube at Z=174.27 cm. (Perhaps a smaller angular range would have been sufficient and would have yielded an even more efficient calculational model, but the idea here was also to include scattering events at or in the vessel nozzle, which dictated the present location and therefore this particular angular range.) In the case of the neutron dosimetry problem, where the dosimeters are located outside the beam tube but inside the pressure vessel, the importance cutoff plane had to be moved back as noted above, and the cone of sampling directions had

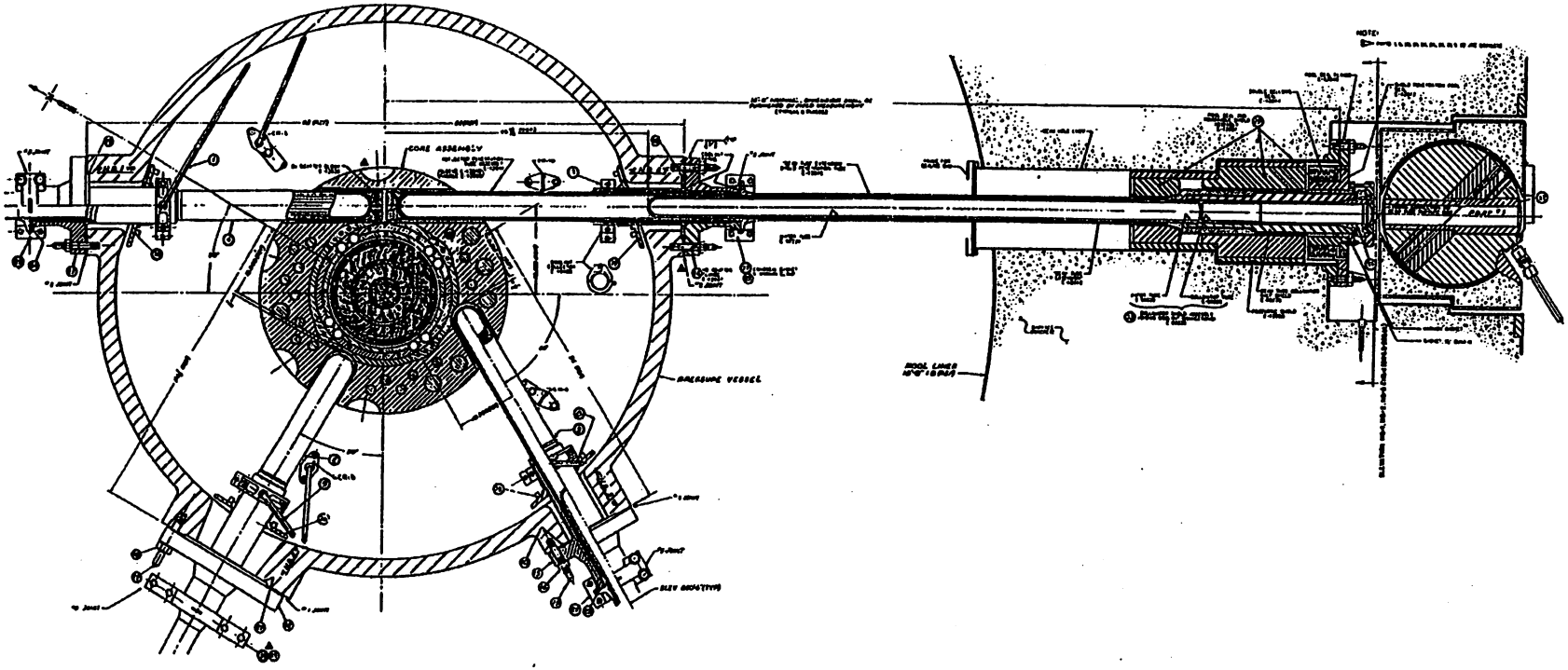


Fig. 3.1. Overview of the original 1960 HB-4 beam tube before the cold source or any of the recently proposed upgrades.

MCNP Plot Window: Origin of plot window located at X=0, Y=0, Z=240 cm in real system;
Size of plot window = ± 250 x ± 250 cm;
Orientation basis vectors: (0,1,0) and (0,0,1) are such that:
+y in model (horz lateral in real world) is to right in plot,
+z in model (horz axis in real world) is up in plot

light green = beryllium refl.
light blue = water in vessel
purple = water in pool / tube
dark green = barytes concrete

orange = carbon steel
yellow = stainless steel
pink = aluminum
light gray = void

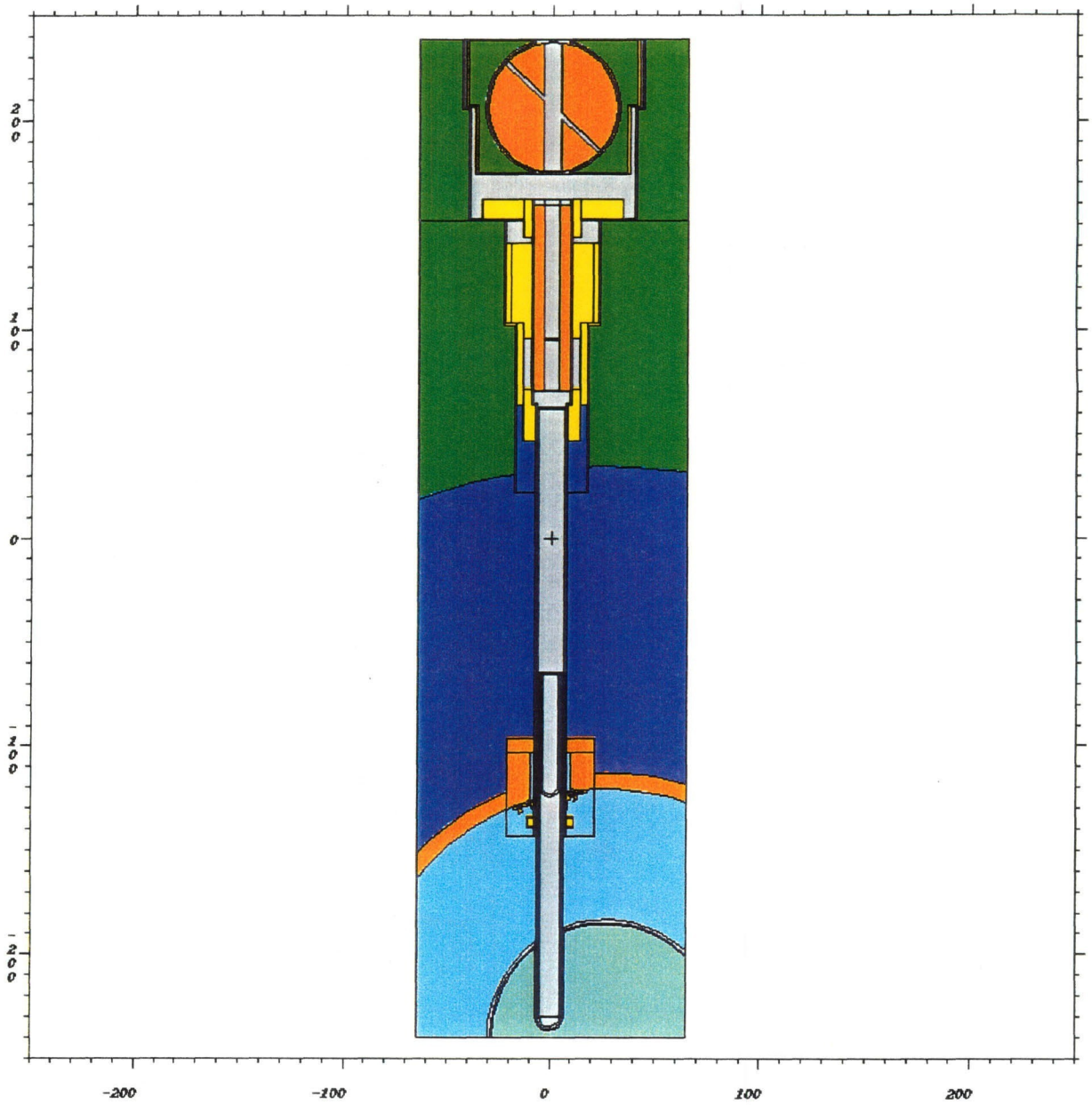


Fig. 3.2. Basic MCNP model used in the HB-3 dosimetry analysis, shown with the 1960 beam tube void and the rotary shutter's large-diameter aperture open.

MCNP Plot Window: Origin of plot window located at X=0, Y=0, Z=240 cm in real system;
Size of plot window = ± 250 x ± 250 cm;
Orientation basis vectors: (0,1,0) and (0,0,1) are such that:
+y in model (horz lateral in real world) is to right in plot,
+z in model (horz axis in real world) is up in plot

light green = beryllium refl.
light blue = water in vessel
purple = water in pool / tube
dark green = barytes concrete

orange = carbon steel
yellow = stainless steel
pink = aluminum
light gray = void

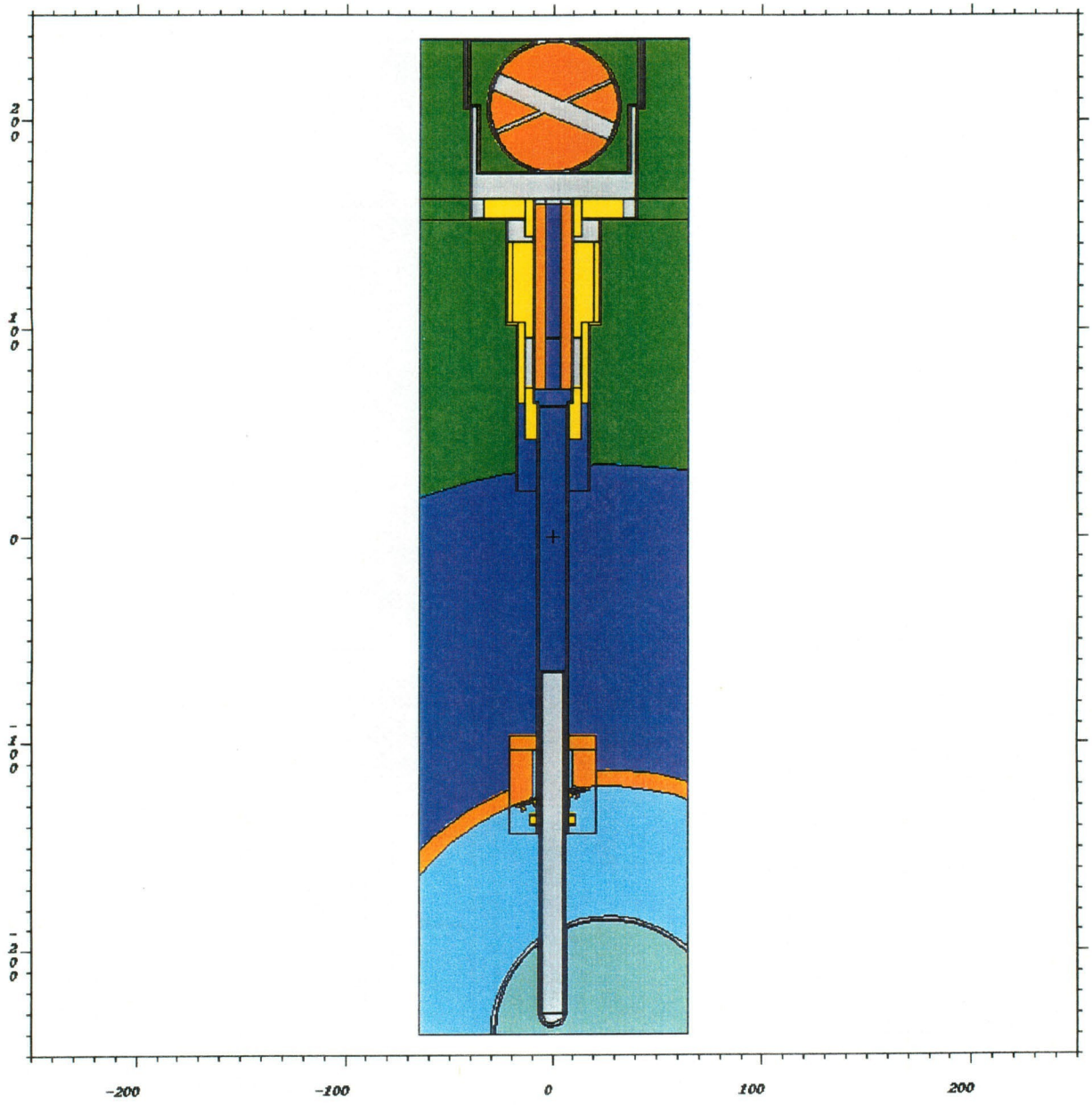


Fig. 3.3. Basic MCNP model used in the final HB-3 gamma shielding analysis, shown with the 1998 water tube and collimator sections both flooded and the shutter closed.

to be expanded to include all starting directions with direction cosines greater than 0.71 (i.e., all neutrons starting within 44.765 degrees of the centerline) so that the model would include the vast majority of fast neutrons (above 27 keV) that stood any chance of impinging on the inner wall of the beam tube within about a foot (in this case, 35.85638 cm) of the first (most upstream) dosimeter. In both the shielding analyses and the dosimetry analysis, the starting weight (wgt) of the source particles was defined on the sdef card such that wgt = [mu(max)-mu(min)]/[(+1)-(-1)] = (1-cos(theta))/2. (To verify that this formulation was correct, simple MCNP test calculations were first performed in a vacuum, using source sampling over these limited angular ranges in conjunction with the corresponding weights; the resulting fluxes were then compared with the simple analytic results, and with other MCNP results using full-range 4*pi sampling and starting weights of 1.0.)

Figures 3.2 and 3.3 show overviews of the same basic calculational model, configured in different ways. Moreover, in constructing the model for the HB-3 beam tube, an attempt was made to make and keep the base MCNP input file as general as possible. In reference to the two typical MCNP input files shown in Appendices B.1 and D.4, for example:

(a) Surfaces for describing both the original 1960 water tube and the newly proposed 1998 water tube design are included the base model. In a particular calculation, if one is describing the one, the material for the other is set to void, and vice versa. (See Cells 2140, 2141, 4305, and 4380 in the MCNP input files)

(b) Whether the water tube is void or flooded is controlled by the materials used in Cells 2145 and 2146 in the MCNP input. Input for both models is included, one needs only to select (uncomment) which set is to be used in a given calculation.

(c) The orientation of the rotary shutter (closed, small aperture open, or large aperture open) is described by Surfaces 3131 and 3132 in the MCNP input. Cards describing all three orientations are in the input, and one needs only to select (uncomment) which set is to be used in a given calculation.

(d) While not presently the case, all of the source definition cards shown in Appendix A.1 (for neutrons or gammas, for one particular beam tube, or for all four beam tubes) may be placed directly in the MCNP input files, and the user could select the point sources to be used for a particular problem simply by changing the one line "sdef" card which determines which set of distribution functions to use in a particular problem.

(e) While never used, the base model in Appendix D.4 has provision for decoupling some regions of the problem from the other regions, thereby allowing one to run the rotary shutter (for example) as a boundary source problem, while only altering one or two lines in the input file. When running the whole problem, for example, one can create an MCNP boundary source just upstream of the rotary shutter. There are 3 XY planar surfaces and 2 infinitesimally small void cells at this location, all of which cut across the entire problem geometry. The boundary source is calculated and stored on the middle surface. In a bootstrapped calculation, one can use that boundary source, set the importance of the first cell just upstream of the boundary source to zero (imp=0) to decouple everything downstream from everything upstream, run the calculation (perhaps with a perturbed shutter design) and tally results on the third surface (downstream of the second void cell) to verify that the flux there is identical to that in the original (larger) problem. Ultimately, that capability was not needed, but it is in the model, and a good 592 MB boundary source at this location is available if needed in the future.

(f) Optimal importance-region biasing for the neutron dosimetry problem is "built in" to both of the MCNP input files shown in the above appendices, yet for the gamma-only transport problem described in Sect 6, one can easily override those specifications by placing "wwinp=wwinp" on the MCNP header card, thus telling the code to go out and use a special geometry-independent weight window file that contains optimal space-energy-directional-dependent biasing parameters based on a global phantom (XYZ) mesh that is completely independent of the geometry specifications needed to describe the physical layout of materials in the problem. This allows the same base geometry model to be used in all of the necessary calculations, even though the biasing requirements may be quite different from one problem to the next. This extremely useful feature is described more fully in Sect 6.

These and other generalizations have been built into the base model which is heavily annotated with comments describing how to make all of the necessary permutations. The key permutations used in the various calculations required for this study are described in subsequent sections.

To describe the exact location and size of every surface and cell (and material) used in the model is beyond the scope of this section. Moreover, such a compilation of information would ultimately have to be a reproduction of all the information contained in the input files shown in Appendices B.1 and D.4. For such details, the reader is therefore referred to the typical input file listings shown in those appendices. Below, we shall first present a series of

pictures (plots made from the actual MCNP input files) to illustrate various aspects of the base model used throughout this study, and to provide the reader with a general orientation. We shall then list the key engineering drawings from which key dimensions and material specifications were taken during the creation of the present base model, along with a brief description of the specific information that was taken from each drawing. In the subsequent sections describing individual calculations, any departure from the base case (and/or any key features of the model that are especially important to the particular calculation) will be noted.

3.1 Pictorial Orientation (Overview)

Figures 3.4-3.8 show various permutations of the base model. These picture plots were made using the MCNP "ip" plotting option and the actual input files for various runs. Whenever model changes are made, plots such as these are created before the calculational run is ever submitted, just to verify that the actual geometry is free of errors and corresponds to what was intended. In the MCNP model, Z=0 cm (corresponding to the core radial plane perpendicular to the beam tube centerline) is at the bottom of each figure, while the surface at Z=478.79 cm (at the top of each figure) corresponds to the downstream surface of the steel-clad concrete housing holding the rotary shutter. So as to include the distant point where Blosser and Thomas made their experimental measurements of the flux in 1968, the model also included a large void region axially, from Z=478.79 cm to Z=700 cm. This geometrically-uninteresting void region was not included in these plots so that the other regions of real interest would be more plainly visible. The origin of the plot window corresponds to MCNP coordinates X=0, Y=0, Z=240 cm where, in reality, Z is the horizontal axis of the beam tube, Y lies in a horizontal plane and extends to the right of the centerline, and X is the vertical coordinate perpendicular to the page. A scale is shown with each figure simply to give one a sense of relative size (in cm). To aid in interpreting these and other plots, the text line labeled "MCNP Plot Window" always shows the location of the plot origin in terms of the actual MCNP coordinates.

The hemisphere defining the outermost surface of the hot tip of the HB-3 beam tube is, in reality, centered at a point 28.5369 cm from the core radial plane perpendicular to the beam tube. In the base MCNP model, however, this midpoint (in the voided beam tube) was repositioned at Z=10.0 cm from the core radial plane perpendicular to the beam tube in order to accommodate one of the equivalent point sources shown in Table 2.2b. Since no external boundary sources are being used, since the central region of the beam tube is void, since we are sampling the point sources only over a very narrow cone of forward directions, and since the aluminum wall of the beam tube is assigned an importance of zero all the way out to Z=118.6879 cm (normally), this accommodation will have no effect on the actual solution; it simply makes the plot look a little different than one would expect based on engineering drawings.

Figure 3.4, is similar to Fig. 3.2 in that the entire beam tube is void. In this case, however, the small beam hole in the rotary shutter is open, as was the case when Blosser and Thomas made their flux measurements at Z=678.1673 cm (not shown in this figure).

Figure 3.5 shows the axial extent of the original 1960 water tube inside the HB-3 beam tube. Note that much of the the light gray area representing the central void in Fig. 3.4 has been replaced by a dark blue/purple area showing the flooded portion of the 1960 water tube. Also note that the 1960 water tube starts near the inner surface of the pressure vessel and extends about one-third of the way up the region now occupied by the the 1998 collimator. This particular model has several approximations: (1) The aluminum walls of the internal water tube were not actually included in this particular (early) model; only the corresponding void or water-filled regions are shown. (2) The hemispherical tip of defining the hot end of the internal water tube is not included because the body of the internal water tube was not included in this (early) model; instead, a flat aluminum disk from Z=116.7841 to Z=117.7366 cm was used to represent the hemispherical tip of the water tube. In several of the later models, shown below, the actual geometry near the tip of the 1960 water tube was represented correctly. (3) The primary focus of the HB-3 analysis was the correct representation of the 1998 water tube and collimator. The 1960 water tube was generally handled in a more approximate fashion, as noted above. Consistent with that, we elected to model the newly proposed 1998 collimator (between the end of the 1998 water tube and the start of the rotary shutter) exactly, and to represent the downstream end of the 1960 water tube by simply placing a second aluminum window (Z=334.7709 to 335.4756 cm) in the normally void rectangular collimator hole, where the 1960 water tube would normally terminate in the old design. In practice, the 3-D MCNP model of the 1960 water tube shown here was never used since other simpler models sufficed. Nevertheless, Fig. 3.5 is included here to give one a sense of perspective for comparison purposes.

Figure 3.6 shows the axial extent of the newly proposed 1998 water tube formed by two aluminum disks welded inside the new beam tube, in the region downstream of the vessel flange. The first aluminum disk is located between Z=174.27 and Z=174.95125 cm, while the second is located between Z=302.1868 and Z=302.5043 cm. To highlight the region that might be filled with water during

MCNP Plot Window: Origin of plot window located at X=0, Y=0, Z=240 cm in real system;
Size of plot window = ± 250 x ± 250 cm;
Orientation basis vectors: (0,1,0) and (0,0,1) are such that:
+y in model (horz lateral in real world) is to right in plot,
+z in model (horz axis in real world) is up in plot

light green = beryllium refl.
light blue = water in vessel
purple = water in pool / tube
dark green = barytes concrete

orange = carbon steel
yellow = stainless steel
pink = aluminum
light gray = void

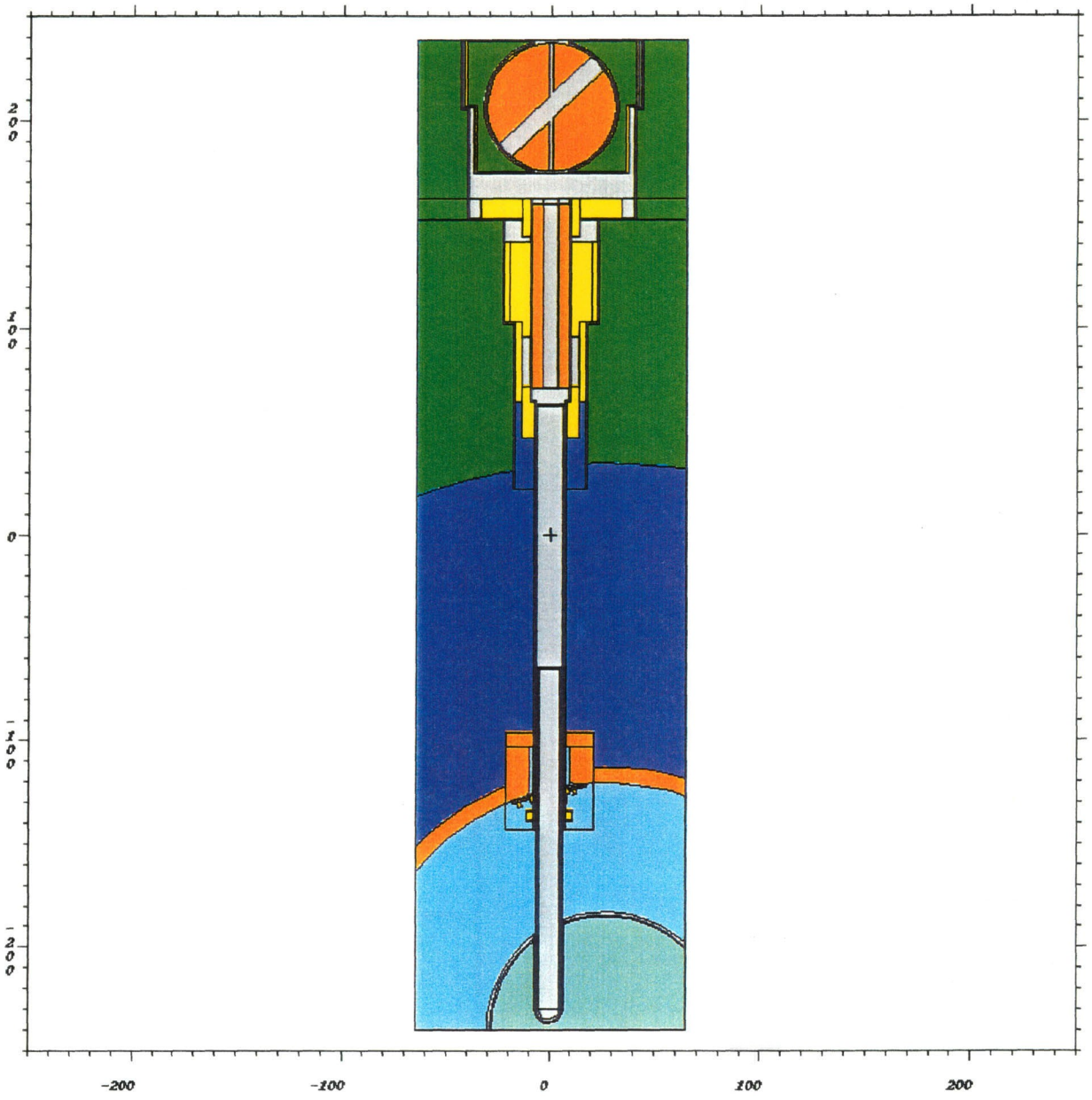


Fig. 3.4. Variation of the basic MCNP model, shown with the HB-3 water tube void and the rotary shutter's small-diameter aperture open.

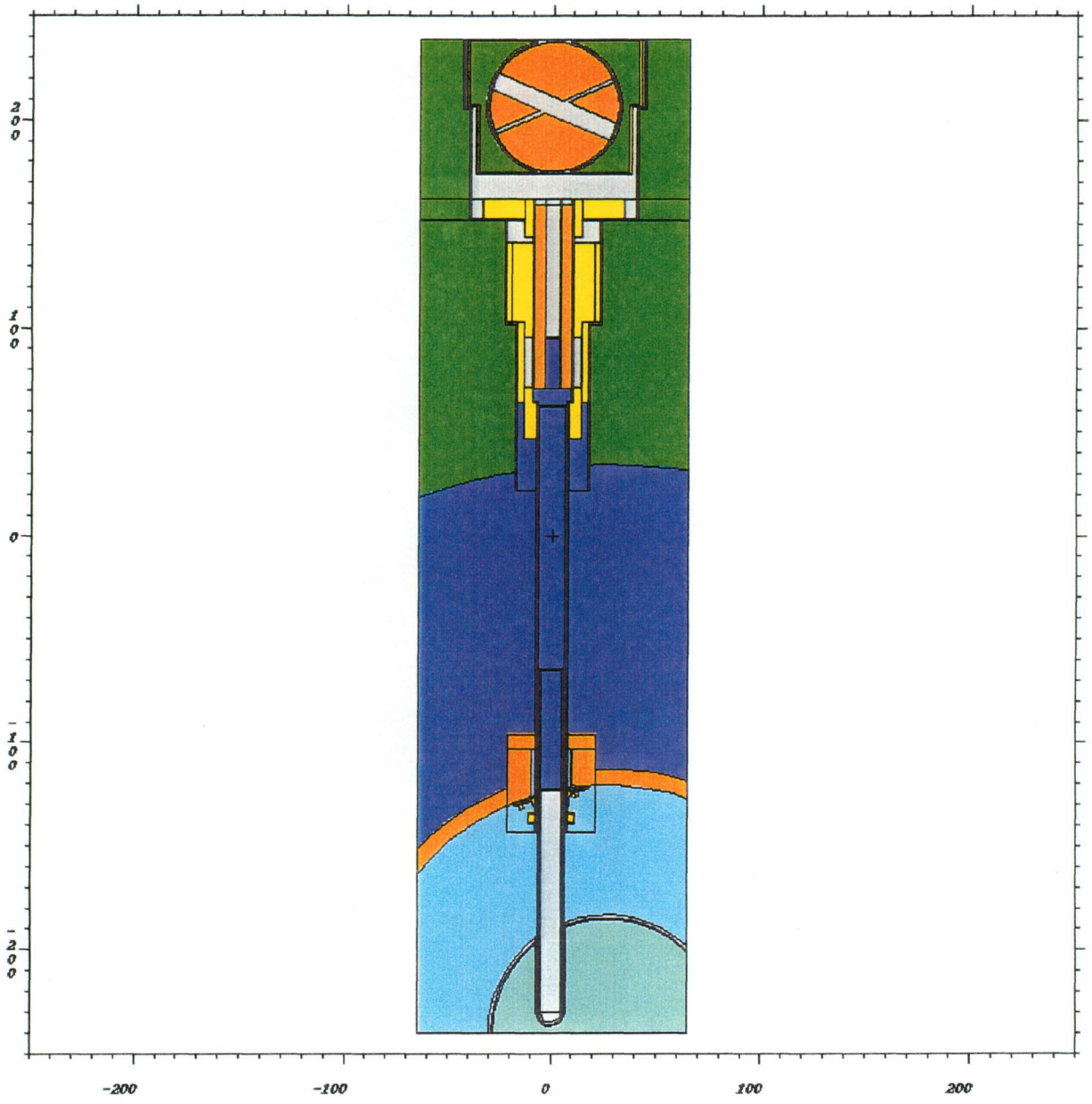


Fig. 3.5. Variation of the basic MCNP model, showing the axial extent of the water in the original (simplified model of the) 1960 water tube.

MCNP Plot Window: Origin of plot window located at X=0, Y=0, Z=240 cm in real system;
Size of plot window = ± 250 x ± 250 cm;
Orientation basis vectors: (0,1,0) and (0,0,1) are such that:
+y in model (horz lateral in real world) is to right in plot,
+z in model (horz axis in real world) is up in plot

light green = beryllium refl.
light blue = water in vessel
purple = water in pool / tube
dark green = barytes concrete

orange = carbon steel
yellow = stainless steel
pink = aluminum
light gray = void

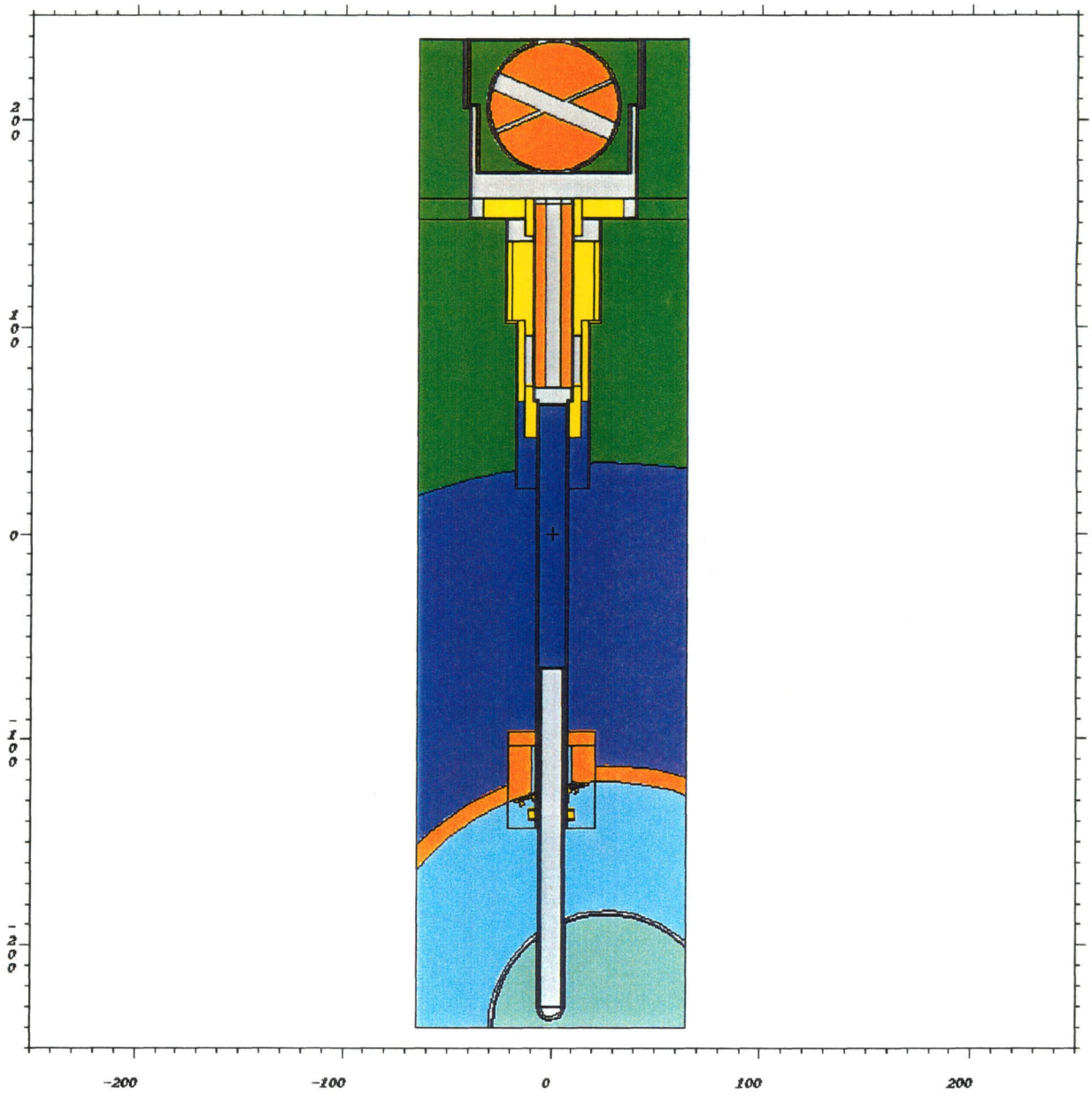


Fig. 3.6. Variation of the basic MCNP model, showing the axial extent of the water in newly proposed 1998 water tube.

MCNP Plot Window: Origin of plot window located at X=0, Y=0, Z=240 cm in real system;
Size of plot window = ± 250 x ± 250 cm;
Orientation basis vectors: (0,1,0) and (0,0,1) are such that:
+y in model (horz lateral in real world) is to right in plot,
+z in model (horz axis in real world) is up in plot

light green = beryllium refl.
light blue = water in vessel
purple = water in pool / tube
dark green = barytes concrete

orange = carbon steel
yellow = stainless steel
pink = aluminum
light gray = void

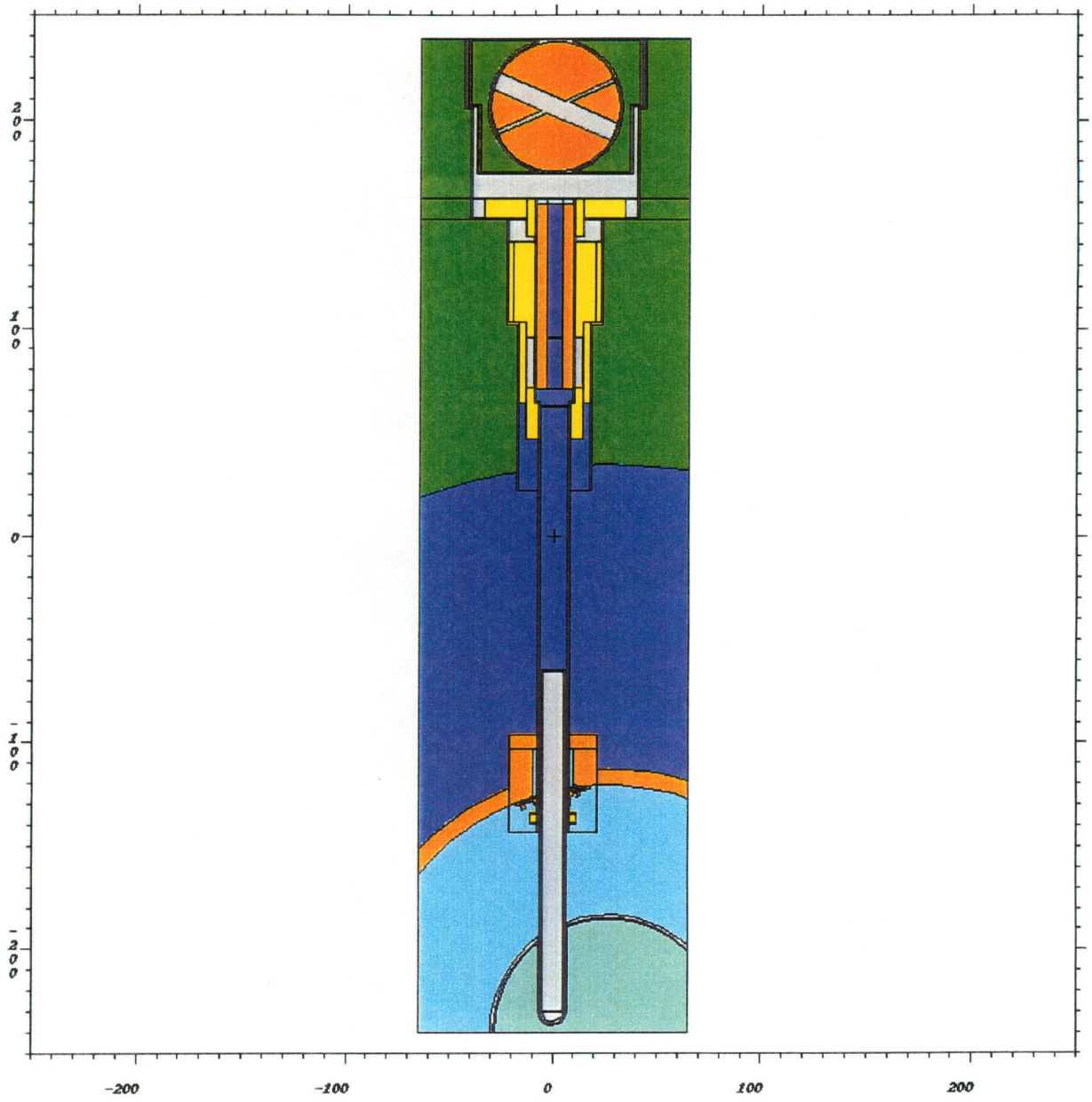


Fig. 3.7. Variation of the basic MCNP model, showing the 1998 water tube and collimator sections both flooded.

MCNP Plot Window: Origin of plot window located at X= -0.01, Y=0, Z=120 cm in real system;
Size of plot window = ± 30 x ± 30 cm;
Orientation basis vectors: (0,1,0) and (0,0,1) are such that:
+y in model (horz lateral in real world) is to right in plot,
+z in model (horz axis in real world) is up in plot

light green = beryllium refl.
light blue = water in vessel
purple = water in pool / tube
dark green = barytes concrete

orange = carbon steel
yellow = stainless steel
pink = aluminum
light gray = void

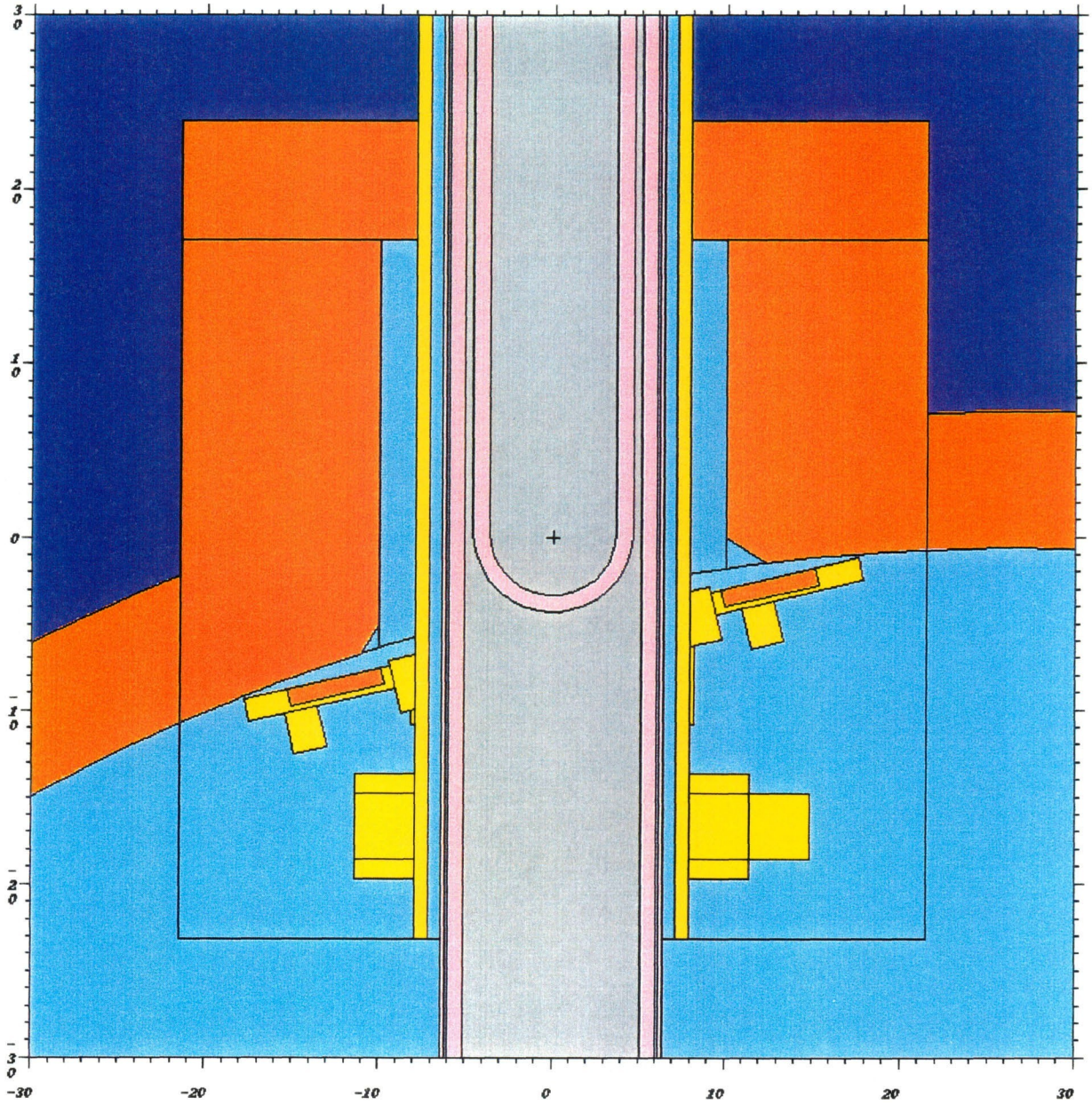


Fig. 3.8. Close-up view of the HB-3 beam tube (and the 1960 internal water tube), the surrounding stainless steel sleeve, the dosimeter holder ring, the coolant collector assembly, all located in the vicinity of the pressure vessel's HB-3 nozzle.

MCNP Plot Window: Origin of plot window located at X=0, Y=0, Z=175 cm in real system;
Size of plot window = ± 12 x ± 12 cm;
Orientation basis vectors: (0,1,0) and (0,0,1) are such that:
+y in model (horz lateral in real world) is to right in plot,
+z in model (horz axis in real world) is up in plot

light green = beryllium refl.
light blue = water in vessel
purple = water in pool / tube
dark green = barytes concrete

orange = carbon steel
yellow = stainless steel
pink = aluminum
light gray = void

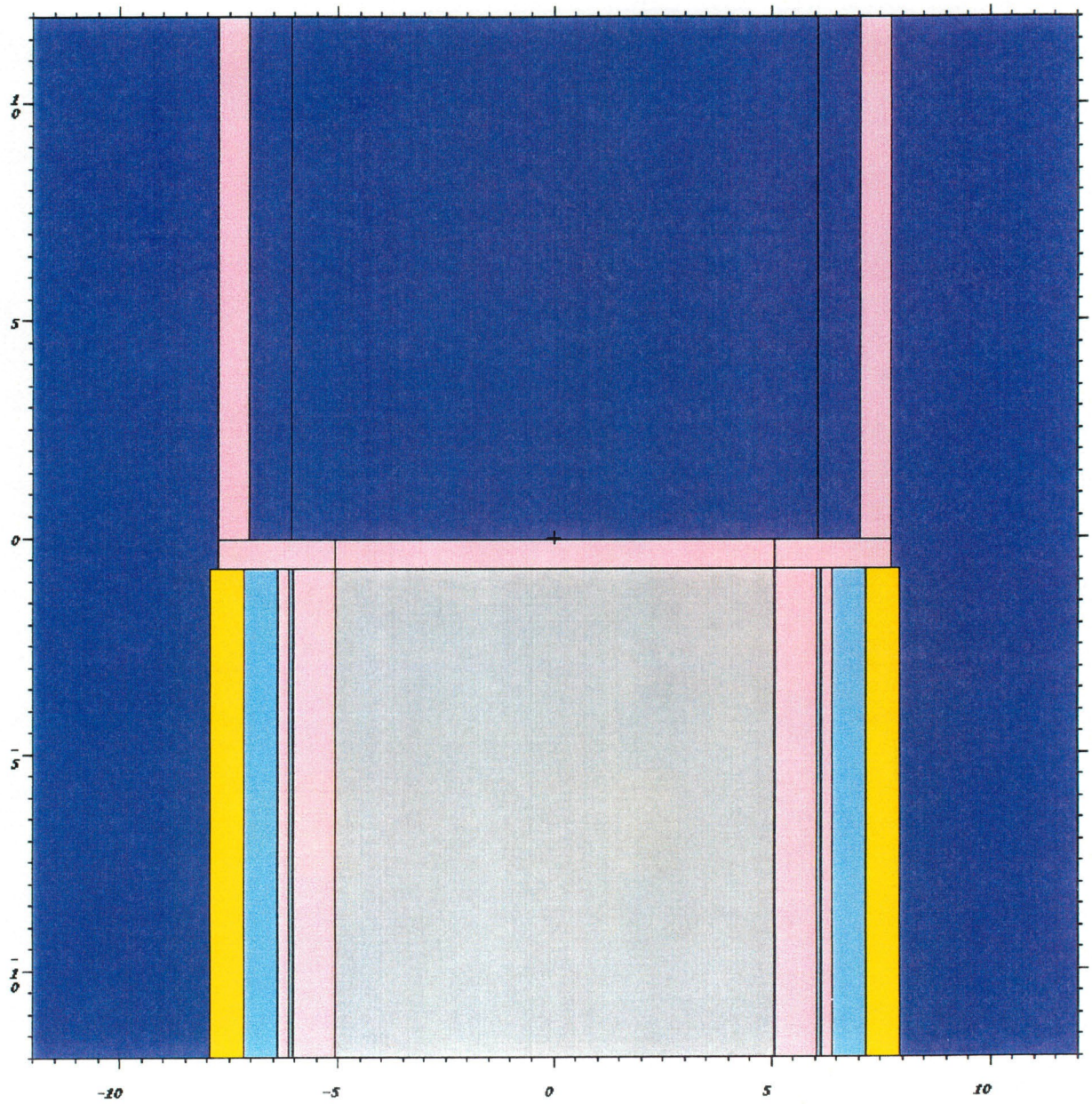


Fig. 3.9. Close-up view the 1998 HB-3 beam tube design in the vicinity of the first aluminum window defining the start of the 1998 water tube.

MCNP Plot Window: Origin of plot window located at X=0, Y=0, Z=332 cm in real system;
Size of plot window = ± 75 x ± 75 cm;
Orientation basis vectors: (0,1,0) and (0,0,1) are such that:
+y in model (horz lateral in real world) is to right in plot,
+z in model (horz axis in real world) is up in plot

light green = beryllium refl.
light blue = water in vessel
purple = water in pool / tube
dark green = barytes concrete

orange = carbon steel
yellow = stainless steel
pink = aluminum
light gray = void

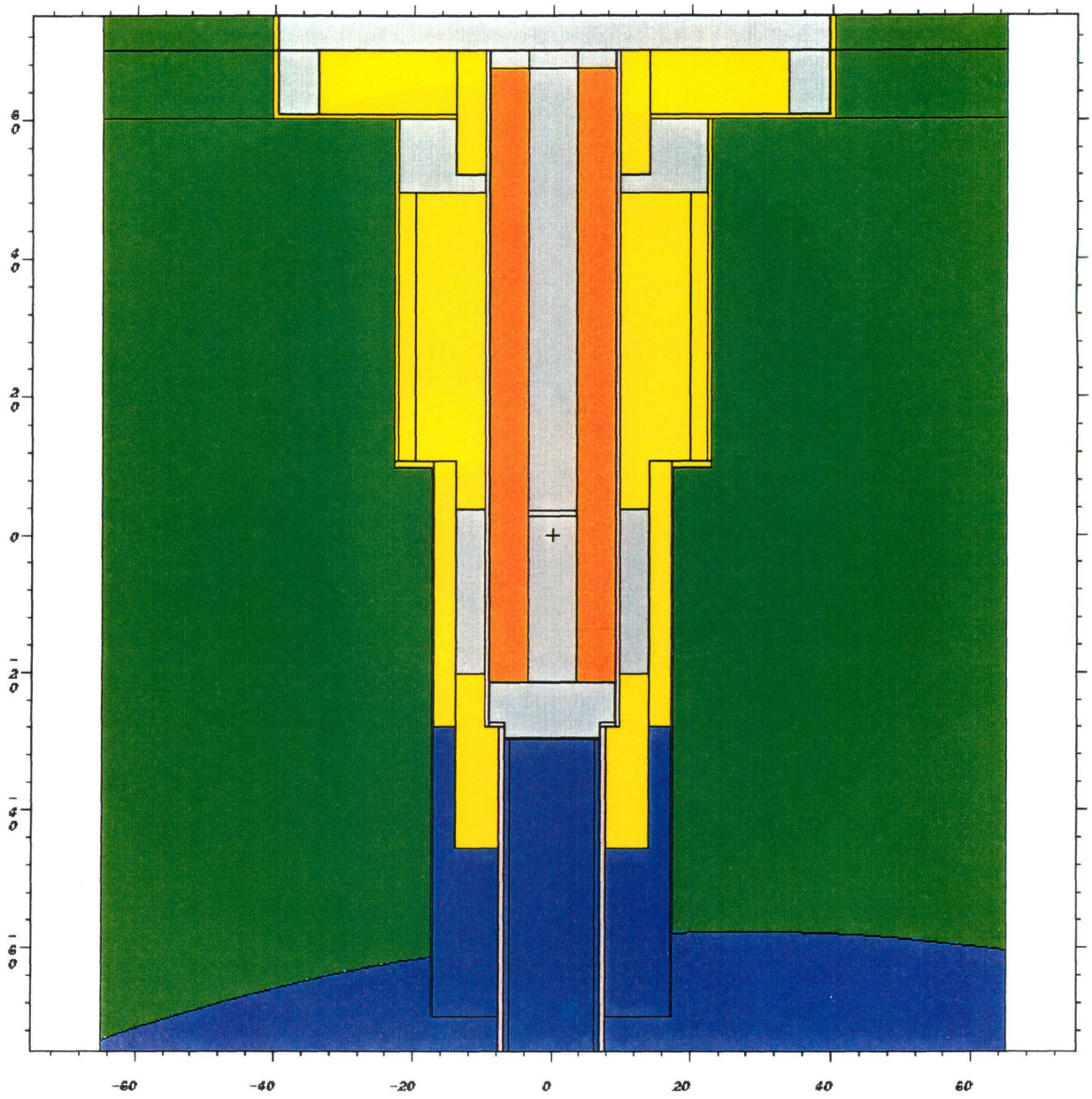


Fig. 3.10. Top view of a horizontal slice through the 1998 collimator design and the attendant radial and eccentric shields, as well as the pool seals, with the water tube flooded but the collimator section dry.

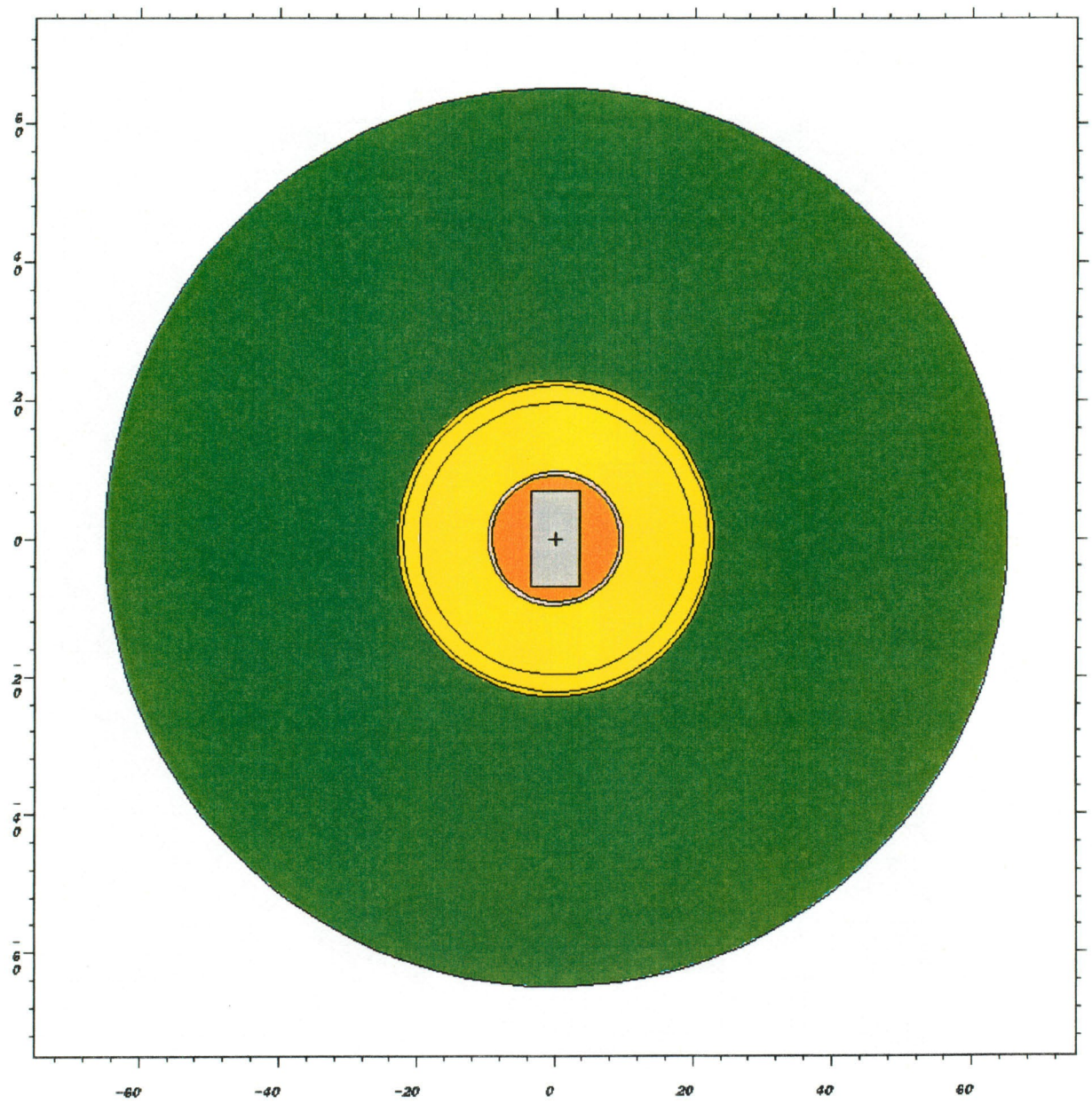


Fig. 3.11. Vertical slice through the MCNP model near the middle of the collimator, showing the rectangular hole down the center of the collimator, the collimator itself, the surrounding beam tube, the radial shield, the eccentric shield, a thin steel liner, and the surrounding biological shield.

MCNP Plot Window: Origin of plot window located at X=0, Y=0, Z=430 cm in real system;
Size of plot window = ± 55 x ± 55 cm;
Orientation basis vectors: (0,1,0) and (0,0,1) are such that:
+y in model (horz lateral in real world) is to right in plot,
+z in model (horz axis in real world) is up in plot

light green = beryllium refl.
light blue = water in vessel
purple = water in pool / tube
dark green = barytes concrete

orange = carbon steel
yellow = stainless steel
pink = aluminum
light gray = void

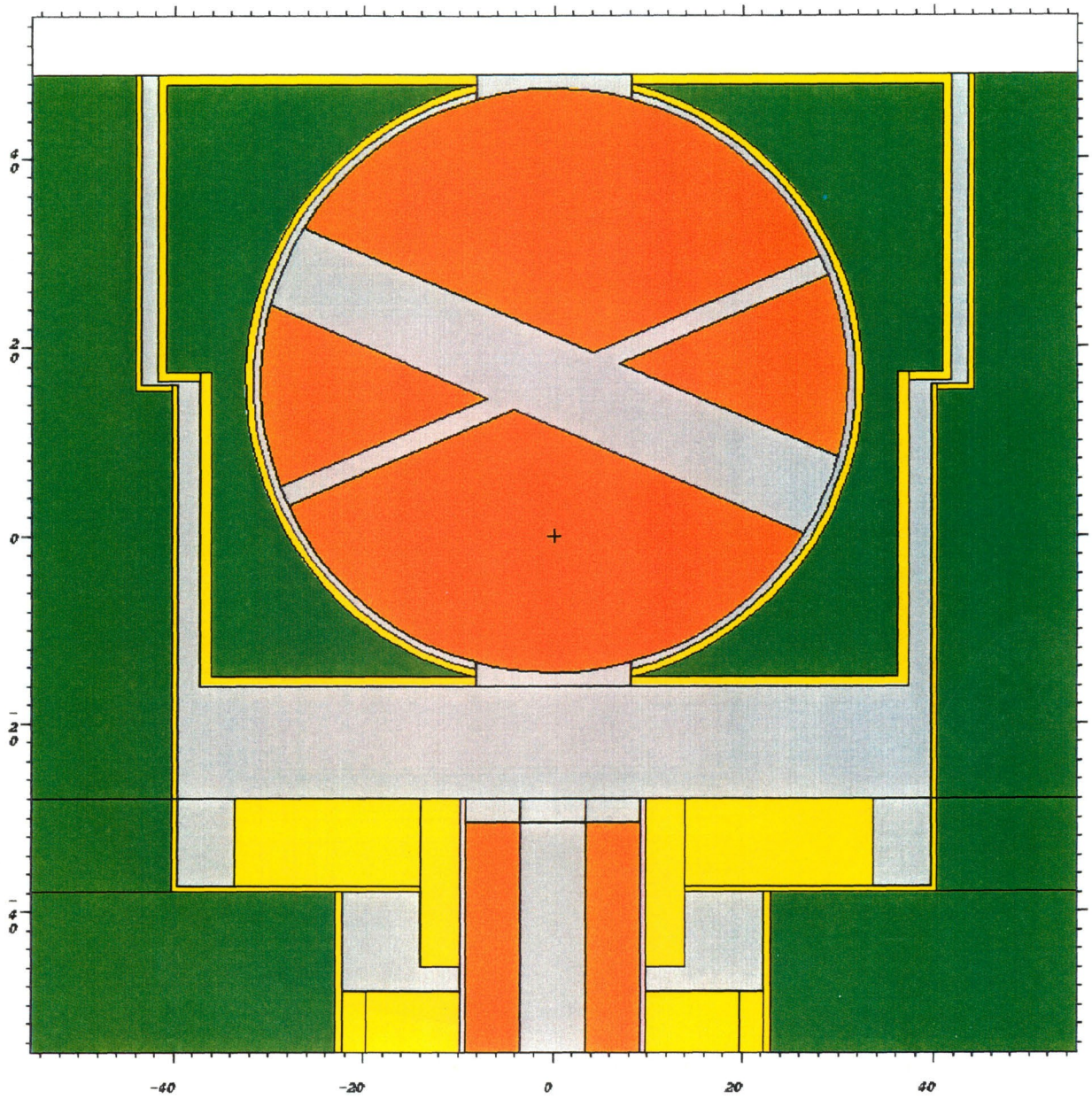


Fig. 3.12. Top view of a horizontal (YZ) slice through the rotary shutter, including the downstream end of the collimator, the steel-line stepped concrete box holding the rotary shutter, and surrounding portions of the biological shield.

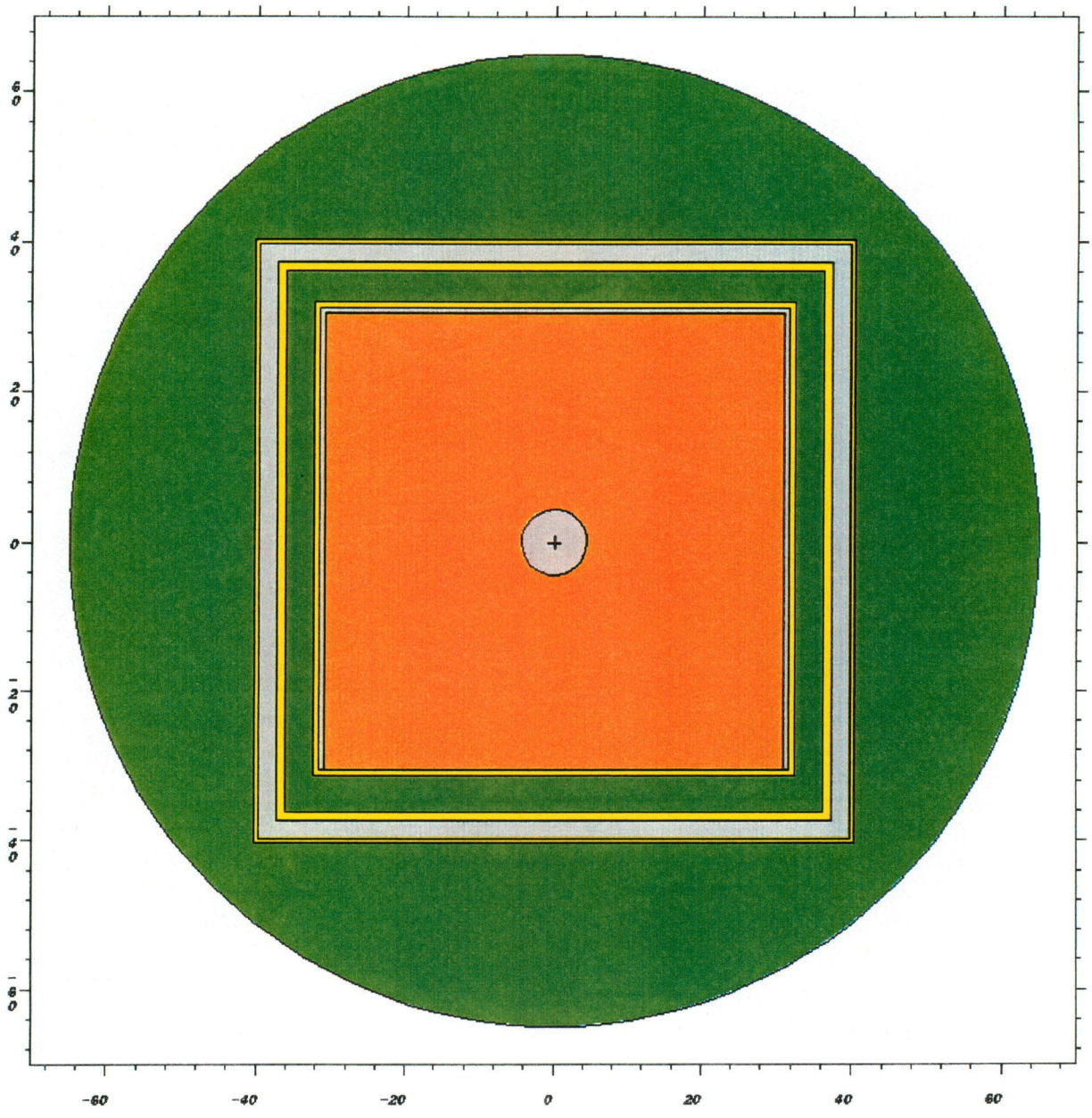


Fig. 3.13. Axial view of a vertical (XY) slice through the rotary shutter assembly and surrounding materials including the biological shield (with the shutter in the open position).

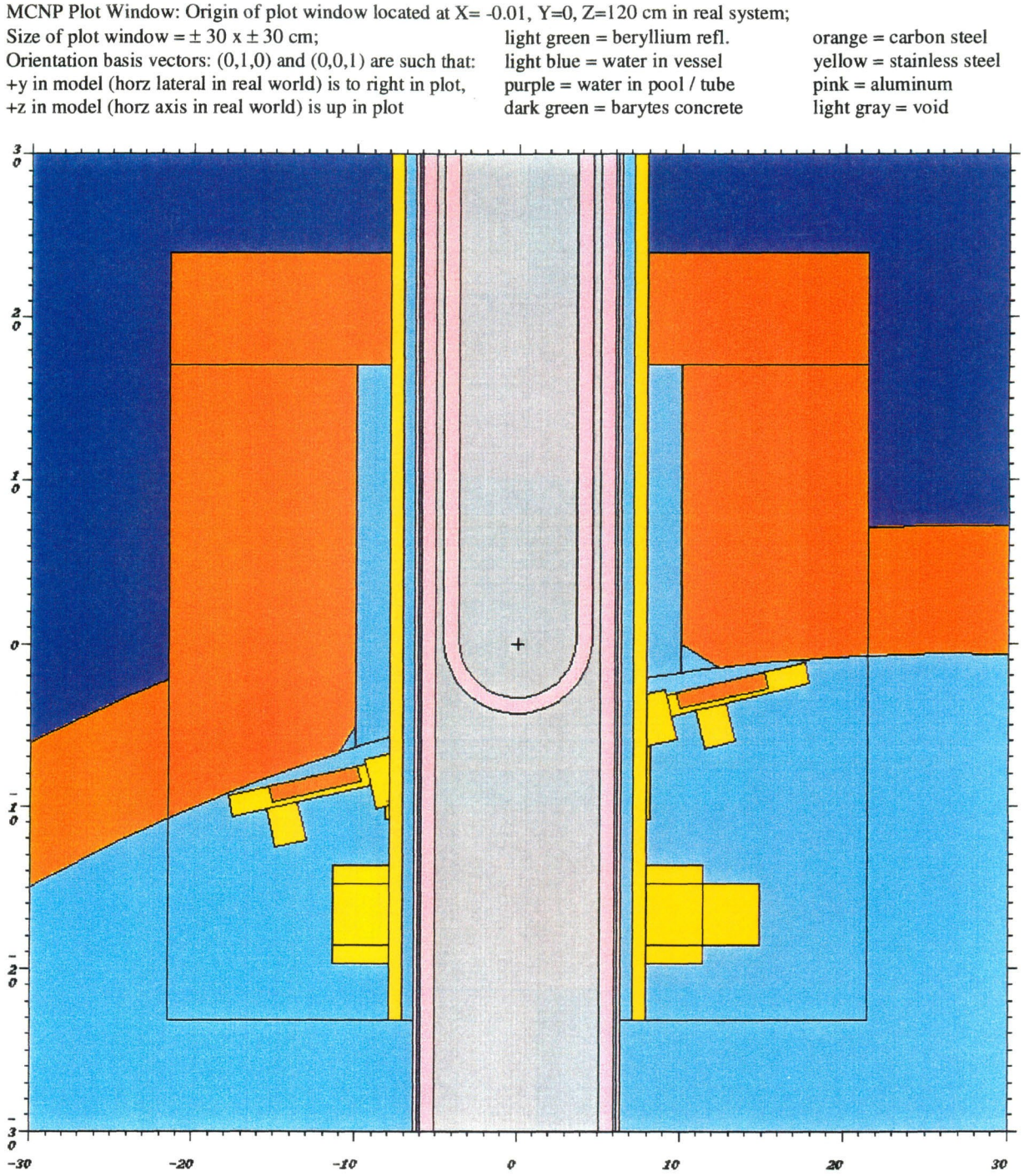


Fig. 3.14. Close-up view of a horizontal (YZ) slice through the HB-3 beam tube (and the 1960 internal water tube), the surrounding stainless steel sleeve, the dosimeter holder ring, and the coolant collector assembly, as modeled in the dosimetry analysis for key 3, positions 3 and 8. In this figure, key 3 position 3 is on the right, and key 3 position 8 is on the left.

MCNP Plot Window: Origin of plot window located at X=0, Y=0, Z=120 cm in real system;
Size of plot window = ± 30 x ± 30 cm;
Orientation basis vectors: (0,0,-1) and (1,0,0) are such that:
+z in model (horz axis in real world) is to left in plot,
+x in model (vert upward in real world) is up in plot

light green = beryllium refl.
light blue = water in vessel
purple = water in pool / tube
dark green = barytes concrete

orange = carbon steel
yellow = stainless steel
pink = aluminum
light gray = void

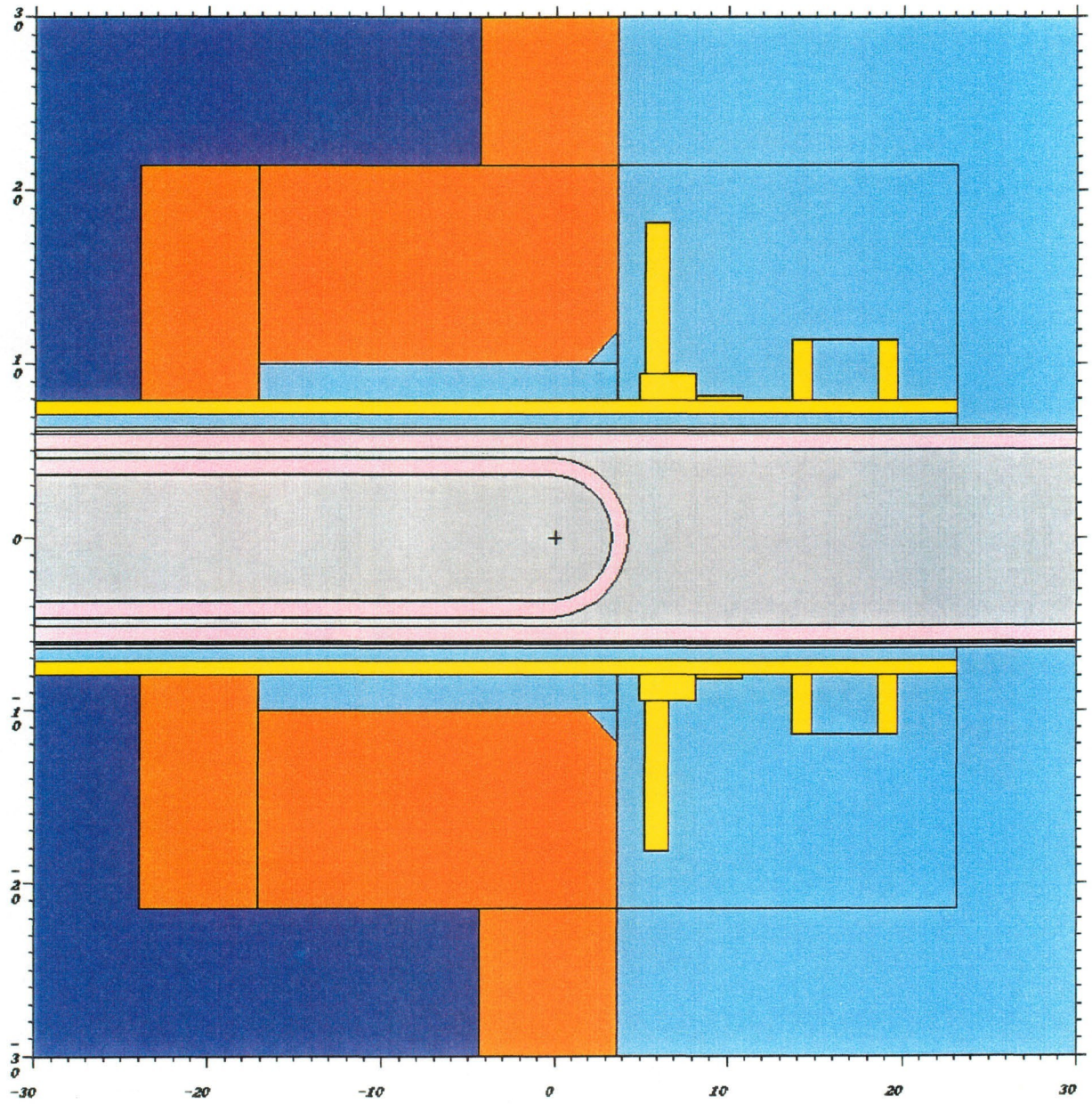


Fig. 3.15. Close-up view of a vertical (XZ) slice through the HB-3 beam tube (and the 1960 internal water tube), the surrounding stainless steel sleeve, the dosimeter holder ring, and the coolant collector assembly, as modeled in the dosimetry analysis for Key 3, positions 3 and 8.

MCNP Plot Window: Origin of plot window located at X=0, Y=0, Z=104 cm in real system;
Size of plot window = ± 20 x ± 20 cm;
Orientation basis vectors: (0,1,0) and (1,0,0) are such that:
+y in model (horz lateral in real world) is to right in plot,
+x in model (vert upward in real world) is up in plot

light green = beryllium refl.
light blue = water in vessel
purple = water in pool / tube
dark green = barytes concrete

orange = carbon steel
yellow = stainless steel
pink = aluminum
light gray = void

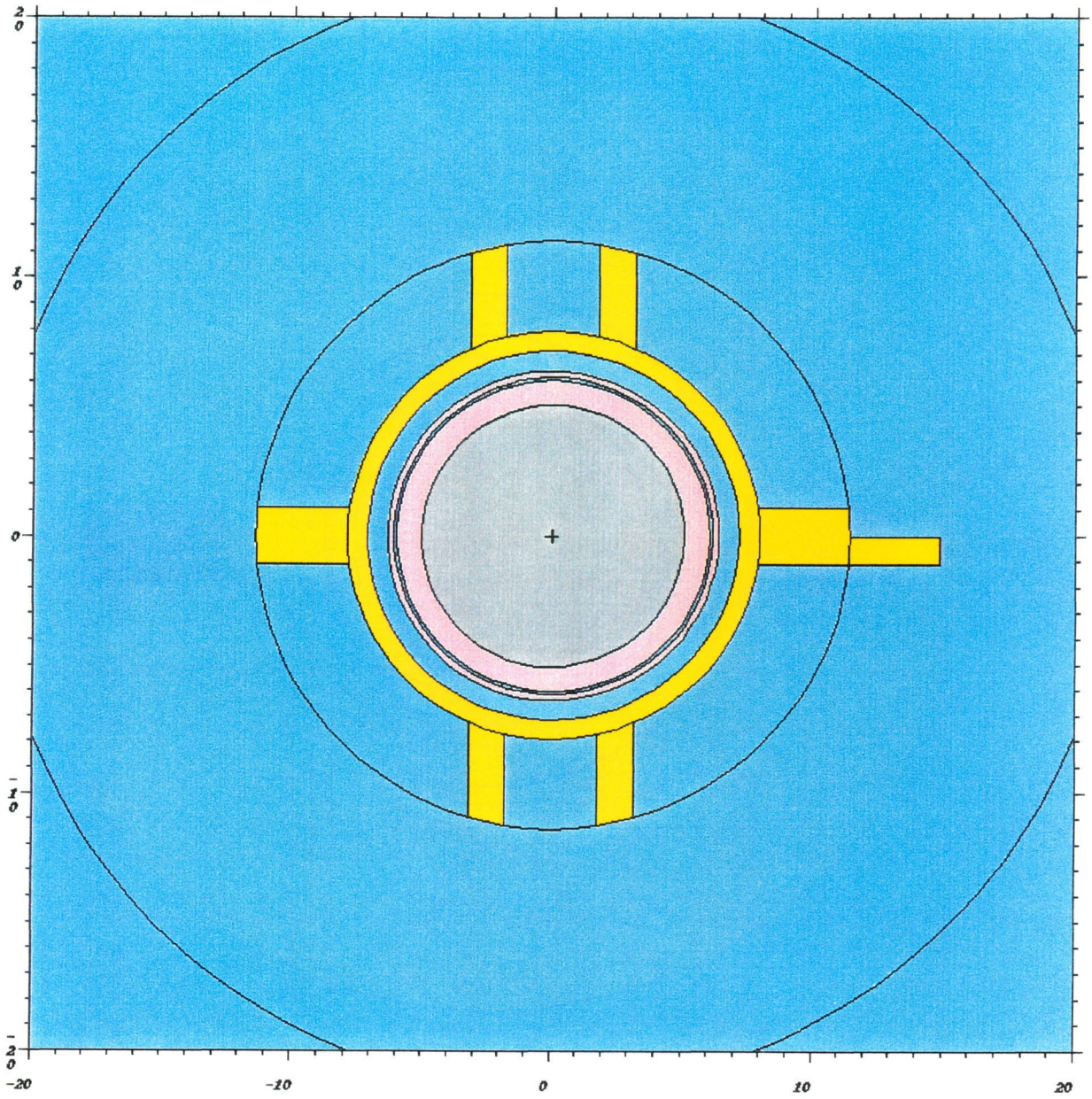


Fig. 3.16. Vertical (XY) slice through the coolant collector assembly mounted near the end of the stainless steel sleeve surrounding the HB-3 beam tube.

MCNP Plot Window: Origin of plot window located at X=0, Y=0, Z=114.14 cm in real system;
Size of plot window = ± 20 x ± 20 cm; Orientation basis vectors: (0, 0.974370, 0.224951) and (1,0,0) are such that this plot is in plane of dosimeters (horz here is really horz), +x in model (vert upward in real world) is up in plot

light green = beryllium refl.
light blue = water in vessel
purple = water in pool / tube
dark green = barytes concrete

orange = carbon steel
yellow = stainless steel
pink = aluminum
light gray = void

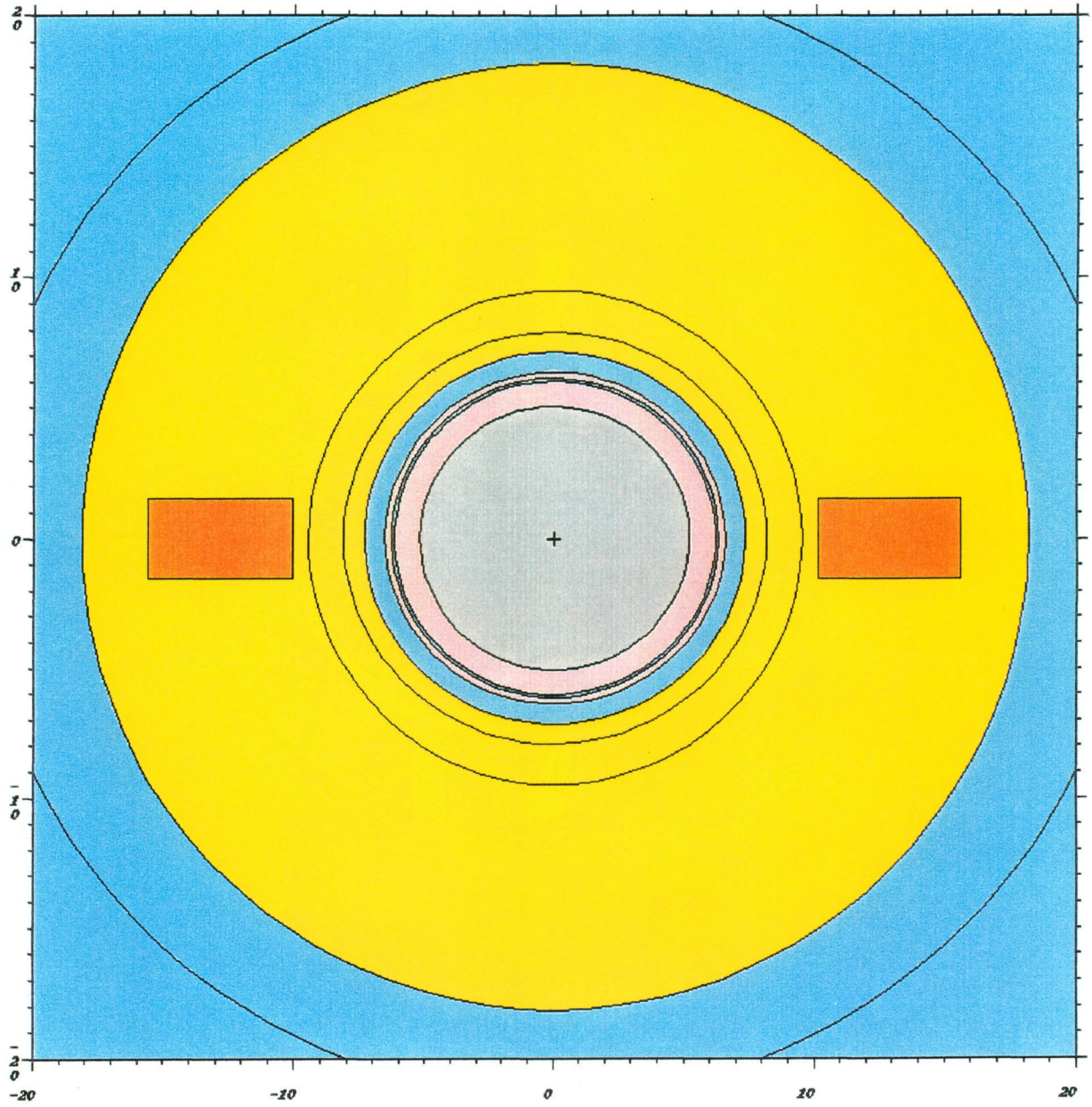


Fig. 3.17. Vertical slice through the rear section of the dosimeter holder ring (in the rotated plane of the holder ring), showing the Charpy V-notch specimens at Key 3, positions 3 and 8.

MCNP Plot Window: Origin of plot window located at X=0, Y=0, Z=111.20 cm in real system;
Size of plot window = ± 20 x ± 20 cm; Orientation basis vectors: (0, 0.974370, 0.224951) and (1,0,0) are such that plot is offset but parallel to plane of dosimeter holder ring, +x in model (vert upward in real world) is up in plot

light green = beryllium refl.
light blue = water in vessel
purple = water in pool / tube
dark green = barytes concrete

orange = carbon steel
yellow = stainless steel
pink = aluminum
light gray = void

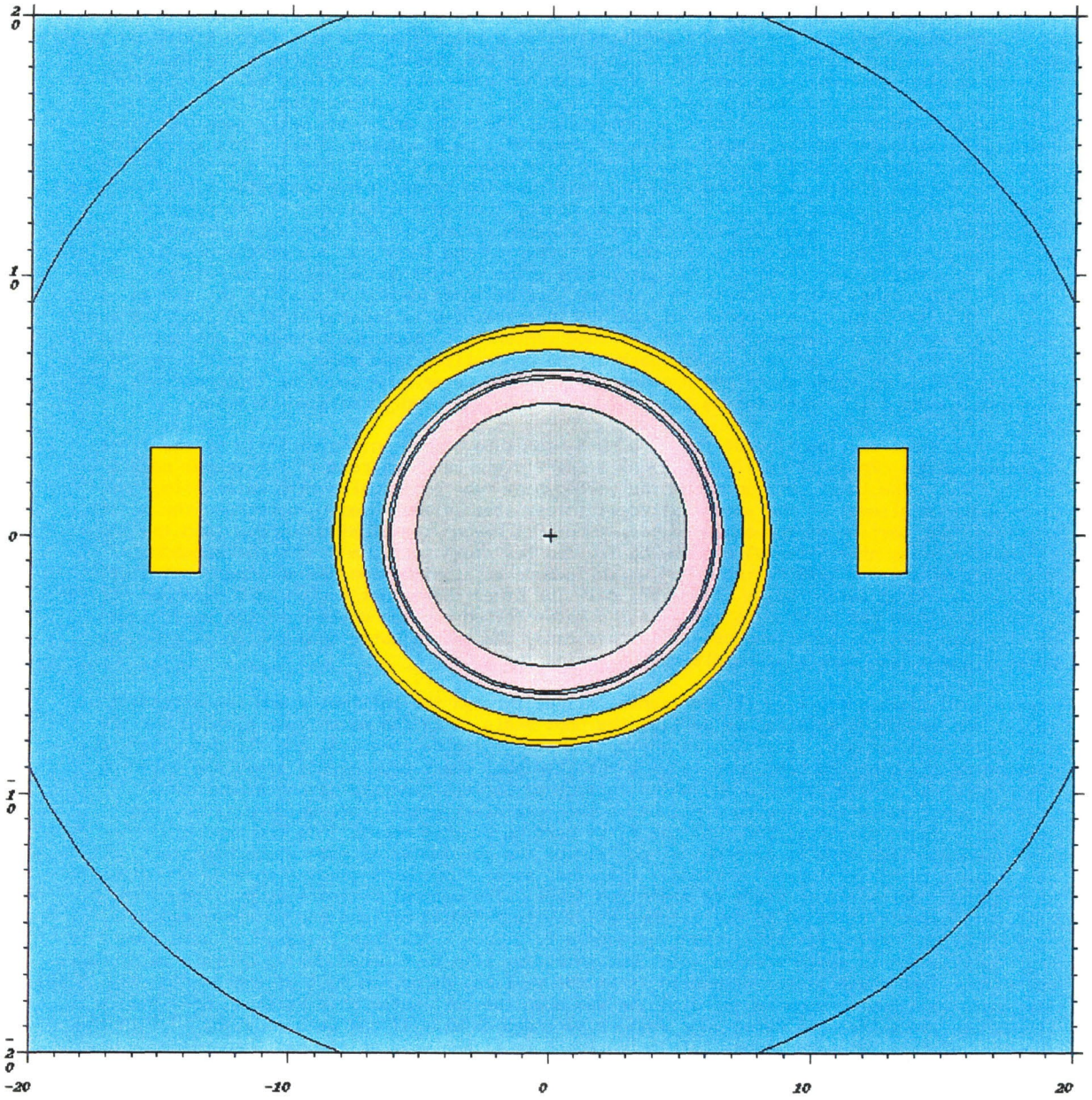


Fig. 3.18. Vertical slice just upstream of the dosimeter holder ring (in a plane rotated parallel to holder ring), showing the bolts and mounting lugs holding the dosimeter ring together, close to the dosimeters of interest.

certain maintenance operations, much of the the light gray area representing the central void in Fig. 3.4 has been replaced by a dark blue/purple area showing the floodable portion of the 1998 water tube. In reality, the central rectangular void in the 1998 collimator would also be flooded during maintenance operations, such that the water would extend all the way to a third aluminum window at Z=399.48 cm, right at the end of the carbon steel collimator (which will be protected from corrosion by a thin black oxide coating). This flooded configuration, which was analyzed in detail in Sect 6, is shown in Fig. 3.7.

Figure 3.8 shows a close up view of the 1960 beam tube and other components in the vicinity of the pressure vessel. The "beam tube" consists of a thick aluminum wall (from R=5.08 cm to R=6.0325 cm), followed by a thin film of water out to R=6.1515625 cm (representing the axial cooling channel grooves), followed by a thin aluminum outer shell extending out to 6.3896875 cm. Near the vessel, the beam tube passes through a water filled stainless steel liner, outside of which is located a coolant collector assembly (near the end), and a dosimetry specimen holder immediately adjacent to the vessel. Both of these will be discussed later. This particular model, which really represents the generalized base model, was first used in MCNP Run HB304M4 to calculate the Ni58(n,p)Co58 and Fe54(n,p)Mn54 reaction rates in the dosimeter wires near the middle of the rear surface of the two sets of Charpy specimens shown here. (See results in Table 2.4.) To obtain good comparisons with measured values, it was necessary to model things in excruciating detail, including the rounded corner on the inner surface of the pressure vessel and the presence of the original 1960 water tube which is void during normal operations. This internal water tube, which is made of aluminum, has an inner radius of 3.65125 cm, and an outer radius of 4.60375 cm. The midpoint of the hemispherical tip is located at Z=120.30375 cm from the core radial plane perpendicular to the tube centerline. Subsequent to this dosimetry analysis, all of the features shown here became part of the generalized base model. In shielding analyses for the 1998 water tube, where the presence of the 1960 water tube would be inappropriate, the aluminum in the cells representing the 1960 water tube was simply replaced by void.

Figure 3.9 shows that portion of the 1998 HB-3 beam tube design in the vicinity of the first aluminum window (Z=174.27 to 174.95125 cm) a short distance downstream of the vessel nozzle in Fig. 3.7. The lower portion shows the voided beam tube (main wall, thin water film, and thin aluminum sleeve) in the water filled stainless steel sleeve used to penetrate the vessel nozzle. That portion of the expanded beam tube just beyond the aluminum window (and the end of the stainless steel sleeve) can now be flooded (as shown here), and thus corresponds to the start of the new 1998 "water tube" which is made of aluminum and has an inner radius of 7.03453 cm and an outer radius of 7.74573 cm. The lines shown just inside this expanded portion of the beam tube can be used to simulate the water-filled cooling coils near the outer edge of the beam tube in the voided case. In this case, the entire water tube region is shown as being flooded (see dark blue/purple region inside the tube).

Figure 3.10 shows a top view (YZ horizontal slice) through the collimator and the attendant radial and eccentric shields, as well as the pool seals, with the water tube flooded but the collimator section dry. Starting at the bottom of the figure, one sees the flooded water-tube section of the expanded beam tube leaving the HFIR pool (dark blue/purple area) and entering the biological shield (green area) which is made of barytes concrete having a density of 3.09725 g/cc. Note that the concrete has a thin stainless steel liner which extends into the pool a short distance, and that the first portion of this recess into the concrete is also flooded. The central cylindrical portion of the collimator is made of carbon steel so as to minimize activation by neutrons. The other steel components (radial shield, eccentric shield, and pool seals are made of stainless steel. The central cylindrical portion of the collimator starts at Z=310.58 cm, extends axially to Z=399.48 cm, and has an outer radius of 9.21131 cm. Along its axis, there extends a 2.75-inch x 5.5-inch rectangular hole (see Fig. 3.11) which is shown here as void, but which may also be flooded during certain maintenance operations, and whose bigger dimension is in the vertical direction (out of the page in Fig. 3.10). The small thin region about a third of the way down the collimator hole is shown here simply to illustrate where the 1960 water tube would have ended axially if one were modeling it. In the analysis of the 1998 water tube, this thin region is either void or flooded, depending on how the rest of the rectangular hole is modeled in a given calculation. Near the top of Fig. 3.10, we see the collimator passing through the final pool seal and a thick steel gasketed flange as it enters the expanded cavity in the biological shield which holds the concrete block containing the rotary shutter.

Figure 3.11 is a vertical slice (XY plane) near the middle of the collimator, and is intended to show the central hole in the central collimator, the surrounding beam tube, the radial shield, the eccentric shield, a thin steel liner, and the surrounding biological shield.

Looking further downstream, Fig. 3.12 shows the last portion of the collimator passing through the final pool seal and thick steel flange in the expanded cavity wherein lies the rotary shutter assembly. The Type 1020 carbon steel shutter (having a vertical axis of rotation) sits inside a large, stainless-steel-lined, stepped block of barytes concrete. When initially designed, the gaps between the concrete block and the biological shield were intentionally quite large so as to provide for easier alignment of the shutter assembly with the beam tube after the biological shield was poured. By the smaller end of the block, the gap between the steel liners

of the block and the biological shield are nearly an inch wide (from Y=37.30625 cm to Y=39.6875 cm, which equals 2.38125 cm), while near the bigger end of the block, the gap between the steel liners of the block and the biological shield are almost three-quarters of an inch wide (from Y=41.75125 cm to Y=43.4975 cm, which equals 1.74625 cm). [While initially of some concern prior to the final shielding analysis (cf Sect 6), it has since been shown that radiation streaming through this stepped gap is negligible when compared to that which comes through the central portion of the assembly.] The carbon steel rotary shutter shield plug in the middle of the assembly has a diameter of 24.375 inches, and is centered at Z=446.405 cm. In Fig. 3.12, it is shown in the closed position. It may, however, be rotated so as to use either the large 3.5-inch-diam beam hole (normally the case) or the smaller 0.875-inch-diam beam hole that was used when Blosser and Thomas made their measurements on HB-3. Upstream and downstream of the rotary shutter, there is a 6-inch-diam break in the stainless steel concrete liners so as not to interfere with the transmission of the beam under normal circumstances. The downstream surface of the stainless steel liner on the barytes concrete block containing the shutter assembly is located at Z=478.79 cm. In the base MCNP model, everything past that point is treated as a void.

Figure 3.13 shows a vertical slice (located at Z=445.0 cm) through the center of the rotary shutter assembly after the shutter had been rotated to the open position. Note that while the bottom of the rotary shutter shield plug was assumed to sit flush against the stainless steel liner on the bottom of the cavity, there is a small 0.3125-inch clearance gap directly above the shield plug, and a similar clearance gap circumferentially around the shield plug.

3.2 Figures Showing Components Affecting the Dosimetry Analysis

Because of the complicated nature of the components affecting the dosimetry analysis, their depiction has been saved to the last. Note, however, that all of the smaller components described here are still present in the base MCNP model used everywhere, even though their presence has essentially no effect of the final shielding analysis.

Figure 3.14 shows a close up view of the 1960 beam tube and other components in the vicinity of the pressure vessel. Near the vessel, the beam tube passes through a water-filled stainless steel liner, outside of which is located a coolant collector assembly (near the end), and a dosimeter specimen holder immediately adjacent to the vessel. Both of these will be discussed later. This particular model, which really represents the generalized base model, was first used in MCNP Run HB304M4 to calculate the Ni58(n,p)Co58 and Fe54(n,p)Mn54 reaction rates in the dosimeter wires near the middle of the rear surface of the two sets of Charpy specimens shown here. (See results in Table 2.4.) To obtain good comparisons with measured values, it was necessary to model things in excruciating detail, including the rounded corner on the inner surface of the pressure vessel and the presence of the original 1960 water tube (see earlier description) which is void during normal operations. In the shielding analyses for the 1998 water tube, where the presence of the 1960 water tube would be inappropriate, the aluminum in the cells representing the 1960 water tube was simply replaced by void.

Figure 3.14 shows a horizontal (YZ) slice through the beam tube in the vicinity of the pressure vessel. For another perspective, Fig. 3.15 shows a vertical (XZ) slice through the beam tube at this same location, while Fig. 3.16 shows an end view (vertical XY slice) of coolant collector mounted near the end of the stainless steel sleeve surrounding the beam tube. Because this component is located just upstream of the dosimeters (see Fig. 3.14), it was included in the model out of concern that its presence might have some impact on the neutrons travelling from the beam tube towards the dosimeters, especially the one at Key 3, position 3. Likewise, an elliptically shaped cone was needed to model a chamfer region (really a 1.0625-inch round) near the intersection of the inner wall of the pressure vessel and the large beam tube hole leading out through the vessel nozzle (cf Fig. 3.14). This was needed, not to be aesthetically pleasing, but to adequately model neutron reflection and attenuation in the vicinity of the dosimeters. In particular, this was needed to accurately calculate a response from the dosimeter at Key 3, position 3, on the HB-2 side of the HB-3 beam tube (just to the right of the beam tube in Fig. 3.14). In reality, the small (0.4184 gram SS302L) dosimeter wire is located near the center of the back surface of the Charpy V-notch specimens (shown as dark orange rectangular blocks) in the dosimeter holder assembly. Engineering drawing M-10070-0E-510-E (Rev 2) shows this particular dosimeter wire as being within 0.375 inches of the rounded steel corner of the pressure vessel adjacent to the nozzle. If this rounded corner were not modeled and "came out straight" forming a sharp corner, the small dosimeter wire would be partially shielded by the steel corner rather than by the water that should be present in this region. Given that many of the neutrons reaching this particular dosimeter have their first collision in the nearby portion of the beam tube just downstream of the dosimeter holder ring and then backscatter through this region to the dosimeter location, the presence of the proper material there actually does make a small but discernible difference. Moreover, because the aluminum wall of the (voided) 1960 water tube was also a major scattering region, contributing to the fast neutron flux in the region of this particular dosimeter, it also had to be included in the dosimetry analysis.

Figure 3.17 is a vertical slice in the plane of the dosimeter holder ring, near the rear surface. It shows the beam tube (aluminum wall, thin water film, and thin aluminum jacket), the surrounding water, the stainless steel sleeve around the beam tube, the central hub of the dosimeter holder, and a broad approximate representation of the stainless steel dosimeter holder itself, including the two (dark orange) rectangular regions representing the Charpy V-notch specimens at Key 3, positions 3 and 8. In the plane of the figure (parallel to the back side of the holder ring), the slot for the Charpy V-notch specimens extends radially 10.10045 cm to 15.59955 cm from the centerline of the holder ring (both critical dimensions), and extends 1.50622 cm above and below the midplane of the system. Each of the two regions shown here contain three carbon steel Charpy V-notch specimens which would lay horizontally in this figure. At the center of each, there is a small V-notch. These are aligned to form a single vertical notch on the rear surface. The small 0.1 gram SS302L dosimeter wire (not explicitly modeled here) lies in this notch. A point detector is used in the MCNP model to obtain the fast flux and energy-integrated dosimeter responses at these locations (Key 3, positions 3 and 8). The actual design of the dosimeter holder (see engineering drawing E-42047) is somewhat more complicated. It consists of two or three pieces. The main body resembles a daisy, with the petals being the body of the holder between which a number of dosimeter specimen packages may be located. On the back (downstream) side, the dosimeters are exposed to the reactor vessel which is nominally only 0.375 inches away. The cover plate (including the central hub which mounts on the stainless steel sleeve) covers only the front (upstream) side of the dosimeter specimens, and resembles a split frisbee, cut in half as if one were slicing a pizza into two large pieces. These pieces (each with a portion of the central hub) are placed around a groove in the sleeve surrounding the beam tube, one from the top and the other from the bottom, and bolted together to form a complete assembly. The bolts, together with the mounting lugs on the top and bottom pieces, measure about 0.75-inch x 0.96-inch x 1.92-inch (high), as shown in Figs. 3.14 and 3.18. Because one is located directly in front of the dosimeter at Key 3 position 3 and the other is located very close the dosimeter at Key 3 position 8, both were included in the 3-D MCNP model. Moreover, the one at position 3 (on the right of the beam tube in Fig. 3.14) did have a small but calculationally observable effect on that dosimeter response. No significant effect was observed at position 8 (on the left of the beam tube) due to its "out of the way" location relative to the beam tube and the dosimeter.

3.3 Older Engineering Drawings Used in Formulating This Model

Dwg E-42027, Rev. D, Sheet 1 (Apr 11, 1995):

This drawing corresponds to the left side of Fig. 3.1 shown above. It shows the relative location of the HFIR core, the pressure vessel, and all four of the "as built" horizontal beam tubes (HB-1,2,3,4). It is most useful insofar as it specifically states the distance from the outside of vessel nozzle boss to the core radial plane perpendicular to each beam tube. Those distances are as follows: 52.0 inches (132.08 cm) for HB-1; 54.5 inches (138.43 cm) for HB-2; 54.0 inches (137.16 cm) for HB-3; 52.0 inches (132.08 cm) for HB-4. Some of the drawings available for the newly revised beam tubes at the start of this study were somewhat generic while others were under development and not yet complete. A preliminary drawing for the new HB-1 beam tube, without most of the key dimensions, was available (see below), but drawings for the new HB-3 beam tube were not available, and it was simply said that it would be "essentially the same" as that for HB-1. Likewise the drawing for the new HB-2 beam tube was only partially complete and did not yet show the second (downstream) aluminum window forming the terminal end of the built-in water tube. Nevertheless, many of the dimensions could be scaled off these generic drawings, with the external surface of the vessel nozzle boss (see E-42027) serving as a common reference point since it was not going to change. Dwg E-42027 Sheet 1 is also useful insofar as it specifically labels the location and orientation of all four beam tube centerlines and the tips of the HB-2 and HB-3 beam tubes. It also shows the location of the hot tip of the internal water tube for the "as built" HB-4 beam tube, while the location of the 1960 water tube in HB-3 may be easily scaled off the drawing. It also shows a crude insert sketch of the coolant collector assembly mounted on the stainless steel sleeve surrounding each beam tube, and references Dwg E-49400 for further details.

Dwg E-42027, Rev. D, Sheet 2 (Apr 11, 1995):

This drawing corresponds to the right side of Fig. 3.1 shown above. It shows the "as built" collimator in the 1960 beam tube, and the rotary shutter. Components such as the removable radial shield assembly, the eccentric shield, and the pool seals, all in the vicinity of the collimator and referenced above in the description of the MCNP model, are clearly labeled in this drawing. While in this study, the 1960 collimator design has been largely ignored and replaced by the 1998 design (see below), many of the details regarding the rotary shutter and the steel-lined concrete housing containing the rotary shutter shield plug were taken from this drawing. Indeed, the dimensions of the void gaps along the sides of this housing were scaled

off this drawing. Once the location of the cavity containing the shutter assembly is firmly located (see Dwg 1546-01-M-5022, Rev 1), Sheet 2 of Dwg E-42027 may be used to fix the location of the second aluminum window in the 1960 water tube inside HB-3. (Note that we cannot use E-42027 directly for HB-3 since this drawing is really for HB-4.) Lastly, this drawing also specifies the biological shield as being made of barytes concrete.

Dwg 1546-01-M-5022, Rev 1 (Apr 4, 1961) and Rev 2 (Sep 18, 1961):

This overview of the entire biological shield clearly shows the locations of the cavities in the shield which are provided for the steel-lined stepped concrete housings holding the rotary shutter assemblies for each of the four beam tubes. Moreover, in the case of HB-3, the outermost extent of this cavity (corresponding to the downstream surface of the steel liner on the concrete housing holding the rotary shutter) is shown as being located 188.5 inches (478.79 cm) from the core radial plane perpendicular to the beam tube. It also shows that the "sealing surface" of the pool seal flange (roughly the midpoint of the thick flange in the MCNP model, just downstream of the collimator and upstream of the rotary shutter assembly) is located 32.5 inches upstream of the previously mentioned surface. Together with the information on Sheet 2 of E-42027, this fixes the location of the second (downstream) aluminum window in the 1960 water tube.

Dwg M-10070-0E-510-E, Rev 2 (Sept 30, 1987):

This drawing is similar to Dwg E-42027, Sheet 1, but shows a few additional details related to the placement of the dosimeter holder around each beam tube, including HB-3. In particular, it specifies that the dosimeter holder is located such that the dosimeter flux wire in the back (downstream) side of the Charpy V-notch specimens is to be located 0.375 inches away from the inner surface of the pressure vessel, as in the MCNP model. It also shows that the inner corner of the vessel wall leading to the large hole through the nozzle will be "rounded" with a curvature of 1.0625 inches. The location of the hot tip of the 1960 water tube was also determined from this drawing. The drawing also shows the thick beam tube flange (joint) on the outside of the vessel nozzle. In the MCNP model, this flange and the vessel nozzle were both combined into one geometry zone. Not related to this study, this drawing also shows the location of the weldments between the vessel nozzles and the pressure vessel itself, as well as the location of Key 3, positions 3 and 8 which were critically important in the dosimetry study.

Dwg. E-49961, Rev C (Apr 25, 1988):

This is the HFIR dosimeter specimen identification chart. It was of no real use in defining the calculational model, but is does show (schematically) the relative locations of the various dosimeter ID numbers in the dosimeter holder rings around each of the four beam tubes, as well as at several other key locations.

Dwg E-49953, Rev A (Oct 12, 1965):

This drawing shows the pressure vessel surveillance specimen mount assembly (i.e., the dosimeter holder assembly) for HB-1, 3, and 4, previously described loosely as a daisy petal arrangement with a split frisbee-like front cover plate. It also shows the orientation of the three Charpy V-notch specimens in each specimen holder. By scaling this large but relatively simple drawing, it is quite clear that the V-notches holding the dosimeter flux wire are located 12.85 cm from the centerline of the assembly. It also shows the split central hub clamp assembly and the mounting hardware, as well as the stubs and bolts mounted on the front face of the split cover plate (see Figs. 3.14 and 3.18) that are used to hold the cover plate together and in place. Dimensions for this component and the mounting hardware were taken from this drawing. Of particular importance to the dosimetry study was the fact that the plane of the dosimeter holder ring is inclined 77.0 degrees relative to the HB-3 centerline. Because the dosimeter flux wires are located 12.85 cm radially out from the centerline of this holder ring, a difference of even one degree can significantly change the amount of water between the dosimeter(s) and the vessel, and can change the calculated dosimeter response(s) by as much as 10%. Interestingly, the dosimeter holder rings for HB-1 and HB-4 are inclined 73.5 degrees with respect to those beam tube centerlines, while that for HB-2 is perpendicular to the beam tube centerline.

Dwg E-49945, Rev C (Apr 25, 1988):

This drawing shows additional details of the 2.73-inch x 1.75-inch surveillance specimen assemblies containing the Charpy V-notch specimens and the 1.18-inch long x 16 gauge (0.065-inch-diam) dosimeter flux wire laid inside the aligned V-notches on the back (downstream) side of the specimen assemblies. (The actual flux wire at Key 3 position 3 only weighed 0.4184 grams, while that at position 8 weighed 0.4172 grams.) These assemblies are then placed in the dosimeter holder ring described above. While

Dwg E-49945 shows the dosimeter flux wires as being SS304L, the actual wires removed and analyzed in counting experiments in Dec 1987 and reported in Table E.12 of Ref 6 (and summarized in Table 2.4 above) were made of SS302L. [See personal communication from C. A. Baldwin#17. Also see page 15 of Ref 18, which is a 1966 document describing the "HFIR Pressure Vessel and Structural Components Surveillance Program."] In the MCNP model, the Charpy specimens were modeled as carbon steel (which they are), while reaction rates in the dosimeter flux wire were calculated by folding the energy-dependent flux (at a point detector located there) with the appropriate energy-dependent reaction cross sections. A point detector was used in place of a volume detector because of the small volume of the flux wire and the detector's extreme sensitivity to spatial position. Over the length of the 2.73-inch long Charpy specimens, for example, both the calculated and measured reaction rates may change by as much as a factor of two. Placing the point detector at exactly the center of the dosimeter flux wire, as opposed to averaging over the volume of the Charpy specimens, was deemed critical if one really wanted the model to accurately calculate the measured reality.

Dwg. M-11511-OH-001-E, Rev 1 (Nov 4, 1992)

The purpose of this drawing is similar to Dwg E-49945 insofar as it shows the construction of some special 2.1-inch x 1.16-inch multi-function dosimetry specimen assemblies to be placed in the dosimetry holder ring around different beam tubes. These dosimeters, however, do not correspond to the types of dosimeters found at Key 3, positions 3 and 8. As a result, this drawing (M-11511-OH-001-E) was not used at all in the development of this particular MCNP dosimetry model. Moreover, Dwg. E-49945 (described above) does describe the particular dosimeters found at Key 3, positions 3 and 8, and is the drawing that was actually used in this model development.

Dwg. E-49400

This drawing shows details of the coolant collector assembly located near the end of the stainless steel sleeve around the beam tube, a short distance inside the vessel, as shown in Figs. 3.14, 3.15, and 3.16. Moreover, the simplified model used here was actually based on the small insert sketch shown on Sheet 1 of Dwg E-42027, as well as larger top views shown there and on Dwg M-10070-OE-510-E, Rev 2. Given that this simplified model did not have any apparent affect on the calculated dosimeter responses (despite initial concerns to the contrary), a more detailed model was not considered justified.

3.4 Newer Engineering Drawings Used in Formulating This Model

This last section lists and briefly describes the newer engineering drawings (and unreleased concept sketches) used to describe the newly proposed 1998 beam tube designs for all four beam tubes. While frequently incomplete, not fully dimensioned, and occasionally even lacking reference drawing numbers, these drawings represent the best available source of information at the time this study was commissioned. Information, as available, is listed here for all four newly designed beam tubes, with extended supplementary discussion only for HB-3 (which was the primary focus of this shielding study, but for which specific detailed drawings were not available).

HB-2 Concept Dwg E-SK-PCH-970801-1, Rev. 1 (Aug 11, 1997):

This drawing shows the newly enlarged beam tube starting in the permanent beryllium reflector and extending out through the pressure vessel, the pool, and the biological shield, to the cavity which will house the (yet to be designed) new shutter mechanism. No mention is made of the five neutron guide tubes to be placed inside this portion of the new HB-2 beam tube since the focus was primarily on the beam tube itself. The drawing focuses on: the two beryllium inserts to be placed inside the hot end of the beam tube, the flange area where the beam tube passes through the pressure vessel, and the flange area where the beam tube enters the cavity in the biological shield which will house the new shutter mechanism. While no axial dimensions or locations are given, radial dimensions for each section of the expanded beam tube are clearly shown. The inner diameter of the beam tube in the beryllium reflector is 7.052 inches, while the outer diameter there is 8.5 inches (including the thin aluminum water jacket). Just outside the beryllium reflector, the beam tube expands to an inside diameter of 9.110 inches, with an outside diameter of 11.0 inches (including the thin aluminum water jacket). These dimensions are maintained through to the outside surface of the flange on the outside of the pressure vessel nozzle, where a 0.3-inch-thick aluminum window (located approximately 199.841 cm from the core centerline) marks the beginning of the water tube portion of the beam tube which there expands to an inside diameter of 12.0 inches (outside diameter of 12.5 inches). A second aluminum window defining the end of the water tube portion of the beam tube is not shown at all. The most useful feature of this drawing is the heavily dimensioned sketch showing the two beryllium pieces (called wings) inserted on the inside of the hot tip of the beam tube. These start at the inner surface of the beam tube

and extend down to a location 21.354 inches from the centerline of the core.

HB-4 Concept Dwg dated Jan 30, 1998 (no drawing number shown):

This drawing shows the newly designed beam tube starting in the permanent beryllium reflector and extending out through the pressure vessel, the pool, and the biological shield, to the cavity which will house the rotary shutter assembly. Except for depicting the cold source vacuum vessel inside the beam tube, no further mention is made of the cold source which will be located near the hot tip of the beam tube. While no axial dimensions or locations are given, radial dimensions for each axial section of the beam tube are clearly shown. The inner diameter of the beam tube in the beryllium reflector is 4.875 inches, while the outer diameter there is 6.0 inches (including the thin aluminum water jacket). Just outside the beryllium reflector, the beam tube expands to an inside diameter of 5.73 inches, with an outside diameter of 7.0 inches (including the thin aluminum water jacket). These dimensions are maintained through to the outside surface of the flange on the outside of the pressure vessel nozzle, where two 0.125-inch-thick aluminum windows (located approximately 214.3364 cm and 218.1452 cm from the core radial plane perpendicular to the beam tube) mark the beginning of the water tube portion of the beam tube which expands just downstream of the flange to in inside diameter of 11.75 inches (outside diameter of 12.5 inches). A third 0.125-inch-thick aluminum window defining the end of the water tube portion of the beam tube is located approximately 373.6654 cm from the core radial plane perpendicular to the beam tube. This location is just a short distance upstream of the cavity in the biological shield which will house the rotary shutter assembly. Unlike HB-1 and HB-3, no collimator section is shown for HB-4.

HB-1 (and HB-3) Concept Dwg dated Jan 30, 1998 (no drawing number shown):

Although this large (E-size) concept drawing has no drawing number shown, it was obtained from Pete Hambaugh on Jan 30, 1998 at the start of this study, and was created by him from a computer file called e:\ham\ustn\allbeam1197.dgn (Jan 29, 1998, 12:55:09 pm). It specifically shows the newly proposed design for the HB-1 beam tube, but says clearly (in 2-inch letters) that HB-3 in the same, although it is believed that the length of the water tube section of the beam tube may be 2.0295 inches (5.155 cm) shorter for HB-3 than for HB-1 based on reasons described below. While no axial dimensions or locations are given, radial dimensions for each axial section of the beam tube are clearly shown. The inner diameter of the beam tube in the beryllium reflector is 4.0 inches (the same as the original 1960 design), while the outer diameter there is 5.0 inches (including the thin aluminum water jacket). These dimensions remain constant all the way through to the outside surface of the flange on the outside of the pressure vessel nozzle, where a 0.2682-inch-thick aluminum window starting 37.11 cm downstream of the outer surface of the vessel nozzle/flange interface marks the beginning of the water tube portion of the beam tube which then expands (just downstream of the flange) to an inside diameter of 5.539 inches (outside diameter of 6.099 inches). A second 0.125-inch-thick aluminum window defining the end of the water tube portion of the beam tube is located just upstream of the collimator in the biological shield (i.e., this window is located approximately 89.9257 cm upstream of the start of the cavity in the biological shield which contains the rotary shutter assembly). The exact locations of the aluminum windows defining the beginning and end of the water tube segment of the beam tube(s) will be discussed later. Further downstream, the primary focus of this drawing is the new conceptual design of the collimator, the radial and eccentric shields around it, and the pool seal upstream and downstream of the collimator itself. In this case, unlike the old 1960 design, the carbon steel collimator resides inside the last segment of the aluminum beam tube which has an inside diameter of 7.753 inches and an outside diameter of 8.253 inches. While no other dimensions in this region are shown, they may be easily scaled from this large drawing. Virtually everything in this portion of the MCNP model (see descriptive text associated with Figs. 3.10 and 3.11) was based on this portion of this drawing.

HB-1 Concept Dwg. M-11537-OH-001-E (Feb 13, 1998):

This drawing, which is completely void of any dimensions except two or three key axial locations not shown on the Jan 30 drawing, shows essentially the same HB-1 configuration as the Jan 30 drawing above. It does show, however, that the distance from the hot tip of the HB-1 beam tube to the downstream surface of the extended collar on the flange holding the beam tube on the vessel nozzle is 59.458 inches, and that the distance from this downstream surface of the extended collar back to the core radial plane perpendicular to the beam tube is 61.975 inches. This information was notably missing from the Jan 30 conceptual drawing. With this information, one can go back and scale the Jan 30 drawing to locate the two aluminum windows defining the beginning and end of the 1998 water tube in HB-1. Taking this approach, and letting Z denote the distance from the any point of interest back to the core radial plane perpendicular to the beam tube, the first 0.68125-cm-thick aluminum window in HB-1 appears to be located between Z=169.19 and 169.87125 cm, while the amount of water (possible) between this and the second aluminum window appears to be 132.391 cm.

Using the information on the Feb 13 conceptual drawing for HB-1 to scale the drawings and determine the location and extent of the water tube section of the beam tube was perfectly

legitimate in the case of the HB-1 beam tube depicted in these drawings.

Unfortunately, the same approach could not be used for the HB-3 beam tube since the few key axial dimensions shown on the Feb 13 conceptual drawing for HB-1 do not apply to HB-3. In the case of HB-3: the beam tube is several cm shorter, its centerline is offset a different distance from the core centerline, and the distance from the vessel nozzle back to the core radial plane perpendicular to the beam tube is different (see Dwg. E-42027). [When it was said that HB-3 was the same as (or similar to) HB-1, the intent was that the first aluminum window and other hardware near the extended collar on the flange mounted to the vessel nozzle was the same as that used in HB-1, and that the second aluminum window by the collimator (and indeed the entire collimator design) was the same as that for HB-1.] Thus, to determine the location of the two aluminum windows defining the beginning and end of the water tube in the HB-3 design, an alternate approach had to be taken. This involved: (1) locating the first window relative to a well established datum plane such as the vessel nozzle/flange interface which is known from Dwg E-42027 to be located at Z=137.16 cm, and (2) locating the second aluminum window relative to another well established datum plane such as the start of the cavity in the biological shield containing the rotary shield plug as shown on Dwg 1546-01-M-5022. From this exercise, it can be deduced that the first 0.68125-cm-thick aluminum window in HB-3 is located between Z=174.27 and 174.95125 cm, that the second 0.3175-cm-thick aluminum window in HB-3 is located between Z=302.1868 and 302.5043 cm from the core radial plane perpendicular to the beam tube, such that the (occasionally) water-filled portion of the beam tube would be 127.23555 cm long, or about 5.155 cm shorter than that in the HB-1 beam tube. It was through this process that the specifications used in the base MCNP model for HB-3 were developed from the conceptual engineering drawings that were available at the time of this study.

4.0 DOSIMETRY ANALYSIS

In the Spring of 1998, a concerted effort was made to calculate dosimeter responses at HFIR Key 3, positions 3 and 8, around the HB-3 beam tube, just inside the pressure vessel. This effort was undertaken partially to help validate the "equivalent point sources" that had been developed for that beam tube (prior to their anticipated use in the HB-3 "water tube" shielding analysis), and partially to see if MCNP could be used for good and reliable neutron dosimetry analyses.

Since most of the modeling approximations and the final results have already been presented in Sects 2.8, 3.2, and 3.3, the approach taken here will be to present a brief review of that information, expand on the theoretical basis for laterally offsetting the equivalent point sources from centerline in final analysis, and then (anti-climatically) presenting a brief review of the historical evolution of the model to its final state, the lessons learned along the way, and some discussion of the sensitivity of the model to various parameters. This brief historical review is considered useful insofar as it provides some supplementary guidance for dosimetry analyses of other beam tubes in the future.

Run HB304M4 is the most detailed geometry model ever developed, representing the dosimeters and other materials in the neighborhood with the greatest fidelity ever. Based on the geometry alone, it is clearly a benchmark calculation. Moreover, with the point sources shifted a little off the centerline as prescribed by an easily defendable theoretical model, it also gives the best C/E ratios ever obtained by any DORT, TORT, or MCNP model.

The complete MCNP input file for the final dosimetry analysis (Run HB304M4) is listed in Appendix B.1 for future reference. It is heavily annotated with explanatory comments on virtually every one of its 1280 lines. Together with the overview presented here and in other sections of this report, the final model is considered thoroughly documented.

4.1 Geometric Model Used in Final Analysis

The full 3-D geometric model of the HB-3 beam tube used in the final dosimetry analysis (MCNP Run HB304M4) is shown in Fig. 3.2. Supplementary views of various components are shown in Figs. 3.8 through 3.18, and discussed at length in Sects 3.1 and 3.2. Those shown in Figs. 3.14 through 3.18 and discussed in Sect 3.2 are of particular interest in the dosimetry analysis. Engineering drawings upon which these models were based are discussed in Sects 3.3 and 3.4. Those of particular interest to the dosimetry analysis are: Dwg. E-42027, Rev. D, Sheet 1; Dwg. M-10070-0E-510-E, Rev 2; Dwg. E-49953, Rev A; Dwg. E-49945, Rev C; and Dwg. E-49400. These are each discussed at length in Sect 3.3. To summarize briefly: The coolant collector was included because of concerns that it might partially scatter or absorb neutrons that would otherwise travel uncollided from the beam tube to the dosimeter locations. (That concern was later shown to be largely unfounded.) The dosimeter holder ring and its exact description were found to be important; that includes the discrete representation of the Charpy specimens, the cover plate, the central hub, and the mounting hardware that holds it together. The exact placement of the point detectors located at the center of the backside (downstream side) of the Charpy specimens was found to be "extremely" important because of strong spatial gradients in the fast flux in this region. Likewise, the presence of the original (dry) 1960 water tube, which was present for years prior to and during the 1987 dosimeter measurements, was important because of local scattering from the main beam. Even the additional water afforded by modeling the 1.0625-inch-radius rounded corner on the inner wall of the vessel near the HB-3 nozzle (as opposed to a sharp steel corner) had a 4-5% effect on the dosimeter response at Key 3, position 3, which is located only 0.375 inches away.

4.2 Other MCNP Modeling Parameters Used in the Final Analysis

The original flux wire dosimeters at Key 3, positions 3 and 8 (which were removed for activation analysis in 1987) were made of SS302L, and weighed 0.4184 grams and 0.4172 grams, respectively. From these activation measurements, experimenters directly determined and reported the saturation activities and reaction rates corresponding to Ni58(n,p)Co58 and Fe54(n,p)Mn54 reactions in the SS302L flux wires (see Table E.12 in Ref 6). From these two respective reaction rates, they could also infer, indirectly, the flux above 1.0 MeV and above 0.1 MeV at the dosimeter locations.

To be assured of calculating all possible reactions even in the vicinity of this lower energy threshold, all neutrons were tracked until their energy fell below 27 keV. In the MCNP source definition, the source probability distribution was therefore set to zero below 27 keV in the dosimetry analysis, and the source normalization values used on the corresponding "fm" tally multiplier cards were set equal to that portion of the total neutron source (n/s) in the beam tube above 27 keV (i.e., not the total source integrated over all energies). By excluding

low-energy neutrons and thermal neutrons, this neutron energy cutoff at 27 keV made it feasible to track the huge numbers of fast neutrons that were needed to generate good statistics at the dosimeter locations. Typically 40 million histories were used in the initial scoping analyses, while 120 million histories were used in the final analysis. This final analysis required approximately 11 CPU hours on each of eight nodes on the ORNL SP2 computer.

In the final model (Run HB304M4), the point detector representing the dosimeter wire at Key 3 position 3 (on the HB-2 side of the HB-3 beam tube), was located at X=0 (vertically), Y=12.52066 cm (horizontally), and Z=117.11062 cm (axially), while the point detector representing the dosimeter wire at Key 3 position 8 (on the HB-4 side of the HB-3 beam tube) was located at X=0, Y= -12.52060 cm, Z=111.32938 cm. Since these are located inside the pressure vessel, at an axial location much further upstream than the start of the 1998 water tube analyzed in the shielding analysis, the "importance cutoff plane" (Surf 1007) described at the beginning of Sect 3 had to be moved back to Z=75.473 cm. (The normal location used in the water tube shielding calculations would have precluded any neutrons from ever reaching the dosimeter locations.) This allowed us to physically track all neutrons impingent on the inner wall of the beam tube downstream of that point [i.e., all those striking the inner wall of the beam tube within a foot or so (14.117 inches) of the most upstream dosimeter] while, in the name of efficiency, killing all other neutrons entering the side wall of the beam tube further upstream where they would not be likely to contribute to the detector response.

For the purpose of estimating fluxes at distant locations down the beam tube(s), the point sources in Table 2.2 are indeed meant to be treated as isotropic over a 4*pi sphere about the point(s) of origin. Nevertheless, in a large Monte Carlo calculation, if one sampled the sources over the entire 4*pi sphere, it would be exceedingly difficult or impossible to generate any meaningful statistics at distant locations. If one is primarily interested in the water tube shielding analysis, for example, it would be much more pragmatic to sample the isotropic point sources only over a narrow cone of directions that have some reasonable likelihood of contributing to the flux in the region of interest. Of course, if we sample the source only over a narrow cone of directions all the time, we must reduce the starting weight of those neutrons by the fraction of the time we would normally have picked directions in that cone if we were really sampling over the entire 4*pi sphere -- i.e., the starting weights must be reduced by the fraction of the 4*pi sphere corresponding to the solid angle subtended by this narrow cone of directions. This is necessary to maintain a fair game. In the water tube shielding analysis, for example, we only sample over a very narrow cone of directions within 15.13 degrees of the centerline where the direction cosines with respect to the centerline are between 0.965335056 and 1.0. Accordingly, the starting weights on the MCNP "sdef" card must then be set to 0.017332472 [= (1.0 - mu(min))/2]. In the case of the neutron dosimetry problem, the dosimeters are located outside the beam tube but inside the pressure vessel. Since this region is somewhat closer to the point sources, the cone of sampling directions had to be expanded so as to include the vast majority of fast neutrons (above 27 keV) that stood any chance of impinging on the inner wall of the beam tube within about a foot or so of the first (most upstream) dosimeter. In the initial scoping analyses, we sampled the isotropic point sources over a somewhat wider cone of directions within 36.87 degrees of the centerline, where the direction cosines with respect to the centerline were between 0.8 and 1.0. This included virtually all of the fast neutrons striking the inner wall of the beam tube within a about a foot or so of the first (most upstream) dosimeter. Accordingly, the starting weights on the MCNP "sdef" card were set to 0.1 [= (1.0-0.8)/2]. In the final reference calculation (Run HB304M4), to verify that this was adequate, we sampled the isotropic point sources over an even slightly wider cone of directions within 44.765 degrees of the centerline, where the direction cosines with respect to the centerline were between 0.71 and 1.0. This included virtually all of the fast neutrons striking the inner wall of the beam tube within 14.117 inches (35.85638 cm) of the first (most upstream) dosimeter, as well as others further upstream that would (in the name of efficiency) be killed by the importance cutoff plane.

In setting the location of the importance cutoff plane relative to the dosimeters (see above), one must be mindful of those tube-wall impact points that are likely to contribute to the dosimeter response: (a) If the importance cutoff plane is located too close to the dosimeters, important neutron histories may be excluded and the solution would be erroneous or poor. (b) If located too far back from the dosimeters, a large amount of time will be spent tracking enormous numbers of neutrons which are not likely to contribute to the dosimeter response, and one may have to settle for many fewer histories than would be required for a good solution. To the extent that CPU time is usually limited, efficiency is as essential for accuracy as having a good basic model. Having fixed the axial location of the importance cutoff plane, and knowing the inner radius of the beam tube (5.08 cm), the angular range over which to sample the source must be determined by considering the location of the most forward (downstream) point source that is likely to make any significant contribution to the result of interest. In Table 2.2a, for example, the most forward source in HB-3 that is likely to make any significant contribution to these fast flux dosimeters is that for VELM group 16 (0.907 to 1.108 MeV) which is located at Z=70.1 cm. The angle subtended by the 5.08-cm-radius hole in the importance plane at Z=75.473 cm, as seen from this most forward source point at Z=70.1 cm, is 43.394 degrees. It is therefore incumbent on the user to sample the source over a cone of similar (or slightly greater) angular extent. It was for that reason that, in the final analysis, the isotropic source was sampled over a cone (of 44.765 degrees) whose direction

cosines were between 0.71 an 1.0. Accordingly, in the final analysis, the starting weights on the MCNP "sdef" card were set to 0.145 [= (1.0-0.71)/2].

Note that the source normalization values used on the "fm" tally multiplier cards must be consistent with the overall source strength, the energy range being sampled, the angular range being sampled, and the starting weights of the neutrons. The scheme outlined in the preceding paragraphs maintains the necessary consistency in a straight-forward fashion.

Most of the early scoping analyses were performed in a strictly analog fashion, meaning that every cell in the MCNP model was assigned an importance of 1.0. To induce splitting and thereby provide better sampling of the fast neutron collisions in the regions around the dosimeters, however, that approach was later changed. While the spatial material configuration was left unaltered, a few existing cells were subdivided so that the geometry could be defined more efficiently and so that everything in the annular region from R=6.3896875 cm to R=21.45 cm, between Z=96.8375 cm and Z=143.9443 cm, could be assigned an importance of two (imp:n=2). In Figs. 3.14 and 3.15, for example this region extends radially from the outer surface of the thin aluminum jacket around the beam tube to the outer radial surface of the vessel nozzle at R=21.45 cm, and axially from the tip of the stainless steel sleeve around the beam tube to the outer (downstream) edge of the vessel nozzle at Z=143.9443 cm. Referring to Fig. 3.14, this region includes: (a) the dosimeters and those cells comprising the dosimeter holder ring; (b) the coolant collector assembly; (c) the water outside the stainless steel sleeve that is within about 20 cm of the dosimeters; (d) that portion of the stainless steel sleeve surrounding the beam tube near the vessel nozzle; (e) the water outside the beam tube but inside the stainless steel sleeve surrounding it (near the vessel nozzle); (f) the entire vessel nozzle and flange; and (g) those portions of the pressure vessel between the nozzle and the dosimeter holder ring. This same scheme was used in the final dosimetry analysis (Run HB304M4).

In the early MCNP scoping analyses, the calculated fluxes above 1.0 MeV and above 0.1 MeV were tallied and compared with previously reported fluxes at the respective dosimeter locations as given in Table E.23 of Ref 6. Unfortunately, those "previously reported fluxes" were really calculated values from a 1988 3-D TORT analysis, to which an "experimental correction" had been applied. In essence, we had been comparing our MCNP fluxes against somebody else's computed values, which is never a terribly reliable thing to do since they could be off as much as we are. Further investigation showed that the actual measured reaction rates in the original dosimeter flux wires were given (unaltered) in Table E.12 of Ref 6. These included the Ni58(n,p)Co58 reactions (above 1.0 Mev) and the Fe54(n,p)Mn54 reactions (above 0.1 MeV). Since comparisons against directly measured data are always preferable to anything else, and since MCNP could be used to compute these results directly, the MCNP point detector tallies were subsequently modified so that the pointwise energy-dependent fluxes would be folded directly with the MCNP pointwise energy-dependent cross sections for these reactions, to obtain the integral reaction rates necessary for direct comparisons with the experimental data. When this was done, it was found that the MCNP dosimeter responses were actually in much better agreement with the experimental data than previously thought. These results are described below.

Lastly, in the final reference dosimetry analysis (Run HB304M4), instead of locating the point sources along the actual centerline of the beam tube as specified in Table 2.2a, the entire line of point sources was shifted laterally (ie, horizontally) to a parallel line 1.6986 cm off the beam tube centerline, but were otherwise left unaltered. This shift was necessary to simulate the fact that neutrons really do enter this tangential beam tube in an asymmetric fashion that cannot be represented by isotropic point sources along the centerline. While this physical reality is totally inconsequential for shielding calculations where one is interested in the flux at great distances down the beam tube, it is marginally important if one is interested in small spatial variations in the flux closer to the core (such as at the dosimeter locations). Moreover, the size of the lateral shift needed to simulate this asymmetric effect can be (and was) determined a priori using the straightforward theoretical model described below. Note that it does not violate any of the assumptions upon which the point sources were originally based, but is simply a supplemental enhancement of the model.

4.3 Theoretical Basis for Laterally Offsetting Sources from the Centerline in the Final Analysis

In the present geometry system described in Sect 3, the hemispherical tip of the HB-3 beam tube is centered about X=0, Y=0, Z=28.5369 cm. It has an inner radius of 5.08 cm, and the outer radius (including the water film and outer aluminum liner) is 6.3897 cm. The tube itself resides in a water-filled cavity of the beryllium reflector which has a thin aluminum liner between the water and the beryllium. The radius of the aluminum/beryllium interface is 6.76 cm.

Most (virtually all) of the fast neutrons streaming any distance down the beam tube, have their last collision (prior to beam tube entry) in the beryllium near the hot tip of the beam tube. Assume, for the sake of argument, that most of these collisions occur 1 cm inside the beryllium, i.e., over a hemispherical surface of 7.76 cm radius, centered at X=0, Y=0, Z=28.5369. (Since actual "average depth" into the beryllium is not terribly important to the following arguments,

and since 1.0 seems reasonable, let us proceed with a hemisphere of 7.76 cm radius.) Now consider a relatively uniform distribution of many points on the hemisphere. This may be generated as follows. Imagine the hemisphere divided into many rings (200), with the smallest ring near the centerline having one surface element in each quadrant, the next having two in each quadrant, the next having 3 in each quadrant, etc., so that one eventually has 80400 (=2*200*201) surface elements, with the spacing of the rings being chosen such that all 80400 surface elements have an equal area. Let [x(i),y(i),z(i)] designate the midpoint for each of the equal-sized surface elements on the hemisphere.

If the fast flux were constant in this entire region, the fast neutron scattering density associated with each surface element would be equal. That is not the case, however, since the 15.52-cm-diam hemisphere sits in the HFIR reflector where the fast and non-thermal fluxes have a steep gradient. Fig. 5.1 on page 15 of Ref 1 shows the thermal and non-thermal flux in the HFIR reflector as a function of radial distance (R) from the core centerline. Moreover, this non-thermal flux (n/s/cm2) in the reflector region is described very well by the following power laws:

if R .le. 33 cm, flux = (9.48470e+20)/(R^4.0464) n/s/cm2
if R .gt. 33 cm, flux = (4.13906e+24)/(R^6.4434) n/s/cm2

In the present geometry system described in Sect 3, the midpoint of the HFIR core sits at X=0, Y=26.67 cm, Z=0, with its vertical centerline at Y=26.67, Z=0. Knowing this, one can compute the distance from the centerline of the core to the midpoint [x(i),y(i),z(i)] of each surface element of the hemisphere, and the resulting fast (non-thermal) flux at each location. From one side of the hemisphere to the other, the flux is seen to vary by more than a factor of four. Assuming that the number of neutrons entering the beam tube from each surface element is proportional to the fast neutron scattering density near each surface element, which in turn is proportional to the fast flux near each surface element, it is clear that points on one side of the hemisphere will contribute to the beam tube flux more heavily than points on the other side of the hemisphere. This is clearly an asymmetrical effect.

Unfortunately, if one is constrained to using isotropic point sources along the centerline of the beam tube (in MCNP, DORT, or most other codes), this very real physical effect cannot be represented.

If one is interested only in representing the overall flux at great distances down the beam tube (near experimental facilities, for example) this asymmetrical effect becomes so slight that it really doesn't matter. That is why, for example, the point sources in Table 2.2 were able to reproduce the Blosser and Thomas measurements with an acceptable degree of accuracy. Likewise, if one is performing shielding analyses where the shield material itself provides even a modest amount of scattering (like the water in the flooded water tube), this asymmetrical effect will be washed out completely. In that case, the only thing that matters is the total current impingent on the shield, and the point sources in Table 2.2 faithfully reproduce that parameter. If, on the other hand, one is interested in accurately calculating dosimeter responses on opposing sides of the beam tube at relative "close-in" locations inside the vessel (like Key 3, positions 3 and 8), one better have a model that accurately reproduces (or at least approximates) the relative outward-directed current on the inner surface of the beam tube in the vicinity of each dosimeter.

Fortunately, the well-founded yet simplistic hemispherical model described above provides a framework which allows one to make a reasonable estimate of the "relative" outward-directed current on the inner surface of the beam tube in the vicinity of each dosimeter.

Most neutrons contributing to a dosimeter response tend to enter the wall of the beam tube just slightly upstream of the dosimeter's axial position. Those contributing to Key 3 position 3 (on the HB-2 side of the HB-3 beam tube) would likely enter the HB-3 beam tube wall around x3=0.0 (vertical midplane), y3=5.08 (location of tube wall), z3=107.0 cm (10 cm upstream of dosimeter), while those contributing to Key 3 position 8 (on the HB-4 side of the HB-3 beam tube) would likely enter the HB-3 beam tube wall around x8=0.0 (vertical midplane), y8= -5.08 cm (location of tube wall), z8=101.5 cm (10 cm upstream of dosimeter).

If D designates the distance from each of the 80400 source points on the hemisphere [x(i),y(i),z(i)] to a given "dosimeter impact point" [(x3,y3,z3) or (x8,y8,z8)] and the fast neutron scattering source S(x,y,z) on each surface element is proportional to the fast flux there (as shown above), then the directional flux at each dosimeter impact point due to each of the (j=1 to 80400) source points, F3(j) or F8(j), may be written as F(j)=S(j)/[4*pi*D(j)*D(j)]. Moreover, the outward-directed current (in the +y direction in the case of the dosimeter at position 3, and in the -y direction in the case of the dosimeter at position 8), can be obtained by folding the directional flux [F(j)] with the dot product of the unit direction vector [d(j)] times the appropriate outward-directed normal vector (+y or -y), and summing over only those terms where the dot product is positive. [Because the source hemisphere has a bigger radius than the beam tube, there will be some terms at each location where the dot product is negative. In reality, those neutrons would never reach the dosimeter (tube wall) impact points, and even if they did, we are only interested in the gross outward-directed current, not the net outward-directed current. That is why the summation is taken over only those directions where the dot product is positive.] This will

yield a quantity proportional to the gross outward-directed current (J3 or J8) impingent on the inner surface of the beam tube wall in the vicinity of the two dosimeters.

In reality, all one really needs to know is the "relative" outward-directed current impingent on the inner wall of the beam tube in the vicinity of the two dosimeters as defined by the ratio:

RCR (relative current ratio) = J8/J3

which is convenient since many of the assumptions made thus far then cancel out and disappear completely. For these particular dosimeter locations around the HB-3 beam tube, the relative current ratio (RCR) was found to be 2.6628.

For the MCNP dosimetry analysis to calculate the dosimeter responses as accurately as possible, all known physical effects must be modeled as accurately as possible. Isotropic point sources along the centerline of a beam tube cannot model this effect. However, if the same isotropic point sources are shifted laterally a short distance to a line parallel to the centerline, this asymmetric effect can be preserved without any significant perturbation of the total scalar fluxes down the centerline of the beam tube, upon which these source terms were based.

Inspection of Table 2.2a, for example, shows that most of the significant fast neutron sources above 0.1 MeV originate in a fairly narrow band of axial locations and may (to first order) be approximated as originating at X=0, Y=0, Z=50 cm (using the present coordinate system). Now consider one single group of neutrons (representing all source neutrons above 0.1 MeV) originating instead, just a short distance away, at an off-centerline location designated as X=0, Y=y0, Z=z0=50 cm where X=0 is the vertical midplane and y0 is the distance by which the source may be offset from the centerline in the horizontal plane (ie, towards the side of the HB-3 tube closest to HB-2). If D is the distance from this new source point to either of the two dosimeter (tube wall) impact points, then a simple analytic expression, F=S/(4*pi*D*D), may be written for the flux at each of the impact points, and the direction cosines with respect to the outward normal(s) can applied to obtain the outward-directed current (j3 or j8) impingent on the inner surface of the beam tube wall in the vicinity of the two dosimeters. From this, one can again write an expression for the "relative" outward-directed current impingent on the inner wall of the beam tube in the vicinity of the two dosimeters as defined by the ratio:

rcr (relative current ratio) = j8/j3

where again, many of the simplifying assumptions cancel out and disappear completely. In this case, however, the expression for rcr may be written directly as:

rcr=((r0+y0)/(r0-y0))*((((z3-z0)^2+(r0-y0)^2)/((z8-z0)^2+(r0+y0)^2))^1.5)

where r0=5.08 is the inner radius of the beam tube, y0 is the yet-to-be-determined offset, and all the other variables have fixed values as defined above. At this point, all that remains is to solve the equation rcr=RCR=2.6628 for the unknown offset (y0) which will preserve the ratio of the outward-directed currents impingent on the two sides of the inner wall of the beam tube in the vicinity of the respective dosimeters. This may be accomplished using a simple binary search algorithm or any other search method. In this case, y0 was found to be 1.6986 cm.

Subsequently, in the final dosimetry analysis for the HB-3 beam tube (MCNP Run HB304M4), all of the equivalent point sources shown in Table 2.2a were shifted laterally, from the beam tube centerline to a line parallel to the centerline, by this amount.

It is important to note that no use whatsoever was made of any measured data in the determination of this prescribed offset. Rather, it is based on a well-founded yet very simple analytic approach that, while approximate, can be easily defended and applied in other similar situations.

The small three page Fortran program (FADIST7.FOR) used to implement the logic described above is included as Appendix B.2. It is by no means a production program, but all of the necessary coding and elements of logic may be found there.

4.4 Final Results and Conclusions

Table 4.1 shows the calculated and measured Ni58(n,p)Co58 reaction rates (due primarily to neutrons above 1.0 Mev), as well as the calculated and measured Fe54(n,p)Mn54 reaction rates (due primarily to neutrons above 0.1 MeV) for the dosimeter flux wires at HFIR Key 3, positions 3 and 8 around the HB-3 beam tube, just inside the pressure vessel, with the HFIR operating at 100 MW. The measured reference reaction rates were taken directly from Table E.12 of Ref 6. While that document also reports "experimentally corrected" (inferred) fluxes based on fluxes from a detailed 3-D TORT calculation multiplied by experimentally determined E/C ratios, it was judged far more appropriate to make the present MCNP comparisons against the most fundamental measured data available -- the originally measured reaction rates in the dosimeters themselves. To that end, the MCNP flux and

reaction rate tallies were defined such that the pointwise-continuous energy-dependent MCNP fluxes at the two dosimeter locations were folded on-line with the MCNP pointwise-continuous energy-dependent Ni58(n,p)Co58 and Fe54(n,p)Mn54 reaction cross sections to obtain the corresponding integral reaction rates. Those integral reaction rates were then compared directly with the measured reaction rates, as shown in Table 4.1.

Insofar as the 120 million neutron histories used in the final MCNP analysis allowed the fractional standard deviations at the dosimeter locations to be reduced to the 3-4% range, certain key conclusions may be drawn with confidence.

The most striking aspect of these results is that all of the C/E ratios are relatively small and lay in a narrow band between 1.17 and 1.25. Another interesting feature of the calculated and measured results is the "flux tilt" between dosimeters at Key 3, positions 3 and 8. The measured Ni58(n,p)Co58 reaction rates at these two positions show the flux above 1 MeV to be 2.37 times higher at position 8 than at position 3, while the Fe54(n,p)Mn54 reaction rates show the flux above 0.1 MeV to be 2.29 times higher at position 8 than at position 3. The calculated values given by MCNP show similar flux tilts of 2.29 and 2.36, respectively, thus increasing our confidence in the MCNP model and the simple theoretical model used a priori to determine the necessary lateral offset of the point sources.

By way of comparison, the geometrically less detailed but far more expensive 1988 TORT analyses yielded an overall "experimentally corrected" average C/E ratio of 0.69 and did not represent the flux tilt as well. Moreover, the experimentally corrected TORT fluxes given in Table E.23 of Ref 6 show a flux tilt of 1.95 (=1.78/0.913) above 1 MeV, and a flux tilt of 1.99 (=3.84/1.93) above 0.1 MeV. [Interestingly, it should be noted that the MCNP model for the entire HB-3 beam tube took 4 weeks to initially set up, with an additional 4 weeks to perfect and complete the dosimetry analysis described above, while the less geometrically detailed 3-D TORT analysis took something in excess of 6 man months. (Actually 6 man-years was spent over an 18 month period analyzing a total of 4 beam tubes.) For neutron dosimetry where one is only interested in results at one or two key locations, it would appear that MCNP would be the code of choice. Nevertheless, because deterministic codes like TORT produce a wealth of results (flux contours, etc) at many points, there remains a vital need for both types of analyses.]

Lastly, it should be noted that the MCNP C/E ratios (1.17 to 1.25) are also consistent with the C/E ratios previously obtained 6.55 meters down the beam tube based on comparisons of the calculated fluxes from MCNP Run HB302 and the 1968 measurements of Blosser and Thomas#5 in this energy range (see Table 2.3). Together, MCNP Runs HB302 and HB304M4 clearly show that the equivalent point sources defined above are wholly adequate for the HB-3 shielding calculations that were to follow.

4.5 Historical Evolution of the Model to Its Final State, Lessons Learned, and Sensitivities

The final MCNP dosimetry analysis (MCNP Run HB304M4) was certainly a success, but it was not the first and only run in the 304 series. Prior to the initial dosimetry analysis, everything shown in Fig. 3.2 was present except the dosimeters, the dosimeter holder ring, the coolant collector, and the detailed model of the 1960 water tube. Models of these components were added and refined during the course of the dosimetry analysis. While the geometric fidelity of the model improved in a monotonic fashion with time, the C/E ratios did not always improve in a monotonic fashion! However, once a component or feature was deemed important enough to include in the model, it was forever present whether it improved the C/E ratios or not. Ultimately, the model that evolved became the base model for all of the other calculations in this report.

Table 4.2 shows a brief summary of how the model evolved, the sensitivity of some key results to various modeling approximations, and the lessons learned along the way. Additional information on each calculation mentioned is available upon request. While anti-climactic, it is hoped that this abbreviated record will serve as a useful guide to other dosimetry analyses that might be performed for other beam tubes in the future.

Lessons learned include the following:

(1) Whenever possible, always compare calculated dosimeter responses (i.e., reaction rates) against directly measured dosimeter reaction rates. Do not waste time trying to compare calculated fluxes against "inferred" fluxes based on other calculational tools, even if some "experimental correction" has been applied. Such comparisons can often be misleading.

(2) For neutron dosimetry, use of the point sources described in Table 2.2a appears to be fully adequate for calculating dosimeter responses to within 50-60%. Offsetting the line of

Table 4.1. Comparison of calculated and measured neutron reaction rates for Ni-58 and Fe-54 dosimeters at HFIR Key 3, positions 3 and 8, around the HB-3 beam tube, just inside the pressure vessel. Calculated reaction rates (based on MCNP Run HB304M4) and measured reaction rates from Table E.12 of ORNL/TM-10444 are all for the HFIR operating at 100 MW.

Tally 35 (Key 3, Pos 8) just on the HB4 side of HB3			Tally 25 (Key 3, Pos 3) just on the HB2 side of HB3		
Ni58(n,p)Co58 reactions/sec/atom			Ni58(n,p)Co58 reactions/sec/atom		
Calculated MCNP Value	Measured Ref Value	C/E ratio	Calculated MCNP Value	Measured Ref Value	C/E ratio
3.838E-16	3.17E-16	1.21	1.674E-16	1.34E-16	1.25
fsd=3%			fsd=4%		
Fe54(n,p)Mn54 reactions/sec/atom			Fe54(n,p)Mn54 reactions/sec/atom		
Calculated MCNP Value	Measured Ref Value	C/E ratio	Calculated MCNP Value	Measured Ref Value	C/E ratio
2.839E-16	2.36E-16	1.20	1.202E-16	1.03E-16	1.17
fsd=3%			fsd=4%		

(a) Ni58(n,p)Co58 reactions are typically used to measure neutron fluxes above 1.0 MeV; Fe54(n,p)Mn54 reactions are typically used to measure neutron fluxes above 0.1 MeV.
(b) Calculated Ni58(n,p)Co58 reactions based on tally multiplier bin 2 for material 71.
(c) Calculated Fe54(n,p)Mn54 reactions based on tally multiplier bin 3 for material 72.
(d) Measured reference values shown are taken from Table E.12 on pp 208 of "Evaluation of HFIR Pressure-Vessel Integrity Considering Radiation Embrittlement" (ORNL/TM-10444) by R.D.Cheverton, J.G.Merkle, and R.K.Nanstad.

Table 4.2. Evolution of the dosimetry model which subsequently became the base MCNP model.

MCNP Run ID	nps	Model Changes and/or Comments on Results	C/E ratios at Key 3 Pos. 8 >1.0 MeV	Pos. 8 >0.1 MeV	Pos. 3 >1.0 MeV	Pos. 3 >0.1 MeV
HB304A	2M	No comment; contained error (starting wts wrong)	---		---	
HB304B	2M	Sampled isotropic source dist from mu=0.8 to 1.0; used volume-averaged flux detectors in water; dosimeters & holder not explicitly modeled	1.61-1.82		2.79-3.73	
HB304C	2M	Permanently switched to using point detectors; point detectors located at center of Charpy(s); model dosimeter holder as solid SS304 ring	1.71-2.48		2.18-3.56	
HB304C2	40M	Same as C (above), but with more histories	1.89-2.59		2.54-4.00	
HB304D	2M	Point detectors moved radially outward 1.9 cm, just to determine sensitivity	1.96-1.85		1.66-2.37	
HB304D2	40M	Same as D (above), but with more histories; --> Note that moving the pt detectors radially out --> by this 1.9 cm caused the flux to drop by 25%. --> This sensitivity is consistent with measurements.	1.45-1.90		1.90-3.13	
HB304E	2M	No comment; not clear what model differences were	1.25-1.31		1.29-3.05	
HB304E2	40M	Same as E (above), but with more histories	0.97-1.42		1.57-2.43	
HB304F2	40M	Started with C2, and added model of coolant collector to see if it blocked some neutrons going to dosimeters; --> Effect of adding this was totally negligible	1.77-2.60		2.55-4.05	
Note: All C/E ratios above were based on comparing the calculated MCNP fluxes with previosly reported fluxes from Table E.23 of ORNL/TM-10444. Those "previously reported fluxes" were "experimentally adjusted" calculated values from 1988 3-D TORT analyses -- i.e., we were essentially comparing against somebody else's computed values, which is not a terribly reliable thing to do since they could be off as much as we are. Beginning with Run HB304F3, we compare the MCNP calculated reaction rates for the Ni58(n,p)Co58 reactions (above 1.0 Mev) and the Fe54(n,p)Mn54 reactions (above 0.1 MeV) against the directly measured reaction rates reported in Table E.12 of ORNL/TM-10444. Thus, the following C/E ratios are much more reliable.						
HB304F3	2M	Same as F2, but detector tallies altered to include the reaction rates shown above.	1.17-1.19		1.22-1.18	
HB304F4	40M	Same as F2, but detector tallies altered to include the reaction rates shown above. --> When MCNP results are compared against directly --> measured values, we see that MCNP is really --> doing MUCH better than previously thought!	0.92-0.92		1.34-1.28	
HB304F5	40M	Started with F4, but moved pt detectors down 0.75 cm from midpoint of Charpy V-notch to bottom edge to see the sensitivity in vertical direction	0.98-0.99		2.00-2.00	
HB304F6	40M	No comment; started with F4, but not clear what the model differences were	1.00-1.02		1.22-1.16	

(continued)

Table 4.2 (cont)

HB304G	40M	Started with F4, but added elliptically shaped cone to model the "rounded corner" on inner surface of pressure vessel next to nozzel entrance (concern was that this could affect results at Key 3, position 3) --> Replacing sharp steel corner with water lowered --> fast flux at Pos 3 by 4-5%, and at Pos 8 by 3-4%	0.89-0.89	1.28-1.22
HB304G2	40M	No comment		
HB304G3	40M	No comment		
HB304H	40M	Started with HB304G, but made following changes: 1) Included explicit model of (dry) 1960 water tube; 2) Made Charpy(s) carbon steel rather than stainless; 3) Modeled bolts & mounting lugs on dosimeter holder; 4) Improved model of dosimeter holder based on E-49953	0.95-0.94	1.72-1.69
HB304H2	40M	No comment; not clear what model differences were		
HB304H3	40M	No comment; not clear what model differences were		
HB304I	40M	Never run; improvements here carried forward to HB304K; Started with HB304H and made following improvements: 1) Maintained same material configuration, but added cells and redefiend boundaries so dosimeter holder, sleeve, the vessel nozzel, part of vessel around dosimeters, and water near dosimeters, would have importance of 2.0; 2) Redefined elliptical cone forming rounded corner (the previous model in HB304G had cut off too much steel and substituted too much water).		
HB304J	40M	Never run; used only for checking model graphically; elliptical cone for rounded corner improved further.		
HB304K	40M	Embodied all the improvements noted above for HB304H, HB304I, and HB304J	1.01-1.00	1.56-1.47
HB304L	40M	Never existed		
HB304M	40M	Started with HB304K, but arbitrarily shifted the line of point sources (previously along tube centerline) 0.54 cm closer to the tube wall on HB-2 side of HB-3 to see sensitivity; exploring a possible physical effect	1.34-1.36	1.61-1.54
HB304M2	60M	Started with HB304K, but arbitrarily shifted the line of point sources 1.05 cm closer to the tube wall; also improved model of dosimeter holder ring so cover plate would be distinctly separate from the Charpy(s); --> Subsequent results from M3 (below) suggest the --> primary cause for improved results was the improved --> model of the dosimeter holder cover plate.	1.17-1.16	1.38-1.29
HB304M3	80M	Started with M2 (above), but arbitrarily shifted the line of point sources 1.5 cm off the centerline; kept improved cover plate model	1.20-1.19	1.31-1.23
HB304M4	120M	FINAL REFERENCE RUN; Started with M3 (above), but: 1) Shifted the line of point sources 1.6986 cm off the centerline based on a "solid theoretical model" emboddied in the FADIST7.FOR program; 2) Changed the MCNP sdef card so as to allow sampling of the isotropic source distribution over a little wider angular range (mu=0.71 to 1.0, rather than 0.8 to 1.0) and reset source starting weights accordingly. To preserve good statistics with these two changes required more histories (120M).	1.21-1.20	1.25-1.17
HB304N	40M	Experimental run to test new idea; subsequently discarded.		

point sources laterally a small distance from the centerline, as prescribed by a simple yet easily defendable theoretical model, allows one to routinely calculate dosimeter responses to within 17-25%. This lateral shift is necessary only for tangential beam tubes where the neutrons are known to enter the beam tube in an asymmetric fashion that cannot be represented by isotropic point sources along the centerline of the beam tube. Use of the supplemental theoretical model described above is defendable and acceptable, and works well.

(3) Neutron dosimetry is extremely position dependent and extremely sensitive to seemingly small changes in the geometry. (See sensitivity discussion below.) This sensitivity is physically real, and requires that the geometry be accurately represented with great precision. While this is possible with Monte Carlo methods, it is doubtful that 2- or 3-D deterministic codes requiring a discrete spatial mesh and an ultra-fine angular quadrature will be able to provide the necessary precision in the near future. The fact that earlier deterministic calculations had C/E ratios as close as 0.69 in the absence of components or details now known to be important is considered fortuitous. Nevertheless, because of the wealth of additional information provided by such analyses (flux contours, etc), there remains a continued need for both deterministic and Monte Carlo results in the future.

(4) For neutron dosimetry, the use of point sources within the beam tube is sufficient to accurately describe the dosimeter responses since virtually all of the fast neutrons reaching the dosimeters do stream down through the beam tube. For gamma dosimetry in the HFIR core, however, this may not be totally adequate since many of the prompt fission gammas (and delayed fission product gammas) reaching the dosimeters stream relatively uncollided through the beryllium and water reflectors. In such cases, a full-core model enhanced by the use of other biasing techniques (such as multiple importance zones, or the use of adjoint-generated geometry-independent multigroup weight windows) may be required. This is not considered to be a major problem in light of the newer advances described later in this report. While physically less important (according to studies by J. V. Pace et al), energetic secondary gammas from thermal neutron (n,g) reactions in various structural components, including the aluminum beam tube, would also have to be included in some fashion. Tracking neutrons all the way down to the thermal energy range at distant locations near the dosimeters could be a formidable problem for Monte Carlo methods. Decoupling and recombining results from the beam tube streaming analysis with those from the global reflector analysis would present a lesser but still serious obstacle. Thus, for gamma dosimetry analyses, one may still be better served by deterministic 3-D methods. That remains to be seen.

Regarding sensitivities:

(1) Exact placement of the dosimeter in the model is critical if one needs results to be accurate to within 20 or 25%. Moving the dosimeter location 1.9 cm (0.75 inches) radially can cause the calculated fast flux to change by 25%. This effect has been seen both calculationally and experimentally. In other experimental measurements where the Charpy specimens have been broken into segments and activation analyses applied to each of multiple segments, it is estimated that the fast flux can change by nearly a factor of two over the short 2-inch length of a Charpy specimen. In the other direction, calculations have shown that the fast flux can change by as little as 5% to as much as 50% over a vertical distance of 0.75 cm, depending on the configuration of other materials affecting the flux gradient around a given dosimeter. Because the fast fluxes at Key 3 position 3 (on the HB-2 side of the HB-3 beam tube) are 2.29 to 2.37 times lower than those at position 8, and because the flux gradients there are somewhat more severe, the results at position 3 are naturally more sensitive to small changes in the model.

(2) Contrary to initial expectations, modeling the coolant collector (near the end of the stainless steel sleeve around the beam tube) did not seem to have any perceivable impact of the dosimeter response. This would suggest that most of the fast neutrons affecting the dosimeter response first enter the inner wall of the beam tube slightly further downstream.

(3) Because the dosimeter flux wires are only 0.375 inches away from the pressure vessel, very small details such as modeling (or failing to model) the 1.0625-inch-radius rounded corner on the inner surface of the vessel adjacent to the nozzle may affect the calculated fast flux by as much as 3-5%. (Since the fsd's associated with that particular sensitivity study were also on the order of 3-5%, it may not be possible to draw this conclusion with a high degree of certainty, but the trend appears to be real insofar as the calculated fast flux dropped by 3-5% when the sharp steel corner was replaced by water associated with the rounded corner.)

(4) Detailed modeling on the dosimeter holder ring appears to be very important. Simply modeling the stainless steel cover plate of the holder as distinct from the carbon steel Charpy specimens appears to have changed the calculated fast fluxes by 15-18%. Moreover, earlier calculations showed that including the explicit model of the (dry) 1960 water tube, explicitly modeling the Charpy(s), and modeling the bolts and mounting lugs on the dosimeter holder, collectively changed the calculated fast fluxes at position 8 by 5%, but changed the calculated fast fluxes at position 3 by as much as 35%. [Because of the location of the dosimeter at Key 3, position 3 (on the HB-2 side of the HB-3 beam tube), the orientation of the dosimeter holder ring itself

relative to the beam tube, the location of the dosimeter relative to the nearby bolts and mounting lugs on the dosimeter holder, and the resulting flux gradients in this region, the results at position 3 generally seem to be much more sensitive to small geometric changes than the results at position 8. This sensitivity is also due to the fact that both the calculated and measured fast fluxes at position 3 (cf Table 4.1) are approximately 2.29 to 2.37 times lower than those at position 8. The smaller the fluxes, the more sensitive they will be to small changes in the local geometry.] Moreover, even the angle of inclination of the dosimeter holder relative to the beam tube has a calculationally discernible effect on the calculated fluxes. At one time, it was thought (incorrectly) that the dosimeter holder ring was inclined at an angle of 76 degrees relative to the beam tube. It was later learned that it is actually inclined at 77.0 degrees (cf Dwg. E-49953, Rev A). This seemingly small change produced small but statistically observable changes in the calculated fast flux. This sensitivity stems from the fact that the dosimeter flux wires are located 12.85 cm (radially) from the center of the dosimeter holder ring. As the angle of inclination is changed from 76 to 77 degrees, the dosimeter at position 8 is rotated back 0.22 cm closer to the vessel and is slightly less exposed to neutrons coming directly from the upstream portion of the nearby beam tube, while the dosimeter at position 3 gets rotated 0.22 cm further out from the vessel and faces the upstream portion of the beam tube a little more directly. The effect is small but observable. (Ironically, neither the Charpy specimens or the dosimeter holder were modeled at all in the 1988 TORT dosimetry analysis!) Paranthetically, it should also be noted for future reference that the dosimeter holder rings around the HB-1 and HB-4 beam tubes are inclined 73.5 degrees relative to the beam tube centerline.

5.0 TREATMENT OF NEUTRONS AND SECONDARY GAMMAS IN THE WATER-TUBE SHIELDING ANALYSIS

To gain a sense of the magnitude of the shielding problem at hand, assume for a moment that the HB-3 water tube is void and the rotary shutter is in the open position. Taking the isotropic point sources in Tables 2.2a and 2.2b, applying the intended 1/[4*pi*(R-R0)^2] approximation to compute the (uncollided) multigroup neutron and gamma fluxes at different points down the beam tube, and folding them with the 1977 ANSI Standard flux-to-dose-rate conversion factors#19, one can then estimate that the resulting neutron and gamma dose rates at Z=478.79 cm (i.e., at the beam tube centerline near the downstream surface of the steel liner of the concrete housing containing the rotary shutter) would be 5.89e+8 mrem/hr and 8.44e+7 mrem/hr, respectively, whereas at Z=399.48 cm (on the downstream surface of the collimator, just upstream of the rotary shutter) they would be 8.95e+8 mrem/hr and 1.33e+8 mrem/hr, respectively. Obviously, these values do not account for any attenuation in the thin aluminum windows, nor do they account for any additional contribution due to secondary gammas produced in any of the components along the way. Nevertheless, they do give one an "order of magnitude" feel for the amount of attenuation that must ultimately be provided by the (flooded) water tube and (closed) shutter if these dose rates are to be reduced to acceptable levels such that maintenance work could be performed downstream of the shutter under these conditions.

While MCNP#4 can handle combined neutron/gamma boundary sources under some conditions (i.e., when a preliminary MCNP calculation has produced a boundary crossing source file to be used in a subsequent bootstrapped MCNP calculation), that is not normally the case. If sources are supplied via the MCNP "sdef" card as shown in Appendix A.1, one may either run: (a) the coupled neutron/gamma problem with the neutron-only source, or (b) the gamma-only problem with the gamma-only source. The latter will be discussed at length in Sect 6, while the former is discussed in this section.

This section focuses on the 1998 water-tube shielding problem; in particular, it focuses on the determination of the neutron and secondary gamma dose rates just downstream of the collimator (i.e., on the fluxes and dose rates impingent on the rotary shutter) when both the water tube and collimator sections are flooded. A brief explanation is given (and expanded upon in Appendix C.1) as to why the use of the MCNP code was abandoned in this phase of the study. Some simple engineering insights are then provided on the neutron shielding problem, which suggest that the neutron dose rate at the location of interest is completely negligible. This was then confirmed by some simple 1-D ANISN#9 calculations in slab geometry. Other results from those calculations were then used to obtain conservative estimates of the secondary gamma production rate, which were then used in a QAD-like procedure to show that their contribution to the overall dose rate at the point of interest was also negligible. This was subsequently confirmed by use of a very simplistic MCNP model. The main conclusion is that the neutron dose rate upstream of the rotary shutter, and the secondary gamma dose rate upstream of the rotary shutter, are both completely negligible, even for the shorter 1998 water tube design. That being the case, the only part of the shielding analysis of any real concern is the transmission and overall attenuation of the original gamma sources down through the flooded portions of the water tube and collimator sections, and their subsequent attenuation in the rotary shutter. These topics are discussed in Sect 6. While seemingly trivial, this gamma shielding problem was, in fact, one of the more difficult shielding problems ever solved at ORNL. In the end, however, even that component of the dose rate on the downstream side of the rotary shutter was found to be negligible relative to the normal dose rate present there due to activation of the shutter itself. The activation analysis and subsequent dose rate calculation are discussed in Sect 7. With these extensive and rigorous analyses serving as benchmarks, the ultimate conclusion is that, in the future, fairly simplistic analytic tools such as the point-kernel technique embodied in QAD#20 may be used (in combination with the equivalent point sources described here in Sect 2) for most day-to-day dose rate assessments involving changes to the water tube(s) or the rotary shutter(s).

5.1 Initial (Since Abandoned) Approach Using MCNP

Calculations in this section, and in the balance of Sect 5, focus on the 1998 water-tube shielding problem. In particular, they focus on the determination of the neutron and secondary gamma dose rates just downstream of the collimator (i.e., on the fluxes and dose rates impingent on the rotary shutter) when both the water tube and collimator sections are flooded as shown in Fig. 3.3.

The HB305 series of runs (HB305A through HB305Q) represented the first serious attempt to solve the overall problem directly, using the MCNP code#4. While these initial attempts failed and were ultimately abandoned in favor of simpler methods which showed the neutron and secondary gamma components of the dose rate to be inconsequential, the lessons learned from these initial attempts are worth mentioning, at least briefly.

The basic geometry model used here for the flooded HB-3 beam tube is shown in Fig. 3.3 and described in Sects 3 and 6. It uses the 1998 water tube design rather than 1960 water tube design. In this case, the water tube and collimator sections are both flooded, as is the small (normally void) region between the two. The Type 1020 carbon steel rotary shutter was in the closed position as shown in Fig. 3.3. Lastly, all of the fine geometric details associated with dosimetry analysis described in

Sect 4 (except the 1960 water tube) were retained in the model. These particular runs were coupled neutron/gamma calculations with a neutron-only source, including neutrons over the entire energy range (0-20 MeV) such that the neutron energy cutoff card previously used in the dosimetry analysis was removed and the source normalization value on the "fm" tally multiplier cards (9.64595e16 n/s) equaled the sum of all the HB-3 point sources shown in Table 2.2a. To be as conservative yet as realistic as possible, the point sources were placed along the centerline of the beam tube. To increase the efficiency of the water tube shielding analysis while still including all neutrons that had any credible chance of contributing to the flux in the water tube, the "importance cutoff plane" described in Sect 2 was located at Z=118.6879 cm, more than 55.58 cm upstream of the start of the 1998 water tube. Consistent with that, the isotropic point sources were only sampled over directions within 15.13 degrees of the beam tube centerline, which required that the starting weight of the neutrons be reduced to 0.017332472 at the source. Additional details are provided in Appendix C.1.

Note that without any sort of axial biasing or geometric splitting, there is simply no chance of solving this problem. If all geometry cells have a neutron importance of 1.0, the weight of the neutrons after they penetrate 10, 15, or at most 20 cm into the water will be so low that they will all be killed by Russian Roulette, and one will get no histories in axial regions beyond that point. As an alternative to complex user-supplied space-energy-dependent weight windows, the user may subdivide the material cells into many smaller "importance cells" and specify the relative neutron importance to be used for each cell. This relative neutron importance controls the relative average weight of particles in adjacent importance cells, and therefore the frequency with which geometric splitting and Russian Roulette are applied. The higher the specified relative neutron importance is, the lower will be the average neutron weight in a cell and the "lower weight limit" beyond which Russian Roulette will be played. Thus, fast neutrons that are being attenuated and loosing weight as they move axially through the water tube will be subjected to Russian Roulette less often, so that a larger number of lower weight particles will then be allowed to penetrate deeper into the shield and provide better statistics at these more distant locations, instead of all being killed at or near the start of the shield.

The first few runs in this series (HB305A to HB305D) attempted to make the best possible use of geometric importance zones to affect an efficient solution of the problem. Run HB305D also used source-energy biasing to affect an efficient solution to the problem. From these runs, it was learned that "in a very real practical sense", the effective use of geometric importance zones to force neutron splitting and reduce uncertainties in "large, geometrically-complex problems" is totally infeasible, even though it often works very nicely in geometrically simpler problems involving thick shields.

The difficulty stems partly from the need to have a very large number of importance zones, and partly (mostly) from the way in which the data must be supplied. For problems in which the flux attenuates by 10 or 11 orders of magnitude, a large number of importance cells (40-50) will be required axially, between the upstream side of the water tube and the downstream side of the water-filled collimator. Note that the specified "importance" (imp:n=2, imp:n=6, etc) should not change by more than a factor of 2 or 3 (and never by more than a factor of 3 or 4) from one importance cell to the next in all three spatial directions. For an efficient solution, or even a semi-efficient solution, 20 to 30 importance cells may also be required in the radial direction, thus resulting in a large number of importance cells in any event. The major difficulty, however, comes from the way in which the neutron (and/or photon) importance is to be specified. Simply put: the large, relatively simple, material cells originally used to specify the problem geometry must now be subdivided into literally dozens or hundreds of little small cells; a separate "cell definition card" must then be prepared to describe each one of these little small cells in terms of all the new surfaces that will be required; and, the neutron (and/or) photon importance must be specified manually on each cell card. In the case of a large, homogeneous shield having only one or two material regions, this is not a problem and the input specifications can be easily automated. In the case of a complex shield which may already require many axial and radial cells just to describe the material configuration (such as the HB-3 beam tube as shown in Fig. 3.3), the problem becomes "enormously" more complicated, time-consuming, and error prone since the (dozens or hundreds) of 3-D surfaces needed to define the (hundreds or thousands) of new importance cells are intermingled with the dozens of surfaces already needed to describe the (dozens or hundreds) of material cells in the original problem. Thus, the input file for an otherwise modestly simple problem can become complicated and extraordinarily voluminous very quickly. Furthermore, parametric calculations involving the relocation of either the source or the detectors of interest would impact the relative neutron importance distribution, such that most or all of the cell cards would have to be regenerated each time, with the new importance values specified for each cell. Some of the other difficulties involved with this approach, and some early related efforts to circumvent these difficulties, are described in Appendix C.1. The approach was subsequently abandoned as being too impractical for deep penetration problems involving complex geometries.

This conclusion was reached just prior to the Radiation Protection and Shielding Conference held in Nashville, TN in late April 1998. There, a paper was presented by John Hendricks and Tom Evans#21 (members of the MCNP code development group at Los Alamos) showing how they were using an undocumented feature of MCNP4B called the "AVATAR patch" that allowed the user to supply "geometry-independent (multigroup) weight windows" to the code via an external file that could be generated off-line by hand or through the use of multidimensional deterministic codes

in adjoint mode. A key advantage of this approach is that space- and energy-dependent weight windows required for successful biasing could be specified in terms of an independent phantom (XYZ) mesh that did not have to be explicitly incorporated into the MCNP problem geometry -- i.e., the geometry specifications required to specify the material configuration in a problem no longer had to be extensively augmented by hundreds or thousands of additional (artificial) geometry zones to accommodate the weight window specifications needed for biasing. This was immediately seen as a major breakthrough since it would allow for the solution of problems that would have, in a practical sense, remained unsolvable without this capability.

In the two or three weeks immediately after the conference, numerous unsuccessful attempts were made to take advantage of this new yet undocumented capability (cf Runs HB305E through HB305Q). While the format of the needed weight window file was known from diagnosing the MCNP Fortran, the meaning of one or two variables was not properly understood, and Runs HB305E through HB305Q were considered failures. By mid-May, this approach was temporarily abandoned in favor of the more elementary approach described here in Sects 5.2 through 5.6, which showed that the neutron and gamma dose rates at the point of interest (downstream of the flooded collimator and/or just upstream of the rotary shutter) to be totally inconsequential.

Nevertheless, the need for a "geometry independent weight window approach" was so compelling that work on it continued on weekends throughout the month May. By that time, we had received from Tom Evans, a description of the necessary weight-window file format and a brief description of each variable in the file. To study the approach, a highly simplified academic problem was defined involving a narrow collimated beam of neutrons impingent on the bottom of a large homogeneous cylindrical tank of water, with the object being to calculate the particle distributions axially along the centerline with sufficient accuracy that the total "neutron plus secondary gamma" dose rate at the upper surface could be calculated within a few percent by volumetric or boundary crossing estimators that rely on the presence of real particles at this location (rather than by point detectors which rely instead on pseudoparticles and which may or may not be terribly reliable). This problem was ultimately solved very successfully with a 10,000-fold increase in calculational efficiency resulting from the use of a 3-D space-energy-direction-dependent weight window file based on a simple 1-D ANISN solution in adjoint mode. The approach used is described at some length in Appendix C.2, with supporting documentation in Appendices C.3, C.4 and C.5.

By the time the "geometry-independent weight window" approach was properly understood and implemented, however, the elementary approach described in Sects 5.2 through 5.6 (for the real HB-3 flooded beam tube problem) had already shown the neutron and secondary gamma dose rates to be totally insignificant. For that reason, and the lack of time, a final rigorous solution of the flooded HB-3 problem (with a neutron-only source) using MCNP and an appropriate weight window file was never attempted again, although we now have every reason to believe, in retrospect, that such an approach could and would be highly successful.

By late June 1998, however, it had also been demonstrated that an MCNP solution for the flooded HB-3 problem with the gamma-only source was also intractable using the standard tools available in MCNP. By taking the adjoint weight-window approach already developed for neutrons and applying it to the gamma problem, however, it was possible to construct a 3-D space-energy-direction-dependent weight window file that could be (and was) used with MCNP4B to obtain an extremely good and highly reliable solution for the real gamma-only flooded HB-3 problem. Moreover, use of this approach allowed us to obtain reliable particle distributions and real boundary crossing estimates (that confirmed our point detector estimates) not only through the flooded sections of the beam tube and collimator, but all the way through the carbon steel rotary shutter assembly! This analysis is described at length in Sect 6.

5.2 Some Engineering Insights on Neutron and Gamma Dose Rates

With the standard MCNP options having been shown to be inadequate in any real practical sense for deep penetration problems involving complex geometries, and with the "geometry-independent weight window" approach not yet working as of mid-May, simpler alternative methods were being sought. Moreover, this unfortunate confluence of circumstances actually called for real thought! The remainder of Sect 5 describes some of the beneficial insights gained from this rare practice.

The two key things of initial interest in the water tube shielding analysis are the neutron and gamma loads (fluxes, currents, dose rates) impingent on the rotary shutter shield plug. The present shutter provides adequate shielding when the water tube section and the section reserved for the collimator are both flooded. (Note that a collimator had been designed for HB-3 in 1960, but never installed.) The question was then this: With the total amount of water shielding in the "1998 water tube and flooded collimator sections" effectively being 1.89 feet (57.6 cm) less than the total amount of water in the original 1960 design, will the neutron or gamma loads impingent on the rotary shutter increase to the point where it must be redesigned?

This simple question gives rise to a number of other (more fundamental) questions:

Q1: What types of radiation must be considered?
A1: Neutrons coming down the beam tube, secondary gammas born in the water-filled beam tube, and the original "primary" gammas coming down the beam tube.

Nomenclature: The term "primary gamma" as used here is really a misnomer since those coming down the beam tube and represented here by the equivalent point sources in Table 2.2b may be fission gammas that have experienced at least one collision in the beryllium reflector, or they may be secondary gammas produced by (n,g) reactions in the beryllium reflector, in the aluminum at the hot tip of the beam tube, or in other components (or other regions of these components), close to the hot tip of the beam tube. For the purpose of this study, however, all gammas represented by the equivalent point sources in Table 2.2b will be referred to as "primary" gammas, whereas all other gammas (subsequently produced by the neutron sources in Table 2.2a) will be referred to as secondary gammas.

Q2: How do neutrons get to the rotary shutter?
A2: First, by going through the water tube where they are heavily attenuated. (Those wandering outside into the concrete would be attenuated even more.) After that, they must go through the collimator section. Some will go up through the water-filled hole in the collimator, while some of the (few) moderately energetic ones still present at the entrance of the collimator may actually stream through the steel body of the collimator itself due to the relatively low neutron cross section in the iron near a few key antiresonances (at 15 keV and 25 keV, for example).

Q3: How do primary gammas get to the rotary shutter?
A3: They tend to stream relatively freely through the low-density materials in the system -- in this case, straight down the centerline, through the water tube and the water-filled hole in the steel collimator. Those entering the concrete further upstream, or the steel sections of the collimator further downstream, are heavily attenuated. The path of least resistance is the water hole up the middle.

Q4: How and where are secondary gammas produced?
A4: Energetic (6-8 MeV) secondary gammas are produced by (n,g) reactions in the aluminum windows at the beginning and end of the water tube, with the former being far more important, and to a lesser extent by (n,g) reactions in the aluminum body of the water tube. A very substantial number of 2.2 MeV secondary gammas are also created by (n,g) reactions with the hydrogen in the water, especially at the start of the water tube where the neutron flux is very high. There are also (n,g) reactions in the steel collimator, but the neutron flux there is so low (having been attenuated by 10 to 11 orders of magnitude) that any secondary gammas produced there are essentially negligible compared to the other gammas that are likely to be present in this region.

Q5: Are these secondary gammas very important?
A5: Yes and no; it depends where you are. Near the hot end of the water tube, the impingent neutron flux is so intense, that enormous numbers of 2.2 MeV secondary gammas are produced in the water, not to mention those produced in the first aluminum window. Here, the number of secondary gammas per unit volume (p/cc) is far greater than the number of primary gammas streaming down the beam tube. Moreover, even the gamma energy density (MeV/cc) associated with the secondary gammas is greater than that associated with the primary gammas streaming down the beam tube. For that reason, the relative importance of the secondary gammas was studied analytically and is discussed at some length (further below). The answer to the basic question, however, is "no" -- these secondary gammas are not terribly important down near the rotary shutter, and they can be ignored for all practical purposes. While it is true that they are created in enormous numbers near the hot end of the water tube, the saving grace is that they are born isotropically over the 4*pi sphere and the resulting secondary gamma flux is substantially reduced as they go from their point of origin (near Z=174 cm) to the rotary shutter (near Z=400 cm). The primary gammas streaming down the beam tube are also intense, very energetic, and certainly not negligible. More importantly, they are already fairly well collimated by the time they get to the hot end of the water tube. Unlike the secondaries which are born there isotropically, the primary gammas streaming through this region are all (pretty much) travelling in a narrow cone of directions pointed straight down the water tube towards the collimator and the rotary shutter. By the time one gets to the rotary shutter, the primary gammas are totally dominant over the relatively few secondary gammas that manage to get there. Simple analyses demonstrating this are presented below.

Other questions that come to mind are:

What form of radiation is dominant at the upstream surface of the rotary shutter: neutrons, secondary gammas, or primary gammas? What are their relative magnitudes? Given that the 1998 water tube is now 1.89 feet shorter than the 1960 water tube, how does this change things? Could it be that things that were negligible before are now dominant? Or, could it be that

things that were negligible before have gone up substantially, but are still negligible relative to other things? Order of magnitude approximations can by used to provide tentative answers to some of these questions, while simple yet conservative 1-D ANISN calculations can be used to provide the necessary confirmation in a more rigorous fashion. In other cases, 1-D ANISN calculations are needed to obtain simple yet realistic source terms that can then be used in combination with point kernel techniques to quickly and easily assess the relative importance of some parameters. The approach here was to use a combination of these tools to first determine which transport phenomena were important and which were not. Later, the most advanced 3-D tools available were used to closely examine those transport phenomena that were clearly important (like the transmission and attenuation of primary gammas through the system).

To begin with the most elementary assessment possible, consider the unshielded neutron and gamma dose rates on the downstream surface of the collimator at Z=399.48 cm, just upstream of the rotary shutter. Taking the isotropic point sources in Tables 2.2a and 2.2b, applying the intended 1/[4*pi*(R-R0)^2] approximation to compute the (uncollided) multigroup neutron and gamma fluxes at different points down the beam tube, and folding them with the 1977 ANSI Standard flux-to-dose-rate conversion factors#19, one can then estimate that the resulting neutron and gamma dose rates at this location (Z=399.48 cm) are 8.95e+8 mrem/hr and 1.33e+8 mrem/hr, respectively. More precisely: the dose rate due to gammas above 6 Mev is 1.900e+7 mrem/hr (97.5% of which come from gammas in the 6-8 MeV range); the dose rate due to gammas between 2 and 6 MeV is 3.498E+7 mrem/hr; and the dose rate due to gammas below 2 MeV is 7.919e+7 mrem/hr. Because the 1/(4*pi*R^2) term has already been applied, the effect of natural divergence from the original point sources has already been included in these neutron and gamma dose rates. All that remains for the shielded case is to apply some simple attenuation factors, like those shown in Table 5.1.

Now consider how neutrons get from the upstream side of the water (at Z=174.95 cm) inside the water tube, to the upstream side of the collimator at Z=310.58 cm, and then how they get from that location to the downstream side of the collimator at Z=399.48 cm. In the first case, they must travel a distance of 135.6 cm through water. To be conservative, let's assume that they're all fast neutrons since fast neutrons experience less attenuation than thermal neutrons. In the second leg of the journey, they may travel through the water-filled rectangular hole in the collimator, or through the steel body of the collimator. (1) By the time they reach the collimator, most neutrons are certainly well thermalized after travelling all the way through the water tube. Thus, it is probably most realistic to use the thermal neutron relaxation length (2.76 cm) through this 88.9 cm of water. (2) To be conservative, however, one might alternately want to assume that they're still all fast neutrons and use the fast neutron relaxation length (10 cm) across this 88.9 cm of water. (3) Lastly, fast or resonance range neutrons may also find less resistance travelling through the steel body of the collimator than thermal neutrons would find travelling through the water, so let us also consider that possibility by using a relaxation length of 6 cm over the 88.9-cm-long steel body of the collimator. Applying these attenuation factors to the unshielded neutron dose rate impingent of the rotary shutter, we see that the shielded dose rate there may be in the range of:

Dose(n)= (8.95e+8 mrem/hr) * exp(-135.63/10.0) * exp(-88.9/2.76) = 1.026e-14 mrem/hr (1)

or = (8.95e+8 mrem/hr) * exp(-135.63/10.0) * exp(-88.9/10.0) = 1.587e-1 mrem/hr (2)

or = (8.95e+8 mrem/hr) * exp(-135.63/10.0) * exp(-88.9/6.0) = 3.675e-7 mrem/hr (3)

Thus, even in the worst case (2), this quick analysis suggests that the direct neutron dose rate impingent on the rotary shutter is probably negligible when the 1998 water tube and collimator sections are both flooded.

Now consider how the primary gammas (from the equivalent point sources in the beam tube) get from the upstream side of the water (at Z=174.95 cm) inside the water tube, to the upstream side of the collimator at Z=310.58 cm, and from there to the downstream side of the collimator at Z=399.48 cm. In the first case, they must again travel a distance of 135.6 cm through water. In the second leg of the journey, the path of least resistance is obviously through the water-filled rectangular hole through the center of the steel collimator, a distance of 88.9 cm. Thus, from beginning to end, these gammas must pass through 224.53 cm of water. It is important to note, however, that gammas of different energies attenuate at different rates, as crudely shown in Table 5.1. Taking the unshielded primary gamma dose rates impingent on the rotary shutter corresponding to each of the three energy ranges noted above, and using the appropriate energy-dependent relaxation lengths shown in Table 5.1, the shielded (primary) gamma dose rate there is given by:

Dose(g) = (1.900e+7 mrem/hr)*exp(-224.53/40.0)
+ (3.498e+7 mrem/hr)*exp(-224.53/30.0)
+ (7.919e+7 mrem/hr)*exp(-224.53/20.3)

Table 5.1. Relaxation lengths for different particles in water and iron.

Material	Relaxation Lengths (cm) for Different Particles				
	Fast Neutrons	Thermal Neutrons	2 MeV Gammas	4 MeV Gammas	8 MeV Gammas
Water	10.0 (a)	2.76 (c)	20.3(d)	30.0 (a)	40.0 (a)
Steel	6.0 (a)	-------	-------	3.7 (b)	4.4 (b)

(a) Taken from Table 10.4 in Sect 10.74 of Ref 22.
(b) Taken from same table, but not needed in this calculation.
(c) Taken from Table 3.1 in Sect 3.40 of Ref 22.
(d) Taken from Example 10.2 in Sect 10.113 of Ref 22.

= (69335 + 19652 + 1245) mrem/hr = 90232 mrem/hr = 90.23 Rem/hr (for 1998 water tube)

which completely overshadows the direct neutron dose rate. Moreover, it is interesting and enlightening to compare this extremely simple estimate with more rigorous MCNP estimates cited later in this report. MCNP Run HB307C (cf Appendix C.6) utilized a highly simplified 3-D model of the HB-3 water tube and collimator where, for example, all of the barytes concrete surrounding the beam tube was replaced by water and the collimator was modeled as a monolithic piece of carbon steel with a water-filled rectangular hole up the middle, and everything past the collimator was treated as an external void. This highly simplified model was employed in a preliminary MCNP analysis of the gamma-only problem so that photon importance regions could be easily specified and used for geometric splitting. While this preliminary model using simple geometric splitting was not sufficiently accurate to yield reliable "boundary crossing" estimates of the space- and energy-dependent photon flux downstream of the collimator, a point detector estimate at that location (based on "pseudo-particle" contributions from each source point and each collision site) did yield a fairly well converged dose rate of 109.31 Rem/hr at this location. Likewise, the final reference benchmark solution provided by MCNP Run HB308G5 showed the primary gamma dose rate at this location to be 103.99 Rem/hr, +/- 0.5%. This particular calculation, described at length in Sect 6, used the full-blown 3-D model of the HB-3 beam tube shown in Fig 3.3, including the pressure vessel, the pool, the concrete biological shield, the beam tube itself, the 1998 water tube, the collimator with the attendant radial and eccentric shields, and the rotary shutter assembly downstream of the collimator. This was a very rigorous analysis employing 3-D broad-group "geometry-independent weight windows" based on a fine-group adjoint analysis. In this 3-D MCNP analysis, we were able to obtain a highly reliable space-energy-direction-dependent boundary source downstream of the collimator (just upstream of the rotary shutter), and the real-particle boundary crossing estimates of the photon flux and dose rates upstream (and downstream) of the rotary shutter were in excellent agreement with the point detector estimates at these same locations. While the ultra simple 3-group gamma shielding calculation above could be (and has been) expanded to include 23-group energy-dependent mass attenuation coefficients whose results agree even better with the rigorous 3-D MCNP results, it was most gratifying to see that even the simplest textbook approaches can, when properly applied, yield surprisingly accurate results!

Parenthetically, it is also interesting to take the same simple 3-group gamma shielding calculation and apply it to the original 1960 water tube. In this case, the water inside the water tube actually starts at Z=117.74 cm, such that the total amount of water between the start of the 1960 water tube and the downstream surface of the collimator is now 281.74 cm instead of 224.53 cm. Applying the same formula as before, one can credibly estimate that the shielded (primary) gamma dose rate downstream of the collimator would then be on the order of:

```
Dose(g) =  (1.900e+7 mrem/hr)*exp(-281.74/40.0)
         + (3.498e+7 mrem/hr)*exp(-281.74/30.0)
         + (7.919e+7 mrem/hr)*exp(-281.74/20.3)

        = (16588 + 2919 + 74) mrem/hr = 19581 mrem/hr = 19.58 Rem/hr  for the 1960 water tube.
```

In this case, MCNP Run HB307D, which uses the same highly simplified 3-D model as HB307C but incorporates the longer 1960 water tube, showed the shielded (primary) gamma dose rate downstream of the collimator to be 26.77 Rem/hr. Thus both methods suggest that the primary gamma dose rate impingent on the rotary shutter downstream of the collimator will be between 4.1 and 4.6 times higher for the shorter 1998 water tube than for the longer (original) 1960 water tube.

Of "key significance" is the fact that the first two simple calculations illustrated above suggest very strongly that the direct neutron dose rate impingent on the rotary shutter (when the 1998 water tube and collimator sections are both flooded) is totally negligible -- both in the absolute sense, and relative to the primary gamma dose rate at this same location. Because the neutron calculation was still very approximate, however, multigroup 1-D ANISN calculations to confirm this tentative conclusion were still deemed appropriate. Moreover, nothing quantitative has been said so far about the effect of secondary gammas produced in the beam tube. The 1-D ANISN calculations described below also address that issue, or at least provide the source terms that can be used in a point kernel analysis to quantitatively resolve the question of their relative importance.

5.3 Use of ANISN to Confirm that the Direct Neutron Dose Rate is Negligible

Table 5.2 briefly describes an ANISN 1-D slab model of the HB-3 water tube and collimator that was used to get a further feel for which transport phenomena were important and which were not. For reasons explained below, one must be very careful to "pick and choose" what things to believe and what things not to believe. Proper inferences can be made about some things, while other results can be terribly misleading because of the 1-D nature of the model. First, however, let us say a few words about the model itself and how it was used before highlighting its weaknesses.

Table 5.2. ANISN 1-D slab model of the HB-3 water tube and collimator that was used to get a rough feel for what w important and what was not. Includes provisions for modeling either the 1960 or the (default) 1998 water tube desig.

Zone No.	# of Mesh	Xmin (cm)	Xmax (cm)	Material	Description / Comments
1	1	115.0	116.7841	Always Void	For 1960 water tube, put boundary source on right of mesh 1
2	3	116.7841	117.7366	Usually Void	For 1960 water tube, first aluminum window would go here
3	112	117.7366	174.27	Usually Void	For 1960 water tube, put water here; For 1998 water tube, put void here, with bndry src on right of mesh 116
4	3	174.27	174.95125	Aluminum	Represents first aluminum window in 1998 water tube; Water in 1998 water tube starts at 174.95125
5	8	174.95125	179.05	Water	1st 4.1-cm-thk water region used to find secondary gamma production rate
6	8	179.05	183.15	Water	2nd 4.1-cm-thk water region used to find secondary gamma production rate
7	8	183.15	187.25	Water	3rd 4.1-cm-thk water region used to find secondary gamma production rate
8	8	187.25	191.35	Water	4th 4.1-cm-thk water region used to find secondary gamma production rate
9	8	191.35	195.45	Water	5th 4.1-cm-thk water region used to find secondary gamma production rate
10	8	195.45	199.55	Water	6th 4.1-cm-thk water region used to find secondary gamma production rate
11	8	199.55	203.65	Water	7th 4.1-cm-thk water region used to find secondary gamma production rate
12	8	203.65	207.75	Water	8th 4.1-cm-thk water region used to find secondary gamma production rate
13	190	207.75	302.1868	Water	Balance of water in 1998 water tube; 1998 water tube ends at 302.1868
14	3	302.1868	302.5043	Aluminum	Represents second aluminum window in 1998 water tube
15	16	302.5043	310.58	Water	Region between end of 1998 water tube and start of collimator; 1998 collimator design starts at 310.58
16	50	310.58	334.7709	Water, SS, or C-Stl	Always water if looking at 1960 design; Use Water, SS or C-stl for alternate 1-D models of 1998 collimator
17	3	334.7709	335.4756	Al, Water, SS, or C-Stl	Would be aluminum (2nd window) only if looking at 1960 design; Use Water, SS or C-stl for alternate 1-D models of 1998 collimator
18	128	335.4756	399.48	Water, SS, or C-stl	Use Water, SS or C-stl for alternate 1-D models of 1998 collimator; 1988 collimator design ends at 399.48
19	3	399.48	401.9445	Always Void	Thin region between end of collimator and end of flange; Neutron & gamma dose rates tabulated for 1st mesh in Zone 19 (mesh #574)
20	15	401.9445	415.44875	Always Void	Void between end of flange and the C-stl rotary shutter shield plug
21	125	415.44875	477.36125	C-stl	Represents C-stl rotary shutter shield plug
22	3	477.36125	478.79	Always Void	Last part of cavity containing the rotary shutter assembly; Monochronometer (not modeled here) starts at 478.49

Pre-mixed materials available in the HB-3 water tube 61n/23g cross section library (xsects.dort-ready.bin.hfir.hb3.watertube.01may98) include the following:

Mixture 1 = ANISN/DORT Material 1 = Water at 1.00 g/cc
Mixture 2 = ANISN/DORT Material 5 = Aluminum 6061 (2.7 g/cc)
Mixture 3 = ANISN/DORT Material 9 = Void (He @ 1.0e-20 atoms/barn*cm)
Mixture 4 = ANISN/DORT Material 13 = SS304 (7.92 g/cc; see page 50 of ORNL/TM-11989)
Mixture 5 = ANISN/DORT Material 17 = Carbon Steel (7.8212 g/cc, 99 wt% Fe, 1 wt% C)
Mixture 6 = ANISN/DORT Material 21 = Barytes Concrete at 3.09725 g/cc
Mixture 7 = ANISN/DORT Material 25 = Regular Concrete
Mixture 8 = ANISN/DORT Material 29 = response functions

Table 5.2 describes the model geometry as clearly as possible. Basically it is a 1-D infinite slab model along the centerline of the HB-3 beam tube. It includes the 1998 water tube, the water-filled collimator, and the rotary shield plug. It also includes the aluminum windows defining the beginning and end of the water tube. Provisions are also present for modeling the 1960 water tube but, for reasons described below, comparisons of results between the 1998 and 1960 models would be misleading and should be avoided. (Thus we'll only discuss the former.) Of greater interest are the eight 4.1-cm-thick slabs used to estimate the secondary gamma production rate near the hot end of the water tube. Lastly, zones 16-18 can be altered to approximate the collimator section as all water, all stainless steel, or all carbon steel.

Appendix C.7 lists the actual ANISN input for this particular model, as well as a small Fortran program for reading the ANISN flux file and calculating the neutron and gamma dose rates just downstream of the collimator. As noted there, this particular file is set up for a "forward mode" Group-Banded ANISN#9 calculation involving a 1-D infinite slab model representing materials along the centerline of the HB-3 beam tube. One of the attractive features of the model is that the nuclear cross section data used for all materials is based on the coupled VELM 61n/23g shielding library#10 using 61 neutron groups and 23 gamma groups. Moreover, the source terms impingent on the upstream side of the first aluminum window (at X=174.27 cm) are also specified in this same 61n/23g group structure. In this case, an S-32 quadrature was used, with the impingent source being zero in all but the most forward direction (direction 33). Moreover, the impingent multigroup source terms in that direction have been properly normalized (based on the quadrature weight for that direction, and the associated direction cosine) to reproduce the impingent currents (n/s/cm2 and p/s/cm2) based on the location of this first aluminum window and the locations and magnitudes of the various 61n/23g source terms shown in Tables 2.2a and 2.2b. In the ANISN input file, these are specified in the 18** array. The internal boundary sources in the 18** array (cf Appendix C.7) are presently set up to include the 61-group neutron source impingent on the new 1998 water tube (at X=174.27 cm), as well as the 23-group gamma source impingent on the new 1998 water tube (at X=174.27 cm). That can, however, be easily altered. By placing "18** 2013z e" at the end of the existing 18** array (the source specification array), one can zero-out all of the neutron sources to run the gamma-only case. [Eliminating the neutrons will also eliminate the secondary gammas, thus allowing one to partially assess their relative importance.] Likewise, by placing "18** a2014 f0" at the end of the existing 18** array, one can easily zero-out all of the primary gamma sources while keeping all the neutron sources. [The resulting (coupled n/g) calculation will allow one to estimate how many secondary gammas are being generated in each energy group, and see where they are being generated (spatially). These secondary gammas can then be treated as source terms in a QAD-like point kernel analysis to realistically determine their relative importance in the real (3-D) HB-3 water tube shielding problem.] Lastly, by simply rearranging the given data for zones 16, 17, and 18 in the GB-ANISN 9$$ array (the material-by-zone array), the collimator section may be modeled as all water, all stainless steel, or all carbon steel.

The first three cases used both the neutron and gamma sources impingent on the 1998 water tube at X=174.27 cm. Case 1 modeled the collimator section as all water, Case 2 modeled it as all stainless steel, and Case 3 modeled it as all carbon steel. Individually, none were terribly realistic, but the objective here was to bracket reality and see which material offered the path of least resistance in terms of conservatively estimating the direct neutron dose rate just downstream of the collimator. [Unlike the 1- or 2-group data in Table 5.1, the 61-group neutron cross section data used here faithfully represents the unusually low cross sections (known as windows) that exist in the energy-dependent iron cross section. These typically occur in very select narrow energy bands (as around 15 keV or 25 keV in iron), and are caused by anti-resonance quantum effects in the nucleus. Neutrons in these narrow energy ranges only see a very low cross section and can therefore travel much further in the iron than neutrons at nearby energies that are heavily attenuated.] While the intent was partly to see which material offered the path of least resistance, the more general hope was to verify that, even with a very conservative 1-D model involving a neutron source of infinite extent [ie, the actual neutron source intensity (n/s/cm2) applied uniformly across the 1-D source plane], the direct neutron dose rate downstream of the collimator would be negligible relative to: (1) the primary plus secondary gamma dose rate in this model and, more importantly, relative to (2) just the primary gamma dose rate downstream of the collimator resulting from a simple but more realistic model of the real (finite) gamma source in water as exemplified by the simple hand calculation shown above or the two 3-D MCNP calculations cited there. Neutron and gamma dose rates just downstream of the collimator, based on these 1-D infinite slab ANISN calculations, are as follows:

	Neutron Dose Rate (mrem/hr)	Gamma Dose Rate (mrem/hr)
Case 1, collimator = all water (in zones 16-18):	4.62647e-2	4.04834e+6 (*)
Case 2, collimator = all SS304 (in zones 16-18):	5.05770e-1	7.58715e-2 (*)
Case 3, collimator = all C-Stl (in zones 16-18):	1.45603e+0	1.13501e-1 (*)

Before discussing the neutron dose rates at all, it should be noted that (1) none of the three gamma dose rates shown here are credible (that is: none of them represent reality, for the reasons described below), and (2) the conservatively high neutron dose rates shown here should therefore be compared against the much more realistic primary gamma dose rates described in Sect 5.2 (90-110 Rem/hr).

First, it is interesting to note that if the collimator were a monolithic block of carbon steel (with no hole), the direct neutron dose rate downstream of the collimator would be about 31 times higher than if it were all water. Undoubtedly this is due to the multiple narrow windows in the energy-dependent iron cross section data which cannot be represented by 1- or 2-group cross section data but which are well represented in the 61n/23g VELM cross section library.

Secondly, it is interesting to note that if the collimator were a monolithic block of stainless steel, the direct neutron dose rate downstream of the collimator would be substantially less than it would be if it were all carbon steel. This is because cross sections for the other nuclides present in the stainless steel would tend to "cover over" the windows in the iron cross section, although their effect is still significant. [In the actual collimator design, it is now known that carbon steel would be used (rather than stainless steel) for the central cylindrical section having the rectangular hole up the middle. That is because this component is immediately adjacent to the neutron beam during normal (dry) operation, and the carbon steel (which is 99 wt% iron and 1 wt% carbon) will become far less activated than the stainless steel. Moreover, the very nuclides which tend to make the stainless a better shield material, also cause activation problems which can become a nuisance during maintenance operations. Thus the central section will be made of carbon steel while stainless will be reserved for use in the surrounding radial and eccentric shields which are further removed from the direct neutron beam and less likely to become as activated.]

Lastly and "most importantly", regardless of which material is used to represent the collimator, the direct neutron dose rate downstream of the collimator (based on this extremely conservative model corresponding to an infinite planar source of neutrons) is negligible in the absolute sense, and completely negligible relative to the 90-110 Rem/hr that would be present there due to the primary gamma sources entering the water tube, based on the very realistic estimates for the latter as given in Sect 5.2. Thus, unless they create a "whole lot" of important secondary gammas, the neutrons can be ignored completely. This issue is discussed in Sect 5.4.

Finally, the 1-D gamma dose rates shown above should probably have been purged from the table, but their intentional presence merits some discussion. Given that the collimator is not really a monolithic block of stainless steel or carbon steel, as necessarily represented in the 1-D model, and that it does have a water-filled hole up the middle that gammas can easily stream through, the gamma dose rates shown here for Cases 2 and 3 are obviously unrealistic and should not be used for anything. Less obvious are the serious deficiencies associated with Case 1 which cause the gamma dose rate there to be unrealistically high. As with the neutrons, this model also includes a gamma (photon) source of infinite extent [ie, the actual gamma source intensity (p/s/cm2) at Z=174.27 cm is applied uniformly across the infinite 1-D source plane]. For an optically thick shield such as steel or lead (Pb), this may not be a bad approximation at distant locations. Because the water is relatively transparent to high energy gammas, however, it is not a very good approximation in this particular case. That is to say: because the water is relatively transparent to high energy photons, the detector in mesh 574 (near Z=400 cm) can still see and feel the effects of not only those source gammas at Z=174.27 cm that would normally enter the 14-cm-diam water tube, but it can also see and feel the effects of many other gammas impingent at many other nearby locations on the infinite 1-D source plane. As a result, the 1-D calculation grossly overestimates the gamma dose rate at the location of interest. Moreover, there is no way to "fix up" a 1-D calculation to simulate this particular physical situation in a realistic fashion, even if one were to go to a spherical model. Using a small spherical source volume at the center of a sphere would overestimate the natural divergence of the source and underestimate the flux and dose rate at the desired location, while use of a larger (hollow) sphere with an internally impingent gamma source would, because of the larger source surface, cause the same difficulty as the infinite planar source, albeit to a lesser and somewhat arbitrary extent. In the case of a 2-D RZ DORT model, which would superficially appear to be a much better model, the solution at the point of interest would, unfortunately, be plagued by ray effects as described in Appendix C.2.7. Moreover, it is a classic case where the more famous codes are not necessarily the best codes for a particular application. Because they can all better represent a small finite gamma source in water, the the simple hand calculation illustrated above, point kernel calculations, and 3-D Monte Carlo models, are all more applicable to this particular application. That is why, for example, after the secondary gamma sources were obtained from the 1-D ANISN model (see below), we then took those gamma sources and put them in a point kernel model to assess their relative importance downstream of the collimator.

One last note of caution is also in order. The 1-D model described in Table 5.2 appears to be fairly flexible insofar as it has provisions for modeling either the 1998 water tube (beginning at Z=174.27 cm) or the 1960 water tube (beginning at Z=116.7841 cm). For the purposes described above, and for the purposes described in Sects 5.4 and 5.5, this model is entirely appropriate.

Use of this 1-D model in scoping calculations to compare the effectiveness of the 1998 water tube as a primary gamma shield to the effectiveness of the 1960 water tube as a primary gamma shield, however, would not be appropriate and could be misleading for the reasons described above -- namely that no 1-D model, whether in slab or spherical geometry, can accurately model all of the necessary characteristics of the gamma source impingent on the end of the small-diameter water tube. Because of the modeling compromises that would be necessary in either case, and the relative transparency of the water to high energy gammas, the calculated fluxes and dose rates in both cases would be sufficiently distorted that even the relative change in the dose rate at the point of interest would not be representative of reality. For such parametric comparisons, one is better advised to use the simple types of hand calculations illustrated above, point kernel calculations, or simple 3-D Monte Carlo models, all of which are more applicable to this particular problem.

5.4 Determination of Secondary Gamma Source Terms Using ANISN

Based on the ratio of neutron and gamma beam intensities impingent on the first aluminum window of the 1998 water tube at Z=174.27, 1.0 neutrons enter the water tube for every 1.4 gammas that enter the water tube. While the impingent (primary) gammas do include a number of 6-8 MeV gammas, the vast majority would appear to be in the 0.6 to 1.0 MeV energy range (cf Table 2.2b). If every neutron entering the water were ultimately thermalized and absorbed by the hydrogen in the water, thereby producing one 2.2 MeV capture gamma for every neutron, it is not at all inconceivable that the gamma energy flux associated with secondary gammas at the hot end of the water tube would exceed the impingent gamma energy flux. [1-D calculations described below have confirmed that, after one accounts for neutrons that are reflected back out of the system, and considers secondary gammas produced during the slowing down process as well as those ultimately produced by thermal neutron capture, there are actually about 1.065 secondary gammas produced for every neutron that "enters and stays in the system".] In addition, one must consider that some of the impingent neutrons, instead of being absorbed by the water where they would produce 2.2 MeV gammas, are actually absorbed in the first aluminum window where they will produce more energetic secondary gammas in the 6-8 MeV range. Given that the secondary gammas are likely to travel much further in the water than their parent neutrons, the effect of secondary gammas must definitely be considered!

To prevent undue concern from developing prematurely, however, two important facts (demonstrated below) should probably be mentioned at this time:

1) Because the secondary gammas are born isotropically near the hot end of the water tube (a considerable distance from the location of interest on the downstream side of the collimator), while the primary gammas impingent on the water tube are already pretty well collimated and travelling directly towards the location of interest, the latter are ultimately far more important.

2) By the time one gets further down the water tube and the water-filled collimator section, most of the lower energy gammas below 2 or 3 MeV which had been impingent on the water tube or born as secondaries near the hot end of the water tube have been pretty well attenuated, while the 6-8 MeV gammas impingent on the water tube have experienced far less attenuation. Thus, despite their fewer numbers, the primary gammas impingent on the water tube in this energy range (6-8 MeV) are the ones that ultimately determine the gamma dose rate impingent on the rotary shutter downstream of the water-filled collimator.

The balance of Sects 5.4 and 5.5 describe the calculations necessary to support these claims.

To begin assessing the effect of secondary gammas on the dose rate downstream of the collimator, consider Case 1 (above) where, with a coupled neutron-gamma source impingent on the first aluminum window of the beam tube (at Z=174.27 cm), the 61n/23g 1-D ANISN slab calculation showed the gamma dose rate at Z=399.48 cm to be 4.04834e+6 mrem/hr. In Case 4, the 18** (multigroup source specification) array was altered so as to "zero out" all of the impingent neutron sources, thereby precluding the production of any secondary gammas. Surprisingly, the calculated gamma dose rate at Z=399.48 cm was then found to be 3.96216e+6 mrem/hr, which is only 2.1% lower!

To investigate further and verify that energetic secondary gammas were indeed being generated in the vast numbers expected (in Case 1), another perturbation was run. In Case 5, the 18** (multigroup source specification) array was altered so as to "zero out" all of the impingent gamma sources while maintaining all of the impingent neutron sources. As with Case 1, the direct neutron dose rate at Z=399.48 cm was again found to be 4.62647e-2 mrem/hr (as expected) and, consistent with the 2.1% change noted above, the secondary gamma dose rate at Z=399.48 cm was found to be 8.61865e+4 mrem/hr. The main purpose of this calculation, however, was to determine the gamma production rates (by energy group) in the first and second aluminum windows of the water tube, and in all the water in between, especially in the first eight 4.1-cm-thick regions (zones 5-12) near the hot end of the water tube. Table 5.3 shows the number of secondary gammas (p/s) produced in each gamma energy group in zones 4 through 14 of this particular 1-D

slab model (Case 5) where the 61-group neutron source impingent on the first aluminum window (zone 4) has the same intensity (n/s/cm2) and energy distribution as the 61-group neutron source impingent on the first aluminum window of the 1998 water tube at Z=174.27 cm. Results shown here were obtained by folding the "volume integrated" 61-group neutron fluxes in each zone (as given by the ANISN balance tables for each zone) with the appropriate elements of the 84 grp x 84 grp macroscopic scattering cross section matrix for water (in zones 5-13), and/or for aluminum (in zones 4 and 14). In the first aluminum window (zone 4) there are a significant number of secondary gammas being generated in the 2-10 MeV energy range, while at the second aluminum window, the neutron flux had been so attenuated that the secondary gamma source there was clearly insignificant. In the case of the water, the huge spike between 2.0 and 2.5 MeV is quite apparent. This is due to thermal neutron capture in the hydrogen, which produces a well-known 2.2 MeV gamma. This secondary gamma production rate at 2.2 MeV appears to decrease by about an order of magnitude every 8.2 cm (or so), with the vast majority clearly being generated in the first 10-20 cm of the water. Note that the secondary gamma production rates (p/s) shown in this table have already been integrated over the volume of each zone, where for the purpose of calculating volumes in an infinite 1-D slab calculation, the code uses a unit area (1 cm x 1 cm) times the thickness of each zone, and the impingent source is automatically assumed to be per unit area. The source terms shown here in Table 5.3 were later used in a point kernel QAD-like code (QADD3) as noted below in Sect 5.5. Before that, however, the other data available from this 1-D slab calculation was used to verify the reasonableness of the secondary gamma production rate, as noted at the bottom of Table 5.3. Here in Case 5, the impingent neutron source at the left of zone 4 was 7.51812e+11 n/s/cm2, when integrated over all energy groups. From the system balance table, however, it is known that the total number of neutrons reflected back to the left (ie, back out of the system) was 5.21766e+11 n/s/cm2, when integrated over all energy. Given that the leakage out the right is totally negligible, this means that the total number of neutrons that remained resident in the system (and were ultimately captured) is given by the difference (impingent-reflected), or 2.30046e+11 n/s/cm2. Table 5.3 also shows the total number of secondary gammas produced in each zone, from which we see the total number of secondary gammas produced in the entire system is 2.44948e+11 p/s (per unit source area). Thus the number of secondary gammas produced in the system per "resident" neutron is 1.065 (=2.44948e+11/2.30046e+11). This is slightly greater than one because of a few secondary gammas produced while the faster neutrons were slowing down. Nevertheless, this value of 1.065 secondary gammas per resident neutron is eminently reasonable and should dispel any fears that the code or data might not be producing as many gammas as it should be. The key thing to note, however, is that the rule should really say that "about one secondary gamma is produced per 'resident' neutron" (as opposed to "per impingent neutron") since many can be reflected back out of the system.

5.5 Primary and Secondary Gamma Dose Rates Based on a QAD-like Procedure

The 1-D ANISN runs (Cases 4 and 5 in Sect 5.4) show clearly that the component of the total gamma dose rate downstream of the collimator due to secondary gamma production is negligible relative to that caused by the well-collimated high-energy primary gammas streaming down the beam tube and impinging on the water tube -- provided the secondary gamma production rate was correctly accounted for. Having shown in Sect 5.4 that the "number of secondary gammas produced per resident neutron" was eminently reasonable, all doubt should be removed. Initially, however, there remained a desire to understand why their contribution to the total gamma dose rate downstream of the collimator was "so" low, given prior speculation to the contrary. To aid in that understanding, a QAD-like point kernel shielding program was written which would utilize the multigroup secondary gamma source terms in Table 5.3, calculate the total gamma dose rate downstream of the collimator based on a more realistic finite geometry, and list the actual and relative contribution from secondary gammas along each segment of the beam tube, as well as the contribution from the original (impingent) primary gammas, along with the relative contribution from each energy group. Because of its simplicity, it could be used to easily make parametric comparisons of the dose rates downstream of either the 1960 or 1998 water tubes, while its multigroup capability would allow us to determine which gamma groups were of greatest ultimate importance -- knowledge that could be potentially useful in source energy biasing of more rigorous MCNP gamma-only calculations. Lastly, because of its multigroup capability and its ability to include secondary gammas, it should be much more accurate that the 3-group formula described above, while at the same time providing a reality check for the still-more-rigorous gamma-only MCNP calculations (Runs HB307C and HB307D) mentioned earlier and described in Appendix C.6.

This useful QAD-like point kernel code (originally called QADD, but recently upgraded to QADD3) is listed in its entirety in Appendix C.8. Some of the key features are described below:

1) The code uses a single water-filled region to simulate the flooded water tube and the flooded hole up the middle of the collimator. If simulating the 1998 water tube, this region extends from Z=174.27 cm to Z=400.0 cm; if simulating the 1960 water tube, this region extends from Z=116.7841 cm to Z=400.0 cm. In both cases we want to calculate the total gamma dose rate at a point (X=0,Y=0,Z=400) located immediately downstream of the flooded collimator section, just

Table 5.3. Number of secondary gammas produced in each gamma energy group in zones 4 through 14 of the 1-D slab model given that the 61-group neutron source impingent on the first aluminum window here (zone 4) has the same intensities (n/s/cm2) as the 61-group neutron source impingent on the first aluminum window of the 1998 water tube at Z=174.27 cm. Results shown here were obtained by folding the "volume integrated" 61-group neutron fluxes in each zone (as given by the ANISN balance tables for each zone) with the 84 grp x 84 grp macroscopic scattering cross section matrix (for H2O in zones 5-13, and AL in zones 4 and 14).

Grp	Emin (MeV)	Emax (MeV)	Zone 4 Aluminum 1 cm x 1 cm x 0.68123 cm	Zone 5 Water 1 cm x 1 cm x 4.1 cm	Zone 6 Water 1 cm x 1 cm x 4.1 cm	Zone 7 Water 1 cm x 1 cm x 4.1 cm	Zone 8 Water 1 cm x 1 cm x 4.1 cm	Zone 9 Water 1 cm x 1 cm x 4.1 cm	Zone 10 Water 1 cm x 1 cm x 4.1 cm	Zone 11 Water 1 cm x 1 cm x 4.1 cm	Zone 12 Water 1 cm x 1 cm x 4.1 cm	Zone 13 Water 1 cm x 1 cm x 94.4368 cm	Zone 14 Aluminum 1 cm x 1 cm x 0.317505 cm
62	10.0	14.0	1.65693E+05	0.00000E+00	0.00000E+00	0.00000E+00	0.00000E+00	0.00000E+00	0.00000E+00	0.00000E+00	0.00000E+00	0.00000E+00	1.68222E-02
63	8.0	10.0	1.03877E+08	8.88559E+03	6.37610E+03	4.55434E+03	3.22882E+03	2.27301E+03	1.59042E+03	1.10705E+03	7.67212E+02	1.68139E+03	5.99439E-01
64	7.5	8.0	4.82814E+09	9.59494E+01	6.89209E+01	4.92781E+01	3.49680E+01	2.46371E+01	1.72517E+01	1.20170E+01	8.33348E+00	1.82933E+01	1.80289E+01
65	7.0	7.5	2.38268E+08	3.91174E+05	2.76269E+05	1.94118E+05	1.35468E+05	9.39502E+04	6.48112E+04	4.45103E+04	3.04543E+04	6.44523E+04	1.12970E+00
66	6.0	7.0	1.18343E+09	3.04019E+06	2.11984E+06	1.46872E+06	1.01054E+06	6.91105E+05	4.70301E+05	3.18745E+05	2.15317E+05	4.40025E+05	5.30501E+00
67	5.0	6.0	1.57892E+09	4.22477E+03	2.79421E+03	1.83745E+03	1.19857E+03	7.76536E+02	5.00467E+02	3.21267E+02	2.05635E+02	3.62459E+02	7.76747E+00
68	4.0	5.0	5.19572E+09	1.61134E+04	1.00417E+04	6.15986E+03	3.73237E+03	2.24836E+03	1.35232E+03	8.14333E+02	4.91786E+02	7.73206E+02	2.19504E+01
69	3.0	4.0	4.68252E+09	6.70271E+06	2.91323E+06	1.26436E+06	6.39792E+05	3.70233E+05	2.31858E+05	1.51024E+05	1.00195E+05	2.04432E+05	2.49267E+01
70	2.5	3.0	2.84097E+09	2.55717E+05	1.40053E+05	7.91040E+04	4.76683E+04	3.02080E+04	1.97580E+04	1.31609E+04	8.85560E+03	1.86359E+04	1.49176E+01
71	2.0	2.5	1.67960E+09	1.38337E+11	5.16124E+10	1.64938E+10	5.42936E+09	1.94765E+09	7.72685E+08	3.36978E+08	1.58952E+08	1.74253E+08	1.68884E+01
72	1.5	2.0	1.14845E+09	2.06225E+04	1.47981E+04	1.05700E+04	7.49358E+03	5.27525E+03	3.69105E+03	2.56923E+03	1.78053E+03	3.90208E+03	8.74875E+00
73	1.0	1.5	9.92435E+08	3.16644E+07	1.18137E+07	3.77533E+06	1.24275E+06	4.45807E+05	1.76865E+05	7.71333E+04	3.63838E+04	3.98865E+04	1.65612E+01
74	0.70	1.0	7.10282E+08	3.70816E+07	1.38360E+07	4.42251E+06	1.45641E+06	5.22848E+05	2.07670E+05	9.07106E+04	4.28715E+04	4.72743E+04	1.01142E+01
75	0.60	0.70	6.83261E+07	0.00000E+00	0.00000E+00	0.00000E+00	0.00000E+00	0.00000E+00	0.00000E+00	0.00000E+00	0.00000E+00	0.00000E+00	3.10489E-01
76	0.51	0.60	4.90984E+07	4.01537E+03	2.83340E+03	1.98907E+03	1.38687E+03	9.61004E+02	6.62406E+02	4.54572E+02	3.10800E+02	6.56607E+02	2.30460E-01
77	0.40	0.51	1.75864E+08	3.61894E+06	2.50670E+06	1.72378E+06	1.17681E+06	7.98498E+05	5.39134E+05	3.62578E+05	2.43076E+05	4.86456E+05	6.92917E-01
78	0.30	0.40	1.30021E+08	3.18702E+03	2.28955E+03	1.63726E+03	1.16199E+03	8.18824E+02	5.73463E+02	3.99523E+02	2.77109E+02	6.08684E+02	5.21942E-01
79	0.15	0.30	6.87302E+07	1.41722E+05	1.00739E+05	7.12619E+04	5.00562E+04	3.49321E+04	2.42419E+04	1.67440E+04	1.15195E+04	2.47550E+04	6.53672E-01
80	0.10	0.15	1.55946E+07	1.35356E+04	9.72390E+03	6.95354E+03	4.93501E+03	3.47757E+03	2.43551E+03	1.69677E+03	1.17688E+03	2.58502E+03	6.43597E-02
81	0.070	0.10	2.82638E+06	0.00000E+00	0.00000E+00	0.00000E+00	0.00000E+00	0.00000E+00	0.00000E+00	0.00000E+00	0.00000E+00	0.00000E+00	1.40324E-02
82	0.045	0.070	1.72677E+07	0.00000E+00	0.00000E+00	0.00000E+00	0.00000E+00	0.00000E+00	0.00000E+00	0.00000E+00	0.00000E+00	0.00000E+00	6.78809E-02
83	0.020	0.045	3.80053E+09	0.00000E+00	0.00000E+00	0.00000E+00	0.00000E+00	0.00000E+00	0.00000E+00	0.00000E+00	0.00000E+00	0.00000E+00	1.40403E+01
84	0.010	0.020	3.08735E+07	0.00000E+00	0.00000E+00	0.00000E+00	0.00000E+00	0.00000E+00	0.00000E+00	0.00000E+00	0.00000E+00	0.00000E+00	1.19169E-01
sum	0.010	14.00	2.95419E+10	1.38420E+11	5.16462E+10	1.65069E+10	5.43514E+09	1.95065E+09	7.74430E+08	3.38060E+08	1.59646E+08	1.75590E+08	1.63670E+02

animpg = 7.51812E+11 = number of neutrons (per cm2) impingent on system
anrefl = 5.21766E+11 = number of neutrons (per cm2) reflected back out to the left, almost immediately
anresi = 2.30046E+11 = number of neutrons (per cm2) resident in system, neglecting the very few that leak out far right side
secgam = 2.44948E+11 = number of secondary gammas produced (per cm2) in system; obtained by summing above data
secgpn = 1.06478E+00 = number of secondary gammas produced in system per resident neutron; where secgpn=secgam/anresi

upstream of the rotary shutter shield plug (not modeled).

2) The code considers two kinds of point sources, those corresponding to the original (primary) gamma sources in the voided beam tube to the left of the water region described above, and secondary gamma sources located throughout the water region.

   a) The original (primary) gamma sources: (iloc=-1)

      These are the original 23-group gamma point sources listed in Table 2.2b. While the code refers to these collectively as "source location -1" (iloc= -1), the point of origin for gammas in each energy group remains as shown in Table 2.2b. These locations and source intensities remain invariant whether one is analyzing the 1998 water tube or the 1960 water tube.

   b) The secondary gamma sources: (iloc=0,1,2,3,4,5,6,7,8)

      1. In the case of the 1998 water tube:

         These correspond to the 23-group secondary gamma sources (p/s) shown in Table 5.3. Source location 0 (iloc=0) in QADD corresponds to the first aluminum window, known as Zone 4 in Table 5.3, while source locations iloc=1 to 8 in the point kernel code correspond to the "midpoints" of Zones 5 through 12 in Table 5.3, while the far less intense sources in Zones 13 and 14 in Table 5.3 are presently ignored. That is: the point sources in the first aluminum window are located at X=0, Y=0, Z=174.61 cm (as in the real 1998 water tube), while the point sources in the first 4.1-cm-thick water region are located at X=0, Y=0, Z=177.0 cm, and those in the remaining seven 4.1-cm-thick increments of water are located at Z=181.1 cm, Z=185.2 cm, etc.

         Since the source terms in Table 5.3 are "per unit area" perpendicular to the impingent neutron source in the 1-D slab calculation, the point kernel code multiplies them by the area of the water tube perpendicular to the impingent neutron source (in this case: pi*r*r, where r=7.03453 cm is the inner radius of the 1998 water tube). This same factor is used when analyzing the 1960 water tube. In both cases, this is intentionally very conservative. Moreover, in both cases, the value of "r" should probably be 5.08 cm, the inner radius of the beam tube itself, since the effective area of the neutron beam producing the secondary gammas is likely to be no bigger than the inside area of the beam tube, regardless of the diameter of the water tube downstream. Nevertheless, this was deemed a small concession to conservatism.

      2. In the case of the 1960 water tube, the secondary gamma sources (p/s) are basically the same as described above, with the following two exceptions:

         a. The source locations (X,Y,Z) are all shifted to the left by an amount, dZ=(174.27-116.7841) cm, so as to be at the corresponding locations in the 1960 water tube model.

         b. The secondary gamma sources are also multiplied by the ratio of the impingent neutron flux for the 1960 water tube to impingent neutron flux for the 1998 water tube. This is because the multigroup secondary gamma source terms in Table 5.3 were based on a 1-D calculation in which the impingent neutron flux (7.51812e11 n/s/cm2) was essentially identical to that impingent on the first aluminum window in the 1998 water tube at Z=174.27 cm (7.55818E+11 n/s/cm2), while in the 1960 water tube case, the first aluminum window is located at Z=116.7841 cm where the impingent neutron flux generating the secondary gammas is significantly higher (4.48493e+12 n/s/cm2).

3) In the 1/(4*pi*R^2) geometric dilution term, the distance used is simply the real distance between each source point and the detector location at (X=0,Y=0,Z=400 cm), while in the exponential attenuation term, the distance used depends on the amount of water between the source point and the detector point. For the secondary gamma point sources located in the water, these two distances are the same, but for the original (primary) gamma point sources, these two distances are different.

4) The energy-dependent mass attenuation coefficients (cm2/g) used here for the hydrogen and oxygen comprising the water (at 1.0 g/cc) correspond to the "Hubble 28-group mass attenuation coefficients for H and O" found in ascii format in the FORT10 dataset in the QAD-CGGP code package#20 distributed by the Radiation Shielding Information Center in Oak Ridge. The actual values of these coefficients at the original 28 gamma energies used in QAD are listed in Appendix C.8. Conversion of those coefficients from that original 28-group structure to the present VELM 23-group gamma structure#10 was accomplished using the group-to-group mapping illustrated in Appendix C.8. This remapping allowed us to calculate the multigroup fluxes at the point of interest (X=0,Y=0,Z=400 cm) in the same group structure as the source terms used throughout the rest of this report, and then apply the VELM 23-gamma-group flux-to-dose-rate conversion factors based on the 1977 ANSI Standard#19. These 23-group flux-to-dose-rate conversion factors are also listed in Appendix C.8.

5) Dose rate "build up factors", traditionally used in many point kernel shielding analyses, were not used in the QADD3 program because their use here would have been inappropriate. Typically they are used when one has a large spatially distributed shield around a volume of radioactive material, and one needs to account for the dose rate coming not just from gammas along a precise, very narrow, line of sight from the source, but also from collisions that occur in the neighboring shield material some distance to either side of a direct line from the source, but nevertheless somewhat close to the surface of the shield. In Monte Carlo parlance, these would be called "last flight" contributions or next to last flight contributions. With most point kernel methods, one takes the direct line of sight attenuated fluxes or dose rates and then multiplies the results by a correction factor or "build up factor" which has been determined in advance (either empirically by experiment, or by extensive higher-order analytic calculations) to obtain the correct "adjusted" result for many typical (simple) situations involving such shields. Indeed, if one had a large pool of water in place of the biological shield and/or the steel collimator and radial and eccentric shields, such an approach would be quite justified. For gammas streaming through the small water-filled rectangular hole in the collimator, however, that is not the case. Directly in front of the small 2.75-inch x 5.5-inch water-filled hole, the gamma dose rate is indeed very high because of gammas streaming through the water. If one goes more than 2 or 3 inches off to the side of the centerline, however, the gamma flux is heavily shielded and drastically lower. Moreover, in this case, one does not have similar contributions from a vast array of nearby points in similar (water-like) materials, and to apply a build-up correction factor based on that assumption would be clearly inappropriate in this particular situation.

6) After calculating the total cumulative gamma dose rate at the point of interest for either the 1960 or 1998 water tube, the total contribution from each source region (iloc=-1,0,1,2,3,4,5,6,7,8) is printed along with the cumulative total. In addition, the fraction of the total gamma dose rate contributed from each source energy group at each source location is also tabulated, sorted, and printed in decreasing order so that one can easily discern the relative importance by energy group and source location.

This handy little program has provided a wealth of helpful information and useful insights.

Table 5.4 shows the QADD3 point kernel estimates of the total gamma dose rate downstream of the flooded collimator section based on both the 1998 water tube design and the original 1960 water tube design. These dose rates would exist just upstream of the rotary shutter when the water tube and collimator sections are both flooded and the HFIR is operating at 100 MW. In each case, Table 5.4 also shows the portion of the total dose rate at Z=400 cm due to (1) the original primary gammas which come from the hot end of the HB-3 beam tube and impinge directly the water tube, (2) the secondary gammas generated by neutrons in the first aluminum window, and (3) secondary gammas generated by neutrons in each of the first eight 4.1-cm increments of the water tube. Note that while the secondary gamma source terms in Table 5.3 were dropping off by about an order of magnitude every 8.2 cm in the water, the dose rate due to these secondary gammas in each increment of water is dropping off somewhat less rapidly since each successive increment experiences less and less attenuation. Nevertheless, it is clear that even these contributions are negligible and decreasing. Moreover, while it was clear from the previous section that the photon energy density due to secondary gammas at the hot end of the water tube was comparable to that coming from the primary (impingent) gammas, it is now equally clear from Table 5.4 that the reason these numerous energetic secondary gammas born near the hot end of the beam tube do not contribute significantly to the dose rate at the point of interest (Z=400 cm) is precisely because they are born isotropically and their areal density (flux) at this distant location is greatly diminished relative to the original primary gammas which were also born isotropically but were fairly well collimated by the time they entered the water tube. Moreover, it is also clear from Table 5.4 that the dose rate contributions from secondary gammas born in the water tube are actually much more negligible than previously indicated by the 1-D slab analyses corresponding to Cases 4 and 5 in Sect 5.4. Based on this finding, and the previous findings regarding the direct neutron dose rates impingent on the rotary shutter, there is simply no further need of any detailed 3-D MCNP water tube shielding analyses for either neutrons or secondary gammas. Detailed rigorous analyses are still required, however, for the gamma-only problem involving the original primary gammas streaming down the beam tube and impinging on the water tube since these do contribute significantly to the dose rate impingent on the rotary shutter.

Before concluding this discussion, however, at least one or two other points are in order.

First, it is informative to review (one last time) what is known about the total gamma dose rate impingent on the rotary shutter based on the three analytic techniques mentioned in this section: the elementary 3-group formula, the point kernel results presented here, and the semi-rigorous (although still not perfect) MCNP results mentioned above and in Appendix C.6. Table 5.5 summarizes the results obtained for the total gamma dose rate at Z=400 cm by these three independent techniques. Note, for example, that all three techniques are in excellent agreement. Moreover, the simple 23-group point kernel technique yields results that are within 1% of the most highly advanced state-of-the-art final MCNP reference run (HB308G5) described in Sect 6. Even more surprising is that the simple 3-group formula presented in Sect 5.2 is within 13-14% of the final reference solution.

Table 5.4. QADD3 point kernel results showing the total gamma dose rate downstream of the flooded collimator section (for the 1998 and 1960 HB-3 water tubes), and estimates of the relative dose rates there due to the original primary (impingent) gammas, secondary gammas in the first aluminum window, and secondary gammas in the first 32.8 cm of water, in eight 4.1-cm increments. These dose rates would exist just upstream of the rotary shutter when the water tube and collimator sections are both flooded and the HFIR is operating at 100 MW.

		For 1998 water tube	For 1960 water tube
Dose rate due to src loc -1 (primary gammas in HB3)	=	1.02952E+05 mrem/hr	2.38587E+04 mrem/hr
Dose rate due to src loc 0 (first aluminum window)	=	6.59302E+01 mrem/hr	5.75822E+01 mrem/hr
Dose rate due to src loc 1 (1st 4.1-cm water seg)	=	1.73852E+01 mrem/hr	6.69047E+00 mrem/hr
Dose rate due to src loc 2 (2nd 4.1-cm water seg)	=	7.92927E+00 mrem/hr	3.03324E+00 mrem/hr
Dose rate due to src loc 3 (3rd 4.1-cm water seg)	=	3.10514E+00 mrem/hr	1.18317E+00 mrem/hr
Dose rate due to src loc 4 (4th 4.1-cm water seg)	=	1.25670E+00 mrem/hr	4.78499E-01 mrem/hr
Dose rate due to src loc 5 (5th 4.1-cm water seg)	=	5.56537E-01 mrem/hr	2.12604E-01 mrem/hr
Dose rate due to src loc 6 (6th 4.1-cm water seg)	=	2.73695E-01 mrem/hr	1.05289E-01 mrem/hr
Dose rate due to src loc 7 (7th 4.1-cm water seg)	=	1.48445E-01 mrem/hr	5.76366E-02 mrem/hr
Dose rate due to src loc 8 (8th 4.1-cm water seg)	=	8.72652E-02 mrem/hr	3.42147E-02 mrem/hr
Total gamma dose rate at Z=400 cm	=	1.03048E+05 mrem/hr	2.39281E+04 mrem/hr

Table 5.5. Gamma dose rates impingent on the rotary shutter as given by the 3-group formula (which did not include secondary gammas, the 23-group point kernel method that did include secondary gammas, and the preliminary MCNP runs (HB307C and HB307D) which did not include secondary gammas.

	For the 1998 water tube	For the 1960 water tube
3-Group Formula:	90.23 Rem/hr	19.58 Rem/hr
Point Kernel Method (QADD3):	103.05 Rem/hr	23.93 Rem/hr
Preliminary MCNP Runs:	109.31 Rem/hr	26.77 Rem/hr
Final MCNP Ref Run (HB308G5): described in Sect 6	103.99 Rem/hr	----- Rem/hr

Table 5.6. Cumulative fractional gamma dose rates at Z=400 cm as given by the QADD3 point kernel code for the "Top 25" contributors, in terms of source location and source energy group, ranked in order of importance, for the 1998 and 1960 HB-3 water tube shielding problem.

For the 1998 water tube:

Rank= 1	Loc=-1	Grp= 3	Cumulative fractional gamma dose rate at Z=400 cm:	0.411054100
Rank= 2	Loc=-1	Grp= 5	Cumulative fractional gamma dose rate at Z=400 cm:	0.704645200
Rank= 3	Loc=-1	Grp= 7	Cumulative fractional gamma dose rate at Z=400 cm:	0.799076600
Rank= 4	Loc=-1	Grp= 6	Cumulative fractional gamma dose rate at Z=400 cm:	0.866660500
Rank= 5	Loc=-1	Grp= 4	Cumulative fractional gamma dose rate at Z=400 cm:	0.908384900
Rank= 6	Loc=-1	Grp= 8	Cumulative fractional gamma dose rate at Z=400 cm:	0.949603500
Rank= 7	Loc=-1	Grp= 2	Cumulative fractional gamma dose rate at Z=400 cm:	0.980754100
Rank= 8	Loc=-1	Grp= 10	Cumulative fractional gamma dose rate at Z=400 cm:	0.991010100
Rank= 9	Loc=-1	Grp= 9	Cumulative fractional gamma dose rate at Z=400 cm:	0.997165000
Rank= 10	Loc=-1	Grp= 11	Cumulative fractional gamma dose rate at Z=400 cm:	0.998673200
Rank= 11	Loc= 0	Grp= 3	Cumulative fractional gamma dose rate at Z=400 cm:	0.999051500
Rank= 12	Loc=-1	Grp= 12	Cumulative fractional gamma dose rate at Z=400 cm:	0.999284000
Rank= 13	Loc= 1	Grp= 10	Cumulative fractional gamma dose rate at Z=400 cm:	0.999452400
Rank= 14	Loc=-1	Grp= 1	Cumulative fractional gamma dose rate at Z=400 cm:	0.999595700
Rank= 15	Loc= 0	Grp= 5	Cumulative fractional gamma dose rate at Z=400 cm:	0.999677500
Rank= 16	Loc= 2	Grp= 10	Cumulative fractional gamma dose rate at Z=400 cm:	0.999754300
Rank= 17	Loc= 0	Grp= 7	Cumulative fractional gamma dose rate at Z=400 cm:	0.999826600
Rank= 18	Loc= 0	Grp= 6	Cumulative fractional gamma dose rate at Z=400 cm:	0.999871900
Rank= 19	Loc= 3	Grp= 10	Cumulative fractional gamma dose rate at Z=400 cm:	0.999901800
Rank= 20	Loc= 0	Grp= 8	Cumulative fractional gamma dose rate at Z=400 cm:	0.999926000
Rank= 21	Loc= 0	Grp= 4	Cumulative fractional gamma dose rate at Z=400 cm:	0.999943800
Rank= 22	Loc= 0	Grp= 2	Cumulative fractional gamma dose rate at Z=400 cm:	0.999958400
Rank= 23	Loc=-1	Grp= 13	Cumulative fractional gamma dose rate at Z=400 cm:	0.999970500
Rank= 24	Loc= 4	Grp= 10	Cumulative fractional gamma dose rate at Z=400 cm:	0.999982500
Rank= 25	Loc= 5	Grp= 10	Cumulative fractional gamma dose rate at Z=400 cm:	0.999987800

For the 1960 water tube:

Rank= 1	Loc=-1	Grp= 3	Cumulative fractional gamma dose rate at Z=400 cm:	0.438447900
Rank= 2	Loc=-1	Grp= 5	Cumulative fractional gamma dose rate at Z=400 cm:	0.751604700
Rank= 3	Loc=-1	Grp= 7	Cumulative fractional gamma dose rate at Z=400 cm:	0.822877600
Rank= 4	Loc=-1	Grp= 6	Cumulative fractional gamma dose rate at Z=400 cm:	0.882121800
Rank= 5	Loc=-1	Grp= 4	Cumulative fractional gamma dose rate at Z=400 cm:	0.926626900
Rank= 6	Loc=-1	Grp= 2	Cumulative fractional gamma dose rate at Z=400 cm:	0.964102400
Rank= 7	Loc=-1	Grp= 8	Cumulative fractional gamma dose rate at Z=400 cm:	0.989245400
Rank= 8	Loc=-1	Grp= 10	Cumulative fractional gamma dose rate at Z=400 cm:	0.993766800
Rank= 9	Loc=-1	Grp= 9	Cumulative fractional gamma dose rate at Z=400 cm:	0.996480200
Rank= 10	Loc= 0	Grp= 3	Cumulative fractional gamma dose rate at Z=400 cm:	0.998000300
Rank= 11	Loc=-1	Grp= 11	Cumulative fractional gamma dose rate at Z=400 cm:	0.998380500
Rank= 12	Loc= 0	Grp= 5	Cumulative fractional gamma dose rate at Z=400 cm:	0.998709400
Rank= 13	Loc= 1	Grp= 10	Cumulative fractional gamma dose rate at Z=400 cm:	0.998987900
Rank= 14	Loc= 0	Grp= 7	Cumulative fractional gamma dose rate at Z=400 cm:	0.999193700
Rank= 15	Loc=-1	Grp= 1	Cumulative fractional gamma dose rate at Z=400 cm:	0.999396000
Rank= 16	Loc= 0	Grp= 6	Cumulative fractional gamma dose rate at Z=400 cm:	0.999545300
Rank= 17	Loc= 2	Grp= 10	Cumulative fractional gamma dose rate at Z=400 cm:	0.999671200
Rank= 18	Loc= 0	Grp= 4	Cumulative fractional gamma dose rate at Z=400 cm:	0.999742700
Rank= 19	Loc= 0	Grp= 2	Cumulative fractional gamma dose rate at Z=400 cm:	0.999808800
Rank= 20	Loc= 0	Grp= 8	Cumulative fractional gamma dose rate at Z=400 cm:	0.999864300
Rank= 21	Loc= 3	Grp= 10	Cumulative fractional gamma dose rate at Z=400 cm:	0.999913000
Rank= 22	Loc=-1	Grp= 12	Cumulative fractional gamma dose rate at Z=400 cm:	0.999949800
Rank= 23	Loc= 4	Grp= 10	Cumulative fractional gamma dose rate at Z=400 cm:	0.999969200
Rank= 24	Loc= 5	Grp= 10	Cumulative fractional gamma dose rate at Z=400 cm:	0.999977700
Rank= 25	Loc= 0	Grp= 9	Cumulative fractional gamma dose rate at Z=400 cm:	0.999983500

Lastly, it is potentially helpful to future MCNP analyses to review some additional QADD3 point kernel results not shown in Table 5.4. Table 5.6, for example, shows the cumulative fractional gamma dose rates at Z=400 cm, as given by the QADD3 point kernel code for the "Top 25" contributors -- i.e., the contributions from each source location and each source energy group as ranked in order of importance, for the 1998 and 1960 HB-3 water tube shielding problems. Valuable insights on how to run future MCNP gamma-only calculations more efficiently can be gained from studying this type of information.

Having looked at "the rankings" in Table 5.6 and being content that one can safely ignore the contributions from all secondary gammas born in source locations 0-8, it may actually be more useful to remove "the rankings" and retally the cumulative fractional total gamma dose rates by energy group, first for source region -1 (the original "primary" gammas streaming down the beam tube), and then all other secondary gamma source regions. This particular sorted list is not exactly the same as Table 5.6, but it is very similar.

For the 1960 water tube, one would see that:

Group 1- 7 sources (of the primary gammas) contribute 96.430% of the final gamma dose
Group 1- 8 sources (of the primary gammas) contribute 98.945% of the final gamma dose
Group 1-11 sources (of the primary gammas) contribute 99.706% of the final gamma dose
Group 1-12 sources (of the primary gammas) contribute 99.710% of the final gamma dose

and that all other sources can be neglected for all practical purposes in a 3-D MCNP analysis. Moreover, in the MCNP analysis, even if does consider only the primary gamma sources in groups 1-12, there still may be some concern about under sampling the energetic gammas in group 1 since the source strength there is so much less than the source strength in the other groups. (cf Table 2.2b). Results in Table 5.6 should alleviate that anxiety, since examination of that data shows that group 1 gammas, while energetic, only contribute about 0.020% of the total gamma dose rate at the desired location (Z=400 cm) just downstream of the water-filled collimator.

Likewise, for the shorter 1998 water tube, one would see that:

Group 1- 8 sources (of the primary gammas) contribute 98.090% of the final gamma dose
Group 1-11 sources (of the primary gammas) contribute 99.882% of the final gamma dose
Group 1-12 sources (of the primary gammas) contribute 99.905% of the final gamma dose

and that all other sources can be neglected for all practical purposes in a 3-D MCNP analysis. In this case, examination of the results in Table 5.6 shows that group 1 gammas, while energetic, only contribute about 0.014% of the total gamma dose rate at the desired location (Z=400 cm) just downstream of the water-filled collimator. [In this case, while their actual contribution (in terms of mrem/hr) does in fact go up because of the shorter water tube, their relative fractional contribution is slightly less because contributions from other energy groups and source locations have gone up more.]

What does this mean in terms of how one might optimize the gamma-only MCNP analysis? First, it means that one can safely ignore all secondary gamma sources. Secondly, it means that even groups 13-23 of the primary gamma source (Table 2.2b) could be safely ignored as well. Third, it means that one might also want to consider ignoring the primary gammas in groups 8-12 as well. Consider this: In a straight analog Monte Carlo simulation, the running time is roughly proportional to the number of histories that must be run. To run "x" number of histories for sources in groups 1-8 would, would require running "y" number of histories in groups 9-12 where, in the absence of any source energy biasing, x and y would be proportional to the number of source gammas (p/s) in these respective energy ranges. From Table 2.2b, we see that the point sources in VELM groups 1-8 represent 7.984211e15 p/s, while the point sources in VELM groups 1-12 represent 2.160073e16 p/s. Therefore, if one includes groups 9-12 (with no source energy biasing), the calculation will take 3 times longer and would change the calculated total gamma dose rate only by a minuscule amount. From Table 5.6, we see that the expected change in the total gamma dose rate at Z=400 cm would only amount to 1.815% in the case of the 1998 water tube, or 0.765% in the case of the 1960 water tube. Moreover, the CPU time would be much better spent running additional histories for sources in groups 1-8.

To take this example one step further, assume one decided to include just the source terms in gamma groups 1-8, instead of all the source terms in groups 1-23, what kind of calculational savings could be realized, and at what cost in terms of precision? Again assuming no source energy biasing, and that one needed "x" number of histories in groups 1-8 to get adequate dose rate statistics in both cases, the amount of running time required would be roughly proportional to the number of source gammas in both calculations:

$$\frac{\text{Sources in VELM groups 1-23} = 1.35399\text{e+}17 \text{ p/s}}{\text{Sources in VELM groups 1- 8} = 7.984211\text{e+}15 \text{ p/s}} \Rightarrow \text{Ratio} = 16.96$$

Thus, by running only VELM source groups 1-8 (which account for 98-99% of the total gamma dose

rate just downstream of the flooded collimator, the calculation should run about 17 times faster than if one tried to include the sources from all 23 gamma groups. Given that even the shorter of the two calculations may take on the order of 1 or 2 CPU days on each of 8 nodes on the ORNL SP2 computer, the choice is clear since the longer more-inclusive calculation would be quite prohibitive. Moreover, this is a good example of where and how an understanding of the physics, gleaned from relatively simple methods, can serve as a valuable guide to more rigorous analyses that would otherwise be doomed to failure. (In practice, the use of broad-group "geometry independent weight windows" based on fine-group adjoint analyses, in conjunction with the 3-D MCNP model, as described in Sect 6 and used in the final analysis, is far more powerful than the simplistic approach outlined here. In the absence of the state-of-the-art techniques described in Sect 6, however, the simplistic considerations outlined here still serve as valuable guidance.)

5.6 Conclusions Regarding Neutron and Secondary Gamma Dose Rates

In absolute terms, and relative to the total dose rate just upstream of the rotary shutter (with the HFIR operating at 100 MW and the HB-3 water tube and collimator sections both flooded), the direct neutron dose rate at that location is totally negligible. This is based on elementary hand calculations, and was confirmed by conservative 1-D slab calculations using the VELM cross section library with 61 neutron energy groups and 23 gamma groups.

Likewise, the dose rate at this location due to secondary gammas produced by the neutrons at the hot end of the water tube under these conditions is also totally negligible when compared to the dose rate at the shutter due to primary gammas streaming down the beam tube and impinging on the water tube. This was also based on a conservative 1-D slab calculation using the VELM cross section library with 61 neutron energy groups and 23 gamma groups. Further investigations with a 23-group point kernel code have confirmed that this is the case because of the isotropic nature of the secondary gamma source terms and the relatively distant location where they are produced. Moreover, separate offline QA checks on the intensities of the secondary gammas produced by the ANISN analysis (and used in both calculations) have shown the secondary gamma production rates to be eminently reasonable.

Since the direct neutron dose rate just upstream of the rotary shutter and the relative gamma dose rate there due to secondary gammas produced in the system are both totally negligible when compared to the gamma dose rate at the shutter due to primary gammas streaming down the beam tube and impinging on the water tube, there is no further need of any detailed 3-D MCNP analyses to further assess those effects. Nevertheless, it should be noted that three different and independent (albeit approximate) calculational techniques have shown that the total gamma dose rate impingent on the rotary shutter will be on the order of 100 Rem/hr when the 1998 water tube and collimator sections are both flooded and the HFIR is operating at 100 MW. Given that this is about four times higher than the 25 Rem/hr calculated there with the 1960 water tube and collimator sections both flooded, detailed state-of-the-art 3-D MCNP calculations for the the gamma-only source are warranted and justified. Moreover, this analysis must include a more rigorous determination of the boundary source just upstream of the shutter (for use in case the shutter must be redesigned), but must go further and accurately calculate the final resulting dose rate downstream of the rotary shutter to determine if it must be redesigned to meet current dose limits. This analysis is described in Sect 6.

6.0 TREATMENT OF PRIMARY GAMMAS IN THE WATER-TUBE SHIELDING ANALYSIS

The total dose rate downstream of the flooded water tube, the flooded collimator, and the rotary shutter assembly, depends on three things: (1) the direct neutron dose rate, (2) the dose rate due to secondary gammas produced by these neutrons, and (3) the dose rate due to primary gammas that penetrate the shielding. [Here the term "primary gammas" is used to refer to those coming from the equivalent point sources in the hot end of the HB-3 beam tube listed in Table 2.2b even though, in reality, many of these are in fact high-energy secondary gammas produced by (n,g) reactions in the aluminum at the tip of the beam tube and other materials near the tip of the tangential beam tube.] As shown in Sect 5, however, the direct neutron dose rate, and the dose rate due to secondary gammas, are both totally negligible downstream of the flooded water tube and collimator sections, even though the total gamma dose rate impingent on the rotary shutter is approximately 100-110 Rem/hr for the 1998 water tube design, or about four times higher than it is with the original 1960 design using the longer water tube. Moreover, the high gamma dose rate at this location has been consistently calculated by three independent analytic techniques: an elementary 3-group analytic formula, a 23-group point kernel analysis, and a preliminary MCNP analysis based on a highly simplified model in which geometric splitting based on the extensive use of photon importance zones permitted a very credible solution to be obtained downstream of the flooded collimator section (cf Appendix C.6). Unfortunately, the use of the MCNP biasing technique applied in Appendix C.6 could not be extended into and through the region corresponding to the geometrically complex rotary shutter assembly, and the boundary source impingent on the rotary shutter lacked the resolution necessary for a detailed streaming analysis in and around the rotary shutter. Nevertheless, it was clear that such an analysis was beyond the capability of the elementary methods and would require the use of a 3-D transport model which could adequately represent the large and small holes in the rotary shutter itself, as well as the small clearance gaps around the cylindrical shutter, and the large 1- and 2-cm clearance gaps between the shutter housing assembly and the biological shield.

Fortunately, by the time the gamma-only water-tube shielding problem was to be addressed, a new and much more powerful analytic biasing technique had been perfected for use with MCNP4B. This technique allows use of broad-group "geometry-independent weight windows" based on the adjoint analysis of a similar but simplified geometry model. These weight windows can then be used in conjunction with the full 3-D MCNP model of the real system in all its glorious detail. The benefits of this approach are described more fully in Appendix C.6.6, while the power of this approach in a simple academic problem was first demonstrated Appendix C.2. Without this approach, the rigorous solution of the gamma-only water-tube shielding problem using MCNP would have been impossible. Moreover, this was the first demonstration of the method in a very difficult yet very real application. The approach taken was to model the entire HB-3 beam tube and rotary shutter assembly exactly as described in Sect 3 and shown in Fig. 3.3, with no approximations. Moreover, Fig.3.3 was created from the actual MCNP input file used in this analysis. This base model includes: the hot end of the beam tube inside the vessel, all of the small geometry regions required for the dosimetry analysis (cf Figs. 3.14 to 3.18), the entire (flooded) water tube including the surrounding pool and portions of the biological shield, the (flooded) collimator section including the radial and eccentric shields and the surrounding concrete (shown without water in Figs. 3.10 and 3.11), and the full 3-D model of the rotary shutter assembly including all the small internal void regions and the surrounding concrete (cf Figs. 3.12 and 3.13). The initial plan was to use this detailed MCNP model in combination with broad-group "geometry-independent weight windows" based on adjoint analyses to generate a much better internal (MCNP) boundary source just downstream of the collimator (at Z=401.9645 cm) that could then be used in a follow-up bootstrapped calculation in which even more histories could be used in the analysis of the rotary shutter assembly. Indeed, just such a boundary source was written and saved. It included the coordinates, direction cosines, energies, and particle weights for over 5.6 million high-energy particles crossing this artificial internal boundary at Z=401.9645 cm. (This boundary source file required over 542 MB of disk space, and was subsequently archived to tape for future reference.) The new method involving the use of broad-group "geometry-independent weight windows" worked so well, however, that no follow-up bootstrapped analysis was ever needed. That is: Because the base model used to generate this boundary source already contained the rotary shutter, the concrete assembly, the streaming paths, and the biological shield, as well as all the point detectors and boundary crossing estimators that we had planned to use in the final analysis, and because the statistics obtained from this initial calculation were so good, and because the (real particle) boundary crossing tallies downstream of the rotary shutter provided a "positive confirmation" of the point detector estimates downstream of the rotary shutter assembly, there was no further need of any further follow-up analysis.

Most of the key elements needed to understand the approach taken here are described elsewhere in this report. "Why this approach was taken" and "obstacles presented by other approaches" are discussed in Sect 5.1, Appendix C.1, and Appendix C.6.6. Those unfamiliar with biasing techniques might also want to review Appendices C.2.1 and C.2.2. Appendix C.2.3 and the balance of Appendix C.2 describe the use of broad-group "geometry-independent weight windows" in conjunction with MCNP4B as applied to a simple problem. Lastly, the format of the broad-group "geometry-independent weight window file" is described in Appendix C.3. This technique and the necessary file format specifications will be formally published by Los Alamos (cf Ref 23) in the next release of the code (MCNP4C) in the year 2000. While it awaits the next formal release

of the code, it has already undergone extensive internal testing at Los Alamos and is presently available as an undocumented feature of the MCNP4B code as released in the spring of 1997.

The remainder of Sect 6 briefly describes the 1-D ANISN model used in the adjoint analysis, and how that resulting broad-group data was used to create a 3-D weight-window file for use in MCNP4B. A few supplementary details regarding the MCNP analysis are then given, followed by an extensive presentation and discussion of the results obtained.

6.1 Discussion of the 1-D ANISN Model Used in the Adjoint Analysis

Table 6.1 briefly describes the ANISN 1-D buckled slab model (of the flooded 1998 HB-3 water tube, flooded collimator, and rotary shutter) that was used in the adjoint analysis of the gamma-only shielding problem to generate broad-group weight window information that could then be used in subsequent 3-D MCNP analyses. It is very similar to (and indeed based upon) the 1-D model previously described in Sect 5.3, with minor changes for this particular application.

Table 6.1 describes the model geometry as clearly as possible. Basically it is a 1-D infinite slab model along the centerline of the HB-3 beam tube, including the 1998 water tube, the water-filled collimator, and the rotary shield plug. It also includes the aluminum windows defining the beginning and end of the water tube. Appendix D.1 lists, among other things, the actual ANISN input for this particular model. Moreover, the GETWING3.SCR script file shown there (and discussed below) also contains an embedded Fortran program which is compiled and executed after the adjoint ANISN calculation has been run. The purpose of that program is to generate properly normalized 1-D broad-group weight window information that is later used in the 3-D weight window file generator (WW308G) which is also discussed below.

This adjoint ANISN calculation#9 is an 84-group calculation using the 61n/23g VELM cross section library#10. Moreover, premixed cross sections for the various materials listed in Table 6.1 were created and cast in an "adjoint format" by the GIP code#24 prior to running this group-banded 1-D adjoint ANISN calculation. Unlike the academic problem in Appendix C.2 where the stated objective of the final MCNP analysis was to calculate the total "neutron plus secondary gamma" dose rate downstream of the shield, the direct neutron dose rate downstream of the shield (in this case) has already been dismissed as being totally negligible, and the final objective was simply to optimize the calculation of the "total gamma dose rate" downstream of the shield. Thus, the "source term" in this adjoint calculation corresponds to the 23-group-gamma flux-to-dose-rate conversion factors [(mrem/hr)/(p/s/cm2)] in the VELM 61n/23g library structure, based on the 1977 ANSI Standard#19. Those adjoint source terms corresponding to the 61 neutron groups were set to zero in this adjoint analysis. This volumetric adjoint source (described by the 17** array in the ANISN input) was placed in mesh interval 719, between X=478.31375 and X=478.79 cm in the 1-D model, the latter corresponding to the downstream surface of the steel-clad concrete assembly holding the rotary shutter in the final 3-D model. Next, because one is ultimately and primarily concerned with the fluxes and dose rates near the center of a finite system due to a narrowly collimated impingent photon beam rather than the response over an "infinite plane" due to an "infinite plane source", this 1-D ANISN calculation was run as a buckled slab whose assumed dimensions in the two transverse directions (dx=dy=27.2 cm) were based on the diameter of the beam and the concept of reflector savings, normally applied to water reflected cores in reactor physics calculations. While it is recognized that the latter is not directly applicable in this particular case, it is far better and more realistic than the alternative. Lastly, it should be noted that "less than full density steel" was intentionally used for the rotary shutter shield plug in this adjoint analysis. In reality, the shield plug is Type 1020 carbon steel with a density of approximately 7.8212 g/cc. Here, however, it must be recognized that the objective of this adjoint calculation is not to calculate the actual transmission through the steel, but to develop a biasing function that would be appropriate for later use in MCNP. In that quest, one has considerable latitude, as long as one does not overbias the solution. (Underbiasing may result in less than optimal efficiency but always permits a correct solution; overbiasing can either increase or (sometimes) decrease the efficiency, but it can also distort the solution. Overbiasing can result if the material appears "too black" in the adjoint calculation used to generate the weight window information.) In the real system, the rotary shutter shield plug has a large 3.5-inch-diam beam hole and a small 0.875-inch-diam beam hole, both of which are inclined at an obtuse angle to the beam centerline when the shutter is in the closed position. These holes provide streaming paths by which at least some radiation can get a "free ride" through part of the shield plug. In addition, clearance gaps circumferentially around the side of the shield plug, near the top of the shield plug, and between the concrete shutter assembly block and the biological shield, also provide streaming paths that could conceivably make the dose rate downstream of the shield bigger than one would expect of it were a monolithic block of steel with no streaming paths. So as not to obtain an adjoint calculation that would overbias the final solution, the density of the steel used in the 1-D adjoint analysis was artificially reduced to 3.6760 g/cc by using a density factor of 0.47 for those mesh intervals, as specified in the ANISN 21** input array (density factors by mesh interval). [With the 1960 water tube and collimator sections both flooded, it was known (cf Sect 5.5) that the gamma dose rate impingent

Table 6.1. ANISN 1-D buckled slab model (of the flooded 1998 HB-3 water tube, flooded collimator, and rotary shutter) used in the adjoint analysis of the gamma-only shielding problem to generate broad-group weight window information that could then be used in subsequent 3-D MCNP analyses.

Zone No.	# of Mesh	Xmin (cm)	Xmax (cm)	Material	Description / Comments
1	1	115.0	116.7841	Void	Void for 1998 water water tube model
2	3	116.7841	117.7366	Void	Void for 1998 water water tube model
3	112	117.7366	174.27	Void	Void for 1998 water water tube model (large number of mesh simply left over from earlier more general model to accomodate 1960 model)
4	3	174.27	174.95125	Aluminum	Represents first aluminum window in 1998 water tube; Water in 1998 water tube starts at 174.95125
5	8	174.95125	179.05	Water	1st 4.1-cm-thk water region
6	8	179.05	183.15	Water	2nd 4.1-cm-thk water region
7	8	183.15	187.25	Water	3rd 4.1-cm-thk water region
8	8	187.25	191.35	Water	4th 4.1-cm-thk water region
9	8	191.35	195.45	Water	5th 4.1-cm-thk water region
10	8	195.45	199.55	Water	6th 4.1-cm-thk water region
11	8	199.55	203.65	Water	7th 4.1-cm-thk water region
12	8	203.65	207.75	Water	8th 4.1-cm-thk water region
13	190	207.75	302.1868	Water	Balance of water in 1998 water tube; 1998 water tube ends at 302.1868
14	3	302.1868	302.5043	Aluminum	Represents second aluminum window in 1998 water tube
15	16	302.5043	310.58	Water	Region between end of 1998 water tube and start of collimator; 1998 collimator design starts at 310.58
16	50	310.58	334.7709	Water	Water used for central (flooded) section of 1998 collimator
17	3	334.7709	335.4756	Water	Water used for central (flooded) section of 1998 collimator
18	128	335.4756	399.48	Water	Water used for central (flooded) section of 1998 collimator
19	3	399.48	401.9445	Void	Thin region between end of collimator and end of flange
20	15	401.9445	415.44875	Void	Void between end of flange and the C-stl rotary shutter shield plug
21	125	415.44875	477.36125	C-stl	Represents C-stl rotary shutter shield plug; in the adjoint analysis, "less than full density steel" was intentionally used here (see text)
22	3	477.36125	478.79	Void	Last part of cavity containing the rotary shutter assembly; Monochronometer (not modeled here) starts at 478.49; Volumetric "adjoint source" placed in last mesh interval (mesh 719) between X=478.31375 and X=478.79 cm.

Pre-mixed materials available in the HB-3 water tube 61n/23g "adjoint" cross section library (adjoint.xsects.dort-ready.bin.hfir.hb3.watertube.14may98) include the following:

Mixture 1 = ANISN/DORT Material 1 = Water at 1.00 g/cc
Mixture 2 = ANISN/DORT Material 5 = Aluminum 6061 (2.7 g/cc)
Mixture 3 = ANISN/DORT Material 9 = Void (He @ 1.0e-20 atoms/barn*cm)
Mixture 4 = ANISN/DORT Material 13 = SS304 (7.92 g/cc; see page 50 of ORNL/TM-11989)
Mixture 5 = ANISN/DORT Material 17 = Carbon Steel (7.8212 g/cc, 99 wt% Fe, 1 wt% C)
Mixture 6 = ANISN/DORT Material 21 = Barytes Concrete at 3.09725 g/cc
Mixture 7 = ANISN/DORT Material 25 = Regular Concrete
Mixture 8 = ANISN/DORT Material 29 = response functions

on the rotary shutter was about 26 Rem/hr and that most of this was due to 8 MeV gammas. We had also been told that the dose rate downstream of the rotary shutter was about 100 mrem/hr. (In retrospect, it was later discovered that the latter is more like 50 mrem/hr, as noted in Sect 7, and that virtually all of this is due to activation sources within the shutter itself as opposed to transmission through the shutter.) Thus, while not totally appropriate in the end, these two values (26 Rem/hr and 100 mrem/hr) provided a semi-credible basis for determining the reduced density of the steel to be used in the adjoint calculation so that we would at least be assured of obtaining a photon importance function that would not overbias the final MCNP solution. Note that having no special biasing in this region (ie, constant weight windows in this region) would be appropriate if there were no attenuation, but that much stronger spatial biasing would be required for an efficient solution if one had solid steel with no streaming paths. Using the reduced density indicated above, while perhaps not grounded in the best set of facts, at least provided a happy medium that would permit a more efficient solution without overbiasing the result. While the density used may not have been optimal, it was both useful and safe for the purpose at hand.]

The 1-D fine-mesh adjoint calculation described above is an 84-group calculation involving 61 neutron groups and 23 gamma groups. Just as a real neutron source can create secondary gammas, the adjoint gamma source can create adjoint neutrons. Thus, adjoint neutron fluxes and adjoint gamma fluxes will both appear in the binary flux file created by ANISN. Unlike the flux file in a standard "forward mode solution", however, it is important to note here that: (a) the first of the 84 records contains the adjoint gamma fluxes for the softest gamma group, while (b) record 23 contains the adjoint gamma flux for the hardest gamma group, (c) record 24 contains the adjoint neutron flux for the slowest neutron group, and (d) record 84 contains the adjoint fluxes for the fastest neutron group. This point is emphasized here since it is quite the reverse of what one would normally expect and obtain in a normal "forward" calculation. After first running the adjoint ANISN calculation, the GETWING3.SCR script in Appendix D.1 then calls the embedded GETWING3.F Fortran program (also shown) which further processes the data, as described below.

6.2 Obtaining Properly Normalized 1-D Broad-Group Weight Windows from the Adjoint Information

Unlike it counterpart in the simple academic problem (cf Appendices C.2 and C.4), the GETWING3.SCR script file in Appendix D.1 does not "directly" produce the 3-D broad-group weight window file later used by MCNP4B. That task is now left to a separate stand-alone follow-up program described below in Sect 6.4. Nevertheless, the GETWING3.F program embedded within GETWING3.SCR script does serve much the same role as its counterpart, and produces (1-D) broad-group weight window data that is then used in the 3-D weight window generator. Within the GETWING3.F program, subroutine SRCJST first calls subroutine GETADJ which reads the adjoint scalar flux file as noted above, as well as the mesh information contained in the ANISN printed output file, and spatially averages the broad-group adjoint fluxes (for six broad neutron groups and four broad gamma groups) over a series of somewhat wider (5-cm-thick) importance zones from X=174.27 cm to X=479.27 cm. These results are listed below in Table 6.2a. Knowing a priori (from the point kernel studies described in Sect 5.5) that the primary gammas sources in the beam tube in VELM groups 1 to 8 (E > 3 MeV) are responsible for 98-99% of the total gamma dose rate impingent on the rotary shutter, and that the other primary gamma sources in Table 2.2b could ultimately be ignored in the final MCNP analysis, it was decided that these particular fine-group adjoint fluxes should be binned together into one broad gamma group by themselves. The fine groups comprising the other broad gamma groups and each of the the broad neutron groups are indicated on in Table 6.2a. (Note that in the final MCNP analysis we "do not" ignore the gamma fluxes in the other energy groups, only the gamma source terms in the other energy groups.)

The next step is to determine the average broad-group weights for neutrons and gammas in each of the 5-cm-thick importance zones. This "average weight" is proportional to the inverse of the corresponding broad-group adjoint flux in each zone. The tricky part, however, is knowing how to properly normalize everything#25. This is clearly shown in subroutine SRCJST of the GETWING3.F program in Appendix D.1. After setting the real neutron sources to zero in that routine, and setting the real gamma sources to a negligibly small value (such as 1.0) for all but the first eight VELM gamma groups above 3 MeV, one basically proceeds as follows:

(1) Look at the broad-group adjoint fluxes back at the location where the (real) source particles would normally impinge on the shield, as well as the equivalent broad-group source terms.

(2) Determine the "source-averaged adjoint flux" (avgadj) at that location by taking the integral over all broad groups of "the real broad-group sources there, times the broad group adjoint fluxes there", and dividing that integral by the sum of all the real broad-group sources at that location. [In this special case where all the sources are either zero or negligibly small except those in the most energetic gamma broad group, the "source averaged adjoint flux" (avgadj) will essentially be identical to the original adjoint flux in the most energetic gamma broad group. Had the source been different, that would not be the case.]

(3) The average (survival) weight assigned to each broad group at that location equals this "source-averaged adjoint flux" divided by the particular broad-group adjoint flux at that location. [In this special case, the average (survival) weight assigned to the most energetic

gamma group in this source region will be 1.0; had the source been different, that would not be the case.] Likewise, the average (survival) weight assigned to each broad group in every other importance mesh equals this same "source-averaged adjoint flux" (avgadj) divided by the local broad-group adjoint flux in the given importance mesh. The upper weight window limit (wthigh) for each broad group in each importance mesh is then typically taken to be ten times the average survival weight, while the lower weight window limit (wtlow) for each broad group in each importance mesh is then typically taken to be one tenth the average survival weight. Table 6.2b shows the resulting lower weight limit for each of the neutron and gamma broad groups in each importance mesh along the axis. [In MCNP, "wthigh" is used to control splitting, and "wtlow" is used for invoking Russian Roulette. As per the "geometry-independent weight window" file specifications in Appendix C.3, only the lower weight window limits are actually specified in this auxiliary file. (That's why we tabulate only that data, and why there is no mention of "wthigh" in the GETWING3.F program.) Within the regular MCNP input, on the "wwn" and "wwp" cards, WSURVN is the ratio of the average (survival) weight to "wtlow", while WUPN is the ratio of the upper weight window limit to "wtlow".]

Focusing on the weight window data in Table 6.2b for the four broad gamma groups, two things should be noted: (a) Back where the (real) gamma source impinges on the water tube (around X=174.27 cm), the values of "wtlow" for these four broad groups are vastly different by orders of magnitude but become much closer as one approaches the downstream side of the rotary shutter (around X=479.27 cm). This is reflective of the fact that low energy gammas back near the source (whether included in the source or present by virtue of slowing down) simply don't contribute significantly to the final solution and, in the name of efficiency, may as well be killed off by Russian Roulette while lower energy gammas present (by virtue of slowing down) near the downstream side of the rotary shutter may indeed contribute to the final solution and should not be killed as readily. (b) The variation of this data along the centerline of the system is markedly different from one broad gamma group to the next. While "wtlow" for some broad gamma groups may change by 14, 18, or even 26 orders of magnitude across the system, values of "wtlow" for the highest energy broad group above 3 MeV only diminishes by 11 orders of magnitude. As long as one can even approximate these sorts of variations from one broad group to the next, across the entire system, with any semi-reasonable degree of fidelity, and as long as the data is properly normalized relative to the starting weights of the particles, the improvement to the overall calculational efficiency can be immense. In developing a weight window file for use in MCNP, it is NOT necessary to replicate small intricate variations down to the tiniest detail; representing only the gross behavior in each energy range is usually sufficient to realize huge gains in calculational efficiency, with essentially no loss of accuracy.

It is important to note, however, that one is not yet done at this point. To work, the starting weight of the particles must be compatible with the weight windows just defined, or one could easily have a situation where all the source particles split like crazy or are immediately killed without going anywhere. To accomplish this, source-energy biasing is required. Fortunately, the adjoint technique provides an analytic tool for defining the optimal source-energy biasing algorithm compatible with the weight windows just established. Continue as follows:

(4) The optimally biased energy distribution for the source (on a broad-group basis) is obtained by taking the (real) broad-group source intensity and dividing it by the average (survival) weight for the corresponding broad-group at the source location. The ratio of the biased source energy distribution to the original source energy distribution (based on the broad group values in both cases) can then be applied to the fine-group source terms to obtain the biased source energy distribution on a fine group basis. By supplying MCNP with the original fine-group source energy distribution as well as the biased fine-group source energy distribution (on the MCNP "sb" card), it will then adjust the starting weights automatically. Moreover, following this procedure will assure that the starting weights used by MCNP are fully compatible with the weight windows supplied in the "geometry-independent weight window" file created by the WW308G.F program below. For the convenience of the user, the GETWING3.SCR script will also print out the original fine-group source energy distribution as well as the biased source energy distribution that the user should supply manually in the MCNP input file. Table 6.2c shows the original and biased source energy distributions on both a broad-group and fine-group basis. [Again, because of this special case in which the only non-zero source of any substance lies in a single broad gamma group, the biased and unbiased source energy distributions are essentially identical, and in the final MCNP analysis we actually ignore all gamma sources below 3 MeV. In a more general case such as that shown in Appendix C.2.5, these distributions could and would be quite different.]

6.3 Other Factors Affecting Proper Normalization

There are still two other things affecting proper normalization that have yet to be discussed. Both are consequences of how the physics is simulated in the MCNP model. The first affects how the WTLOW data supplied in the weight window file is normalized, while the other does not.

Table 6.2a. Spatially-averaged broad-group neutron and gamma adjoint fluxes for the HB-3 gamma-only problem as summarized by GETWING3.SCR. In this 1-D adjoint analysis, the adjoint source between X=478.31 and X=478.79 cm corresponded to the VELM 23-group (ANSI Std) Gamma-Flux-to-Dose-Rate conversion factors, with 0.0 for all the Neutron-Flux-to-Dose-Rate conversion factors. Because it was an adjoint calculation, the adjoint neutron flux is nonzero.

Neutron and Gamma Adjoint Fluxes: where adjoint is based on just the gamma dose rate at X= 478.790 cm, and buckling DY=DZ= 27.20 cm
mnXX-YY = MCNP neutron grp numbers, mgXX-YY = MCNP gamma grp numbers
vnXX-YY = VELM neutron grp numbers, vgXX-YY = VELM gamma grp numbers

		Emax:	4.13990E-07	1.06770E-05	1.23410E-03	1.22770E-01	1.10800E+00	1.49180E+01	3.00000E-01	1.00000E+00	3.00000E+00	1.40000E+01
		imp	mn01-01	mn02-05	mn06-13	mn14-31	mn32-46	mn47-61	mg01-06	mg07-11	mg12-15	mg16-23
xmin	xmax	mesh	vn61-61	vn57-60	vn49-56	vn31-48	vn16-30	vn01-15	vg18-23	vg13-17	vg09-12	vg01-08
174.27	179.27	1	2.35650E-16	6.21847E-16	9.02720E-16	1.55231E-15	9.25418E-16	8.37683E-15	2.01141E-29	1.05289E-21	1.26399E-16	5.20915E-13
179.27	184.27	2	5.69204E-17	2.40488E-16	5.20679E-16	1.21907E-15	9.65215E-16	1.22326E-14	4.11412E-29	1.85484E-21	1.94049E-16	7.04533E-13
184.27	189.27	3	4.84531E-17	1.95200E-16	3.98844E-16	9.25554E-16	8.04382E-16	1.73533E-14	8.44863E-29	3.31200E-21	3.01108E-16	9.60188E-13
189.27	194.27	4	7.09434E-17	2.83000E-16	5.65534E-16	1.27247E-15	1.05431E-15	2.44704E-14	1.73120E-28	5.91323E-21	4.67211E-16	1.30886E-12
194.27	199.27	5	1.08713E-16	4.33271E-16	8.63948E-16	1.93696E-15	1.58700E-15	3.38971E-14	3.40735E-28	1.02296E-20	7.08220E-16	1.75598E-12
199.27	204.27	6	1.68190E-16	6.70252E-16	1.33622E-15	2.99475E-15	2.45008E-15	4.70673E-14	6.75960E-28	1.77912E-20	1.07698E-15	2.36028E-12
204.27	209.27	7	2.65373E-16	1.05753E-15	2.10826E-15	4.72491E-15	3.86493E-15	6.63619E-14	1.37924E-27	3.16790E-20	1.66833E-15	3.21632E-12
209.27	214.27	8	4.15818E-16	1.65706E-15	3.30348E-15	7.40360E-15	6.05604E-15	9.31497E-14	2.78277E-27	5.59071E-20	2.56748E-15	4.36406E-12
214.27	219.27	9	6.48660E-16	2.58496E-15	5.15333E-15	1.15495E-14	9.44738E-15	1.30418E-13	5.57668E-27	9.81228E-20	3.93484E-15	5.90537E-12
219.27	224.27	10	1.01202E-15	4.03299E-15	8.04012E-15	1.80193E-14	1.47399E-14	1.82798E-13	1.11767E-26	1.72247E-19	6.03207E-15	7.99505E-12
224.27	229.27	11	1.57904E-15	6.29264E-15	1.25450E-14	2.81158E-14	2.29991E-14	2.56517E-13	2.24004E-26	3.02402E-19	9.24917E-15	1.08293E-11
229.27	234.27	12	2.46381E-15	9.81853E-15	1.95743E-14	4.38701E-14	3.58869E-14	3.60424E-13	4.48903E-26	5.30928E-19	1.41844E-14	1.46745E-11
234.27	239.27	13	3.84477E-15	1.53218E-14	3.05459E-14	6.84602E-14	5.60030E-14	5.07180E-13	8.99651E-26	9.32310E-19	2.17589E-14	1.98952E-11
239.27	244.27	14	6.00035E-15	2.39121E-14	4.76720E-14	1.06844E-13	8.74040E-14	7.14890E-13	1.80304E-25	1.63738E-18	3.33865E-14	2.69867E-11
244.27	249.27	15	9.59255E-15	3.82273E-14	7.62111E-14	1.70809E-13	1.39733E-13	1.02828E-12	3.75699E-25	2.96638E-18	5.24331E-14	3.72179E-11
249.27	254.27	16	1.52840E-14	6.09086E-14	1.21431E-13	2.72159E-13	2.22648E-13	1.47951E-12	7.76323E-25	5.34544E-18	8.21065E-14	5.12732E-11
254.27	259.27	17	2.38593E-14	9.50828E-14	1.89564E-13	4.24868E-13	3.47586E-13	2.09988E-12	1.55583E-24	9.39229E-18	1.26082E-13	6.96574E-11
259.27	264.27	18	3.72515E-14	1.48453E-13	2.95970E-13	6.63365E-13	5.42734E-13	2.98981E-12	3.11825E-24	1.65065E-17	1.93668E-13	9.46851E-11
264.27	269.27	19	5.81685E-14	2.31813E-13	4.62174E-13	1.03592E-12	8.47707E-13	4.27364E-12	6.24966E-24	2.90145E-17	2.97568E-13	1.28773E-10
269.27	274.27	20	9.08553E-14	3.62089E-13	7.21968E-13	1.61845E-12	1.32535E-12	6.14039E-12	1.25255E-23	5.10099E-17	4.57337E-13	1.75225E-10
274.27	279.27	21	1.42047E-13	5.66184E-13	1.12929E-12	2.53298E-12	2.07998E-12	8.88738E-12	2.51064E-23	8.97052E-17	7.03139E-13	2.38574E-10
279.27	284.27	22	2.22895E-13	8.88981E-13	1.77572E-12	3.99255E-12	3.31084E-12	1.30036E-11	5.03287E-23	1.57798E-16	1.08142E-12	3.25012E-10
284.27	289.27	23	3.55149E-13	1.42018E-12	2.85437E-12	6.48201E-12	5.52885E-12	1.93314E-11	1.00888E-22	2.77621E-16	1.66365E-12	4.42993E-10
289.27	294.27	24	6.02832E-13	2.43568E-12	5.00797E-12	1.17150E-11	1.03640E-11	2.92985E-11	2.02300E-22	4.88603E-16	2.56031E-12	6.04166E-10
294.27	299.27	25	1.27251E-12	5.26560E-12	1.10811E-11	2.57569E-11	2.12862E-11	4.47225E-11	4.05949E-22	8.60193E-16	3.94153E-12	8.24444E-10
299.27	304.27	26	3.42460E-12	1.25881E-11	2.28373E-11	4.72095E-11	3.49214E-11	6.64607E-11	8.19893E-22	1.51503E-15	6.06427E-12	1.12613E-09
304.27	309.27	27	2.81050E-12	1.14282E-11	2.31414E-11	5.18679E-11	4.15505E-11	9.15409E-11	1.66510E-21	2.69941E-15	9.41507E-12	1.54990E-09
309.27	314.27	28	3.42464E-12	1.37014E-11	2.75499E-11	6.24322E-11	5.19609E-11	1.33150E-10	3.46065E-21	4.90016E-15	1.48418E-11	2.15328E-09
314.27	319.27	29	5.27076E-12	2.10130E-11	4.19311E-11	9.41142E-11	7.73163E-11	2.00323E-10	7.04108E-21	8.75047E-15	2.31296E-11	2.96949E-09
319.27	324.27	30	8.12798E-12	3.23944E-11	6.45971E-11	1.44823E-10	1.18585E-10	3.03008E-10	1.38522E-20	1.51982E-14	3.52751E-11	4.03141E-09
324.27	329.27	31	1.28606E-11	5.12554E-11	1.02200E-10	2.29106E-10	1.87517E-10	4.77809E-10	2.83033E-20	2.72210E-14	5.50607E-11	5.56586E-09
329.27	334.27	32	2.02912E-11	8.08705E-11	1.61255E-10	3.61496E-10	2.95875E-10	7.64593E-10	5.73732E-20	4.85205E-14	8.57240E-11	7.67718E-09
334.27	339.27	33	3.19247E-11	1.27237E-10	2.53715E-10	5.68784E-10	4.65561E-10	1.24327E-09	1.16007E-19	8.62691E-14	1.33122E-10	1.05673E-08
339.27	344.27	34	5.05251E-11	2.01372E-10	4.01554E-10	9.00241E-10	7.36920E-10	2.07499E-09	2.36237E-19	1.54471E-13	2.07987E-10	1.46187E-08
344.27	349.27	35	7.93691E-11	3.16337E-10	6.30821E-10	1.41429E-09	1.15781E-09	3.50625E-09	4.75518E-19	2.74093E-13	3.22701E-10	2.01242E-08
349.27	354.27	36	1.24728E-10	4.97130E-10	9.91381E-10	2.22276E-09	1.81987E-09	6.05280E-09	9.57103E-19	4.86680E-13	5.01024E-10	2.77232E-08
354.27	359.27	37	1.96119E-10	7.81693E-10	1.55893E-09	3.49547E-09	2.86250E-09	1.06788E-08	1.92660E-18	8.64921E-13	7.78542E-10	3.82227E-08
359.27	364.27	38	3.08591E-10	1.23003E-09	2.45326E-09	5.50142E-09	4.50764E-09	1.92564E-08	3.87851E-18	1.53867E-12	1.21088E-09	5.27427E-08
364.27	369.27	39	4.86075E-10	1.93767E-09	3.86548E-09	8.67136E-09	7.11806E-09	3.54931E-08	7.80814E-18	2.74015E-12	1.88509E-09	7.28377E-08

(continued)

Table 6.2a (cont)

xmin	xmax	Emax: imp mesh	4.13990E-07 mn01-01 vn61-61	1.06770E-05 mn02-05 vn57-60	1.23410E-03 mn06-13 vn49-56	1.22770E-01 mn14-31 vn31-48	1.10800E+00 mn32-46 vn16-30	1.49180E+01 mn47-61 vn01-15	3.00000E-01 mg01-06 vg18-23	1.00000E+00 mg07-11 vg13-17	3.00000E+00 mg12-15 vg09-12	1.40000E+01 mg16-23 vg01-08
369.27	374.27	40	7.67666E-10	3.06126E-09	6.11192E-09	1.37291E-08	1.13477E-08	6.69129E-08	1.57216E-17	4.88634E-12	2.93798E-09	1.00678E-07
374.27	379.27	41	1.22328E-09	4.88509E-09	9.78594E-09	2.21037E-08	1.87301E-08	1.29183E-07	3.16611E-17	8.72712E-12	4.58473E-09	1.39286E-07
379.27	384.27	42	2.01917E-09	8.11048E-09	1.64685E-08	3.80196E-08	3.46788E-08	2.55764E-07	6.37757E-17	1.56156E-11	7.16443E-09	1.92873E-07
384.27	389.27	43	3.80438E-09	1.55932E-08	3.31132E-08	8.15331E-08	8.33189E-08	5.18732E-07	1.28523E-16	2.80070E-11	1.12139E-08	2.67324E-07
389.27	394.27	44	1.02908E-08	4.39600E-08	1.00524E-07	2.63044E-07	2.53143E-07	1.06559E-06	2.59218E-16	5.03808E-11	1.75834E-08	3.70833E-07
394.27	399.27	45	4.60290E-08	1.93485E-07	4.12197E-07	8.85248E-07	5.74321E-07	2.16166E-06	5.23990E-16	9.09568E-11	2.76075E-08	5.14582E-07
399.27	404.27	46	9.56304E-08	3.69069E-07	7.03839E-07	1.13858E-06	5.54639E-07	3.00003E-06	7.29484E-16	1.20461E-10	3.42633E-08	6.02957E-07
404.27	409.27	47	9.56304E-08	3.69069E-07	7.03839E-07	1.13858E-06	5.54639E-07	3.00003E-06	7.29484E-16	1.20461E-10	3.42633E-08	6.02957E-07
409.27	414.27	48	9.56304E-08	3.69069E-07	7.03839E-07	1.13858E-06	5.54639E-07	3.00003E-06	7.29484E-16	1.20461E-10	3.42633E-08	6.02957E-07
414.27	419.27	49	1.15808E-07	4.78116E-07	8.94636E-07	1.13889E-06	5.02553E-07	3.69216E-06	1.66481E-15	1.90480E-10	4.67160E-08	7.81894E-07
419.27	424.27	50	2.28653E-07	1.00193E-06	1.77995E-06	1.46559E-06	4.93139E-07	6.63029E-06	1.27505E-14	6.47794E-10	1.09903E-07	1.61650E-06
424.27	429.27	51	4.83229E-07	2.14679E-06	3.55740E-06	2.32088E-06	6.54792E-07	1.21352E-05	1.00138E-13	2.26554E-09	2.63588E-07	3.40294E-06
429.27	434.27	52	1.03120E-06	4.61849E-06	7.01657E-06	3.93045E-06	1.01014E-06	2.23522E-05	7.86521E-13	7.98888E-09	6.34347E-07	7.19496E-06
434.27	439.27	53	2.21926E-06	9.96427E-06	1.36464E-05	6.78278E-06	1.65793E-06	4.14075E-05	6.17893E-12	2.84439E-08	1.53344E-06	1.53037E-05
439.27	444.27	54	4.82965E-06	2.15193E-05	2.61094E-05	1.17250E-05	2.78613E-06	7.71635E-05	4.85601E-11	1.02424E-07	3.72857E-06	3.28177E-05
444.27	449.27	55	1.06725E-05	4.63817E-05	4.89735E-05	2.01490E-05	4.72667E-06	1.44761E-04	3.81918E-10	3.73814E-07	9.13782E-06	7.11771E-05
449.27	454.27	56	2.40854E-05	9.92791E-05	8.96184E-05	3.42200E-05	8.05773E-06	2.73672E-04	3.00832E-09	1.38685E-06	2.26430E-05	1.56875E-04
454.27	459.27	57	5.59040E-05	2.09295E-04	1.58834E-04	5.70075E-05	1.37856E-05	5.21806E-04	2.37762E-08	5.25397E-06	5.70239E-05	3.53958E-04
459.27	464.27	58	1.41367E-04	4.44798E-04	2.76553E-04	9.42893E-05	2.43660E-05	1.04078E-03	2.17886E-07	2.23155E-05	1.55938E-04	8.70934E-04
464.27	469.27	59	3.63145E-04	8.75310E-04	4.43904E-04	1.46383E-04	4.28320E-05	2.07061E-03	1.91885E-06	9.66602E-05	4.41887E-04	2.26274E-03
469.27	474.27	60	8.65588E-04	1.42958E-03	6.00341E-04	1.98961E-04	7.20126E-05	3.94212E-03	1.81768E-05	4.45318E-04	1.35781E-03	6.53636E-03
474.27	479.27	61	1.18659E-03	1.28117E-03	4.76627E-04	1.78834E-04	9.36265E-05	5.73700E-03	2.34383E-03	5.03039E-03	1.02074E-02	4.68343E-02

Table 6.2b. Space- and energy-dependent weight window lower limits (WTLOW) along the centerline of the flooded HB-3 system [for the six broad neutron weight-window groups and four broad gamma weight-window groups(*)] in the gamma-only shielding analysis of the flooded HB-3 system, as calculated by GETWING3.SCR based on the associated 1-D adjoint analysis and the source-weight renormalization procedures in GETWING3.SCR. In the final gamma-only shielding analysis, MCNP4B only uses the four-group weight-window data for the gammas, although similar data for one dummy neutron group must also be supplied to satisfy file format requirements. For the 3-D broad-group weight-window lower limits used in final MCNP4B analysis, see discussion in text.

WTLOW for the 6 broad neutron groups and 4 broad gamma groups based on 1-D adjoint & Tang's source-weight renormalization procedure.
Use these values for the gamma-only MCNP4B transport analysis using a gamma-only source (with WTHI=100*WTLOW & WTSURV=WTAVG=10*WTLOW)
For a coupled n/g calc, or a neutron-only calc, values would be different.

mnXX-YY = MCNP neutron grp numbers, mgXX-YY = MCNP gamma grp numbers
vnXX-YY = VELM neutron grp numbers, vgXX-YY = VELM gamma grp numbers

		Emax:	4.13990E-07	1.06770E-05	1.23410E-03	1.22770E-01	1.10800E+00	1.49180E+01	3.00000E-01	1.00000E+00	3.00000E+00	1.40000E+01
		imp	mn01-01	mn02-05	mn06-13	mn14-31	mn32-46	mn47-61	mg01-06	mg07-11	mg12-15	mg16-23
xmin	xmax	mesh	vn61-61	vn57-60	vn49-56	vn31-48	vn16-30	vn01-15	vg18-23	vg13-17	vg09-12	vg01-08
174.27	179.27	1	2.21054E+02	8.37689E+01	5.77050E+01	3.35573E+01	5.62897E+01	6.21852E+00	2.58980E+15	4.94748E+07	4.12119E+02	1.00000E-01
179.27	184.27	2	9.15165E+02	2.16608E+02	1.00045E+02	4.27306E+01	5.39688E+01	4.25841E+00	1.26616E+15	2.80841E+07	2.68445E+02	7.39376E-02
184.27	189.27	3	1.07509E+03	2.66862E+02	1.30606E+02	5.62815E+01	6.47597E+01	3.00183E+00	6.16568E+14	1.57281E+07	1.72999E+02	5.42514E-02
189.27	194.27	4	7.34268E+02	1.84069E+02	9.21103E+01	4.09375E+01	4.94084E+01	2.12876E+00	3.00899E+14	8.80931E+06	1.11495E+02	3.97991E-02
194.27	199.27	5	4.79164E+02	1.20228E+02	6.02947E+01	2.68935E+01	3.28238E+01	1.53675E+00	1.52880E+14	5.09222E+06	7.35527E+01	2.96652E-02
199.27	204.27	6	3.09718E+02	7.77193E+01	3.89844E+01	1.73943E+01	2.12611E+01	1.10675E+00	7.70630E+13	2.92793E+06	4.83681E+01	2.20700E-02
204.27	209.27	7	1.96295E+02	4.92578E+01	2.47083E+01	1.10249E+01	1.34780E+01	7.84961E-01	3.77681E+13	1.64435E+06	3.12237E+01	1.61960E-02
209.27	214.27	8	1.25275E+02	3.14361E+01	1.57687E+01	7.03597E+00	8.60158E+00	5.59223E-01	1.87193E+13	9.31751E+05	2.02890E+01	1.19365E-02
214.27	219.27	9	8.03063E+01	2.01518E+01	1.01083E+01	4.51030E+00	5.51385E+00	3.99420E-01	9.34095E+12	5.30881E+05	1.32385E+01	8.82103E-03
219.27	224.27	10	5.14728E+01	1.29164E+01	6.47895E+00	2.89087E+00	3.53405E+00	2.84968E-01	4.66071E+12	3.02423E+05	8.63575E+00	6.51547E-03
224.27	229.27	11	3.29892E+01	8.27816E+00	4.15237E+00	1.85275E+00	2.26494E+00	2.03072E-01	2.32548E+12	1.72259E+05	5.63202E+00	4.81025E-03
229.27	234.27	12	2.11427E+01	5.30543E+00	2.66122E+00	1.18740E+00	1.45155E+00	1.44528E-01	1.16042E+12	9.81140E+04	3.67244E+00	3.54979E-03
234.27	239.27	13	1.35487E+01	3.39982E+00	1.70535E+00	7.60902E-01	9.30155E-01	1.02708E-01	5.79019E+11	5.58736E+04	2.39404E+00	2.61830E-03
239.27	244.27	14	8.68141E+00	2.17845E+00	1.09271E+00	4.87546E-01	5.95985E-01	7.28664E-02	2.88909E+11	3.18139E+04	1.56026E+00	1.93027E-03
244.27	249.27	15	5.43041E+00	1.36268E+00	6.83516E-01	3.04970E-01	3.72792E-01	5.06587E-02	1.38652E+11	1.75607E+04	9.93484E-01	1.39963E-03
249.27	254.27	16	3.40824E+00	8.55240E-01	4.28982E-01	1.91401E-01	2.33963E-01	3.52085E-02	6.71003E+10	9.74503E+03	6.34438E-01	1.01596E-03
254.27	259.27	17	2.18328E+00	5.47854E-01	2.74797E-01	1.22606E-01	1.49866E-01	2.48069E-02	3.34814E+10	5.54619E+03	4.13157E-01	7.47824E-04
259.27	264.27	18	1.39837E+00	3.50894E-01	1.76003E-01	7.85262E-02	9.59798E-02	1.74230E-02	1.67054E+10	3.15582E+03	2.68973E-01	5.50155E-04
264.27	269.27	19	8.95527E-01	2.24713E-01	1.12710E-01	5.02851E-02	6.14499E-02	1.21890E-02	8.33509E+09	1.79536E+03	1.75057E-01	4.04522E-04
269.27	274.27	20	5.73346E-01	1.43864E-01	7.21521E-02	3.21861E-02	3.93040E-02	8.48342E-03	4.15882E+09	1.02120E+03	1.13902E-01	2.97283E-04
274.27	279.27	21	3.66721E-01	9.20046E-02	4.61275E-02	2.05653E-02	2.50442E-02	5.86129E-03	2.07483E+09	5.80696E+02	7.40842E-02	2.18345E-04
279.27	284.27	22	2.33705E-01	5.85969E-02	2.93354E-02	1.30472E-02	1.57336E-02	4.00594E-03	1.03502E+09	3.30116E+02	4.81694E-02	1.60276E-04
284.27	289.27	23	1.46675E-01	3.66794E-02	1.82497E-02	8.03632E-03	9.42176E-03	2.69465E-03	5.16331E+08	1.87635E+02	3.13116E-02	1.17590E-04
289.27	294.27	24	8.64113E-02	2.13869E-02	1.04017E-02	4.44657E-03	5.02621E-03	1.77796E-03	2.57497E+08	1.06613E+02	2.03458E-02	8.62205E-05
294.27	299.27	25	4.09360E-02	9.89279E-03	4.70094E-03	2.02243E-03	2.44719E-03	1.16477E-03	1.28320E+08	6.05579E+01	1.32161E-02	6.31838E-05
299.27	304.27	26	1.52110E-02	4.13817E-03	2.28099E-03	1.10341E-03	1.49168E-03	7.83794E-04	6.35345E+07	3.43832E+01	8.58990E-03	4.62569E-05
304.27	309.27	27	1.85346E-02	4.55815E-03	2.25101E-03	1.00431E-03	1.25369E-03	5.69051E-04	3.12842E+07	1.92974E+01	5.53278E-03	3.36097E-05
309.27	314.27	28	1.52108E-02	3.80190E-03	1.89081E-03	8.34369E-04	1.00251E-03	3.91225E-04	1.50525E+07	1.06306E+01	3.50977E-03	2.41917E-05
314.27	319.27	29	9.88310E-03	2.47901E-03	1.24231E-03	5.53493E-04	6.73745E-04	2.60038E-04	7.39823E+06	5.95299E+00	2.25216E-03	1.75423E-05
319.27	324.27	30	6.40891E-03	1.60804E-03	8.06406E-04	3.59690E-04	4.39276E-04	1.71915E-04	3.76053E+06	3.42747E+00	1.47672E-03	1.29214E-05
324.27	329.27	31	4.05048E-03	1.01631E-03	5.09700E-04	2.27369E-04	2.77796E-04	1.09021E-04	1.84048E+06	1.91365E+00	9.46073E-04	9.35911E-06
329.27	334.27	32	2.56719E-03	6.44135E-04	3.23038E-04	1.44100E-04	1.76059E-04	6.81297E-05	9.07940E+05	1.07360E+00	6.07665E-04	6.78524E-06
334.27	339.27	33	1.63170E-03	4.09405E-04	2.05315E-04	9.15840E-05	1.11890E-04	4.18988E-05	4.49036E+05	6.03825E-01	3.91307E-04	4.92951E-06
339.27	344.27	34	1.03100E-03	2.58682E-04	1.29725E-04	5.78639E-05	7.06881E-05	2.51045E-05	2.20506E+05	3.37225E-01	2.50455E-04	3.56334E-06

(continued)

Table 6.2b (cont)

xmin	xmax	Emax: imp mesh	4.13990E-07 mn01-01 vn61-61	1.06770E-05 mn02-05 vn57-60	1.23410E-03 mn06-13 vn49-56	1.22770E-01 mn14-31 vn31-48	1.10800E+00 mn32-46 vn16-30	1.49180E+01 mn47-61 vn01-15	3.00000E-01 mg01-06 vg18-23	1.00000E+00 mg07-11 vg13-17	3.00000E+00 mg12-15 vg09-12	1.40000E+01 mg16-23 vg01-08
344.27	349.27	35	6.56319E-04	1.64671E-04	8.25773E-05	3.68324E-05	4.49915E-05	1.48568E-05	1.09547E+05	1.90050E-01	1.61423E-04	2.58850E-06
349.27	354.27	36	4.17641E-04	1.04784E-04	5.25444E-05	2.34356E-05	2.86237E-05	8.60619E-06	5.44262E+04	1.07034E-01	1.03970E-04	1.87899E-06
354.27	359.27	37	2.65612E-04	6.66393E-05	3.34148E-05	1.49026E-05	1.81979E-05	4.87803E-06	2.70380E+04	6.02269E-02	6.69091E-05	1.36284E-06
359.27	364.27	38	1.68804E-04	4.23497E-05	2.12336E-05	9.46874E-06	1.15563E-05	2.70515E-06	1.34308E+04	3.38549E-02	4.30195E-05	9.87653E-07
364.27	369.27	39	1.07168E-04	2.68836E-05	1.34761E-05	6.00731E-06	7.31822E-06	1.46765E-06	6.67144E+03	1.90104E-02	2.76335E-05	7.15173E-07
369.27	374.27	40	6.78570E-05	1.70164E-05	8.52294E-06	3.79425E-06	4.59049E-06	7.78497E-07	3.31338E+03	1.06606E-02	1.77303E-05	5.17407E-07
374.27	379.27	41	4.25834E-05	1.06634E-05	5.32310E-06	2.35669E-06	2.78116E-06	4.03238E-07	1.64528E+03	5.96892E-03	1.13620E-05	3.73990E-07
379.27	384.27	42	2.57985E-05	6.42274E-06	3.16309E-06	1.37012E-06	1.50211E-06	2.03670E-07	8.16793E+02	3.33585E-03	7.27085E-06	2.70083E-07
384.27	389.27	43	1.36925E-05	3.34066E-06	1.57313E-06	6.38900E-07	6.25206E-07	1.00421E-07	4.05308E+02	1.85995E-03	4.64528E-06	1.94862E-07
389.27	394.27	44	5.06197E-06	1.18498E-06	5.18197E-07	1.98033E-07	2.05779E-07	4.88852E-08	2.00957E+02	1.03395E-03	2.96253E-06	1.40471E-07
394.27	399.27	45	1.13171E-06	2.69227E-07	1.26375E-07	5.88439E-08	9.07011E-08	2.40979E-08	9.94132E+01	5.72706E-04	1.88686E-06	1.01231E-07
399.27	404.27	46	5.44717E-07	1.41143E-07	7.40105E-08	4.57514E-08	9.39196E-08	1.73636E-08	7.14087E+01	4.32436E-04	1.52033E-06	8.63934E-08
404.27	409.27	47	5.44717E-07	1.41143E-07	7.40105E-08	4.57514E-08	9.39196E-08	1.73636E-08	7.14087E+01	4.32436E-04	1.52033E-06	8.63933E-08
409.27	414.27	48	5.44717E-07	1.41143E-07	7.40105E-08	4.57515E-08	9.39196E-08	1.73636E-08	7.14087E+01	4.32436E-04	1.52033E-06	8.63934E-08
414.27	419.27	49	4.49809E-07	1.08952E-07	5.82265E-08	4.57389E-08	1.03654E-07	1.41087E-08	3.12897E+01	2.73474E-04	1.11507E-06	6.66222E-08
419.27	424.27	50	2.27819E-07	5.19913E-08	2.92656E-08	3.55431E-08	1.05632E-07	7.85660E-09	4.08546E+00	8.04137E-05	4.73978E-07	3.22248E-08
424.27	429.27	51	1.07799E-07	2.42649E-08	1.46431E-08	2.24447E-08	7.95543E-08	4.29261E-09	5.20197E-01	2.29930E-05	1.97625E-07	1.53078E-08
429.27	434.27	52	5.05152E-08	1.12789E-08	7.42407E-09	1.32533E-08	5.15686E-08	2.33048E-09	6.62302E-02	6.52050E-06	8.21182E-08	7.24000E-09
434.27	439.27	53	2.34724E-08	5.22783E-09	3.81724E-09	7.67996E-09	3.14197E-08	1.25802E-09	8.43051E-03	1.83138E-06	3.39704E-08	3.40385E-09
439.27	444.27	54	1.07858E-08	2.42068E-09	1.99513E-09	4.44276E-09	1.86968E-08	6.75079E-10	1.07272E-03	5.08585E-07	1.39709E-08	1.58730E-09
444.27	449.27	55	4.88090E-09	1.12310E-09	1.06367E-09	2.58531E-09	1.10208E-08	3.59845E-10	1.36395E-04	1.39351E-07	5.70065E-09	7.31857E-10
449.27	454.27	56	2.16278E-09	5.24697E-10	5.81259E-10	1.52225E-09	6.46479E-09	1.90343E-10	1.73158E-05	3.75611E-08	2.30056E-09	3.32057E-10
454.27	459.27	57	9.31802E-10	2.48891E-10	3.27962E-10	9.13765E-10	3.77868E-09	9.98292E-11	2.19091E-06	9.91469E-09	9.13503E-10	1.47169E-10
459.27	464.27	58	3.68484E-10	1.17113E-10	1.88360E-10	5.52465E-10	2.13787E-09	5.00507E-11	2.39077E-07	2.33432E-09	3.34053E-10	5.98111E-11
464.27	469.27	59	1.43446E-10	5.95120E-11	1.17349E-10	3.55859E-10	1.21618E-09	2.51576E-11	2.71472E-08	5.38914E-10	1.17884E-10	2.30215E-11
469.27	474.27	60	6.01805E-11	3.64384E-11	8.67699E-11	2.61818E-10	7.23367E-10	1.32141E-11	2.86582E-09	1.16976E-10	3.83643E-11	7.96949E-12
474.27	479.27	61	4.39002E-11	4.06593E-11	1.09292E-10	2.91283E-10	5.56375E-10	9.07992E-12	2.22250E-11	1.03554E-11	5.10332E-12	1.11225E-12

Table 6.2c. Original MCNP4B source intensities(*) and the new recommended (biased) source intensities that are consistent with the recommended weight windows for the HB-3 gamma-only problem (when 1998 water tube and collimator sections are both flooded) as determined by GETWING3.SCR.

Emax:	4.13990E-07	1.06770E-05	1.23410E-03	1.22770E-01	1.10800E+00	1.49180E+01	3.00000E-01	1.00000E+00	3.00000E+00	1.40000E+01
	mn01-01	mn02-05	mn06-13	mn14-31	mn32-46	mn47-61	mg01-06	mg07-11	mg12-15	mg16-23
	vn61-61	vn57-60	vn49-56	vn31-48	vn16-30	vn01-15	vg18-23	vg13-17	vg09-12	vg01-08
S0:	0.00000E+00	0.00000E+00	0.00000E+00	0.00000E+00	0.00000E+00	0.00000E+00	4.52970E-05	5.00745E-05	5.28339E-05	9.80429E+10
SB:	0.00000E+00	0.00000E+00	0.00000E+00	0.00000E+00	0.00000E+00	0.00000E+00	1.74905E-21	1.01212E-13	1.28201E-08	9.80429E+10
R:	1.00000E+00	1.00000E+00	1.00000E+00	1.00000E+00	1.00000E+00	1.00000E+00	3.86130E-17	2.02123E-09	2.42649E-04	1.00000E+00

mnXX-YY = MCNP neutron grp numbers, mgXX-YY = MCNP gamma grp numbers
vnXX-YY = VELM neutron grp numbers, vgXX-YY = VELM gamma grp numbers

S0 = The original MCNP source intensities (summed into broad energy groups)
SB = The recommended (biased) MCNP source intensities (summed into broad groups), consistent with the above weight windows
R = The ratio of these two (SB/S0), used to determine the calculate the fine-group biased sources to the used in MCNP

Unbiased fine-group gamma sources in MCNP order (grp 1=low E, grp 23=high E):

1.00000E+00	1.00000E+00	1.00000E+00	1.00000E+00	1.00000E+00
1.00000E+00	1.00000E+00	1.00000E+00	1.00000E+00	1.00000E+00
1.00000E+00	1.00000E+00	1.00000E+00	1.00000E+00	1.00000E+00
2.34929E+15	1.98361E+15	6.75453E+14	1.23378E+15	1.60183E+14
1.51983E+15	6.19421E+13	1.23250E+11		

Biased fine-group gamma sources in MCNP order (grp 1=low E, grp 23=high E):
Use these values for the gamma-only mcnp transport analysis involving a gamma-only source.
(For a coupled n/g calc, or a neutron-only calc, values would be different)

3.86130E-17	3.86130E-17	3.86130E-17	3.86130E-17	3.86130E-17
3.86130E-17	2.02123E-09	2.02123E-09	2.02123E-09	2.02123E-09
2.02123E-09	2.42649E-04	2.42649E-04	2.42649E-04	2.42649E-04
2.34929E+15	1.98361E+15	6.75453E+14	1.23378E+15	1.60183E+14
1.51983E+15	6.19421E+13	1.23250E+11		

In addition:

On your WWP:N card, make sure you have WTHI= 100*WTLO and WTSURV= 10*WTLO
On your WWP:P card, make sure you have WTHI= 100*WTLO and WTSURV= 10*WTLO

(*) In this particular case, this particular table is pointless since the biased source given by GETWING3.SCR is ultimately identical to the original unbiased source specified in GETWING3.SCR. It is shown here, however, so as to be completely analogous to Table C2.1c in Appendix C.2 where that was not the case. Explanation as to why this table is pointless in this case: Generally one would enter the actual gamma sources for all 23 gamma groups directly from Table 2.2b. (These total 1.35399E+17 p/s.) In Sect 5.5, however, the point kernel method showed the contribution to the dose rate downstream of the flooded collimator "due to gammas in VELM source groups 9 to 23 (E < 3.0 MeV)" to be completely negligible (less than 2%) at that location. It would therefore be even more negligible at points in and beyond the shutter. It was then decided to ignore these completely. In GETWING3.F (embedded within GETWING3.SCR) we assign these groups a dummy source strength of 1.0 p/s as shown above, as opposed to their much larger real values shown in Table 2.2b. [Likewise in MCNP4B, we assign them a value of zero. This allows us to completely avoid sampling from those groups that are known a priori not to contribute to the dose rate of interest in any meanigful fashion. Note that the real sources above 3 MeV total 7.984211E+15 p/s, and that value was therefore necessarily used on all the MCNP "fm" multiplier cards.] Thus, the only source of any significance known by GETWING3.F is in VELM groups 1 to 8. But, since they are (by design) all in the same broad gamma-weight-window group, and the sources in all other broad gamma-weight-window groups are completely negligible, the ratio of the biased and unbiased sources as calculated by GETWING3.F turns out to be 1.00000 in this particular case. If other gamma groups had non-negligible sources, this would not be the case.

(1) Much has already been said about the various MCNP models used for the 1998 water tube shielding analyses using a neutron source. For reasons that are explained in Sects 3.0 and 4.2 and cited again in Sects 5.1, C.1.2, and C.6.3, it should be noted that:

> "... Efficiency demanded that we track only those particles that had a reasonable chance of (impinging directly on the water tube, or regions immediately upstream of the water tube and) contributing to the dose rate at locations much further downstream.
>
> "... Consistent with that, the isotropic point sources were only sampled over directions within 15.13 degrees of the beam tube centerline, which required that the starting weight of the particles (as specified on the MCNP "sdef" card) be reduced to 0.017332472 at the source.

While those statements were made in reference to the neutron sources, the same applies to the gamma sources in the gamma-only water tube shielding analysis described below. Moreover, if the starting weights of the particles (as specified on the MCNP "sdef" card) are going to be reduced from 1.0 to 0.017332472 at the source, then all the other weights associated with weight window biasing must be reduced by a similar factor. Specifically, the values of WTLOW shown in Table 6.2b (and Table 6.3, below) must be reduced by a similar factor. In the WW308G 3-D weight window generator described below and listed in Appendix D.2, this is accomplished by setting the parameter "WTCONE" equal to the same "WGT" specified on the MCNP "sdef" card (0.017332472).

(2) As already noted above and demonstrated in Sect 5.5, the gamma source terms below 3 MeV have a (completely) negligible effect on the dose rate downstream of the flooded collimator, and thus an even more negligible effect on the dose rate downstream of the rotary shutter. One way to account for their presence, if one were inclined to waste (cpu) time doing so, would be to include the source terms from all 23 VELM gamma groups in both the MCNP analysis and in Subroutine SRCJST of the GETWING3.F program described above. If that were done, the biased and unbiased fine-group source-energy distributions produced by that routine and shown in Table 6.2c would clearly be different, with the biased source-energy distribution being optimized for that particular problem. Moreover, even the values of WTLOW shown in Table 6.2b (and Table 6.3 below) would be different in anticipation of the fact that MCNP will use the biased and unbiased source-energy distributions to (internally) adjust the starting weights of the particles in each energy group. Subroutine SRCJST in the GETWING3.F program is designed to be fully consistent with the known internal adjustments made by the MCNP code (based on the biased and unbiased distributions), so that the user need not (and should not) make any further adjustments to the WTLOW data (except, of course, to multiply by WTCONE if necessary). In this case, the value used on the MCNP "fm" tally multiplier cards should be equal to the total photon source summed over all 23 gamma groups (1.35399E+17 p/s). As optimized as this procedure may be, it would still start (and then promptly kill) many photons in the lower energy gamma groups that are not going to contribute to the ultimate solution. The approach taken here (based on our "a priori" knowledge of the problem) is even more efficient and might, in a sense, be considered the ultimate in source-energy biasing. This approach completely ignores all source gammas below 3 MeV in the MCNP source definition and assigns them a completely negligible value in Subroutine SRCJST of the GETWING3.F program described above. In this case, the value used on the MCNP "fm" tally multiplier cards should be equal to the total photon source summed over just the first eight VELM gamma groups above 3 MeV (7.984211E+15 p/s). Because the other lower-energy gamma sources are not known to either Subroutine SRCJST in the GETWING3.F program or to MCNP (since the sources below 3 MeV are set to zero or not represented at all), the weight window data produced by GETWING3 will remain fully consistent with that needed by MCNP, so that the user again need not (and should not) make any further adjustments to the WTLOW data (except, of course, to multiply by WTCONE if necessary). Moreover, if one were to keep only the gamma sources above 3 MeV (as in this case), but shifted the broad group boundaries (say by putting VELM gamma groups 7 and 8 into a different broad (weight window) group, the WTLOW curves produced by GETWING3.F and the biased source-energy distribution produced by GETWING3.F for use in MCNP would both be different, but the data produced by GETWING3 would remain fully consistent with that needed by MCNP, so that the user again need not (and should not) make any further adjustments to the WTLOW data (except, of course, to multiply by WTCONE if necessary). In that case, the value used on the MCNP "fm" tally multiplier cards should again be equal to the total photon source summed over just the first eight VELM gamma groups above 3 MeV (7.984211E+15 p/s).

6.4 Obtaining 3-D Broad-Group Weight Windows for Use in MCNP

Just as a sunset can be painted many ways by different artists, approximate but efficient weight window files may also be created in many different ways as long as certain fundamental guidelines like those set forth above are observed. In the limit, of course, one would always like to have a fine-mesh, fine-group, fine-quadrature, deterministic adjoint solution as someday might be possible with TORT#8 or THREEDANT#26. A weight window file based on such an adjoint solution would clearly be optimal. (But then, if one had such an adjoint solution, one could simply "fold in" the source terms to get the desired answer immediately. Moreover, if one had the capability of performing such a rigorous adjoint calculation, one could certainly

perform the same calculation in the forward mode and bypass the need for the adjoint altogether.) The unfortunate fact is that practical considerations pertaining to the use of these deterministic techniques, at present, would require modeling compromises far more limiting than those imposed by MCNP. [A partial list of difficulties that might/would be encountered in the use of these codes on this particular problem would include: (a) the inability to represent the HB-3 beam tube with its horizontal centerline while simultaneously representing the rotary shutter with its vertical centerline; (b) the impossibly large number of mesh required to represent the fine details of the geometry, including all the streaming paths that may be important; (c) problems with ray effects; (d) not having enough quadrature directions to adequately represent gamma streaming through the water tube; etc, etc.] Still, while a final solution to the HB-3 water tube shielding problem is beyond the capabilities of these codes at this time, there is little doubt that a better (truly 3-D, albeit still approximate) adjoint solution adequate for biasing purposes could have been obtained using that approach if one had the time and resources to devote to that pursuit. Fortunately, the development of an adequate weight window biasing scheme in this particular case does not require that degree of rigor. The key features of any set of weight windows needed to simulate the physics in this case are described under item (3) in Sect 6.2 above. Moreover, "As long as one can even approximate these sorts of variations (in the weight windows) from one broad group to the next, across the entire system, with any semi-reasonable degree of fidelity, and as long as the data is properly normalized relative to the starting weights of the particles ..., it is NOT necessary (for the final MCNP weight windows) to replicate all the small intricate variations (in photon importance) down to the tiniest detail; representing only the gross behavior in each energy range is usually sufficient to realize huge gains in calculational efficiency, with essentially no loss of accuracy." In that sense, it cannot be argued that the approach outlined below is unique or optimal, BUT: (a) it does accurately preserve the key weight window properties needed to simulate the physics, especially along the centerline of the system; (b) it does provide a semi-realistic and efficient approximation for the weight windows at less important locations further removed from the centerline; (c) it has been found to provide a tremendous boost to the calculational efficiency, without which no solution would have been possible; (d) the statistics associated with all detectors are quite good; and (e) statistically acceptable boundary crossing estimates of the fluxes and dose rates even downstream of the rotary shutter did provide a "positive confirmation" of the point detector responses in this same area. By any measure, the approach taken here is certainly acceptable if not optimal. With that understanding, let us begin. .

Table 6.3 shows the space- and energy-dependent weight window lower limits (WTLOW) for the four broad gamma weight-window groups along the centerline of the system in the gamma-only shielding analysis of the flooded HB-3 system, as calculated by GETWING3.SCR based on the associated 1-D adjoint analysis and the source-weight renormalization procedures described in Sect 6.2. This same data was also shown in Table 6.2b. In this case, however, Table 6.3 also shows the "ratio" of those values of "wtlow" from one 5-cm-thick importance mesh to the next. The most striking feature is the constancy of those ratios from mesh-to-mesh for any given broad group, for any given material. This, of course, is simply reflective of the exponential attenuation characteristic of any given broad group in any given material. (From Z=174.27 cm to about Z=399.27 cm, the key material is water, while from about Z=419.27 cm to about Z=474.27 cm, the key material is the "less than full density steel" used to represent the rotary shutter shield plug in the adjoint analysis.) For later reference, let "rw" denote the ratio of those values of wtlow from one 5-cm-thick importance mesh to the next "in the water", and let "rs" denote the ratio of those values of wtlow from one 5-cm-thick importance mesh to the next "in the steel". Typical average values of these ratios, of course, differ from one broad weight-window group to the next. In the case of the water, for example, "rw" may be as high as 0.73 in the 3-14 MeV energy range, or as low as 0.50 in the energy range below 0.3 MeV. Table 6.4 summarizes some typical average values for "rw" and "rs" for each of four broad energy groups. [Note that these are "derived quantities" based on an adjoint calculation for a particular response function in a given configuration. Thus, unlike basic cross section data, they are not invariant and could easily be different from one application to the next. The values shown here, however, are good for this particular application.] To begin constructing a broad-group weight-window file for later use in MCNP, one would start by identifying the group-specific value of wtlow (w0) that should be used for each broad group, in the source zone, in the actual MCNP analysis. Specifically, the values of "wtlow" shown for each broad group in (Table 6.2b and) Table 6.3 must be multiplied by whatever starting weight (wgt) is specified on the MCNP "sdef" card. Recall, for example, that to improve the efficiency of the Monte Carlo calculation, it only made sense (in these water-tube shielding calculations) to sample the isotropic source distributions over a very narrow cone of starting directions within 15.13 degrees of the centerline whose direction cosines were between 0.965335056 and 1.0; to keep the MCNP calculation properly scaled (without having to make adjustments for this particular effect on all the "fm" tally multiplier cards), the user-supplied starting weight of the photons (wgt) on the MCNP "sdef" card was reduced (from its default value of 1.0) to

wgt = wtcone = 0.017332472 = (1.0-0.965335056)/2.

Thus, if the user-supplied starting weights are reduced by this factor, then, to remain compatible, all of the weight-window information in "all" of the broad weight window groups must be reduced by this same factor. Specifically, all the values of "wtlow" shown in Tables 6.2b and 6.3 must be reduced by this same factor, including the broad group values of "wtlow" in the first importance mesh [wtlow(1st)], from Z=174.27 to Z=179.27 cm, where the incident photon beam first impinges on the water in the water tube. If "w0" denotes the corrected value of wtlow in this first importance mesh, then for each broad group, one has:

Table 6.3. Space- and energy-dependent weight window lower limits (WTLOW) along the centerline of the system [for the gamma groups(*) in the gamma-only problem], as well as the ratio of those values from one importance mesh to the next (calculated by GETWING3.F based on the associated 1-D adjoint analysis).

zmin	zmax	imp mesh	Below 0.3 MeV mg01-06(*) vg18-23	Ratio	0.3 to 1.0 MeV mg07-11(*) vg13-17	Ratio	1.0 to 3.0 MeV mg12-15(*) vg09-12	Ratio	3.0-14.0 MeV mg16-23(*) vg01-08	Ratio
174.27	179.27	1	2.58980E+15	.0000	4.94748E+07	.0000	4.12119E+02	.0000	1.00000E-01	.0000
179.27	184.27	2	1.26616E+15	.4889	2.80841E+07	.5676	2.68445E+02	.6514	7.39376E-02	.7394
184.27	189.27	3	6.16568E+14	.4870	1.57281E+07	.5600	1.72999E+02	.6445	5.42514E-02	.7337
189.27	194.27	4	3.00899E+14	.4880	8.80931E+06	.5601	1.11495E+02	.6445	3.97991E-02	.7336
194.27	199.27	5	1.52880E+14	.5081	5.09222E+06	.5780	7.35527E+01	.6597	2.96652E-02	.7454
199.27	204.27	6	7.70630E+13	.5041	2.92793E+06	.5750	4.83681E+01	.6576	2.20700E-02	.7440
204.27	209.27	7	3.77681E+13	.4901	1.64435E+06	.5616	3.12237E+01	.6455	1.61960E-02	.7338
209.27	214.27	8	1.87193E+13	.4956	9.31751E+05	.5666	2.02890E+01	.6498	1.19365E-02	.7370
214.27	219.27	9	9.34095E+12	.4990	5.30881E+05	.5698	1.32385E+01	.6525	8.82103E-03	.7390
219.27	224.27	10	4.66071E+12	.4990	3.02423E+05	.5697	8.63575E+00	.6523	6.51547E-03	.7386
224.27	229.27	11	2.32548E+12	.4990	1.72259E+05	.5696	5.63202E+00	.6522	4.81025E-03	.7383
229.27	234.27	12	1.16042E+12	.4990	9.81140E+04	.5696	3.67244E+00	.6521	3.54979E-03	.7380
234.27	239.27	13	5.79019E+11	.4990	5.58736E+04	.5695	2.39404E+00	.6519	2.61830E-03	.7376
239.27	244.27	14	2.88909E+11	.4990	3.18139E+04	.5694	1.56026E+00	.6517	1.93027E-03	.7372
244.27	249.27	15	1.38652E+11	.4799	1.75607E+04	.5520	9.93484E-01	.6367	1.39963E-03	.7251
249.27	254.27	16	6.71003E+10	.4839	9.74503E+03	.5549	6.34438E-01	.6386	1.01596E-03	.7259
254.27	259.27	17	3.34814E+10	.4990	5.54619E+03	.5691	4.13157E-01	.6512	7.47824E-04	.7361
259.27	264.27	18	1.67054E+10	.4989	3.15582E+03	.5690	2.68973E-01	.6510	5.50155E-04	.7357
264.27	269.27	19	8.33509E+09	.4989	1.79536E+03	.5689	1.75057E-01	.6508	4.04522E-04	.7353
269.27	274.27	20	4.15882E+09	.4990	1.02120E+03	.5688	1.13902E-01	.6507	2.97283E-04	.7349
274.27	279.27	21	2.07483E+09	.4989	5.80696E+02	.5686	7.40842E-02	.6504	2.18345E-04	.7345
279.27	284.27	22	1.03502E+09	.4988	3.30116E+02	.5685	4.81694E-02	.6502	1.60276E-04	.7340
284.27	289.27	23	5.16331E+08	.4989	1.87635E+02	.5684	3.13116E-02	.6500	1.17590E-04	.7337
289.27	294.27	24	2.57497E+08	.4987	1.06613E+02	.5682	2.03458E-02	.6498	8.62205E-05	.7332
294.27	299.27	25	1.28320E+08	.4983	6.05579E+01	.5680	1.32161E-02	.6496	6.31838E-05	.7328
299.27	304.27	26	6.35345E+07	.4951	3.43832E+01	.5678	8.58990E-03	.6500	4.62569E-05	.7321
304.27	309.27	27	3.12842E+07	.4924	1.92974E+01	.5612	5.53278E-03	.6441	3.36097E-05	.7266
309.27	314.27	28	1.50525E+07	.4812	1.06306E+01	.5509	3.50977E-03	.6344	2.41917E-05	.7198
314.27	319.27	29	7.39823E+06	.4915	5.95299E+00	.5600	2.25216E-03	.6417	1.75423E-05	.7251
319.27	324.27	30	3.76053E+06	.5083	3.42747E+00	.5758	1.47672E-03	.6557	1.29214E-05	.7366
324.27	329.27	31	1.84048E+06	.4894	1.91365E+00	.5583	9.46073E-04	.6407	9.35911E-06	.7243
329.27	334.27	32	9.07940E+05	.4933	1.07360E+00	.5610	6.07665E-04	.6423	6.78524E-06	.7250
334.27	339.27	33	4.49036E+05	.4946	6.03825E-01	.5624	3.91307E-04	.6440	4.92951E-06	.7265
339.27	344.27	34	2.20506E+05	.4911	3.37225E-01	.5585	2.50455E-04	.6400	3.56334E-06	.7229
344.27	349.27	35	1.09547E+05	.4968	1.90050E-01	.5636	1.61423E-04	.6445	2.58850E-06	.7264
349.27	354.27	36	5.44262E+04	.4968	1.07034E-01	.5632	1.03970E-04	.6441	1.87899E-06	.7259
354.27	359.27	37	2.70380E+04	.4968	6.02269E-02	.5627	6.69091E-05	.6435	1.36284E-06	.7253
359.27	364.27	38	1.34308E+04	.4967	3.38549E-02	.5621	4.30195E-05	.6430	9.87653E-07	.7247
364.27	369.27	39	6.67144E+03	.4967	1.90104E-02	.5615	2.76335E-05	.6423	7.15173E-07	.7241
369.27	374.27	40	3.31338E+03	.4967	1.06606E-02	.5608	1.77303E-05	.6416	5.17407E-07	.7235
374.27	379.27	41	1.64528E+03	.4966	5.96892E-03	.5599	1.13620E-05	.6408	3.73990E-07	.7228
379.27	384.27	42	8.16793E+02	.4964	3.33585E-03	.5589	7.27085E-06	.6399	2.70083E-07	.7222
384.27	389.27	43	4.05308E+02	.4962	1.85995E-03	.5576	4.64528E-06	.6389	1.94862E-07	.7215
389.27	394.27	44	2.00957E+02	.4958	1.03395E-03	.5559	2.96253E-06	.6378	1.40471E-07	.7209
394.27	399.27	45	9.94132E+01	.4947	5.72706E-04	.5539	1.88686E-06	.6369	1.01231E-07	.7206
399.27	404.27	46	7.14087E+01	.7183	4.32436E-04	.7551	1.52033E-06	.8057	8.63934E-08	.8534
404.27	409.27	47	7.14087E+01	1.0000	4.32436E-04	1.0000	1.52033E-06	1.0000	8.63933E-08	1.0000
409.27	414.27	48	7.14087E+01	1.0000	4.32436E-04	1.0000	1.52033E-06	1.0000	8.63934E-08	1.0000
414.27	419.27	49	3.12897E+01	.4382	2.73474E-04	.6324	1.11507E-06	.7334	6.66222E-08	.7711
419.27	424.27	50	4.08546E+00	.1306	8.04137E-05	.2940	4.73978E-07	.4251	3.22248E-08	.4837
424.27	429.27	51	5.20197E-01	.1273	2.29930E-05	.2859	1.97625E-07	.4169	1.53078E-08	.4750
429.27	434.27	52	6.62302E-02	.1273	6.52050E-06	.2836	8.21182E-08	.4155	7.24000E-09	.4730
434.27	439.27	53	8.43051E-03	.1273	1.83138E-06	.2809	3.39704E-08	.4137	3.40385E-09	.4701
439.27	444.27	54	1.07272E-03	.1272	5.08585E-07	.2777	1.39709E-08	.4113	1.58730E-09	.4663
444.27	449.27	55	1.36395E-04	.1271	1.39351E-07	.2740	5.70065E-09	.4080	7.31857E-10	.4611
449.27	454.27	56	1.73158E-05	.1270	3.75611E-08	.2695	2.30056E-09	.4036	3.32057E-10	.4537
454.27	459.27	57	2.19091E-06	.1265	9.91469E-09	.2640	9.13503E-10	.3971	1.47169E-10	.4432
459.27	464.27	58	2.39077E-07	.1091	2.33432E-09	.2354	3.34053E-10	.3657	5.98111E-11	.4064
464.27	469.27	59	2.71472E-08	.1136	5.38914E-10	.2309	1.17884E-10	.3529	2.30215E-11	.3849
469.27	474.27	60	2.86582E-09	.1056	1.16976E-10	.2171	3.83643E-11	.3254	7.96949E-12	.3462
474.27	479.27	61	2.22250E-11	.0078	1.03554E-11	.0885	5.10332E-12	.1330	1.11225E-12	.1396

(*) vgXX-YY are the VELM gamma group numbers comprising this broad gamma group, and mgXX-YY are the corresponding MCNP source groups (on si & sp cards); RATIO is the ratio of wtlow in mesh (i+1) to wtlow in mesh (i); ratio=1.0000 around z=409.27 cm since there are two void regions back to back. Assumes that WTLOW=WTAVG/10, and WTHI=10*WTAVG. Also note that these weights apply if and only if the user-assigned starting weights in MCNP were 1.0 and one let the code handle adjustments for source-energy biasing. However, if we also do directional source biasing and (as in the water-tube shielding problem) set the starting weights to 0.017332472 (for example), then the above weights must be multiplied by this same factor before being used in such an MCNP calculation.

w0 = wtcone * wtlow(1st, in Table 6.3)

The final values of w0 for each broad weight-window group are shown in Table 6.4, along with the corresponding mesh-to-mesh reduction factors in water and steel (rw and rs) for this particular case where each importance mesh is 5 cm thick. By starting with "w0" and multiplying by the appropriate value of "rw" multiple times (ie, once for each importance mesh up to the end of the water in the water-filled collimator), and then multiplying by the appropriate value of "rs" multiple times (ie, once for each importance mesh through the rotary shutter shield plug), one can simply and easily reconstruct the values of "wtlow" that should be used along the centerline for each of the broad group weight windows in the final MCNP analysis. [Note that use of these simple factors (rw and rs), and the fact that we ignore the small void between the end of the collimator and the start of the rotary shutter, will introduce some minor approximations, but these are "very" minor when contrasted with the "several orders of magnitude" difference between different broad groups or the 11 to 26 orders of magnitude change seen in any given broad group across the entire system.] Plots of this broad group data as a function of axial position are given in Sect 6.6, along with a brief physical interpretation of how this data is used in MCNP to improve the efficiency of the final calculation. Also note that none of the simplifying assumptions described above (in connection with the adjoint analysis or the weight window determination) exist in the actual MCNP model. The steel used there in the rotary shutter shield plug is "real" steel (7.8212 g/cc), void regions are treated as void regions, and the entire geometric model (including all materials) are treated in painstaking detail as described in Sect 3 and shown in Fig. 3.3, etc. It is only in the determination of the weight window parameters that one is free to take some liberty.

Having the broad-group weight-window parameters along the centerline is nice, but to realize the efficiencies that are necessary to solve the real problem (in any acceptable amount of time) will require a fuller description that includes all spatial points in the real 3-D MCNP model. As noted previously, the real MCNP model extends from R=0 to R=65.0 cm, and from Z=0 to Z=700 cm, with everything past Z=478.79 cm (just downstream of the shutter assembly) being treated as an internal void in which point detectors could be located if necessary. Thus, the 3-D phantom mesh used to describe the importance regions associated with the "geometry-independent weight windows" must fully enclose this entire region. In this case, the importance mesh measures 27 x 27 x 142 and goes from:

X= -67.5 cm to X= +67.5 cm (vertically) in 27 increments of 5.0 cm each,
Y= -67.5 cm to Y= +67.5 cm (horizontally) in 27 increments of 5.0 cm each,
Z= -5.73 cm to X= +704.27 cm (axially) in 142 increments of 5.0 cm each.

For those mesh that are on the centerline or whose centroids are within 10.61 cm of the centerline (ie: IX=13,14,15; JY=13,14,15), the scheme described above is excellent and well-defined. For those mesh that are further removed from the centerline, one must be a little more creative, while still applying sound judgement based on an understanding of the underlying physics.

Just as the importance increases (and the values of "wtlow" decrease) by a factor of "rw" as one moves from the impingent source region (Z=174.27 cm), down through the water tube, towards the shutter, the importance will physically decrease (and the values of "wtlow" should increase) as one moves radially outward further and further from the centerline. (In Appendix C.2.5 where there was nothing but a homogeneous tank of water, all mesh that were equidistant from the detector at the top of the tank were assigned the same weight window parameters. This made sense for that particular problem. Here, however, photons that are some distance from the centerline of the water tube and scatter towards the ultimate detector (at R=0, Z=478.79 cm) would eventually encounter the biological shield (and/or steel shields around the collimator) and be heavily attenuated before ever reaching the rotary shutter; ie, those photons that are some distance from the centerline of the water tube (in this case) would be relatively unimportant. Thus, the scheme previously used in Appendix C.2.5 would not make sense in this particular application.) In this case, since the importance must decrease as one moves radially out from the centerline, and "wtlow" must increase as one moves out from the centerline, it is simply assumed that the value of "wtlow" should be divided by the value of "rw" every time one moves out another 5 cm further from the centerline, at least as long as one remains in the pool water surrounding the first long portion of the water tube (174.27 cm < Z < 274.27 cm). The formalism actually used in the WW308G program is illustrated in Table 6.5.

As the water tube begins to pass through the concrete biological shield, the same logic applies. Those photons further removed from the centerline are less important and the corresponding values assigned to "wtlow" should increase as one moves further outward radially, except that in this case, the value of "wtlow" should be divided by the value of "rc" every time one moves out another 5 cm further from the centerline, into the concrete. Unfortunately, the value of "rc" (the mesh-to-mesh wtlow reduction factor for the concrete) has not yet been defined and, since there were no concrete zones in the 1-D adjoint model, there is no analogously rigorous way to define what it should be. To introduce a thick concrete zone into the 1-D model would perturb the problem

Table 6.4. Key parameters used by the WW308G program to generate the 3-D broad group weight window file finally used by MCNP4B in the gamma-only shielding analysis of the flooded 1998 water tube, collimator, and rotary shutter assembly. These parameters are based on the 1-D adjoint analysis and normalization procedures described in Sects 6.1 and 6.2, and summarized in Table 6.3, as well as the other MCNP normalization notes given in item 1 of Sect 6.3.

Energy range for broad gamma group weight window:	E < 0.3 MeV	0.3-1.0 MeV	1.0-3.0 MeV	3.0-14.0 MeV
Corresponding VELM gamma groups in WW broad group:	18-23	13-17	9-12	1-8
Starting weight of gammas in each broad group in MCNP (after adjusting "wgt" on the "sdef" card for directional source biasing)	---	---	---	wgt=0.017332472
wtlow in source region (w0), where w0=(value in Table 6.3)*WTCONE w0=(value in Table 6.3)*(0.017332472) as noted in item 1 of Sect 6.3	w0=4.48876e+13	w0=8.57521e+5	w0=7.14304	w0=1.7332472e-3
Ratio of "wtlow" from one 5-cm-thick importance mesh to the next in water (based on Table 6.3)	rw=0.50	rw=0.57	rw=0.65	rw=0.73
Ratio of "wtlow" from one 5-cm-thick importance mesh to the next in the half-density steel (based on Table 6.3)	rs=0.13	rs=0.28	rs=0.40	rs=0.46
Ratio of "wtlow" from one 5-cm-thick importance mesh to the next in barytes concrete, where rc=sqrt(rs*sqrt(rs*rw)) (approximation; see Appendix D.3)	rc=0.18	rc=0.33	rc=0.45	rc=0.51

Table 6.5. Spatial definition of the 3-D lower weight window limits, and the location of the magnet points, as a function of importance mesh location (x,y,z) for the gamma-only MCNP4B analysis of the 1998 water tube problem. Here: r=sqrt(x*x+y*y); x is vertical position, y is horizontal position, z is axial position.

z < 174.27 cm AXIALLY UPSTREAM OF THE START OF THE WATER TUBE	174.27 < z < 274.27 AXIALLY IN FIRST PART OF WATER TUBE SECT, UPSTREAM OF CONCRETE BIO SHIELD; SURROUNDED BY POOL WATER	274.27 < z < 309.27 AXIALLY IN LAST PART OF WATER TUBE, JUST BEFORE COLLIMATOR; SURROUNDED BY CONCRETE BIO SHIELD	309.27 < z < 404.27 AXIALLY IN REGION ALIGNED WITH THE COLLIMATOR SECTION	404.27 < z < 479.27 AXIALLY IN ROTARY SHUTTER ASSEMBLY, OR THE CONCRETE SHIELD AROUND ASSEMBLY
r < 10.61 cm radially inside or near central void in beam tube wt=w0 xd=0, yd=0, zd=1000.0 cm (xd,xy,zd) is a distant point along centerline; biasing almost parallel to the centerline	r < 10.61 cm radially inside or near flooded water tube n=1+int((z-174.27)/5.0) wt=w0*(rw**n) xd=0, yd=0, zd=1000.0 cm (xd,xy,zd) is a distant point along centerline; biasing almost parallel to the centerline	r < 10.61 cm radially inside or near flooded water tube n=1+int((z-174.27)/5.0) wt=w0*(rw**n) xd=0, yd=0, zd=330.0 cm (xd,xy,zd) biased towards a point on the centerline a short distance inside the collimator	r < 10.61 cm radially inside or near flooded rectangular hole n=1+int((z-174.27)/5.0) wt=w0*(rw**n) xd=0, yd=0, zd=405.0 cm (xd,xy,zd) biased towards point on centerline, just beyond collimator exit	r < 30.0 cm radially inside or near carbon steel shield plug nr=1+int((404.27-2.5-174.27)/5.0) wr=w0*(rw**nr)/2.0 wr=ref wt upstream of shield plug n2=1+int((z-404.27)/5.0) wt=wr*(rs**n2) for (yd,zd), see sketch; xd=0 if -12.5 < x < 12.5, xd=x otherwise
10.61 cm < r radially outside central region; in pool water, or the vessel nozzel, or the water inside vessel; mostly water in vessel; treat nozzel as water for biasing purposes m=1+int((r-10.61)/5.0) wt=w0/(rw**m) xd=0, yd=0, zd=200.0 cm (xd,xy,zd) biased towards a point on the centerline, just upstream of the start of the water tube	10.61 cm < r radially outside central region, in pool water n=1+int((z-174.27)/5.0) m=1+int((r-10.61)/5.0) wt=w0*(rw**(n-m)) xd=0, yd=0, zd=320.0 cm (xd,xy,zd) biased towards a point on the centerline near start of collimator	10.61 cm < r radially outside central region, in concrete n=1+int((z-174.27)/5.0) m=1+int((r-10.61)/5.0) wt=w0*(rw**n)/(rc**m) xd=0, yd=0, zd=z (xd,xy,zd) biased radially straight in, towards centerline	10.61 cm < r < 23.00 cm radially outside central region, in steel shields n=1+int((z-174.27)/5.0) m=1+int((r-10.61)/5.0) wt=w0*(rw**n)/(rs**m) xd=0, yd=0, zd=z (xd,xy,zd) biased radially straight in, towards water along the centerline	30.0 cm < r < 50.0 cm radially in surrounding concrete assembly (mostly) nr=1+int((404.27-2.5-174.27)/5.0) wr=w0*(rw**nr)/2.0 wr=ref wt upstream of shield plug n2=1+int((z-404.27)/5.0) wt=wr*(rc**n2) for (yd,zd), see sketch; xd=0 if -12.5 < x < 12.5, xd=x otherwise
			23.00 cm < r further out radially, in the concrete n=1+int((z-174.27)/5.0) m=1+int((r-10.61)/5.0) wt=w0*((rw**n)/(rs**4))/(rc**(m-4)) xd=x, yd=y, zd=1000.0 (xd,xy,zd) biased towards a very distant point, straight ahead axially	50.0 cm < r radially far out, in concrete bio shield nr=1+int((404.27-2.5-174.27)/5.0) wr=w0*(rw**nr)/2.0 wr=ref wt upstream of shield plug n2=1+int((z-404.27)/5.0) m2=1+int((r-50.0)/5.0) wt=wr*(rc**(n2-m2)) for (yd,zd), see sketch; xd=0 if -12.5 < x < 12.5, xd=x otherwise

too severely, and to introduce only a thin concrete region into the 1-D model would not allow one to determine the needed asymptotic value. Indeed, this is where a 2-D or 3-D adjoint solution would have been nice to have. All is not lost, however. One can still rely in engineering judgement. Obviously the correct value will lie somewhere between that for water (rw) and that (rs) for the half-density steel (3.6760 g/cc) used in the adjoint analysis. Moreover, given that the barytes concrete has a density of 3.09725 g/cc, it is quite likely that the correct value for "rc" will be much closer to that for "rs". With that in mind, a very simplistic formula was proposed and used to estimate the correct value of "rc" for each of the four broad weight-window energy groups. Quite simply, It is:

rc = sqrt(rs*sqrt(rs*rw)) = (rs^0.75)*(rw^0.25)

Values of "rc" for each of the four broad gamma groups of interest are shown in Table 6.4. While this may seem fairly arbitrary (and it is), it must be remembered that virtually all of the important high-energy gammas stream up through the water tube and very very few ever get through the concrete. Thus, one does not need to know this particular parameter very accurately. Nevertheless, some approximate value is needed if one is going to use weight windows to kill off the low importance gammas that enter the concrete, scatter about, and have the potential for greatly slowing down the calculation to the point where one could no longer run as many histories as necessary to fully resolve the contributions of other high-importance gammas. With respect to the form and accuracy of this particular approximation, it is actually not as arbitrary nor as approximate as one might first expect. A low-order justification for the assumed mesh-to-mesh weight reduction factor in barytes concrete (rc) is provided in Appendix D.3. The quantitative arguments presented there suggest that the actual value in the high-energy range (3-14 MeV) may actually be accurate to within about 2%, while the value in the low-energy range (below 0.3 MeV) may actually be accurate to within about 5%. Moreover, both are quite acceptable for the intended purpose of setting weight window lower limits and playing Russian Roulette in the concrete regions far from the centerline which ultimately do not contribute much to the final solution anyway. [Had the concrete been located in a much more critical portion of the problem, it would have been included in the 1-D (or a 2-D) adjoint analysis.] For now, the approximation given above is deemed wholly adequate for the present purpose.

Thus, as one moves radially outward from the water tube into the surrounding concrete shield, the values of "wtlow" are divided by the value of "rc" every time one moves out another 5 cm further from the centerline, into the concrete, just as shown in Table 6.5.

Further down the centerline, one begins to enter the water-filled rectangular hole down through the middle of the collimator. For those importance mesh whose centroids are within 10.61 cm of the centerline (ie: IX=13,14,15; JY=13,14,15), the weight windows used are the same as those directly along the centerline, as described above. Moving radially outward from there, some importance mesh are located in the steel comprising the central collimator, the radial shield, and/or the eccentric shield. In this region (R < 23 cm), the values of "wtlow" are divided by the value of "rs" every time one moves out another 5 cm further from the centerline. Once in the surrounding concrete, the values of "wtlow" are divided by the value of "rc" every time one moves out another 5 cm further from the centerline, into the concrete.

In the last axial region of any real interest, one begins to enter the region occupied by the rotary shutter shield plug, the surrounding concrete assembly, and the surrounding biological shield. The approach taken is the same as in earlier regions, except the central region of highest importance has been expanded to include those importance mesh whose centroids are within 30.0 cm of the centerline. This expansion of the high importance region, while it may lead to some loss of efficiency, was deemed prudent in order to account for the possibly more divergent nature of the radiation in this area caused by the void region just upstream of the shutter and the multiple streaming paths around and through the shutter. For these central importance regions, the weight windows used are the same as those directly along the centerline, as described above. (Note, as shown in Table 6.5, that a small adjustment in the axially-dependent weights downstream of Z=404.27 cm is made to account for the small void region between the end of the water-filled collimator and the start of the rotary shutter.) Moving radially outward from R=30 cm, through the concrete block holding the shutter, and then through the concrete biological shield, the values of "wtlow" are divided by the value of "rc" every time one moves out another 5 cm further from the centerline, into the concrete. This increase in "wtlow" as a function of radius is again a reflection of the gradually lower importance associated with particles in this region.

In the void beyond the downstream edge of the steel-lined concrete assembly holding the rotary shutter (ie, beyond Z=478.27 cm), the 3-D broad-group weight window generator code (WW308G.F, shown in Appendix D.2) simply assigns each importance mesh the same weight window parameters used in the last axial importance mesh along the centerline of the system. Since splitting and Russian Roulette can occur not only at collision sites (of which there are none in a void), but also at importance mesh boundaries (which do exist), holding all weight window parameters constant beyond this point will prevent any needless splitting that might otherwise occur in this final void region. Moreover, since the values of "wtlow" in the last mesh along the centerline are the lowest in the system, one can also be assured that none of the particles emerging from the downstream surface of the shield will be killed by Russian Roulette as might

occur if some other (higher) value of "wtlow" were used in this region.

Following the prescriptions described above and illustrated in Table 6.5, the 3-D broad-group weight window generator code (WW308G.F) shown in Appendix D.2 will prepare and write the necessary weight window file for MCNP4B in accordance with the format given in Appendix C.3. The "wtlow" data for each broad group, in each of the 27 x 27 x 142 importance mesh intervals, is written in ascii format within this weight-window file, and is, when used in combination with the handful of parameters on the MCNP "wwn" and "wwp" cards, fully sufficient to describe the weight windows, throughout the entire problem. In addition to that data, however, MCNP4B also allows the weight-window file to contain additional supplemental data that would normally correspond to the directional adjoint currents (aJx,aJy,aJz) in each importance mesh and each broad energy group. This supplemental data can be used for "on the fly directional biasing" at each collision site, or whenever a particle crosses an importance mesh boundary. Section 6.5 describes how similarly useful information is generated by WW308G.F and supplied to MCNP4B in place of this more rigorous data to achieve the same effect.

6.5 Magnet Points and On-The-Fly Directional Biasing

Some directions are more important than others ...
... and the most important direction from a given point usually depends on where you are.

Fortunately, if one has the directional adjoint currents (aJx,aJy,aJz) from a rigorous 3-D adjoint analysis such as TORT#8 or THREEDANT#26, information about "the most important direction" at each spatial location (for each broad group) is readily available, and MCNP4B#4 is smart enough to take advantage of this information and use it intelligently -- if it is supplied as auxiliary data in the weight-window input file. Moreover, a plot of small arrows showing a field of unit vectors aligned with the directional adjoint current would show the path of adjoint particles flowing away from the adjoint source. Conversely, if one reverses the direction of the arrows at each location, they would point in "the most important direction" (ie, the direction which, if taken by real particles, would be the most likely to contribute to the response of interest). The 3-D directional adjoint currents (aJx,aJy,aJz) by spatial mesh and energy group, which may be entered as auxiliary data in the weight-window input file (cf Appendix C.3), are used in precisely that fashion. If the optional adjoint directional currents are supplied, it appears that their sole purpose is to determine the unit vector corresponding to the adjoint current in each mesh, in each broad energy group (see lines 125 to 140, of MCNP4B subroutine WWVAL). At each collision site, the outgoing direction cosines of a particle after a collision are folded with the direction cosines forming the adjoint current vector for that spatial mesh and energy range. The resulting dot product is then applied in an exponential transform to significantly increase the assigned weight of the particle if it is travelling in a direction of high importance or to significantly decrease its assigned weight if it is traveling in the opposite direction, with a graded adjustment being made for intermediate directions. [This capability, as well as being able to use a "geometry-independent weight-window file" at all, has existed as an undocumented feature of MCNP4B since the time of its release, and is part of what is known as the "AVATAR patch". AVATAR stands for the "Automatic Variance and Time-of-Analysis Reduction" programmatic effort underway at Los Alamos#27 in which MCNP geometries could be automatically parsed into a crude XYZ mesh on which a 3-D THREEDANT adjoint analysis could be performed, and the resulting weight-window file (based on the adjoint solution) would then be passed back to MCNP which would then use that information to accelerate the Monte Carlo solution of the original problem with all of the fine geometric modeling details still in tact. Tentatively, the features described and used here will be announced in the next release of MCNP (MCNP4C) in the year 2000, and the rest of the highly-automated AVATAR system will then be made available (for a fee) at that time.]

Also fortunate is the fact that one does not need to have access to the latest 3-D discrete-ordinate codes in order to figure out which directions are the most important in most cases. In the case of the academic water tank problem in Appendix C.2, for example, it was clear that within each importance mesh, the most important direction was the one that pointed from that (x,y,z) location to the detector at the top of the water tank. Thus, in lieu of 3-D directional adjoint currents (aJx,aJy,aJz) for each broad group at each mesh location, it was sufficient to substitute a series of unit vectors (Ux,Uy,Uz) that pointed in the direction adjoint particles would flow -- ie, from the detector at the top of the tank, back toward the centroid of each importance mesh. Moreover, by using a broad-group "geometry-independent weight-window" file with this directional information, the water tank problem was made to run over 10,000 times faster than would have been possible without that information.

In the present case, the situation is much the same, except that most important direction at any given location depends upon where you are. Photons scattering in the water tube or in the reactor pool outside the water tube might be biased toward one "magnet point" whereas photons scattering in the water-filled collimator or in the concrete block surrounding the rotary shutter should be biased towards other "magnet points". Different regions of the problem may have different magnet points, and the magnet point for a given region may indeed lie outside that region in some cases. In all cases, the unit vectors (Ux,Uy,Uz) that should be used in place of the directional adjoint currents (aJx,aJy,aJz) should point "from" the magnet point,

back "towards" the center of the importance mesh in question.

Let us start with the water in the water tube and/or the water in the reactor pool outside the vessel (cf Fig. 3.3). Photons scattering anywhere in this region are only going to contribute to the final solution if they make it through the hole in the biological shield through which the water tube passes. Thus, those that are already inside the water tube should be biased "straight ahead" towards some arbitrary magnet point "way down" the beam tube, say (X=0,Y=0,Z=1000). On the other hand, this would not be a particularly good magnet point for photons scattering anywhere in the reactor pool since the "straight ahead" direction, or anything close to it like the magnet point at (X=0,Y=0,Z=1000), would preferentially bias many of them straight into the concrete biological shield where they would have very little likelihood of contributing to the final solution. Instead, those photons scattering in the reactor pool water outside the water tube should be biased towards a point along the centerline that is at or just slightly upstream of where the water tube first penetrates the biological shield (around Z=275 cm), since these are the only ones that stand any real chance of contributing to the final solution. Thus, in this case, a much more reasonable "magnet point" might be around (X=0,Y=0,Z=275 cm). On the other hand, scattering events deep in the pool water far from the centerline are far less numerous and far less important that those that occur just a short distance into the pool water (10, 15, 20, or 25 cm radially beyond the water tube). For those, especially the ones that occur between Z=250 and Z=275 cm, biasing towards this particular magnet point would improve the representation of gamma leakage into the inner cylindrical wall of the biological shield (which is not particularly important), but it would do little to improve the representation of gammas that scatter in more important directions that are somewhat more parallel to the tube centerline. As a compromise, and in deference to the importance of those particular scattering events, the "magnet point" for importance mesh in the pool water outside the water tube was moved slightly further down the beam tube to a point (X=0,Y=0,Z=320 cm) just beyond the start of the collimator. Appropriate magnet points for other regions of the problem are listed in Table 6.5, with a limited amount of discussion in the text that follows.

Before continuing, the term "biased towards" should first be clarified since it will be used repeatedly in the following discussions. When a photon or any particle undergoes a scattering event, the outgoing direction is fixed by the appropriate scattering law and the associated scattering probability distribution. The outgoing direction selected, as such, is not directly affected by any "on-the-fly directional biasing" applied by these routines in MCNP. The outgoing direction selected subsequent to a particular event will be the same whether this technique is invoked or not. What will change, is the weight assigned to a given "numerical particle" subsequent to a scattering event, based on the direction it happens to be going. Those travelling in an important direction will be assigned a bigger weight (and therefore represent more real photons available for future tracking) while those travelling in unimportant directions (away from the magnet point) will be assigned a smaller weight (and therefore represent fewer photons that the code will have to waste time tracking in the future). Thus, the code is not changing or altering scattering laws, the angle of scatter, or the directions in which particles emerge from a collision; by assigning those in some directions more weight than others, however, it is choosing more wisely those to which it will devote more calculational resources following in the future as tracking continues.

Having clarified that finepoint, consider photons a little further downstream, where the water tube penetrates the biological shield (Z=274.27 to Z=309.27 cm). For importance mesh close to the centerline, any scattered radiation should obviously be biased toward points further down the centerline, i.e., towards the entrance of the water-filled hole through the collimator. For these mesh, the chosen "magnet point" (X=0,Y=0,Z=330 cm) was located still further downstream, just a little deeper inside the collimator (axially). But what about importance mesh further out radially, say 5, 10, 15 or 20 cm inside the concrete biological shield? If scattering events in the concrete were biased toward the magnet point at (X=0,Y=0,Z=330 cm), those gammas would have to pass through a large amount of barytes concrete to get to that particular location. A few may indeed get there that way, but most would not. Of those that do scatter in the concrete, especially those that are fairly close to the water tube, the ones that are most likely to contribute to the result of interest (in and beyond the rotary shutter) are the ones that scatter back towards the water tube and then scatter again down the water tube, towards the collimator and rotary shutter -- ie, for those that scatter in the biological shield (especially those that are only a short distance beyond the water tube), the "path of least resistance" is back towards the water tube. Thus, for those importance mesh in the concrete biological shield at some general point (x,y,z), the most appropriate "magnet point" might well be a axially-floating one located at (X=0,Y=0,Z=z). While a better floating magnet point might well be at some other floating location further downstream (Z=z+dz, where one could debate "dz"), the choice of an axially-floating magnet point at (X=0,Y=0,Z=z) is clearly better (for importance mesh in the concrete) than the one at (X=0,Y=0,Z=320 cm) which would bias these gammas towards and through a large amount of concrete where many would likely be killed and their overall contribution would be negligible.

In the next axial region, in and adjacent to the collimator, the arguments are much the same. Those in the water along the centerline, or in regions within 10 or 11 cm of the centerline,

should be biased towards a point on the centerline just downstream of the collimator exit. Those in the 12 or 13 cm of steel (in the collimator itself, or the radial shield, or the eccentric shield) should be biased back along the path of least resistance towards the centerline using an axially-floating magnet point at (X=0,Y=0,Z=z) for the same reasons described above. Lastly, one must consider the concrete radially beyond the steel shields. There will be relatively few gammas in this region (because of the steel shields), so the directions into which they are biased are almost irrelevant. Nevertheless, the concrete is far less dense than the steel, and just a short distance ahead (axially) is the large cavity in which sits the rotary shutter assembly. Knowing that axial leakage into this cavity at more distant radial locations may contribute to streaming around the edges of the concrete block holding the rotary shutter, a "straight-ahead floating magnet point" was used. Thus, for importance mesh located at some arbitrary position (x,y,z), the corresponding magnet point was taken to be at (X=x,Y=y,Z=1000 cm). These magnet points are all clearly defined in Table 6.5

Lastly, the magnet points for the regions in and around the rotary shutter shield plug are too complex to describe in Table 6.5 and are instead illustrated in Fig. 6.1. [Again, it should be recalled the rotary shutter shield plug is made on Type 1020 carbon steel, and that in the real MCNP model, it has a density of 7.8212 g/cc (not the half-density steel intentionally used in the adjoint analysis.] Radiation streaming uncollided through the steel (which is actually responsible for most of the downstream dose) will not be affected by the choice of magnet points in the steel, while all scattering events in the last (downstream) half of the shield plug will always be biased towards the point(s) of interest shown along the centerline of the system. Prior to the completion of this analysis, however, there was some concern about scattered radiation streaming (a) through the rather large 1- and 2-cm clearance gaps between the biological shield and the concrete assembly holding the rotary shutter, (b) in the clearance gaps circumferentially around the rotary shutter [ie, between the steel shutter and the inner steel liner of the concrete block assembly holding the shutter, and (c) through the large-diameter beam hole in the rotary shutter. So as not to overlook contributions from scattered radiation streaming through these regions, every possible effort was made to bias as much radiation as reasonably credible into and through these particular regions. This was accomplished by dividing the top, middle, and bottom sections of the rotary shutter, the concrete block assembly, and portions of the surrounding biological shield, into a number of different spatial regions, each with their own magnet points as shown in Fig. 6.1 and identified explicitly in the logic of Subroutine GETWT in the WW308G.F weight-window generator program listed in Appendix D.2. [In the final analysis, the dose rate near the clearance gap on one side of the assembly was indeed found to twice as big as the corresponding dose rate on the other side, but both were negligible relative to that along the centerline, which itself was completely negligible.]

Sketch A in Fig. 6.1 shows the vertical mid-section of the rotary shutter assembly, between X= -12.5 cm and X= +12.5 cm. This section contains the large- and small-diam beam holes through the shutter. Not only was there concern about scattered radiation streaming through the 2.3813-cm-wide clearance gaps along the sides of the concrete assembly block between Z=414 cm and Z=446 cm, as well as the 1.7463-cm-wide clearance gaps along the sides of the concrete assembly between Z=446.4 cm and Z=478.79 cm, but there was also some concern about scattered radiation streaming diagonally through the large-diameter beam hole when the shutter was in the closed position. The fear was that some of the scattered radiation coming through the water-filled hole in the collimator and leaving the central hole in a direction 40 degrees removed from the centerline (to the upper right in Fig. 6.1) would be travelling nearly tangent to the clearance gap between the rotary shutter shield plug and the surrounding concrete assembly block, and pass through very little concrete (perhaps as little as 13 cm) before scattering in a region near the one end of the large-diameter beam hole in the shutter. Some of that scattered radiation could conceivably stream out through the clearance gaps along side the concrete block assembly, while anything scattering in a direction parallel to the large-diameter beam hole could then get "a free ride" through most of the shield plug where upon exiting, it might scatter back towards the centerline (almost tangent to the circumferential clearance gap), or scatter in a more forward direction out through the 1.7463-cm-wide clearance gap along side the concrete block assembly on that side of the beam hole. [As it turns out, the dose rate at both of these final destinations is negligible, however, the dose rate by the clearance gap on this one side of the block (near the exit of the beam hole) is indeed about a factor of two bigger than the dose rate by the clearance gap on the other side of the block.] In any event, considerations such as these led to the rotary shutter assembly being divided into multiple regions with multiple magnet points as illustrated in Fig. 6.1. Also note that while the arrows in Fig. 6.1 are intended to show the possible paths of least resistance along which scattered radiation might preferentially travel, the directional unit vectors (Ux,Uy,Uz) supplied for each importance mesh in the weight-window file [in place of the directional adjoint currents (aJx,aJy,aJz)] would actually point in the opposite direction [ie, "from" the respective magnet points "towards" the center of each importance mesh in the corresponding region]. It should also be noted that the magnet points in Sketch "A" were all located at the vertical

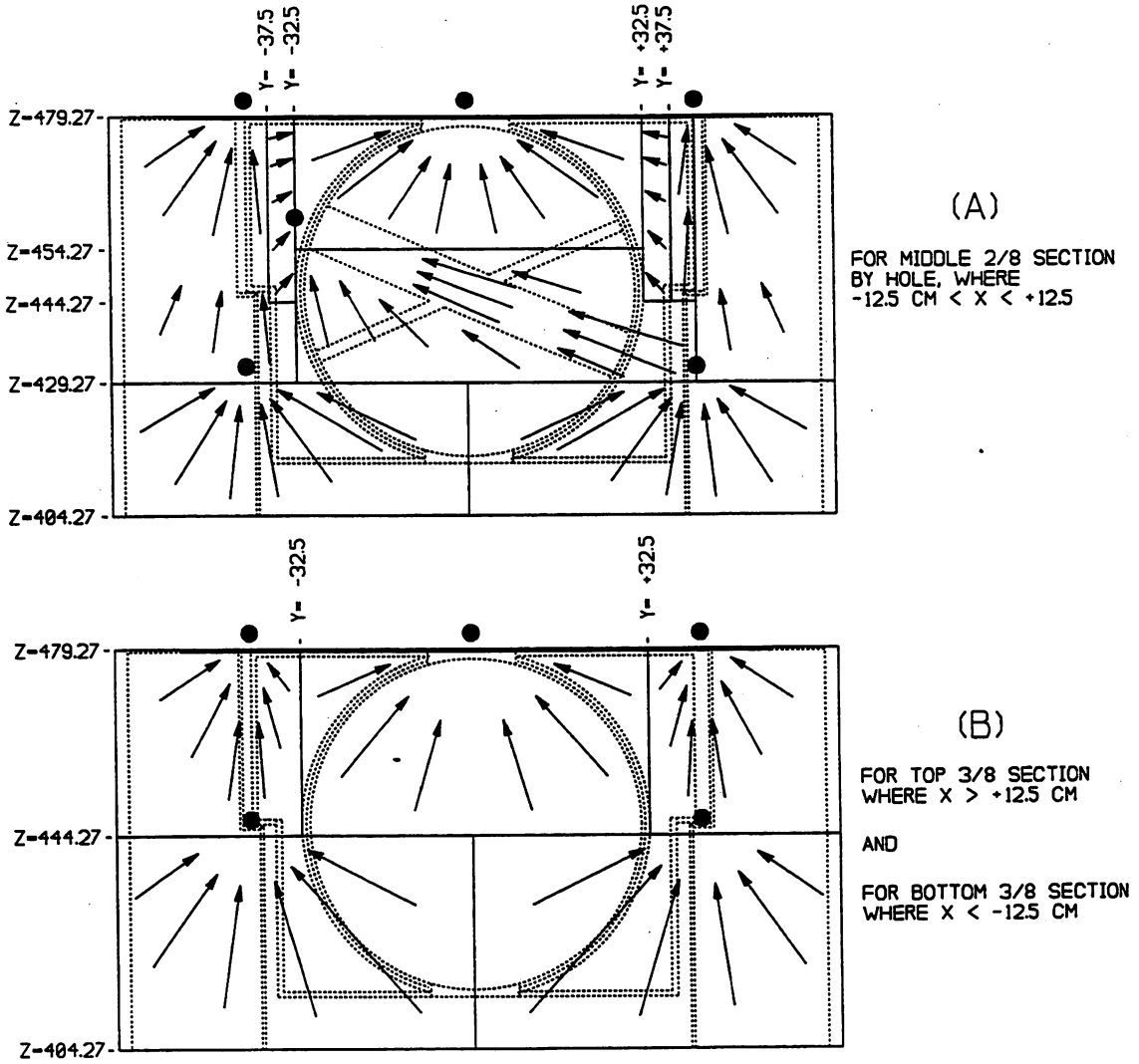


Fig. 6.1. Magnet points for the regions in and around the rotary shutter.

midplane (X=0) in the plane of the figure, while those in Sketch B were assumed to be floating in the vertical (X) direction so as to correspond to same vertical (X) location as the centroid of the given importance mesh interval. In both cases, the horizontal (Y) and axial (Z) locations of the magnet points were as shown in Fig. 6.1. More precise information may be found in Subroutine GETWT of the WW308G.F 3-D weight window generator program listed in Appendix D.2.

This concludes the discussion of the 3-D broad-group weight window generator program (WW308G.F) which then writes the (large) ascii weight-window file in accordance with the format described in Appendix C.3 so that it could then be used directly in MCNP4B Run HB308G for the final gamma-only shielding analysis of the HB-3 beam tube and rotary shutter with the water tube and collimator sections both flooded and the shutter in the closed position as shown in Fig. 3.3.

6.6 Role of the Broad Group Weight Windows in Accelerating the Final MCNP Calculation

Obviously the purpose of the 3-D broad-group weight windows in the final MCNP analysis is to speed up the calculation by placing far less emphasis on things that are unimportant so that the time saved can be used to run even more histories while emphasizing those things that are important, thereby resulting in good and reliable answers (for those things that were prejudged to be important) with reasonable overall running times. For large complicated problems such as this, the 3-D broad-group weight windows make the difference between getting good and reliable answers after a period of time versus getting none at all. But how do they work? Physically speaking, what gets short-changed, and what doesn't? Before describing the final MCNP model and the final results, it might be good to dwell on these questions momentarily.

Figure 6.2 shows the average (survival) weight for each of the four broad gamma weight-window groups along the centerline of the system as calculated by the 3-D broad-group weight window generator program (WW308G) described above. [Actually, that program only generates and stores values for the lower weight window cutoff (wtlow), below which Russian Roulette is played. However, in WW308G and in MCNP Run HB308G, it is assumed that the average (survival) weight within a given weight window is given by wtavg=10*wtlow, and that the weight window upper limit (wthigh) above which splitting will occur is given by wthigh=100*wtlow.] Except for the fact that this plot shows "wtavg" instead of "wtlow" and that both values have already been multiplied by WTCONE (=0.017332472) as indicated in Sect 6.3, the plots here are otherwise virtually identical to the data shown in Table 6.3. Several things should be noted:

1) Throughout most of the shield configuration, the curves differ by several/many orders of magnitude, although they do tend to converge near the end of the shield on the far right.

2) If and when the average (survival) weight shown here is very high, the importance of the corresponding particle is very low. Thus, low energy particles back near the source (on the left) are very unimportant, while closer to the detector (on the right) the importance of even low energy particles increases dramatically, both in absolute terms and in relation to other groups (although higher energy groups are still more important).

3) The importance of gammas in different energy groups changes by many orders of magnitude across the length of the shield, and at different rates for different energy groups -- an important physical effect that cannot be modeled efficiently (or at all) if one simply had weight windows for one broad group or (worse yet) tried to "get by" with energy-independent geometric splitting instead. With enough histories, those MCNP calculations would still yield valid energy-dependent fluxes, but it would take an extraordinarily large number of histories and an extraordinary amount of CPU time, to the point of being prohibitive for all practical purposes. In this case, the importance of the high-energy photons above 3 MeV changes by 11 orders of magnitude across the shield while the importance of low-energy photons below 0.3 Mev changes by 26 orders of magnitude across the shield.

Figure 6.3 is very similar except that is shows the lower weight window cutoff limit (wtlow) for each broad weight-window group along the centerline of the system. (Here the data is the same as in Fig. 6.2, just an order of magnitude lower since wtavg=10*wtlow.) To begin visualizing how this affects the efficiency of the calculation (and what gets ignored), assume for the moment that there are no upper limits to the broad group weight windows, or that they are so high that they never come into play and particle splitting never occurs. Now imagine a high-energy source gamma in the 3-14 MeV energy range (the only kind we model) starting off on the left with a starting weight of 0.017332472 (because we're starting all particles in the very narrow cone of directions previously described). As it travels to the right, through the system, it may slow down to the next lower energy range (1-3 MeV) or either of the other two. If it were to slow down to the 1-3 MeV range "before" getting past Z=245 cm, its weight (even if it were not diminished at all) would still be below the lower weight window cutoff for the 1-3 MeV broad group. Thus, if it slowed down "too soon", it would not automatically keep on going; moreover, if it slowed down to this energy range before getting past Z=245 cm, it would be subjected to Russian Roulette which it may or may not survive. In that sense, the lower weight window cutoff curve for the second broad group defines an "automatic acceptance

point" (Z=245 cm in this case), beyond which previously uncollided particles slowing down into this energy range will automatically be accepted and tracked further, but before which they will be subjected to Russian Roulette and possibly/probably killed. Likewise, a previously uncollided source particle slowing down into the third broad group (0.3-1.0 MeV) will not be automatically accepted or tracked any further unless it did so somewhere downstream of Z=335 cm; if it slowed down to that energy range (0.3-1.0 MeV) anywhere upstream of that location, it would be subjected to Russian Roulette where it would possibly/probably be killed. (The closer to the source the slowing-down event occurs, the more likely it is that the particle will be killed since its survival is dependent on the ratio of the particle weight to the local value of "wtlow" for the group into which it would be slowing down.) Lastly, previously uncollided high-energy source particles slowing down below 0.3 MeV will not be automatically accepted and tracked further unless the slowing down event occurred somewhere downstream of Z=415 cm. Based on these examples, it starts to become clear that a lot of the efficiency comes from the fact that the code simply kills off and refuses to track a lot of low-energy particle histories that are generated too far back in the shield to be of any ultimate importance. This does give raise one very important note of caution: If one has an MCNP calculation that has been optimally biased to efficiently calculate some particular parameter of great interest such as the total gamma dose rate downstream of the rotary shutter, then one cannot come in "after the fact" and arbitrarily insert other detectors elsewhere in the problem that may be sensitive to particles in some other energy range, and necessarily expect to get good or correct results. If this new detector is primarily sensitive to the same type of particle (ie, the same physical type of particle, in the same energy range) that the problem was previously optimized for, the result may indeed be correct and highly accurate. However, if the detector is primarily sensitive to particles in some other energy range that were systematically and preferentially killed off in the name of optimizing the earlier calculation for which the weight windows were designed, then the result returned by this new detector could not only be poorly converged, it could be plain wrong and almost no number of additional histories would help. A classic example of this would be if someone were to take a calculation that had been optimized for fast neutron shielding and later reran the same calculation after inserting a new detector to measure the thermal neutron heating rate in some region of the problem where the thermal neutrons had been "optimized out". Another example would the incremental volumetric multigroup gamma flux tallies (every 5 cm) along the HB-3 water tube and water-filled section of the collimator. In the preliminary MCNP analyses described in Appendix C.6, the total gamma flux along most of the water tube was known with a fair degree of accuracy, but the high-energy gamma fluxes that would ultimately contribute most to the dose rates further downstream were known with less and less precision as one progressed down the water tube and water-filled collimator. In this case, most of the gamma flux in the first and middle sections of the water tube came from a lot of low-energy gamma noise that ultimately would not contribute much to the final dose rate further downstream. In the final reference analysis (Run HB308G, using the broad group weight windows developed here), the reverse is almost true. The high-energy gamma flux throughout the water tube, and down near the end of the water tube and water-filled collimator (and even throughout the rotary shutter) is known with excellent precision, but the "total" gamma flux in the first and middle sections of the water tube (most of which is the low energy gamma noise that doesn't contribute much to the final dose rate further downstream) is ironically known with less precision than before, precisely because these unimportant low-energy gammas have been systematically and preferentially killed off in the name of efficiency as one goes back closer to the source. Thus, while the broad-group weight-window technique is very powerful, it must be used with a great deal of caution.

While Fig. 6.3 begins to illustrate how unimportant particle histories are eliminated in order to improve the efficiency of the calculation, it does not tell the whole story. The effect of weight windows in a real calculation is actually somewhat more pronounced. Weight "windows" are always defined in terms of three parameters: wtavg, wtlow, and wthigh, where "wthigh" is the upper limit on the weight window. (In this case: wtavg=10*wtlow, and wthigh=100*wtlow.) Everyone understands how the upper limit is used to control splitting and improve calculational statistics. [Particles traveling through the shield eventually reach a point where their own weight is greater than the specified upper weight limit in a given region, and the particle is split into two or more pieces whose weights are close to the specified average (survival) weight for the new region; as those particles travel further into the shield, they enter subsequent regions where the specified upper weight limit is still lower, and those particles split again; etc, etc. Thus, even in the presence of strong absorption or leakage, this constant splitting at lower and lower weight levels as one progresses through the shield will tend to maintain the "number" of increasingly lower weight "numerical particles" reaching the detector so that the response (based on the integral over the number of such particles times their respective weights) will still be based on a large "number" of low weight particles, and still exhibit good statistics.] Less commonly understood and often overlooked, is the vital role the upper weight limit also serves (indirectly) in helping to eliminate "even more" of the unimportant particle histories. Consider Fig. 6.4 which shows the weight window bands (wtlow, wtavg, and wthigh) for all four broad weight-window groups as a function of distance down the centerline. In this case, the weight window band for the high-energy gammas between 3 and 14 MeV has been "shaded in" for easier viewing. As before, high-energy source particles start on the left (travelling to the right), with a starting weight of 0.017332472. After traveling no more than about 40 cm in the water, they will enter a spatial region where the upper weight limit is less than their starting weight, and even those that had remained uncollided will be split into several pieces, each with a lower weight that is closer to the average weight for the new region. As they continue travelling further to the right, the same thing will happen again and again. The

point is that the original 3-14 MeV source neutrons traveling to the right, even if they remain uncollided, can never have a weight greater than "wthigh" for the shaded region. Now assume one of these 3-14 MeV photons whose weight equals "wthigh" experiences a collision and slows down to the next broad group (1-3 MeV). Even if it lost no weight in the collision, it will not be automatically accepted and tracked in this lower energy group unless the collision occurred somewhere down past Z=335 cm; if this slowing down event occurred prior to getting that far (ie, upstream of Z=335 cm), the particle weight will be less than "wtlow" for the new energy group and the code will play Russian Roulette whereupon the particle will possibly/probably be killed. The point here is that the presence of the upper weight window limit has pushed the "automatic acceptance point" forward considerably, from Z=245 cm in the previous example (with no upper weight limit) to Z=335 cm in the present (more realistic) case. This, of course will make the calculation even "more efficient" than previously thought since a lot of particles that slowed down from the first broad group to the second broad group in the earlier example and were automatically accepted for further tracking (if the slowing down event occurred downstream of Z=245 cm in the earlier example), will no longer be "automatically accepted" in this second example; some will, of course survive Russian Roulette and be tracked, but the vast majority between Z=245 cm and Z=335 cm will now be killed in Russian Roulette. Moreover, in the case of previously uncollided photons slowing down from the 3-14 MeV group to the 0.3-1.0 MeV energy group, the very existence of the upper weight window limit (wthigh=100*wtlow) has pushed the "automatic acceptance point" forward from Z=335 cm in the earlier example (cf Fig. 6.3) to around Z=445 cm in the present example (cf Fig. 6.4), even though the initial starting weight and the "wtlow" and "wtavg" specifications were left unchanged. [The dashed lines in Fig. 6.4 also show how the "automatic acceptance point" for transitions from the second group (1-3 MeV) to the third group (0.3-1.0 MeV) is now at Z=420 cm, and how the "automatic acceptance point" for transitions from the third group (0.3-1.0 MeV) to the fourth group (below 0.3 MeV) is now at Z=468 cm.] The present weight windows, actually used in WW308G and MCNP Run HB308G, and used here for illustrative purposes, are defined such that wtlow=wtavg/10 and wthigh=10*wtavg. J. S. Tang#25 and others have found that this type of weight window is generally suitable for many types of shielding analyses. Having a narrower weight window such as might be defined by wtlow=wtavg/3 and wthigh=1.67*wtavg (which correspond to the defaults in the MCNP manual), would push the "automatic acceptance points" even further downstream. While that would indeed make for a more efficient solution, it is not necessarily one that should be recommended. At some point, legitimate concerns arise over whether one is throwing away too much in the name of efficiency. [Note that nothing is ever really "thrown away"; Russian Roulette is played and surviving particle weights are always adjusted so as to maintain a fair game. Nevertheless, some statistics in less important energy ranges and/or spatial regions of the problem may eventually become compromised more than one might like.] Unfortunately, there is no single weight window size that can be recommended for all problems. The best that one can do is to become familiar with the physical effects these parameters can have, so that one is ever mindful of what is being "thrown away", compromised, or short-changed in the name of efficiency. Moreover, the fact that some particles always survive Russian Roulette will mitigate some of the concerns described above to some degree. Close examination of the results obtained from the final reference run (MCNP4B Run HB308G) using the set of weight windows described above strongly suggests that the values used here were wholly adequate for this particular application.

6.7 General Review of the 3-D MCNP Model Used in the Final Gamma-Only Shielding Analysis (Run HB308G)

The final gamma-only shielding analysis (Run HB308G) for the HB-3 beam tube and rotary shutter used the newly proposed 1998 version of the beam tube in which the water tube was defined by aluminum windows welded inside the expanded portion of the beam tube itself (unlike the original 1960 design which had a physically separate water tube that was slid inside the beam tube). The analysis was performed with the 1998 water tube and collimator sections both flooded, and the rotary shutter in the closed position. The total amount of water in the new water tube and collimator sections was approximately 1.89 feet less than in the original 1960 design. The final gamma-only shielding analysis described here did not include neutrons, secondary gammas, or activation gammas, since the fluxes and dose rates due to neutrons upstream of the rotary shutter, and the fluxes and dose rates due to secondary gammas upstream of the rotary shutter, had already been found (cf Sect 5.6) to be completely negligible relative to those caused by high-energy gammas coming from the hot end of the beam tube, streaming through the water in the water tube and flooded collimator sections, and subsequently impinging on the rotary shutter. Calculated and measured dose rates downstream of the rotary shutter due to activation of the shutter itself are discussed in Sect. 7.

The final gamma-only shielding analysis (Run HB308G) uses the most comprehensive geometric model ever developed. The approach taken was to model the entire HB-3 beam tube and rotary shutter assembly exactly as described in Sect 3 and shown in Fig. 3.3, with no approximations. Moreover, Fig. 3.3 was created from the actual MCNP input file used in this analysis. Basically, the model includes everything within 65 cm (radially) of the beam tube centerline, starting at the radial plane perpendicular to the beam tube (which is defined as Z=0), and extending axially outward along the beam tube centerline to the outermost downstream surface of the steel clad concrete assembly holding the rotary shutter. This outermost downstream surface is located at Z=478.79 cm. An

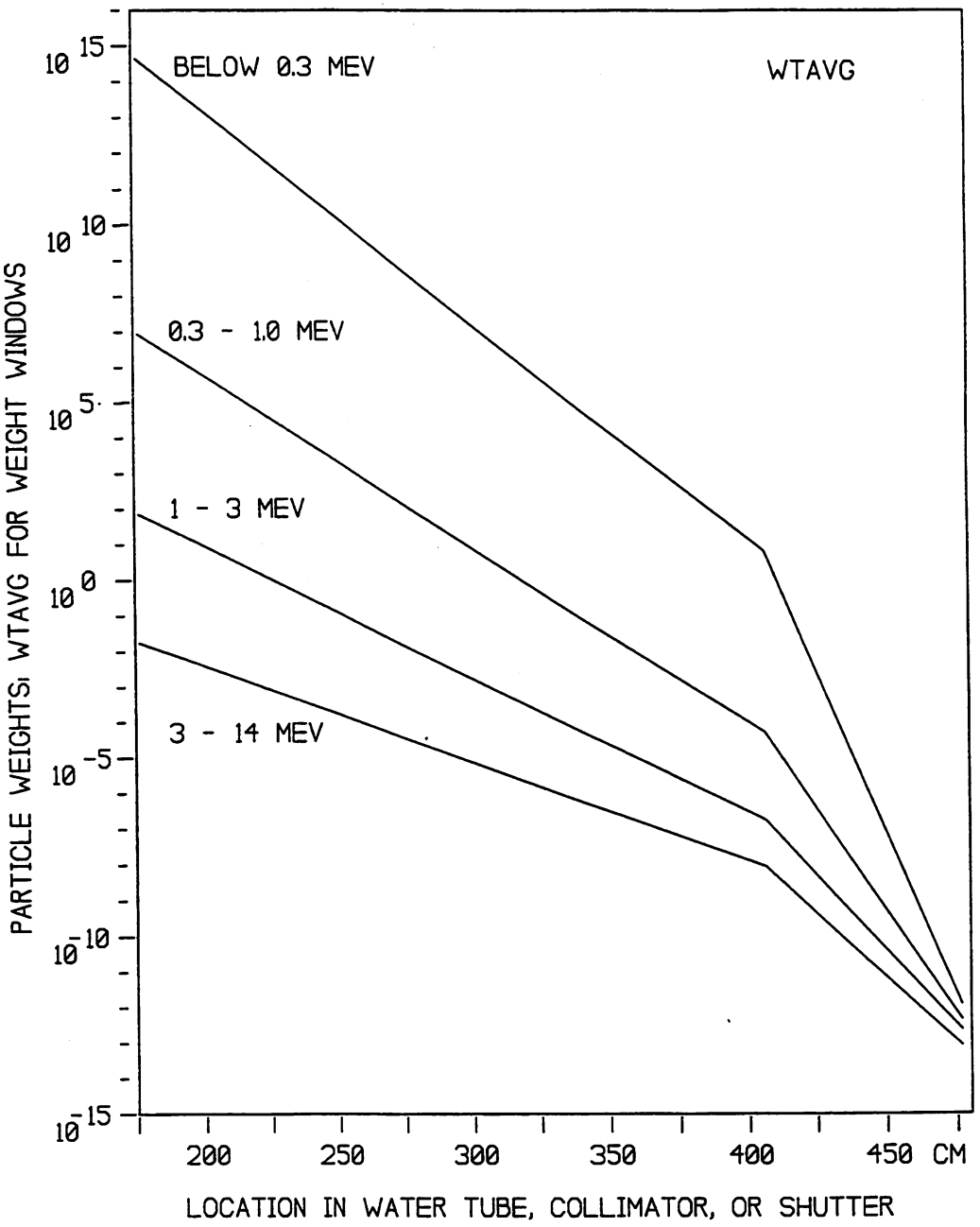


Fig. 6.2. Values of WTAVG for each of the four broad gamma weight-window groups along the centerline of the flooded HB-3 beam tube and shutter. Plot assumes that wtavg=10*wtlow.

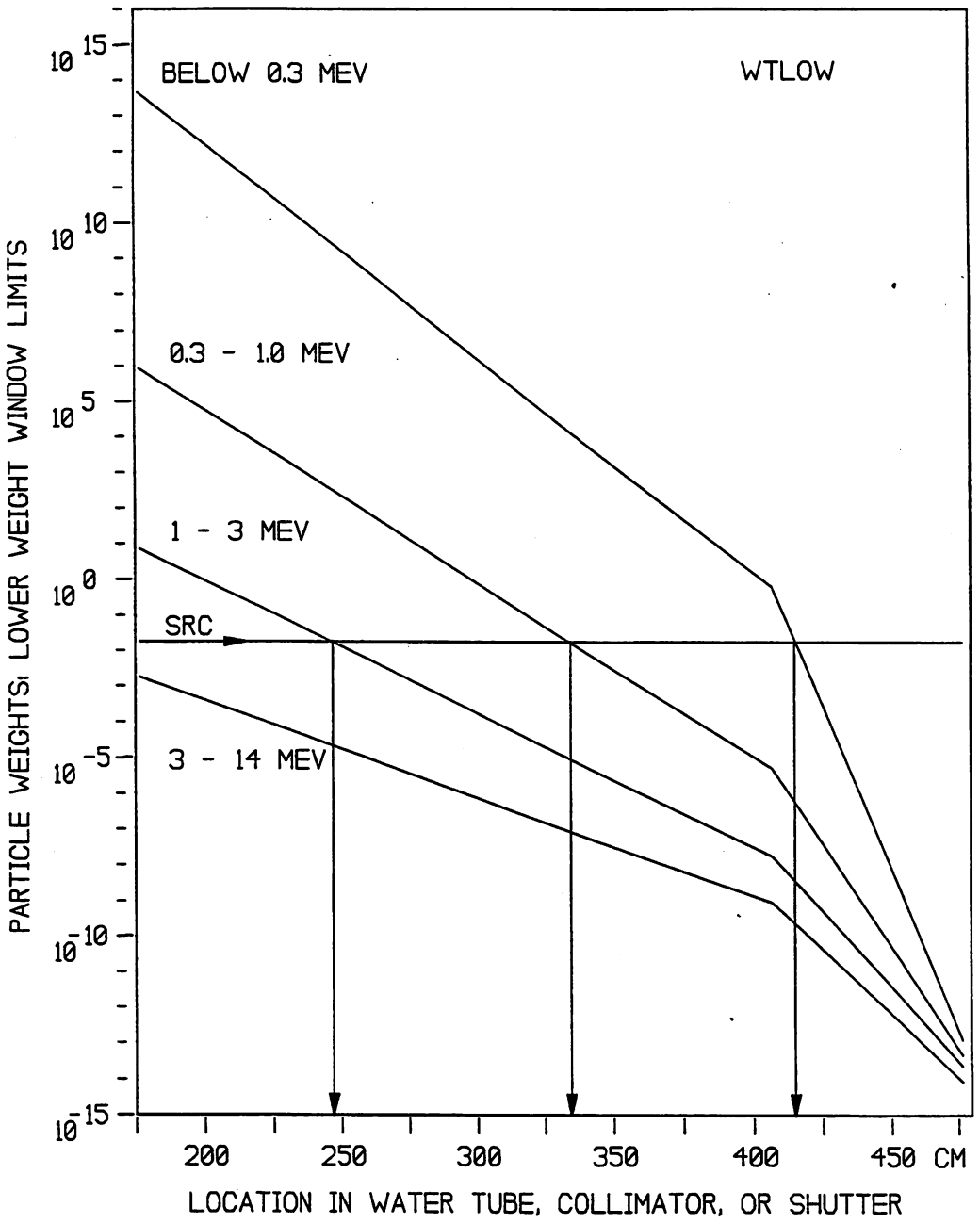


Fig. 6.3. Values of WTLOW for each of the four broad gamma weight-window groups along the centerline of the flooded HB-3 beam tube and shutter. Plot shows "where in the shield" a high energy source photon slowing down to lower energy groups would no longer be subjected to Russian Roulette (due to "wtlow" cutoff), if there were no upper weight-window limits.

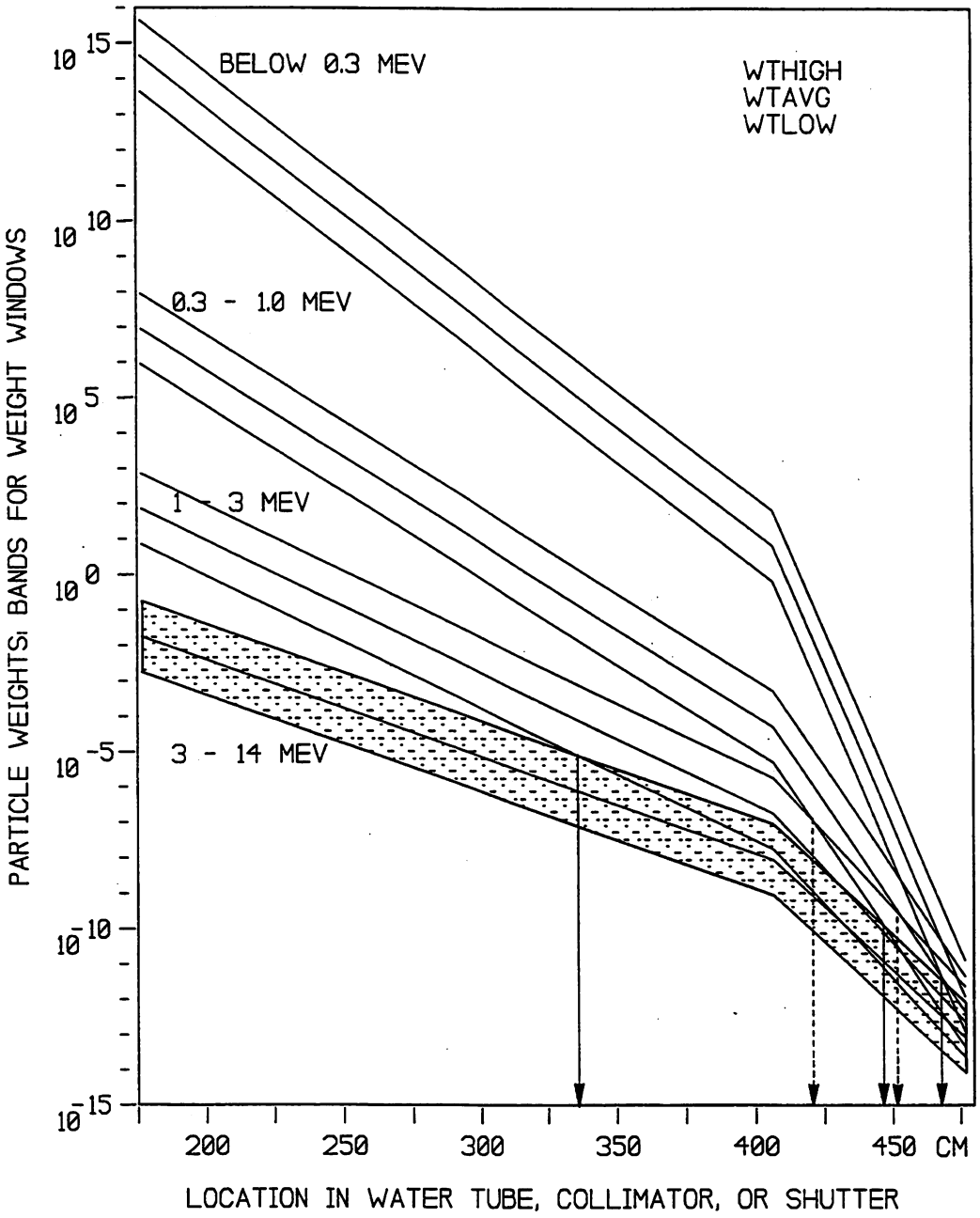


Fig. 6.4. Values of WTLOW, WTAVG, and WTHIGH for each of the four broad gamma weight-window groups along the centerline of the flooded HB-3 beam tube and shutter. Plot shows "where in the shield" a high energy source photon slowing down to lower energy groups would no longer be subjected to Russian Roulette (due to "wtlow" cutoff), for the real case where the weight window is fully defined and wthigh=100*wtlow.

additional void region extending from there, out to Z=700 cm, is also included in the model so as to accommodate point detectors sometimes located in this region. Because the source terms used are the previously described equivalent point sources located inside the beam tube, the external surfaces at Z=0, Z=700 cm, and R=65 cm may all be treated as external voids (ie, black boundaries). To be more specific, this model includes:

a) the hot end of the beam tube inside the vessel,

b) all of the small geometry regions required for the dosimetry analysis (cf Figs. 3.14 to 3.18),

c) the entire (flooded) water tube including the surrounding pool and portions of the biological shield,

d) the (flooded) collimator section including the radial and eccentric shields and surrounding concrete (shown without water in Figs. 3.10 and 3.11), and

e) the full 3-D model of the rotary shutter assembly including all the small internal void regions and the surrounding concrete (cf Figs. 3.12 and 3.13).

These figures show different views of different sections of the overall configuration, and each figure is described at some length in Sect 3. The text associated with each figure usually includes some discussion of the materials and key dimensions for each major component. Older engineering drawings used in formulating this model include:

Dwg E-42027, Rev. D, Sheet 1 (Apr 11, 1995)
Dwg E-42027, Rev. D, Sheet 2 (Apr 11, 1995)
Dwg 1546-01-M-5022, Rev 1 (Apr 4, 1961) and Rev 2 (Sep 18, 1961)
Dwg M-10070-OE-510-E, Rev 2 (Sept 30, 1987)
Dwg E-49961, Rev C (Apr 25, 1988)
Dwg E-49953, Rev A (Oct 12, 1965)
Dwg E-49945, Rev C (Apr 25, 1988)
Dwg M-11511-OH-001-E, Rev 1 (Nov 4, 1992)
Dwg E-49400

while newer engineering drawings used in formulating this model include:

HB-2 Concept Dwg E-SK-PCH-970801-1, Rev. 1 (Aug 11, 1997)
HB-4 Concept Dwg dated Jan 30, 1998 (no drawing number shown)
HB-1 (and HB-3) Concept Dwg dated Jan 30, 1998 (no drawing number shown)
HB-1 Concept Dwg. M-11537-OH-001-E (Feb 13, 1998).

In Sects 3.3 and 3.4, separate paragraphs about each of these drawings tell specifically what useful information was gleaned from each drawing and how rare (but occasional) conflicts were resolved. [While the newer drawings on HB-2 and HB-4 did not relate to the HB-3 analysis, they do provide valuable information pertaining to the new designs for these beam tubes. At the time of this study, separate new drawings specifically for HB-3 were not yet available, but most of the information on the HB-1 drawings was said to be directly applicable to HB-3. Only in one or two instances did conflicts have to be resolved, and these are clearly documented in Sect 3.]

As one might surmise, the final 3-D model is quite detailed. The actual MCNP input file for Run HB308G is listed in Appendix D.4 for future reference. It is 2560 lines long, with some of the last few comments in the header records having been added after the calculation had been run. Of these 2560 lines, approximately 1735 are needed just to describe the various cells and surfaces used to model the material regions associated with the geometry (even in spite of the fact that use of the "geometry-independent weight-window" file allowed us to keep the number of cells down to the bare minimum needed to describe just the basic geometry).

To describe the exact location and size of every surface and cell (and material) used in the model is beyond the scope of this section. Moreover, such a compilation of information would ultimately have to be a reproduction of all the information contained in the input file already listed in Appendix D.4. For such details, the reader is therefore referred to that appendix. As is standard practice, the input file shown there (and used in the actual analysis) is heavily annotated with explanatory comments on virtually every one of the 2560 lines. It is deemed to be "self-documenting".

Before discussing other (more analytic) aspects of this particular calculation, the following list of a few key dimensions, and the assumptions used in the water tube shielding analysis, is provided for quick and easy reference:

a) Point sources are located in the void portion of the HB-3 beam tube, as listed in Table 2.2b. For reasons noted in Sect 5.5, only those gamma sources in VELM groups 1 to 8 (above 3 MeV) were used in this analysis.

b) The first 0.68125-cm-thick aluminum window defining the start of the water tube is located between Z=174.27 cm and Z=174.95125 cm. The second 0.3175-cm-thick aluminum window defining the end of the water tube is located between Z=302.1868 cm and Z=302.5043 cm. The region between these windows is

flooded with water at 1.0 g/cc. The inner diameter of the water tube in this region (including the water-filled cooling coils along the inner surface) is 14.06906 cm.

c) The carbon steel collimator starts at Z=310.58 cm. The region between the second aluminum window and the start of the collimator is flooded with water at 1.0 g/cc.

d) The carbon steel collimator starts at Z=310.58 cm and extends axially to Z=399.48 cm. The diameter of the carbon steel collimator itself is 18.42262 cm. It is surrounded radially by a thin aluminum tube, a stainless steel radial shield, a stainless steel eccentric shield, and a thin stainless steel bio shield liner. The barytes concrete bio shield begins 22.9315 cm from the beam tube centerline.

e) The carbon steel collimator has a 2.75-inch (horizontal) x 5.5-inch (vertical), water-filled rectangular hole running axially along the centerline, the entire length of the collimator.

f) Downstream of the collimator is a large rectangular cavity in the biological shield which contains a stainless-steel-lined, stepped, concrete block which contains the rotary shutter shield plug. This concrete block assembly begins at Z=414.02 cm and extends out to Z=478.79 cm. The space between the end of the collimator and the start of the concrete block assembly (and the rotary shutter) is void.

g) Between the end of the collimator and the concrete block assembly is a large void space, measuring about 14.54 cm (axially) x 79.375 cm x 79.375 cm. This void space is surrounded vertically and horizontally by the biological shield. Around the sides of the internal concrete block assembly (between it and the biological shield) is a 2.38125-cm-thick clearance gap through which radiation may stream. The block is stepped and later expands. After the expansion, the clearance gap between it and the biological shield is 1.74625 cm thick. This last clearance gap (on all four sides) extends axially to the surface of the block at Z=478.79 cm where it will be directly exposed to personnel during certain maintenance operations.

h) The rotary shutter shield plug is made of Type 1020 low activation carbon steel, has a diameter of 61.9125 cm (24.375 inches), and is centered at X=0,Y=0,Z=446.405 cm. Its density was assumed to be 7.8212 g/cc in this MCNP analysis. It sits inside the previously described concrete block assembly which has a stainless-steel-lined central hole whose inner diameter measures 63.50 cm so that the circumferential clearance gap between the rotary shutter shield plug and the steel liner is 0.79375-cm-wide.

i) The rotary shutter shield plug has a large 3.5-inch-diameter beam hole and a smaller 0.875-inch-diameter beam hole which are oriented as shown in Figs 3.3 and 3.12 when the shutter is in the closed position as modeled here.

j) The central beam hole in the concrete block assembly leading to and from the rotary shutter shield plug measures 6.5 inches in diameter. Dose rates downstream of this last hole will certainly be needed since this area (and the rotary shutter itself) can be directly exposed to workers during certain maintenance operations.

6.8 Other Aspects of the 3-D MCNP Model Used in the Final Gamma-Only Shielding Analysis (Run HB308G)

Besides the physical description of the problem, there are a number of other aspects of the calculation that should be discussed at least briefly.

6.8.1 Use of the Weight Window File and Importance Specifications

The biggest difference between this MCNP calculation and most of the others in this report is the use of broad-group weight windows as supplied to MCNP4B in the form of a large, auxiliary, ascii-based, 3-D, broad-group, "geometry-independent weight-window" file created by the WW308G.F program listed in Appendix D.2. The merits of adjoint-based broad-group weight windows (in terms of accelerating the variance reduction) have already been described in the preceding subsections, while the urgent and desperate need for the ability to specify such weight windows in a "geometry-independent" fashion (that does not require hundreds or thousands of changes to the cell specifications) has been discussed at length in Appendices C.1 and C.2.2, and elsewhere throughout this report. Without the ability to specify 3-D broad group weight windows in a "geometry-independent" fashion, the solution of deep penetration shielding problems involving geometrically complex configurations would either be impossible, or next to impossible for all practical purposes. Yet, the use of the "geometry-independent weight window" file remains, for now, an undocumented feature of the MCNP4B code. (Note that it was not available at all in earlier versions.) To use the large ascii-based weight window file described above, just two things are required in the MCNP4B input:

1) On the very first record, one must have a parameter of the form: wwinp='filename'. In this case, the weight-window file produced by WW308G was simply called "wwinp", so the first header record

looked like:

message: outp=hb308.o runtpe=hb308.r wssa=hb308.s wwinp=wwinp

2) Down in the MCNP parameter specification cards, the fifth parameter on the "wwn" and "wwp" cards must be negative. Only if the fifth parameter is negative, will MCNP4B actually read and use the data in the auxiliary weight window file. In this case, those cards were as follows:

```
wwp:n  100  10  50  0  -1
wwp:p  100  10  50  0  -1
```

The first parameter says to make wthigh=100*wtlow; the second parameter says to make wtavg=10*wtlow (where "wtlow" for each broad group and each 3-D importance mesh is now taken from the weight window file); the third parameter says that no particle shall ever be split more than 50:1 or rouletted more heavily than 1:50; the fourth parameter (0) says to apply the weight window information at every collision site, as well as every time a particle crosses an importance mesh boundary; and the fifth parameter (-1) is simply a data flag triggering the use of the auxiliary "geometry-independent weight-window" file.

Use of the "geometry-independent weight-window" file gives one the freedom to specify the geometry in the simplest possible terms. Spatial "cells" are now needed only to specify different material regions; unlike in the past, no additional cells are needed in the MCNP input to specify different importance regions. Thus, the present model can be fully specified with as few as 88 cells, as shown in Appendix D.4. Without this new capability, many thousands of cells would have been required (literally). A few additional comments regarding the present cells are warranted at this point:

For each cell that is specified, an importance value (imp:n=0,1,2,3,4 or imp:p=0,1,2,3,4) is still required. Because of the frequent need to run neutron-only problems, one recommended scheme is to always specify an "imp:n=" value on each cell card, but not the "imp:p=" value. When a coupled n/g calculation or a gamma-only calculation is needed, go to "MCNP print table 60", strip off a list of cells in the order read by MCNP, and then go back and include a separate "imp:p=" card with the values for all the cells given collectively in one place. This makes the data much easier to manage. In this case, the "imp:p=" data looks like:

```
imp:p  $ obtained from MCNP output table when I ran a fake MCNP run with neutrons;
       $ here imp:p=imp:n in all 88 cells;  note that the non-zero values will be
       $ ignored as soon as the wwinp file is read, but it must be entered anyway
       1 0 1 1 1 1 1 1 1 1 0 1 1 1 1 1 1 1 1 2
       2 2 2 2 1 1 1 1 1 1 1 2 2 1 2 2 2 2 2 2
       2 2 2 2 2 2 2 2 1 1 1 1 1 1 1 1 1 1 1 1
       1 1 1 1 1 1 1 1 1 1 1 1 1 1 1 1 1 1 1 1
       1 1 1 1 1 1 1 0
```

While Run HB308G is a gamma-only calculation (as specified by the MCNP "mode p" parameter card), the presence of the "imp:n=" data does not hurt a thing. [Note that the "wwinp" file MUST also include dummy weight window information for one dummy broad group of neutrons, even though this data is never used in a gamma-only calculation.]

In this particular input file for Run HB308G, the imp:n=2 and imp:p=2 values (in some cells around the dosimeters) represent old "legacy" information left over from the dosimetry analysis. They are irrelevant here. In fact, all non-zero values specified for various cells are now irrelevant in the sense that they will now be ignored completely since the MCNP4B code will, if the "wwinp" is specified, use the 3-D broad-group weight window information for each (phantom) XYZ importance mesh in that file in place of importance data specified in the MCNP input. The only MCNP cells with importance values of any significance are those in which the user specifies an importance of zero. Those cells will still be honored and treated as infinitely black absorbers such that particle tracking will stop immediately whenever a particle enters one of these cells. This is frequently used to flag external non-reentrant boundaries. In this particular problem, it is also used for a portion of the aluminum beam tube wall below the importance cutoff plane (Surf 1007), located at Z=118.6879 cm. Its use in that capacity is described below and elsewhere throughout this report.

6.8.2 Creating, Saving, and Using and Internal Boundary Source Downstream of the Collimator

Initially it was thought that one would be fortunate if this all-inclusive model, including the entire HB-3 beam tube and the complete rotary shutter assembly, could simply be used to generate a good internal boundary source located just downstream of the water tube and flooded collimator sections, but upstream of the rotary shutter. Such a boundary source, similar to (but much more detailed and complete than) that described in Appendix C.6.5, would have to include an enormous number of high-energy gammas if the corresponding space-energy-direction-dependent distribution were going to have sufficient resolution to then describe the transport of gamma radiation through the rotary shutter assembly, which would be necessary in order to obtain accurate dose rates at

various locations of interest downstream of that assembly. Moreover, it was anticipated that this boundary source, once saved, could then be used in a follow-up ("bootstrapped") analysis of the rotary shutter assembly using the same geometry as in this problem, but with far more photon histories. Such an internal boundary source would also be good to have in case the shutter itself had to be redesigned at some future time (a distinct possibility that would be partially dependent on the outcome of the present analyses). Ultimately, the present analysis proved so successful, and the quality of the results so reliable (and the dose rates so low), that a separate follow-up analysis of the rotary shutter using this boundary source was never required. Nevertheless, a good and reliable, binary-formatted, MCNP particle-crossing boundary source was saved at Z=401.9645 cm, and could be used in the future if the shutter is ever redesigned and has to be reanalyzed. This internal boundary source file includes the coordinates, direction cosines, energies, and particle weights for over 5.6 million high-energy particles crossing this artificial internal boundary at Z=401.9645 cm. Since it required over 542 MB of disk space, it was subsequently archived to tape for future reference.

To obtain this internal boundary source and facilitate its use in the future, two or three minor modifications to the problem geometry were introduced in Run HB308G. Basically, the configuration was "sliced in half" at this axial location by three new (artificial) plane surfaces:

Surface number 4196 (pz) at Z=401.9545, located 0.01 cm upstream of boundary source
Surface number 4197 (pz) at Z=401.9645, corresponding to the boundary source location
Surface number 4198 (pz) at Z=401.9745, located 0.01 cm downstream of boundary source
and now used for F1 tallies

Surface number 4195 (pz), an existing surface at Z=401.9445, corresponds to the downstream side of the flange around pool seal (B). Three new "void" cells were then introduced:

Cell 9981, between Surfs 4195 and 4196;
Cell 9982, between Surfs 4196 and 4197;
Cell 9983, between Surfs 4197 and 4198.

In Run HB308G, the binary-formatted MCNP particle-crossing internal boundary source file would be written for those photons crossing the middle surface (4197), while a detailed printed listing of F1 tally results for surface 4198 would also be prepared and saved. These F1 tallies show the energy- and direction-dependent gamma leakage corresponding to each of the 23 VELM energy groups, and each of the angular-dependent "direction bins" shown for the preliminary model in Appendix C.6, for the area directly in front of the water-filled rectangular hole in the collimator (Segment 5), and each of the four other larger areas comprising the remainder of Surface 4198.

In the event that the shutter is ever redesigned, minor changes could easily be made to its representation in the present model. To run such a follow-up analysis, one could then use this slightly-modified input file with the following three changes:

1) Comment out the "sdef" source specification cards now found in Run HB308G. These correspond to the equivalent point sources in the beam tube and would no longer be needed.

2) The boundary source file generated here in Run HB308G would be applied at Surface 4197 by simply changing the "wssa" parameter card to a "rssa" parameter card.

3) On the specification card for Cell 9981, set imp:n=0 and imp:p=0. This will cause Cell 9981 to be treated as an infinitely black absorber, so that particles reflected back into this region would be killed immediately and tracked no further. This will effectively "decouple" the rotary shutter analysis from all the existing beam tube geometry which may then be left in place, unchanged.

Such a follow-up analysis would also produce an F1 gamma-leakage tally edit on surface 4198, which may then be compared to the one produced in Run HB308G for quality assurance purposes. The two should be identical.

6.8.3 Source Terms Included, and Values Used on the "fm" Multiplier Cards

As shown in Sect 5.5 for the 1998 water tube, over 99% of the total gamma dose rate just upstream of the rotary shutter is due to the original gamma point sources above 3 MeV, corresponding to VELM gamma energy groups 1 to 8. Further downstream, the percentage of the total gamma dose rate due to these high-energy gamma sources will be even more predominant. For that reason, those particular gamma sources (shown in Table 2.2b) above 3 MeV are the only ones included in this analysis. Based on that, the value entered on all the "fm" tally multiplier cards should correspond to just the total gamma source above 3 Mev (7.984211e+15 p/s) rather than the total gamma source summed over all energies (1.35399E+17 p/s). Because of the way the broad gamma group weight windows were designed, with one broad weight window spanning all eight VELM gamma source groups above 3 MeV, there is no need (in this case) to enter a biased source-energy distribution (see discussion of Table 6.2c in Sect 6.2). [Had the weight windows been designed with different energy boundaries, one would have

needed to specify the original (unbiased) source-energy distribution as well as a biased source-energy distribution based on the results of the GETWING3.F program which properly renormalizes the biased source-energy distribution in a fashion consistent with both the adjoint-based weight windows and the use of that data in the MCNP program.]

6.8.4 Source Direction Biasing and Starting Weights

It would be totally unproductive and wasteful to start particles in directions that stood no chance entering the water tube directly or after one or two shallow angle scattering events. Thus, the isotropic source terms given in Table 2.2b are only sampled over a narrow cone of starting directions within 15.13 degrees of the beam tube centerline (whose direction cosines are between 0.965335056 and 1.0). Rather than adjust all the "fm" tally multipliers each time this cone is altered, it was far easier to simply reset the starting weights in a fashion consistent with the fractional solid angle over which particles will really be sampled. For an isotropic source which is only sampled between direction cosines mu(max) and mu(min), the corresponding starting weight based on this fractional solid angle is given by wgt=[mu(max)-mu(min)]/[cos(0 deg)-cos(180 deg)], or in this case: wgt = 0.017332472 = (1.0-0.965335056)/2. Note that the broad group weight windows in the weight-window file must be (and have been) determined in a fashion consistent with the starting weights of the particles in the MCNP analysis. [Otherwise, source particles impingent on the water tube would either start "splitting like crazy" or be killed upon impact, neither of which is terribly useful. In this case, had the weight windows still been based on a starting weight of 1.0, most (virtually all) gammas would be killed by Russian Roulette upon entering the water tube, and very little response (with correspondingly poor statistics) would have been seen downstream of that location. On the other hand, when properly normalized, everything works amazingly well.]

6.8.5 The Importance Cutoff Plane

The importance cutoff plane defines an axial location (Z=118.6879 cm in this case) below which any photons striking the aluminum wall of the beam tube would be immediately killed and tracked no further. Photons traveling uncollided through the central void of the 10.16-cm-ID beam tube would remain unaffected, as would photons striking the aluminum wall of the beam tube at axial locations downstream of the importance cutoff plane. Because the importance cutoff plane defined by surface 1007 is located at Z=118.6879 cm, close to the inner wall of the vessel and a full 55.58 cm upstream of the start of the water tube, shallow-angle scattering events in the tube wall anywhere close to the water tube (and collisions in the vessel nozzle) will all be properly accounted for in the present gamma-only shielding analysis.

The concept of an importance cutoff plane and the role served by it were already described briefly in Sects 2.7 and 3.0. The necessity of moving it for the dosimetry analyses is described in Sect 4.2. It is also mentioned briefly in Sect 5.1 and Appendices C.1.2 and C.6.3. The original need for it stems back to the "intended use of the equivalent point sources in the beam tubes". In Sect 2.7, it is noted that:

> "While it is fine to include the hot tip of the beam tube and the surrounding beryllium in the model for illustrative purposes, that portion of the aluminum beam tube within a foot or two of any point source should be assigned an importance of zero so that as particles pass from the internal void into the body of the beam tube in this imp=0 region, they vanish immediately. If this were not the case, radiation from the equivalent point sources inside the beam tube would scatter in the adjacent materials and contribute further to the fluxes and dose rates farther downstream when, in fact, the effects of such scattering events near the hot end of the beam tube have already been represented in the global analyses and incorporated in the determination of the equivalent point sources. To not use a zero importance zone in this region would cause the subsequent calculations to effectively count many scattering events two or more times."

Sampling the source only over a narrow range of directions within 15.13 degrees of the centerline partially alleviates that concern, but not entirely. Given that the beam tube has an inner radius of only 5.08 cm, some source particles could still impact the beam tube wall within 18.79 cm of their point of origin. Thus, the need for the importance cutoff plane still remains. But "how and why" was a directional cone of 15.13 degrees chosen in the first place? It was originally set during the time the dosimetry analyses were being performed, and later retained in the beam tube shielding analyses. [Moreover, it could and perhaps should be narrowed down considerably more in future shielding analyses.] At the time it was originally set (in the dosimetry analyses), we looked at the locations of the most axially-advanced neutron sources in the beam tube (cf Table 2.2a) and asked "What angular range would be necessary to envelope everything within a few centimeters of the dosimeters (in all directions) as seen from the most axially-advanced neutron source in the beam tube?". The answer was "all source particles within 15.13 degrees of the centerline." It greatly improved the efficiency and worked quite well. When it came time to begin the early shielding analyses, the original objective was (and still is) to include everything that stands a semi-reasonable chance of "making it through" the vessel nozzle. For the most axially-advanced

point sources, the original cone of 15.13 degrees could have been narrowed down a bit, but not much. Unfortunately, the same cone of angular directions must be used for all point sources in the model. In deference to the most axially-advanced point sources, we did not really want to narrow it down any further. Yet, because the equivalent point sources are distributed up and down the beam tube centerline, and because the beam tube is thin and the vessel water outside the beam tube is relatively transparent to gammas passing through the beam tube, it was recognized that many of the source gammas in this 15.13 degree cone would simply fly off through the vessel water and strike the vessel, thus burning up valuable computer time but never contributing to the final solution downstream of the collimator or rotary shield plug. Only those that passed through the beam tube near the vessel nozzle could do that. In recognition of that, plus the need to not "doubly account" for scattering events in the beam tube wall close to the core, plus the still present desire to use a source cone of 15.13 degrees for at least some source points (and therefore for all source points), the idea of an "importance cutoff plane" was invented. It still allows one to sample over all necessary directions (even for the most axially-advanced point sources), yet particles that have no chance of making it through the vessel nozzle are killed on their first flight before any real computer time is wasted.

6.8.6 List of the Flux, Leakage, and Dose Rate Tallies in Run HB308G

The final gamma-only shielding analysis corresponding to Run HB308G (with the 1998 HB-3 water tube and collimator sections both flooded, the rotary shutter closed, and the HFIR operating at 100 MW) included the following MCNP output tallies:

Tally 15: Gamma fluxes (p/s/cm2) midway between the collimator and the shutter
Tally 25: Gamma dose rate (mrem/hr) midway between the collimator and the shutter

Tally 35: Gamma fluxes (p/s/cm2) 0.5 cm past the concrete block containing the shutter
Tally 45: Gamma dose rate (mrem/hr) 0.5 cm past the concrete block containing the shutter

Tally 55: Gamma fluxes (p/s/cm2) 1.5 feet past the concrete block containing the shutter
Tally 65: Gamma dose rate (mrem/hr) 1.5 feet past the concrete block containing the shutter

Tally 75: Gamma fluxes (p/s/cm2) 3.0 feet past the concrete block containing the shutter
Tally 85: Gamma dose rate (mrem/hr) 3.0 feet past the concrete block containing the shutter

Tally 184: Approximate gamma dose rate (mrem/hr) axially, through the water tube, in each of 30 equal volume segments, with dz=4.24119 cm

Tally 194: Approximate gamma dose rate (mrem/hr) axially, through the collimator hole, in each of 20 equal volume segments, with dz=4.44500 cm

Tally 201: Primary gamma leakage (p/s) at upstream entrance of the collimator hole; L(z-) and L(z+) only; given for each of 5 spatial regions

Tally 211: Primary gamma leakage (p/s) 2.4945 cm downstream of the collimator hole exit; L(z-) and L(z+) only; given for each of 5 spatial regions; see segment 5

Tally 221: Primary gamma leakage (p/s) 2.4945 cm downstream of the collimator hole exit; given for many angular bins, in each of 5 spatial regions; see segment 5

Tally 231: Primary gamma leakage (p/s) on downstream surface of the concrete block holding the shutter; L(z-) and L(z+) only; given for each of 10 spatial regions

Tally 212: Primary gamma dose rate (mrem/hr) 2.4945 cm downstream of the collimator hole exit; given for each of 5 spatial regions; see segment 5

Tally 232: Primary gamma dose rate (mrem/hr) on downstream surface of the concrete block holding the shutter; given for each of 10 spatial regions; see segment 10

The key results of programmatic interest are described in Sect 6.9, while a few of the more detailed tally results are discussed separately in Appendix D.5.

Tallies 184 and 194 were included so that one could monitor how well the code was tracking photons through the flooded water tube and flooded collimator. If statistics here were not good to excellent, then all other results farther downstream would be meaningless.

Despite potentially good statistics, for any of the above point detectors to be at all "trustworthy", Segment 5 of Tally 184 and Segment 5 of Tally 194 would have to be well converged in all the higher-energy groups. Likewise, for those point detectors downstream of the concrete block assembly holding the rotary shutter to be very trustworthy, one or more of segments 5-10 in Tally 231 would have to be at least fairly well converged also. If these conditions are not met, then the point detector values may not be trustworthy,

even though they may appear to have good statistics.

Only if Tally 212 (the boundary crossing estimate of the primary gamma dose rate downstream of the collimator hole) has good statistics, is it possible to have a high degree of confidence in the point detector estimates. If the boundary crossing estimate in Tally 212 is well converged, then the point detector represented by Tally 25 will be even more accurate; if the boundary crossing estimate in Tally 212 is not well converged, the point detector estimate given by Tally 25 may or may not be any good (even if its statistics appear to be good).

Only if Segment 10 of Tally 232 (the boundary crossing estimate of the primary gamma dose rate downstream of the central 6.5-inch-diam disk directly in front of the shutter) has good statistics, is it possible to have a high degree of confidence in the point detector estimates. If Tally 232 is well converged in segments 5-10, then the point detector estimates corresponding to Tallies 45, 65 and 85 will be very accurate; if these portions of Tally 232 are not well converged, the point detector estimates corresponding to Tallies 45, 65 and 85 may or may not be any good (even if their statistics appear to be good).

6.8.7 Comments in the Header Records of Run HB308G Shown in Appendix D.4

Run HB308G was the last in a series of attempts to analyze the gamma-only shielding problem. In the end, it was fantastically successful. But, it was not the first in the series. As a complex calculational model evolves (usually resulting in a series of calculations), notes describing all changes (including successes and failures) are maintained in the header record file for future reference. After the final successful completion of the series, comments pertaining to the last successful run are updated one last time, but all previous comments are retained for future reference. Thus, in browsing through Appendix D.4, most readers would be encouraged to skip directly to the last set of comments pertaining specifically to Run HB308G. Most key things of interest are summarized here in Sect 6.

The final gamma-only shielding analysis (Run HB308G) was in fact a multipart calculation that was run in stages, sometimes several days or weeks apart. Periodically during each step, a "restart file" was dumped to disk so that if the computer should fail for any reason, the calculation could be restarted from the last dump file. A restart file was also created at the end of each calculational step. Input files for the subsequent continuation runs consist of only 3 or 4 lines, giving the name of the most recent restart file and the number of histories (NPS) to which the calculation is to be extended.

HB308G1 initially ran 240,000 histories between 06/21/98 16:21:40 and 06/21/98 21:50:35. These experienced a total of 58,312,798 collisions (each of which contribute marginally to the point detector tallies). More importantly, 374,828 real particle tracks were recorded crossing surface 4197, just downstream of the flooded collimator and upstream of the rotary shutter. Information regarding the coordinates, direction cosines, energy, and weight of each particle crossing this surface was saved as part of the internal boundary source file being generated and saved in binary format for possible future use. Indications were that every 1,000,000 source particle histories would take approximately 22.84 wall-clock hours on each of 8 nodes on the ORNL SP2 computer. This was considered quite encouraging given the complex nature of the problem and the fact good and meaningful results were being obtained.

HB308G2 extended NPS up to 1,000,000 histories and finished with dump 126 at 06/23/98 02:08:24. These experienced a total of 212,701,257 collisions (used in point detector estimates) and, more importantly, actually allowed 1,411,263 real particle tracks to cross surface 4197.

HB308G3 extended NPS up to 2,000,000 histories and finished with dump 251 at 06/24/98 06:19:21. These experienced a total of 415,638,456 collisions (used in point detector estimates) and, more importantly, actually allowed 2,769,376 real particle tracks to cross surface 4197. Cumulative results up to this point were considered more than adequate, and the calculation was temporarily halted for two weeks. For the sake of generating a still better boundary source for future reference, however, additional continuation runs were submitted in July.

HB308G4 extended NPS up to 3,000,000 histories and finished with dump 376 at 07/08/98 11:24:20. These experienced a total of 635,895,583 collisions (used in point detector estimates) and, more importantly, actually allowed 4,244,571 real particle tracks to cross surface 4197.

HB308G5 extended NPS up to 4,000,000 histories and finished with dump 501 at 07/09/98 06:29:49. These experienced a total of 855,219,125 collisions (used in point detector estimates) and, more importantly, actually allowed 5,688,819 real particle tracks to cross surface 4197. The objective here was to drive the key fsd's (fractional standard deviations) for both the point detectors and the boundary crossing tallies down to the 3-4% range before terminating the calculations. Moreover, the final internal boundary source file named "HB308G.S" now contained detailed information for 5,688,819 real particle tracks, primarily in the high energy range, and had grown to occupy about 542 MB of disk space. For that reason, the calculation was finally halted and the internal boundary source was archived to tape for future reference.

6.9 Results from the final gamma-only shielding analysis (MCNP4B Run HB308G5)

The key results of programmatic interest are summarized in Fig. 6.5. Everything else in the remainder of Sect 6 and Appendix D.5 may be regarded at supplemental supporting information.

6.9.1 Point Detector Results Along the Centerline

Figure 6.5 shows that the dose rate immediately downstream of the rotary shutter at Z=479.29 cm is 0.8934 mrem/hr +/- 3.4%. This is based on point detector Tally 45, and is for the standard case where the 1998 HB-3 water tube and collimator sections are both flooded, the rotary shutter is closed, and the HFIR is operating at 100 MW. Note, however, that this is the calculated dose rate due to gammas initially streaming down the beam tube and impinging on the flooded water tube. It does not include the dose rate due to activation gammas in the shutter itself or any surrounding materials. [The dose rate due to activation of the shutter is actually much higher, and is discussed separately in Sect 7.] Fig. 6.5 also shows that the dose rate along the centerline, 1.5 feet from the downstream surface of the steel-lined concrete block assembly holding the shutter is only 0.3033 mrem/hr +/- 1.1%, while the dose rate 3.0 feet from this surface is only 0.2088 mrem/hr +/- 0.6%. Based on the supporting information described below, a high degree of confidence should be associated with these calculated values, prior expectations not withstanding. Fig. 6.5 also shows that the dose rate in the void between the flooded collimator and the rotary shield plug (at Z=407.464 cm) is significantly higher, at 103.99 Rem/hr +/- 0.5%. Note that this value is about four times higher than that which would exist at this location with the old 1960 water tube and collimator sections both flooded (cf Sect 5.5 and/or Appendix C.6).

Detailed fluxes and dose rates, by energy group, for detectors at the four locations shown in Fig. 6.5 are given in Table 6.6. Note that for the three detector locations downstream of the rotary shutter, the fluxes and dose rates in each energy bin are amazingly and uniformly well converged to within about 3 or 4% for most groups, and even more tightly converged for the more important high-energy groups, with the aggregate total dose rates being converged within 3.4%, 1.1%, and 0.6% as one moves further downstream. [The "curiously poor" low-energy fsd's for the one detector upstream of the rotary shutter are explained in Sect 6.9.2.3; in a biased calculation such as this, they are totally irrelevant and are to be expected.]

The extremely good convergence of the point detector responses downstream of the shutter across the entire energy spectrum (and the ability to confirm those responses with statistically meaningful results from other types of detectors) is a direct and important consequence of the 3-D broad-group weight-window biasing technique used in this analysis, wherein these weight windows were based on a fine-group 1-D adjoint analysis, described earlier in Sect 6. With simple geometric splitting, it is doubtful that any useful solution could have been obtained downstream of the rotary shutter. Moreover, with no biasing of any kind, experience has shown that the statistics would have deteriorated severely by the time the photons had penetrated 30 or 40 cm into the water tube, and that few if any would have been tracked past this point. [Moreover, in a neutron shielding problem with no biasing, virtually no neutrons would ever be tracked more than 10, 15, or 20 cm into the water; all would be killed by Russian Roulette.] In light of this, the use of the 3-D broad-group weight windows as calculated above and supplied to MCNP4B using the still undocumented "geometry-independent weight window" file (cf Appendix C.3) must be regarded as having been fantastically successful.

6.9.1.1 Confirmation of Dose Rate Upstream of Shutter

Point detector 25 showed that the peak dose rate along the centerline in the void between the collimator and the rotary shutter was 103.991 Rem/hr +/- 0.5%. Boundary crossing estimates of the dose rate just downstream of the water-filled collimator (cf Sect 6.9.2) confirm that result, as do volumetric track length estimates of the dose rate in the last 4.445-cm increment of water in the water-filled collimator (cf Sect 6.9.3). Independent methods [including: (1) a simple 3-group hand calculation, (2) a 23-group point kernel calculation, and (3) a preliminary MCNP analysis that did not use weight-window biasing] all indicate the general reasonableness of this result as well. A summary of those comparisons is given in Sect 6.9.4.

6.9.1.2 Confirmation of Dose Rate Downstream of Shutter

Point detector 45 showed the peak dose rate just downstream of the shutter along the centerline to be 0.8934 mrem/hr +/- 3.4%. Later in Sect 6.9.5, results of real boundary crossing estimates for the gamma fluxes and dose rates downstream of the entire shield configuration will be used to show that the point detector responses described above are not only well converged, but physically meaningful

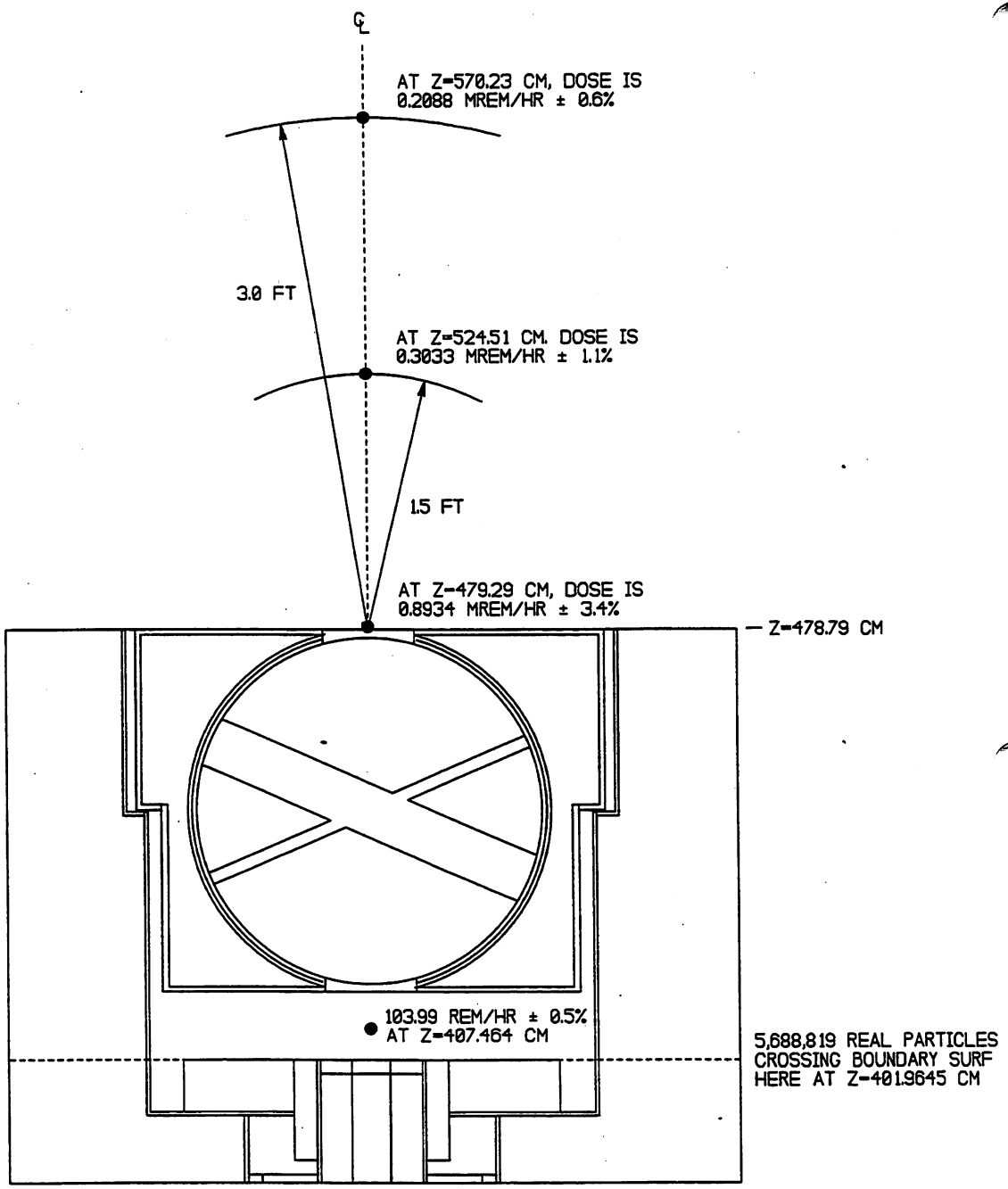


Fig. 6.5. Centerline dose rates upstream and downstream of the rotary shutter in HB-3 when the 1998 water tube and collimator sections are both flooded, the shutter is closed, and the HFIR is operating at 100 MW.

Table 6.6. Gamma fluxes and dose rates at key axial locations along the HB-3 centerline, with the 1998 water tube and collimator sections both flooded, the shutter closed, and HFIR at 100 MW. Results based on the gamma sources streaming down beam tube; does not include contributions from any activation sources.

Emin (MeV)	Emax (MeV)	Tally 15 p/s/cm2	Tally 15 fsd	Tally 35 p/s/cm2	Tally 35 fsd	Tally 55 p/s/cm2	Tally 55 fsd	Tally 75 p/s/cm2	Tally 75 fsd
0.010	0.020	1.63689E+04	.1070	3.10908E-02	.3279	4.17939E-03	.1012	1.49223E-03	.0956
0.020	0.045	8.24280E+04	.0784	8.95259E-02	.1573	2.06201E-02	.0563	7.70814E-03	.0525
0.045	0.070	7.54374E+04	.0640	2.88657E-01	.1086	5.53663E-02	.0505	1.96471E-02	.0468
0.070	0.10	8.24296E+04	.1374	1.37137E+00	.0707	1.26160E-01	.0452	4.41100E-02	.0433
0.10	0.15	1.69743E+05	.2269	6.89966E+00	.0516	3.87411E-01	.0408	1.29379E-01	.0401
0.15	0.30	7.68251E+05	.1067	2.61180E+01	.0457	1.38887E+00	.0397	4.68471E-01	.0402
0.30	0.40	2.12749E+05	.0601	1.29217E+01	.0460	7.88284E-01	.0397	2.70250E-01	.0413
0.40	0.51	1.77907E+05	.0392	1.19315E+01	.0447	7.26765E-01	.0392	2.54700E-01	.0422
0.51	0.60	3.76940E+05	.0276	1.41605E+01	.0460	6.52241E-01	.0400	2.27304E-01	.0457
0.60	0.70	6.79724E+04	.0687	6.23365E+00	.0607	4.66485E-01	.0397	1.67804E-01	.0411
0.70	1.0	1.63007E+05	.0806	1.49145E+01	.0449	1.18527E+00	.0389	4.29510E-01	.0403
1.0	1.5	1.94608E+05	.0269	1.81373E+01	.0450	1.57304E+00	.0390	5.98771E-01	.0411
1.5	2.0	1.81662E+05	.0264	1.35185E+01	.0432	1.26556E+00	.0376	4.99514E-01	.0407
2.0	2.5	1.90650E+05	.0236	1.08295E+01	.0434	1.09471E+00	.0369	4.37278E-01	.0472
2.5	3.0	2.28072E+05	.0225	9.09896E+00	.0414	9.61987E-01	.0360	3.77692E-01	.0443
3.0	4.0	1.14987E+06	.0103	1.60157E+01	.0402	1.95479E+00	.0290	8.76913E-01	.0294
4.0	5.0	1.90375E+06	.0077	1.54745E+01	.0388	2.95183E+00	.0163	1.72791E+00	.0107
5.0	6.0	1.56224E+06	.0106	1.45054E+01	.0421	3.29578E+00	.0174	1.95841E+00	.0106
6.0	7.0	3.33878E+06	.0060	2.03711E+01	.0334	9.29078E+00	.0113	6.59730E+00	.0061
7.0	7.5	1.02485E+06	.0136	7.65129E+00	.0559	3.27672E+00	.0283	1.79465E+00	.0165
7.5	8.0	5.16310E+06	.0031	2.30835E+01	.0191	1.76437E+01	.0071	1.39046E+01	.0044
8.0	10.0	3.39638E+05	.0265	1.82227E+00	.1408	1.08948E+00	.0444	7.98230E-01	.0242
10.0	14.0	9.89672E+02	.1267	3.32275E-03	.1273	2.64000E-03	.1266	2.14293E-03	.1262
	Total:	1.74714E+07	.0102	2.45471E+02	.0392	5.02027E+01	.0154	3.15937E+01	.0094

Emin (MeV)	Emax (MeV)	Tally 25 mrem/hr	Tally 25 fsd	Tally 45 mrem/hr	Tally 45 fsd	Tally 65 mrem/hr	Tally 65 fsd	Tally 85 mrem/hr	Tally 85 fsd
0.010	0.020	3.06711E+01	.1147	2.92534E-05	.4416	4.68351E-06	.1275	1.60612E-06	.1132
0.020	0.045	4.76112E+01	.0784	5.17110E-05	.1573	1.19104E-05	.0563	4.45230E-06	.0525
0.045	0.070	2.07196E+01	.0640	7.92824E-05	.1086	1.52069E-05	.0505	5.39626E-06	.0468
0.070	0.10	2.19625E+01	.1374	3.65387E-04	.0707	3.36140E-05	.0452	1.17527E-05	.0433
0.10	0.15	5.56198E+01	.2269	2.26081E-03	.0516	1.26943E-04	.0408	4.23936E-05	.0401
0.15	0.30	4.35414E+02	.1067	1.48026E-02	.0457	7.87158E-04	.0397	2.65511E-04	.0402
0.30	0.40	1.86355E+02	.0601	1.13186E-02	.0460	6.90490E-04	.0397	2.36723E-04	.0413
0.40	0.51	1.93065E+02	.0392	1.29480E-02	.0447	7.88685E-04	.0392	2.76400E-04	.0422
0.51	0.60	4.82371E+02	.0276	1.81212E-02	.0460	8.34672E-04	.0400	2.90881E-04	.0457
0.60	0.70	9.79958E+01	.0687	8.98706E-03	.0607	6.72532E-04	.0397	2.41923E-04	.0411
0.70	1.0	2.86290E+02	.0806	2.61944E-02	.0449	2.08168E-03	.0389	7.54348E-04	.0403
1.0	1.5	4.50634E+02	.0269	4.19987E-02	.0450	3.64252E-03	.0390	1.38651E-03	.0411
1.5	2.0	5.31724E+02	.0264	3.95687E-02	.0432	3.70429E-03	.0376	1.46208E-03	.0407
2.0	2.5	6.61290E+02	.0236	3.75633E-02	.0434	3.79711E-03	.0369	1.51674E-03	.0472
2.5	3.0	9.03074E+02	.0225	3.60283E-02	.0414	3.80908E-03	.0360	1.49551E-03	.0443
3.0	4.0	5.31480E+03	.0103	7.40261E-02	.0402	9.03524E-03	.0290	4.05318E-03	.0294
4.0	5.0	1.03061E+04	.0077	8.37726E-02	.0388	1.59800E-02	.0163	9.35420E-03	.0107
5.0	6.0	9.67166E+03	.0106	8.98017E-02	.0421	2.04038E-02	.0174	1.21243E-02	.0106
6.0	7.0	2.31261E+04	.0060	1.41100E-01	.0334	6.43526E-02	.0113	4.56962E-02	.0061
7.0	7.5	7.66413E+03	.0136	5.72187E-02	.0559	2.45043E-02	.0283	1.34209E-02	.0165
7.5	8.0	4.05138E+04	.0031	1.81132E-01	.0191	1.38447E-01	.0071	1.09106E-01	.0044
8.0	10.0	2.97917E+03	.0265	1.59842E-02	.1408	9.55647E-03	.0444	7.00175E-03	.0242
10.0	14.0	1.09062E+01	.1267	3.66167E-05	.1273	2.90928E-05	.1266	2.36151E-05	.1262
	Total:	1.03991E+05	.0052	8.93389E-01	.0339	3.03309E-01	.0108	2.08773E-01	.0061

Tallies 15 & 25 = Gamma fluxes & dose rates at Z=407.464 cm, midway between collimator and rotary shutter
Tallies 35 & 45 = Gamma fluxes & dose rates at Z=479.290 cm, 0.5 cm past conc block assy holding shutter
Tallies 55 & 65 = Gamma fluxes & dose rates at Z=524.510 cm, 1.5 feet past conc block assy holding shutter
Tallies 75 & 85 = Gamma fluxes & dose rates at Z=570.230 cm, 3.0 feet past conc block assy holding shutter
Note: Because of the broad-group weight window biasing scheme used, low energy fluxes and dose rates below 0.3 or 1.0 MeV are actually known with greater certainty at and beyond Z=479.29 cm than at Z=407.464 cm.

and correct. In that context, the boundary crossing estimate of the area-averaged dose rate for the 6.5-inch-diam hole downstream of the shutter provides "positive confirmation" of the point detector response described above. The importance and significance of that confirmation (in terms of the physics used in the calculational model) is also discussed at some length in Sect 6.9.5. Lastly, independent low-order hand calculations described in Sect 6.10 have also been used to confirm the general reasonableness this result based on simple direct-line attenuation through the steel.

6.9.2 Boundary Crossing Data Just Downstream of Collimator

6.9.2.1 Binary Particle History File Available for Future Use

As with the preliminary MCNP analyses in Appendix C.6, a detailed description of the boundary flux just downstream of the flooded collimator has been prepared and saved for future reference. In this case, however, the internal boundary flux file (actually a boundary crossing history file or "wssa" file) at Z=401.9645 cm has been saved which contains the coordinates, direction cosines, energies and weights of the 5,688,819 photons crossing this surface in Run HB308G5. This particular binary file, which requires 542 MB of disk space, can then be used as an internal boundary source file in subsequent follow-up shielding analyses of this rotary shutter (or any similar shutter design in the future) by using the procedures outlined in Sect 6.8.2 above.

6.9.2.2 Boundary Crossing Estimate of Dose Rate Confirms Point Detector

Supplemental data in Appendix D.5 describe the results of "segmented area" boundary crossing tallies for a similar parallel surface (Surf 4198) at Z=401.9745 cm, which is located 2.4945 cm downstream of the collimator exit. Surface crossing Tallies 211 and 212 are "segmented" in the sense that the 130-cm-diam disk comprising this planar surface has been divided into five segments (cf Fig. D5.1), one of which corresponds to the 2.75-inch x 5.5-inch water-filled rectangular hole in the collimator immediately upstream of this axial location. Table D5.1 gives the integrated gamma leakage rate (in the forward hemisphere) across each of the five segments comprising the larger surface, while Table D5.2 gives the area-averaged dose rate for each of the five segments. Of the latter, only the results for the small 2.75-inch x 5.5-inch area directly downstream of the hole in the collimator are of any real interest. Results for this area (segment 5) show that the gamma dose rate at this location is 110.861 Rem/hr +/- 2.7%. This result is significant for three reasons: (1) it is very well converged in the most important high-energy gamma groups; (2) boundary crossing tallies such as this only count "real particles", thus indicating by virtue of its tight convergence that the region is indeed being adequately sampled in the most important high-energy gamma groups; and (3) it is in excellent agreement with the earlier point detector estimate of 103.991 Rem/hr +/-0.52% in the same void region, at Z=407.464 cm, midway between the collimator and the rotary shutter.

6.9.2.3 Brief Discussion of Supplemental Tabulated Data Available in Appendix D.5

As in Appendix C.6, a detailed printed listing of gamma leakage through the downstream exit of the 2.75-inch x 5.5-inch flooded hole in the collimator, in each of 23 energy bins and 7 directional bins, was also tallied and saved in Run HB308G5. Because that information was not of any immediate programmatic interest, and because some of it requires further explanation, that tally data has been relegated to Appendix D.5.

Just as the fluxes and dose rates for the point detector in the void between the collimator and the rotary shutter exhibited "curiously poor" fsd's below 0.3 MeV (see Tallies 15 and 25 in Table 6.6), the boundary crossing estimates of the low-energy gamma leakage downstream of the collimator exit (cf Table D5.3) also exhibited "curiously poor" statistics below 3 Mev, poorer statistics below 1 Mev, and no statistics below 0.3 MeV. In this particular calculation, this curious behavior is nothing to become alarmed about. Moreover, in a biased calculation such as Run HB308G, this is intentionally the case by design (not by accident), and it is a direct result of the broad-group weight windows used to improve the efficiency of the calculation. Why the point detector appears to have done better in the unimportant low-energy range than the boundary crossing detector can also be easily explained, although neither set of results "in the low energy range, at this particular axial location" should be taken too seriously. To explain:

Assume (as in this MCNP calculation and the preceding 1-D adjoint analysis) that the primary thing of interest is the gamma dose rate downstream of the rotary shutter. Close to the downstream exit of the rotary shutter, "all" gammas are tracked because "there" all gammas are important and can easily contribute directly to the local dose rate at this "primary point of interest". As one moves back through the shield (from the downstream side of the shutter, to the upstream side of the shutter, through the water in the collimator, and through the water in the flooded water tube), gammas of all energies become somewhat less important (because they are less likely to contribute to the dose rate

of interest downstream of the shutter), but the low-energy gammas become less and less important far more rapidly because they are the most readily attenuated and are the least likely to contribute to the dose rate of interest downstream of the shutter. Thus, as one moves back further in the shield (from the downstream side of the shutter towards the source), it makes less and less sense to spend valuable computer time tracking unimportant low-energy gammas that stand little chance of contributing to the dose rate of interest downstream of the shutter -- especially when the computer time could be better spent tracking the more important high-energy gammas that do have a better chance of making a real contribution there. Thus, as one moves further back towards the source, the code uses Russian Roulette to more and more often to preferentially kill off the low-importance low-energy gammas (while of course increasing the weight of the few survivors to maintain a fair game). To see this in a more quantitative fashion and understand how the weight window parameters used (wtlow, wtavg, and wthigh) will determine "what is killed where", see the rather enlightening discussion in Sect 6.6 associated with Figs. 6.3 and 6.4. (Additional comments are also provided in Appendix D.5.) The key point is this: Given that the "quantity of primary interest" is the total gamma dose rate downstream of the rotary shutter, and that the broad-group weight-window biasing scheme has been optimized for that purpose, most of the very low energy gammas "below 0.3 MeV, in the region upstream of the shutter" are simply not worth tracking and are killed by Russian Roulette, even though higher-energy gammas at this same location may be worth tracking and will likely survive Russian Roulette or even be "automatically accepted for further tracking" without being subjected to Russian Roulette at all.

Real particle counters (including volumetric track length counters and boundary crossing tallies such as that used at the downstream exit of the collimator) are, therefore, keenly sensitive to special local effects caused by the use of weight windows (see additional caveats and cautions in Appendix D.5). If unimportant low-energy particles in a particular portion of the problem are intentionally not being tracked or are mostly being killed by Russian Roulette under the enlightened direction of the broad-group weight-window biasing scheme being used, then these types of detectors in these particular regions may well see nothing at all in those energy ranges. While point detectors are also affected by the same considerations, their response in a given energy range at a given spatial location will be less "black and white" since they can also sense "pseudoparticles" of all energies coming from collisions at distant sites where particles in this energy range are, in fact, being tracked and may be undergoing collisions. That is why the point detectors used in Tallies 15 and 25 just upstream of the rotary shutter are registering results below 0.3 MeV while the nearby boundary crossing tallies just downstream of the collimator exit may be sensing nothing in this same energy range (below 0.3 MeV) as shown in Table D5.3.

For purists who would like to see a more complete description of the gamma leakage downstream of the collimator exit over the entire energy range, a composite table like that shown in Table D5.4 may be constructed which shows the more tightly converged high-energy results above 3 MeV from Run HB308G, in combination with the more tightly converged low-energy results below 3 MeV from Run HB307C (cf Appendix C.6) which did not use weight windows and therefore did not incur this artificial loss of low-energy particles.

Because of the necessity for lengthy explanations such as this, some results not of any direct programmatic interest have been banished to Appendix D.5.

6.9.3 Axial Variation of Dose Rates in Water, Based on Segmented Volume Tallies

Tallies 184 and 194 are "volume detectors" that use the real particle track length in a given region to calculate the average flux or other dependent quantity in the given region. Tally 184 is a segmented volume detector used to calculate the approximate gamma dose rate in each of 30 equal (4.2412-cm-thick) regions, axially down the water tube from Z=174.9513 cm to Z=302.1868 cm, while Tally 194 is a segmented volume detector used to calculate the approximate gamma dose rate in each of 20 equal (4.445-cm-thick) regions, through the water-filled rectangular hole in the collimator, from Z=310.58 cm to Z=399.48 cm. Results for both are shown in Table 6.7.

6.9.3.1 Volumetric Track Length Estimate of Dose Rate Confirms Point Detector

As shown in Table 6.7, the average gamma dose rate in the last 4.445-cm segment of water in the water-filled collimator (from Z=395.035 to Z=399.480 cm) was 120.735 Rem/hr +/- 2.7%. As with the boundary crossing estimate at the collimator exit, this volumetric track length estimate of the gamma dose rate in this region is significant for three reasons: (1) it is very well converged; (2) volumetric track length estimates such as this only count "real particles", thus indicating by virtue of its tight convergence that the region is indeed being adequately sampled in the most important high-energy gamma groups; and (3) it is in excellent agreement with (or at least very consistent with) the earlier point detector estimate of 103.991 Rem/hr +/-0.52% at Z=407.464 cm, in the void midway between the collimator and the rotary shutter. To make the comparison fair, of course, the "average" value of 120.735 Rem/hr "within" this last 4.445 cm increment of water would

Table 6.7. Approximate(**) gamma dose rates and fractional standard deviations, up through the 1998 HB3 water tube and the flooded rectangular hole in the collimator with the HFIR operating at 100 MW. Because Tallies 184 and 194 are segmented volume detectors, they indicate the presence of real particles tracking through the region. The fact that the fsd's are small and almost constant (rather than growing, or being 10 or 20 times bigger) is extremely good, and indicates that there is now excellent population control over the most important photons, and that the weight windows are about as good as they can be. This is necessary if the solution further downstream is to be credible. For detailed energy and angular distribution of gammas, 2.4945 cm downstream of collimator exit, see Appendix D.5.

Zmin (cm)	Zmax (cm)	Above surf	Below surf	Tally 184 mrem/hr	fsd
174.9513	179.1924	5100	-5101	4.79653E+08	.0079
179.1924	183.4336	5101	-5102	4.20084E+08	.0116
183.4336	187.6748	5102	-5103	3.53748E+08	.0072
187.6748	191.9160	5103	-5104	3.01415E+08	.0111
191.9160	196.1572	5104	-5105	2.47087E+08	.0111
196.1572	200.3984	5105	-5106	2.06311E+08	.0139
200.3984	204.6395	5106	-5107	1.71117E+08	.0160
204.6395	208.8807	5107	-5108	1.40542E+08	.0072
208.8807	213.1219	5108	-5109	1.18525E+08	.0132
213.1219	217.3631	5109	-5110	1.01732E+08	.0198
217.3631	221.6043	5110	-5111	8.48348E+07	.0174
221.6043	225.8455	5111	-5112	7.25931E+07	.0240
225.8455	230.0867	5112	-5113	5.88593E+07	.0126
230.0867	234.3278	5113	-5114	4.97336E+07	.0143
234.3278	238.5690	5114	-5115	4.22599E+07	.0162
238.5690	242.8102	5115	-5116	3.54105E+07	.0117
242.8102	247.0514	5116	-5117	3.01512E+07	.0117
247.0514	251.2926	5117	-5118	2.57778E+07	.0120
251.2926	255.5338	5118	-5119	2.20608E+07	.0126
255.5338	259.7750	5119	-5120	1.86652E+07	.0126
259.7750	264.0161	5120	-5121	1.58087E+07	.0127
264.0161	268.2573	5121	-5122	1.34985E+07	.0128
268.2573	272.4985	5122	-5123	1.16335E+07	.0143
272.4985	276.7397	5123	-5124	9.99517E+06	.0145
276.7397	280.9809	5124	-5125	8.60419E+06	.0225
280.9809	285.2221	5125	-5126	7.24780E+06	.0143
285.2221	289.4633	5126	-5127	6.22696E+06	.0149
289.4633	293.7044	5127	-5128	5.32575E+06	.0151
293.7044	297.9456	5128	-5129	4.62638E+06	.0163
297.9456	302.1868	5129	-5130	4.04428E+06	.0241

Zmin (cm)	Zmax (cm)	Above surf	Below surf	Tally 194 mrem/hr	fsd
310.5800	315.0250	5140	-5141	2.46532E+06	.0177
315.0250	319.4700	5141	-5142	2.15109E+06	.0259
319.4700	323.9150	5142	-5143	1.86015E+06	.0364
323.9150	328.3600	5143	-5144	1.48316E+06	.0177
328.3600	332.8050	5144	-5145	1.25324E+06	.0184
332.8050	337.2500	5145	-5146 *	1.06383E+06	.0192
337.2500	341.6950	5146	-5147	8.98548E+05	.0199
341.6950	346.1400	5147	-5148	7.67443E+05	.0205
346.1400	350.5850	5148	-5149	6.55737E+05	.0211
350.5850	355.0300	5149	-5150	5.52912E+05	.0210
355.0300	359.4750	5150	-5151	4.70904E+05	.0216
359.4750	363.9200	5151	-5152	4.04357E+05	.0222
363.9200	368.3650	5152	-5153	3.46170E+05	.0228
368.3650	372.8100	5153	-5154	2.98821E+05	.0234
372.8100	377.2550	5154	-5155	2.56774E+05	.0239
377.2550	381.7000	5155	-5156	2.21575E+05	.0243
381.7000	386.1450	5156	-5157	1.90829E+05	.0250
386.1450	390.5900	5157	-5158	1.63317E+05	.0255
390.5900	395.0350	5158	-5159	1.40187E+05	.0260
395.0350	399.4800	5159	-5160	1.20735E+05	.0266

a) In Tally 184, each segment of Cell 2145 was 4.2412 cm thick and had a volume of 493.55788 cc.
b) In Tally 194, each segment of Cell 4300 was 4.4450 cm thick and had a volume of 433.74510 cc.
* This particular value has been adjusted manually to account for the fact that Cell 4305 (which is also water, but is embedded in Cell 4300) diminished the volume of this tally segment by 68.7649 cc.
** These are labeled "approximate" because, with the broad-group weight window biasing scheme used, the low energy gammas below 1.0 or 3.0 MeV are known with less and less certainty as one goes back closer to the source, where the low energy gammas are ultimately ignored completely.

have to be reduced by about 8% (to about 111.8 Rem/hr) to account for attenuation over the last half of this 4.445-cm-thick segment of water. Having done that, the comparison looks very good indeed.

6.9.3.2 Why These Dose Rates Must Be Regarded as Approximate

Before proceeding, it should be noted that the gamma dose rates in Table 6.7 are labeled "approximate". They are labeled "approximate" because, as explained in Sect 6.9.2.3 and earlier in Sect 6.6, many of the lower-energy gammas produced by slowing down in the upstream regions back closer to the source are intentionally being killed by Russian Roulette and not being tracked. [In this context, nothing is ever really "thrown away", and the weights of those surviving Russian Roulette are, of course, being adjusted to maintain a fair game. As one goes back closer to the source, however, the odds of surviving Russian Roulette become so diminishingly small (cf Figs 6.3 and 6.4), that for all practical purposes, none are ever really tracked, and their contributions to the dose rate as measured by the volumetric track length estimators are (for all practical purposes) totally missing.] The second reason that these gamma dose rates are labeled "approximate", especially back near the source, is that in Run HB308G, all of the gamma point sources below 3 MeV were totally ignored and not even included in the calculation. This was and is fully justifiable on the grounds that (for this particular configuration) they would be responsible for less than 2% of the total gamma dose rate impingent on the rotary shutter (as shown in Sect 5.5). Justifiable as it may be, it still means that calculated dose rates in the water tube and flooded collimator sections must be regarded as "approximate", with the approximation becoming better and better as one moves from the source towards the rotary shutter.

6.9.3.3 Significance of this Approximate Data

If this data is approximate, why did we bother to tabulate and report it? The answer is simple: it is a prime diagnostic tool and a key indicator of how good (or how poor) the results further downstream may be.

It is relatively easy to accurately calculate the dose rate downstream of the flooded water tube and the flooded collimator sections (viz the simple calculations in Sect 5.5 and Appendix C.6). It is quite another matter, however, to perform a good 3-D analysis of the rotary shutter assembly where multidimensional streaming may be important and must be assessed. Simple tools and 2-D deterministic analyses must be abandoned, and even 3-D deterministic methods are extremely limited in their ability to deal with such problems. Ultimately, one must turn to 3-D Monte Carlo analyses. To be meaningful, such a calculation must first be able to transport an extremely large number of high-energy particles to a location just upstream of the rotary shutter so that the distribution there can be well-characterized and sampled in all directions, especially at the higher energies. Where do those high-energy gammas come from? They come from the source ... and, to be useful, they must be transported without any loss of integrity or statistical degradation from the source region to the region of interest (in this case, just upstream of the rotary shutter). And how can one really be assured that this is really being done? We monitor the progress every inch of the way.

The fact that results in Table 6.7 made no attempt to account for low-energy gammas from the source, and only a statistically poor attempt to account for gammas that have slowed down to low energies, is irrelevant; that was not the intended purpose. The gamma dose rate, based on the 1977 ANSI Std Flux-to-Dose-Rate conversion factors#19, is heavily weighted to account for the presence of high-energy gammas. As such, it was a good (and probably the single most useful) barometer of statistical variations associated with the high-energy gamma fluxes. If the high-energy gamma sources were heavily sampled in all directions of importance (ie, if one had a large number of histories in the high-energy range that were concentrated in the narrow cone of directions that stood a reasonable chance of making a contribution far downstream), and if the uncertainties (fsd's) associated with the high-energy gamma fluxes near the source were low, and if the broad-group weight window approach was successful in maintaining low fsd's for these high-energy gammas along the entire length of the water tube and the water-filled collimator (as characterized by this barometer), then and only then could one be assured of having a good and full representation of the high-energy gamma fluxes downstream of the collimator, as would be necessary for a meaningful shielding analysis of the rotary shutter further downstream. Note, for example, that in the case of a neutron analysis with no special biasing, the neutrons tend to "fizzle out" in the first 10, 15 or 20 cm of water in the water tube, with only 2 out of 250,000 neutron histories even making it that far. In the case of a gamma analysis with no special biasing, most gamma histories never make it through 30 or 40 cm of water before being killed by Russian Roulette. Even in the preliminary gamma-only analyses (cf Appendix C.6), where extensive use was made of geometric splitting to preserve the gamma population down the length of the water tube and collimator, the unimportant low-energy gamma noise was preserved at a high level, and some high-energy gammas did manage to get through all the way to the end of the water-filled collimator, but the statistics associated with those all-important high-energy gammas had experienced severe degradation, and simply tallying the total gamma flux as a function of axial location was a woefully inadequate indicator that masked over the degradation that had actually occurred in the high energy range. (In that case, a sufficient number of particles had traversed the water-filled collimator that the dose rate at the downstream end (and the statistics associated with it) were deemed acceptable,

but the number of histories there, particularly in the higher energies, was not deemed adequate for going forward from there with a shielding analysis of the shutter based on that data. Look, for example, at the gamma leakage terms for Segment 5 in Table C6.8; beginning at around 4, 5, or 6 Mev where the fsd's are already in the 7-10% range, they increase to 19% in the most important 7-7.5 MeV energy range, and go up to 34.5% in the 8-10 MeV range. Uncertainties in the angular distribution(s) were even larger. If at all possible, these are not the kinds of uncertainties that one would like to have at the "outset" of a shielding calculation. Moreover, for other reasons explained in Appendix C.6.6, there was no good vehicle for moving forward from that point with a follow-up bootstrapped shielding calculation of the rotary shutter even if one had wanted to.) The point of these anecdotes is this: Having some sort of barometer for measuring uncertainties associated with the high-energy gammas as they traverse the water tube and water-filled collimator is an invaluable diagnostic tool that can be used to verify that the high-energy population is well controlled (ie: not dying out, and not overbiased) as it migrates through the system from the source to the ultimate detector of interest. The gamma dose rate as it is calculated here, even though it does not always account for all the low-energy gammas that might be present, is still a very good and convenient tool for that purpose. Moreover, the very small and fairly constant fsd's shown in Table 6.7 are judged to be absolutely excellent (a truly amazing and remarkable tribute to the 3-D broad-group weight-window biasing scheme used here). The availability and inspection of this type of data, coupled with a careful inspection of the high-energy gamma leakage terms downstream of the collimator, provides the best possible defense against poor sampling of high-energy particles just upstream of the rotary shutter shield configuration.

6.9.4 Summary of Independent Checks on the Dose Rate Just Upstream of the Shutter

Table 6.8 summarizes various estimates of the calculated gamma dose rate along the centerline, in or near the void space between the collimator and the rotary shutter, when the 1998 HB-3 water tube and collimator sections are both flooded and the HFIR is operating at 100 MW. All are highly consistent.

The first three are based on the present weight-window-biased calculation, MCNP4B Run HB308G, but have used different algorithms for calculating the dose rate at slightly different locations. The first two, using a volumetric track length detector in the last 4.445 cm of water inside the water-filled collimator, and using a boundary crossing tally to calculate the average dose rate over a 2.75-inch x 5.5-inch area directly downstream of the flooded hole in the collimator, are meaningful and virtuous insofar as they only count real particles that have been successfully transported to this region and are presently being tracked. Only by looking at these detector results as a function of energy and making sure that the fsd's for the high-energy gammas are good, can one verify that a large statistically-meaningful population of real "numerical particles" actually exists in a given energy range at a given location. Only then can this population of "numerical particles" faithfully represent the real distribution of photons in all elements of phase space (physical location, energy, and direction), and only then can adequate sampling in the local region be guaranteed. Moreover, only then can one have full confidence in any point detector tallies in the region. Point detector tallies may indeed still be correct without this independent confirmation, but one can never be sure without it. Given that real particle detectors (volumetric track length detectors or boundary crossing tallies) yield dose rates that are reasonably close to the point detector estimates and exhibit the virtuous characteristics described above (and that is a very important "if"), then the point detector tallies will likely be much more accurate since they can also sample small uncollided contributions from distant sources and as well as millions of distant collision sites (855.3 million collision sites in this particular calculation).

The role of volumetric track length detectors and boundary crossing tallies as diagnostic tools and "confidence builders" cannot be overstated, but their importance goes far beyond that. Had they not indicated the presence of a large thriving population of photons in the high-energy range that were still being actively tracked in this region and which could be adequately sampled in all elements of phase space, then it would have been impossible to go forward from this point with any sort of Monte Carlo shielding analysis of the rotary shutter shield assembly, point detector responses not withstanding. Point detectors responses are based on tracking "invisible" pseudoparticles from each source point and each collision site, to the point detector site of interest. The appropriate 1/(4*pi*R^2) term is applied in each case, as is the appropriate exponential attenuation factor along the entire optical (line of sight) path from each source or collision site to the detector site. However, the "pseudoparticles" remain invisible to everything else in the calculation. They are not recorded by volumetric track length detectors or by boundary crossing tallies; they do not cause collisions or reaction rates of any type to occur anywhere in the problem; their tracks are invisible, and they cannot be tracked beyond the point detector to which they are going. For all practical purposes, in the real world they don't exist. The fact that a point detector upstream of the rotary shutter can see these pseudoparticles and can calculate a response based upon them does not necessarily mean that the real shutter will ever see any real particles. The only particles the real shutter will ever see in the shielding analysis are real particles that left real particle tracks as recorded by the real (volumetric or boundary crossing) tallies. Thus, if one plans to continue forward from this point with a real shielding analysis of the rotary shutter, it is not only reassuring but "imperative" that one use these tallies to verify the existence of a large number of real particle tracks (especially high-energy ones) in the region upstream of the shutter.

Table 6.8. Various estimates of the gamma dose rate (Rem/hr) between the end of the water-filled collimator and the rotary shutter.

Results from MCNP4B Run HB308G:

Description of Detector and Exact Location	Dose Rate	
Volume detector in last 4.4450 cm of water (Z=395.0350 to Z=399.4800 cm) inside the water-filled collimator (cf Table 6.7)	120.735 Rem/hr	+/- 2.66%
Boundary crossing tally for the rectangular 2.75-inch x 5.5-inch central portion of a plane, 0.24945 cm downstream of collimator exit; plane located at Z=401.9745 cm (Tally 212, Segment 5; cf Table D5.2);	110.861 Rem/hr	+/- 2.70%
Point detector located on the centerline, at Z=407.464 cm, in void space between the collimator and the rotary shutter (Tally 15; cf Table 6.6)	103.991 Rem/hr	+/- 0.52%

Results from earlier independent calculations:

Description of Methodology Used		
3-group hand calculation described in Sect 5.2; based on attenuation through 224.53 cm of water	90.232 Rem/hr	---------
23-group point kernel calculation described in Sect 5.5	103.048 Rem/hr	---------
Point detector located on centerline at Z=407.464 cm (downstream of collimator, shutter not modeled); based on preliminary, highly simplified model in MCNP Run HB307C; only used simple geometric splitting (see Tally 25, in Table C6.5, Appendix C.6)	109.310 Rem/hr	+/- 1.14%

Point detectors can be good indicators (and frequently the best indicators) of fluxes and dose rates at locations that might otherwise the difficult to calculate for various other reasons, "but that's about all they're good for" generally. To be fair, if one had access to point detector information from enough locations, and was both creative and ambitious enough to create a space-energy-direction-dependent source distribution manually from that information (a fine and noble but underappreciated tradition), the calculational benefits could also be tremendous. That approach has also been used quite successfully in other HFIR-related applications, but was not chosen as the optimal course of action in this particular problem.

Lastly, Table 6.8 also shows three other estimates of the calculated dose rate at this location, based on three completely independent calculational techniques previously described in Sect 5 and/or Appendix C.6. These include a 3-group hand calculation based of the attenuation of the original point sources through 224.53 cm of water, a 23-group point kernel calculation that came within 1% of the best (recommended) point detector estimate above, and an earlier value from a highly-simplified preliminary MCNP model (described in Appendix C.6) which only used simple energy-independent geometric splitting. Results of all three methods are in good agreement with each other, and with the results of the present calculation. The latter is especially important because it erases any doubt regarding the various normalization parameters needed in this calculation and/or in the generation of the 3-D broad-group weight windows used in this calculation.

6.9.5 Boundary Crossing Data Downstream of Entire Shield Configuration

Figure 6.6 shows a sketch of the end of the entire shield configuration at Z=478.79 cm, as would be seen if one were standing outside the system (where the monochrometer drum would normally be located), looking back towards the steel-lined concrete block assembly holding the rotary shutter. The small numbers, 1 through 10, indicate the surface segment numbers corresponding to Tallies 231 and 232, the results of which are summarized below in Tables 6.9 and 6.10. Segment 10 (in the center) corresponds to the 6.5-inch-diameter hole coming out from the rotary shutter and through the concrete block assembly holding shutter, while segment 9 is the remainder of the 83.5025 cm x 83.5025 cm face of the steel-lined concrete block assembly holding the rotary shutter. Segments 5 to 8 are the 1.74625-cm clearance gaps between the concrete block assembly and the biological shield, while segments 1 to 4 represent portions of the steel-clad biological shield beyond that, out to a radius of 65 cm. Most of the key results of interest (based on Tally 232) are summarized directly on Fig. 6.6.

In addition to the "area-averaged" dose rates for each of the 10 segments comprising this planar surface at Z=478.79 cm, Table 6.9 also shows the integrated gamma leakage (p/s) across each segment. From this, it is quite clear that most of the gamma leakage is indeed coming from Segments 9 and 10, with almost half of that coming from Segment 10, the 6.5-inch-diam hole directly downstream of the rotary shutter. Because the leakage through each of the other 8 segments is relatively low, their statistics are marginal. For boundary crossing tallies such as these, fractional standard deviations of 0.10 are generally considered quite good and acceptable. With fsd's between 23% and 39% (mostly around 25%), the calculated dose rates are likely to be accurate to within about a factor of two since the actual uncertainties vary in a non-linear fashion with the fsd's. Nevertheless, this is considered wholly sufficient for the present purpose. Even after making allowances for this higher uncertainty, one can say with reasonable confidence that the dose rates in and around the clearance gaps are well below those at the centerline, and one can say with absolute confidence that they are definitely not orders of magnitude above the dose rate at the centerline. Moreover, asymmetric variations in the external dose rates and gamma leakage rates shown in Fig. 6.6 and discussed in Sect 6.9.5.3 are wholly consistent with expectations and clearly indicate that this model (with the biasing scheme used) is sensitive to internal streaming effects (in and around the rotary shutter) to the point that, if these effects were significant, their presence would be clearly and readily identifiable in the tally output with far greater precision. As it is, internal streaming effects are already clearly and readily identifiable beyond any shadow of statistical doubt, but the magnitude of the associated dose rates are well below the threshold of concern.

Lastly, Table 6.10 focuses on the two key areas of primary interest, Segments 9 and 10. For each of these areas, Table 6.10 lists the integrated gamma leakage rates (p/s) by energy group, and the area-averaged gamma dose rates (mrem/hr) by energy group. Of particular interest here is the fact that the "average" dose rate across the 6.5-inch-diam hole is 0.4596 mrem/hr +/- 3.7%. Just as the total leakage rate and total gamma dose rate for each segment are both well converged (to within 3.7% for segment 10, and to within 5.5 or 6.0% for segment 9), so also are the contributions from all the key energy groups. [Unlike the region upstream of the shutter where "key energy groups" meant anything above 5 or 6 MeV (typically radiation in the 7-10 MeV range), the expression here means "anything that contributes significantly to the dose rate at this location" since there is no more shielding to go through and any radiation that gets here is automatically folded with the 1977 ANSI Std flux-to-dose-rate conversion factors to calculate the total dose rate. Thus, in this case, if most of the dose comes from the intermediate energy groups (0.7 to 6 Mev for the main face, or 1 to 8 MeV for the central hole), then these are by definition the "key energy groups" for these locations.]

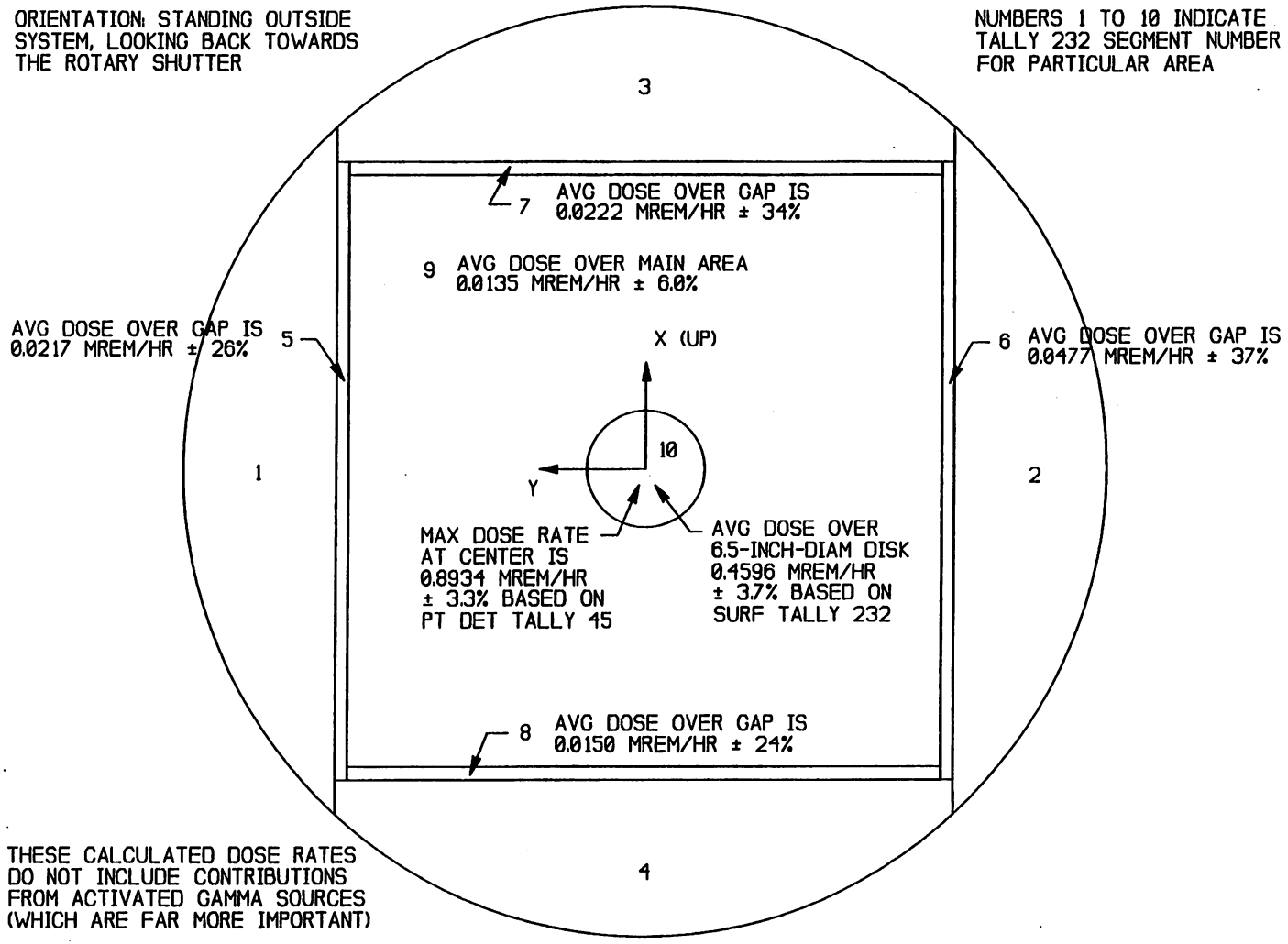


Fig. 6.6. External dose rates averaged over different portions of the downstream surface of the entire shield configuration (at Z=478.79 cm), including the central 6.5-inch-diam hole downstream of the shutter, the main face of the concrete block assembly holding the rotary shutter, and each of the four 1.74625-cm-wide clearance gaps between the biological shield and the concrete block assembly, when the 1998 water tube and collimator sections are both flooded, the shutter is closed, and the HFIR is operating at 100 MW.

Table 6.9. Integrated gamma leakage rates (p/s) and area-averaged gamma dose rates (mrem/hr) for various portions of a plane surface immediately downstream of the entire shield configuration (ie, at Z=478.79 cm, corresponding to the downstream surface of the stainless steel liner on the concrete block assembly holding the rotary shutter). The locations of the various area segments are illustrated in Fig. 6.6, where segment 10 is the 6.5-inch-diam hole in the middle, directly downstream of the shutter, and segment 9 corresponds to the remainder of the central block. These values were calculated by Tallies 231 and 232 in Run HB308G. More detailed results may be found in Appendix D.5.

Segment Number	Description	Area	Integrated Gamma Leakage photons/sec	fsd	Average Gamma Dose Rate mrem/hr	fsd
1	Portion of concrete biological shield on left	1438.21 cm2	3.17051e+3	.2392	8.50096e-3	.2559
2	Portion of concrete biological shield on right	1438.21 cm2	9.01193e+3	.3904	2.63248e-2	.4254
3	Portion of concrete biological shield on top	1414.34 cm2	3.68030e+3	.2432	1.02264e-2	.2589
4	Portion of concrete biological shield on bottom	1414.34 cm2	2.90242e+3	.2266	7.81712e-3	.2387
5	Gap on left, between bio shield and central block	151.915 cm2	1.00144e+3	.2389	2.17049e-2	.2638
6	Gap on right, between bio shield and central block	151.915 cm2	2.06711e+3	.3601	4.77339e-2	.3710
7	Gap on top, between bio shield and central block	145.816 cm2	9.61594e+2	.2933	2.22012e-2	.3380
8	Gap on bottom, between bio shield and central block	145.816 cm2	6.95966e+2	.2372	1.49776e-2	.2425
9	Face of concrete block holding shutter (excluding 10) ..	6758.58 cm2	2.70641e+4	.0546	1.35404e-2	.0597
10	6.5-inch-diam hole leading directly to rotary shutter ..	214.084 cm2	2.57918e+4	.0365	4.59621e-1	.0374

Note that:

(1) These estimates are based on real boundary crossing tallies. That is significant, because volumetric track length tallies and boundary crossing tallies only sense real particles; when one can get good statistics, these types of tallies are considered much more reliable than point detectors which sense pseudoparticles.
(2) A large fraction of the total gamma leakage (p/s) comes through the small 6.5-inch-diam hole in the middle (segment 10), as well as through the main face (segment 9). Both well converged. That is very important.
(3) While the dose rate directly in front of the central hole (segment 10) is dominent, average dose rates for the other areas appear low because of the large areas over which they were averaged. To assess relative contributions from these regions, look at the integrated leakage terms or point detector responses further from the surface.
(4) The "average" dose rate over the central 6.5-inch-diam hole (segment 10) is only 1.944 times lower than the "peak" value at the centerline given by point detector Tally 45. The fact that the two are in such excellent agreement is "positive confirmation" that the point detector values are trustworthy.
(5) See other notes in main text.

The fact that the total dose rates are so well converged and that the corresponding dose rates in each of the key energy groups are so uniformly well converged, is a tribute to the 3-D broad-group weight window biasing scheme used, and means that one can indeed have a great deal of confidence in these particular results.

6.9.5.1 Boundary Crossing Estimate of Dose Rate Confirms Point Detector

As indicated on Fig. 6.6, the "average" dose rate across the central 6.5-inch-diam hole downstream of the shutter is 0.4596 mrem/hr +/- 3.7%. Results for this region (Segment 10 of Tally 232 in Table 6.10) also show that the constituent dose rates in each of the key energy groups are similarly and uniformly well converged, thus justifying a high level of confidence in this particular result. The fact that it has excellent statistics and is based on a boundary crossing tally which only senses the presence of real particles, warrants an added degree of confidence in this result. Given that radiation passing through the steel shutter is likely to be very forward-directed and concentrated along the centerline, this value of 0.4596 mrem/hr, averaged across the entire 6.5-inch-diam disk, is highly consistent with point detector Tally 45 which registered a "peak" dose rate of 0.8944 mrem/hr +/- 3.4% along the centerline.

6.9.5.2 Significance of This Confirmation

Point detector estimates of fluxes or dose rates, by themselves, may or may not warrant a high degree of confidence. If, due to tracking difficulties or insufficient biasing, collisions in nearby material regions closest to the point detector are not adequately sampled, the point detector response may or may not be valid, even if it appears to be well converged; in that case, there is often no way to tell for sure (although other edits, such as "collisions by cell", may provide some limited reassurance). The only way to be sure that those local regions closest to the detector are being adequately sampled in all the key energy ranges, is to use a volumetric track length counter in that region, or a boundary crossing tally between the point detector and the region of interest. These two types of detectors will only measure the presence of real particle tracks in the region. If they show an absence of real particle tracks in the region of interest or the energy ranges of interest, then the point detector tally may or may not be yielding a correct result. [Indeed, it may still be correct, but there's no way to prove it; alternately, it could be wrong.] On the other hand, if the volumetric track length detector or the boundary crossing tally does show that the population in this region of space-energy phase space is being adequately represented by a statistically large and meaningful number of real particle tracks, then one can be assured that this element of phase space is being adequately sampled. In that happy event, the point detector response is likely to be more accurate (and better converged) that the volumetric track length counter or the boundary crossing tally since it can also sense millions of extremely small contributions from every collision anywhere in the system as well as uncollided contributions from every source point.

Thus, the significance of the boundary crossing estimate of the dose rate averaged across the 6.5-inch-diam hole is not so much that it was "close" to the point detector estimate (although we were certainly pleased that this was the case), but that the boundary crossing estimate of the total dose rate was well-converged and that all the constituent dose rates were well converged in a uniform fashion for each of the key energy groups of interest, thus guaranteeing that the fluxes and collisions in the material regions close to the point detector were adequately sampled. That being the case, this point detector estimate of the peak dose rate along the centerline (0.8934 mrem/hr +/-3.3%) is beyond reproach, and a high degree of confidence in that result is clearly warranted.

6.9.5.3 Asymmetric Variations Indicative of Streaming Through and Around the Shutter

While probably of less interest from a programmatic viewpoint, this section is included in abbreviated form to (1) highlight the power of the methodology now being used and (2) to provide as much reassurance as possible that if important streaming effects were present, they would have been clearly and readily identifiable in the tally outputs with far greater precision than is presently the case. As it is, internal streaming effects are already clearly and readily identifiable beyond any shadow of statistical doubt, but the magnitudes of the associated dose rates are well below the threshold of concern. Because of that, follow-up calculations to better calculate the local dose rates directly in front of the clearance gaps have never been undertaken, although that could easily be done by using the existing boundary source file upstream of the shutter, the existing weight-window file, and the existing MCNP model after the addition of appropriate point detectors at these locations. The key point to be demonstrated here is that the present model is sophisticated and powerful enough that even weak streaming effects like those found here were detectable and did not go unnoticed. Had they been more pronounced, they would have received further attention.

Table 6.10. Integrated gamma leakage rates (p/s) and area-averaged gamma dose rates (mrem/hr) by energy group, at Z=478.29 cm, immediately downstream of the 6.5-inch-diam hole and the remainder of the square (83.5 cm x 83.5 cm) face of the concrete block assembly holding the rotary shutter (see segments 10 and 9, respectively, in Fig. 6.6). These values were calculated by Tallies 231 and 232 in Run HB308G, with the 1998 HB-3 water tube and collimator sections flooded, the shutter closed, and the HFIR at 100 MW.

Emin (MeV)	Emax (MeV)	Segment 10 (6.5-inch hole; 214.084 cm2) mrem/hr	fsd	photons/sec	fsd	Segment 9 (Remainder of face; 6758.58 cm2) mrem/hr	fsd	photons/sec	fsd
0.010	0.020	9.63548e-6	.2006	2.33257e+0	.1428	8.22639e-7	.3894	2.80732e+0	.2651
0.020	0.045	4.37461e-5	.0794	1.47449e+1	.0794	9.82171e-7	.0851	9.49487e+0	.0880
0.045	0.070	5.65988e-5	.0583	3.76023e+1	.0549	1.44273e-6	.0753	2.79090e+1	.0783
0.070	0.10	2.50063e-4	.0436	1.42192e+2	.0431	6.74252e-6	.0583	1.04838e+2	.0597
0.10	0.15	1.59958e-3	.0405	6.59894e+2	.0384	4.71959e-5	.0551	5.48003e+2	.0529
0.15	0.30	1.03948e-2	.0368	2.50157e+3	.0372	3.78841e-4	.0507	2.46285e+3	.0510
0.30	0.40	8.11035e-3	.0366	1.32099e+3	.0370	3.59998e-4	.0515	1.55019e+3	.0520
0.40	0.51	9.31381e-3	.0366	1.24438e+3	.0370	4.38628e-4	.0536	1.53628e+3	.0538
0.51	0.60	1.23883e-2	.0369	1.36578e+3	.0374	4.90946e-4	.0586	1.45508e+3	.0590
0.60	0.70	6.26229e-3	.0358	6.64158e+2	.0362	3.46807e-4	.0509	9.75231e+2	.0502
0.70	1.0	1.83411e-2	.0355	1.68859e+3	.0357	1.00310e-3	.0502	2.51209e+3	.0512
1.0	1.5	2.84631e-2	.0353	2.16100e+3	.0354	1.52432e-3	.0495	3.31417e+3	.0517
1.5	2.0	2.60992e-2	.0350	1.67111e+3	.0349	1.37897e-3	.0509	2.61635e+3	.0534
2.0	2.5	2.47421e-2	.0347	1.38697e+3	.0346	1.30285e-3	.0721	2.21142e+3	.0779
2.5	3.0	2.37765e-2	.0343	1.19483e+3	.0342	1.09610e-3	.0447	1.67637e+3	.0455
3.0	4.0	4.60422e-2	.0334	2.02812e+3	.0332	1.84037e-3	.0464	2.49730e+3	.0470
4.0	5.0	4.67043e-2	.0332	1.79384e+3	.0331	1.32412e-3	.0540	1.58123e+3	.0547
5.0	6.0	4.74763e-2	.0360	1.61421e+3	.0360	1.01366e-3	.0938	1.07907e+3	.0941
6.0	7.0	6.01868e-2	.0444	1.84814e+3	.0444	5.33744e-4	.1100	5.13961e+2	.1100
7.0	7.5	2.46268e-2	.0626	7.02803e+2	.0627	1.18871e-4	.1812	1.06657e+2	.1807
7.5	8.0	5.88834e-2	.0603	1.60594e+3	.0603	3.17169e-4	.7272	2.71564e+2	.7262
8.0	10.0	5.85047e-3	.2340	1.42562e+2	.2340	1.47016e-5	.3629	1.12521e+1	.3630
10.0	14.0	0.00000e+0	.0000	0.00000e+0	.0000	0.00000e+0	.0000	0.00000e+0	.0000
	Total:	4.59621e-1	.0374	2.57918e+4	.0365	1.35404e-2	.0597	2.70641e+4	.0546

Note that while these estimates are based on real boundary crossing tallies, they are well converged due to the broad-group weight window biasing scheme used in this analysis. More importantly, note that the the "average" dose rate over the central 6.5-inch-diam hole (segment 10) is only 1.944 times lower than the "peak" value at the centerline given by point detector Tally 45. The fact that the two are in such excellent agreement is "positive confirmation" that the point detector values are trustworthy.

6.9.5.3.1 Clear Right-to-Left Variations Indicative of Streaming in the Shutter Beam Hole

When the shutter is in the closed position, the centerline of the large 3.5-inch-diam beam hole through the shutter is rotated 66.75 degrees away from the centerline of the beam tube. As indicated in the top view of the shutter shown in Fig. 6.1a, this will facilitate radiation streaming from right-to-left in plane of that figure, which means from left-to-right when viewed from the outside as shown in Fig. 6.6. Thus, one would expect that the dose rates and leakage rates for the clearance gap and biological shield on the right side of Fig. 6.6 (cf Segments 6 and 2) would be somewhat larger than for the corresponding regions on the left (cf Segments 5 and 1). In fact, that is the case, and the calculational results clearly show that effect. Even though the fluxes and dose rates for these regions are 10, 20, or even 50 times less than those along the centerline, and even though the fsd's in these segments are therefore relatively large (on the order of 25-30%), Table 6.11a clearly shows that the dose rates and leakage rates for the clearance gap on the right are about 2.13 times bigger than those on the left, while the dose rates and leakage rates for that portion of the biological shield on the right are about 2.97 times bigger than those on the left. Given that these ratios are much bigger than anything one might expect due to random variations based on these fsd's, and given that all four ratios tabulated in Table 6.11a are pretty consistent with each other and wholly consistent with what one would expect based on the geometric configuration, it is safe to conclude that preferential directional streaming within the shutter shield plug does exist and is being accounted for within the model. Moreover, it is comforting to know that the present model (with this weight-window biasing scheme) is sophisticated and powerful enough that these effects are clearly and readily identifiable even though the external manisfistations of internal streaming are well below the threshold of concern in this particular case. It means, for example, that all the key phenomena are already being adequately sampled and therefore, had the geometric configuration permitted substantially more streaming, the effects would have been even more clearly and readily identifiable (viz, calculated external dose rates would have been much larger, and the associated uncertainties would have been much smaller).

6.9.5.3.2 Slight Top-to-Bottom Variations Indicative of Streaming in the Gap Above the Shutter

Likewise, to a lesser but still observable extent, there is a similar asymmetric variation in the external dose rates and leakage rates in the vertical direction caused by the position of the rotary shutter shield plug inside the cavity. Fig. 3.13 shows the MCNP model of the carbon steel rotary shield plug sitting atop the stainless steel liner inside the concrete block housing assembly. While a 5/16-inch clearance gap was assumed circumferentially around the carbon steel shield plug, and a similar 5/16-inch clearance gap was assumed atop the carbon steel shield plug, no such clearance gap was assumed on the bottom since the carbon steel shield plug was assumed to be sitting flush against the bottom liner. While no attempt was made to bias the gamma flux up or down vertically in this MCNP calculation, the effect of that clearance gap near the top, while small, is still calculationally observable. Table 6.11b shows, for example, that the dose rates and leakage rates for the clearance gap on the top are about 1.43 times bigger than those on the bottom, while the dose rates and leakage rates for that portion of the biological shield on the top are about 1.29 times bigger than those on the bottom. While these ratios are arguably not much bigger than the associated fsd's shown in Table 6.9, it is significant that all four ratios tabulated in Table 6.11b are very consistent with each other and wholly consistent with what one would expect based on the geometric configuration. Based on this, it would be reasonable to conclude that there is some internal streaming in the clearance gap above the carbon steel shield plug, and that this is being accounted for within the model. Again, it is comforting to know that the present model is capable of detecting such effects even though the external manifestations of internal streaming, in this particular case, are well below the threshold of concern. Moreover, it indicates again, that all the key phenomena are indeed being sampled and therefore, had the geometric configuration permitted substantially more streaming, the effects would have been even more clearly and readily identifiable.

6.10 Simple Checks for Reasonableness

The following calculations are not complex or elegant. They are basically handbook calculations similar in nature to what was likely used in the original 1960 design analysis. Nevertheless, they appear to give results that are in very good agreement with those from MCNP Run HB308G.

6.10.1 External Dose Rate at the Centerline Due to Direct Transmission

This is a check on the transmission through the carbon steel portion of the rotary shutter as shown in Fig. 6.7. The starting point will be the known or assumed dose rate upstream of the rotary shutter. It is assumed that the dose rate here is 110 Rem/hr, and that most of the dose comes from gammas in the 7.5 to 8.0 MeV energy range. This is a safe and very reasonable assumption that needs no further

Table 6.11a. Asymmetric right-to-left variations in external dose rates and leakage rates. Because these asymmetric variations: (1) are quite large [ie, far in excess of any uncertainties], (2) are so consistent with each other, and (3) are fully consistent with the (slanted) orientation of the large beam hole through the shutter, these results are clearly indicative of internal streaming through the beam hole in the shutter, and clearly demonstrate the model's sensitivity to such multidimensional effects even when the effects are quite small. Had they been more important, the fsd's would have been smaller.

	Dose Rate (mrem/hr)	Ratio	Leakage (p/s)	Ratio
Segment 6: (R) Clear. Gap	0.0477339		2067.11	
Segment 5: (L) Clear. Gap	0.0217049		1001.44	
Ratio	--------->	2.20	------->	2.06
Segment 2: (R) Bio Shield	0.0263248		9011.93	
Segment 1: (L) Bio Shield	0.0085010		3170.51	
Ratio	--------->	3.10	------->	2.84

Table 6.11b. Asymmetric top-to-bottom variations in external dose rates and leakage rates. It is true that these asymmetric variations are less pronounced than those in Table 6.11a, and only slightly bigger than the associated fsd's. Nevertheless, because these asymmetric variations: (1) are all so consistent with each other, and (2) are all consistent with the model having a 5/16-inch clearance gap above the carbon steel shutter but not having any such clearance gap on the bottom, these results are indicative of internal streaming over the top, and demonstrate the model's sensitivity to such effects even when the effects are quite small. Had they been more important, the fsd's would have been smaller.

	Dose Rate (mrem/hr)	Ratio	Leakage (p/s)	Ratio
Segment 7: (T) Clear. Gap	0.0222012		961.594	
Segment 8: (B) Clear. Gap	0.0149776		695.966	
Ratio	--------->	1.48	------->	1.38
Segment 3: (T) Bio Shield	0.0102264		3680.30	
Segment 4: (B) Bio Shield	0.0078171		2902.42	
Ratio	--------->	1.31	------->	1.27

verification. Section 6.9.4 summarizes the independent checks that have already been performed on the dose rate just upstream of the shutter. These included: a simple 3-group hand calculation, a 23-group point kernel analysis, a highly-simplified preliminary MCNP analysis that did not use weight windows or any unconventional methods, and three different types of tallies in this final reference analysis (MCNP4B Run HB308G). Having said that, the hand calculation for the dose rate downstream of the shutter is very straightforward:

1) The Type 1020 carbon steel rotary shutter has a radius of 30.95625 cm.

2) The large beam hole has a radius of 4.445 cm.

3) Accounting for the fact that the hole is at an angle of 66.75 degrees relative to the system centerline when the shutter is closed, the amount of steel the gammas coming straight through the system along the centerline would have to pass through is 52.24 cm.

4) Upstream of the shutter, the dose rate (with system flooded, etc) is about 110 Rem/hr.

5) Most of the harder gamma flux impingent on the shutter is between 7.5-8.0 MeV.

6) The mass attenuation coefficient (u) for 8 MeV gammas in steel is 0.0298 cm2/g. This value was taken from page 138 of the 1970 edition of the Radiological Health Handbook (Ref 28).

7) Multiplying by the density (7.82 g/cc) and the thickness (52.24 cm), one obtains: u*rho*t=12.17 (dimensionless).

Since this is a small-diameter "highly collimated" beam of photons, a "buildup factor" of 1.0 is probably the most reasonable thing to use.

If one had a larger "distributed source" and u*rho*t=12.17, a more reasonable buildup factor might be 6.28 (see page 147 of Ref 28).

Depending on which buildup factor is used, one obtains:

Dose2 = Dose1 * exp(-u*rho*t) * (Buildup Factor)

= (110.0e3) * exp(-12.17) * (1.0) = 0.57 mrem/hr (no buildup factor)

= (110.0e3) * exp(-12.17) * (6.78)= 3.87 mrem/hr (with buildup factor)

By way of comparison, the best MCNP estimate of the peak dose rate 0.5 cm downstream of the rotary shutter along the system centerline (cf Tally 45) was 0.8934 mrem/hr +/- 3.4%. By any measure, this must be considered fairly reasonable!

Thinking in terms of "beam attenuation" is indeed a useful concept for estimating fluxes and dose rates along the centerline. Unfortunately, it is not very helpful when trying to estimates dose rates at points off the centerline. Likewise, because the flux at the exit of the collimator is very forward peaked, the use of an isotropic source with the standard exp(-u*rho*t)/(4*pi*R^2) approach is not directly applicable either, and must be modified. Before calculating the dose rate at an off-center location, we must first define several new concepts, and then revisit the centerline problem described above and reevaluate the result with a different, slightly more general, approach.

6.10.2 Equivalent Point Source

For calculations of the dose rate at other locations not on the centerline, it is conceptually easier to have some simple but useful expression for the source in terms of the known dose rate. Moreover, because of the strong directional dependence of the source emanating from the water-filled hole in the collimator, a directional dependence must be included as well. In the simplistic derivation of this alternative methodology, we will first assume the source is isotropic, but in the final analysis, the "constant" used to represent the actual source intensity (NO, p/s) will depend on the direction of interest.

Unlike the simple straight ahead analysis above, where the dose rate could simply be multiplied by a set attenuation factor, calculations involving one or more scattering events require one to think in terms of collision densities. Instead of working with dose rates, it is conceptually easier to think in terms of fluxes, currents, particle densities, and scattering densities, etc. Before that can happen, one must have some simple but useful expression for the source in terms of the known dose rate. In this case, we define the initial source (NOO) in terms of the initial dose rate (DO), the initial flux (FO), the area of the source (ASO), and a flux-to-dose-rate conversion factor (FTD) that we really don't need to know since it will ultimately cancel out in the final shielding calculation for the final dose rate. To be a

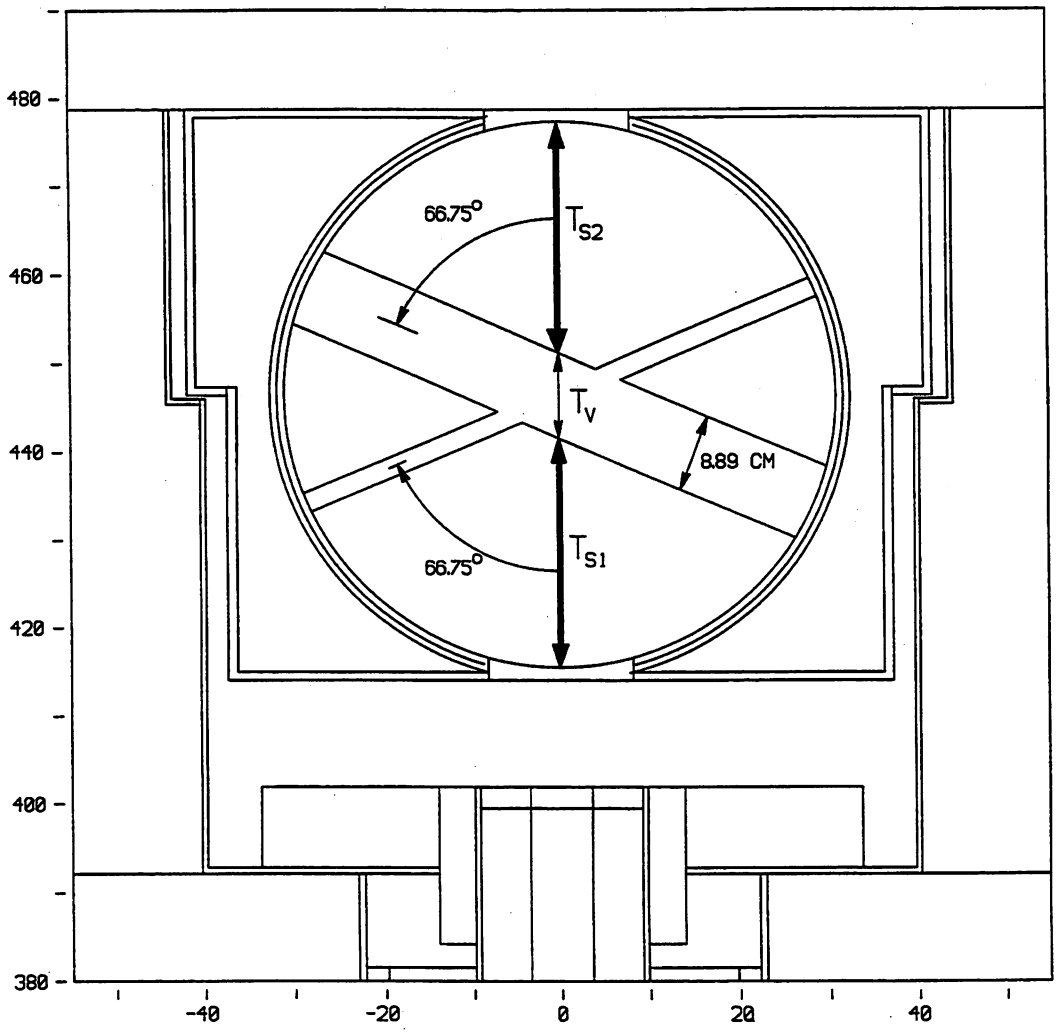


Fig. 6.7. Top view of the rotary shutter showing the amount of steel along the centerline, as used in the simple analytic determination of the dose rate downstream of the shutter.

little more precise, let NFH be the number of particles emitted from a source over the "forward hemisphere" (such as the number of photons emitted over the forward hemisphere at the end of the collimator hole), and let N00 be the corresponding number of particles (p/s) emitted over the entire 4*pi sphere if the equivalent point source were isotropic (or at least symmetric), such that N00=2*NFH. In this example, AS0 would be the area of the 2.75-inch x 5.5-inch hole in the collimator (97.58 cm2). Having defined these quantities, we now have:

D0 = F0 * FTD = (NFH/AS0) * FTD = ((N00/2)/AS0) * FTD = N00 * FTD / (2*AS0), or more usefully:

N00 = D0 * (2*AS0/FTD) where D0 and AS0 are known and FTD will eventually cancel out.

This last expression is a useful simple expression for "an" equivalent point source in "photons/sec".

Unfortunately, it cannot be used directly in any real shielding analysis because it does not yet account for the strong directional variations in source intensity. Instead, the quantity that should/must be used as the equivalent point source (N0) in all shielding calculations is defined by:

N0 = N00 * AFIR = D0 * AFIR * (2*AS0/FTD)

where AFIR is the "angular flux intensity ratio" for the direction of interest (described below).

6.10.3 Angular Flux Intensity Ratio

N00 is a useful expression if the radiation coming from the collimator were isotropic. Unfortunately it is not. The greatest gamma intensity is straight ahead, while the gamma intensity in other directions is substantially less. Most initial scattering points of interest in the following work are located along directions that are 30 to 50 degrees away from the beam tube centerline (as measured from the collimator exit). Table D5.4 lists the total gamma leakage from the collimator exit in the forward hemisphere (0-90 degrees) as L(0-90), while the corresponding total leakage through a cone spanning the range 30 to 60 degrees off centerline is listed there as L(30-60). With these leakage values, the corresponding angular flux per steradian in the range of interest is (to first order):

Aflux(30-60) = (L(30-60)/ubar) / (2*pi*[cos(30)-cos(60)]), where ubar=[cos(30)+cos(60)]/2 = 0.68301270

such that

Aflux(30-60) = L(30-60) * 4.000 / (2*pi)

Likewise, since the total leakage is so forward peaked and the leakage-weighted "ubar" is essentially 1.0, the "average" angular flux per steradian in the forward hemisphere is:

Aflux(0-90) = L(0-90) / (2*pi*[cos(0)-cos(90)]) = L(0-90) / (2*pi)

so that the "angular flux intensity ratio" (AFIR) needed to account for this effect is given by:

AFIR = (Local angular flux, 30-60 degrees) / (Average angular flux) = 4.000 * L(30-60) / L(0-90) .

By summing the leakage rates in Table D5.4 over various energy ranges, we see that:

for E > 1.000 MeV, L(30-60)=3.44478e+7 p/s, L(0-90)=1.64717e+9 p/s, which yields AFIR=0.083653
for E > .510 MeV, L(30-60)=6.40698e+7 p/s, L(0-90)=1.72771e+9 p/s, which yields AFIR=0.148335
for E > .010 MeV, L(30-60)=1.18504e+8 p/s, L(0-90)=1.89858e+9 p/s, which yields AFIR=0.249668

While the last value may be the most conservative, it would also be very unrealistic, since most of the dose downstream of the shield comes from photons that were above 1 MeV at the time they left the collimator. Indeed, most of that dose comes from those that were between 4 and 8 MeV at that time, which would yield a still smaller value of AFIR. Thus, using the first "angular flux intensity ratio" shown here would be a conservative compromise that's more representative of reality.

In the elementary off-centerline shielding calculations that follow, the above source (N00) must therefore be multiplied by the appropriate "angular flux intensity ratio" (AFIR) to account for the angular distribution at the exit of the collimator. In this case,

AFIR = 4.000 * L(30-60) / L(0-90) = 4.000 * (3.445e+7) / (1.647e+9) = 0.08365

will be taken as a constant in subsequent scattering/streaming calculations in which the initial scattering events of interest occur in regions downstream of the collimator that are 35-50 degrees off the centerline.

To estimate the "direct dose" downstream of the entire rotary shutter shield assembly, either at the centerline or at other locations across the external face, however, one will need to use a

value of AFIR that is more appropriate to the particular angular direction characteristic of that point. Table D5.4 gives the gamma leakage rate from the hole in the collimator, by energy group, for each of seven directional bins. It is important to recognize that this is very forward peaked and changes markedly from one directional range to the next. For the simplistic analyses that follow, it is especially important to take note of the variations above 1 MeV. For E > 1 MeV, the total leakage rate from the hole in the collimator (over the entire forward hemisphere, 0-90 degrees) is L(0-90)=1.64717e+9 p/s, and the average leakage per steradian is L(0-90)/[2*pi*(cos(0)-cos(90)]. Likewise, the average leakage per steradian in each of the other directional bins can be computed as L(xx-yy)/[2*pi*cos(xx)-cos(yy)], and the average angular flux per steradian (above 1 MeV) can, to first order, be obtained by dividing that quantity by "ubar", the average cosine for the angular range. The (approximate) "angular flux intensity ratio" (AFIR) is then defined as before:

AFIR = ((L(xx-yy)/ubar(xx,yy))/(cos(xx)-cos(yy)))/L(0-90), where ubar(xx,yy)=0.5*(cos(xx)+cos(yy)).

For E > 1 MeV, theta = 0-90 deg, L(0-90) = 1.64717e+9
For E > 1 MeV, theta = 0- 2 deg, L(0- 2) = 1.18009e+9, and AFIR = 1.17643e+3
For E > 1 MeV, theta = 2- 5 deg, L(2- 5) = 1.43669e+8, and AFIR = 2.73501e+1
For E > 1 MeV, theta = 5-10 deg, L(5-10) = 1.15578e+8, and AFIR = 6.22122e+0
For E > 1 MeV, theta = 10-20 deg, L(10-20) = 1.20065e+8, and AFIR = 1.67906e+0
For E > 1 MeV, theta = 20-30 deg, L(20-30) = 5.28592e+7, and AFIR = 4.82489e-1
For E > 1 MeV, theta = 30-60 deg, L(30-60) = 3.44478e+7, and AFIR = 8.36534e-2
For E > 1 MeV, theta = 60-90 deg, L(60-90) = 4.63110e+5, and AFIR = 2.24924e-3

Note that the angular flux intensity ratio (AFIR) varies by almost six orders of magnitude over the forward hemisphere. While a value of 0.08365 may indeed be appropriate for some of the initial scattering regions of interest, a value of 1176.4 would be more appropriate for estimating the external dose rate along the centerline. Moreover, if one were trying to estimate the "direct" component of the dose rate on the external surface of the shield configuration (Z=478.79 cm), at the midplane, directly in front of one of the clearance gaps (a point that is 30 deg off the centerline, as measured from the collimator exit), a value somewhere between 0.48248 and 0.08365 would be appropriate. In this case, we'll use the numerical average, 0.2831, with the caveat that the actual dose rate due to this component of the flux may actually be up to a factor of 2 higher. In all cases, the equivalent point source to be used in the simple analytic shielding calculations is given by:

N0 = D0 * AFIR * (2*AS0/FTD)

where D0 is the dose rate at the exit of the collimator (110.0e+3 mrem/hr), AS0 is the area of the 2.75-inch x 5.5-inch rectangular hole in the collimator (97.58 cm2), FTD is a flux-to-dose-rate factor that will ultimately cancel out prior to calculation the final dose rate, and AFIR is the angular flux intensity ratio as described above.

6.10.4 More General Method of Estimating External Dose Rate at the Centerline Due to Transmission

With the above as prologue, the uncollided flux and direct dose rate at the point of interest (X=0,Y=0,Z=478.79 cm) may be calculated as for any other point source in an attenuating media:

f = N0 * exp(-u*rho*t) / (4*pi*d^2)

D = f * FTD = FTD * [N0] * exp(-u*rho*t) / (4*pi*d^2)

= FTD * [D0 * AFIR * (2*AS0/FTD)] * exp(-u*rho*t) / (4*pi*d^2)

= D0 * AFIR * exp(-u*rho*t) * (2*AS0) / (4*pi*d^2)

where d is the distance (79.31 cm) from the exit of the collimator (X=0,Y=0,Z=399.48 cm) to the point of interest (X=0,Y=0,Z=Z=478.79 cm),

AS0 is the area of the rectangular hole in the collimator (97.58 cm2),

t is the total amount of steel (52.24 cm) the gammas must pass through when traversing the rotary shutter shield plug along the centerline as shown in Fig. 6.7,

rho is the mass density (7.82 g/cc) of the steel comprising the carbon steel shield plug

u is the mass attenuation coefficient (0.0298 cm2/g) for 8 MeV gammas in steel

AFIR is the appropriate "angular flux intensity ratio" (1176.4) for the given direction (along the centerline, in this case) as described at the end of Sect 6.10.3, and

D0 is the dose rate at the exit of the water-filled collimator (110.0e+3 mrem/hr)

Inserting all the above values then yields a dose rate of 1.65 mrem/hr at the external surface, along the centerline. This is in good agreement with the simple "beam analysis" in Sect 6.10.1 where the dose rate was simply folded with the exponential attenuation factor, exp(-12.17). In that case, the simple analytic "beam formula" gave 0.57 mrem/hr when no buildup factor was used, and 3.87 mrem/hr when a buildup factor was used. All three simple analytic values are, of course, crude estimates. [By way of comparison, the best MCNP estimate of the peak dose rate 0.5 cm downstream of the rotary shutter along the system centerline (cf Tally 45) was 0.8934 mrem/hr +/- 3.4%.] The advantage of the present formulation, unlike that in Sect 6.10.1, is that: (1) it can account for the variation in the source strength as a function of direction (via the AFIR parameter), (2) it does have a 4*pi*d^2 divergence term in the denominator which (physically) is necessary and more descriptive of reality, and (3) it can be used to evaluate the direct (uncollided) component of the dose rate at other points along the external surface (such as at the midplane, directly in front of the clearance gaps, or anywhere else).

Finally, while the above formulation was derived in an elementary fashion to take advantage of the limited data available in this case, its physical interpretation is directly analogous to what one would normally derive in a more mathematical world. Basically, it corresponds to integrating the attenuated angular flux at the point of interest over only those directions lying in that portion of the unit sphere [ASO/(4*pi*d^2)] corresponding to the finite source as seen from the point of interest, to obtain the scalar flux (at the point of interest), which is then folded with the flux-to-dose-rate conversion factor to obtain the dose rate in a very traditional fashion. [The extra factor of 2 seen multiplying ASO in our expression for the final dose rate has nothing to do with this solid angle, but is a legacy term that needs to remain because of the way in which the equivalent point source was inferred from the dose rate at the collimator exit. Note that the dose rate at the collimator exit depends primarily (almost exclusively) on fluxes in the forward hemisphere only. To obtain the equivalent point source strength over a fictitious 4*pi sphere, the simplistic derivation assumed that the fluxes in both hemispheres were symmetric, and, for consistency, the corresponding dose rate used to obtain the equivalent point source had to be multiplied by this factor of 2. Alternately, this factor of 2 may be viewed as a direct consequence of the way in which the angular flux intensity ratio (AFIR) has been defined. Here it is defined as the ratio of the angular flux in a given direction to the average angular flux in the forward hemisphere. Had it been defined as the ratio of the angular flux in a given direction to the average angular flux over the 4*pi sphere (where the fluxes in the backward hemisphere are effectively zero by comparison to those in the forward hemisphere), the values of AFIR would have been a factor of 2 higher, and the need for this extra factor of 2 in our expression for the final dose rate would have disappeared completely.]

6.10.5 Direct External Dose at the Midplane, in Front of a Tall Thin Clearance Gap

Consider the gamma dose rate at the midplane, directly downstream of the tall thin clearance gap shown on the left in Fig. 6.8 (or on the right in Fig. 6.6). One can certainly visualize multiple ways radiation could reach that point: (1) the direct uncollided dose coming from the emerging source at the exit of the collimator; (2) radiation that basically scatters just once, close to where the concrete block assembly is stepped (just upstream of the clearance gap), and (3) radiation that leaves the collimator while travelling to the right, passes through a minimal amount of concrete, scatters once in the concrete near the close end of the rotary shutter's large beam hole, streams down the beam hole, and then scatters in the concrete around the clearance gap before streaming out through the void. The first component will be described in this section, while the second will be described in Sect 6.10.7, and the third will be left as an exercise for the reader.

The limited objective in this section is determine the uncollided component of the dose rate at this point due to radiation coming directly from the emerging source at the exit of the collimator. Only if this "direct dose" is found to be really negligible, will it later be possible to say whether or not the configuration exhibits any streaming effects and whether MCNP is able to accurately account for those effects.

The approach taken here is essentially the same as that taken in Sect 6.10.4, except that the angular flux intensity ratio (AFIR) used here is now much less (0.2831), as indicated at the end of Sect 6.10.3, because the direct line from the collimator exit (X=0,Y=0,Z=399.48) to the point of interest (X=0,Y=-42.62438,Z=478.79) is now about 30 degrees away from the centerline. As indicated in Fig. 6.8, this line of sight from the collimator exit to the point of interest now passes through a total of 21.4 cm of concrete and 45.8 cm of carbon steel, while the total distance (d) between the two points is 90.0 cm. As in the above case, the uncollided flux and direct dose rate at the point of interest may again be calculated as for any other point source in an attenuating media:

f = NO * exp[-(ucon*rhocon*tcon+ustl*rhostl*tstl)] / (4*pi*d^2)

D = f * FTD = FTD * [NO] * exp[-(ucon*rhocon*tcon+ustl*rhostl*tstl)] / (4*pi*d^2)

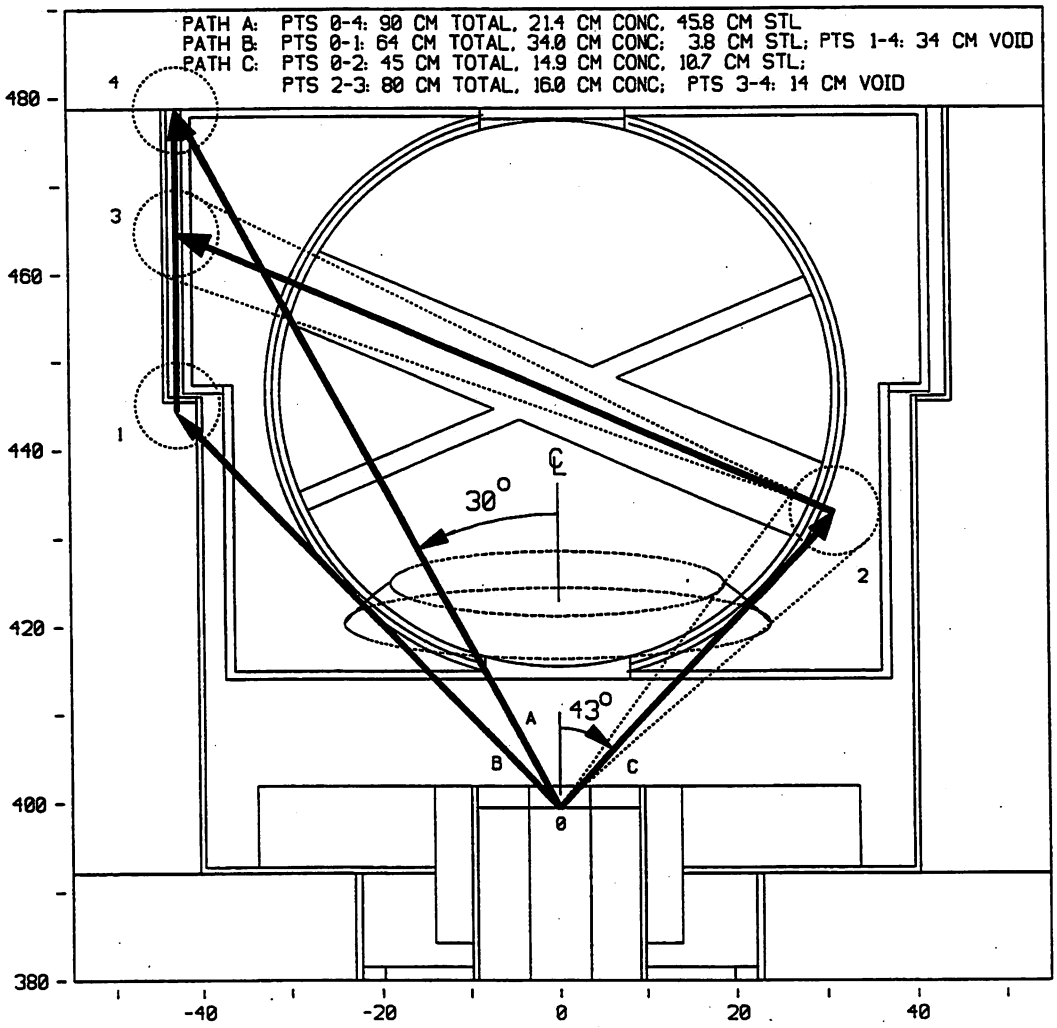


Fig. 6.8. Three different paths by which gammas emerging from the collimator exit may contribute to the dose rate downstream of the void clearance gap between the biological shield and the concrete block assembly holding the rotary shutter. Note that while Paths A and B are clearly defined, Path C represents just one of many alternate paths.

= FTD * [D0 * AFIR * (2*AS0/FTD)] * exp[-(ucon*rhocon*tcon+ustl*rhostl*tstl)] / (4*pi*d^2)

= D0 * AFIR * exp[-(ucon*rhocon*tcon+ustl*rhostl*tstl)] * (2*AS0) / (4*pi*d^2)

where d is the distance (90.0 cm) from the exit of the collimator (X=0,Y=0,Z=399.48 cm) to the point of interest (X=0,Y=-42.62438,Z=478.79),

AS0 is the area of the rectangular hole in the collimator (97.58 cm2),

tstl is the total amount of steel (45.8 cm) the gammas must pass through when traversing the rotary shutter shield plug and metal liners in this direction.

tcon is the total amount of barytes concrete (21.4 cm) the gammas must pass through when going in this direction and traversing the concrete block assembly holding the rotary shutter

rhostl is the mass density (7.82 g/cc) of the steel comprising the carbon steel shield plug

rhocon is the mass density (3.097 g/cc) of the barytes concrete comprising the block assembly

ustl is the mass attenuation coefficient (0.0298 cm2/g) for 8 MeV gammas in steel

ucon is the mass attenuation coefficient (0.0245 cm2/g) for 8 MeV gammas in concrete

AFIR is the appropriate "angular flux intensity ratio" (0.2831) for the given direction (30 degrees off centerline, in this case) as described at the end of Sect 6.10.3, and

D0 is the dose rate at the exit of the water-filled collimator (110.0e+3 mrem/hr)

Inserting all the above values then yields a dose rate of 2.726e-4 mrem/hr on the external surface, at the midplane, directly downstream of the tall thin clearance gap between the biological shield and the concrete block assembly holding the rotary shutter. While the optical thickness used in the exponential attenuation term is almost the same here (12.30) as in the previous case along the centerline (12.17), the large decrease in the "direct dose" seen here is due to the large decrease in the angular flux intensity ratio as one deviates from the centerline (cf Sect 6.10.3). While the value of AFIR used here at 30 degrees was the numerical average of two widely disparate values (0.482489 in the 20 to 30 degree range, and 0.0836534 in the 30-60 degree range), the largest credible value (0.482489) would only increase the calculated dose rate obtained here by a factor of 1.7. Moreover, the detailed energy-dependent and angular-dependent leakage terms, upon which the angular flux intensity ratio is based, are generally all converged to within 3 to 5% as shown in Table D5.4. The conclusion to which one is then drawn is that the direct (uncollided) component of the dose rate at this particular location is indeed very negligible, and on the order of 2.726e-4 mrem/hr.

In Sect 6.10.7, we will attempt to estimate the dose rate here and along the entire length of the clearance gap (near the external surface) due to gammas that have experienced their first collision in the neighborhood of the stepped region between the biological shield and the concrete block holding the rotary shutter assembly, and have subsequently streamed out through the void clearance gap. The object of that analysis will be twofold: (1) to determine if any significant streaming effects should be expected and, if so, (2) to verify whether or not MCNP is correctly estimating the magnitude of those effects. Before that can be done, however, a simple analytic algorithm must first be developed that will allow one to roughly estimate such effects. Once developed in Sect 6.10.6, its use in this particular application will be explained in Sect 6.10.7.

6.10.6 Methodology for Treating Scattering: The Strength of Scattering Source(s)

Everyone knows that in a void, some distance (d) from a small scattering source (NS1 photons/sec), the flux (f) can be calculated as f=NS1/(4*pi*d^2).

Now assume the point of interest is in a void clearance gap downstream of the configuration, and the scattering source of interest is a small volume element of the shielding material upstream of the gap. What is the scattering source (NS1)? One must have it to proceed with any estimate.

Consider the situation in Fig. 6.9 where one has a huge block of shielding material and one needs to know the actual number of particles scattering (NS1) in a small spherical volume element of radius "r" located some distance (R) from the origin where one has a point source emitting N0 particles/sec. Furthermore, let that small spherical volume element be sandwiched between two big spheres of radii RM1 and RM2 (both in centimeters). If "u" denotes the mass attenuation coefficient (cm2/g) and "rho" denotes the density (g/cc), then

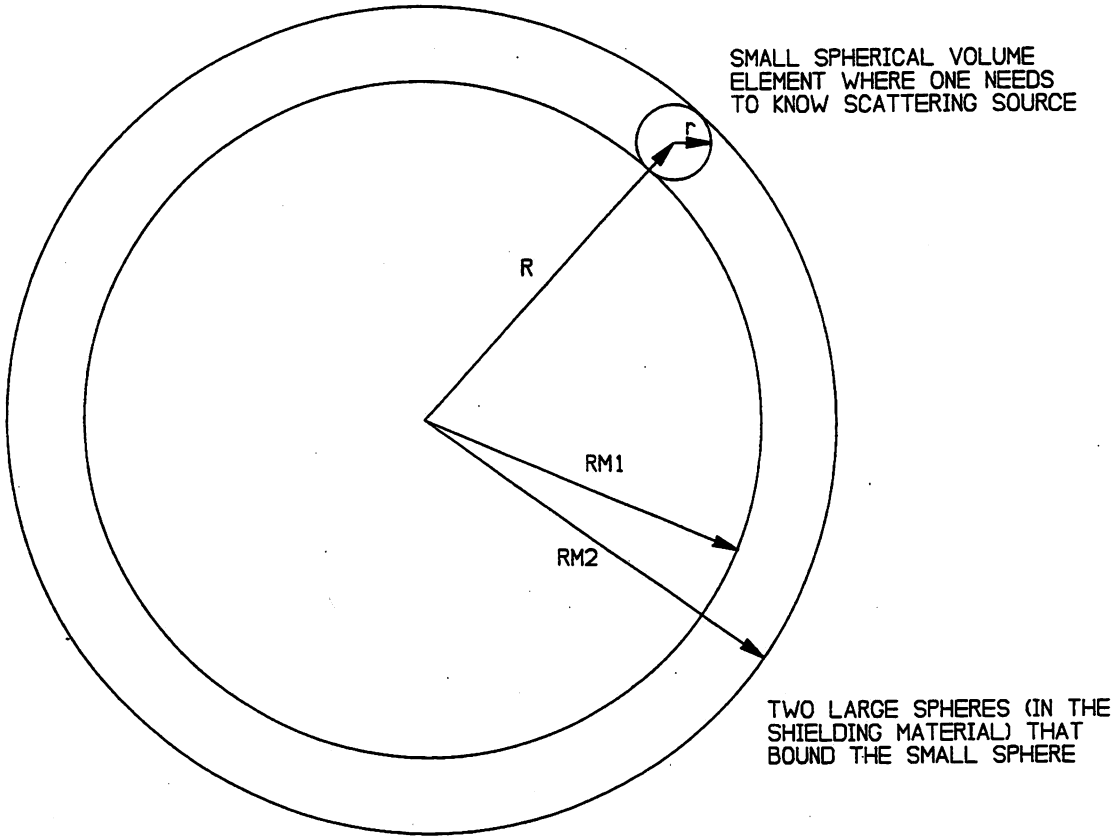


Fig. 6.9. Two large spherical shells (in a bulk shielding material, centered about a point source) which bound a small spherically-shaped volume element in which the scattering rate is to be determined.

N1 = N0 * exp(-u*rho*RM1) is the "number" of particles reaching the first large sphere, and

N2 = N0 * exp(-u*rho*RM2) id the "number" of particles reaching the second large sphere.

Note that we are not concerned about fluxes or currents, only the "number" of particles (p/s), and the only thing that affects that is the exponential attenuation.

But what happens to those particles that "made it" to the first large sphere but did not "make it" to the second large sphere? They experienced a collision, and are likely scattered. Thus, the total number of collisions (=scattering events) between the two shells (TNSshell) is given by:

TNSshell = N2 - N1 = N0 * [exp(-u*rho*RM1) - exp(-u*rho*RM2]

= N0 * [exp(-u*rho*RM1) - exp(-u*rho*(RM1+2*r)]

= N0 * exp(-u*rho*RM1) * [1.0 - exp(-2*u*rho*r)]

At this point, several things must be recognized. First, as stated before, "r" is the radius of the small sphere where we eventually want to know the scattering density. Secondly, RM1 does not necessarily have to be the inner radius of the large sphere. More appropriately stated, it is really the amount ("thickness") of the shielding material that the original source particles (N0) must go through before reaching the first large sphere. Part of this big inner sphere may be void, for example. Thus, let us define "TM1" as the "thickness of the material" (between N0 and the inner big sphere), and make that substitution. Lastly, consider the approximation:

exp(x) =?= 1.0 + x which is really good iff x << 1.0, such that

[1.0 - exp(-x)] =?= x which is really good iff x << 1.0.

In our case, u is typically 0.025 cm2/g, rho is about 3.1 g/cc for the barytes concrete, and the small scattering sphere of interest is typically 4.445 cm in radius, such that x=2*u*rho*r is about 0.689 and the rigorous expression [1.0-exp(-x)] equals 0.498 rather than 0.689 as given by the approximate expression. Moreover, that is close enough for our purposes and it's conservative. If anyone is really concerned about it, they can always use smaller volume elements (ie, smaller values of "r"), in which case the approximation becomes better and better very quickly (it just means that you then have to calculate scattered contributions from more volume elements). Making these substitutions, we then see that the total "number" of scattering events between the two large spherical shells (TNSshell) is given by:

TNSshell = N0 * exp(-u*rho*TM1) * (2*u*rho*r)

This would be the total scattering source (p/s) between the two large spherical shells. The total scattering source for the small spherical volume element of interest (of radius "r") then simply depends on the volume fraction (VF) of the large spherical shell occupied by this small volume element:

VF = (4/3)*pi*r^3 / [(4/3)*pi*(RM2^3-RM1^3)] = r^3 / [(R+r)^3-(R-r)^3)] = r^3 / [6*R^2*r + 2*r^3]

but, since r << R, this simplifies to:

VF = r^3 / [6*r*R^2] = (1/6)*(r/R)^2

and the total scattering source (NS1 photons/sec) in this small volume element of interest simplifies to:

NS1 = TNSshell * VF = N0 * exp(-u*rho*TM1) * (u*rho*r/3) * (r/R)^2

If there were a thin void of some sort (like a clearance gap) extending out from this volume element, and one needed to calculate the flux (f) and dose rate (D) some distance away, one could then proceed in the traditional fashion:

f = NS1 / (4*pi*d^2) and

D = f * FTD = FTD * [NS1] / (4*pi*d^2)

= FTD * [(N0) * exp(-u*rho*TM1) * (u*rho*r/3) * (r/R)^2] / (4*pi*d^2)

= FTD * [(D0*AFIR*(2*AS0/FTD)) * exp(-u*rho*TM1) * (u*rho*r/3) * (r/R)^2] / (4*pi*d^2)

= D0 * AFIR * [exp(-u*rho*TM1) * (u*rho*r/3) * (r/R)^2] * (2*AS0) / (4*pi*d^2))

In reality, of course, this would only be the dose rate, D(i), at the point of interest due to the NS1(i) photons/sec scattering in volume element "i". If the point of interest in the gap or void could see multiple volume elements, then one would have to sum over all "i".

Now assume that one needed to have the number of second generation scattering events "NS2(j)" in some other volume element further downstream that could see first generation scattering events "NS1(i)" in volume elements further upstream. In this case, the expression for each NS2 would be the same as the previous expression for NS1, except that it would be recursive in the sense that everywhere the original expression had NO, one would now have NS1(i), and one would have to sum over all NS1(i), etc, etc. This recursiveness becomes confusing and laborious very quickly. The good news is that the terms converge very quickly and a "ricochet" problem with more than two "bounces" is usually a "non-problem" in the sense that everything is generally negligible by that time. Moreover, to first order, contributions from "the first bounce" are usually the only contributions that one needs to worry about. Beyond that, one really needs a computer (and good cross section data, etc).

6.10.7 Contributions from "The First Bounce" Scattered Sources Streaming Through the Gap

Armed with this approximation, as crude and elementary as it might be, one is now in a position to estimate the first-order streaming effects downstream of the clearance gap (between the biological shield and the concrete block assembly holding the rotary shutter) due to gammas that may have first scattered in the region upstream of this clearance gap where the biological shield and concrete block assembly are "stepped" in order to minimize streaming (cf region 1 in Fig. 6.8). In particular, we will be looking at Path B in Fig. 6.8. In this example, we will first consider scattering from a single small volume element at the midplane (cf region 1) to a single detector at the midplane (cf region 4). With the aid of a small program, we will then look at the contribution from a series of 9 such volume elements (stacked vertically up and down the stepped region, into and out of the plane of the figure) to this given detector location at the midplane, and then from each and every volume element to each of 9 different detectors stacked vertically up and down the vertical extent of this tall thin clearance gap so that we can see the variation in the vertical direction and compute the average dose rate over the length of the gap which can then be directly compared with the MCNP estimate shown in Fig. 6.6.

To begin, let us consider all scattering events within about 2 inches of the stepped region in Fig. 6.8. More precisely, let us consider a stack of nine 4-inch x 4-inch x 4-inch volume elements stacked vertically at this location and centered at the midplane. Each one would have an equivalent radius (r) of 6.30276 cm. (In the numbering scheme later used, volume element 0 corresponds to the one at the midplane, while number -4 corresponds to the one at the bottom, and number 4 corresponds to the one at the top.) Here we will first focus only on contributions from the volume element at the midplane to the detector at the midplane. Based on the above formulation in Sect 6.10.6, the portion of the dose rate at this detector due to this volume element is given by:

$$D(0) = D0 * AFIR * [\exp(-urt) * (ucon*rhocon*r/3) * (r/R)^2] * (2*AS0) / (4*pi*d^2)$$

where $urt = ucon*rhocon*tcon + ustl*rhostl*tstl$

where d is the distance (34.0 cm) from the center of this particular volume element (where scattering is being modeled) to the detector of interest at (X=0,Y=-42.62438,Z=478.79)

AS0 is the area of the rectangular hole in the collimator (97.58 cm2),

r is the equivalent radius (6.30276 cm) of this 4-inch x 4-inch x 4-inch volume element where scattering is being modeled

R is the distance (64.0 cm) from the exit of the collimator (X=0,Y=0,Z=399.48 cm) to the center of this particular volume element (where scattering is being modeled)

tcon is the total amount of barytes concrete (34.0 cm) the gammas must pass through when travelling from the collimator exit to the center of this particular volume element as shown in Fig. 6.8.

tstl is the total amount of steel (3.8 cm) the gammas must pass through when travelling from the collimator exit to the center of this particular volume element. This steel is associated with the various steel liners. As shown in Fig. 6.8, most gammas traveling in this direction will "just miss" the carbon steel shield plug.

rhocon is the mass density (3.097 g/cc) of the barytes concrete comprising the block assembly

rhostl is the mass density (7.82 g/cc) of the steel comprising the carbon steel shield plug

ucon is the mass attenuation coefficient (0.0245 cm2/g) for 8 MeV gammas in concrete

ustl is the mass attenuation coefficient (0.0298 cm2/g) for 8 MeV gammas in steel

AFIR is the appropriate "angular flux intensity ratio" (0.08365) for the given direction; in this case the line from the collimator exit to the volume element of interest is approximately 43 degrees away from the beam tube centerline, and the appropriate value for this direction (0.08365) was obtained as noted in Sect 6.10.3.

D0 is the dose rate at the exit of the water-filled collimator (110.0e+3 mrem/hr)

Inserting all the above values then yields a dose rate of 5.9748e-3 mrem/hr at the point of interest, due to scattering events in this particular volume element. Likewise, the streaming contributions to this detector from scattering events in each of the eight other volume elements described above (4 below the midplane and 4 above the midplane) may be calculated in a similar fashion. Assuming AFIR remains constant over this range (for lack of any more detailed knowledge), the only things that change with the position of the volume element are the amounts of concrete and steel used in the exponential attenuation term (tcon and tslt simply increase as the angle changes), and the distance (d) from the center of each volume element to the detector. Table 6.12 lists a simple 1-page program for doing just that sort of analysis. In addition to calculating the scattered dose rate for this detector at the midplane from all 9 volume elements (and the resulting total), it also does a similar set of calculations for all 9 detectors spaced up and down over the length of the tall thin clearance gap. Lastly, it also calculates the "direct" dose rate at each detector due to uncollided gammas coming straight from the collimator exit. It does not, however, account for scattered radiation streaming through the 3.5-inch-diam beam hole in the rotary shutter. Nevertheless, the results are fascinating.

Based on this simplistic analysis, Table 6.13 shows the scattered dose rate, the direct dose rate, and total dose rate (mrem/hr) at the nine different (vertical) detector locations directly in front of one of the tall thin clearance gaps between the biological shield and the concrete block assembly holding the rotary shutter. One of the most revealing things in the table is that the direct dose rate is two or more orders of magnitude lower than the dose rate due to radiation that scattered in these nine particular volume elements of interest and subsequently streamed out through the clearance gap. Basically, that says that all the radiation that gets there is due to streaming (albeit, a very small amount). Secondly, the results obtained by this simple analytic model were surprisingly close to those obtained by MCNP. Note, for example, that MCNP4B Run HB308G calculated an average total dose rate of 0.0217 mrem/hr +/- 26% for the tall thin gap on the left of Fig. 6.6, and an average total dose rate of 0.0477 mrem/hr +/- 37% for the tall thin gap on the right. By way of comparison, Table 6.13 shows the average dose rate to be 0.0240 mrem/hr which, perhaps fortuitously, is within a just half a standard deviation of the lower MCNP result. Moreover, given that the simple analytic model described above does not account for scattered radiation streaming through the 3.5-inch-diam beam hole in the rotary shutter, it should indeed be more characteristic of the lower MCNP value (and it is!). More realistically speaking, had the low-order analytic method been within a factor of 2 or 3 (or maybe even within a factor of 10) of the MCNP result at this difficult-to-calculate location, it would have been sufficient to certify the acceptability of the MCNP result, especially since the dose rates obtained by both methods are so low. The fact that they appear to agree within 10% is remarkable.

6.10.8 Concluding Remarks on Scattered Radiation and Streaming

In Sect 6.9.5.3.1, it was noted that the MCNP dose rates in front of the clearance gap on the right of Fig. 6.6 were about 2.13 times larger than those on the left. Obviously this is due to scattered radiation (from somewhere) streaming through the large beam hole in the shutter. Since MCNP did so well in calculating the dose rate on the other side where this is not a contributing factor, there is every reason to believe that it is also calculating this asymmetry correctly. Path C in Fig. 6.8 suggests one possible explanation for the asymmetry seen on the one side, but it is not likely the real reason. The theory put forth in Sect 6.10.6 can and has been applied to estimate the additional dose rate at location 4 in Fig. 6.8 due to the third leg of Path C. While the second leg of path C does contribute to the general dose rate in the biological shield to the left of that location, the dilution associated with the 1/(4*pi*d^2) term after the second scattering event makes its contribution to the dose rate at location 4 relatively negligible. (For the same reason, the additional dose rate along the centerline due to the path shown in Fig. 6.10 is completely negligible as well.) Moreover, for that same reason, it is far more likely that the previously described asymmetry in the dose rates for the right and left clearance gaps is due to a series of "first collision" events somewhere in the system. Figure 6.11 suggests another possible explanation using "first bounce" theory. While qualitatively more plausible, its effect has also been evaluated using the above equation, and the dilution associated with the 1/(4*pi*d^2) term after the first scattering event also makes this particular contribution relatively negligible. While the difference in dose rates in front of the right and left clearance gaps is very small (but real), the particular paths shown in Fig. 6.11 do not appear to be the explanation. Moreover, for scattering events along path D to make a noticeable contribution at location 6, not only is a single scattering event required, but the second leg of the path must be considerably shorter. Scattering events along the sides of the beam hole near the beam tube centerline (where the gamma flux is much higher) have also been evaluated, but they, by themselves, cannot fully explain the noted asymmetry either. While there is little doubt that this

Table 6.12. Simplistic program to calculate the local dose rate up and down on the external (downstream) face of the HB-3 shield configuration, directly in front of the void clearance gap between the biological shield and the concrete block assembly holding the rotary shutter, as well as the average dose rate over the long narrow gap. Accounts for direct dose rate from source, as well as scattering in concrete upstream of the clearance gap, but does not account for streaming through the 3.5-inch-diam beam hole in the shutter.

```
c       SCATSRC.FOR -- Simple program to calculate dose up and down in gap beside block
c
        dimension d(-4:4)
        pi=acos(-1.0)
        d0=110.0e3     ! mrem/hr initial dose rate in front of collimator hole
        as0=97.58      ! cm2     area of the 2.75"x5.5" collimator hole
        afir=0.08365   ! angular flux intensity ratio (unitless) for scatter reg at 43 deg off centerline
        afirdd=0.2831  ! angular flux intensity ratio (unitless) for direct dose at 30 deg off centerline
        ucon=0.0245    ! cm2/g   mass attenuation coef for barytes concrete (at 8 MeV)
        ustl=0.0298    ! cm2/g   mass attenuation coef for steel (at 8 MeV)
        rhocon=3.097   ! g/cc    density for barytes concrete
        rhostl=7.82    ! g/cc    density for steel
        tstl0=45.8     ! cm  thickness of steel    between src & det (at midplane)
        tcon0=21.4     ! cm  thickness of concrete between src & det (at midplane)
        t0c=34.0       ! cm  thickness of concrete between src & 1 st scatter pt (at midplane)
        t0s=3.8        ! cm  thickness of steel    between src & 1 st scatter pt (at midplane)
        ra0=64.0       ! cm  distance (thru void+conc) to 1st scatter pt (at midplane)
        rb0=34.0       ! cm  distance from 1st scatter pt to det (at midplane)
        rc0=90.0       ! cm  distance from src to det (at midplane)
        r=6.30276      ! cm  equiv radius of a 4"x4"x4" cube (of conc at scatter pts)
        dh=10.16       ! cm  vertical spacing between scattering pts considered
c
        do j=4,-4,-1
           hd=j*dh       ! height of det "j" above midplane
           write (*,10) j,hd
10         format (/,' for det',i3,' hd=',f7.2,/)
c       compute dose from gammas that scatter in conc & then stream thru gap to det "j":
        sum=0.0
        do i=4,-4,-1
           h=i*dh        ! height of scatter pt "i" above midplane
           ra=sqrt(ra0*ra0+h*h)            ! dist from src to scatter pt "i"
           rb=sqrt(rb0*rb0+(h-hd)*(h-hd))  ! dist from scatter pt "i" to det "j"
           tm1c=t0c*ra/ra0                 ! thickness of conc  from src to scatter pt "i"
           tm1s=t0s*ra/ra0                 ! thickness of steel from src to scatter pt "i"
           urt=ucon*rhocon*tm1c+ustl*rhostl*tm1s
           d(i)=exp(-urt)*(ucon*rhocon*r/3.0)*(r/ra)**2
           d(i)=d0*afir*d(i)*2.0*as0/(4.0*pi*rb*rb)  ! dose from scatter pt "i" to det "j"
           write (*,11) i,d(i)
11         format (' segment=',i2,' dose(i)=',f12.8,' mrem/hr')
           sum=sum+d(i)  ! running sum of dose from all scatter pts "i" to det "j"
        enddo
        sd=sum           ! final   sum of dose from all scatter pts "i" to det "j"
c
c       compute direct dose to det "j" (from src, thru concrete & part of steel shutter)
        rc=sqrt(rc0*rc0+hd*hd)          ! dist from src to det "j"
        urtstl=ustl*rhostl*tstl0*rc/rc0  ! adjust thickness for det "j" location
        urtcon=ucon*rhocon*tcon0*rc/rc0  ! adjust thickness for det "j" location
        urttot=urtstl+urtcon
        dd=d0*afirdd*exp(-urttot)*2.0*as0/(4.0*pi*rc0*rc0)  ! direct dose from src to det "j"
        td=dd+sd  ! total dose = direct dose + scattered dose
c
        write (*,12) sd,dd,td
12      format ('   total scat dose =',f12.8,' mrem/hr',/,
     *          '       direct dose =',f12.8,' mrem/hr',/,
     *          '       total  dose =',f12.8,' mrem/hr',/)
        tdsum=tdsum+td      ! running sum of total dose for all detectors
        enddo               ! end (j) loop on det location
c
        tdavg=tdsum/9.0     ! "avg" total dose up & down the gap
        write (*,13) tdavg
13      format (/,'   total dose avgd =',f12.8,' mrem/hr')
        stop
        end
```

Table 6.13. Scattered dose rate, direct dose rate, and total dose rate (mrem/hr) at nine different verticle locations directly in front of one of the tall thin clearance gaps between the biological shield and the concrete block assembly holding the rotary shutter. These values were calculated by the simplistic program (SCATSRC.FOR) shown in Table 6.12. It accounts for the direct dose coming from the source (at the collimator exit), through a portion of the steel shutter and the concrete block assembly, to each detector point. It also accounts for dose at each detector from each of nine different 4-inch x 4-inch x 4-inch scattering regions in the concrete, near the rear of this last segment of the void clearance gap where the concrete block assembly is stepped.

Det Location-->	40.64 cm above midplane	30.48 cm above midplane	20.32 cm above midplane	10.16 cm above midplane	00.00 cm above midplane	10.16 cm below midplane	20.32 cm below midplane	30.48 cm below midplane	40.64 cm below midplane
Vert. location of scatter pt.									
+40.64 cm	.00224600	.00206189	.00165490	.00124525	.00092477	.00069484	.00053291	.00041782	.00033448
+30.48 cm	.00307920	.00335416	.00307920	.00247142	.00185964	.00138104	.00103767	.00079584	.00062397
+20.32 cm	.00337240	.00420177	.00457697	.00420177	.00337240	.00253760	.00188451	.00141597	.00108597
+10.16 cm	.00309395	.00411178	.00512298	.00558044	.00512298	.00411178	.00309395	.00229768	.00172641
00.00 cm	.00246005	.00331260	.00440235	.00548501	.00597480	.00548501	.00440235	.00331260	.00246005
-10.16 cm	.00172641	.00229768	.00309395	.00411178	.00512298	.00558044	.00512298	.00411178	.00309395
-20.32 cm	.00108597	.00141597	.00188451	.00253760	.00337240	.00420177	.00457697	.00420177	.00337240
-30.48 cm	.00062397	.00079584	.00103767	.00138104	.00185964	.00247142	.00307920	.00335416	.00307920
-40.64 cm	.00033448	.00041782	.00053291	.00069484	.00092477	.00124525	.00165490	.00206189	.00224600
Total Scat'd Dose (all 9)=	.01802245	.02196950	.02538544	.02770914	.02853438	.02770914	.02538545	.02196950	.01802245
Direct Dose From Source =	.00008248	.00013729	.00020006	.00025216	.00027264	.00025216	.00020006	.00013729	.00008248
Total Dose =	.01810494	.02210679	.02558551	.02796130	.02880702	.02796130	.02558551	.02210679	.01810494

AVG TOTAL DOSE = .02403601 mrem/hr (when total dose at detectors are averaged over all detector positions)

Note that MCNP4B Run HB308G gave an average total dose rate of 0.0217 mrem/hr +/- 26% for the tall thin gap on one side, and an average total dose rate of 0.0477 mrem/hr +/- 37% for the tall thin gap on the other side.

asymmetry exists, one can only speculate that it is due to a large number of small contributions from scattering events all along the inner wall of the rotary shutter beam hole, with those on the right (resulting from higher flux levels) subsequently being more heavily diluted by the 1/(4*pi*d^2) term in the second leg of the journey, and those on the left (resulting from lower flux levels) subsequently being less diluted by the 1/(4*pi*d^2) term in the second leg of the journey. Because the asymmetry is relatively small (about a factor of 2), and because the corresponding dose rates are totally negligible in any event (less than 0.05 mrem/hr), this small but real asymmetry is only of minor academic interest and will be pursued no further.

The important facts demonstrated in the previous subsection are these: (1) streaming effects associated with the clearance gaps will increase the dose rate that would otherwise be present by about two orders of magnitude; (2) MCNP and the simple analytic method illustrated in Sect 6.10.7 both show this effect, and both yield essentially the same result; and (3) the dose rates obtained by both methods are totally negligible (less than 0.05 mrem/hr).

6.11 Concluding Remarks on the Final Gamma-Only Shielding Analysis

The final gamma-only shielding analysis (Run HB308G) for the HB-3 beam tube and rotary shutter used the newly proposed 1998 version of the beam tube in which the water tube was defined by aluminum windows welded inside the expanded portion of the beam tube itself (unlike the original 1960 design which had a physically separate water tube that was slid inside the beam tube). This analysis was performed with the 1998 water tube and collimator sections both flooded, the rotary shutter in the closed position, and the HFIR operating at 100 MW. The total amount of water in the new water tube and collimator sections was approximately 1.89 feet less than in the original 1960 design. The final gamma-only shielding analysis described here did not include neutrons, secondary gammas, or activation gammas, since the fluxes and dose rates due to neutrons upstream of the rotary shutter, and the fluxes and dose rates due to secondary gammas upstream of the rotary shutter, had already been found (cf Sect 5.6) to be completely negligible relative to those caused by high-energy gammas coming from the hot end of the beam tube, streaming through the water in the water tube and flooded collimator sections, and subsequently impinging on the rotary shutter. Calculated and measured dose rates downstream of the rotary shutter, due to activation of the shutter itself, are discussed separately in Sect 7.

This particular analysis (Run HB308G) uses the most comprehensive geometric model ever developed. The approach taken was to model the entire HB-3 beam tube and rotary shutter assembly exactly as described in Sect 3 and shown in Fig. 3.3, with no approximations. Moreover, Fig. 3.3 was created from the actual MCNP input file used in this analysis. Basically, the model includes everything within 65 cm (radially) of the beam tube centerline, starting at the radial plane perpendicular to the beam tube (which is defined as Z=0), and extending axially outward along the beam tube centerline to a location well beyond the rotary shutter. The outermost downstream surface of the steel clad concrete block assembly holding the rotary shutter is located at Z=478.79 cm. Dose rates were calculated at several locations on this surface, including the midpoint at the centerline, and several lateral locations in front of the 1.74625-cm clearance gaps between the biological shield and the concrete block assembly holding the rotary shutter. Dose rates were also calculated at several other axial locations along the centerline, downstream of the rotary shutter.

The dose rate on the centerline, immediately downstream of the shutter (at Z=479.29 cm) was found to be 0.8934 mrem/hr +/- 3.4%. At 1.5 feet from the surface of the rotary shutter housing (at Z=524.51 cm), the centerline dose rate was found to be 0.3033 mrem/hr +/- 1.1%, while at 3.0 feet from this surface (at Z=570.23 cm) the centerline dose rate was found to be 0.2088 mrem/hr +/- 0.6%. The dose rate at the closest point was calculated using a point detector estimate, but verified using a much more rigorous boundary crossing tally which exhibited exceptionally good statistics in every energy range of interest. The dose rate at the closest point was also verified using simple analytic approximations.

Streaming effects associated with the 1.74625-cm clearance gaps between the biological shield and the concrete block assembly holding the shutter caused the dose rates in front of those locations to be two orders of magnitude higher than they otherwise would have been without any clearance gaps. MCNP and a simple analytic method used to check those results both saw this same effect, and both gave essentially the same result. Fortunately, the dose rates obtained by both methods downstream of the clearance gaps (even with streaming) were totally negligible (less than 0.05 mrem/hr). In the case of MCNP, the average dose rate for the gap on the right side of the configuration (0.0477 mrem/hr) was found to be 2.13 times higher than on the left (0.0217 mrem/hr) due to streaming through the large beam hole in the rotary shutter which is rotated 66.75 degrees from the beam tube centerline when the shutter is in the closed position. In addition, the average dose rate for the clearance gap above the concrete block assembly holding the rotary shutter (0.0222 mrem/hr) was found to be marginally higher than for the clearance gap on the bottom (0.0150 mrem/hr) due to a small amount of streaming in the 5/16-inch clearance gap above the carbon steel shield plug inside the rotary shutter assembly. While not of any programmatic significance because of their low values, these small, physically justifiable, asymmetric variations are indicative of the small details that can be seen with this detailed 3-D model when used in combination with the 3-D broad-group weight window file which was developed for this analysis using

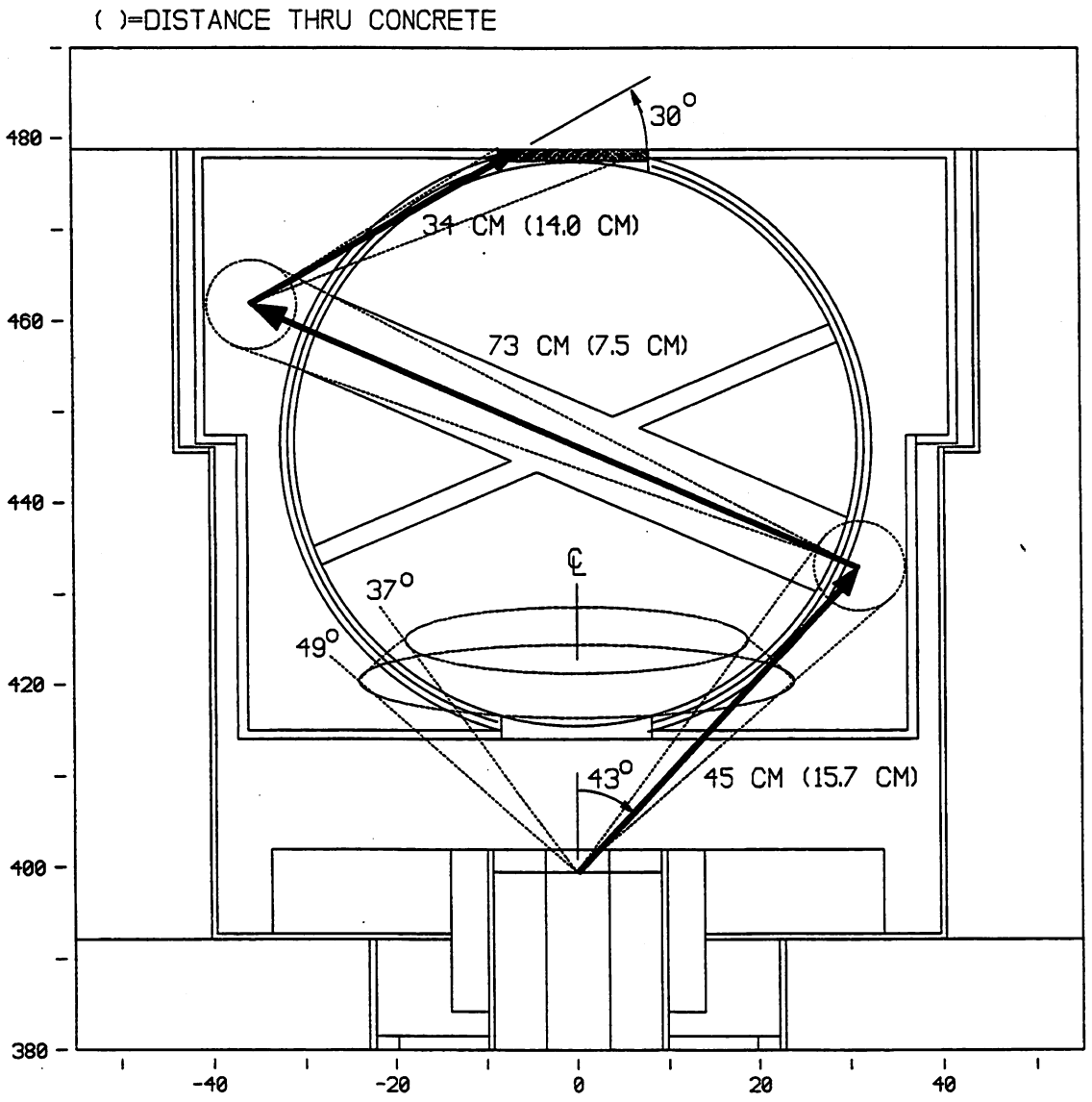


Fig. 6.10. One possible path by which scattered radiation might conceivably increase the dose rate along the centerline, directly downstream of the rotary shutter. Note, however, that in most cases where the radiation has scattered twice, the associated dose rate even a short distance from the second scattering event is usually negligible compared to that from radiation that has scattered just once, and even more negligible compared to the direct (uncollided) dose rate. In this particular case, the additional dose rate associated with this path is completely negligible relative to the direct (uncollided) dose rate.

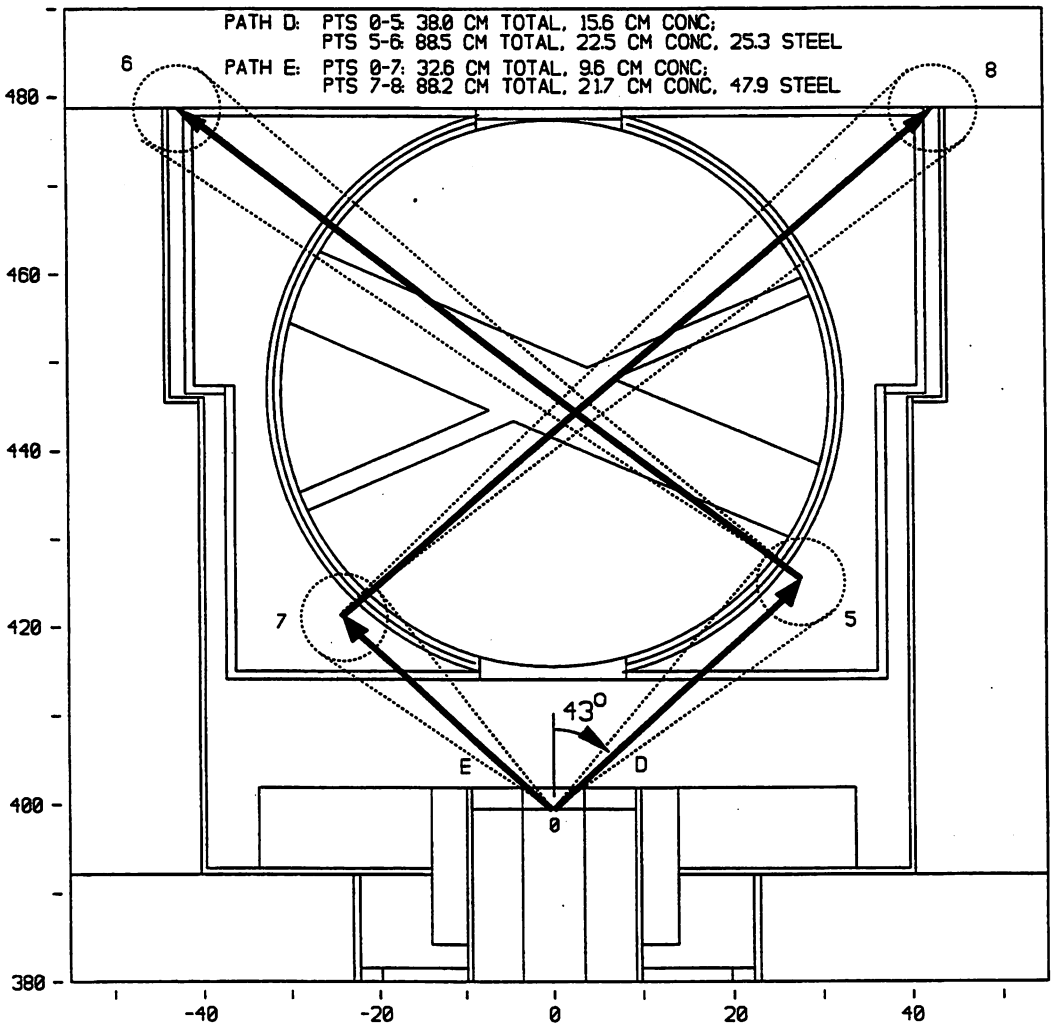


Fig. 6.11. Two of many possible paths showing how radiation that has passed through only a minimal amount of shielding material and scattered just once may preferentially tend to increase the dose rate downstream of the shield on one side of the shutter more than on the other side.

a fine-group 1-D adjoint analysis.

A useful by-product of this analysis was a very detailed boundary source file for a surface perpendicular to the centerline, just upstream of the rotary shutter assembly. This binary file is an MCNP boundary crossing history file (at Z=401.9645 cm) which contains the coordinates, direction cosines, energies and weights of the 5,688,819 photons crossing this surface in Run HB308G5. This particular file, which requires 542 MB of disk space, can then be used as an internal boundary source file in subsequent follow-up shielding analyses of this rotary shutter (or any similar shutter design in the future) by using the procedures outlined in Sect 6.8.2.

Rigorous solution of this particular problem required a host of biasing techniques including: use of only the most energetic source groups (a form of source-energy biasing); directional biasing of the source; on-the-fly directional biasing that was location dependent; and the extensive use of 3-D broad-group weight windows based on a preliminary 1-D adjoint analysis. The last was, by far, the most important. Without it, the rigorous solution of this problem would have been totally impossible. A large portion of Sect 6 was intentionally devoted to explaining how this weight window file was generated because it was the first time that such an elaborate approach has ever been undertaken at ORNL, at least for this sort of problem. The other feature unique to this analysis is that it was the first time (at ORNL) that a "geometry-independent weight window" file has ever been used with MCNP. This allows for the specification of the 3-D broad-group weight windows in an external file using a regular Cartesian mesh that is independent of the geometry cells needed to describe the material configuration. This feature has been tested at LANL and is currently available as an undocumented feature of the MCNP4B code; its availability will be announced formally with MCNP4C which will be part of a larger code system (to be released in the year 2000) aimed at automating the type of variance reduction techniques described here. We are indebted to Dr. Tom Evans of Los Alamos who first made us aware of this capability within MCNP4B and subsequently provided supplemental memos on how to take advantage of this feature. Without the availability of "geometry independent" weight windows, the rigorous solution of this geometrically complex deep penetration problem would also have been impossible.

7.0 ACTIVATION ANALYSIS AND RESULTING DOSE RATES

Analyses in Sects 5 and 6 have shown conclusively that, with the 1998 HB-3 water tube and collimator sections both flooded, the rotary shutter closed, and the HFIR operating at 100 MW, the total (contact) dose rate downstream of the rotary shutter (due to neutrons and gammas streaming down the beam tube from the operating reactor) would only be about 1 mrem/hr. (More precisely: at Z=479.29 cm, the dose rate was estimated to be 0.8934 mrem/hr +/-3.4%. This particular centerline location is 0.5 cm beyond the downstream surface of the metal liner on the concrete block assembly holding the rotary shutter.) There remained, however, vague but persistent recollections that measured dose rates during past maintenance operations were actually much higher, but the origin of the radiation was not known. (Results of measurements during the Spring 1998 outage are described below, in Sect 7.5). It was assumed that these higher dose rates were due to activation, but no calculations had been performed to assess those effects. The calculations described here in Sect 7 do address those effects. Moreover, it has subsequently been found that activation of the shutter itself is responsible for virtually all of the radiation dose at this location.

Once it is established that activation is responsible for virtually all of the dose at this location (as has now been done), then the calculations in this section become irrelevant from a programmatic viewpoint. That is to say: The amount of activation experienced by the collimator and rotary shutter with the new 1998 water tube in place will be no greater and no less than that experienced with the existing 1960 water tube design. The amount of activation depends only on the number of neutrons entering these components (over their lifetime and recent past) under normal conditions -- i.e., when the water tube and collimator sections are both dry, the shutter is open, and the HFIR is operating at 100 MW. As such, this does not depend on which water tube design is in use. Nevertheless, these calculations were still necessary and important in order to establish that this was, in fact, the case. (Had this not been the case, it would have implied a serious error in the previous analyses, and the acceptability of the 1998 water tube design might still be in question.) In that sense, the calculations described below, and their results, form an important part of the historical record.

The calculations described here focus exclusively on the activation of the carbon steel rotary shutter shield plug and the downstream dose rates resulting from that activation. This was sufficient for the present purpose.

Virtually all of the steel and aluminum components shown in Figs. 3.10 and 3.12 will be come activated to some degree. Around the collimator this includes: the radial and eccentric (stainless steel) shields, the various stainless steel pools seals, the various stainless steel liners, and the central collimator itself, which is made of carbon steel. Likewise, the stainless steel liners in and around the concrete block assembly holding the rotary shutter, and the stainless steel liner on the inner surface of the biological shield around the shutter assembly housing, will also become activated, especially those surfaces on the back (upstream) side of the concrete block assembly. Lastly, and most importantly, the Type 1020 carbon steel rotary shutter will also become highly activated after years of exposure. Outside the shield configuration of concern here, the steel face of the monochrometer drum (which normally abuts the shield configuration shown here) will also become activated. The two primary components, however, are the carbon steel collimator and the Type 1020 carbon steel rotary shutter, since they are the two components that are normally immediately adjacent to the neutron beam during regular operation when the beam tube is dry and the shutter is in the open position. Since the intensity of the neutron beam (and the radial leakage associated with its natural divergence) does not change dramatically over the length of the collimator or the beam hole in the shutter, these two components will become almost equally activated (to within a factor of 2 or so) on a "per unit length" basis, although the leading (upstream) edge on the collimator that directly faces the broader neutron beam will obviously become much more activated. Because of the length of the collimator, however, it will provide significant self-shielding against the activation gammas coming from the leading edge. Moreover, when the rotary shutter is in the closed position, it will provide significant shielding against all activation gammas coming from the collimator as well as activation gammas coming from all other components further upstream. The main problem will be activation gammas coming from the shutter itself, specifically from regions within the first few centimeters of the large beam hole. Because the inner surface of the beam hole is in immediate (albeit tangential) contact with the neutron beam, it will become highly activated. Unfortunately, even when the shutter is in the closed position and the axis of its beam hole is turned 66.75 degrees with respect to the beam tube axis as shown in Fig. 3.12, the one end of the shutter beam hole is never far away from the external surface of the shield configuration, and the amount of steel available for self-attenuation between the internal surface of the beam hole and the outside world is minimal. (If the shutter only had one beam hole such that it could be turned 90 degrees when closed, this situation could definitely be improved. Unfortunately, with the present design, one is simply "stuck" with this minor problem for which there is no real fix.) Thus, it was prejudged that the rotary shutter itself was likely the biggest contributing factor to the activation dose downstream of the shield configuration (at least when the monochrometer drum is pulled back far enough so as not to be a big factor). For that reason, this study focused exclusively on the activation of the rotary shutter shield plug and the downstream dose rate resulting from that activation. If it could be established (as it now has been) that activation of this component alone was responsible for all or most of the dose measured during maintenance operations, then there would be no impediment to accepting the well-founded conclusion from the previous section that the transmitted component of the dose rate would be negligible (or at least less than 1 mrem/hr) with the 1998 water tube and collimator sections

flooded, the shutter closed, and the HFIR operating at 100 MW, and that, under those conditions, the total dose rate (including activation) should be essentially the same as with the existing 1960 design.

This study involves three or four key steps: (1) identification of the key radioactive nuclides responsible for the activation dose, and the (twelve) nuclear reaction processes by which these are created; (2) running a 3-D MCNP neutron-only beam tube analysis to determine all of the necessary reaction rates in each of 39 1-cm-thick cylindrical shells around rotary shutter beam hole under normal conditions with the shutter open; (3) performing a detailed activation analysis for each of these 39 regions so as to determine the concentration levels after 30 years of exposure and at various times (0-60 days) after a subsequent shutdown; and (4) putting the resulting gamma source terms for each region back into the 3-D MCNP model, rotating the shutter to the closed position with the sources in place, and performing the attendant 3-D gamma shielding analysis. Each aspect of this analysis will be briefly described in the following sections. Comparisons with the most recently measured values will then be made. Lastly, results from a few scoping studies will be presented in which the merits of using a low-activation steel in the forthcoming design are discussed. For completeness, additional supplementary details may found in each of several related appendices:

E.1: Details of MCNP Run HB309, used to calculate all the necessary reaction rates.
E.2: A listing of the ad hoc activation program (ACTSRC.FOR) described above.
E.3: A listing of a utility program (SI.FOR) needed to create the necessary MCNP source-term probability distributions from the information obtained by ACTSRC.FOR.
E.4: Details of MCNP Run HB310, used to calculate the resulting dose rates.

7.1 Key Radioactive Nuclides and Nuclear Reaction Processes By Which They Are Formed

The rotary shutter shield plug is made of Type 1020 carbon steel. As such, it is mostly iron, but also contains a small specified amount of manganese as an alloying agent, and likely contains small unspecified trace amounts of cobalt by default. Figure 7.1 shows how naturally occurring isotopes of these elements can serve as precursors to the production of four key radioactive nuclides: Fe-59, Co-60, Mn-56, and Mn-54. [The data shown in Fig. 7.1 was taken primarily from General Electric's Chart of the Nuclides#29, with supplemental data from the ICRP Table of Isotopes#30.]

Because the Fe-59 emits energetic gammas (average E=1.19 MeV), has a 44.51 day halflife, and is always present after any significant exposure to neutron radiation, its effect on activation dose rates is usually important for weeks and months after shutdown, during which time maintenance operations are most likely to be performed. It also serves as a precursor to Co-59 production, and therefore to Co-60 production. Small, frequently undocumented, trace amounts of cobalt naturally found in most iron ores are also major activation sources, as noted below.

Page 6.30 of "Marks' Standard Handbook for Mechanical Engineers" (Ref 31) indicates that Type 1020 carbon steel typically contains 0.30-0.60 wt% manganese. For the purpose of this analysis, the steel was therefore assumed to contain 0.45 wt% Mn-55, the only naturally occurring isotope. The small quantities of Mn-54, formed by (n,p) reactions in Fe-54, are minor contributors to the overall dose rate. Somewhat larger quantities of Mn-56, formed by (n,g) reactions in Mn-55, can contribute more significantly to the overall dose rate, especially in the first few hours after shutdown, but, because of its short 2.578 hour halflife, its effect is generally negligible beyond the first one or two days after shutdown.

Most steels also contain some small trace amounts of cobalt which may or may not appear in metallurgical fact sheets. Even extremely small trace quantities can be a major source of radioactivity for years after exposure. Moreover, even if the original steel is free of any cobalt (which is almost never the case), it will be generated anyway by the following sequence: Naturally occurring Fe-58 will experience (n,g) reactions and produce Fe-59 which will then beta decay (with a halflife of 44.51 days) to form Co-59, which will then experience (n,g) reactions to form the radioactive isotope, Co-60. Thus, even if there was no cobalt present initially, this process will create small amounts over time. More importantly, if there is even a small trace amount of natural cobalt (Co-59) initially present, the amount of Co-60 produced by direct (n,g) capture will generally be even more significant. In this case, no information could be found on the cobalt content of Type 1020 steel, undoubtedly because it is present in such minute quantities as to be metallurgically insignificant. Still, it is best to include it in the activation analysis if one has any reasonable basis for estimating the amount present. To that end, it was noted (cf pp. 106 of Ref 6) that the main HFIR pressure vessel initially contained 0.015 wt% Co-59. That same reference also indicated that the HB-1 and HB-4 vessel nozzles initially contained 0.005 wt% Co-59 and that the HB-2 and HB-3 vessel nozzles initially contained 0.03 wt% Co-59. On that basis, the present activation analysis assumed that the Type 1020 steel used for the rotary shutter nominally contained 0.015 wt% Co-59. The subsequent (nominal) dose rate calculations are also based on that assumption in the activation analysis. [Alternate (hypothetical) activation and dose rate calculations described in Sect 7.6 examine the possible merits of using specialty steels where the cobalt content is more tightly controlled.]

Figure 7.1 shows how these and other naturally occurring isotopes of these elements can serve as precursors to the production of four key radioactive nuclides: Fe-59, Co-60, Mn-56, and Mn-54. In particular, it

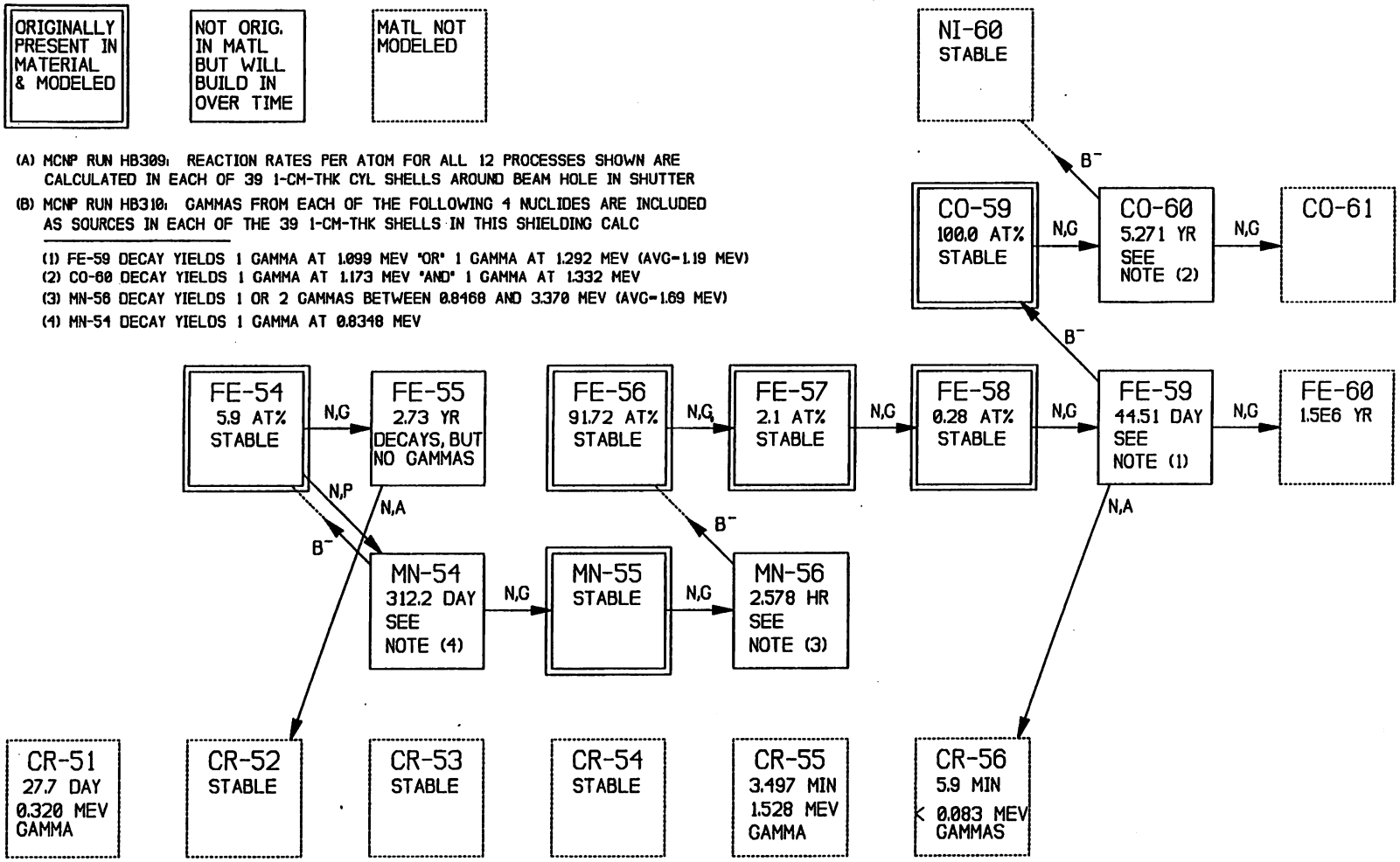


Fig. 7.1. Nuclear processes leading to the production of four key radioactive nuclides (Fe-59, Co-60, Mn-56, and Mn-54) in Type 1020 carbon steel. Identified here are 12 individual reaction rates that must be known to perform the necessary activation analysis.

shows the following 12 reaction rates to be of key importance in any activation analysis:

Fe54(n,g)Fe55, Fe54(n,p)Mn54, Fe55(n,a)Cr52, Mn54(n,g)Mn55, Mn55(n,g)Mn56,

Fe56(n,g)Fe57, Fe57(n,g)Fe58, Fe58(n,g)Fe59, Fe59(n,g)Fe60, Fe59(n,a)Cr56,

Co59(n,g)Co60, and Co60(n,g)Co61.

7.2 Determination of the Spatially-Dependent Reaction Rates Using MCNP Run HB309

While it would have been possible to perform a 3-D MCNP beam tube neutron-only analysis to determine the fast, epithermal, and thermal flux levels throughout different regions of the rotary shutter, and then have allowed ORIGEN-S#32 to fold its 1-group or 3-group cross sections with the MCNP fluxes to do the activation analyses (one region at a time for each of the 39 regions of interest), the alternate approach described below is more efficient and more accurate. Armed with preliminary knowledge of which reaction rates are important, it is both possible and convenient when running MCNP to let it fold the pointwise-energy-dependent fluxes (in each cell or tally segment of interest) directly with the pointwise-energy-dependent cross sections for these various reactions to obtain the best possible estimate of the average "reaction rate per unit atom density" for each process, in each cell or tally segment of interest. [Here, reaction rate per unit atom density = the "pointwise-energy-dependent flux (in n/s/cm2) times the pointwise-energy-dependent microscopic cross section (in barns)," integrated over all energy, and spatially averaged over a volumetric cell or tally segment of interest. It is such that when one multiplies by the atomic density of the nuclide in "atoms/(barn*cm)" the result is in "reactions/sec/cc".] The advantage of this approach, when one has a large representative neutron population from which to sample, is that it does not depend on some previously calculated "group-averaged" cross section data which may or may not be appropriate for the local spectrum; with this approach, all local spectral effects are accounted for directly. Moreover, with these more accurate local reaction rates in hand, it is then a simple matter to write a small activation program that can, in a single run, do all the activation analyses for all 39 regions of interest, and list the resulting decay gamma source terms for each of the 39 regions at any decay time desired.

The role of MCNP Run HB309 was to determine these 12 nuclear reaction rates under nominal conditions, in (the steel portion of) each of the 39 1-cm-thick cylindrical shells concentrically centered around the 3.5-inch-diam beam hole in the rotary shutter, when the water tube and collimator sections are both void, the shutter is open, and the HFIR is operating at 100 MW.

Appendix E.1 shows the modifications needed to convert the input file for MCNP Run HB308G (listed in Appendix D.4) to the form needed for this neutron-only analysis in Run HB309. To summarize very briefly, it should be noted that Run HB309 is a neutron-only analysis with 20 million histories. The source includes all 61 VELM neutron groups for the HB-3 beam tube as specified in Table 2.2a. This represents a total of 9.64595e+16 n/s. All neutrons were started within a narrow cone of 15.13 degrees about the centerline, and the starting weights were adjusted accordingly, as shown in item 3 of Appendix E.1 (ie, only starting direction cosines between 0.965335056 and 1.0 were sampled, and all source particles had starting weights of 0.017332472 since source energy biasing was not used). All neutrons were tracked, including thermal neutrons, until they leaked from the system, were absorbed, or killed by Russian Roulette (ie, no energy cutoffs were used). From a material viewpoint, the geometry was identical to that shown in Fig. 3.2, with the water tube and collimator sections both void and the shutter's 3.5-inch-diam beam hole in the open position. Because the water tube and collimator sections were void, no weight windows or other fancy biasing techniques were needed. Moreover, since the primary interest was in neutron reactions in portions of the carbon steel rotary shutter close to the large beam hole, it was possible to obtain good statistics by simply running a large number of histories (20 million) in this narrow cone of starting directions. [In Run HB309, the 20 million neutrons that were started subsequently experienced a total of 550.8 million collisions, and the calculation only required about 7 hours of CPU time on each of 8 nodes on the ORNL SP2 computer.]

To obtain the desired information, several other minor additions were required. As shown in item 7 of Appendix E.1, a number of new dummy materials (m71 through m82) were added. Each represents a single nuclide from the list in Sect 7.1, and each was assigned a number density of 1.0 atoms/(barn*cm). These are only used in various tallies to obtain the desired reaction rates "per unit number density" in each region of the rotary shutter. To obtain information for different regions of the steel comprising the rotary shutter (Cell 3090), a number of auxiliary surfaces (Surf 5171 through 5208) had to be introduced, as described in item 6 of Appendix E.1. These were used in the tally specifications to segment the shutter into the 39 cylindrical shells described above. Note that no new cells were actually introduced; these surfaces are only used in the segmented volume tallies described in item 8 of Appendix E.1.

Lastly, because the large 3.5-inch-diam beam hole has a horizontal axis while the 24.375-inch-diam rotary shutter has a vertical axis, and because the rotary shutter is also penetrated by a small 0.875-inch-diam horizontal beam hole whose axis is inclined 46.5 degrees with respect to the large beam hole, the actual volume of steel in each of these 39 "cylindrical shells" around the large beam hole is somewhat irregular

and had to be computed manually (offline) in advance of Run HB309. Moreover, the actual volume of steel in each of these 39 segments also had to be entered manually on the tally specification cards so that the volume-averaged fluxes and reaction rates as subsequently calculated by Run HB309 would be correct. While different methods may be used to calculate such irregular volumes, a standard stochastic method was used in this case. Here the volume of steel in each of the 36 innermost segments was converged to within 0.03% (typically), while the 3 outermost segments were converged to within 0.12%, 0.17%, and 0.3% respectively. The resulting segment volumes are shown in Table 7.1. Note that because the outermost shells just "clip the outside corners" of the steel shutter, their volumes are very small.

Based on Run HB309, Table 7.1 shows the volume-averaged estimates of the total, fast, intermediate, and thermal neutron fluxes in (the steel portion of) each segment of the rotary shutter under nominal conditions where the water tube and collimator sections were both void, the shutter was wide open, and the HFIR was at 100 MW. Note that the total, fast, and intermediate neutron fluxes are generally converged to within about 3% for most of the shutter segments, and always to within 10 or 11%, except for the outermost three or four segments where the volumes are rapidly becoming smaller, the fluxes are down by two orders of magnitude, and any resulting activation is minimal. Unlike the fast fluxes which vary slowly by position, the thermal fluxes responsible for most activation vary much more rapidly as one moves back away from the central beam hole, falling off by:

1 order of magnitude from R=5 cm to R=10 cm (where the fsd's are under 2%),
2 orders of magnitude from R=5 cm to R=14 cm (where the fsd's are under 4%),
3 orders of magnitude from R=5 cm to R=22 cm (where the fsd's are under 9%).

By the time the fractional standard deviations (fsd's) exceed 15%, the fluxes are even smaller and the volume of steel in successive segments is also getting smaller and smaller (because the shutter has a vertical axis while these concentric shells around the beam hole have a horizontal axis). Thus, as shown in Appendix E.1, most of the key activation rates are known to within a few percent.

Lastly, Table 7.2 shows each of the 12 key reaction rates (per unit atom density) in each of the 39 segments of the rotary shutter under nominal conditions. To be more specific, this table gives the "reactions/sec/cc" that would exist in the steel portion of each 1-cm-thick cylindrical shell segment of the shutter (going out from the 3.5-inch-diam beam hole) if the density of the given nuclide were 1.0 atoms/(barn*cm). These multiregion reaction rates are then used directly in the multiregion activation analysis described in Sect 7.3 and/or Appendix E.2. More detailed results showing the fractional standard deviations associated with each reaction rate (in each of the 39 segments) are given in Appendix E.1. Also note that the most important segments for activation purposes are the first few closest to the beam hole, where the flux has not been attenuated much.

7.3 Activation Program Used to Determine the Gamma Source Terms 7 Days After Shutdown

Appendix E.2 lists the small ad hoc activation program (ACTSRC.FOR) used to obtain the decay gamma source terms due to activation in (the steel portion of) each of the 39 1-cm-thick cylindrical shells concentrically centered around the 3.5-inch-diam beam hole through the HB-3 rotary shutter, while Table 7.3 summarizes the buildup/depletion equations used during the irradiation period, as illustrated in Fig. 7.1. Note that the same equations are used after shutdown; the only difference is that, then, all the reaction rates (the "x" data in Table 7.3) are set to zero, and smaller time steps are used. Since the program is short and heavily annotated, descriptive comments here will be held to a minimum. Nevertheless, a few comments are in order:

1) The nuclear reaction rate data for each of the 12 processes in each of the 39 shells comprising the shutter was based on MCNP Run HB309, as described above and listed in Table 7.2. That data is built into the program in the form of data statements. Near the top of the program, all those reaction rates are multiplied once by a constant factor of "1.0e-24 cm2/barn" so that all nuclide number densities used in the buildup and depletion equations throughout the program can then be in units of atoms/cc.

2) Time steps of 7 days (6.048e+5 seconds) are generally used throughout the assumed 30 year irradiation period, while time steps of 1 day (8.64e+4 seconds) are generally used for the subsequent decay period, 0 to 60 days after shutdown. The only exceptions are for the equations involving Mn-55 and Mn-56. Because of the much shorter halflife of Mn-56 (9281 sec), time steps of 3024 seconds were used for these two nuclides during the 30-year irradiation period, and time steps of 2880 seconds were used for these two nuclides during the 60-day decay period. While decay gamma source terms from each of the four primary radioactive nuclides are tabulated on a daily basis throughout this 60-day decay period after shutdown, only those at 7 days after shutdown were subsequently used in the MCNP gamma shielding analysis (Run HB310).

Table 7.1. Broad-group neutron fluxes (n/s/cm2) in each segment of the rotary shutter under nominal conditions, and the actual volume(*) of each of the 39 1-cm-thick cylindrical segments going outward from the 3.5-inch beam hole. These results are based on Run HB309 where the water tube and collimator sections were both void, the shutter was wide open, and the HFIR was at 100 MW.

Segment Number	Dist(cm) from centerline of big beam hole		Rot.Shutter Cell 3090 Segment Vol	Thermal Flux below 0.414 eV		Intermediate Flux 0.414 eV to 0.1 MeV		Fast Neutron Flux above 0.1 MeV		Total Neutron Flux (All Energies)	
seg	rmin	rmax	volume (cc)	N-Flux	fsd	N-Flux	fsd	N-Flux	fsd	N-Flux	fsd
1	4.445	5.445	1.89858E+03	2.74732E+09	.0088	2.02708E+09	.0167	7.73721E+08	.0259	5.54812E+09	.0084
2	5.445	6.445	2.27981E+03	1.84566E+09	.0084	1.66341E+09	.0163	5.90820E+08	.0259	4.09989E+09	.0086
3	6.445	7.445	2.65511E+03	1.36593E+09	.0089	1.42750E+09	.0162	5.11630E+08	.0247	3.30506E+09	.0090
4	7.445	8.445	3.02744E+03	6.96965E+08	.0108	1.05363E+09	.0174	3.67896E+08	.0271	2.11850E+09	.0107
5	8.445	9.445	3.39342E+03	3.37267E+08	.0133	8.08969E+08	.0188	2.60845E+08	.0272	1.40708E+09	.0126
6	9.445	10.445	3.75537E+03	1.90977E+08	.0163	6.74424E+08	.0197	2.19476E+08	.0275	1.08488E+09	.0141
7	10.445	11.445	4.11116E+03	1.10171E+08	.0197	5.60476E+08	.0205	1.90583E+08	.0282	8.61231E+08	.0154
8	11.445	12.445	4.45690E+03	6.72172E+07	.0238	4.76992E+08	.0213	1.66833E+08	.0287	7.11041E+08	.0165
9	12.445	13.445	4.79709E+03	4.03766E+07	.0290	4.02304E+08	.0223	1.48498E+08	.0297	5.91178E+08	.0177
10	13.445	14.445	5.12661E+03	2.62801E+07	.0348	3.49902E+08	.0230	1.30761E+08	.0304	5.06943E+08	.0186
11	14.445	15.445	5.44592E+03	1.81081E+07	.0405	3.05466E+08	.0241	1.19669E+08	.0313	4.43243E+08	.0195
12	15.445	16.445	5.75543E+03	1.22659E+07	.0457	2.65727E+08	.0252	1.05416E+08	.0315	3.83409E+08	.0204
13	16.445	17.445	6.05497E+03	9.25039E+06	.0544	2.35619E+08	.0261	9.65105E+07	.0323	3.41380E+08	.0211
14	17.445	18.445	6.33840E+03	6.90746E+06	.0612	2.08903E+08	.0267	8.79522E+07	.0327	3.03762E+08	.0215
15	18.445	19.445	6.60982E+03	5.33066E+06	.0682	1.82957E+08	.0281	7.82697E+07	.0335	2.66558E+08	.0225
16	19.445	20.445	6.86725E+03	4.35552E+06	.0718	1.63203E+08	.0292	7.13853E+07	.0348	2.38944E+08	.0236
17	20.445	21.445	7.10540E+03	3.50262E+06	.0815	1.45159E+08	.0299	6.48972E+07	.0355	2.13559E+08	.0241
18	21.445	22.445	7.32554E+03	2.71110E+06	.0869	1.32135E+08	.0313	6.13374E+07	.0361	1.96184E+08	.0250
19	22.445	23.445	7.53004E+03	2.31448E+06	.0946	1.18128E+08	.0316	5.43873E+07	.0375	1.74829E+08	.0256
20	23.445	24.445	7.70707E+03	2.15837E+06	.1055	1.06460E+08	.0327	4.84026E+07	.0391	1.57021E+08	.0265
21	24.445	25.445	7.85115E+03	1.97678E+06	.1022	9.47021E+07	.0337	4.57820E+07	.0394	1.42461E+08	.0272
22	25.445	26.445	7.96738E+03	1.63389E+06	.1014	8.52979E+07	.0344	4.08429E+07	.0400	1.27775E+08	.0275
23	26.445	27.445	8.04809E+03	1.38260E+06	.1114	7.89053E+07	.0362	3.83933E+07	.0418	1.18681E+08	.0290
24	27.445	28.445	8.08235E+03	1.44871E+06	.1105	7.24254E+07	.0367	3.30346E+07	.0429	1.06909E+08	.0299
25	28.445	29.445	8.05935E+03	1.41795E+06	.1202	6.51446E+07	.0384	3.08990E+07	.0452	9.74616E+07	.0313
26	29.445	30.445	7.95535E+03	1.22925E+06	.1200	6.18837E+07	.0390	2.74878E+07	.0462	9.06007E+07	.0319
27	30.445	31.445	6.44147E+03	1.13551E+06	.1436	5.78272E+07	.0438	2.49149E+07	.0500	8.38777E+07	.0355
28	31.445	32.445	4.99352E+03	6.93888E+05	.2174	5.26223E+07	.0516	2.38801E+07	.0589	7.71962E+07	.0412
29	32.445	33.445	4.08671E+03	4.54804E+05	.2911	4.75744E+07	.0568	2.19426E+07	.0671	6.99718E+07	.0462
30	33.445	34.445	3.36986E+03	3.69736E+05	.3667	4.22995E+07	.0648	1.88337E+07	.0824	6.15029E+07	.0536
31	34.445	35.445	2.76096E+03	1.26607E+05	.4321	3.80259E+07	.0725	1.69396E+07	.0870	5.50922E+07	.0583
32	35.445	36.445	2.23160E+03	3.85593E+04	.5617	3.51092E+07	.0837	1.65887E+07	.1004	5.17364E+07	.0667
33	36.445	37.445	1.76511E+03	1.04516E+05	.8487	3.16187E+07	.0978	1.39530E+07	.1120	4.56763E+07	.0784
34	37.445	38.445	1.35264E+03	3.01327E+04	.9999	2.50538E+07	.0997	1.15256E+07	.1304	3.66095E+07	.0841
35	38.445	39.445	9.88281E+02	5.47862E+04	.9999	2.44744E+07	.1160	1.16599E+07	.1615	3.61891E+07	.0987
36	39.445	40.445	6.71165E+02	2.42782E+04	.9999	2.20308E+07	.1412	1.23392E+07	.1804	3.43942E+07	.1139
37	40.445	41.445	4.01009E+02	0.00000E+00	.0000	2.09847E+07	.1754	7.56120E+06	.2365	2.85459E+07	.1454
38	41.445	42.445	1.86544E+02	0.00000E+00	.0000	1.97000E+07	.2063	7.22905E+06	.3785	2.69290E+07	.1837
39	42.445	43.4433	3.97575E+01	0.00000E+00	.0000	9.80637E+06	.4708	1.15976E+07	.5075	2.14040E+07	.3495

(*) Because the large 3.5-inch-diam beam hole has a horizontal axis while the 24.375-inch-diam rotary shutter has a vertical axis, and because the rotary shutter is also penetrated by a small 0.875-inch-diam horizontal beam hole whose axis is inclined 46.5 degrees with respect to the large beam hole, the actual volume of steel in each of these 39 "cylindrical shells" around the large beam hole had to be computed a priori (offline) and supplied to MCNP manually so that the volume-averaged fluxes and reaction rates calculated by MCNP for each of these 39 steel segments would be correct. Because the outermost shells just "clip the outside corners" of the steel shutter, their volumes are very small.

Table 7.2. Key reaction rates (per unit atom density) in each segment of the rotary shutter under nominal conditions. This table gives the "reactions/sec/cc" that would exist in the steel portion of each 1-cm-thick cylindrical shell segment of the shutter (going out from the 3.5-inch beam hole) if the density of the nuclide was 1.0 atoms/(barn*cm). Based on Run HB309 where the water tube and collimator sections were both void, the shutter was wide open, and the HFIR was at 100 MW.

Seg.	Fe54(n,g)	Fe54(n,p)	Fe55(n,a)	Mn54(n,g)	Mn55(n,g)	Fe56(n,g)	Fe57(n,g)	Fe58(n,g)	Fe59(n,g)	Fe59(n,a)	Co59(n,g)	Co60(n,g)
1	5.99198e+09	1.20292e+07	2.02828e+05	1.26622e+10	1.84169e+10	3.36721e+09	3.19633e+09	1.57216e+09	2.14995e+09	3.32113e+03	5.78845e+10	3.16042e+09
2	4.14389e+09	6.67175e+06	1.35130e+05	8.62084e+09	1.25220e+10	2.25370e+09	2.14003e+09	1.14615e+09	1.44126e+09	1.34551e+03	4.06547e+10	2.20321e+09
3	3.13285e+09	5.25048e+06	1.22644e+05	6.51046e+09	9.38180e+09	1.67026e+09	1.58950e+09	8.48714e+08	1.07228e+09	2.51155e+03	3.06994e+10	1.69199e+09
4	1.72564e+09	2.58757e+06	5.63003e+04	3.56730e+09	5.16367e+09	8.73702e+08	8.45299e+08	4.32341e+08	5.62506e+08	3.30643e+02	1.76769e+10	9.72573e+08
5	9.50033e+08	1.10414e+06	7.41870e+03	1.96939e+09	2.77038e+09	4.41938e+08	4.33831e+08	2.31799e+08	2.86986e+08	1.71738e+00	1.04784e+10	5.77529e+08
6	6.12330e+08	8.03867e+05	4.30735e+03	1.30528e+09	1.82913e+09	2.69553e+08	2.63626e+08	1.50153e+08	1.74651e+08	0.00000e+00	7.29654e+09	4.08203e+08
7	4.13005e+08	6.54756e+05	1.09205e+03	9.02419e+08	1.23859e+09	1.68245e+08	1.69071e+08	8.94690e+07	1.10666e+08	0.00000e+00	5.34792e+09	2.97571e+08
8	2.95404e+08	4.41701e+05	5.56648e+02	6.61735e+08	8.55010e+08	1.15170e+08	1.16809e+08	6.46687e+07	7.44673e+07	0.00000e+00	4.09892e+09	2.27118e+08
9	2.08192e+08	3.78326e+05	2.73019e+02	4.94689e+08	6.40729e+08	7.62715e+07	7.88794e+07	5.18197e+07	5.04288e+07	0.00000e+00	3.11880e+09	1.79749e+08
10	1.58984e+08	2.53326e+05	1.62800e+02	3.86573e+08	5.04035e+08	5.46814e+07	5.81192e+07	3.51538e+07	3.64339e+07	0.00000e+00	2.74753e+09	1.45030e+08
11	1.27956e+08	2.03298e+05	1.51162e+02	3.14478e+08	3.92140e+08	4.23195e+07	4.55823e+07	2.67623e+07	2.78752e+07	0.00000e+00	2.22914e+09	1.22003e+08
12	1.04389e+08	1.62342e+05	5.13810e+01	2.59155e+08	3.35307e+08	3.23935e+07	3.51442e+07	3.00751e+07	2.18257e+07	0.00000e+00	1.70038e+09	1.01511e+08
13	8.83181e+07	9.57636e+04	8.32803e-01	2.16017e+08	2.73264e+08	2.76522e+07	2.91652e+07	3.66566e+07	1.78110e+07	0.00000e+00	1.43644e+09	8.67970e+07
14	7.62692e+07	7.33266e+04	0.00000e+00	1.84598e+08	2.27944e+08	2.20551e+07	2.46814e+07	2.40311e+07	1.49781e+07	0.00000e+00	1.15434e+09	7.54545e+07
15	6.45517e+07	8.56045e+04	0.00000e+00	1.55570e+08	1.92078e+08	1.76561e+07	2.06657e+07	1.43074e+07	1.23244e+07	0.00000e+00	1.03716e+09	6.46226e+07
16	5.46605e+07	5.96741e+04	0.00000e+00	1.34916e+08	1.72462e+08	1.46348e+07	1.77527e+07	1.27613e+07	1.05036e+07	0.00000e+00	8.20952e+08	5.65885e+07
17	4.79391e+07	4.36338e+04	0.00000e+00	1.16707e+08	1.58814e+08	1.27331e+07	1.46638e+07	2.23069e+07	8.87970e+06	0.00000e+00	7.84838e+08	4.90034e+07
18	4.19608e+07	3.66938e+04	0.00000e+00	1.04449e+08	1.38011e+08	1.07375e+07	1.31289e+07	1.09186e+07	7.65916e+06	0.00000e+00	6.02624e+08	4.47282e+07
19	3.36966e+07	3.31433e+04	0.00000e+00	9.18358e+07	1.10222e+08	9.74353e+06	1.16829e+07	6.67290e+06	6.63824e+06	0.00000e+00	5.61004e+08	3.87558e+07
20	2.94455e+07	2.71341e+04	0.00000e+00	8.01191e+07	9.73559e+07	9.28538e+06	1.13470e+07	1.23014e+07	5.85553e+06	0.00000e+00	5.46825e+08	3.40701e+07
21	2.71815e+07	1.70733e+04	0.00000e+00	7.10371e+07	8.52599e+07	8.09216e+06	1.08416e+07	5.22684e+06	5.42374e+06	0.00000e+00	4.63993e+08	3.05252e+07
22	2.36507e+07	1.25406e+04	0.00000e+00	6.24565e+07	7.89212e+07	6.72191e+06	8.76487e+06	5.80662e+06	4.71597e+06	0.00000e+00	3.46108e+08	2.70076e+07
23	2.09731e+07	1.37422e+04	0.00000e+00	5.80331e+07	7.39348e+07	5.83975e+06	7.26148e+06	6.27061e+06	4.13551e+06	0.00000e+00	4.29789e+08	2.48438e+07
24	1.87989e+07	6.98949e+03	0.00000e+00	5.33454e+07	6.10265e+07	5.30684e+06	6.93971e+06	6.00283e+06	3.84405e+06	0.00000e+00	3.42289e+08	2.26819e+07
25	1.86951e+07	6.42573e+03	0.00000e+00	4.80855e+07	6.61182e+07	4.89180e+06	6.17780e+06	5.91870e+06	3.52275e+06	0.00000e+00	2.56266e+08	2.15119e+07
26	1.58571e+07	9.50111e+03	0.00000e+00	4.57404e+07	5.89068e+07	4.45160e+06	5.27628e+06	4.47121e+06	3.19568e+06	0.00000e+00	2.45520e+08	2.10725e+07
27	1.38394e+07	2.73547e+03	0.00000e+00	4.29561e+07	5.39730e+07	3.90635e+06	4.86002e+06	2.85362e+06	2.88050e+06	0.00000e+00	2.86070e+08	2.05226e+07
28	1.19015e+07	1.59773e+03	0.00000e+00	3.69811e+07	3.89956e+07	3.36825e+06	5.20521e+06	1.96904e+06	2.25836e+06	0.00000e+00	2.64852e+08	1.67992e+07
29	9.08576e+06	6.43392e+02	0.00000e+00	3.02216e+07	3.61343e+07	2.54684e+06	5.25065e+06	2.53224e+06	1.89263e+06	0.00000e+00	1.72396e+08	1.38844e+07
30	8.42691e+06	1.59097e+02	0.00000e+00	2.74636e+07	2.99655e+07	1.98251e+06	3.97629e+06	4.48026e+06	1.52881e+06	0.00000e+00	1.17480e+08	1.38453e+07
31	5.61515e+06	1.51799e+02	0.00000e+00	2.49245e+07	3.16423e+07	2.16223e+06	2.23946e+06	1.98723e+06	1.09491e+06	0.00000e+00	1.87061e+08	1.34534e+07
32	5.37685e+06	1.80963e+02	0.00000e+00	2.55141e+07	2.99357e+07	1.60233e+06	3.02018e+06	1.74243e+06	1.03533e+06	0.00000e+00	2.08958e+08	1.26163e+07
33	5.13309e+06	2.74708e+02	0.00000e+00	2.15737e+07	1.87112e+07	1.60190e+06	3.40241e+06	7.31046e+05	1.02367e+06	0.00000e+00	2.95190e+08	1.00471e+07
34	4.02939e+06	3.34009e+02	0.00000e+00	1.41898e+07	1.51089e+07	2.55469e+06	1.84750e+06	5.80676e+06	7.86281e+05	0.00000e+00	1.55585e+08	6.81065e+06
35	4.37901e+06	6.53157e+01	0.00000e+00	1.35236e+07	1.29813e+07	1.23464e+06	2.21092e+06	6.43253e+05	9.12764e+05	0.00000e+00	3.65217e+08	5.00097e+06
36	3.45857e+06	2.51263e+01	0.00000e+00	1.13716e+07	9.25437e+06	8.49530e+05	2.70400e+06	4.54047e+05	7.76966e+05	0.00000e+00	1.77113e+08	5.05343e+06
37	2.60602e+06	7.91661e+00	0.00000e+00	7.43682e+06	4.44866e+06	5.14348e+05	3.18876e+06	3.32985e+05	4.84942e+05	0.00000e+00	1.06684e+07	4.13671e+06
38	1.78521e+06	1.51097e-01	0.00000e+00	5.15752e+06	2.29941e+06	2.57386e+05	3.15490e+06	1.66274e+05	2.77516e+05	0.00000e+00	5.70826e+06	3.52430e+06
39	3.94089e+05	2.08653e-01	0.00000e+00	1.19179e+06	2.80385e+05	3.11991e+04	1.33737e+06	5.19141e+04	9.67132e+04	0.00000e+00	1.72262e+06	1.43811e+06

Note: More detailed results showing the fractional standard deviations associated with each reaction rate (in each of the 39 segments) are given in Appendix E.1. Also note that the most important segments for activation purposes are the first few closest to the beam hole, where the flux has not been attenuated much.

Table 7.3. Buildup/depletion equations used during irradiation. Note that the same equations are used after shutdown, except that then all the reaction rates ("x" data) are set to zero.

```
      dt=7.0d0            ! delta-t = 1 week = 7 days
      dt=dt*8.64d4        ! delta-t in seconds
c
      tburn=30.0d0        ! tburn= 30 years (appx)
      tburn=tburn*52.0d0  ! tburn in weeks
      tburn=tburn*7.0d0   ! tburn in days
      tburn=tburn*8.64d4  ! tburn in seconds
c
      nburn=nint(tburn/dt) ! irradiate for this many timesteps
c
c     From here on, all densities will be in "atoms/cc" and all times will be in "sec"
c
      dcf59=1.80241d-7  ! decay constant ("per sec") for Fe-59  (T-half=44.51 days)
      dcc60=4.16705d-9  ! decay constant ("per sec") for Co-60  (T-half=5.271 years)
      dcm56=7.46861d-5  ! decay constant ("per sec") for Mn-56  (T-half=2.578 hours)
      dcm54=2.56968d-8  ! decay constant ("per sec") for Mn-54  (T-half=312.2 days)
c
      do i=1,nburn
      iyr=i/52
      iwk=i-52*iyr
c     ------------------------------------------------------------------------
      delm54=  afe54*xf54np - amn54*xm54ng - dcm54*amn54
c
      nmicro=200
      dtsm=dt/dfloat(nmicro)  ! small timestep required for these 2 nuclides
      do j=1,nmicro           ! because of the small half-life of Mn-56
         delm55= amn54*xm54ng - amn55*xm55ng
         delm56= amn55*xm55ng - dcm56*amn56
         amn55=amn55+delm55*dtsm
         amn56=amn56+delm56*dtsm
      enddo
c
      delf54= -afe54*xf54np - afe54*xf54ng
      delf55=  afe54*xf54ng - afe55*xf55na
      delf56= -afe56*xf56ng
      delf57=  afe56*xf56ng - afe57*xf57ng
      delf58=  afe57*xf57ng - afe58*xf58ng
      delf59=  afe58*xf58ng - afe59*xf59ng - afe59*xf59na -dcf59*afe59
c
      delc59=  dcf59*afe59  - aco59*xc59ng
      delc60=  aco59*xc59ng - aco60*xc60ng - dcc60*aco60
c     ------------------------------------------------------------------------
      amn54=amn54+delm54*dt
c
c     amn55=amn55+delm55*dt  ! now done inside short-time loop above instead
c     amn56=amn56+delm56*dt  ! now done inside short-time loop above instead
c
      afe54=afe54+delf54*dt
      afe55=afe55+delf55*dt
      afe56=afe56+delf56*dt
      afe57=afe57+delf57*dt
      afe58=afe58+delf58*dt
      afe59=afe59+delf59*dt
c
      aco59=aco59+delc59*dt
      aco60=aco60+delc60*dt
c     ------------------------------------------------------------------------
      enddo
c
```

Note: Nuclid ID's prefaced by "a" (such as afe54) denote the "amount" in atoms/cc, while ID's prefaced by "del" mean the "change in the amount per second" during the given time step.

3) Two key assumptions are that the Type 1020 carbon steel rotary shutter initially contained:

0.45 wt% Mn-55 (Type 1020 carbon steel typically contains 0.30-0.60 wt% Mn-55; see pp 6.30 of Ref 31)

0.015 wt% Co-59 (HFIR vessel has this amount [see pp 106 of Ref 6], while the HB-1 and HB-4 nozzles have 0.005 wt%, and the HB-2 and HB-3 nozzles have 0.03 wt%)

4) The four primary radioactive nuclides are:

Mn-54, where each decay produces 1 gamma at 0.8348 MeV;

Mn-56, where each decay produces 1 or 2 gammas between 0.8468 MeV and 3.370 MeV, with an "average" energy per decay of 1.69 MeV. Note that Mn-56 is basically gone after 2-4 days.

Fe-59, where each decay produces 1 gamma at 1.099 MeV "OR" 1 gamma at 1.292 MeV, plus some low-energy gammas, such that the "average" energy per decay is 1.19 MeV.

Co-60, where each decay produces 1 gamma at 1.173 MeV "AND" 1 gamma at 1.332 MeV. Note that Co-60 always yields 2 gammas per disintegration#30.

The decay rates for each nuclide are accurately calculated and tabulated by this activation program. To simplify the description of the decay gamma sources in the subsequent MCNP shielding analysis, however, it is convenient to tabulate an "equivalent" gamma source at a single energy (1.25 MeV) based on the decay rates of these four radioactive nuclides and the respective gamma energies. If "del" denotes the decay rate (atoms/s/cc) for each nuclide at the decay time of interest (typically 7 days after shutdown), then the "equivalent gamma source" may be written as:

Equivalent Gamma Source (p/s/cc) at 1.25 MeV =

(delc60*1.173 + delc60*1.332 + delf59*1.19 + delm54*0.8348 + delm56*1.69) / 1.25

Since all the key decay energies are clustered about 1.25 MeV anyway, with the Co-60 and Fe-59 nuclides being the predominant ones by far, this convenient approximation should be wholly adequate.

Table 7.4 shows a typical set of results for the first 1-cm-thick cylindrical shell of the rotary shutter adjacent to the 3.5-inch-diam beam hole (ie, that portion of the steel from r=4.445 cm to r=5.445 cm). The first section of the table shows the concentrations (atoms/cc) of the various nuclides shown in Fig. 7.1 during the 30-year irradiation period. Note that some nuclides like Fe-59 and Mn-56 reach saturation long before the end of the first year, while others like Mn-54 take 3 to 8 years to reach saturation, and others like Co-60 (a strong gamma emitter) and Fe-55 (a non-gamma emitter) continue to build in over the entire 30-year period. The second section of the table shows the concentrations of these same nuclides over the first 60 days following a subsequent shutdown. While the radioactive Mn-56 is essentially gone after 2 to 4 days, the radioactive Fe-59 with its 44.51-day halflife, the radioactive Mn-54 with its 312.2 day halflife, and the Co-60 with its 5.271-year halflife diminish much more slowly. The third section of the table is undoubtedly more useful since it shows the disintegration rate for each of these four nuclides as a function of time over the first 60 days after shutdown, as well as the equivalent gamma source at 1.25 MeV, as described above. In terms of the disintegration rate, the Fe-59 is almost an order of magnitude more important than the Mn-54, but only about half as important as the Co-60. Moreover, given that the Co-60 yields two high-energy gammas per disintegration but that the Fe-59 only yields one of comparable energy, the radiation dose caused by the Co-60 is nearly four times more important than that caused by the Fe-59. [In this case, the amount of Co-60 present is a direct consequence of the fact that the original steel was assumed to contain 0.015 wt% Co-59. Without that initial Co-59 present, some Co-59 and Co-60 would "build in" anyway, but the amount would be far less, and the dose from Fe-59 may dominate. Cases with varying amounts of Co-59 initially present are examined in Sect 7.6.] The most interesting feature of this table is the equivalent gamma source as a function of time, as shown in the lower right-hand corner of the table. Because it is primarily due to the Co-60 with its 5.271-year halflife, and to a lesser extent due to the Fe-59 with its 44.51-day half life, the equivalent gamma source changes very little with time over the first 60 days after shutdown. While the subsequent gamma shielding analyses in MCNP Run HB310 are based on the gamma sources at 7 days after shutdown, the resulting dose rates (to within 10%) would be equally applicable to almost any time during a typical 1- to 2-month outage.

Lastly, Table 7.5 shows the disintegration rates for each of the four radioactive nuclides, and the corresponding equivalent gamma source (p/s/cc) at 1.25 MeV, for (the steel portion of) each of the 39 1-cm-thick cylindrical shells centered around the 3.5-inch-diam beam hole in the rotary shutter, 7 days after shutdown. Given the actual volume of steel in each of these 39 cylindrical shells (cf Table 7.1), Table 7.5 also shows the integrated equivalent gamma source (p/s) at 1.25 MeV in each of the 39 shells, 7 days after shutdown. Summing these integrated values over all 39 shells gives a total equivalent activation gamma source of 1.61388e+10 p/s, 7 days after shutdown. This is the value that was then used in the subsequent MCNP gamma shielding calculation (Run HB310).

Table 7.4. Time-dependent results from the (ACTSRC) activation program for the first (innermost) 1-cm-thick shell next to the shutter's large beam hole, assuming the steel initially contained 0.45 wt% Mn-55 and 0.015 wt% Co-59.

DURING IRRADIATION: Concentrations (atoms/cc)

Yr/Wk	Mn-54	Mn-55	Mn-56	Fe-54	Fe-55	Fe-56	Fe-57	Fe-58	Fe-59	Co-59	Co-60
0 0	0.000e+00	3.858e+20	0.000e+00	4.926e+21	0.000e+00	7.658e+22	1.753e+21	2.338e+20	0.000e+00	1.199e+19	0.000e+00
1 0	1.285e+12	3.858e+20	9.513e+10	4.926e+21	9.283e+14	7.658e+22	1.753e+21	2.338e+20	2.034e+12	1.199e+19	2.048e+13
2 0	1.854e+12	3.858e+20	9.513e+10	4.926e+21	1.857e+15	7.658e+22	1.753e+21	2.338e+20	2.039e+12	1.199e+19	3.844e+13
3 0	2.106e+12	3.858e+20	9.513e+10	4.926e+21	2.785e+15	7.658e+22	1.753e+21	2.338e+20	2.039e+12	1.199e+19	5.419e+13
4 0	2.217e+12	3.858e+20	9.513e+10	4.926e+21	3.713e+15	7.658e+22	1.753e+21	2.338e+20	2.039e+12	1.199e+19	6.800e+13
5 0	2.267e+12	3.858e+20	9.513e+10	4.926e+21	4.642e+15	7.658e+22	1.753e+21	2.338e+20	2.039e+12	1.199e+19	8.012e+13
6 0	2.289e+12	3.858e+20	9.513e+10	4.926e+21	5.570e+15	7.658e+22	1.753e+21	2.338e+20	2.039e+12	1.199e+19	9.075e+13
7 0	2.298e+12	3.858e+20	9.513e+10	4.926e+21	6.498e+15	7.658e+22	1.753e+21	2.338e+20	2.039e+12	1.199e+19	1.001e+14
8 0	2.303e+12	3.858e+20	9.513e+10	4.926e+21	7.427e+15	7.658e+22	1.753e+21	2.338e+20	2.039e+12	1.199e+19	1.082e+14
9 0	2.305e+12	3.858e+20	9.513e+10	4.926e+21	8.355e+15	7.658e+22	1.753e+21	2.338e+20	2.039e+12	1.199e+19	1.154e+14
10 0	2.305e+12	3.858e+20	9.513e+10	4.926e+21	9.283e+15	7.658e+22	1.753e+21	2.338e+20	2.039e+12	1.199e+19	1.217e+14
15 0	2.306e+12	3.858e+20	9.513e+10	4.926e+21	1.392e+16	7.658e+22	1.753e+21	2.338e+20	2.039e+12	1.199e+19	1.433e+14
20 0	2.306e+12	3.858e+20	9.513e+10	4.926e+21	1.857e+16	7.658e+22	1.754e+21	2.338e+20	2.039e+12	1.199e+19	1.545e+14
25 0	2.306e+12	3.858e+20	9.513e+10	4.926e+21	2.321e+16	7.658e+22	1.754e+21	2.338e+20	2.039e+12	1.199e+19	1.603e+14
30 0	2.306e+12	3.858e+20	9.513e+10	4.926e+21	2.785e+16	7.658e+22	1.754e+21	2.338e+20	2.039e+12	1.199e+19	1.633e+14

AFTER SHUTDOWN: Concentrations (atoms/cc)

At end of day	Mn-54	Mn-55	Mn-56	Fe-54	Fe-55	Fe-56	Fe-57	Fe-58	Fe-59	Co-59	Co-60
1	2.301e+12	3.858e+20	6.650e+07	4.926e+21	2.785e+16	7.658e+22	1.754e+21	2.338e+20	2.007e+12	1.199e+19	1.632e+14
2	2.296e+12	3.858e+20	4.649e+04	4.926e+21	2.785e+16	7.658e+22	1.754e+21	2.338e+20	1.976e+12	1.199e+19	1.632e+14
3	2.291e+12	3.858e+20	3.250e+01	4.926e+21	2.785e+16	7.658e+22	1.754e+21	2.338e+20	1.945e+12	1.199e+19	1.631e+14
4	2.286e+12	3.858e+20	2.272e-02	4.926e+21	2.785e+16	7.658e+22	1.754e+21	2.338e+20	1.915e+12	1.199e+19	1.630e+14
5	2.281e+12	3.858e+20	1.588e-05	4.926e+21	2.785e+16	7.658e+22	1.754e+21	2.338e+20	1.885e+12	1.199e+19	1.630e+14
6	2.275e+12	3.858e+20	1.110e-08	4.926e+21	2.785e+16	7.658e+22	1.754e+21	2.338e+20	1.856e+12	1.199e+19	1.629e+14
7	2.270e+12	3.858e+20	7.759e-12	4.926e+21	2.785e+16	7.658e+22	1.754e+21	2.338e+20	1.827e+12	1.199e+19	1.629e+14
8	2.265e+12	3.858e+20	5.424e-15	4.926e+21	2.785e+16	7.658e+22	1.754e+21	2.338e+20	1.799e+12	1.199e+19	1.628e+14
9	2.260e+12	3.858e+20	3.791e-18	4.926e+21	2.785e+16	7.658e+22	1.754e+21	2.338e+20	1.771e+12	1.199e+19	1.627e+14
10	2.255e+12	3.858e+20	2.650e-21	4.926e+21	2.785e+16	7.658e+22	1.754e+21	2.338e+20	1.743e+12	1.199e+19	1.627e+14
15	2.230e+12	3.858e+20	4.424e-37	4.926e+21	2.785e+16	7.658e+22	1.754e+21	2.338e+20	1.611e+12	1.199e+19	1.624e+14
20	2.206e+12	3.858e+20	7.384e-53	4.926e+21	2.785e+16	7.658e+22	1.754e+21	2.338e+20	1.490e+12	1.199e+19	1.621e+14
30	2.157e+12	3.858e+20	2.057e-84	4.926e+21	2.785e+16	7.658e+22	1.754e+21	2.338e+20	1.273e+12	1.199e+19	1.615e+14
40	2.110e+12	3.858e+20	5.731-116	4.926e+21	2.785e+16	7.658e+22	1.754e+21	2.338e+20	1.088e+12	1.199e+19	1.609e+14
50	2.063e+12	3.858e+20	1.597-147	4.926e+21	2.785e+16	7.658e+22	1.754e+21	2.338e+20	9.304e+11	1.199e+19	1.604e+14
60	2.018e+12	3.858e+20	4.448-179	4.926e+21	2.785e+16	7.658e+22	1.754e+21	2.338e+20	7.952e+11	1.199e+19	1.598e+14

AFTER SHUTDOWN: at end of day	Disintegretions/sec/cc				Equivalent Gamma Source (p/s/cc) at 1.25 MeV and Total Gamma Source (p/s) for this shell	
	Mn-54	Mn-56	Fe-59	Co-60	(p/s/cc)	(p/s)
1	5.926e+04	6.328e+03	3.676e+05	6.804e+05	1.762e+06	3.344e+09
2	5.913e+04	4.423e+00	3.618e+05	6.801e+05	1.747e+06	3.317e+09
3	5.899e+04	3.092e-03	3.562e+05	6.799e+05	1.741e+06	3.305e+09
4	5.886e+04	0.000e+00	3.506e+05	6.796e+05	1.735e+06	3.294e+09
5	5.873e+04	0.000e+00	3.452e+05	6.794e+05	1.729e+06	3.283e+09
6	5.860e+04	0.000e+00	3.398e+05	6.792e+05	1.724e+06	3.272e+09
7	5.847e+04	0.000e+00	3.345e+05	6.789e+05	1.718e+06	3.262e+09
8	5.834e+04	0.000e+00	3.293e+05	6.787e+05	1.713e+06	3.251e+09
9	5.821e+04	0.000e+00	3.242e+05	6.784e+05	1.707e+06	3.241e+09
10	5.808e+04	0.000e+00	3.191e+05	6.782e+05	1.702e+06	3.231e+09
15	5.744e+04	0.000e+00	2.950e+05	6.770e+05	1.676e+06	3.182e+09
20	5.681e+04	0.000e+00	2.728e+05	6.757e+05	1.652e+06	3.136e+09
30	5.556e+04	0.000e+00	2.332e+05	6.733e+05	1.608e+06	3.054e+09
40	5.434e+04	0.000e+00	1.993e+05	6.709e+05	1.570e+06	2.982e+09
50	5.314e+04	0.000e+00	1.703e+05	6.685e+05	1.537e+06	2.919e+09
60	5.197e+04	0.000e+00	1.456e+05	6.661e+05	1.508e+06	2.863e+09

Table 7.5. Disintegration rates for the four key radioactive nuclides, and the equivalent gamma source (p/s/cc) at 1.25 MeV, for the steel portion of each of the 39 1-cm-thick cylindrical shells around the shutter's large beam hole, 7 days after shutdown (subsequent to 30 years of irradiation), assuming the steel initially contained 0.45 wt% Mn-55 and 0.015 wt% Co-59. Table also shows the total (volume-integrated) equivalent gamma source in each shell, based on the actual volume of steel in each shell, as shown in Table 7.1.

At end of 7th day after shutdown:	Disintegretions/sec/cc				Equivalent Gamma Source (p/s/cc) at 1.25 MeV and Total Gamma Source (p/s) for this shell	
	Mn-54	Mn-56	Fe-59	Co-60	(p/s/cc)	(p/s)
Shell 1	5.847e+04	0.000e+00	3.345e+05	6.789e+05	1.718e+06	3.262e+09
Shell 2	3.243e+04	0.000e+00	2.439e+05	4.768e+05	1.209e+06	2.757e+09
Shell 3	2.552e+04	0.000e+00	1.806e+05	3.601e+05	9.105e+05	2.418e+09
Shell 4	1.258e+04	0.000e+00	9.199e+04	2.073e+05	5.115e+05	1.548e+09
Shell 5	5.367e+03	0.000e+00	4.932e+04	1.229e+05	2.968e+05	1.007e+09
Shell 6	3.908e+03	0.000e+00	3.195e+04	8.558e+04	2.045e+05	7.681e+08
Shell 7	3.183e+03	0.000e+00	1.904e+04	6.272e+04	1.459e+05	6.000e+08
Shell 8	2.147e+03	0.000e+00	1.376e+04	4.808e+04	1.109e+05	4.942e+08
Shell 9	1.839e+03	0.000e+00	1.103e+04	3.658e+04	8.503e+04	4.079e+08
Shell 10	1.231e+03	0.000e+00	7.480e+03	3.223e+04	7.252e+04	3.718e+08
Shell 11	9.882e+02	0.000e+00	5.694e+03	2.615e+04	5.848e+04	3.185e+08
Shell 12	7.891e+02	0.000e+00	6.399e+03	1.994e+04	4.659e+04	2.681e+08
Shell 13	4.655e+02	0.000e+00	7.800e+03	1.685e+04	4.150e+04	2.513e+08
Shell 14	3.564e+02	0.000e+00	5.113e+03	1.354e+04	3.224e+04	2.043e+08
Shell 15	4.161e+02	0.000e+00	3.044e+03	1.216e+04	2.755e+04	1.821e+08
Shell 16	2.901e+02	0.000e+00	2.715e+03	9.629e+03	2.207e+04	1.516e+08
Shell 17	2.121e+02	0.000e+00	4.746e+03	9.205e+03	2.311e+04	1.642e+08
Shell 18	1.784e+02	0.000e+00	2.323e+03	7.068e+03	1.650e+04	1.208e+08
Shell 19	1.611e+02	0.000e+00	1.420e+03	6.580e+03	1.465e+04	1.103e+08
Shell 20	1.319e+02	0.000e+00	2.617e+03	6.414e+03	1.543e+04	1.189e+08
Shell 21	8.299e+01	0.000e+00	1.112e+03	5.442e+03	1.202e+04	9.437e+07
Shell 22	6.096e+01	0.000e+00	1.235e+03	4.059e+03	9.352e+03	7.451e+07
Shell 23	6.680e+01	0.000e+00	1.334e+03	5.041e+03	1.142e+04	9.188e+07
Shell 24	3.398e+01	0.000e+00	1.277e+03	4.015e+03	9.284e+03	7.504e+07
Shell 25	3.123e+01	0.000e+00	1.259e+03	3.006e+03	7.243e+03	5.838e+07
Shell 26	4.618e+01	0.000e+00	9.514e+02	2.880e+03	6.707e+03	5.336e+07
Shell 27	1.330e+01	0.000e+00	6.072e+02	3.355e+03	7.311e+03	4.709e+07
Shell 28	7.766e+00	0.000e+00	4.190e+02	3.106e+03	6.629e+03	3.310e+07
Shell 29	3.127e+00	0.000e+00	5.388e+02	2.022e+03	4.567e+03	1.866e+07
Shell 30	7.734e-01	0.000e+00	9.533e+02	1.378e+03	3.669e+03	1.237e+07
Shell 31	7.379e-01	0.000e+00	4.228e+02	2.194e+03	4.800e+03	1.325e+07
Shell 32	8.796e-01	0.000e+00	3.707e+02	2.451e+03	5.265e+03	1.175e+07
Shell 33	1.335e-00	0.000e+00	1.555e+02	3.462e+03	7.087e+03	1.251e+07
Shell 34	1.624e-00	0.000e+00	1.236e+03	1.825e+03	4.834e+03	6.539e+06
Shell 35	3.175e-01	0.000e+00	1.369e+02	4.284e+03	8.715e+03	8.613e+06
Shell 36	1.221e-01	0.000e+00	9.661e+01	2.077e+03	4.255e+03	2.856e+06
Shell 37	3.848e-02	0.000e+00	7.085e+01	1.251e+02	3.182e+02	1.276e+05
Shell 38	7.345e-04	0.000e+00	3.538e+01	6.695e+01	1.679e+02	3.131e+04
Shell 39	1.014e-03	0.000e+00	1.105e+01	2.020e+01	5.101e+01	2.028e+03

For Mn-54, each decay = 1 gamma at 0.8348 MeV
For Mn-56, each decay = 1 or 2 gammas between 0.8468 MeV and 3.370 MeV; avg=1.69 MeV; basically gone after 2-4 days
For Fe-59, each decay = 1 gamma at 1.099 MeV "OR" 1 gamma at 1.292 MeV, plus some low energy gammas; avg=1.19 MeV
For Co-60, each decay = 1 gamma at 1.173 MeV "AND" 1 gamma at 1.332 MeV (always 2 gammas per disintegration)

Equivalent Gamma Source (p/s/cc) at 1.25 MeV =

(delc60*1.173 + delc60*1.332 + delf59*1.19 + delm54*0.8348 + delm56*1.69) / 1.25

7.4 Gamma Shielding Analysis Based on Activation Sources in the Shutter (Run HB310)

MCNP Run HB310 was a gamma-only shielding analysis used to determine dose rate(s) downstream of the rotary shutter due to activation sources in the shutter itself, 7 days after shutdown (following an irradiation period of 30 years under nominal conditions). In this case, the shutter is in the closed position, and the equivalent gamma sources (at 1.25 MeV) in each of the 39 1-cm-thick shells around the large beam hole in the shutter have been rotated into their proper positions along with the shutter itself.

7.4.1 Overview of Model, Including Source Term Specifications

The input file for Run HB310 was created by making a series of modifications to Run HB308G. However, because of the importance of this problem, the number and nature of the modifications required, and the fact that it is a fundamentally a different problem, the full input listing for Run HB310 is given in Appendix E.4. The first part of that file itemizes the changes required. The following text summarizes just a few of the key changes required to calculate the dose rate due to the activation sources in the rotary shutter.

Plots of the MCNP model used here would be identical with Fig. 3.7, with the rotary shutter in the closed position as shown in Figs. 3.12 and 6.5. This is because Run HB310 uses the same base geometry model used throughout this report. In reality, this is a much simpler problem and, as noted in Sect 6.8.2 and shown in Fig. 6.5, everything of interest here (the rotary shutter, the concrete block assembly holding the shutter, and that portion of the surrounding biological shield downstream of Z=401.9645 cm) is effectively "decoupled" from everything upstream of that location by specifying an importance of zero in Cell 9981 immediately adjacent to that location. While the internal boundary source described in Sect 6.8.2 is not used at all in this particular problem (where all the sources are in the rotary shutter itself), the presence of this zero-importance region at Z=401.9645 cm prevents activation gammas (coming from the shutter) from tracking anywhere upstream of this location, thus increasing the efficiency of the calculation immensely, to the point that no weight window files or special biasing techniques of any sort are required in Run HB310. [Even without any such biasing, the 40 million source particles sampled and tracked in this calculation only required 8.28 CPU hours on each of 8 nodes on the ORNL SP2.]

The physical description of the equivalent gamma source in each of the 39 1-cm-thick concentric cylindrical shells around the 3.5-inch-diam hole in the shutter at 7 days after shutdown is well characterized by the location of the shells in Table 7.1, the volume of steel in each of those shells as shown in Table 7.1, the equivalent gamma source density (p/s/cc) in the steel portions of those shells as shown in Table 7.5, and the total volume-integrated equivalent gamma source (p/s) in each shell as shown in Table 7.5. By summing the last set of values over all 39 shells, it can be seen that the total volume-integrated equivalent gamma source for the entire rotary shutter (ie, the total activation gamma source) is 1.61388e+10 p/s.

While accurately modeling that source within MCNP is straightforward, it does require a degree on conceptual clarity that may or may not be apparent to the casual reader. First, the easy part: The steel portion of the rotary shutter (not including the large and small beam holes) is designated as Cell 3090 in this particular MCNP model. To describe the spatial variation of the activation source within MCNP does not require the definition of any new cells. Instead, the spatial variation of this monoenergetic source is described in terms of a radial probability distribution within a "sampling volume" that must fully enclose Cell 3090. In this case, the "sampling volume" is a finite horizontal cylinder, 62 cm long, having an outer radius of 43.4433 cm, whose center is located at center of the rotary shield plug, at (X=0, Y=0, Z=446.405 cm). [Here, as throughout all the MCNP models in this report, Y and Z lie in the horizontal plane, while X denotes the vertical direction.] Likewise, the axis of the sampling volume is coincident with the axis of the large beam hole when the shutter is in the closed position, meaning that it is rotated 66.75 degrees with respect to the beam tube centerline such that its direction cosines with respect to the X, Y,and Z directions are (0.0, -0.9187912, 0.3947439). [The midpoint location "pos", and the direction cosines "axs", are parameters that must be supplied on the MCNP "sdef" source definition card.] Moreover, the axial distribution, defined by the "ext=d1" parameter on the MCNP "sdef" card and the associated "si1" axial bins and "sp1" sampling probabilities, are used to tell the code to sample the distribution uniformly in the axial direction from a location 31 cm on one side of the midpoint to a location 31 cm on the other side of the midpoint. That was easy. Likewise, the "rad=d2" parameter on the MCNP "sdef" card and the associated "si2" radial bins and "sp2" sampling probabilities are used to tell the code how to sample the source in the radial direction (ie, in the radial direction relative to the axis of the sampling volume). This is where conceptual clarity is important. If the rotary shutter had no holes, and it had the same size and shape and orientation as the sampling volume, then there is no question that the (unnormalized) sampling probabilities for each radial shell in the sampling volume would simply be the volume of the given radial shell times the source density (p/s/cc). Unfortunately, none of those conditions are true in this case. The size and shape and orientation of the shutter are all different from those of the sampling volume, and the shutter does have holes. Nevertheless, it is important that the equivalent gamma source densities (p/s/cc) "for the steel portion" of each radial shell as listed in Table 7.5 still be multiplied by the "full volume" of each sampling shell [Vol(samp)=(62 cm)*pi*(r(i+1)*r(i+1)-r(i)*r(i))]

rather than just the volume of the steel in each shell (shown in Table 7.1). At first glance, that might appear to dramatically increase the total source or shift the distribution, but neither of these is really true. While coordinate triplets (x,y,z) in the bigger (outermost) sampling shells will be tested much more often, the fact is that all those outside the steel comprising Cell 3090 will be rejected. In the case of the outermost sampling shells which just "clip the corners" of the rotary shutter, many potential (x,y,z) source points will be tested, but few will be chosen, and the fraction that are chosen will accurately represent the total source in that radial shell. Use of the the total activation gamma source (1.61388e+10 p/s) on the "fm" tally multiplier cards will accurately represent the total source strength in any event, but failure to follow the above guidelines would distort the spatial distribution. This fine point is therefore important. To aid in the correct preparation of the radial MCNP source probability distribution data [ie, the "si2" radial bins and the "sp2" (unnormalized) radial probabilities], the SI.FOR program in Appendix E.3 was written in June 1998. It correctly implements the above requirements, but goes a step beyond that. Each of the 39 radial sampling bins, for example, has been further subdivided radially into three pieces of equal volume, and the total source in the innermost piece is assumed to be 6% higher than the average of the three, while the total source in the outermost piece is assumed to be 6% lower than the average of the three, and the total source in the central piece is left unchanged. This slight tilt is rather arbitrary and probably makes very little difference in the final dose rate downstream of the shutter, but was intentionally chosen so as to smooth out the step discontinuities in the source terms stemming from the binning of the original results into 39 1-cm-thick radial shells in Run HB309. Thus, the radial source probability distribution produced by SI.FOR (in Appendix E.3) and used by MCNP Run HB310, as shown in Appendix E.4 [see the (si2,sp2) distribution], is actually expressed in terms of 117 discrete radial shells.

7.4.2 Final Results: Activation Dose Rates Downstream of the Rotary Shutter

The key results of programmatic interest from MCNP Run HB310 are summarized in Fig. 7.2. Everything else in the remainder of Sect 7.4.2 may be regarded as supplemental information, presented for the sake of completeness, in a fashion parallel to that in Sect 6.

7.4.2.1 Point Detector Results Along the Centerline

Figure 7.2 shows that the dose rate immediately downstream of the rotary shutter at Z=479.29 cm is 42.78 mrem/hr +/- 1.2%. Note that this due exclusively to the activation sources in the carbon steel rotary shutter shield plug, 7 days after shutdown, assuming the shutter is in the closed position. More importantly, it should be noted that the dose rate due to these activation sources is far greater than the 0.8934 mrem/hr +/- 3.4% (cf Table 6.6) due to the direct transmission and attenuation of radiation streaming down the beam tube when the 1998 HB-3 water tube and collimator sections are both flooded, the rotary shutter is closed, and the HFIR is operating at 100 MW. Put another way: this calculation shows that these activation sources in the shutter itself are responsible for virtually all of dose at this location. Because the activation levels will be independent of the water-tube design used, it means that with the newly proposed design changes (to the HB-3 beam tube and water tube), the dose rates downstream of the rotary shutter should be virtually the same as with the original 1960 design if the shutter itself is left unchanged. [Moreover, if the new rotary shutter has only one large 3.5-inch-diam beam hole and no small beam hole, then it may be turned 90-degrees with respect to the beam tube (when closed) rather than 66.75 degrees as is now the case, and the resulting dose rates should be even less than presently calculated.] Lastly, and most importantly, recent experimental measurements of the contact dose rate here, after shutdown, are in excellent agreement with this calculated value, thereby confirming these conclusions. Measurements by Health Physics personnel at HFIR on Feb. 20, 1998, subsequent to a recent shutdown, show that the measured "contact dose rate" (along the centerline, on the downstream surface of the shutter, when the shutter was in the closed position) was 50 mrem/hr, which is in excellent agreement with the 43 mrem/hr calculated here. Other comparisons with measurements are discussed in Sect 7.5.

Figure 7.2 also shows that the calculated dose rate along the centerline, 1.5 feet from the downstream surface of the steel-lined concrete block assembly holding the shutter is only 5.597 mrem/hr +/- 0.41%, while the dose rate 3.0 feet from this location is only 2.108 mrem/hr +/- 0.25%. [If and when the radioactive monochrometer drum is located nearby, the actual dose rates at these locations (15-20 mrem/hr) may be somewhat higher than calculated here since this calculation did not account for the presence of the (movable) monochrometer drum or anything else downstream of the steel-lined concrete block assembly holding the shutter in the biological shield (ie, it did not account for any movable experimental equipment downstream of Z=478.79 cm).]

Detailed fluxes and dose rates, by energy group, for detectors at the three locations shown in Fig. 7.2 are given in Table 7.6. Note that these dose rates are converged to within 1.2%, 0.41%, and 0.25%, respectively.

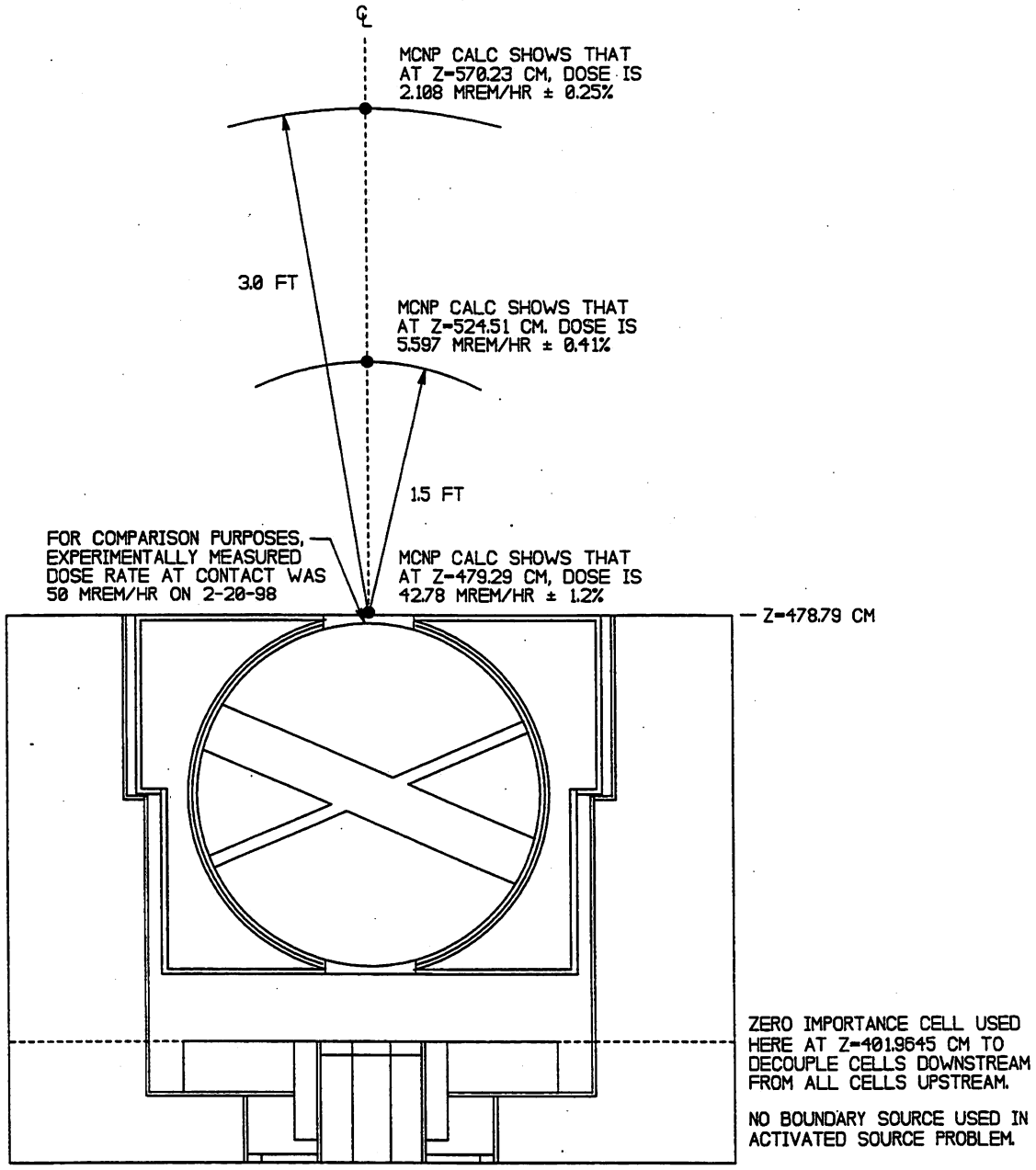


Fig. 7.2. Centerline dose rates downstream of the HB-3 rotary shutter due to activation sources in the shutter itself, 7 days after shutdown, subsequent to operating at 100 MW for 30 years.

Table 7.6. Gamma fluxes and dose rates at key axial locations along the HB-3 centerline (with the shutter closed), due to activation sources in the rotary shutter, 7 days after shutdown, subsequent to operating at 100 MW for 30 years. In the associated activation analysis the carbon steel rotary shutter was assumed to initially contain 0.45 wt% Mn-55 and 0.015 wt% Co-59.

Emin (MeV)	Emax (MeV)	Tally 35 0.5 cm downstream p/s/cm2	fsd	Tally 55 1.5 ft downstream p/s/cm2	fsd	Tally 75 3.0 ft downstream p/s/cm2	fsd
0.010	0.020	9.10565e-1	.6177	9.42180e-2	.2497	3.44430e-2	.2433
0.020	0.045	2.17396e+0	.8590	6.61779e-1	.2268	3.32686e-1	.2508
0.045	0.070	3.42002e+0	.3098	1.42005e+0	.1634	4.96694e-1	.1637
0.070	0.10	1.76063e+2	.1311	1.33744e+1	.0383	4.28843e+0	.0375
0.10	0.15	1.05632e+3	.0392	9.79839e+1	.0280	2.95287e+1	.0146
0.15	0.30	4.98857e+3	.0234	4.92588e+2	.0080	1.56487e+2	.0109
0.30	0.40	2.51109e+3	.0303	3.51090e+2	.0115	1.16871e+2	.0076
0.40	0.51	1.99570e+3	.0310	3.45111e+2	.0118	1.23789e+2	.0068
0.51	0.60	1.37837e+3	.0375	2.43600e+2	.0077	9.29327e+1	.0101
0.60	0.70	1.33454e+3	.0407	2.38566e+2	.0073	9.20591e+1	.0068
0.70	1.00	3.33642e+3	.0365	6.10335e+2	.0170	2.38856e+2	.0047
1.00	1.50	1.10754e+4	.0147	1.24017e+3	.0033	4.75018e+2	.0034
	Total:	2.78589e+4	.0117	3.63499e+3	.0041	1.33069e+3	.0027

Emin (MeV)	Emax (MeV)	Tally 45 0.5 cm downstream mrem/hr	fsd	Tally 65 1.5 ft downstream mrem/hr	fsd	Tally 85 3.0 ft downstream mrem/hr	fsd
0.010	0.020	3.15500e-6	.7526	2.43927e-5	.4708	1.32843e-5	.5359
0.020	0.045	1.25570e-3	.8590	3.82250e-4	.2268	1.92163e-4	.2508
0.045	0.070	9.39341e-4	.3098	3.90030e-4	.1634	1.36422e-4	.1637
0.070	0.10	4.69102e-2	.1311	3.56348e-3	.0383	1.14261e-3	.0375
0.10	0.15	3.46124e-1	.0392	3.21064e-2	.0280	9.67567e-3	.0146
0.15	0.30	2.82732e+0	.0234	2.79179e-1	.0080	8.86905e-2	.0109
0.30	0.40	2.19956e+0	.0303	3.07534e-1	.0115	1.02372e-1	.0076
0.40	0.51	2.16574e+0	.0310	3.74515e-1	.0118	1.34336e-1	.0068
0.51	0.60	1.76390e+0	.0375	3.11735e-1	.0077	1.18926e-1	.0101
0.60	0.70	1.92401e+0	.0407	3.43940e-1	.0073	1.32722e-1	.0068
0.70	1.0	5.85975e+0	.0365	1.07193e+0	.0170	4.19503e-1	.0047
1.0	1.5	2.56461e+1	.0147	2.87174e+0	.0033	1.09995e+0	.0034
	Total:	4.27816e+1	.0119	5.59704e+0	.0041	2.10766e+0	.0025

Tallies 35 & 45 are at Z=479.290 cm, 0.5 cm past concrete block assembly holding the shutter.
Tallies 55 & 65 are at Z=524.510 cm, 1.5 feet past concrete block assembly holding the shutter.
Tallies 75 & 85 are at Z=570.230 cm, 3.0 feet past concrete block assembly holding the shutter.
All results are based on MCNP Run HB310 with 40 million histories and no special biasing.
These 40 million histories experienced a total of 281 million collisions.

7.4.2.2 Boundary Crossing Data Downstream of Entire Shield Configuration

Figure 7.3 shows a sketch of the end of the entire shield configuration at Z=478.79 cm, as would be seen if one were standing outside the system (where the monochrometer drum would normally be located), looking back towards the steel-lined concrete block assembly holding the rotary shutter. The small numbers, 1 through 10, indicate the surface segment numbers corresponding to Tallies 231 and 232, the results of which are summarized below in Tables 7.7 and 7.8. Segment 10 (in the center) corresponds to the 6.5-inch-diameter hole coming out from the rotary shutter through the concrete block assembly holding shutter, while segment 9 is the remainder of the 83.5025 cm x 83.5025 cm face of the steel-lined concrete block assembly holding the rotary shutter. Segments 5 to 8 are the 1.74625-cm clearance gaps between the concrete block assembly and the biological shield, while segments 1 to 4 represent portions of the steel-clad biological shield beyond that, out to a radius of 65 cm. Most of the key results of interest (based on Tally 232) are summarized directly on Fig. 7.3. In addition to the "area-averaged" dose rates for each of the 10 segments comprising this planar surface at Z=478.79 cm, Table 7.7 also shows the integrated gamma leakage (p/s) across each surface segment, while Table 7.8 shows both types of data on a group-by-group basis for Segments 9 and 10.

Unlike the previous case in Sect 6 where the source upstream of the shutter was a tightly focused beam from the collimator and the results downstream of the shutter were fairly peaked around the centerline, the isotropic activation sources in this present calculation are spatially distributed over a much larger volume in concentric shells around the shutter's large beam hole. As a result, most of the gamma leakage now comes from Segment 9, the large face of the concrete block holding the rotary shutter, and localized peaking near the centerline is much less noticeable. Indeed, if there is any peaking at all, it is just to the right of the centerline where the amount of steel (and concrete) between the large beam hole and the outer face of the assembly is less than at any other location. For that reason, the average dose rate over the 6.5-inch-diam hole (43.16 mrem/hr +/- 1.3%) is very similar to (but just slightly higher than) the point detector estimate of 42.78 mrem/hr +/- 1.2% at the centerline. [Recall that for the previous case in Sect 6, the flux near the centerline was necessarily more peaked, and the ratio of the peak-to-average dose rate was 1.944.] Moreover, the fact that the boundary crossing estimate of the dose rate and the point detector estimate of the dose rate are in excellent agreement with each other, and that both are in very good agreement with the measured contact dose rate of 50 mrem/hr, suggests that these results (and the other results obtained here) are quite credible.

Average dose rates downstream of the four 1.74625-cm clearance gaps between the concrete block assembly and the biological shield are shown in Fig. 7.3 and Table 7.7, while Tables 7.9a and 7.9b compare those values in a more pointed fashion. Because the source gammas are now coming from concentric shells around the large beam hole "inside" the shutter itself, rather than from the collimator region upstream of the shutter as was the case in Sect 6, there is no appreciable internal streaming in the clearance gap between the top of the shutter and the concrete housing. As a result, the top-to-bottom asymmetry previously seen in Sect 6 is essentially non-existent in this particular case (cf Table 7.9b). A clear right-to-left asymmetry does exist, however, with the dose rates on the right being more than an order of magnitude greater than those on the left, as shown in Table 7.9a. While streaming through the system diagonally along the axis of the large beam tube hole (cf Fig. 7.3) is undoubtedly still responsible for a large part of this difference, it is not the whole cause in this case. (Recall that in this model, the activation sources in the carbon steel are distributed uniformly along the axis of the large beam hole through the shutter.) Indeed, the fundamental cause of the asymmetry in this case is the simple fact that source gammas starting in the steel near the one end of the large beam hole simply have to pass through far less material (mostly concrete) to escape from the system than would source gammas starting in the steel near the other end of the large collimator hole (cf Fig. 7.3).

7.4.3 Simple Checks for Reasonableness

It is possible to estimate the overall activity and the overall gamma source within the rotary shutter using very elementary methods. As shown in the following subsection, the overall gamma source can be estimated to within about 15% using very simple logic. Unfortunately, elementary methods cannot be used to accurately estimate the dose rate outside the shutter, primarily because the dose rate there is critically dependent on the spatial distribution of the gamma sources within the shutter (which cannot be ascertained by elementary methods). If one were willing to assume that the distribution given by the activation program using the spatially-dependent MCNP reaction rates was indeed correct (a reasonable assumption, given that the total is correct), then undoubtedly simple point kernel methods could be used to good affect if one were willing to invest the effort. In this case, that was not necessary since direct experimental measurements provided the needed confirmation.

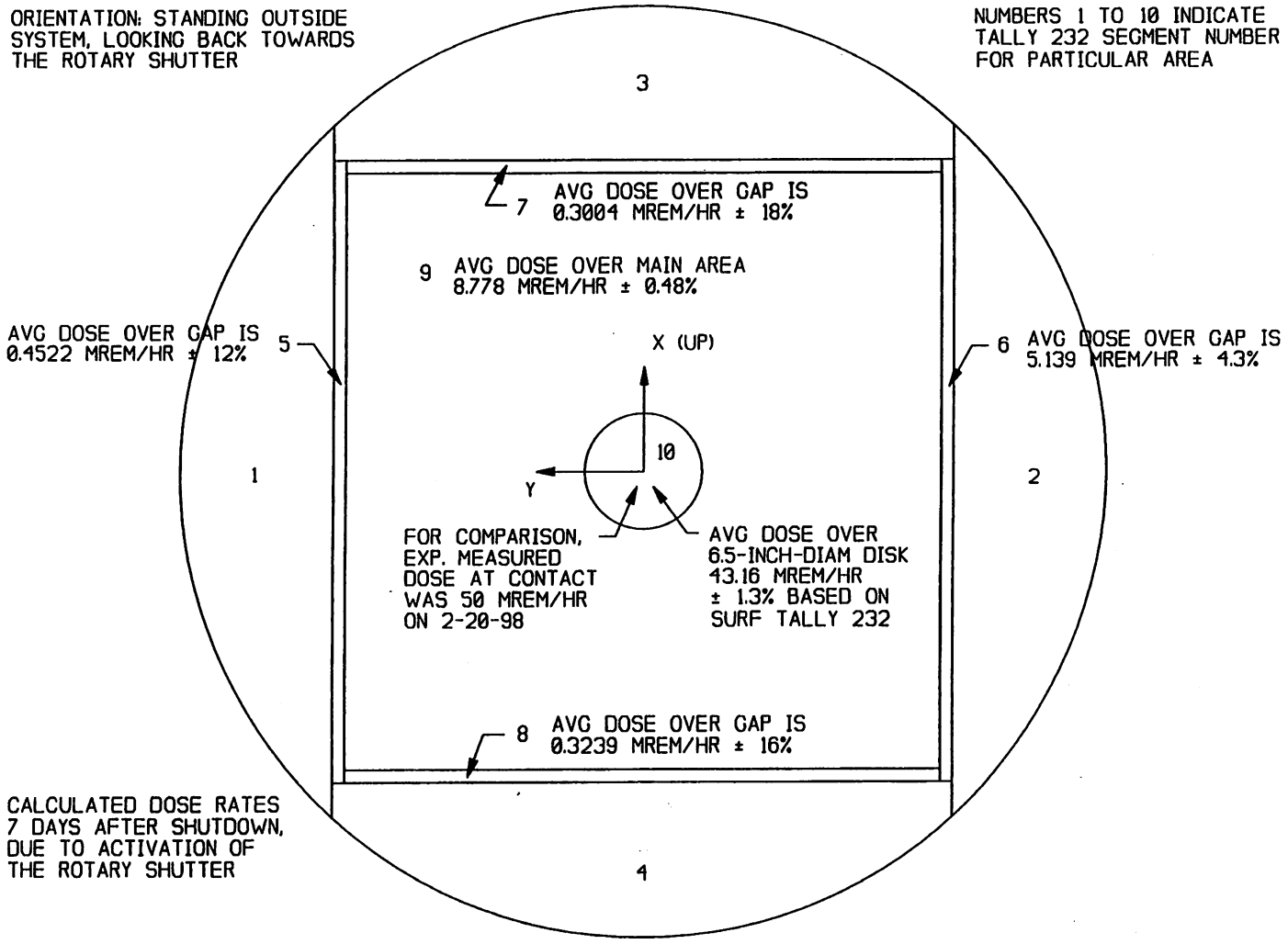


Fig. 7.3. External dose rates averaged over different portions of the downstream surface of the entire shield configuration at Z=478.79 cm (including the central 6.5-inch-diam hole downstream of the shutter, the main face of the concrete block assembly holding the rotary shutter, and each of the four 1.74625-cm-wide clearance gaps between the biological shield and the concrete block assembly), due to activation sources in the rotary shutter, 7 days after shutdown, subsequent to operating at 100 MW for 30 years.

Table 7.7. Integrated gamma leakage rates (p/s) and area-averaged gamma dose rates (mrem/hr) for various portions of a plane surface immediately downstream of the entire shield configuration (ie, at Z=478.79 cm, corresponding to the downstream surface of the stainless steel liner on the concrete block assembly holding the rotary shutter) due to activation sources in the rotary shutter, 7 days after shutdown, subsequent to operating at 100 MW for 30 years. In the associated activation analysis the carbon steel rotary shutter was assumed to initially contain 0.45 wt% Mn-55 and 0.015 wt% Co-59. The locations of the various area segments are illustrated in Fig. 7.3, where segment 10 is the 6.5-inch-diam hole in the middle, directly downstream of the shutter, and segment 9 corresponds to the remainder of the central block. Values are based on Tallies 231 and 232 in Run HB310 with 40 million histories.

Segment Number	Description	Area	Integrated Gamma Leakage photons/sec	fsd	Average Gamma Dose Rate mrem/hr	fsd
1	Portion of concrete biological shield on left	1438.21 cm2	8.43252e+4	.0692	1.40591e-1	.0837
2	Portion of concrete biological shield on right	1438.21 cm2	9.20719e+5	.0209	1.74357e+0	.0265
3	Portion of concrete biological shield on top	1414.34 cm2	5.52754e+4	.0854	1.15428e-1	.1091
4	Portion of concrete biological shield on bottom	1414.34 cm2	5.60823e+4	.0854	1.23049e-1	.1378
5	Gap on left, between bio shield and central block	151.915 cm2	4.55921e+4	.0941	4.52217e-1	.1227
6	Gap on right, between bio shield and central block	151.915 cm2	3.66754e+5	.0332	5.13936e+0	.0437
7	Gap on top, between bio shield and central block	145.816 cm2	1.89631e+4	.1459	3.00386e-1	.1825
8	Gap on bottom, between bio shield and central block	145.816 cm2	2.13839e+4	.1374	3.23933e-1	.1597
9	Face of concrete block holding shutter (excluding 10) ..	6758.58 cm2	2.67662e+7	.0039	8.77772e+0	.0048
10	6.5-inch-diam hole leading directly to rotary shutter ..	214.084 cm2	3.69740e+6	.0105	4.31643e+1	.0131

Note that:

(1) These estimates are based on real boundary crossing tallies. That is significant, because volumetric track length tallies and boundary crossing tallies only sense real particles; when one can get good statistics, these types of tallies are considered much more reliable than point detectors which sense pseudoparticles.
(2) While the dose rate directly in front of the central hole (segment 10) is dominent, average dose rates for the other areas appear low because of the large areas over which they were averaged. To assess relative contributions from these regions, look at the integrated leakage terms or point detector responses further from the surface.
(3) The average dose rate over the central 6.5-inch-diam hole (segment 10) is 43.164 mrem/hr, while the corresponding point detector (Tally 45 in Table 7.6) is 42.782 mrem/hr. Unlike the values in Run HB308G for the transmitted component of the gamma flux where some radial peaking was expected and observed, the two values here are nearly equal because the decay gamma sources in the shutter are "distributed" over a much bigger volume. The fact that the two detectors here are in such excellent agreement indicates that the point detector values are trustworthy.
(4) See other notes in main text.

Table 7.8. Integrated gamma leakage rates (p/s) and area-averaged gamma dose rates (mrem/hr) by energy group at Z=478.29 cm [immediately downstream of the 6.5-inch-diam hole and the remainder of the square (83.5 cm x 83.5 cm) face of the concrete block assembly holding the rotary shutter], due to activation sources in the rotary shutter, 7 days after shutdown, subsequent to operating at 100 MW for 30 years. In the associated activation analysis the carbon steel rotary shutter was assumed to initially contain 0.45 wt% Mn-55 and 0.015 wt% Co-59. The locations of surface segments 9 and 10 are shown in Fig. 7.3. These leakage rates and area-averaged dose rates were calculated by Tallies 231 and 232 in Run HB310.

Emin (MeV)	Emax (MeV)	Segment 10 (6.5-inch hole; 214.084 cm2) mrem/hr	fsd	photons/sec	fsd	Segment 9 (Remainder of face; 6758.58 cm2) mrem/hr	fsd	photons/sec	fsd
0.010	- 0.020	0.00000e+0	.0000	4.03470e+2	.9999	0.00000e+0	.0000	8.06940e+2	.7071
0.020	- 0.045	0.00000e+0	.0000	0.00000e+0	.0000	4.54291e-4	.2894	4.84164e+3	.2887
0.045	- 0.070	1.83722e-3	.5815	1.21041e+3	.5774	5.38428e-4	.2127	9.68328e+3	.2041
0.070	- 0.10	4.24818e-2	.1593	2.01735e+4	.1414	6.03063e-3	.0897	8.87634e+4	.0674
0.10	- 0.15	4.07880e-1	.0881	1.33952e+5	.0549	6.03678e-2	.0331	6.68146e+5	.0246
0.15	- 0.30	2.94054e+0	.0367	6.12064e+5	.0257	5.54159e-1	.0151	3.50293e+6	.0107
0.30	- 0.40	2.26294e+0	.0439	3.34880e+5	.0347	5.76592e-1	.0176	2.54428e+6	.0126
0.40	- 0.51	2.09926e+0	.0485	2.54590e+5	.0398	6.84438e-1	.0170	2.57374e+6	.0125
0.51	- 0.60	2.00805e+0	.0600	1.99718e+5	.0449	5.65214e-1	.0190	1.91043e+6	.0145
0.60	- 0.70	1.84919e+0	.0539	1.75509e+5	.0479	6.33347e-1	.0174	1.99112e+6	.0142
0.70	- 1.00	5.67723e+0	.0355	4.40993e+5	.0302	1.78488e+0	.0107	4.90498e+6	.0091
1.00	- 1.50	2.58749e+1	.0181	1.52391e+6	.0163	3.91170e+0	.0074	8.56648e+6	.0069
	Total:	4.31643e+1	.0131	3.69740e+6	.0105	8.77772e+0	.0048	2.67662e+7	.0039

Note that the calculated dose rate directly downstream of the 6.5-inch-diam hole was 43.2 mrem/hr, while the experimentally measured contact dose rate at this location was 50 mrem/hr. This measurement, next to the HB-3 rotary shutter, was made at 2:52 pm on Feb 20, 1998, during a recent shutdown.

Table 7.9a. Clear asymmetric right-to-left variations in external dose rates and leakage rates for Run HB310, based on the decay gamma activation sources in the rotary shutter, 7 days after shutdown. Note that the uncertainties (fsd's) in the dose rates and leakages shown here were reasonably small (typically between 3% and 12%), so that it can be said with certainty that the huge right-to-left asymmetries shown here are quite real. These asymmetries are also fully consistent with the (slanted) orientation of the large beam hole through the shutter. Thus, these asymmetries are clearly indicative of internal streaming through the large beam hole in the shutter, around which the activated gamma sources are primarily concentrated.

	Dose Rate (mrem/hr)	Ratio	Leakage (p/s)	Ratio
Segment 6: (R) Clear. Gap	5.13936		366754.	
Segment 5: (L) Clear. Gap	0.45222		45592.	
Ratio	-------->	11.36	------->	8.04
Segment 2: (R) Bio Shield				
Segment 1: (L) Bio Shield	1.74357		920719.	
Ratio	0.14059		84325.	
	-------->	12.40	------->	10.92

Table 7.9b. Non-existence of asymmetric top-to-bottom variations in external dose rates and leakage rates for Run HB310, based on the decay gamma activation sources in the rotary shutter, 7 days after shutdown. Note that the uncertainties (fsd's) in the dose rates and leakages shown here were typically between 9% and 16%. Thus, the quantities being compared here are "statistically identical" and no significant top-to-bottom asymmetries would appear to exist in this particular problem with the spatially-distributed activation sources, 7 days after shutdown.

	Dose Rate (mrem/hr)	Ratio	Leakage (p/s)	Ratio
Segment 7: (T) Clear. Gap	0.300386		18963.1	
Segment 8: (B) Clear. Gap	0.323933		21383.9	
Ratio	-------->	0.93	------->	0.89
Segment 3: (T) Bio Shield	0.115428		55275.4	
Segment 4: (B) Bio Shield	0.123049		56082.3	
Ratio	-------->	0.94	------->	0.99

7.4.3.1 Estimate of Total Gamma Source Within the Shutter

The shutter becomes activated due to (1) neutron absorption along the length of the inner surface of the large beam hole and (2) due to neutron absorption on the leading edge (upstream face) of the shutter, in the region just outside the large beam hole, that normally faces the collimator. Each will be discussed in turn.

In this simplified activation analysis, we will ignore decay gammas from Mn-56 and Mn-54. If one is primarily interested in dose rates for maintenance purpose, say a week or so after shutdown, the gamma sources from the iron and cobalt sources will be very close to their values at shutdown since their halflives are 44.51 days and 5.271 years, respectively. With a halflife of only 2.578 hours, the Mn-56 will be virtually gone 1 or 2 days after shutdown, and totally gone 7 days after shutdown, so that it can justifiably be ignored. Decay gammas from Mn-54, however, are another matter since Mn-54 has a halflife of 312.2 days. It will not disappear readily. Because it is only produced in relatively small quantities by high-energy Fe54(n,p)Mn54 reactions, and because Mn54(n,g)Mn55 reactions help to deplete some of the Mn-54 that is produced, it has not traditionally been considered a major activation source (when compared with Fe-59 and Co-60). Indeed, at 7 days after shutdown, Table 7.5 suggests that decay gammas from Mn-54 only account for 1.68% of all decay gammas in Shell 10, and at most 3.34% of all decay gammas even in the innermost shell (Shell 1). For that reason [and because high-energy (n,p) cross section data for Fe-54 is not readily available in a simple 1-, 2-, or 3-group format], we will also ignore the Mn-54 in this simplified activation analysis where the main goal is to verify the gamma source from the key isotopes of iron and cobalt, at or shortly after shutdown.

With respect to the iron and cobalt, it is necessary only to consider the activation due to the initial Co-59 in the system (which may be treated as a fixed quantity), and the initial amount of Fe-58 in the system (which may be treated as a fixed quantity). While it is true that the amount of Fe-58 will be augmented slightly by (n,g) captures in Fe-57, and/or (n,g) captures in Fe-56 and subsequent (n,g) captures in Fe-57, the incremental amount of Fe-58 produced by either method is negligible compared to the amount (0.28 at%) of Fe-58 initially in the system. Moreover, since Fe-58 experiences negligibly little depletion over a 30 year irradiation period, its density may be treated as a constant in this activation analysis. It is significant only insofar at it produces radioactive Fe-59 which is initially not present at all. Likewise, the production of Co-59 from decay of Fe-59 would be significant only if one had no Co-59 initially in the system. Given that there is a trace amount (0.015 wt%) initially present, any additional incremental amount produced by Fe-59 is so small that it may also be neglected. Since the amount of Co-59 does not deplete significantly over a 30 year irradiation period, its density may also be treated as constant in this activation analysis. It is significant only insofar as it produces radioactive Co-60 which is initially not present at all. Lastly, since the amount of Co-60 present at any given time will be 5 to 6 orders of magnitude less than Co-59, and since the amount of Fe-59 will be about 8 orders of magnitude less than Fe-58, the destruction rates for Co-60 and Fe-59 by (n,g) capture will be many orders of magnitude less than their respective production rates, and can be safely ignored. With respect to nuclides in the carbon steel forming the rotary shutter, the following notation will be used:

Density NO(all Fe)= 8.34943e+22 atoms/cc, microscopic absorption cross section = x(avg Fe) = 2.62 barns
Density NO(Fe-58) = 0.0028*NO(all Fe), microscopic absorption cross section = x(Fe-58) = 1.35 barns
Density NO(Co-59) = 1.19882E+19 atoms/cc, microscopic absorption cross section = x(Co-59) = 37.0 barns

Halflife of Co-60 = TCo60(1/2) = 5.271 years, Decay constant (lambda) = DCo60 = 4.16705e-9/sec
Halflife of Fe-59 = TFe59(1/2) = 44.51 days, Decay constant (lambda) = DFe59 = 1.80241e-7/sec

Irradiation time = Tirr = 30 years = 9.46e+8 sec

Here, the microscopic cross section for Co-59 was taken from Table 7.3 ("Induced activities in metals present in structural materials") as given in Sect 7.36 of Ref 22 by Glasstone and Sesonske, while the cross section for "all iron" was taken from Table A.2 of that same reference, and that for Fe-58 was taken from the Chart of the Nuclides#29.

First, let us consider only those neutrons inside the beam hole that are available to activate materials there. Using the neutron point sources for HB-3 in Table 2.2a and the 1/(4*pi*R^2) approximation, the flux entering the beam hole (Flux1) at Z=415.44875 cm is 6.51026e+10 n/s/cm2, while the flux going out the other end (Flux2) at Z=477.36125 cm is 4.67075e+10 n/s/cm2. The area of the 3.5-inch-diam beam hole (Ahole) is 62.07167 cm2. The fluxes may be treated as currents, and number of neutrons available for absorption (NA) in the material is given by

NA = Ahole*(Flux1-Flux2) = 1.1418e+12 n/s

The production rate of Co-60, is then NA times the fraction that get absorbed by the Co-59 as opposed to anything else (mostly Fe). Thus, the production rate of Co-60 is given by:

P(Co-60) = NA * NO(Co-59)*x(Co-59) / [NO(all Fe)*x(avg Fe)] = 2.31522e+9 atoms/sec.

The solution to the differential equation

d[N(Co-60)]/dt = P(Co-60) - DCo60*N(Co-60) where DCo60 = lambda = decay constant, is then

N(Co-60) = P(Co-60)*(1.0-exp(-DCo60*t)/DCo60

and after multiplying both sides by DCo60 (the decay constant) we see that the decay rate, DR(Co-60), at the end of a 30 year irradiation period (and for many weeks thereafter) is given by

DR(Co-60) = P(Co-60)*(1.0-exp(-DCo60*Tirr) = P(Co-60)*(0.98059) = 2.27028e+9 atoms/sec

Since Co-60 gives off 2 gammas per decay#30, the corresponding gamma emission rate, GER(Co-60), is

GER(Co-60) = 4.54057e+9 p/s .

These gammas are distributed more-or-less uniformly along the entire length of the 61.9125-cm-long beam hole. Likewise, for the Fe-59, we have:

P(Fe-59) = NA * NO(Fe-58)*x(Fe-58) / [NO(all Fe)*x(avg Fe)] = 1.64735e+9 atoms/sec,

and since Fe-59 effectively only gives off 1 gamma per decay,

GER(Fe-59) = P(Fe-59)*(1.0-exp(-DFe59*Tirr) = P(Fe-59)*(1.0000) = 1.64735e+9 p/s.

Thus, the total gamma emission rate (distributed more-or-less uniformly along the length of the beam hole) is:

GER(Hole) = GER(Co-60)+GER(Fe-59) = 6.18792e+9 p/s .

As noted above, however, that is not the entire gamma source. It is only the gamma source due to neutrons inside the beam hole. It does not account for neutrons impinging on the leading edge (upstream face) of the shutter in the region just beyond the 3.5-inch-diam beam hole. Most (virtually all) of the neutron radiation reaching the rotary shutter comes through the 2.75-inch x 5.5-inch rectangular hole in the collimator. This area extends beyond the 3.5-inch-diam hole as shown in Fig. 7.4. Even if the neutron beam were perfectly collimated (which its not), the area of the shutter (AS) that is impacted by the beam outside the hole would be 42.613 cm2. Given that the flux (Flux1) at this axial location (Z=415.44875 cm) is 6.51026e+10 n/s/cm2, and that approximately half will be reflected back (and therefore not absorbed), the total number of neutrons available (NA2) to activate materials in this region of the shutter is

NA2 = 0.5*AS*Flux1 = 1.387108e12 n/s,

the production rate for Co-60 in this region is

P2(Co-60) = NA2 * NO(Co-59)*x(Co-59) / [NO(all Fe)*x(avg Fe)] = 2.81260e+9 atoms/sec,

and the total gamma emission rate here (GER2) due to gammas from the Co-60 is

GER2(Co-60) = 2.0*P2(Co-60)*(1.0-exp(-DCo60*Tirr) = 5.51607e+9 atoms/sec.

Likewise, for the Fe-59, we have:

P2(Fe-59) = NA2 * NO(Fe-58)*x(Fe-58) / [NO(all Fe)*x(avg Fe)] = 2.001247e+9 atoms/sec,

and since Fe-59 effectively only gives off 1 gamma per decay, the gamma emission rate for the Fe-59 in this region, GER2(Fe-59) is given by:

GER2(Fe-59) = P2(Fe-59)*(1.0-exp(-DFe59*Tirr) = P2(Fe-59)*(1.0000) = 2.001247e+9 p/s.

Summing over all four terms, the total gamma emission rate for the shutter can then be estimated as:

GER(Total) = GER(Co-60) + GER(Fe-59) + GER2(Co-60) + GER2(Fe-59) = 1.37e+10 p/s.

Results of the detailed activation analysis produced by the ACTSRC.FOR program based on 12 different reaction rates in each of 39 shells about the beam hole (as calculated by MCNP Run HB309) are shown in Table 7.5. If one sums the total resulting gamma source (p/s) over all 39 shells in Table 7.5, the resulting (total) gamma source is 1.61e+10 p/s, which is within 15% of the much more approximate value of 1.37e+10 p/s obtained here. Moreover, had the Mn-54 and its resulting decay gammas been included in the simplified analysis, the approximate gamma source from this simplified analysis would have been 2 to 3% higher, such that the approximate and rigorous gamma source terms would only have differed by 12 to 13%. This small difference may be due to uncertainties in the 1-group cross section data used here, or due to uncertainties in the reflected albedo from the shutter (0.5), but is more likely due to the fact

that the area of the shutter impacted by the neutron beam was assumed to correspond exactly to the area of the 2.75-inch x 5.5-inch hole in the collimator when, in fact, there is some small divergence and the area impacted is likely to be slightly larger than that shown in Fig. 7.4. The key point demonstrated by this elementary analysis, however, is that the decay gamma source terms used in the final shielding analysis (as determined by the ACTSRC.FOR activation program using the spatially-dependent reaction rates from MCNP Run HB309) are eminently reasonable.

7.4.3.2 Estimate of the Activation Gamma Dose Rate Downstream of the Shutter

Figure 7.5 illustrates an elementary approach that did not work and should not be trusted in this case. Here the approach was to take the gamma sources along the beam tube hole, GER(hole), and distribute them evenly among the four point sources illustrated in Fig. 7.5, while the gamma sources for the leading edge, GER2(Co-60) and GER2(Fe-59), would be added in with those from region 1 in Fig. 7.5. Knowing the total distance from each source point to the detector point, and the total amount of steel along each of the four paths, an attempt was made to calculate the contribution from each point source as S(i)*exp(-u*rho*t)/(4*pi*R^2), and sum to get the total. The result was a deceptively low (and erroneous) dose rate of 0.017 mrem/hr at the detector point, just downstream of the shutter. At the risk of sounding very inexperienced, it was decided to include this one example as a classic illustration of how poorly things can go when one over-simplifies a problem.

The tragic flaw here, of course, is the implicit assumption that all gammas are born on the centerline. Had one assumed them to be born on the inner surface of the hole, the results would have been much the same. While the gamma source is indeed peaked in the regions around the hole, the reality is that they do have a spatial distribution, and this spatial distribution is very important (cf Table 7.5). As one goes out to more distant radial shells, the gamma source will become less and less, but the amount of attenuation between the detector point and "that portion of each shell closest to the detector" will go down much faster, thus making those sources in those portions of the more distant shells more and more important. By going out 10 cm from the inner surface, the total source in each shell (p/s) will be about a factor of 10 lower than on the inner surface, but those born in that portion of shell 10 closest to the detector point will experience 70 times less attenuation than those born on the inner wall. Moreover, by going out 20 cm from the inner surface, the total source in each shell (p/s) will be about a factor of 20 lower than on the inner surface, but those born in that portion of shell 20 closest to the detector will experience 4900 times less attenuation than those born on the inner wall. Thus, if one wants to estimate the dose rate outside the shutter, it is imperative that one have a good description of the spatial distribution for the source and treat it rigorously. While elementary point kernel codes like QAD could treat a known distribution quite well, there is no ultra-simple elementary method for obtaining the distribution in the first place.

Thus, in this case, one must simply be content in the knowledge that the overall gamma source obtained (by the ACTSRC.FOR program using spatially-dependent MCNP reaction rates) is correct. Fortunately, thanks to recent measurements by Health Physics personnel at HFIR, the dose rates downstream of the shutter (as calculated by MCNP Run HB310) have since been confirmed by direct experimental measurements, so that confirmation by elementary analytic techniques becomes moot.

7.5 Comparison of Calculated Activation Dose Rate Against Recent Experimental Measurements

Table 7.10 and Fig. 7.6 show the results of a recent radiation survey#11 in the region(s) downstream of the HB-3 rotary shutter subsequent to the Feb 1998 shutdown of the HFIR reactor. These measurements were made during a maintenance operation in which the monochrometer drum had been rolled back a short distance from the biological shield and the saddle shield was being removed.

The only measurement of direct interest here is the one that was made inside the cavity where the beam tube and crystal are located (ie, inside the 6.5-inch-diam hole leading to the rotary shutter). There, the maximum measured dose rate at contact (with the closed shutter, at Z=477.36 cm) was 50 mrem/hr. This is in good to excellent agreement with the calculated values. As shown in Table 7.7 and Fig. 7.3, the average dose rate calculated over the 6.5-inch-diam hole at Z=478.79 cm was 43.16 mrem/hr +/- 1.3%, while, as shown in Table 7.6 and Fig. 7.2, the point detector along the centerline at Z=479.29 cm showed the dose rate to be 42.78 mrem/hr +/-1.2%. This is significant because:

a) The experimentally measured value of 50 mrem/hr (at contact with the rotary shutter) confirms the accuracy of the activation analysis and the subsequent gamma shielding analysis using those activation sources.

b) Since the measurement was made after shutdown, it also tends to confirm the previous suspicion that most of the dose at this location is indeed due to activation.

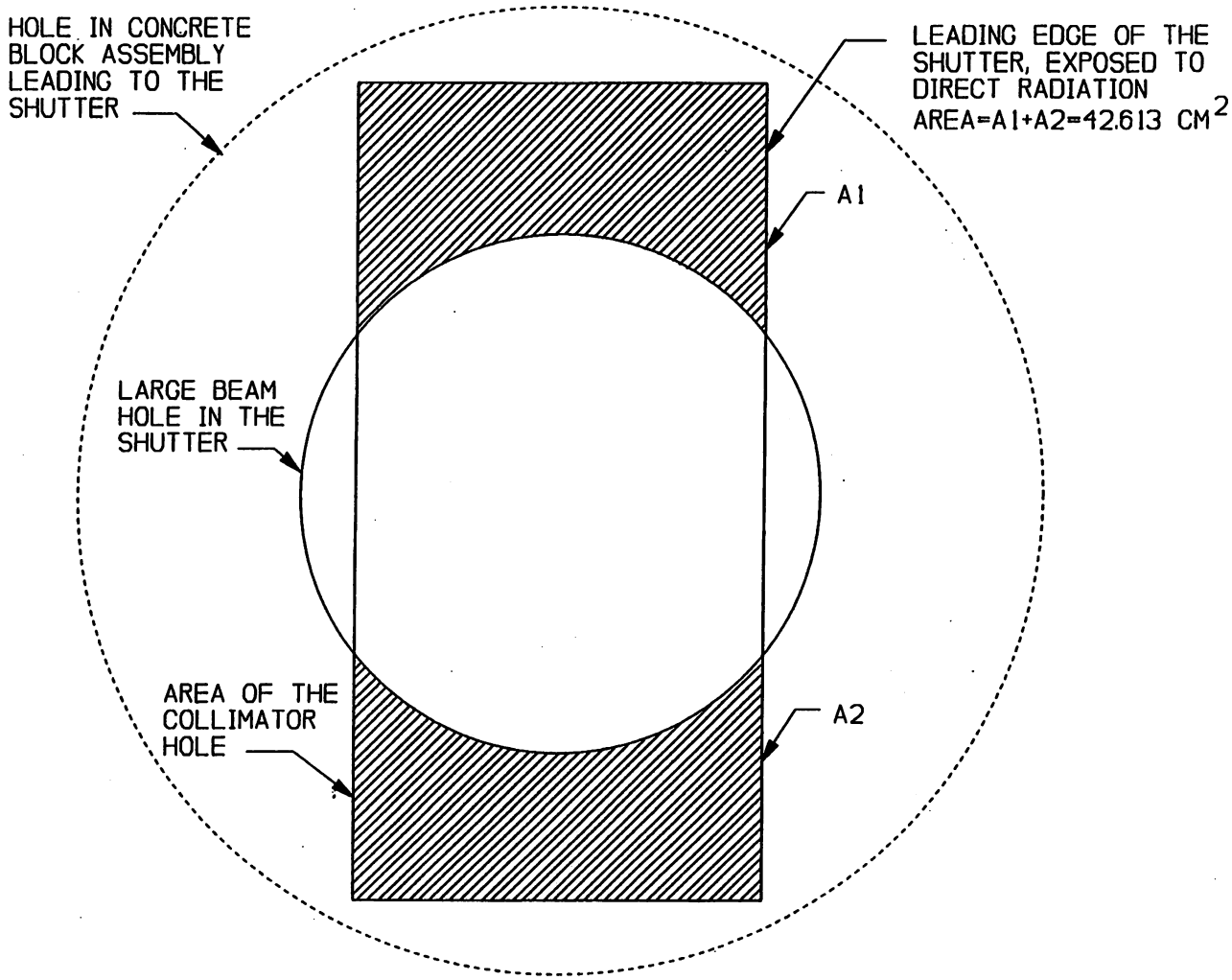


Fig. 7.4. Portion of the rotary shutter, beyond the 3.5-inch-diam beam hole, that is directly exposed to the highly collimated neutron beam coming from the 2.75-inch x 5.5-inch rectangular hole in the collimator under normal operating conditions.

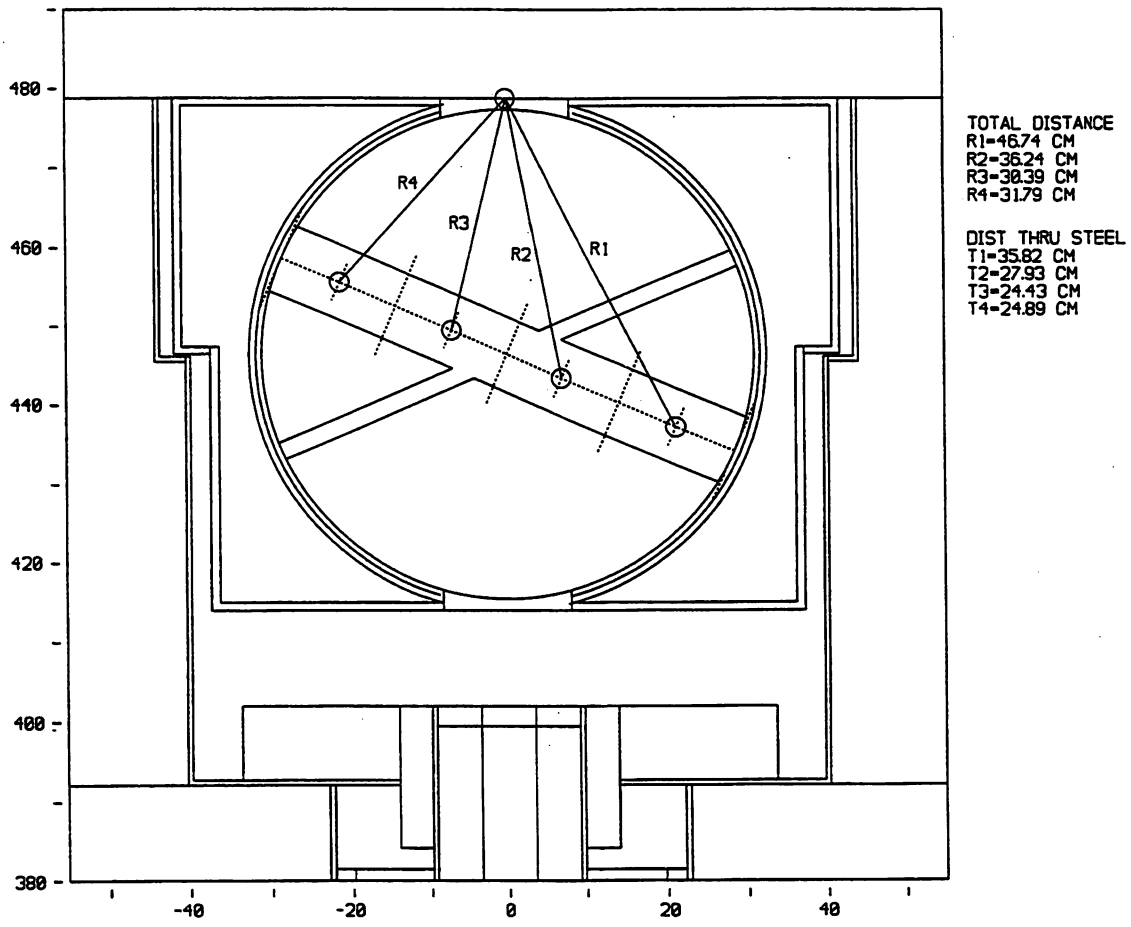


Fig. 7.5. An elementary point source representation of the activation sources in the rotary shutter that proved woefully inadequate for representing the actual spatial distribution of the decay gamma sources, and could lead to very misleading estimates of the activation dose rate downstream of the shutter. See discussion in main text.

Table 7.10. Results of radiological survey HFIR-98-1712 in the region downstream of the HB-3 rotary shutter after shutdown (Feb 1998).

Subject: HB-3 radiological survey
To: Jim Bucholz
From: Roger L. Davis
Date: Wed, 24 Jun 1998 09:50:44

Jim, here is the survey data that you requested.
I highlighted the actual cavity survey in red.

Survey No. HFIR-98-1712
Date: 2/20/98
Time: 14:52
Building: 7900
Location: Beam Room at HB-3
Descr: Contamination and Radiation survey upon removal of saddle shield from HB-3.
Radiological Conditions: The reactor is shutdown.

The Max dose rate found on the saddle shield block on the side that faces the reactor is 280 mr/hr on contact, and 18 mr/hr at 30 cm.

--> Max dose rate inside the cavity where the beam tube and crystal are located is
--> 50 mr/hr contact, and 20 mr/hr at 1 foot, general area of 15 mr/hr.

Max dose rate on the drum (between the saddle shield and the drum) is 50/12 mr/hr.

Max dose rate on the saddle shield (on the side facing the drum) is 60/15 mr/hr.

All LAS's in the troughs, on the drum and saddle shield, and on all accessible surfaces NDGMT.

LAS inside the beam port on the saddle shield = 30,000 dpm beta/gamma.

I will send you a paper copy of the actual survey by plant mail.
If you have any other questions feel free to call me.

Roger L. Davis
Office of Radiation Protection
HP Complex Leader, Research Reactors

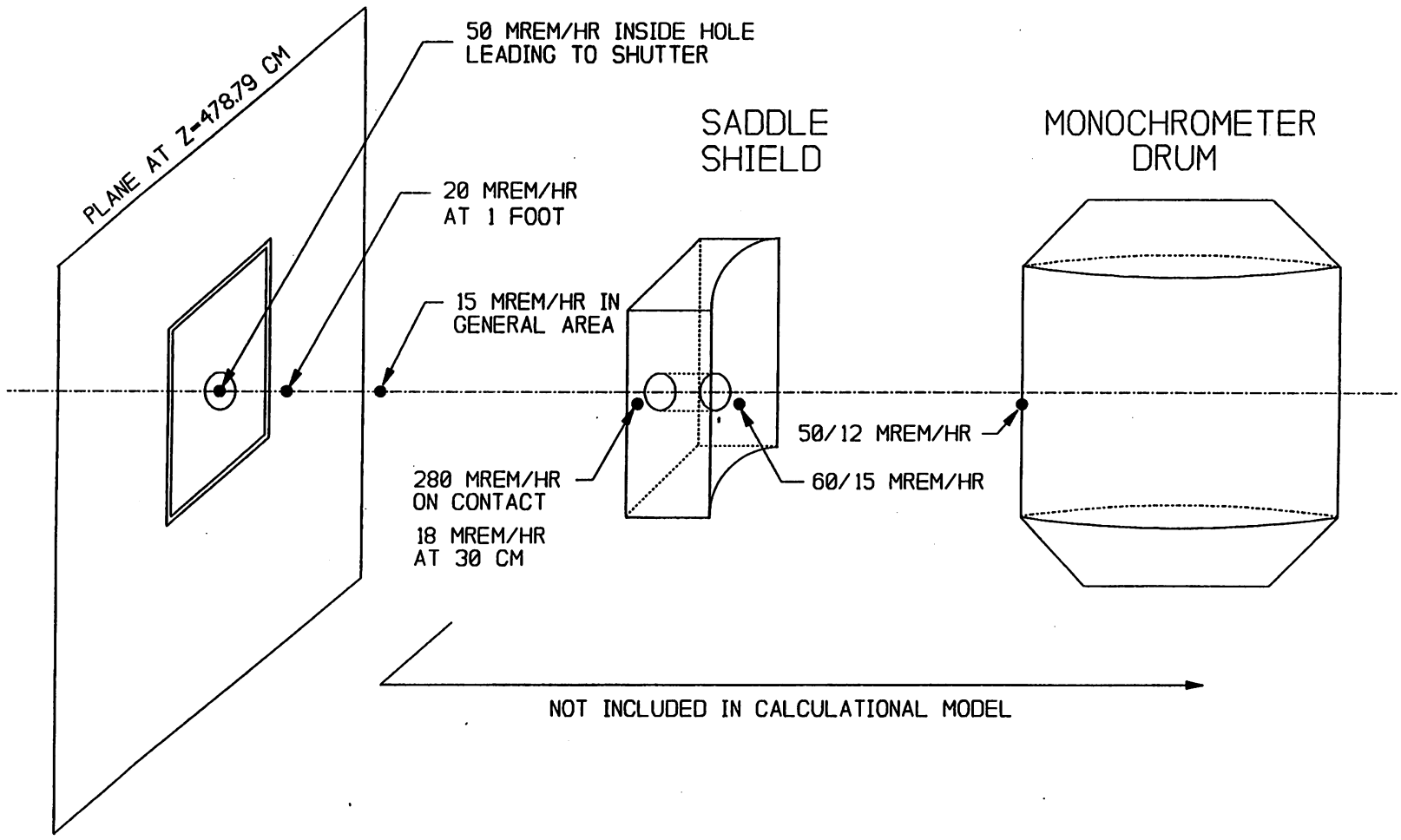


Fig. 7.6. Location of experimentally measured activation dose rates after shutdown. See Table 7.10 for a copy of the memo describing the actual measurements made on Feb 20, 1998.

c) Given that (1) the amount of activation is independent of the water tube design [since activation occurs under nominal conditions when the water tube is void], and that (2) the portion of the dose rate here due radiation streaming down the beam tube, through the flooded 1998 water tube and collimator sections, and through the closed shutter, is less than 1 mrem/hr when the HFIR is operating at 100 MW [cf Sect 6.11], one is forced to conclude that the total dose rate here, under these conditions, will be essentially unaffected by the newly proposed design changes.

The remaining dose rates described in Table 7.10 and illustrated in Fig. 7.6 are certainly of general interest, but cannot be directly compared to anything in this analytic study since the monochrometer drum and saddle shield (both downstream of the rotary shutter) were not included in the calculational model. Moreover, even the experimentally measured dose rate of 20 mrem/hr at 1 foot from the downstream surface of the concrete block assembly holding the rotary shutter (ie, 1 foot downstream of the surface at Z=478.79 cm) cannot and should not be directly compared against values in Table 7.6. In the analytic study, everything downstream of Z=478.79 cm was ignored and treated as void, and the only activation sources considered were those in the rotary shutter itself. Thus, except for radiation coming from the shutter itself, the general area background radiation would have been zero in this model. Even so, the calculated dose rate 1.5 feet from the plane at Z=478.79 cm was 5.597 mrem/hr +/- 0.41%, while the calculated dose rate 3.0 feet from this plane was 2.108 mrem/hr +/-0.25%. With the activated monochrometer drum and/or saddle shield present at the time the measurements were made, the general area background radiation was measured and found to be about 15 mrem/hr while the dose rate 1 foot from the plane at Z=478.79 cm was found to be 5 mrem/hr higher (ie, 20 mrem/hr). While this increase is highly consistent with the calculated value at 1.5 feet from the plane, direct comparisons should probably not be made since it is not exactly clear where this "general area background radiation" was measured or where (exactly) the saddle shield or monochrometer drum were located at the time the measurements were made. Nevertheless, given the excellent comparisons between the calculated and measured dose rates within 1 or 2 cm of the shutter itself, it is reasonable to believe that similarly good results could have been obtained on the surface of the saddle shield and/or monochrometer drum had similar activation analyses been performed for those components.

7.6 Parametric Variations as a Function of Initial Cobalt Content

The key results and conclusions of this activation study are summarized in Sect 7.4.2 and Sect 7.5, respectively. The parametric variations reported here in Sect 7.6 represent a few small extensions that were requested to aid in developing specifications for possible future procurements.

Shortly after the completion of this study in early July 1998, it was announced that new rotary shutter shield plugs, perhaps with only one rectangular beam hole instead of the two circular beam holes, might be ordered and manufactured for the HFIR Upgrade Program. As such, there was some interest in knowing how much the activation dose rate downstream of the shutter could be reduced after shutdown if the shutter were made with a low-activation steel having little or no Co-59 initially in the steel. (Note that even if there was no cobalt initially present, Fig. 7.1 shows that a small amount of Co-59 and Co-60 would still be generated from the iron during irradiation, and that activated decay gammas resulting from the production of Fe-59 would also be inevitable.) So that a cost/benefit study could be undertaken by RRD staff prior to procurement, a series of activation studies were undertaken using small variations of the previously described activation program (ACTSRC.FOR) listed in Appendix E.2. In these cases, the initial Co-59 concentration was varied from 0.005 wt% to 0.030 wt% in increments of 0.005 wt%; initial Co-59 concentrations of 0.001 wt% and 0.000 wt% were also included as limiting cases. In each case, the 12 key reaction rates (per unit atom density), in each of the 39 1-cm-thick shells around the large beam hole in the shutter, were assumed to the be same as those shown in Table 7.2.

Table 7.11 shows the results of these activation studies. In particular, it shows the total equivalent gamma source (photons/sec at 1.25 MeV, seven days after shutdown) in each of the 39 1-cm-thick shells around the large beam hole in the shutter as a function of the amount (wt%) of Co-59 initially present in the steel. While no new shielding calculations were performed to determine the actual dose rates downstream of the shutter, one can estimate the relative dose rates by comparing the total source terms (p/s) shown in Table 7.11 against those for the reference case which yielded a dose rate of 43 mrem/hr and had 0.015 wt% Co-59 initially present in the steel. The following are a few casual observations based on Table 7.11:

1) With 0.030 wt% Co-59 initially in the steel, the total source in the 1-cm-thick cylindrical shell closest to the big hole (shell 1) would be 5.845E+9 p/s at 1.25 MeV at 7 days after shutdown, while with 0.015 wt% Co-59 initially in the steel, it would be 3.262E+9 p/s, and with no Co-59 initially in the steel, it would be 6.788E+8 p/s.

2) Instead of looking at only the activation in just the first (innermost) shell where the activation is highest, one should also look at the activation levels 10 to 15 cm further out since, by virtue of their location, they may actually contribute more to the dose rate downstream of the shutter. Fortunately, those activation levels are "almost" directly proportional to activation level in the first shell except at very low initial Co-59 concentrations (0.000 wt% and 0.001 wt%) where some

Table 7.11. Total volume-integrated equivalent gamma source (p/s at 1.25 MeV) in each of the 39 cylindrical shells around the 3.5-inch hole in the rotary shutter, 7 days after shutdown, as a function of the initial Co-59 concentration (wt%) in the steel.

	Rmin (cm)	Rmax (cm)	VOL (cc)	Initial Co-59 concentration (wt%) in the steel forming the rotary shutter							
				0.000 wt% (p/s)	0.001 wt% (p/s)	0.005 wt% (p/s)	0.010 wt% (p/s)	0.015 wt% (p/s)	0.020 wt% (p/s)	0.025 wt% (p/s)	0.030 wt% (p/s)
Shell 1	4.445	5.445	1.89858e+03	6.788e+08	8.510e+08	1.540e+09	2.401e+09	3.262e+09	4.123e+09	4.984e+09	5.845e+09
Shell 2	5.445	6.445	2.27981e+03	5.787e+08	7.239e+08	1.305e+09	2.031e+09	2.757e+09	3.483e+09	4.209e+09	4.936e+09
Shell 3	6.445	7.445	2.65511e+03	5.017e+08	6.295e+08	1.140e+09	1.779e+09	2.418e+09	3.056e+09	3.695e+09	4.333e+09
Shell 4	7.445	8.445	3.02744e+03	2.906e+08	3.744e+08	7.099e+08	1.129e+09	1.548e+09	1.968e+09	2.387e+09	2.806e+09
Shell 5	8.445	9.445	3.39342e+03	1.715e+08	2.272e+08	4.501e+08	7.287e+08	1.007e+09	1.286e+09	1.564e+09	1.843e+09
Shell 6	9.445	10.445	3.75537e+03	1.240e+08	1.670e+08	3.387e+08	5.534e+08	7.681e+08	9.828e+08	1.197e+09	1.412e+09
Shell 7	10.445	11.445	4.11116e+03	8.324e+07	1.177e+08	2.555e+08	4.278e+08	6.000e+08	7.723e+08	9.445e+08	1.117e+09
Shell 8	11.445	12.445	4.45690e+03	6.477e+07	9.340e+07	2.079e+08	3.510e+08	4.942e+08	6.373e+08	7.804e+08	9.236e+08
Shell 9	12.445	13.445	4.79709e+03	5.624e+07	7.969e+07	1.735e+08	2.907e+08	4.079e+08	5.251e+08	6.423e+08	7.596e+08
Shell 10	13.445	14.445	5.12661e+03	4.072e+07	6.279e+07	1.511e+08	2.614e+08	3.718e+08	4.822e+08	5.925e+08	7.029e+08
Shell 11	14.445	15.445	5.44592e+03	3.312e+07	5.214e+07	1.282e+08	2.233e+08	3.185e+08	4.136e+08	5.087e+08	6.038e+08
Shell 12	15.445	16.445	5.75543e+03	3.810e+07	5.343e+07	1.148e+08	1.914e+08	2.681e+08	3.448e+08	4.215e+08	4.981e+08
Shell 13	16.445	17.445	6.05497e+03	4.684e+07	6.047e+07	1.150e+08	1.831e+08	2.513e+08	3.194e+08	3.876e+08	4.557e+08
Shell 14	17.445	18.445	6.33840e+03	3.236e+07	4.383e+07	8.969e+07	1.470e+08	2.043e+08	2.617e+08	3.190e+08	3.763e+08
Shell 15	18.445	19.445	6.60982e+03	2.099e+07	3.174e+07	7.470e+07	1.284e+08	1.821e+08	2.358e+08	2.896e+08	3.433e+08
Shell 16	19.445	20.445	6.86725e+03	1.908e+07	2.792e+07	6.325e+07	1.074e+08	1.516e+08	1.958e+08	2.399e+08	2.841e+08
Shell 17	20.445	21.445	7.10540e+03	3.311e+07	4.185e+07	7.680e+07	1.205e+08	1.642e+08	2.079e+08	2.516e+08	2.953e+08
Shell 18	21.445	22.445	7.32554e+03	1.707e+07	2.399e+07	5.166e+07	8.625e+07	1.208e+08	1.554e+08	1.900e+08	2.246e+08
Shell 19	22.445	23.445	7.53004e+03	1.099e+07	1.761e+07	4.409e+07	7.718e+07	1.103e+08	1.434e+08	1.765e+08	2.096e+08
Shell 20	23.445	24.445	7.70707e+03	1.988e+07	2.649e+07	5.290e+07	8.592e+07	1.189e+08	1.520e+08	1.850e+08	2.180e+08
Shell 21	24.445	25.445	7.85115e+03	8.748e+06	1.446e+07	3.729e+07	6.583e+07	9.437e+07	1.229e+08	1.515e+08	1.800e+08
Shell 22	25.445	26.445	7.96738e+03	9.695e+06	1.402e+07	3.130e+07	5.291e+07	7.451e+07	9.612e+07	1.177e+08	1.393e+08
Shell 23	26.445	27.445	8.04809e+03	1.058e+07	1.600e+07	3.768e+07	6.478e+07	9.188e+07	1.190e+08	1.461e+08	1.732e+08
Shell 24	27.445	28.445	8.08235e+03	1.001e+07	1.435e+07	3.169e+07	5.336e+07	7.504e+07	9.671e+07	1.184e+08	1.401e+08
Shell 25	28.445	29.445	8.05935e+03	9.830e+06	1.307e+07	2.601e+07	4.219e+07	5.838e+07	7.456e+07	9.074e+07	1.069e+08
Shell 26	29.445	30.445	7.95535e+03	7.450e+06	1.051e+07	2.275e+07	3.806e+07	5.336e+07	6.866e+07	8.397e+07	9.927e+07
Shell 27	30.445	31.445	6.44147e+03	3.781e+06	6.668e+06	1.822e+07	3.266e+07	4.709e+07	6.153e+07	7.597e+07	9.041e+07
Shell 28	31.445	32.445	4.99352e+03	2.018e+06	4.090e+06	1.238e+07	2.274e+07	3.310e+07	4.347e+07	5.383e+07	6.419e+07
Shell 29	32.445	33.445	4.08671e+03	2.105e+06	3.209e+06	7.625e+06	1.314e+07	1.866e+07	2.418e+07	2.970e+07	3.522e+07
Shell 30	33.445	34.445	3.36986e+03	3.060e+06	3.680e+06	6.162e+06	9.263e+06	1.237e+07	1.547e+07	1.857e+07	2.167e+07
Shell 31	34.445	35.445	2.76096e+03	1.113e+06	1.922e+06	5.159e+06	9.206e+06	1.325e+07	1.730e+07	2.135e+07	2.539e+07
Shell 32	35.445	36.445	2.23160e+03	7.889e+05	1.520e+06	4.442e+06	8.096e+06	1.175e+07	1.540e+07	1.906e+07	2.271e+07
Shell 33	36.445	37.445	1.76511e+03	2.630e+05	1.079e+06	4.345e+06	8.428e+06	1.251e+07	1.659e+07	2.067e+07	2.476e+07
Shell 34	37.445	38.445	1.35264e+03	1.592e+06	1.922e+06	3.241e+06	4.890e+06	6.539e+06	8.188e+06	9.837e+06	1.149e+07
Shell 35	38.445	39.445	9.88281e+02	1.290e+05	6.946e+05	2.957e+06	5.785e+06	8.613e+06	1.144e+07	1.427e+07	1.710e+07
Shell 36	39.445	40.445	6.71165e+02	6.178e+04	2.481e+05	9.931e+05	1.924e+06	2.856e+06	3.787e+06	4.719e+06	5.650e+06
Shell 37	40.445	41.445	4.01009e+02	2.706e+04	3.376e+04	6.058e+04	9.410e+04	1.276e+05	1.611e+05	1.947e+05	2.282e+05
Shell 38	41.445	42.445	1.86544e+02	6.283e+03	7.952e+03	1.463e+04	2.297e+04	3.131e+04	3.965e+04	4.800e+04	5.634e+04
Shell 39	42.445	43.443	3.97575e+01	4.181e+02	5.254e+02	9.547e+02	1.491e+03	2.028e+03	2.564e+03	3.101e+03	3.638e+03

Note: The radii shown here defining these 39 concentric cylindrical shells are measured from the centerline of the 3.5-inch-diam hole in the rotary shutter, while the volumes shown correspond to the actual amount of steel in the rotary shutter that lies within each of these shells. Because the shutter has a vertical axis and the beam hole has a horizontal axis, the outermost shells just "clip the corners" of the rotary shutter, and the corresponding amount of steel actually in these shells is relatively small. The sources all lie in the steel portion(s) of these shells. Assumed irradiation period prior to shutdown was 30 years.

small non-linearities do start to become apparent due to the increased relative importance of the buildup chains shown in Fig. 7.1.

3) For most initial cobalt concentrations of interest (between 0.005 wt% and 0.030 wt%), the gamma sources vary almost linearly with the amount of Co-59 initially present:

   a) For the reference case with 0.015 wt% Co-59 initially present, the resulting dose rate immediately downstream of the shutter was about 43 mrem/hr.

   b) From Table 7.11, it is clear that if the amount of Co-59 initially present were 2.0 times higher (ie, 0.030 wt%), the total gamma source would be 1.8 to 1.9 times higher, while

   c) If the amount of Co-59 initially present were 3.0 times lower (ie, 0.005 wt%), the total gamma source rate would be 2.2 to 2.4 times lower.

4) For very low initial Co-59 concentrations (0.000 wt% and 0.001 wt%), the relationship is no longer linear:

   a) If the initial amount of Co-59 is reduced by a factor of 15 (from 0.015 wt%, down to 0.001 wt%), the total gamma source would only be 4 to 5 times lower, while

   b) If the initial Co-59 is reduced to zero, the total gamma source would be about 5 to 8 times lower than for the case with 0.015 wt% Co-59.

Given that the reference case of 0.015 wt% Co-59 initially present in the steel yields a contact dose rate of only 43 mrem/hr (7 days after shutdown, subsequent to operating for 30 years), paying a steep premium to be overly restrictive on the material specifications may not be worthwhile. Indeed, it would likely make little sense unless the saddle shield were also replaced by a low-activation steel.

7.7 Conclusions Regarding the Activation Analysis and All Other Shielding Calculations in This Report

Assuming an initial Co-59 concentration of 0.015 wt% initially in the steel forming the rotary shutter shield plug, decay gamma source terms from activation of the shutter itself were calculated for various decay times, including 7 days after shutdown, following 30 years of continuous operation. After the first day or two, shortlived sources from the decay of Mn-56 are essentially gone. With halflives of 312.2 days, 44.51 days, and 5.271 years, for Mn-54, Fe-59, and Co-60, respectively, the remaining decay gamma source terms and resulting dose rates change very slowly over the next few weeks. The dose rate 7 days after shutdown was therefore taken as a representative time. Of the radioactive sources, Co-60 is the most important (by far). During the first few weeks or months, Fe-59 is the next most important, with the Mn-54 being a distant third.

Calculated dose rates 1.43 cm and 1.93 cm downstream of the rotary shutter, due to activation of the shutter alone, were 43.16 and 42.78 mrem/hr, respectively. This is in good to excellent agreement with the experimentally measured contact dose rate of 50 mrem/hr, as measured during the Feb 1998 shutdown.

This dose rate due to activation would be present whenever the shutter is closed, whether the HFIR is operating or not. Because this inherent activation of the shutter is the result of neutrons streaming down the beam tube during years of normal operation when the water tube is normally void, the intensity of this activation source and the resulting dose rate (43 mrem/hr) will be independent of water tube design (ie, it will be essentially the same whether one switches to the new 1998 design or continues to use the original 1960 design).

More importantly, this dose rate due to activation alone (43-50 mrem/hr) is far greater than the 0.8934 mrem/hr (cf Sect 6) that results from direct transmission of radiation down the beam tube and through the shutter when the new (shorter) 1998 water tube and collimator sections are both flooded, the shutter is closed, and the HFIR is operating at 100 MW.

For these reasons, one is forced to conclude that the total dose rate downstream of the shutter, under these conditions, will remain in the 43-50 mrem/hr range and will be independent of water-tube design (ie, it will be essentially the same whether one switches to the new 1998 design or continues to use the original 1960 design). That is the main conclusion of this entire report.

Other miscellaneous observations and conclusions related to the activation study include the following:

Fabricating new rotary shutters with a type of steel with absolutely no cobalt initially present would likely reduce the activation dose rate by a factor of 5 to 8, but the availability of such a steel is questionable and may not be worth the additional cost even if it were available. This would have to be evaluated prior to procurement. Carbon steel with as little as 0.005 wt% cobalt has been available in the past and, in fact, corresponds to the measured cobalt content in the HB-1 and HB-4 vessel nozzles (see pp. 106 of Ref 6). If still available, use of such a material in the new rotary shutter shield plugs would likely reduce the activation dose by about a factor of 2.2 or 2.4.

Switching to a new rotary shutter design which only has one beam hole and could therefore be turned 90 degrees when closed (rather than 66.75 degrees as in the present design) will, in fact, reduce the dose rate somewhat, although the extent of that decrease has not been evaluated.

REFERENCES

1. R. D. Cheverton and T. M. Sims, "HFIR Core Nuclear Design," ORNL-4621 (July 1971).

2. D. L. Selby et al., "High Flux Isotope Reactor Cold Neutron Source Reference Design Concept," ORNL/TM-13498 (May 1998).

3. J. A. Bucholz, "HFIR Upgrade Reflector Impact on Core Nuclear Performance," RRD Calc C-HFIR-97-25, ORNL (Sept 30, 1997).

4. J. F. Briesmeister, Ed, "MCNP - A General Monte Carlo N-Particle Transport Code, Version 4B," LA-12625-M Vers 4B, Los Alamos National Laboratory (March 1997); Code is available from the Radiation Shielding Information Center at ORNL as Code Package CCC-660 (April 1997).

5. T. V. Blosser and G. E. Thomas, Jr., "Neutron Flux and Neutron and Gamma Ray Spectra Measurements at the HFIR, USAEC Report ORNL-TM-2221 (June 1968).

6. R. D. Cheverton, J. G. Merkle, and R. K. Nanstad, "Evaluation of HFIR Pressure-Vessel Integrity Considering Radiation Embrittlement," ORNL/TM-10444 (April 1988).

7. W. A. Rhoades and R. L. Childs, "The DORT Two-Dimensional Discrete Ordinate Transport Code," Nuclear Science and Engineering, Vol 99, pp 88 (May 1988); Version 2.12.14 of DORT is available from the Radiation Shielding Information Center at ORNL as part of Code Package CCC-543 (Jan 1995).

8. W. A. Rhoades and R. L. Childs, "TORT: A Three-Dimensional Discrete Ordinates Neutron/Photon Transport Code," Nuclear Science and Engineering, Vol 107, pp 397 (April 1991); Version 2.12.14 of TORT is available from the Radiation Shielding Information Center at ORNL as part of Code Package CCC-543 (Jan 1995).

9. R. L. Childs and D. E. Cullen, "GBANISN: One-Dimensional Discrete Ordinates Transport Code System with Anisotropic Scattering, with the Group-Band Option," available from the Radiation Shielding Information Center at ORNL as Code Package CCC-628 (July 1995).

10. C. Y. Fu and D. T. Ingersoll, "VELM61 and VELM22: Multigroup Cross-Section Libraries for Sodium-Cooled Reactor Shield Analysis," ORNL/TM 10302 (April 1987).

11. R. L. Davis, "HFIR Radiation Survey No. HFIR-98-1712 around HB-3, February 20, 1998," as contained in personal correspondence to J. A. Bucholz (June 24, 1998).

12. A. T. Lucas, "Cold Source Reference Design," Paper 3 in the Proceedings of the "HFIR Cold Source Project Review," at the Oak Ridge National Lab, Oak Ridge, TN, May 29-30, 1997.

13. J. A. Bucholz, "Physics Analysis," Paper 2 in the Proceedings of the "HFIR Cold Source Project Review," at the Oak Ridge National Lab, Oak Ridge, TN, May 29-30, 1997.

14. D. R. Vondy, T. B. Fowler, and G. W. Cunningham, III, "The Bold Venture Computation System for Nuclear Reactor Core Analysis, Version III," ORNL-5711 (June 1981).

15. R. T. Primm, III, "Reactor Physics Input to the Safety Analysis Report for the High Flux Isotope Reactor," ORNL/TM-11956 (March 1992).

16. J. A. Bucholz, "C/E Dosimetry Results for HB-2, Using a Finite Line Source in MCNP Run GF208," personal correspondence to J. V. Pace, III (Oct 22, 1997).

17. C. A. Baldwin, "HFIR Surveillance Dosimeters, Request No. 2323 Datasheet, dated Nov. 18, 1986," forwarded as personal communication to J. A. Bucholz in April 1998.

18. J. R. McWherter et al., "HFIR Pressure Vessel and Structural Components Surveillance Program," ORNL-TM-1372 (January 1966).

19. M. E. Battat et al., "American National Standard Neutron and Gamma-Ray Flux-to-Dose-Rate Factors," ANSI/ANS-6.1.1-1977, pub by the American Nuclear Society (March 1997).

20. D. K. Trubey and V. R. Cain, "QAD-CGGP: A Combinatorial Geometry Version of QAD-P5A, A Point Kernel Code System for Neutron and Gamma-Ray Shielding Calculations Using the GP Buildup Factors," available from the Radiation Shielding Information Center at ORNL as Code Package CCC-493 (July 1986).

21. T. M. Evans and J. M. Hendricks, "An Enhanced Geometry-Independent Mesh Weight Window Generator for MCNP," page I-165 of the "1998 ANS Radiation Protection and Shielding Division Topical Conference on Technologies for the New Century," in Nashville, Tennessee (April 19-23, 1998).

22. S. Glasstone and A. Sesonske, "Nuclear Reactor Engineering," pub. by Van Nostrand Co. (1967 ed).

23. T. M. Evans, "AVATAR (Patch Verification)," Los Alamos Internal Memo XTM:TME-97-133(U), from T. M. Evans to John Hendricks, dated May 22, 1997.

24. W. A. Rhoades, "The GIP Program for Preparation of Group-Organized Cross Section Libraries," described on pp. 53-56 of the "AXMIX: ANISN Cross Section Code" document, available from the Radiation Shielding Information Center at ORNL as Code Package PSR-75 (Oct 1984).

25. J. S. Tang and T. J. Hoffman, "Monte Carlo Shielding Analyses Using an Automated Biasing Procedure," pp 329-342, Vol 99, Nuclear Science and Engineering (1988).

26. R. E. Alcouffe et al., "THREEDANT: A Code Package for Three-Dimensional, Diffusion-Accelerated, Neutral-Particle Transport," as contained in Sect 6 of "DANTSYS: A Diffusion-Accelerated Neutral-Particle Transport Code System," Los Alamos Report LA-12969-M (June 1995), available from the Radiation Shielding Information Center at ORNL as Code Package CCC-547 (March 1997).

27. K. A. Van Riper, T. J. Urbatsch, et al., "AVATAR: Automatic Variance Reduction in Monte Carlo Calculations," Los Alamos Report LA-UR-97-919, presented at the "Joint International Conference on Mathematical Methods and Supercomputing in Nuclear Applications" (CONF-971005-10) in Saratoga Springs, NY (Oct 6-10, 1997).

28. J. C. Villforth and G. R. Shultz, "Radiological Health Handbook," compiled by the U.S. Bureau of Radiological Health, Public Health Service, and published by the U.S. Department of Health, Education, and Welfare (January 1970).

29. F. W. Walker, J. R. Parrington, and F. Feiner, "Nuclides and Isotopes" (Chart of the Nuclides), Fourteenth Edition, pub. by General Electric Co. (1989).

30. M. R. Ford et al., "Radionuclide Transformations: Energy and Intensity of Emissions," pub. by Pergamon Press for the International Commission on Radiological Protection, as ICRP Publication 38 (1983).

31. T. Baumeister, Ed., "Marks' Standard Handbook for Mechanical Engineers," Eighth Edition, pub. by McGraw-Hill Book Co (1978).

32. O. W. Hermann and R. M. Westfall, "ORIGEN-S: SCALE System Module to Calculate Fuel Depletion, Actinide Transmutation, Fission Product Buildup and Decay, and Associated Radiation Source Terms," as contained in Vol. 2, Sect. F7 of "SCALE: A Modular Code System for Performing Standardized Computer Analyses for Licensing Evaluation," ORNL/NUREG/CSD-2/V2/R5 (March 1997).

Additional References Cited in the Various Appendices

33. J. C. Wagner, "A3MCNP - Automatic Adjoint Accelerated MCNP," as described on the following web page: http://gracie.psu.edu/~wagner/research/a3mcnp/Research_a3mcnp.html (Dec 1997).

34. J. C. Wagner, "Acceleration of Monte Carlo Shielding Calculations with an Automated Variance Reduction Technique and Parallel Processing," PhD Thesis, Nuclear Engineering Dept, The Pennsylvania State University (1997).

35. J. C. Wagner and A. Haghighat, "Automatic Variance Reduction of Monte Carlo Shielding Calculations Using the Discrete Ordinates Adjoint Function," Nuclear Science and Engineering (Feb 1998).

36. J. A. Bucholz, "Design and Pre-Experimental Analysis of the Proposed Borated Pin-Array Experiments for the MHTGR," ORNL/NPR-92/1 (Jan 1992).

37. R. L. Childs, "GRTUNCL: A First Collision Source Program" (1982) for use with DORT, as described in Sect 5 of the "TORT-DORT, Two- and Three-Dimensional Discrete Ordinates Transport Code System, Version 2.12.14," available from the Radiation Shielding Information Center at ORNL as Code Package CCC-543 (Jan 1995).

Appendix A.1

Neutron and Gamma Source Terms in MCNP Format for Each Beam Tube

Section 2 describes the necessity of performing shielding analyses separately for each of the four beam tubes (HB-1,2,3,4), as opposed to trying to incorporate such analyses into one giant global model for the entire HFIR reactor system. Based on beam tube fluxes obtained from a series of large global analyses, Tables 2.2a and 2.2b describe the equivalent point sources that can be used to represent the neutron and gamma sources in these individual calculations. In an MCNP calculation, these source terms are represented by the SDEF card and the associated distribution functions. In a single calculation, one can only represent the neutron source "or" the gamma source within a single beam tube. The balance of Appendix A.1 shows explicitly how these source terms may be represented in an MCNP calculation for a single beam tube where the Z axis corresponds to the beam tube centerline, and Z=0.0 corresponds to the radial plane (extending out from the core) that is perpendicular to the beam tube centerline. In any given beam tube analysis one may retain any or all of the source distribution cards shown below, but only one of the 8 sdef cards shown below may be active in any given calculation.

```
sdef  erg=d51  pos ferg d61  $ source def for neutrons in HB-1
c       sdef  erg=d52  pos ferg d62  $ source def for neutrons in HB-2
c       sdef  erg=d53  pos ferg d63  $ source def for neutrons in HB-3
c       sdef  erg=d54  pos ferg d64  $ source def for neutrons in HB-4
c
c       sdef  erg=d71  pos ferg d81  $ source def for gammas in HB-1
c       sdef  erg=d72  pos ferg d82  $ source def for gammas in HB-2
c       sdef  erg=d73  pos ferg d83  $ source def for gammas in HB-3
c       sdef  erg=d74  pos ferg d84  $ source def for gammas in HB-4
c
c       ------------------------------------------------------------------------
c       Begin distributions needed to describe the neutron sources in the four beam tubes
c       ------------------------------------------------------------------------
si51  h  1.0000e-11  $ this one Emin(MeV), followed by Emax(MeV) for the 61 VELM neut grps (low to high E for MCNP):
         4.1399e-7    1.1253e-6    2.3824e-6    5.0435e-6    1.0677e-5    $ VELM n-groups 61, 60, 59, 58, 57,
         2.2603e-5    4.7851e-5    1.0130e-4    1.6702e-4    2.7536e-4    $ VELM n-groups 56, 55, 54, 53, 52,
         4.5400e-4    7.4852e-4    1.2341e-3    2.0347e-3    2.2487e-3    $ VELM n-groups 51, 50, 49, 48, 47,
         2.6126e-3    3.0354e-3    3.7074e-3    5.5308e-3    9.1188e-3    $ VELM n-groups 46, 45, 44, 43, 42,
         1.5034e-2    2.3579e-2    2.4788e-2    2.6058e-2    2.7000e-2    $ VELM n-groups 41, 40, 39, 38, 37,
         2.8501e-2    3.4307e-2    5.2475e-2    5.6562e-2    8.6517e-2    $ VELM n-groups 36, 35, 34, 33, 32,
         1.2277e-1    1.4996e-1    1.8316e-1    2.2371e-1    2.7324e-1    $ VELM n-groups 31, 30, 29, 28, 27,
         2.9452e-1    2.9721e-1    2.9849e-1    3.0197e-1    3.8774e-1    $ VELM n-groups 26, 25, 24, 23, 22,
         4.9787e-1    5.2340e-1    6.0810e-1    7.4274e-1    9.0718e-1    $ VELM n-groups 21, 20, 19, 18, 17,
         1.1080e+0    1.3534e+0    1.6530e+0    2.0190e+0    2.2313e+0    $ VELM n-groups 16, 15, 14, 13, 12,
         2.3457e+0    2.4660e+0    3.0119e+0    3.6788e+0    4.4933e+0    $ VELM n-groups 11, 10,  9,  8,  7,
         5.4881e+0    6.7032e+0    8.1873e+0    1.0000e+1    1.2214e+1    $ VELM n-groups  6,  5,  4,  3,  2,
         1.4918e+1                                                       $ VELM n-group   1
sp51  d     0.0  $ dummy 0, followed by neut src terms (n/s) for HB-1:
         5.31877e+16  1.32866e+15  8.60077e+14  8.45061e+14  7.81961e+14  $ VELM n-groups 61, 60, 59, 58, 57,
         8.06771e+14  7.62547e+14  7.57662e+14  5.20223e+14  4.87720e+14  $ VELM n-groups 56, 55, 54, 53, 52,
         5.07730e+14  5.17013e+14  4.80954e+14  4.33392e+14  6.66316e+13  $ VELM n-groups 51, 50, 49, 48, 47,
         1.60061e+14  1.08823e+14  1.68435e+14  3.29352e+14  3.59507e+14  $ VELM n-groups 46, 45, 44, 43, 42,
         4.57210e+14  3.67329e+14  5.62891e+13  5.39204e+13  4.22279e+13  $ VELM n-groups 41, 40, 39, 38, 37,
         7.80191e+13  2.18288e+14  2.32623e+14  5.36186e+13  4.18163e+14  $ VELM n-groups 36, 35, 34, 33, 32,
         2.42117e+14  2.56507e+14  1.86655e+14  1.79164e+14  2.47877e+14  $ VELM n-groups 31, 30, 29, 28, 27,
         9.40518e+13  7.91646e+12  4.33179e+12  9.72508e+12  2.83441e+14  $ VELM n-groups 26, 25, 24, 23, 22,
         2.71588e+14  6.25375e+13  1.69143e+14  2.16209e+14  2.17359e+14  $ VELM n-groups 21, 20, 19, 18, 17,
         3.00075e+14  2.46072e+14  2.62407e+14  1.96210e+14  7.75874e+13  $ VELM n-groups 16, 15, 14, 13, 12,
         2.95862e+13  2.69013e+13  6.93878e+13  5.41415e+13  4.48929e+13  $ VELM n-groups 11, 10,  9,  8,  7,
         2.62833e+13  9.85249e+12  3.53515e+12  1.08706e+12  3.99094e+11  $ VELM n-groups  6,  5,  4,  3,  2,
         3.08026e+09                                                     $ VELM n-group   1
ds61  l     $ neutron starting positions (x,y,z) in HB-1:
         0 0  72.3    0 0  54.0    0 0  54.8    0 0  52.3    0 0  54.8    $ VELM n-groups 61, 60, 59, 58, 57,
         0 0  50.1    0 0  51.6    0 0  51.5    0 0  47.5    0 0  49.7    $ VELM n-groups 56, 55, 54, 53, 52,
         0 0  49.8    0 0  44.9    0 0  46.9    0 0  52.2    0 0  56.6    $ VELM n-groups 51, 50, 49, 48, 47,
         0 0  44.7    0 0  64.4    0 0  46.0    0 0  45.9    0 0  57.5    $ VELM n-groups 46, 45, 44, 43, 42,
         0 0  42.4    0 0  50.5    0 0  36.6    0 0  48.1    0 0  42.4    $ VELM n-groups 41, 40, 39, 38, 37,
         0 0  36.0    0 0  41.4    0 0  39.0    0 0  50.6    0 0  45.1    $ VELM n-groups 36, 35, 34, 33, 32,
         0 0  47.7    0 0  45.5    0 0  35.6    0 0  55.0    0 0  48.7    $ VELM n-groups 31, 30, 29, 28, 27,
         0 0  41.3    0 0  52.3    0 0  38.2    0 0  43.2    0 0  45.3    $ VELM n-groups 26, 25, 24, 23, 22,
         0 0  52.4    0 0  39.2    0 0  49.6    0 0  52.1    0 0  60.0    $ VELM n-groups 21, 20, 19, 18, 17,
         0 0  42.6    0 0  51.4    0 0  50.8    0 0  48.7    0 0  44.1    $ VELM n-groups 16, 15, 14, 13, 12,
         0 0  44.0    0 0  46.1    0 0  48.9    0 0  55.1    0 0  45.3    $ VELM n-groups 11, 10,  9,  8,  7,
         0 0  64.4    0 0  56.0    0 0  52.9    0 0  58.3    0 0  39.7    $ VELM n-groups  6,  5,  4,  3,  2,
         0 0  79.2                                                        $ VELM n-group   1
c       ---------------------------------
si52  h  1.0000e-11  $ this one Emin(MeV), followed by Emax(MeV) for the 61 VELM neut grps (low to high E for MCNP):
         4.1399e-7    1.1253e-6    2.3824e-6    5.0435e-6    1.0677e-5    $ VELM n-groups 61, 60, 59, 58, 57,
         2.2603e-5    4.7851e-5    1.0130e-4    1.6702e-4    2.7536e-4    $ VELM n-groups 56, 55, 54, 53, 52,
         4.5400e-4    7.4852e-4    1.2341e-3    2.0347e-3    2.2487e-3    $ VELM n-groups 51, 50, 49, 48, 47,
         2.6126e-3    3.0354e-3    3.7074e-3    5.5308e-3    9.1188e-3    $ VELM n-groups 46, 45, 44, 43, 42,
         1.5034e-2    2.3579e-2    2.4788e-2    2.6058e-2    2.7000e-2    $ VELM n-groups 41, 40, 39, 38, 37,
         2.8501e-2    3.4307e-2    5.2475e-2    5.6562e-2    8.6517e-2    $ VELM n-groups 36, 35, 34, 33, 32,
         1.2277e-1    1.4996e-1    1.8316e-1    2.2371e-1    2.7324e-1    $ VELM n-groups 31, 30, 29, 28, 27,
         2.9452e-1    2.9721e-1    2.9849e-1    3.0197e-1    3.8774e-1    $ VELM n-groups 26, 25, 24, 23, 22,
         4.9787e-1    5.2340e-1    6.0810e-1    7.4274e-1    9.0718e-1    $ VELM n-groups 21, 20, 19, 18, 17,
         1.1080e+0    1.3534e+0    1.6530e+0    2.0190e+0    2.2313e+0    $ VELM n-groups 16, 15, 14, 13, 12,
         2.3457e+0    2.4660e+0    3.0119e+0    3.6788e+0    4.4933e+0    $ VELM n-groups 11, 10,  9,  8,  7,
         5.4881e+0    6.7032e+0    8.1873e+0    1.0000e+1    1.2214e+1    $ VELM n-groups  6,  5,  4,  3,  2,
         1.4918e+1                                                       $ VELM n-group   1
```

```
sp52  d     0.0  $ dummy 0, followed by neut src terms (n/s) for HB-2:
          1.27996e+17  4.56223e+15  3.25137e+15  2.82574e+15  3.12475e+15  $ VELM n-groups 61, 60, 59, 58, 57,
          2.91875e+15  2.95904e+15  2.82080e+15  1.88854e+15  1.73245e+15  $ VELM n-groups 56, 55, 54, 53, 52,
          1.84391e+15  1.75804e+15  1.77021e+15  1.83135e+15  3.38748e+14  $ VELM n-groups 51, 50, 49, 48, 47,
          4.86574e+14  5.09912e+14  6.79285e+14  1.48446e+15  1.74494e+15  $ VELM n-groups 46, 45, 44, 43, 42,
          1.76510e+15  1.62195e+15  1.61758e+14  1.93557e+14  1.22345e+14  $ VELM n-groups 41, 40, 39, 38, 37,
          2.74072e+14  6.93489e+14  1.13406e+15  2.45790e+14  1.70292e+15  $ VELM n-groups 36, 35, 34, 33, 32,
          1.13709e+15  9.30940e+14  8.76802e+14  1.06795e+15  1.19915e+15  $ VELM n-groups 31, 30, 29, 28, 27,
          4.36229e+14  4.40442e+13  2.08255e+13  5.38008e+13  1.80933e+15  $ VELM n-groups 26, 25, 24, 23, 22,
          1.52963e+15  4.24300e+14  1.07362e+15  1.59906e+15  1.70706e+15  $ VELM n-groups 21, 20, 19, 18, 17,
          2.01784e+15  2.02508e+15  3.11387e+15  3.79686e+15  1.67723e+15  $ VELM n-groups 16, 15, 14, 13, 12,
          8.22294e+14  7.86217e+14  1.84949e+15  1.79911e+15  2.01809e+15  $ VELM n-groups 11, 10,  9,  8,  7,
          1.55944e+15  9.82537e+14  5.63371e+14  2.48357e+14  7.93888e+13  $ VELM n-groups  6,  5,  4,  3,  2,
          1.09787e+13                                                     $ VELM n-group   1
ds62  l     $ neutron starting positions (x,y,z) in HB-2:
          0 0  93.7    0 0  80.1    0 0  79.0    0 0  76.1    0 0  73.6   $ VELM n-groups 61, 60, 59, 58, 57,
          0 0  73.9    0 0  71.9    0 0  76.9    0 0  76.5    0 0  75.9   $ VELM n-groups 56, 55, 54, 53, 52,
          0 0  67.6    0 0  71.4    0 0  67.6    0 0  66.1    0 0  77.8   $ VELM n-groups 51, 50, 49, 48, 47,
          0 0  78.3    0 0  68.6    0 0  68.4    0 0  70.0    0 0  71.9   $ VELM n-groups 46, 45, 44, 43, 42,
          0 0  66.5    0 0  61.6    0 0  62.9    0 0  73.3    0 0  75.0   $ VELM n-groups 41, 40, 39, 38, 37,
          0 0  63.7    0 0  67.0    0 0  65.8    0 0  69.3    0 0  67.0   $ VELM n-groups 36, 35, 34, 33, 32,
          0 0  73.2    0 0  76.3    0 0  67.6    0 0  66.1    0 0  73.8   $ VELM n-groups 31, 30, 29, 28, 27,
          0 0  70.1    0 0  80.0    0 0  52.3    0 0  77.1    0 0  64.6   $ VELM n-groups 26, 25, 24, 23, 22,
          0 0  68.4    0 0  64.7    0 0  75.6    0 0  70.6    0 0  72.1   $ VELM n-groups 21, 20, 19, 18, 17,
          0 0  64.9    0 0  69.8    0 0  68.9    0 0  62.2    0 0  58.8   $ VELM n-groups 16, 15, 14, 13, 12,
          0 0  61.6    0 0  54.6    0 0  56.4    0 0  56.4    0 0  56.4   $ VELM n-groups 11, 10,  9,  8,  7,
          0 0  53.4    0 0  54.3    0 0  37.5    0 0  37.2    0 0  50.3   $ VELM n-groups  6,  5,  4,  3,  2,
          0 0  34.5                                                       $ VELM n-group   1
c         ---------------------------------
si53  h   1.0000e-11  $ this one Emin(MeV), followed by Emax(MeV) for the 61 VELM neut grps (low to high E for MCNP):
          4.1399e-7    1.1253e-6    2.3824e-6    5.0435e-6    1.0677e-5   $ VELM n-groups 61, 60, 59, 58, 57,
          2.2603e-5    4.7851e-5    1.0130e-4    1.6702e-4    2.7536e-4   $ VELM n-groups 56, 55, 54, 53, 52,
          4.5400e-4    7.4852e-4    1.2341e-3    2.0347e-3    2.2487e-3   $ VELM n-groups 51, 50, 49, 48, 47,
          2.6126e-3    3.0354e-3    3.7074e-3    5.5308e-3    9.1188e-3   $ VELM n-groups 46, 45, 44, 43, 42,
          1.5034e-2    2.3579e-2    2.4788e-2    2.6058e-2    2.7000e-2   $ VELM n-groups 41, 40, 39, 38, 37,
          2.8501e-2    3.4307e-2    5.2475e-2    5.6562e-2    8.6517e-2   $ VELM n-groups 36, 35, 34, 33, 32,
          1.2277e-1    1.4996e-1    1.8316e-1    2.2371e-1    2.7324e-1   $ VELM n-groups 31, 30, 29, 28, 27,
          2.9452e-1    2.9721e-1    2.9849e-1    3.0197e-1    3.8774e-1   $ VELM n-groups 26, 25, 24, 23, 22,
          4.9787e-1    5.2340e-1    6.0810e-1    7.4274e-1    9.0718e-1   $ VELM n-groups 21, 20, 19, 18, 17,
          1.1080e+0    1.3534e+0    1.6530e+0    2.0190e+0    2.2313e+0   $ VELM n-groups 16, 15, 14, 13, 12,
          2.3457e+0    2.4660e+0    3.0119e+0    3.6788e+0    4.4933e+0   $ VELM n-groups 11, 10,  9,  8,  7,
          5.4881e+0    6.7032e+0    8.1873e+0    1.0000e+1    1.2214e+1   $ VELM n-groups  6,  5,  4,  3,  2,
          1.4918e+1                                                       $ VELM n-group   1
sp53  d     0.0  $ dummy 0, followed by neut src terms (n/s) for HB-3:
          6.30365e+16  2.25679e+15  1.52979e+15  1.30212e+15  1.55274e+15  $ VELM n-groups 61, 60, 59, 58, 57,
          1.58981e+15  1.54759e+15  1.45876e+15  9.03837e+14  9.69821e+14  $ VELM n-groups 56, 55, 54, 53, 52,
          9.50610e+14  8.74122e+14  8.53691e+14  8.87245e+14  2.04908e+14  $ VELM n-groups 51, 50, 49, 48, 47,
          2.76622e+14  2.54975e+14  3.36538e+14  7.55438e+14  8.76077e+14  $ VELM n-groups 46, 45, 44, 43, 42,
          9.84217e+14  7.42049e+14  6.69650e+13  1.12860e+14  5.24714e+13  $ VELM n-groups 41, 40, 39, 38, 37,
          1.21873e+14  3.03507e+14  4.96958e+14  1.29680e+14  8.89397e+14  $ VELM n-groups 36, 35, 34, 33, 32,
          5.59006e+14  4.29193e+14  3.63241e+14  4.33245e+14  7.35199e+14  $ VELM n-groups 31, 30, 29, 28, 27,
          2.12840e+14  1.38494e+13  7.68584e+12  3.65651e+13  6.29256e+14  $ VELM n-groups 26, 25, 24, 23, 22,
          5.85513e+14  1.49367e+14  3.61470e+14  5.35177e+14  6.65098e+14  $ VELM n-groups 21, 20, 19, 18, 17,
          5.40055e+14  7.09512e+14  8.07055e+14  8.54720e+14  3.12945e+14  $ VELM n-groups 16, 15, 14, 13, 12,
          2.00073e+14  1.35333e+14  2.41078e+14  1.61947e+14  2.06360e+14  $ VELM n-groups 11, 10,  9,  8,  7,
          1.36477e+14  7.32282e+13  3.05242e+13  8.64293e+12  6.92602e+12  $ VELM n-groups  6,  5,  4,  3,  2,
          2.74800e+09                                                     $ VELM n-group   1
ds63  l     $ neutron starting positions (x,y,z) in HB-3:
          0 0  80.2    0 0  57.3    0 0  65.2    0 0  76.1    0 0  54.5   $ VELM n-groups 61, 60, 59, 58, 57,
          0 0  48.2    0 0  56.5    0 0  55.4    0 0  56.0    0 0  51.1   $ VELM n-groups 56, 55, 54, 53, 52,
          0 0  53.8    0 0  52.6    0 0  61.2    0 0  60.5    0 0  43.0   $ VELM n-groups 51, 50, 49, 48, 47,
          0 0  49.5    0 0  55.0    0 0  65.1    0 0  53.3    0 0  52.7   $ VELM n-groups 46, 45, 44, 43, 42,
          0 0  50.7    0 0  54.0    0 0  69.0    0 0  46.7    0 0  62.6   $ VELM n-groups 41, 40, 39, 38, 37,
          0 0  67.5    0 0  79.8    0 0  52.9    0 0  56.7    0 0  47.4   $ VELM n-groups 36, 35, 34, 33, 32,
          0 0  45.7    0 0  45.6    0 0  42.5    0 0  48.9    0 0  34.2   $ VELM n-groups 31, 30, 29, 28, 27,
          0 0  42.4    0 0  63.8    0 0  53.7    0 0  42.3    0 0  49.6   $ VELM n-groups 26, 25, 24, 23, 22,
          0 0  58.8    0 0  52.9    0 0  50.3    0 0  56.8    0 0  44.1   $ VELM n-groups 21, 20, 19, 18, 17,
          0 0  70.1    0 0  46.8    0 0  59.7    0 0  50.2    0 0  52.1   $ VELM n-groups 16, 15, 14, 13, 12,
          0 0  33.3    0 0  43.5    0 0  65.3    0 0  56.9    0 0  47.9   $ VELM n-groups 11, 10,  9,  8,  7,
          0 0  62.6    0 0  59.5    0 0  42.9    0 0  68.7    0 0  31.1   $ VELM n-groups  6,  5,  4,  3,  2,
          0 0  99.9                                                       $ VELM n-group   1
c         ---------------------------------
si54  h   1.0000e-11  $ this one Emin(MeV), followed by Emax(MeV) for the 61 VELM neut grps (low to high E for MCNP):
```

```
        4.1399e-7    1.1253e-6    2.3824e-6    5.0435e-6    1.0677e-5    $ VELM n-groups 61, 60, 59, 58, 57,
        2.2603e-5    4.7851e-5    1.0130e-4    1.6702e-4    2.7536e-4    $ VELM n-groups 56, 55, 54, 53, 52,
        4.5400e-4    7.4852e-4    1.2341e-3    2.0347e-3    2.2487e-3    $ VELM n-groups 51, 50, 49, 48, 47,
        2.6126e-3    3.0354e-3    3.7074e-3    5.5308e-3    9.1188e-3    $ VELM n-groups 46, 45, 44, 43, 42,
        1.5034e-2    2.3579e-2    2.4788e-2    2.6058e-2    2.7000e-2    $ VELM n-groups 41, 40, 39, 38, 37,
        2.8501e-2    3.4307e-2    5.2475e-2    5.6562e-2    8.6517e-2    $ VELM n-groups 36, 35, 34, 33, 32,
        1.2277e-1    1.4996e-1    1.8316e-1    2.2371e-1    2.7324e-1    $ VELM n-groups 31, 30, 29, 28, 27,
        2.9452e-1    2.9721e-1    2.9849e-1    3.0197e-1    3.8774e-1    $ VELM n-groups 26, 25, 24, 23, 22,
        4.9787e-1    5.2340e-1    6.0810e-1    7.4274e-1    9.0718e-1    $ VELM n-groups 21, 20, 19, 18, 17,
        1.1080e+0    1.3534e+0    1.6530e+0    2.0190e+0    2.2313e+0    $ VELM n-groups 16, 15, 14, 13, 12,
        2.3457e+0    2.4660e+0    3.0119e+0    3.6788e+0    4.4933e+0    $ VELM n-groups 11, 10,  9,  8,  7,
        5.4881e+0    6.7032e+0    8.1873e+0    1.0000e+1    1.2214e+1    $ VELM n-groups  6,  5,  4,  3,  2,
        1.4918e+1                                                      $ VELM n-group   1
sp54  d    0.0  $ dummy 0, followed by neut src terms (n/s) for HB-4:
        4.52747e+16  9.92916e+14  7.22306e+14  6.83147e+14  6.71028e+14  $ VELM n-groups 61, 60, 59, 58, 57,
        6.52905e+14  6.53783e+14  6.46494e+14  4.03643e+14  3.61966e+14  $ VELM n-groups 56, 55, 54, 53, 52,
        3.81395e+14  3.70852e+14  3.56115e+14  3.27352e+14  6.72898e+13  $ VELM n-groups 51, 50, 49, 48, 47,
        8.59309e+13  1.00723e+14  1.17327e+14  2.72559e+14  3.16192e+14  $ VELM n-groups 46, 45, 44, 43, 42,
        3.03564e+14  2.97379e+14  6.36810e+13  3.81986e+13  2.60682e+13  $ VELM n-groups 41, 40, 39, 38, 37,
        4.67136e+13  1.35653e+14  1.83967e+14  5.45132e+13  3.09633e+14  $ VELM n-groups 36, 35, 34, 33, 32,
        2.16102e+14  1.59338e+14  1.26213e+14  1.69151e+14  2.03836e+14  $ VELM n-groups 31, 30, 29, 28, 27,
        6.34254e+13  8.20767e+12  2.48863e+12  8.16811e+12  2.52780e+14  $ VELM n-groups 26, 25, 24, 23, 22,
        2.34828e+14  5.15963e+13  1.53089e+14  2.04653e+14  2.12911e+14  $ VELM n-groups 21, 20, 19, 18, 17,
        2.40525e+14  2.56365e+14  2.15642e+14  2.01888e+14  7.15232e+13  $ VELM n-groups 16, 15, 14, 13, 12,
        2.86747e+13  2.56186e+13  7.37185e+13  6.39971e+13  4.25672e+13  $ VELM n-groups 11, 10,  9,  8,  7,
        4.06939e+13  1.97320e+13  4.80519e+12  1.11369e+12  5.13981e+12  $ VELM n-groups  6,  5,  4,  3,  2,
        3.25386e+10                                                    $ VELM n-group   1
ds64  l    $ neutron starting positions (x,y,z) in HB-4:
        0 0  86.8    0 0  64.8    0 0  61.0    0 0  49.9    0 0  48.5    $ VELM n-groups 61, 60, 59, 58, 57,
        0 0  58.6    0 0  46.9    0 0  49.5    0 0  45.3    0 0  49.7    $ VELM n-groups 56, 55, 54, 53, 52,
        0 0  50.9    0 0  46.4    0 0  46.6    0 0  46.5    0 0  53.9    $ VELM n-groups 51, 50, 49, 48, 47,
        0 0  59.1    0 0  40.2    0 0  51.5    0 0  47.3    0 0  44.9    $ VELM n-groups 46, 45, 44, 43, 42,
        0 0  44.2    0 0  43.9    0 0  10.0    0 0  40.0    0 0  51.5    $ VELM n-groups 41, 40, 39, 38, 37,
        0 0  23.0    0 0  48.6    0 0  49.1    0 0  29.3    0 0  49.6    $ VELM n-groups 36, 35, 34, 33, 32,
        0 0  47.3    0 0  51.8    0 0  51.2    0 0  41.2    0 0  42.1    $ VELM n-groups 31, 30, 29, 28, 27,
        0 0  63.7    0 0  21.1    0 0  46.2    0 0  45.4    0 0  45.3    $ VELM n-groups 26, 25, 24, 23, 22,
        0 0  45.6    0 0  42.5    0 0  53.7    0 0  54.4    0 0  49.6    $ VELM n-groups 21, 20, 19, 18, 17,
        0 0  42.6    0 0  43.5    0 0  54.9    0 0  52.8    0 0  59.8    $ VELM n-groups 16, 15, 14, 13, 12,
        0 0  48.2    0 0  52.9    0 0  71.1    0 0  62.3    0 0  68.7    $ VELM n-groups 11, 10,  9,  8,  7,
        0 0  73.9    0 0  59.2    0 0  63.6    0 0  50.0    0 0  51.4    $ VELM n-groups  6,  5,  4,  3,  2,
        0 0  10.0                                                        $ VELM n-group   1
c
c       ------------------------------------------------------------------------
c       Begin distributions needed to describe the gamma sources in the four beam tubes
c       ------------------------------------------------------------------------
si71  h  1.0000e-2   $ this one Emin(MeV), followed by Emax(MeV) for the 23 VELM gamma grps (low to high E for MCNP):
        2.0000e-2    4.5000e-2    7.0000e-2    1.0000e-1    1.5000e-1    $ VELM g-groups 23, 22, 21, 20, 19,
        3.0000e-1    4.0000e-1    5.1000e-1    6.0000e-1    7.0000e-1    $ VELM g-groups 18, 17, 16, 15, 14,
        1.0000e+0    1.5000e+0    2.0000e+0    2.5000e+0    3.0000e+0    $ VELM g-groups 13, 12, 11, 10,  9,
        4.0000e+0    5.0000e+0    6.0000e+0    7.0000e+0    7.5000e+0    $ VELM g-groups  8,  7,  6,  5,  4,
        8.0000e+0    1.0000e+1    1.4000e+1                              $ VELM g-groups  3,  2,  1
sp71  d    0.0  $ dummy 0, followed by gamma src terms (p/s) for HB-1:
        2.41702e+12  1.19589e+15  8.84390e+15  1.11793e+16  1.18909e+16  $ VELM g-groups 23, 22, 21, 20, 19,
        1.50947e+16  4.76182e+15  3.74129e+15  2.01818e+15  1.16662e+15  $ VELM g-groups 18, 17, 16, 15, 14,
        2.07064e+15  2.27631e+15  4.40082e+15  3.59955e+15  1.17847e+15  $ VELM g-groups 13, 12, 11, 10,  9,
        1.90084e+15  1.80302e+15  7.06655e+14  7.05919e+14  1.02398e+14  $ VELM g-groups  8,  7,  6,  5,  4,
        2.26137e+15  3.04858e+13  6.73779e+09                          $ VELM g-groups  3,  2,  1
ds81  l    $ gamma starting positions (x,y,z) in HB-1:
        0 0  91.7    0 0  77.5    0 0  82.9    0 0  82.7    0 0  82.5    $ VELM g-groups 23, 22, 21, 20, 19,
        0 0  82.5    0 0  83.0    0 0  81.6    0 0  86.0    0 0  86.0    $ VELM g-groups 18, 17, 16, 15, 14,
        0 0  88.0    0 0  87.0    0 0  78.4    0 0  80.3    0 0  79.9    $ VELM g-groups 13, 12, 11, 10,  9,
        0 0  78.3    0 0  72.9    0 0  79.3    0 0  81.0    0 0  82.6    $ VELM g-groups  8,  7,  6,  5,  4,
        0 0  68.0    0 0  90.2    0 0  87.2                              $ VELM g-groups  3,  2,  1
c       ---------------------------------
si72  h  1.0000e-2   $ this one Emin(MeV), followed by Emax(MeV) for the 23 VELM gamma grps (low to high E for MCNP):
        2.0000e-2    4.5000e-2    7.0000e-2    1.0000e-1    1.5000e-1    $ VELM g-groups 23, 22, 21, 20, 19,
        3.0000e-1    4.0000e-1    5.1000e-1    6.0000e-1    7.0000e-1    $ VELM g-groups 18, 17, 16, 15, 14,
        1.0000e+0    1.5000e+0    2.0000e+0    2.5000e+0    3.0000e+0    $ VELM g-groups 13, 12, 11, 10,  9,
        4.0000e+0    5.0000e+0    6.0000e+0    7.0000e+0    7.5000e+0    $ VELM g-groups  8,  7,  6,  5,  4,
        8.0000e+0    1.0000e+1    1.4000e+1                              $ VELM g-groups  3,  2,  1
sp72  d    0.0  $ dummy 0, followed by gamma src terms (p/s) for HB-2:
        4.95649e+14  8.70290e+15  4.73267e+16  6.39484e+16  8.95231e+16  $ VELM g-groups 23, 22, 21, 20, 19,
        1.31735e+17  6.18177e+16  6.00657e+16  4.22019e+16  4.06972e+16  $ VELM g-groups 18, 17, 16, 15, 14,
```

```
        1.05252e+17  1.19189e+17  7.21632e+16  4.92481e+16  2.56328e+16  $ VELM g-groups 13, 12, 11, 10,  9,
        3.03766e+16  1.57178e+16  7.53651e+15  5.21478e+15  8.92992e+14  $ VELM g-groups  8,  7,  6,  5,  4,
        7.67819e+15  4.75524e+14  4.72146e+12                            $ VELM g-groups  3,  2,  1
ds82  l     $ gamma starting positions (x,y,z) in HB-2:
        0 0  69.3    0 0  69.9    0 0  80.7    0 0  83.8    0 0  79.4   $ VELM g-groups 23, 22, 21, 20, 19,
        0 0  78.1    0 0  73.3    0 0  71.0    0 0  74.2    0 0  68.6   $ VELM g-groups 18, 17, 16, 15, 14,
        0 0  64.0    0 0  61.0    0 0  70.2    0 0  73.6    0 0  67.5   $ VELM g-groups 13, 12, 11, 10,  9,
        0 0  67.2    0 0  75.2    0 0  72.4    0 0  79.5    0 0  81.1   $ VELM g-groups  8,  7,  6,  5,  4,
        0 0  84.9    0 0  87.0    0 0  41.1                            $ VELM g-groups  3,  2,  1
c       ---------------------------------
si73  h  1.0000e-2   $ this one Emin(MeV), followed by Emax(MeV) for the 23 VELM gamma grps (low to high E for MCNP):
        2.0000e-2    4.5000e-2    7.0000e-2    1.0000e-1    1.5000e-1   $ VELM g-groups 23, 22, 21, 20, 19,
        3.0000e-1    4.0000e-1    5.1000e-1    6.0000e-1    7.0000e-1   $ VELM g-groups 18, 17, 16, 15, 14,
        1.0000e+0    1.5000e+0    2.0000e+0    2.5000e+0    3.0000e+0   $ VELM g-groups 13, 12, 11, 10,  9,
        4.0000e+0    5.0000e+0    6.0000e+0    7.0000e+0    7.5000e+0   $ VELM g-groups  8,  7,  6,  5,  4,
        8.0000e+0    1.0000e+1    1.4000e+1                             $ VELM g-groups  3,  2,  1
sp73  d     0.0  $ dummy 0, followed by gamma src terms (p/s) for HB-3:
        8.72837e+12  2.84514e+15  1.65029e+16  1.67705e+16  1.82855e+16  $ VELM g-groups 23, 22, 21, 20, 19,
        2.56708e+16  1.03805e+16  7.17665e+15  4.80101e+15  4.03975e+15  $ VELM g-groups 18, 17, 16, 15, 14,
        7.31636e+15  5.27935e+15  4.23989e+15  2.66951e+15  1.42777e+15  $ VELM g-groups 13, 12, 11, 10,  9,
        2.34929e+15  1.98361e+15  6.75453e+14  1.23378e+15  1.60183e+14  $ VELM g-groups  8,  7,  6,  5,  4,
        1.51983e+15  6.19421e+13  1.23250e+11                            $ VELM g-groups  3,  2,  1
ds83  l     $ gamma starting positions (x,y,z) in HB-3:
        0 0  10.0    0 0  61.9    0 0  68.1    0 0  82.1    0 0  83.9   $ VELM g-groups 23, 22, 21, 20, 19,
        0 0  84.5    0 0  81.6    0 0  84.7    0 0  88.8    0 0  83.2   $ VELM g-groups 18, 17, 16, 15, 14,
        0 0  86.8    0 0  93.6    0 0  96.9    0 0  99.2    0 0  96.6   $ VELM g-groups 13, 12, 11, 10,  9,
        0 0  92.6    0 0  93.2    0 0  96.4    0 0  93.9    0 0  96.0   $ VELM g-groups  8,  7,  6,  5,  4,
        0 0  94.4    0 0  99.9    0 0  97.4                            $ VELM g-groups  3,  2,  1
c       ---------------------------------
si74  h  1.0000e-2   $ this one Emin(MeV), followed by Emax(MeV) for the 23 VELM gamma grps (low to high E for MCNP):
        2.0000e-2    4.5000e-2    7.0000e-2    1.0000e-1    1.5000e-1   $ VELM g-groups 23, 22, 21, 20, 19,
        3.0000e-1    4.0000e-1    5.1000e-1    6.0000e-1    7.0000e-1   $ VELM g-groups 18, 17, 16, 15, 14,
        1.0000e+0    1.5000e+0    2.0000e+0    2.5000e+0    3.0000e+0   $ VELM g-groups 13, 12, 11, 10,  9,
        4.0000e+0    5.0000e+0    6.0000e+0    7.0000e+0    7.5000e+0   $ VELM g-groups  8,  7,  6,  5,  4,
        8.0000e+0    1.0000e+1    1.4000e+1                             $ VELM g-groups  3,  2,  1
sp74  d     0.0  $ dummy 0, followed by gamma src terms (p/s) for HB-4:
        3.54722e+13  1.10320e+15  9.00884e+15  1.23622e+16  1.35354e+16  $ VELM g-groups 23, 22, 21, 20, 19,
        1.77459e+16  6.62631e+15  4.47890e+15  2.84838e+15  1.69776e+15  $ VELM g-groups 18, 17, 16, 15, 14,
        3.37424e+15  3.46054e+15  6.18428e+15  7.78940e+15  1.57823e+15  $ VELM g-groups 13, 12, 11, 10,  9,
        2.70895e+15  2.64709e+15  9.17647e+14  1.00541e+15  1.98826e+14  $ VELM g-groups  8,  7,  6,  5,  4,
        2.38110e+15  4.71480e+13  4.55814e+09                            $ VELM g-groups  3,  2,  1
ds84  l     $ gamma starting positions (x,y,z) in HB-4:
        0 0  93.1    0 0  77.0    0 0  85.9    0 0  88.1    0 0  90.4   $ VELM g-groups 23, 22, 21, 20, 19,
        0 0  88.3    0 0  82.8    0 0  89.1    0 0  92.7    0 0  94.7   $ VELM g-groups 18, 17, 16, 15, 14,
        0 0  97.6    0 0  97.9    0 0  86.1    0 0  80.1    0 0  86.0   $ VELM g-groups 13, 12, 11, 10,  9,
        0 0  83.3    0 0  78.1    0 0  84.7    0 0  85.8    0 0  89.5   $ VELM g-groups  8,  7,  6,  5,  4,
        0 0  76.1    0 0  99.9    0 0  99.9                            $ VELM g-groups  3,  2,  1
c       ---------------------------------
```

Appendix A.2

Comparison of the Approximate Fluxes and Dose Rates Resulting from Use of the Equivalent Point Sources, Against the Original Fluxes and Dose Rates Calculated Directly by MCNP

Section 2 describes how the equivalent point sources for each neutron and gamma energy group were determined based on the calculated MCNP fluxes at several points down a beam tube. That methodology is embodied in a small Fortran utility program called "MULT-ISO.FOR." In addition, it also calculates and prints the ratios of the approximate fluxes using these sources [Flux(x,g)=S(x0,g)/[4*pi*(x-x0)^2]] to the original MCNP fluxes for each group, at each of the original points, in each beam tube, as well as the resulting differences (APPX flux - MCNP flux) in terms of FSD's (fractional standard deviations in the original MCNP fluxes). Lastly, it also prints an overall "quality indicator" for the resulting group-dependent fluxes at each point in each beam tube. These quality factors are designated as follows:

OK if (1) the approximate fluxes at each point are within 10% of the original fluxes
OR (2) the approximate fluxes at all deviant points are still within 2 FSD's of the original flux

? if (1) the approximate flux at any point is 10-15% different than the original flux
AND (2) the approximate flux at the deviant point is more than 2 FSD's away from the original flux

?? if (1) the approximate flux at any point is 15-20% different than the original flux
AND (2) the approximate flux at the deviant point is more than 2 FSD's away from the original flux

??? if (1) the approximate flux at any point is more than 20% different than the original flux
AND (2) the approximate flux at the deviant point is 2-3 FSD's away from the original flux

???? if (1) the approximate flux at any point is more than 20% different than the original flux
AND (2) the approximate flux at the deviant point is more than 3 FSD's away from the original flux

These flux ratios, relative flux differences in FSD's, and the corresponding quality factors, are shown below in Tables A.2.1, A.2.2, A.2.3, and A.2.4 for points along HB-1, HB-2, HB-3, and HB-4 respectively. Values shown in these tables are for the 4 points in HB-1, HB-3, and HB-4 (cf Table 2.1), and the 7 points in HB-2 (cf Table 2.1). As shown by the flux ratios there, the approximate fluxes are generally within 10% of the original MCNP fluxes and seldom differ by more than 2 FSD's. In those few cases where the fluxes do differ by more than this amount, it is generally because of stochastic noise in the fine-group MCNP fluxes -- ie, if the flux ratio is high in one fine-group, it is generally low by a similar offsetting amount in the adjacent energy group(s). In general, the agreement shown here is considered to be good to excellent.

Lastly, for each point in each beam tube (cf Table 2.1), the utility program described above will calculate the fast and total neutron dose rates and the total gamma dose rates: (1) based on the original MCNP fluxes, (2) based on the approximate fluxes obtained using these isotropic multigroup point-source terms, and (3) the ratio of the (APPX/MCNP) dose rates at each point. These results are shown in Table A.2.5. All dose rates are in mrem/hr. Generally the dose rates based on the approximate flux values (using the equivalent point sources) are within 5 to 10% of those calculated directly by MCNP. For shielding calculations where other uncertainties may be between 50% and a factor or 2, the approximate fluxes and dose rates resulting from use of these equivalent point source terms are considered wholly adequate.

Table A.2.1. Comparison of the approximate and original MCNP fluxes at each detector location in HB-1 shown in Table 2.1.

Beam Tube	VELM-N Group	Intensity of Pt Src (n/s)	Src Loc x0 (cm)	Flux Ratio (Appx/MCNP) at Points A, B, C, D	Flux Diff in FSD's at Points A, B, C, D	Quality
HB-1	ign= 1	3.08026E+09	79.2 cm	1.0002 .9998 1.0000 1.0000	.00 .00 .00 .00	OK
HB-1	ign= 2	3.99094E+11	39.7 cm	1.0004 .9275 1.0346 1.0667	.00 .14 .06 .10	OK
HB-1	ign= 3	1.08706E+12	58.3 cm	.9989 1.0670 .9808 .9454	.00 .19 .05 .12	OK
HB-1	ign= 4	3.53515E+12	52.9 cm	.9999 .9747 .9984 1.0326	.00 .10 .01 .11	OK
HB-1	ign= 5	9.85249E+12	56.0 cm	1.0015 .9679 1.0004 1.0353	.01 .23 .00 .23	OK
HB-1	ign= 6	2.62833E+13	64.4 cm	.9291 1.0345 1.0002 .9949	.19 .24 .00 .03	OK
HB-1	ign= 7	4.48929E+13	45.3 cm	1.0004 .9945 .9984 1.0071	.00 .05 .01 .06	OK
HB-1	ign= 8	5.41415E+13	55.1 cm	.9997 1.0082 .9878 1.0045	.00 .09 .14 .05	OK
HB-1	ign= 9	6.93878E+13	48.9 cm	.9999 1.0093 1.0036 .9865	.00 .12 .04 .16	OK
HB-1	ign=10	2.69013E+13	46.1 cm	1.0000 .9709 .9998 1.0311	.00 .26 .00 .28	OK
HB-1	ign=11	2.95862E+13	44.0 cm	.9996 1.0163 .9938 .9891	.00 .13 .04 .07	OK
HB-1	ign=12	7.75874E+13	44.1 cm	1.0004 1.0373 .9014 1.0167	.01 .49 .56 .15	OK
HB-1	ign=13	1.96210E+14	48.7 cm	1.0275 .5488 1.0250 1.0388	.49 .99 .54 .82	OK
HB-1	ign=14	2.62407E+14	50.8 cm	.9875 1.0090 .9950 .9999	.09 .21 .12 .00	OK
HB-1	ign=15	2.46072E+14	51.4 cm	.7913 1.0451 1.0111 1.0000	1.02 1.08 .26 .00	OK
HB-1	ign=16	3.00075E+14	42.6 cm	1.0007 .8904 .4426 1.1942	.01 .47 .88 3.01	??
HB-1	ign=17	2.17359E+14	60.0 cm	.9354 1.1059 .5627 1.0002	.24 2.15 .95 .00	?
HB-1	ign=18	2.16209E+14	52.1 cm	.7860 1.0485 1.0186 .9995	1.20 1.17 .43 .01	OK
HB-1	ign=19	1.69143E+14	49.6 cm	1.0745 .4080 1.0493 1.0495	.64 .93 .85 .91	OK
HB-1	ign=20	6.25375E+13	39.2 cm	1.0464 .5575 1.0318 1.0793	.52 .93 .30 .95	OK
HB-1	ign=21	2.71588E+14	52.4 cm	1.0097 .9543 1.0134 .9999	.06 .33 .29 .00	OK
HB-1	ign=22	2.83441E+14	45.3 cm	.9399 1.0334 1.0000 .9884	.52 .86 .00 .27	OK
HB-1	ign=23	9.72508E+12	43.2 cm	.9991 .9858 1.0861 .9398	.00 .08 .47 .32	OK
HB-1	ign=24	4.33179E+12	38.2 cm	.9996 1.0294 .8696 1.1412	.00 .11 .56 .60	OK
HB-1	ign=25	7.91646E+12	52.3 cm	1.0084 .9555 1.0394 1.0083	.03 .23 .18 .04	OK
HB-1	ign=26	9.40518E+13	41.3 cm	1.0689 .4209 1.0662 1.0582	.65 .90 .83 .78	OK
HB-1	ign=27	2.47877E+14	48.7 cm	1.0559 .7847 1.0090 1.0175	.54 .82 .19 .36	OK
HB-1	ign=28	1.79164E+14	55.0 cm	1.0887 .5178 1.0625 1.0048	.47 .88 1.26 .09	OK
HB-1	ign=29	1.86655E+14	35.6 cm	1.0004 1.0125 1.0395 .8732	.01 .19 .70 .76	OK
HB-1	ign=30	2.56507E+14	45.5 cm	.9213 1.0524 .9059 .9997	.40 1.05 .51 .00	OK
HB-1	ign=31	2.42117E+14	47.7 cm	.8121 1.0323 1.0194 .9998	.86 .67 .42 .00	OK
HB-1	ign=32	4.18163E+14	45.1 cm	1.0006 1.0028 1.0012 .9954	.01 .08 .03 .12	OK
HB-1	ign=33	5.36186E+13	50.6 cm	.9996 1.0465 1.0089 .9440	.00 .49 .09 .52	OK
HB-1	ign=34	2.32623E+14	39.0 cm	.9991 1.0162 .9955 .9879	.01 .33 .09 .22	OK
HB-1	ign=35	2.18288E+14	41.4 cm	1.0147 .7500 1.0126 1.0415	.29 .98 .25 .81	OK
HB-1	ign=36	7.80191E+13	36.0 cm	1.0010 .9361 1.0282 1.0443	.01 .68 .30 .44	OK
HB-1	ign=37	4.22279E+13	42.4 cm	1.0012 .8790 1.0085 1.1163	.01 .74 .07 .85	OK
HB-1	ign=38	5.39204E+13	48.1 cm	.9369 1.0476 .9834 1.0002	.28 .49 .16 .00	OK
HB-1	ign=39	5.62891E+13	36.6 cm	1.0002 .9883 .9969 1.0130	.00 .08 .03 .11	OK
HB-1	ign=40	3.67329E+14	50.5 cm	1.0216 .9031 1.0185 1.0007	.23 .60 .43 .01	OK
HB-1	ign=41	4.57210E+14	42.4 cm	1.0006 .9682 1.0822 .6267	.01 .27 1.86 .91	OK
HB-1	ign=42	3.59507E+14	57.5 cm	.8728 1.0095 1.0219 .9996	.46 .09 .46 .01	OK
HB-1	ign=43	3.29352E+14	45.9 cm	.9996 1.0060 1.0008 .9928	.01 .14 .02 .15	OK
HB-1	ign=44	1.68435E+14	46.0 cm	1.0005 .9968 .9972 1.0063	.01 .06 .05 .10	OK
HB-1	ign=45	1.08823E+14	64.4 cm	1.0064 .9825 1.0078 1.0004	.02 .12 .10 .01	OK
HB-1	ign=46	1.60061E+14	44.7 cm	1.0006 1.2937 1.2199 .1532	.00 4.77 3.25 .97	????
HB-1	ign=47	6.66316E+13	56.6 cm	.9356 1.0302 .9996 1.0000	.35 .39 .00 .00	OK
HB-1	ign=48	4.33392E+14	52.2 cm	1.0021 .9974 1.0011 1.0002	.01 .05 .03 .00	OK

HB-1	ign=49	4.80954E+14	46.9 cm	.9990	1.0517	.9400	.9647	.01	1.47	.79	.52	OK
HB-1	ign=50	5.17013E+14	44.9 cm	1.0003	.7540	1.0969	.7071	.01	.82	2.47	.83	OK
HB-1	ign=51	5.07730E+14	49.8 cm	1.0012	1.0175	.6677	1.0513	.01	.25	.99	1.29	OK
HB-1	ign=52	4.87720E+14	49.7 cm	1.0020	.8257	.9942	1.0521	.01	1.03	.09	1.40	OK
HB-1	ign=53	5.20223E+14	47.5 cm	1.0008	.9992	1.0079	.9920	.01	.02	.22	.21	OK
HB-1	ign=54	7.57662E+14	51.5 cm	1.0086	.8288	1.0340	1.0000	.10	.97	1.11	.00	OK
HB-1	ign=55	7.62547E+14	51.6 cm	.9636	1.0447	1.0001	.9478	.35	1.71	.01	1.21	OK
HB-1	ign=56	8.06771E+14	50.1 cm	.7542	1.0273	1.0199	.9999	1.05	.73	.69	.00	OK
HB-1	ign=57	7.81961E+14	54.8 cm	.9999	.8944	1.0237	.9992	.00	.66	.78	.02	OK
HB-1	ign=58	8.45061E+14	52.3 cm	.9988	1.0186	1.0065	.9763	.02	.46	.19	.61	OK
HB-1	ign=59	8.60077E+14	54.8 cm	1.0021	1.0197	.8696	1.0249	.02	.27	.85	.71	OK
HB-1	ign=60	1.32866E+15	54.0 cm	.9992	.9860	1.0231	.9786	.01	.16	.71	.51	OK
HB-1	ign=61	5.31877E+16	72.3 cm	1.0007	.8910	.9512	1.1101	.03	1.86	.53	2.90	?

Beam Tube	VELM-G Group	Intensity of Pt Src (p/s)	Src Loc x0 (cm)	Flux Ratio (Appx/MCNP) at Points A, B, C, D				Flux Diff in FSD's at Points A, B, C, D				Quality
HB-1	igg= 1	6.73779E+09	87.2 cm	.9990	1.0012	1.0000	1.0000	.00	.00	.00	.00	OK
HB-1	igg= 2	3.04858E+13	90.2 cm	1.0085	.8778	1.0897	1.0961	.06	2.36	1.48	1.39	?
HB-1	igg= 3	2.26137E+15	68.0 cm	.9996	1.0646	.9624	.8264	.01	.75	.16	.44	OK
HB-1	igg= 4	1.02398E+14	82.6 cm	1.0029	1.0332	.8513	1.0563	.02	.49	.85	.53	OK
HB-1	igg= 5	7.05919E+14	81.0 cm	1.0014	.8711	1.1245	.9841	.02	2.96	3.89	.09	?
HB-1	igg= 6	7.06655E+14	79.3 cm	1.0008	.8941	1.1345	.9489	.01	1.47	2.09	.20	?
HB-1	igg= 7	1.80302E+15	72.9 cm	.9998	.8778	.8689	1.1340	.01	2.84	.91	4.85	?
HB-1	igg= 8	1.90084E+15	78.3 cm	1.0033	.7770	.9817	1.1937	.05	2.98	.19	4.75	??
HB-1	igg= 9	1.17847E+15	79.9 cm	1.0003	.6869	.8886	1.2200	.01	2.66	.89	5.95	????
HB-1	igg=10	3.59955E+15	80.3 cm	1.0009	.9014	.8276	1.0754	.03	1.70	1.77	4.29	OK
HB-1	igg=11	4.40082E+15	78.4 cm	1.0005	.8708	1.1014	.9741	.02	2.03	2.76	.19	?
HB-1	igg=12	2.27631E+15	87.0 cm	1.0002	.7631	1.0129	1.2936	.00	3.35	.11	5.53	????
HB-1	igg=13	2.07064E+15	88.0 cm	1.0034	.8396	.8141	1.1689	.08	2.98	1.44	6.12	??
HB-1	igg=14	1.16662E+15	86.0 cm	1.0020	.9013	1.1194	.9940	.03	.89	1.11	.04	OK
HB-1	igg=15	2.01818E+15	86.0 cm	1.0021	.8312	1.1075	.9239	.04	1.19	2.01	.38	?
HB-1	igg=16	3.74129E+15	81.6 cm	1.0023	.9384	1.0619	1.0227	.05	.52	.35	.17	OK
HB-1	igg=17	4.76182E+15	83.0 cm	1.0028	.9108	1.0311	1.0107	.08	.68	.45	.24	OK
HB-1	igg=18	1.50947E+16	82.5 cm	1.0014	.9558	.9851	1.0295	.06	.69	.16	.85	OK
HB-1	igg=19	1.18909E+16	82.5 cm	.9986	.9584	.9845	1.0321	.05	.53	.29	.93	OK
HB-1	igg=20	1.11793E+16	82.7 cm	.9978	.9774	1.0476	.9837	.07	.24	1.02	.64	OK
HB-1	igg=21	8.84390E+15	82.9 cm	1.0003	.9510	1.0220	1.0018	.01	.45	.40	.07	OK
HB-1	igg=22	1.19589E+15	77.5 cm	1.0011	.9971	1.0571	.9543	.02	.02	1.10	.99	OK
HB-1	igg=23	2.41702E+12	91.7 cm	.9939	1.2219	.9888	.8303	.01	.60	.03	.37	OK

Table A.2.2. Comparison of the approximate and original MCNP fluxes at each detector location in HB-2 shown in Table 2.1.

Beam Tube	VELM-N Group	Intensity of Pt Src (n/s)	Src Loc x0 (cm)	Flux Ratio (Appx/MCNP) at Points U', U, V, W, Z, Z', Z''							Flux Diff in FSD's at Points U', U, V, W, Z, Z', Z''							Quality
HB-2	ign= 1	1.09787E+13	34.5 cm	1.0590	.7694	.8609	.9478	.9704	1.2277	1.3276	.17	.42	.27	.10	.05	.47	.64	OK
HB-2	ign= 2	7.93888E+13	50.3 cm	.5890	1.3223	1.3662	1.3793	1.4058	.6932	.7081	1.31	1.53	1.65	1.69	1.82	.97	.89	OK
HB-2	ign= 3	2.48357E+14	37.2 cm	1.0435	.8676	.9581	1.0000	1.0219	.9808	1.1716	.41	.97	.28	.00	.13	.08	1.13	OK
HB-2	ign= 4	5.63371E+14	37.5 cm	.6766	1.0005	1.1351	1.1780	1.2096	.8938	.9697	2.09	.01	1.33	1.73	2.01	.86	.25	???
HB-2	ign= 5	9.82537E+14	54.3 cm	.9995	1.0259	.9471	.9602	.9558	1.0428	1.0719	.00	.32	.64	.60	.67	.67	1.13	OK
HB-2	ign= 6	1.55944E+15	53.4 cm	.9994	.9998	.9832	.9741	.9737	1.0320	1.0433	.01	.00	.34	.55	.56	.67	.89	OK
HB-2	ign= 7	2.01809E+15	56.4 cm	.7758	.9995	1.0186	1.0596	1.0568	.9605	.9796	1.10	.00	.27	1.39	1.37	.92	.48	OK
HB-2	ign= 8	1.79911E+15	56.4 cm	.9998	1.0756	1.0593	.5906	.9597	1.0014	1.0045	.00	.97	1.39	.98	.65	.03	.10	OK
HB-2	ign= 9	1.84949E+15	56.4 cm	1.0295	.9348	.9781	1.0181	1.0199	.9923	.9998	.40	.62	.34	.38	.43	.17	.01	OK
HB-2	ign=10	7.86217E+14	54.6 cm	1.0002	.9659	1.0552	1.0592	1.0466	.9298	.9458	.00	.32	1.06	1.28	1.00	1.50	1.16	OK
HB-2	ign=11	8.22294E+14	61.6 cm	.9889	1.0490	.9879	.9984	1.0038	1.0001	.9928	.08	.33	.14	.03	.07	.00	.14	OK
HB-2	ign=12	1.67723E+15	58.8 cm	.9370	1.1340	.9956	.9905	1.0144	.9683	.9998	.67	1.72	.09	.18	.39	.88	.01	OK
HB-2	ign=13	3.79686E+15	62.2 cm	.9998	1.0281	.9447	1.0385	.9866	.3809	1.0560	.00	.35	.71	1.01	.19	.99	2.35	OK
HB-2	ign=14	3.11387E+15	68.9 cm	1.1365	1.0004	.9034	.8806	.9680	1.0176	1.0437	1.67	.00	.90	1.34	.96	.60	1.51	OK
HB-2	ign=15	2.02508E+15	69.8 cm	.9260	1.1550	.9611	.9610	1.0313	.9619	1.0005	.66	2.11	.51	.42	.97	1.05	.01	??
HB-2	ign=16	2.01784E+15	64.9 cm	.9986	1.0325	1.0118	.9893	.7354	.6834	1.0991	.01	.32	.24	.24	.97	.92	2.62	OK
HB-2	ign=17	1.70706E+15	72.1 cm	1.0015	1.1441	.8827	.8011	.9306	1.0443	1.0322	.01	1.54	.88	.92	1.04	1.14	.82	OK
HB-2	ign=18	1.59906E+15	70.6 cm	.9258	1.0007	1.0216	.9929	1.0099	1.0182	.9917	.59	.01	.32	.13	.23	.41	.18	OK
HB-2	ign=19	1.07362E+15	75.6 cm	1.1978	.9191	1.0294	1.0251	.4109	1.0697	.9995	1.05	.46	.34	.51	1.02	1.38	.01	OK
HB-2	ign=20	4.24300E+14	64.7 cm	.9376	1.0012	1.0745	1.0137	.9712	1.0110	.9593	.44	.01	1.05	.19	.39	.14	.43	OK
HB-2	ign=21	1.52963E+15	68.4 cm	1.0002	.8687	1.0848	1.0207	1.0003	.9898	.9462	.00	.75	2.01	.51	.01	.23	1.20	OK
HB-2	ign=22	1.80933E+15	64.6 cm	1.1007	.8250	.7854	.9538	.9999	1.0694	1.0416	1.13	1.16	1.11	.63	.00	1.64	.96	OK
HB-2	ign=23	5.38008E+13	77.1 cm	1.0034	.8628	1.2007	.9291	.8346	1.1162	1.0933	.01	.31	1.22	.44	1.05	.59	.60	OK
HB-2	ign=24	2.08255E+13	52.3 cm	.6839	1.0041	1.3075	1.0001	1.2864	.8876	.8396	1.19	.02	1.91	.00	1.54	.41	.40	OK
HB-2	ign=25	4.40442E+13	80.0 cm	1.0002	.9273	1.1025	.8895	.8505	1.2522	.9947	.00	.12	.53	.55	.75	1.47	.03	OK
HB-2	ign=26	4.36229E+14	70.1 cm	1.0000	.9412	.5156	1.2517	1.1776	.9456	.8527	.00	.24	.80	3.48	2.29	.72	1.85	??
HB-2	ign=27	1.19915E+15	73.8 cm	1.3532	.6382	.6658	1.0136	1.0044	1.0340	1.0006	3.53	1.54	.80	.22	.09	.72	.01	????
HB-2	ign=28	1.06795E+15	66.1 cm	.8324	1.0669	.9197	1.0768	1.0634	.9712	.9999	1.19	.57	.31	.86	.86	.36	.00	OK
HB-2	ign=29	8.76802E+14	67.6 cm	.8334	1.0012	1.1852	.8525	1.0788	.5362	.9942	1.04	.01	3.16	.59	1.37	1.02	.10	??
HB-2	ign=30	9.30940E+14	76.3 cm	1.0001	1.3523	1.2440	.9161	1.0428	.1780	1.0846	.00	3.09	4.37	.60	.72	1.28	1.45	????
HB-2	ign=31	1.13709E+15	73.2 cm	1.0012	.9063	1.1757	.9677	1.0483	.6757	.9601	.01	.48	2.55	.34	.94	.95	.75	??
HB-2	ign=32	1.70292E+15	67.0 cm	1.0000	.8573	1.0923	1.0502	1.0322	.9527	.9446	.00	1.04	2.05	1.10	.70	1.05	1.21	OK
HB-2	ign=33	2.45790E+14	69.3 cm	1.0006	.8310	1.0168	.9817	.9247	1.1455	1.0638	.00	.71	.16	.19	.73	1.31	.57	OK
HB-2	ign=34	1.13406E+15	65.8 cm	1.0000	.9076	1.1368	1.0289	.9024	.9970	.9507	.00	.62	2.30	.33	.60	.06	.89	?
HB-2	ign=35	6.93489E+14	67.0 cm	.8599	1.0009	1.2462	.6601	1.1195	.9375	.9133	.87	.00	3.86	.83	1.60	.89	1.19	????
HB-2	ign=36	2.74072E+14	63.7 cm	.5901	1.0831	1.0346	1.2687	1.1191	.9497	1.0000	1.44	.24	.15	2.33	.80	.45	.00	???
HB-2	ign=37	1.22345E+14	75.0 cm	.8276	1.0013	1.0871	1.1748	1.0885	.9181	.8941	.63	.01	.49	1.06	.52	.45	.53	OK
HB-2	ign=38	1.93557E+14	73.3 cm	1.0996	1.0009	.8521	.9805	1.0203	1.0604	1.0211	.31	.00	.72	.14	.14	.44	.15	OK
HB-2	ign=39	1.61758E+14	62.9 cm	.9981	1.0511	.8042	1.1503	1.1309	.9090	.9452	.01	.32	.69	1.05	.95	.68	.41	OK
HB-2	ign=40	1.62195E+15	61.6 cm	.9990	.6172	1.0594	1.0918	1.0890	.9264	.9714	.01	1.58	1.07	1.83	1.75	1.07	.55	OK
HB-2	ign=41	1.76510E+15	66.5 cm	1.0881	.9657	.7249	.8891	1.1035	.9272	1.0001	1.01	.30	.76	.55	2.03	.74	.00	?
HB-2	ign=42	1.74494E+15	71.9 cm	1.2120	.8971	.7674	.9405	1.0776	.7196	1.0008	2.09	.48	.66	.37	1.47	.94	.02	???
HB-2	ign=43	1.48446E+15	70.0 cm	1.0761	1.0010	.9708	.7979	.6180	1.0680	1.0322	.76	.01	.18	.77	.88	1.34	.62	OK
HB-2	ign=44	6.79285E+14	68.4 cm	.7790	1.0011	1.1729	1.0909	1.0339	.9694	.9357	1.54	.01	2.40	1.02	.33	.42	.85	??
HB-2	ign=45	5.09912E+14	68.6 cm	.9990	1.0208	1.0963	.4562	1.1086	1.0414	.9764	.01	.15	1.13	1.18	1.34	.52	.29	OK
HB-2	ign=46	4.86574E+14	78.3 cm	.9988	1.0402	1.0640	.9107	.9531	1.0512	1.0021	.01	.15	.70	.70	.58	.59	.02	OK
HB-2	ign=47	3.38748E+14	77.8 cm	1.2485	.9855	1.0000	.6507	.9354	1.1175	1.0315	1.22	.05	.00	1.04	.71	1.26	.32	OK
HB-2	ign=48	1.83135E+15	66.1 cm	1.1542	.8573	1.0798	.6574	1.0013	.9255	1.0010	2.22	1.23	1.82	.93	.02	.74	.02	??

HB-2	ign=49	1.77021E+15	67.6 cm	.9369	1.0019	1.0807	1.0450	1.0306	.7888	.9494	.57	.02	1.59	.97	.66	1.09	1.01	OK
HB-2	ign=50	1.75804E+15	71.4 cm	1.0024	.8798	.7211	1.0516	1.0264	1.0517	.9959	.02	.86	1.20	1.12	.58	1.13	.09	OK
HB-2	ign=51	1.84391E+15	67.6 cm	.9994	.8664	1.0592	1.0554	1.0352	.9784	.9565	.01	1.20	1.03	1.19	.75	.45	.92	OK
HB-2	ign=52	1.73245E+15	75.9 cm	1.0227	.9995	.8897	.9667	.9453	1.0862	1.0381	.21	.00	.71	.63	1.17	1.87	.79	OK
HB-2	ign=53	1.88854E+15	76.5 cm	.9994	1.0121	1.0389	.9832	.9997	.7530	1.0395	.00	.09	.34	.22	.01	.76	.86	OK
HB-2	ign=54	2.82080E+15	76.9 cm	.9990	1.1735	.6158	1.0044	1.0332	1.0223	.9764	.01	1.85	1.36	.05	.67	.58	.59	OK
HB-2	ign=55	2.95904E+15	71.9 cm	1.0255	.9670	.9251	.9788	.9983	1.0489	1.0005	.28	.40	.70	.33	.04	1.31	.01	OK
HB-2	ign=56	2.91875E+15	73.9 cm	1.0000	.9984	.6462	1.0570	.9992	1.0366	.9818	.00	.02	1.23	1.57	.02	.97	.47	OK
HB-2	ign=57	3.12475E+15	73.6 cm	1.0016	.9757	.8682	1.0392	.9483	1.0458	.9988	.02	.21	.98	.69	.43	1.19	.03	OK
HB-2	ign=58	2.82574E+15	76.1 cm	.9945	1.0010	1.0368	1.0155	.9988	1.0163	.9575	.06	.01	.41	.29	.03	.38	.93	OK
HB-2	ign=59	3.25137E+15	79.0 cm	1.0810	.9999	.8138	.8788	1.0137	1.1121	.7482	.75	.00	.94	.81	.18	2.58	.83	?
HB-2	ign=60	4.56223E+15	80.1 cm	1.2096	.8844	.9685	.6963	.9622	1.0452	1.0192	2.42	.78	.31	1.15	.71	1.11	.53	???
HB-2	ign=61	1.27996E+17	93.7 cm	1.1922	.9031	.6130	.8507	.9922	.9999	1.1103	9.91	4.33	6.84	2.12	.11	.00	11.38	?

Beam Tube	VELM-G Group	Intensity of Pt Src (n/s)	Src Loc x0 (cm)	Flux Ratio (Appx/MCNP) at Points U', U, V, W, Z, Z', Z''							Flux Diff in FSD's at Points U', U, V, W, Z, Z', Z''							Quality
HB-2	igg= 1	4.72146E+12	41.1 cm	1.3029	.8933	.8162	.8140	.8184	1.4401	1.5618	.96	.32	.50	.47	.44	.94	1.07	OK
HB-2	igg= 2	4.75524E+14	87.0 cm	1.0375	.7570	.9858	1.0558	1.0232	1.1005	.9992	.42	2.13	.28	.99	.38	1.53	.01	???
HB-2	igg= 3	7.67819E+15	84.9 cm	1.1814	.8755	.9279	.7652	1.0185	1.0156	1.0003	5.81	3.16	1.87	1.33	1.33	1.14	.02	?
HB-2	igg= 4	8.92992E+14	81.1 cm	1.1827	.9519	.9638	1.0583	1.1193	.4710	1.0005	2.24	.53	.48	.68	1.29	1.24	.01	??
HB-2	igg= 5	5.21478E+15	79.5 cm	1.0535	.8252	.9027	1.0389	1.0451	.9999	1.0135	1.72	2.15	1.29	1.02	1.16	.00	.30	??
HB-2	igg= 6	7.53651E+15	72.4 cm	1.0567	.9114	.9222	1.0002	1.0622	.9971	1.0291	1.71	2.21	1.54	.01	1.97	.06	.70	OK
HB-2	igg= 7	1.57178E+16	75.2 cm	1.0764	.9600	.9372	1.0207	.9539	.9995	1.0087	2.59	1.28	1.49	.68	.45	.01	.33	OK
HB-2	igg= 8	3.03766E+16	67.2 cm	1.0382	.9465	.9510	1.0196	.9861	.9814	1.0566	2.02	2.48	1.71	.63	.24	.44	2.69	OK
HB-2	igg= 9	2.56328E+16	67.5 cm	1.0870	.9936	.9114	.9707	1.0006	.9507	1.0241	4.03	.21	2.43	.88	.03	1.09	1.23	OK
HB-2	igg=10	4.92481E+16	73.6 cm	1.0301	.9857	.8848	1.0057	1.0669	.9825	.9603	1.85	.89	3.30	.19	4.26	.45	.85	?
HB-2	igg=11	7.21632E+16	70.2 cm	1.0770	1.0000	.8774	.9855	1.0354	.9404	1.0150	4.75	.00	3.89	.60	1.54	1.81	1.09	?
HB-2	igg=12	1.19189E+17	61.0 cm	1.0133	.9491	.9789	1.0308	1.0570	.9599	.9449	1.00	2.79	1.05	1.57	3.00	.81	.46	OK
HB-2	igg=13	1.05252E+17	64.0 cm	1.0176	.9874	.9445	.9920	.9829	.9052	1.0455	1.05	.68	1.75	.23	.65	1.13	3.83	OK
HB-2	igg=14	4.06972E+16	68.6 cm	1.1316	.9908	.9535	.9186	.9637	1.0015	1.0008	4.84	.27	1.10	1.40	1.38	.06	.05	?
HB-2	igg=15	4.22019E+16	74.2 cm	1.1146	1.0005	.8974	.8844	.7786	1.0326	1.0047	4.02	.02	2.10	1.34	1.34	1.66	.34	?
HB-2	igg=16	6.00657E+16	71.0 cm	1.0311	.9995	.9127	.9460	.9043	.9945	1.0438	1.14	.01	1.66	1.03	1.47	.08	3.68	OK
HB-2	igg=17	6.18177E+16	73.3 cm	1.0703	.9720	.8942	.9819	.8498	1.0007	1.0425	2.88	.83	1.61	.22	.95	.01	1.36	OK
HB-2	igg=18	1.31735E+17	78.1 cm	1.0543	.9901	.9136	1.0006	.8410	1.1429	1.0133	1.75	.38	1.61	.01	1.08	1.91	.09	OK
HB-2	igg=19	8.95231E+16	79.4 cm	1.0534	.9783	.8649	1.0014	.9598	.9705	1.2128	.99	.67	1.41	.01	.28	.19	2.25	???
HB-2	igg=20	6.39484E+16	83.8 cm	1.1077	1.0009	.8093	.9250	.6125	.9049	1.0946	2.39	.02	2.82	1.25	1.67	.89	6.96	??
HB-2	igg=21	4.73267E+16	80.7 cm	1.0613	1.0012	.8165	1.0131	.8009	1.0635	1.0365	1.53	.03	2.55	.19	1.29	1.56	1.67	??
HB-2	igg=22	8.70290E+15	69.9 cm	1.0220	.9995	.9458	1.0367	.9738	.9726	1.0180	.31	.01	.46	.53	.33	.26	.31	OK
HB-2	igg=23	4.95649E+14	69.3 cm	2.0094	.7467	.6130	.6695	.7497	2.4128	2.6771	1.57	.30	.52	.43	.30	1.74	2.12	???

Table A.2.3. Comparison of the approximate and original MCNP fluxes at each detector location in HB-3 shown in Table 2.1.

Beam Tube	VELM-N Group	Intensity of Pt Src (n/s)	Src Loc x0 (cm)	Flux Ratio (Appx/MCNP) at Points K, L, M, N				Flux Diff in FSD's at Points K, L, M, N				Quality
HB-3	ign= 1	2.74800E+09	99.9 cm	.6048	.7065	2.2014	11.2841	.63	.29	1.20	10.29	????
HB-3	ign= 2	6.92602E+12	31.1 cm	.9998	.9957	1.0114	.9933	.00	.01	.02	.01	OK
HB-3	ign= 3	8.64293E+12	68.7 cm	1.0011	.9222	1.0135	1.0733	.00	.14	.02	.13	OK
HB-3	ign= 4	3.05242E+13	42.9 cm	.9996	1.0283	1.0032	.9694	.00	.09	.01	.09	OK
HB-3	ign= 5	7.32282E+13	59.5 cm	1.0005	.9940	1.0068	.9991	.00	.03	.03	.00	OK
HB-3	ign= 6	1.36477E+14	62.6 cm	1.0000	1.0205	.9944	.9859	.00	.12	.03	.09	OK
HB-3	ign= 7	2.06360E+14	47.9 cm	1.0008	.9923	.9997	1.0076	.01	.06	.00	.06	OK
HB-3	ign= 8	1.61947E+14	56.9 cm	1.0009	.9594	1.0149	1.0289	.01	.40	.15	.27	OK
HB-3	ign= 9	2.41078E+14	65.3 cm	.8750	1.1168	1.0000	.9475	.41	1.02	.00	.43	OK
HB-3	ign=10	1.35333E+14	43.5 cm	1.0174	.7914	1.0036	1.1068	.15	.69	.02	.78	OK
HB-3	ign=11	2.00073E+14	33.3 cm	1.1073	.4373	1.0351	1.2249	.83	.85	.13	1.30	OK
HB-3	ign=12	3.12945E+14	52.1 cm	.7987	1.0520	1.0106	.9997	.60	.66	.13	.00	OK
HB-3	ign=13	8.54720E+14	50.2 cm	.9660	1.0193	1.0002	.9959	.29	.38	.00	.08	OK
HB-3	ign=14	8.07055E+14	59.7 cm	.4903	1.0910	1.0289	.9999	1.00	1.66	.53	.00	OK
HB-3	ign=15	7.09512E+14	46.8 cm	1.0082	.9092	1.0176	1.0268	.14	.79	.30	.45	OK
HB-3	ign=16	5.40055E+14	70.1 cm	1.0009	.9951	1.0191	.9838	.00	.03	.28	.24	OK
HB-3	ign=17	6.65098E+14	44.1 cm	1.0096	.8874	1.0142	1.0365	.17	.87	.24	.60	OK
HB-3	ign=18	5.35177E+14	56.8 cm	.9998	1.0062	1.0080	.9871	.00	.07	.11	.18	OK
HB-3	ign=19	3.61470E+14	50.3 cm	.9847	1.0351	.9997	.9767	.15	.53	.00	.35	OK
HB-3	ign=20	1.49367E+14	52.9 cm	.9847	1.0147	.9944	1.0000	.09	.15	.06	.00	OK
HB-3	ign=21	5.85513E+14	58.8 cm	.4254	1.0937	1.0292	.9999	.86	1.67	.50	.00	OK
HB-3	ign=22	6.29256E+14	49.6 cm	.9916	1.0150	1.0001	.9925	.07	.19	.00	.12	OK
HB-3	ign=23	3.65651E+13	42.3 cm	1.0047	.9079	1.0413	1.0359	.02	.31	.18	.15	OK
HB-3	ign=24	7.68584E+12	53.7 cm	1.0498	.8890	1.0589	1.0538	.12	.36	.17	.15	OK
HB-3	ign=25	1.38494E+13	63.8 cm	.9993	1.2042	1.0371	.8246	.00	.78	.14	.65	OK
HB-3	ign=26	2.12840E+14	42.4 cm	1.0006	.9936	.9706	1.0353	.01	.06	.29	.36	OK
HB-3	ign=27	7.35199E+14	34.2 cm	1.0004	1.0854	1.2451	.2501	.01	.76	3.77	.93	????
HB-3	ign=28	4.33245E+14	48.9 cm	1.0003	1.0021	1.0574	.8625	.00	.02	.83	.69	OK
HB-3	ign=29	3.63241E+14	42.5 cm	1.0004	.9988	1.0050	.9957	.01	.02	.06	.05	OK
HB-3	ign=30	4.29193E+14	45.6 cm	.9990	1.0022	.9999	.9989	.01	.03	.00	.01	OK
HB-3	ign=31	5.59006E+14	45.7 cm	1.0016	.9799	1.0155	1.0003	.02	.24	.23	.00	OK
HB-3	ign=32	8.89397E+14	47.4 cm	.9991	1.0102	.9980	.9920	.01	.18	.03	.13	OK
HB-3	ign=33	1.29680E+14	56.7 cm	.9855	1.0305	1.0001	.9777	.06	.21	.00	.15	OK
HB-3	ign=34	4.96958E+14	52.9 cm	.9996	.9950	1.0103	.9941	.00	.06	.15	.08	OK
HB-3	ign=35	3.03507E+14	79.8 cm	.9982	.9908	1.0313	.9742	.00	.04	.36	.30	OK
HB-3	ign=36	1.21873E+14	67.5 cm	.5951	1.1198	1.0501	.9996	.64	.86	.33	.00	OK
HB-3	ign=37	5.24714E+13	62.6 cm	.5493	1.1607	1.0320	.9997	.69	1.19	.24	.00	OK
HB-3	ign=38	1.12860E+14	46.7 cm	.9762	1.0339	.9998	.9867	.14	.26	.00	.11	OK
HB-3	ign=39	6.69650E+13	69.0 cm	.5744	1.1559	1.0252	1.0000	.63	1.08	.17	.00	OK
HB-3	ign=40	7.42049E+14	54.0 cm	.9978	1.0164	1.0000	.9845	.02	.28	.00	.26	OK
HB-3	ign=41	9.84217E+14	50.7 cm	.9552	1.0364	.9999	.9931	.48	.63	.00	.11	OK
HB-3	ign=42	8.76077E+14	52.7 cm	.9451	1.0429	1.0000	.9799	.33	.70	.00	.31	OK
HB-3	ign=43	7.55438E+14	53.3 cm	.5688	1.0688	1.0477	1.0001	.88	.99	.66	.00	OK
HB-3	ign=44	3.36538E+14	65.1 cm	.9517	1.0378	1.0000	.9789	.14	.37	.00	.21	OK
HB-3	ign=45	2.54975E+14	55.0 cm	1.0560	.7953	1.0603	1.0003	.35	.70	.58	.00	OK
HB-3	ign=46	2.76622E+14	49.5 cm	1.0007	.9826	.9763	1.0447	.01	.17	.23	.42	OK
HB-3	ign=47	2.04908E+14	43.0 cm	.9997	.9993	1.0224	.9795	.00	.01	.21	.19	OK
HB-3	ign=48	8.87245E+14	60.5 cm	.6631	1.0795	1.0243	.9996	1.09	1.35	.41	.01	OK

HB-3	ign=49	8.53691E+14	61.2 cm	.9892	1.0287	1.0000	.9779	.06	.47	.00	.38	OK
HB-3	ign=50	8.74122E+14	52.6 cm	1.0006	.9969	1.0028	.9997	.01	.05	.05	.01	OK
HB-3	ign=51	9.50610E+14	53.8 cm	.8268	1.0346	1.0217	.9999	.76	.59	.35	.00	OK
HB-3	ign=52	9.69821E+14	51.1 cm	.9999	.9899	1.0076	1.0029	.00	.17	.13	.05	OK
HB-3	ign=53	9.03837E+14	56.0 cm	.8576	1.0396	1.0083	.9995	.74	.75	.15	.01	OK
HB-3	ign=54	1.45876E+15	55.4 cm	1.0137	.9713	1.0135	1.0002	.10	.34	.25	.00	OK
HB-3	ign=55	1.54759E+15	56.5 cm	.8994	1.1358	.4510	.9993	.53	3.02	.93	.01	?
HB-3	ign=56	1.58981E+15	48.2 cm	1.0002	1.0150	.7313	1.0446	.00	.31	.88	.93	OK
HB-3	ign=57	1.55274E+15	54.5 cm	1.0001	1.0367	.8523	1.0165	.00	.78	.92	.33	OK
HB-3	ign=58	1.30212E+15	76.1 cm	1.1613	.7512	1.0236	1.0076	.53	.69	.32	.14	OK
HB-3	ign=59	1.52979E+15	65.2 cm	1.0754	.7114	.9043	1.0989	.33	1.00	.49	1.80	OK
HB-3	ign=60	2.25679E+15	57.3 cm	1.0011	1.0987	.3061	1.0612	.01	2.16	.97	1.25	OK
HB-3	ign=61	6.30365E+16	80.2 cm	1.0002	.8239	.6271	1.1036	.00	1.28	1.49	4.33	?

Beam Tube	VELM-G Group	Intensity of Pt Src (p/s)	Src Loc x0 (cm)	Flux Ratio (Appx/MCNP) at Points K, L, M, N				Flux Diff in FSD's at Points K, L, M, N				Quality
HB-3	igg= 1	1.23250E+11	97.4 cm	1.0667	.6105	1.1429	2.2851	.24	.85	.24	2.19	???
HB-3	igg= 2	6.19421E+13	99.9 cm	.7891	.7976	1.6401	2.3230	4.72	1.23	6.24	8.64	????
HB-3	igg= 3	1.51983E+15	94.4 cm	1.0009	.9027	1.0132	1.0365	.01	1.12	.30	.97	OK
HB-3	igg= 4	1.60183E+14	96.0 cm	1.0013	.8708	.9207	1.2630	.01	.59	.36	1.35	OK
HB-3	igg= 5	1.23378E+15	93.9 cm	1.0017	.9970	1.0042	.9984	.03	.07	.07	.03	OK
HB-3	igg= 6	6.75453E+14	96.4 cm	1.0033	.8302	1.0251	1.1585	.05	1.81	.30	2.12	??
HB-3	igg= 7	1.98361E+15	93.2 cm	1.0637	.8106	.3029	1.3504	.84	.68	1.72	7.72	????
HB-3	igg= 8	2.34929E+15	92.6 cm	1.0009	.8638	.9611	1.1203	.02	1.11	.33	1.80	OK
HB-3	igg= 9	1.42777E+15	96.6 cm	1.0006	.7797	1.0134	1.1141	.01	1.09	.11	1.44	OK
HB-3	igg=10	2.66951E+15	99.2 cm	1.0030	.8058	.8843	1.1311	.07	1.83	.48	3.11	?
HB-3	igg=11	4.23989E+15	96.9 cm	1.0036	.7856	1.0140	1.0595	.06	1.36	.25	1.50	OK
HB-3	igg=12	5.27935E+15	93.6 cm	1.0011	.9201	1.0415	1.0011	.02	.77	.83	.02	OK
HB-3	igg=13	7.31636E+15	86.8 cm	1.0008	.9211	1.0296	.9936	.02	.40	.59	.16	OK
HB-3	igg=14	4.03975E+15	83.2 cm	1.0005	.7520	1.0730	.9838	.01	.93	1.73	.38	OK
HB-3	igg=15	4.80101E+15	88.8 cm	1.0018	.8154	1.0634	.9827	.02	.99	1.81	.49	OK
HB-3	igg=16	7.17665E+15	84.7 cm	.9991	1.0266	1.0472	.9331	.01	.31	1.48	1.59	OK
HB-3	igg=17	1.03805E+16	81.6 cm	1.0002	1.0859	1.0099	.9619	.00	1.49	.23	1.54	OK
HB-3	igg=18	2.56708E+16	84.5 cm	.9977	1.1050	.9685	.9519	.04	1.79	.56	.95	OK
HB-3	igg=19	1.82855E+16	83.9 cm	.9975	1.0416	1.0093	.9820	.04	.76	.17	.85	OK
HB-3	igg=20	1.67705E+16	82.1 cm	.9610	1.1525	1.0001	.9267	.53	4.46	.00	3.08	??
HB-3	igg=21	1.65029E+16	68.1 cm	.6864	1.0934	1.0428	.9997	1.91	1.76	1.23	.01	OK
HB-3	igg=22	2.84514E+15	61.9 cm	1.0646	.8781	1.0004	1.0139	.53	.66	.00	.25	OK
HB-3	igg=23	8.72837E+12	10.0 cm	1.0468	1.0014	.9818	.9709	.06	.00	.02	.03	OK

Table A.2.4. Comparison of the approximate and original MCNP fluxes at each detector location in HB-4 shown in Table 2.1.

Beam Tube	VELM-N Group	Intensity of Pt Src (n/s)	Src Loc x0 (cm)	Flux Ratio (Appx/MCNP) at Points E, F, G, H				Flux Diff in FSD's at Points E, F, G, H				Quality
HB-4	ign= 1	3.25386E+10	10.0 cm	1.0000	1.0000	1.0000	1.0000	.00	.00	.00	.00	OK
HB-4	ign= 2	5.13981E+12	51.4 cm	1.0002	.9849	1.0099	1.0053	.00	.02	.01	.01	OK
HB-4	ign= 3	1.11369E+12	50.0 cm	1.0004	1.0800	1.0302	.9067	.00	.14	.05	.16	OK
HB-4	ign= 4	4.80519E+12	63.6 cm	.9993	1.0229	.9951	.9810	.00	.10	.02	.08	OK
HB-4	ign= 5	1.97320E+13	59.2 cm	1.0002	.9599	1.0022	1.0405	.00	.17	.01	.17	OK
HB-4	ign= 6	4.06939E+13	73.9 cm	1.0043	.9924	1.0002	1.0035	.01	.02	.00	.01	OK
HB-4	ign= 7	4.25672E+13	68.7 cm	.9991	.9927	1.0113	.9960	.00	.06	.11	.04	OK
HB-4	ign= 8	6.39971E+13	62.3 cm	1.0076	.9791	1.0138	1.0003	.04	.16	.13	.00	OK
HB-4	ign= 9	7.37185E+13	71.1 cm	.5378	1.1390	1.0508	.9998	.92	1.32	.59	.00	OK
HB-4	ign=10	2.56186E+13	52.9 cm	1.0000	.9875	.9893	1.0252	.00	.12	.10	.23	OK
HB-4	ign=11	2.86747E+13	48.2 cm	.9999	.9953	.9791	1.0276	.00	.04	.16	.21	OK
HB-4	ign=12	7.15232E+13	59.8 cm	.6649	1.0484	1.0568	.9999	.83	.61	.72	.00	OK
HB-4	ign=13	2.01888E+14	52.8 cm	1.0121	.9606	1.0002	1.0111	.20	.42	.00	.23	OK
HB-4	ign=14	2.15642E+14	54.9 cm	.9434	1.0408	1.0001	.9825	.44	.89	.00	.38	OK
HB-4	ign=15	2.56365E+14	43.5 cm	.9532	1.0427	.9775	.9997	.55	.90	.27	.00	OK
HB-4	ign=16	2.40525E+14	42.6 cm	1.0001	1.0426	.9108	.9925	.00	.90	.69	.11	OK
HB-4	ign=17	2.12911E+14	49.6 cm	.9985	1.0109	.9999	.9910	.02	.21	.00	.19	OK
HB-4	ign=18	2.04653E+14	54.4 cm	.9999	1.0277	1.0009	.9749	.00	.57	.02	.56	OK
HB-4	ign=19	1.53089E+14	53.7 cm	1.0007	1.0643	.5839	1.0317	.00	1.10	.94	.58	OK
HB-4	ign=20	5.15963E+13	42.5 cm	1.0006	.9867	1.0095	1.0046	.01	.16	.10	.05	OK
HB-4	ign=21	2.34828E+14	45.6 cm	.8365	1.0331	1.0156	1.0000	.94	.79	.37	.00	OK
HB-4	ign=22	2.52780E+14	45.3 cm	.9863	1.0235	.9999	.9885	.23	.49	.00	.24	OK
HB-4	ign=23	8.16811E+12	45.4 cm	.9999	1.0498	1.0369	.9239	.00	.22	.16	.33	OK
HB-4	ign=24	2.48863E+12	46.2 cm	.9997	1.0150	1.0676	.9216	.00	.06	.24	.26	OK
HB-4	ign=25	8.20767E+12	21.1 cm	1.0004	1.2324	.8021	1.0807	.00	1.20	1.07	.39	OK
HB-4	ign=26	6.34254E+13	63.7 cm	.5048	1.1103	1.0508	.9999	.77	1.13	.54	.00	OK
HB-4	ign=27	2.03836E+14	42.1 cm	1.0000	1.0399	.9024	1.0017	.00	.81	.73	.03	OK
HB-4	ign=28	1.69151E+14	41.2 cm	.9577	1.0308	.9999	.9969	.50	.60	.00	.06	OK
HB-4	ign=29	1.26213E+14	51.2 cm	.6586	1.0560	1.0306	1.0001	.98	.97	.58	.00	OK
HB-4	ign=30	1.59338E+14	51.8 cm	.6357	1.0774	1.0298	1.0001	1.32	1.58	.62	.00	OK
HB-4	ign=31	2.16102E+14	47.3 cm	.8342	1.0805	.9637	1.0001	.86	1.63	.46	.00	OK
HB-4	ign=32	3.09633E+14	49.6 cm	.8253	1.0366	1.0196	.9999	.97	.70	.52	.00	OK
HB-4	ign=33	5.45132E+13	29.3 cm	1.0495	.7407	1.0164	1.0624	.49	.92	.17	.65	OK
HB-4	ign=34	1.83967E+14	49.1 cm	.8194	1.0465	1.0155	1.0000	1.08	1.03	.34	.00	OK
HB-4	ign=35	1.35653E+14	48.6 cm	.8060	1.0508	1.0211	.9998	1.00	.91	.40	.00	OK
HB-4	ign=36	4.67136E+13	23.0 cm	1.0394	.9130	1.0000	1.0576	.36	.81	.00	.57	OK
HB-4	ign=37	2.60682E+13	51.5 cm	.5526	1.1820	1.0366	1.0001	.88	1.55	.30	.00	OK
HB-4	ign=38	3.81986E+13	40.0 cm	1.0004	.9859	.9885	1.0235	.00	.13	.11	.25	OK
HB-4	ign=39	6.36810E+13	10.0 cm	1.0206	1.1789	.3192	1.1822	.18	1.55	.91	1.61	OK
HB-4	ign=40	2.97379E+14	43.9 cm	.9995	1.0023	1.0054	.9931	.01	.04	.12	.15	OK
HB-4	ign=41	3.03564E+14	44.2 cm	.9906	1.0095	.9998	.9993	.19	.22	.00	.02	OK
HB-4	ign=42	3.16192E+14	44.9 cm	.9998	1.0509	.9689	.9326	.00	1.22	.39	.71	OK
HB-4	ign=43	2.72559E+14	47.3 cm	.9839	1.0253	1.0000	.9848	.19	.57	.00	.36	OK
HB-4	ign=44	1.17327E+14	51.5 cm	.9481	1.0361	1.0001	.9953	.46	.58	.00	.08	OK
HB-4	ign=45	1.00723E+14	40.2 cm	1.0055	.9937	1.0001	1.0014	.08	.10	.00	.02	OK
HB-4	ign=46	8.59309E+13	59.1 cm	.9995	1.0173	1.0073	.9787	.00	.24	.12	.34	OK
HB-4	ign=47	6.72898E+13	53.9 cm	.9009	1.0589	1.0001	.9834	.49	.78	.00	.19	OK
HB-4	ign=48	3.27352E+14	46.5 cm	.9511	1.0440	.9999	.9822	.62	1.21	.00	.50	OK

HB-4	ign=49	3.56115E+14	46.6 cm	1.0313	.8762	1.0117	1.0089	.64	1.03	.32	.24	OK
HB-4	ign=50	3.70852E+14	46.4 cm	1.0039	.9715	1.0155	1.0001	.05	.48	.45	.00	OK
HB-4	ign=51	3.81395E+14	50.9 cm	.8807	1.0198	1.0209	.9999	.79	.33	.59	.00	OK
HB-4	ign=52	3.61966E+14	49.7 cm	.9855	1.0300	.9999	.9776	.18	.89	.00	.66	OK
HB-4	ign=53	4.03643E+14	45.3 cm	1.0259	.9548	1.0048	1.0002	.60	.69	.14	.00	OK
HB-4	ign=54	6.46494E+14	49.5 cm	.8701	1.0252	1.0116	.9998	.96	.74	.39	.01	OK
HB-4	ign=55	6.53783E+14	46.9 cm	.8952	1.0236	1.0141	.9998	1.17	.81	.53	.01	OK
HB-4	ign=56	6.52905E+14	58.6 cm	.9352	1.0931	1.0001	.7526	.39	2.87	.00	1.66	OK
HB-4	ign=57	6.71028E+14	48.5 cm	1.0002	1.0018	1.0234	.9404	.00	.04	.88	.84	OK
HB-4	ign=58	6.83147E+14	49.9 cm	.8210	1.0343	1.0189	.9999	1.49	1.17	.71	.01	OK
HB-4	ign=59	7.22306E+14	61.0 cm	.9998	.9780	1.0240	.9844	.00	.19	.63	.41	OK
HB-4	ign=60	9.92916E+14	64.8 cm	.9992	.8923	1.0296	.9926	.01	.70	1.11	.29	OK
HB-4	ign=61	4.52747E+16	86.8 cm	1.0000	1.1039	1.0346	.9508	.00	4.54	3.39	7.03	?

Beam Tube	VELM-G Group	Intensity of Pt Src (p/s)	Src Loc x0 (cm)	Flux Ratio (Appx/MCNP) at Points E, F, G, H				Flux Diff in FSD's at Points E, F, G, H				Quality
HB-4	igg= 1	4.55814E+09	99.9 cm	.8584	1.3044	1.0000	1.0000	.20	.30	.00	.00	OK
HB-4	igg= 2	4.71480E+13	99.9 cm	.9867	.9548	1.0501	1.0209	.14	1.13	1.00	.38	OK
HB-4	igg= 3	2.38110E+15	76.1 cm	.9997	1.0338	.9750	.9601	.01	1.47	.46	.91	OK
HB-4	igg= 4	1.98826E+14	89.5 cm	1.0052	.9950	1.0021	1.0000	.03	.05	.02	.00	OK
HB-4	igg= 5	1.00541E+15	85.8 cm	1.0178	.9201	1.0223	1.0363	.36	2.11	.81	1.18	OK
HB-4	igg= 6	9.17647E+14	84.7 cm	1.0000	.8871	1.0587	.9756	.00	.87	1.49	.41	OK
HB-4	igg= 7	2.64709E+15	78.1 cm	1.0007	.9956	1.0111	.9910	.02	.11	.44	.34	OK
HB-4	igg= 8	2.70895E+15	83.3 cm	1.0000	.9229	1.0487	1.0046	.00	1.59	1.73	.07	OK
HB-4	igg= 9	1.57823E+15	86.0 cm	.9999	.9751	.9913	1.0220	.00	.52	.17	.72	OK
HB-4	igg=10	7.78940E+15	80.1 cm	.9994	1.0086	1.0137	.9913	.02	.31	.71	.98	OK
HB-4	igg=11	6.18428E+15	86.1 cm	.9990	.9532	1.0644	.9595	.03	1.49	2.66	.88	OK
HB-4	igg=12	3.46054E+15	97.9 cm	.9993	.9042	1.0888	.9793	.01	1.70	2.39	.30	OK
HB-4	igg=13	3.37424E+15	97.6 cm	1.0015	.9991	.9332	1.0296	.03	.02	.66	.71	OK
HB-4	igg=14	1.69776E+15	94.7 cm	1.0012	.8875	1.0619	.9686	.02	1.27	2.01	.47	OK
HB-4	igg=15	2.84838E+15	92.7 cm	.9998	1.0239	.9993	.9779	.00	.32	.01	.29	OK
HB-4	igg=16	4.47890E+15	89.1 cm	.9991	1.1548	.9356	.7091	.02	4.11	.77	1.93	??
HB-4	igg=17	6.62631E+15	82.8 cm	.9992	1.0674	1.0001	.9422	.02	1.11	.00	.96	OK
HB-4	igg=18	1.77459E+16	88.3 cm	1.0011	1.0922	1.0055	.9141	.04	2.89	.21	2.65	OK
HB-4	igg=19	1.35354E+16	90.4 cm	1.0011	1.0952	1.0142	.9092	.02	2.37	.49	2.43	OK
HB-4	igg=20	1.23622E+16	88.1 cm	.9986	1.0745	1.0261	.9410	.03	1.63	.75	2.09	OK
HB-4	igg=21	9.00884E+15	85.9 cm	.9998	1.0941	1.0063	.9012	.00	1.79	.12	1.59	OK
HB-4	igg=22	1.10320E+15	77.0 cm	1.0006	1.1461	1.0347	.6196	.00	1.60	.73	1.30	OK
HB-4	igg=23	3.54722E+13	93.1 cm	1.0019	.8268	1.0240	1.2173	.00	.27	.04	.35	OK

Table A.2.5. Comparison of the approximate and original MCNP dose rates (mrem/hr) at each detector location shown in Table 2.1.

		Point A	Point B	Point C	Point D
	Fast Neut Dose Rate				
HB-1	(1) Approximate ...	1.09258E+10	2.20131E+09	9.18284E+08	5.01071E+08
HB-1	(2) Original	1.14719E+10	2.56451E+09	1.07434E+09	4.97757E+08
HB-1	(3) Ratio	.95240	.85837	.85474	1.00666
	Total Neut Dose Rate				
HB-1	(1) Approximate ...	2.68656E+10	3.88086E+09	1.51664E+09	8.04996E+08
HB-1	(2) Original	2.74000E+10	4.44955E+09	1.70339E+09	7.71546E+08
HB-1	(3) Ratio	.98050	.87219	.89037	1.04335
	Gamma Dose Rate				
HB-1	(1) Approximate ...	1.71724E+10	1.15099E+09	3.84734E+08	1.90518E+08
HB-1	(2) Original	1.71535E+10	1.29644E+09	3.95315E+08	1.86706E+08
HB-1	(3) Ratio	1.00110	.88781	.97323	1.02041

		Point U'	Point U	Point V	Point W	Point Z	Point Z'	Point Z''
	Fast Neut Dose Rate							
HB-2	(1) Approximate ...	1.23119E+11	9.04096E+10	1.85714E+10	7.80103E+09	4.27204E+09	4.27204E+09	1.05187E+09
HB-2	(2) Original	1.23930E+11	9.03869E+10	1.93720E+10	8.28019E+09	4.52263E+09	5.34416E+09	1.03711E+09
HB-2	(3) Ratio	.99345	1.00025	.95867	.94213	.94459	.79938	1.01424
	Total Neut Dose Rate							
HB-2	(1) Approximate ...	1.89953E+11	1.26422E+11	2.19247E+10	8.96842E+09	4.85924E+09	4.85924E+09	1.18051E+09
HB-2	(2) Original	1.79991E+11	1.30263E+11	2.48424E+10	9.65250E+09	5.11445E+09	5.93140E+09	1.15295E+09
HB-2	(3) Ratio	1.05535	.97051	.88255	.92913	.95010	.81924	1.02390
	Gamma Dose Rate							
HB-2	(1) Approximate ...	6.36297E+10	4.47516E+10	8.06451E+09	3.26557E+09	1.75731E+09	1.75731E+09	4.21980E+08
HB-2	(2) Original	5.99046E+10	4.64616E+10	8.77781E+09	3.32854E+09	1.79608E+09	1.80979E+09	4.18235E+08
HB-2	(3) Ratio	1.06218	.96320	.91874	.98108	.97841	.97100	1.00895

Table A.2.5 (cont)

		Point K	Point L	Point M	Point N
	Fast Neut Dose Rate				
HB-3	(1) Approximate ...	1.95405E+10	4.87886E+09	2.18219E+09	1.23285E+09
HB-3	(2) Original	2.36341E+10	4.98574E+09	2.21887E+09	1.33685E+09
HB-3	(3) Ratio	.82679	.97856	.98347	.92221
	Total Neut Dose Rate				
HB-3	(1) Approximate ...	3.08903E+10	6.54149E+09	2.81786E+09	1.56584E+09
HB-3	(2) Original	3.49822E+10	7.00380E+09	3.23257E+09	1.63858E+09
HB-3	(3) Ratio	.88303	.93399	.87171	.95561
	Gamma Dose Rate				
HB-3	(1) Approximate ...	1.51070E+10	1.39536E+09	4.91145E+08	2.48536E+08
HB-3	(2) Original	1.51157E+10	1.55203E+09	5.67854E+08	2.39294E+08
HB-3	(3) Ratio	.99943	.89906	.86491	1.03862

		Point E	Point F	Point G	Point H
	Fast Neut Dose Rate				
HB-4	(1) Approximate ...	4.15302E+09	1.06506E+09	4.79354E+08	2.71535E+08
HB-4	(2) Original	4.61695E+09	1.03982E+09	4.97649E+08	2.73103E+08
HB-4	(3) Ratio	.89952	1.02427	.96324	.99426
	Total Neut Dose Rate				
HB-4	(1) Approximate ...	9.98399E+09	1.88661E+09	7.90611E+08	4.33920E+08
HB-4	(2) Original	1.04479E+10	1.78403E+09	7.98496E+08	4.43888E+08
HB-4	(3) Ratio	.95559	1.05750	.99013	.97754
	Gamma Dose Rate				
HB-4	(1) Approximate ...	5.44182E+09	7.75991E+08	2.96665E+08	1.55505E+08
HB-4	(2) Original	5.43837E+09	7.81736E+08	2.92136E+08	1.61607E+08
HB-4	(3) Ratio	1.00064	.99265	1.01550	.96224

Appendix B.1

Input Listing for the Final (Reference) HB-3 Dosimetry Analysis,

MCNP Run HB304M4

```
message:  outp=hb304.o  runtpe=hb304.r

Isolated model of HB-3 using equivalent point sources
c
c     ------------------------------------------------------------------------------------------------------------------
c
c       HB304 is a "special" variant of HB301 used only to get fast fluxes at the two dosimeter locations.
c
c             Would like to have this info so as to compare with values published in Tables E.12 and E.23 (on
c             pp 208 & 221) of ORNL/TM-10444, "Evaluation of HFIR Pressure-Vessel Integrity Considering Radiation
c             Embrittlement" (1988).   Note that fluxes on pp 208 (E>1 MeV and E>0.1 MeV) are those calculated
c             by Bob Child's DORT/TORT runs;  the "real" fluxes there should either (a) be inferred from
c             the Ni58(n,p)Co58 and Fe54(n,p)Mn54 decay data, OR (b) be inferred by dividing his published
c             fluxes by the C/E ratios for the decay data, to get the real fluxes.  Moreover, in Table E.23
c             they applied method (b).  Dwgs M-10070-0E-510-E, Rev 2 (1986) and Dwg E-49961, Rev C (1988)
c             show the positions of the various "coupons" in the ring around HB-3 corresponding to Key 3.
c
c             Cell 2134 (just slightly on HB-4 side of HB-3) corresponds to Key 3 Position 8 where the "real"
c             fluxes using Method B are: Flux(E>1 MeV)=1.78+9 n/s/cm2 and Flux(E>0.1 MeV)=3.84+9 n/s/cm2
c
c             Cell 2135 (just slightly on HB-2 side of HB-3) corresponds to Key 3 Position 3 where the "real"
c             fluxes using Method B are: Flux(E>1 MeV)=0.913+9 n/s/cm2 and Flux(E>0.1 MeV)=1.93+9 n/s/cm2
c
c             It will be interesting to see how well (or how poorly) our MCNP results compare with these values!
c
c
c             Modifications needed to get HB304 from HB301 are as follows:
c
c             1) To save time, run as "mode n" rather than "mode n p"
c
c             2) Use the following "cut:n" card to avoid tracking neutrons below 27 keV: (ie, keep only neutron grps 1-36)
c                cut:n  time(shakes) energy(MeV)  WC1   WC2   SWTM
c                cut:n    1.0e20       0.027     -0.5  -0.25   0.0  $ cutoff:  don't track any neutrons below 27 keV
c
c             3) On the si53, sp53, and ds63 cards describing the source, comment out all info pertaining to neutron
c                groups 37-61 since everything in these groups is below 27 keV; keep only info for grps 1-36 (above 27 keV)
c
c             4) On the fm14 & fm15 multiplier cards, use fm14=fm15=1.20830e16 n/s = sum of equivalent point
c                sources (n/s) over grps 1-36 only (ie, E>27 keV; use for dosimetry calc only) in HB-3 for HFIR at 100 MW
c
c             5) Change location of "importance cutoff plane" (Surf 1007) from Z=118.6879 cm (used to increase efficiency
c                of the water tube calcs, but is downstream of the dosimeters) to Z=75.473 cm which is more like 31.6546 cm
c                upstream of first dosimeter.  Belief is that most of the fast neutrons reaching the dosimeters are those
c                that strike the inner wall of the beam tube in the viscinity of the dosimeters, and that all others can,
c                for all practical purposes, be ignored.  [Surf 1007 is used in Cell 10110 (inner Al wall of beam tube)
c                to kill all neutrons below this location, ie: not within most forward-directed cone.]
c
c             6) On the sdef card, we need to "open up" the allowed angular distribution a little wider for the
c                dosimetry calc;  setting mu(min)=0.8 will allow neutrons from even the most forward equiv pt source
c                (at Z=68.7 cm) to hit the beam tube at Z=75.473 cm, which is well (31.654 cm) upstream of the first
c                dosimeter which is located at Z=107.1276 cm.  To accomplish this we need to do 2 things associated
c                with the sdef card:  (a) on the si3 (ang dist) card, set mu(min)=0.8, and (b) on the sdef card
c                itself, set wgt=0.1 =(mumax-mumin)/2
c
c                wgt=0.1  $ use this with mu(min)=0.8 in d3 for dosimetry calc only;  wgt = [mu(max)-mu(min)]/[(+1)-(-1)] = [1.0-0.8]/2 = 0.1
c                si3   h  0.8  1.0  $ open up angular distribution for dosime   run;  mu boundaries (i.e, cosine boundaries wrt vec)
c
c             7) Change dosimeter specimens from carbon steel to water;  spec   ns (including foils) are really much smaller
```

```
c        than the big chunks of metal originally envisioned. To do this, change Cells 2134 & 2135 to matl=7, den=-1.0 g/cc
c
c     8) Set up volume-averaged flux detectors for the two dosimeter cells (Cells 2134 & 2135); get N-fluxes by energy;
c        Cell 2134 = just slightly on HB-4 side of HB-3,  Cell 2135 = just slightly on HB-2 side of HB-3
c        May(?) later want to calculate activation rates here directly, or refine desc of dosimeter package inside dxtran sphere.
c
c     9) May(?) want to run as many as nps=5,000,000 histories to get good statistics;
c        will try 2,000,000 first; should go fast because of energy cutoff card above;
c        2,000,000 was subsequently found to be ok with dxtran spheres
c
c    10) May(?) want to have 3.2 cm radius dxtran spheres around each dosimeter so as to get better statistics
c        without having to run as many histories; found to work well with 2,000,000 histories
c
c    11) All the modifications previously used to create HB302 from HB301 should also be incorporated in HB304.
c        HB302 was a "special" varient of HB301;  HB302 was intented to get comparisons with the June 1968
c        Blosser & Thomas measurements. HB302 thus differed from HB301 insofar as:
c
c        a) Aluminum windows 1 and 2 were placed in their 1960 axail locations (see Cells 2140, 2141, 4305, 4380)
c        b) We used the small hole in the rotary shutter since that's what they used on HB-3 (see Surfs 3131 & 3132)
c        c) The was no water in the water tubes; they were void in this calc (see Cells 2145 & 2146)
c        d) Use pt det 15 to get results at B&T measurement point, 655.6626 from tip of HB-3 (ie, at Z=678.1673 cm)
c
c        While HB302 has been already run, and our results compared quite well with measurements (C/E=1.45 generally),
c        the main purpose of including it again here in Run HB304 is simply to verify that I haven't screwed up the
c        source normalization by only looking at the fast groups.  I am pretty sure there is no problem with above
c        appraoch, but want to keep this B&T comparison in the calc as a reference point to verify there is no problem.
c
c        Update:  After this had been verified, I subsequently used Surfs 3131 & 3132 to turn the rotary shutter's
c        big 3.5" beam hole to the open position (prior to the final dosimetry analysis) since this has been the
c        position most commonly used from 1968 thru 1988 (and still is).
c
c    12) Delete the oversimplified spherical representation of the 2 dosimeters (Key 3 Positions 3 & 8)
c        and model then more precisely as particular rectangular regions on the ss304 dosimeter specimen
c        holder ring [see Dwg M-10070-0E-510-E Rev 2 (1987), as well as Dwg E-49961 Rev C (1988), and
c        Dwg M-115-11-0H-001-E, Rev 1 (1992)].  To affect this change:
c        a) Delete the oversimplified dosimeter cells (2134 & 2135) described by surfaces 2121 & 2126,
c           as well as the corresponding exclusion zones in the pool water (Cell 2130).
c        b) Include (instead):  Surfs 2510-2562, Transformation 40, and Cells 2581-2593 (all below).
c        c) Include the following new exclusion regions in the pool water (Cells 2130 & 2133):
c           #(-2530  2531  -2532)  #(-2520  2521  -2522)  #(-2510  2511  -2521)
c           to exclude from the water: the dosimeter holder ring, and the thick and thin inner sleeves
c        d) Use separate volume-averaged tallies (as shown below) for Key 3 Posn 3 and Key 3 Posn 8
c           so that each can be clearly labeled.
c        e) Revise the dxtran spheres around these two dosimeters as shown below.
c           (Update: dxtran spheres later had to be discarded; went with pt detectors embedded within dosimeters)
c           (Update: to get good statistics, we then needed 40,000,000 histories; these take 4 hrs, 35 min wallclock)
c
c    13) It recently became apparent (3-27-98) that there is a rather large 2-plate collar assembly holding a cooling
c        tube on the ss sleeve outside the beam tube, close to dosimeter ring.  Moreover, this collar assembly may
c        shield some of the dosimeters (Key 3, Positions 3 and 8 in particular) from some of the neutrons coming down
c        the HB-3 beam tube. To model this, we had to add Cells 2761-2781 (below) as well as Surfs 2701-2748 (below).
c        In addition, the following two new exclusions requirements had to be included in the description of
c        the water (Cell 2130) between the aluminum reflector container and the pressure vessel:
c        #(-2701  2742  -2748)                    $ exclude bulk of this 2-plate collar assembly
c        #(-2702 2701 2744 -2746 2711 -2710 2720)  $ exclude horz spacer plate extension (Cell 2727)
c        Also need the following new exclusion region added to the description of the water (Cell 2133)
c        just outside the ss sleeve around the beam tube:
c        #( 2742  -2748)  $ water outside ss sleeve, excluding bulk of 2-plate collar assembly
```

```
c                ------------------------------------
c                Update on "2-plate collar" assembly:  This is really called a "coolant collector". A very small insert sketch
c                of one is shown up near HB-4 on Dwg E-42027, Sheet 1, while the ref dwg no. for this part in Dwg E-49400.
c                I was unaware of these sketches/drawings when I created the above model.  Note however, that the approximate
c                model that I did create and use was really not too bad and, since it (as a whole) was found to have very little
c                impact on the fluxes at the dosimeter locations, any further refinements are probably unwarrented.  JAB 4-4-98
c
c             14) Material m71 was added to get the Ni58(n,p)Co58 reaction rate [(n,p)=103] in the dosimeters
c                Material m72 was added to get the Fe54(n,p)Mn54 reaction rate [(n,p)=103] in the dosimeters
c                Tallies f25:n and f35:n were modified to calculate fluxes as well as these reaction rates in dosimeters.
c
c             15) In reality, the inner edge of the HB3 vessel hole (where it penetrates the inner surface of the
c                pressure vessel) is slightly rounded and has a curvature of 1.0625 inches (all the way around
c                this elliptically shaped hole).  Because this is rounded, the steel that would otherwise be there
c                in this little corner element is really gone and replaced by water.  Because of its very close
c                proximity to the dosimeter at Key 3 Position 3, the erroneous use of steel instead of water will
c                likely cause one to slightly overestimate the fast flux at this dosimeter location.  I believe
c                (4-2-98) that it is important to model this with water to correctly moderate those neutrons which
c                hit the beam tube downstream of this location and then backscatter toward the dosimeter and pass
c                thru this region.  While I cannot "round the edge", I can certainly replace the rounded edge by a
c                chamfer (ie knock off the sharp steel corner around this ring and replace it by water) by using an
c                elliptically shaped cone whose size and position are carefully calculated to preserve the correct
c                amount of water (ie, so that the amount of water in this chamfer ring is the same as what would be
c                in this ring if the corners were actually rounded with the correct radius).  To model this, we
c                will need:  three new surfaces (Surfs 2110, 2111, and 2112, shown below), one new transformation
c                (*tr42, shown below), and one new water-filled cell (Cell 2134, shown below).  In addition, the
c                main pressure vessel cell (Cell 2150) must now exclude everything inside (ie, include stuff only
c                outside) the elliptically shaped cone defined by Surf 2110.  These changes were first incorporated
c                in Run HB304G on 2 Apr 98. -- J.A. Bucholz (update: this made a small difference, but very little)
c
c             16) If/when doing dosimetry calcs for the old 1960 design, it was decided that one should probably use
c                a better (more realistic) model of the old (1960) water tube since this may have a small effect on
c                backscatter toward the dosimeters.  To do this, we added surfaces 2161-2165 below;  must also:
c                Replace Cell 2140 with one of the following, depending whether you're modeling the old (1960) water tube or not:
c                2140  23  -2.7       (2161 -2162 2163 -2153):(2164 -2165 -2163)  imp:n=1  $ aluminum: part-length model of old (1960) water tube: 1st sph w
indow & cyl section
c                2140  61  -3.2325-4  (2161 -2162 2163 -2153):(2164 -2165 -2163)  imp:n=1  $ int void: part-length model of old (1960) water tube: 1st sph w
indow & cyl section
c                Delete the old exclusion spec for Cell 1010:
c                #(2151  -2152)  imp:n=1    $ tube void region (above) excluding 1st aluminum window in 1960 design (see cell 2140)
c                and replace it with the following new exclusion spec for Cell 1010:
c                #((2161 -2162 2163 -2153):(2164 -2165 -2163)) imp:n=1    $ tube void region (above) excluding part-length model of old (1960) water tube
c
c             17) While the dosimeter strips are really SS302, they are very tiny (typically 0.417 grams).  The bulk of
c                the 1.16"x2.1" dosimeter package is comprised of three carbon steel Charpy V-notch specimens, with the
c                tiny dosimeter strips laying perpendicularly across these specimens in the V-notches.  Since the bulk
c                of each dosimeter package is carbon steel, Cells 2581 & 2582 were changed to matl m50 at 7.8212 g/cc.
c
c             18) Just upstream of the dosimeters located at Key 3, Positions 3 and 8, are what appear to be two stainless
c                steel pegs.  The one in front of Position 3 is of particular concern since it directly shields the
c                dosimeter from neutrons scattering in the nearby beam tube.  The one in front of Position 8 is of
c                less concern since it is more "off to the side".  Nevertheless, both should be modeled.  While I'll
c                refer to these as "square pegs", each is really a large bolt going thru two thick tabs that stick out
c                from the top and bottom halves of the dosimeter holder assembly front plate (see Dwg E49953, Rev A,
c                dated 30 Jun 1965).  To model these, we will need 7 new surfaces (2533,2543,2544,2553,2554,2563,2564),
c                and 2 new cells (2583 & 2584).  In addition, Cell 2130 (and perhaps Cell 2133) will need the following
c                two exclusion statements:
c                #(2533  -2531  2553  -2554  2543  -2544) $ large water region above), excluding ss square peg just upstream of dosimeter at 3, Positio
```

```
ns 3
c               #(2533  -2531  2564  -2563  2543  -2544) $ large water region (above), excluding ss square peg just upstream of dosimeter at Key 3, Positio
ns 8
c
c            19) On 3 Apr 98, Pete Hambaugh gave me a full size dwg of the "Pressure Vessel Surveillance Specimen Mount
c                Assembly for HB-1, 3, and 4", Dwg E-49953, Rev A, dated 6-30-98.  This is a very good drawing of the
c                assembly;  it is much better than the little sketches I was using, and clarifies a number of questions.
c                Thus: For Run HB304H (3 Apr 98) and all subsequent runs, Surfaces 2510-2564 (associated with the dosimeters
c                and the dosimeter specimen holder at Key 3 around HB-3) were all revised based on newly available data shown
c                on this drawing.  In particular, we can now model (with confidence) the large bolts and ss tabs (collectively
c                referred to above and below as the "ss square pegs" which sit very close to the dosimeters in Positions 3 & 8
c                of Key 3.  Transformation tr40 was also revised as shown below, based on that newly available.  Lastly,
c                point detectors 25 and 35 (below) were repositioned so as to correspond to what are the newly revised
c                midpoints of the dosimeter locations, based on this newly available data.
c
c            20) On 4 Apr 98, I made a number of small modeling improvements to improve the overall calculational
c                efficiency and reliability.  While a number of geometry cells were redefined, the actual physical
c                distribution of materials was not changed at all.  (1) The way the water outside the ss sleeve
c                (radially beyond the beam tube) was broken up into cells was changed in order to (a) reduce the
c                number of exclusion regions required (especially in cell 2130) and to (b) allow for a new importance
c                region in the water outside the ss sleeve but inside the vessel in the vicinity of the dosimeters.
c                To accomplish this, one new water cell (Cell 2135) was added while Cells 2130 & 2133 were modified.
c                (2) To allow the nozzel and that portion of the vessel near the dosimeters to have a higher importance,
c                the cell corresponding to the nozzel was extended thru the vessel wall, while the region now called
c                the vessel was pushed back (radially) the same offsetting amount.  This required the modification
c                of Cells 2150 & 2151.  (3) To allow better statistical sampling in those regions close to the
c                dosimeters, I decided to use  imp:n=2  for a number of cells including:
c                ---------------------------------------
c                Cells 2131                                        <-- for the water outside the beam tube but inside the ss sleeve surrounding it, near the v
essel nozzel
c                Cells 2132                                        <-- for the ss sleeve surrounding the beam tube near the vessel nozzel
c                Cells 2133, 2134 & 2135                           <-- for the water outside the ss sleeve that is within about 20 cm of the dosimeters
c                Cells 2151 & 2152                                 <-- for the newly defined vessel nozzle region and flange
c                Cells 2581, 2582, 2583, 2584, 2591, 2592 & 2593 <-- for the dosimeters & those cells comprising the dosimeter holder ring
c                Cells 2761, 2762, 2771, 2772, 2773, 2774 & 2781 <-- for cells associated with the 2-plate collar holding the cooling tube
c                ---------------------------------------
c                Hopefully these improvements will lead to better fsd's without adding too much to the calculational overhead.
c
c
c            21) The following error was corrected by JAB on 6 Apr, just prior to submitting Run HB304K:
c                ------------------------------------------------------------------------------------
c                bad surf:   2110   42  sq  0.9262159  0.9880902  -1.0  0  0  0  0  0  0  0  $ elliptical cone used to define chamfer between HB3 vessel hol
e and inner surf of pressure vessel
c                bad tranf:  *tr42  $ use tr42 to locate and position the elliptical cone used to define chamfer between HB3 vessel hole and inner surf of p
ressure vessel
c                bad tranf:         0.0  -2.14265  128.18364   $ location of local origin (center of elliptical cone), relative to the global origin (cm) in
 HB-3 model
c                bad tranf:           0    90.0000    90.0000  $ degrees from global x,y,z axes to local x axis
c                bad tranf:          90    12.6575   -77.3425  $ degrees from global x,y,z axes to local y axis
c                bad tranf:          90   102.6575    12.6575  $ degrees from global x,y,z axes to local z axis
c
c                The above specification was used in Runs HB304G & HB304H. Subsequent graphical analysis of the flare at the midplane (x=0)
c                showed that this elliptical cone chamfer was NOT a good representation of the rounded corners, and (in fact) cut off too
c                much steel from the vessel and substituted too much water.  The graphical analysis was reworked, using some CAD work
c                and some equations this time, and the following was found to be a much more accurate representation.  -- JAB, 5 Apr 98
c
c                Input files for HB304I & HB304J were also no good. These were failed attempts to fix the problem.  Those two cases
c                (I&J) were never run since similar problems were noticed during the graphical checkout step before final submission.
```

```
c
c               Run HB304K (whose correct input is shown below) was the firt run which had this correct. TR42 also changed. -- JAB 6 Apr 98
c               The following corrections to Surf 2110 and Trans *tr42 were made by JAB on 6 Apr 98, just prior to submitting Run HB304K:
c
c               2110   42  sq  0.928252  1.0  -1.0  0  0  0  0  0  0  0  $ elliptical cone used to define chamfer between HB3 vessel hole and inner surf of
 pressure vessel
c               *tr42  $ use tr42 to locate and position the elliptical cone used to define chamfer between HB3 vessel hole and inner surf of pressure vess
el
c                     0.0  -2.02265  127.62367   $ location of local origin (center of elliptical cone), relative to the global origin (cm) in HB-3 model
c                       0    90.0000    90.0000  $ degrees from global x,y,z axes to local x axis
c                      90    12.6929   -77.3071  $ degrees from global x,y,z axes to local y axis
c                      90   102.6929    12.6929  $ degrees from global x,y,z axes to local z axis
c
c
c           22) Numerical experiment in Run HB304M:
c
c               Shift sources 0.54 cm to right of beam tube centerline to account for the anisotropic effect
c               of more neutrons entering the one side of the beam tube than the other -- JAB, 4-7-98  3 am
c
c               In Run HB304M2:  Shift sources 1.05 cm to right of beam tube centerline to account for the anisotropic
c               effect of more neutrons entering the one side of the beam tube than the other;  also need to increase
c               nps by 50% (from 40M to 60M) to preserve statistics at Posn 3, since shifting the source this much will
c               cause fewer neutrons to impact the Key 3 Posn 3 (HB-2 side) of the HB-3 beam tube due to the shift in
c               direction cosines relative to the outward normal of the circular beam tube.  -- JAB, 4-7-98  6 pm
c
c               In Run HB304M3:  Shift sources 1.5 cm to right of beam tube centerline to account for the anisotropic
c               effect of more neutrons entering the one side of the beam tube than the other;  also need to increase
c               nps by from 60M to 80M) to preserve statistics at Posn 3, since shifting the source this much will
c               cause fewer neutrons to impact the Key 3 Posn 3 (HB-2 side) of the HB-3 beam tube due to the shift in
c               direction cosines relative to the outward normal of the circular beam tube.  -- JAB, 4-7-98  6 pm
c
c               In Run HB304M4:  Shift sources 1.6986 cm to right of beam tube centerline to account for the anisotropic
c               effect of more neutrons entering the one side of the beam tube than the other;  also need to increase
c               nps by from 60M to 80M) to preserve statistics at Posn 3, since shifting the source this much will
c               cause fewer neutrons to impact the Key 3 Posn 3 (HB-2 side) of the HB-3 beam tube due to the shift in
c               direction cosines relative to the outward normal of the circular beam tube.
c               ----------------------------------------
c               Important note:  Rather than trying to find an offset that might match the known dosimetry results better,
c               this particular offset (of 1.6986 cm) was based on a theoretical model which considered the RATIO of
c               ("the radial outward component of the current (from HB3, in direction of HB4) at Z=101.5 cm" to the
c               "the radial outward component of the current (from HB3, in direction of HB2) at Z=107.0 cm") based on
c               80400 source points on a hemispherical shell (R=7.76 cm) 1.0 cm into the Be (just past the hot end of the
c               beam tube) and Cheverton's known fast flux distribution as a function of radial distance from the core
c               centerline (see HFIR Nuclear Design document) in this region, which changes by a factor of 4 from one side
c               of the hemisphere to the other.  See FADIST7.FOR for more details about the methodology used to determine
c               this offset.  -- JAB, 4-15-98  11 am
c               ----------------------------------------
c               On the sdef card, we now need to "open up" the allowed angular distribution a little wider for the
c               dosimetry calc;  setting mu(min)=0.71 will allow neutrons from even the most forward equiv pt source
c               (at Z=68.7 cm) to hit the beam tube at Z=75.473 cm, which is well (31.654 cm) upstream of the first
c               dosimeter which is located at Z=107.1276 cm.  To accomplish this we need to do 2 things associated
c               with the sdef card:  (a) on the si3 (ang dist) card, set mu(min)=0.71, and (b) on the sdef card
c               itself, set wgt=0.145 =(mumax-mumin)/2
c
c               wgt=0.145  $ use this with mu(min)=0.71 in d3 for dosimetry calc only;  wgt = [mu(max)-mu(min)]/[(+1)-(-1)] = [1.0-0.8]/2 = 0.145
c               si3   h  0.71  1.0  $ open up angular distribution for dosimetry run;  mu boundaries (i.e, cosine boundaries wrt vec)
c               ----------------------------------------
c               In Run HB304M4, will also increase nps to 120,000,000 to preserve statistics after mu is opened up from 0.8 to 0.71
```

```
c              ----------------------------------------
c
c           23) Added 4-7-98:  Use of Surf 2534 (instead of Surf 2531) in the definition of Cells 2581 & 2582 allows the
c               portion "of the ss304 cover plate of dosimeter holder ring directly upstream of the dosimeters" to be modeled
c               separate from the carbon steel Charpy specimens in the 1-cm-thk dosimeter capsules (Cells 2581 & 2582).
c               To do this also requires that the exclusion specs for Cell 2591 (the holder ring) be modified as follows:
c               #(2534  2551  -2552  2541  -2542)   $ Key 3 dosimetry specimen holder ring (ss304), excluding dosimeter at Key 3, Position 3
c               #(2534  2562  -2561  2541  -2542)   $ Key 3 dosimetry specimen holder ring (ss304), excluding dosimeter at Key 3, Position 8
c
c     ------------------------------------------------------------------------------------------------------------
c
c     Used to study shielding effectiveness of water tube (work performed by Jim Bucholz for Mike Farrah, Mar/Apr 1998):
c
c       Ref 1:  Dwg of HB-1 (e:\ham\ustn\allbeam1197.dgn Jan 29, 1998 12:55:09), where HB-3 is said to be the same.
c       Ref 2:  Dwg M-11537-OH-001-E, Feb 13, 1998, 10:30:22, dwg of HB-1 (essentially the same as Ref 1, but smaller)
c       Ref 3:  Dwg E-42027, Sheet 1, Apr 11, 1995, showing location on HB-3 & 1st aluminum window in vessel, as built
c       Ref 4:  Dwg E-42027, Sheet 2, Apr 11, 1995, showing typical beam tube collimator & rotary shutter, as built
c       Ref 5:  Dwg 1546-01-M-5022, Rev Sep 18, 1961, showing concrete around HB-3 beam tube collimator & rotary shutter
c
c       Distance from outside of vessel nozzel boss to radial plane
c       perpendicular to beam tube (as specifically stated in Ref 3):
c         HB-1:  52.0 inches = 132.08 cm
c         HB-2:  54.5 inches = 138.43 cm
c         HB-3:  54.0 inches = 137.16 cm
c         HB-4:  52.0 inches = 132.08 cm
c
c       Notes regarding length of the 1998 water tube:
c
c       The location of the 1st aluminum window relative to the vessel nozzel boss (cf Ref 1 & 2) is believed to be
c       correctly modeled here.  Likewise, the 2nd aluminum window relative to the beam tube collimator assembly
c       (cf Ref 1 & 2) is believed to be correctly modeled here.  Given the location of the beam tube collimator
c       assembly (Ref 1 & 2) relative to the concrete biological shield specifically around HB-3 as shown in Ref 5,
c       however, the length of the new HB-3 water tube [from Surf 2154 at Z=174.95125 cm, to Surf 4110 at Z=302.1868 cm
c       (total length of water when flooded = 127.23555 cm)] is about 2.03 inches shorter than shown for HB-1 on Refs
c       1 & 2, and about 89.8 cm shorter than the water tube originally in HB-3. Note, however, that this 2" difference
c       in water tube length between HB-1 and HB-3 is wholly consistent with the data in Ref 3 above if the vessel
c       flange hardware and collimator hardware are the same for HB-1 and HB-3 -- J. A. Bucholz, 3-21-98
c
c
c     BEGIN CELLS:
c
c     HB-3 (Tangential tube); sign on some surfs changed to accomodate this local model
c
1000  61  -3.2325-4  -1000        -1006        imp:n=1    $ endcap void region replaced with He at 2 atm (3.2325-4 g/cc)
1001  24  -2.7       -1001  1000  -1006        imp:n=0    $ endcap inner Al wall (imp=0 to kill all inward-directed neutrons)
1002  5   -0.98465   -1002  1001  -1006        imp:n=1    $ endcap water
1003  24  -2.7       -1003  1002  -1006        imp:n=1    $ endcap outer Al wall
1004  5   -0.98465   -1004  1003  -1006        imp:n=1    $ endcap water jacket
1005  24  -2.7       -1005  1004  -1006        imp:n=1    $ endcap Al Be liner
c
1010  61  -3.2325-4  -2153  -1010  1006                   $ tube void region replaced with He at 2 atm (3.2325-4 g/cc)
c         #(2151  -2152)   $ obsolete (too approximate)   $ tube void region (above) excluding 1st aluminum window in 1960 design (see cell 2140)
          #((2161 -2162 2163 -2153):(2164 -2165 -2163))   $ tube void region (above) excluding part-length model of old (1960) water tube: 1st sph window &
cyl section
          imp:n=1                                         $ tube void region (above)
1011  24  -2.7       -2153  -1011  1010  1007  imp:n=1    $ tube inner Al wall (surf 8051 is the "importance cutoff plane")
10110 24  -2.7       -2153  -1011  1010  1006 -1007  imp:n=0    $ tube inner Al wall (used to kill all neutrons not within most forward-directed cone
1012  5   -0.98465   -2153  -1012  1011  1006  imp:n=1    $ tube water
```

```
1013  24  -2.7       -2153  -1013  1012  1006  imp:n=1    $ tube outer Al wall
1014  5   -0.98465   -2012  -1014  1013  1006  imp:n=1    $ tube water jacket [now cut off at cage (2012) as it should be]
1015  24  -2.7       -2012  -1015  1014  1006  imp:n=1    $ tube Al Be liner  [now cut off at cage (2012) as it should be]
c
c
c     Main cylindrical components outside HB-3:
c
2024 108  1.23156-1  -9999 9997 -2010  1005  #(-1015 1006) imp:n=1  $ permanent Be refl (0.123156 atoms/b*cm; typical comp, center ring); exclude HB-3
2110  5   -0.98465   -9999 9997  2010 -2011  1015  imp:n=1 $ water between Be refl and aluminum reflector container
2120  23  -2.7       -9999 9997  2011 -2012  1015  imp:n=1 $ aluminum refl container
c
c
2130  7   -0.9899  -9999 9997  2012 -2013   $ large water region between aluminum refl container and the pressure vessel
                    1013  #(-2101 2150)     $ large water region (above); excluding beam tube & regions around beam tube near vessel
c                   2121   2126             $ large water region (above); excluding the two small dosimeter locations (obsolete model)
c                 #(-2530  2531  -2532)      $ large water region (above); excluding the dosimeter holder ring (and dosimeters)
c                 #(-2520  2521  -2522)      $ large water region (above); excluding thick inner hub   of the holder ring
c                 #(-2510  2511  -2521)      $ large water region (above); excluding thin inner sleeve of the holder ring
c                 #(-2702 2701 2744 -2746 2711 -2710 2720)  $ large water region (above); excluding horz spacer plate extension (Cell 2727) on 2-plate collar
 assembly
c                 #(-2701  2742  -2748)      $ large water region (above); excluding bulk of 2-plate collar assy on ss sleeve outside beam tube close to dosi
meter ring
c                 #(2533  -2531  2553  -2554  2543  -2544) $ large water region (above), excluding ss square peg just upstream of dosimeter at Key 3, Positio
ns 3
c                 #(2533  -2531  2564  -2563  2543  -2544) $ large water region (above), excluding ss square peg just upstream of dosimeter at Key 3, Positio
ns 8
                    imp:n=1                $ large water region (above)
2131  7   -0.9899    1013  -2130  2150  -2153  imp:n=2 $ water between beam tube and ss sleeve near vessel
2132  40  -7.92      2130  -2131  2150  -2153  imp:n=2 $ ss sleeve around beam tube, near vessel
2133  7   -0.9899    2131  -2101  2150  -2013  $ water just outside ss sleeve but inside main pressure vessel, in vicinity of dosimeters
c                    2121   2126              $ water just outside ss sleeve (above), excluding dosimeter locations
                  #(-2530  2531  -2532)       $ water just outside ss sleeve (above); excluding the dosimeter holder ring (and dosimeters)
                  #(-2520  2521  -2522)       $ water just outside ss sleeve (above), excluding thick inner hub   of the holder ring
                  #(-2510  2511  -2521)       $ water just outside ss sleeve (above), excluding thin inner sleeve of the holder ring
c                 #( 2742  -2748)             $ water just outside ss sleeve (above), large water region (above); excluding bulk of 2-plate collar assy on s
s sleeve outside beam tube close to dosimeter ring
                  #(-2702 2701 2744 -2746 2711 -2710 2720)  $ large water region (above); excluding horz spacer plate extension (Cell 2727) on 2-plate collar
 assembly
                  #(-2701  2742  -2748)      $ large water region (above); excluding bulk of 2-plate collar assy on ss sleeve outside beam tube close to dosi
meter ring
                  #(2533  -2531  2553  -2554  2543  -2544) $ water just outside ss sleeve (above), excluding ss square peg just upstream of dosimeter at Key
3, Positions 3
                  #(2533  -2531  2564  -2563  2543  -2544) $ water just outside ss sleeve (above), excluding ss square peg just upstream of dosimeter at Key
3, Positions 8
                    imp:n=2                 $ water just outside ss sleeve (above)
2134  7   -0.9899   2013 -2016  2100  -2110  2112  imp:n=2  $ water in elliptical cone chamfer ring where hb3 vessel hole penetrates inner wall of vessel
2135  7   -0.9899   2131 -2100 -2105   2013        imp:n=2  $ water outside ss sleeve but inside vessel nozzel
c
c
c     Note regarding dosimeters: the two cards shown below clearly define the location of the actual dosimeters presently
c     in use around HB-3.  Nevertheless, without further (questionable) changes to the model, the results here are probably
c     not even worth tabulating.  Reason:  The equivalent point sources used in this HB-3 analysis (of the voided & flooded
c     water tube) were based on global model point detectors at Z=120.6879, 185.9844, 251.2809 & 316.5774 cm from the radial
c     plane perpendicular to the HB-3 beam tube.  Moreover, for the analysis of the HB-3 water tube (the primary purpose of
c     this study), we spray neutron isotropically only over a very narrow forward-directed cone [cos(theta).gt. 0.965335056]
c     that in[illegible]es this region of interest, and assign the inner wall of the [illegible]eam tube an importance of 0.0 for all locations
c     below [illegible] 1007 at Z=118.6879 cm (see cell 10110).  This is done prim[illegible] in the name of efficiency in this water tube
c     analysis, but also because points below this would be outside the axia[illegible]ge where we know our equivalent point sources
```

```
c     give good results.  Unfortunately, these two dosimeters are located at Z=107.1276 cm and 112.9905 cm respectively (see
c     surfaces 2121 and 2126).  Thus, with the present model, these two dosimeters probably won't see any neutrons except for
c     a few stray ones that might backscatter into this region.  If one really wants to check fluxes at these dosimeters, one
c     would have to lower plane 1007 in cell 10110, and open up the angular range on the sdef card to the point where our
c     equivalent point sources may or may not still be valid.  At any rate, doing so would greatly decrease the efficiency
c     of the water tube analysis that we originally wanted to focus on.  --  J.A. Bucholz, 3-20-98(a)
c
c     Updated thoughts:  Neutron group 16 in the VELM library goes from 0.907 Mev to 1.108 Mev.  Virtually all of the
c     equivalent point neutron sources for these first 16 energy groups lie between Z=31 and Z=70 cm (indeed, most lie
c     between Z=45 cm and Z=60 cm).  Thus, if we use an energy cutoff card set at 1 MeV (as typically done for dosimetry
c     calcs), we could probably make the modifications described above without seriously impacting the quality of the
c     results at the dosimeter locations.  [Efficiency of the water tube calc would go to pot, but if we use this ECUT
c     card for the dosimetry, we would (by definition) not be interested in the water tube results in this calc anyway].
c     Thus, we can probably do the dosimetry study -- at least for fast neutrons above 1 MeV.  Nevertheless, a better
c     course of action might be to take this geometry model, then apply the approach I took last fall with HB-2 (involving
c     a finite line source with all neutrons in a prescribed direction wrt the axis). It gave absolutely excellent results,
c     very quickly.  --  J.A. Bucholz, 3-20-98(b)
c
c       $ obsolete $ 2134  50  -7.8212  -2121   imp:n=1   $ dosimeter (modeled as carbon steel; really Charpy V-notch specimens) just slightly on HB-4 side
of HB-3
c       $ obsolete $ 2135  50  -7.8212  -2126   imp:n=1   $ dosimeter (modeled as carbon steel; really Charpy V-notch specimens) just slightly on HB-2 side
of HB-3
c       $ obsolete $ 2134  7  -1.0000  -2121   imp:n=1   $ dosimeter (now modeled as water; specimens are quite small) just slightly on HB-4 side of HB-3
c       $ obsolete $ 2135  7  -1.0000  -2126   imp:n=1   $ dosimeter (now modeled as water; specimens are quite small) just slightly on HB-2 side of HB-3
c       The above (oversimplified) dosimeter cells have been replaced by Cells 2581 and 2582, along with Cells 2591-2593 for the dosimeter holder assembly (
ring)
c
c     ---------------------------------
c     Use the following two if looking at the old 1960 HB-3 design:   (must also set options on Cells 4305 & 4380 below)
c     $ obsolete $ 2140  23  -2.7       -1010  2151  -2152  imp:n=1  $ aluminum: 1st window at start of water tube (old 1960 location)
2140  23  -2.7       (2161 -2162 2163 -2153):(2164 -2165 -2163)  imp:n=1  $ aluminum: part-length model of old (1960) water tube: 1st spherical window & cyl
indrical section
2141  61  -3.2325-4  -1010  2153  -2154  imp:n=1  $ int void: 1st window at start of water tube (new 1998 location)
c
c     Use the following two if looking at the new 1998 HB-3 design:   (must also set options on Cells 4305 & 4380 below)
c       $ obsolete $ 2140  61  -3.2325-4  -1010  2151  -2152  imp:n=1  $ int void: 1st window at start of water tube (old 1960 location)
c       2140  61  -3.2325-4  (2161 -2162 2163 -2153):(2164 -2165 -2163)  imp:n=1  $ int void: part-length model of old (1960) water tube: 1st spherical wind
ow & cylindrical section
c       2141  23  -2.7       -1010  2153  -2154  imp:n=1  $ aluminum: 1st window at start of water tube (new 1998 location)
c     ---------------------------------
c
2144  24  -2.7  -2136  1010  2153 -2154  imp:n=1  $ aluminum ring joining regular section of beam tube to expanded section
c
c     ---------------------------------
c     Use the following two if beam tube is void, as in normal operation:
2145  61  -1.0e-20   -2134  2154 -4110         imp:n=1  $ void inside main cavity of expanded beam tube outside vessel (if void, as in normal operation)
2146  61  -1.0e-20   -2135  2134  2154  -4110  imp:n=1  $ void in pneumatic tube coils located just inside outer wall of expanded beam tube outside vessel
c
c     Use the following two if beam tube is flooded for maintenance work:
c       2145   8   -1.0000   -2134  2154 -4110         imp:n=1  $ water inside main cavity of expanded beam tube outside vessel (if flooded for maintenance)
c       2146   8   -1.0000   -2135  2134  2154  -4110  imp:n=1  $ water in pneumatic tube coils located just inside outer wall of expanded beam tube outside
 vessel
c     ---------------------------------
c
2147  24  -2.7  -2136  2135  2154  -4125  imp:n=1  $ aluminum body of expanded section of the new HB-3 beam tube outside vessel
c
c     ---------------------------------
c       In the name of simplification, lets combine the inner & outer SS liners with the main vessel, and treat all as carbon steel
```

```
c       2140  40  8.62373-2  -9999 9997  2013 -2014  2100  imp:n=1  $ pressure vessel's inner liner
c       2150  50  8.74142-2  -9999 9997  2014 -2015  2100  imp:n=1  $ main pressure vessel (thick carbon steel)
c       2160  40  8.62373-2  -9999 9997  2015 -2016  2100  imp:n=1  $ pressure vessel's outer liner
c       2150  50  -7.8212    -9999 9997  2013 -2016  2100  imp:n=1  $ main pressure vessel (thick carbon steel + inner & outer liners)
2150  50  -7.8212    -9999  9997  2013 -2016  2101        imp:n=1  $ main pressure vessel (thick carbon steel + inner & outer liners)
2151  50  -7.8212     2100 -2101 -2105  2013  9997                 $ vessel nozzel boss around HB-3
                  #(-2110 -2111)                          imp:n=2  $ vessel nozzel boss around HB-3 (above); excluding HB3 chamfer (surf 2110)
2152  50  -7.8212    -2101  2131  2105 -2106               imp:n=2  $ carbon steel flange on vessel nozzel boss by HB-3
c     ------------------------------
2170  8   -1.0000    -9999 9997  2016 -2017          $ water pool between pressure vessel and concrete bioshield
                     #(-2136  2153)  #(-2131 -2153)   $ water pool (above) excluding expanded section of HB-3 beam tube
                     #(4100  -4225)                   $ water pool (above) excluding everything inside ss sleeve (water & beam tube) where beam tube enters
concrete bioshield
                     #(-2101 -2106)  imp:n=1          $ water pool (above) excluding vessel boss (and flange) around HB-3
c
c
c     Cells associated with dosimeters & dosimeter specimen holder at Key 3 around HB-3 (see Dwg E-49953, Rev A, 6-30-65):
c     ------------------------------------------------------------------------------------------------------------
c     $ obsolete $ 2581  40 -7.92   2531  -2532  2551  -2552  2541  -2542  imp:n=1  $ dosimeter at Key 3, Position 3, just slightly on HB-2 side of HB-3 (mo
deled as ss304)
c     $ obsolete $ 2582  40 -7.92   2531  -2532  2562  -2561  2541  -2542  imp:n=1  $ dosimeter at Key 3, Position 8, just slightly on HB-4 side of HB-3 (mo
deled as ss304)
c
c     $ obsolete $ 2581  50  -7.8212  2531  -2532  2551  -2552  2541  -2542  imp:n=2  $ dosimeter at Key 3, Position 3, just slightly on HB-2 side of HB-3 (
modeled as carbon steel)
c     $ obsolete $ 2582  50  -7.8212  2531  -2532  2562  -2561  2541  -2542  imp:n=2  $ dosimeter at Key 3, Position 8, just slightly on HB-4 side of HB-3 (
modeled as carbon steel)
c
c     $ added 4-7-98:  Use of surf 2534 (instead of 2531) allows the ss304 cover plate of dosimeter holder ring to
c     $ added 4-7-98:  be modeled be separate from the carbon steel Charpy specimens in 1-cm-thk dosimeter capsules
2581  50  -7.8212  2534  -2532  2551  -2552  2541  -2542  imp:n=2  $ dosimeter at Key 3, Position 3, just slightly on HB-2 side of HB-3 (modeled as carbon s
teel)
2582  50  -7.8212  2534  -2532  2562  -2561  2541  -2542  imp:n=2  $ dosimeter at Key 3, Position 8, just slightly on HB-4 side of HB-3 (modeled as carbon s
teel)
c
2583  40  -7.92  2533  -2531  2553  -2554  2543  -2544  imp:n=2  $ ss square peg just upstream of dosimeter at Key 3, Position 3
2584  40  -7.92  2533  -2531  2564  -2563  2543  -2544  imp:n=2  $ ss square peg just upstream of dosimeter at Key 3, Position 8
c
2591  40 -7.92   2520  -2530  2531  -2532          $ Key 3 dosimetry specimen holder ring (ss304)
              #(2534  2551  -2552  2541  -2542)   $ Key 3 dosimetry specimen holder ring (ss304), excluding dosimeter at Key 3, Position 3
              #(2534  2562  -2561  2541  -2542)   $ Key 3 dosimetry specimen holder ring (ss304), excluding dosimeter at Key 3, Position 8
              imp:n=2                            $ Key 3 dosimetry specimen holder ring (ss304)
2592  40 -7.92  -2520  2521  -2522  2131  imp:n=2  $ short thick ss304 cylindrical sleeve on Key 3 dosimetry specimen holder
2593  40 -7.92  -2510  2131  -2521  2511  imp:n=2  $ long  thin  ss304 cylindrical sleeve on Key 3 dosimetry specimen holder
c     ------------------------------------------------------------------------------------------------------------
c
c
c     Cells associated with the 2-plate collar holding cooling tube on ss sleeve outside beam tube close to dosimeter ring
c     ------------------------------------------------------------------------------------------------------------
2761  40 -7.92  -2701 2131 2742 -2744  imp:n=2  $ 1st (upstream)   ss plate of 2-plate collar assembly
2762  40 -7.92  -2701 2131 2746 -2748  imp:n=2  $ 2nd (downstream) ss plate of 2-plate collar assembly
c
2771  40 -7.92  -2701 2131 2744 -2746 2711 -2712              imp:n=2  $ horizontal ss spacer plates (right & left, top & bottom, treated as one cell)
2772  40 -7.92  -2702 2701 2744 -2746 2711 -2710 2720        imp:n=2  $ horizontal ss spacer plate extension (on one side only); must exclude this from ve
ssel water (Cell 2130)
2773  40 -7.9    2701 2131 2744 -2746 2724 -2728 #(2722 -2726) imp:n=2  $ ver    l   ss spacer plates (right & left, top & bottom, treated as    cell)
2774   7 -0.9    -2701 2131 2744 -2746 2722 -2726             imp:n=2  $ wa    etween vertical spacer plates
c
```

```
2781   7 -0.9899  -2701  2131  2744  -2746          $ water between main upstream & downstream plates of 2-plate collar assembly
                  #(2711  -2712)  #(2724  -2728)    $ water (above), excluding horizontal & vertical spacers
                  imp:n=2                           $ water between main upstream & downstream plates of 2-plate collar assembly
c     ------------------------------------------------------------------------------------------------------------------------
c
c
c       Intermediate notes using COMJOM-like notation to describe the cells in and around the HB-3 shield plug:
c
c       box1 = (3083 -3073 3023 -3033 3006 -3001)
c       box2 = (3082 -3072 3022 -3032 3005 -3001)
c       box3 = (3103 -3093 3043 -3053 3010 -3002)
c       box4 = (3102 -3092 3042 -3052 3009 -3002)
c       box5 = (3081 -3071 3021 -3031 3004 -3001)
c       box6 = (3080 -3070 3020 -3030 3003 -3002)
c       box7 = (3101 -3091 3041 -3051 3008 -3002)
c       box8 = (3100 -3090 3040 -3050 3007 -3002)
c
c       cyl9  = (-3120 3061 -3062)
c       cyl10 = (-3121 3061 -3063)
c       cyl11 = (-3122 3060 -3064)
c       cyl12 = (-3110)
c
c       Cell 3001 = bconc den  (former cell 3001)  #box3  #box1   imp:n=1  $ revised model of barytes concrete forming bioshield
c       Cell 3010 = ss  den  box1  #box2  #box3   imp:n=1  $ ss liner on bioshield near big (downstream) side of removable block containing shield plug
c       Cell 3020 = ss  den  box3  #box4  #box2   imp:n=1  $ ss liner on bioshield near small (upstream) side of removable block containing shield plug
c       Cell 3030 = ss  den  box5  #box6  #box7  #cyl12   imp:n=1  $ ss liner on big (downstream) side of removable concrete block containing shield plug
c       Cell 3040 = ss  den  box7  #box8  #box6  #cyl12   imp:n=1  $ ss liner on small (upstream) side of removable concrete block containing shield plug
c       Cell 3050 = void den  (box4 OR box2)  #box7  #box5   imp:n=1  $ void immediately upstream of (and around) the removable concrete block containing sh
ield plug
c       Cell 3060 = bconc den  (box8 OR box6)  #cyl11  #cyl12   imp:n=1  $ barytes concrete forming bulk of the removable concrete block containing shield p
lug
c       Cell 3070 = ss  den  cyl11  #cyl10  #cyl12   imp:n=1  $ ss liner inside the removable concrete block containing shield plug
c       cccc    Cell 3080 = void den  (box7 OR box5) inside cyl12  #cyl10   imp:n=1  $ void near centerline, upstream and downstream of shield plug, inside
removable concrete block
c       Cell 3080 = void den  (box7 OR box5) inside cyl12  #cyl9   imp:n=1  $ void near centerline, upstream and downstream of shield plug, inside removable
 concrete block
c       Cell 3090 = cstl den  cyl9   imp:n=1  $ carbon steel forming the actual shield plug
c       Cell 3100 = void den  cly10  #cyl9   imp:n=1  $ void gap around the cylindrical shield plug
c
c       Final MCNP description of the cells in and around the HB-3 shield plug:
c     ------------------------------------------------------------------------------------------------------------------------
c
3000  61  -1.0e-20   -9999 3001 -9998  9990  imp:n=1       $ void downstream of the HB-3 shield plug (shutter); excl small sph around pt where Blosser & Tho
mas made measurements
c
c     Barytes concrete bioshield from the upstream edge of the cavity containing the removable concrete block containing
c     the HB-3 shield plug (really surf 3010), out to the downstream edge of the removable block containing the shield plug:
3001  62  -3.09725   -9999 3010 -3001                     $ barytes concrete bioshield (outermost part)
                    #(3103 -3093 3043 -3053 3010 -3002)   $ barytes concrete bioshield (outermost part)
                    #(3083 -3073 3023 -3033 3006 -3001)   $ barytes concrete bioshield (outermost part)
                    imp:n=1                               $ barytes concrete bioshield (outermost part)
c
c     Barytes concrete bioshield from beyond pool liner (liner not modeled) out to upstream edge of removable block containing shield plug (really surf 3010
)
3002  62  -3.09725   -9999 9997 -3010  2017  2136  $ barytes concrete bioshield (from pool liner to shutter assembly cavity)
                    #(4155  -3010  -4265)   4225  $ barytes concrete (above) excluding everything inside ss bioshield liner around collimator assembly
                    imp:n=1                       $ barytes concrete bioshield (from pool liner to shutter assembly cavity)
c
```

```
c     -------------------------
c
3010  40  -7.92  (3083 -3073 3023 -3033 3006 -3001)   $ ss liner on bioshield near big (downstream) side of removable block containing shield plug
                #(3082 -3072 3022 -3032 3005 -3001)  $ ss liner on bioshield near big (downstream) side of removable block containing shield plug
                #(3103 -3093 3043 -3053 3010 -3002)  $ ss liner on bioshield near big (downstream) side of removable block containing shield plug
                imp:n=1                              $ ss liner on bioshield near big (downstream) side of removable block containing shield plug
c
3020  40  -7.92  (3103 -3093 3043 -3053 3010 -3002)   $ ss liner on bioshield near small (upstream) side of removable block containing shield plug
                #(3102 -3092 3042 -3052 3009 -3002)  $ ss liner on bioshield near small (upstream) side of removable block containing shield plug
                #(3082 -3072 3022 -3032 3005 -3001)  $ ss liner on bioshield near small (upstream) side of removable block containing shield plug
                4240  imp:n=1                        $ ss liner on bioshield near small (upstream) side of removable block containing shield plug (excl end
 of collimator assy)
c
3030  40  -7.92  (3081 -3071 3021 -3031 3004 -3001)   $ ss liner on big (downstream) side of removable concrete block containing shield plug
                #(3080 -3070 3020 -3030 3003 -3002)  $ ss liner on big (downstream) side of removable concrete block containing shield plug
                #(3101 -3091 3041 -3051 3008 -3002)  $ ss liner on big (downstream) side of removable concrete block containing shield plug
                3110  imp:n=1                        $ ss liner on big (downstream) side of removable concrete block containing shield plug
c
3040  40  -7.92  (3101 -3091 3041 -3051 3008 -3002)   $ ss liner on small (upstream) side of removable concrete block containing shield plug
                #(3100 -3090 3040 -3050 3007 -3002)  $ ss liner on small (upstream) side of removable concrete block containing shield plug
                #(3080 -3070 3020 -3030 3003 -3002)  $ ss liner on small (upstream) side of removable concrete block containing shield plug
                3110  imp:n=1                        $ ss liner on small (upstream) side of removable concrete block containing shield plug
c
3050  61  -1.0e-20  ((3102 -3092 3042 -3052 3009 -3002): $ void immediately upstream of (and around) the removable concrete block containing shield plug
                     (3082 -3072 3022 -3032 3005 -3001)) $ void immediately upstream of (and around) the removable concrete block containing shield plug
                    #(3101 -3091 3041 -3051 3008 -3002)  $ void immediately upstream of (and around) the removable concrete block containing shield plug
                    #(3081 -3071 3021 -3031 3004 -3001)  $ void immediately upstream of (and around) the removable concrete block containing shield plug
                    #(-4195  -4245)                      $ void (above) excluding downstream end of collimator assembly and flange
                    imp:n=1                              $ void immediately upstream of (and around) the removable concrete block containing shield plug
c
3060  62  -3.09725  ((3100 -3090 3040 -3050 3007 -3002): $ barytes concrete forming bulk of the removable concrete block containing shield plug
                     (3080 -3070 3020 -3030 3003 -3002)) $ barytes concrete forming bulk of the removable concrete block containing shield plug
                    #(-3122 3060 -3064)  3110   imp:n=1  $ barytes concrete forming bulk of the removable concrete block containing shield plug
c
3070  40  -7.92   -3122  3060  -3064  3110  3007  -3002  $ ss liner inside the removable concrete block containing shield plug
                 #(-3121 3061 -3063)           imp:n=1  $ ss liner inside the removable concrete block containing shield plug
c
c       3080  61  -1.0e-20  -3110  3008  -3001  3121    imp:n=1  $ void near centerline, upstream and downstream of shield plug, inside removable concrete b
lock
3080  61  -1.0e-20  -3110  3008  -3001  3120    imp:n=1  $ void near centerline, upstream and downstream of shield plug, inside removable concrete block
c
3090  50   -7.8212   -3120  3061  -3062  3131  3132     imp:n=1  $ carbon steel forming the shield plug (ie, the rotary shutter)
3091  61  -1.0e-20   -3120  (-3131:-3132)  imp:n=1  $ beam holes thru the rotary shutter); for orientation, see surfs 3131 & 3132
c
3100  61  -1.0e-20  -3121  3061  -3063  3007  -3002      $ void gap around the cylindrical shield plug
                     3110  #(-3120 3061 -3062)  imp:n=1  $ void gap around the cylindrical shield plug
c     ---------------------------------------------------------------------------------------------------------------------------------------------
c
c
c     Cells used for the description of the collimator assembly (etc) inside the concrete:
c     ---------------------------------------------------------------------------------------------------------------------------------------------
c
4300  61  -1.0e-20  4130 -4190 4210 -4211 4212 -4213                    $ rectangular hole up thru collimator
                   #(4140 -4145)                                imp:n=1  $ exclusion used to allow simulating 2nd aluminum window in 1960 design (see cells
 4305 & 4380)
c     ---------------------------------
4305  23  -2.      4140 -4145 4210 -4211 4212 -4213     imp:n=1  $ aluminum      IFF simulating 2nd aluminum window in 1960 design (downstr      nd of water
 tube)
```

```
c       4305  61  -1.0e-20  4140 -4145 4210 -4211 4212 -4213            imp:n=1  $ void here IF modeling 2nd aluminum window in 1998 design (downstream end
 of water tube not here)
c     -------------------------
4310  40  -7.92     4130  -4190 -4230  #(4210 -4211 4212 -4213)  imp:n=1  $ ss body of central collimator with rectangular hole
4315  61  -1.0e-20  4190  -4195  4210   -4211 4212 -4213         imp:n=1  $ thin rect void reg (5.5"x2.75") immediately downstream of colimator <-- get axia
l leakage here
4316  61  -1.0e-20  4190  -4195 -4230  #(4210 -4211 4212 -4213)  imp:n=1  $ thin void immediately downstream of steel body of collimator (excl rect hole)
4320  24   -2.7     4125  -4195  4230  -4235                    imp:n=1  $ aluminum: expanded section of beam tube along side the collimator
4321  24   -2.7     4125  -4126  2135  -4230                    imp:n=1  $ aluminum step where beam tube expands again, just upstream of collimator
4330  40  -7.92     4180  -4195  4235  -4240                    imp:n=1  $ ss pool seal (B) downstream of collimator
4335  40  -7.92     3009  -4195  4240  -4245                    imp:n=1  $ ss flange around pool seal (B) downstream of collimator
4340  61  -1.0e-20  4170  -3010  4235  -4260  #(4180 -4240)      imp:n=1  $ void downstream of removable shield and eccentric shield
c       4345  41  -7.92     4150  -4170  4235  -4255  #(4250 -4160)      imp:n=1  $ ss removable shield, radially outside beam tube, next to collimator
4345  40  -7.92     4150  -4170  4235  -4255  #(4250 -4160)      imp:n=1  $ ss removable shield, radially outside beam tube, next to collimator
4350  40  -7.92     4160  -4170  4255  -4260                    imp:n=1  $ ss eccentric shield, radially outside removable shield
4355  40  -7.92     4160  -3010  4260  -4265                    imp:n=1  $ ss bioshield liner, between eccentric shield and concrete bioshield
4356  40  -7.92     4155  -4160  4220  -4265                    imp:n=1  $ ss liner on step expansion of bioshield, just upstream of removable shiled
4360  61  -1.0e-20  4135  -4150  4235  -4250                    imp:n=1  $ void just upstream of removable shield around collimator
4365  40  -7.92     4120  -4160  4250  -4220                    imp:n=1  $ ss pool seal (A2) upstream of collimator
4370  40  -7.92     4105  -4135  2136  -4250  #(4125 -4235)      imp:n=1  $ ss pool seal (A1) upstream of collimator
4375  61  -1.0e-20  4115  -4130 -4230         #(2135 -4126)      imp:n=1  $ void just upstream of collimator (before 2nd aluminum window in 1998 design)
c     -------------------------
4380  61  -1.0e-20  4110  -4115  -2135                  imp:n=1  $ void here IFF simulating 2nd aluminum window in 1960 design (downstream end of water tub
e not here)
c       4380  23   -2.7     4110  -4115  -2135                    imp:n=1  $ aluminum here IF one wants to model 2nd aluminum window in 1998 design (
downstream end of water tube)
c     -------------------------
4385  8  -1.0000  4100  -4120  2136  -4220  #(4105 -4250)        imp:n=1  $ water between beam tube & ss sleeve extending from concrete bioshield into pool
4390  40   -7.92  4100  -4155  4220  -4225                      imp:n=1  $ ss sleeve / bioshield liner extending from bioshield into the pool
c     ------------------------------------------------------------------------------------------------------------------------------------------------
c
9990  61  -1.0e-20    -9990   imp:n=1   $ small sph around pt where Blosser & Thomas made measurements;  for illustrative purposes only;  may put pt det ins
ide
9999  0  #(-9999 9997 -9998)  imp:n=0   $ external void; everything not inside the (1.3 m diam x 7.0 m long) cylinder modeled here
c
c     END CELLS (next line must be blank)

c     BEGIN SURFACES:
c
c      HB-3 (Tangential tube); described here as if the Z axis now corresponds to HB-3 axis
c
c      The following correspond to the real "physical" location of the spherical tip of the HB-3 beam tube:
c      1000   sz   28.5369   5.08         $ Spherical void OD
c      1001   sz   28.5369   6.03250      $ Spherical inner Al wall OD
c      1002   sz   28.5369   6.15250      $ Spherical water OD
c      1003   sz   28.5369   6.3896875    $ Spherical outer Al wall OD
c      1004   sz   28.5369   6.5497075    $ Spherical water jacket OD
c      1005   sz   28.5369   6.7605275    $ Spherical Al Be liner OD
c      1006   pz   28.5369                $ Plane at end of Cylindrical tube
c
c      Here, the hot tip has been artificially extended inward 18.5369 cm to accomodate innermost equiv point src at Z=10 cm:
1000   sz   10.0   5.08         $ Spherical void OD
1001   sz   10.0   6.03250      $ Spherical inner Al wall OD
1002   sz   10.0   6.15250      $ Spherical water OD
1003   sz   10.0   6.3896875    $ Spherical outer Al wall OD
1004   sz   10.0   6.5497075    $ Spherical water jacket OD
1005   sz   10.0   6.7605275    $ Spherical Al Be liner OD
1006   pz   10.0                $ Plane at end of Cylindrical tube
```

```
c       1007   pz   118.6879            $ Plane below which all importances are zero; located 2 cm upstream of first pt det used to get pt srcs
1007   pz   75.473    $ Plane below which all importances are zero; use this for dosimetry only; located 31.6546 cm upstream of first dosimeter
c
c      Cylindrical part of HB-3; described here as if the Z axis now corresponds to HB-3 axis
1010   cz   5.08                  $ Cylindrical void OD
1011   cz   6.03250               $ Cylindrical inner Al wall OD
1012   cz   6.1515625             $ Cylindrical water OD
1013   cz   6.3896875             $ Cylindrical outer Al wall OD
1014   cz   6.5497075             $ Cylindrical water jacket OD
1015   cz   6.7605275             $ Cylindrical Al Be liner OD
c
c
c      If the Z axis now corresponds to HB-3, then the main cylinders for core, vessel, etc, are described as:
c      Sidewall thicknesses from per comm. with Dick Rothrock (01-11-95); Sidewall dimensions from 1971 report
2010   c/x  26.67  0.0     54.61      $ outer radius--permanent Be refl. reg.
2011   c/x  26.67  0.0     55.245     $ outer radius--water gap
2012   c/x  26.67  0.0     56.8325    $ outer radius--aluminum reflector cage
2013   c/x  26.67  0.0    119.38      $ outer radius--water
2014   c/x  26.67  0.0    119.6975    $ outer radius--inner pressure vessel clad
2015   c/x  26.67  0.0    127.0       $ outer radius--pressure vessel
2016   c/x  26.67  0.0    127.254     $ outer radius--outer pressure vessel clad
2017   c/x  26.67  0.0    274.32      $ outer radius--H2O pool (pool/pool-liner interface at r=274.32 cm; pool diam=18 ft)
c
c      Note: for now, will model boss & flange on HB-3, but will ignore some of the finer details.  Will assume, for example,
c      that the vessel is tight against HB-3, thus ignoring the slightly larger hole actually present in vessel for HB-3, and
c      the sleeve (hydraulic seal) around HB-3 near vessel.  These may be added later (?).
2100   cz   10.0680   $ inner radius of vessel nozzel (boss) around HB-3 beam tube (see dwg E-42027)
2101   cz   21.45     $ outer radius of vessel nozzel (boss) around HB-3 beam tube (see dwg E-42027)
2105   pz  137.16     $ plane defining end of boss on pressure vessel around HB-3 (see dwg E-42027); in model, use 2106 instead
2106   pz  143.9443   $ plane defining end of thick flange mounted on boss on pressure vessel around HB-3 (see dwg E-42027)
c
c      wrong:  2110   42  sq  0.9262159  0.9880902  -1.0  0  0  0  0  0  0  0  $ elliptical cone used to define chamfer between HB3 vessel hole and inner su
rf of pressure vessel
c      The above specification was used in Runs HB304G & HB304H. Subsequent graphical analysis of the flare at the midplane (x=0)
c      showed that this elliptical cone chamfer was NOT a good representation of the rounded corners, and (in fact) cut off too
c      much steel from the vessel and substituted too much water.  The graphical analysis was reworked, using some CAD work
c      and some equations this time, and the following was found to be a much more accurate representation.  -- JAB, 5 Apr 98
c      Input files for HB304I & HB304J were also no good. These were failed attempts to fix the problem.  Those two cases
c      (I&J) were never run since similar problems were noticed during the graphical checkout step before final submission.
c      Run HB304K (whose correct input is shown below) was the firt run which had this correct. TR42 also changed. -- JAB 6 Apr 98
2110   42  sq  0.928252  1.0  -1.0  0  0  0  0  0  0  0  $ elliptical cone used to define chamfer between HB3 vessel hole and inner surf of pressure vessel
2111   42  pz  -0.001  $ plane used to help define which side of the double elliptical cone we want (cone reduces to a point at z=0, but use z=-0.001 to avo
id roundoff)
2112   42  pz  -15.0   $ plane used to define the upstream axial extent of the elliptical cone we want to consider (must be somewhere beyond z=-12.78829; z=
-15 is arbitrary)
c
c      Note regarding dosimeters:  these are really Charpy V-notch specimens, measuring 0.75"x0.75"x1.5";  locations were taken from dwg E-42027
2121   s  0.0  -13.480  107.1276  1.48893  $ sphere simulating dosimeter just slightly on HB-4 side of HB-3   (see above note)
2126   s  0.0   12.284  112.9905  1.48893  $ sphere simulating dosimeter just slightly on HB-2 side of HB-3   (see above note)
c
2130   cz  7.16174    $ inner radius of ss sleeve around HB-3 beam tube, near vessel
2131   cz  7.9338     $ outer radius of ss sleeve around HB-3 beam tube, near vessel
c
2134   cz  6.08626    $ inner radius of pneumatic tubes/coils inside expanded section of the HB-3 beam tube outside the vessel
2135   cz  7.03453    $ pneumatic tube / beam tube interface for the expanded section of the HB-3 beam tube outside the vessel
2136   cz  7.[illegible]3    $ outer radius of the expanded section of the HB-3 beam tube outside the vessel
c
2150   pz   96.8375   $ plane defining end of ss sleeve around beam tube, near vessel
```

```
2151   pz  116.7841   $ upstream   side of aluminum window forming start of water tube in original HB-3 design (as built)
2152   pz  117.7366   $ downstream side of aluminum window forming start of water tube in original HB-3 design (as built)
2153   pz  174.27     $ upstream   side of aluminum window forming start of water tube in proposed HB-3 design
2154   pz  174.95125  $ downstream side of aluminum window forming start of water tube in proposed HB-3 design
c
c      The following surfaces are used for a part-length model of the old (1960) water tube.
c      In this part-length model, the downstream end is defined by surf 2153 which is the
c      upstream surface of the 1-st aluminum window defining the start of the 1998 water tube.
2161   cz  3.65125            $ inner radius of cylindrical portion of old (1960) water tube
2162   cz  4.60375            $ outer radius of cylindrical portion of old (1960) water tube
2163   pz  120.30375          $ plane between cylindrical & spherical portion of old (1960) water tube, near upstream end
2164   sz  120.30375  3.65125 $ inner radius of spherical portion of old (1960) water tube, near upstream end
2165   sz  120.30375  4.60375 $ outer radius of spherical portion of old (1960) water tube, near upstream end
c
c
c      Surfaces associated with dosimeters & dosimeter specimen holder at Key 3 around HB-3
c      ------------------------------------------------------------------------------
c      2510   cz  8.41005  $ outer radius of thin cylindrical sleeve on Key 3 dosimetry specimen holder
c      2511   pz  107.056  $ upstream extent of thin cylindrical sleeve on Key 3 dosimetry specimen holder
c      c
c      2520   40  cz  9.36625   $ outer radius      of thick cylindrical sleeve on Key 3 dosimetry specimen holder
c      2521   40  pz  -1.5875   $ upstream   extent of thick cylindrical sleeve on Key 3 dosimetry specimen holder
c      2522   40  pz   1.5875   $ downstream extent of thick cylindrical sleeve on Key 3 dosimetry specimen holder
c      c
c      2530   40  cz  18.57375  $ outer radius      of Key 3 dosimetry specimen holder (ring)
c      2531   40  pz  -0.635    $ upstream   extent of Key 3 dosimetry specimen holder = upstream   surf of all capsule positions in Key 3
c      2532   40  pz   0.635    $ downstream extent of Key 3 dosimetry specimen holder = downstream surf of all capsule positions in Key 3
c      2533   40  pz   -2.54    $ upstream face of small square pegs directly upstream of dosimeters in Key 3, Positions 3 & 8 (downstream face=surf 2531)
c      c
c      2541   px  -1.4732       $ bottom (-X) surf of capsules in Key 3, positions 3 & 8 (specifically); no transformation req'd
c      2542   px   1.4732       $ top    (+X) surf of capsules in Key 3, positions 3 & 8 (specifically); no transformation req'd
c      2543   px  -1.905        $ bottom (-X) surf of small square pegs directly upstream of dosimeters in Key 3, Positions 3 & 8; no transformation req'd;
-X location only a guess
c      2544   px   1.905        $ top    (+X) surf of small square pegs directly upstream of dosimeters in Key 3, Positions 3 & 8; no transformation req'd;
+X location only a guess
c      c
c      2551   40  py   10.993   $ innermost (-Y) surf of capsule in Key 3, Position 3 (specifically); ie, capsule on HB-2 side of HB-3
c      2552   40  py   16.327   $ outermost (+Y) surf of capsule in Key 3, Position 3 (specifically); ie, capsule on HB-2 side of HB-3
c      2553   40  py   10.7675  $ innermost (-Y) surf of square peg just upstream of dosimeter at Key 3, Position 3 (specifically)
c      2554   40  py   12.6725  $ outermost (+Y) surf of square peg just upstream of dosimeter at Key 3, Position 3 (specifically)
c      c
c      2561   40  py  -10.993   $ innermost (+Y) surf of capsule in Key 3, Position 8 (specifically); ie, capsule on HB-4 side of HB-3
c      2562   40  py  -16.327   $ outermost (-Y) surf of capsule in Key 3, Position 8 (specifically); ie, capsule on HB-4 side of HB-3
c      2563   40  py  -13.9075  $ innermost (+Y) surf of square peg just upstream of dosimeter at Key 3, Position 8 (specifically)
c      2564   40  py  -15.8125  $ outermost (-Y) surf of square peg just upstream of dosimeter at Key 3, Position 8 (specifically)
c      ------------------------------------------------------------------------------
c
c
c      Surfaces associated with dosimeters & dosimeter specimen holder at Key 3 around HB-3. (Note: These were all revised
c      as follows by JAB on 3 Apr 98 for Run HB304H, based on newly available data shown on Dwg E-49953, Rev A, 6-30-65):
c      ------------------------------------------------------------------------------------------------------------------
2510   cz  8.17193  $ outer radius of thin cylindrical sleeve on Key 3 dosimetry specimen holder
2511   pz  109.17   $ upstream extent of thin cylindrical sleeve on Key 3 dosimetry specimen holder
c
2520   40  cz   9.5      $ outer radius      of thick cylindrical sleeve on Key 3 dosimetry specimen holder
2521   40  pz  -2.3      $ upstream   extent of thick cylindrical sleeve on Key 3 dosimetry specimen holder
2522   40  pz   0.8      $ downstream extent of thick cylindrical sleeve on Key 3 dosimetry specimen holder
c
```

```
2530   40  cz  18.16      $ outer radius      of Key 3 dosimetry specimen holder (ring)
2531   40  pz  -0.8175    $ upstream   extent of Key 3 dosimetry specimen holder ring (ie, just upstream on the 0.3175 cm cover plate, but no water)
2532   40  pz   0.50      $ downstream extent of Key 3 dosimetry specimen holder ring = downstream surf of all capsule positions in Key 3 (capsules are 0.394
"=1.00075 cm thk)
2533   40  pz  -3.25      $ upstream face of small square pegs directly upstream of dosimeters in Key 3, Positions 3 & 8 (downstream face=surf 2531)
2534   40  pz  -0.50      $ upstream face of 1-cm-thk dosimeter capsules (Key 3, Positions 3 & 8) inside dosimeter holder ring
c
2541   px  -1.50622       $ bottom (-X) surf of capsules in Key 3, positions 3 & 8 (specifically); no transformation req'd
2542   px   1.50622       $ top    (+X) surf of capsules in Key 3, positions 3 & 8 (specifically); no transformation req'd
2543   px  -1.50          $ bottom (-X) surf of small square pegs directly upstream of dosimeters in Key 3, Positions 3 & 8; no transformation req'd; -X loca
tion only a guess
2544   px   3.37          $ top    (+X) surf of small square pegs directly upstream of dosimeters in Key 3, Positions 3 & 8; no transformation req'd; +X loca
tion only a guess
c
2551   40  py   10.10045 $ innermost (-Y) surf of capsule in Key 3, Position 3 (specifically); ie, capsule on HB-2 side of HB-3
2552   40  py   15.59955 $ outermost (+Y) surf of capsule in Key 3, Position 3 (specifically); ie, capsule on HB-2 side of HB-3
2553   40  py   11.0475  $ innermost (-Y) surf of square peg just upstream of dosimeter at Key 3, Position 3 (specifically)
2554   40  py   12.9525  $ outermost (+Y) surf of square peg just upstream of dosimeter at Key 3, Position 3 (specifically)
c
2561   40  py  -10.10045 $ innermost (+Y) surf of capsule in Key 3, Position 8 (specifically); ie, capsule on HB-4 side of HB-3
2562   40  py  -15.59955 $ outermost (-Y) surf of capsule in Key 3, Position 8 (specifically); ie, capsule on HB-4 side of HB-3
2563   40  py  -14.1475  $ innermost (+Y) surf of square peg just upstream of dosimeter at Key 3, Position 8 (specifically)
2564   40  py  -16.0525  $ outermost (-Y) surf of square peg just upstream of dosimeter at Key 3, Position 8 (specifically)
c      ------------------------------------------------------------------------------------------------------------------------
c
c
c     Surfaces associated with the 2-plate collar holding cooling tube on ss sleeve outside beam tube close to dosimeter ring
c     ------------------------------------------------------------------------------------------------------------------------
2701  cz  11.40      $ outer radius of 2-plate collar (surf 2131 defines inner radius)
2702  cz  14.88      $ outer radius of the one spacer plate extension
c
2710  px   0.0       $ horizontal midplane = top surface of the one spacer plate extension
2711  px  -1.11125   $ bottom surface of the horizontal spacer plates
2712  px   1.11125   $ top surface of the horizontal spacer plates
c
2720  py   0.0       $ vertical plane up middle (needed to uniquely define spacer plate extension)
2722  py  -1.80      $ right surface of vertical spacer plates on left
2724  py  -3.22      $ left  surface of vertical spacer plates on left
2726  py   1.80      $ left  surface of vertical spacer plates on right
2728  py   3.22      $ right surface of vertical spacer plates on right
c
2742  pz  100.3275   $ upstream   surface of 1st (upstream)   plate
2744  pz  101.43875 $ downstream surface of 1st (upstream)   plate
2746  pz  105.24875 $ upstream   surface of 2nd (downstream) plate
2748  pz  106.36     $ downstream surface of 2nd (downstream) plate
c     ------------------------------------------------------------------------------------------------------------------------
c
c
c      Surfaces describing the cells in and around the HB-3 shield plug (ie, the rotary shutter):
c      ------------------------------------------------------------------------------------------------------------------------
3001   pz  478.79     $ plane defining end of concrete just past downstream edge of removable concrete block containing HB-3 shield plug (see dwgs 1546-01-M
-5022 and E-42027)
3002   pz  477.8375   $ upstream surf of ss block liner downstream of shutter
3003   pz  447.3575   $ downstream side of ss liner on removable block near midsection of removable concrete block containing shield plug
3004   pz  446.405    $ upstream   side of ss liner on removable block near midsection of removable concrete block containing shield plug
3005   pz  44[illegible]75   $ downstream side of ss liner on bioshield near midsect[illegible] of removable concrete block containing shield plug
3006   pz  44[illegible]25   $ upstream   side of ss liner on bioshield near midsec[illegible] of removable concrete block containing shield plug
3007   pz  414.[illegible]725   $ downstream side of ss liner on upstream side of remov[illegible]e concrete block containing shield plug
```

```
3008   pz  414.02     $ upstream   side of ss liner on upstream side of removable concrete block containing shield plug
3009   pz  392.7475   $ downstream side of ss liner on bioshield (upstream of removable concrete block containing shield plug)
3010   pz  392.1125   $ upstream   side of ss liner on bioshield (upstream of removable concrete block containing shield plug)
c
3020   py  -40.79875  $ inner surf (-Y) of ss liner on big (downstream) side of removable concrete block containing shield plug
3021   py  -41.75125  $ outer surf (-Y) of ss liner on big (downstream) side of removable concrete block containing shield plug
3022   py  -43.4975   $ inner surf (-Y) of ss liner on bioshield near big (downstream) side of removable concrete block containing shield plug
3023   py  -44.1325   $ outer surf (-Y) of ss liner on bioshield near big (downstream) side of removable concrete block containing shield plug
c
3030   py   40.79875  $ inner surf (+Y) of ss liner on big (downstream) side of removable concrete block containing shield plug
3031   py   41.75125  $ outer surf (+Y) of ss liner on big (downstream) side of removable concrete block containing shield plug
3032   py   43.4975   $ inner surf (+Y) of ss liner on bioshield near big (downstream) side of removable concrete block containing shield plug
3033   py   44.1325   $ outer surf (+Y) of ss liner on bioshield near big (downstream) side of removable concrete block containing shield plug
c
3040   py  -36.195    $ inner surf (-Y) of ss liner on small (upstream) side of removable concrete block containing shield plug
3041   py  -37.30625  $ outer surf (-Y) of ss liner on small (upstream) side of removable concrete block containing shield plug
3042   py  -39.6875   $ inner surf (-Y) of ss liner on bioshield near small (upstream) side of removable concrete block containing shield plug
3043   py  -40.3225   $ outer surf (-Y) of ss liner on bioshield near small (upstream) side of removable concrete block containing shield plug
c
3050   py   36.195    $ inner surf (+Y) of ss liner on small (upstream) side of removable concrete block containing shield plug
3051   py   37.30625  $ outer surf (+Y) of ss liner on small (upstream) side of removable concrete block containing shield plug
3052   py   39.6875   $ inner surf (+Y) of ss liner on bioshield near small (upstream) side of removable concrete block containing shield plug
3053   py   40.3225   $ outer surf (+Y) of ss liner on bioshield near small (upstream) side of removable concrete block containing shield plug
c
3060   px  -31.27375  $ bot surf of lower ss liner for cylindrical cavity containing shield plug
3061   px  -30.48     $ top surf of lower ss liner for cylindrical cavity containing shield plug = bottom surf of shield plug
3062   px   30.48     $ top surf of shield plug
3063   px   31.27375  $ bot surf of upper ss liner for cylindrical cavity containing shield plug
3064   px   32.0675   $ top surf of upper ss liner for cylindrical cavity containing shield plug
c
3070   px   40.79875  $ inner surf (+X) of ss liner on big (downstream) side of removable concrete block containing shield plug
3071   px   41.75125  $ outer surf (+X) of ss liner on big (downstream) side of removable concrete block containing shield plug
3072   px   43.4975   $ inner surf (+X) of ss liner on bioshield near big (downstream) side of removable concrete block containing shield plug
3073   px   44.1325   $ outer surf (+X) of ss liner on bioshield near big (downstream) side of removable concrete block containing shield plug
c
3080   px  -40.79875  $ inner surf (-X) of ss liner on big (downstream) side of removable concrete block containing shield plug
3081   px  -41.75125  $ outer surf (-X) of ss liner on big (downstream) side of removable concrete block containing shield plug
3082   px  -43.4975   $ inner surf (-X) of ss liner on bioshield near big (downstream) side of removable concrete block containing shield plug
3083   px  -44.1325   $ outer surf (-X) of ss liner on bioshield near big (downstream) side of removable concrete block containing shield plug
c
3090   px   36.195    $ inner surf (+X) of ss liner on small (upstream) side of removable concrete block containing shield plug
3091   px   37.30625  $ outer surf (+X) of ss liner on small (upstream) side of removable concrete block containing shield plug
3092   px   39.6875   $ inner surf (+X) of ss liner on bioshield near small (upstream) side of removable concrete block containing shield plug
3093   px   40.3225   $ outer surf (+X) of ss liner on bioshield near small (upstream) side of removable concrete block containing shield plug
c
3100   px  -36.195    $ inner surf (-X) of ss liner on small (upstream) side of removable concrete block containing shield plug
3101   px  -37.30625  $ outer surf (-X) of ss liner on small (upstream) side of removable concrete block containing shield plug
3102   px  -39.6875   $ inner surf (-X) of ss liner on bioshield near small (upstream) side of removable concrete block containing shield plug
3103   px  -40.3225   $ outer surf (-X) of ss liner on bioshield near small (upstream) side of removable concrete block containing shield plug
c
3110   cz   8.255     $ cyl (along z axis) defining void in removable concrete block, upstream and downstream of the shield plug
c
3120   c/x  0.0  446.405  30.95625  $ outer radius of carbon steel shield plug (ie, rotary shutter); also see surfs 3131 & 3132
3121   c/x  0.0  446.405  31.75     $ outer radius of void around shield plug = inner radius of ss liner in removable concrete block
3122   c/x  0.0  446.405  32.54375  $ outer radius of ss liner in removable concrete block containing shield plug
c
c      ------------------------------------------------------------------------------------------------------------------------------
c
```

```
3131  11  cz  4.445    $ the big 3.5"diam beam hole in the rotary shutter;  use this when big hole is turned to "open" position
3132  21  cz  1.11125  $ small 0.875"diam beam hole in the rotary shutter;  use this when big hole is turned to "open" position
c
c       3131  12  cz  4.445    $ the big 3.5"diam beam hole in the rotary shutter;  use this when small hole is turned to "open" position
c       3132  22  cz  1.11125  $ small 0.875"diam beam hole in the rotary shutter;  use this when small hole is turned to "open" position
c
c       3131  13  cz  4.445    $ the big 3.5"diam beam hole in the rotary shutter;  use this when shutter is turned to "closed" position
c       3132  23  cz  1.11125  $ small 0.875"diam beam hole in the rotary shutter;  use this when shutter is turned to "closed" position
c
c      ------------------------------------------------------------------------------------------------------------------------------------
c
c
c
c     Axial surfaces used for the description of the collimator assembly (etc) inside the concrete:
c     ---------------------------------------------------------------------------
4100  pz  261.9474  $ max upstream axial location of narrow ss sleeve extending thru concrete into pool
4105  pz  286.385   $ upstream axial surf of pool seal (A1)
4110  pz  302.1868  $ upstream   surf of 2nd aluminum window defining end of water tube in 1998 design
4115  pz  302.5043  $ downstream surf of 2nd aluminum window defining end of water tube in 1998 design
4120  pz  304.0467  $ upstream axial surf of pool seal (A2)
4125  pz  304.1     $ step A for 2nd expansion of beam tube just upstream of collimator
4126  pz  304.735   $ step B for 2nd expansion of beam tube just upstream of collimator
4130  pz  310.58    $ upstream surface of collimator
4135  pz  311.785   $ downstream surf of pool seal (A1)
4140  pz  334.7709  $ upstream   surf of 2nd aluminum window defining end of water tube in 1960 design
4145  pz  335.4756  $ downstream surf of 2nd aluminum window defining end of water tube in 1960 design
4150  pz  335.7967  $ upstream surf of removable shield
4155  pz  341.8292  $ upstream   side of ss liner in bioshield near step
4160  pz  342.7817  $ downstream side of ss liner in bioshield near step = upstream surf of eccentric shield
4170  pz  381.5167  $ downstream surf of removable shield and eccentric shield
4180  pz  384.1645  $ upstream   side of pool seal (B)
4190  pz  399.48    $ downstream side of collimator
4195  pz  401.9445  $ downstream side of pool seal (B) = downstream side of flange around pool seal (B)
c
c
c     Box surfaces corresponding to rectangular-shaped hole in collimator:
c     ---------------------------------------------------------------
c     Here (like everywhere in this MCNP model of HB-3),
c     Z=central axis; Y is really horizontal; X is really vertical
4210  py  -3.4925   $ ymin
4211  py   3.4925   $ ymax
4212  px  -6.9850   $ xmin
4213  px   6.9850   $ xmax
c
c
c     Radial surfaces used for the description of the collimator assembly (etc) inside the concrete:
c     ---------------------------------------------------------------------------
4220  cz  17.2099   $ inner radius of narrow ss sleeve extending thru concrete into pool
4225  cz  17.4742   $ outer radius of narrow ss sleeve extending thru concrete into pool
4230  cz   9.21131  $ outer radius of collimator = inner radius of (again) expanded aluminum beam tube
4235  cz   9.84631  $ outer radius of (again) expanded aluminum beam tube = inner radius of removable shield
4240  cz  13.97     $ outer radius of pool seal (B)
4245  cz  33.655    $ outer radius of flange holding pool seal (B)
4250  cz  14.0339   $ outer radius of pool seal (A1) = inner radius of pool seal (A2)
4255  cz  19.7564   $ outer radius of removable shield = inner radius of eccentric shield
4260  cz  22.       $ outer radius of eccentric shield = inner radius of ss bioshield liner (in this axail section)
4265  cz  22.       $ outer radius of ss bioshield liner (in this axail sect
c
```

```
c
c
9990   s  0.0  0.0  678.1673  1.11125 $ small sph (R=radius of small shutter hole), located at pt where Blosser & Thomas made measurements in June 1968 (cf
ORNL-TM-2221)
c
9997   pz    0.0   $ External void boundary (location corresponds to the real radial plane perpendicular to the real beam tube)
9998   pz  700.0   $ External void boundary (far enough out to emcompass point where Blosser & Thomas made measurements in 1968)
9999   cz   65.0   $ External void boundary (radial extent of this model)
c
c
c     END SURFACES (next line must be blank)

c     PROBLEM PARAMETERS:
c       mode   p
c       mode   n p
mode   n
c       nps    2000000
c       nps    40000000
c       nps    60000000
c       nps    80000000
nps    120000000
c      cut:n  time(shakes) energy(MeV)   WC1   WC2   SWTM
cut:n          1.0e20          0.027     -0.5  -0.25   0.0  $ cutoff:  don't track any neutrons below 27 keV
print  60      $ Table 60 shows vol, mass, n-imp by cell; see pp 3-117 of manual for description of other useful tables you may want
prdmp  0   80000  0  4  0   $ make restart file after every 80000 histories in fixed src calc; save only the 4 most recent restart files
c
c
c     EQUIVALENT POINT SOURCES:
c
c       sdef  erg=d73  pos ferg d83  $ source def for gammas in HB-3 (total p/s = 1.35399E+17)
sdef   erg=d53  pos ferg d63  $ source def for neutrons in HB-3 (total n/s = 9.64595E+16);  total n/s above 27 keV = 1.20830e16
       par=1            $ par=1 for neut, par=2 for photons
       vec  0  0  1     $ reference vector if directional-dependent source is used
       dir=d3           $ angular distribution wrt vec (Caution: choice of angular distribution sampled will dictate choice of wgt)
c      wgt=1.7332472-2  $ use this with d3;  wgt = [mu(max)-mu(min)]/[(+1)-(-1)] = [1.0000000000-0.965335056]/2 = 1.7332472-2
c      wgt=0.1    $ use this with mu(min)=0.8 in d3 for dosimetry calc only;  wgt = [mu(max)-mu(min)]/[(+1)-(-1)] = [1.0-0.8]/2 = 0.1
       wgt=0.145  $ use this with mu(min)=0.71 in d3 for HB304M4 dosimetry calc only;  wgt = [mu(max)-mu(min)]/[(+1)-(-1)] = [1.0-0.8]/2 = 0.145
c      -------------------
c      Ang Dist: to spray isotropically across central void of HB-3 beam tube
c      si3   h  0.965335056   1.0  $ angular distribution;  mu boundaries (i.e, cosine boundaries wrt vec)
c      si3   h  0.8  1.0  $ open up angular distribution for dosimetry run;  mu boundaries (i.e, cosine boundaries wrt vec)
si3    h  0.71  1.0  $ open up angular distribution for HB304M4 dosimetry run;  mu boundaries (i.e, cosine boundaries wrt vec)
sp3    d  0  1  $ angular distribution; particle emmission probabilities by bin; first value (below lowest bin bound) must be zero
c      -------------------
c
c        ------------------------------------------------------------------------
c        Begin distributions needed to describe the neutron sources in the HB-3 beam tube
c        ------------------------------------------------------------------------
si53   h  1.0000e-11  $ this one Emin(MeV), followed by Emax(MeV) for the 61 VELM neut grps (lowest to highest energy for MCNP):
c          4.1399e-7    1.1253e-6    2.3824e-6    5.0435e-6    1.0677e-5    $ VELM n-groups 61, 60, 59, 58, 57,
c          2.2603e-5    4.7851e-5    1.0130e-4    1.6702e-4    2.7536e-4    $ VELM n-groups 56, 55, 54, 53, 52,
c          4.5400e-4    7.4852e-4    1.2341e-3    2.0347e-3    2.2487e-3    $ VELM n-groups 51, 50, 49, 48, 47,
c          2.6126e-3    3.0354e-3    3.7074e-3    5.5308e-3    9.1188e-3    $ VELM n-groups 46, 45, 44, 43, 42,
c          1.5034e-2    2.3579e-2    2.4788e-2    2.6058e-2    2.7000e-2    $ VELM n-groups 41, 40, 39, 38, 37,
         2.8501e-2    3.4307e-2    5.2475e-2    5.6562e-2    8.6517e-2    $ VELM n-groups 36, 35, 34, 33, 32,
         1.2277e-1    1.4996e-1    1.8316e-1    2.2371e-1    2.7324e-1    $ VELM n-groups 31, 30, 29, 28, 27,
         2.9452e-1    2.9721e-1    2.9849e-1    3.0197e-1    3.8774e-1    $ VELM n-groups 26, 25, 24, 23, 22,
         4.9787e-1    5.2340e-1    6.0810e-1    7.4274e-1    9.0718e-1    $ VELM n-groups 21, 20, 19, 18, 17,
```

```
        1.1080e+0    1.3534e+0    1.6530e+0    2.0190e+0    2.2313e+0    $ VELM n-groups 16, 15, I4, 13, 12,
        2.3457e+0    2.4660e+0    3.0119e+0    3.6788e+0    4.4933e+0    $ VELM n-groups 11, 10,  9,  8,  7,
        5.4881e+0    6.7032e+0    8.1873e+0    1.0000e+1    1.2214e+1    $ VELM n-groups  6,  5,  4,  3,  2,
        1.4918e+1                                                       $ VELM n-group   1
sp53  d     0.0  $ dummy 0, followed by neut src terms (n/s) for HB-3:
c        6.30365e+16  2.25679e+15  1.52979e+15  1.30212e+15  1.55274e+15  $ VELM n-groups 61, 60, 59, 58, 57,
c        1.58981e+15  1.54759e+15  1.45876e+15  9.03837e+14  9.69821e+14  $ VELM n-groups 56, 55, 54, 53, 52,
c        9.50610e+14  8.74122e+14  8.53691e+14  8.87245e+14  2.04908e+14  $ VELM n-groups 51, 50, 49, 48, 47,
c        2.76622e+14  2.54975e+14  3.36538e+14  7.55438e+14  8.76077e+14  $ VELM n-groups 46, 45, 44, 43, 42,
c        9.84217e+14  7.42049e+14  6.69650e+13  1.12860e+14  5.24714e+13  $ VELM n-groups 41, 40, 39, 38, 37,
        1.21873e+14  3.03507e+14  4.96958e+14  1.29680e+14  8.89397e+14  $ VELM n-groups 36, 35, 34, 33, 32,
        5.59006e+14  4.29193e+14  3.63241e+14  4.33245e+14  7.35199e+14  $ VELM n-groups 31, 30, 29, 28, 27,
        2.12840e+14  1.38494e+13  7.68584e+12  3.65651e+13  6.29256e+14  $ VELM n-groups 26, 25, 24, 23, 22,
        5.85513e+14  1.49367e+14  3.61470e+14  5.35177e+14  6.65098e+14  $ VELM n-groups 21, 20, 19, 18, 17,
        5.40055e+14  7.09512e+14  8.07055e+14  8.54720e+14  3.12945e+14  $ VELM n-groups 16, 15, 14, 13, 12,
        2.00073e+14  1.35333e+14  2.41078e+14  1.61947e+14  2.06360e+14  $ VELM n-groups 11, 10,  9,  8,  7,
        1.36477e+14  7.32282e+13  3.05242e+13  8.64293e+12  6.92602e+12  $ VELM n-groups  6,  5,  4,  3,  2,
        2.74800e+09                                                     $ VELM n-group   1
ds63  1     $ neutron starting positions (x,y,z) in HB-3:
c        0 0  80.2    0 0  57.3    0 0  65.2    0 0  76.1    0 0  54.5    $ VELM n-groups 61, 60, 59, 58, 57,
c        0 0  48.2    0 0  56.5    0 0  55.4    0 0  56.0    0 0  51.1    $ VELM n-groups 56, 55, 54, 53, 52,
c        0 0  53.8    0 0  52.6    0 0  61.2    0 0  60.5    0 0  43.0    $ VELM n-groups 51, 50, 49, 48, 47,
c        0 0  49.5    0 0  55.0    0 0  65.1    0 0  53.3    0 0  52.7    $ VELM n-groups 46, 45, 44, 43, 42,
c        0 0  50.7    0 0  54.0    0 0  69.0    0 0  46.7    0 0  62.6    $ VELM n-groups 41, 40, 39, 38, 37,
c        0 0  67.5    0 0  79.8    0 0  52.9    0 0  56.7    0 0  47.4    $ VELM n-groups 36, 35, 34, 33, 32,
c        0 0  45.7    0 0  45.6    0 0  42.5    0 0  48.9    0 0  34.2    $ VELM n-groups 31, 30, 29, 28, 27,
c        0 0  42.4    0 0  63.8    0 0  53.7    0 0  42.3    0 0  49.6    $ VELM n-groups 26, 25, 24, 23, 22,
c        0 0  58.8    0 0  52.9    0 0  50.3    0 0  56.8    0 0  44.1    $ VELM n-groups 21, 20, 19, 18, 17,
c        0 0  70.1    0 0  46.8    0 0  59.7    0 0  50.2    0 0  52.1    $ VELM n-groups 16, 15, 14, 13, 12,
c        0 0  33.3    0 0  43.5    0 0  65.3    0 0  56.9    0 0  47.9    $ VELM n-groups 11, 10,  9,  8,  7,
c        0 0  62.6    0 0  59.5    0 0  42.9    0 0  68.7    0 0  31.1    $ VELM n-groups  6,  5,  4,  3,  2,
c        0 0  99.9                                                       $ VELM n-group   1
c       Shift sources 1.5 cm to right of beam tube centerline to account for the anisotropic effect
c       of more neutrons entering the one side of the beam tube than the other:   -- JAB, 4-7-98
      0 1.6986 67.5  0 1.6986 79.8  0 1.6986 52.9  0 1.6986 56.7  0 1.6986 47.4    $ VELM n-groups 36, 35, 34, 33, 32,
      0 1.6986 45.7  0 1.6986 45.6  0 1.6986 42.5  0 1.6986 48.9  0 1.6986 34.2    $ VELM n-groups 31, 30, 29, 28, 27,
      0 1.6986 42.4  0 1.6986 63.8  0 1.6986 53.7  0 1.6986 42.3  0 1.6986 49.6    $ VELM n-groups 26, 25, 24, 23, 22,
      0 1.6986 58.8  0 1.6986 52.9  0 1.6986 50.3  0 1.6986 56.8  0 1.6986 44.1    $ VELM n-groups 21, 20, 19, 18, 17,
      0 1.6986 70.1  0 1.6986 46.8  0 1.6986 59.7  0 1.6986 50.2  0 1.6986 52.1    $ VELM n-groups 16, 15, 14, 13, 12,
      0 1.6986 33.3  0 1.6986 43.5  0 1.6986 65.3  0 1.6986 56.9  0 1.6986 47.9    $ VELM n-groups 11, 10,  9,  8,  7,
      0 1.6986 62.6  0 1.6986 59.5  0 1.6986 42.9  0 1.6986 68.7  0 1.6986 31.1    $ VELM n-groups  6,  5,  4,  3,  2,
      0 1.6986 99.9                                                     $ VELM n-group   1
c       ------------------------------------------------------------------------------
c       Begin distributions needed to describe the gamma sources in the HB-3 beam tube
c       ------------------------------------------------------------------------------
si73  h  1.0000e-2   $ this one Emin(MeV), followed by Emax(MeV) for the 23 VELM gamma grps (lowest to highest energy for MCNP):
        2.0000e-2    4.5000e-2    7.0000e-2    1.0000e-1    1.5000e-1    $ VELM g-groups 23, 22, 21, 20, 19,
        3.0000e-1    4.0000e-1    5.1000e-1    6.0000e-1    7.0000e-1    $ VELM g-groups 18, 17, 16, 15, 14,
        1.0000e+0    1.5000e+0    2.0000e+0    2.5000e+0    3.0000e+0    $ VELM g-groups 13, 12, 11, 10,  9,
        4.0000e+0    5.0000e+0    6.0000e+0    7.0000e+0    7.5000e+0    $ VELM g-groups  8,  7,  6,  5,  4,
        8.0000e+0    1.0000e+1    1.4000e+1                              $ VELM g-groups  3,  2,  1
sp73  d     0.0  $ dummy 0, followed by gamma src terms (p/s) for HB-3:
        8.72837e+12  2.84514e+15  1.65029e+16  1.67705e+16  1.82855e+16  $ VELM g-groups 23, 22, 21, 20, 19,
        2.56708e+16  1.03805e+16  7.17665e+15  4.80101e+15  4.03975e+15  $ VELM g-groups 18, 17, 16, 15, 14,
        7.31636e+15  5.27935e+15  4.23989e+15  2.66951e+15  1.42777e+15  $ VELM g-groups 13, 12, 11, 10,  9,
        2.3[illegible]+15  1.98361e+15  6.75453e+14  1.23378e+15  1.60183e+14  $ VELM g-groups  8,  7,  6,  5,  4,
        1.5[illegible]+15  6.19421e+13  1.23250e+11                     $ VELM g-groups  3,  2,  1
ds83  1     $ gamma starting positions (x,y,z) in HB-3:
```

```
        0 0  10.0    0 0  61.9    0 0  68.1    0 0  82.1    0 0  83.9    $ VELM g-groups 23, 22, 21, 20, 19,
        0 0  84.5    0 0  81.6    0 0  84.7    0 0  88.8    0 0  83.2    $ VELM g-groups 18, 17, 16, 15, 14,
        0 0  86.8    0 0  93.6    0 0  96.9    0 0  99.2    0 0  96.6    $ VELM g-groups 13, 12, 11, 10,  9,
        0 0  92.6    0 0  93.2    0 0  96.4    0 0  93.9    0 0  96.0    $ VELM g-groups  8,  7,  6,  5,  4,
        0 0  94.4    0 0  99.9    0 0  97.4                               $ VELM g-groups  3,  2,  1
c       -----------------------------------
c
c
c
c      BEGIN-TRANSFORMATIONS:
c
c      Transformations that can/should be used for the holes in the beam tube shield plug (ie, the rotary shutter):
c         When big   hole is turned to "open" position:  use tr11 for big hole in shutter, and tr21 for small hole
c         When small hole is turned to "open" position:  use tr12 for big hole in shutter, and tr22 for small hole
c         When shutter    is turned to "off"  position:  use tr13 for big hole in shutter, and tr23 for small hole
c      ------------------------------------------------------------------------------------------------------------
*tr11  $ use tr11 for big hole in shutter, when big hole is turned to "open" position
       0.0  0.0  446.405  $ location of local origin (center of shutter), relative to the global origin (cm) in HB-3 model
         0    90   90     $ degrees from global x,y,z axes to local x axis
        90     0   90     $ degrees from global x,y,z axes to local y axis
        90    90    0     $ degrees from global x,y,z axes to local z axis
c
*tr12  $ use tr12 for big hole in shutter, when small hole is turned to "open" position
       0.0  0.0  446.405  $ location of local origin (center of shutter), relative to the global origin (cm) in HB-3 model
         0    90    90    $ degrees from global x,y,z axes to local x axis
        90  -46.5  -136.5 $ degrees from global x,y,z axes to local y axis
        90   43.5  -46.5  $ degrees from global x,y,z axes to local z axis
c
*tr13  $ use tr13 for big hole in shutter, when shutter is turned to "off" position
       0.0  0.0  446.405    $ location of local origin (center of shutter), relative to the global origin (cm) in HB-3 model
         0    90      90    $ degrees from global x,y,z axes to local x axis
        90  -113.25 -203.25 $ degrees from global x,y,z axes to local y axis
        90  -23.25  -113.25 $ degrees from global x,y,z axes to local z axis
c
*tr21  $ use tr21 for small hole in shutter, when big hole is turned to "open" position
       0.0  0.0  446.405    $ location of local origin (center of shutter), relative to the global origin (cm) in HB-3 model
         0    90    90      $ degrees from global x,y,z axes to local x axis
        90   46.5 -43.5     $ degrees from global x,y,z axes to local y axis
        90  136.5  46.5     $ degrees from global x,y,z axes to local z axis
c
*tr22  $ use tr22 for small hole in shutter, when small hole is turned to "open" position
       0.0  0.0  446.405    $ location of local origin (center of shutter), relative to the global origin (cm) in HB-3 model
         0    90   90       $ degrees from global x,y,z axes to local x axis
        90     0   90       $ degrees from global x,y,z axes to local y axis
        90    90    0       $ degrees from global x,y,z axes to local z axis
c
*tr23  $ use tr23 for small hole in shutter, when shutter is turned to "off" position
       0.0  0.0  446.405    $ location of local origin (center of shutter), relative to the global origin (cm) in HB-3 model
         0    90     90     $ degrees from global x,y,z axes to local x axis
        90  -66.75 -156.75  $ degrees from global x,y,z axes to local y axis
        90   23.25  -66.75  $ degrees from global x,y,z axes to local z axis
c
c       *tr40  $ use tr40 to locate and position the Key 3 dosimetry specimen holder relative to HB-3 beam tube
c              0.0  0.0  113.64     $ location of local origin (center of shutter), relative to the global origin (cm) in HB-3 model
c                0    90   90       $ degrees from global x,y,z axes to local x axis
c               90    14  -76       $ degrees from global x,y,z axes to local y axis
c               90   104   14       $ degrees from global x,y,z axes to local z axis
c
c       *tr40 was revised as follows by JAB on 3 Apr 98 for Run HB304H, based on newly available data shown on Dwg E-49953, Rev A, 6-30-65:
```

```
*tr40  $ use tr40 to locate and position the Key 3 dosimetry specimen holder relative to HB-3 beam tube
       0.0  0.0  114.22     $ location of local origin (center of shutter), relative to the global origin (cm) in HB-3 model
         0    90   90       $ degrees from global x,y,z axes to local x axis
        90    13  -77       $ degrees from global x,y,z axes to local y axis
        90   103   13       $ degrees from global x,y,z axes to local z axis
c
c       $ incorrect & obsolete:   *tr42  $ use tr42 to locate and position the elliptical cone used to define chamfer between HB3 vessel hole and inner surf
 of pressure vessel
c       $ incorrect & obsolete:          0.0  -2.14265  128.18364   $ location of local origin (center of elliptical cone), relative to the global origin (c
m) in HB-3 model
c       $ incorrect & obsolete:            0    90.0000    90.0000  $ degrees from global x,y,z axes to local x axis
c       $ incorrect & obsolete:           90    12.6575   -77.3425  $ degrees from global x,y,z axes to local y axis
c       $ incorrect & obsolete:           90   102.6575    12.6575  $ degrees from global x,y,z axes to local z axis
c
c       The following correction to *tr42 was made by JAB on 6 Apr 98, just prior to submitting Run HB304K:
c
*tr42  $ use tr42 to locate and position the elliptical cone used to define chamfer between HB3 vessel hole and inner surf of pressure vessel
       0.0  -2.02265  127.62367   $ location of local origin (center of elliptical cone), relative to the global origin (cm) in HB-3 model
         0    90.0000    90.0000  $ degrees from global x,y,z axes to local x axis
        90    12.6929   -77.3071  $ degrees from global x,y,z axes to local y axis
        90   102.6929    12.6929  $ degrees from global x,y,z axes to local z axis
c      ------------------------------------------------------------------------------------------------------------------------
c      END-TRANSFORMATIONS
c
c
c      BEGIN MATERIAL DESCRIPTIONS:
c
c       Water gaps in removable reflector region     --Avg. Density= 0.98465 g/cm^3
m5      1001.50c     6.63485-02    8016.50c    3.31742-02
mt5     lwtr.01t
c
c       Water Reflector --Density= 0.9899 g/cm^3
m7      1001.50c     6.67022-02    8016.50c    3.33511-02
mt7     lwtr.01t
c
c       H2O Pool  --Density= 1.0000 g/cm^3
m8      1001.50c     6.73828-02    8016.50c    3.36914-02
mt8     lwtr.01t
c
c       Aluminum reflector container (outside Be reflector; 2.7 g/cc)
m23     13027.52c   5.85482-02   1001.50c  3.45716-04  12000.50c  6.68986-04
        14000.50c   3.47363-04  22000.50c  2.54704-05  24000.50c  6.09789-05
        25055.50c   2.21974-05  26000.55c  1.01905-04  29000.50c  8.74557-05
c
c       Aluminum liners in Be reflectors (2.7 g/cc)
m24     13027.52c   5.85482-02   1001.50c  3.45716-04  12000.50c  6.68986-04
        14000.50c   3.47363-04  22000.50c  2.54704-05  24000.50c  6.09789-05
        25055.50c   2.21974-05  26000.55c  1.01905-04  29000.50c  8.74557-05
c
c       ss liner of pressure vessel, bioshield liner, and other components -- SCALE SS304 (7.92 g/cc;  69.5 w/o Fe, 19.0 w/o Cr, 9.5 w/o Ni,  2.0 w/o Mn)
m40     26000.55c  5.93541-02   24000.50c  1.74281-02
        28000.50c  7.71883-03   25055.50c  1.73629-03
c
c       ss (same as above, but diff color on plot) used for removable shield around collimator -- SCALE SS304 (7.92 g/cc; 69.5 w/o Fe, 19.0 w/o Cr, 9.5 w/o
Ni, 2.0 w/o Mn)
m41     26000      5.93541-02   24000.50c  1.74281-02
        28000      7.71883-03   25055.50c  1.73629-03
c
```

```
c       carbon steel in main body of pressure vessel -- SCALE Carbon Steel (7.8212 g/cc;  99.0 w/o Fe, 1.0 w/o C)
m50     26000.55c  8.34929-02    6012.50c  3.92134-03
c
c       Void in reflector components
m60     1001.50c   1.00000-15   8016.50c   1.00000-15
c
c       Void regions in the HB-1,2,and 3 beam tubes (m60 @ 2.0e-15 atoms/b-cm) have been replaced with helium-filled regions
c       where m61 = He (void) at T=300 deg.K and P=2 atm, where rho=3.2325e-4 g/cc, N(He)=4.86816e-5 atoms/(barn*cm)
c       Note: cold source vacuum vessel in HB-4 now has a true void (see m610) as of July 1996.
c       ------------------------
c       Helium void inside beam tubes HB-1,2,3 (He at T=300 deg.K, P=2 atm); cold source vacuum vessel in HB-4 now has a true void (see m610)
m61     2004.50c  4.86816e-5  $  add-jab122395:  For He at T=300 deg.K and P=2 atm, rho=3.2325e-4 g/cc, N(He)=4.86816e-5 atoms/(barn*cm)
c
c       Barytes concrete at 3.09725 g/cc (used for biological shield); shown below are atoms/(barn*cm) by nuclide
m62      1001.50c  1.681e-2   5010.50c  3.378e-4   5011.56c  1.368e-3
         8016.50c  4.195e-2  11023.50c  3.193e-4  12000.50c  1.549e-4
        13027.52c  7.534e-4  14000.50c  1.260e-3  16032.50c  5.401e-3
        20000.50c  3.273e-3  22000.50c  1.336e-4  25055.50c  1.713e-4
        26000.55c  6.875e-4  56138.50c  5.394e-3
c       real concentration for ba-138 = 3.8787e-3 atoms/(barn*cm); it is available;
c       other nuclide concentrations for which there is no mcnp xsect data:
c       ba-134=1.3037e-4;  ba-135=3.5557e-4;  ba-136=4.2364e-4;  ba-137=6.0575e-4
c       total number density for all barium nuclides in barytes concrete: 5.394030e-3
c       total number density for all nuclides in barytes concrete:  7.801382e-2
c       while this barytes concrete (for ANS project) was 3.09725 g/cc, it can
c       sometimes be made as dense as 3.5 g/cc; see book by Schaffer
c
c
m71     28058.24y  1.0  $ Ni58;  this material (m71) is used only to get the Ni58(n,p)Co58 reaction rate [(n,p)=103] in the dosimeters
m72     26054.24y  1.0  $ Fe54;  this material (m72) is used only to get the Fe54(n,p)Mn54 reaction rate [(n,p)=103] in the dosimeters
c
c
c       Typical beryllium used in permanent reflector (with he-3 and li-6, based in center ring, cell 9024)
m108    4009.50c   1.21135-01   1001.50c   1.34766-03   8016.50c   6.73828-04
        3006.50c   4.80664-8    2003.50c   1.39911-9
mt108   be.01t
c
c
c     ---------------------------------------------------------------------------------------------------------------------
c     *** start detectors used to get fluxes at different points down HB-3 beam tube; for HFIR at 100 MW
c     ---------------------------------------------------------------------------------------------------------------------
c
c       dxt:n  $ dxtran spheres used to improve statistics in oversimplified dosimeter cells
c              0.0  -13.480  107.1276  1.5  3.0  $ dxtran sphere around 1.48893 cm radius cell simulating dosimeter just slightly on HB-4 side of HB-3   (se
e above note)
c              0.0   12.284  112.9905  1.5  3.0  $ dxtran sphere around 1.48893 cm radius cell simulating dosimeter just slightly on HB-2 side of HB-3   (se
e above note)
c              0.0   0.0     0.0                  $ defaults weights (dwc1, dwc2, dpwt) for dxtran spheres
c
c       dxt:n  $ dxtran spheres used to improve statistics in more rigorous dosimeter cells
c              0.0   13.25424  116.94465  3.2  5.0  $ dxtran sphere around dosimeter at Key 3, Position 3, just slightly on HB-4 side of HB-3
c              0.0  -13.25424  110.33535  3.2  5.0  $ dxtran sphere around dosimeter at Key 3, Position 8, just slightly on HB-2 side of HB-3   (see above n
ote)
c              0.0   0.0     0.0                    $ defaults weights (dwc1, dwc2, dpwt) for dxtran spheres
c
c       fc14   N-Flux (n/s/cm2) at 2 dosimeter locations adjacent to HB-3 (at 100 MW)
c       f14:n  2134  $ dosimeter (modeled as carbon steel; really Charpy V-notch specimens) just slightly on HB-4 side of HB-3
c              2135  $ dosimeter (modeled as carbon steel; really Charpy V-notch specimens) just slightly on HB-2 side of HB-3
```

```
c       c       fm14   9.64595e16  $ sum of equivalent point sources (n/s) in HB-3 for HFIR at 100 MW (Sn=7.5573e18 n/s in global calc);  will yield fluxes
in n/s/cm2
c       fm14   1.20830e16  $ sum of equivalent point sources (n/s) for grps 1-36 (E>27 keV; use for dosimetry calc only) in HB-3 for HFIR at 100 MW (Sn=7.55
73e18 n/s in global calc);  will yield fluxes in n/s/cm2
c       e14    $ Emax(ig) in MeV; corresponds to no particular group structure; chosen for dosimetry calcs
c              0.027  0.1  1.0  20.0
c
c
fc15   N-Flux (n/s/cm2) at 655.6626 from tip of HB-3 at 100 MW
f15:n  0.0  0.0  678.1673  0.5   $ neut flux at pt 655.6629 cm from real tip of HB-3 beam tube, where Blosser & Thomas made measurements in June 1968 (cf OR
NL-TM-2221)
c       fm15   9.64595e16  $ sum of equivalent point sources (n/s) in HB-3 for HFIR at 100 MW (Sn=7.5573e18 n/s in global calc);  will yield fluxes in n/s/c
m2
fm15   1.20830e16  $ sum of equivalent point sources (n/s) for grps 1-36 (E>27 keV; use for dosimetry calc only) in HB-3 for HFIR at 100 MW (Sn=7.5573e18 n/
s in global calc);  will yield fluxes in n/s/cm2
e15    $ Emax(ig) in MeV; corresponds to no particular group structure; chosen to facilitate comparison with Blosser & Thomas measurements
       0.4e-6  1.0e-6  1.9e-6  4.0e-6  6.0e-6  25.0e-6  100.0e-6  170.0e-6
       640.0e-6  2.4e-3  3.8e-3  2.0e-2  0.1  1.0  2.9  6.3  8.1  20.0
c      Note 1:  Comparisons with B&T are fair only if we use aluminum windows 1 & 2 for 1960 design AND use small hole in rotary shutter.
c      Note 2:  B&T tabulated their results with HFIR power normalized to 1.0 MW;  here we have it at 100.0 MW;  must renormalize later.
c      Note 3:  Many of B&T's results are n/s/cm2/eV, therefore must divide some of our results by delta-E later, where appropriate.
c      Note 4:  The energy ranges above were selected after consulting the B&T report, as well as the barn book to check width of certain resonances.
c
c
c       fc24   N-Flux (n/s/cm2) for dosimeter at Key 3, Position 3 (100 MW)
c       f24:n  2581  $ dosimeter at Key 3, Position 3, just slightly on HB-2 side of HB-3
c       c       fm24   9.64595e16  $ sum of equivalent point sources (n/s) in HB-3 for HFIR at 100 MW (Sn=7.5573e18 n/s in global calc);  will yield fluxes
in n/s/cm2
c       fm24   1.20830e16  $ sum of equivalent point sources (n/s) for grps 1-36 (E>27 keV; use for dosimetry calc only) in HB-3 for HFIR at 100 MW (Sn=7.55
73e18 n/s in global calc);  will yield fluxes in n/s/cm2
c       e24    $ Emax(ig) in MeV; corresponds to no particular group structure; chosen for dosimetry calcs
c              0.027  0.1  1.0  20.0
c
c
c       fc34   N-Flux (n/s/cm2) for dosimeter at Key 3, Position 8 (100 MW)
c       f34:n  2582  $ dosimeter at Key 3, Position 8, just slightly on HB-4 side of HB-3
c       c       fm34   9.64595e16  $ sum of equivalent point sources (n/s) in HB-3 for HFIR at 100 MW (Sn=7.5573e18 n/s in global calc);  will yield fluxes
in n/s/cm2
c       fm34   1.20830e16  $ sum of equivalent point sources (n/s) for grps 1-36 (E>27 keV; use for dosimetry calc only) in HB-3 for HFIR at 100 MW (Sn=7.55
73e18 n/s in global calc);  will yield fluxes in n/s/cm2
c       e34    $ Emax(ig) in MeV; corresponds to no particular group structure; chosen for dosimetry calcs
c              0.027  0.1  1.0  20.0
c
c
c      Note use of dxtran spheres with tallies 24 & 34 seemed to be a problem for the code;
c      kept getting messages saying "bank is full"; therefore try using point detectors instead,
c      and get rid of all the dxtran cards above.
c
fc25   N-Flux (n/s/cm2) for dosimeter at Key 3, Position 3 (100 MW)
c      f25:n  0.0    13.25424  116.94465  0.5  $ midpoint of dosimeter (in Cell 2581) at Key 3, Position 3, just slightly on HB-4 side of HB-3
c      f25:n  0.0    14.54813  117.26726  0.5  $ dosimeter (in Cell 2581) at Key 3, Position 3, just slightly on HB-4 side of HB-3
c      f25:n  0.0    15.84202  117.58986  0.5  $ outer edge of dosimeter (in Cell 2581) at Key 3, Position 3, just slightly on HB-4 side of HB-3
c      fm25   9.64595e16  $ sum of equivalent point sources (n/s) in HB-3 for HFIR at 100 MW (Sn=7.5573e18 n/s in global calc);  will yield fluxes in n/s/cm
2
c      Midpoint location was revised as follows on 3 Apr 98 (for Runs HB304H & later) based on the very detailed, newly available, information on Dwg E-4995
3, Rev A (6-3    65):
f25:n  0.0      2066  117.11062  0.45  $ midpoint of dosimeter (in Cell 258.  Key 3, Position 3, just slightly on HB-4 side of HB-3
c      f25:n  0.75311  12.52066  117.11062  0.45  $ 0.75311 cm above midpoint o  dosimeter (in Cell 2581) at Key 3, Position 3, just slightly HB-4 side o
```

```
f HB-3
c      f25:n -0.75311  12.52066  117.11062  0.45  $ 0.75311 cm below midpoint of dosimeter (in Cell 2581) at Key 3, Position 3, just slightly on HB-4 side o
f HB-3
fm25   (1.20830e16)  $ sum of equivalent point sources (n/s) for grps 1-36 (E>27 keV; use for dosimetry calc only) in HB-3 for HFIR at 100 MW (Sn=7.5573e18
n/s in global calc);  will yield fluxes in n/s/cm2
       (1.20830e-8  71  103)  $ to get number of (n,p) "reactions/sec" in Ni58;  note that src had to be multiplied by 1e-24 to convert (n,p) xsect 103 from
 barns to cm2
       (1.20830e-8  72  103)  $ to get number of (n,p) "reactions/sec" in Fe54;  note that src had to be multiplied by 1e-24 to convert (n,p) xsect 103 from
 barns to cm2
e25    $ Emax(ig) in MeV; corresponds to no particular group structure; chosen for dosimetry calcs
       0.027  0.1  1.0  20.0  t
c
c
fc35   N-Flux (n/s/cm2) for dosimeter at Key 3, Position 8 (100 MW)
c      f35:n  0.0  -13.25424  110.33535  0.5  $ midpoint of dosimeter (in Cell 2582) at Key 3, Position 8, just slightly on HB-2 side of HB-3
c      f35:n  0.0  -14.54813  110.01274  0.5  $ dosimeter (in Cell 2582) at Key 3, Position 8, just slightly on HB-2 side of HB-3
c      f35:n  0.0  -15.84202  109.69014  0.5  $ outer edge of dosimeter (in Cell 2582) at Key 3, Position 8, just slightly on HB-2 side of HB-3
c      fm35   9.64595e16  $ sum of equivalent point sources (n/s) in HB-3 for HFIR at 100 MW (Sn=7.5573e18 n/s in global calc);  will yield fluxes in n/s/cm
2
c      Midpoint location was revised as follows on 3 Apr 98 (for Runs HB304H & later) based on the very detailed, newly available, information on Dwg E-4995
3, Rev A (6-30-1965):
f35:n  0.0  -12.52066  111.32938  0.45  $ midpoint of dosimeter (in Cell 2582) at Key 3, Position 8, just slightly on HB-2 side of HB-3
c      f35:n  0.75311  -12.52066  111.32938  0.45  $ 0.75311 cm above midpoint of dosimeter (in Cell 2582) at Key 3, Position 8, just slightly on HB-2 side
of HB-3
c      f35:n -0.75311  -12.52066  111.32938  0.45  $ 0.75311 cm below midpoint of dosimeter (in Cell 2582) at Key 3, Position 8, just slightly on HB-2 side
of HB-3
fm35   (1.20830e16)  $ sum of equivalent point sources (n/s) for grps 1-36 (E>27 keV; use for dosimetry calc only) in HB-3 for HFIR at 100 MW (Sn=7.5573e18
n/s in global calc);  will yield fluxes in n/s/cm2
       (1.20830e-8  71  103)  $ to get number of (n,p) "reactions/sec" in Ni58;  note that src had to be multiplied by 1e-24 to convert (n,p) xsect 103 from
 barns to cm2
       (1.20830e-8  72  103)  $ to get number of (n,p) "reactions/sec" in Fe54;  note that src had to be multiplied by 1e-24 to convert (n,p) xsect 103 from
 barns to cm2
e35    $ Emax(ig) in MeV; corresponds to no particular group structure; chosen for dosimetry calcs
       0.027  0.1  1.0  20.0  t
c
c      ------------------------------------------------------------------------------------------------------------------------
c      ********** end of model **********
c      ------------------------------------------------------------------------------------------------------------------------
```

Appendix B.2

FADIST7.FOR: A simple Fortran program to determine the "relative" outward-directed current impingent on the inner wall of the HB-3 beam tube in the vicinity of the two dosimeters, and to determine a lateral offset that will allow a line of isotropic point sources "near" the centerline to reproduce that asymmetric effect based on the logic described in Sect 4.

```
c       ********************************************************************************
c       ********************************************************************************
c
c       FADIST.FOR -- little test program to get the "Fast Angular flux Distribution"
c                     at an equivalent source point in the HB3 beam tube; JAB, 8 Apr 98
c
c       ********************************************************************************
c       ********************************************************************************
c
        implicit double precision (a-h,o-z)
        implicit integer*4  (i-n)
        double precision dfloat,dacos,dsqrt,dsin,dcos
        dimension sum(0:180)
        dimension suma(180),sumb(180)
        dimension umina(180),uminb(180)
        dimension umaxa(180),umaxb(180)
        dimension xx(41),yy(41),zz(41),contrb(41),contrd(41)
c
        open (6,file='fadist7.out',status='unknown')
c
        zero=0.0d0
        one=1.0d0
        two=2.0d0
        half=0.5d0
c
        pi=dacos(-one)
        twopi=pi+pi
        fourpi=twopi+twopi
        conv=180.0d0/pi
c
        rtube=5.08d0
c
        xclsph=zero
        yclsph=zero
        zclsph=28.5369d0
        rsph=7.76d0
c
        xclcor=zero
        yclcor=26.67d0
        zclcor=zero
c
        nr=3    ! used only for QA ! number of eta-level rings into which the hemisphere is divided
        nr=200                     ! number of eta-level rings into which the hemisphere is divided
        ne=2*nr*(nr+1)             ! total number of equal-area surface elements the hemisphere is divided into
        nfs=2*ne                   ! total number of equal-area surface elements corresponding to full 4*pi sphere
        fs=nfs
c
ccc        call getxyz (xx,yy,zz)     ! get location of 41 receptor points (on disk at Z=75.473 cm)
cccc
ccc        do 30 ipt=1,41             ! now calculate contribution to each
ccc        xrecp=xx(ipt)              ! defined in subr getxyz
ccc        yrecp=yy(ipt)              ! defined in subr getxyz
ccc        zrecp=zz(ipt)              ! defined in subr getxyz
c
        ipt=1
        xrecp=
        yrecp=5.08d0
```

```
      zrecp=107.0d0  ! pt on inner wall of tube (right side), 10 cm upstream of dosimeter on HB2 side of HB3
c     Result: outward (+y) current= 1.583568E+13;  inward (-y) current= 1.866867E+12
c
      ipt=1
      xrecp=zero
      yrecp=-5.08d0
      zrecp=101.5d0  ! pt on inner wall of tube (left side), 10 cm upstream of dosimeter on HB4 side of HB3
c     Result: outward (-y) current= 4.218403E+13;  inward (+y) current= 4.559646E+11
c
c     **********************************************************************
c     **********************************************************************
c
c           implicit double precision (a-h,o-z)
c     c
c     c      do i=0,507
c     c      epsi=dfloat(i)/100.0d0
c     c      do i=1690,1700
c     c      epsi=dfloat(i)/1000.0d0
c           do i=16980,16990
c           epsi=dfloat(i)/10000.0d0
c           dum1=(107.0d0-50.0d0)**2 + (5.08d0-epsi)**2
c           dum2=(101.5d0-50.0d0)**2 + (5.08d0+epsi)**2
c           dum=dum1/dum2
c           dum=dum*dsqrt(dum)
c           dum=dum*(5.08d0+epsi)/(5.08d0-epsi)
c           write (*,11) epsi,dum
c     11    format (1x,f8.5,f12.5)
c           enddo
c     c
c           stop
c           end
c
c           shows that epsi=1.6986 cm yields dum=4.218e13/1.584e13=2.6628
c           therefore, my line of pount sources should be offset to y=1.6986 cm
c
c     **********************************************************************
c     **********************************************************************
c
      contrb(ipt)=zero
      contrd(ipt)=zero
c
      do ir=1,nr
         n2=2*ir*(ir+1)              ! number of equal-area surface elements in this and all lower eta-levels
         n1=2*(ir-1)*ir              ! number of equal-area surface elements in all lower eta-levels
         umax=one-dfloat(2*n1)/fs
         umin=one-dfloat(2*n2)/fs
         umid=(umin+umax)/two        ! cos of angle from midpoint of sphere to midpoint of ring corresponding to midpoint of eta-level
         smid=dsqrt(one-umid*umid)   ! sin of angle from midpoint of sphere to midpoint of ring corresponding to midpoint of eta-level
         rring=rsph*smid             ! radius of disk located at midpoint of this eta-level
         zr=zclsph-rsph*umid         ! axial (z) location corresponding to midpoint of eta-level ring, and all elements on it
         nth=4*ir                    ! number of equal-area surface elements in this eta-level ring
         dth=twopi/dfloat(nth)
         th0=-dth/two
ccc      write (6,81) umid,smid,rring  ! used only for QA with nr=3
81       format (1x,' umid=',f12.8,' smid=',f12.8,' rring=',f12.8)
c
         do ith=1,nth
           th=th0+dth*dfloat(ith)
```

```
            dx=rring*dsin(th)
            dy=rring*dcos(th)
            xr=xclsph+dx
            yr=yclsph+dy
            dist=dsqrt((yr-yclcor)*(yr-yclcor)+(zr-zclcor)*(zr-zclcor)) ! dist from centerline of core to this point on scattering sphere
            fflx=9.48470d20/(dist**4.0464d0)                            ! fast flux vs radial dist from core centerline, in Cheverton's report
            if (dist.gt.33.0d0) fflx=4.13906d24/(dist**6.4434d0)  ! fast flux vs radial dist from core centerline, in Cheverton's report
            dist2=((xr-xrecp)*(xr-xrecp)
     *         +(yr-yrecp)*(yr-yrecp)+(zr-zrecp)*(zr-zrecp)) ! dist**2 from point on scattering sphere to point detector
            cosz=(zrecp-zr)/dsqrt(dist2)                        ! used to get current thru disk element in z-direction (might as well be 1.0 always)
            cosx=(xrecp-xr)/dsqrt(dist2)                        ! used to get current thru disk element in x-direction (might as well be 1.0 always)
            cosy=(yrecp-yr)/dsqrt(dist2)                        ! used to get current thru disk element in y-direction (might as well be 1.0 always)
c
           if (cosy.lt.0)   ! right or left (horizontally)
     *       contrb(ipt)=contrb(ipt)+dabs(cosy)*fflx/(fourpi*dist2) ! leakage thru disk element (ipt) in z-direction
           if (cosy.gt.0)
     *       contrd(ipt)=contrd(ipt)+dabs(cosy)*fflx/(fourpi*dist2) ! leakage thru disk element (ipt) in z-direction
c
ccc           if (cosx.lt.0)  ! +x=up, -x=down
ccc     *       contrb(ipt)=contrb(ipt)+dabs(cosx)*fflx/(fourpi*dist2) ! leakage thru disk element (ipt) in z-direction
ccc           if (cosx.gt.0)
ccc     *       contrd(ipt)=contrd(ipt)+dabs(cosx)*fflx/(fourpi*dist2) ! leakage thru disk element (ipt) in z-direction
c
ccc        if (cosz.lt.0)  ! z=axial
ccc  *       contrb(ipt)=contrb(ipt)+dabs(cosz)*fflx/(fourpi*dist2) ! leakage thru disk element (ipt) in z-direction
ccc        if (cosz.gt.0)
ccc  *       contrd(ipt)=contrd(ipt)+dabs(cosz)*fflx/(fourpi*dist2) ! leakage thru disk element (ipt) in z-direction
c
         enddo
       enddo
30     continue
c
       do ipt=1,41
          write (6,84) ipt,ravg,xx(ipt),yy(ipt),zz(ipt),
     *      contrb(ipt),contrd(ipt)
84        format (1x,i3,4f16.6,1pe15.6,1pe15.6)
       enddo
c
       stop
       end
c      ************************************************************
c      ************************************************************
       subroutine getxyz (xx,yy,zz)
c
       implicit double precision (a-h,o-z)
       implicit integer*4  (i-n)
       double precision dfloat,dacos,dsqrt,dsin,dcos
       dimension xx(41),yy(41),zz(41)
c
ccc    open (6,file='bozo.out',status='unknown')
c
       zero=0.0d0
       one=1.0d0
       two=2.0d0
       half=0.5d0
c
       pi=da[illegible]-one)
       twopi=pi+pi
```

```
      fourpi=twopi+twopi
      conv=180.0d0/pi
c
      rsph=7.76d0
      rtube=5.08d0
c
      ipt=1
      ravg=zero
      xx(ipt)=zero
      yy(ipt)=zero
      zz(ipt)=75.473d0
ccc   write (6,84) ipt,ravg,xx(ipt),yy(ipt),zz(ipt)
c
      adisk=pi*rtube*rtube
      ap=adisk/41.0d0
      nrd=4
c
      do ir=1,nrd
         n2=1+2*ir*(ir+1)      ! number of equal-area surface elements in this and all inner rings of disk
         n1=1+2*(ir-1)*ir      ! number of equal-area surface elements in all other inner rings of disk
         n1p=n1+1
         ravg=dsqrt((ap*dfloat(n1+n2)/two)/pi)
         nth=4*ir              ! number of equal-area surface elements in this eta-level ring
         dth=twopi/dfloat(nth)
         th0=-dth
         do ith=1,nth
            ipt=ipt+1
            th=th0+dth*dfloat(ith)
            xx(ipt)=ravg*dsin(th)
            yy(ipt)=ravg*dcos(th)
            zz(ipt)=zz(1)
ccc         write (6,84) ipt,ravg,xx(ipt),yy(ipt),zz(ipt)
84          format (1x,i3,4f16.6)
         enddo
      enddo
c
c
      return
      end
```

Appendix C.1

Initial (Since Abandoned) Attempt to Use MCNP for the Neutron and Secondary Gammas in the Shielding Analysis of the 1998 Water-Tube Problem

Appendix C.1

Initial (Since Abandoned) Attempt to Use MCNP for the Neutron and Secondary Gammas

in the Shielding Analysis of the 1998 Water-Tube Problem

C.1.1 Overview; Lessons Learned; Ultimate Success from Initial Failures

Sect 5 focused on the 1998 water-tube shielding problem; in particular, it focused on the determination of the neutron and secondary gamma dose rates just downstream of the collimator (i.e., on the fluxes and dose rates impingent on the rotary shutter) when both the water tube and collimator sections were flooded as shown in Fig. 3.3. The HB305 series of runs (HB305A through HB305Q) represented a serious attempt to solve this portion of the overall problem directly, using the MCNP code. While these initial attempts failed and were ultimately abandoned in favor of simpler methods which showed these components of the dose rate to be inconsequential, the lessons learned from these initial attempts are well worth documenting, at least briefly, for future reference. The first few runs in this series (HB305A to HB305D) attempted to make the best possible use of geometric importance zones (and later source-energy biasing in Run HB305D) to affect an efficient solution of the problem. From these runs, it was learned that "in a very real practical sense", the effective use of importance zones to force geometric splitting and reduce uncertainties in "large, geometrically-complex problems" is totally infeasible, even though it often works very nicely in geometrically simpler problems involving thick shields. This conclusion was reached just prior to the Radiation Protection and Shielding Conference held in Nashville, TN in late April 1998. There, a paper was presented by John Hendricks and Tom Evans#21 (members of the MCNP code development group at Los Alamos) showing how they were using an undocumented feature of the code that allowed the user to supply "geometry-independent (multigroup) weight windows" to the code via an external file that could be generated off-line by hand or through the use of multidimensional deterministic codes in adjoint mode. A key advantage of this approach is that space- and energy-dependent weight windows required for successful biasing could be specified in terms of an independent phantom (XYZ) mesh that did not have to be explicitly incorporated into the MCNP problem geometry -- i.e., the geometry specifications required to specify the material configuration in a problem no longer had to be extensively augmented by hundreds or thousands of additional (artificial) geometry zones to accommodate the weight-window specifications needed for biasing. This was immediately seen as a major breakthrough since it would allow for the solution of problems that would have, in a practical sense, remained unsolvable without this capability. In the two or three weeks after the conference, Runs HB305E through HB305Q (each with their own weight window files) were set up and tried in an attempt to take advantage of this new capability. While the format of the needed weight window file(s) were known from diagnosing the MCNP Fortran, the meaning of one or two variables was not properly understood, and Runs HB305 through HB305Q were considered failures. By mid-May, this approach was temporarily abandoned in favor of the more elementary approach described in Sect 5 which showed the neutron and gamma dose rates at the point of interest (downstream of the flooded collimator and/or just upstream of the rotary shutter) to be totally inconsequential. Nevertheless, the need for a "geometry-independent weight-window approach" was so compelling that work on it continued on weekends throughout the month May. By that time, we had received from Tom Evans, a description of the necessary weight-window file format and a brief description of each variable in the file. To study the approach, a highly simplified academic problem was defined involving a narrow collimated beam of neutrons impingent on the bottom of a large homogeneous cylindrical tank of water, with the object being to accurately calculate the neutron distribution axially along the centerline as well as the particle flux and dose rate emerging from the upper surface. This problem was successfully solved (with a speed-up factor of 10,000) using a space-energy-direction-dependent weight window file based on a simple ANISN solution in adjoint mode, and is described in Appendix C.2. By the time this was done, the elementary approach described in Sect 5 (for the real HB-3 flooded beam tube problem) had already shown the neutron and secondary gamma dose rates to be totally insignificant. For that reason, and the lack of time, a final rigorous solution of the flooded HB-3 problem (with a neutron-only source) using MCNP and an appropriate weight window file was never attempted again, although we have every reason to believe in retrospect that such an approach could and would be highly successful. A short time later (late June / early July), it was demonstrated that an MCNP solution for the flooded HB-3 problem with the gamma-only source was also intractable using the standard tools available in MCNP. By taking the adjoint weight window approach already developed for neutrons and applying it to the gamma problem, however, we were able to construct a 3-D space-energy-direction-dependent weight window file that could be (and was) used with MCNP(4b) to obtain an extremely good and highly reliable solution for the real gamma-only flooded HB-3 problem. Moreover, use of this approach allowed us to obtain reliable particle distributions and real boundary crossing estimates (that confirmed our point detector estimates) not only through the flooded sections of the beam tube and collimator, but all the way through the carbon steel rotary shutter assembly! This analysis is described at length in Sect 6.

The balance of Appendix C.1 briefly describes the minor perturbations to the base model corresponding to the flooded beam tube configuration shown in Fig. 3.3, and documents why the use of spatially-dependent geometric splitting as attempted in Runs HB305A-HB305D is hopelessly futile in a geometrically-complex problem such as this.

C.1.2 Basic Model of the Flooded HB-3 Tube Used in the HB305 Series of Runs

The basic model for the flooded HB-3 beam tube is shown in Fig. 3.3 and described in Sects 3 and 6. It uses the 1998 water tube design rather than 1960 water tube design. In this case, the water tube and collimator sections are both flooded, as is the small (normally void) region between the two. The Type 1020 carbon steel rotary shutter was in the closed position as shown in Fig. 3.3. Lastly, all of the fine geometric details associated with the dosimetry analysis described in Sect 4 (except the 1960 water tube) are retained in the present model.

This was a coupled neutron/gamma calculation with a neutron-only source, including neutrons over the entire energy range (0-20 MeV) such that the neutron energy cutoff card previously used in the dosimetry analysis was removed and the source normalization value (9.64595e16 n/s) on the "fm" tally multiplier cards now equals the sum of all the HB-3 point sources shown in Table 2.2a. Likewise, the si53, sp53, and ds63 cards describing the neutron-only source again include information pertaining to all 61 neutron groups, and the point sources were again placed back on the centerline of the beam tube so as to be as conservative as reasonably possible. As noted in Sect 2, the "importance cutoff plane" (Surf 1007) was located at Z=118.6879 cm in order to increase the efficiency of the water tube shielding analysis. Likewise, the isotropic point sources were only sampled over 15.13 degrees of the beam tube centerline (ie, over direction cosines between 0.965335056 and 1.0), which required that the starting weight of the neutrons be reduced to 0.017332472 [=(1.0-0.965335056)/2].

Note that without any sort of axial biasing or geometric splitting, there is simply no chance of solving this problem. If all geometry cells have a neutron importance of 1.0, the weight of the neutrons after they penetrate 10, 15, or at most 20 cm into the water will be so low that they will all be killed by Russian Roulette and one will get no histories in axial regions beyond that point. As an alternative to complex user-supplied space-energy-dependent weight windows, the user may subdivide the material cells into many smaller "importance cells" and specify the relative neutron importance to be used for each cell. This relative neutron importance controls the relative average weight of particles in adjacent importance cells, and therefore the frequency with which geometric splitting and Russian Roulette are applied. The higher the relative neutron importance is, the lower will be the average neutron weight in a cell and the lower weight limit beyond which Russian Roulette will be played. Thus, fast neutrons that are being attenuated and loosing weight as they move axially through the water tube will be subjected to Russian Roulette less often, so that a larger number of lower weight particles will then be allowed to penetrate deeper into the shield and provide better statistics at these more distant locations instead of all being killed at or near the start of the shield.

C.1.3 Additional Changes Required to Add Importance Cells Needed for Geometric Splitting

To obtain adequate statistics throughout the problem, the number density of the ("ever-lower-weight") statistical particles being tracked must remain approximately constant throughout the problem in the direction of interest (axially), even though the product of their number density times their average weight (product=numden*avgwgt, which represents the "real" neutron population density) will attenuate. In the real world, of course, the neutron and secondary gamma population will attenuate in more-or-less the same fashion as the fast neutrons, which have a relaxation length of about 10 cm in water. Because of natural divergence and scattering, however, the actual neutron flux (axially) will diminish somewhat faster and will be the product of the exponential term [exp(-dZ/10)] times the 1/(4*pi*dZ^2) term such that, from the point of impact at the beginning of the water tube (Z=174.27 cm) to the end of the water tube (Z=302.1868 cm), it is not unreasonable for the fast neutron flux to attenuate by a factor of 1.4e-11. If the density of "ever-lower-weight" statistical particles must remain approximately constant, then the average statistical "weight" of the particles in each region of the problem must decrease approximately in proportion to the expected fast flux, and the average neutron "importance" in each axial region must vary inversely with the average statistical weight of the particles. Moreover, if the average importance from one axial importance zone to the next is not supposed to change by more than a factor of 3, and those at beginning of the water tube have an importance of 2 or 3, then the number of axial importance zones is pretty well determined. In this case, we used a few more axial importance zones (31) across the length of the water tube so that the zone-to-zone importance ratio (2.31) would be somewhat less than the recommended maximum -- that is: we assumed that the relative neutron importance would change by a factor of 2.31 from one 4.1-cm-thick axial importance zone to the next in this particular problem. Likewise, about 20 or 22 additional axial importance zones of similar size were used along the length of the water-filled collimator from Z=302.1868 cm to Z=399.48 cm, thus giving us about 53 axial importance zones over the region of interest in this problem.

While the relative neutron importance increases axially as one moves from the impingent source (on the upstream end of the water tube) to the point of interest (downstream of the water-filled

collimator), the relative neutron importance also decreases as one moves radially outward from the centerline of the beam tube. If one does not allow for this radial decrease, one will end up tracking an enormous number particles in distant radial regions that never really contribute to the flux at the point of interest. Thus, for a calculation to be reasonably efficient, one must take the cells necessary to describe the material configuration and subdivide them both radially and axially into a number of "importance cells" where the neutron importance specified manually on each cell description card increases axially but decreases radially. If the shield is relatively simple and homogeneous, this is not difficult and one can write a simple Fortran program to prepare the necessary cell description cards for each of the hundreds (or thousands) of cells that will be required to obtain an efficient solution. In the case of the originally proposed HB-2 backstop involving a relatively homogeneous slab shield, this approach was used with very good results. (In that case, the 3-D MCNP results were confirmed by 2-D RZ DORT calculations, as well as by simpler semi-analytic methods.)

In the case of a complex shield which may already require many axial and radial cells just to describe the material configuration (such as the HB-3 beam tube as shown in Fig. 3.3), the problem becomes "enormously" more complicated, time-consuming, and error prone since the (dozens or hundreds) of 3-D surfaces needed to define the (hundreds or thousands) of new importance cells are intermingled with the dozens of surfaces already needed to describe the (dozens or hundreds) of material cells in the original problem. Moreover, virtually all of the original material cells have to be subdivided in accordance with this superset of 3-D surfaces in order to describe the thousands of importance cells needed (each having a material ID, a material density, and an assigned neutron importance), without violating the original material description of the problem. The input file for an otherwise modestly simple problem can become complicated and extraordinarily voluminous very quickly. Because of the intermingled nature of the surfaces required, most of this input must be prepared by hand (which becomes intractable very quickly) or by a special input preparation program which one would have to rewrite on an ad hoc basis for every problem to be solved. Furthermore, relocating either the source or the detector points of interest would impact the relative neutron importance distribution, such that most or all of the cell cards would have to be regenerated with the new importance values specified for each cell. Even if this is not the case, but a calculation is run and the statistics are found to be too poor or the running time simply too prohibitive, the importance distribution may have to be changed anyway, and all the cell cards regenerated again, even if the material configuration or source distribution did not change!

As unattractive (and potentially infeasible) as this might be, it was the only alternative available at the time this water-tube shielding analysis was initiated in April 1998. Moreover, because of these considerations, it was not at all clear at the time this study was initiated, whether it even could be brought to a successful conclusion or not.

To begin investigating the feasibility of the water-tube shielding problem on a "limited" basis, without a full implementation of all the necessary radial and axial variations described above, it was decided that we would initially take only the six or seven basic material cells lying on or close to the centerline of the beam tube, and subdivide them into a number of importance cells (with the neutron importance increasing axially), while leaving the rest of the cells and their importance values essentially untouched. This would tend to keep the population of "ever-smaller-weight" particles basically constant down along the centerline of the problem, thus affording good statistical results near the end of the collimator. As noted above, this is a very traditional concept and is well-founded. As for leaving the other radial zones untouched: The thought (later found to be fatal) was that if some low-weight particles from some advanced axial zone were to leak out radially from this central region, they would enter zones where the neutron importance was relatively/very low (ie, where the average neutron weight would be relatively very high), and would immediately be killed by Russian Roulette. Since the ratio of the escaping neutron weight to the local average weight in such zones would be very low, it would almost be akin to making all the other radial zones (outside the six or seven of interest) a black void. Because of this, it was known that this would not yield a correct solution, but if the approach appeared promising, the level of effort needed to implement a full-blown description of all the radial and axial importance zones throughout the entire problem could be justified, subsequent to which the correct solution would then be obtained. The six or seven material cells to be subdivided into multiple importance cells in this trial run were as follows:

From the start of the 1998 water tube at Z=174.27 cm to the end of the water tube at Z=302.1868 cm:

Cell 2145 (the water inside the 1998 HB-3 water tube)..... was replaced with 31 new cells,
Cell 2146 (the pneumatic tube coils inside the 1998 water tube)... was replaced with 31 new cells,
Cell 2147 (the expanded aluminum body of the 1998 water tube)..... was replaced with 31 new cells.

From the end of the water tube at Z=302.1868 cm to the start of the collimator at Z=310.58 cm:

Cell 4375 (the previously void region just upstream of collimator) was replaced with 2 new cells.

From about Z=302.1868 or Z=310.58 cm, to the end of the collimator at Z=399.48 or Z=401.9445 cm:

Cell 4300 (the water-filled rectangular hole up thru collimator).. was replaced with 20 new cells,
Cell 4310 (the steel body of the central collimator)..... was replaced with 20 new cells,
Cell 4320 (the expanded aluminum beam tube adjacent to collimator) was replaced with 22 new cells.

These 157 new importance cells, and the "neutron importance" assigned to each, are further described in Table C1.1. Note that in addition to these 157 new cells, the MCNP input file had to be augmented with the addition of several dozen new surfaces needed to describe these new cells. (In a full-blown implementation, each of the 100+ original material cells in the problem would have to be subdivided in a similar fashion. Specification of those new importance cells would, in turn, require a few new axial surfaces and a number of new radial surfaces. More intimidating, is the fact that each of the several thousand new importance cells that would be created would each have to have their own cell specification card, like those shown in Table C1.1.)

In addition:

a) Cell 4321 (representing the aluminum step where beam tube expands a second time) must have the same importance as Cell 6182 (imp:n=3.7E+11) or all of the (low-weight) neutrons that have been successfully transported to this point would be killed if they entered Cell 4380 and found a low-importance region there.

b) Cell 4380 (representing the 2nd aluminum window in the 1998 water tube) must have the same importance as Cell 6182 (imp:n=3.7E+11) or all of the (low-weight) neutrons that have successfully been transported to this point would be killed if they entered Cell 4380 and found a low-importance region there.

c) Cells 4315 and 4316 (previously representing the small void regions just downstream of the collimator and the rectangular hole in the collimator) must both have the same importance as Cell 6224 (imp:n=9.3E+18) or all of the (low-weight) neutrons that have been successfully transported to this point would be killed if they entered these cells and found a low-importance region there.

These types of considerations must generally be studied individually and implemented by hand. In a complex 3-D problem, there is no "magic button" one can push or any input flag one can set to relieve the user of the responsibility of considering such details on a case-by-case basis.

While this does represent a lot of changes in order to accommodate the flooded 1998 water tube, this only represents a fraction of the changes that would eventually be required. Here, for example, we have simply provided for different importance zones along the middle of the system -- ie, for the aluminum water tube (aluminum and water regions separately), the rectangular hole in the collimator, the steel collimator itself, and the aluminum cylinder surrounding the collimator. If this begins to look at all tractable, then one would have to expand these importance regions in the radial direction to get the right answer. The limited use made of different importance regions described above was intended to see if this approach will work, but that's all. Presently, those neutrons that stray outside the regions described above will enter very low importance regions and likely be killed, when in fact, the surrounding regions should have importances that diminish gradually in the radial direction so that these neutrons are not all killed at once, and so that some of them have a chance of returning without being fat particles. (The term "fat particle" refers to a particle whose weight, for whatever reason, is unusually and disturbingly large relative to that of most others in a given region.) From that viewpoint, this was simply a test case -- not a reference case.

C.1.4 Initial Results, Other Variations, and the Necessary Conclusion

Despite initial success with the above approach a year earlier on a similar problem involving a simpler (more homogeneous) shield, the test cases here were a dismal failure. Run HB305A was for the purpose of checking the basic geometry only. Runs HB305B, HB305C, and HB305D were actually submitted for testing. Run HB305B was exactly as described above. In Run HB305C, the values used for the neutron importance in the various axial importance zones were changed a little. In Run HB305D, source-energy biasing was used to force sampling in the fast energy groups more often, and in the thermal groups less often, with the MCNP automatically making the necessary self-consistent changes in the starting weights for the neutrons in these various energy ranges, as appropriate. Unfortunately, none of these ever ran to completion. Moreover, they all exhibited the same fatal characteristic: they would run nicely for a while (maybe several hours), and then get "hung up" and go into what appeared to be a state of suspended animation for a day or more, during which time there was no choice but to cancel each one.

After some thought and diagnosis, it eventually became apparent what was happening in these calculational runs. The difficulty stemmed from the fact that we did not alter or reduce the specified neutron importance in the other radial regions (outside the central regions of interest)

at each axial level. More precisely, the difficulty stemmed from the previously noted assumption that low-weight neutrons at advanced axial locations which leak from the central zones into the surrounding radial zones where the neutron importance is lower (and the average weight is higher) will generally/always be killed by Russian Roulette. While that is generally true, the few that survive Russian Roulette are then assigned the (higher) average weight corresponding to this new region, and those that subsequently cross back into the central (lower-weight) zones are then split into a zillion pieces that must then be tracked. Say, for example, that a neutron in a central axial zone where the average weight might be 1.0e-4 leaks radially outward and (1 time in 10,000) survives Russian Roulette and is reassigned a weight of 1.0; if that same neutron then scatters back into the central region where the average weight is 1.0e-4, it will be split into 10,000 progeny, each of which must then be tracked in the MCNP model before the code can proceed to the next source neutron. Now consider a similar situation further down the water tube where one such neutron might beget 1,000,000 or 10,000,000 progeny, or more! Obviously, the potential is there for the code to get "hung up" for a long time if one of the low-weight neutrons from the central region leaks out radially and happens to survive Russian Roulette.

This is no fault of the code. Users are warned, and we have always known, that discontinuities in the neutron importance from one cell to the next should never exceed a factor of about 3 or 4. In this particular case, however, we were simply willing to "take the chance" in order to test the feasibility of this approach prior to investing the effort required for a full-blown implementation of all the radial and axial importance cells that would be necessary for the final analysis. It didn't work. No shortcuts allowed. Thus, there were basically three options left at the time these initial test calculations were being performed:

1) For testing purposes, make all the surrounding radial regions a black void by assigning them a neutron importance of zero. This was considered too unrealistic, but may have allowed the initial testing to go forward. Ultimately, however, one would have to turn to options (2) or (3) below.

2) Allow the axial importance regions to extend radially across the entire problem geometry, without decreasing the neutron importance in the radial direction. This would have required more importance cells than used in the present HB305B model, but likely would have worked based on our prior experience. The disadvantage, of course, is that, without a radial decrease in the neutron importance, the code would have spent an enormous amount of time (perhaps a prohibitive amount of time) tracking particles in distant radial locations that have no realistic chance of ever contributing to the solution at the point of interest.

3) Spend the time and effort necessary to subdivide all of the material cells into the (literally) thousands of smaller importance zones required for the full-blown implementation described above, and then hope that the assumed importance distribution was adequate so we wouldn't have to do it again. Moreover, if one later wanted to solve the 1960 water-tube problem instead of the 1998 water problem, or perform any parametric analyses, this would have to done over again each time with the appropriate values -- clearly not an exciting or attractive prospect even if the approach could be made to work.

In lieu of this extremely unattractive and error-prone approach, it was decided to temporarily abandon the use of MCNP for the water-tube shielding analysis, at least as far as the neutron source was concerned, and turn instead to the more elementary analytic techniques described in Sect 5. In the mean time, while those elementary techniques showed the neutron and secondary gamma dose rates to be totally insignificant, work on advanced techniques using undocumented features of the MCNP4B code was being conducted on the side which would circumvent the difficulties described above and allow the existing code to be used much more effectively on geometrically-complex deep penetration shielding problems of this nature. Those efforts were mentioned briefly in Sect C.1.1, and are elaborated upon extensively in Appendix C.2 and in Sect 6 of the main report where this new, previously unavailable and still undocumented, approach was used in the successful solution of the 1998 water-tube shielding problem for the case with a gamma-only source. Moreover, it is now believed that such an approach could also be used for this same problem with the neutron-only source. That, however, has not been done since the need this detailed analysis has since been dismissed.

Table C1.1. List of 307 additional new "importance" cells needed to replace just six or seven of the simple "material" cells near the centerline in the flooded HB-3 water-tube shielding analysis, as taken from the MCNP input for Run HB305B.

```
c      Cell 2145 (corresponding to the water in the 1998 water tube), formerly described as:
c      2145   8   -1.0000   -2134  2154 -4110          imp:n=1  $ water inside main cavity of expanded beam tube outside vessel (if flooded for maintenance)
c      has been replaced with cells 6120 thru 6180:
c      ---------------------------------------------------
6120   8   -1.0000   -2134  2154  -5122  imp:n=4.5E+00  $  Z < 178.45    $ surf 2154 at Z=174.95125 cm
6122   8   -1.0000   -2134  5122  -5124  imp:n=1.0E+01  $  Z < 182.62
6124   8   -1.0000   -2134  5124  -5126  imp:n=2.3E+01  $  Z < 186.80
6126   8   -1.0000   -2134  5126  -5128  imp:n=5.1E+01  $  Z < 190.97
6128   8   -1.0000   -2134  5128  -5130  imp:n=1.2E+02  $  Z < 195.15
6130   8   -1.0000   -2134  5130  -5132  imp:n=2.6E+02  $  Z < 199.32
6132   8   -1.0000   -2134  5132  -5134  imp:n=5.8E+02  $  Z < 203.50
6134   8   -1.0000   -2134  5134  -5136  imp:n=1.3E+03  $  Z < 207.67
6136   8   -1.0000   -2134  5136  -5138  imp:n=3.0E+03  $  Z < 211.85
6138   8   -1.0000   -2134  5138  -5140  imp:n=6.7E+03  $  Z < 216.02
6140   8   -1.0000   -2134  5140  -5142  imp:n=1.5E+04  $  Z < 220.20
6142   8   -1.0000   -2134  5142  -5144  imp:n=3.4E+04  $  Z < 224.37
6144   8   -1.0000   -2134  5144  -5146  imp:n=7.6E+04  $  Z < 228.55
6146   8   -1.0000   -2134  5146  -5148  imp:n=1.7E+05  $  Z < 232.72
6148   8   -1.0000   -2134  5148  -5150  imp:n=3.8E+05  $  Z < 236.90
6150   8   -1.0000   -2134  5150  -5152  imp:n=8.6E+05  $  Z < 241.07
6152   8   -1.0000   -2134  5152  -5154  imp:n=1.9E+06  $  Z < 245.25
6154   8   -1.0000   -2134  5154  -5156  imp:n=4.4E+06  $  Z < 249.42
6156   8   -1.0000   -2134  5156  -5158  imp:n=9.8E+06  $  Z < 253.60
6158   8   -1.0000   -2134  5158  -5160  imp:n=2.2E+07  $  Z < 257.77
6160   8   -1.0000   -2134  5160  -5162  imp:n=5.0E+07  $  Z < 261.9474  $ 5162 same as surf 4100
6162   8   -1.0000   -2134  5162  -5164  imp:n=1.1E+08  $  Z < 266.02
6164   8   -1.0000   -2134  5164  -5166  imp:n=2.5E+08  $  Z < 270.09
6166   8   -1.0000   -2134  5166  -5168  imp:n=5.7E+08  $  Z < 274.17
6168   8   -1.0000   -2134  5168  -5170  imp:n=1.3E+09  $  Z < 278.24
6170   8   -1.0000   -2134  5170  -5172  imp:n=2.9E+09  $  Z < 282.31
6172   8   -1.0000   -2134  5172  -5174  imp:n=6.5E+09  $  Z < 286.385   $ 5174 same as surf 4105
6174   8   -1.0000   -2134  5174  -5176  imp:n=1.5E+10  $  Z < 290.34
6176   8   -1.0000   -2134  5176  -5178  imp:n=3.3E+10  $  Z < 294.29
6178   8   -1.0000   -2134  5178  -5180  imp:n=7.4E+10  $  Z < 298.24
6180   8   -1.0000   -2134  5180  -4110  imp:n=1.7E+11  $  Z < 302.1868  $ 4110 same as surf 5182
c      ---------------------------------------------------
c
c      *** IMPORTANT (when water tube is flooded):  Cell 4321 (representing aluminum step where beam tube expands again)
c      *** IMPORTANT (when water tube is flooded):  MUST have the same importance as Cell 6182 below (imp:n=3.7E+11) or all of
c      *** IMPORTANT (when water tube is flooded):  the (low weight) neutrons we've worked so hard to transport so far to this point
c      *** IMPORTANT (when water tube is flooded):  will be killed if they enter Cell 4380 and find a low importance region there
c
c      *** IMPORTANT (when water tube is flooded):  Cell 4380 (representing the 2nd aluminum window in the 1998 water tube)
c      *** IMPORTANT (when water tube is flooded):  MUST have the same importance as Cell 6182 below (imp:n=3.7E+11) or all of
c      *** IMPORTANT (when water tube is flooded):  the (low weight) neutrons we've worked so hard to transport so far to this point
c      *** IMPORTANT (when water tube is flooded):  will be killed if they enter Cell 4380 and find a low importance region there
c
c      Cell 4375 (previously corresponding to void just upstream of collimator), formerly described as:
c      4375  61  -1.0e-20  4115  -4130 -4230        #(2135 -4126)      imp:n=1  $ void just upstream of collimator (before 2nd aluminum window in 1998 design)
c      has been replaced with cells 6182 thru 6184:
c      ---------------------------------------------------
6182   8   -1.0000   4115  -5184 -4230  #(2135 -4126)  imp:n=3.7E+11  $  Z < 306.38,  water-filled former void just upstream of collimator (before 2nd aluminum wind
6184   8   -1.0000   5184  -4130 -4230                 imp:n=8.4E+11  $  Z < 310.58,  4130 same as surf 5186,  water-filled former void just upstream of collimator
```

Table C1.1 (cont)

```
c      *** NOTE ***  For the case of the 1998 water tube, where both the water tube and the collimator
c      *** NOTE ***  section are flooded, Cell 4305 is not needed and should be commented out
c
c      Cell 4300 (previously void rectangular hole up thru collimator), formerly described as:
c      4300  61  -1.0e-20  4130 -4190 4210 -4211 4212 -4213 #(4140 -4145) imp:n=1   $ rectangular hole up thru collimator
c      has been replaced with cells 6186 thru 6224:  (now water-filled)
c      ------------------------------------------------------
6186  8  -1.0000  4210 -4211 4212 -4213  4130  -5188  imp:n=1.9E+12  $  Z < 315.04     ! 4130 same as surf 5186
6188  8  -1.0000  4210 -4211 4212 -4213  5188  -5190  imp:n=4.2E+12  $  Z < 319.51
6190  8  -1.0000  4210 -4211 4212 -4213  5190  -5192  imp:n=9.5E+12  $  Z < 323.97
6192  8  -1.0000  4210 -4211 4212 -4213  5192  -5194  imp:n=2.1E+13  $  Z < 328.44
6194  8  -1.0000  4210 -4211 4212 -4213  5194  -5196  imp:n=4.8E+13  $  Z < 332.90
6196  8  -1.0000  4210 -4211 4212 -4213  5196  -5198  imp:n=1.1E+14  $  Z < 337.37
6198  8  -1.0000  4210 -4211 4212 -4213  5198  -5200  imp:n=2.4E+14  $  Z < 341.8292  ! same as surf 4155
6200  8  -1.0000  4210 -4211 4212 -4213  5200  -5202  imp:n=5.5E+14  $  Z < 346.24
6202  8  -1.0000  4210 -4211 4212 -4213  5202  -5204  imp:n=1.2E+15  $  Z < 350.65
6204  8  -1.0000  4210 -4211 4212 -4213  5204  -5206  imp:n=2.8E+15  $  Z < 355.06
6206  8  -1.0000  4210 -4211 4212 -4213  5206  -5208  imp:n=6.3E+15  $  Z < 359.47
6208  8  -1.0000  4210 -4211 4212 -4213  5208  -5210  imp:n=1.4E+16  $  Z < 363.88
6210  8  -1.0000  4210 -4211 4212 -4213  5210  -5212  imp:n=3.2E+16  $  Z < 368.29
6212  8  -1.0000  4210 -4211 4212 -4213  5212  -5214  imp:n=7.1E+16  $  Z < 372.70
6214  8  -1.0000  4210 -4211 4212 -4213  5214  -5216  imp:n=1.6E+17  $  Z < 377.11
6216  8  -1.0000  4210 -4211 4212 -4213  5216  -5218  imp:n=3.6E+17  $  Z < 381.5167  ! same as surf 4170
6218  8  -1.0000  4210 -4211 4212 -4213  5218  -5220  imp:n=8.1E+17  $  Z < 386.81
6220  8  -1.0000  4210 -4211 4212 -4213  5220  -5222  imp:n=1.8E+18  $  Z < 392.1125  ! same as surf 3010
6222  8  -1.0000  4210 -4211 4212 -4213  5222  -5224  imp:n=4.1E+18  $  Z < 397.03
6224  8  -1.0000  4210 -4211 4212 -4213  5224  -4190  imp:n=9.3E+18  $  Z < 399.48     ! 4195 same as surf 5226
c
c      *** IMPORTANT (when water tube is flooded):  Cells 4315 & 4316 (previously representing the small void regions just
c      *** IMPORTANT (when water tube is flooded):  downstream of the collimator and the rectangular hole in the collimator)
c      *** IMPORTANT (when water tube is flooded):  BOTH should perhaps (?) be replaced by aluminum (3rd aluminum window ??), and
c      *** IMPORTANT (when water tube is flooded):  BOTH MUST have the same importance as Cell 6224 above (imp:n=9.3E+18) or all of
c      *** IMPORTANT (when water tube is flooded):  the (low weight) neutrons we've worked so hard to transport so far to this point
c      *** IMPORTANT (when water tube is flooded):  will be killed if they enter these cells and find a low importance region there
c      *** IMPORTANT (when water tube is flooded):  Also: Should probably now calc leakage across Surf 4195 instead of Surf 4190,
c      *** IMPORTANT (when water tube is flooded):  however, since I have no details, leave cells void & stay with Surf 4190
c
c      Cell 2146 (corresponding to the pneumatic tube coils inside the 1998 water tube), formerly described as:,
c      2146   8   -1.0000   -2135  2134  2154  -4110  imp:n=1  $ water in pneumatic tube coils located just inside outer wall of expanded beam tube outside vessel
c      has been replaced with cells 6320 thru 6380:
c      ------------------------------------------------------
6320   8   -1.0000   2134  -2135  2154  -5122  imp:n=4.5E+00  $  Z < 178.45    $ surf 2154 at Z=174.95125 cm
6322   8   -1.0000   2134  -2135  5122  -5124  imp:n=1.0E+01  $  Z < 182.62
6324   8   -1.0000   2134  -2135  5124  -5126  imp:n=2.3E+01  $  Z < 186.80
6326   8   -1.0000   2134  -2135  5126  -5128  imp:n=5.1E+01  $  Z < 190.97
6328   8   -1.0000   2134  -2135  5128  -5130  imp:n=1.2E+02  $  Z < 195.15
6330   8   -1.0000   2134  -2135  5130  -5132  imp:n=2.6E+02  $  Z < 199.32
6332   8   -1.0000   2134  -2135  5132  -5134  imp:n=5.8E+02  $  Z < 203.50
6334   8   -1.0000   2134  -2135  5134  -5136  imp:n=1.3E+03  $  Z < 207.67
6336   8   -1.0000   2134  -2135  5136  -5138  imp:n=3.0E+03  $  Z < 211.85
6338   8   -1.0000   2134  -2135  5138  -5140  imp:n=6.7E+03  $  Z < 216.02
6340   8   -1.0000   2134  -2135  5140  -5142  imp:n=1.5E+04  $  Z < 220.20
6342   8   -1.0000   2134  -2135  5142  -5144  imp:n=3.4E+04  $  Z < 224.37
6344   8   -1.0000   2134  -2135  5144  -5146  imp:n=7.6E+04  $  Z < 228.55
6346   8   -1.0000   2134  -2135  5146  -5148  imp:n=1.7E+05  $  Z < 232.72
6348       -1.0000   2134  -2135  5148  -5150  imp:n=3.8E+05  $  Z < 236.90
```

Table C1.1 (cont)

```
6350   8   -1.0000   2134  -2135  5150  -5152  imp:n=8.6E+05  $  Z < 241.07
6352   8   -1.0000   2134  -2135  5152  -5154  imp:n=1.9E+06  $  Z < 245.25
6354   8   -1.0000   2134  -2135  5154  -5156  imp:n=4.4E+06  $  Z < 249.42
6356   8   -1.0000   2134  -2135  5156  -5158  imp:n=9.8E+06  $  Z < 253.60
6358   8   -1.0000   2134  -2135  5158  -5160  imp:n=2.2E+07  $  Z < 257.77
6360   8   -1.0000   2134  -2135  5160  -5162  imp:n=5.0E+07  $  Z < 261.9474  $ 5162 same as surf 4100
6362   8   -1.0000   2134  -2135  5162  -5164  imp:n=1.1E+08  $  Z < 266.02
6364   8   -1.0000   2134  -2135  5164  -5166  imp:n=2.5E+08  $  Z < 270.09
6366   8   -1.0000   2134  -2135  5166  -5168  imp:n=5.7E+08  $  Z < 274.17
6368   8   -1.0000   2134  -2135  5168  -5170  imp:n=1.3E+09  $  Z < 278.24
6370   8   -1.0000   2134  -2135  5170  -5172  imp:n=2.9E+09  $  Z < 282.31
6372   8   -1.0000   2134  -2135  5172  -5174  imp:n=6.5E+09  $  Z < 286.385   $ 5174 same as surf 4105
6374   8   -1.0000   2134  -2135  5174  -5176  imp:n=1.5E+10  $  Z < 290.34
6376   8   -1.0000   2134  -2135  5176  -5178  imp:n=3.3E+10  $  Z < 294.29
6378   8   -1.0000   2134  -2135  5178  -5180  imp:n=7.4E+10  $  Z < 298.24
6380   8   -1.0000   2134  -2135  5180  -4110  imp:n=1.7E+11  $  Z < 302.1868  $ 4110 same as surf 5182
c      ----------------------------------------------------
c
c      Cell 4310 (corresponding to ss body of central collimator with rectangular hole), formerly described as:
c      4310  40  -7.92  4130  -4190 -4230  #(4210 -4211 4212 -4213)  imp:n=1  $ ss body of central collimator with rectangular hole
c      has been replaced with cells 6386 thru 6424:
c      ----------------------------------------------------
6386  40  -7.92  -4230  #(4210 -4211 4212 -4213)  4130  -5188  imp:n=1.9E+12  $  Z < 315.04    ! 4130 same as surf 5186
6388  40  -7.92  -4230  #(4210 -4211 4212 -4213)  5188  -5190  imp:n=4.2E+12  $  Z < 319.51
6390  40  -7.92  -4230  #(4210 -4211 4212 -4213)  5190  -5192  imp:n=9.5E+12  $  Z < 323.97
6392  40  -7.92  -4230  #(4210 -4211 4212 -4213)  5192  -5194  imp:n=2.1E+13  $  Z < 328.44
6394  40  -7.92  -4230  #(4210 -4211 4212 -4213)  5194  -5196  imp:n=4.8E+13  $  Z < 332.90
6396  40  -7.92  -4230  #(4210 -4211 4212 -4213)  5196  -5198  imp:n=1.1E+14  $  Z < 337.37
6398  40  -7.92  -4230  #(4210 -4211 4212 -4213)  5198  -5200  imp:n=2.4E+14  $  Z < 341.8292  ! same as surf 4155
6400  40  -7.92  -4230  #(4210 -4211 4212 -4213)  5200  -5202  imp:n=5.5E+14  $  Z < 346.24
6402  40  -7.92  -4230  #(4210 -4211 4212 -4213)  5202  -5204  imp:n=1.2E+15  $  Z < 350.65
6404  40  -7.92  -4230  #(4210 -4211 4212 -4213)  5204  -5206  imp:n=2.8E+15  $  Z < 355.06
6406  40  -7.92  -4230  #(4210 -4211 4212 -4213)  5206  -5208  imp:n=6.3E+15  $  Z < 359.47
6408  40  -7.92  -4230  #(4210 -4211 4212 -4213)  5208  -5210  imp:n=1.4E+16  $  Z < 363.88
6410  40  -7.92  -4230  #(4210 -4211 4212 -4213)  5210  -5212  imp:n=3.2E+16  $  Z < 368.29
6412  40  -7.92  -4230  #(4210 -4211 4212 -4213)  5212  -5214  imp:n=7.1E+16  $  Z < 372.70
6414  40  -7.92  -4230  #(4210 -4211 4212 -4213)  5214  -5216  imp:n=1.6E+17  $  Z < 377.11
6416  40  -7.92  -4230  #(4210 -4211 4212 -4213)  5216  -5218  imp:n=3.6E+17  $  Z < 381.5167  ! same as surf 4170
6418  40  -7.92  -4230  #(4210 -4211 4212 -4213)  5218  -5220  imp:n=8.1E+17  $  Z < 386.81
6420  40  -7.92  -4230  #(4210 -4211 4212 -4213)  5220  -5222  imp:n=1.8E+18  $  Z < 392.1125  ! same as surf 3010
6422  40  -7.92  -4230  #(4210 -4211 4212 -4213)  5222  -5224  imp:n=4.1E+18  $  Z < 397.03
6424  40  -7.92  -4230  #(4210 -4211 4212 -4213)  5224  -4190  imp:n=9.3E+18  $  Z < 399.48    ! 4195 same as surf 5226
c
c      Cell 2147 (corresponding to the aluminum body of the expanded section of the new HB-3 beam tube forming the 1998 water tube), formerly described as:
c      2147  24  -2.7  -2136  2135  2154  -4125  imp:n=1  $ aluminum body of expanded section of the new HB-3 beam tube outside vessel
c      has been replaced with cells 6520 thru 6580:
c      ----------------------------------------------------
6520   24  -2.7   2135  -2136  2154  -5122  imp:n=4.5E+00  $  Z < 178.45    $ surf 2154 at Z=174.95125 cm
6522   24  -2.7   2135  -2136  5122  -5124  imp:n=1.0E+01  $  Z < 182.62
6524   24  -2.7   2135  -2136  5124  -5126  imp:n=2.3E+01  $  Z < 186.80
6526   24  -2.7   2135  -2136  5126  -5128  imp:n=5.1E+01  $  Z < 190.97
6528   24  -2.7   2135  -2136  5128  -5130  imp:n=1.2E+02  $  Z < 195.15
6530   24  -2.7   2135  -2136  5130  -5132  imp:n=2.6E+02  $  Z < 199.32
6532   24  -2.7   2135  -2136  5132  -5134  imp:n=5.8E+02  $  Z < 203.50
6534   24  -2.7   2135  -2136  5134  -5136  imp:n=1.3E+03  $  Z < 207.67
```

Table C1.1 (cont)

```
6536   24  -2.7   2135  -2136  5136  -5138  imp:n=3.0E+03  $  Z < 211.85
6538   24  -2.7   2135  -2136  5138  -5140  imp:n=6.7E+03  $  Z < 216.02
6540   24  -2.7   2135  -2136  5140  -5142  imp:n=1.5E+04  $  Z < 220.20
6542   24  -2.7   2135  -2136  5142  -5144  imp:n=3.4E+04  $  Z < 224.37
6544   24  -2.7   2135  -2136  5144  -5146  imp:n=7.6E+04  $  Z < 228.55
6546   24  -2.7   2135  -2136  5146  -5148  imp:n=1.7E+05  $  Z < 232.72
6548   24  -2.7   2135  -2136  5148  -5150  imp:n=3.8E+05  $  Z < 236.90
6550   24  -2.7   2135  -2136  5150  -5152  imp:n=8.6E+05  $  Z < 241.07
6552   24  -2.7   2135  -2136  5152  -5154  imp:n=1.9E+06  $  Z < 245.25
6554   24  -2.7   2135  -2136  5154  -5156  imp:n=4.4E+06  $  Z < 249.42
6556   24  -2.7   2135  -2136  5156  -5158  imp:n=9.8E+06  $  Z < 253.60
6558   24  -2.7   2135  -2136  5158  -5160  imp:n=2.2E+07  $  Z < 257.77
6560   24  -2.7   2135  -2136  5160  -5162  imp:n=5.0E+07  $  Z < 261.9474  $ 5162 same as surf 4100
6562   24  -2.7   2135  -2136  5162  -5164  imp:n=1.1E+08  $  Z < 266.02
6564   24  -2.7   2135  -2136  5164  -5166  imp:n=2.5E+08  $  Z < 270.09
6566   24  -2.7   2135  -2136  5166  -5168  imp:n=5.7E+08  $  Z < 274.17
6568   24  -2.7   2135  -2136  5168  -5170  imp:n=1.3E+09  $  Z < 278.24
6570   24  -2.7   2135  -2136  5170  -5172  imp:n=2.9E+09  $  Z < 282.31
6572   24  -2.7   2135  -2136  5172  -5174  imp:n=6.5E+09  $  Z < 286.385   $ 5174 same as surf 4105
6574   24  -2.7   2135  -2136  5174  -5176  imp:n=1.5E+10  $  Z < 290.34
6576   24  -2.7   2135  -2136  5176  -5178  imp:n=3.3E+10  $  Z < 294.29
6578   24  -2.7   2135  -2136  5178  -5180  imp:n=7.4E+10  $  Z < 298.24
c      6580   24  -2.7   2135  -2136  5180  -4110  imp:n=1.7E+11  $  Z < 302.1868  $ 4110 same as surf 5182
6580   24  -2.7   2135  -2136  5180  -4125  imp:n=1.7E+11  $
c      ---------------------------------------------------
c
c      Cell 4320 (aluminum: expanded section of beam tube along side the collimator), formerly described as:
c      4320  24  -2.7  4125  -4195  4230  -4235  imp:n=1  $ aluminum: expanded section of beam tube along side the collimator
c      has been replaced with cells 6582 thru 6624:
c      ---------------------------------------------------
6582  24  -2.7   4230  -4235  4125  -5184  imp:n=3.7E+11  $  Z < 306.38
6584  24  -2.7   4230  -4235  5184  -5186  imp:n=8.4E+11  $  Z < 310.58    ! same as surf 4130
6586  24  -2.7   4230  -4235  5186  -5188  imp:n=1.9E+12  $  Z < 315.04
6588  24  -2.7   4230  -4235  5188  -5190  imp:n=4.2E+12  $  Z < 319.51
6590  24  -2.7   4230  -4235  5190  -5192  imp:n=9.5E+12  $  Z < 323.97
6592  24  -2.7   4230  -4235  5192  -5194  imp:n=2.1E+13  $  Z < 328.44
6594  24  -2.7   4230  -4235  5194  -5196  imp:n=4.8E+13  $  Z < 332.90
6596  24  -2.7   4230  -4235  5196  -5198  imp:n=1.1E+14  $  Z < 337.37
6598  24  -2.7   4230  -4235  5198  -5200  imp:n=2.4E+14  $  Z < 341.8292  ! same as surf 4155
6600  24  -2.7   4230  -4235  5200  -5202  imp:n=5.5E+14  $  Z < 346.24
6602  24  -2.7   4230  -4235  5202  -5204  imp:n=1.2E+15  $  Z < 350.65
6604  24  -2.7   4230  -4235  5204  -5206  imp:n=2.8E+15  $  Z < 355.06
6606  24  -2.7   4230  -4235  5206  -5208  imp:n=6.3E+15  $  Z < 359.47
6608  24  -2.7   4230  -4235  5208  -5210  imp:n=1.4E+16  $  Z < 363.88
6610  24  -2.7   4230  -4235  5210  -5212  imp:n=3.2E+16  $  Z < 368.29
6612  24  -2.7   4230  -4235  5212  -5214  imp:n=7.1E+16  $  Z < 372.70
6614  24  -2.7   4230  -4235  5214  -5216  imp:n=1.6E+17  $  Z < 377.11
6616  24  -2.7   4230  -4235  5216  -5218  imp:n=3.6E+17  $  Z < 381.5167  ! same as surf 4170
6618  24  -2.7   4230  -4235  5218  -5220  imp:n=8.1E+17  $  Z < 386.81
6620  24  -2.7   4230  -4235  5220  -5222  imp:n=1.8E+18  $  Z < 392.1125  ! same as surf 3010
6622  24  -2.7   4230  -4235  5222  -5224  imp:n=4.1E+18  $  Z < 397.03
6624  24  -2.7   4230  -4235  5224  -4195  imp:n=9.3E+18  $  Z < 401.9445  ! 4195 same as surf 5226
```

Appendix C.2

MCNP4B Solution of an Academic 3-D Problem Involving the Transmission of a Narrow Collimated Beam of Neutrons Impingent on the Bottom of a Large Cylindrical Tank of Water, Using Geometry-Independent Space-Energy-Direction-Dependent Weight Windows Based on a Simple 1-D Deterministic Adjoint Flux Calculation

Appendix C.2

MCNP4B Solution of an Academic 3-D Problem Involving the Transmission of a Narrow Collimated Beam of Neutrons Impingent on the Bottom of a Large Cylindrical Tank of Water, Using Geometry-Independent Space-Energy-Direction-Dependent Weight Windows Based on a Simple 1-D Deterministic Adjoint Flux Calculation

C.2.1 General Comments on Biasing Techniques

Deep penetration problems in geometrically complex shield configurations are classic in the annals of Monte Carlo history. Solution of deep penetration problems generally require the use of one or more forms of biasing. Weight windows in one form or another are typically used to control and maintain the neutron population throughout the various geometric regions comprising the shield. This may be done directly by having the user specify energy-dependent limits on the weight window (wthigh, wtlow, and wtavg) to be used in each of many small importance cells comprising the shield, or indirectly in an energy-independent fashion by having the user specify the relative neutron importance in each of many small importance cells comprising the shield. In both cases, neutron splitting and Russian Roulette are used to control the local population. In the first case, splitting and Russian Roulette depend on the "absolute" weight of a neutron in a given energy range in a given importance cell. If the neutron has a weight greater than the upper limit (wthigh) for that particular energy range and spatial location, it is split into two or more pieces whose weights lie within the specified weight window. Each piece is then tracked separately. This prevents any one neutron history from dominating the flux solution in a given region (which could lead to very unreliable results). Likewise, if the "absolute" weight of a neutron in a given energy range in a given cell is below the lower limit (wtlow) for that particular energy range and spatial location, a numerical game of Russian Roulette is played. The probability of survival depends on its absolute weight relative to the average weight for that energy range in that particular cell. If it survives, its weight is reset to the specified average weight for that energy range in that particular cell, and tracking continues as if nothing had happened, otherwise it is killed. This prevents enormous numbers of extremely low-weight particles that cannot realistically contribute to the solution from being tracked indefinitely and burning up valuable computer time that could be more usefully spent tracking more important particles. When the user instead elects to specify the "relative neutron importance" on the various cell cards (a simpler procedure requiring far less knowledge on the part of the user), neutron splitting and Russian Roulette are again applied with the same objectives in mind, but they are applied in a slightly different fashion. In this case, neutron splitting is commonly referred to as geometric splitting since it is energy independent and is applied whenever a particle crosses a cell boundary. In this case, the application of neutron splitting and Russian Roulette does not depend on the "absolute" weight of the neutron, but simply on the user-specified importance in the cell the neutron is coming from and the cell to which it is going. In that sense, all neutrons are treated equally. If a neutron is coming from a low-importance region to a high-importance region, it will be split into multiple pieces, each with a proportionately lower weight so that the population represented by the sum of the weights will be maintained. If a neutron is coming from a high-importance region to a low-importance region, the probability of its survival again depends on the ratio of the user-specified importance in the cell the neutron is coming from and the cell to which it is going. If the neutron survives, its original weight is multiplied by the ratio of the higher cell importance to the lower cell importance. Quite independent of whether one specifies the relative neutron importance on each cell card and uses geometric splitting, or whether one specifies a complete set of energy-dependent weight windows for every geometry cell, many other things such as neutron scattering and absorption events at each collision site will also affect the weight of a neutron throughout its history. Moreover, it is the sum of the weighted neutron track lengths in any given cell that will ultimately determine the flux in that cell. The number of neutron tracks in a given cell, however, will determine the statistical uncertainty of the result. To the extent that one can use the above mechanisms to hold the total population constant throughout the problem (which generally means increasing the number of low weight particles deep in the shield near regions of interest), the final solution will be more reliable.

C.2.2 Difficulties With Traditional Biasing Techniques

Both of the mechanisms described above for handling deep penetration problems are well known and have been around for many years. The difficulty with both approaches in geometrically complex problems comes from the fact that this information (the weight window specifications or the relative neutron importance specifications) must be supplied for each of many small importance cells throughout the problem. If these cells and cell boundary surfaces could be specified independently of the cells and surfaces needed to specify the material configuration, the task would not be nearly as daunting. Historically, until recently, that has not been the case. The cells and constituent surfaces needed to specify the many small importance regions that might be required were also used to specify the material configuration. Large, relatively simple cells that might otherwise be adequate to specify the entire material configuration would frequently have to be split individually into dozens of smaller 3-D cells to form the importance regions needed for an adequate solution. In geometrically complex shields where a hundred or more material cells might needed to specify the geometry alone, one can ill-afford to split each into the many (sometimes dozens) of additional

smaller cells that might be required to specify the importance zones. Some of these difficulties are outlined more extensively in Appendix C.1.3. Moreover, even if one is mentally nimble enough to visualize the full 3-D problem and create input files describing all of the surfaces and dual purpose cells that might be necessary to describe the problem without violating other constraints such as the maximum allowable ratio of neutron importances in adjacent cells (ratio should always be less than 3), the very existence of all the otherwise unnecessary geometry specifications makes the model much more difficult to understand and adds a certain degree of unavoidable calculational overhead to the tracking algorithms and running time. More importantly, a whole range of important but geometrically-complex deep penetration problems simply become infeasible in any practical sense.

C.2.3 Recent Developments: Geometry-Independent Weight Windows

In the last two or three years, there have been two independent, yet essentially identical, efforts to circumvent the well-known difficulty described above -- one by John Wagner and Alireza Haghighat at the Pennsylvania State University#33-35, and one by John Hendricks, Tom Evans, Ken Van Riper, and Todd Urbatsch at Los Alamos#21,27. In both cases, a modified version of the MCNP code is used in which neutrons are essentially tracked simultaneously in two "separate" geometry systems, so to speak. (1) The first uses the same traditional surfaces and cells that have always been specified by the user in the regular MCNP input file to describe the location of the material cells required to specify the entire configuration in the simplest possible fashion. Tracking in this system is used to determine the materials the neutrons are passing through and the types of collision events (absorption, scattering, etc) that take place while the neutron is in a given material cell. (2) The second "geometry system", if you wish to call it that, has nothing to do with the material description of the problem; it is simply a set of XYZ mesh intervals (or R-Z-Theta mesh intervals), expressed in terms of the problem's global coordinate system, which fully encapsulate the shield configuration. This is often referred to as a "phantom mesh" since it never appears directly in the MCNP input file and is completely independent of the surface and cell specifications used to describe the problem's material geometry. This variable XYZ mesh, for example, is specified at the beginning of a separate stand-alone ascii-based weight-window file created by the user or some alternate code system. (Indeed, that's why its called a "geometry-independent" weight window file.) The modified version of MCNP is simply given the name of this new file (as a parameter on the existing message header record in the regular MCNP input file), and the modified version of the code uses this alternative broad-group weight window information whenever a neutron crosses into any of the corresponding phantom mesh or experiences a collision in any of the corresponding phantom mesh. [Here at ORNL, this same type of "geometry-independent weight window" approach was previously implemented into the existing MORSE code by J. A. Bucholz back in 1991 for the analysis of the proposed borated pin-array experiments for the NPR Program at the Tower Shielding Reactor#36. This (then) non-standard approach was described at the end of Sect 7.6 in Ref 36, while all of the necessary Fortran routines needed for fully implementing the approach were listed in Appendix D of that document.] In the present Los Alamos formulation, the "geometry-independent weight window" file contains some header information describing the number of different particle types (neutron, photons, or electrons for which information is supplied) and the number of broad energy groups used for biasing each, the specifications for the 3-D (XYZ or RZT) phantom mesh for which weight windows will be supplied, the weight-window lower bound (wtlow) for each 3-D mesh (by broad group), and optionally, the directional adjoint currents (aJx, aJy, aJz) for each 3-D mesh (by broad energy group) as produced by a THREEDANT#26 adjoint analysis of (a generally much cruder model of) the shield configuration. [In the Penn State approach, the 3-D TORT code#8 from ORNL is used instead of THREEDANT for this same type of adjoint analysis.] If the optional adjoint directional currents are supplied, it appears that their sole purpose is to determine the unit vector corresponding to the adjoint current in each mesh, in each broad energy group (see lines 125 to 140, of MCNP4B#4 subroutine WWVAL). At each collision site, the outgoing direction cosines of a particle after a collision are folded with the direction cosines forming the adjoint current vector for that spatial mesh and energy range. The resulting dot product is then applied in an exponential transform to significantly increase the assigned weight of the outgoing particle if it is travelling in a direction of high importance, or to significantly decrease its assigned weight if it is traveling in the opposite direction, with a graded adjustment being made for intermediate directions. In any event, once one is familiar with both the content and the format specifications for the "geometry-independent weight window" file, one can manually construct (through the use of simple Fortran programs) similarly useful 3-D weight window files based on results from simpler 1-D ANISN adjoint calculations that represent the main characteristics of the problem at hand. By using engineering judgement based of a thorough understanding of a given problem, it is often also possible to supply artificially-constructed directional information which simulates the biasing effects that would normally be based more rigorously on the 3-D directional adjoint currents if that information were available. Both types of information (with or without the directional data) are tremendously valuable in accelerating the solution of otherwise difficult Monte Carlo shielding problems. In one academic-based problem described below, a good calculation with perfectly acceptable results was made to run 10,000 times faster than an earlier calculation which had yielded essentially useless results!

In a paper#21 at the ANS Radiation Protection and Shielding Conference in Nashville (April 1997), Tom Evans of the Los Alamos MCNP development group indicated that a version of MCNP (MCNP4C) with the capabilities described above, as well as some other enhancements, would be released in the year 2000, along with other codes and code systems now under development for use in hybrid shielding calculations. When asked how those codes and code systems were being tested, he indicated that all the hooks and logic for reading and

using the type of "geometry-independent weight window" file described above already exist (and have existed for some time) as an undocumented feature of the MCNP4B code which has been publicly available since early 1997 and in use at ORNL since July 1997. Subsequent to the meeting, he later forwarded a set of notes (to be included in the FY 2000 documentation) describing the content and format specifications for the "geometry-independent weight window" file corresponding to XYZ and R-Z-Theta geometries. An enhanced explanation of the information pertinent to the former is included in Appendix C.3 below.

C.2.4 Definition on an Academic Problem for Testing Purposes

To verify that we knew and correctly understood how to generate the necessary information and utilize this "newly-found and still undocumented" capability which held great promise as the only practical method of solving many realistic problems of engineering interest that were otherwise intractable (cf Appendix C.1), we first decided to apply it to a relatively simple "academically-idealized" version of the HB-3 water-tube problem. There it was originally thought that only the 127.23555-cm-long portion of the 1998 water tube from Z=174.95125 to Z=302.1868 cm would be flooded. It was known that without biasing of some sort, the neutrons were (numerically) not progressing much beyond the first 10, 15, or 20 cm of water, and that all earlier attempts at using radial and axial importance cells had failed (cf Appendix C.1). Use of the phantom mesh in the geometry-independent weight window file should work whether one has a simple geometry or a complex geometry (although it is really only needed in the latter case). Thus, for testing purposes, an exceedingly simple "academic" version of the problem was devised. Basically, it involved only the transmission of a narrow collimated beam of neutrons (10-cm-diam) impingent on the bottom of a large (130-cm-diam) cylindrical tank of water extending from Z=175 cm to Z=300 cm. No concrete or aluminum or steel components were included in this academic version of the problem, only the idealized tank of water described above. The neutron-only source was the same 61-group neutron source previously used in the actual HB-3 beam tube analysis (cf Table 2.2a), except that: (a) for the sake of simplification, the point sources for all energy groups were assumed to be located at a single location (X=0, Y=0, Z=50 cm); and (b) the source would now be collimated, not by water or barytes concrete around an empty tube as in the real HB-3 analysis, but by a 130-cm-diam black absorber having a 10-cm-diam hole up the middle, through which neutrons from the point source would stream and become collimated before reaching the bottom of the water tank. This geometry is illustrated in Fig. C2.1, and can be simply modeled in its entirety by the following 6 cells and 7 surfaces:

```
=======================================================================================
Simple "academic model" used for testing geometry-independent weight windows
c
c    CELLS:
101  61  -1.0e-20   -1001         9997  -1003  imp:n=1  $ void inside  central source tube
102  61  -1.0e-20    1001  -9999  9997  -1003  imp:n=0  $ void outside central source tube
201   8   -1.0000   -1002         1003  -1004  imp:n=1  $ water shield, central portion
202   8   -1.0000    1002  -9999  1003  -1004  imp:n=1  $ water shield, outside central portion
300  61  -1.0e-20   -9999   1004        -9998  imp:n=1  $ void beyond water shield
900   0  #(-9999 9997 -9998)                   imp:n=0  $ external void

c     SURFACES:
1001  cz   5.0   $ Cylindrical void OD
1002  cz  10.0   $ radius of central region of interest
1003  pz  175.0  $ start of water
1004  pz  300.0  $ end of water
9997  pz    0.0  $ External void boundary (far enough down to include all point sources)
9998  pz  700.0  $ External void boundary (far enough out to encompass pt detectors if desired)
9999  cz   65.0  $ External void boundary (radial extent of this model)
=======================================================================================
```

The complete MCNP input file (WWT08), which is 280 lines long primarily because of all the diagnostic detectors used, is described below and listed in Appendix C.5.

The objective was to calculate, as accurately as possible, the total "neutron plus secondary gamma" dose rate averaged over a 20-cm-diam disk on the downstream surface of the water tank (at Z=300 cm). To test the ability of the model and the associated geometry-independent weight window file to transport real particles through the entire system, these dose rate estimates were to be based on real boundary crossing tallies at this location (not point detector tallies). To further verify that real particles were actually progressing up through the system, volume-averaged estimates of the total neutron flux and total gamma flux were calculated and displayed for each of twenty-five distinct volume elements (each 5-cm-thick x 20-cm-diam) up along the central portion of the system from Z=175 cm to Z=300 cm.

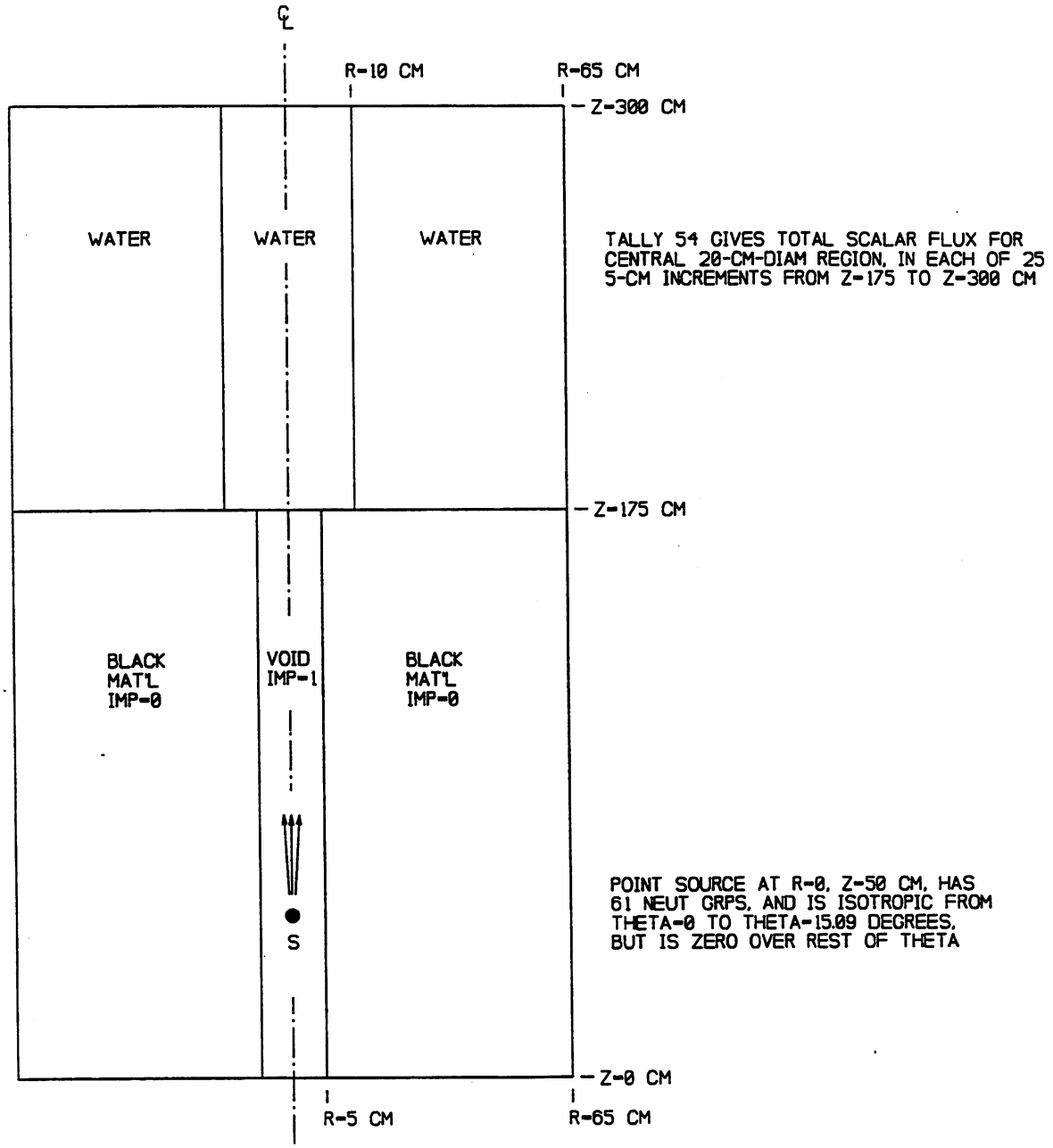


Fig. C2.1. Simple "academic" model used for testing the use of geometry-independent weight windows. This problem (not drawn to scale) involves the transmission of a narrow collimated beam of neutrons (10-cm-diam) impingent on the bottom of a large (130-cm-diam) cylindrical tank of water extending from Z=175 cm to Z=300 cm. Main parameters of interest include the total "neutron plus secondary gamma" dose rate over a 20-cm-diam disk at the top, and the total neutron and gamma fluxes in each of twenty-five 5-cm-thick axial segments in the 20-cm-diam region up the middle.

C.2.5 Use of a 1-D Adjoint Calculation to Generate a 3-D Broad-Group Weight Window File

Appendix C.4 lists the complete contents of a self-contained, fully-automated, script file (GETWIN8.SCR) for generating the geometry-independent broad-group weight window file (wwinp) needed by the MCNP4B code for this particular problem. At the core of this script file is the input for a 1-D Group-Banded ANISN#9 adjoint calculation which generates the fine-group adjoint information used by the other Fortran routines (see the GETWIN8.F program) in the remainder of the script.

This adjoint ANISN calculation is an 84-group calculation and uses the 61n/23g VELM cross section library#10. Because the stated objective of the final MCNP analysis was to calculate the total "neutron plus secondary gamma" dose rate downstream of the water tank at Z=300 cm, the "source term" in this adjoint calculation corresponds to the 61-group-neutron and 23-group-gamma flux-to-dose-rate conversion factors [(mrem/hr)/(n/s/cm2) and (mrem/hr)/(p/s/cm2)] based on the 1977 ANSI Standard#19. These are input as source terms in a thin 0.01-cm-thick mesh (number 251) on the right of the buckled 1-D slab ANISN model. (See the 17** array in the ANISN input). The other 250 0.5-cm-thick mesh intervals in the ANISN model correspond to that portion of the water tank between Z=175 cm and Z=300 cm in the MCNP model. (Lastly, because one is ultimately concerned with the response over a small-diameter disk due to a narrowly collimated beam rather than the response over an infinite plane due to an infinite plane source, this ANISN calculation was run as a buckled slab whose assumed dimensions in the two transverse directions (dx=dy=27.2 cm) were based on the diameter of the beam and the concept of reflector savings, normally applied to water reflected cores in reactor physics calculations.) The ANISN calculation then computes the 84-group neutron and gamma fluxes in each of the 251 mesh intervals of interest and writes those fluxes in "adjoint order" on a binary flux file. (Here the first of the 84 records contains the adjoint gamma fluxes for the softest gamma group, while record 23 contains the adjoint gamma fluxes for the hardest gamma group, record 24 contains the adjoint neutron fluxes for the slowest neutron group, and record 84 contains the adjoint fluxes for the fastest neutron group. This point is emphasized here since it is quite the reverse of what one would normally expect and obtain in a normal "forward" calculation.) After completion of the ANISN calculation, the GETWIN8.SCR script then calls the embedded GETWIN8.F Fortran program (also shown) which further processes the data.

Within the GETWIN8.F program, subroutine SRCJST first calls subroutine GETADJ which reads the adjoint scalar flux file as noted above, as well as the mesh information contained in the ANISN printed output file, and spatially averages the broad-group adjoint fluxes (for six neutron groups and four gamma groups) over each of the 25 wider (5-cm-thick) importance zones. These more meaningful results are listed below in Table C2.1a.

The average broad-group weight for neutrons and gammas in each of the 5-cm-thick importance zones is proportional to the inverse of the corresponding broad-group adjoint flux in such a zone. The tricky part, however, is knowing how to properly normalize everything#25. This is clearly shown in subroutine SRCJST of the GETWIN8.F program in Appendix C.4. Basically, one proceeds as follows:

1) Look at the broad-group adjoint fluxes back at the location where the (real) source particles would normally impinge on the shield, as well as the equivalent broad-group source terms.

2) Determine the "source-averaged adjoint flux" (avgadj) at that location by taking the integral over all broad groups of "the real broad-group sources there, times the broad group adjoint fluxes there", and dividing that integral by the sum of all the real broad-group sources at that location.

3) The average (survival) weight assigned to each broad group at that location equals this "source-averaged adjoint flux" divided by the particular broad-group adjoint flux at that location. Likewise, the average (survival) weight assigned to each broad group in every other importance mesh equals this same "source-averaged adjoint flux" (avgadj) divided by the local broad-group adjoint flux in the given importance mesh. The lower weight window limit (wtlow) for each broad group in each importance mesh is then typically taken to be one tenth the average survival weight. Table C2.1b shows the resulting lower weight limit for each of the neutron and gamma broad groups in each importance mesh along the axis.

   It is important to note, however, that one is not yet done at this point. To work, the starting weight of the neutrons must be compatible with the weight windows just defined, or one could easily have a situation where all the source neutrons split like crazy or are immediately killed without going anywhere. To accomplish this, source-energy biasing is required. Fortunately, the adjoint technique provides an analytic tool for defining the optimal source-energy biasing algorithm compatible with the weight windows just established. Continue as follows:

4) The optimally biased energy distribution for the source (on a broad-group basis) is obtained by taking the (real) broad-group source intensity and dividing it by the average (survival) weight for the corresponding broad-group at the source location. The ratio of the biased source energy

Table C2.1a. Spatially-averaged broad-group neutron and adjoint fluxes for the academic problem as summarized by GETWIN8.SCR.

Neutron and Gamma Adjoint Fluxes in water, where adjoint is based on total n+g dose at X= 300.000 cm, and buckling DY=DZ= 27.20 cm
mnXX-YY = MCNP neutron grp numbers, mgXX-YY = MCNP gamma grp numbers
vnXX-YY = VELM neutron grp numbers, vgXX-YY = VELM gamma grp numbers

		Emax:	4.13990E-07	1.06770E-05	1.23410E-03	1.22770E-01	1.10800E+00	1.49180E+01	3.00000E-01	1.00000E+00	4.00000E+00	1.40000E+01
		imp	mn01-01	mn02-05	mn06-13	mn14-31	mn32-46	mn47-61	mg01-06	mg07-11	mg12-16	mg17-23
xmin	xmax	mesh	vn61-61	vn57-60	vn49-56	vn31-48	vn16-30	vn01-15	vg18-23	vg13-17	vg08-12	vg01-07
175.00	180.00	1	9.81737E-10	3.84592E-09	7.49249E-09	1.63987E-08	1.32706E-08	2.47022E-08	1.92692E-12	1.37135E-10	1.10285E-08	3.53542E-07
180.00	185.00	2	2.14677E-09	8.52375E-09	1.68595E-08	3.74009E-08	3.00442E-08	4.55406E-08	4.03542E-12	2.49004E-10	1.68611E-08	4.89117E-07
185.00	190.00	3	3.45650E-09	1.37712E-08	2.74379E-08	6.14311E-08	5.00895E-08	7.47089E-08	8.23914E-12	4.50294E-10	2.57917E-08	6.77464E-07
190.00	195.00	4	5.43922E-09	2.16778E-08	4.32243E-08	9.68926E-08	7.92752E-08	1.19546E-07	1.67768E-11	8.14177E-10	3.94952E-08	9.39605E-07
195.00	200.00	5	8.54544E-09	3.40592E-08	6.79195E-08	1.52275E-07	1.24659E-07	1.91520E-07	3.41752E-11	1.47290E-09	6.05648E-08	1.30528E-06
200.00	205.00	6	1.34313E-08	5.35340E-08	1.06761E-07	2.39376E-07	1.96000E-07	3.09621E-07	6.96925E-11	2.66639E-09	9.30220E-08	1.81654E-06
205.00	210.00	7	2.11261E-08	8.42061E-08	1.67939E-07	3.76575E-07	3.08391E-07	5.06554E-07	1.42310E-10	4.83041E-09	1.43121E-07	2.53311E-06
210.00	215.00	8	3.32584E-08	1.32569E-07	2.64411E-07	5.92948E-07	4.85683E-07	8.39988E-07	2.91021E-10	8.75692E-09	2.20619E-07	3.54010E-06
215.00	220.00	9	5.24127E-08	2.08927E-07	4.16743E-07	9.34652E-07	7.65753E-07	1.41341E-06	5.96074E-10	1.58863E-08	3.40781E-07	4.95938E-06
220.00	225.00	10	8.27008E-08	3.29677E-07	6.57665E-07	1.47517E-06	1.20894E-06	2.41552E-06	1.22298E-09	2.88401E-08	5.27583E-07	6.96634E-06
225.00	230.00	11	1.30685E-07	5.20991E-07	1.03944E-06	2.33185E-06	1.91167E-06	4.19590E-06	2.51382E-09	5.23927E-08	8.18829E-07	9.81485E-06
230.00	235.00	12	2.06878E-07	8.24802E-07	1.64581E-06	3.69285E-06	3.02871E-06	7.41230E-06	5.17724E-09	9.52466E-08	1.27441E-06	1.38748E-05
235.00	240.00	13	3.28198E-07	1.30861E-06	2.61167E-06	5.86137E-06	4.80978E-06	1.33219E-05	1.06848E-08	1.73279E-07	1.98972E-06	1.96893E-05
240.00	245.00	14	5.22040E-07	2.08174E-06	4.15558E-06	9.32907E-06	7.66043E-06	2.43666E-05	2.21006E-08	3.15489E-07	3.11769E-06	2.80633E-05
245.00	250.00	15	8.33092E-07	3.32260E-06	6.63445E-06	1.48995E-05	1.22451E-05	4.53704E-05	4.58218E-08	5.74933E-07	4.90541E-06	4.02025E-05
250.00	255.00	16	1.33495E-06	5.32513E-06	1.06370E-05	2.38998E-05	1.96646E-05	8.60387E-05	9.52467E-08	1.04890E-06	7.75593E-06	5.79372E-05
255.00	260.00	17	2.15044E-06	8.58025E-06	1.71477E-05	3.85537E-05	3.17736E-05	1.66306E-04	1.98536E-07	1.91638E-06	1.23347E-05	8.40911E-05
260.00	265.00	18	3.48829E-06	1.39232E-05	2.78455E-05	6.26650E-05	5.17756E-05	3.28105E-04	4.15140E-07	3.50850E-06	1.97580E-05	1.23111E-04
265.00	270.00	19	5.71314E-06	2.28157E-05	4.56804E-05	1.02956E-04	8.54527E-05	6.62241E-04	8.71301E-07	6.44317E-06	3.19378E-05	1.82191E-04
270.00	275.00	20	9.49108E-06	3.79385E-05	7.61066E-05	1.71999E-04	1.44176E-04	1.37256E-03	1.83755E-06	1.18904E-05	5.22484E-05	2.73392E-04
275.00	280.00	21	1.61431E-05	6.46505E-05	1.30219E-04	2.96026E-04	2.54455E-04	2.93833E-03	3.90297E-06	2.21228E-05	8.69075E-05	4.17999E-04
280.00	285.00	22	2.87232E-05	1.15542E-04	2.34972E-04	5.41749E-04	4.97761E-04	6.55734E-03	8.39237E-06	4.17668E-05	1.48178E-04	6.56565E-04
285.00	290.00	23	5.62788E-05	2.28779E-04	4.75786E-04	1.13094E-03	1.21403E-03	1.54925E-02	1.85098E-05	8.11554E-05	2.63230E-04	1.07678E-03
290.00	295.00	24	1.34208E-04	5.55965E-04	1.19420E-03	2.91568E-03	4.31392E-03	4.00774E-02	4.35668E-05	1.68776E-04	5.08148E-04	1.92109E-03
295.00	300.00	25	4.29402E-04	1.76790E-03	3.61867E-03	8.98086E-03	3.69541E-02	1.46413E-01	1.54494E-04	4.96719E-04	1.41180E-03	4.86643E-03
300.00	305.00	26	9.38563E-04	4.44065E-03	8.46623E-03	2.94963E-02	2.26125E-01	5.53246E-01	8.01714E-04	1.74881E-03	4.80507E-03	1.53926E-02

Table C2.1b. Space- and energy-dependent weight window lower limits (based on adjoint fluxes for the academic problem) as summarized by GETWIN8.SCR.

WTLO for the 6 broad neutron groups and 4 broad gamma groups based on 1-D adjoint & Jabo's procedure with WTHI= 100*WTLO & WTSURV=WTAVG= 10*WTLO
Use these values for the coupled n/g mcnp transport analysis involving a neutron-only source.
(With a n/g source, or a gamma-only source, values would be differnet)
mnXX-YY = MCNP neutron grp numbers, mgXX-YY = MCNP gamma grp numbers
vnXX-YY = VELM neutron grp numbers, vgXX-YY = VELM gamma grp numbers

		Emax:	4.13990E-07	1.06770E-05	1.23410E-03	1.22770E-01	1.10800E+00	1.49180E+01	3.00000E-01	1.00000E+00	4.00000E+00	1.40000E+01
		imp	mn01-01	mn02-05	mn06-13	mn14-31	mn32-46	mn47-61	mg01-06	mg07-11	mg12-16	mg17-23
xmin	xmax	mesh	vn61-61	vn57-60	vn49-56	vn31-48	vn16-30	vn01-15	vg18-23	vg13-17	vg08-12	vg01-07
175.00	180.00	1	4.85301E-01	1.23881E-01	6.35887E-02	2.90534E-02	3.59017E-02	1.92872E-02	2.47253E+02	3.47423E+00	4.32006E-02	1.34761E-03
180.00	185.00	2	2.21932E-01	5.58953E-02	2.82593E-02	1.27387E-02	1.58579E-02	1.04618E-02	1.18064E+02	1.91337E+00	2.82566E-02	9.74078E-04
185.00	190.00	3	1.37838E-01	3.45967E-02	1.73642E-02	7.75565E-03	9.51173E-03	6.37725E-03	5.78261E+01	1.05806E+00	1.84725E-02	7.03266E-04
190.00	195.00	4	8.75930E-02	2.19781E-02	1.10225E-02	4.91718E-03	6.00992E-03	3.98539E-03	2.83986E+01	5.85177E-01	1.20632E-02	5.07062E-04
195.00	200.00	5	5.57535E-02	1.39885E-02	7.01475E-03	3.12879E-03	3.82194E-03	2.48767E-03	1.39410E+01	3.23469E-01	7.86658E-03	3.65009E-04
200.00	205.00	6	3.54723E-02	8.89973E-03	4.46265E-03	1.99033E-03	2.43080E-03	1.53878E-03	6.83628E+00	1.78683E-01	5.12177E-03	2.62277E-04
205.00	210.00	7	2.25521E-02	5.65800E-03	2.83696E-03	1.26519E-03	1.54491E-03	9.40546E-04	3.34788E+00	9.86331E-02	3.32891E-03	1.88084E-04
210.00	215.00	8	1.43253E-02	3.59389E-03	1.80188E-03	8.03507E-04	9.80965E-04	5.67196E-04	1.63713E+00	5.44070E-02	2.15955E-03	1.34583E-04
215.00	220.00	9	9.09012E-03	2.28041E-03	1.14324E-03	5.09749E-04	6.22182E-04	3.37085E-04	7.99293E-01	2.99904E-02	1.39808E-03	9.60681E-05
220.00	225.00	10	5.76098E-03	1.44517E-03	7.24438E-04	3.22972E-04	3.94097E-04	1.97241E-04	3.89571E-01	1.65200E-02	9.03058E-04	6.83914E-05
225.00	230.00	11	3.64569E-03	9.14483E-04	4.58362E-04	2.04318E-04	2.49226E-04	1.13548E-04	1.89528E-01	9.09359E-03	5.81852E-04	4.85426E-05
230.00	235.00	12	2.30299E-03	5.77639E-04	2.89485E-04	1.29016E-04	1.57307E-04	6.42767E-05	9.20255E-02	5.00215E-03	3.73850E-04	3.43384E-05
235.00	240.00	13	1.45168E-03	3.64079E-04	1.82427E-04	8.12843E-05	9.90561E-05	3.57635E-05	4.45900E-02	2.74955E-03	2.39450E-04	2.41978E-05
240.00	245.00	14	9.12645E-04	2.28865E-04	1.14650E-04	5.10703E-05	6.21947E-05	1.95529E-05	2.15577E-02	1.51016E-03	1.52817E-04	1.69772E-05
245.00	250.00	15	5.71891E-04	1.43393E-04	7.18127E-05	3.19768E-05	3.89086E-05	1.05011E-05	1.03976E-02	8.28684E-04	9.71249E-05	1.18509E-05
250.00	255.00	16	3.56895E-04	8.94697E-05	4.47907E-05	1.99348E-05	2.42282E-05	5.53748E-06	5.00214E-03	4.54228E-04	6.14289E-05	8.22334E-06
255.00	260.00	17	2.21554E-04	5.55273E-05	2.77844E-05	1.23578E-05	1.49948E-05	2.86483E-06	2.39975E-03	2.48614E-04	3.86258E-05	5.66573E-06
260.00	265.00	18	1.36582E-04	3.42190E-05	1.71101E-05	7.60293E-06	9.20198E-06	1.45209E-06	1.14766E-03	1.35795E-04	2.41137E-05	3.86998E-06
265.00	270.00	19	8.33934E-05	2.08820E-05	1.04298E-05	4.62761E-06	5.57545E-06	7.19433E-07	5.46812E-04	7.39446E-05	1.49177E-05	2.61505E-06
270.00	275.00	20	5.01985E-05	1.25582E-05	6.26014E-06	2.77000E-06	3.30456E-06	3.47116E-07	2.59279E-04	4.00692E-05	9.11870E-06	1.74269E-06
275.00	280.00	21	2.95134E-05	7.36943E-06	3.65874E-06	1.60945E-06	1.87238E-06	1.62146E-07	1.22071E-04	2.15361E-05	5.48212E-06	1.13981E-06
280.00	285.00	22	1.65872E-05	4.12350E-06	2.02763E-06	8.79444E-07	9.57162E-07	7.26571E-08	5.67704E-05	1.14071E-05	3.21530E-06	7.25652E-07
285.00	290.00	23	8.46567E-06	2.08252E-06	1.00137E-06	4.21276E-07	3.92443E-07	3.07527E-08	2.57397E-05	5.87068E-06	1.80997E-06	4.42464E-07
290.00	295.00	24	3.55000E-06	8.56956E-07	3.98961E-07	1.63405E-07	1.10442E-07	1.18879E-08	1.09358E-05	2.82289E-06	9.37596E-07	2.48003E-07
295.00	300.00	25	1.10954E-06	2.69494E-07	1.31661E-07	5.30503E-08	1.28927E-08	3.25406E-09	3.08387E-06	9.59170E-07	3.37469E-07	9.79030E-08
300.00	305.00	26	5.07625E-07	1.07290E-07	5.62751E-08	1.61525E-08	2.10696E-09	8.61168E-10	5.94274E-07	2.72436E-07	9.91531E-08	3.09524E-08

Table C2.1c. Original MCNP source intensities and the new recommended (biased) source intensities that are consistent with the recommended weight windows for the academic problem as determined by GETWIN8.SCR.

Emax:	4.13990E-07	1.06770E-05	1.23410E-03	1.22770E-01	1.10800E+00	1.49180E+01	3.00000E-01	1.00000E+00	4.00000E+00	1.40000E+01
	mn01-01	mn02-05	mn06-13	mn14-31	mn32-46	mn47-61	mg01-06	mg07-11	mg12-16	mg17-23
	vn61-61	vn57-60	vn49-56	vn31-48	vn16-30	vn01-15	vg18-23	vg13-17	vg08-12	vg01-07
S0:	3.21042E+11	3.38246E+10	4.65916E+10	4.10023E+10	2.90184E+10	1.97852E+10	0.00000E+00	0.00000E+00	0.00000E+00	0.00000E+00
SB:	6.61533E+10	2.73040E+10	7.32703E+10	1.41127E+11	8.08274E+10	1.02582E+11	0.00000E+00	0.00000E+00	0.00000E+00	0.00000E+00
R:	2.06058E-01	8.07224E-01	1.57261E+00	3.44194E+00	2.78538E+00	5.18478E+00	1.00000E+00	1.00000E+00	1.00000E+00	1.00000E+00

mnXX-YY = MCNP neutron grp numbers, mgXX-YY = MCNP gamma grp numbers
vnXX-YY = VELM neutron grp numbers, vgXX-YY = VELM gamma grp numbers

S0 = The original MCNP source intensities (summed into broad energy groups)
SB = The recommended (biased) MCNP source intensities (summed into broad groups), consistent with the above weight windows
R = The ratio of these two (SB/S0), used to determine the calculate the fine-group biased sources to the used in MCNP

Unbiased fine-group neutron sources in MCNP order (grp 1=low E, grp 61=high E):

6.30365E+16	2.25679E+15	1.52979E+15	1.30212E+15	1.55274E+15
1.58981E+15	1.54759E+15	1.45876E+15	9.03837E+14	9.69821E+14
9.50610E+14	8.74122E+14	8.53691E+14	8.87245E+14	2.04908E+14
2.76622E+14	2.54975E+14	3.36538E+14	7.55438E+14	8.76077E+14
9.84217E+14	7.42049E+14	6.69650E+13	1.12860E+14	5.24714E+13
1.21873E+14	3.03507E+14	4.96958E+14	1.29680E+14	8.89397E+14
5.59006E+14	4.29193E+14	3.63241E+14	4.33245E+14	7.35199E+14
2.12840E+14	1.38494E+13	7.68584E+12	3.65651E+13	6.29256E+14
5.85513E+14	1.49367E+14	3.61470E+14	5.35177E+14	6.65098E+14
5.40055E+14	7.09512E+14	8.07055E+14	8.54720E+14	3.12945E+14
2.00073E+14	1.35333E+14	2.41078E+14	1.61947E+14	2.06360E+14
1.36477E+14	7.32282E+13	3.05242E+13	8.64293E+12	6.92602E+12
2.74800E+09				

Biased fine-group neutron sources in MCNP order (grp 1=low E, grp 61=high E):
Use these values for the coupled n/g mcnp transport analysis involving a neutron-only source.
(With a n/g source, or a gamma-only source, values would be differnet)

1.29892E+16	1.82174E+15	1.23488E+15	1.05110E+15	1.25341E+15
2.50015E+15	2.43375E+15	2.29406E+15	1.42138E+15	1.52515E+15
1.49494E+15	1.37465E+15	1.34252E+15	3.05384E+15	7.05280E+14
9.52115E+14	8.77608E+14	1.15834E+15	2.60017E+15	3.01540E+15
3.38761E+15	2.55408E+15	2.30489E+14	3.88457E+14	1.80603E+14
4.19479E+14	1.04465E+15	1.71050E+15	4.46350E+14	3.06125E+15
1.92406E+15	1.19547E+15	1.01176E+15	1.20675E+15	2.04781E+15
5.92841E+14	3.85759E+13	2.14080E+13	1.01848E+14	1.75272E+15
1.63088E+15	4.16044E+14	1.00683E+15	1.49067E+15	1.85255E+15
1.50426E+15	3.67866E+15	4.18440E+15	4.43153E+15	1.62255E+15
1.03733E+15	7.01672E+14	1.24994E+15	8.39660E+14	1.06993E+15
7.07603E+14	3.79672E+14	1.58261E+14	4.48117E+13	3.59099E+13
1.42478E+10				

On your WWP:N card, make sure you have WTHI= 100*WTLO and WTSURV= 10*WTLO
On your WWP:P card, make sure you have WTHI= 100*WTLO and WTSURV= 10*WTLO

---

distribution to the original source energy distribution (based on the broad group values in both cases) can then be applied to the fine-group source terms to obtain the biased source energy distribution on a fine group basis. By supplying MCNP with the original fine-group source energy distribution as well as the biased fine-group source energy distribution (on the MCNP "sb" card), it will then adjust the starting weights automatically. Moreover, following this procedure will assure that the starting weights used by MCNP are fully compatible with the weight windows supplied in the "geometry-independent weight window" file created by the GETWIN8.SCR script. For the convenience of the user, the GETWIN8.SCR script will also print out the original fine-group source energy distribution as well as the biased source energy distribution that the user should supply manually in the MCNP input file. Table C2.1c shows the original and biased source energy distributions on both a broad-group and fine-group basis.

Lastly, the GETWIN8.F program (embedded in the GETWIN8.SCR script) calls subroutine WTWIN which writes out the large ascii-based 3-D weight-window file (wwinp) that will actually be used by MCNP4B. Since the MCNP model extends from Z=0 to Z=300 cm, and from R=0 to R=65 cm, the phantom mesh containing the 3-D XYZ importance zones must extend somewhat beyond that in all directions. In this case, we had:

27 equally space importance mesh intervals from X= -67.5 cm to X= 67.5 cm
27 equally space importance mesh intervals from Y= -67.5 cm to Y= 67.5 cm
65 equally space importance mesh intervals from Z= 0.0 cm to Z=325.0 cm .

The discussion above describes how the lower weight window bounds (wtlow) were determined for each of the 6 broad neutron groups and 4 broad gamma groups for those importance mesh intervals located along the centerline of the system from Z=175 cm to Z=300 cm. These were based directly on the 1-D ANISN adjoint calculation. For the remainder of the 47,385 importance zones: (a) Values of wtlow for Z < 175 cm were assumed to be the same as those in the zone closest to the impingent source, although values for the black absorber regions (where one has imp:n=0) don't matter anyway; (b) Values of wtlow for Z > 300 cm were assumed to be the same as those for the last importance region, although (because this region is void with no other materials beyond it) these values don't matter either; (c) Values of wtlow for the vast majority of the other 18,200 importance mesh intervals in the water tank, but not directly along the centerline, were based on the distance from the detector of interest (X=0, Y=0, Z=300) to the midpoint of the given importance mesh interval. Thus, the weight values for each mesh were based on a corresponding mesh equidistant from the detector along the centerline. This was based on the first order belief, applicable only to a homogeneous shield, that particles a certain distance from the detector in any direction "which are travelling toward the detector" should be as important as particles the same distance from the detector along the centerline "which are travelling toward the detector". To be sure that the full meaning of this last phrase was properly applied by the code, a set of fictitious directional adjoint currents were also entered in the weight window file. In a large infinite media, the adjoint current would extend radially outward in all three directions from the adjoint source which corresponds physically to the "real" detector at (X=0, Y=0, Z=300). Thus, in place of the directional adjoint currents from a true XYZ adjoint solution, we inserted unit vectors (aJx, aJy, aJz) in each of the 47,385 importance mesh intervals which pointed from the detector at (X=0,Y=0,Z=300) back toward the centroid of each importance mesh interval. Because MCNP is known to use only the unit vector corresponding to the directional adjoint current in its "collision site directional biasing algorithm" (rather than the absolute magnitude of the adjoint current), this substitution was wholly acceptable. [Moreover, even in more complex geometries involving dissimilar materials and/or streaming paths, if one can adequately visualize the "path of least resistance" from any given collision site to the detector of interest (which may not be a straight line), then the use of local directional unit vectors pointing in the opposite direction (ie, the way adjoint particles would move) provides an extra degree of acceleration that would not be available without this valuable information.]

Finally, it should be noted that the large ascii-based 3-D geometry-independent weight window file written by subroutine WTWIN is wholly compatible with the format prescribed in Appendix C.3, and that this file can now be read and used directly by MCNP4B. Except for zero importance regions (imp:n=0) representing a black absorber or external void, all of the other importance data (imp:n=1) necessarily still included on the MCNP cell cards will be disregarded and functionally replaced by the broad-group weight window information in this new "geometry-independent weight window" file (wwinp). All that remains is to update the source distribution in one's MCNP input file so as to include both the original fine-group "unbiased" source energy distribution and the new fine-group "biased" source energy distribution shown in Table C2.1c. The final 280-line MCNP input file (WWT08), with the original and biased source terms, and all of the necessary diagnostic flux tallies, is listed in Appendix C.5.

C.2.6 Results Obtained from MCNP4B When Using a Geometry-Independent Weight Window File

Cell 202 in the final model (see Appendix C.5) is a thin flat, 20-cm-diam disk, located at the top of the water tank, between Z=299.99 cm and Z=300.0 cm. This "volume detector", used in Tallies 64 and 74, was chosen so as to determine whether or not the geometry-independent weight window approach described above would permit a sufficient number of real particles to transport to this location (in an acceptable amount of CPU time), and whether the total "neutron plus secondary gamma" dose could be accurately determined based on the number of real particles actually reaching that location. [If not, results could still be obtained through the use of point detectors, but that practice is sometimes less reliable. Generally,

point detectors are to be used to obtain results at distant points in a void. When there remains an adequate number of collisions in the outermost portion of the shield material closest to the void, point detectors provide a good and reliable tool for estimating the fluxes and dose rates at distant points. When the point of interest is close to the shield, and there is some question as to whether or not there exists an adequate number of collisions in the outermost regions to provide adequate sampling, the use of point detectors may be questioned; the point detector responses may still be quite good - or they may not be. In such cases, the only way to confirm the adequacy of the solution is to somehow drive a sufficient number of particles to that region, so that either a volumetric track length detector or a boundary crossing detector (ie, something that counts real particles) will provide the needed confirmation.]

In this case, Tally 74 showed the total secondary gamma dose rate in Cell 202 to be 6185.8 mrem/hr with a fractional standard deviation of +/- 1.6% (ie, +/- 99.0 mrem/hr), while Tally 64 showed the total neutron dose rate to be much lower (62.06 mrem/hr, +/- 20.8% = +/- 12.9 mrem/hr). Combined statistically, this yields a total "neutron plus secondary gamma" dose rate of 6247.9 mrem/hr +/-1.6%. This is considered "excellent" insofar as volume detector estimates with fsd's of 10% are normally considered very good and reliable, while volume detector fsd's of 15% are often considered acceptable.

More to the point, Table C2.2 shows the total neutron flux and the secondary gamma flux axially up through the centermost 20-cm-diam water region, in 5-cm increments from Z=175 cm to Z=300 cm. Since most of the total "neutron plus secondary gamma" dose rate (i.e., 99% of it) downstream of the water tank comes from gammas, it is significant (and by no means accidental) that the gamma fluxes in this adjoint-biased calculation are known with greatest precision in that portion of the water tank closest to the detector. (Moreover, in this particular calculation there were over 200,000 gamma tracks in Cell 202.) Because the neutrons were known a priori from the adjoint analysis to contribute relatively little in terms of the direct neutron dose rate at Z=300 cm, there were fewer of them (approximately 4,000 neutron tracks in Cell 202). Still, given that the neutron flux attenuates by over 8 order of magnitude across the water tank, it was extremely encouraging that reasonable statistics were still found to exist throughout most or all of the entire water tank. To put the quality of these results in some perspective, one must consider the original state of affairs:

a) In the original unbiased calculation where no weight window file was used (MCNP Run WWT01), most neutrons never made it more than 15 or 20 cm into the water before being being killed by Russian Roulette; of the 240,000 neutron histories in that original pilot calculation, only 2 individual neutrons made it 20-25 cm into the water, and only 1 made it 25-30 cm into the water. Here, by comparison, over 4000 made it through 125 cm of water.

b) Several earlier attempts at solving the original HB-3 water tube problem using geometric splitting (see MCNP Runs HB305B-HB305D in Appendix C.1) resulted in total failure and had to be abandoned.

c) Another earlier attempt (MCNP Run WWT05) which used one common set of weight windows for all neutron groups and no special biasing for gammas (because it was originally thought they probably didn't need it) produced some relatively useless results for the neutrons and virtually no results for the gammas. In this particular case, the one-group weight windows were not based on a rigorous adjoint analysis, but simply on the overall expected attenuation of fast neutrons in water, with no special provisions at all for the gammas. While the performance was much better than in previous cases, it still took 38 hours on each of 8 nodes on the ORNL SP2 to run 96,000 neutron histories. The fsd's on the total neutron flux between Z=295 and Z=300 cm were around 0.85 (that is 85%), while even at Z=210 to 215 cm, the fsd's on the total neutron flux were over 50%, and there were no results at all for the gammas because they were killed almost at birth by Russian Roulette.

d) The present calculation (as noted above) was based on a real (albeit simple 1-D) adjoint analysis, where the weight windows for 6 broad neutron groups and 4 broad gamma groups were derived from the resulting adjoint fluxes, and the source-energy biasing was wholly consistent with the weight windows used. This additional degree of rigor had a tremendous payoff. Compared to the previous case, for example, we were now able to run 1,000 times more histories (96 million instead of 96 thousand) in "one-tenth" the time (now just 4.5 hours on each of 8 nodes instead of 38 hours on each of 8 nodes). No matter how you look at it, that's a 10,000-fold increase in calculational efficiency!

   Moreover, the present calculation produced results that are quite credible in comparison with other calculational methods, and yielded very good to excellent statistics for the parameter of greatest importance (the gamma fluxes closest to the detector). Lastly, because of the efficiencies provided by this adjoint biasing, it would not have been really necessary to run 96 million histories. That many were used this case simply to produce a benchmark-quality result. In reality, an fsd of 5.1% on the total dose rate had been achieved after 9.6 million histories taking less than 27 minutes, while an fsd of 3.6% had been achieved after 19.8 million histories taking less than 54 minutes. Of these, the former would be adequate for most engineering purposes.

Lastly, while not shown here, it should be noted that virtually all of the gammas in this calculation are below 2.5 MeV. That is because virtually all of the secondary gammas produced in water come from (n,g) reactions with hydrogen which produce gammas at 2.2 MeV. For the real HB-3 water-tube shielding problem using the gamma-only point sources in the beam tube, the gamma dose rates are "much higher" and,

Table C2.2. Total neutron and secondary gamma flux up through the central 20-cm-diam region of the academic problem, from MCNP Run WWT08 with 96 million histories.

	Tally 54 (neutrons)		Tally 44 (gammas)	
Z (cm)	(n/s/cm2)	fsd	(p/s/cm2)	fsd
295-300	1.79460E+03	.2048	7.47002E+06	.0129
290-295	3.94075E+03	.1984	1.18945E+07	.0130
285-290	6.97304E+03	.1789	1.67140E+07	.0138
280-285	1.19808E+04	.1620	2.25377E+07	.0151
275-280	2.04571E+04	.1479	2.99008E+07	.0166
270-275	3.65306E+04	.1362	4.00931E+07	.0183
265-270	6.55155E+04	.1274	5.38954E+07	.0214
260-265	1.22114E+05	.1148	7.02508E+07	.0235
255-260	2.32813E+05	.1102	9.18429E+07	.0258
250-255	4.10427E+05	.1015	1.21931E+08	.0280
245-250	7.23337E+05	.0850	1.67082E+08	.0301
240-245	1.35499E+06	.0746	2.26124E+08	.0417
235-240	2.65535E+06	.0651	3.07086E+08	.0503
230-235	5.10029E+06	.0536	4.31771E+08	.0543
225-230	9.75876E+06	.0477	5.58796E+08	.0589
220-225	2.08210E+07	.0393	8.97730E+08	.0690
215-220	4.47850E+07	.0314	1.11336E+09	.0656
210-215	1.01862E+08	.0245	1.31550E+09	.0525
205-210	2.39651E+08	.0190	2.05202E+09	.0645
200-205	6.05299E+08	.0150	2.92876E+09	.0703
195-200	1.76305E+09	.0121	4.20838E+09	.0422
190-195	5.85581E+09	.0091	7.49931E+09	.1067
185-190	2.26818E+10	.0062	1.35832E+10	.0934
180-185	1.00728E+11	.0040	2.45322E+10	.0265
175-180	3.56075E+11	.0021	3.73733E+10	.0123

after passing through one or two meters of water, most of the residual gammas are in the 6-8 MeV range.

Before concluding this discussion of adjoint-biased Monte Carlo solutions using geometry-independent weight windows, one or two additional remarks are in order. To the experienced user, these remarks are likely to be obvious, while for the inexperienced user, they are probably worth noting.

The irony of (and the saving grace of) adjoint-biased Monte Carlo solutions is that "not all results are calculated equally well". This is by design. More specifically, the desired calculational efficiencies are realized by not wasting time calculating things that are known a priori (by virtue of the adjoint analysis) to have a small or negligible effect on the result of interest. In Table C2.2, for example, it may at first seem ironic and even peculiar that the gamma fluxes closer to the impingent neutron source have larger uncertainties (fsd's) than those further downstream. Upon reflection, however, there is a reason for that -- they are less important. Secondary gammas created close to the source are by definition further from the detector. As such, there may be more of them, but, because they have more opportunities to scatter and slow down to lower energies (and/or be absorbed), and because of the 1/(4*pi*R^2) effect, they actually contribute less to the final detector response than those created closer to the detector. Had the adjoint been run as an infinite 1-D slab (rather than a buckled slab) the 1/(4*pi*R^2) effect would be removed, but the other effects would still have been present and the overall trend would have been the same. To understand how this translates into calculational efficiency and why the gamma fsd's closer to the detector are lower than those closer to the source, one must consider the adjoint fluxes in Table C2.1a and the lower weight cutoffs in Table C2.1b relative to the actual weights of gammas at any point in the problem (not shown). As one goes back from the detector towards the source, the importance (indicated by the adjoint flux) becomes smaller and smaller, and the lower weight cutoff becomes larger and larger. Back near the source, the birth weight of gammas is high, but the lower weight cutoff is also high so that many are killed by Russian Roulette. Indeed, that is by intent, since we really don't want to spend time tracking millions of gammas there that will not contribute significantly to the final result at the detector. Depending on how many are tracked there, the fsd's there can be relatively poor. Progressing a little closer to the detector, the birth weight of the gammas will be somewhat lower (because the average weight of the neutrons there will be lower), but the lower weight cutoff (wtlow) curve for the gammas diminishes even faster than the birth weight curve, so that more of those born closer to the detector will survive Russian Roulette and be tracked longer. This is the reason that the gamma fsd's tend to improve as one gets closer to the detector. It is not mysterious, just tightly controlled.

Folklore wisdom says: "Be careful what you wish for ... you just might get it!". The same is certainly true in adjoint-biased Monte Carlo work. (a) If the adjoint calculation is performed using both the neutron and gamma flux-to-dose-rate conversion factors as the adjoint source, then the Monte Carlo calculation will give most favored treatment to those things that contribute most to the total "neutron plus secondary gamma" dose rate. Given that secondary gammas comprise most of the dose rate, those neutrons that contribute little to the secondary gamma birth rate and little to the direct neutron dose rate will receive relatively little attention. Close to the source where a lot of thermal neutrons are creating a lot of secondary gammas, the neutrons will receive a lot of attention. Further down through the shield, where the neutrons have attenuated 5 or 6 orders of magnitude, the spectrum is somewhat harder but the neutrons are so few in number that neither the fast neutrons remaining or the relatively few gammas that could then be produced by them (after they slow down to thermal) could contribute much to the overall dose rate. Thus, they tend to receive relatively little attention and their fsd's tend to be relatively high. In practice, the wtlow curve for these faster neutrons tends to diminish (axially) more slowly than the average weight of the fast neutrons progressing through the shield, so that as one proceeds through the shield, more are killed by Russian Roulette, fewer are tracked, and the fsd's deteriorate once they are no longer important. (b) Alternately, if one really wanted to obtain the best estimate of the total neutron flux at the end of the problem by the detector, then one should use an adjoint source of 1.0 for all the neutron groups and an adjoint source of 0.0 for all the gamma groups in the 1-D ANISN adjoint calculation, and use the corresponding set of weight windows and biased source terms in the MCNP calculations. (c) Lastly, if one really wanted to obtain the best estimate of just the neutron dose rate at Z=300, then one should use the neutron flux-to-dose-rate conversion factors as the adjoint source (with zeroes for all the gamma adjoint sources), and then use those resulting weight windows and biased source terms in the MCNP calculation. The primary difference between the latter two cases is that the lower weight window limits for the thermal groups in case (c) would be somewhat higher, thus causing the code to kill more of them more frequently (resulting in poorer thermal fsd's) so that a larger fraction of the total computer time could be spent tracking faster neutrons that would be more likely to contribute to the total neutron dose rate. Thus, there is no magic bullet. If one is really interested in optimizing several different calculational parameters, or results at several different locations, it will may be necessary to run several different adjoint calculations and then rerun the same MCNP calculation with a different "geometry-independent weight window" file each time. Nevertheless, this is infinitely easier and vastly superior to the only previous alternative described in Appendix C.1.

C.2.7 Verification of The MCNP Results

Several types of verification calculations have been made so as to provide a check of reasonableness. Unfortunately, none are considered of benchmark quality, but collectively, they suggest that the present MCNP result is of high quality and should itself (perhaps) be considered the reference solution. The

following briefly describes some of the alternative solutions examined:

(a) In the first approach, a coupled 61n/23g 1-D (slab) forward ANISN calculation was first performed using the impingent neutron-only source, to get the secondary gamma source density distribution axially in the water. Here the source density in any given gamma group, in any given 4.1-cm-thick axial slab, was taken to be the gamma absorption rate, plus the gamma out-leakage, minus the gamma in-leakage. Because of the rapidly attenuating neutron flux, these secondary gamma sources rapidly become negligible after the first 20, 30, or 40. cm of water. We then considered an imaginary cylindrical volume element (whose radius was equal to that of the impingent neutron beam) running axially through all of the 4.1-cm-thick slab zones used in the 1-D model. The volume of this cylindrical core element (in each of the 4.167-cm-thick slabs), times the multigroup gamma source density in each slab, defines a multigroup source (p/s) which may then be treated as a multigroup point source at the center of each volume element in a simple QAD-like#20 point kernel shielding analysis for the cylindrical element. From that, one can determine the total secondary gamma dose rate at the end of the 125-cm-long cylindrical element due to all of the point sources collectively or individually. The dose rates obtained in this fashion were slightly below the MCNP result before the application of the buildup factors normally used in point kernel analyses, and slightly higher than the MCNP result after the application of the necessary buildup factors. Note that while the relatively crude point kernel method lacks the statue and rigor of more-often-used discrete ordinate methods, it is also free of the ray effects that often plague such methods when one is modeling small and/or highly localized gamma sources in water.

(b) In the second approach, we used a simple back-of-the-envelope method from undergraduate school. In particular, the gamma mass attenuation coefficient for 2 MeV gammas, and the corresponding energy-flux-to-dose-rate conversion factor, were taken directly from a similar example in Section 10.113 of Ref 22 by Glasstone and Sesonske, which was based on a simple shielding analysis involving the ORNL Bulk Shielding Reactor. The logic goes like this: (1) Based on the point sources in Table 2.2a, the neutron flux on the bottom of the water tank at Z=175 cm in this academic problem is 7.448e11 n/s/cm2. (2) The allowable impact area (A) is A=pi*5*5 = 78.54 cm2, such that the total neutron source is 5.850e13 n/s. (3) The mean free path of fast neutrons in water is 10 cm. (4) Assume that the majority of neutrons thermalize and are absorbed in the first 10-20 cm of water at the bottom of the water tank (say at Z=190 cm) where they produce 2.2 MeV gammas from (n,g) reactions in hydrogen. (5) The unattenuated gamma energy flux at Z=300 cm would then be:

gamma energy flux = 2.2*(5.850e13)/[4*pi*(300-190)^2]= 8.464e8 MeV/s/cm2

(6) For 2 MeV photons, 620 MeV/s/cm2 is equivalent to 1 mrem/hr, so the unattenuated gamma dose rate here would be 8.464e8/620 = 1.365e6 mrem/hr. (7) At this energy, the mass attenuation coefficient for water is 0.0493/cm, so the attenuated gamma dose rate at Z=300 cm would be:

D = (1.365e6 mrem/hr)*exp[-0.0493*(300-190)] = 6025 mrem/hr

By way of comparison, the detailed MCNP calculation gave 6186 mrem/hr.

(c) The other classic solution method often used for benchmark analysis involves a rigorous 2-D RZ deterministic solution using the DORT code. It also confirms the "reasonableness" of the MCNP result, but is not necessarily the best benchmark available since discrete ordinate methods often suffer from ray effects when modeling small and/or highly localized gamma sources in water. Using the GRTUNCL code#37 to determine the first collision scattering moments throughout the problem due to the point neutron sources would help somewhat, but would do little to reduce the ray effects due to the gammas which stream preferentially along quadrature directions in the relatively transparent water. Using a higher-order directional quadrature set will also help somewhat, but will never eliminate the characteristic "dip" one sees along the centerline in such problems. In the present case, the flux from the neutron point sources at (X=0,Y=0, Z=50 cm) were transported analytically to the bottom surface of the water tank where a spatially-distributed, highly forward-directed internal boundary flux file was written for each of the 61 neutron energy groups. It was non-zero from R=0 to R=5 cm, and zero everywhere else. This particular model used 65 radial mesh intervals of 1 cm each, and 125 axial mesh intervals of 1 cm each from Z=175 cm to Z=300 cm. A thin axial mesh of 0.01 cm thickness was also used on the bottom (to allow for the necessary internal boundary source) and on the top, over which the fluxes and dose rates could be averaged for various radial regions of interest. In this case, a standard symmetric S12 quadrature with 48 upward directions and 48 downward directions was used. In retrospect, a higher-order directional quadrature could have and probably should have been used, but the results would have been qualitatively the same. In this particular case, the average neutron dose rate over the 20-cm-diam disk at the top was also found to be negligible (< 10 mrem/hr). Likewise the gamma dose rate was in semi-reasonable agreement with the MCNP gamma dose rate, if a 21.7% difference can be considered semi-reasonable. In the case of the DORT results, the average gamma dose rate over the 20-cm-diam disk at the top was 4844.9 mrem/hr, or about 21.7% lower than the MCNP result. In this case, this is not considered to be a bad reflection on the MCNP result (which is actually believed to be more trustworthy), but a poignant reminder of the nastiness that can be perpetrated by ray effects in discrete ordinate calculations when one has localized gamma sources in water. Examining the DORT gamma dose rate as a function of radial position along the top, we see that:

```
at  Z=300 cm,  R=  0.5 cm,  the DORT Gamma Dose =   4552.48 mrem/hr
at  Z=300 cm,  R=  4.5 cm,  the DORT Gamma Dose =   4790.50 mrem/hr
at  Z=300 cm,  R=  9.5 cm,  the DORT Gamma Dose =   5045.99 mrem/hr
at  Z=300 cm,  R= 14.5 cm,  the DORT Gamma Dose =   5573.61 mrem/hr
at  Z=300 cm,  R= 19.5 cm,  the DORT Gamma Dose =   7688.80 mrem/hr
at  Z=300 cm,  R= 24.5 cm,  the DORT Gamma Dose =  10171.10 mrem/hr
at  Z=300 cm,  R= 29.5 cm,  the DORT Gamma Dose =   6198.56 mrem/hr
at  Z=300 cm,  R= 34.5 cm,  the DORT Gamma Dose =   3991.98 mrem/hr
at  Z=300 cm,  R= 39.5 cm,  the DORT Gamma Dose =   3209.04 mrem/hr
```

This unnatural ripple, known as a ray effect, is (of course) physically impossible. Nevertheless, it is the reason the average DORT gamma dose rate over the 20-cm-diam disk at the center is lower than the more realistic MCNP value of 6186 mrem/hr. Numerically, the type of unnatural ray effect exhibited here is quite understandable and quite predictable. The large unnatural peak at R=24.5 cm, for example, is directly traceable to the angular quadrature used in the S12 DORT solution. Neutrons enter the bottom of the water tank at Z=175 cm. Most become thermal 10-20 cm into the water (say at Z=190 cm), whereupon they give birth to most of the secondary gammas that are created. The angular direction between this birth point and the large ripple at the top is given by cos(theta)=cos(arctan(24.5/(300-190)))=0.976 which is almost identical to the direction cosine of the most forward direction in the quadrature set (cos(theta)=0.96922). With a more highly-biased quadrature set where the most-forward direction were a little closer to the centerline, this peak would tend to shift radially inward and become less pronounced (while simultaneously raising the flux and the calculated dose rate at the centerline), but the characteristic dip near the centerline would never disappear completely since there are no quadrature sets with a transport direction exactly along the vertical axis. Moreover, because of the geometry, the materials, and the nature of the source, this seemingly simple problem is actually a fairly difficult one that is classically known as the "pencil beam problem" in academic circles. If for example, the secondary gamma source were more widely distributed over a wider area, the dips in the flux caused by one portion of the more widely distributed spatial source would be "filled in" by contributions or peaks from adjacent source elements, and the flux at the top would begin to appear much flatter. With a narrowly collimated beam source only over a small portion of the bottom surface, however, defects in the solution have no place to hide and we see these types of ray effects. Moreover, even preprocessing the point neutron source using the GRTUNCL code#37 to calculate the first collision source is not likely to help tremendously in this particular case since the problem does not stem directly from the neutron distribution, but from the spatial distribution of the secondary gammas which will still be highly localized around the centerline near the bottom of the problem. GRTUNCL will of course help, but not tremendously in this case.

Thus, unfortunately, the DORT approach (like the other approaches) serves as a good "check for reasonableness", but does not provide a rigorous benchmark. Moreover, given that the MCNP calculation used 96 million histories and those neutrons and gammas experienced over 700 million collisions, each at different points in the configuration, it would appear far more reasonable in this case to view the MCNP result as the reference solution.

General comment: It was because of the known potential difficulties with ray effects in discrete ordinate methods that MCNP was originally chosen as the preferred solution method for the original HB-3 water tube shielding problem. While ray effects are visible and bothersome in this particular academic problem, they would be far less visible but equally incorrect in the real water tube problem. Moreover, as one proceeds even further in the real problem, down through the narrow water-filled rectangular hole in the collimator beyond the water tube, the seriousness of ray effect errors along the centerline would be compounded much more, and the underestimation of the flux along the centerline would become much more serious and devious. "Devious" because, with the peaks and dips smoothed over by contributions from the surrounding radial and eccentric shields, the ripples would not be as apparent and the flux plots would appear normal to the untrained eye. In spite all the histories and all the elaborate biasing techniques needed to get good and reliable results with MCNP, Monte Carlo methods are at least free of these difficulties and are ultimately better suited for this particular type of analysis, if and when properly used.

C.2.8 Conclusion

Success is usually relative. Yet by any measure, this weight-window-biased MCNP calculation was a success, and given the proper perspective, it should be considered a tremendous success! In short:

1) It worked, and it worked well!

2) It provided a rigorous and self-consistent methodology for space-energy biasing of both the flux and the source.

3) It did not require us to "add to or change" any of the geometry specifications in the basic material model.

4) It is general and can be applied with equal ease to geometrically complex problems.

5) It can be used for neutron-only problems, gamma-only problems, or coupled n/g problems like this.

6) It can be easily changed to optimize the MCNP results for other responses (fluxes, dose rates, heating rates, etc) at other locations, without perturbing the basic model.

Appendix C.3

Informal notes on the format of the "geometry-independent weight window" file to be used with MCNP4B

Subsequent to the ANS Radiation Protection and Shielding Conference in Nashville in late April 1998, and conversations with Tom Evans of Los Alamos at that conference, the following set of informal notes on the format of the "geometry-independent weight window" file to be used with MCNP4B was distilled from careful inspection of Subroutine WWFILE in the MCNP4B code, which was already operational at ORNL. Clarification on the meaning of a couple of parameters was subsequently provided by Dr. Evans and incorporated in these notes. Formal documentation of these features will be provided by Los Alamos in the next version of the code, MCNP4C, to be released in the year 2000.

The ability to read and use the type of "geometry-independent weight window" file described here was originally installed in MCNP4B as an undocumented and untested feature, referred to as the "AVATAR patch". Prior to the time the code was finally released by Los Alamos and installed at ORNL, the AVATAR patch had actually undergone a considerable amount of internal testing and verification at Los Alamos. Much of this testing is described in an internal LANL memo from T. M. Evans to J. Hendricks, XTM:TME-97-133(U), dated May 22, 1997. It is now externally available upon request and has since been posted on the LANL web pages as a postscript file. Pages 5-7 of that memo, briefly describe much of the same information contained in this appendix. Users wishing to supply weight window information in R-Z-Theta geometries, however, would be better advised to obtain and read the original LANL memo since the present appendix only deals with weight window information supplied in a variable Cartesian (XYZ) phantom mesh.

INFORMAL NOTES ON THE FORMAT OF THE "GEOMETRY-INDEPENDENT WEIGHT WINDOW" FILE TO BE USED WITH MCNP4B

Notes by J.A.Bucholz, last updated 5-26-98

Notes on the format and structure of the user-supplied MCNP4B "wwinp" file:

a) this ascii file is read & used by MCNP when the 5th parameter on the WWP:n or WWP:p card is negative

b) you'll need to put wwinp=filename on the MCNP message card so code knows the name of the file to look for

c) this will replace all the non-zero importances that you may have supplied in your MCNP input file;
cells where you previously specified an importance of 0 will still be recognized as 0

Structure of this ascii file is as follows:

Record 1: format (4i10)

IF IV NI NR

IF -- type of adjoint entered later in this file

Set IF=1 to "read in" and use scalar adjoint: flux(i) for each fine mesh (NX*NY*NZ)
IF=2 to "read in" and use directional adjoints: flux(i), Jx(i), Jy(i), Jz(i) for each fine mesh (NX*NY*NZ)
IF=3 to "read in" directional adjoints: flux(i), Jx(i), Jy(i), Jz(i) for each fine mesh (NX*NY*NZ)
but (when IF=3) only "use" scalar info

Note: While I refer to the scalar adjoint flux ["flux(i)"], it is NOT really the adjoint "flux" that will be entered. To be more precise, one will really enter the "LOWER weight window bound(s)" based on the scalar adjoint flux. These lower weight window bounds are entered on Records 7.2 or 7.3 below.

I'll probably use IF=1 most of the time, or IF=2 when I feel directional biasing might be beneficial.

IV -- version number; I have no idea what this is used for (can't tell from Fortran);
Tom Evans says its not used for anything and to set IV=0

NI -- number of different particle types for which energy-dependent
weight windows will be read

NI must be .le. 12

controls length of IA(i) array to be read next

Set NI=1 for neutron-only problems (frequently used)

Set NI=1 for gamma-only problems

Set NI=2 for neutron/gamma problems (frequently used)

Set NI=3 for neutron/gamma/electron problems (seldom used)

NR -- number of parameters to be read in the RA(i) array below, where
WWM(i)=RA(i), and WWM array is described on pages E-26 and E-41
of MCNP4B manual

RA(NR) is a flag that should generally be set to 1

NR must be .le. 15

--> NOTE: in Subroutine WWFILE that we have in our MCNP4B, NR must be .le. 15
In reality, however, our version is obsolete and RA should be dimensioned to 16.
See patch file from Tom Evans. This doesn't matter if you're always using
cartesian geometry, but you'll need to patch the routine if you want to specify
the weight window file in a cylindrical RZth geometry. -- JAB, 5-25-98.

Set NR=10 for cartesian XYZ adjoints; that's all I'll talk about below

Set NR=16 for cylindrical RZth geometry adjoints; I'll skip any discussion of this for now
(see description of WWM array on page E-26 & E-41); will also need to patch WWFILE

Record 2: format (7i10)

IA(ip), ip=1,NI IA(ip)=number of energy-dependent weight windows for particle type ip

---

NWW(ip)=IA(ip) for ip.le.NI
NWW(ip)=0 for ip.gt.NI

NWW(ip)=IA(ip) = number of energy-dependent weight windows
for particle type ip

If NI=2 (for a coupled neutron/gamma problem) then

IA(1) = number of energy-dependent weight windows for neutrons
IA(2) = number of energy-dependent weight windows for gammas

If you have a real adjoint (from DORT or TORT) this could be
the number of neutron or gamma energy groups.

If I'm just entering my own heuristic guess for these things
I'll just set IA(1)=1 and IA(2)=0 or IA(2)=1

Record 3: format (6g13.5)

RA(i), i=1,NR

WWM(i)=RA(i) for i.le.NR
WWM(i)=0.0 for i.gt.NR

See description of WWM(i) array on pp E-26 and E-41 of manual

For cartesian XYZ adjoints where NR=10:

WWM(1) = RA(1) = NX = total number of fine mesh in X direction
WWM(2) = RA(2) = NY = total number of fine mesh in Y direction
WWM(3) = RA(3) = NZ = total number of fine mesh in Z direction

WWM(4) = RA(4) = XMIN(0) = X location of lower left corner of global mesh describing cartesian importance cells
WWM(5) = RA(5) = YMIN(0) = Y location of lower left corner of global mesh describing cartesian importance cells
WWM(6) = RA(6) = ZMIN(0) = Z location of lower left corner of global mesh describing cartesian importance cells

WWM(7) = RA(7) = NCX = number of coarse mesh in X direction
WWM(8) = RA(8) = NCY = number of coarse mesh in Y direction
WWM(9) = RA(9) = NCZ = number of coarse mesh in Z direction

WWM(10) = RA(10) = NWGEOM = 1 = a flag saying "that's all" (if NR=10 for cartesian XYZ adjoints)

Note: if NR=16 for cylindrical RZth geometries, then one would have WWM(10) = RA(10) = NWGEOM = 2
and there would be six more parameters, WWM(11) ... WWM(16), which I'm not going to discuss.
Anyone interested in this should go read Tom Evans' memo (Ref 23).

BEGIN GEOMETRIC MESH DATA: (I will describe info for cartesian mesh only)

See Subroutine WWFILE (in MCNP4B) for more details. That is where this file is read. From DO-loop 120 in Subroutine IWTWND you can see/verify how the fine mesh are numbered internally. From Function WWVAL you can see how this info is accessed internally when MCNP needs values.

Record 4: format (6g13.5)

X-mesh data as follows:

XO, NFXC(1),XMAXC(1),ratioXC(1), NFXC(2),XMAXC(2),ratioXC(2), ..., NFXC(NCX),XMAXC(NCX),ratioXC(NCX)

that is:

xo, data for coarse mesh 1, data for coarse mesh 2, ..., data for coarse mesh NCX,

where

XO = location of left most plane (globally)

NFXC(i) = number of fine mesh intervals in coarse mesh i <-- used in Subroutine WWVAL

XMAXC(i)= location of rightmost plane in coarse mesh i <-- used in Subroutine WWVAL

ratioXC(i)= fine mesh ratio in course mesh i <-- required; may(?) allow for logarithmically denser or sparser fine mesh inside a given course mesh; not sure if used or not; I always enter 1.0

Note: For cylindrical RZth geometry, this would instead be the data for the R direction

Record 5: format (6g13.5)

Y-mesh data as follows:

YO, NFYC(1),YMAXC(1),ratioYC(1), NFYC(2),YMAXC(2),ratioYC(2), ..., NFYC(NCY),YMAXC(NCY),ratioYC(NCY)

that is:

yo, data for coarse mesh 1, data for coarse mesh 2, ..., data for coarse mesh NCY,

where

YO = location of left most plane (globally)

NFYC(i) = number of fine mesh intervals in coarse mesh i <-- used in Subroutine WWVAL

YMAXC(i)= location of rightmost plane in coarse mesh i <-- used in Subroutine WWVAL

ratioYC(i)= fine mesh ratio in course mesh i <-- required; may(?) allow for logarithmically denser or sparser fine mesh inside a given course mesh; not sure if used or not; I always enter 1.0

Note: For cylindrical RZth geometry, this would instead be the data for the Z direction

Record 6: format (6g13.5)

Z-mesh data as follows:

ZO, NFZC(1),ZMAXC(1),ratioZC(1), NFZC(2),ZMAXC(2),ratioZC(2), ..., NFZC(NCZ),ZMAXC(NCZ),ratioZC(NCZ)

that is:

zo, data for coarse mesh 1, data for coarse mesh 2, ..., data for coarse mesh NCZ,

where

ZO = location of left most plane (globally)

NFZC(i) = number of fine mesh intervals in coarse mesh i <-- used in Subroutine WWVAL

ZMAXC(i)= location of rightmost plane in coarse mesh i <-- used in Subroutine WWVAL

ratioZC(i)= fine mesh ratio in course mesh i <-- required; may(?) allow for logarithmically denser or sparser fine mesh inside a given course mesh; not sure if used or not; I always enter 1.0

Note: For cylindrical RZth geometry, this would instead be the data for the theta direction; in this case, data would be in "revolutions" so that 0.125 would correspond to 45-degrees, etc.

Record 7 data is described below; note that this is really a whole series of records:

```
+-------- FIRST ENTER THE UPPER ENERGY BOUNDS & WEIGHT WINDOW INFO BELOW FOR PARTICLE TYPE 1 (neutrons)
         THEN  ENTER THE UPPER ENERGY BOUNDS & WEIGHT WINDOW INFO BELOW FOR PARTICLE TYPE 2 (gammas)    if NI=2 or NI=3
         THEN  ENTER THE UPPER ENERGY BOUNDS & WEIGHT WINDOW INFO BELOW FOR PARTICLE TYPE 3 (electrons) iff NI=3 (seldom used)

         Note:  The upper energy bounds & weight window info are read for each particle type (ip=1,NI).
         The weight window info (energy bins & adjoint info by fine mesh) are stored in separate (internal)
         array locations for each particle type.  See Subroutine WWFILE (in MCNP4B) for more details.
         That is where this file is read.  From DO-loop 120 in Subroutine IWTWND you can see/verify how
         the fine mesh are numbered internally.  From Function WWVAL you can see how this info is accessed
         internally when MCNP needs values.


   BEGIN READING ENERGY-DEPENDENT WEIGHT WINDOW INFORMATION


   Record 7.1:  Read "(6g13.5)"  (EMAX(ie),ie=1,NWW(ip))  <-- upper energy bounds (MeV) for energy-dependent
                                                              weight window "ie",  for particle type "ip"


   If (as the first parameter on Record 1) you had IF=1, THEN your file should contain only the info shown on Record 7.2a,
   while if you had IF=2 or IF=3, THEN forget about Record 7.2a and instead enter the info shown below as Record 7.2b

   ---------------------------

   Record 7.2a: Read "(6g13.5)"  ((((aFlx),i=1,NX),j=1,NY),k=1,NZ)  for energy-dependent weight window 1
                Read "(6g13.5)"  ((((aFlx),i=1,NX),j=1,NY),k=1,NZ)  for energy-dependent weight window 2
                Read "(6g13.5)"  ((((aFlx),i=1,NX),j=1,NY),k=1,NZ)  for energy-dependent weight window 3
                  :                                                                                  :
                Read "(6g13.5)"  ((((aFlx),i=1,NX),j=1,NY),k=1,NZ)  for energy-dependent weight window NWW(ip)

   ---------------------------

   Record 7.2b: Read "(6g13.5)"  ((((aFlx,aJx,aJy,aJz),i=1,NX),j=1,NY),k=1,NZ)  for energy-dependent weight window 1
                Read "(6g13.5)"  ((((aFlx,aJx,aJy,aJz),i=1,NX),j=1,NY),k=1,NZ)  for energy-dependent weight window 2
                Read "(6g13.5)"  ((((aFlx,aJx,aJy,aJz),i=1,NX),j=1,NY),k=1,NZ)  for energy-dependent weight window 3
                  :                                                                                                :
                Read "(6g13.5)"  ((((aFlx,aJx,aJy,aJz),i=1,NX),j=1,NY),k=1,NZ)  for energy-dependent weight window NWW(ip)

   ---------------------------
   See definitions and supplemental notes on next page.
   ---------------------------
```

```
---------------------------

      The above lines read the energy-dependent adjoint flux (importance) and adjoint currents in each FINE mesh
      (for particle type "ip"), where:

      aFlx = adjflx(i,j,k) = energy-dependent adjoint flux (importance) in each FINE mesh (for particle type "ip")
      aJx  = adj Jx(i,j,k) = energy-dependent adjoint current (Jx) in each FINE mesh (for particle type "ip")
      aJy  = adj Jy(i,j,k) = energy-dependent adjoint current (Jy) in each FINE mesh (for particle type "ip")
      aJz  = adj Jz(i,j,k) = energy-dependent adjoint current (Jz) in each FINE mesh (for particle type "ip")

  --> IMPORTANT NOTE:  To be more precise, the parameter denoted here as "aFlx" is NOT really
      the energy-dependent adjoint flux (importance) in each FINE mesh (for particle type "ip").
      More correctly stated, it is the corresponding "lower weight window bound" based on the
      scalar adjoint flux.  These things are inversely proportional.
      The lower  the scalar adjoint flux, the higher the "lower weight window bound"; while
      the higher the scalar adjoint flux, the lower  the "lower weight window bound".
      At LANL, they have an option in THREEDANT that actually writes the "lower weight window bound(s)"
      in the WWINP file based on the THREEDANT adjoint solution.  However you get it, the key
      thing to note here is that the parameter denoted here as "aFlx" should instead really be
      the "lower weight window bound" in each FINE mesh (for particle type "ip").

      Furthermore:  you may want to rescale this data before using it in MCNP4B so as to BE SURE
      that the "lower weight window bound(s)" in your source region are (well) below the weight
      of your starting source particles.  If the "lower weight window bound(s)" in the source
      region are above the weights assigned to your source particles, they may be killed at birth
      by Russian Roulette -- most unproductive!  Be especially careful to check this if you are now
      (or later) applying any source-energy biasing (SB Card) which might automatically reduce the
      starting weights of particles in energy groups you wish to sample more heavily!!!

  --> Update (9-5-98):  Notes in Appendix C.2 of this H8-3 Shielding Report describe how the lower
      weight window bounds should be calculated from the adjoint information and properly renormalized
      back to the real MCNP source (i.e., all broad groups multiplied by the same factor), and how the
      "optimally biased" fine-group source energy distribution should be calculated from the original
      fine-group source energy distribution in a fashion consistent with the weight window specifications.

      Note:  It is always possible (and many times desirable) to set  aJx = aJy = aJz = 0.0
             The code knows how to handle this, and it works just fine.
             If you're thinking of doing this, however, you might as well
             set IF=1 and use the shorter file format and save the space.

      Note:  If one wants to more sophisticated, however, the last few lines of Function Subroutine WWVAL
             can also apply a directional biasing based on the adjoint currents.  This has the potential
             for being very powerful.  For "heuristic adjoints" that one might create by hand (where the
             directional adjoint currents are not really known), I believe we can gain the same benefit by
             letting (aJx,aJy,aJz) be the direction cosines of a unit vector that points "FROM the detector
             of interest, TO the centroid of the geometry mesh interval (i,j,k)".  -- JAB, 4-29-98

             If the "dot product of this and the direction cosines of a real neutron" is negative (ie, if
             a real neutron is travelling towards the detector), Function Subroutine WWVAV makes wwval very
             big, while if the dot product is positive (ie, if a real neutron is travelling away from the
             detector, Function Subroutine WWVAL makes wwval relatively small.  -- JAB, 4-29-98
```

Appendix C.4

GETWIN8.SCR: A fully self-contained script file for automatically generating the broad-group weight window file used by MCNP4B in the solution of the academic water tank problem described in Appendix C.2

Embedded within this script file is the input for the 1-D ANISN adjoint analysis and the necessary Fortran program (GETWIN8.F) for reading the resulting adjoint flux file, creating the necessary 3-D broad-group "geometry-independent weight window" file, and consistently determining the biased source-energy distribution to be used in the MCNP analysis. Details are discussed in Appendix C.2.

```
#  ***************************************************************************************************
#  ***************************************************************************************************
#
#  Korn-Shell script file to run GBANISN and generate the MCNP4B "wwinp" file on the sp2
#
#  ***************************************************************************************************
#  ***************************************************************************************************

export RTNDIR=$PWD
# export TMPDIR=/u/mnt8/$LOGNAME/temp$RANDOM
export TMPDIR=/work1/$LOGNAME/temp$RANDOM

echo  $TMPDIR
mkdir $TMPDIR
cd $TMPDIR


cat >getwin8.f <<'END-GETWIN'
c       ************************************************************************
c       ************************************************************************
c
c       GETWIN8.F -- Updated version of GETWIN.SCR
c
c       After the larger script (GETWIN8.SCR) runs the GBANISN adjoint calc to
c       calculate the fine-group (61n/23g) adjoint flux everywhere (based on
c       the total n+g flux-to-dose-rate conversion factors as the adj source),
c       this particular Fortran routine will:
c
c       Call Subroutine SRCJST which, in turn, calls Subroutine GETADJ which
c       reads the anisn scalar adjoint fluxes on fort.15, as well as anisn mesh
c       info in the GBAOUTPUT printed output file.  GETADJ then calculates and
c       prints the broad group adjoint fluxes (for 6 neut grps & 4 gamma grps)
c       as averaged over a wider (geometry-independent) mesh spaced every "dx" cm
c       (as specified there by the user; typically in 5-cm increments).  GETADJ
c       then return to Subroutine SRCJST.
c
c       SRCJST then calculates the unbiased and "biased" source distribution to
c       be in MCNP, and tabulates the corresponding space/energy-dependent weight
c       windows (values of WTLO) to be used in a coupled n/g MCNP calc with a
c       neutron-only source.
c
c       This information is printed out in a file called "GETADJ.OUT".
c
c       Lastly, this program calls Subroutine WTWIN which writes out the large
c       (ascii) weight-window file (wwinp) that will actually be used by MCNP4B.
c
c       ************************************************************************
c       ************************************************************************
c
c       IMPORTANT SUBSTATIVE CHANGE:
c
c       In version GETWIN8.SCR (dated 7-29-98), as opposed to earlier versions
c       (like GETWIN.SCR dated 5-26-98 for the academic neutron in water problem),
c       we now recognize the correct order of the group-dependent adjoint fluxes
c       being read off the GBANISN flux tape.  See comments in Subroutine GETADJ.
c
c
c       ************************************************************************
```

```
c      ************************************************************************
c
       dimension xmini(3000),xmaxi(0:3000)      ! xmin & xmax for each importance zone
       dimension emaxi(10)      ! maximum energy (MeV) of the 6 broad neut groups & the 4 broad gamma groups
       dimension wtlo(3000,10)  ! wtlo(mesh,ig) for a given importance mesh, and broad group (calculated here)
c
       whi2lo=10000.  ! Jabo recommends wthi=10000*wtlo & wtsurv=wtavg=100*wtlo  (as the biggest weight window)
       wav2lo=100.    ! Jabo recommends wthi=10000*wtlo & wtsurv=wtavg=100*wtlo  (as the biggest weight window)
c
       whi2lo=100.    ! Jabo recommends wthi=  100*wtlo & wtsurv=wtavg= 10*wtlo  (as the best    weight window)
       wav2lo=10.     ! Jabo recommends wthi=  100*wtlo & wtsurv=wtavg= 10*wtlo  (as the best    weight window)
c
       xsrc=174.951   ! location where the "real" (forward) source would impinge on the 1-D buckled slab model (used for several things)
       xsrc=116.7841  ! point where the old 1960 water tube began
       xsrc=174.27    ! point where the new 1998 water tube begins
       xsrc=175.0
c
       xdet=400.0     ! location of adjoint source in anisn model (not used, only printed, but user MUST specify for QA purposes)
       xdet=300.0     ! location of adjoint source in anisn model (not used, only printed, but user MUST specify for QA purposes)
       dx=4.1         ! thickness on each importance zone to be used in mcnp
       dx=5.0         ! thickness on each importance zone to be used in mcnp
       dydz=26.3      ! transverse dimensions used for buckling in anisn  (not used, only printed, but user MUST specify for QA purposes)
       dydz=27.2      ! transverse dimensions used for buckling in anisn  (not used, only printed, but user MUST specify for QA purposes)
c
c      Also note:  For this particular "academic problem" se place all the point sources at x0(ig)=50.0 cm (impinge at xsrc=175.0 cm)
c
       call srcjst (xsrc,xdet,dx,dydz,
     *  whi2lo,wav2lo,imi,xmini,xmaxi,emaxi,wtlo)  ! calculate weight window info
c
       call wtwin (imi,xmini,xmaxi,emaxi,wtlo)     ! write out weight window file for Cartesian XYZ geometry
c
       stop
       end
c
c
       subroutine srcjst (xsrc,xdet,dx,dydz,
     *  whi2lo,wav2lo,imi,xmini,xmaxi,emaxi,wtlo)
c      ************************************************************************
c      ************************************************************************
c
c      Calculates the biased source distribution for MCNP as well
c      as the space/energy-dependent weight windows to be used in a
c      coupled n/g MCNP calc with a neutron-only source.
c
c      The neutron-only source used here is for the HB3 water tube.
c
c      The user must supply the following information:
c
c           xsrc = location (cm) where the "real" (forward) source would impinge on the 1-D buckled slab model (used for several things)
c           xdet = location (cm) of adjoint source in anisn model (not used, only printed, but user MUST specify for QA purposes)
c           dx   = thickness (cm) of each importance zone to be used in mcnp
c           dydz = transverse dimensions (cm) DY=DZ=dyzy used for buckling in anisn (not used, only printed;  MUST specify for QA purposes)
c           whi2lo=ratio of WTHIGH/WTLOW to be used in setting up weight windows; must use same values in MCNP run
c           wav2lo=ratio of WTAVG/WTLOW = WTSURV/WTLOW to be used in setting up weight windows; must use same values in MCNP run
c
c
c      This routine calculates and returns the following parameters:
c
```

```
c           imi = number of 5-cm coarse importance mesh intervals
c           xmini(3000),xmaxi(0:3000) = xmin & xmax for each importance zone,  i=1,imi  (imi.le.3000)
c           emaxi(10)       ! maximum energy (MeV) of the 6 broad neut groups & the 4 broad gamma groups
c           wtlo(3000,10)   ! ((wtlo(mesh,ig),mesh=1,imi),ig=1,10) for a given importance mesh, and broad group (calculated here)
c
c       ------------------------------------------------------------
c
c       Ref: "Monte Carlo Shielding Analyses Using an Automated Biasing
c       Procedure" by J. S. Tang and T. J. Hoffman, Nuclear Science and
c       Engineering, Vol 99, pp 329-342 (1988)
c
c       ***********************************************************************
c       ***********************************************************************
c
        dimension xmini(3000),xmaxi(0:3000)       ! xmin & xmax for each importance zone
        dimension emaxi(10)       ! maximum energy (MeV) of the 6 broad neut groups & the 4 broad gamma groups
        dimension wtlo(3000,10)   ! wtlo(mesh,ig) for a given importance mesh, and broad group (calculated here)
c
        dimension adjnf1(3000,6) ! allows for 6 neutron imp grps  and up to 3000 coarse imp mesh
        dimension adjgf1(3000,4) ! allows for 4 gamma   imp grps  and up to 3000 coarse imp mesh
c
        dimension s0(10),sb(10),ratio(10),a(10),wtavg(10)
        dimension ptsrc(84),x0(84),src(84),srcb(84)
        dimension srcm(61),srcbm(61)  ! unbiased & biased sources in MCNP order (grp 1=low E, grp 61=high E)
c
        data ptsrc/  ! for neut in HB3 (velm grp=1,61), gammas in HB3 (velm grp=1,23); fast=grp 1
     *  2.74800E+09, 6.92602E+12, 8.64293E+12, 3.05242E+13, 7.32282E+13,
     *  1.36477E+14, 2.06360E+14, 1.61947E+14, 2.41078E+14, 1.35333E+14,
     *  2.00073E+14, 3.12945E+14, 8.54720E+14, 8.07055E+14, 7.09512E+14,
     *  5.40055E+14, 6.65098E+14, 5.35177E+14, 3.61470E+14, 1.49367E+14,
     *  5.85513E+14, 6.29256E+14, 3.65651E+13, 7.68584E+12, 1.38494E+13,
     *  2.12840E+14, 7.35199E+14, 4.33245E+14, 3.63241E+14, 4.29193E+14,
     *  5.59006E+14, 8.89397E+14, 1.29680E+14, 4.96958E+14, 3.03507E+14,
     *  1.21873E+14, 5.24714E+13, 1.12860E+14, 6.69650E+13, 7.42049E+14,
     *  9.84217E+14, 8.76077E+14, 7.55438E+14, 3.36538E+14, 2.54975E+14,
     *  2.76622E+14, 2.04908E+14, 8.87245E+14, 8.53691E+14, 8.74122E+14,
     *  9.50610E+14, 9.69821E+14, 9.03837E+14, 1.45876E+15, 1.54759E+15,
     *  1.58981E+15, 1.55274E+15, 1.30212E+15, 1.52979E+15, 2.25679E+15,
     *  6.30365E+16, 1.23250E+11, 6.19421E+13, 1.51983E+15, 1.60183E+14,
     *  1.23378E+15, 6.75453E+14, 1.98361E+15, 2.34929E+15, 1.42777E+15,
     *  2.66951E+15, 4.23989E+15, 5.27935E+15, 7.31636E+15, 4.03975E+15,
     *  4.80101E+15, 7.17665E+15, 1.03805E+16, 2.56708E+16, 1.82855E+16,
     *  1.67705E+16, 1.65029E+16, 2.84514E+15, 8.72837E+12/
        data x0 / ! for neut in HB3 (velm grp=1,61), gammas in HB3 (velm grp=1,23); fast=grp 1
     *   99.9, 31.1, 68.7, 42.9, 59.5, 62.6, 47.9, 56.9, 65.3, 43.5,
     *   33.3, 52.1, 50.2, 59.7, 46.8, 70.1, 44.1, 56.8, 50.3, 52.9,
     *   58.8, 49.6, 42.3, 53.7, 63.8, 42.4, 34.2, 48.9, 42.5, 45.6,
     *   45.7, 47.4, 56.7, 52.9, 79.8, 67.5, 62.6, 46.7, 69.0, 54.0,
     *   50.7, 52.7, 53.3, 65.1, 55.0, 49.5, 43.0, 60.5, 61.2, 52.6,
     *   53.8, 51.1, 56.0, 55.4, 56.5, 48.2, 54.5, 76.1, 65.2, 57.3,
     *   80.2, 97.4, 99.9, 94.4, 96.0, 93.9, 96.4, 93.2, 92.6, 96.6,
     *   99.2, 96.9, 93.6, 86.8, 83.2, 88.8, 84.7, 81.6, 84.5, 83.9,
     *   82.1, 68.1, 61.9, 10.0/
c
        open (30,file='getadj.out',status='unknown')                    ! ascii file with summary adjoint info
c
        khi21[illegible]t(whi21o)
        kav21[illegible]t(wav21o)
```

```
c
      pi=acos(-1.0)
      x=xsrc       ! point where the point source streaming thru void first impinges on the water tube (input by user)
c
      do i=1,10
      s0(i)=0.0
      enddo
c
      do i=1,84
c
         x0(i)=50.0  ! override the above for the special "ACADEMIC" case ONLY
c
         dum=4.0*pi*(x-x0(i))*(x-x0(i))
         src(i)=ptsrc(i)/dum           ! real unbiased src, (n/s/cm2) or (p/s/cm2), impingent on water tube
c
         if (i.eq.61)                s0(1)=s0(1)+src(i)    ! Unbiased SRC  for  VELM neutr grps 61-61 = MCNP neutr grps 01-01
         if (i.ge.57 .and. i.le.60)  s0(2)=s0(2)+src(i)    ! Unbiased SRC  for  VELM neutr grps 57-60 = MCNP neutr grps 02-05
         if (i.ge.49 .and. i.le.56)  s0(3)=s0(3)+src(i)    ! Unbiased SRC  for  VELM neutr grps 49-56 = MCNP neutr grps 06-13
         if (i.ge.31 .and. i.le.48)  s0(4)=s0(4)+src(i)    ! Unbiased SRC  for  VELM neutr grps 31-48 = MCNP neutr grps 14-31
         if (i.ge.16 .and. i.le.30)  s0(5)=s0(5)+src(i)    ! Unbiased SRC  for  VELM neutr grps 16-30 = MCNP neutr grps 32-46
         if (i.ge.01 .and. i.le.15)  s0(6)=s0(6)+src(i)    ! Unbiased SRC  for  VELM neutr grps 01-15 = MCNP neutr grps 47-61
c
         j=i-61
c
         if (j.ge.18 .and. j.le.23)  s0(7)=s0(7)+src(i)     ! Unbiased SRC  for  VELM gamma grps 18-23 = MCNP gamma grps 01-06
         if (j.ge.13 .and. j.le.17)  s0(8)=s0(8)+src(i)     ! Unbiased SRC  for  VELM gamma grps 13-17 = MCNP gamma grps 07-11
         if (j.ge.08 .and. j.le.12)  s0(9)=s0(9)+src(i)     ! Unbiased SRC  for  VELM gamma grps 08-12 = MCNP gamma grps 12-16
         if (j.ge.01 .and. j.le.07)  s0(10)=s0(10)+src(i)   ! Unbiased SRC  for  VELM gamma grps 01-07 = MCNP gamma grps 17-23
c
      enddo
c
      do i=7,10
         s0(i)=0.0   ! use 0.0 here when running the MCNP n/g problem with no external gamma sources
      enddo
c
c     ====================================
      call getadj (xsrc,xdet,dx,dydz,          ! go get GBANISN broad group adjoint fluxes for each importance mesh
     *  imi,xmini,xmaxi,emaxi,adjnfl,adjgfl)  ! go get GBANISN broad group adjoint fluxes for each importance mesh
c     ====================================
c
      do i=1,10
      ratio(i)=0.0
      enddo
c
c     --------- Now begin procedure outlined in Jabo Tang's NS&E paper:
c
      mesh=1
      do i=1,6
      a(i)=adjnfl(mesh,i)   ! get adjoint fluxes for the 6 neutron groups in imp mesh 1, the 1st mesh the "real" source hits
      enddo
      do i=7,10
      a(i)=adjgfl(mesh,i-6)   ! get adjoint fluxes for the 4 gamma groups in imp mesh 1, the 1st mesh the "real" source hits
      enddo
c
      sums0=0.0
      sums0a=0.0
      do i=1,10
         sums0a=sums0a+s0(i)*a(i)
```

```
         sums0=sums0+s0(i)
       enddo
       avgadj=sums0a/sums0              ! "Source-Averaged" Adjoint
c
       write (30,'(////)')
       do i=1,10
         sb(i)=s0(i)*a(i)/avgadj        ! Biased MCNP source distribution
         wtavg(i)=avgadj/a(i)
         wtlo(mesh,i)=wtavg(i)/wav2lo   ! See Jabo's recommendation (above)
       enddo
       write (30,'(a1)') char(12)
c      write (30,11) mesh,(wtlo(mesh,i),i=1,10)
c11    format (1x,i3,2x,1p,10e13.5)
       write (30,11) mesh,(wtlo(mesh,i),ratio(i),i=1,10)
11     format (1x,i3,2x,10(1p,e13.5,0p,f7.4))
c
       do i=1,10
       ratio(i)=wtlo(mesh,i)
       enddo
c
       do mesh=2,imi
         m=mesh
         do i=1,6
         a(i)=adjnfl(m,i)   ! get adjoint fluxes for the 6 neutron groups in import mesh "m"
         enddo
         do i=7,10
         a(i)=adjgfl(m,i-6)   ! get adjoint fluxes for the 4 gamma groups in import mesh "m"
         enddo
c        ----------------
         do i=1,10
           wtavg(i)=avgadj/a(i)
           wtlo(mesh,i)=wtavg(i)/wav2lo  ! See Jabo's recommendation (above)
         enddo
c        ----------------
         do i=1,10
         ratio(i)=wtlo(mesh,i)/ratio(i)
         enddo
c        write (30,11) mesh,(wtlo(mesh,i),i=1,10)
         write (30,11) mesh,(wtlo(mesh,i),ratio(i),i=1,10)
         do i=1,10
         ratio(i)=wtlo(mesh,i)
         enddo
       enddo
c
c      ------------------------------------------------------
c
       write (30,'(a1)') char(12)
       write (30,401)  khi2lo,kav2lo,(emaxi(i),i=1,10)
401    format (17x,'WTLO for the 6 broad neutron groups',
     *  ' and 4 broad gamma groups based on 1-D adjoint & Jabo''s',
     *  ' procedure with WTHI=',i5,'*WTLO & WTSURV=WTAVG=',i3,'*WTLO',
     *  /,17x,'Use these values for the coupled n/g mcnp transport',
     *  ' analysis involving a neutron-only source.',/,17x,
     *  '(With a n/g source, or a gamma-only source, values',
     *  ' would be differnet)',/,17x,
     *  'mnXX-yy = MCNP neutron grp numbers,   ',
     *  'mgXX-yy = MCNP gamma grp numbers',/,17x,
     *  'vnXX-yy = VELM neutron grp numbers,   ',
```

```
*    'vgXX-YY = VELM gamma grp numbers',//,17x,
*    'Emax:',1pe12.5,9e13.5,/,17x,
*    'imp      mn01-01      mn02-05      mn06-13      mn14-31',
*      '       mn32-46      mn47-61      mg01-06      mg07-11',
*      '       mg12-16      mg17-23',/,
*    '  xmin     xmax   mesh',
*        '     vn61-61      vn57-60      vn49-56      vn31-48',
*      '       vn16-30      vn01-15      vg18-23      vg13-17',
*      '       vg08-12      vg01-07',/)
     do jx=1,imi
        write (30,402) xmini(jx),xmaxi(jx),jx,
*         (wtlo(jx,ig),ig=1,10)
402     format (1x,f6.2,f8.2,i5,1x,1p,10e13.5)
     enddo
c
c    ------------------------------------------------------
c
     do i=1,10
     ratio(i)=1.0
     if (s0(i).gt.0.0)  ratio(i)=sb(i)/s0(i)
     enddo
c
     write (30,'(a1)') char(12)
     write (30,12) (s0(i),i=1,10)
     write (30,13) (sb(i),i=1,10)
     write (30,14) (ratio(i),i=1,10)
c
12   format (///,1x,' s0',2x,1p,10e13.5)
13   format (///,1x,' sb',2x,1p,10e13.5)
14   format (///,1x,' r ',2x,1p,10e13.5)
c
c
c
     do i=1,84
        src(i)=ptsrc(i)          ! return to original point sources (rather than impingent sources)
        if (i.gt.61) src(i)=0.0
c
        if (i.eq.61)               srcb(i)=src(i)*sb(1)/s0(1)  ! Biased SRC  for  VELM neutr grps 61-61 = MCNP neutr grps 01-01
        if (i.ge.57 .and. i.le.60) srcb(i)=src(i)*sb(2)/s0(2)  ! Biased SRC  for  VELM neutr grps 57-60 = MCNP neutr grps 02-05
        if (i.ge.49 .and. i.le.56) srcb(i)=src(i)*sb(3)/s0(3)  ! Biased SRC  for  VELM neutr grps 49-56 = MCNP neutr grps 06-13
        if (i.ge.31 .and. i.le.48) srcb(i)=src(i)*sb(4)/s0(4)  ! Biased SRC  for  VELM neutr grps 31-48 = MCNP neutr grps 14-31
        if (i.ge.16 .and. i.le.30) srcb(i)=src(i)*sb(5)/s0(5)  ! Biased SRC  for  VELM neutr grps 16-30 = MCNP neutr grps 32-46
        if (i.ge.01 .and. i.le.15) srcb(i)=src(i)*sb(6)/s0(6)  ! Biased SRC  for  VELM neutr grps 01-15 = MCNP neutr grps 47-61
c
ccc        j=i-61
cccc
ccc        if (j.ge.18 .and. j.le.23)  srcb(i)=src(i)*sb(7)/s0(7)   ! Unbiased SRC  for  VELM gamma grps 18-23 = MCNP gamma grps 01-06
ccc        if (j.ge.13 .and. j.le.17)  srcb(i)=src(i)*sb(8)/s0(8)   ! Unbiased SRC  for  VELM gamma grps 13-17 = MCNP gamma grps 07-11
ccc        if (j.ge.08 .and. j.le.12)  srcb(i)=src(i)*sb(9)/s0(9)   ! Unbiased SRC  for  VELM gamma grps 08-12 = MCNP gamma grps 12-16
ccc        if (j.ge.01 .and. j.le.07)  srcb(i)=src(i)*sb(10)/s0(10) ! Unbiased SRC  for  VELM gamma grps 01-07 = MCNP gamma grps 17-23
c
     enddo
c
     do i=1,61
     k=62-i
     srcm(i)=src(k)    ! unbiased sources in MCNP order (grp 1=low E, grp 61=high E)
     srcbm(i)=srcb(k)  !   biased sources in MCNP order (grp 1=low E, grp 61=high E)
     enddo
```

```
c
      write (30,41)
41    format (///,' Unbiased neutron sources in MCNP order',
     *  ' (grp 1=low E, grp 61=high E):',/)
      write (30,42)  (srcm(i),i=1,61)
42    format (5x,1p,5e13.5)
c
      write (30,43)
43    format (/,' Biased neutron sources in MCNP order',
     *  ' (grp 1=low E, grp 61=high E):',/,
     *  ' Use these values for the coupled n/g mcnp transport',
     *  ' analysis involving a neutron-only source.',/,
     *  ' (With a n/g source, or a gamma-only source, values',
     *  ' would be differnet)',/)
      write (30,42)  (srcbm(i),i=1,61)
      write (30,44)  khi2lo,kav2lo,khi2lo,kav2lo
44    format (/,' In addition:',//,
     * ' On your  WWP:N  card, make sure you have',
     * '  WTHI=',i5,'*WTLO  and WTSURV=',i3,'*WTLO',/,
     * ' On your  WWP:P  card, make sure you have',
     * '  WTHI=',i5,'*WTLO  and WTSURV=',i3,'*WTLO')
c
c
      return
      end
c
c
      subroutine getadj (xsrc,xdet,dx,dydz,
     *  imi,xmini,xmaxi,emaxi,adjnfl,adjgfl)
c     ****************************************************************************
c     ****************************************************************************
c
c     Tallies the GBANISN adjoint flux into 6 broad neutron groups and 4 broad
c     gamma groups, for each 5-cm coarse importance mesh composed of any number
c     of fine mesh in the GBANISN adj calc using the VELM 61n/23g lib
c
c     The user must supply the following information:
c
c          xsrc = location (cm) where the "real" (forward) source would impinge on the 1-D buckled slab model (used for several things)
c          xdet = location (cm) of adjoint source in anisn model (not used, only printed, but user MUST specify for QA purposes)
c          dx   = thickness (cm) of each importance zone to be used in mcnp
c          dydz = transverse dimensions (cm) DY=DZ=dyzy used for buckling in anisn (not used, only printed;  MUST specify for QA purposes)
c
c     This subroutine will return:  imi, xmini, xmaxi, emaxi, adjnfl, adjgfl  where
c
c          imi = number of 5-cm coarse importance mesh intervals
c          dimension xmini(3000),xmaxi(0:3000)  ! xmin & xmax for each importance zone, i=1,imi  (imi.le.3000)
c          dimension emaxi(10)       ! maximum energy (MeV) of the 6 broad neut groups & the 4 broad gamma groups
c          dimension adjnfl(3000,6) ! allows for 6 neutron imp grps  and up to 3000 coarse imp mesh
c          dimension adjgfl(3000,4) ! allows for 4 gamma   imp grps  and up to 3000 coarse imp mesh
c
c                                              -- J.A. Bucholz, 20 May 1998
c
c     ****************************************************************************
c     ****************************************************************************
c
c     This s     e was recently updated to account for fact the results on '
c     gbanis     djoint scalar flux tape" are in "adjoint order", i.e. ....
```

```
c
c       ... the results in grp  1 on the tape really correspond to the adjoint flux for the lowest  energy gamma group,
c       ... the results in grp 23 on the tape really correspond to the adjoint flux for the highest energy gamma group,
c       ... the results in grp 24 on the tape really correspond to the adjoint flux for the lowest  energy neutron group, and
c       ... the results in grp 84 on the tape really correspond to the adjoint flux for the highest energy neutron group.
c
c       This conclusion was verified by extensive testing on 13 June 1998.
c       Prior to this time, I had failed to appreciate this fact.
c
c       Note:  The above observations were made on 13 June 1998 when I was busy working on the HB308 series of calcs
c       with a gamma-only source (see the H2O-TUBE.308 subdirectory, where everything is throroghly documented). Because
c       of the intensive involvement on that "much more important" problem, I was simply "too busy" to go back to the
c       "academic problem" (from May 1998) with the neutron-only-source n/g problem (in this ACADEMIC.111 subdirectory)
c       and make the necessary corrections at that time.  On 29 July 1998, however, I did have a little extra time, so
c       I did go back to the ACADEMIC.111 subdirectory, took the GETWIN.SCR script, copied it into GETWIN8.SCR and made
c       the necessary changes here in Subroutine GETADJ of GETWIN8.SCR for the academic neutron-only-source n/g problem.
c
c                                                                                       -- J.A. Bucholz, 29 July 1998
c       ************************************************************************
c       ************************************************************************
c
        dimension flux(3000),emax0(84),emaxi(10)
        dimension xmina(3000),xmida(3000)        ! xmin & midpoint for each anisn mesh; xmin read from anisn printed output file
        dimension xmini(3000),xmaxi(0:3000)      ! xmin & xmax for each importance zone
        dimension vola(3000)                     ! volume of each fine mesh in the 1-D slab anisn calc
        dimension voli(3000)                     ! total vol of all fine mesh whose midpoints lie inside a given imp zone (may differ slightly from actual v
ol of imp zone)
        character*32 linchk
        character*1  lin1
        equivalence (lin1,linchk)
c
c       double precision adjnfl(3000,6),adjgfl(3000,4)  ! allows for 6 neutron imp grps & 4 gamma imp grps; total=10
        dimension adjnfl(3000,6),adjgfl(3000,4)  ! allows for 6 neutron imp grps & 4 gamma imp grps; total=10
        dimension igmin(10),igmax(10)
        data igmin/ 1, 16, 31, 49, 57, 61, 62, 69, 74, 79 /  ! VELM group numbers corresponding to each importance group
        data igmax/15, 30, 48, 56, 60, 61, 68, 73, 78, 84 /  ! VELM group numbers corresponding to each importance group
c
c       Emax in MeV for VELM neutron grps ig=1,61 followed by
c       Emax in MeV for VELM gamma   grps ig=1,23
        data emax0/
     * 1.4918E+01, 1.2214E+01, 1.0000E+01, 8.1873E+00, 6.7032E+00,
     * 5.4881E+00, 4.4933E+00, 3.6788E+00, 3.0119E+00, 2.4660E+00,
     * 2.3457E+00, 2.2313E+00, 2.0190E+00, 1.6530E+00, 1.3534E+00,
     * 1.1080E+00, 9.0718E-01, 7.4274E-01, 6.0810E-01, 5.2340E-01,
     * 4.9787E-01, 3.8774E-01, 3.0197E-01, 2.9849E-01, 2.9721E-01,
     * 2.9452E-01, 2.7324E-01, 2.2371E-01, 1.8316E-01, 1.4996E-01,
     * 1.2277E-01, 8.6517E-02, 5.6562E-02, 5.2475E-02, 3.4307E-02,
     * 2.8501E-02, 2.7000E-02, 2.6058E-02, 2.4788E-02, 2.3579E-02,
     * 1.5034E-02, 9.1188E-03, 5.5308E-03, 3.7074E-03, 3.0354E-03,
     * 2.6126E-03, 2.2487E-03, 2.0347E-03, 1.2341E-03, 7.4852E-04,
     * 4.5400E-04, 2.7536E-04, 1.6702E-04, 1.0130E-04, 4.7851E-05,
     * 2.2603E-05, 1.0677E-05, 5.0435E-06, 2.3824E-06, 1.1253E-06,
     * 4.1399E-07, 1.4000E+01, 1.0000E+01, 8.0000E+00, 7.5000E+00,
     * 7.0000E+00, 6.0000E+00, 5.0000E+00, 4.0000E+00, 3.0000E+00,
     * 2.5000E+00, 2.0000E+00, 1.5000E+00, 1.0000E+00, 7.0000E-01,
     * 6.0000E-01, 5.1000E-01, 4.0000E-01, 3.0000E-01, 1.5000E-01,
     * 1.0000E-01, 7.0000E-02, 4.5000E-02, 2.0000E-02/
c
```

```
c
c       ---------------------------------------------------------
c       read anisn mesh from anisn printed output file:
c
        open (12,file='gbaoutput',status='old',form='formatted')       ! anisn printed output file
c
200     read (12,'(a32)')  linchk
        if (linchk.ne.'  int.  zone number     radius  ') go to 200
201     read (12,'(a32)')  linchk
        read (linchk,'(i6,18,e18.5)') mesha,mzone,xmina(mesha)
        if (mzone.gt.0)  go to 201
        im=mesha-1  ! number of anisn mesh intervals
        close (12)
c
        do i=1,im
        xmida(i)=(xmina(i)+xmina(i+1))/2.0  ! get midpoint of each anisn mesh
        vola(i)=xmina(i+1)-xmina(i)
        enddo
c
        xmaxi(0)=xmina(1)
        xmaxi(0)=xsrc
        i=0
203     i=i+1
        xmini(i)=xmaxi(i-1)
        xmaxi(i)=xmini(i)+dx  ! increment by thickness of each importance zone to be used in mcnp
        if (xmaxi(i).lt.xmina(mesha)) go to 203
        imi=i  ! number of mcnp importance zones corresponding to anisn model
c
c       ---------------------------------------------------------
c
        do ig=1,6
           do ix=1,imi
              adjnfl(ix,ig)=0.0d0
           enddo
        enddo
c
        do ig=1,4
           do ix=1,imi
              adjgfl(ix,ig)=0.0d0
           enddo
        enddo
c
c
c       get total volume of all anisn fine mesh (ix) whose midpoints lie inside a given importance mesh (jx):
        do jx=1,imi
           voli(jx)=0.0
           do ix=1,im
           if (xmida(ix).ge.xmini(jx) .and. xmida(ix).le.xmaxi(jx))
     *        voli(jx)=voli(jx)+vola(ix)
           enddo
        enddo
c
c       ---------------------------------------------------------
c
        open (15,file='fort.15',status='old',form='unformatted')       ! anisn flux moment file (fort.15)
c
c       ---------------------------------------------------------
c
```

```
c  deleted by jab on 7-29-98:          do ig=1,61   ! tally neutrons
c  deleted by jab on 7-29-98:  c
c  deleted by jab on 7-29-98:             do jg=1,6
c  deleted by jab on 7-29-98:             if (ig.ge.igmin(jg) .and. ig.le.igmax(jg)) igg=7-jg  ! igg=mcnp broad group (1=slow, 6=fast)
c  deleted by jab on 7-29-98:             enddo
c  deleted by jab on 7-29-98:  c
c  deleted by jab on 7-29-98:             read (15) (flux(ix),ix=1,im)
c  deleted by jab on 7-29-98:  c
c  deleted by jab on 7-29-98:             do jx=1,imi                                                    ! for every coarse importance mesh
c  deleted by jab on 7-29-98:                do ix=1,im                                                  ! check the location of each anisn fine mesh
c  deleted by jab on 7-29-98:                if (xmida(ix).ge.xmini(jx) .and. xmida(ix).le.xmaxi(jx))    ! and stuff the anisn adjoint flux in the right i
mp mesh
c  deleted by jab on 7-29-98:       *          adjnfl(jx,igg)=adjnfl(jx,igg)+flux(ix)*vola(ix)/voli(jx)   ! while accounting for relative volume of each me
sh
c  deleted by jab on 7-29-98:                enddo
c  deleted by jab on 7-29-98:             enddo
c  deleted by jab on 7-29-98:  c
c  deleted by jab on 7-29-98:          enddo
c  deleted by jab on 7-29-98:  c
c  deleted by jab on 7-29-98:  c       ------------------------------------------------------
c  deleted by jab on 7-29-98:  c
c  deleted by jab on 7-29-98:          do ig=62,84   ! tally gammas
c  deleted by jab on 7-29-98:  c
c  deleted by jab on 7-29-98:             do jg=7,10
c  deleted by jab on 7-29-98:             if (ig.ge.igmin(jg) .and. ig.le.igmax(jg)) igg=11-jg  ! igg=mcnp broad group (1=soft, 4=hard)
c  deleted by jab on 7-29-98:             enddo
c  deleted by jab on 7-29-98:  c
c  deleted by jab on 7-29-98:             read (15) (flux(ix),ix=1,im)
c  deleted by jab on 7-29-98:  c
c  deleted by jab on 7-29-98:             do jx=1,imi                                                    ! for every coarse importance mesh
c  deleted by jab on 7-29-98:                do ix=1,im                                                  ! check the location of each anisn fine mesh
c  deleted by jab on 7-29-98:                if (xmida(ix).ge.xmini(jx) .and. xmida(ix).le.xmaxi(jx))    ! and stuff the anisn adjoint flux in the right i
mp mesh
c  deleted by jab on 7-29-98:       *          adjgfl(jx,igg)=adjgfl(jx,igg)+flux(ix)*vola(ix)/voli(jx)   ! while accounting for relative volume of each me
sh
c  deleted by jab on 7-29-98:                enddo
c  deleted by jab on 7-29-98:             enddo
c  deleted by jab on 7-29-98:  c
c  deleted by jab on 7-29-98:          enddo
c
c       ------------------------------------------------------
c
c       This routine was recently updated (as shown above and below) to account for fact the results on the
c       gbanisn "adjoint scalar flux tape" are in "adjoint order", i.e. ....
c
c       ... the results in grp  1 on the tape really correspond to the adjoint flux for the lowest  energy gamma group,
c       ... the results in grp 23 on the tape really correspond to the adjoint flux for the highest energy gamma group,
c       ... the results in grp 24 on the tape really correspond to the adjoint flux for the lowest  energy neutron group, and
c       ... the results in grp 84 on the tape really correspond to the adjoint flux for the highest energy neutron group.
c
c       This conclusion was verified by extensive testing on 13 June 1998.
c       Prior to this time, I had failed to appreciate this fact.
c
c       Note:  The above observations were made on 13 June 1998 when I was busy working on the HB308 series of calcs
c       with a gamma-only source (see the H2O-TUBE.308 subdirectory, where everything is throroghly documented). Because
c       of the intensive involvement on that "much more important" problem, I was simply "too busy" to go back to the
c       "academic problem" (from May 1998) with the neutron-only-source n/g problem (in this ACADEMIC.111 subdirectory)
c       and make the necessary corrections at that time.  On 29 July 1998, however, I did have a little extra time, so
```

```
c       I did go back to the ACADEMIC.111 subdirectory, took the GETWIN.SCR script, copied it into GETWIN8.SCR and made
c       the necessary changes here in Subroutine GETADJ of GETWIN8.SCR for the academic neutron-only-source n/g problem.
c
c                                                                                    -- J.A. Bucholz, 29 July 1998
c
c       The necessary modifications (dated 7-29-98) are as follows:
c       -----------------------------------------------------
c                     ! tally gammas
        do iag=1,23   ! on velm adjoint calc tape fort.15, group  iag=  1,  2,  3,  4, .... 21, 22, 23
           ig=85-iag  ! really corresponds to "real" velm  group   ig= 84, 83, 82, 81, .... 64, 63, 62
c
           do jg=7,10
           if (ig.ge.igmin(jg) .and. ig.le.igmax(jg)) igg=11-jg  ! igg=mcnp broad group (1=soft, 4=hard)
           enddo
c
           read (15) (flux(ix),ix=1,im)
c
           do jx=1,imi                                                    ! for every coarse importance mesh
              do ix=1,im                                                  ! check the location of each anisn fine mesh
              if (xmida(ix).ge.xmini(jx) .and. xmida(ix).le.xmaxi(jx))    ! and stuff the anisn adjoint flux in the right imp mesh
     *          adjgfl(jx,igg)=adjgfl(jx,igg)+flux(ix)*vola(ix)/voli(jx) ! while accounting for relative volume of each mesh
              enddo
           enddo
c
        enddo
c
c       -----------------------------------------------------
c                     ! tally neutrons
        do iag=24,84  ! on velm adjoint calc tape fort.15, group  iag= 24, 25, 26, 27, .... 82, 83, 84
           ig=85-iag  ! really corresponds to "real" velm  group   ig= 61, 60, 59, 58, ....  3,  2,  1
c
           do jg=1,6
           if (ig.ge.igmin(jg) .and. ig.le.igmax(jg)) igg=7-jg  ! igg=mcnp broad group (1=slow, 6=fast)
           enddo
c
           read (15) (flux(ix),ix=1,im)
c
           do jx=1,imi                                                    ! for every coarse importance mesh
              do ix=1,im                                                  ! check the location of each anisn fine mesh
              if (xmida(ix).ge.xmini(jx) .and. xmida(ix).le.xmaxi(jx))    ! and stuff the anisn adjoint flux in the right imp mesh
     *          adjnfl(jx,igg)=adjnfl(jx,igg)+flux(ix)*vola(ix)/voli(jx) ! while accounting for relative volume of each mesh
              enddo
           enddo
c
        enddo
c
c       -----------------------------------------------------
c       End of modifications dated 7-29-98.
c
c
        impg=0
        do i=6,1,-1
        impg=impg+1
        emaxi(impg)=emax0(igmin(i))  ! emax for each braod (neutron) importance group (impg=1,6)
        enddo
        do i=10,7,-1
        impg=impg+1
        emaxi(impg)=emax0(igmin(i))  ! emax for each braod (gamma) importance group (impg=7,10)
```

```
      enddo
c     ------------------------------------------------------
c
      write (30,'(a1)') char(12)
      write (30,401)  xdet,dydz,(emaxi(i),i=1,10)
401   format (17x,'Neutron and Gamma Adjoint Fluxes in water,',
     *  ' where adjoint is based on total n+g dose at X=',f8.3,
     *  ' cm, and buckling DY=DZ=',f6.2,' cm',/,17x,
     *  'mnXX-YY = MCNP neutron grp numbers,   ',
     *  'mgXX-YY = MCNP gamma grp numbers',/,17x,
     *  'vnXX-YY = VELM neutron grp numbers,   ',
     *  'vgXX-YY = VELM gamma grp numbers',//,17x,
     *  'Emax:',1pe12.5,9e13.5,/,17x,
     *  'imp     mn01-01      mn02-05      mn06-13      mn14-31',
     *    '      mn32-46      mn47-61      mg01-06      mg07-11',
     *    '      mg12-16      mg17-23',/,
     *  '  xmin     xmax   mesh',
     *       '    vn61-61      vn57-60      vn49-56      vn31-48',
     *    '      vn16-30      vn01-15      vg18-23      vg13-17',
     *    '      vg08-12      vg01-07',/)
      do jx=1,imi
         write (30,402) xmini(jx),xmaxi(jx),jx,
     *      (adjnfl(jx,ig),ig=1,6),(adjgfl(jx,ig),ig=1,4)
402      format (1x,f6.2,f8.2,i5,1x,1p,10e13.5)
      enddo
c
c
      return
      end
c
c
      subroutine wtwin (imi,zmini,zmaxi,emaxi,wtlo)
c
c     ********************************************************************
c     ********************************************************************
c
c     WTWIN.F
c
c     A utility program to write out a (wwinp) weight-window file that
c     can be used by MCNP4B -- in this case for the simple idealized
c     academic problem where we have a narrowly collimated beam on
c     neutrons impingent on the bottom of a 130-cm-diam x 125-cm-thick
c     tank of water (Z=175 cm to Z=300 cm) and we want to get the total
c     neutron+gamma dose rate across a 20-cm-diam disk at the top,
c     assuming due to the 61-neutron-group source at the bottom
c     (similar to the 1998 HB3 beam tube when flooded).
c
c     Required input supplied by calling routine:
c
c     imi = number of coarse mesh importance zones (based on fine mesh 1-D GBANISN calc, as processed by Subroutine GETADJ)
c     dimension xmini(3000),xmaxi(0:3000)  ! xmin & xmax for each importance zone (X used in GBANISN & GETADJ.F;  now called Z)
c     dimension emaxi(10)       ! Emax(MeV) for each of the 6 broad neutron groups & each of the 4 broad gamma groups
c     dimension wtlo(3000,10)   ! wtlo(mesh,ig) for a given importance mesh, and broad group (calculated in Subroutine SRCJST)
c
c     ********************************************************************
c     ********************************************************************
c
      dimension zmini(3000),zmaxi(0:3000)  ! zmin & zmax for each importance zone (Z used in this subroutine in place of X)
```

```
c
      dimension emaxi(10)      ! Emax(MeV) for each of the 6 broad neutron groups & each of the 4 broad gamma groups
      dimension wtlo(3000,10)  ! wtlo(mesh,ig) for a given importance mesh, and broad group (calculated in Subroutine SRCJST)
c
c     For this particular "academic" problem, the following 4 arrays don't have to be this big, but that's ok:
c     (u,v,w) = unit vector going from detector point to mesh point; needed iff one wants "in flight" angular biasing
      dimension u(33,33,172)       ! x-direction cosine for above unit vector; used for "on the fly" directional biasing
      dimension v(33,33,172)       ! y-direction cosine for above unit vector; used for "on the fly" directional biasing
      dimension w(33,33,172)       ! z-direction cosine for above unit vector; used for "on the fly" directional biasing
      dimension imindx(33,33,172)  ! importance mesh index (tells what 1-D importance mesh values to use in each 3-D XYZ mesh)
c
      dimension mhead(4),ia(3),ra(10),geomx(4),geomy(4),geomz(4)  ! wwinp header info & phantom mesh geometry specs
c
ccc   data from earlier runs, not applicable in this "academic" case:
ccc   data mhead/ 2, 0, 1, 10 /
ccc   data ia/    1, 0, 0 /
ccc   data ra/ 33.0, 33.0, 172.0, -67.65, -67.65, -2.03, 4*1.0 /
ccc   data geomx/ -67.65, 33.0,  67.65, 1.0 /
ccc   data geomy/ -67.65, 33.0,  67.65, 1.0 /
ccc   data geomz/ -2.03, 172.0, 703.17, 1.0 /
c
      data mhead/ 2, 0, 2, 10 /  ! see explanation below
      data ia/    6, 4, 0 /      ! number of energy-dependent weight window set to be entered for neutrons, gammas, electrons
      data ra/ 27.0, 27.0, 65.0, -67.5, -67.5, 0.0, 4*1.0 /
      data geomx/ -67.5, 27.0,  67.5, 1.0 /
      data geomy/ -67.5, 27.0,  67.5, 1.0 /
      data geomz/   0.0, 65.0, 325.0, 1.0 /
c
      data xd,yd,zd/ 0.0, 0.0, 300.0 /  ! location of detector towards which we want to bias particles
c
c     ------------------------------------
c
c     open (7,file='wts3d.398',status='unknown')  !  <-- 7 = ascii file ("wwinp") needed by MCNP
      open (7,file='wwinp',status='unknown')      !  <-- 7 = ascii file ("wwinp") needed by MCNP
      open (6,file='wts3d.prn',status='unknown')  !  <-- 6 = debug print file
c
      mhead(1)=1   ! write and use "weights only" for each mesh
      mhead(1)=2   ! write and use "weights & directional info" for each mesh
      mhead(1)=3   ! write "weights & directional info" for each mesh, but only use weights
c
      mhead(1)=2   ! write and use "weights & directional info" for each mesh
      mhead(2)=0   ! dummy version number; always enter 0
      mhead(3)=2   ! number of different particle types for which energy-dependent weight windows will be read (2 for coupled n/g problem)
      mhead(4)=10  ! number of parameters to be read in RA array;  10 for cartesian XYZ specs, 15 for RZth specs
c
      nptype=mhead(3)
c
c     ------------------------------
c     The values of "wtlo" entered in the data statements above must all be multiplied by the same
c     wgt=1.7332472e-2  that appears on my MCNP sdef card to account for the fact that I am only going
c     to spray neutrons isotropically across a very narrow cone of directions (ie, only the central
c     void of HB-3 beam tube, where  MIN cos = cos(theta max) = cos(15.13023 deg) = 0.965335056
c     If there were no other biasing, this spec on the sdef card:
c     wgt = [mu(max)-mu(min)]/[(+1)-(-1)] = [1.0000000000-0.965335056]/2 = 1.7332472e-2
c     would cause this to be the starting weight for all neutrons emitted by my point source.
c     ------------------------------
c     In rea[illegible] presence of the SB (source-energy biasing) data in my MCNP [illegible]ut deck (as calculated
c     by the [illegible]ADJ.F program in my GETADJ.SCR script file) will cause the a[illegible]ing weights to be different
```

```
c       in each broad energy group, and would make those weights compatible with the "wtlo" weight window data
c       found in the above data statements.  The narrow-cone cosine-effect, however, must still be accounted
c       for separately, and that's what the following loop does.
c       ------------------------------
        wtcone=1.7332472e-2
        do 11 ie=1,10
        do 11 iz=1,imi
11      wtlo(iz,ie)=wtcone*wtlo(iz,ie)
c
c       ----------------------------------
c
c       Following info needed iff mhead(1)=2 or mhead(1)=3
c       such that one wants to write "in flight" directional biasing
c       info (ie, direction cosines from detector to each mesh).
c       For simplistic situations involving bulk shielding, this
c       very simplistic definition is good enough.  For more complex
c       situations with multiple streaming paths, one would really
c       want to enter the adjoint currents (aJx,aJy,aJz) instead.
c       See DO-LOOP 20 below.
c
c       The following (at least "imindx") is also needed if I want to assign
c       weight window info to cartesian mesh intervals "automatically" using
c       my simplistic "spherical shell" assignment algorithm.
c       See DO-LOOP 20 below.
c       ----------------------------------
        anx=ra(1)  ! total number of fine mesh in x-direction
        any=ra(2)  ! total number of fine mesh in x-direction
        anz=ra(3)  ! total number of fine mesh in x-direction
c
        nx=nint(anx)
        ny=nint(any)
        nz=nint(anz)
c
        xminn=ra(4)
        yminn=ra(5)
        zminn=ra(6)
c
        xmaxx=geomx(3)
        ymaxx=geomy(3)
        zmaxx=geomz(3)
c
        dx=(xmaxx-xminn)/anx
        dy=(ymaxx-yminn)/any
        dz=(zmaxx-zminn)/anz
c
c       ----------------------------------
c
        do 20 k=1,nz
        z=zminn+dz*(0.5+float(k-1))
c
        do 20 j=1,ny
        y=yminn+dy*(0.5+float(j-1))
c
        do 20 i=1,nx
        x=xminn+dx*(0.5+float(i-1))
c
        dist2=(x-xd)*(x-xd)+(y-yd)*(y-yd)+(z-zd)*(z-zd)
        dist=sqrt(dist2)      ! distance from detector location to center of each impotrance mesh
```

```
c
c       Set up importance region "index numbers" for each importance mesh interval;
c       When we get around to assigning actual energy-dependent weight windows, we'll
c       use these index numbers.  Here, I am simply going to assign weight window
c       index numbers to each 3-D XYZ mesh based on each mesh's distance from the detector
c       of interest -- ie, basically assign the same weight window values to all mesh
c       intervals within a given "spherical shell" (distance) from the detector location.
c       Note, however, that we must distinguish between those mesh that are between the
c       detector and the source, and those mesh that are downstream of the detector.
c       ----------------------------------
        indx=0
        if (z.le.zd) zloc=zd-dist  ! for mesh between the detector and the source
        if (z.gt.zd) zloc=zd+dist  ! for mesh that are downstream of the detector
        do iz=1,imi                ! imi=number of coarse mesh importance zones;  check each one
           if (zloc.ge.zmini(iz) .and. zloc.le.zmaxi(iz)) indx=iz  ! select importance region index number
        enddo
        if (indx.eq.0 .and. z.le.zd) indx=1
        if (indx.eq.0 .and. z.ge.zd) indx=imi
        imindx(i,j,k)=indx    ! used to assign weight window values to cartesian mesh using my simplified spherical shell algorithm
c
c       The following unit vectors will be used in place of rigorous
c       directional adjoint currents (aJx, aJy, aJz) for "on the fly"
c       directional biasing in MCNP4B:
c       ----------------------------------
        u(i,j,k)=(x-xd)/dist  ! (u,v,w) is a unit vector pointing from the detector to the center of each mesh
        v(i,j,k)=(y-yd)/dist  ! (u,v,w) is a unit vector pointing from the detector to the center of each mesh
        w(i,j,k)=(z-zd)/dist  ! (u,v,w) is a unit vector pointing from the detector to the center of each mesh
20      continue
c       ----------------------------------
c
c
c       Begin writing the wwinp file:
c       ----------------------------------
        write (7,'(4i10)')       (mhead(i),i=1,4)
        write (7,'(7i10)')       (ia(i),i=1,3)
        write (7,'(1p,6e13.5)') (ra(i),i=1,10)
        write (7,'(1p,6e13.5)') (geomx(i),i=1,4)
        write (7,'(1p,6e13.5)') (geomy(i),i=1,4)
        write (7,'(1p,6e13.5)') (geomz(i),i=1,4)
c       ----------------------------------
c
        write (7,'(1p,6e13.5)') (emaxi(i),i=1,6)  ! for the 6 broad neutron groups
c
        do ie=1,6  ! write weight window info for each of the 6 broad neutron groups
           write (7,'(1p,6e13.5)')
     *       (((wtlo(imindx(i,j,k),ie),
     *         u(i,j,k),v(i,j,k),w(i,j,k),
     *         i=1,nx),j=1,ny),k=1,nz)
        enddo
c
c       ----------------------------------
c
        write (7,'(1p,6e13.5)') (emaxi(i),i=7,10)    ! for the 4 broad gamma groups
c
        do ie=7,10  ! write weight window info for each of the 4 broad gamma groups
           write (7,'(1p,6e13.5)')
     *       (((wtlo(imindx(i,j,k),ie),
     *         u(i,j,k),v(i,j,k),w(i,j,k),
```

```
     *          i=1,nx),j=1,ny),k=1,nz)
          enddo
c         ---------------------------------
c
          return
          end
END-GETWIN



cat >gbainput1 <<'END-GBAINPUT1'
gbanisn: 1-d slab model of hb3 water tube & collimator
/
/*********************************
/
/ see description of revised input in section 6 of
/ charles slater's memo to dist, dated 4/7/88
/
/*********************************
/
15$$  /  15$$ = integer parameters
  1   /  id  = problem id number;  if .gt. 1000000, disadvantage factors will be computed by group for each material in calc
  1 / 0   /  ith = 0/1 = forward/adjoint calc
  3   /  isct = maximum order of scatter found in any zone
 32   /  isn = order of angular quadrature
  1   /  ige = 1/2/3 = slab/cyl/spherical geometry
  0   /  ibl = 0/1/2/3 = vacuum/reflection/periodic/white(albedo) = left boundary condition
  0   /  ibr = 0/1/2/3 = vacuum/reflection/periodic/white(albedo) = right boundary condition
  1 / 22   /  izm = number of zones or regions (same material)
251 / 719   /  im  = number of mesh intervals
  0   /  ievt = 0/1/2/3/4/5/6 = fixed src / k-calc / alpha / conc search / zone width search / outer radius search / buckling search
      /  ------- 10 -------
 84   /  igm = number of energy groups
  3   /  iht = position of sigt in xsect table
  4   /  ihs = position of g-g (self-scatter) in xsect table
 87   /  ihm =length of xsect table
  0   /  ms = mixing table length (10$$, 11$$, 12** arrays)
  0   /  mcr = number of xsect sets read from cards (14** array)
 32   /  mtp = number of xsect sets to be read from tape (13$$ array)
 32   /  mt  = total number of xsect sets (number entered + any mixtures created)
  0   /  idfm = 0/1 = density factors not used / density factors used (if used, enter 21** array)
  0   /  ipvt = 0/1/2 = no effect / enter initial keff (as pv in 16**) / enter initial alpha (as pv in 16**);  see page 25 for more notes
      /  ------- 20 -------
  1 / 0   /  iqm  = 0/1 = no effect / enter distributed source (in 17** array)
  0 / 1   /  ipm  = 0/1/im = no effect / enter shell src by grp and angle (18**) / enter shell src by interval, grp, and angle
  0 / 116   /  ipp  = interval number which contains shell src if ipm=1;  otherwise, set ipp=0
200   /  iim  = inner (spatial) iteration maximum
  0   /  id1  = -1/0/1/2/3 = no scalar flux or dist src print/ no effect / print angular flux / punch scalar flux / print angular flx and punch scalar flx
  1   /  id2  = 0/1/2 = no effect / read mtp xsect sets from tape in gip format / use xsects and fixed src from previous problem
  0   /  id3  = 0/N = no effect / compute N activities by zone, where N is any positive integer
  0   /  id4  = 0/1 = no effect / compute N activities by interval (where N=id3)
  1   /  icm  = outer (energy) iteration maximum
      /         icm note: if there is no fission, one may set icm=1 in "gbanisn" and it will cycle thru each of the thermal
      /         groups once and then repeat that cycle up to iim times (where iim is the "inner" iteration max) to converge
      /         the upscatter terms -- i.e., with group-banded anisn (and the bands properly defined in the 1$$ array)
      /         icm.gt.1 is not needed to converge upscatter, although icm.gt.1 would be needed if one allows fission.
  1   /  idat1= 0/1/2 = all data in core/ xsects & fixed sources stored on tape / fluxes & currents on tape also
      /         ****  must set idat1=1 if xsects come from a gip tape  ****
```

```
      /  ------- 30 -------
  0   /  idat2= 0 for no effect; idat2.gt.0, enter 24$$ array to select Sn, or diff theory, or inf hom media option by group for first "idat2" outers
  0   /  ifg = 0/1/2/3/4 = no effect/ do xsect weighting / read wtg xsects from prev calc / write wtd xsects (fort.10) / read & write
  3   /  iflu= 0/1/2/3/4 = (wtd diff model) = sometimes step/ linear only/ step only/ wtd diff / wtg with neg flx fixup
  1   /  ifn = 0/1/2 = enter fission guess (2**) / enter flux guess (3**) / use flux from prev case
  1   /  iprt= 0/1 = print xsects / don't print xsects
  2   /  ixtr= 0/1/2/3 as noted below:
      /     ixtr=0 no effect; start problem from scratch (requires 3** flux guess array in data block f)
      /     ixtr=1 read flux guess (on unit nt14); set ifn=1 and do not enter 3** array; do not include data block f at all
      /     ixtr=2 write flux soln (on unit nt15)
      /     ixtr=3 read flux guess on one unit (nt14), write flux solution on another unit (nt15)
  e   /  note: ixtr is now last parameter in 15$$ (not nbuf or nsav)
/
16**       /   16** = floating point parameters
    0      /   ev   = first guess for keff (usually 0.0)
    0      /   evm  = eigenvalue modifier
  1e-4     /   eps  = epsilon (accuracy desired)
  1.420892 /  0      /   bf   = buckling factor (normally 1.420892 if buckling is used; otherwise 0)
   27.2    /  0      /   dy   = cylinder or plane height for buckling correction
   27.2    /  0      /   dz   = plane depth for buckling correction
    0      /   dfm1 = transverse dimension for void streaming
    0      /   xnf  = source normalization factor (typ: 1 for keff, 0 for fixed src);  n/cm3 for sphere; n/cm2 for slab; n/cm(of height) for cyl
    0      /   pv   = enter:  0 / keff0 / alpha0, depending on value of ipvt (param 20 in 15$$ array)
   0.5     /   ryf  = lamda2 relaxation factor (normally 0.5)
           /  ------- 10 -------
  1e-4     /   xlal = point flux convergence criteria if .gt. 0
    0      /   xlah = upper limit for abs(1.0-lamda1) used in linear search
    0      /   eql  = eigenvalue change epsilon
    0      /   xnpm = new parameter modifier
   e
59$$    /  59$$ = array of unit numbers to be used (may skip entire array and take defaults)
    8   /  nt1  = 1st flux and current scratch unit if idat1=2 (default: fort.8)
    9   /  nt2  = 2nd flux and current scratch unit if idat1=2 (default: fort.9)
    1   /  nt3  = 1st xsect and source scratch unit if idat1.gt.0  (default: fort.1)
    2   /  nt4  = 2nd xsect and source scratch unit if idat1.gt.0  (default: fort.2)
    3   /  nt5  = angular flux output unit (default: fort.3)
    4   /  nt6  = anisn-formatted (nuclide oriented) binary xsect library (default: fort.4) if idat1.ne.1
    4   /  nt7  = gip-formatted    (group  oriented) binary xsect library (default: fort.4) if idat1=1
    2   /  nt8  = few-group xsect library output unit if ifg=3 or ifg=4 (default: fort.2)
    2   /  nt9  = few-group xsect library input  unit if ifg=2 or ifg=4 (default: fort.2)
   14   /  nt14 = flux guess input unit if ixtr=1 or ixtr=3 (default: fort.14)
   15   /  nt15 = flux output unit if ixtr=2 or ixtr=3 (default: fort.15)
    6   /  nt99 = unit number for fido edit of input (default: fort.6)
   e
60$$    /   60$$ new array required for canisn, janisn, and gbanisn (but not regualr anisn); only has one entry (kwrd)
  2400  /   kwrd = thousands of real*4 words to be alocated for storage;  typ:  400 req'd for s4;  500 for s8;  900 for s16
   e
 t      / end of data block b;  t is always required   (there is no data block a; that's the title card)
/
/
/
1$$     /  number of groups in each band; if nbands.lt.igm (as usually the case) fill with zeros; igm entries required anyway
   f1   /  use this for VELM 61n/23g
/  14r1  25  44r1  f0  / use this for ANSLV 39n/44g; yields 1 grp per band in 1st 14 bands, and 25 groups in band 15; and 1 grp per band in the 44 gamma ban
ds
/
/ these 2$$ a[illegible]* arrays here were only needed in a very special burnup-dep[illegible]nt version of the group-banded anisn code
/ that bob chi[illegible] wrote especially for jim bucholz on the mhtgr project in 19[illegible] these two arrays are not part of the
```

```
/ regular group-banded anisn code and should not be entered (they're listed here only as a reminder to me)
/ 2$$  24  e  /  2$$ number of burnup intervals (used only in bob child's version)     ..... this 2$$ not standard
/ 3**  2.  e  /  3** length of burnup intervals in years (used only in bob's version) ..... this 3** not standard
 t      / end of data block c;  t is always required   (this data block has only the 1$$ array and is reqd by std gb-anisn)
/
/
/ 13$$ id numbers for nuclides or macroscopic materials in 'premixed' xsect library
/      but "only if" supplied in anisn-formatted (nuclide oriented) binary library;
/      this array allows the code to strip off just the nuclides it needs from tape;
/      not needed should not be entered if idat1=1 and input xsects are from gip tape
/ 13$$ / mtp entries; not needed when input xsects are from gip tape
/ 14** cross sections entered off cards if mcr.gt.0
/  t      / end of data block d;  t is required if 13$$ or 14** are entered; otherwise this t should be skipped
/
/
/
/ 17** fixed source specifications (im*igm entries reqd if iqm=1)
/   source in each mesh interval for group 1
/   source in each mesh interval for group 2
/   source in each mesh interval for group 3
/     :     :  :    :      :      :    :   :
/   source in each mesh interval for group 27
/   ... these may all be renormalized using xnf
/ 17**  /  values are n/s/cc;  remember to use "lower case" e's for exponents, not upper case e's
/      144r0  18r7.02795e+12   36r6.55051e+12  18r8.15472e+12  183r0   /  group  1  (halfway up top sect of ans core)   1.9097700e-02
/      144r0  18r7.22984e+13   36r6.73868e+13  18r8.38897e+13  183r0   /  group  2  (halfway up top sect of ans core)   2.1556070e-01
/      144r0  18r8.24511e+13   36r7.68498e+13  18r9.56702e+13  183r0   /  group  3  (halfway up top sect of ans core)   4.3961270e-01
/      144r0  18r4.65807e+13   36r4.34163e+13  18r5.40488e+13  183r0   /  group  4  (halfway up top sect of ans core)   5.6619070e-01
/      144r0  18r6.05776e+13   36r5.64623e+13  18r7.02897e+13  183r0   /  group  5  (halfway up top sect of ans core)   7.3080370e-01
/      144r0  18r6.35937e+13   36r5.92735e+13  18r7.37895e+13  183r0   /  group  6  (halfway up top sect of ans core)   9.0361270e-01
/      144r0  18r3.04993e+13   36r2.84274e+13  18r3.53892e+13  183r0   /  group  7  (halfway up top sect of ans core)   9.8649130e-01
/      144r0  18r4.61450e+12   36r4.30101e+12  18r5.35432e+12  183r0   /  group  8  (halfway up top sect of ans core)   9.9903070e-01
/      144r0  18r3.33162e+11   36r3.10529e+11  18r3.86576e+11  183r0   /  group  9  (halfway up top sect of ans core)   9.9993600e-01
/      144r0  18r2.47229e+10   36r2.30433e+10  18r2.86866e+10  183r0   /  group 10  (halfway up top sect of ans core)   1.0000030e+00
/       f0
/ 17** fixed source specifications (im*igm entries reqd if iqm=1)
/ volumetric source:  (src(i,g),i=1,im=719),g=1,84)
/
/ the following flux-to-dose-rate factors are now being treated as an adjoint source: (note: must use adjoint dort-ready xsects)
17**   / volumetric source:  (src(i,g),i=1,im=251),g=1,84)
    250z 1.9465e-1  250z 1.5977e-1  250z 1.4706e-1  / flux-to-dose-rate conv factors for neutron groups 1, 2, 3
    250z 1.4723e-1  250z 1.5118e-1  250z 1.5411e-1  / flux-to-dose-rate conv factors for neutron groups 4, 5, 6
    250z 1.4596e-1  250z 1.3694e-1  250z 1.2849e-1
    250z 1.2527e-1  250z 1.2562e-1  250z 1.2615e-1
    250z 1.2721e-1  250z 1.2864e-1  250z 1.3008e-1
    250z 1.2975e-1  250z 1.1804e-1  250z 1.0554e-1
    250z 9.5577e-2  250z 9.0488e-2  250z 8.3046e-2
    250z 6.6330e-2  250z 5.8498e-2  250z 5.8080e-2
    250z 5.7731e-2  250z 5.5626e-2  250z 4.9373e-2
    250z 4.1241e-2  250z 3.4447e-2  250z 2.8773e-2
    250z 2.2781e-2  250z 1.6688e-2  250z 1.3503e-2
    250z 1.1148e-2  250z 8.7422e-3  250z 7.9520e-3
    250z 7.6770e-3  250z 7.4241e-3  250z 7.1386e-3
    250z 5.8975e-3  250z 4.0874e-3  250z 3.5585e-3
    250z 3.5825e-3  250z 3.6062e-3  250z 3.6229e-3
    250z 3.6387e-3  250z 3.6528e-3  250z 3.6908e-3
    250z 3.7629e-3  250z 3.8453e-3  250z 3.9356e-3
    250z 4.0311e-3  250z 4.1289e-3  250z 4.2492e-3
```

```
    250z 4.3820e-3  250z 4.4897e-3  250z 4.5583e-3
    250z 4.5742e-3  250z 4.5250e-3  250z 4.3706e-3  / flux-to-dose-rate conv factors for neutron groups 58,59,60
    250z 3.7090e-3  250z 1.1020e-2  250z 8.7716e-3  / f-to-d conv factors for neut-group 61 and gamma-grps 1 & 2
    250z 7.8468e-3  250z 7.4783e-3  250z 6.9265e-3  / flux-to-dose-rate conv factors for gamma groups 3, 4, 5
    250z 6.1909e-3  250z 5.4136e-3  250z 4.6221e-3
    250z 3.9596e-3  250z 3.4686e-3  250z 2.9270e-3
    250z 2.3156e-3  250z 1.7563e-3  250z 1.4417e-3
    250z 1.2797e-3  250z 1.0852e-3  250z 8.7594e-4
    250z 5.6676e-4  250z 3.2767e-4  250z 2.6644e-4
    250z 2.7466e-4  250z 5.7761e-4  250z 2.1439e-3  / flux-to-dose-rate conv factors for gamma groups 21,22,23
/ 17**  a15312  f0  / use this to zero-out the adjoint source for gammas if we only care about the direct neutron dose rate
/
/ 18** shell source specifications (not reqd if ipm=0,  mm*igm entries reqd if ipm.eq.1,  mm*im*igm entries reqd if ipm.gt.1)
/   note: for adjoint calcs, the angular dependent adjoint source must
/   be supplied as if it were reflected thru the origin)
/   Below:  Source(33)=ScalarFlux(monodirectional)/Weight(33)
/ 18**  / based on full 100 MW power n/g from core, including decay fission gammas from core.
/       The following angular fluxes for quadrature direction 33 = (scalar flux)/(weight 33).
/
/   1-D slab GBANISN sources impingent on the old 1960 water tube and/or the new 1998 water
/   tube in the HFIR HB3 beam tube, based on the equivalent point sources in SRC-DESC.SUM;
/   these forward-directed shell sources in direction 33 (of an S32 1-D slab quad set) were
/   computed using the utility program SRC1D.FOR as:
/   SRC(grp ig, direction 33)= (PtSrc(ig)/[4*pi*(X-X0)^2])/weight(33)
/   where the multigroup PtSrc for HB3 is given in ref dataset SRC-DESC.SUM,
/   where X0(ig), the effective center of emmission for group (ig) in HB3, is
/   given in SRC-DESC.SUM (X0=dist in cm from the plane perpendicular to the tube),
/   where x = x1=116.7841 cm = the point where the old 1960 water tube began
/   and   x = x2=174.27   cm = the point where the new 1998 water tube begins
/
/   impingent neutron src on old 1960 water tube (at X=116.7841 cm), for neutrons in HB3 (velm grp=1,61),  fast=grp 01
/    32z 1.13006e+08 32z 1.10592e+10 32z 4.38227e+10 32z 6.55516e+10
/    32z 2.61608e+11 32z 5.44950e+11 32z 5.09834e+11 32z 5.29409e+11
/    32z 1.06623e+12 32z 2.95410e+11 32z 3.36529e+11 32z 8.76827e+11
/    32z 2.26008e+12 32z 2.90345e+12 32z 1.69825e+12 32z 2.90497e+12
/    32z 1.47587e+12 32z 1.74368e+12 32z 9.58689e+11 32z 4.29052e+11
/    32z 2.04155e+12 32z 1.63431e+12 32z 7.72646e+10 32z 2.26409e+10
/    32z 5.78337e+10 32z 4.50956e+11 32z 1.26373e+12 32z 1.10214e+12
/    32z 7.71693e+11 32z 9.92951e+11 32z 1.29692e+12 32z 2.16579e+12
/    32z 4.21110e+11 32z 1.42750e+12 32z 2.60124e+12 32z 5.88214e+11
/    32z 2.09517e+11 32z 2.69366e+11 32z 3.43813e+11 32z 2.20686e+12
/    32z 2.64203e+12 32z 2.50082e+12 32z 2.19740e+12 32z 1.47693e+12
/    32z 7.83043e+11 32z 7.16313e+11 32z 4.41240e+11 32z 3.28332e+12
/    32z 3.23922e+12 32z 2.48747e+12 32z 2.80919e+12 32z 2.63519e+12
/    32z 2.86782e+12 32z 4.53851e+12 32z 4.99220e+12 32z 3.96223e+12
/    32z 4.69230e+12 32z 9.22237e+12 32z 6.73971e+12 32z 7.47705e+12
/    32z 5.52139e+14
/  impingent gamma src on old 1960 water tube (at X=116.7841 cm), for gammas in HB3 (velm grp=61,84), fast=grp 63
/    32z 3.84536e+09 32z 2.54725e+12 32z 3.55596e+13 32z 4.34705e+12
/    32z 2.76192e+13 32z 1.90569e+13 32z 4.18079e+13 32z 4.70888e+13
/    32z 4.10847e+13 32z 1.01212e+14 32z 1.25714e+14 32z 1.15144e+14
/    32z 9.54013e+13 32z 4.19883e+13 32z 7.18706e+13 32z 8.17303e+13
/    32z 9.83029e+13 32z 2.88737e+14 32z 1.98233e+14 32z 1.63428e+14
/    32z 8.16257e+13 32z 1.10727e+13 32z 8.97349e+09
/  impingent neutron src on new 1998 water tube (at X=174.27 cm), for neutrons in HB3 (velm grp=1,61),  fast=grp 01
/    32z 5.824[illegible]+06 32z 3.96115e+09 32z 9.09120e+09 32z 2.07345e+10
/    32z 6.51[illegible]10 32z 1.28300e+11 32z 1.51488e+11 32z 1.37816e+11
/    32z 2.380[illegible]11 32z 9.27745e+10 32z 1.18026e+11 32z 2.45799e+11
```

```
/    32z 6.50926e+11 32z 7.20780e+11 32z 5.11900e+11 32z 5.83437e+11
/    32z 4.60156e+11 32z 4.54658e+11 32z 2.75728e+11 32z 1.18870e+11
/    32z 5.14801e+11 32z 4.74618e+11 32z 2.46126e+10 32z 6.19803e+09
/    32z 1.33040e+10 32z 1.43484e+11 32z 4.39295e+11 32z 3.23138e+11
/    32z 2.45247e+11 32z 3.03906e+11 32z 3.96441e+11 32z 6.47767e+11
/    32z 1.09982e+11 32z 3.95492e+11 32z 3.98678e+11 32z 1.25329e+11
/    32z 4.93277e+10 32z 8.12988e+10 32z 7.08402e+10 32z 6.01394e+11
/    32z 7.55624e+11 32z 6.94913e+11 32z 6.05180e+11 32z 3.31031e+11
/    32z 2.10124e+11 32z 2.08309e+11 32z 1.39402e+11 32z 8.03580e+11
/    32z 7.82793e+11 32z 6.92223e+11 32z 7.67867e+11 32z 7.49416e+11
/    32z 7.57499e+11 32z 1.21027e+12 32z 1.30806e+12 32z 1.17264e+12
/    32z 1.26895e+12 32z 1.58393e+12 32z 1.50752e+12 32z 1.93367e+12
/    32z 8.35086e+13
/  impingent gamma src on new 1998 water tube (at X=174.27 cm), for gammas in HB3 (velm grp=61,84), fast=grp 63
/    32z 2.44520e+08 32z 1.31290e+11 32z 2.79299e+12 32z 3.06526e+11
/    32z 2.23919e+12 32z 1.30586e+12 32z 3.53816e+12 32z 4.12907e+12
/    32z 2.77455e+12 32z 5.55316e+12 32z 8.30330e+12 32z 9.51037e+12
/    32z 1.12103e+13 32z 5.71012e+12 32z 7.70454e+12 32z 1.04867e+13
/    32z 1.41704e+13 32z 3.73438e+13 32z 2.62482e+13 32z 2.31424e+13
/    32z 1.71632e+13 32z 2.64146e+12 32z 3.79191e+09
/
/  end of source specifications
/  18**  2013z e  / zero-out all neutron sources to run gamma-only calc
/
 t  / end of data block e;  t is required if 17** or 18** are entered; otherwise this t should be skipped
/
/
/
/ 2**  fission density; im entries required; enter only if ifn=0 (34th param in 15$$) and ixtr=0 (36th param in 15$$ array)
/ 3**  flux guess ((flx(i,g),i=1,im),g=1,igm); enter only if ifn=1 (34th param in 15$$) and ixtr=0 (36th param in 15$$ array)
3** f0              / setting ifn=1 and filling 3** with f0 is recommended for shielding work
 t  / end of data block f;  t is required if 2** or 3** are entered; otherwise this t should be skipped
/
/
/
1**  / chi(g) fission spectrum; igm entries; not needed if no fissionable material present (if not needed, manual says enter f0)
       f0
/
5**  / avg velocity for each energy group; usually not needed (if not needed, manual says enter f0)
       f0
/
6**   / 1-D xsdrnpm quadrature weights (ige=1 isn=32  mm=  33)
    0.00000e+00  6.78811e-03  1.55634e-02  2.37896e-02  3.11572e-02
    3.73990e-02  4.22891e-02  4.56509e-02  4.73627e-02  4.73627e-02
    4.56509e-02  4.22891e-02  3.73990e-02  3.11572e-02  2.37896e-02
    1.55634e-02  6.78811e-03  6.78811e-03  1.55634e-02  2.37896e-02
    3.11572e-02  3.73990e-02  4.22891e-02  4.56509e-02  4.73627e-02
    4.73627e-02  4.56509e-02  4.22891e-02  3.73990e-02  3.11572e-02
    2.37896e-02  1.55634e-02  6.78811e-03
7**   / 1-D xsdrnpm direction cosines  (ige=1 isn=32  mm=  33)
   -1.00000e+00 -9.94700e-01 -9.72288e-01 -9.32816e-01 -8.77702e-01
   -8.08938e-01 -7.29008e-01 -6.40802e-01 -5.47506e-01 -4.52494e-01
   -3.59198e-01 -2.70992e-01 -1.91062e-01 -1.22298e-01 -6.71844e-02
   -2.77125e-02 -5.29953e-03  5.29953e-03  2.77125e-02  6.71844e-02
    1.22298e-01  1.91062e-01  2.70992e-01  3.59198e-01  4.52494e-01
    5.47506e-01  6.40802e-01  7.29008e-01  8.08938e-01  8.77702e-01
    9.32816e-01  9.72288e-01  9.94700e-01
/
```

```
/ 4**  / location of each interval boundary; im+1 entries required
/ 4**  0.0  24i10.01  35.56  35.57   / mesh boundaries
/ 4**  0.0  24i10.01  19.06  19.07   / mesh boundaries
/ 4**  0.0  24i10.01  27.95  27.96   / mesh boundaries
/ 4**  8.0 3i9.0 3i10.0 15i12.54 3i109.06 2i111.6 31i112.6 143.08  / mesh boundaries
/ 4**  / 720 mesh boundaries required here (for these 719 mesh intervals):
/      115.0  2i116.7841  111i117.7366  2i174.27  7i174.95125  7i179.05
/      7i183.15  7i187.25  7i191.35  7i195.45  7i199.55  7i203.65
/      189i207.75  2i302.1868  15i302.5043  49i310.58  2i334.7709
/      127i335.4756  2i399.48  14i401.9445  124i415.44875
/      2i477.36125  478.79
4**  / 252 mesh boundaries required here (for these 251 mesh intervals):
     249i175.0  300.0  300.1
/
/ 8$$  / zone numbers by mesh interval (im entries required)
/      1  3r2  112r3  3r4  8r5  8r6  8r7  8r8  8r9  8r10  8r11  8r12
/      190r13  3r14  16r15  50r16  3r17  128r18  3r19  15r20  125r21
/      3r22
8$$  / zone numbers by mesh interval (im entries required)
     251r1
/
/ 9$$    /  material numbers by zone (izm entries required); material numbers should correspond to p0 components only
/   9    /  1st zone always void; 1.7841 cm thick (thickness doesn't matter in slab geometry)
/   9    /  2nd zone void here;  1st aluminum window in 1960 design would go here
/   9    /  3rd zone void here;  use water if looking at 1960 design
/   5    /  4th zone aluminum = 1st window in 1998 design;  would be water for 1960 design
/   1    /  5th zone water (first 4.1 cm in 1998 design)
/   1    /  6th zone water (next 4.1 cm in 1998 design)
/   1    /  7th zone water (next 4.1 cm in 1998 design)
/   1    /  8th zone water (next 4.1 cm in 1998 design)
/   1    /  9th zone water (next 4.1 cm in 1998 design)
/   1    / 10th zone water (next 4.1 cm in 1998 design)
/   1    / 11th zone water (next 4.1 cm in 1998 design)
/   1    / 12th zone water (next 4.1 cm in 1998 design)
/   1    / 13th zone water (remainder of water in 1998 water tube design)
/   5    / 14th zone aluminum = 2nd window in 1998 design;  would be water for 1960 design
/   1    / 15th zone water
//  ------------------------------ may wish to make next 3 zones: all water (1), all stainless steel (13), or all carbon steel (17)
/   1    / 16th zone water here; may later try stainless steel or carbon steel;
/   1    / 17th zone water here; may later try stainless steel or carbon steel; use aluminum iff modeling 1960 water tube design
/   1    / 18th zone water here; may later try stainless steel or carbon steel;
//  ------------------------------ previous 3 zones represent the collimator section
/   9    / 19th zone thin void at end of collimator (need incoming flux here)
/   9    / 20th zone void upstream of carbon steel shutter drum
/  17    / 21th zone carbon steel shutter drum
/   9    / 22th zone thin void
9$$  f1 /  material numbers by zone (izm entries required); material numbers should correspond to p0 components only
/
/  end of 9$$ array (although user may use the "plugdef" file to redefine the entire 9$$ array
/
/  list of possible materials (with this HB3 water tube xsect lib) includes the following:
/
/   mix  1  (ANISN/DORT MATL  1) = Water at 1.00 g/cc
/   mix  2  (ANISN/DORT MATL  5) = Aluminum 6061 (2.7 g/cc)
/   mix  3  (ANISN/DORT MATL  9) = Void (He @ 1.0e-20 atoms/barn*cm)
/   mix  4  (ANISN/DORT MATL 13) = SS304 (7.92 g/cc;  see page 50 of ORNL/TM-11989)
/   mix  5  (ANISN/DORT MATL 17) = Carbon Steel (7.8212 g/cc, 99 wt% Fe, 1 wt'
/   mix  6  (ANISN/DORT MATL 21) = Barytes Concrete at 3.09725 g/cc
```

```
/   mix  7  (ANISN/DORT MATL 25) = Regular Concrete
/   mix  8  (ANISN/DORT MATL 29) = response functions
/
END-GBAINPUT1



cat >gbainput2 <<'END-GBAINPUT2'
/
/
/ note: anisn reads macroscopic cross sections for materials that
/ have been premixed elsewhere (in this case materials 1 to 52).
/ it also allows us to use these to create some secondary materials
/ (like materials 53, 57, 61, 65, 69, and 73), as described below:
/ ================================================================
/
/10$$ / mixture numbers in mixing table:
/       4r-53 4r-57 4r-61 4r-65 4r-69 4r-73   / irrelevant here, but shown as an example
/
/11$$ / component numbers (like nuclid numbers) in mixing table:
/       0 41 45 49 5q4                        / irrelevant here, but shown as an example
/
/12** / number densities (atoms/barn*cm):
/       reset   ss      b-10        b-11      / irrelevant here, but shown as an example
/         0    1.0   6.79702e-3   1.67426e-3  / densities for 1st row of pins (mix 53):
/         0    1.0   6.79702e-3   1.67426e-3  / densities for 2nd row of pins (mix 57):
/         0    1.0   6.79702e-3   1.67426e-3  / densities for 3rd row of pins (mix 61):
/         0    1.0   6.79702e-3   1.67426e-3  / densities for 4th row of pins (mix 65):
/         0    1.0   6.79702e-3   1.67426e-3  / densities for 5th row of pins (mix 69):
/         0    1.0   6.79702e-3   1.67426e-3  / densities for 6th row of pins (mix 73):
/ ================================================================
/
/
/ 16$$ is peculiar to gb-anisn;  always use f1 to specify that all
/ angular fluxes should always be continuous across media boundaries
16$$ f1
/
/ 19$$ order of scatter by zone
  19$$ f3
/
/ 20** radius modifiers by zone (required iff ievt=4)
/
/ 21** density factors by interval (required iff idfm=1)
/
/ 22$$ material numbers used for activities; refers to p0 components; use minus sign; id3 entries required (iff id3.gt.0)
/ 22$$ -49  / material number for b-10
/
/ 23$$ xsect table position for activities; id3 entries required (iff id3.gt.0)
/ 23$$ 1    / absorption in b-10
/
/ 24$$ calculation type markers; igm entries required, but iff idat2=1;  0/1/2 = sn / diff-th / inf-hom-media
/
/ 25**  right boundary albedo by group; igm entries required, if ibr=3 (otherwise not required)
/
/ 26**  left  boundary albedo by group; igm entries required, if ibl=3 (otherwise not required)
/
/ 27$$  few group parameters; 5 entries required, but only if ifg=1 (otherwise array not needed)
/       /  icon = 0/1/2 = no effect / micro xsects desired / macro xsects desired;   (minus implies cell weighting)
```

```
/       /  ihtf = position of sigma total in weighted xsects
/       /  ihsf = position of g-to-g scatter in weighted xsects;  (minus implies upscatter removal)
/       /  ihmf = table length of weighted xsects
/       /  ipun = -1/0/1 = write nuclide tape on fort.10 / no effect / punch wtd xsects (free-form on fort.7)
/   e   /  end of 27$$
/
/ 28$$  /  broad-group number for each fine group; igm entries required, if ifg=1 (otherwise not required)
/        5r1  7r2  10r3  3r4  6r5  10r6  12r7  7r8  9  / broad adjoint groups for neutrons
/        7r10  5r11  5r12  6r13                        / broad adjoint groups for gammas
/
 t  / end of data block g;  this t is always required
END-GBAINPUT2


#  cat  gbainput1  $RTNDIR/plugdef  gbainput2  > gbainput
cat  gbainput1  gbainput2  > gbainput

#  ln -s  /u/mnt4/jab/hfir/water-tube.hb3/dort.xsects/xsects.dort-ready.bin.hfir.hb3.watertube.01may98  fort.4  # link dort-ready xsects to fort.4 for use i
n GBANISN
#  ln -s  /u/mnt4/jab/hfir/water-tube.hb3/dort.xsects/adjoint.xsects.dort-ready.bin.hfir.hb3.watertube.14may98  fort.4  # link dort-ready xsects to fort.4 f
or use in GBANISN

ln -s  /work1/jab/dort.xsects/adjoint.xsects.dort-ready.bin.hfir.hb3.watertube.14may98  fort.4  # link dort-ready xsects to fort.4 for use in GBANISN

#   For this particular library:
#
#   mix  1  (ANISN/DORT MATL  1) = Water at 1.00 g/cc
#   mix  2  (ANISN/DORT MATL  5) = Aluminum 6061 (2.7 g/cc)
#   mix  3  (ANISN/DORT MATL  9) = Void (He @ 1.0e-20 atoms/barn*cm)
#   mix  4  (ANISN/DORT MATL 13) = SS304 (7.92 g/cc;  see page 50 of ORNL/TM-11989)
#   mix  5  (ANISN/DORT MATL 17) = Carbon Steel (7.8212 g/cc, 99 wt% Fe, 1 wt% C)
#   mix  6  (ANISN/DORT MATL 21) = Barytes Concrete at 3.09725 g/cc
#   mix  7  (ANISN/DORT MATL 25) = Regular Concrete
#   mix  8  (ANISN/DORT MATL 29) = response functions

gbanisn  <gbainput  >gbaoutput
xlf getwin8.f -o getwin8
getwin8

#  cp -p gbaoutput $RTNDIR/gbaoutput.175-300cm.buck
#  cp -p fort.15 $RTNDIR/gbadjnt.fort.15.175-300cm.buck
#  cp -p getadj.out $RTNDIR/getadj.out.175-300cm.buck

cp -p getadj.out $RTNDIR/getadj.out
cp -p wwinp $RTNDIR/wwinp

#  cat  $RTNDIR/plugdef getdose.out >>  $RTNDIR/results

rm *           # dangerous !!! be careful what subdirectory you are in
cd $RTNDIR
rmdir $TMPDIR

#  !!!
#  echo  "Job will be run in "  $TMPDIR
```

Appendix C.5

Listing of the MCNP4B input file (WWT08) used in the solution of the academic water tank problem described in Appendix C.2. Note that successful solution of this problem requires the use of the 3-D broad-group "geometry-independent weight window" file described in Appendices C.2 and C.4.

```
message:  outp=wwt08.o  runtpe=wwt08.r  wwinp=wwinp

Academic test of geometry-independent weight windows
c
c     BEGIN CELLS:
c
101  61  -1.0e-20   -1001         9997  -1003  imp:n=1  imp:p=1   $ void inside  central source tube
102  61  -1.0e-20    1001  -9999  9997  -1003  imp:n=0  imp:p=0   $ void outside central source tube
c
201   8   -1.0000   -1002         1003  -1004  imp:n=1  imp:p=1   $ water shield, central portion  <-- want flux dist axially in here
202   8   -1.0000   -1002         1004  -1005  imp:n=1  imp:p=1   $ water shield, central portion  <-- want dose rates in this last 0.1 cm
203   8   -1.0000    1002  -9999  1003  -1005  imp:n=1  imp:p=1   $ water shield, outside central portion
c
300  61  -1.0e-20   -9999   1005        -9998  imp:n=1  imp:p=1   $ void beyond water shield
c
900   0  #(-9999 9997 -9998)                  imp:n=0  imp:p=0   $ external void
c
c     END CELLS (next line must be blank)

c     BEGIN SURFACES:
1001  cz   5.0   $ Cylindrical void OD
1002  cz  10.0   $ radius of central region of interest
1003  pz  175.0  $ start of water
1004  pz  299.99 $ almost at end of water (added so I could have a volumetric n+g dose rate tally in last 0.01 cm)
1005  pz  300.0  $ end of water
c
c      9997   pz    0.0  $ External void boundary (location corresponds to the real radial plane perpendicular to the real beam tube)
9997   pz    0.1  $ External void boundary (Z=0.0 corresponds to the real radial plane perpendicular to the real beam tube)
c      9998   pz  700.0  $ External void boundary (far enough out to encompass point where Blosser & Thomas made measurements in 1968)
9998   pz  324.9  $ External void boundary (shortened up so wwinp file won't have to be so big)
9999   cz   65.0  $ External void boundary (radial extent of this model)
c
c     Surfaces used for tally segment dividers:
5120  pz  175.0   $ same as surf 1003
5121  pz  180.0
5122  pz  185.0
5123  pz  190.0
5124  pz  195.0
5125  pz  200.0
5126  pz  205.0
5127  pz  210.0
5128  pz  215.0
5129  pz  220.0
5130  pz  225.0
5131  pz  230.0
5132  pz  235.0
5133  pz  240.0
5134  pz  245.0
5135  pz  250.0
5136  pz  255.0
5137  pz  260.0
5138  pz  265.0
5139  pz  270.0
5140  pz  275.0
5141  pz  280.0
5142  pz  285.0
5143  pz  290
5144  pz  295
```

```
5145  pz  300.0   $ same as surf 1005
c
c     END SURFACES (next line must be blank)

c     PROBLEM PARAMETERS:
mode   n p
c      mode   n
c      nps    240000
c      nps    100000
c      nps    96000
c      nps    24000000
nps    96000000
c      cut:n  time(shakes) energy(MeV)   WC1   WC2   SWTM
c      cut:n         1.0e20          0.027     -0.5  -0.25   0.0  $ cutoff:  don't track any neutrons below 27 keV
print  60      $ Table 60 shows vol, mass, n-imp by cell; see pp 3-117 of manual for description of other useful tables you may want
prdmp  0   480000  0  4  0   $ make restart file after every 80000 histories in fixed src calc; save only the 4 most recent restart files
c      prdmp  0   80000  0  4  0   $ make restart file after every 80000 histories in fixed src calc; save only the 4 most recent restart files
c      prdmp  0   8000  0  4  0   $ make restart file after every 80000 histories in fixed src calc; save only the 4 most recent restart files
c      wwp:n  5  3  5  0  -1       $ 5th parameter is negative to make MCNP4B read the weight window importance file (wwinp)
c      wwp:n  5  3  5  0  1
c      ------------------------------------------------------------------------------------
c      To be consistent with the wwinp file & the biased source dist
c      (see GETADJ.FOR, as embedded in GATADJ.SCR), make sure you have
c      WUPN=WTHI= 100*WTLOW  and  WTSURV=WTAVG= 10*WTLOW  on the WWP:n and WWP:p  cards
c      ------------------------------------------------------------------------------------
c      WWP:n  wupn  wsurvn  mxspln  mwhere  switchn
c       wwp:n  100  10  100  0  -1       $ 5th parameter is negative to make MCNP4B read the weight window importance file (wwinp)
c       wwp:p  100  10  100  0  -1       $ 5th parameter is negative to make MCNP4B read the weight window importance file (wwinp)
wwp:n  100  10  50  0  -1       $ 5th parameter is negative to make MCNP4B read the weight window importance file (wwinp)
wwp:p  100  10  50  0  -1       $ 5th parameter is negative to make MCNP4B read the weight window importance file (wwinp)
c       wwp:n  100  10  10  0  -1       $ 5th parameter is negative to make MCNP4B read the weight window importance file (wwinp)
c       wwp:p  100  10  10  0  -1       $ 5th parameter is negative to make MCNP4B read the weight window importance file (wwinp)
c      ------------------------------------------------------------------------------------
c
c
c     EQUIVALENT POINT SOURCES:
c
sdef   erg=d53  pos 0 0 50  $ source def for neutrons in HB-3 (total n/s = 9.64595E+16);  total n/s above 27 keV = 1.20830e16
       par=1            $ par=1 for neut, par=2 for photons
       vec  0  0  1     $ reference vector if directional-dependent source is used
       dir=d3           $ angular distribution wrt vec (Caution: choice of angular distribution sampled will dictate choice of wgt)
       wgt=1.7332472-2  $ use this with d3;  wgt = [mu(max)-mu(min)]/[(+1)-(-1)] = [1.0000000000-0.965335056]/2 = 1.7332472-2
c      -------------------
c     Ang Dist: to spray isotropically across central void of HB-3 beam tube
si3    h  0.965335056   1.0  $ angular distribution;  mu boundaries (i.e, cosine boundaries wrt vec)
sp3    d  0  1  $ angular distribution; particle emmission probabilities by bin; first value (below lowest bin bound) must be zero
c      -------------------
c
c        ---------------------------------------------------------------------------
c        Begin distributions needed to describe the neutron sources in the HB-3 beam tube
c        ---------------------------------------------------------------------------
si53   h  1.0000e-11  $ this one Emin(MeV), followed by Emax(MeV) for the 61 VELM neut grps (lowest to highest energy for MCNP):
          4.1399e-7    1.1253e-6    2.3824e-6    5.0435e-6    1.0677e-5    $ VELM n-groups 61, 60, 59, 58, 57,
          2.2603e-5    4.7851e-5    1.0130e-4    1.6702e-4    2.7536e-4    $ VELM n-groups 56, 55, 54, 53, 52,
          4.5400e-4    7.4852e-4    1.2341e-3    2.0347e-3    2.2487e-3    $ VELM n-groups 51, 50, 49, 48, 47,
          2.6126e-3    3.0354e-3    3.7074e-3    5.5308e-3    9.1188e-3    $ VELM n-groups 46, 45, 44, 43, 42,
          1.5034e-2    2.3579e-2    2.4788e-2    2.6058e-2    2.7000e-2    $ VELM n-groups 41, 40, 39, 38, 37,
          2.8501e-2    3.4307e-2    5.2475e-2    5.6562e-2    8.6517e-2    $ VELM n-groups 36, 35, 34, 33, 32,
```

```
        1.2277e-1    1.4996e-1    1.8316e-1    2.2371e-1    2.7324e-1    $ VELM n-groups 31, 30, 29, 28, 27,
        2.9452e-1    2.9721e-1    2.9849e-1    3.0197e-1    3.8774e-1    $ VELM n-groups 26, 25, 24, 23, 22,
        4.9787e-1    5.2340e-1    6.0810e-1    7.4274e-1    9.0718e-1    $ VELM n-groups 21, 20, 19, 18, 17,
        1.1080e+0    1.3534e+0    1.6530e+0    2.0190e+0    2.2313e+0    $ VELM n-groups 16, 15, 14, 13, 12,
        2.3457e+0    2.4660e+0    3.0119e+0    3.6788e+0    4.4933e+0    $ VELM n-groups 11, 10,  9,  8,  7,
        5.4881e+0    6.7032e+0    8.1873e+0    1.0000e+1    1.2214e+1    $ VELM n-groups  6,  5,  4,  3,  2,
        1.4918e+1                                                      $ VELM n-group   1
sp53  d     0.0  $ dummy 0, followed by neut src terms (n/s) for HB-3:
c       Unbiased neutron sources in MCNP order (grp 1=low E, grp 61=high E):
        6.30365e+16  2.25679e+15  1.52979e+15  1.30212e+15  1.55274e+15  $ VELM n-groups 61, 60, 59, 58, 57,
        1.58981e+15  1.54759e+15  1.45876e+15  9.03837e+14  9.69821e+14  $ VELM n-groups 56, 55, 54, 53, 52,
        9.50610e+14  8.74122e+14  8.53691e+14  8.87245e+14  2.04908e+14  $ VELM n-groups 51, 50, 49, 48, 47,
        2.76622e+14  2.54975e+14  3.36538e+14  7.55438e+14  8.76077e+14  $ VELM n-groups 46, 45, 44, 43, 42,
        9.84217e+14  7.42049e+14  6.69650e+13  1.12860e+14  5.24714e+13  $ VELM n-groups 41, 40, 39, 38, 37,
        1.21873e+14  3.03507e+14  4.96958e+14  1.29680e+14  8.89397e+14  $ VELM n-groups 36, 35, 34, 33, 32,
        5.59006e+14  4.29193e+14  3.63241e+14  4.33245e+14  7.35199e+14  $ VELM n-groups 31, 30, 29, 28, 27,
        2.12840e+14  1.38494e+13  7.68584e+12  3.65651e+13  6.29256e+14  $ VELM n-groups 26, 25, 24, 23, 22,
        5.85513e+14  1.49367e+14  3.61470e+14  5.35177e+14  6.65098e+14  $ VELM n-groups 21, 20, 19, 18, 17,
        5.40055e+14  7.09512e+14  8.07055e+14  8.54720e+14  3.12945e+14  $ VELM n-groups 16, 15, 14, 13, 12,
        2.00073e+14  1.35333e+14  2.41078e+14  1.61947e+14  2.06360e+14  $ VELM n-groups 11, 10,  9,  8,  7,
        1.36477e+14  7.32282e+13  3.05242e+13  8.64293e+12  6.92602e+12  $ VELM n-groups  6,  5,  4,  3,  2,
        2.74800e+09                                                    $ VELM n-group   1
c
c
sb53  d     0.0  $ dummy 0, followed by "biased" neut src terms (n/s) for HB-3:
c       ---------------------------------------------------------------------------
c       Biased neutron sources in MCNP order (grp 1=low E, grp 61=high E);
c       Calculated using GETADJ.SCR and GBANISN in adjoint mode, where the
c       adjoint source at Z=300 cm was the total n+g flux-to-dose-rate factors;
c       Use these values for the coupled n/g mcnp calc with a neutron-only source.
c       (With a n/g source, or a gamma-only source, values would be differnet).
c       Note that this can/should only be used with the corresponding weight
c       window file prepared by GETWIN8.SCR where the space/energy weights for the
c       neutron groups AND the gamma groups using the data in GETADJ.OUT.
c       ---------------------------------------------------------------------------
c       To work well (or even to work "at all") everything MUST be self-consistent !!!!!
c       ---------------------------------------------------------------------------
c       The following values were used on 26 May 98, before the group ordering on the gbanisn adjoint flux tape was properly understood:
c       2.26004e+15  3.24361e+14  2.19872e+14  1.87149e+14  2.23170e+14  $ VELM n-groups 61, 60, 59, 58, 57,
c       4.63275e+14  4.50972e+14  4.25087e+14  2.63381e+14  2.82609e+14  $ VELM n-groups 56, 55, 54, 53, 52,
c       2.77011e+14  2.54722e+14  2.48768e+14  5.94834e+14  1.37376e+14  $ VELM n-groups 51, 50, 49, 48, 47,
c       1.85455e+14  1.70942e+14  2.25624e+14  5.06467e+14  5.87346e+14  $ VELM n-groups 46, 45, 44, 43, 42,
c       6.59846e+14  4.97490e+14  4.48952e+13  7.56645e+13  3.51783e+13  $ VELM n-groups 41, 40, 39, 38, 37,
c       8.17070e+13  2.03479e+14  3.33174e+14  8.69411e+13  5.96276e+14  $ VELM n-groups 36, 35, 34, 33, 32,
c       3.74773e+14  6.35195e+15  5.37588e+15  6.41192e+15  1.08808e+16  $ VELM n-groups 31, 30, 29, 28, 27,
c       3.14998e+15  2.04968e+14  1.13749e+14  5.41155e+14  9.31284e+15  $ VELM n-groups 26, 25, 24, 23, 22,
c       8.66545e+15  2.21060e+15  5.34967e+15  7.92049e+15  9.84329e+15  $ VELM n-groups 21, 20, 19, 18, 17,
c       7.99269e+15  1.56382e+14  1.77881e+14  1.88386e+14  6.89753e+13  $ VELM n-groups 16, 15, 14, 13, 12,
c       4.40975e+13  2.98284e+13  5.31353e+13  3.56943e+13  4.54832e+13  $ VELM n-groups 11, 10,  9,  8,  7,
c       3.00805e+13  1.61400e+13  6.72775e+12  1.90496e+12  1.52654e+12  $ VELM n-groups  6,  5,  4,  3,  2,
c       6.05679e+08                                                    $ VELM n-group   1
c       The following values were used on 29 July 98, after the group ordering on the gbanisn adjoint flux tape was properly understood:
        1.29892E+16  1.82174E+15  1.23488E+15  1.05110E+15  1.25341E+15  $ VELM n-groups 61, 60, 59, 58, 57,
        2.50015E+15  2.43375E+15  2.29406E+15  1.42138E+15  1.52515E+15  $ VELM n-groups 56, 55, 54, 53, 52,
        1.49494E+15  1.37465E+15  1.34252E+15  3.05384E+15  7.05280E+14  $ VELM n-groups 51, 50, 49, 48, 47,
        9.52115E+14  8.77608E+14  1.15834E+15  2.60017E+15  3.01540E+15  $ VELM n-groups 46, 45, 44, 43, 42,
        3.387[illegible]15  2.55408E+15  2.30489E+14  3.88457E+14  1.80603E+14  $ VE[illegible]n-groups 41, 40, 39, 38, 37,
        4.19[illegible]14  1.04465E+15  1.71050E+15  4.46350E+14  3.06125E+15  $ V[illegible]-groups 36, 35, 34, 33, 32,
```

```
        1.92406E+15  1.19547E+15  1.01176E+15  1.20675E+15  2.04781E+15  $ VELM n-groups 31, 30, 29, 28, 27,
        5.92841E+14  3.85759E+13  2.14080E+13  1.01848E+14  1.75272E+15  $ VELM n-groups 26, 25, 24, 23, 22,
        1.63088E+15  4.16044E+14  1.00683E+15  1.49067E+15  1.85255E+15  $ VELM n-groups 21, 20, 19, 18, 17,
        1.50426E+15  3.67866E+15  4.18440E+15  4.43153E+15  1.62255E+15  $ VELM n-groups 16, 15, 14, 13, 12,
        1.03733E+15  7.01672E+14  1.24994E+15  8.39660E+14  1.06993E+15  $ VELM n-groups 11, 10,  9,  8,  7,
        7.07603E+14  3.79672E+14  1.58261E+14  4.48117E+13  3.59099E+13  $ VELM n-groups  6,  5,  4,  3,  2,
        1.42478E+10                                                     $ VELM n-group   1
c
c
c      BEGIN-TRANSFORMATIONS:
c      END-TRANSFORMATIONS
c
c
c      BEGIN MATERIAL DESCRIPTIONS:
c
c       H2O Pool  --Density= 1.0000 g/cm3
m8      1001.50c     6.73828-02    8016.50c    3.36914-02
mt8     lwtr.01t
c
c       Helium void
m61     2004.50c  1.0e-20
c
c      ------------------------------------------------------------------------------------------------------------------------
c      *** start detectors used to get fluxes at different points down HB-3 beam tube; for HFIR at 100 MW
c      ------------------------------------------------------------------------------------------------------------------------
c
fc44   G-flux axially up thru central water region
f44:p  201
fm44   9.64595E+16  $ total (n/s) over all energies
c      fm44   1.20830E+16  $ total (n/s) above 27 keV
fs44         $ 25 roughly even "5-cm-long" axial segments of interest
      -5120  -5121  -5122  -5123  -5124  -5125  -5126  -5127  -5128  -5129
      -5130  -5131  -5132  -5133  -5134  -5135  -5136  -5137  -5138  -5139
      -5140  -5141  -5142  -5143  -5144  -5145
c      sd54   1e20  314.16  24r  1e20   $ vol of each 5-cm axial segment in cm3 (original spec, but incorrect)
sd44   1e20  1570.80  24r  1e20   $ vol of each 5-cm axial segment in cm3 (correction)
c
c
fc54   N-flux axially up thru central water region
f54:n  201
fm54   9.64595E+16  $ total (n/s) over all energies
c      fm54   1.20830E+16  $ total (n/s) above 27 keV
fs54         $ 25 roughly even "5-cm-long" axial segments of interest
      -5120  -5121  -5122  -5123  -5124  -5125  -5126  -5127  -5128  -5129
      -5130  -5131  -5132  -5133  -5134  -5135  -5136  -5137  -5138  -5139
      -5140  -5141  -5142  -5143  -5144  -5145
c      sd54   1e20  314.16  24r  1e20   $ vol of each 5-cm axial segment in cm3 (original spec, but incorrect)
sd54   1e20  1570.80  24r  1e20   $ vol of each 5-cm axial segment in cm3 (correction)
c
c
fc64   N-dose rate (mrem/hr) in last 0.01 cm of central water region
f64:n  202
fm64   9.64595E+16  $ total (n/s) over all energies
e64    $ Neutron energy boundaries (Emax, in MeV) from VELM 61n/23g structure:
       1.00001e-11  4.13994e-07  1.12535e-06  2.38237e-06  5.04348e-06
       1.06770e-05  2.26033e-05  4.78512e-05  1.01301e-04  1.67017e-04
       2.75364e-04  4.53999e-04  7.48518e-04  1.23410e-03  2.03468e-03
       2.24867e-03  2.61259e-03  3.03539e-03  3.70744e-03  5.53084e-03
```

```
      9.11882e-03  1.50344e-02  2.35786e-02  2.47875e-02  2.60584e-02
      2.70001e-02  2.85011e-02  3.43067e-02  5.24752e-02  5.65622e-02
      8.65169e-02  1.22773e-01  1.49956e-01  1.83156e-01  2.23708e-01
      2.73237e-01  2.94518e-01  2.97211e-01  2.98491e-01  3.01974e-01
      3.87742e-01  4.97870e-01  5.23397e-01  6.08101e-01  7.42735e-01
      9.07180e-01  1.10803e+00  1.35335e+00  1.65299e+00  2.01897e+00
      2.23130e+00  2.34570e+00  2.46597e+00  3.01194e+00  3.67879e+00
      4.49329e+00  5.48811e+00  6.70320e+00  8.18730e+00  1.00000e+01
      1.22140e+01  1.49183e+01
em64  $ Neutron flux-to-dose-rate conversion factors [(mrem/hr)/(n/s/cm2)] for the VELM 61n/23g xsect library,
c     calculated as prescribed in ANSI/ANS-6.1.1-1977, with groups arranged here in order of "increasing"
c     energy for use in MCNP;  first value here corresponds to non-existant group below 1.0e-11 MeV:
      0.00000e+00  3.70900e-03  4.37060e-03  4.52500e-03  4.57420e-03
      4.55830e-03  4.48970e-03  4.38200e-03  4.24920e-03  4.12890e-03
      4.03110e-03  3.93560e-03  3.84530e-03  3.76290e-03  3.69080e-03
      3.65280e-03  3.63870e-03  3.62290e-03  3.60620e-03  3.58250e-03
      3.55850e-03  4.08740e-03  5.89750e-03  7.13860e-03  7.42410e-03
      7.67700e-03  7.95200e-03  8.74220e-03  1.11480e-02  1.35030e-02
      1.66880e-02  2.27810e-02  2.87730e-02  3.44470e-02  4.12410e-02
      4.93730e-02  5.56260e-02  5.77310e-02  5.80800e-02  5.84980e-02
      6.63300e-02  8.30460e-02  9.04880e-02  9.55770e-02  1.05540e-01
      1.18040e-01  1.29750e-01  1.30080e-01  1.28640e-01  1.27210e-01
      1.26150e-01  1.25620e-01  1.25270e-01  1.28490e-01  1.36940e-01
      1.45960e-01  1.54110e-01  1.51180e-01  1.47230e-01  1.47060e-01
      1.59770e-01  1.94650e-01
c
c
fc74  G-dose rate (mrem/hr) in last 0.01 cm of central water region
f74:p 202
fm74  9.64595E+16  $ total (n/s) over all energies
e74   $ Gamma energy boundaries (Emax, in MeV) from VELM 61n/23g structure:
      1.00000e-02  2.00000e-02  4.50000e-02  7.00000e-02  1.00000e-01
      1.50000e-01  3.00000e-01  4.00000e-01  5.10000e-01  6.00000e-01
      7.00000e-01  1.00000e+00  1.50000e+00  2.00000e+00  2.50000e+00
      3.00000e+00  4.00000e+00  5.00000e+00  6.00000e+00  7.00000e+00
      7.50000e+00  8.00000e+00  1.00000e+01  1.40000e+01
em74  $ Gamma flux-to-dose-rate conversion factors [(mrem/hr)/(p/s/cm2)] for the VELM 61n/23g xsect library,
c     calculated as prescribed in ANSI/ANS-6.1.1-1977, with groups arranged here in order of "increasing"
c     energy for use in MCNP;  first value here corresponds to non-existant group below 1.0e-2 MeV:
      0.00000e+00  2.14390e-03  5.77610e-04  2.74660e-04  2.66440e-04
      3.27670e-04  5.66760e-04  8.75940e-04  1.08520e-03  1.27970e-03
      1.44170e-03  1.75630e-03  2.31560e-03  2.92700e-03  3.46860e-03
      3.95960e-03  4.62210e-03  5.41360e-03  6.19090e-03  6.92650e-03
      7.47830e-03  7.84680e-03  8.77160e-03  1.10200e-02
c
c     ------------------------------------------------------------------------------------------------------------------------
c     ********** end of model **********
c     ------------------------------------------------------------------------------------------------------------------------
```

Appendix C.6

Preliminary, highly simplified, MCNP models once used for exploratory gamma-only analyses of the HB-3 beam tube using the newly proposed 1998 water tube design concept, as well as the original 1960 design concept.

Appendix C.6

Preliminary, highly simplified, MCNP models once used for exploratory gamma-only analyses of the HB-3 beam tube using the newly proposed 1998 water tube design concept, as well as the original 1960 design concept.

C.6.1 Reason for Including These Calculations in This Appendix

This appendix describes a preliminary, highly simplified, MCNP model (Run HB307C) once used for an exploratory gamma-only analysis of the HB-3 beam tube using the newly proposed 1998 water tube design concept, as well as a similar preliminary model (Run HB307D) used with the original 1960 water tube in place. These models were not deemed important enough to include in the main body of the report for several reasons:

1) They were preliminary exploratory calculations, and do not represent the final model or the final results.

2) These models are highly simplified in many respects (as noted below); for example, they only extend radially out to R=17.4742 cm (instead of R=65 cm), and they completely ignore some of the material surrounding the beam tube such as the biological shield; likewise, the rotary shutter is not included at all.

3) While point detector estimates of the dose rate downstream of the collimator (with the water tube and collimator both flooded) do appear to be fairly accurate, and while a serious attempt was made to obtain a good energy and direction-dependent boundary source downstream of the collimator, the results obtained lacked the statistical resolution necessary in off-normal directions to be considered reliable in later bootstrapped calculations using that source. Moreover, while the format used for reporting those results looks nice in tabular form, it is not entirely clear how (or even if) it could be utilized as user-supplied input to a follow-up bootstrapped analysis. A regular (binary) MCNP internal boundary source file would actually be far more useful.

Nevertheless, these models do merit some degree of serious attention and are deemed important enough to include (at least in an appendix) for several other valid reasons:

1) As a follow-up to Appendix C.1, these gamma-only models further illustrate the benefits derived from, and the frustrations associated with, the use of "importance zones" to control geometric splitting and improve statistical accuracy. Not withstanding the fact that this approach is "difficult to impossible" to implement in geometrically complex deep penetration problems and that more advanced, yet undocumented, methods (such as broad-group "geometry-independent weight windows" (cf Appendix C.2) work far better, the use of "importance zones" with geometric splitting can be very useful in the solution of simple situations. Moreover, some broad guidance is provided below as to how their use may be implemented intelligently in a simplified model such as this.

2) Because the point detector estimates of the dose rate downstream of the collimator (with the water tube and collimator both flooded) obtained by this method do appear to be fairly accurate based on the statistics obtained, and because they are in good agreement with the results obtained by the totally independent point kernel method (typically within 6-11%, as shown in Table 5.5), the two methods are considered mutually confirmatory. As such, some discussion of these simplified MCNP models is necessary if the results are to be used for that purpose.

3) Examination of the results presented here serves to illustrate those things one must consider when deciding whether to accept "an answer" as being valid or not. Moreover, it is not always sufficient to simply have good statistics. Point detectors, for example, may have good or even excellent statistics, but if the neutron or gamma collisions in the immediate neighborhood are not adequately sampled, the results may or may not be valid (see discussion in the first two parts of Appendix C.2). More to the point here: If the point detector shows most of the dose as coming from 8 MeV gammas (due either to the uncollided flux coming from the original sources, or due to collisions at distant locations) but the boundary crossing counter tally shows little or no gammas in this energy range (as can often happen if the number of "real" gammas numerically transported to the immediate neighborhood is so low that good local sampling cannot take place), then one can have the most unfortunate situation where one naively believes the results "because the point detector responses look reasonable", but where the boundary source based on the boundary crossing tally is totally deficient in representing the gammas in the energy range that really count, and any use of that boundary source in a follow-up bootstrapped calculation could/would yield totally misleading results.

For these reasons, an abbreviated discussion of these highly-simplified "preliminary" MCNP models and their associated results was considered worth including in this appendix.

C.6.2 Reason for Looking at These Highly Simplified Models

One of the lessons learned from the HB305 series of calculations described in Appendix C.1 was that the use of importance zones to invoke geometric splitting was cumbersome to the point of being totally impractical for geometrically complex problems like the full HB-3 model shown in Fig. 3.3, even though it was known to work well in many cases and was not too cumbersome for simpler geometries. While gamma-only shielding analyses would require fewer importance zones, thus partially alleviating the difficulties described in Appendix C.1, there was no illusion left that this approach would prove practical. Moreover, by mid-May 1998, the use of broad-group "geometry independent weight windows" based on adjoint analyses had only been available as a possibility for two weeks, was still under development, and still had not yet been demonstrated. As an alternative, use of elementary handbook formulations, multigroup 1-D ANISN transport analyses, and a 23-group point kernel approach had been used to determine what features of the problem were important and which ones were not. Yet, there remained a need for some sort of 3-D gamma-only analysis. This was needed for two reasons: (1) to verify the total gamma dose rate downstream of the collimator as initially given by the 23-group point kernel approach, and (2) to determine the space-energy-direction-dependent flux on a surface downstream of the flooded collimator that could be used as a boundary source in a follow-up (bootstrapped) analysis of the rotary shutter. Clearly the point kernel approach could not supply all the information needed for the latter. Knowing that the dominant thing at the downstream exit of the collimator would be the gammas streaming through the water-filled hole and that nothing upstream of the collimator really mattered (in the gamma-only analysis) except the water in the water tube, a "highly-simplified" 3-D MCNP model was developed that would model only these essential characteristics. By keeping the model "highly-simplified", it was hoped that use of importance zones would not prove too cumbersome and that their use alone might yield a satisfactory solution for the key things that were needed.

C.6.3 Description of the Highly Simplified Model(s)

Figure C6.1 shows an isometric view of the simplified model that was created with these considerations in mind. It is very simple, and all of the key parameters and dimensions are shown on the figure itself. Moreover, the 12 cells and 15 surfaces shown in Table C6.1 are fully sufficient to describe the basic geometry for the case involving the 1998 water tube if one did not have to worry about importance zones, while the 13 cells and 15 surfaces shown in Table C6.2 are fully sufficient to describe the basic geometry for the case involving the 1960 water tube if one did not have to worry about importance zones. [Importance zones, and the final models using them, will be discussed later.]

The key simplifications used in this model are as follows:

1) Everything beyond R=17.4742 cm was eliminated. [In the real model (cf Fig. 3.3), R=17.4742 cm corresponds to the outer radius of the stainless steel sleeve around the HB-3 beam tube as it enters the biological shield.] It was believed that the gammas entering and successfully passing through the water-filled rectangular hole in the collimator would come primarily from the original sources along the centerline of the system and/or from scattering events close to the centerline, so that scattering events at more radially-distant locations could be safely ignored. This eliminates the need to spend precious CPU time tracking gammas (especially low-energy gammas) at these more distant radial locations. It also eliminated the need to have a series of radial importance zones beyond that point which would likely be necessary to affect an efficient solution, but which would severely "add to" and complicate the amount of input required. On the other hand, while scattering events beyond this radial location may contribute negligibly to the gamma flux directly entering the hole in the collimator in directions that are likely to get through, the fact that a vacuum boundary condition is applied to the outer radial surface will cause a certain amount of unrealistic radial leakage and the remaining gamma flux will now be (slightly) buckled in the radial direction. That is: the gamma flux, even along the centerline (which may scatter towards the collimator), will now be slightly lower than it would have been otherwise. In the case of neutrons which are highly diffusive in water, this sort of approximation would clearly not be acceptable. In this case, however, the water is relatively transparent to high energy gammas, and the gammas (unlike neutrons) tend to travel much greater distances along straight lines, more like x-rays. Under these conditions, the R=17.4742 cm approximation is not considered too unrealistic.

2) The rotary shutter assembly and all shielding materials surrounding it were eliminated since the primary focus here was on the determination of the boundary flux "leaving" the collimator section. Note that reflection from the shutter back to the collimator and then back again toward the shutter will physically increase the flux in this region slightly, but that would clearly be a second- or third-order effect. Moreover, in the simplified model, I instead chose to include a single void region downstream of the collimator (from Z=399.48 cm to Z=415.44875 cm) so that a point detector could be placed at a location (R=0, Z=407.46438 cm) which would correspond to a point midway between the collimator exit and the rotary shutter shield plug if the latter were present. This

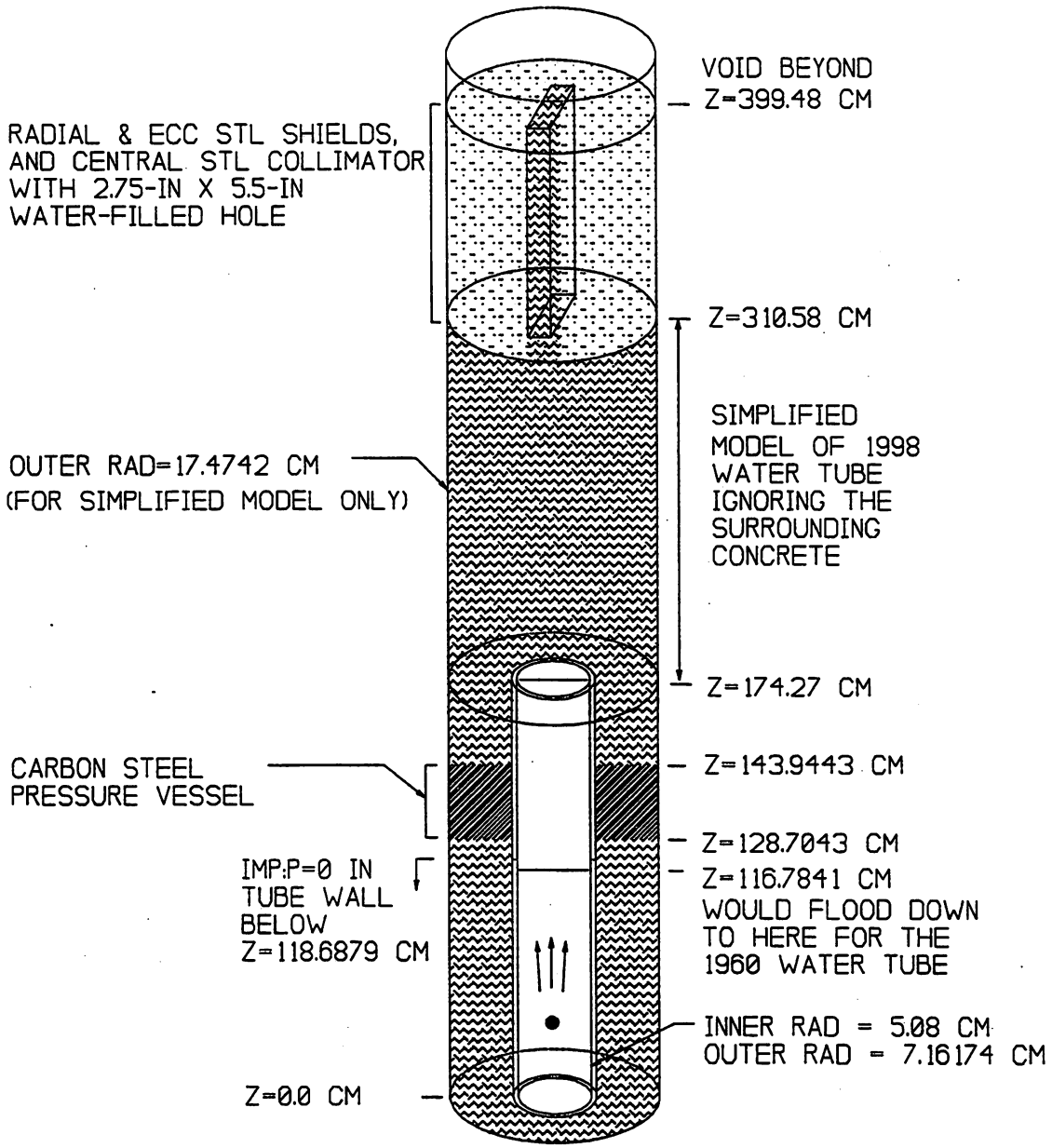


Fig. C6.1. Isometric view of the highly-simplified model of the HB-3 water tube and collimator sections used in the preliminary gamma-only shielding analyses corresponding to MCNP Runs HB307C and HB307D.

Table C6.1. Simplest possible geometry description (with no special importance zones) for the highly simplified, preliminary, gamma-only MCNP model for the HB-3 beam tube using the 1998 water tube design.

```
c     BEGIN CELLS:
c
100  61  -3.2325-4  -1010   9997 -2153         imp:p=1  $ void up center of beam tube (upstream of where water begins)
111  24  -2.7        1010  -2130  9997  -1007  imp:p=0  $ aluminum wall of beam tube (upstream of importance cutoff plane)
112   8  -1.0000     2130  -4225  9997  -1007  imp:p=0  $ water outside beam tube (upstream of importance cutoff plane)
121  24  -2.7        1010  -2130  1007  -2153  imp:p=1  $ aluminum wall of beam tube (downstream of importance cutoff plane)
122   8  -1.0000     2130  -4225  1007  -2107  imp:p=1  $ water outside beam tube (downstream of importance cutoff plane, inside vessel)
201  50  -7.8212     2130  -4225  2107  -2106  imp:p=1  $ carbon steel vessel nozzel flange (appx model; arbitrarily 6" thick)
202   8  -1.0000     2130  -4225  2106  -2153  imp:p=1  $ water outside beam tube (downstream of vessel flange)
c
c    Cell 300 goes from Z=174.27 to Z=310.58; it may have to be subdivided into a number of axial importance zones
300  8  -1.0000    2153  -4130  -4225 imp:p=1 $ water in water tube (from start, up "to" collimator)
c
c    Cells 400 & 500 go from Z=174.27 to Z=310.58; they may have to be subdivided into a number of axial importance zones
400  8  -1.0000  4130 -4190  4212  -4213  4210 -4211  imp:p=1  $ water in rectangular hole up thru collimator
500  40  -7.92  4130 -4190 -4225 #(4212 -4213  4210 -4211) imp:p=1   $ stainless steel model of collimator (with rectangular hole)
c
800  60  -1.0e-20  4190  -9998  -4225  imp:p=1  $ internal void downstream of collimator, but upstream of shutter drum
900   0          #(-4225   9997  -9998) imp:p=0  $ enternal void
c
c     END CELLS (next line must be blank)

c     BEGIN SURFACES:
c
1010  cz   5.08    $ inner radius of voided portion of beam tube
2130  cz   7.16174 $ inner radius of ss sleeve around HB-3 beam tube, near vessel; used as outer radius of beam tube in this model
4225  cz  17.4742  $ outer radius of narrow ss sleeve extending thru concrete into pool; radial boundary to ext void in this model
c
c     Box surfaces corresponding to rectangular-shaped hole in collimator:
c     Here (like everywhere in this MCNP model of HB-3),
c     Z=central axis; Y is really horizontal; X is really vertical
4210  py  -3.4925   $ ymin
4211  py   3.4925   $ ymax
4212  px  -6.9850   $ xmin
4213  px   6.9850   $ xmax
c
9997  pz    0.0     $ external void boundary (location corresponds to the real radial plane perpendicular to the real beam tube)
1007  pz  118.6879  $ plane below which all importances are zero; located 2 cm upstream of first pt det used to get pt srcs
2107  pz  128.7043  $ arb plane defining upstream side of thick flange in this model (flange arbitrarily taken to be 6" thick here)
2106  pz  143.9443  $ plane defining end of thick flange mounted on boss on pressure vessel around HB-3 (see dwg E-42027)
2153  pz  174.27    $ upstream   side of aluminum window forming start of water tube in proposed HB-3 design
4130  pz  310.58    $ upstream surface of collimator
4190  pz  399.48    $ downstream side of collimator
9998  pz  415.44875 $ upstream side of shutter drum; taken as ext void boundary in this model
c
c     END SURFACES (next line must be blank)
```

Table C6.2. Simplest possible geometry description (with no special importance zones) for the highly simplified, preliminary, gamma-only MCNP model for the HB-3 beam tube using the 1960 water tube design.

```
c     BEGIN CELLS:
c
100   61  -3.2325-4  -1010   9997 -1060          imp:p=1  $ void up center of beam tube (upstream of where water begins)
c
c    Cell 1000 goes from to Z=116.7841 to Z=174.27; it may have to be subdivided into a number of axial importance zones
1000   8  -1.0000    -1010   1060 -2153          imp:p=1  $ water from start of 1960 water tube to start of 1998 water tube
c
111   24  -2.7        1010  -2130  9997  -1007  imp:p=0  $ aluminum wall of beam tube (upstream of importance cutoff plane)
112    8  -1.0000     2130  -4225  9997  -1007  imp:p=0  $ water outside beam tube (upstream of importance cutoff plane)
c
c    Cell 1100 goes from to Z=118.6879 to Z=174.27; it may have to be subdivided into a number of axial importance zones
1100  24  -2.7        1010  -2130  1007  -2153  imp:p=1  $ aluminum wall of beam tube (downstream of importance cutoff plane)
c
c    Cell 1200 goes from to Z=118.6879 to Z=128.7043; it may have to be subdivided into a number of axial importance zones
1200   8  -1.0000     2130  -4225  1007  -2107  imp:p=1  $ water outside beam tube (downstream of importance cutoff plane, inside vessel)
c
c    Cell 1300 goes from to Z=128.7043 to Z=143.9443; it may have to be subdivided into a number of axial importance zones
1300  50  -7.8212     2130  -4225  2107  -2106  imp:p=1  $ carbon steel vessel nozzel flange (appx model; arbitrarily 6" thick)
c
c    Cell 1400 goes from to Z=143.9443 to Z=175.27; it may have to be subdivided into a number of axial importance zones
1400   8  -1.0000     2130  -4225  2106  -2153  imp:p=1  $ water outside beam tube (downstream of vessel flange)
c
c    Cell 1500 goes from Z=174.27 to Z=310.58; it may have to be subdivided into a number of axial importance zones
1500  8  -1.0000    2153  -4130  -4225 imp:p=1 $ water in water tube (from start, up "to" collimator)
c
c    Cells 1600 & 1700 go from Z=174.27 to Z=310.58; they may have to be subdivided into a number of axial importance zones
1600  8  -1.0000  4130 -4190  4212  -4213  4210 -4211  imp:p=1  $ water in rectangular hole up thru collimator
1700  40  -7.92  4130 -4190 -4225 #(4212 -4213  4210 -4211) imp:p=1   $ stainless steel model of collimator (with rectangular hole)
c
800  60  -1.0e-20  4190  -9998  -4225  imp:p=1  $ internal void downstream of collimator, but upstream of shutter drum
900   0          #(-4225   9997  -9998) imp:p=0  $ enternal void
c
c     END CELLS (next line must be blank)

c     BEGIN SURFACES:  (continued on next page)
```

Table C6.2 (cont)

```
c     BEGIN SURFACES:
c
1010  cz   5.08     $ inner radius of voided portion of beam tube
2130  cz   7.16174  $ inner radius of ss sleeve around HB-3 beam tube, near vessel; used as outer radius of beam tube in this model
4225  cz  17.4742   $ outer radius of narrow ss sleeve extending thru concrete into pool; radial boundary to ext void in this model
c
c     Box surfaces corresponding to rectangular-shaped hole in collimator:
c     Here (like everywhere in this MCNP model of HB-3),
c     Z=central axis; Y is really horizontal; X is really vertical
4210  py  -3.4925   $ ymin
4211  py   3.4925   $ ymax
4212  px  -6.9850   $ xmin
4213  px   6.9850   $ xmax
c
9997  pz    0.0     $ external void boundary (location corresponds to the real radial plane perpendicular to the real beam tube)
1060  pz  116.7841  $ start of water tube in 1960 design
1007  pz  118.6879  $ plane below which all importances are zero; located 2 cm upstream of first pt det used to get pt srcs
2107  pz  128.7043  $ arb plane defining upstream side of thick flange in this model (flange arbitrarily taken to be 6" thick here)
2106  pz  143.9443  $ plane defining end of thick flange mounted on boss on pressure vessel around HB-3 (see dwg E-42027)
2153  pz  174.27    $ upstream   side of aluminum window forming start of water tube in proposed HB-3 design
4130  pz  310.58    $ upstream surface of collimator
4190  pz  399.48    $ downstream side of collimator
9998  pz  415.44875 $ upstream side of shutter drum; taken as ext void boundary in this model
c
c     END SURFACES (next line must be blank)
```

location was also chosen (as opposed to a location directly at the exit of the water-filled hole) for two reasons: (a) so it would be far enough back from the collimator that gammas coming from the surrounding steel (if any) could also be seen, and (b) so that it would be far enough back in the void so that contributions from any nearby collisions in the water or the steel would not be adversely (ie, disproportionately) affected by the 1/(4*pi*R^2) term used by the code in calculating the response to a detector from each collision site. If collisions occur too close to a point detector, this can sometimes be a problem. By keeping the point detector back some distance from any real material, this problem can be avoided.

3) The collimator with its radial shield, eccentric shield, and pools seals (cf Fig. 3.10) was highly simplified. In this case, these components were treated as a monolithic steel cylinder with a 2.75-inch x 5.5-inch water-filled rectangular hole up the middle, and the surrounding biological shield was completely ignored. The key feature is obviously the rectangular hole.

4) Further upstream (cf Fig. 3.3), the flooded water tube is surrounded by the pool water between the pressure vessel and the biological shield. In the simplified model, the aluminum walls of the water tube have been eliminated, leaving nothing but water in this region. [Closer to the biological shield, just slightly upstream of the collimator, the aluminum walls of the water tube and the surrounding stainless steel sleeve, and the concrete beyond the stainless steel sleeve, have all been eliminated as well.] The resulting model, just upstream of the collimator, has "one big water region" which can easily be subdivided into as many importance regions as necessary.

5) The 1998 water tube starts at Z=174.27 cm, and below that, the tube is void. [Note that the thin aluminum windows at both ends of the water tube have also been eliminated since (a) they provide very little gamma attenuation and, (b) in this gamma-only calculation for primary gammas streaming down the beam tube, secondary gammas are not being considered at all.] A highly simplified model of the voided aluminum beam tube itself (ID=10.16 cm, OD=14.32348 cm) is included below Z=174.27 cm. In the case of the 1960 water tube, the portion of the tube above Z=116.7841 cm would also be flooded.

6) As shown in Fig. C6.1, the pressure vessel and vessel nozzle have also been simplified and are now represented by a thick, flat, steel plate with a single hole up through the middle for the beam tube. All the elaborate geometry for the dosimetry analysis (cf Fig. 3.14) just inside the vessel has also been eliminated.

7) Lastly, in addition to the point detector mentioned in item 2 (at Z=407.46488 cm, midway between the collimator exit and the rotary shutter), a boundary crossing surface detector (F1 tally) was also placed across the entire system at the collimator exit (Z=399.48 cm). It was divided into five "segments", with segment 5 corresponding to the rectangular hole in the collimator. This was used to calculate the directional-dependent multigroup gamma leakage (p/s) across the entire system, as well as that coming from the small 2.75-inch x 5.5-inch water-filled rectangular hole in the collimator which is responsible for the vast majority of high-energy gammas impingent on the rotary shutter.

With these simplifications, the model shown in Fig. C6.1 can be readily subdivided into any number of axial importance zones in a straightforward fashion as needed, without the cumbersome constraints and considerations that afflict geometrically more complex problem descriptions. In the case of the 1998 water tube, for example, the problem may be divided into the 23 axial importance zones shown in Fig. C6.2 and listed in the first part of Table C6.3, while in the case of the original (longer) 1960 water tube, the problem may be divided into the 29 axial importance zones shown in Fig. C6.3 and listed in the second part of Table C6.3. Unfortunately, while the basic geometry specifications in Tables C6.1 and C6.2 (and the importance zone specifications shown in Table C6.3) are extremely simple and easy to visualize, the actual MCNP input required to implement these importance zones, even for this ultra-simple model, is a little more complex. The actual MCNP input file for Run HB307C with the 1998 water tube is listed in Appendix C.6.7, while the actual MCNP input file for Run HB307D with the 1960 water tube is listed in Appendix C.6.8. Since this is an abbreviated appendix, the heavily annotated input files are simply presented without much further explanation, except as noted below:

1) While the neutron and gamma sources are both listed in the input files, only the gamma sources specified by the si73, sp73, and ds83 cards are actually used. This data is taken directly from Table 2.2b. The total gamma source, summed over all 23 groups is 1.35399e+17 p/s. This same value must be used on all the "fm" tally multiplier cards.

2) While each of the gamma point sources in Table 2.2b are to be treated as if they are isotropic, it is far more efficient in these MCNP calculations to sample these isotropic source distributions only over those starting directions whose direction cosines with respect to the tube centerline are between 0.965335056 and 1.0 (ie, to sample only over those starting directions that are within about 15.13 degrees of the centerline) since these are the only ones that are likely to contribute to the response of interest. Accordingly, the starting weights assigned to these gammas must be set to 0.017332472, as given by

   wgt = [mu(max)-mu(min)]/[(+1)-(-1)] = [1.0000000000-0.965335056]/2 = 0.017332472

   The need for this is discussed in Sects 4.2 and 5.1 of the main report, and in Appendix C.1.2.

3) Consistent with that, the importance cutoff plane in these two gamma-only shielding calculations is located at Z=118.6879 cm. Above that location, the importance assigned to the aluminum wall of the beam tube is 1.0 (or greater), while below that location, the aluminum wall of the beam tube is assigned an importance of zero so that gammas impinging on the inner wall of the beam tube below that location will be killed immediately and tracked no further. The role of the importance cutoff plane, and how it should be consistent with the range of starting directions sampled, is also discussed in Sects 4.2 and 5.1 of the main report, and in Appendix C.1.2.

C.6.4 Discussion of Importance Zones in This Model

Having dispensed with the minimal obligatory explanations, it would be good to dwell briefly on how the importance zones shown in Figs. C6.2 and C6.3 and Table C6.3 were chosen. Note, for example, that while the ratio of importances from one zone to the next in Run HB307C was approximately 1.8 in all cases (and approximately 1.7 in all cases for Run HB307D), the spacing between importance zones is not uniform and tends to get bigger as one gets further from the source.

First, it should be said that the determination of importance zone data to be used in a given calculation is as much an art as a science. Secondly, it should be noted that their exact determination is not terribly critical, as long as one is reasonably close. That is to say: As long as one is reasonably close and uses reasonable judgement, the values chosen will not affect the absolute value of the solution itself, but only the efficiency with which it is reached. One key guideline is that the specified importance should not vary by more than a factor of 3 or 4 from one importance mesh to the next at any location in all three spatial directions. To those who think in adjoint mode, it is clear that the importance should increase in regions closer to the detector of interest. To the rest of us, it is clear that the (real) particle flux decreases exponentially as one gets further from the source and that the importance assigned a zone should vary inversely with that decrease (ie, the assigned importance should increase exponentially). A much more rigorous discussion on importance zones and geometric splitting, and on the alternative use of space-(energy-direction)-dependent weight windows is provided in Appendix C.2.1.

Importance zones are used to control the numerical particle density -- specifically, the population of artificial "numerical particles" (of ever increasingly lower weight) used to represent the gammas in each water-filled cell along the centerline in this particular MCNP model. To obtain good statistics and a reasonably efficient solution, this population density should be held basically constant (within an order of magnitude or so) while the progressively lower and lower weights ascribed to the numerical particles reflect the decrease in the real gamma flux. If the numerical particle density becomes too low, flux estimates will suffer from poor statistics; if it grows too fast (say, due to an over-zealous attempt to get good statistics), lots of extra computer time will be required to track these extra particles, and the efficiency of the calculation will deteriorate severely. Thus, it is best to hold the density of "numerical particles" approximately constant, within an order of magnitude or so, all the way from the source to the detector.

To use importance regions, one must specify the thickness of each importance zone throughout the problem, and the "importance" to be assigned to each zone. Both must be specified. Since both are somewhat arbitrary but must work together harmoniously, how is that done?

If each zone is about half a mean free path thick, then the flux across an importance zone will drop by a factor of exp(-0.5) and the "importance" will increase by a factor of 1.65=exp(+0.5) which is well within the guidelines set forth above. This suggests that if all importance zones were about "half a mean free path thick", then the assigned importance should increase by a constant factor of 1.65 from one importance zone to the next. But what is the mean free path of gammas in water? It depends on the average energy of the gammas, and that depends on where you are in the system. Inspection of Table 2.2b shows that while there are some high energy gammas impingent on the water tube, the average energy of the impingent gammas is somewhere between 0.5 MeV and 1.0 MeV, where the gammas have mean free paths of between 10 and 14 cm, say 12 cm on the average. As shown by the simple 3-group analytic approximation in Sect 5.2, the average energy of gammas emerging from the downstream end of the water-filled collimator is likely to be somewhere between 4 and 8 MeV, where the mean free paths are between 30 and 40 cm, say 35 cm on the average. Applying the above criteria, the importance zones should therefore vary from about 6 cm in thickness near the source end of the water tube to about 17.5 cm in thickness near the exit of the collimator if one wants to increase the importance by a constant factor from one importance zone to the next. Of course, the rigid locations of the planar surfaces required to specify the actual geometry, and the necessity of having an integer number of importance zones between such planes, will limit one's ability to increase the spacing in a uniform logarithmic fashion, but one can and should try. In Table C6.3, for example, the thickness of these importance zones for the 1998 water tube increases from about 6.4 cm near the source, to 8.4 cm, to 12.1 cm, to 16.5 cm near the exit of the collimator, while for the 1960 water tube, they increase from about 5.0 cm near the source, to 7.6 cm, to 8.3 cm, to 11.0 cm, to 13.0 cm, to 15.7 cm near the collimator exit. [Note that while the importance zones

MCNP Plot Window: Origin of plot window located at X=0, Y=0, Z=210 cm in real system;
Size of plot window = ± 110 x ± 220 cm;.
Orientation basis vectors: (0,1,0) and (0,0,1) are such that:
+y in model (horz lateral in real world) is to right in plot,
+z in model (horz axis in real world) is up in plot

yellow = stainless steel
orange = carbon steel
pink = aluminum

light blue = water
light gray = void

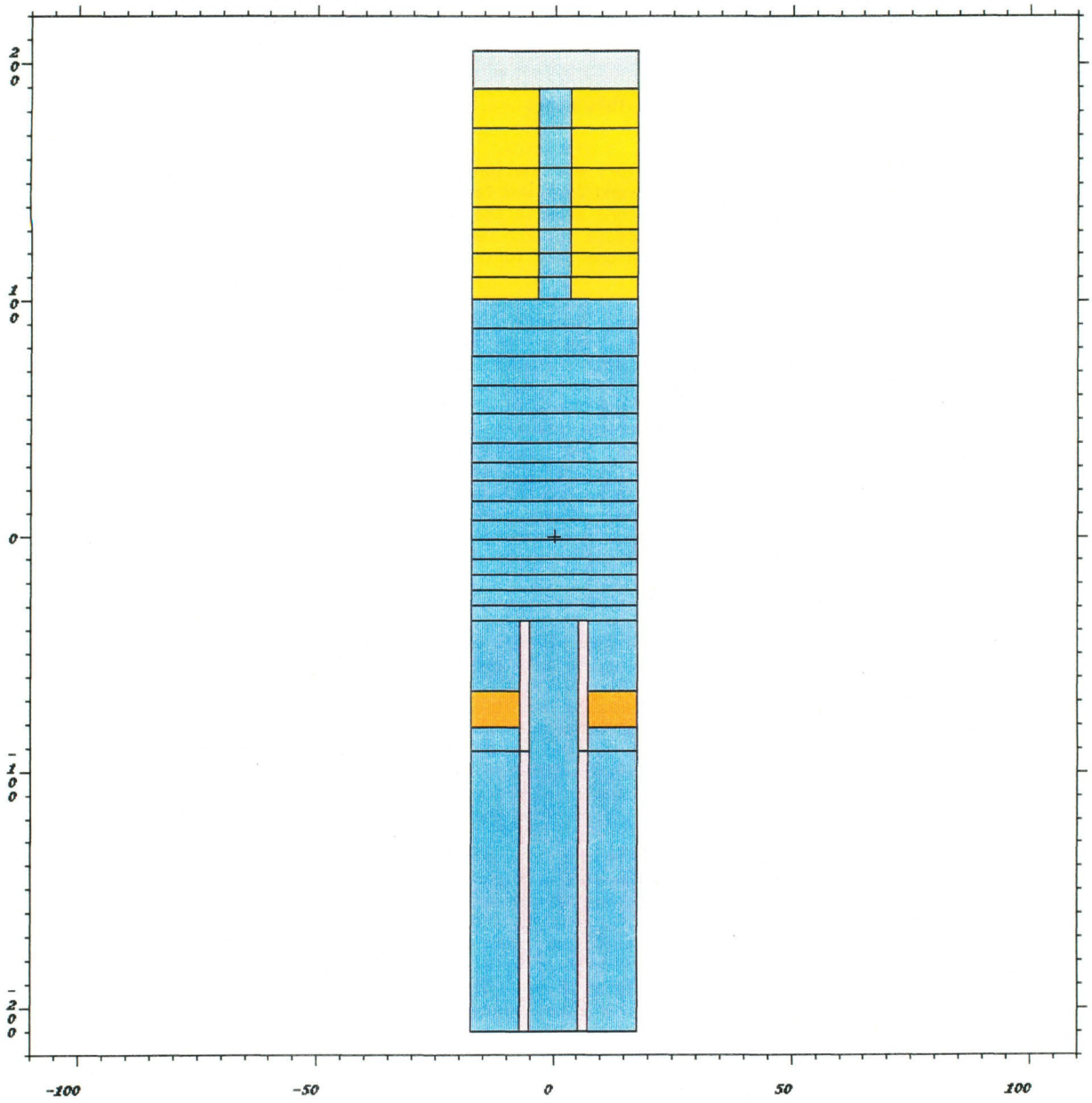


Fig. C6.2. Highly-simplified preliminary model of the 1998 HB-3 water tube and collimator sections used in MCNP Run HB307C.

MCNP Plot Window: Origin of plot window located at X=0, Y=0, Z=210 cm in real system;
Size of plot window = ± 110 x ± 220 cm;
Orientation basis vectors: (0,1,0) and (0,0,1) are such that:
+y in model (horz lateral in real world) is to right in plot,
+z in model (horz axis in real world) is up in plot

yellow = stainless steel
orange = carbon steel
pink = aluminum

light blue = water
light gray = void

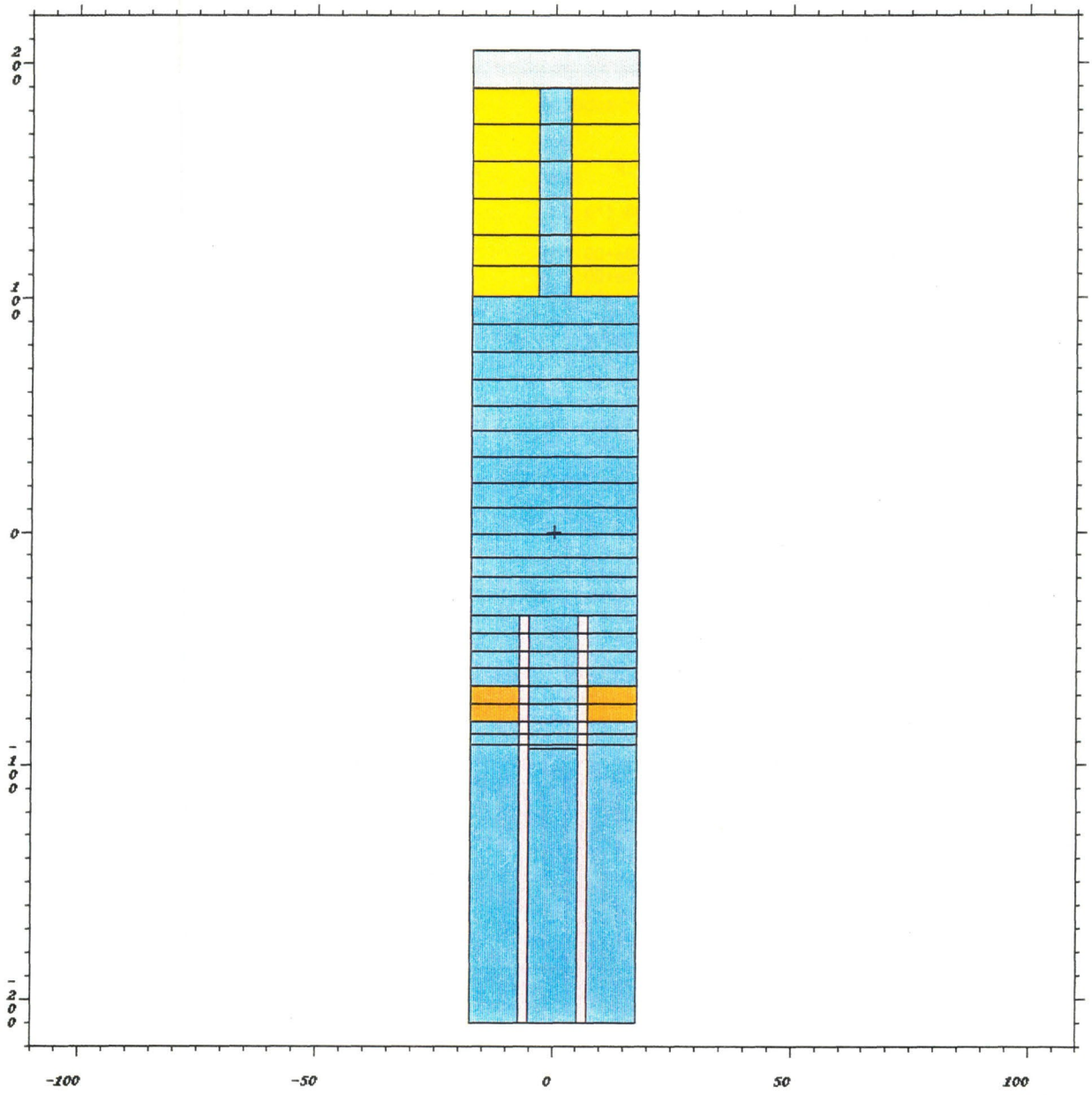


Fig. C6.3. Highly-simplified preliminary model of the 1960 HB-3 water tube and collimator sections used in MCNP Run HB307D.

Table C6.3. Axially-dependent photon importance zones used in MCNP Run HB307C with the new (shorter) 1998 water tube starting at Z=174.27 cm, and in MCNP Run HB307D with the original (longer) 1960 water tube starting at 116.7841 cm

In Run HB307C with 1998 water tube			In Run HB307D with 1998 water tube		
Zmin (cm)	Zmax (cm)	IMP:P	Zmin (cm)	Zmax (cm)	IMP:P
0.0	174.27	1.00 (*)	0.0	116.7841	1.00 (*)
174.27	180.7	1.80e+00	116.7841	118.6879	1.00e+00
180.7	187.1	3.24e+00	118.6879	123.70	1.70e+00
187.1	193.6	5.83e+00	123.70	128.7043	2.89e+00
193.6	200.0	1.05e+01	128.7043	136.32	4.91e+00
200.0	208.3	1.89e+01	136.32	143.9443	8.35e+00
208.3	216.7	3.40e+01	143.9443	151.53	1.42e+01
216.7	225.0	6.12e+01	151.53	159.11	2.41e+01
225.0	233.7	1.10e+02	159.11	166.69	4.10e+01
233.7	241.7	1.98e+02	166.69	174.27	6.98e+01
241.7	250.0	3.57e+02	174.27	182.60	1.19e+02
250.0	262.1	6.43e+02	182.60	190.94	2.02e+02
262.1	274.2	1.16e+03	190.94	199.27	3.43e+02
274.2	286.3	2.08e+03	199.27	209.27	5.83e+02
286.3	298.5	3.75e+03	209.27	220.27	9.90e+02
298.5	310.58	6.75e+03	220.27	231.27	1.68e+03
310.58	320.4	1.21e+04	231.27	242.27	2.86e+03
320.4	330.3	2.19e+04	242.27	253.27	4.87e+03
330.3	340.1	3.93e+04	253.27	264.27	8.27e+03
340.1	350.0	7.08e+04	264.27	275.27	1.41e+04
350.0	366.5	1.27e+05	275.27	287.04	2.39e+04
366.5	383.0	2.29e+05	287.04	298.81	4.06e+04
383.0	399.48	4.13e+05	298.81	310.58	6.91e+04
			310.58	323.58	1.17e+05
399.48	415.44875	4.13e+05	323.58	336.58	2.00e+05
			336.58	352.31	3.39e+05
* Except in the beam tube wall, where IMP:P=0 below Z=118.6879			352.31	368.03	5.77e+05
			368.03	383.76	9.81e+05
			383.76	399.48	1.67e+06
			399.48	415.44875	1.67e+06
			* Except in the beam tube wall, where IMP:P=0 below Z=118.6879		

are becoming thicker as one moves further from the source and approaches the detector (which may seem counter intuitive), the actual importance is still increasing at an ever increasing rate as one approaches the detector.] Having tentatively established the location and thickness of each importance zone, the next two questions are: how does one set the rate of change in the assigned importance from one importance zone to the next (ie, the ratio), and how does one verify that it is okay?

Since the importance zones are each approximately a "half a mean free path thick", the ratio ideally ought to be 1.65=exp(+0.5). Nevertheless, at this early stage before any calculations are performed, there may by some uncertainty in the energy spectrum as a function of distance down the water tube (and hence the mean free path at any location). In addition, there may be still other questions about the effect of any natural divergence that might be present (which will also affect the numerical particle density). At this point, it is best to make the importance ratio a little bigger than you expect it should be, run a pilot calculation or two to see what happens, and then make any necessary adjustments based in the information described below. In this case, the pilot run (HB307A) for the 1998 water tube was identical to final run (HB307C) except that an importance ratio of 2.0 was used between adjacent importance zones in the pilot run, while in the final run, the importance ratio was reduced to 1.8 between adjacent zones. Both used 2 million histories. Likewise, the pilot run (HB307B) for the 1960 water tube was identical to the final run (HB307D) except that an importance ratio of 2.0 was used between adjacent importance zones in the pilot run, while in the final run, the importance ratio was reduced to 1.7 between adjacent zones. In this case, the pilot run used 2 million histories, while in the final run, the number was increased to 5 million histories to improve the statistical accuracy.

To determine the acceptability of using an importance ratio of 2 (or any assumed ratio), the data in Table C6.4 is most helpful. Taken from "MCNP Print Table 126," it shows the population of "numerical particles" (the ever increasingly lower-weight particles) representing the gammas in each water-filled cell along the centerline in the various MCNP runs. Moreover, since this table shows the population (rather than the population density), one must really make comparisons between similar cells.

In the case of pilot run HB307A for the 1998 water tube, for example, we can look at all the cells between the start of the water tube at Z=174.27 cm and the start of the collimator at Z=310.58 cm (where all the cells have a radius of 17.4742 cm) and see that an importance ratio of 2.0 between cells was really too large and caused the "numerical particle density" to artificially grow too fast, by a factor of 78.3 over the length of the region, while in the collimator section (Z=310.58 cm to 399.48 cm) it grew by a more acceptable factor of only 2.5 over the length of the region. "Population control" is the job of the importance ratio. Reducing the importance ratio (between adjacent importance zones) to 1.8 in the final run (HB307C) seemed to control the population much better. There, the population increased by only a factor of 17.9 across the length of the water tube, and by a only a factor of 1.33 across the length of the water filled collimator. While one could have done better by using a still lower importance ratio (perhaps 1.65), the population control demonstrated in Run HB307C was considered quite acceptable -- ie, it was not diminishing to the point where statistics would become poor, and it was not artificially growing out of control to the point where it would impact calculational efficiency too adversely.

[At this point, it would be good to recall that the term "numerical particle density" really refers to the the density of "numerical particles" used internally within the code, and does not correspond to the real photon density. Moreover, it is the integral of the "numerical particle density times the average numerical particle weight" that corresponds to the real photon density. In two otherwise similar calculations that are biased differently, the "numerical particle density" in a given cell may be very high in one case and very low in the other, but the average particle weight may be very low in the first case and very high in the second case, such that the two calculations yield the same (real) photon flux. The key difference is that in the first case (which may be less efficient), the statistics will be quite good so that one can have a high level of confidence in the result, whereas in the other case, the statistics will be much poorer and one may not be able to have as much confidence in the result, even though the two calculations may yield the same real flux (very nearly). Properly implemented, "good biasing will not affect the result, only the efficiency with which it is obtained."]

In the case of pilot run HB307B for the 1960 water tube, the data in Table C6.4 was again very useful in determining the appropriate importance ratio and in verifying its acceptability once it was determined. In the 10.16-cm-diam portion of the 1960 water tube, for example, one can look at all the (similar) cells between Z=116.7841 cm and Z=174.27 cm and see that an importance ratio of 2.0 had caused the population to artificially grow by a factor of 2.54 across this short region. Likewise, in the region between Z=174.27 cm and Z=310.58 cm (where all the cells have a radius of 17.4742 cm), one also sees that an importance ratio of 2.0 between cells was again too large and caused the "numerical particle density" to artificially grow too fast, by a factor of 36.6 over the length of the region. Only in the collimator section (Z=310.58 cm to 399.48 cm) was it reasonably constant, growing by only a factor of 1.14 over the length of the region. Reducing the importance ratio (between adjacent importance zones) to 1.7 in Run HB307D seemed to control the population much better, with the population decreasing by only a factor of 1.23 across the first region, growing by a factor of 5.21 across the second, and decreasing by a factor of 1.78 across the third -- overall, quite remarkable. While one could perhaps do better, the population control

Table C6.4. Population of "numerical particles" (ever increasingly lower-weight particles) representing the gammas in each water-filled cell along the centerline in various MCNP runs. Runs HB307A and HB307C were for the 1998 water tube model, while Runs HB307B and HB307D were for the original (longer) 1960 water tube. Data shown is taken from MCNP Print Table 126, "photon activity in each cell".

cell	HB307A (2M) 1998 W.Tube population	HB307C (2M) 1998 W.Tube population	
----------	----------	----------	Z=174.27 cm
301	354585	315013	
302	522654	418171	
303	735074	530188	big water
304	1011720	657448	region
305	1411603	826727	where
306	1819977	957220	R=17.4742
307	2398283	1135028	cm
308	3262110	1388833	
309	4457666	1706729	
310	6406763	2213283	
311	9390256	2920848	
312	11989198	3350996	
313	15612858	3912222	
314	20717599	4669575	
315	27780829	5628258	
----------	----------	----------	Z=310.58 cm
401	6611728	1194444	
402	7236547	1177849	water in
403	8330752	1211174	rectangular
404	10578428	1373538	hole in
405	14779665	1724710	collimator
406	15574741	1648657	
407	16548724	1584309	
----------	----------	----------	Z=399.48 cm

cell	HB307B (2M) 1960 W.Tube population	HB307D (5M) 1960 W.Tube population	
----------	----------	----------	Z=116.7841 cm
1001	129931	2013590	
1002	211966	2789359	water inside
1003	251488	2810499	10.16-cm-diam
1004	303359	2883304	part of 1960
1005	286551	2322314	water tube
1006	281599	1938155	
1007	295579	1723785	
1008	330599	1642062	
----------	----------	----------	Z=174.27 cm
1501	1786047	6378430	
1502	2488378	7548536	
1503	3509576	9049368	big water
1504	5039333	11038789	region
1505	6754982	12565165	where
1506	8568638	13543794	R=17.4742
1507	11003972	14830770	cm
1508	14411121	16531105	
1509	19193043	18669722	
1510	25863946	21479141	
1511	35485652	24956717	
1512	47841899	28596954	
1513	65288285	33236548	
----------	----------	----------	Z=310.58 cm
1601	14805227	6788285	
1602	13208499	5254607	water in
1603	13817089	4744579	rectangular
1604	14500298	4194883	hole in
1605	15787049	3946292	collimator
1606	16887164	3806567	
----------	----------	----------	Z=399.48 cm

demonstrated in Run HB307D was considered quite acceptable -- ie, it was not diminishing to the point where statistics would become poor, and it was not artificially growing out of control to the point where it would impact calculational efficiency too adversely.

C.6.5 Key Results

Table C6.5 shows the gamma fluxes and dose rates at a point midway between the collimator and rotary shutter when the water tube and collimator sections are both flooded and the HFIR is operating at 100 MW. Results are shown for Run HB307C, which used 2 million histories and is based on the 1998 water tube, as well as for Run HB307D, which used 5 million histories and incorporates the original 1960 water tube design. In both cases, the flux and dose rate estimates are based on Tallies 15 and 25, respectively. These point detectors are located at X=0, Y=0, Z=407.464 cm (in the void region just downstream of the water-filled collimator). Note that the rotary shutter itself was not actually included in these models. Moreover, the energy-dependent fluxes and dose rates shown here correspond to the gamma energy spectrum at the detector location.

The first and most interesting thing to note is that the gamma dose rate at this location (due to the original "primary" gammas streaming down the beam tube and impinging on the water tube) is approximately 4.1 times higher for the shorter 1998 water tube than for the original (longer) 1960 water tube. In the case of the older (longer) water tube, the dose rate there was 26.77 Rem/hr, while for the newly proposed (shorter) water tube it was 109.31 Rem/hr. Both point detector estimates appear to be well converged, with statistical deviations of about 0.85% to 1.14%, respectively, although the boundary crossing estimators associated with the gamma leakage at this location suggest that the actual uncertainties (discussed later) may be more like 10-15%.

The second thing to note from Table C6.5 is that about half of the dose comes from gammas that are ultimately in the 7.5 to 8.0 MeV range, while about half the dose comes from gammas that are ultimately in the 3 (or 4) to 7.5 MeV energy range. This corresponds to just the 7 or 8 most energetic gamma source groups. This, in turn, means two things: (a) the calculation could probably be made a lot more efficient by just analyzing these energy groups, and (b) the actual uncertainty relative to reality is more closely linked to uncertainties in the original source terms in these particular groups (cf Table 2.2b) than to the uncertainties in this transport calculation. [Note that for tangential beam tubes, gamma sources in this energy range come primarily from (n,g) reactions in the aluminum at the hot end of the beam tube as calculated by the large global analyses described in Sect 2, while for the radial beam tube (HB-2), gamma sources in this energy range are more likely to come directly from prompt and delayed fission gammas in the core.]

Lastly, these findings are in qualitatively good agreement with the simple 3-group analytic formula presented in Sect 5.2, whose results were known a priori. More importantly, these findings are in excellent agreement with results from the totally independent 23-group point kernel approach which was developed concurrently to cross check the MCNP results. Table 5.5, which compares the results obtained by these two methods shows that: (a) for the 1998 water tube, the point kernel method in QADD3 yielded a dose rate of 103.05 Rem/hr at this location, which is very close to the 109.31 Rem/hr obtained by MCNP Run HB307C; (b) for the 1960 water tube, the point kernel method in QADD3 yielded a dose rate of 23.93 Rem/hr at this location, which is very close to the 26.77 Rem/hr obtained by MCNP Run HB307D. Moreover, based on the 23-group point kernel approach, one is compelled to reach the same conclusion with respect to the relative importance of the various gamma source groups. In Sect 5.5, which discusses the findings of the point kernel method in more detail, it is noted that: (a) for the 1998 water tube, the primary gamma sources in VELM groups 1-8 (just those above 3.0 MeV) contribute 98.090% of the final gamma dose at the location of interest (impingent on the rotary shutter, just downstream of the water-filled collimator); while (b) for the 1960 water tube, the primary gamma sources in VELM groups 1-8 contribute 98.945% of the final gamma dose at the location of interest. Implications for running the MCNP calculations more efficiently, based on this knowledge, are discussed in Sect 5.5. There it is shown that, by ignoring all lower energy gammas, the MCNP calculations could be made to run about 17 times faster than the present calculations, even if the importance regions in this simplified problem were left unchanged. Moreover, if one were to focus exclusively on gammas on the 3-8 MeV range, then the mean free path would be more constant throughout the problem and somewhat longer than the mean free path assumed here at the hot end of the water tube, such one could get by with fewer importance regions and less geometric splitting, thus resulting in even further gains in calculational efficiency. [Generally, this would not maintain a constant (total) gamma population throughout the problem, but it would maintain a more constant population of "numerical particles" representing the higher-energy gammas that really contribute to the final result. Moreover, if the gamma sources in the other groups were set to zero at the start, then even the total population would appear to be constant within the limits described above.]

Additional results of interest are shown in Tables C6.6 and C6.7. The first shows the gamma leakage rates (p/s), in various energy and angular ranges, on the downstream (exit) side of the 2.75-inch x 5.5-inch rectangular hole through the collimator when the 1998 water tube and collimator sections are both flooded and the HFIR is operating at 100 MW. These results are from Run HB307C, which used 2 million histories and was based on the new (shorter) 1998 water tube design. Table C6.7 shows the corresponding results from Run

Table C6.5. Gamma fluxes and dose rates at a point midway between the collimator and rotary shutter when the water tube and collimator sections are both flooded and the HFIR is operating at 100 MW. Results are shown for Run HB307C, which used 2 million histories and is based on the 1998 water tube, as well as for Run HB307D, which used 5 million histories and is for the original 1960 water tube. In both cases, the flux and dose rate estimates are based on Tallies 15 and 25, point detectors which are located at X=0, Y=0, Z=407.464 cm (in a void region just downstream of the water-filled collimator). Note that the rotary shutter itself was not actually included in these models. Moreover, the energy-dependent fluxes and dose rates shown here correspond to the gamma energies at this detector location.

		Results from Tallies 15 & 25 of Run HB307C for the proposed (shorter) 1998 water tube				Results from Tallies 15 & 25 of Run HB307D for the original (longer) 1960 water tube			
Emin (MeV)	Emax (MeV	G-Flux (p/s/cm2)	fsd	G-Dose (mrem/hr)	fsd	G-Flux (p/s/cm2)	fsd	G-Dose (mrem/hr)	fsd
0.000 -	0.010	0.00000E+00	.0000	0.00000E+00	.0000	0.00000E+00	.0000	0.00000E+00	.0000
0.010 -	0.020	1.31885E+04	.1536	2.53493E+01	.1635	4.06284E+03	.1236	7.50793E+00	.1160
0.020 -	0.045	7.66123E+04	.0947	4.42520E+01	.0947	2.25621E+04	.0947	1.30321E+01	.0947
0.045 -	0.070	7.51274E+04	.0853	2.06345E+01	.0853	2.28770E+04	.0700	6.28341E+00	.0700
0.070 -	0.10	8.80572E+04	.0687	2.34620E+01	.0687	2.46462E+04	.0540	6.56674E+00	.0540
0.10 -	0.15	1.48767E+05	.0629	4.87463E+01	.0629	4.15198E+04	.0498	1.36048E+01	.0498
0.15 -	0.30	3.06887E+05	.0588	1.73931E+02	.0588	8.34084E+04	.0471	4.72726E+01	.0471
0.30 -	0.40	1.24954E+05	.0576	1.09452E+02	.0576	3.46754E+04	.0439	3.03736E+01	.0439
0.40 -	0.51	1.23737E+05	.0625	1.34279E+02	.0625	3.15359E+04	.0439	3.42228E+01	.0439
0.51 -	0.60	1.54585E+05	.0608	1.97822E+02	.0608	4.11664E+04	.0421	5.26806E+01	.0421
0.60 -	0.70	6.58593E+04	.0663	9.49493E+01	.0663	1.74080E+04	.0519	2.50971E+01	.0519
0.70 -	1.0	1.58518E+05	.0570	2.78405E+02	.0570	4.04917E+04	.0425	7.11156E+01	.0425
1.0 -	1.5	2.15834E+05	.0463	4.99785E+02	.0463	5.30227E+04	.0371	1.22779E+02	.0371
1.5 -	2.0	2.41709E+05	.0345	7.07482E+02	.0345	5.13129E+04	.0299	1.50193E+02	.0299
2.0 -	2.5	3.15030E+05	.0271	1.09271E+03	.0271	5.92829E+04	.0234	2.05629E+02	.0234
2.5 -	3.0	3.90983E+05	.0266	1.54814E+03	.0266	7.22261E+04	.0202	2.85986E+02	.0202
3.0 -	4.0	1.24757E+06	.0210	5.76639E+03	.0210	2.29964E+05	.0149	1.06292E+03	.0149
4.0 -	5.0	2.01818E+06	.0163	1.09256E+04	.0163	4.06580E+05	.0115	2.20106E+03	.0115
5.0 -	6.0	1.69435E+06	.0234	1.04895E+04	.0234	4.15572E+05	.0143	2.57277E+03	.0143
6.0 -	7.0	3.59676E+06	.0162	2.49130E+04	.0162	8.89728E+05	.0100	6.16270E+03	.0100
7.0 -	7.5	9.91370E+05	.0302	7.41376E+03	.0302	3.02390E+05	.0200	2.26136E+03	.0200
7.5 -	8.0	5.29945E+06	.0086	4.15837E+04	.0086	1.34149E+06	.0072	1.05264E+04	.0072
8.0 -	10.0	3.66893E+05	.0478	3.21824E+03	.0478	1.03207E+05	.0453	9.05291E+02	.0453
10.0 -	14.0	0.00000E+00	.0000	0.00000E+00	.0000	3.93554E+02	.4127	4.33697E+00	.4127
	Total:	1.77144E+07	.0152	1.09310E+05	.0114	4.28952E+06	.0118	2.67692E+04	.0085
	Total:			109.31 Rem/hr				26.77 Rem/hr	

HB307D which used 5 million histories and was based on the original (longer) 1960 water tube design. Results in the first column are based on Tally 51 and show the total leakage (p/s) for all gammas integrated over the entire forward hemisphere (0 to 90 degrees). Results in the other columns are based on Tally 41 and show the total leakage (p/s) within discrete angular ranges (0-2 degrees of the centerline, 2-5 degrees of the centerline, etc). These results from Tallies 41 and 51 are based on "real" boundary crossing counters, not point detectors. Also note that these are "leakage" rates (p/s) by energy group, not fluxes or currents. One can divide by the area of the hole to get currents, but the fluxes are not immediately available from this data since the effect of individual particle direction cosines with respect to the exit surface have already been applied to get the leakage rates. Moreover, the detailed results in Tables C6.6 and C6.7 would likely only be useful in the event that one had to construct a space-energy-angle-dependent boundary source by hand for use in a subsequent bootstrapped shielding analysis of the rotary shutter using some alternate analytic technique (QAD, DORT, TORT, etc). [If one anticipated using MCNP in the subsequent calculation, it would be far better and easier to let the preliminary MCNP calculation write a binary "surface source file" which could then be used in the follow-up shielding analysis if necessary.] Nevertheless, two things should be noted:

(1) The zeros in the lower right hand corner of these tables corresponding to high-energy gammas emerging at large angles with respect to the centerline do not necessarily denote poor statistics or any anomaly with the analysis. Moreover, this is actually a consequence of the basic physics. The Compton and Klein-Nishina scattering laws establish a unique relationship between the angle of scatter and the amount of energy lost in a scattering event. High-energy gammas scattering through large angles necessarily end up at lower energies. Thus this result is to be expected.

(2) In the higher energy range of primary interest (6-8 MeV), the calculational uncertainties based on the associated fsd's (fractional standard deviations) are substantially higher than what one would be led to believe based on the point detector responses cited above. While the point detector total dose rates had fsd's on the order of 1%, the boundary crossing tallies for the total gamma leakage in the 6-8 MeV range have fsd's on the order of 10-12% for the 1998 water tube (see column 1 of Table C6.6, based on Run HB307C with 2 million histories), and on the order of 6-8% for the 1960 water tube (see column 1 of Table C6.7, based on Run HB307D with 5 million histories), while the results in the 8-10 MeV range have uncertainties in the 27-35% range, depending on the model. While those in this higher energy range (8-10 MeV) contribute only marginally to the dose rate at this particular location just downstream of the collimator (cf Table C6.5), they may have a somewhat larger role in determining the dose rate downstream of the rotary shutter in any subsequent bootstrapped calculation. Thus, despite the good point detector flux and dose rates estimates, and despite the good uncertainties on the overall gamma leakage rate (especially in the less important gamma energy ranges), the quality of these boundary crossing tallies in the higher energy ranges is probably a little less than normally desirable if these results were to be used as boundary source terms in a follow-up bootstrapped shielding analysis for the rotary shutter.

Lastly, it is useful or at least interesting to compare the total gamma leakage through the water-filled rectangular hole, with the total gamma leakage through the rest of the steel collimator assembly. Table C6.8 shows the total integrated gamma leakage rates (p/s) across the entire downstream surface of the collimator at Z=399.48 cm, when the 1998 water tube and collimator sections are both flooded and the HFIR is operating at 100 MW (based on Run HB307C), while Table C6.9 shows the corresponding gamma leakage rates when the 1960 water tube and collimator sections are both flooded (based on Run HB307D). More specifically, these tables show the gamma leakage rates through each of five different segments of the 34.9484-cm-diam disk (at Z=399.48 cm) corresponding to the downstream end of the collimator, with the five different segments being defined as shown in Fig. C6.4. Segment 5 corresponds to the area immediately in front of the 2.75-inch x 5.5-inch water-filled rectangular hole, while segments 1 to 4 correspond to different portions of the steel collimator surrounding the rectangular hole. In the case of the 1998 water tube, the gamma leakage through the water-filled hole accounts for 87.0% of the total gamma leakage (over all energies), but about 97.8% of all the high-energy gamma leakage. In the case of the 1960 water tube, the gamma leakage through the water-filled hole accounts for 86.2% of the total gamma leakage (over all energies), but about 95.4% of all the high-energy gamma leakage.

C.6.6 Conclusions and Possible Improvements

In the case of the 1998 water tube, Run HB307C showed the dose rate downstream of the collimator to be 109.31 Rem/hr when the water tube and collimator sections are both flooded and the HFIR is operating at 100 MW. In the case of the 1960 water tube, Run HB307D showed the dose rate downstream of the collimator to be 26.77 Rem/hr when the water tube and collimator sections are both flooded. These results are in very good agreement with those from a totally independent 23-group point kernel analysis which showed the corresponding dose rates to be 103.05 Rem/hr and 23.93 Rem/hr, respectively. As shown by both methods, 98% to 99% of the total gamma dose rate downstream of the collimator comes from the original (primary) gamma sources in VELM groups 1 through 8. This means that the ultimate uncertainty of the calculated dose rate relative to reality is keenly dependent of the uncertainty associated with these particular source terms. As shown above and in Sect 5.2, it also means that the same MCNP calculations described here could have been made to run 17 times faster if all other source terms had been ignored, with no significant

Table C6.6. Gamma leakage (p/s) and corresponding fsd's, in various energy and angular ranges(*), on the downstream (exit) side of the 2.75-inch x 5.5-inch rectangular hole through the collimator when the 1998 water tube and collimator sections are both flooded and the HFIR is operating at 100 MW. Results are shown for Run HB307C, which used 2 million histories and was based on the new (shorter) 1998 water tube design. (See recommended values in Table D5.4)

Emin (MeV)	Emax (MeV)	Range: 0-90 deg (p/s)	fsd	Range: 0-2 deg (p/s)	fsd	Range: 2-5 deg (p/s)	fsd	Range: 5-10 deg (p/s)	fsd	Range: 10-20 deg (p/s)	fsd	Range: 20-30 deg (p/s)	fsd	Range: 30-60 deg (p/s)	fsd	Range: 60-90 deg (p/s)	fsd
0.010	- 0.020	1.90358e+6	.0710	1.90358e+5	.1424	3.94921e+5	.1035	4.94362e+5	.0972	4.31857e+5	.0967	1.78993e+5	.1280	1.78993e+5	.1375	3.40939e+4	.2887
0.020	- 0.045	1.08476e+7	.0612	6.79038e+5	.1005	1.94051e+6	.0780	2.53432e+6	.0703	2.24452e+6	.0645	1.11089e+6	.0732	1.82687e+6	.0685	5.11409e+5	.0926
0.045	- 0.070	1.34898e+7	.0579	7.24496e+5	.0910	1.96608e+6	.0779	2.44056e+6	.0680	2.61955e+6	.0609	1.61662e+6	.0670	3.21335e+6	.0609	9.09172e+5	.0789
0.070	- 0.10	1.65498e+7	.0544	6.84720e+5	.1004	1.83539e+6	.0704	2.31555e+6	.0650	2.95481e+6	.0611	2.23315e+6	.0582	4.89248e+6	.0582	1.63367e+6	.0700
0.10	- 0.15	2.86673e+7	.0539	7.69955e+5	.0924	2.45476e+6	.0692	3.36678e+6	.0625	4.75610e+6	.0579	4.07991e+6	.0561	9.90997e+6	.0557	3.32984e+6	.0620
0.15	- 0.30	5.46128e+7	.0533	1.64219e+6	.0812	4.53449e+6	.0695	6.07156e+6	.0585	8.44393e+6	.0535	7.28474e+6	.0547	1.91892e+7	.0548	7.44668e+6	.0545
0.30	- 0.40	2.30162e+7	.0536	7.01767e+5	.0901	2.05984e+6	.0723	2.82127e+6	.0633	3.60259e+6	.0594	3.12244e+6	.0584	8.10867e+6	.0559	2.59966e+6	.0596
0.40	- 0.51	2.17889e+7	.0533	6.08009e+5	.0973	1.97177e+6	.0708	2.62807e+6	.0612	3.52304e+6	.0582	3.26449e+6	.0597	7.11427e+6	.0564	2.67922e+6	.0597
0.51	- 0.60	3.37558e+7	.0569	5.39821e+5	.1091	1.62230e+6	.0756	2.44624e+6	.0650	4.48904e+6	.0587	5.11693e+6	.0590	1.33961e+7	.0618	6.14543e+6	.0586
0.60	- 0.70	1.27881e+7	.0494	4.20492e+5	.1089	1.29273e+6	.0731	1.65071e+6	.0713	1.84960e+6	.0626	1.45467e+6	.0599	3.44065e+6	.0514	2.67922e+6	.0560
0.70	- 1.0	3.39917e+7	.0467	1.09953e+6	.0832	3.18210e+6	.0664	3.90376e+6	.0572	4.49472e+6	.0540	3.56282e+6	.0510	1.27852e+7	.0433	4.96351e+6	.0561
1.0	- 1.5	4.75156e+7	.0436	1.81266e+6	.0692	4.25038e+6	.0606	5.11409e+6	.0540	6.35000e+6	.0463	5.73631e+6	.0421	2.38004e+7	.0454	4.51745e+5	.1012
1.5	- 2.0	4.45523e+7	.0395	3.60259e+6	.0756	3.90944e+6	.0590	4.34129e+6	.0476	6.42387e+6	.0410	6.82447e+6	.0380	1.94392e+7	.0494	1.13646e+4	.5000
2.0	- 2.5	5.04022e+7	.0384	1.10294e+7	.0909	4.06570e+6	.0589	4.63393e+6	.0443	7.20519e+6	.0389	1.24841e+7	.0442	1.09839e+7	.0640	0.00000e+0	.0000
2.5	- 3.0	4.95271e+7	.0444	1.06458e+7	.1333	4.38959e+6	.0645	5.12261e+6	.0461	1.03930e+7	.0441	1.76067e+7	.0518	1.36944e+6	.0787	0.00000e+0	.0000
3.0	- 4.0	1.53775e+8	.0554	7.18160e+7	.0977	1.34387e+7	.0514	1.54957e+7	.0450	3.12386e+7	.0470	2.14849e+7	.0656	3.01163e+5	.1223	0.00000e+0	.0000
4.0	- 5.0	2.11871e+8	.0738	1.30355e+8	.1080	2.05700e+7	.0882	1.91295e+7	.0561	4.01882e+7	.0582	1.62799e+6	.1022	0.00000e+0	.0000	0.00000e+0	.0000
5.0	- 6.0	1.83079e+8	.0965	1.02972e+8	.1569	2.37010e+7	.1066	2.81502e+7	.0642	2.82298e+7	.0723	2.55705e+4	.3333	0.00000e+0	.0000	0.00000e+0	.0000
6.0	- 7.0	4.15767e+8	.1072	3.30237e+8	.1262	4.08815e+7	.0989	3.91938e+7	.0676	5.45503e+6	.1161	0.00000e+0	.0000	0.00000e+0	.0000	0.00000e+0	.0000
7.0	- 7.5	9.73410e+7	.1898	5.75079e+7	.3107	2.94771e+7	.0885	1.01486e+7	.1052	2.07405e+5	.5207	0.00000e+0	.0000	0.00000e+0	.0000	0.00000e+0	.0000
7.5	- 8.0	4.31933e+8	.1172	4.15895e+8	.1195	1.48650e+7	.1217	1.12794e+6	.2485	4.54586e+4	.9396	0.00000e+0	.0000	0.00000e+0	.0000	0.00000e+0	.0000
8.0	- 10.0	7.18729e+7	.3444	6.80004e+7	.3502	2.82127e+6	.2935	1.04839e+6	.4696	2.84116e+3	.9999	0.00000e+0	.0000	0.00000e+0	.0000	0.00000e+0	.0000
10.0	- 14.0	0.00000e+0	.0000	0.00000e+0	.0000	0.00000e+0	.0000	0.00000e+0	.0000	0.00000e+0	.0000	0.00000e+0	.0000	0.00000e+0	.0000	0.00000e+0	.0000
	Total:	2.00905e+9	.0533	1.21193e+9	.0626	1.85624e+8	.0428	1.64179e+8	.0438	1.75149e+8	.0471	9.88156e+7	.0471	1.39950e+8	.0497	3.33950e+7	.0515

* Results in the first column are based on Tally 51 and show the total leakage (p/s) for all gammas integrated over the entire forward hemisphere (0 to 90 degrees). Results in the other columns are based on Tally 41 and show the total leakage (p/s) within discrete angular ranges (0-2 degrees of the centerline, 2-5 degrees of the centerline, etc). These results from Tallies 41 and 51 are based on "real" boundary crossing counters, not point detectors. Also note that these are "leakage" rates (p/s) by energy group, not fluxes or currents. One can divide by the area of the hole to get currents, but the fluxes are not immediately available from this data since the effect of individual particle direction cosines with respect to the exit surface have already been applied to get the leakage rates.

Table C6.7. Gamma leakage (p/s) and corresponding fsd's, in various energy and angular ranges(*), on the downstream (exit) side of the 2.75-inch x 5.5-inch rectangular hole through the collimator when the 1960 water tube and collimator sections are both flooded and the HFIR is operating at 100 MW. Results are shown for Run HB307D, which used 5 million histories and was based on the original 1960 water tube design.

Emin (MeV)	Emax (MeV)	Range: 0-90 deg (p/s)	fsd	Range: 0-2 deg (p/s)	fsd	Range: 2-5 deg (p/s)	fsd	Range: 5-10 deg (p/s)	fsd	Range: 10-20 deg (p/s)	fsd	Range: 20-30 deg (p/s)	fsd	Range: 30-60 deg (p/s)	fsd	Range: 60-90 deg (p/s)	fsd
0.010	0.020	5.18544e+5	.0479	4.04717e+4	.0926	1.16918e+5	.0676	1.39122e+5	.0647	1.24788e+5	.0616	4.97465e+4	.0817	4.15960e+4	.0917	5.90213e+3	.2182
0.020	0.045	2.80183e+6	.0417	1.92803e+5	.0652	5.13485e+5	.0512	6.17194e+5	.0455	6.16351e+5	.0429	3.06911e+5	.0489	4.38444e+5	.0458	1.16637e+5	.0633
0.045	0.070	3.38389e+6	.0393	1.85777e+5	.0634	4.94655e+5	.0511	6.07638e+5	.0441	6.41927e+5	.0423	4.04436e+5	.0445	8.05500e+5	.0402	2.43955e+5	.0508
0.070	0.10	4.20428e+6	.0372	1.63573e+5	.0622	4.73857e+5	.0499	6.40803e+5	.0439	7.29335e+5	.0407	5.52552e+5	.0405	1.24001e+6	.0385	4.04155e+5	.0445
0.10	0.15	7.16378e+6	.0364	2.27935e+5	.0590	6.26188e+5	.0475	8.39227e+5	.0413	1.18099e+6	.0384	1.02753e+6	.0378	2.47805e+6	.0373	7.83859e+5	.0402
0.15	0.30	1.37045e+7	.0367	4.17365e+5	.0550	1.23130e+6	.0449	1.55114e+6	.0405	2.13095e+6	.0376	1.78863e+6	.0386	4.79169e+6	.0368	1.79340e+6	.0379
0.30	0.40	5.81332e+6	.0368	2.00110e+5	.0611	5.61546e+5	.0474	7.30178e+5	.0419	9.19046e+5	.0403	7.92010e+5	.0411	1.92662e+6	.0373	6.83804e+5	.0401
0.40	0.51	5.36391e+6	.0375	1.72848e+5	.0644	4.97465e+5	.0488	6.57385e+5	.0427	8.84757e+5	.0413	7.50695e+5	.0411	1.75181e+6	.0390	6.48953e+5	.0389
0.51	0.60	8.63116e+6	.0391	1.28442e+5	.0658	4.26640e+5	.0474	6.25626e+5	.0438	1.21190e+6	.0413	1.27627e+6	.0411	3.39822e+6	.0406	1.56406e+6	.0431
0.60	0.70	3.09215e+6	.0343	1.25631e+5	.0674	3.40637e+5	.0512	3.92632e+5	.0462	4.40692e+5	.0421	3.28833e+5	.0434	7.94258e+5	.0359	6.69470e+5	.0362
0.70	1.0	8.06456e+6	.0329	3.06630e+5	.0526	8.05781e+5	.0470	9.33661e+5	.0411	1.09864e+6	.0371	8.35854e+5	.0375	2.86675e+6	.0297	1.21724e+6	.0380
1.0	1.5	1.10817e+7	.0307	4.10901e+5	.0500	1.04440e+6	.0415	1.18605e+6	.0378	1.43900e+6	.0336	1.25209e+6	.0316	5.63738e+6	.0301	1.11859e+5	.0626
1.5	2.0	9.75538e+6	.0286	4.95217e+5	.0468	8.85038e+5	.0410	9.94087e+5	.0360	1.33641e+6	.0291	1.41426e+6	.0253	4.62868e+6	.0324	1.68632e+3	.4082
2.0	2.5	9.82114e+6	.0260	1.06744e+6	.0548	8.82790e+5	.0354	9.31412e+5	.0318	1.51853e+6	.0261	2.56518e+6	.0252	2.85579e+6	.0415	0.00000e+0	.0000
2.5	3.0	1.04808e+7	.0260	1.79087e+6	.0719	1.02416e+6	.0339	1.06997e+6	.0294	1.93365e+6	.0254	4.28101e+6	.0332	3.81109e+5	.0574	0.00000e+0	.0000
3.0	4.0	2.78516e+7	.0281	9.00159e+6	.0622	3.11042e+6	.0274	3.13600e+6	.0240	6.78323e+6	.0268	5.73406e+6	.0431	8.62835e+4	.0739	0.00000e+0	.0000
4.0	5.0	4.42632e+7	.0413	2.38485e+7	.0670	5.12923e+6	.0315	4.52862e+6	.0291	1.03197e+7	.0360	4.37039e+5	.0748	0.00000e+0	.0000	0.00000e+0	.0000
5.0	6.0	4.79326e+7	.0551	2.51731e+7	.0937	7.69413e+6	.0577	7.35771e+6	.0360	7.69778e+6	.0469	9.83688e+3	.1917	0.00000e+0	.0000	0.00000e+0	.0000
6.0	7.0	9.59239e+7	.0631	7.22508e+7	.0788	1.14150e+7	.0380	1.06039e+7	.0418	1.65428e+6	.0781	0.00000e+0	.0000	0.00000e+0	.0000	0.00000e+0	.0000
7.0	7.5	3.02273e+7	.1002	1.87775e+7	.1574	8.52998e+6	.0430	2.83330e+6	.0694	8.65646e+4	.3567	0.00000e+0	.0000	0.00000e+0	.0000	0.00000e+0	.0000
7.5	8.0	1.25912e+8	.0771	1.21465e+8	.0781	4.11294e+6	.0729	3.19558e+5	.1922	1.43337e+4	.5983	0.00000e+0	.0000	0.00000e+0	.0000	0.00000e+0	.0000
8.0	10.0	1.44538e+7	.2653	1.32137e+7	.2713	8.70705e+5	.1877	3.69305e+5	.3351	0.00000e+0	.0000	0.00000e+0	.0000	0.00000e+0	.0000	0.00000e+0	.0000
10.0	14.0	0.00000e+0	.0000	0.00000e+0	.0000	0.00000e+0	.0000	0.00000e+0	.0000	0.00000e+0	.0000	0.00000e+0	.0000	0.00000e+0	.0000	0.00000e+0	.0000
	Total:	4.90445e+8	.0363	2.89657e+8	.0433	5.07873e+7	.0237	4.10645e+7	.0294	4.27629e+7	.0325	2.38069e+7	.0329	3.41222e+7	.0336	8.24499e+6	.0356

* Results in the first column are based on Tally 51 and show the total leakage (p/s) for all gammas integrated over the entire forward hemisphere (0 to 90 degrees). Results in the other columns are based on Tally 41 and show the total leakage (p/s) within discrete angular ranges (0-2 degrees of the centerline, 2-5 degrees of the centerline, etc). These results from Tallies 41 and 51 are based on "real" boundary crossing counters, not point detectors. Also note that these are "leakage" rates (p/s) by energy group, not fluxes or currents. One can divide by the area of the hole to get currents, but the fluxes are not immediately available from this data since the effect of individual particle direction cosines with respect to the exit surface have already been applied to get the leakage rates.

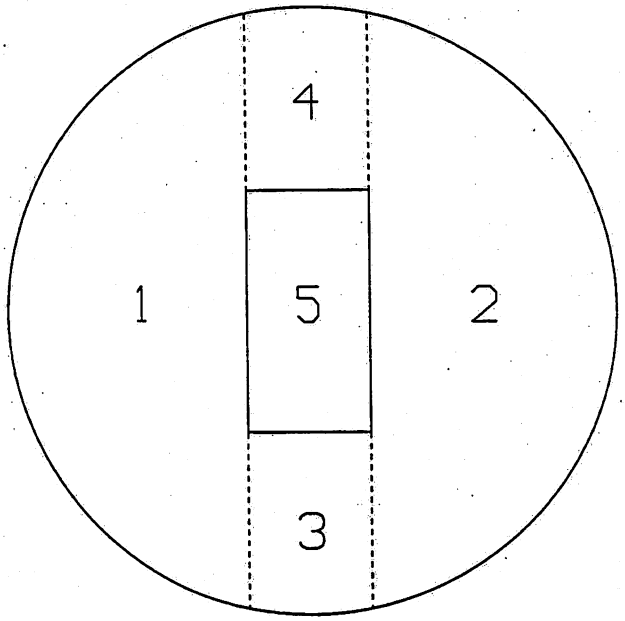


Fig. C6.4. Segmented areas used to tally the total gamma leakage (by energy group) at Z=399.48 cm in Tables C6.8 and C6.9.

Table C6.8. Total integrated gamma leakage (p/s) across the entire downstream surface of the collimator at Z=399.48 cm, including the water-filled rectangular hole (segment 5), when the 1998 water tube and collimator sections are both flooded and the HFIR is operating at 100 MW. These results are taken from Tally 51 of Run HB307C which used 2 million histories. Collectively, area segments 1 to 5 cover the entire 34.9484-cm-diam surface at Z=399.48 cm (as described in Fig. C6.4), while segment 5 corresponds to area directly downstream of the 2.75-inch x 5.5-inch water-filled rectangular hole.

Emin (MeV)	Emax (MeV)	Segment 1 (p/s)	fsd	Segment 2 (p/s)	fsd	Segment 3 (p/s)	fsd	Segment 4 (p/s)	fsd	Segment 5 (p/s)	fsd
0.010	0.020	1.13646e+4	.5000	8.52348e+3	.5773	1.13646e+4	.5000	1.42058e+4	.4472	1.90358e+6	.0710
0.020	0.045	5.11409e+4	.2357	5.68232e+4	.2345	2.27293e+4	.3953	3.97763e+4	.2857	1.08476e+7	.0612
0.045	0.070	1.42058e+5	.1549	1.56264e+5	.1595	5.96644e+4	.2284	8.52348e+4	.2211	1.34898e+7	.0579
0.070	0.10	5.59709e+5	.0904	6.39261e+5	.0946	2.84116e+5	.1175	3.12528e+5	.1681	1.65498e+7	.0544
0.10	0.15	2.84116e+6	.0617	2.83264e+6	.0706	1.03702e+6	.0867	1.42626e+6	.1116	2.86673e+7	.0539
0.15	0.30	9.92418e+6	.0544	1.07879e+7	.0688	4.23617e+6	.0739	4.56291e+6	.0950	5.46128e+7	.0533
0.30	0.40	5.28456e+6	.0563	5.48912e+6	.0642	2.09394e+6	.0769	2.40362e+6	.0900	2.30162e+7	.0536
0.40	0.51	5.07716e+6	.0538	5.02317e+6	.0622	1.99734e+6	.0742	2.25588e+6	.0947	2.17889e+7	.0533
0.51	0.60	5.31297e+6	.0560	5.67664e+6	.0733	2.24736e+6	.0810	2.73320e+6	.1103	3.37558e+7	.0569
0.60	0.70	2.71047e+6	.0558	2.66217e+6	.0631	1.18476e+6	.0721	1.35523e+6	.0900	1.27881e+7	.0494
0.70	1.0	7.16825e+6	.0492	7.63136e+6	.0528	2.89230e+6	.0666	3.20199e+6	.0774	3.39917e+7	.0467
1.0	1.5	9.39856e+6	.0470	9.52073e+6	.0528	4.00320e+6	.0589	4.42369e+6	.0705	4.75156e+7	.0436
1.5	2.0	7.41543e+6	.0477	7.61147e+6	.0503	3.36962e+6	.0598	3.44349e+6	.0682	4.45523e+7	.0395
2.0	2.5	6.37557e+6	.0491	6.53467e+6	.0496	2.83264e+6	.0634	2.97470e+6	.0683	5.04022e+7	.0384
2.5	3.0	5.15671e+6	.0488	5.31297e+6	.0510	2.54000e+6	.0637	2.58262e+6	.0699	4.95271e+7	.0444
3.0	4.0	8.76498e+6	.0497	9.07467e+6	.0516	4.71633e+6	.1004	5.37832e+6	.1071	1.53775e+8	.0554
4.0	5.0	7.10006e+6	.0823	6.53751e+6	.0883	3.52872e+6	.0946	4.06854e+6	.1225	2.11871e+8	.0738
5.0	6.0	7.02903e+6	.2208	6.47217e+6	.1337	2.65649e+6	.1098	3.87534e+6	.2994	1.83079e+8	.0965
6.0	7.0	5.11409e+6	.2625	4.09127e+6	.1061	2.69910e+6	.3137	7.15120e+6	.4637	4.15767e+8	.1072
7.0	7.5	1.45752e+6	.1701	1.24159e+6	.1469	7.30178e+5	.3543	7.33020e+5	.2419	9.73410e+7	.1898
7.5	8.0	6.39261e+5	.2200	5.38684e+6	.5572	7.30178e+5	.3690	2.45476e+6	.5532	4.31933e+8	.1172
8.0	10.0	2.32975e+5	.4427	1.42058e+5	.6112	1.10805e+5	.5864	4.26174e+4	.6633	7.18729e+7	.3444
10.0	14.0	0.00000e+0	.0000	0.00000e+0	.0000	0.00000e+0	.0000	0.00000e+0	.0000	0.00000e+0	.0000
	Total:	9.77672e+7	.0545	1.02890e+8	.0715	4.39840e+7	.0712	5.55191e+7	.1194	2.00905e+9	.0533

Table C6.9. Total integrated gamma leakage (p/s) across the entire downstream surface of the collimator at Z=399.48 cm, including the water-filled rectangular hole (segment 5), when the 1960 water tube and collimator sections are both flooded and the HFIR is operating at 100 MW. These results are taken from Tally 51 of Run HB307D which used 5 million histories. Collectively, area segments 1 to 5 cover the entire 34.9484-cm-diam surface at Z=399.48 cm (as described in Fig. C6.4), while segment 5 corresponds to area directly downstream of the 2.75-inch x 5.5-inch water-filled rectangular hole.

Emin (MeV)	Emax (MeV)	Segment 1 (p/s)	fsd	Segment 2 (p/s)	fsd	Segment 3 (p/s)	fsd	Segment 4 (p/s)	fsd	Segment 5 (p/s)	fsd
0.010	0.020	1.12422e+3	.5000	1.12422e+3	.5000	2.81054e+3	.5292	1.96738e+3	.4286	5.18544e+5	.0479
0.020	0.045	1.71443e+4	.1664	1.43337e+4	.1400	1.01179e+4	.3579	6.18318e+3	.2132	2.80183e+6	.0417
0.045	0.070	4.38444e+4	.1189	3.70991e+4	.1039	2.92296e+4	.2062	2.64191e+4	.1435	3.38389e+6	.0393
0.070	0.10	1.55142e+5	.0826	1.52050e+5	.0644	8.01003e+4	.1371	7.75709e+4	.0883	4.20428e+6	.0372
0.10	0.15	6.95327e+5	.0490	6.97857e+5	.0430	3.12813e+5	.0870	3.27428e+5	.0642	7.16378e+6	.0364
0.15	0.30	2.52105e+6	.0442	2.49632e+6	.0410	1.08515e+6	.0664	1.13967e+6	.0575	1.37045e+7	.0367
0.30	0.40	1.32404e+6	.0426	1.32826e+6	.0420	5.73350e+5	.0619	5.87965e+5	.0550	5.81332e+6	.0368
0.40	0.51	1.25266e+6	.0431	1.20263e+6	.0396	5.37656e+5	.0654	5.51147e+5	.0555	5.36391e+6	.0375
0.51	0.60	1.38054e+6	.0516	1.36929e+6	.0452	6.61882e+5	.0882	6.87177e+5	.0685	8.63116e+6	.0391
0.60	0.70	6.73124e+5	.0415	6.59914e+5	.0405	3.04943e+5	.0616	2.72341e+5	.0578	3.09215e+6	.0343
0.70	1.0	1.78244e+6	.0359	1.74085e+6	.0345	7.45917e+5	.0523	7.78519e+5	.0478	8.06456e+6	.0329
1.0	1.5	2.33359e+6	.0347	2.23438e+6	.0336	9.61204e+5	.0483	9.69355e+5	.0440	1.10817e+7	.0307
1.5	2.0	1.78216e+6	.0338	1.79284e+6	.0335	7.95101e+5	.0447	7.75709e+5	.0419	9.75538e+6	.0286
2.0	2.5	1.52978e+6	.0341	1.45586e+6	.0338	6.81837e+5	.0446	6.74248e+5	.0426	9.82114e+6	.0260
2.5	3.0	1.27570e+6	.0345	1.28526e+6	.0334	6.12416e+5	.0444	5.96396e+5	.0443	1.04808e+7	.0260
3.0	4.0	2.21105e+6	.0334	2.17592e+6	.0409	1.08093e+6	.0428	1.14248e+6	.0496	2.78516e+7	.0281
4.0	5.0	1.69054e+6	.0367	1.76923e+6	.0474	9.28040e+5	.0508	1.17031e+6	.1405	4.42632e+7	.0413
5.0	6.0	1.84765e+6	.1974	1.62505e+6	.1422	8.81666e+5	.1030	7.69525e+5	.0522	4.79326e+7	.0551
6.0	7.0	1.79734e+6	.1711	1.33163e+6	.1063	7.85264e+5	.1414	1.66777e+6	.2650	9.59239e+7	.0631
7.0	7.5	3.95162e+5	.1091	3.88416e+5	.0747	2.99041e+5	.2337	4.16241e+5	.5400	3.02273e+7	.1002
7.5	8.0	1.94658e+6	.4957	7.87513e+5	.4720	2.45922e+6	.6194	8.51312e+5	.5553	1.25912e+8	.0771
8.0	10.0	3.85044e+4	.5036	1.07644e+5	.5396	3.70991e+4	.4178	2.61380e+4	.4686	1.44538e+7	.2653
10.0	14.0	0.00000e+0	.0000	0.00000e+0	.0000	0.00000e+0	.0000	0.00000e+0	.0000	0.00000e+0	.0000
	Total:	2.66945e+7	.0622	2.46535e+7	.0435	1.38658e+7	.1396	1.35159e+7	.0790	4.90445e+8	.0363

degradation in the final results. Moreover, by using only these particular source terms and running for the same amount of time, the associated calculational uncertainties could have been reduced still further. That, however, was not done for a couple of reasons:

1) The model would still have suffered from all the approximations and simplifications described in Sect C.6.2 above. While those simplifications do attempt to model all of the key characteristics that were judged to be important in this analysis, it is, in the end, a highly-simplified "preliminary" model that somehow, someday, somebody would eventually challenge. Moreover, it generally falls into the category of a "special purpose model" whose geometric description and importance regions necessarily differ from the base model that we had hoped to use for all of the HB-3 beam tube analyses.

2) The model itself is incomplete and would have to be bootstrapped to separate model of the rotary shutter assembly in order to estimate the fluxes and dose rates downstream of the rotary shutter. While the gamma leakage terms by energy group and direction (as shown in Tables C6.6 and C6.7) may be useful for specifying source terms to be used with other codes, it would be difficult or impossible to use them directly as input to a follow-up MCNP analysis of the rotary shutter. If that were the intended use, it would be better to rerun the calculations from scratch and save a binary MCNP "surface source file" at the downstream end of the collimator that could then be used in a follow-up calculation. Moreover, the present boundary crossing tallies at the downstream end of the collimator, while not bad, were somewhat deficient in the highest energy gamma groups, with fsd's of 10-12% in the 6-8 MeV energy range for the 1998 water tube. A good boundary source should be better defined with more resolution in this energy range. [While Run HB307C for the 1998 water tube actually saw 0.8 million "numerical particles" exit the collimator section (with many of these being lower energy gammas), the final model (Run HB308G5, described in Sect 6) actually saw 5.6 million "numerical particles" exit the collimator section, where most of them had been properly biased toward higher energies that would be more likely to contribute to the dose rate downstream of the rotary shutter.]

3) While running the preliminary model with many more histories and using only the higher energy sources (corresponding to VELM groups 1 to 8) would have produced a better boundary source downstream of the collimator that could have been bootstrapped to an MCNP model of the rotary shutter assembly, one would ultimately be faced with one of two serious obstacles:

   a) If source terms like those shown in Table C6.6 and C6.7 were to be input manually, there is no convenient mechanism for doing this. In fact, there is no mechanism at all. The only apparent way this could be done would be to write a new user-supplied source routine, and then recompile and relink the MCNP code to use it. While this is commonly done at ORNL for the MORSE code which was written here "in-house" where everyone is familiar with the internal workings of the code, Los Alamos strongly discourages novice users from doing this with MCNP unless one has a strong, familiar, intimate knowledge of the internal workings of the code. While I believe this could have been done without too much difficulty, it would have required a lot of additional QA for which neither time or money was available.

   b) If a binary MCNP "surface source file" were written and used with a follow-up MCNP analysis of the rotary shutter, one would have been saddled with the nightmarish need to use a large number of importance cells in a geometrically complex region of the problem, with all the attendant difficulties described in Appendix C.1. That is to say: without a detailed knowledge of (or even a listing of) the "particle weights by energy" emerging from the collimator section, the use of energy-dependent weight windows for biasing in the rotary shutter would have been impossible. Use of such weights must be correctly and consistently coupled with the weights of the incoming source particles. The only alternative then is to continue using energy-independent geometric splitting based on user-supplied importance zones. In the first place, this is not terribly desirable because one ends up tracking a lot of lower-energy particles that don't contribute significantly to the final dose rate downstream of a thick shield. In the second place, the use of user-supplied importance zones in geometrically complex regions is horribly complicated insofar as it requires literally thousands of changes to an otherwise simple input file; it is very time-consuming (in terms of manpower); and, because of the complicated nature of the resulting problem, the process is very error-prone. Appendix C.1 describes the reason for these difficulties in more detail. Moreover, the hope of circumventing those difficulties was one of the reasons this preliminary, highly-simplified model of the water tube and collimator was created in the first place. Unfortunately, if one continues down this path and attempts to bootstrap a binary MCNP "surface source file" onto the full 3-D model of the rotary shutter assembly with all its complexity and all its 3-D streaming paths, there will be no way to circumvent these difficulties in the subsequent calculation.

For these reasons, use of the highly-simplified preliminary model described here was ultimately discontinued. In lieu of this approach using a highly simplified model with energy-independent geometric splitting based on user-supplied importance zones, a new and much more powerful technique was adopted in the final gamma-only shielding analysis described in Sect 6. It employs broad-group "geometry-independent weight windows" based on a preliminary adjoint analysis. Its first successful use in MCNP4B at ORNL is described in Appendix C.2. [That particular application was for an academic type problem in which the goal was to calculate the total "neutron plus gamma" dose rate at the top

of a 130-cm-diam x 125-cm-thick tank of water having a narrow 10-cm-diam beam of neutrons impingent on the bottom surface. In many respects, it was not unlike the 1998 HB-3 water tube problem. Moreover, this powerful technique was able to make this particular academic problem run up to 10,000 times faster than would have otherwise have been possible.] One of the most attractive features of this approach is that, unlike the use of importance regions where one must often make hundreds or thousands of changes to an input file describing some complex geometry, the use of this new approach requires no significant changes to an existing MCNP input file. This allows us to take the original base model of the HB-3 beam tube described in Fig. 3.3 [including the hot end of the tube, all of the small geometry regions required for the dosimetry analysis, the entire water tube (including the biological shield), the entire collimator section (including the radial and eccentric shields, and surrounding concrete), and the full 3-D model of the rotary shutter assembly] and solve the entire problem all at once -- with no significant changes required in the MCNP input file to accommodate the biasing scheme, and no need for a separate bootstrapped shielding analysis. Moreover, with the broad-group 3-D adjoint-based weight windows (that are supplied in a geometry-independent format in an auxiliary file), this new approach is so powerful that, for the final gamma-only shielding problem, it was indeed possible to obtain good and reliable results throughout the entire configuration, including good and reliable boundary crossing estimates of the gamma fluxes and dose rates downstream of the rotary shutter. See Sect 6 for details.

Appendix C.6.7

Listing of the input file for MCNP Run HB307C, which was a preliminary (highly simplified) MCNP model once used for an exploratory analysis of the HB-3 beam tube using the newly proposed 1998 water tube design concept.

```
message:  outp=hb307.o  runtpe=hb307.r

Simplified model of HB-3 using equivalent point sources
c
c       ------------------------------------------------------------------------------------------------------------
c
c       HB307 is a series of "simplified geometry" calcs to get gamma transport in flooded water tube.
c
c             HB307A.I -- for the 1998 water tube design
c             HB307B.I -- for the 1960 water tube design (I killed this due to time, after 320000 histories)
c             HB307B2.I -- for the 1960 water tube design (continuation run to print results after 320000 histories & stop)
c             HB307C.I -- for the 1998 water tube design <-- this deck; like HB307A.I but different imp values
c
c       ------------------------------------------------------------------------------------------------------------
c
c       Used to study shielding effectiveness of water tube (work performed by Jim Bucholz for Mike Farrah, Mar/Apr 1998):
c
c       Ref 1:  Dwg of HB-1 (e:\ham\ustn\allbeam1197.dgn Jan 29, 1998 12:55:09), where HB-3 is said to be the same.
c       Ref 2:  Dwg M-11537-OH-001-E, Feb 13, 1998, 10:30:22, dwg of HB-1 (essentially the same as Ref 1, but smaller)
c       Ref 3:  Dwg E-42027, Sheet 1, Apr 11, 1995, showing location on HB-3 & 1st aluminum window in vessel, as built
c       Ref 4:  Dwg E-42027, Sheet 2, Apr 11, 1995, showing typical beam tube collimator & rotary shutter, as built
c       Ref 5:  Dwg 1546-01-M-5022, Rev Sep 18, 1961, showing concrete around HB-3 beam tube collimator & rotary shutter
c
c       Distance from outside of vessel nozzel boss to radial plane
c       perpendicular to beam tube (as specifically stated in Ref 3):
c         HB-1:  52.0 inches = 132.08 cm
c         HB-2:  54.5 inches = 138.43 cm
c         HB-3:  54.0 inches = 137.16 cm
c         HB-4:  52.0 inches = 132.08 cm
c
c       Notes regarding length of the 1998 water tube:
c
c       The location of the 1st aluminum window relative to the vessel nozzel boss (cf Ref 1 & 2) is believed to be
c       correctly modeled here.  Likewise, the 2nd aluminum window relative to the beam tube collimator assembly
c       (cf Ref 1 & 2) is believed to be correctly modeled here.  Given the location of the beam tube collimator
c       assembly (Ref 1 & 2) relative to the concrete biological shield specifically around HB-3 as shown in Ref 5,
c       however, the length of the new HB-3 water tube [from Surf 2154 at Z=174.95125 cm, to Surf 4110 at Z=302.1868 cm
c       (total length of water when flooded = 127.23555 cm)] is about 2.03 inches shorter than shown for HB-1 on Refs
c       1 & 2, and about 89.8 cm shorter than the water tube originally in HB-3. Note, however, that this 2" difference
c       in water tube length between HB-1 and HB-3 is wholly consistent with the data in Ref 3 above if the vessel
c       flange hardware and collimator hardware are the same for HB-1 and HB-3 -- J. A. Bucholz, 3-21-98
c
c       ------------------------------------------------------------------------------------------------------------
c
c     BEGIN CELLS:
c
100  61  -3.2325-4  -1010    9997 -2153          imp:p=1  $ void up center of beam tube (upstream of where water begins)
111  24  -2.7         1010  -2130  9997  -1007  imp:p=1  $ aluminum wall of beam tube (upstream of importance cutoff plane)
112   8  -1.0000      2130  -4225  9997  -1007  imp:p=0  $ water outside beam tube (upstream of importance cutoff plane)
121  24  -2.7         1010  -2130  1007  -2153  imp:p=1  $ aluminum wall of beam tube (downstream of importance cutoff plane)
122   8  -1.0000      2130  -4225  1007  -2107  imp:p=1  $ water outside beam tube (downstream of importance cutoff plane, inside vessel)
201  50  -7.8212      2130  -4225  2107  -2106  imp:p=1  $ carbon steel vessel nozzel flange (appx model; arbitrarily 6" thick)
202   8  -1.0000      2130  -4225  2106  -2153  imp:p=1  $ water outside beam tube (downstream of vessel flange)
c
c    Cell 300 goes from Z=174.27 to Z=310.58; it may have to be subdivided into a number of axial importance zones
c    300  8  -1.0000    2153  -4130  -4225 imp:p=1 $ water in water tube (from start, up "to" collimator)
301  8  -1.000     153  -6001  -4225  imp:p=1.80e+00  $  imp:p=2       $ water     ater tube (from start, up "to" collimator)
302  8  -1.000     001  -6002  -4225  imp:p=3.24e+00  $  imp:p=4       $ water     ater tube (from start, up "to" collimator)
```

```
303  8  -1.0000  6002  -6003  -4225  imp:p=5.83e+00  $  imp:p=8       $ water in water tube (from start, up "to" collimator)
304  8  -1.0000  6003  -6004  -4225  imp:p=1.05e+01  $  imp:p=16      $ water in water tube (from start, up "to" collimator)
305  8  -1.0000  6004  -6005  -4225  imp:p=1.89e+01  $  imp:p=32      $ water in water tube (from start, up "to" collimator)
306  8  -1.0000  6005  -6006  -4225  imp:p=3.40e+01  $  imp:p=64      $ water in water tube (from start, up "to" collimator)
307  8  -1.0000  6006  -6007  -4225  imp:p=6.12e+01  $  imp:p=128     $ water in water tube (from start, up "to" collimator)
308  8  -1.0000  6007  -6008  -4225  imp:p=1.10e+02  $  imp:p=256     $ water in water tube (from start, up "to" collimator)
309  8  -1.0000  6008  -6009  -4225  imp:p=1.98e+02  $  imp:p=512     $ water in water tube (from start, up "to" collimator)
310  8  -1.0000  6009  -6010  -4225  imp:p=3.57e+02  $  imp:p=1024    $ water in water tube (from start, up "to" collimator)
311  8  -1.0000  6010  -6011  -4225  imp:p=6.43e+02  $  imp:p=2048    $ water in water tube (from start, up "to" collimator)
312  8  -1.0000  6011  -6012  -4225  imp:p=1.16e+03  $  imp:p=4096    $ water in water tube (from start, up "to" collimator)
313  8  -1.0000  6012  -6013  -4225  imp:p=2.08e+03  $  imp:p=8192    $ water in water tube (from start, up "to" collimator)
314  8  -1.0000  6013  -6014  -4225  imp:p=3.75e+03  $  imp:p=16384   $ water in water tube (from start, up "to" collimator)
315  8  -1.0000  6014  -4130  -4225  imp:p=6.75e+03  $  imp:p=32768   $ water in water tube (from start, up "to" collimator)
c
c    Cells 400 & 500 go from Z=174.27 to Z=310.58; they may have to be subdivided into a number of axial importance zones
c    400  8  -1.0000  4130 -4190  4212  -4213  4210 -4211  imp:p=1  $ water in rectangular hole up thru collimator
401  8  -1.0000  4130 -6016  4212  -4213  4210 -4211 imp:p=1.21e+04  $  imp:p=65536    $ water in rectangular hole up thru collimator
402  8  -1.0000  6016 -6017  4212  -4213  4210 -4211 imp:p=2.19e+04  $  imp:p=131072   $ water in rectangular hole up thru collimator
403  8  -1.0000  6017 -6018  4212  -4213  4210 -4211 imp:p=3.93e+04  $  imp:p=262144   $ water in rectangular hole up thru collimator
404  8  -1.0000  6018 -6019  4212  -4213  4210 -4211 imp:p=7.08e+04  $  imp:p=524288   $ water in rectangular hole up thru collimator
405  8  -1.0000  6019 -6020  4212  -4213  4210 -4211 imp:p=1.27e+05  $  imp:p=1048576  $ water in rectangular hole up thru collimator
406  8  -1.0000  6020 -6021  4212  -4213  4210 -4211 imp:p=2.29e+05  $  imp:p=2097152  $ water in rectangular hole up thru collimator
407  8  -1.0000  6021 -4190  4212  -4213  4210 -4211 imp:p=4.13e+05  $  imp:p=4194304  $ water in rectangular hole up thru collimator
c
c    500  40  -7.92  4130 -4190 -4225 #(4212 -4213  4210 -4211) imp:p=1   $ stainless steel model of collimator (with rectangular hole)
501  40  -7.92  4130 -6016 -4225 #(4212 -4213  4210 -4211) imp:p=1.21e+04  $  imp:p=65536    $ stainless steel model of collimator (with rectangular hole)
502  40  -7.92  6016 -6017 -4225 #(4212 -4213  4210 -4211) imp:p=2.19e+04  $  imp:p=131072   $ stainless steel model of collimator (with rectangular hole)
503  40  -7.92  6017 -6018 -4225 #(4212 -4213  4210 -4211) imp:p=3.93e+04  $  imp:p=262144   $ stainless steel model of collimator (with rectangular hole)
504  40  -7.92  6018 -6019 -4225 #(4212 -4213  4210 -4211) imp:p=7.08e+04  $  imp:p=524288   $ stainless steel model of collimator (with rectangular hole)
505  40  -7.92  6019 -6020 -4225 #(4212 -4213  4210 -4211) imp:p=1.27e+05  $  imp:p=1048576  $ stainless steel model of collimator (with rectangular hole)
506  40  -7.92  6020 -6021 -4225 #(4212 -4213  4210 -4211) imp:p=2.29e+05  $  imp:p=2097152  $ stainless steel model of collimator (with rectangular hole)
507  40  -7.92  6021 -4190 -4225 #(4212 -4213  4210 -4211) imp:p=4.13e+05  $  imp:p=4194304  $ stainless steel model of collimator (with rectangular hole)
c
800  60  -1.0e-20  4190  -9998  -4225  imp:p=4.13e+05  $  imp:p=4194304  $ internal void downstream of collimator, but upstream of shutter drum
900   0          #(-4225   9997  -9998) imp:p=0  $ enternal void
c
c     END CELLS (next line must be blank)

c     BEGIN SURFACES:
c
1010  cz   5.08     $ inner radius of voided portion of beam tube
2130  cz   7.16174 $ inner radius of ss sleeve around HB-3 beam tube, near vessel; used as outer radius of beam tube in this model
4225  cz  17.4742  $ outer radius of narrow ss sleeve extending thru concrete into pool; radial boundary to ext void in this model
c
c     Box surfaces corresponding to rectangular-shaped hole in collimator:
c     Here (like everywhere in this MCNP model of HB-3),
c     Z=central axis; Y is really horizontal; X is really vertical
4210  py  -3.4925   $ ymin
4211  py   3.4925   $ ymax
4212  px  -6.9850   $ xmin
4213  px   6.9850   $ xmax
c
9997  pz    0.0     $ external void boundary (location corresponds to the real radial plane perpendicular to the real beam tube)
1007  pz  118.6879  $ plane below which all importances are zero; located 2 cm upstream of first pt det used to get pt srcs
2107  pz  128.7043  $ arb plane defining upstream side of thick flange in this model (flange arbitrarily taken to be 6" thick here)
2106  pz  143.9443  $ plane defining end of thick flange mounted on boss on pressure vessel around HB-3 (see dwg E-42027)
2153  pz  174.27    $ upstream   side of aluminum window forming start of water tube in proposed HB-3 design
4130  pz  310.58    $ upstream surface of collimator
```

```
4190  pz  399.48    $ downstream side of collimator
9998  pz  415.44875 $ upstream side of shutter drum; taken as ext void boundary in this model
c
6001  pz  180.7     $ importance surface
6002  pz  187.1     $ importance surface
6003  pz  193.6     $ importance surface
6004  pz  200.0     $ importance surface
6005  pz  208.3     $ importance surface
6006  pz  216.7     $ importance surface
6007  pz  225.0     $ importance surface
6008  pz  233.7     $ importance surface
6009  pz  241.7     $ importance surface
6010  pz  250.0     $ importance surface
6011  pz  262.1     $ importance surface
6012  pz  274.2     $ importance surface
6013  pz  286.3     $ importance surface
6014  pz  298.5     $ importance surface
6016  pz  320.4     $ importance surface
6017  pz  330.3     $ importance surface
6018  pz  340.1     $ importance surface
6019  pz  350.0     $ importance surface
6020  pz  366.5     $ importance surface
6021  pz  383.0     $ importance surface
c
c     END SURFACES (next line must be blank)

c     PROBLEM PARAMETERS:
mode   p
c       mode   n
c       mode   n p
nps    2000000
c       nps    40000000
c       nps    60000000
c       nps    80000000
c       nps    120000000
c      cut:n  time(shakes) energy(MeV)   WC1   WC2   SWTM
c      cut:n         1.0e20          0.027     -0.5  -0.25   0.0  $ cutoff:  don't track any neutrons below 27 keV
print  60      $ Table 60 shows vol, mass, n-imp by cell; see pp 3-117 of manual for description of other useful tables you may want
prdmp  0   80000  0  4  0   $ make restart file after every 80000 histories in fixed src calc; save only the 4 most recent restart files
c
c
c     EQUIVALENT POINT SOURCES:
c
sdef  erg=d73  pos ferg d83  $ source def for gammas in HB-3 (total p/s = 1.35399e+17)
      par=2            $ par=1 for neut, par=2 for photons
c     sdef  erg=d53  pos ferg d63  $ source def for neutrons in HB-3 (total n/s = 9.64595e+16);  total n/s above 27 keV = 1.20830e16
c     par=1            $ par=1 for neut, par=2 for photons
      vec  0  0  1     $ reference vector if directional-dependent source is used
      dir=d3           $ angular distribution wrt vec (Caution: choice of angular distribution sampled will dictate choice of wgt)
      wgt=1.7332472-2  $ use this with d3;  wgt = [mu(max)-mu(min)]/[(+1)-(-1)] = [1.0000000000-0.965335056]/2 = 1.7332472-2
c     wgt=0.1    $ use this with mu(min)=0.8 in d3 for dosimetry calc only;  wgt = [mu(max)-mu(min)]/[(+1)-(-1)] = [1.0-0.8]/2 = 0.1
c     wgt=0.145  $ use this with mu(min)=0.71 in d3 for HB304M4 dosimetry calc only;  wgt = [mu(max)-mu(min)]/[(+1)-(-1)] = [1.0-0.8]/2 = 0.145
c     -------------------
c     Ang Dist: to spray isotropically across central void of HB-3 beam tube
si3   h  0.965335056   1.0  $ angular distribution;  mu boundaries (i.e, cosine boundaries wrt vec)
c     si3   h  0.8  1.0  $ open up angular distribution for dosimetry run;  mu boundaries (i.e, cosine boundaries wrt vec)
c     si3   h  0.71  1.0  $ open up angular distribution for HB304M4 dosimetry run;  mu boundaries (i.e, cosine boundaries wrt vec)
sp3   d  0  1     $ angular distribution; particle emmission probabilities by bi      irst value (below lowest bin bound) must be zero
```

```
c     ------------------
c
c
c       ------------------------------------------------------------------------------
c       Begin distributions needed to describe the neutron sources in the HB-3 beam tube
c       ------------------------------------------------------------------------------
si53  h  1.0000e-11  $ this one Emin(MeV), followed by Emax(MeV) for the 61 VELM neut grps (lowest to highest energy for MCNP):
         4.1399e-7    1.1253e-6    2.3824e-6    5.0435e-6    1.0677e-5    $ VELM n-groups 61, 60, 59, 58, 57,
         2.2603e-5    4.7851e-5    1.0130e-4    1.6702e-4    2.7536e-4    $ VELM n-groups 56, 55, 54, 53, 52,
         4.5400e-4    7.4852e-4    1.2341e-3    2.0347e-3    2.2487e-3    $ VELM n-groups 51, 50, 49, 48, 47,
         2.6126e-3    3.0354e-3    3.7074e-3    5.5308e-3    9.1188e-3    $ VELM n-groups 46, 45, 44, 43, 42,
         1.5034e-2    2.3579e-2    2.4788e-2    2.6058e-2    2.7000e-2    $ VELM n-groups 41, 40, 39, 38, 37,
         2.8501e-2    3.4307e-2    5.2475e-2    5.6562e-2    8.6517e-2    $ VELM n-groups 36, 35, 34, 33, 32,
         1.2277e-1    1.4996e-1    1.8316e-1    2.2371e-1    2.7324e-1    $ VELM n-groups 31, 30, 29, 28, 27,
         2.9452e-1    2.9721e-1    2.9849e-1    3.0197e-1    3.8774e-1    $ VELM n-groups 26, 25, 24, 23, 22,
         4.9787e-1    5.2340e-1    6.0810e-1    7.4274e-1    9.0718e-1    $ VELM n-groups 21, 20, 19, 18, 17,
         1.1080e+0    1.3534e+0    1.6530e+0    2.0190e+0    2.2313e+0    $ VELM n-groups 16, 15, 14, 13, 12,
         2.3457e+0    2.4660e+0    3.0119e+0    3.6788e+0    4.4933e+0    $ VELM n-groups 11, 10,  9,  8,  7,
         5.4881e+0    6.7032e+0    8.1873e+0    1.0000e+1    1.2214e+1    $ VELM n-groups  6,  5,  4,  3,  2,
         1.4918e+1                                                      $ VELM n-group   1
sp53  d     0.0  $ dummy 0, followed by neut src terms (n/s) for HB-3:
         6.30365e+16  2.25679e+15  1.52979e+15  1.30212e+15  1.55274e+15  $ VELM n-groups 61, 60, 59, 58, 57,
         1.58981e+15  1.54759e+15  1.45876e+15  9.03837e+14  9.69821e+14  $ VELM n-groups 56, 55, 54, 53, 52,
         9.50610e+14  8.74122e+14  8.53691e+14  8.87245e+14  2.04908e+14  $ VELM n-groups 51, 50, 49, 48, 47,
         2.76622e+14  2.54975e+14  3.36538e+14  7.55438e+14  8.76077e+14  $ VELM n-groups 46, 45, 44, 43, 42,
         9.84217e+14  7.42049e+14  6.69650e+13  1.12860e+14  5.24714e+13  $ VELM n-groups 41, 40, 39, 38, 37,
         1.21873e+14  3.03507e+14  4.96958e+14  1.29680e+14  8.89397e+14  $ VELM n-groups 36, 35, 34, 33, 32,
         5.59006e+14  4.29193e+14  3.63241e+14  4.33245e+14  7.35199e+14  $ VELM n-groups 31, 30, 29, 28, 27,
         2.12840e+14  1.38494e+13  7.68584e+12  3.65651e+13  6.29256e+14  $ VELM n-groups 26, 25, 24, 23, 22,
         5.85513e+14  1.49367e+14  3.61470e+14  5.35177e+14  6.65098e+14  $ VELM n-groups 21, 20, 19, 18, 17,
         5.40055e+14  7.09512e+14  8.07055e+14  8.54720e+14  3.12945e+14  $ VELM n-groups 16, 15, 14, 13, 12,
         2.00073e+14  1.35333e+14  2.41078e+14  1.61947e+14  2.06360e+14  $ VELM n-groups 11, 10,  9,  8,  7,
         1.36477e+14  7.32282e+13  3.05242e+13  8.64293e+12  6.92602e+12  $ VELM n-groups  6,  5,  4,  3,  2,
         2.74800e+09                                                    $ VELM n-group   1
ds63  l     $ neutron starting positions (x,y,z) in HB-3:
         0 0  80.2    0 0  57.3    0 0  65.2    0 0  76.1    0 0  54.5    $ VELM n-groups 61, 60, 59, 58, 57,
         0 0  48.2    0 0  56.5    0 0  55.4    0 0  56.0    0 0  51.1    $ VELM n-groups 56, 55, 54, 53, 52,
         0 0  53.8    0 0  52.6    0 0  61.2    0 0  60.5    0 0  43.0    $ VELM n-groups 51, 50, 49, 48, 47,
         0 0  49.5    0 0  55.0    0 0  65.1    0 0  53.3    0 0  52.7    $ VELM n-groups 46, 45, 44, 43, 42,
         0 0  50.7    0 0  54.0    0 0  69.0    0 0  46.7    0 0  62.6    $ VELM n-groups 41, 40, 39, 38, 37,
         0 0  67.5    0 0  79.8    0 0  52.9    0 0  56.7    0 0  47.4    $ VELM n-groups 36, 35, 34, 33, 32,
         0 0  45.7    0 0  45.6    0 0  42.5    0 0  48.9    0 0  34.2    $ VELM n-groups 31, 30, 29, 28, 27,
         0 0  42.4    0 0  63.8    0 0  53.7    0 0  42.3    0 0  49.6    $ VELM n-groups 26, 25, 24, 23, 22,
         0 0  58.8    0 0  52.9    0 0  50.3    0 0  56.8    0 0  44.1    $ VELM n-groups 21, 20, 19, 18, 17,
         0 0  70.1    0 0  46.8    0 0  59.7    0 0  50.2    0 0  52.1    $ VELM n-groups 16, 15, 14, 13, 12,
         0 0  33.3    0 0  43.5    0 0  65.3    0 0  56.9    0 0  47.9    $ VELM n-groups 11, 10,  9,  8,  7,
         0 0  62.6    0 0  59.5    0 0  42.9    0 0  68.7    0 0  31.1    $ VELM n-groups  6,  5,  4,  3,  2,
         0 0  99.9                                                        $ VELM n-group   1
c       Shift sources 1.6986 cm to right of beam tube centerline (in Run HB304M4) to account for the anisotropic
c       effect of more neutrons entering the one side of the beam tube than the other:   -- JAB, 4-15-98
c     0 1.6986 67.5  0 1.6986 79.8  0 1.6986 52.9  0 1.6986 56.7  0 1.6986 47.4    $ VELM n-groups 36, 35, 34, 33, 32,
c     0 1.6986 45.7  0 1.6986 45.6  0 1.6986 42.5  0 1.6986 48.9  0 1.6986 34.2    $ VELM n-groups 31, 30, 29, 28, 27,
c     0 1.6986 42.4  0 1.6986 63.8  0 1.6986 53.7  0 1.6986 42.3  0 1.6986 49.6    $ VELM n-groups 26, 25, 24, 23, 22,
c     0 1.6986 58.8  0 1.6986 52.9  0 1.6986 50.3  0 1.6986 56.8  0 1.6986 44.1    $ VELM n-groups 21, 20, 19, 18, 17,
c     0 1.6986 70.1  0 1.6986 46.8  0 1.6986 59.7  0 1.6986 50.2  0 1.6986 52.1    $ VELM n-groups 16, 15, 14, 13, 12,
c     0 1.6986 33.3  0 1.6986 43.5  0 1.6986 65.3  0 1.6986 56.9  0 1.6986 47.9    $ VELM n-groups 11, 10,  9,  8,  7,
c     0 1.6986 62.6  0 1.6986 59.5  0 1.6986 42.9  0 1.6986 68.7  0 1.6986 31.1    $ VELM n-groups  6,  5,  4,  3,  2,
c     0 1.6986 99.9                                                    $ VELM n-group   1
c       ------------------------------------------------------------------------------
```

```
c        Begin distributions needed to describe the gamma sources in the HB-3 beam tube
c        ------------------------------------------------------------------------------
si73  h  1.0000e-2   $ this one Emin(MeV), followed by Emax(MeV) for the 23 VELM gamma grps (lowest to highest energy for MCNP):
         2.0000e-2    4.5000e-2    7.0000e-2    1.0000e-1    1.5000e-1    $ VELM g-groups 23, 22, 21, 20, 19,
         3.0000e-1    4.0000e-1    5.1000e-1    6.0000e-1    7.0000e-1    $ VELM g-groups 18, 17, 16, 15, 14,
         1.0000e+0    1.5000e+0    2.0000e+0    2.5000e+0    3.0000e+0    $ VELM g-groups 13, 12, 11, 10,  9,
         4.0000e+0    5.0000e+0    6.0000e+0    7.0000e+0    7.5000e+0    $ VELM g-groups  8,  7,  6,  5,  4,
         8.0000e+0    1.0000e+1    1.4000e+1                              $ VELM g-groups  3,  2,  1
sp73  d     0.0  $ dummy 0, followed by gamma src terms (p/s) for HB-3:
         8.72837e+12  2.84514e+15  1.65029e+16  1.67705e+16  1.82855e+16  $ VELM g-groups 23, 22, 21, 20, 19,
         2.56708e+16  1.03805e+16  7.17665e+15  4.80101e+15  4.03975e+15  $ VELM g-groups 18, 17, 16, 15, 14,
         7.31636e+15  5.27935e+15  4.23989e+15  2.66951e+15  1.42777e+15  $ VELM g-groups 13, 12, 11, 10,  9,
         2.34929e+15  1.98361e+15  6.75453e+14  1.23378e+15  1.60183e+14  $ VELM g-groups  8,  7,  6,  5,  4,
         1.51983e+15  6.19421e+13  1.23250e+11                           $ VELM g-groups  3,  2,  1
ds83  l     $ gamma starting positions (x,y,z) in HB-3:
         0 0  10.0    0 0  61.9    0 0  68.1    0 0  82.1    0 0  83.9    $ VELM g-groups 23, 22, 21, 20, 19,
         0 0  84.5    0 0  81.6    0 0  84.7    0 0  88.8    0 0  83.2    $ VELM g-groups 18, 17, 16, 15, 14,
         0 0  86.8    0 0  93.6    0 0  96.9    0 0  99.2    0 0  96.6    $ VELM g-groups 13, 12, 11, 10,  9,
         0 0  92.6    0 0  93.2    0 0  96.4    0 0  93.9    0 0  96.0    $ VELM g-groups  8,  7,  6,  5,  4,
         0 0  94.4    0 0  99.9    0 0  97.4                              $ VELM g-groups  3,  2,  1
c        ----------------------------------
c
c
c      BEGIN-TRANSFORMATIONS:
c      END-TRANSFORMATIONS
c
c
c      BEGIN MATERIAL DESCRIPTIONS:
c
c       Water gaps in removable reflector region     --Avg. Density= 0.98465 g/cm^3
m5       1001.50c     6.63485-02    8016.50c    3.31742-02
mt5      lwtr.01t
c
c       Water Reflector --Density= 0.9899 g/cm^3
m7       1001.50c     6.67022-02    8016.50c    3.33511-02
mt7      lwtr.01t
c
c       H2O Pool  --Density= 1.0000 g/cm^3
m8       1001.50c     6.73828-02    8016.50c    3.36914-02
mt8      lwtr.01t
c
c       Aluminum reflector container (outside Be reflector; 2.7 g/cc)
m23      13027.52c   5.85482-02   1001.50c  3.45716-04  12000.50c  6.68986-04
         14000.50c   3.47363-04  22000.50c  2.54704-05  24000.50c  6.09789-05
         25055.50c   2.21974-05  26000.55c  1.01905-04  29000.50c  8.74557-05
c
c       Aluminum liners in Be reflectors (2.7 g/cc)
m24      13027.52c   5.85482-02   1001.50c  3.45716-04  12000.50c  6.68986-04
         14000.50c   3.47363-04  22000.50c  2.54704-05  24000.50c  6.09789-05
         25055.50c   2.21974-05  26000.55c  1.01905-04  29000.50c  8.74557-05
c
c       ss liner of pressure vessel, bioshield liner, and other components -- SCALE SS304 (7.92 g/cc;  69.5 w/o Fe, 19.0 w/o Cr, 9.5 w/o Ni,  2.0 w/o Mn)
m40      26000.55c  5.93541-02   24000.50c  1.74281-02
         28000.50c  7.71883-03   25055.50c  1.73629-03
c
c       ss (same as above, but diff color on plot) used for removable shield around collimator -- SCALE SS304 (7.92 g/cc; 69.5 w/o Fe, 19.0 w/o Cr, 9.5 w/o
Ni, 2.0 w/o Mn)
m41      26000.55c  5.93541-02   24000.50c  1.74281-02
```

```
        28000.50c  7.71883-03   25055.50c  1.73629-03
c
c       carbon steel in main body of pressure vessel -- SCALE Carbon Steel (7.8212 g/cc;  99.0 w/o Fe, 1.0 w/o C)
m50     26000.55c  8.34929-02    6012.50c  3.92134-03
c
c       Void in reflector components
m60     1001.50c   1.00000-15   8016.50c   1.00000-15
c
c       Void regions in the HB-1,2,and 3 beam tubes (m60 @ 2.0e-15 atoms/b-cm) have been replaced with helium-filled regions
c       where m61 = He (void) at T=300 deg.K and P=2 atm, where rho=3.2325e-4 g/cc, N(He)=4.86816e-5 atoms/(barn*cm)
c       Note: cold source vacuum vessel in HB-4 now has a true void (see m610) as of July 1996.
c       ------------------------
c       Helium void inside beam tubes HB-1,2,3 (He at T=300 deg.K, P=2 atm); cold source vacuum vessel in HB-4 now has a true void (see m610)
m61     2004.50c  4.86816e-5  $  add-jab122395:  For He at T=300 deg.K and P=2 atm, rho=3.2325e-4 g/cc, N(He)=4.86816e-5 atoms/(barn*cm)
c
c       Barytes concrete at 3.09725 g/cc (used for biological shield); shown below are atoms/(barn*cm) by nuclide
m62      1001.50c  1.681e-2   5010.50c  3.378e-4   5011.56c  1.368e-3
         8016.50c  4.195e-2  11023.50c  3.193e-4  12000.50c  1.549e-4
        13027.52c  7.534e-4  14000.50c  1.260e-3  16032.50c  5.401e-3
        20000.50c  3.273e-3  22000.50c  1.336e-4  25055.50c  1.713e-4
        26000.55c  6.875e-4  56138.50c  5.394e-3
c       real concentration for ba-138 = 3.8787e-3 atoms/(barn*cm); it is available;
c       other nuclide concentrations for which there is no mcnp xsect data:
c       ba-134=1.3037e-4;  ba-135=3.5557e-4;  ba-136=4.2364e-4;  ba-137=6.0575e-4
c       total number density for all barium nuclides in barytes concrete: 5.394030e-3
c       total number density for all nuclides in barytes concrete:  7.801382e-2
c       while this barytes concrete (for ANS project) was 3.09725 g/cc, it can
c       sometimes be made as dense as 3.5 g/cc; see book by Schaffer
c
c
m71     28058.24y  1.0  $ Ni58;  this material (m71) is used only to get the Ni58(n,p)Co58 reaction rate [(n,p)=103] in the dosimeters
m72     26054.24y  1.0  $ Fe54;  this material (m72) is used only to get the Fe54(n,p)Mn54 reaction rate [(n,p)=103] in the dosimeters
c
c
c       Typical beryllium used in permanent reflector (with he-3 and li-6, based in center ring, cell 9024)
m108    4009.50c   1.21135-01   1001.50c   1.34766-03   8016.50c   6.73828-04
        3006.50c   4.80664-8    2003.50c   1.39911-9
mt108   be.01t
c
c
c      ---------------------------------------------------------------------------------------------------------------
c      *** start detectors used to get fluxes at different points down HB-3 beam tube; for HFIR at 100 MW
c      ---------------------------------------------------------------------------------------------------------------
c
fc15   G-Flux (p/s/cm2) midway between collimator & shutter at 100 MW
f15:p  0.0  0.0  407.46438  0.5   $ G-Flux (p/s/cm2) midway between collimator & shutter at 100 MW
fm15   1.35399e+17  $ sum of equivalent point sources (p/s) in HB-3 for HFIR at 100 MW (Sn=7.5573e18 n/s in global calc);  will yield fluxes in p/s/cm2
e15    $  Emax(MeV) for the 23 VELM gamma grps (lowest to highest energy for MCNP):
       2.0000e-2    4.5000e-2    7.0000e-2    1.0000e-1    1.5000e-1    $ VELM g-groups 23, 22, 21, 20, 19,
       3.0000e-1    4.0000e-1    5.1000e-1    6.0000e-1    7.0000e-1    $ VELM g-groups 18, 17, 16, 15, 14,
       1.0000e+0    1.5000e+0    2.0000e+0    2.5000e+0    3.0000e+0    $ VELM g-groups 13, 12, 11, 10,  9,
       4.0000e+0    5.0000e+0    6.0000e+0    7.0000e+0    7.5000e+0    $ VELM g-groups  8,  7,  6,  5,  4,
       8.0000e+0    1.0000e+1    1.4000e+1                              $ VELM g-groups  3,  2,  1
c
fc25   G-Dose (mrem/hr) midway between collimator & shutter at 100 MW
f25:p  0.0  0.0  407.46438  0.5   $ G-Dose (mrem/hr) midway between collimator & shutter at 100 MW
fm25   1.35399e+17  $ sum of equivalent point sources (p/s) in HB-3 for HFIR at 100 MW (Sn=7.5573e18 n/s in global calc);  will yield fluxes in p/s/cm2
e25    $ Gamma energy boundaries (Emax, in MeV) from VELM 61n/23g structure:
```

```
      1.00000e-02  2.00000e-02  4.50000e-02  7.00000e-02  1.00000e-01
      1.50000e-01  3.00000e-01  4.00000e-01  5.10000e-01  6.00000e-01
      7.00000e-01  1.00000e+00  1.50000e+00  2.00000e+00  2.50000e+00
      3.00000e+00  4.00000e+00  5.00000e+00  6.00000e+00  7.00000e+00
      7.50000e+00  8.00000e+00  1.00000e+01  1.40000e+01
em25  $ Gamma flux-to-dose-rate conversion factors [(mrem/hr)/(p/s/cm2)] for the VELM 61n/23g xsect library,
c     calculated as prescribed in ANSI/ANS-6.1.1-1977, with groups arranged here in order of "increasing"
c     energy for use in MCNP;  first value here corresponds to non-existant group below 1.0e-2 MeV:
      0.00000e+00  2.14390e-03  5.77610e-04  2.74660e-04  2.66440e-04
      3.27670e-04  5.66760e-04  8.75940e-04  1.08520e-03  1.27970e-03
      1.44170e-03  1.75630e-03  2.31560e-03  2.92700e-03  3.46860e-03
      3.95960e-03  4.62210e-03  5.41360e-03  6.19090e-03  6.92650e-03
      7.47830e-03  7.84680e-03  8.77160e-03  1.10200e-02
c
c      fc41   Secondary G-Leakage (p/s) at downstream exit of collimator hole
c      fm41   9.64595e16  $ use for n/g calc; = sum of equivalent point sources (n/s) in HB-3 for HFIR at 100 MW (Sn=7.5573e18 n/s in global calc);  will y
ield fluxes in n/s/cm2
fc41  Primary G-Leakage (p/s) at downstream exit of collimator hole
fm41  1.35399e17  $ use for g-only calc; = sum of equivalent point sources (p/s) in HB-3 for HFIR at 100 MW (Sn=7.5573e18 n/s in global calc);  will yield
fluxes in n/s/cm2
f41:p  4190   $ surf at downstream exit of collimator hole
fs41  -4210  4211  -4212  4213  $ the fifth edit ("the remainder") is the leakage (p/s) thru the central rectangular hole in the collimator at downstream ex
it
sd41   1  1  1  1  1           $ enter area of 1.0 cm2 for all segments (including "remainder") to get "leakage (p/s)" instead of "current (p/s/cm2)"
c41  -0.99939083  $  0 -  2 deg wrt -Z axis
     -0.99619470  $  2 -  5 deg wrt -Z axis
     -0.98480775  $  5 - 10 deg wrt -Z axis
     -0.93969262  $ 10 - 20 deg wrt -Z axis
     -0.86602540  $ 20 - 30 deg wrt -Z axis
     -0.5         $ 30 - 60 deg wrt -Z axis
      0.0         $ 60 - 90 deg wrt -Z axis
      0.5         $ 60 - 90 deg wrt +Z axis
      0.86602540  $ 30 - 60 deg wrt +Z axis
      0.93969262  $ 20 - 30 deg wrt +Z axis
      0.98480775  $ 10 - 20 deg wrt +Z axis
      0.99619470  $  5 - 10 deg wrt +Z axis
      0.99939083  $  2 -  5 deg wrt +Z axis
      1.0         $  0 -  2 deg wrt +Z axis
e41   $  Emax(MeV) for the 23 VELM gamma grps (lowest to highest energy for MCNP):
      2.0000e-2    4.5000e-2    7.0000e-2    1.0000e-1    1.5000e-1    $ VELM g-groups 23, 22, 21, 20, 19,
      3.0000e-1    4.0000e-1    5.1000e-1    6.0000e-1    7.0000e-1    $ VELM g-groups 18, 17, 16, 15, 14,
      1.0000e+0    1.5000e+0    2.0000e+0    2.5000e+0    3.0000e+0    $ VELM g-groups 13, 12, 11, 10,  9,
      4.0000e+0    5.0000e+0    6.0000e+0    7.0000e+0    7.5000e+0    $ VELM g-groups  8,  7,  6,  5,  4,
      8.0000e+0    1.0000e+1    1.4000e+1                              $ VELM g-groups  3,  2,  1
fq41  c e s   $ each cosine = new table;  energy grp down vertically;  spatial segments across horizontally
c
c
c      fc51   Secondary G-Leakage (p/s) at downstream exit of collimator hole
c      fm51   9.64595e16  $ use for n/g calc; = sum of equivalent point sources (n/s) in HB-3 for HFIR at 100 MW (Sn=7.5573e18 n/s in global calc);  will y
ield fluxes in n/s/cm2
fc51   Primary G-Leakage (p/s) at downstream exit of collimator hole
fm51   1.35399e17  $ use for g-only calc; = sum of equivalent point sources (p/s) in HB-3 for HFIR at 100 MW (Sn=7.5573e18 n/s in global calc);  will yield
fluxes in n/s/cm2
f51:p  4190   $ surf at downstream exit of collimator hole
fs51  -4210  4211  -4212  4213  $ the fifth edit ("the remainder") is the leakage (p/s) thru the central rectangular hole in the collimator at downstream ex
it
sd51   1  1  1  1  1           $ enter area of 1.0 cm2 for all segments (including "remainder") to get "leakage (p/s)" instead of "current (p/s/cm2)"
c51    0.0  1.0  $ only L(z-) and L(z+)
```

```
e51   $  Emax(MeV) for the 23 VELM gamma grps (lowest to highest energy for MCNP):
      2.0000e-2    4.5000e-2    7.0000e-2    1.0000e-1    1.5000e-1    $ VELM g-groups 23, 22, 21, 20, 19,
      3.0000e-1    4.0000e-1    5.1000e-1    6.0000e-1    7.0000e-1    $ VELM g-groups 18, 17, 16, 15, 14,
      1.0000e+0    1.5000e+0    2.0000e+0    2.5000e+0    3.0000e+0    $ VELM g-groups 13, 12, 11, 10,  9,
      4.0000e+0    5.0000e+0    6.0000e+0    7.0000e+0    7.5000e+0    $ VELM g-groups  8,  7,  6,  5,  4,
      8.0000e+0    1.0000e+1    1.4000e+1                              $ VELM g-groups  3,  2,  1
fq51  c e s   $ each cosine = new table;  energy grp down vertically;  spatial segments across horizontally
c
c
c       fc61   Secondary G-Leakage (p/s) at upstream entrance of collimator hole
c       fm61   9.64595e16  $ use for n/g calc; = sum of equivalent point sources (n/s) in HB-3 for HFIR at 100 MW (Sn=7.5573e18 n/s in global calc);  will y
ield fluxes in n/s/cm2
fc61   Primary G-Leakage (p/s) at upstream entrance of collimator hole
fm61   1.35399e17  $ use for g-only calc; = sum of equivalent point sources (p/s) in HB-3 for HFIR at 100 MW (Sn=7.5573e18 n/s in global calc);  will yield
fluxes in n/s/cm2
f61:p  4130   $ surf at upstream entrance of collimator hole
fs61  -4210  4211  -4212  4213  $ the fifth edit ("the remainder") is the leakage (p/s) thru the central rectangular hole in the collimator at downstream ex
it
sd61   1  1  1  1  1            $ enter area of 1.0 cm2 for all segments (including "remainder") to get "leakage (p/s)" instead of "current (p/s/cm2)"
c61    0.0  1.0    $ only L(z-) and L(z+)
e61   $  Emax(MeV) for the 23 VELM gamma grps (lowest to highest energy for MCNP):
      2.0000e-2    4.5000e-2    7.0000e-2    1.0000e-1    1.5000e-1    $ VELM g-groups 23, 22, 21, 20, 19,
      3.0000e-1    4.0000e-1    5.1000e-1    6.0000e-1    7.0000e-1    $ VELM g-groups 18, 17, 16, 15, 14,
      1.0000e+0    1.5000e+0    2.0000e+0    2.5000e+0    3.0000e+0    $ VELM g-groups 13, 12, 11, 10,  9,
      4.0000e+0    5.0000e+0    6.0000e+0    7.0000e+0    7.5000e+0    $ VELM g-groups  8,  7,  6,  5,  4,
      8.0000e+0    1.0000e+1    1.4000e+1                              $ VELM g-groups  3,  2,  1
fq61  c e s   $ each cosine = new table;  energy grp down vertically;  spatial segments across horizontally
c
c      ------------------------------------------------------------------------------------------------------------------------
c      ********** end of model **********
c      ------------------------------------------------------------------------------------------------------------------------
```

Appendix C.6.8

Listing of the input file for MCNP Run HB307D, which was a preliminary (highly simplified) MCNP model once used for an exploratory analysis of the HB-3 beam tube using the original 1960 water tube design concept.

```
message:  outp=hb307.o  runtpe=hb307.r

Simplified model of HB-3 using equivalent point sources
c
c       ------------------------------------------------------------------------------------------------------------
c
c       HB307 is a series of "simplified geometry" calcs to get gamma transport in flooded water tube.
c
c             HB307A.I -- for the 1998 water tube design; nps=2000000
c             HB307B.I -- for the 1960 water tube design; nps=2000000 (I killed this due to time, after 320000 histories)
c             HB307B2.I -- for the 1960 water tube design (continuation run to print results after 320000 histories & stop)
c             HB307C.I -- for the 1998 water tube design <-- this deck; like HB307A.I but different imp values & nps=2000000
c             HB307D.I -- for the 1960 water tube design <-- this deck; like HB307B.I but different imp values & nps=5000000
c
c       ------------------------------------------------------------------------------------------------------------
c
c       Used to study shielding effectiveness of water tube (work performed by Jim Bucholz for Mike Farrah, Mar/Apr 1998):
c
c       Ref 1:  Dwg of HB-1 (e:\ham\ustn\allbeam1197.dgn Jan 29, 1998 12:55:09), where HB-3 is said to be the same.
c       Ref 2:  Dwg M-11537-OH-001-E, Feb 13, 1998, 10:30:22, dwg of HB-1 (essentially the same as Ref 1, but smaller)
c       Ref 3:  Dwg E-42027, Sheet 1, Apr 11, 1995, showing location on HB-3 & 1st aluminum window in vessel, as built
c       Ref 4:  Dwg E-42027, Sheet 2, Apr 11, 1995, showing typical beam tube collimator & rotary shutter, as built
c       Ref 5:  Dwg 1546-01-M-5022, Rev Sep 18, 1961, showing concrete around HB-3 beam tube collimator & rotary shutter
c
c       Distance from outside of vessel nozzel boss to radial plane
c       perpendicular to beam tube (as specifically stated in Ref 3):
c         HB-1:  52.0 inches = 132.08 cm
c         HB-2:  54.5 inches = 138.43 cm
c         HB-3:  54.0 inches = 137.16 cm
c         HB-4:  52.0 inches = 132.08 cm
c
c       Notes regarding length of the 1998 water tube:
c
c       The location of the 1st aluminum window relative to the vessel nozzel boss (cf Ref 1 & 2) is believed to be
c       correctly modeled here.  Likewise, the 2nd aluminum window relative to the beam tube collimator assembly
c       (cf Ref 1 & 2) is believed to be correctly modeled here.  Given the location of the beam tube collimator
c       assembly (Ref 1 & 2) relative to the concrete biological shield specifically around HB-3 as shown in Ref 5,
c       however, the length of the new HB-3 water tube [from Surf 2154 at Z=174.95125 cm, to Surf 4110 at Z=302.1868 cm
c       (total length of water when flooded = 127.23555 cm)] is about 2.03 inches shorter than shown for HB-1 on Refs
c       1 & 2, and about 89.8 cm shorter than the water tube originally in HB-3. Note, however, that this 2" difference
c       in water tube length between HB-1 and HB-3 is wholly consistent with the data in Ref 3 above if the vessel
c       flange hardware and collimator hardware are the same for HB-1 and HB-3 -- J. A. Bucholz, 3-21-98
c
c       ------------------------------------------------------------------------------------------------------------
c
c     BEGIN CELLS:
c
100    61  -3.2325-4  -1010    9997 -1060          imp:p=1  $ void up center of beam tube (upstream of where water begins)
c
c     Cell 1000 goes from to Z=116.7841 to Z=174.27; it may have to be subdivided into a number of axial importance zones
c     1000    8  -1.0000    -1010   1060 -2153          imp:p=1  $ water from start of 1960 water tube to start of 1998 water tube
1001    8  -1.0000    -1010  1060  -7021  imp:p=1.00e+00  $  imp:p=1    $ water from start of 1960 water tube to start of 1998 water tube
1002    8  -1.0000    -1010  7021  -7022  imp:p=1.70e+00  $  imp:p=2    $ water from start of 1960 water tube to start of 1998 water tube
1003    8  -1.0000    -1010  7022  -7023  imp:p=2.89e+00  $  imp:p=4    $ water from start of 1960 water tube to start of 1998 water tube
1004    8  -1.0000    -1010  7023  -7024  imp:p=4.91e+00  $  imp:p=8    $ water from start of 1960 water tube to start of 1998 water tube
1005    8  -1.0000    -1010  7024  -7025  imp:p=8.35e+00  $  imp:p=16   $ water from start of 1960 water tube to start of 1998 water tube
1006    8  -1.0       -1010  7025  -7026  imp:p=1.42e+01  $  imp:p=32   $ water [illegible]m start of 1960 water tube to start of 1998 water tube
1007    8  -1.[illegible]  -1010  7026  -7027  imp:p=2.41e+01  $  imp:p=64   $ water [illegible] start of 1960 water tube to start of 1998 water tube
```

```
1008   8  -1.0000   -1010  7027  -7028  imp:p=4.10e+01  $  imp:p=128  $ water from start of 1960 water tube to start of 1998 water tube
1009   8  -1.0000   -1010  7028  -2153  imp:p=6.98e+01  $  imp:p=256  $ water from start of 1960 water tube to start of 1998 water tube
c
c
111   24  -2.7        1010  -2130  9997  -1007  imp:p=0  $ aluminum wall of beam tube (upstream of importance cutoff plane)
112    8  -1.0000     2130  -4225  9997  -1007  imp:p=0  $ water outside beam tube (upstream of importance cutoff plane)
c
c
c    Cell 1100 goes from to Z=118.6879 to Z=174.27; it may have to be subdivided into a number of axial importance zones
c    1100  24  -2.7        1010  -2130  1007  -2153  imp:p=1  $ aluminum wall of beam tube (downstream of importance cutoff plane)
1101  24  -2.7   1010  -2130  1007  -7022  imp:p=1.70e+00  $ imp:p=2    $ aluminum wall of beam tube (downstream of importance cutoff plane)
1102  24  -2.7   1010  -2130  7022  -7023  imp:p=2.89e+00  $ imp:p=4    $ aluminum wall of beam tube (downstream of importance cutoff plane)
1103  24  -2.7   1010  -2130  7023  -7024  imp:p=4.91e+00  $ imp:p=8    $ aluminum wall of beam tube (downstream of importance cutoff plane)
1104  24  -2.7   1010  -2130  7024  -7025  imp:p=8.35e+00  $ imp:p=16   $ aluminum wall of beam tube (downstream of importance cutoff plane)
1105  24  -2.7   1010  -2130  7025  -7026  imp:p=1.42e+01  $ imp:p=32   $ aluminum wall of beam tube (downstream of importance cutoff plane)
1106  24  -2.7   1010  -2130  7026  -7027  imp:p=2.41e+01  $ imp:p=64   $ aluminum wall of beam tube (downstream of importance cutoff plane)
1107  24  -2.7   1010  -2130  7027  -7028  imp:p=4.10e+01  $ imp:p=128  $ aluminum wall of beam tube (downstream of importance cutoff plane)
1108  24  -2.7   1010  -2130  7028  -2153  imp:p=6.98e+01  $ imp:p=256  $ aluminum wall of beam tube (downstream of importance cutoff plane)
c
c    Cell 1200 goes from to Z=118.6879 to Z=128.7043; it may have to be subdivided into a number of axial importance zones
c    1200   8  -1.0000     2130  -4225  1007  -2107  imp:p=1  $ water outside beam tube (downstream of importance cutoff plane, inside vessel)
1201   8  -1.0000   2130  -4225  1007  -7022  imp:p=1.70e+00  $ imp:p=2  $ water outside beam tube (downstream of importance cutoff plane, inside vessel)
1202   8  -1.0000   2130  -4225  7022  -2107  imp:p=2.89e+00  $ imp:p=4  $ water outside beam tube (downstream of importance cutoff plane, inside vessel)
c
c    Cell 1300 goes from to Z=128.7043 to Z=143.9443; it may have to be subdivided into a number of axial importance zones
c    1300  50  -7.8212     2130  -4225  2107  -2106  imp:p=1  $ carbon steel vessel nozzel flange (appx model; arbitrarily 6" thick)
1301  50  -7.8212   2130  -4225  2107  -7024  imp:p=4.91e+00  $ imp:p=8    $ carbon steel vessel nozzel flange (appx model; arbitrarily 6" thick)
1302  50  -7.8212   2130  -4225  7024  -2106  imp:p=8.35e+00  $ imp:p=16   $ carbon steel vessel nozzel flange (appx model; arbitrarily 6" thick)
c
c    Cell 1400 goes from to Z=143.9443 to Z=175.27; it may have to be subdivided into a number of axial importance zones
c    1400   8  -1.0000     2130  -4225  2106  -2153  imp:p=1  $ water outside beam tube (downstream of vessel flange)
1401   8  -1.0000   2130  -4225  2106  -7026  imp:p=1.42e+01  $ imp:p=32   $ water outside beam tube (downstream of vessel flange)
1402   8  -1.0000   2130  -4225  7026  -7027  imp:p=2.41e+01  $ imp:p=64   $ water outside beam tube (downstream of vessel flange)
1403   8  -1.0000   2130  -4225  7027  -7028  imp:p=4.10e+01  $ imp:p=128  $ water outside beam tube (downstream of vessel flange)
1404   8  -1.0000   2130  -4225  7028  -2153  imp:p=6.98e+01  $ imp:p=256  $ water outside beam tube (downstream of vessel flange)
c
c    Cell 1500 goes from Z=174.27 to Z=310.58; it may have to be subdivided into a number of axial importance zones
c    1500  8  -1.0000    2153  -4130  -4225 imp:p=1 $ water in water tube (from start, up "to" collimator)
1501  8  -1.0000   2153  -7030  -4225  imp:p=1.19e+02  $ imp:p=512      $ water in water tube (from start, up "to" collimator)
1502  8  -1.0000   7030  -7031  -4225  imp:p=2.02e+02  $ imp:p=1024     $ water in water tube (from start, up "to" collimator)
1503  8  -1.0000   7031  -7032  -4225  imp:p=3.43e+02  $ imp:p=2048     $ water in water tube (from start, up "to" collimator)
1504  8  -1.0000   7032  -7033  -4225  imp:p=5.83e+02  $ imp:p=4096     $ water in water tube (from start, up "to" collimator)
1505  8  -1.0000   7033  -7034  -4225  imp:p=9.90e+02  $ imp:p=8192     $ water in water tube (from start, up "to" collimator)
1506  8  -1.0000   7034  -7035  -4225  imp:p=1.68e+03  $ imp:p=16384    $ water in water tube (from start, up "to" collimator)
1507  8  -1.0000   7035  -7036  -4225  imp:p=2.86e+03  $ imp:p=32768    $ water in water tube (from start, up "to" collimator)
1508  8  -1.0000   7036  -7037  -4225  imp:p=4.87e+03  $ imp:p=65536    $ water in water tube (from start, up "to" collimator)
1509  8  -1.0000   7037  -7038  -4225  imp:p=8.27e+03  $ imp:p=131072   $ water in water tube (from start, up "to" collimator)
1510  8  -1.0000   7038  -7039  -4225  imp:p=1.41e+04  $ imp:p=262144   $ water in water tube (from start, up "to" collimator)
1511  8  -1.0000   7039  -7040  -4225  imp:p=2.39e+04  $ imp:p=524288   $ water in water tube (from start, up "to" collimator)
1512  8  -1.0000   7040  -7041  -4225  imp:p=4.06e+04  $ imp:p=1048576  $ water in water tube (from start, up "to" collimator)
1513  8  -1.0000   7041  -4130  -4225  imp:p=6.91e+04  $ imp:p=2097152  $ water in water tube (from start, up "to" collimator)
c
c    Cells 1600 & 1700 go from Z=174.27 to Z=310.58; they may have to be subdivided into a number of axial importance zones
c    1600  8  -1.0000  4130 -4190  4212  -4213  4210 -4211  imp:p=1  $ water in rectangular hole up thru collimator
1601  8  -1.0000  4130  -7043  4212  -4213  4210 -4211  imp:p=1.17e+05  $ imp:p=4194304    $ water in rectangular hole up thru collimator
1602  8  -1.0000  7043  -7044  4212  -4213  4210 -4211  imp:p=2.00e+05  $ imp:p=8388608    $ water in rectangular hole up thru collimator
1603  8  -1.0000  7044  -7045  4212  -4213  4210 -4211  imp:p=3.39e+05  $ imp:p=16777216   $ water in rectangular hole up thru collimator
1604  8  -1.0000  7045  -7046  4212  -4213  4210 -4211  imp:p=5.77e+05  $ imp:p=33554432   $ water in rectangular hole up thru collimator
```

```
1605  8  -1.0000  7046  -7047  4212  -4213  4210 -4211  imp:p=9.81e+05  $ imp:p=67108864   $ water in rectangular hole up thru collimator
1606  8  -1.0000  7047  -4190  4212  -4213  4210 -4211  imp:p=1.67e+06  $ imp:p=134217728  $ water in rectangular hole up thru collimator
c
c    Cells 1600 & 1700 go from Z=174.27 to Z=310.58; they may have to be subdivided into a number of axial importance zones
c    1700  40  -7.92  4130 -4190 -4225 #(4212 -4213  4210 -4211) imp:p=1   $ stainless steel model of collimator (with rectangular hole)
1701  40  -7.92  4130  -7043  -4225  #(4212 -4213  4210 -4211)  imp:p=1.17e+05  $ imp:p=4194304    $ stainless steel model of collimator (with rectangular h
ole)
1702  40  -7.92  7043  -7044  -4225  #(4212 -4213  4210 -4211)  imp:p=2.00e+05  $ imp:p=8388608    $ stainless steel model of collimator (with rectangular h
ole)
1703  40  -7.92  7044  -7045  -4225  #(4212 -4213  4210 -4211)  imp:p=3.39e+05  $ imp:p=16777216   $ stainless steel model of collimator (with rectangular h
ole)
1704  40  -7.92  7045  -7046  -4225  #(4212 -4213  4210 -4211)  imp:p=5.77e+05  $ imp:p=33554432   $ stainless steel model of collimator (with rectangular h
ole)
1705  40  -7.92  7046  -7047  -4225  #(4212 -4213  4210 -4211)  imp:p=9.81e+05  $ imp:p=67108864   $ stainless steel model of collimator (with rectangular h
ole)
1706  40  -7.92  7047  -4190  -4225  #(4212 -4213  4210 -4211)  imp:p=1.67e+06  $ imp:p=134217728  $ stainless steel model of collimator (with rectangular h
ole)
c
c
c    800  60  -1.0e-20  4190  -9998  -4225  imp:p=1  $ internal void downstream of collimator, but upstream of shutter drum
800  60  -1.0e-20  4190  -9998  -4225  imp:p=1.67e+06  $ imp:p=134217728  $ internal void downstream of collimator, but upstream of shutter drum
900   0          #(-4225   9997  -9998) imp:p=0  $ enternal void
c
c     END CELLS (next line must be blank)

c     BEGIN SURFACES:
c
1010  cz   5.08    $ inner radius of voided portion of beam tube
2130  cz   7.16174 $ inner radius of ss sleeve around HB-3 beam tube, near vessel; used as outer radius of beam tube in this model
4225  cz  17.4742  $ outer radius of narrow ss sleeve extending thru concrete into pool; radial boundary to ext void in this model
c
c     Box surfaces corresponding to rectangular-shaped hole in collimator:
c     Here (like everywhere in this MCNP model of HB-3),
c     Z=central axis; Y is really horizontal; X is really vertical
4210  py  -3.4925   $ ymin
4211  py   3.4925   $ ymax
4212  px  -6.9850   $ xmin
4213  px   6.9850   $ xmax
c
9997  pz    0.0     $ external void boundary (location corresponds to the real radial plane perpendicular to the real beam tube)
1060  pz  116.7841  $ start of water tube in 1960 design
1007  pz  118.6879  $ plane below which all importances are zero; located 2 cm upstream of first pt det used to get pt srcs
2107  pz  128.7043  $ arb plane defining upstream side of thick flange in this model (flange arbitrarily taken to be 6" thick here)
2106  pz  143.9443  $ plane defining end of thick flange mounted on boss on pressure vessel around HB-3 (see dwg E-42027)
2153  pz  174.27    $ upstream   side of aluminum window forming start of water tube in proposed HB-3 design
4130  pz  310.58    $ upstream surface of collimator
4190  pz  399.48    $ downstream side of collimator
9998  pz  415.44875 $ upstream side of shutter drum; taken as ext void boundary in this model
c
7020  pz  116.7841   $  importance surface;  above here,  imp:p=1  (same as surf 1060)
7021  pz  118.6879   $  importance surface;  above here,  imp:p=2  (same as surf 1007)
7022  pz  123.70     $  importance surface;  above here,  imp:p=4
7023  pz  128.7043   $  importance surface;  above here,  imp:p=8  (same as surf 2107)
7024  pz  136.32     $  importance surface;  above here,  imp:p=16
7025  pz  143.9443   $  importance surface;  above here,  imp:p=32  (same as surf 2106)
7026  pz  151.53     $  importance surface;  above here,  imp:p=64
7027  pz  159.       $  importance surface;  above here,  imp:p=128
7028  pz  166.       $  importance surface;  above here,  imp:p=256
```

```
7029  pz  174.27      $  importance surface;  above here,  imp:p=512  (same as surf 2153)
7030  pz  182.60      $  importance surface;  above here,  imp:p=1024
7031  pz  190.94      $  importance surface;  above here,  imp:p=2048
7032  pz  199.27      $  importance surface;  above here,  imp:p=4096
7033  pz  209.27      $  importance surface;  above here,  imp:p=8192
7034  pz  220.27      $  importance surface;  above here,  imp:p=16384
7035  pz  231.27      $  importance surface;  above here,  imp:p=32768
7036  pz  242.27      $  importance surface;  above here,  imp:p=65536
7037  pz  253.27      $  importance surface;  above here,  imp:p=131072
7038  pz  264.27      $  importance surface;  above here,  imp:p=262144
7039  pz  275.27      $  importance surface;  above here,  imp:p=524288
7040  pz  287.04      $  importance surface;  above here,  imp:p=1048576
7041  pz  298.81      $  importance surface;  above here,  imp:p=2097152
7042  pz  310.58      $  importance surface;  above here,  imp:p=4194304 (same as surf 4130)
7043  pz  323.58      $  importance surface;  above here,  imp:p=8388608
7044  pz  336.58      $  importance surface;  above here,  imp:p=16777216
7045  pz  352.31      $  importance surface;  above here,  imp:p=33554432
7046  pz  368.03      $  importance surface;  above here,  imp:p=67108864
7047  pz  383.76      $  importance surface;  above here,  imp:p=134217728
7048  pz  399.48      $  importance surface;  above here,  imp:p=268435456 (same as surf 4190)
c
c     END SURFACES (next line must be blank)

c     PROBLEM PARAMETERS:
mode   p
c       mode   n
c       mode   n p
c       nps    2000000
nps    5000000
c       nps    40000000
c       nps    60000000
c       nps    80000000
c       nps    120000000
c      cut:n  time(shakes) energy(MeV)   WC1   WC2   SWTM
c      cut:n         1.0e20          0.027     -0.5  -0.25   0.0  $ cutoff:  don't track any neutrons below 27 keV
print  60      $ Table 60 shows vol, mass, n-imp by cell; see pp 3-117 of manual for description of other useful tables you may want
prdmp  0   80000  0  4  0   $ make restart file after every 80000 histories in fixed src calc; save only the 4 most recent restart files
c
c
c     EQUIVALENT POINT SOURCES:

--->  The remaining 272 lines of input beyond this point for MCNP Run HB307D are literally identical with    <---
--->  the corresponding input for MCNP Run HB307C shown in Appendix C.6.7, and will not be reporduced here.  <---
```

Appendix C.7

GBA.SCR: A script file used for submitting and running a series of "forward mode" Group-Banded ANISN calculations involving a 1-D infinite slab model of the HB-3 beam tube including the 1998 water tube, the water-filled collimator, and the rotary shutter shield plug, as described in Sect 5.3 and Table 5.2.

This script file was used for submitting and running a series of "forward mode" Group-Banded ANISN calculations involving a 1-D infinite slab model of the HB-3 beam tube including the 1998 water tube, the water-filled collimator, and the rotary shutter shield plug, as described in Sect 5.3 and Table 5.2. All the necessary GB-ANISN input data for several different variations of this problem is included in this file. After completion of the GB-ANISN calculation, the embedded GETDOSE program will read the ANISN flux file and use the 61n/23g fluxes in mesh 574 to calculate the neutron and gamma dose rates in the thin void region just downstream of the collimator which ends at Z=399.48 cm.

This model uses pre-mixed cross section data for water, aluminum 6061, void, ss304, and/or carbon steel, as described below in the 9$$ array (material-by-zone) specifications. Barytes concrete and regular concrete are also available, but not used here. Cross sections are based on the coupled VELM 61n/23g shielding library using 61 neutron groups and 23 gamma groups.

By simply rearranging data for zones 16, 17, and 18 in the GB-ANISN 9$$ array (the material-by-zone array), the collimator section may be modeled as all water, stainless steel, or carbon steel. The default variation shown here is set for the all water case.

Boundary sources in the 18** array are presently set up to include the 61-group impingent neutron source on new 1998 water tube (at X=174.27 cm), as well as the 23-group impingent gamma source on the new 1998 water tube (at X=174.27 cm).

By placing "18** 2013z e" at the end of the existing 18** array (the source specification array), one can easily zero-out all of the neutron sources to run the gamma-only case. Eliminating the neutrons will also eliminate the secondary gammas, thus allowing one to partially assess their relative importance.

By placing "18** a2014 f0" at the end of the existing 18** array (the source specification array), one can easily zero-out all of the primary gamma sources while keeping all the neutron sources. The resulting (coupled n/g) calculation will allow one to estimate how many secondary gammas are being generated in each energy group, and where they are being generated (spatially). These secondary gammas can then be treated as source terms in a QAD-like point kernel analysis to realistically determine their relative importance in the real (3-D) HB-3 water tube shielding problem.

```
#  ***************************************************************************************************
#  ***************************************************************************************************
#
#  Korn-Shell script file (GBA.SCR) to execute GBANISN job on my workstation (jabdb)
#  ---------------------------------------------------------------------------------
#
#  File is set up for a "forward mode" Group-Banded ANISN calculation involving
#  a 1-D infinite slab model of the HB-3 beam tube including the 1998 water tube,
#  water-filled collimator, and rotary shield plug, as described in Table 5.2 of
#  the HB-3 Shielding Report.
#
#  After completion of the GB-ANISN calculation, the GETDOSE program will read the
#  ANISN flux file and use the 61n/23g fluxes in mesh 574 to calculate the neutron
#  and gamma dose rates in the thin void region just downstream of the collimator
#  which ends at Z=399.48 cm.
#
#  Model uses pre-mixed cross section data for water, aluminum 6061, void, ss304,
#  and/or carbon steel, as described in the GB-ANISN input just below the 9$$ array
#  (material-by-zone) specifications.  Barytes concrete and regular concrete are
#  also available, but not used here.  Cross sections are based on the coupled VELM
#  61n/23g shielding library using 61 neutron groups and 23 gamma groups.
#
#  By simply rearranging data for zones 16, 17, and 18 in the GB-ANISN 9$$ array
#  (the material-by-zone array), the collimator section may be modeled as all water,
#  stainless steel, or carbon steel.  Presently set up for the all water case.
#
#  Boundary sources in the 18** array are presently set up to include the
#  61-group impingent neutron source on new 1998 water tube (at X=174.27 cm), as well as the
#  23-group impingent  gamma  source on new 1998 water tube (at X=174.27 cm).
#
#  By placing   18**  2013z e
#  at the end of the existing 18** array (the source specification array), one can easily zero-out
#  all of the neutron sources to run the gamma-only case.  Eliminating the neutrons will also
#  eliminate the secondary gammas, thus allowing one to partially assess their relative importance.
#
#  By placing   18**  a2014 f0
#  at the end of the existing 18** array (the source specification array), one can easily zero-out
#  all of the primary gamma sources while keeping all the neutron sources.  The resulting (coupled n/g)
#  calculation will allow one to estimate how many secondary gammas are being generated in each energy
#  group, and where they are being generated (spatially).  These secondary gammas can then be treated
#  as source terms in a QAD-like point kernal analysis to realistically determine their relative
#  importance in the real (3-D) HB-3 water tube shielding problem.
#
#  ***************************************************************************************************
#  ***************************************************************************************************

export RTNDIR=$PWD
export TMPDIR=/u/mnt8/$LOGNAME/temp$RANDOM

echo  $TMPDIR
mkdir $TMPDIR
cd $TMPDIR


cat >getdose.f <<'END-GETDOSE'
        double precision dosen,doseg
        dimension dosef(84)
c
```

```
c       Multigroup neutron & gamma flux-to-dose-rate conversion factors for the VELM
c       61n/23g cross section library, calculated as prescribed in ANSI/ANS-6.1.1-1977
c       and given here in units of (mrem/hr)/(n/s/cm2) or (mrem/hr)/(p/s/cm2).
        data dosef/
     *  1.9465E-01, 1.5977E-01, 1.4706E-01, 1.4723E-01, 1.5118E-01,
     *  1.5411E-01, 1.4596E-01, 1.3694E-01, 1.2849E-01, 1.2527E-01,
     *  1.2562E-01, 1.2615E-01, 1.2721E-01, 1.2864E-01, 1.3008E-01,
     *  1.2975E-01, 1.1804E-01, 1.0554E-01, 9.5577E-02, 9.0488E-02,
     *  8.3046E-02, 6.6330E-02, 5.8498E-02, 5.8080E-02, 5.7731E-02,
     *  5.5626E-02, 4.9373E-02, 4.1241E-02, 3.4447E-02, 2.8773E-02,
     *  2.2781E-02, 1.6688E-02, 1.3503E-02, 1.1148E-02, 8.7422E-03,
     *  7.9520E-03, 7.6770E-03, 7.4241E-03, 7.1386E-03, 5.8975E-03,
     *  4.0874E-03, 3.5585E-03, 3.5825E-03, 3.6062E-03, 3.6229E-03,
     *  3.6387E-03, 3.6528E-03, 3.6908E-03, 3.7629E-03, 3.8453E-03,
     *  3.9356E-03, 4.0311E-03, 4.1289E-03, 4.2492E-03, 4.3820E-03,
     *  4.4897E-03, 4.5583E-03, 4.5742E-03, 4.5250E-03, 4.3706E-03,
     *  3.7090E-03, 1.1020E-02, 8.7716E-03, 7.8468E-03, 7.4783E-03,
     *  6.9265E-03, 6.1909E-03, 5.4136E-03, 4.6221E-03, 3.9596E-03,
     *  3.4686E-03, 2.9270E-03, 2.3156E-03, 1.7563E-03, 1.4417E-03,
     *  1.2797E-03, 1.0852E-03, 8.7594E-04, 5.6676E-04, 3.2767E-04,
     *  2.6644E-04, 2.7466E-04, 5.7761E-04, 2.1439E-03/
c
        open (15,status='old',form='unformatted')       ! anisn flux moment file (fort.15)
        open (13,file='getdose.out',status='unknown')   ! 1-line of output showing dose rates
c
        nmesh=574  ! get fluxes here, even though we may have more mesh intervals'
c
        dosen=0.0d0
        doseg=0.0d0
        n1=nmesh-1
c
        do ig=1,61
           read (15) (dummy,mesh=1,n1),flux
           dosen=dosen+flux*dosef(ig)
        enddo
c
        do ig=62,84
           read (15) (dummy,mesh=1,n1),flux
           doseg=doseg+flux*dosef(ig)
        enddo
c
        write (13,10) dosen,doseg
10      format (' DOSE(N)=',1pe13.5,'   DOSE(G)=',1pe13.5)
c
        stop
        end
END-GETDOSE


cat >gbainput <<'END-GBAINPUT'
gbanisn: 1-d slab model of hb3 water tube & collimator
/
/*********************************
/
/ see description of revised input in section 6 of
/ charles slater's memo to dist, dated 4/7/88
/
/*********************************
```

```
/
15$$  /  15$$ = integer parameters
  1   /  id  = problem id number;  if .gt. 1000000, disadvantage factors will be computed by group for each material in calc
  0   /  ith = 0/1 = forward/adjoint calc
  3   /  isct = maximum order of scatter found in any zone
 32   /  isn = order of angular quadrature
  1   /  ige = 1/2/3 = slab/cyl/spherical geometry
  0   /  ibl = 0/1/2/3 = vacuum/reflection/periodic/white(albedo) = left boundary condition
  0   /  ibr = 0/1/2/3 = vacuum/reflection/periodic/white(albedo) = right boundary condition
 22   /  izm = number of zones or regions (same material)
719   /  im  = number of mesh intervals
  0   /  ievt = 0/1/2/3/4/5/6 = fixed src / k-calc / alpha / conc search / zone width search / outer radius search / buckling search
      /  ------- 10 -------
 84   /  igm = number of energy groups
  3   /  iht = position of sigt in xsect table
  4   /  ihs = position of g-g (self-scatter) in xsect table
 87   /  ihm =length of xsect table
  0   /  mp = mixing table length (10$$, 11$$, 12** arrays)
  0   /  mcr = number of xsect sets read from cards (14** array)
 32   /  mtp = number of xsect sets to be read from tape (13$$ array)
 32   /  mt  = total number of xsect sets (number entered + any mixtures created)
  0   /  idfm = 0/1 = density factors not used / density factors used (if used, enter 21** array)
  0   /  ipvt = 0/1/2 = no effect / enter initial keff (as pv in 16**) / enter initial alpha (as pv in 16**);  see page 25 for more notes
      /  ------- 20 -------
  0   /  iqm  = 0/1 = no effect / enter distributed source (in 17** array)
  1   /  ipm  = 0/1/im = no effect / enter shell src by grp and angle (18**) / enter shell src by interval, grp, and angle
116   /  ipp  = interval number which contains shell src if ipm=1;  otherwise, set ipp=0
200   /  iim  = inner (spatial) iteration maximum
  0   /  id1  = -1/0/1/2/3 = no scalar flux or dist src print/ no effect / print angular flux / punch scalar flux / print angular flx and punch scalar flx
  1   /  id2  = 0/1/2 = no effect / read mtp xsect sets from tape in gip format / use xsects and fixed src from previous problem
  0   /  id3  = 0/N = no effect / compute N activities by zone, where N is any positive integer
  0   /  id4  = 0/1 = no effect / compute N activities by interval (where N=id3)
  1   /  icm  = outer (energy) iteration maximum
      /         icm note: if there is no fission, one may set icm=1 in "gbanisn" and it will cycle thru each of the thermal
      /         groups once and then repeat that cycle up to iim times (where iim is the "inner" iteration max) to converge
      /         the upscatter terms -- i.e., with group-banded anisn (and the bands properly defined in the 1$$ array)
      /         icm.gt.1 is not needed to converge upscatter, although icm.gt.1 would be needed if one allows fission.
  1   /  idat1= 0/1/2 = all data in core/ xsects & fixed sources stored on tape / fluxes & currents on tape also
      /         ****  must set idat1=1 if xsects come from a gip tape  ****
      /  ------- 30 -------
  0   /  idat2= 0 for no effect; idat2.gt.0, enter 24$$ array to select Sn, or diff theory, or inf hom media option by group for first "idat2" outers
  0   /  ifg = 0/1/2/3/4 = no effect/ do xsect weighting / read wtg xsects from prev calc / write wtd xsects (fort.10) / read & write
  3   /  iflu= 0/1/2/3/4 = (wtd diff model) = sometimes step/ linear only/ step only/ wtd diff / wtg with neg flx fixup
  1   /  ifn = 0/1/2 = enter fission guess (2**) / enter flux guess (3**) / use flux from prev case
  1   /  iprt= 0/1 = print xsects / don't print xsects
  2   /  ixtr= 0/1/2/3 as noted below:
      /     ixtr=0 no effect; start problem from scratch (requires 3** flux guess array in data block f)
      /     ixtr=1 read flux guess (on unit nt14); set ifn=1 and do not enter 3** array; do not include data block f at all
      /     ixtr=2 write flux soln (on unit nt15)
      /     ixtr=3 read flux guess on one unit (nt14), write flux solution on another unit (nt15)
  e   /  note: ixtr is now last parameter in 15$$ (not nbuf or nsav)
/
16**       /   16** = floating point parameters
    0      /   ev   = first guess for keff (usually 0.0)
    0      /   evm  = eigenvalue modifier
  1e-4     /   eps  = epsilon (accuracy desired)
    0      /        = buckling factor (normally 1.420892 if buckling is used;    erwise 0)
    0      /        = cylinder or plane height for buckling correction
```

```
    0       /   dz   = plane depth for buckling correction
    0       /   dfm1 = transverse dimension for void streaming
    0       /   xnf  = source normalization factor (typ: 1 for keff, 0 for fixed src);  n/cm3 for sphere; n/cm2 for slab; n/cm(of height) for cyl
    0       /   pv   = enter:  0 / keff0 / alpha0, depending on value of ipvt (param 20 in 15$$ array)
  0.5       /   ryf  = lamda2 relaxation factor (normally 0.5)
            /  ------- 10 -------
 1e-4       /   xlal = point flux convergence criteria if .gt. 0
    0       /   xlah = upper limit for abs(1.0-lamda1) used in linear search
    0       /   eql  = eigenvalue change epsilon
    0       /   xnpm = new parameter modifier
   e
59$$    /  59$$ = array of unit numbers to be used (may skip entire array and take defaults)
    8   /  nt1  = 1st flux and current scratch unit if idat1=2 (default: fort.8)
    9   /  nt2  = 2nd flux and current scratch unit if idat1=2 (default: fort.9)
    1   /  nt3  = 1st xsect and source scratch unit if idat1.gt.0  (default: fort.1)
    2   /  nt4  = 2nd xsect and source scratch unit if idat1.gt.0  (default: fort.2)
    3   /  nt5  = angular flux output unit (default: fort.3)
    4   /  nt6  = anisn-formatted (nuclide oriented) binary xsect library (default: fort.4) if idat1.ne.1
    4   /  nt7  = gip-formatted    (group  oriented) binary xsect library (default: fort.4) if idat1=1
    2   /  nt8  = few-group xsect library output unit if ifg=3 or ifg=4 (default: fort.2)
    2   /  nt9  = few-group xsect library input  unit if ifg=2 or ifg=4 (default: fort.2)
   14   /  nt14 = flux guess input unit if ixtr=1 or ixtr=3 (default: fort.14)
   15   /  nt15 = flux output unit if ixtr=2 or ixtr=3 (default: fort.15)
    6   /  nt99 = unit number for fido edit of input (default: fort.6)
   e
60$$    /   60$$ new array required for canisn, janisn, and gbanisn (but not regualr anisn); only has one entry (kwrd)
 2400   /   kwrd = thousands of real*4 words to be alocated for storage;  typ:  400 req'd for s4;  500 for s8;  900 for s16
   e
 t      / end of data block b;  t is always required   (there is no data block a; that's the title card)
/
/
/
1$$     /  number of groups in each band; if nbands.lt.igm (as usually the case) fill with zeros; igm entries required anyway
   f1   /  use this for VELM 61n/23g
/  14r1  25  44r1  f0  / use this for ANSLV 39n/44g; yields 1 grp per band in 1st 14 bands, and 25 groups in band 15; and 1 grp per band in the 44 gamma ban
ds
/
/ these 2$$ and 3** arrays here were only needed in a very special burnup-dependent version of the group-banded anisn code
/ that bob childs wrote especially for jim bucholz on the mhtgr project in 1988;  these two arrays are not part of the
/ regular group-banded anisn code and should not be entered (they're listed here only as a reminder to me)
/ 2$$  24  e  /  2$$ number of burnup intervals (used only in bob child's version)     ..... this 2$$ not standard
/ 3**  2.  e  /  3** length of burnup intervals in years (used only in bob's version) ..... this 3** not standard
 t      / end of data block c;  t is always required   (this data block has only the 1$$ array and is reqd by std gb-anisn)
/
/
/ 13$$ id numbers for nuclides or macroscopic materials in 'premixed' xsect library
/      but "only if" supplied in anisn-formatted (nuclide oriented) binary library;
/      this array allows the code to strip off just the nuclides it needs from tape;
/      not needed should not be entered if idat1=1 and input xsects are from gip tape
/ 13$$ / mtp entries; not needed when input xsects are from gip tape
/ 14** cross sections entered off cards if mcr.gt.0
/  t      / end of data block d;  t is required if 13$$ or 14** are entered; otherwise this t should be skipped
/
/
/
/ 17** fixed source specifications (im*igm entries reqd if iqm=1)
/   source in each mesh interval for group 1
/   source in each mesh interval for group 2
```

```
/   source in each mesh interval for group 3
/     :     :  :    :      :      :    :   :
/   source in each mesh interval for group 27
/   ... these may all be renormalized using xnf
/ 17**  /  values are n/s/cc;  remember to use "lower case" e's for exponents, not upper case e's
/      144r0  18r7.02795e+12   36r6.55051e+12  18r8.15472e+12  183r0   /  group  1  (halfway up top sect of ans core)   1.9097700e-02
/      144r0  18r7.22984e+13   36r6.73868e+13  18r8.38897e+13  183r0   /  group  2  (halfway up top sect of ans core)   2.1556070e-01
/      144r0  18r8.24511e+13   36r7.68498e+13  18r9.56702e+13  183r0   /  group  3  (halfway up top sect of ans core)   4.3961270e-01
/      144r0  18r4.65807e+13   36r4.34163e+13  18r5.40488e+13  183r0   /  group  4  (halfway up top sect of ans core)   5.6619070e-01
/      144r0  18r6.05776e+13   36r5.64623e+13  18r7.02897e+13  183r0   /  group  5  (halfway up top sect of ans core)   7.3080370e-01
/      144r0  18r6.35937e+13   36r5.92735e+13  18r7.37895e+13  183r0   /  group  6  (halfway up top sect of ans core)   9.0361270e-01
/      144r0  18r3.04993e+13   36r2.84274e+13  18r3.53892e+13  183r0   /  group  7  (halfway up top sect of ans core)   9.8649130e-01
/      144r0  18r4.61450e+12   36r4.30101e+12  18r5.35432e+12  183r0   /  group  8  (halfway up top sect of ans core)   9.9903070e-01
/      144r0  18r3.33162e+11   36r3.10529e+11  18r3.86576e+11  183r0   /  group  9  (halfway up top sect of ans core)   9.9993600e-01
/      144r0  18r2.47229e+10   36r2.30433e+10  18r2.86866e+10  183r0   /  group 10  (halfway up top sect of ans core)   1.0000030e+00
/        f0
/ 18** shell source specifications (not reqd if ipm=0,  mm*igm entries reqd if ipm.eq.1,  mm*im*igm entries reqd if ipm.gt.1)
/   note: for adjoint calcs, the angular dependent adjoint source must
/   be supplied as if it were reflected thru the origin)
/   Below:  Source(33)=ScalarFlux(monodirectional)/Weight(33)
18**  / based on full 100 MW power n/g from core, including decay fission gammas from core.
/       The following angular fluxes for quadrature direction 33 = (scalar flux)/(weight 33).
/
/   1-D slab GBANISN sources impingent on the old 1960 water tube and/or the new 1998 water
/   tube in the HFIR HB3 beam tube, based on the equivalent point sources in SRC-DESC.SUM;
/   these forward-directed shell sources in direction 33 (of an S32 1-D slab quad set) were
/   computed using the utility program SRC1D.FOR as:
/   SRC(grp ig, direction 33)= (PtSrc(ig)/[4*pi*(X-X0)^2])/weight(33)
/   where the multigroup PtSrc for HB3 is given in ref dataset SRC-DESC.SUM,
/   where X0(ig), the effective center of emmission for group (ig) in HB3, is
/   given in SRC-DESC.SUM (X0=dist in cm from the plane perpendicular to the tube),
/   where x = x1=116.7841 cm = the point where the old 1960 water tube began
/   and   x = x2=174.27   cm = the point where the new 1998 water tube begins
/
/   impingent neutron src on old 1960 water tube (at X=116.7841 cm), for neutrons in HB3 (velm grp=1,61),  fast=grp 01
/    32z 1.13006e+08 32z 1.10592e+10 32z 4.38227e+10 32z 6.55516e+10
/    32z 2.61608e+11 32z 5.44950e+11 32z 5.09834e+11 32z 5.29409e+11
/    32z 1.06623e+12 32z 2.95410e+11 32z 3.36529e+11 32z 8.76827e+11
/    32z 2.26008e+12 32z 2.90345e+12 32z 1.69825e+12 32z 2.90497e+12
/    32z 1.47587e+12 32z 1.74368e+12 32z 9.58689e+11 32z 4.29052e+11
/    32z 2.04155e+12 32z 1.63431e+12 32z 7.72646e+10 32z 2.26409e+10
/    32z 5.78337e+10 32z 4.50956e+11 32z 1.26373e+12 32z 1.10214e+12
/    32z 7.71693e+11 32z 9.92951e+11 32z 1.29692e+12 32z 2.16579e+12
/    32z 4.21110e+11 32z 1.42750e+12 32z 2.60124e+12 32z 5.88214e+11
/    32z 2.09517e+11 32z 2.69366e+11 32z 3.43813e+11 32z 2.20686e+12
/    32z 2.64203e+12 32z 2.50082e+12 32z 2.19740e+12 32z 1.47693e+12
/    32z 7.83043e+11 32z 7.16313e+11 32z 4.41240e+11 32z 3.28332e+12
/    32z 3.23922e+12 32z 2.48747e+12 32z 2.80919e+12 32z 2.63519e+12
/    32z 2.86782e+12 32z 4.53851e+12 32z 4.99220e+12 32z 3.96223e+12
/    32z 4.69230e+12 32z 9.22237e+12 32z 6.73971e+12 32z 7.47705e+12
/    32z 5.52139e+14
/  impingent gamma src on old 1960 water tube (at X=116.7841 cm), for gammas in HB3 (velm grp=61,84), fast=grp 63
/    32z 3.84536e+09 32z 2.54725e+12 32z 3.55596e+13 32z 4.34705e+12
/    32z 2.76192e+13 32z 1.90569e+13 32z 4.18079e+13 32z 4.70888e+13
/    32z 4.10847e+13 32z 1.01212e+14 32z 1.25714e+14 32z 1.15144e+14
/    32z 9.5401[illegible]e+13 32z 4.19883e+13 32z 7.18706e+13 32z 8.17303e+13
/    32z 9.83[illegible]13 32z 2.88737e+14 32z 1.98233e+14 32z 1.63428e+14
/    32z 8.16[illegible]13 32z 1.10727e+13 32z 8.97349e+09
```

```
/  impingent neutron src on new 1998 water tube (at X=174.27 cm), for neutrons in HB3 (velm grp=1,61),  fast=grp 01
     32z 5.82455e+06 32z 3.96115e+09 32z 9.09120e+09 32z 2.07345e+10
     32z 6.51723e+10 32z 1.28300e+11 32z 1.51488e+11 32z 1.37816e+11
     32z 2.38004e+11 32z 9.27745e+10 32z 1.18026e+11 32z 2.45799e+11
     32z 6.50926e+11 32z 7.20780e+11 32z 5.11900e+11 32z 5.83437e+11
     32z 4.60156e+11 32z 4.54658e+11 32z 2.75728e+11 32z 1.18870e+11
     32z 5.14801e+11 32z 4.74618e+11 32z 2.46126e+10 32z 6.19803e+09
     32z 1.33040e+10 32z 1.43484e+11 32z 4.39295e+11 32z 3.23138e+11
     32z 2.45247e+11 32z 3.03906e+11 32z 3.96441e+11 32z 6.47767e+11
     32z 1.09982e+11 32z 3.95492e+11 32z 3.98678e+11 32z 1.25329e+11
     32z 4.93277e+10 32z 8.12988e+10 32z 7.08402e+10 32z 6.01394e+11
     32z 7.55624e+11 32z 6.94913e+11 32z 6.05180e+11 32z 3.31031e+11
     32z 2.10124e+11 32z 2.08309e+11 32z 1.39402e+11 32z 8.03580e+11
     32z 7.82793e+11 32z 6.92223e+11 32z 7.67867e+11 32z 7.49416e+11
     32z 7.57499e+11 32z 1.21027e+12 32z 1.30806e+12 32z 1.17264e+12
     32z 1.26895e+12 32z 1.58393e+12 32z 1.50752e+12 32z 1.93367e+12
     32z 8.35086e+13
/  impingent gamma src on new 1998 water tube (at X=174.27 cm), for gammas in HB3 (velm grp=61,84), fast=grp 63
     32z 2.44520e+08 32z 1.31290e+11 32z 2.79299e+12 32z 3.06526e+11
     32z 2.23919e+12 32z 1.30586e+12 32z 3.53816e+12 32z 4.12907e+12
     32z 2.77455e+12 32z 5.55316e+12 32z 8.30330e+12 32z 9.51037e+12
     32z 1.12103e+13 32z 5.71012e+12 32z 7.70454e+12 32z 1.04867e+13
     32z 1.41704e+13 32z 3.73438e+13 32z 2.62482e+13 32z 2.31424e+13
     32z 1.71632e+13 32z 2.64146e+12 32z 3.79191e+09
/
/  end of source specifications
/  18**  2013z e  / zero-out all neutron sources to run gamma-only calc
/  18**  a2014 f0  / zero-out all primary gamma sources (so we can see where neurons are generating gammas)
/
 t  / end of data block e;  t is required if 17** or 18** are entered; otherwise this t should be skipped
/
/
/
/ 2**  fission density; im entries required; enter only if ifn=0 (34th param in 15$$) and ixtr=0 (36th param in 15$$ array)
/ 3**  flux guess ((flx(i,g),i=1,im),g=1,igm); enter only if ifn=1 (34th param in 15$$) and ixtr=0 (36th param in 15$$ array)
3** f0              / setting ifn=1 and filling 3** with f0 is recommended for shielding work
 t  / end of data block f;  t is required if 2** or 3** are entered; otherwise this t should be skipped
/
/
/
1**  / chi(g) fission spectrum; igm entries; not needed if no fissionable material present (if not needed, manual says enter f0)
       f0
/
5**  / avg velocity for each energy group; usually not needed (if not needed, manual says enter f0)
       f0
/
6**   / 1-D xsdrnpm quadrature weights (ige=1 isn=32  mm=  33)
    0.00000e+00  6.78811e-03  1.55634e-02  2.37896e-02  3.11572e-02
    3.73990e-02  4.22891e-02  4.56509e-02  4.73627e-02  4.73627e-02
    4.56509e-02  4.22891e-02  3.73990e-02  3.11572e-02  2.37896e-02
    1.55634e-02  6.78811e-03  6.78811e-03  1.55634e-02  2.37896e-02
    3.11572e-02  3.73990e-02  4.22891e-02  4.56509e-02  4.73627e-02
    4.73627e-02  4.56509e-02  4.22891e-02  3.73990e-02  3.11572e-02
    2.37896e-02  1.55634e-02  6.78811e-03
7**   / 1-D xsdrnpm direction cosines  (ige=1 isn=32  mm=  33)
   -1.00000e+00 -9.94700e-01 -9.72288e-01 -9.32816e-01 -8.77702e-01
   -8.08938e-01 -7.29008e-01 -6.40802e-01 -5.47506e-01 -4.52494e-01
   -3.59198e-01 -2.70992e-01 -1.91062e-01 -1.22298e-01 -6.71844e-02
```

```
   -2.77125e-02 -5.29953e-03  5.29953e-03  2.77125e-02  6.71844e-02
    1.22298e-01  1.91062e-01  2.70992e-01  3.59198e-01  4.52494e-01
    5.47506e-01  6.40802e-01  7.29008e-01  8.08938e-01  8.77702e-01
    9.32816e-01  9.72288e-01  9.94700e-01
/
/ 4**  / location of each interval boundary; im+1 entries required
/ 4**  0.0  24i10.01  35.56  35.57   / mesh boundaries
/ 4**  0.0  24i10.01  19.06  19.07   / mesh boundaries
/ 4**  0.0  24i10.01  27.95  27.96   / mesh boundaries
/ 4**  8.0 3i9.0 3i10.0 151i12.54 3i109.06 2i111.6 31i112.6 143.08  / mesh boundaries
4**  / 720 mesh boundaries required here (for these 719 mesh intervals):
     115.0  2i116.7841  111i117.7366  2i174.27  7i174.95125  7i179.05
     7i183.15  7i187.25  7i191.35  7i195.45  7i199.55  7i203.65
     189i207.75  2i302.1868  15i302.5043  49i310.58  2i334.7709
     127i335.4756  2i399.48  14i401.9445  124i415.44875
     2i477.36125  478.79
/
8$$  / zone numbers by mesh interval (im entries required)
     1  3r2  112r3  3r4  8r5  8r6  8r7  8r8  8r9  8r10  8r11  8r12
     190r13  3r14  16r15  50r16  3r17  128r18  3r19  15r20  125r21
     3r22
/
9$$    /  material numbers by zone (izm entries required); material numbers should correspond to p0 components only
   9   /  1st zone always void; 1.7841 cm thick (thickness doesn't matter in slab geometry)
   9   /  2nd zone void here;  1st aluminum window in 1960 design would go here
   9   /  3rd zone void here;  use water if looking at 1960 design
   5   /  4th zone aluminum = 1st window in 1998 design;  would be water for 1960 design
   1   /  5th zone water (first 4.1 cm in 1998 design)
   1   /  6th zone water (next 4.1 cm in 1998 design)
   1   /  7th zone water (next 4.1 cm in 1998 design)
   1   /  8th zone water (next 4.1 cm in 1998 design)
   1   /  9th zone water (next 4.1 cm in 1998 design)
   1   / 10th zone water (next 4.1 cm in 1998 design)
   1   / 11th zone water (next 4.1 cm in 1998 design)
   1   / 12th zone water (next 4.1 cm in 1998 design)
   1   / 13th zone water (remainder of water in 1998 water tube design)
   5   / 14th zone aluminum = 2nd window in 1998 design;  would be water for 1960 design
   1   / 15th zone water
/  ------------------------------ may wish to make next 3 zones: all water (1), all stainless steel (13), or all carbon steel (17)
/
   a16 /
  13   / 16th zone stainless steel
  13   / 17th zone stainless steel
  13   / 18th zone stainless steel
/
   a16 /
  17   / 16th zone carbon steel
  17   / 17th zone carbon steel
  17   / 18th zone carbon steel
/
   a16 /
   1   / 16th zone water here; may later try stainless steel or carbon steel;
   1   / 17th zone water here; may later try stainless steel or carbon steel; use aluminum iff modeling 1960 water tube design
   1   / 18th zone water here; may later try stainless steel or carbon steel;
/
/  ------------------------------ previous 3 zones represent the collimator section
   9   / 19th zone thin void at end of collimator (need incoming flux here)
   9   / 20th zone void upstream of carbon steel shutter drum
```

```
  17   / 21th zone carbon steel shutter drum
   9   / 22th zone thin void
/
/  end of 9$$ array
/  list of possible materials (with this HB3 water tube xsect lib) includes the following:
/
/   mix  1  (ANISN/DORT MATL  1) = Water at 1.00 g/cc
/   mix  2  (ANISN/DORT MATL  5) = Aluminum 6061 (2.7 g/cc)
/   mix  3  (ANISN/DORT MATL  9) = Void (He @ 1.0e-20 atoms/barn*cm)
/   mix  4  (ANISN/DORT MATL 13) = SS304 (7.92 g/cc;  see page 50 of ORNL/TM-11989)
/   mix  5  (ANISN/DORT MATL 17) = Carbon Steel (7.8212 g/cc, 99 wt% Fe, 1 wt% C)
/   mix  6  (ANISN/DORT MATL 21) = Barytes Concrete at 3.09725 g/cc
/   mix  7  (ANISN/DORT MATL 25) = Regular Concrete
/   mix  8  (ANISN/DORT MATL 29) = response functions
/
/
/ note: anisn reads macroscopic cross sections for materials that
/ have been premixed elsewhere (in this case materials 1 to 52).
/ it also allows us to use these to create some secondary materials
/ (like materials 53, 57, 61, 65, 69, and 73), as described below:
/ ================================================================
/
/10$$ / mixture numbers in mixing table:
/       4r-53 4r-57 4r-61 4r-65 4r-69 4r-73   / irrelevant here, but shown as an example
/
/11$$ / component numbers (like nuclid numbers) in mixing table:
/       0 41 45 49 5q4                        / irrelevant here, but shown as an example
/
/12** / number densities (atoms/barn*cm):
/       reset   ss      b-10        b-11      / irrelevant here, but shown as an example
/         0    1.0   6.79702e-3   1.67426e-3  / densities for 1st row of pins (mix 53):
/         0    1.0   6.79702e-3   1.67426e-3  / densities for 2nd row of pins (mix 57):
/         0    1.0   6.79702e-3   1.67426e-3  / densities for 3rd row of pins (mix 61):
/         0    1.0   6.79702e-3   1.67426e-3  / densities for 4th row of pins (mix 65):
/         0    1.0   6.79702e-3   1.67426e-3  / densities for 5th row of pins (mix 69):
/         0    1.0   6.79702e-3   1.67426e-3  / densities for 6th row of pins (mix 73):
/ ================================================================
/
/
/ 16$$ is peculiar to gb-anisn;  always use f1 to specify that all
/ angular fluxes should always be continuous across media boundaries
16$$ f1
/
/ 19$$ order of scatter by zone
  19$$ f3
/
/ 20** radius modifiers by zone (required iff ievt=4)
/
/ 21** density factors by interval (required iff idfm=1)
/
/ 22$$ material numbers used for activities; refers to p0 components; use minus sign; id3 entries required (iff id3.gt.0)
/ 22$$ -49  / material number for b-10
/
/ 23$$ xsect table position for activities; id3 entries required (iff id3.gt.0)
/ 23$$ 1    / absorption in b-10
/
/ 24$$ calculation type markers; igm entries required, but iff idat2=1;  0/1/2 = sn / diff-th / inf-hom-media
/
```

```
/ 25**  right boundary albedo by group; igm entries required, if ibr=3 (otherwise not required)
/
/ 26**  left  boundary albedo by group; igm entries required, if ibl=3 (otherwise not required)
/
/ 27$$  few group parameters; 5 entries required, but only if ifg=1 (otherwise array not needed)
/       /  icon = 0/1/2 = no effect / micro xsects desired / macro xsects desired;   (minus implies cell weighting)
/       /  ihtf = position of sigma total in weighted xsects
/       /  ihsf = position of g-to-g scatter in weighted xsects;  (minus implies upscatter removal)
/       /  ihmf = table length of weighted xsects
/       /  ipun = -1/0/1 = write nuclide tape on fort.10 / no effect / punch wtd xsects (free-form on fort.7)
/   e   /  end of 27$$
/
/ 28$$ broad-group number for each fine group; igm entries required, if ifg=1 (otherwise not required)
/
 t  / end of data block g;  this t is always required
END-GBAINPUT


ln -s  /u/mnt4/jab/hfir/water-tube.hb3/dort.xsects/xsects.dort-ready.bin.hfir.hb3.watertube.01may98  fort.4  # link dort-ready xsects to fort.4 for use in G
BANISN
#   For this particular library:
#
#   mix  1  (ANISN/DORT MATL  1) = Water at 1.00 g/cc
#   mix  2  (ANISN/DORT MATL  5) = Aluminum 6061 (2.7 g/cc)
#   mix  3  (ANISN/DORT MATL  9) = Void (He @ 1.0e-20 atoms/barn*cm)
#   mix  4  (ANISN/DORT MATL 13) = SS304 (7.92 g/cc;  see page 50 of ORNL/TM-11989)
#   mix  5  (ANISN/DORT MATL 17) = Carbon Steel (7.8212 g/cc, 99 wt% Fe, 1 wt% C)
#   mix  6  (ANISN/DORT MATL 21) = Barytes Concrete at 3.09725 g/cc
#   mix  7  (ANISN/DORT MATL 25) = Regular Concrete
#   mix  8  (ANISN/DORT MATL 29) = response functions

gbanisn  <gbainput  >gbaoutput
xlf getdose.f -o getdose
getdose

#  cp -p fort.15  $RTNDIR/fort.15
cp -p gbaoutput   $RTNDIR/gbaoutput
cp -p getdose.out $RTNDIR/getdose.out

rm *           # dangerous !!! be careful what subdirectory you are in
cd $RTNDIR
rmdir $TMPDIR

#  !!!
#  echo  "Job will be run in "  $TMPDIR
```

Appendix C.8

QADD3: A QAD-like point kernel shielding code used to estimate the gamma dose rate at Z=400 cm, just downstream of the collimator section, when the HB-3 water tube and collimator sections are both flooded. It includes the effects of the secondary gammas generated by the neutrons. This program, and the associated results for the 1960 and 1998 water tube designs, are fully described in Sect 5.5.

```
c      ********************************************************************************************************************
c      ********************************************************************************************************************
c
c      QADD.FOR ..... Originally written May 7, 1998
c
c      Upgraded version called QADD2.FOR ..... June 16, 1998  ..... Same data, Same Results; More Features (E-Dist)
c
c      Upgraded version called QADD3.FOR ..... Sept 12, 1998  ..... Made Secondary Gamma Sources more rigorous;
c                                                                   Made no significant effect on conlcusions.
c
c      ********************************************************************************************************************
c
c      QADD.FOR
c
c        Uses simple QAD-like mass attenuation coefficients (for each eenrgy group) to calc the gamma dose rate
c        downstream of the collimator for both the long and short water tube models, and tabulates the resulting
c        dose rates due to several gamma sources:
c
c       (-1) the original equivalent point sources down the beam tube,
c        (0) the contribution due to secondary gammas produced in the first aluminum window, and:
c        (1) the contribution due to secondary gammas produced in the first  4.1 cm of water in the water tube,
c        (2) the contribution due to secondary gammas produced in the second 4.1 cm of water in the water tube,
c         :   :       :       : :     :       :     :     : :   :       : : :   : :   :   :
c        (8) the contribution due to secondary gammas produced in the eighth 4.1 cm of water in the water tube.
c
c        The secondary gamma source terms in the 1st aluminum window and each of the 8 water segments was
c        computed "a priori" using the GBANISN data from Calc 5 (GBA3.SCR) above. (Note, however, that the
c        source terms in QADD = the ANISN secondary source terms (above) times the cross sectional area of
c        the water tube (pi*7.03cm*7.03cm) since the raw ANISN terms are for a 1 cm x 1 cm area.)
c
c                                                                   -- J. A. Bucholz  (May 7, 1998)
c
c      ********************************************************************************************************************
c
c      Note:  Basically, QADD2.FOR is identical to QADD.FOR, except that we now tally the contributions to the
c      dose rate by source ENERGY as well as by source LOCATION, and later reorder that list in order of final
c      importance.  From the original QADD.FOR, for example, we know that most of the dose rate at x=400 cm down
c      the beam tube (ie, at the end of the flooded water tube & flooded collimator) comes from the primary gammas
c      streaming down the beam tube and impinging on the water tube.  Before we spend a whole lot of time in MCNP
c      tracking a lot of gammas that might not be important in the end, we'de like to know which groups are the
c      most important so that we can focus more on them.
c                                                                   -- J. A. Bucholz  (June 16, 1998)
c      Results for the 1960 water tube:
c      --------------------------------
c      Group 1- 7 sources (of the primary gammas) contribute  96.627%  of the final gamma dose
c      Group 1- 8 sources (of the primary gammas) contribute  99.147%  of the final gamma dose
c      Group 1-11 sources (of the primary gammas) contribute  99.910%  of the final gamma dose
c      Group 1-12 sources (of the primary gammas) contribute  99.963%  of the final gamma dose
c      All other sources can be neglected
c      Also note:  While in our MCNP calc we might tend to undersample VELM Group 1, QADD2 shows
c      that the Group 1 sources only contribute  0.020%  of the final gamma dose
c
c      Results for the 1960 water tube:
c      --------------------------------
c      Group 1- 8 sources (of the primary gammas) contribute  98.051%  of the final gamma dose
c      Group 1-11 sources (of the primary gammas) contribute  99.842%  of the final gamma dose
c      Group  [illegible] sources (of the primary gammas) contribute  99.914%  of the [illegible]al gamma dose
c      All ot[illegible]ources can be neglected
```

```
c       Also note:  While in our MCNP calc we might tend to undersample VELM Group 1, QADD2 shows
c       that the Group 1 sources only contribute  0.014%  of the final gamma dose
c
c       Other comments:
c       ---------------
c
c       Sources in VELM groups 1- 8 = 7.984211e15 p/s
c       Sources in VELM groups 1-12 = 2.160073e16 p/s
c       Therefore, if we include groups 9-12 (not recommended), the calc will
c       take 3 times longer and change the results for the 1960 water tube by
c       only 1% (2% in the case of the 1998 water tube).  CPU time would be
c       much better spent running additional histories on groups 1-8.
c
c       Sources in VELM groups 1-23 = 1.35399e17 p/s
c       ------------------------------------------  ==> Ratio = 16.96
c       Sources in VELM groups 1- 8 = 7.984211e15 p/s
c
c       --> Thus, by running only VELM source groups 1-8 (which account for 98-99% of
c       --> the final dose just downstream of the flooded collimator, we should be
c       --> able to run about 17 times faster than if we tried to accomodate all of
c       --> the 23 source groups.
c
c       ********************************************************************************************************************
c
c       Note:  Basically, QADD3.FOR is identical to QADD2.FOR, except that the secondary gamma sources in the
c       first aluminum window (iloc=0) and the eight 4.1-cm-thick water zones of 1998 beam tube (iloc=1 to 8)
c       were all updated on Sept 12, 1998.  As before, they are still based on GBA3.OUT (produced by GBA3.SCR).
c       The secondary gamma source terms in QADD.FOR and QADD2.FOR (both identical), were determined in an
c       approximate fashion from the balance table data in GBA3.OUT, by saying:
c       "secondary gamma production rate (g,izn) = absorption rate (g,izn) + absval[leakage rate (g,izn)]"
c       which is note really true on a groupwise basis.  What is true is the following:
c       "inscatter rate (g,izn) = absorption rate (g,izn) + leakage rate (g,izn) + outscatter rate (g,ign)"
c       However, the balance table "inscatter rate" for any given gamma group includes slowing down from higher
c       gamma groups, as well as sec gam prod via inscatter from neut grps.  The approximation shown above is
c       generally conservative (ie, leads to slightly higher than real estimates of sec gam prod rate in each
c       group, but is not rigorously defendable in strict sense.  For the purposes of the HB3 Shielding Report,
c       I decided to clean this up a little, and do things is a more rigorous fashion on Saturday Sept 12, 1998.
c       The secondary gamma source terms used here in QADD3 were obtained by folding the "volume integrated"
c       61-group neutron fluxes in each zone (as given by the GBA3.OUT ANISN balance tables for each zone)
c       with the 84 grp x 84 grp macroscopic scattering cross section matrix (for H2O in zones 5-13, and AL
c       in zones 4 and 14) which I pulled off the binary dort-ready xsect file using the XSECTGET.F program.
c       As expected, these new production rates are very close to the original production rates in those
c       important zones close to the hot end of the water tube, but notably lower in those zones further down the
c       tube where the secondary production rate had really fallen off.  Since the secondary gammas are still make
c       a totally negligible contribution to the total gamma dose rate downstream of the collimator at Z=400 cm,
c       none of the previous observations really change (except maybe the size of the small contribution(s) from
c       the last few water regions).  Use of these new secondary gamma source terms, however, is more rigorous.
c
c       While I was updating things in QADD3, I also added logic to rescale the secondary gamma source terms
c       (ie, those in zones 0 thru 8) for the 1960 water tube, while leaving those for the 1998 water tube
c       basically unchanged.  This rescaling for the 1960 case is really necessary since the sec gam src terms
c       are proportional to the impingent neutron flux, which is bigger for the 1960 water tube which starts
c       closer to the core.  The overall impingent source terms used for rescaling at each location were easliy
c       obtained using the FLUXTUBE program in the VOIDTUBE subdirectory, which uses the source terms shown in
c       Tables 2.2a and 2.2b of the HB3 Shielding Report and uses 1/[4*pi*(R-R0)^2] to get flux at desired point.
c
c       See key results / conclusions at end of this program listing.
c                                                                   -- J. A. Bucholz  (Sept 12, 1998)
```

```
c
c       ***************************************************************************************************************
c       ***************************************************************************************************************
c
        double precision dist,uw2,var,dexp,atten,dum,dose
c
        dimension eu(28),uh(28),uo(28),uw1(28),uw2(23),dosef(23)
c
        dimension src(-1:8,23),x0(-1:8,23),gdose(-1:8)
        dimension msrc(230),mloc(230),gd(230)      ! original list
        dimension msrc2(230),mloc2(230),gd2(230)   ! ordered  list
c
c       23-group gamma flux-to-dose-rate conversion factors for the VELM
c       61n/23g cross section library, calculated as prescribed in ANSI/ANS-6.1.1-1977
c       and given here in units of (mrem/hr)/(p/s/cm2):
        data dosef/  1.1020E-02, 8.7716E-03, 7.8468E-03, 7.4783E-03,
     *   6.9265E-03, 6.1909E-03, 5.4136E-03, 4.6221E-03, 3.9596E-03,
     *   3.4686E-03, 2.9270E-03, 2.3156E-03, 1.7563E-03, 1.4417E-03,
     *   1.2797E-03, 1.0852E-03, 8.7594E-04, 5.6676E-04, 3.2767E-04,
     *   2.6644E-04, 2.7466E-04, 5.7761E-04, 2.1439E-03/
c
        data (x0(-1,ig),ig=1,23)/  ! location of equivalent point sources down beam tube
     *   97.4, 99.9, 94.4, 96.0, 93.9, 96.4, 93.2, 92.6, 96.6, 99.2,
     *   96.9, 93.6, 86.8, 83.2, 88.8, 84.7, 81.6, 84.5, 83.9, 82.1,
     *   68.1, 61.9, 10.0/
c
        data (src(-1,ig),ig=1,23)/  ! equivalent point sources down beam tube
     *   1.23250E+11,6.19421E+13,1.51983E+15,1.60183E+14,1.23378E+15,
     *   6.75453E+14,1.98361E+15,2.34929E+15,1.42777E+15,2.66951E+15,
     *   4.23989E+15,5.27935E+15,7.31636E+15,4.03975E+15,4.80101E+15,
     *   7.17665E+15,1.03805E+16,2.56708E+16,1.82855E+16,1.67705E+16,
     *   1.65029E+16,2.84514E+15,8.72837E+12/
c
c
c       Original secondary gamma source terms in QADD.FOR and QADD2.FOR (both identical, from May 7 1998):
c       ---------------------------------------------------------------------------------------
c       These were determined in an approximate fashion from the balance table data in GBA3.OUT, by saying:
c       secondary gamma production rate (g,izn) = absorption rate (g,izn) + absval[leakage rate (g,izn)]
c       which is not really true on a groupwise basis.  What is true is the following:
c       inscatter rate (g,izn) = absorption rate (g,izn) + leakage rate (g,izn) + outscatter rate (g,ign)
c       However, the balance table inscatter rate for any given gamma group includes slowing down from higher
c       gamma groups, as well as sec gam prod via inscatter from neut grps.  Thus, these appx source terms are
c       generally conservative (ie, lead to slightly higher than real estimates of sec gam prod rate in each
c       group), but are not rigorously defendable in strict sense. I have since replaced these, as noted below.
c       ---------------------------------------------------------------------------------------
ccc        data (x0(0,ig),ig=1,23)/ 23*174.61 /  ! location of equivalent point sources from 1st aluminum window
ccc        data (src(0,ig),ig=1,23)/  ! gamma sources in 1st aluminum window (GBA Zone 4, Vol=0.6812290 cc)
ccc     *   1.52119e+5,9.49803e+7,4.39514e+9,2.25731e+8,1.09412e+9,
ccc     *   1.45544e+9,4.71986e+9,4.28904e+9,2.60488e+9,9.45107e+9,
ccc     *   2.19089e+9,2.31261e+9,1.82538e+9,6.01854e+8,1.43029e+9,
ccc     *   1.12324e+9,1.33012e+9,2.64326e+9,1.21299e+9,1.07793e+9,
ccc     *   3.99505e+9,4.28805e+9,5.69539e+7/
cccc
ccc        data (x0(1,ig),ig=1,23)/ 23*177.00 /  ! location of equivalent point sources from 1st 4.1 cm seg of water
ccc        data (src(1,ig),ig=1,23)/  ! gamma sources in 1st 4.1 cm of water in beam tube (GBA Zone 5, Vol= 4.0987700 cc)
ccc     *   1.6[illegible]83e+4,1.09840e+7,5.42355e+8,1.63231e+7,1.13015e+8,
ccc     *   1[illegible]3e+8,6.21265e+8,5.25754e+8,3.23723e+8,9.68642e+10,
ccc     *   4.[illegible]2e+9,5.42074e+9,4.15433e+9,1.78017e+9,2.39142e+9,
```

```
ccc     *   3.07340e+9,3.77259e+9,6.97578e+9,3.49430e+9,2.60277e+9,
ccc     *   3.28269e+9,2.75080e+9,1.13091e+8/
cccc
ccc         data (x0(2,ig),ig=1,23)/ 23*181.10 /  ! location of equivalent point sources from 2nd 4.1 cm seg of water
ccc         data (src(2,ig),ig=1,23)/  ! gamma sources in 2nd 4.1 cm of water in beam tube (GBA Zone 6, Vol= 4.0999900 cc)
ccc     *   1.02564e+4,6.78600e+6,3.28314e+8,1.20888e+7,7.22342e+7,
ccc     *   1.01109e+8,3.66292e+8,3.18730e+8,1.94526e+8,1.98954e+10,
ccc     *   2.94048e+9,3.32397e+9,2.56706e+9,1.09069e+9,1.36305e+9,
ccc     *   1.87315e+9,2.25184e+9,4.72183e+9,2.83074e+9,2.60706e+9,
ccc     *   4.01766e+9,3.96962e+9,1.61267e+8/
cccc
ccc         data (x0(3,ig),ig=1,23)/ 23*185.2 /  ! location of equivalent point sources from 3rd 4.1 cm seg of water
ccc         data (src(3,ig),ig=1,23)/  ! gamma sources in 3rd 4.1 cm of water in beam tube (GBA Zone 7, Vol= 4.1000100 cc)
ccc     *   7.66288e+3,4.98325e+6,2.37529e+8,1.00054e+7,5.46602e+7,
ccc     *   7.51202e+7,2.60663e+8,2.31762e+8,1.40667e+8,4.10689e+9,
ccc     *   1.09656e+9,1.34347e+9,1.10571e+9,4.79185e+8,5.38636e+8,
ccc     *   8.20898e+8,9.80167e+8,2.69841e+9,1.86256e+9,2.17054e+9,
ccc     *   4.12940e+9,4.59859e+9,1.88303e+8/
cccc
ccc         data (x0(4,ig),ig=1,23)/ 23*189.3 /  ! location of equivalent point sources from 4th 4.1 cm seg of water
ccc         data (src(4,ig),ig=1,23)/  ! gamma sources in 4th 4.1 cm of water in beam tube (GBA Zone 8, Vol= 4.1000100 cc)
ccc     *   6.04443e+3,3.87213e+6,1.82167e+8,8.52183e+6,4.35797e+7,
ccc     *   5.89384e+7,1.97067e+8,1.78063e+8,1.07673e+8,8.14221e+9,
ccc     *   1.30132e+8,2.73781e+8,2.97207e+8,1.40821e+8,1.16069e+8,
ccc     *   2.46944e+8,3.11889e+8,1.43110e+9,1.10975e+9,1.66755e+9,
ccc     *   3.90174e+9,4.79952e+9,1.97921e+8/
cccc
ccc         data (x0(5,ig),ig=1,23)/ 23*193.4 /  ! location of equivalent point sources from 5th 4.1 cm seg of water
ccc         data (src(5,ig),ig=1,23)/  ! gamma sources in 5th 4.1 cm of water in beam tube (GBA Zone 9, Vol= 4.0999900 cc)
ccc     *   4.91243e+3,3.10371e+6,1.44263e+8,7.35750e+6,3.57049e+7,
ccc     *   4.76075e+7,1.53944e+8,1.40889e+8,8.49380e+7,7.34933e+9,
ccc     *   3.13287e+8,2.45094e+8,1.12907e+8,3.20392e+7,8.20402e+7,
ccc     *   4.04003e+7,1.38072e+7,6.85287e+8,6.05672e+8,1.23159e+9,
ccc     *   3.51875e+9,4.70525e+9,1.95078e+8/
cccc
ccc         data (x0(6,ig),ig=1,23)/ 23*197.5 /  ! location of equivalent point sources from 6th 4.1 cm seg of water
ccc         data (src(6,ig),ig=1,23)/  ! gamma sources in 6th 4.1 cm of water in beam tube (GBA Zone 10, Vol= 4.1000100 cc)
ccc     *   4.07028e+3,2.53806e+6,1.16631e+8,6.40317e+6,2.97490e+7,
ccc     *   3.91719e+7,1.22816e+8,1.13615e+8,6.83064e+7,5.82293e+9,
ccc     *   4.94062e+8,4.77642e+8,3.09551e+8,1.15797e+8,1.67570e+8,
ccc     *   1.74248e+8,1.57907e+8,2.54948e+8,2.88114e+8,8.91346e+8,
ccc     *   3.08636e+9,4.42566e+9,1.84230e+8/
cccc
ccc         data (x0(7,ig),ig=1,23)/ 23*201.6 /  ! location of equivalent point sources from 7th 4.1 cm seg of water
ccc         data (src(7,ig),ig=1,23)/  ! gamma sources in 7th 4.1 cm of water in beam tube (GBA Zone 11, Vol= 4.0999900)
ccc     *   3.41875e+3,2.10498e+6,9.56778e+7,5.60261e+6,2.50738e+7,
ccc     *   3.26508e+7,9.94537e+7,9.28679e+7,5.56867e+7,4.46939e+9,
ccc     *   5.46888e+8,5.63974e+8,3.92939e+8,1.52206e+8,1.97972e+8,
ccc     *   2.29575e+8,2.15248e+8,6.10179e+7,2.03704e+8,6.38536e+8,
ccc     *   2.66044e+9,4.04370e+9,1.68848e+8/
cccc
ccc         data (x0(8,ig),ig=1,23)/ 23*205.7 /  ! location of equivalent point sources from 8th 4.1 cm seg of water
ccc         data (src(8,ig),ig=1,23)/  ! gamma sources in 8th 4.1 cm of water in beam tube (GBA Zone 12, Vol= 4.1000100)
ccc     *   2.90103e+3,1.76439e+6,7.93548e+7,4.92169e+6,2.13132e+7,
ccc     *   2.74807e+7,8.14467e+7,7.66907e+7,4.58700e+7,3.41457e+9,
ccc     *   5.38069e+8,5.75335e+8,4.15349e+8,1.62972e+8,2.00901e+8,
ccc     *   2.43844e+8,2.29236e+8,1.80016e+8,2.74146e+8,5.17570e+8,
ccc     *   2.26784e+9,3.61776e+9,1.51420e+8/
```

```
c     ------------------------------------------------------------------------------------------------
c
c
c
c     Updated secondary gamma source terms (from Sept 12, 1998) follow:
c     ------------------------------------------------------------------------------------------------
c     Number of secondary gammas produced in each gamma energy group in zones 4 through 14 of the 1-D slab model
c     given that the 61-group neutron source impingent on the first aluminum window here (zone 4) has the same
c     intensities (n/s/cm2) as the 61-group neutron source impingent on the first aluminum window of the 1998
c     water tube at Z=174.27 cm.  Results shown here were obtained by folding the "volume integrated" 61-group
c     neutron fluxes in each zone (as given by the ANISN balance tables for each zone) with the 84 grp x 84 grp
c     macroscopic scattering cross section matrix (for H2O in zones 5-13, and AL in zones 4 and 14).
c     ------------------------------------------------------------------------------------------------
      data (x0(0,ig),ig=1,23)/ 23*174.61 /  ! location of equivalent point sources from 1st aluminum window
      data (src(0,ig),ig=1,23)/  ! gamma sources in 1st aluminum window (GBA Zone 4, Vol=0.6812290 cc)
     * 1.65693e+05, 1.03877e+08, 4.82814e+09, 2.38268e+08, 1.18343e+09,
     * 1.57892e+09, 5.19572e+09, 4.68252e+09, 2.84097e+09, 1.67960e+09,
     * 1.14845e+09, 9.92435e+08, 7.10282e+08, 6.83261e+07, 4.90984e+07,
     * 1.75864e+08, 1.30021e+08, 6.87302e+07, 1.55946e+07, 2.82638e+06,
     * 1.72677e+07, 3.80053e+09, 3.08735e+07/
c
      data (x0(1,ig),ig=1,23)/ 23*177.00 /  ! location of equivalent point sources from 1st 4.1 cm seg of water
      data (src(1,ig),ig=1,23)/  ! gamma sources in 1st 4.1 cm of water in beam tube (GBA Zone 5, Vol= 4.0987700 cc)
     * 0.00000e+00, 8.88559e+03, 9.59494e+01, 3.91174e+05, 3.04019e+06,
     * 4.22477e+03, 1.61134e+04, 6.70271e+06, 2.55717e+05, 1.38337e+11,
     * 2.06225e+04, 3.16644e+07, 3.70816e+07, 0.00000e+00, 4.01537e+03,
     * 3.61894e+06, 3.18702e+03, 1.41722e+05, 1.35356e+04, 0.00000e+00,
     * 0.00000e+00, 0.00000e+00, 0.00000e+00/
c
      data (x0(2,ig),ig=1,23)/ 23*181.10 /  ! location of equivalent point sources from 2nd 4.1 cm seg of water
      data (src(2,ig),ig=1,23)/  ! gamma sources in 2nd 4.1 cm of water in beam tube (GBA Zone 6, Vol= 4.0999900 cc)
     * 0.00000e+00, 6.37610e+03, 6.89209e+01, 2.76269e+05, 2.11984e+06,
     * 2.79421e+03, 1.00417e+04, 2.91323e+06, 1.40053e+05, 5.16124e+10,
     * 1.47981e+04, 1.18137e+07, 1.38360e+07, 0.00000e+00, 2.83340e+03,
     * 2.50670e+06, 2.28955e+03, 1.00739e+05, 9.72390e+03, 0.00000e+00,
     * 0.00000e+00, 0.00000e+00, 0.00000e+00/
c
      data (x0(3,ig),ig=1,23)/ 23*185.2 /  ! location of equivalent point sources from 3rd 4.1 cm seg of water
      data (src(3,ig),ig=1,23)/  ! gamma sources in 3rd 4.1 cm of water in beam tube (GBA Zone 7, Vol= 4.1000100 cc)
     * 0.00000e+00, 4.55434e+03, 4.92781e+01, 1.94118e+05, 1.46872e+06,
     * 1.83745e+03, 6.15986e+03, 1.26436e+06, 7.91040e+04, 1.64938e+10,
     * 1.05700e+04, 3.77533e+06, 4.42251e+06, 0.00000e+00, 1.98907e+03,
     * 1.72378e+06, 1.63726e+03, 7.12619e+04, 6.95354e+03, 0.00000e+00,
     * 0.00000e+00, 0.00000e+00, 0.00000e+00/
c
      data (x0(4,ig),ig=1,23)/ 23*189.3 /  ! location of equivalent point sources from 4th 4.1 cm seg of water
      data (src(4,ig),ig=1,23)/  ! gamma sources in 4th 4.1 cm of water in beam tube (GBA Zone 8, Vol= 4.1000100 cc)
     * 0.00000e+00, 3.22882e+03, 3.49680e+01, 1.35468e+05, 1.01054e+06,
     * 1.19857e+03, 3.73237e+03, 6.39792e+05, 4.76683e+04, 5.42936e+09,
     * 7.49358e+03, 1.24275e+06, 1.45641e+06, 0.00000e+00, 1.38687e+03,
     * 1.17681e+06, 1.16199e+03, 5.00562e+04, 4.93501e+03, 0.00000e+00,
     * 0.00000e+00, 0.00000e+00, 0.00000e+00/
c
      data (x0(5,ig),ig=1,23)/ 23*193.4 /  ! location of equivalent point sources from 5th 4.1 cm seg of water
      data (src(5,ig),ig=1,23)/  ! gamma sources in 5th 4.1 cm of water in beam tube (GBA Zone 9, Vol= 4.0999900 cc)
     * 0.00000e+00, 2.27301e+03, 2.46371e+01, 9.39502e+04, 6.91105e+05,
     * 7.76536e+02, 2.24836e+03, 3.70233e+05, 3.02080e+04, 1.94765e+09,
     * 5.2752[illegible], 4.45807e+05, 5.22848e+05, 0.00000e+00, 9.61004e+02,
     * 7.9849[illegible], 8.18824e+02, 3.49321e+04, 3.47757e+03, 0.00000e+00,
```

```
     *  0.00000e+00, 0.00000e+00, 0.00000e+00/
c
        data (x0(6,ig),ig=1,23)/ 23*197.5 /  ! location of equivalent point sources from 6th 4.1 cm seg of water
        data (src(6,ig),ig=1,23)/  ! gamma sources in 6th 4.1 cm of water in beam tube (GBA Zone 10, Vol= 4.1000100 cc)
     *  0.00000e+00, 1.59042e+03, 1.72517e+01, 6.48112e+04, 4.70301e+05,
     *  5.00467e+02, 1.35232e+03, 2.31858e+05, 1.97580e+04, 7.72685e+08,
     *  3.69105e+03, 1.76865e+05, 2.07670e+05, 0.00000e+00, 6.62406e+02,
     *  5.39134e+05, 5.73463e+02, 2.42419e+04, 2.43551e+03, 0.00000e+00,
     *  0.00000e+00, 0.00000e+00, 0.00000e+00/
c
        data (x0(7,ig),ig=1,23)/ 23*201.6 /  ! location of equivalent point sources from 7th 4.1 cm seg of water
        data (src(7,ig),ig=1,23)/  ! gamma sources in 7th 4.1 cm of water in beam tube (GBA Zone 11, Vol= 4.0999900)
     *  0.00000e+00, 1.10705e+03, 1.20170e+01, 4.45103e+04, 3.18745e+05,
     *  3.21267e+02, 8.14333e+02, 1.51024e+05, 1.31609e+04, 3.36978e+08,
     *  2.56923e+03, 7.71333e+04, 9.07106e+04, 0.00000e+00, 4.54572e+02,
     *  3.62578e+05, 3.99523e+02, 1.67440e+04, 1.69677e+03, 0.00000e+00,
     *  0.00000e+00, 0.00000e+00, 0.00000e+00/
c
        data (x0(8,ig),ig=1,23)/ 23*205.7 /  ! location of equivalent point sources from 8th 4.1 cm seg of water
        data (src(8,ig),ig=1,23)/  ! gamma sources in 8th 4.1 cm of water in beam tube (GBA Zone 12, Vol= 4.1000100)
     *  0.00000e+00, 7.67212e+02, 8.33348e+00, 3.04543e+04, 2.15317e+05,
     *  2.05635e+02, 4.91786e+02, 1.00195e+05, 8.85560e+03, 1.58952e+08,
     *  1.78053e+03, 3.63838e+04, 4.28715e+04, 0.00000e+00, 3.10800e+02,
     *  2.43076e+05, 2.77109e+02, 1.15195e+04, 1.17688e+03, 0.00000e+00,
     *  0.00000e+00, 0.00000e+00, 0.00000e+00/
c
c       data (x0(9,ig),ig=1,23)/ 23*209.8(...) /  ! location of equivalent point sources in 94.4368 cm of water between Z=207.75 and Z=302.1868 cm (mostly n
ear 209.8)
c       data (src(9,ig),ig=1,23)/  ! gamma sources in 94.4368 cm of water in beam tube (GBA Zone 13, Vol= 94.4368)
c    *  0.00000e+00, 1.68139e+03, 1.82933e+01, 6.44523e+04, 4.40025e+05,
c    *  3.62459e+02, 7.73206e+02, 2.04432e+05, 1.86359e+04, 1.74253e+08,
c    *  3.90208e+03, 3.98865e+04, 4.72743e+04, 0.00000e+00, 6.56607e+02,
c    *  4.86456e+05, 6.08684e+02, 2.47550e+04, 2.58502e+03, 0.00000e+00,
c    *  0.00000e+00, 0.00000e+00, 0.00000e+00/
c
c       data (x0(10,ig),ig=1,23)/ 23*302.35 /  ! location of equivalent point sources in second (0.3175-cm-thk) aluminum window
c       data (src(10,ig),ig=1,23)/  ! gamma sources in 0.3175 cm of water in beam tube (GBA Zone 14, Vol= 0.3175)
c    *  1.68222e-02, 5.99439e-01, 1.80289e+01, 1.12970e+00, 5.30501e+00,
c    *  7.76747e+00, 2.19504e+01, 2.49267e+01, 1.49176e+01, 1.68884e+01,
c    *  8.74875e+00, 1.65612e+01, 1.01142e+01, 3.10489e-01, 2.30460e-01,
c    *  6.92917e-01, 5.21942e-01, 6.53672e-02, 6.43597e-02, 1.40324e-02,
c    *  6.78809e-02, 1.40403e+01, 1.19169e-01/
c       ------------------------------------------------------------------------------------------------------
c
        data eu / ! energies (MeV) for which mass attenuation coefficients are available
     *  1.000E-2,1.500E-2,2.000E-2,3.000E-2,4.000E-2,5.000E-2,6.000E-2,
     *  8.000E-2,1.000E-1,1.500E-1,2.000E-1,3.000E-1,4.000E-1,5.000E-1,
     *  6.000E-1,8.000E-1,1.000E+0,1.500E+0,2.000E+0,3.000E+0,4.000E+0,
     *  5.000E+0,6.000E+0,8.000E+0, 1.000E+1,1.500E+1,2.000E+1,3.000E+1/
c
        data uh / ! mass attenuation coefficients (cm2/gm) for hydrogen (taken from QAD database)
     *  3.854E-1,3.765E-1,3.695E-1,3.571E-1,3.458E-1,3.355E-1,3.261E-1,
     *  3.091E-1,2.944E-1,2.651E-1,2.429E-1,2.113E-1,1.893E-1,1.729E-1,
     *  1.599E-1,1.405E-1,1.263E-1,1.027E-1,8.777E-2,6.923E-2,5.807E-2,
     *  5.049E-2,4.498E-2,3.746E-2, 3.254E-2,2.539E-2,2.153E-2,1.748E-2/
c
        data uo / ! mass attenuation coefficients (cm2/gm) for oxygen (taken from QAD database)
     *  5.613E+0,1.691E+0,7.823E-1,3.398E-1,2.366E-1,1.990E-1,1.807E-1,
```

```
     *  1.621E-1,1.514E-1,1.344E-1,1.227E-1,1.066E-1,9.543E-2,8.713E-2,
     *  8.062E-2,7.080E-2,6.366E-2,5.184E-2,4.457E-2,3.595E-2,3.099E-2,
     *  2.777E-2,2.553E-2,2.263E-2, 2.089E-2,1.866E-2,1.770E-2,1.706E-2/
c
c
c       Assume water = 1.0 g/cc so that M(H)=2/18 g/cc and M(O)=16/18 g/c
        amh=2.0/18.0   ! g/cc
        amo=16.0/18.0  ! g/cc
        do ig=1,28
           uw1(ig)=amh*uh(ig) + amo*uo(ig)  ! attenuation coef "per cm of thickness" in water (using QAD energy structure)
        enddo
c
c       Convert attenuation coefficients "per cm of water" to VELM group structure & call the VELM set uw2(ig)
c       ------------------------------------------------------------------------------------------------------
c                              !   QAD   QAD          VELM GAMMA ENERGY GROUPS        USE THIS
c                              !   GRP   ENERGY                                       QAD DATA
c                              !
        uw2( 1)=uw1(26)        !    1    .010      ig=  1  10.0000 to 14.0000 MeV     26   15.0
        uw2( 2)=uw1(25)        !    2    .015      ig=  2   8.0000 to 10.0000 MeV     25   10.0
        uw2( 3)=uw1(24)        !    3    .02       ig=  3   7.5000 to  8.0000 MeV     24   8.0
        uw2( 4)=uw1(24)        !    4    .03       ig=  4   7.0000 to  7.5000 MeV     24   8.0
        uw2( 5)=uw1(24)        !    5    .04       ig=  5   6.0000 to  7.0000 MeV     24   8.0
        uw2( 6)=uw1(23)        !    6    .05       ig=  6   5.0000 to  6.0000 MeV     23   6.0
        uw2( 7)=uw1(22)        !    7    .06       ig=  7   4.0000 to  5.0000 MeV     22   5.0
        uw2( 8)=uw1(21)        !    8    .08       ig=  8   3.0000 to  4.0000 MeV     21   4.0
        uw2( 9)=uw1(20)        !    9    .10       ig=  9   2.5000 to  3.0000 MeV     20   3.0
        uw2(10)=uw1(20)        !   10    .15       ig= 10   2.0000 to  2.5000 MeV     20   3.0
        uw2(11)=uw1(19)        !   11    .2        ig= 11   1.5000 to  2.0000 MeV     19   2.0
        uw2(12)=uw1(18)        !   12    .3        ig= 12   1.0000 to  1.5000 MeV     18   1.5
        uw2(13)=uw1(17)        !   13    .4        ig= 13    .7000 to  1.0000 MeV     17   1.0
        uw2(14)=uw1(16)        !   14    .5        ig= 14    .6000 to   .7000 MeV     16    .8
        uw2(15)=uw1(15)        !   15    .6        ig= 15    .5100 to   .6000 MeV     15    .6
        uw2(16)=uw1(14)        !   16    .8        ig= 16    .4000 to   .5100 MeV     14    .5
        uw2(17)=uw1(13)        !   17   1.0        ig= 17    .3000 to   .4000 MeV     13    .4
        uw2(18)=uw1(12)        !   18   1.5        ig= 18    .1500 to   .3000 MeV     12    .3
        uw2(19)=uw1(10)        !   19   2.0        ig= 19    .1000 to   .1500 MeV     10    .15
        uw2(20)=uw1( 9)        !   20   3.0        ig= 20    .0700 to   .1000 MeV      9    .10
        uw2(21)=uw1( 7)        !   21   4.0        ig= 21    .0450 to   .0700 MeV      7    .06
        uw2(22)=uw1( 5)        !   22   5.0        ig= 22    .0200 to   .0450 MeV      5    .04
        uw2(23)=uw1( 3)        !   23   6.0        ig= 23    .0100 to   .0200 MeV      3    .02
c                              !   24   8.0
c                              !   25   10.0
c                              !   26   15.0
c                              !   27   20.0
c                              !   28   30.0
c       ------------------------------------------------------------------------------------------------------
c
        pi=acos(-1.0)
        rtube=7.03453  ! very conservative; 7.03453 is inner radius of 1998 water tube; should probably use rtube=5.08 cm = inner radius of 1960 & 1998 beam
 tube
ccc     rtube=5.08     ! should probably use rtube=5.08 cm = inner radius of 1960 & 1998 beam tube (since that's the size of the neutron beam!)
        area=pi*rtube*rtube
c       src(0,ig), above, are the secondary gamma sources in a 1 cm x 1 cm x 0.6812290 cm volume element of aluminum
c       (src(iloc,ig),iloc=1,8), above, are the secondary gamma sources in a 1 cm x 1 cm x 4.1 cm volume element of water
c       based on the 1-D Slab GBANISN calc (Case 5).  To get the total source (p/s) in the corresponding section of the
c       expanded beam tube / water tube, one must multiply by the cross sectional area of the water tube.  This total
c       source can then be treated as an eqivalent iostropic point source.
c       ------------------------------------------
```

```
      do iloc=0,8
      do ig=1,23
      src(iloc,ig)=area*src(iloc,ig)
      enddo
      enddo
c
      x=400.0  ! point where dose rate is wanted (just downstream of collimator)
c
      do 999 iyr=1960,1998,38
      write (*,'(1x)')
c
      gdoset=0.0
c
      do i=1,230
         msrc(i)=0
         mloc(i)=0
         msrc2(i)=0
         mloc2(i)=0
         gd(i)=0.0
         gd2(i)=0.0
      enddo
c
      ii=0
      do iloc=-1,8
      gdose(iloc)=0.0
         do ig=1,23
            ii=ii+1
            dist= x - x0(iloc,ig)
            if (iloc.ge.0 .and. iyr.eq.1960) ! adjust dist from sec gamma sources to detector depending where the water tube starts
     *           dist=dist+(174.27-116.7841) ! (use default locations/distances for 1998 design, or longer distances for 1960 design)
c           116.7841  !  for 1960 water tube, 1st aluminum window would start here
c           174.27    !  for 1998 water tube, 1st aluminum window would start here
            dum=4.0*pi*dist*dist
            distw=dist
            if (iloc.eq.-1 .and. iyr.eq.1998) distw=x-174.27   ! orig sources in beam tube unattenuated until they hit water tube
            if (iloc.eq.-1 .and. iyr.eq.1960) distw=x-116.7841 ! orig sources in beam tube unattenuated until they hit water tube
            var=distw*uw2(ig)
            atten=dexp(-var)
            dose=dosef(ig)*src(iloc,ig)*atten/dum
c           ------------------------------------ begin 9-12-98 update:
            simp1d=7.51812e+11 ! impingent neutron intensity (n/s/cm2) in 1-D calc used to get secondary gamma production rates
            simp98=7.55818e+11 ! impingent neutron intensity (n/s/cm2) on 1998 water tube at Z=174.27 cm   (from fluxtube.for)
            simp60=4.48493e+12 ! impingent neutron intensity (n/s/cm2) on 1960 water tube at Z=116.7841 cm (from fluxtube.for)
            srcrr=1.0          ! note that primary gamma source terms along beam tube centerline (iloc=-1) are still ok & not affected
            if (iloc.ge.0 .and. iyr.eq.1960) srcrr=simp60/simp1d
            if (iloc.ge.0 .and. iyr.eq.1998) srcrr=simp98/simp1d
            dose=dosef(ig)*srcrr*src(iloc,ig)*atten/dum
c           ------------------------------------ end of 9-12-98 update:
               gd(ii)=dose
               msrc(ii)=ig
               mloc(ii)=iloc
            gdose(iloc)=gdose(iloc)+dose
         enddo
      gdoset=gdoset+gdose(iloc)
      enddo
c
c     ----------------------------------------
c
```

```
      do i=1,230
      gd(i)=gd(i)/gdoset  ! convert to fractional dose contribution
      enddo
c
      do j=1,230
         bigest=-1.0
         do i=1,230
            if (gd(i).gt.bigest) then
                bigest=gd(i)
                k=i
            endif
         enddo
         gd2(j)=gd(k)
         msrc2(j)=msrc(k)
         mloc2(j)=mloc(k)
         gd(k)=-2.0
      enddo
c
      do i=2,230
      gd2(i)=gd2(i)+gd2(i-1)  ! get cummulative fractional gamma dose
      enddo
c
      write (*,'(1x)')
      do i=1,230
      write (*,15) iyr,i,mloc2(i),msrc2(i),gd2(i)
15    format (' year=',i4,'  rank=',i3,'  loc=',i2,'  grp=',i3,
     *  '  cummulative fractional gamma dose=',f12.9)
      enddo
      write (*,'(1x)')
c
c     ----------------------------------------
c
      do iloc=-1,8
      write (*,11) iyr,iloc,gdose(iloc),gdoset
11    format (' year=',i4,'  src loc=',i3,'   dose from this src=',
     *  1pe13.5,' mrem/hr,   total gamma dose=',1pe13.5,' mrem/hr')
      enddo
c
999   continue
c
      stop
      end
c
c     ********************************************************************************************************************
c     ********************************************************************************************************************
c
c     Original QADD.FOR and QADD2.FOR results are as follows:  (These are OBSOLETE;  see QADD3 results instead.)
c
c     year=1960  src loc= -1   dose from this src=  2.38587E+04 mrem/hr,   total gamma dose=  2.38743E+04 mrem/hr
c     year=1960  src loc=  0   dose from this src=  8.88175E+00 mrem/hr,   total gamma dose=  2.38743E+04 mrem/hr
c     year=1960  src loc=  1   dose from this src=  1.91506E+00 mrem/hr,   total gamma dose=  2.38743E+04 mrem/hr
c     year=1960  src loc=  2   dose from this src=  9.86765E-01 mrem/hr,   total gamma dose=  2.38743E+04 mrem/hr
c     year=1960  src loc=  3   dose from this src=  7.09310E-01 mrem/hr,   total gamma dose=  2.38743E+04 mrem/hr
c     year=1960  src loc=  4   dose from this src=  7.00675E-01 mrem/hr,   total gamma dose=  2.38743E+04 mrem/hr
c     year=1960  src loc=  5   dose from this src=  6.61132E-01 mrem/hr,   total gamma dose=  2.38743E+04 mrem/hr
c     year=1960  src loc=  6   dose from this src=  6.20159E-01 mrem/hr,   total gamma dose=  2.38743E+04 mrem/hr
c     year=1960  src loc=  7   dose from this src=  5.84906E-01 mrem/hr,   total gamma dose=  2.38743E+04 mrem/hr
c     year=1960  src loc=  8   dose from this src=  5.56148E-01 mrem/hr,   total gamma dose=  2.38743E+04 mrem/hr
```

```
c
c       year=1998  src loc= -1   dose from this src=  1.02952E+05 mrem/hr,   total gamma dose=  1.03074E+05 mrem/hr
c       year=1998  src loc=  0   dose from this src=  6.08418E+01 mrem/hr,   total gamma dose=  1.03074E+05 mrem/hr
c       year=1998  src loc=  1   dose from this src=  1.98900E+01 mrem/hr,   total gamma dose=  1.03074E+05 mrem/hr
c       year=1998  src loc=  2   dose from this src=  8.53448E+00 mrem/hr,   total gamma dose=  1.03074E+05 mrem/hr
c       year=1998  src loc=  3   dose from this src=  5.38053E+00 mrem/hr,   total gamma dose=  1.03074E+05 mrem/hr
c       year=1998  src loc=  4   dose from this src=  5.95492E+00 mrem/hr,   total gamma dose=  1.03074E+05 mrem/hr
c       year=1998  src loc=  5   dose from this src=  5.83342E+00 mrem/hr,   total gamma dose=  1.03074E+05 mrem/hr
c       year=1998  src loc=  6   dose from this src=  5.56064E+00 mrem/hr,   total gamma dose=  1.03074E+05 mrem/hr
c       year=1998  src loc=  7   dose from this src=  5.29238E+00 mrem/hr,   total gamma dose=  1.03074E+05 mrem/hr
c       year=1998  src loc=  8   dose from this src=  5.06782E+00 mrem/hr,   total gamma dose=  1.03074E+05 mrem/hr
c
c       Therefore, shortening the HB3 water tube by 1.886 ft (ie, moving the start of the water tube from
c       X=116.7841 cm in 1960 design, out to X=174.27 cm in 1998 design) causes the dose rate at the end
c       of the collimator to go up by a factor of 4.317 (from 23.87 Rem/hr to 103.07 Rem/hr)
c
c       Note that this is far less than initially feared.
c
c       Also note:
c
c       On 12 May 1998, MCNP Run HB307D for the long  (1960) water tube gave  26.77 Rem/hr (see tally 25) +/- 0.85% (nps=5,000,000)
c       On 11 May 1998, MCNP Run HB307C for the short (1998) water tube gave 109.31 Rem/hr (see tally 25) +/- 1.14% (nps=2,000,000)
c
c       These more rigorous results suggust that the results of my little QADD.FOR program shown above (as run on 7 May 1998)
c       were really pretty darn good.  How about that!
c
c       ************************************************************************************************************
c       ************************************************************************************************************
c
c       QADD3 results from Sept 12, 1998 are as follows:
c
c       year=1960  src loc= -1   dose from this src=  2.38587E+04 mrem/hr,   total gamma dose=  2.39281E+04 mrem/hr
c       year=1960  src loc=  0   dose from this src=  5.75822E+01 mrem/hr,   total gamma dose=  2.39281E+04 mrem/hr
c       year=1960  src loc=  1   dose from this src=  6.69047E+00 mrem/hr,   total gamma dose=  2.39281E+04 mrem/hr
c       year=1960  src loc=  2   dose from this src=  3.03324E+00 mrem/hr,   total gamma dose=  2.39281E+04 mrem/hr
c       year=1960  src loc=  3   dose from this src=  1.18317E+00 mrem/hr,   total gamma dose=  2.39281E+04 mrem/hr
c       year=1960  src loc=  4   dose from this src=  4.78499E-01 mrem/hr,   total gamma dose=  2.39281E+04 mrem/hr
c       year=1960  src loc=  5   dose from this src=  2.12604E-01 mrem/hr,   total gamma dose=  2.39281E+04 mrem/hr
c       year=1960  src loc=  6   dose from this src=  1.05289E-01 mrem/hr,   total gamma dose=  2.39281E+04 mrem/hr
c       year=1960  src loc=  7   dose from this src=  5.76366E-02 mrem/hr,   total gamma dose=  2.39281E+04 mrem/hr
c       year=1960  src loc=  8   dose from this src=  3.42147E-02 mrem/hr,   total gamma dose=  2.39281E+04 mrem/hr
c
c       year=1998  src loc= -1   dose from this src=  1.02952E+05 mrem/hr,   total gamma dose=  1.03048E+05 mrem/hr
c       year=1998  src loc=  0   dose from this src=  6.59302E+01 mrem/hr,   total gamma dose=  1.03048E+05 mrem/hr
c       year=1998  src loc=  1   dose from this src=  1.73852E+01 mrem/hr,   total gamma dose=  1.03048E+05 mrem/hr
c       year=1998  src loc=  2   dose from this src=  7.92927E+00 mrem/hr,   total gamma dose=  1.03048E+05 mrem/hr
c       year=1998  src loc=  3   dose from this src=  3.10514E+00 mrem/hr,   total gamma dose=  1.03048E+05 mrem/hr
c       year=1998  src loc=  4   dose from this src=  1.25670E+00 mrem/hr,   total gamma dose=  1.03048E+05 mrem/hr
c       year=1998  src loc=  5   dose from this src=  5.56537E-01 mrem/hr,   total gamma dose=  1.03048E+05 mrem/hr
c       year=1998  src loc=  6   dose from this src=  2.73695E-01 mrem/hr,   total gamma dose=  1.03048E+05 mrem/hr
c       year=1998  src loc=  7   dose from this src=  1.48445E-01 mrem/hr,   total gamma dose=  1.03048E+05 mrem/hr
c       year=1998  src loc=  8   dose from this src=  8.72652E-02 mrem/hr,   total gamma dose=  1.03048E+05 mrem/hr
c
c       ------------------------------------------------
c       Comments regarding 9-12-98 update:
c
c       To see effect of the secondary gamma source term update of 9-12-98, look at the results for the 1998 water tube.
c       Secondary gamma source terms for the first aluminum window (loc=0) and the first water region (loc=1) changed
```

```
c       very little (because in this more important region the previous approximation was really pretty good), and so
c       their contribution to the total gamma dose rate at Z=400 cm changed very little.  On the other hand, further
c       down the beam tube where the neutron flux and secondary gamma production rate is lower and less important, the
c       previous approximation was overly conservative.  The new secondary gamma production rates in these zones is more
c       realistic and the resulting contributions to the gamma dose rate at Z=400 cm is notably lower.  The saving grace
c       is that compared to everything else, these contribution were negligible before and are even more negligible now.
c
c       Contributions from secondary gammas in the hot end of the 1960 water tube "appear" bigger now, but for a different
c       reason.  In QADD.FOR and QADD2.FOR, the secondary gamma production terms had never been scaled up in proportion to
c       the higher impingent neutron flux at Z=116.7841 cm (ie, they were relocated, but never scaled up as they should have
c       been).  In QADD3, this oversight has been corrected.  Even with that, however, their contribution to the total gamma
c       dose rate at Z=400 cm is still totally negligible.
c
c       ------------------------------------------------
c       General comments on these 9-12-98 results:
c
c       Thus, despite these minor corrections in QADD3 the basic conclusions previously reached remain unchanged.
c       To repeat:
c
c       Shortening the HB3 water tube by 1.886 ft (ie, moving the start of the water tube from X=116.7841 cm
c       in the 1960 design, out to X=174.27 cm in 1998 design) causes the dose rate at the end of the collimator
c       to go up by a factor of 4.306 (from 23.93 Rem/hr to 103.05 Rem/hr).
c
c       Note that this is far less than initially feared (in Feb 98).  Results are very similar to those obtained from MCNP:
c
c       On 12 May 1998, MCNP Run HB307D for the long  (1960) water tube gave  26.77 Rem/hr (see tally 25) +/- 0.85% (nps=5,000,000)
c       On 11 May 1998, MCNP Run HB307C for the short (1998) water tube gave 109.31 Rem/hr (see tally 25) +/- 1.14% (nps=2,000,000)
c
c       These more rigorous results suggust that the results of my little QADD3.FOR program shown above (as run on 12 Sept 1998),
c       and the original QADD.FOR program (as run on 7 May 1998), were really pretty darn good.  How about that!
c
c       ********************************************************************************************************************
c       ********************************************************************************************************************
```

Appendix D.1

GETWING3.SCR: A script file for performing a 1-D adjoint shielding analysis (of the HB-3 water tube, collimator, and rotary shutter) and generating properly normalized broad-group weight window information that is later used in the 3-D weight window generator (WW308G.F) which then produces the actual weight-window file used in the MCNP4B Run HB308G gamma-only shielding analysis where the 1998 water tube and collimator sections are both flooded, the shutter is closed, and the HFIR is operating at 100 MW (cf Sect 6).

In addition to fully describing and running the 1-D ANISN adjoint analysis, this script also contains an embedded Fortran program (GETWING3.F) which is compiled and executed after the adjoint ANISN calculation has been run. The purpose of the GETWING3.F program is to read the adjoint flux file and, from that and the forward-mode source specifications, generate the "properly normalized" 1-D broad-group weight window information that is later used in the stand-alone 3-D weight-window file generator (WW308G). Sect 6.1 describes the 1-D ANISN model used in the adjoint analysis, while Sects 6.2 and 6.3 describe the normalization procedures that are used for the broad-group weight windows themselves. [For more general cases where the actual (forward) source does not lie entirely in a single broad group (as it does here), this program would also calculate and print the optimal "biased" source-energy distribution to be used with this weight-window data in the MCNP analysis. It is extremely important that the biased source-energy distribution used be determined in a fashion that is wholly consistent with the broad-group weight-window data being used, and this program will guarantee the needed consistency. In this particular case, that was not an issue because of the way the broad groups were initially chosen.] Lastly, Sect 6.4 describes how the spatially-dependent broad-group weight window data generated and printed by this program was adapted for use in the 3-D broad-group weight window generator program (WW308G).

```
#  ***************************************************************************************************
#  ***************************************************************************************************
#
#  Korn-Shell script file to run GBANISN and generate preliminary weight-window info for MCNP4B
#
#  ***************************************************************************************************
#  ***************************************************************************************************

export RTNDIR=$PWD
export TMPDIR=/u/mnt8/$LOGNAME/temp$RANDOM
# export TMPDIR=/work1/$LOGNAME/temp$RANDOM

echo  $TMPDIR
mkdir $TMPDIR
cd $TMPDIR


cat >getwin.f <<'END-GETWIN'
c       ************************************************************************
c       ************************************************************************
c
c       GETWING.F ... originally writted 6-13-1998 (see comments below)
c
c       GETWING2.F ... Upgraded version, 1 pm, 6-20-1998 (see comments below)
c
c   --> GETWING3.F ... Upgraded version, 3 pm, 6-20-1998 (see comments below)
c
c       ************************************************************************
c       ************************************************************************
c
c       GETWING.F
c
c       After the larger script (GETWIN.SCR) runs the GBANISN adjoint calc to
c       calculate the fine-group (61n/23g) adjoint flux everywhere (based on
c       the total n+g flux-to-dose-rate conversion factors as the adj source,
c       where the neutron flux-to-dose factors have been set to zero here),
c       this particular Fortran routine will:
c
c       Call Subroutine SRCJST which, in turn, calls Subroutine GETADJ which
c       reads the anisn scalar adjoint fluxes on fort.15, as well as anisn mesh
c       info in the GBAOUTPUT printed output file.  GETADJ then calculates and
c       prints the broad group adjoint fluxes (for 6 neut grps & 4 gamma grps)
c       as averaged over a wider (geometry-independent) mesh spaced every "DX" cm
c       (as specified there by the user; typically in 5-cm increments).  GETADJ
c       then return to Subroutine SRCJST.
c
c       SRCJST then calculates the unbiased and "biased" source distribution to be
c       used in MCNP, and tabulates the corresponding space/energy-dependent weight
c       windows (values of WTLO) to be used the MCNP calc.
c
c       This information is printed out in a file called "GETADJ.OUT".
c
c       Lastly, this program calls Subroutine WTWIN which writes out the large
c       (ascii) weight-window file (wwinp) that will actually be used by MCNP4B.
c       UPDATE:  Subroutine WTWIN no longer used in GETWING3.F (see note), and that
c       UPDATE:  functionality has been moved to a stand-alone routine, WW308G.F,
c       UPDATE:  which is run later and uses data based on the "GETADJ.OUT" f'
c
```

```
c      ************************************************************************
c
c      In version (GETWING.SCR, dated 6-13-98), as opposed to some earlier versions,
c      we now recognize the correct order of the group-dependent adjoint fluxes
c      being read off the GBANISN flux tape.  See comments in Subroutine GETADJ.
c
c      ************************************************************************
c
c      GETWING2.SCR:  this particular version has the following added features:
c
c      1) We recognize the correct order of the group-dependent adjoint fluxes
c         being read off the GBANISN flux tape.  See comments in Subroutine GETADJ.
c
c      2) This version is set up for the "gamma-only" analysis of the full HB3 beam tube,
c         including the rotary shutter (shield plug)
c
c      3) While it is set up for the "gamma-only" MCNP analysis which is to follow,
c         I have learned that the wwinp file must contain at least one dummy neutron group;
c         therefore, I've gone ahead and written out wwinp data for all 6 neutron groups
c         and all 4 gamma groups, even though this wwinp file should only be used for
c         the "gamma-only" MCNP analysis
c
c      4) This particular version has a few lines of special coding in subroutine wtwin
c         which calls subroutine getwt to extract "location-dependent (xd,yd,zd)'s"
c         which are then used to set up the directional biasing information; this
c         enhancement is expected to be very useful for the region in and around the
c         rotary shutter (shield plug).
c                                                    -- JAB, 6-20-98, 1 pm
c
c      ************************************************************************
c
c      GETWING3.F
c
c      1) Important change:  This version uses the same 1-D group-banded anisn adjoint
c         as GETWING2.SCR, but here in Subroutine SRCJST, I have:
c
c         a) set ptsrc(ig)=natural value for VELM grps 62-69 (ie, VELM gamma groups 1-8),
c         b) BUT have set ptsrc=1.0 (a negligibly small value) for all the other gamma groups (VELM gamma groups 9-23)
c
c      2) By commenting out the call to Subroutine WTWIN (no longer shown or used here), the task of writing a 3-D weight window file
c         (for the gamma-only analysis of the HB-3 beam tube and shutter with the 1998 water tube and collimator sections both flooded)
c         was removed from here on 6-20-1998 and placed (instead) in an off-line stand-alone program called WW308G.F which utilizes
c         broad-group mesh-to-mesh wtlow attenuation factors based on the printed output tables in the GETADJ.OUT file produced by
c         Subroutine GETADJ which is called by Subroutine SRCJST above.
c
c                                                    -- JAB, 6-20-98, 3 pm
c
c      ************************************************************************
c      ************************************************************************
c
      dimension xmini(3000),xmaxi(0:3000)      ! xmin & xmax for each importance zone
      dimension emaxi(10)      ! maximum energy (MeV) of the 6 broad neut groups & the 4 broad gamma groups
      dimension wtlo(3000,10)  ! wtlo(mesh,ig) for a given importance mesh, and broad group (calculated here)
c
      whi2lo=10000.  ! Jabo recommends wthi=10000*wtlo & wtsurv=wtavg=100*wtlo  (as the biggest weight window)
      wav2lo=100.    ! Jabo recommends wthi=10000*wtlo & wtsurv=wtavg=100*wtlo  (as the biggest weight window)
c
      whi2lo=100.    ! Jabo recommends wthi=  100*wtlo & wtsurv=wtavg= 10*wtlo  (as the best    weight window)
```

```
      wav2lo=10.      ! Jabo recommends wthi=  100*wtlo & wtsurv=wtavg= 10*wtlo  (as the best    weight window)
c
      xsrc=174.951    ! location where the "real" (forward) source would impinge on the 1-D buckled slab model (used for several things)
      xsrc=116.7841   ! point where the old 1960 water tube began
      xsrc=175.0
      xsrc=174.27     ! point where the new 1998 water tube begins
c
      xdet=400.0      ! location of adjoint source in anisn model (not used, only printed, but user MUST specify for QA purposes)
      xdet=300.0      ! location of adjoint source in anisn model (not used, only printed, but user MUST specify for QA purposes)
      xdet=478.79     ! location of adjoint source in anisn model (not used, only printed, but user MUST specify for QA purposes)
      dx=4.1          ! thickness on each importance zone to be used in mcnp
      dx=5.0          ! thickness on each importance zone to be used in mcnp
      dydz=26.3       ! transverse dimensions used for buckling in anisn  (not used, only printed, but user MUST specify for QA purposes)
      dydz=27.2       ! transverse dimensions used for buckling in anisn  (not used, only printed, but user MUST specify for QA purposes)
c
      isrc=0  ! for a neutron-only MCNP calc with a neutron-only source; adjoint based on just the n-dose rate (not fully implemented)
      isrc=1  ! for a coupled n/g MCNP calc with a neutron-only source;  adjoint based on total  n+g dose rate (works a-ok)
      isrc=2  ! for a gamma-only MCNP calc with a gamma-only source;     adjoint based on just the g-dose rate (working on this now)
c
      call srcjst (isrc,xsrc,xdet,dx,dydz,
     *  whi2lo,wav2lo,imi,xmini,xmaxi,emaxi,wtlo)  ! calculate weight window info
c
c     ------------------------------------------------------
c     By commenting out the call to Subroutine WTWIN (no longer shown or used here), the task of writing a 3-D weight window file
c     (for the gamma-only analysis of the HB-3 beam tube and shutter with the 1998 water tube and collimator sections both flooded)
c     was removed from here on 6-20-1998 and placed (instead) in an off-line stand-alone program called WW308G.F which utilizes
c     broad-group mesh-to-mesh wtlow attenuation factors based on the printed output tables in the GETADJ.OUT file produced by
c     Subroutine GETADJ which is called by Subroutine SRCJST above.  -- JAB, 6-20-98
c       call wtwin (imi,xmini,xmaxi,emaxi,wtlo)      ! write out weight window file for Cartesian XYZ geometry
c     ------------------------------------------------------
c
      stop
      end
c
c
      subroutine srcjst (isrc,xsrc,xdet,dx,dydz,
     *  whi2lo,wav2lo,imi,xmini,xmaxi,emaxi,wtlo)
c     **********************************************************************
c     **********************************************************************
c
c     Calculates the biased source distribution for MCNP, as well as the
c     space/energy-dependent weight windows to be used in the MCNP calc.
c
c     The gamma-only source used here is for the full (complete) HB3 water tube when flooded.
c
c     The user must supply the following information:
c
c          isrc=0 for a neutron-only MCNP calc with a neutron-only source; adjoint based on just the n-dose rate
c          isrc=1 for a coupled n/g MCNP calc with a neutron-only source;  adjoint based on total  n+g dose rate
c          isrc=2 for a gamma-only MCNP calc with a gamma-only source;     adjoint based on just the g-dose rate
c
c          xsrc = location (cm) where the "real" (forward) source would impinge on the 1-D buckled slab model (used for several things)
c          xdet = location (cm) of adjoint source in anisn model (not used, only printed, but user MUST specify for QA purposes)
c          dx   = thickness (cm) of each importance zone to be used in mcnp
c          dydz = transverse dimensions (cm) DY=DZ=dyzy used for buckling in anisn (not used, only printed;  MUST specify for QA purposes)
c          whi2lo=ratio of WTHIGH/WTLOW to be used in setting up weight windows; must use same values in MCNP run
c          wav2lo=ratio of WTAVG/WTLOW = WTSURV/WTLOW to be used in setting up weight windows; must use same values in MCNP run
c
```

```
c
c       This routine calculates and returns the following parameters:
c
c            imi = number of "DX-cm-thick" (typ 5-cm-thick) coarse importance mesh intervals
c            xmini(3000),xmaxi(0:3000) = xmin & xmax for each importance zone,  i=1,imi  (imi.le.3000)
c            emaxi(10)       ! maximum energy (MeV) of the 6 broad neut groups & the 4 broad gamma groups
c            wtlo(3000,10)   ! ((wtlo(mesh,ig),mesh=1,imi),ig=1,10) for a given importance mesh, and broad group (calculated here)
c
c       ---------------------------------------------------------
c
c       Ref: "Monte Carlo Shielding Analyses Using an Automated Biasing
c       Procedure" by J. S. Tang and T. J. Hoffman, Nuclear Science and
c       Engineering, Vol 99, pp 329-342 (1988)
c
c       ***********************************************************************
c       ***********************************************************************
c
        dimension xmini(3000),xmaxi(0:3000)       ! xmin & xmax for each importance zone
        dimension emaxi(10)       ! maximum energy (MeV) of the 6 broad neut groups & the 4 broad gamma groups
        dimension wtlo(3000,10)   ! wtlo(mesh,ig) for a given importance mesh, and broad group (calculated here)
c
        dimension adjnfl(3000,6) ! allows for 6 neutron imp grps  and up to 3000 coarse imp mesh
        dimension adjgfl(3000,4) ! allows for 4 gamma   imp grps  and up to 3000 coarse imp mesh
c
        dimension s0(10),sb(10),ratio(10),a(10),wtavg(10)
        dimension ptsrc(84),x0(84),src(84),srcb(84)
        dimension srcm(61),srcbm(61)  ! unbiased & biased sources in MCNP order (grp 1=low E, grp 61=high E)
c
        data ptsrc/  ! for neut in HB3 (velm grp=1,61), gammas in HB3 (velm grp=1,23); fast=grp 1
     *  2.74800E+09, 6.92602E+12, 8.64293E+12, 3.05242E+13, 7.32282E+13,
     *  1.36477E+14, 2.06360E+14, 1.61947E+14, 2.41078E+14, 1.35333E+14,
     *  2.00073E+14, 3.12945E+14, 8.54720E+14, 8.07055E+14, 7.09512E+14,
     *  5.40055E+14, 6.65098E+14, 5.35177E+14, 3.61470E+14, 1.49367E+14,
     *  5.85513E+14, 6.29256E+14, 3.65651E+13, 7.68584E+12, 1.38494E+13,
     *  2.12840E+14, 7.35199E+14, 4.33245E+14, 3.63241E+14, 4.29193E+14,
     *  5.59006E+14, 8.89397E+14, 1.29680E+14, 4.96958E+14, 3.03507E+14,
     *  1.21873E+14, 5.24714E+13, 1.12860E+14, 6.69650E+13, 7.42049E+14,
     *  9.84217E+14, 8.76077E+14, 7.55438E+14, 3.36538E+14, 2.54975E+14,
     *  2.76622E+14, 2.04908E+14, 8.87245E+14, 8.53691E+14, 8.74122E+14,
     *  9.50610E+14, 9.69821E+14, 9.03837E+14, 1.45876E+15, 1.54759E+15,
     *  1.58981E+15, 1.55274E+15, 1.30212E+15, 1.52979E+15, 2.25679E+15,
     *  6.30365E+16, 1.23250E+11, 6.19421E+13, 1.51983E+15, 1.60183E+14,
     *  1.23378E+15, 6.75453E+14, 1.98361E+15, 2.34929E+15, 1.42777E+15,
     *  2.66951E+15, 4.23989E+15, 5.27935E+15, 7.31636E+15, 4.03975E+15,
     *  4.80101E+15, 7.17665E+15, 1.03805E+16, 2.56708E+16, 1.82855E+16,
     *  1.67705E+16, 1.65029E+16, 2.84514E+15, 8.72837E+12/
        data x0 / ! for neut in HB3 (velm grp=1,61), gammas in HB3 (velm grp=1,23); fast=grp 1
     *   99.9, 31.1, 68.7, 42.9, 59.5, 62.6, 47.9, 56.9, 65.3, 43.5,
     *   33.3, 52.1, 50.2, 59.7, 46.8, 70.1, 44.1, 56.8, 50.3, 52.9,
     *   58.8, 49.6, 42.3, 53.7, 63.8, 42.4, 34.2, 48.9, 42.5, 45.6,
     *   45.7, 47.4, 56.7, 52.9, 79.8, 67.5, 62.6, 46.7, 69.0, 54.0,
     *   50.7, 52.7, 53.3, 65.1, 55.0, 49.5, 43.0, 60.5, 61.2, 52.6,
     *   53.8, 51.1, 56.0, 55.4, 56.5, 48.2, 54.5, 76.1, 65.2, 57.3,
     *   80.2, 97.4, 99.9, 94.4, 96.0, 93.9, 96.4, 93.2, 92.6, 96.6,
     *   99.2, 96.9, 93.6, 86.8, 83.2, 88.8, 84.7, 81.6, 84.5, 83.9,
     *   82.1, 68.1, 61.9, 10.0/
c
        do i=1,84
```

```
      if (i.le.61) ptsrc(i)=1.0     ! DEBUG CASE
      if (i.ge.70) ptsrc(i)=1.0     ! DEBUG CASE
      enddo
c
      open (30,file='getadj.out',status='unknown')                    ! ascii file with summary adjoint info
c
      khi2lo=nint(whi2lo)
      kav2lo=nint(wav2lo)
c
      pi=acos(-1.0)
      x=xsrc        ! point where the point source streaming thru void first impinges on the water tube (input by user)
c
      do i=1,10
      s0(i)=0.0
      enddo
c
      do i=1,84
c
ccc      x0(i)=50.0  ! use this to override the above for the special "ACADEMIC" case ONLY
c
         dum=4.0*pi*(x-x0(i))*(x-x0(i))
         src(i)=ptsrc(i)/dum           ! real unbiased src, (n/s/cm2) or (p/s/cm2), impingent on water tube
c
         if (i.eq.61)                s0(1)=s0(1)+src(i)    ! Unbiased SRC  for  VELM neutr grps 61-61 = MCNP neutr grps 01-01
         if (i.ge.57 .and. i.le.60)  s0(2)=s0(2)+src(i)    ! Unbiased SRC  for  VELM neutr grps 57-60 = MCNP neutr grps 02-05
         if (i.ge.49 .and. i.le.56)  s0(3)=s0(3)+src(i)    ! Unbiased SRC  for  VELM neutr grps 49-56 = MCNP neutr grps 06-13
         if (i.ge.31 .and. i.le.48)  s0(4)=s0(4)+src(i)    ! Unbiased SRC  for  VELM neutr grps 31-48 = MCNP neutr grps 14-31
         if (i.ge.16 .and. i.le.30)  s0(5)=s0(5)+src(i)    ! Unbiased SRC  for  VELM neutr grps 16-30 = MCNP neutr grps 32-46
         if (i.ge.01 .and. i.le.15)  s0(6)=s0(6)+src(i)    ! Unbiased SRC  for  VELM neutr grps 01-15 = MCNP neutr grps 47-61
c
         j=i-61
c
         if (j.ge.18 .and. j.le.23)  s0(7)=s0(7)+src(i)     ! Unbiased SRC  for  VELM gamma grps 18-23 = MCNP gamma grps 01-06
         if (j.ge.13 .and. j.le.17)  s0(8)=s0(8)+src(i)     ! Unbiased SRC  for  VELM gamma grps 13-17 = MCNP gamma grps 07-11
         if (j.ge.09 .and. j.le.12)  s0(9)=s0(9)+src(i)     ! Unbiased SRC  for  VELM gamma grps 09-12 = MCNP gamma grps 12-15
         if (j.ge.01 .and. j.le.08)  s0(10)=s0(10)+src(i)   ! Unbiased SRC  for  VELM gamma grps 01-08 = MCNP gamma grps 16-23
c
      enddo
c
c
      do i=1,10
         if (isrc.le.1 .and. i.ge.7) s0(i)=0.0   ! if this is an MCNP neutron-only or n/g calc, zero-out gamma sources
         if (isrc.eq.2 .and. i.le.6) s0(i)=0.0   ! if this is an MCNP gamma-only calc, zero-out neutron sources
      enddo
c
c     ====================================
      call getadj (isrc,xsrc,xdet,dx,dydz,     ! go get GBANISN broad group adjoint fluxes for each importance mesh
     *  imi,xmini,xmaxi,emaxi,adjnf1,adjgf1)  ! go get GBANISN broad group adjoint fluxes for each importance mesh
c     ====================================
c
      do i=1,10
      ratio(i)=0.0
      enddo
c
c     --------- Now begin procedure outlined in Jabo Tang's NS&E paper:
c
      mesh=
      do i=1,
```

```
      a(i)=adjnfl(mesh,i)   ! get adjoint fluxes for the 6 neutron groups in imp mesh 1, the 1st mesh the "real" source hits
      enddo
      do i=7,10
      a(i)=adjgfl(mesh,i-6)   ! get adjoint fluxes for the 4 gamma groups in imp mesh 1, the 1st mesh the "real" source hits
      enddo
c
      sums0=0.0
      sums0a=0.0
      do i=1,10
         sums0a=sums0a+s0(i)*a(i)
         sums0=sums0+s0(i)
      enddo
      avgadj=sums0a/sums0              ! "Source-Averaged" Adjoint
c
      write (30,'(////)')
      do i=1,10
        sb(i)=s0(i)*a(i)/avgadj        ! Biased MCNP source distribution
ccc      if (a(i).lt.1.0e-20) a(i)=1.0e-20          ! new 6-11-98
         wtavg(i)=avgadj/a(i)
         wtlo(mesh,i)=wtavg(i)/wav2lo  ! See Jabo's recommendation (above)
      enddo
      write (30,10) char(12)
10    format (a1,/,' MESH, WTLOW for each broad group (across) and',
     *  ' each imp mesh (down page), and RATIO of wtlow from',
     *  ' one mesh to the next:',/)
c     write (30,11) mesh,(wtlo(mesh,i),i=1,10)
c11   format (1x,i3,2x,1p,10e13.5)
      write (30,11) mesh,(wtlo(mesh,i),ratio(i),i=1,10)
11    format (1x,i3,2x,10(1p,e13.5,0p,f7.4))
c
      do i=1,10
      ratio(i)=wtlo(mesh,i)
      enddo
c
      do mesh=2,imi
         m=mesh
         do i=1,6
         a(i)=adjnfl(m,i)   ! get adjoint fluxes for the 6 neutron groups in import mesh "m"
         enddo
         do i=7,10
         a(i)=adjgfl(m,i-6)   ! get adjoint fluxes for the 4 gamma groups in import mesh "m"
         enddo
c        ----------------
         do i=1,10
ccc         if (a(i).lt.1.0e-20) a(i)=1.0e-20       ! new 6-11-98
            wtavg(i)=avgadj/a(i)
            wtlo(mesh,i)=wtavg(i)/wav2lo  ! See Jabo's recommendation (above)
         enddo
c        ----------------
         do i=1,10
         ratio(i)=wtlo(mesh,i)/ratio(i)
         enddo
c        write (30,11) mesh,(wtlo(mesh,i),i=1,10)
         write (30,11) mesh,(wtlo(mesh,i),ratio(i),i=1,10)
         do i=1,10
         ratio(i)=wtlo(mesh,i)
         enddo
      enddo
```

```
c
c     ------------------------------------------------------
c
      write (30,'(a1)') char(12)
c
      if (isrc.eq.0) write (30,301)  khi2lo,kav2lo,(emaxi(i),i=1,10)
301   format (17x,'WTLO for the 6 broad neutron groups',
     *  ' and 4 broad gamma groups based on 1-D adjoint & Jabo''s',
     *  ' procedure with WTHI=',i5,'*WTLO & WTSURV=WTAVG=',i3,'*WTLO',
     *  /,17x,'Use these values for the neutron-only mcnp transport',
     *  ' analysis involving a neutron-only source.',/,17x,
     *  ' (For coupled n/g calcs, or gamma-only calcs, values',
     *  ' would be different)',/,17x,
     *  'mnXX-YY = MCNP neutron grp numbers,   ',
     *  'mgXX-YY = MCNP gamma grp numbers',/,17x,
     *  'vnXX-YY = VELM neutron grp numbers,   ',
     *  'vgXX-YY = VELM gamma grp numbers',//,17x,
     *  'Emax:',1pe12.5,9e13.5,/,17x,
     *  'imp     mn01-01      mn02-05      mn06-13      mn14-31',
     *    '      mn32-46      mn47-61      mg01-06      mg07-11',
     *    '      mg12-15      mg16-23',/,
     *  '  xmin    xmax   mesh',
     *      '    vn61-61      vn57-60      vn49-56      vn31-48',
     *    '      vn16-30      vn01-15      vg18-23      vg13-17',
     *    '      vg09-12      vg01-08',/)
c
      if (isrc.eq.1) write (30,401)  khi2lo,kav2lo,(emaxi(i),i=1,10)
401   format (17x,'WTLO for the 6 broad neutron groups',
     *  ' and 4 broad gamma groups based on 1-D adjoint & Jabo''s',
     *  ' procedure with WTHI=',i5,'*WTLO & WTSURV=WTAVG=',i3,'*WTLO',
     *  /,17x,'Use these values for the coupled n/g mcnp transport',
     *  ' analysis involving a neutron-only source.',/,17x,
     *  ' (For a neutron-only calc or gamma-only calc, values',
     *  ' would be different)',/,17x,
     *  'mnXX-YY = MCNP neutron grp numbers,   ',
     *  'mgXX-YY = MCNP gamma grp numbers',/,17x,
     *  'vnXX-YY = VELM neutron grp numbers,   ',
     *  'vgXX-YY = VELM gamma grp numbers',//,17x,
     *  'Emax:',1pe12.5,9e13.5,/,17x,
     *  'imp     mn01-01      mn02-05      mn06-13      mn14-31',
     *    '      mn32-46      mn47-61      mg01-06      mg07-11',
     *    '      mg12-15      mg16-23',/,
     *  '  xmin    xmax   mesh',
     *      '    vn61-61      vn57-60      vn49-56      vn31-48',
     *    '      vn16-30      vn01-15      vg18-23      vg13-17',
     *    '      vg09-12      vg01-08',/)
c
      if (isrc.eq.2) write (30,501)  khi2lo,kav2lo,(emaxi(i),i=1,10)
501   format (17x,'WTLO for the 6 broad neutron groups',
     *  ' and 4 broad gamma groups based on 1-D adjoint & Jabo''s',
     *  ' procedure with WTHI=',i5,'*WTLO & WTSURV=WTAVG=',i3,'*WTLO',
     *  /,17x,'Use these values for the gamma-only mcnp transport',
     *  ' analysis involving a gamma-only source.',/,17x,
     *  ' (For a coupled n/g calc, or a neutron-only calc, values',
     *  ' would be different)',/,17x,
     *  'mnXX-YY = MCNP neutron grp numbers,   ',
     *  'mgXX-YY = MCNP gamma grp numbers',/,17x,
     *  'vnXX-YY = VELM neutron grp numbers,   ',
```

```
      *   'vgXX-YY = VELM gamma grp numbers',//,17x,
      *   'Emax:',1pe12.5,9e13.5,/,17x,
      *   'imp      mn01-01      mn02-05      mn06-13      mn14-31',
      *     '      mn32-46      mn47-61      mg01-06      mg07-11',
      *     '      mg12-15      mg16-23',/,
      *   '  xmin     xmax   mesh',
      *       '     vn61-61      vn57-60      vn49-56      vn31-48',
      *     '      vn16-30      vn01-15      vg18-23      vg13-17',
      *     '      vg09-12      vg01-08',/)
c
      do jx=1,imi
         write (30,402) xmini(jx),xmaxi(jx),jx,
     *      (wtlo(jx,ig),ig=1,10)
402      format (1x,f6.2,f8.2,i5,1x,1p,10e13.5)
      enddo
c
c     ------------------------------------------------------
c
      do i=1,10
      ratio(i)=1.0
      if (s0(i).gt.0.0)  ratio(i)=sb(i)/s0(i)
      enddo
c
      write (30,'(a1)') char(12)
      write (30,12) (s0(i),i=1,10)
      write (30,13) (sb(i),i=1,10)
      write (30,14) (ratio(i),i=1,10)
c
12    format (///,1x,' s0',2x,1p,10e13.5)
13    format (///,1x,' sb',2x,1p,10e13.5)
14    format (///,1x,' r ',2x,1p,10e13.5)
c
c
c
      do i=1,84
         src(i)=ptsrc(i)          ! return to original point sources (rather than impingent sources)
         if (isrc.le.1 .and. i.ge.62) src(i)=0.0  ! for neutron-only or n/g mcnp calc
         if (isrc.eq.2 .and. i.le.61) src(i)=0.0  ! for gamma-only mcnp calc
c
         if (i.eq.61)               srcb(i)=src(i)*sb(1)/s0(1)   ! Biased SRC  for  VELM neutr grps 61-61 = MCNP neutr grps 01-01
         if (i.ge.57 .and. i.le.60) srcb(i)=src(i)*sb(2)/s0(2)   ! Biased SRC  for  VELM neutr grps 57-60 = MCNP neutr grps 02-05
         if (i.ge.49 .and. i.le.56) srcb(i)=src(i)*sb(3)/s0(3)   ! Biased SRC  for  VELM neutr grps 49-56 = MCNP neutr grps 06-13
         if (i.ge.31 .and. i.le.48) srcb(i)=src(i)*sb(4)/s0(4)   ! Biased SRC  for  VELM neutr grps 31-48 = MCNP neutr grps 14-31
         if (i.ge.16 .and. i.le.30) srcb(i)=src(i)*sb(5)/s0(5)   ! Biased SRC  for  VELM neutr grps 16-30 = MCNP neutr grps 32-46
         if (i.ge.01 .and. i.le.15) srcb(i)=src(i)*sb(6)/s0(6)   ! Biased SRC  for  VELM neutr grps 01-15 = MCNP neutr grps 47-61
c
         j=i-61
c
         if (j.ge.18 .and. j.le.23) srcb(i)=src(i)*sb(7)/s0(7)   ! Biased SRC  for  VELM gamma grps 18-23 = MCNP gamma grps 01-06
         if (j.ge.13 .and. j.le.17) srcb(i)=src(i)*sb(8)/s0(8)   ! Biased SRC  for  VELM gamma grps 13-17 = MCNP gamma grps 07-11
         if (j.ge.09 .and. j.le.12) srcb(i)=src(i)*sb(9)/s0(9)   ! Biased SRC  for  VELM gamma grps 09-12 = MCNP gamma grps 12-15
         if (j.ge.01 .and. j.le.08) srcb(i)=src(i)*sb(10)/s0(10) ! Biased SRC  for  VELM gamma grps 01-08 = MCNP gamma grps 16-23
c
      enddo
c
c     ------------------------------------------------------------------------------------
c
      if (isrc.eq.0) then     ! isrc=0 for a neutron-only MCNP calc with a neutron-only source; adjoint based on just the n-dose rate
```

```
      do i=1,61
         k=62-i
         srcm(i)=src(k)    ! unbiased neutron sources in MCNP order (grp 1=low E, grp 61=high E)
         srcbm(i)=srcb(k)  !   biased neutron sources in MCNP order (grp 1=low E, grp 61=high E)
      enddo
      write (30,341)
341   format (///,' Unbiased neutron sources in MCNP order',
     *  ' (grp 1=low E, grp 61=high E):',/)
      write (30,342)  (srcm(i),i=1,61)
342   format (5x,1p,5e13.5)
      write (30,343)
343   format (/,' Biased neutron sources in MCNP order',
     *  ' (grp 1=low E, grp 61=high E):',/,
     *  ' Use these values for the neutron-only mcnp transport',
     *  ' analysis involving a neutron-only source.',/,
     *  ' (For coupled n/g calcs, or gamma-only calcs, values',
     *  ' would be different)',/)
      write (30,342)  (srcbm(i),i=1,61)
      write (30,344)  khi2lo,kav2lo
344   format (/,' In addition:',//,
     *  ' Delete   WWP:P  card completely, and ...',/,
     *  ' On your  WWP:N  card, make sure you have',
     *  '  WTHI=',i5,'*WTLO  and WTSURV=',i3,'*WTLO')
   endif
c
c  ------------------------------------------------------------------------------------
c
   if (isrc.eq.1) then     ! isrc=1 for a coupled n/g MCNP calc with a neutron-only source; adjoint based on total n+g dose rate
      do i=1,61
         k=62-i
         srcm(i)=src(k)    ! unbiased neutron sources in MCNP order (grp 1=low E, grp 61=high E)
         srcbm(i)=srcb(k)  !   biased neutron sources in MCNP order (grp 1=low E, grp 61=high E)
      enddo
      write (30,441)
441   format (///,' Unbiased neutron sources in MCNP order',
     *  ' (grp 1=low E, grp 61=high E):',/)
      write (30,442)  (srcm(i),i=1,61)
442   format (5x,1p,5e13.5)
      write (30,443)
443   format (/,' Biased neutron sources in MCNP order',
     *  ' (grp 1=low E, grp 61=high E):',/,
     *  ' Use these values for the coupled n/g mcnp transport',
     *  ' analysis involving a neutron-only source.',/,
     *  ' (For a neutron-only calc or gamma-only calc, values',
     *  ' would be different)',/)
      write (30,442)  (srcbm(i),i=1,61)
      write (30,444)  khi2lo,kav2lo,khi2lo,kav2lo
444   format (/,' In addition:',//,
     *  ' On your  WWP:N  card, make sure you have',
     *  '  WTHI=',i5,'*WTLO  and WTSURV=',i3,'*WTLO',/,
     *  ' On your  WWP:P  card, make sure you have',
     *  '  WTHI=',i5,'*WTLO  and WTSURV=',i3,'*WTLO')
   endif
c
c  ------------------------------------------------------------------------------------
c
   if (isrc.eq.2) then     ! isrc=2 for a gamma-only MCNP calc with a gamma-only source; adjoint based on just the g-dose rate
      do i=1,23
```

```
            k=85-i
            srcm(i)=src(k)    ! unbiased gamma sources in MCNP order (grp 1=low E, grp 23=high E)
            srcbm(i)=srcb(k)  !   biased gamma sources in MCNP order (grp 1=low E, grp 23=high E)
          enddo
c
          write (30,541)
541       format (///,' Unbiased gamma sources in MCNP order',
     *      ' (grp 1=low E, grp 23=high E):',/)
          write (30,542)  (srcm(i),i=1,23)
542       format (5x,1p,5e13.5)
c
          write (30,543)
543       format (/,' Biased gamma sources in MCNP order',
     *      ' (grp 1=low E, grp 23=high E):',/,
     *      ' Use these values for the gamma-only mcnp transport',
     *      ' analysis involving a gamma-only source.',/,
     *      ' (For a coupled n/g calc, or a neutron-only calc, values',
     *      ' would be different)',/)
          write (30,542)  (srcbm(i),i=1,23)
          write (30,544)  khi2lo,kav2lo
544       format (/,' In addition:',//,
     *     ' Delete   WWP:N  card completely, and ...',/,
     *     ' On your  WWP:P  card, make sure you have',
     *      '  WTHI=',i5,'*WTLO  and WTSURV=',i3,'*WTLO')
        endif
c
c       ------------------------------------------------------------------------------------------
c
        return
        end
c
c
        subroutine getadj (isrc,xsrc,xdet,dx,dydz,
     *   imi,xmini,xmaxi,emaxi,adjnfl,adjgfl)
c       ***************************************************************************
c       ***************************************************************************
c
c       Tallies the GBANISN adjoint flux into 6 broad neutron groups and 4 broad gamma groups,
c       for each "DX-cm-thick" (typ 5-cm-thick) coarse importance mesh composed of any number
c       of fine mesh in the GBANISN adj calc using the VELM 61n/23g lib
c
c       The user must supply the following information:
c
c            isrc = 0 for an MCNP calc with a neutron-only source; adjoint based on just the n-dose rate
c            isrc = 1 for an MCNP calc with a neutron-only source; adjoint based on total  n+g dose rate
c            isrc = 2 for an MCNP calc with a gamma-only source;   adjoint based on just the g-dose rate
c
c            xsrc = location (cm) where the "real" (forward) source would impinge on the 1-D buckled slab model (used for several things)
c            xdet = location (cm) of adjoint source in anisn model (not used, only printed, but user MUST specify for QA purposes)
c            dx   = thickness (cm) of each importance zone to be used in mcnp
c            dydz = transverse dimensions (cm) DY=DZ=dyzy used for buckling in anisn (not used, only printed;  MUST specify for QA purposes)
c
c       This subroutine will return:  imi, xmini, xmaxi, emaxi, adjnfl, adjgfl  where
c
c            imi = number of "DX-cm-thick" (typ 5-cm-thick) coarse importance mesh intervals
c            dimension xmini(3000),xmaxi(0:3000)  ! xmin & xmax for each importance zone, i=1,imi  (imi.le.3000)
c            dimension emaxi(10)       ! maximum energy (MeV) of the 6 broad neut groups & the 4 broad gamma groups
c            dimension adjnfl(3000,6) ! allows for 6 neutron imp grps  and up to 3000 coarse imp mesh
```

```
      dimension adjgfl(3000,4) ! allows for 4 gamma   imp grps  and up to 3000 coarse imp mesh

                                                -- J.A. Bucholz, 20 May 1998

      ************************************************************************

      This routine was recently updated to account for fact the results on the
      gbanisn "adjoint scalar flux tape" are in "adjoint order", i.e. ....

      ... the results in grp  1 on the tape really correspond to the adjoint flux for the lowest  energy gamma group,
      ... the results in grp 23 on the tape really correspond to the adjoint flux for the highest energy gamma group,
      ... the results in grp 24 on the tape really correspond to the adjoint flux for the lowest  energy neutron group, and
      ... the results in grp 84 on the tape really correspond to the adjoint flux for the highest energy neutron group.

      This conclusion was verified by extensive testing on 13 June 1998.
      Prior to this time, I had failed to appreciate this fact.

                                                -- J.A. Bucholz, 13 June 1998

      ************************************************************************
      ************************************************************************

      dimension fluxim(84)
      dimension flux(3000),emax0(84),emaxi(10)
      dimension xmina(3000),xmida(3000)        ! xmin & midpoint for each anisn mesh; xmin read from anisn printed output file
      dimension xmini(3000),xmaxi(0:3000)      ! xmin & xmax for each importance zone
      dimension vola(3000)                     ! volume of each fine mesh in the 1-D slab anisn calc
      dimension voli(3000)                     ! total vol of all fine mesh whose midpoints lie inside a given imp zone (may differ slightly from actual v
l of imp zone)
      character*48 typadj(0:2)                 ! alphanumeric string (set below) indicating type of adjoint;  based on isrc = 0, 1 or 2
      character*32 linchk                      ! used to extract gbanisn mesh when reading gbaoutput file
      character*1  lin1
      equivalence (lin1,linchk)

      double precision adjnfl(3000,6),adjgfl(3000,4)  ! allows for 6 neutron imp grps & 4 gamma imp grps; total=10
      dimension adjnfl(3000,6),adjgfl(3000,4)  ! allows for 6 neutron imp grps & 4 gamma imp grps; total=10
      dimension igmin(10),igmax(10)
      data igmin/ 1, 16, 31, 49, 57, 61, 62, 70, 74, 79 /  ! VELM group numbers corresponding to each importance group
      data igmax/15, 30, 48, 56, 60, 61, 69, 73, 78, 84 /  ! VELM group numbers corresponding to each importance group

      Emax in MeV for VELM neutron grps ig=1,61 followed by
      Emax in MeV for VELM gamma   grps ig=1,23
      data emax0/
     * 1.4918E+01, 1.2214E+01, 1.0000E+01, 8.1873E+00, 6.7032E+00,
     * 5.4881E+00, 4.4933E+00, 3.6788E+00, 3.0119E+00, 2.4660E+00,
     * 2.3457E+00, 2.2313E+00, 2.0190E+00, 1.6530E+00, 1.3534E+00,
     * 1.1080E+00, 9.0718E-01, 7.4274E-01, 6.0810E-01, 5.2340E-01,
     * 4.9787E-01, 3.8774E-01, 3.0197E-01, 2.9849E-01, 2.9721E-01,
     * 2.9452E-01, 2.7324E-01, 2.2371E-01, 1.8316E-01, 1.4996E-01,
     * 1.2277E-01, 8.6517E-02, 5.6562E-02, 5.2475E-02, 3.4307E-02,
     * 2.8501E-02, 2.7000E-02, 2.6058E-02, 2.4788E-02, 2.3579E-02,
     * 1.5034E-02, 9.1188E-03, 5.5308E-03, 3.7074E-03, 3.0354E-03,
     * 2.6126E-03, 2.2487E-03, 2.0347E-03, 1.2341E-03, 7.4852E-04,
     * 4.5400E-04, 2.7536E-04, 1.6702E-04, 1.0130E-04, 4.7851E-05,
     * 2.2603E-05, 1.0677E-05, 5.0435E-06, 2.3824E-06, 1.1253E-06,
     * 4.1399E-07, 1.4000E+01, 1.0000E+01, 8.0000E+00, 7.5000E+00,
     * 7.0000E+00, 6.0000E+00, 5.0000E+00, 4.0000E+00, 3.0000E+00,
     * 2.5000E+00, 2.0000E+00, 1.5000E+00, 1.0000E+00, 7.0000E-01,
```

```
     * 6.0000E-01, 5.1000E-01, 4.0000E-01, 3.0000E-01, 1.5000E-01,
     * 1.0000E-01, 7.0000E-02, 4.5000E-02, 2.0000E-02/
c
      data typadj/                                              ! used only in write statement
     *   ' where adjoint is based on just the n-dose at X=',    ! isrc=0
     *   ' where adjoint is based on total  n+g dose at X=',    ! isrc=1
     *   ' where adjoint is based on just the g-dose at X='  /  ! isrc=2
c
c
c     ------------------------------------------------------
c     read anisn mesh from anisn printed output file:
c
      open (12,file='gbaoutput',status='old',form='formatted')       ! anisn printed output file
c
200   read (12,'(a32)')  linchk
      if (linchk.ne.'  int.  zone number     radius  ') go to 200
201   read (12,'(a32)')  linchk
      read (linchk,'(i6,i8,e18.5)') mesha,mzone,xmina(mesha)
      if (mzone.gt.0)  go to 201
      im=mesha-1  ! number of anisn mesh intervals
      close (12)
c
      do i=1,im
      xmida(i)=(xmina(i)+xmina(i+1))/2.0  ! get midpoint of each anisn mesh
      vola(i)=xmina(i+1)-xmina(i)
      enddo
c
      xmaxi(0)=xmina(1)
      xmaxi(0)=xsrc
      i=0
203   i=i+1
      xmini(i)=xmaxi(i-1)
      xmaxi(i)=xmini(i)+dx  ! increment by thickness of each importance zone to be used in mcnp
      if (xmaxi(i).lt.xmina(mesha)) go to 203
      imi=i  ! number of mcnp importance zones corresponding to anisn model
c
c     ------------------------------------------------------
c
      do ig=1,6
         do ix=1,imi
            adjnfl(ix,ig)=0.0d0
         enddo
      enddo
c
      do ig=1,4
         do ix=1,imi
            adjgfl(ix,ig)=0.0d0
         enddo
      enddo
c
c
c     get total volume of all anisn fine mesh (ix) whose midpoints lie inside a given importance mesh (jx):
      do jx=1,imi
         voli(jx)=0.0
         do ix=1,im
         if (xmida(ix).ge.xmini(jx) .and. xmida(ix).le.xmaxi(jx))
     *       voli(jx)=voli(jx)+vola(ix)
         enddo
```

```
      enddo
c
c     ------------------------------------------------------
c
      open (15,file='fort.15',status='old',form='unformatted')       ! anisn flux moment file (fort.15)
c
c     ------------------------------------------------------
c                    ! tally gammas
      do iag=1,23    ! on velm adjoint calc tape fort.15, group  iag=  1,  2,  3,  4, .... 21, 22, 23
         ig=85-iag   ! really corresponds to "real" velm  group   ig= 84, 83, 82, 81, .... 64, 63, 62
c
         do jg=7,10
         if (ig.ge.igmin(jg) .and. ig.le.igmax(jg)) igg=11-jg  ! igg=mcnp broad group (1=soft, 4=hard)
         enddo
c
         read (15) (flux(ix),ix=1,im)
         fluxim(iag)=flux(im)
c
         do jx=1,imi                                                    ! for every coarse importance mesh
            do ix=1,im                                                  ! check the location of each anisn fine mesh
            if (xmida(ix).ge.xmini(jx) .and. xmida(ix).le.xmaxi(jx))    ! and stuff the anisn adjoint flux in the right imp mesh
     *        adjgfl(jx,igg)=adjgfl(jx,igg)+flux(ix)*vola(ix)/voli(jx)  ! while accounting for relative volume of each mesh
            enddo
         enddo
c
      enddo
c
c     ------------------------------------------------------
c                    ! tally neutrons
      do iag=24,84   ! on velm adjoint calc tape fort.15, group  iag= 24, 25, 26, 27, .... 82, 83, 84
         ig=85-iag   ! really corresponds to "real" velm  group   ig= 61, 60, 59, 58, ....  3,  2,  1
c
         do jg=1,6
         if (ig.ge.igmin(jg) .and. ig.le.igmax(jg)) igg=7-jg  ! igg=mcnp broad group (1=slow, 6=fast)
         enddo
c
         read (15) (flux(ix),ix=1,im)
         fluxim(iag)=flux(im)
c
         do jx=1,imi                                                    ! for every coarse importance mesh
            do ix=1,im                                                  ! check the location of each anisn fine mesh
            if (xmida(ix).ge.xmini(jx) .and. xmida(ix).le.xmaxi(jx))    ! and stuff the anisn adjoint flux in the right imp mesh
     *        adjnfl(jx,igg)=adjnfl(jx,igg)+flux(ix)*vola(ix)/voli(jx)  ! while accounting for relative volume of each mesh
            enddo
         enddo
c
      enddo
c
c     ------------------------------------------------------
ccc   write (30,742) (ig,fluxim(ig),ig=1,84)
742   format (' On TAPE, group ig=',i3,'  flux(im)=',1pe13.5)
c     ------------------------------------------------------
      impg=0
      do i=6,1,-1
      impg=impg+1
      emaxi(impg)=emax0(igmin(i))  ! emax for each braod (neutron) importance group (impg=1,6)
      enddo
      do i=1,6,-1
```

```
        impg=impg+1
        emaxi(impg)=emax0(igmin(i))  ! emax for each braod (gamma) importance group (impg=7,10)
        enddo
c       ------------------------------------------------------
c
        write (30,401) char(12),typadj(isrc),xdet,dydz,(emaxi(i),i=1,10)
401     format (a1,/,17x,'Neutron and Gamma Adjoint Fluxes: ',
     *   a48,f8.3,' cm, and buckling DY=DZ=',f6.2,' cm',/,17x,
     *   'mnXX-YY = MCNP neutron grp numbers,   ',
     *   'mgXX-YY = MCNP gamma grp numbers',/,17x,
     *   'vnXX-YY = VELM neutron grp numbers,   ',
     *   'vgXX-YY = VELM gamma grp numbers',//,17x,
     *   'Emax:',1pe12.5,9e13.5,/,17x,
     *   'imp     mn01-01      mn02-05      mn06-13      mn14-31',
     *     '      mn32-46      mn47-61      mg01-06      mg07-11',
     *     '      mg12-15      mg16-23',/,
     *   '  xmin    xmax   mesh',
     *       '    vn61-61      vn57-60      vn49-56      vn31-48',
     *     '      vn16-30      vn01-15      vg18-23      vg13-17',
     *     '      vg09-12      vg01-08',/)
        do jx=1,imi
           write (30,402) xmini(jx),xmaxi(jx),jx,
     *        (adjnfl(jx,ig),ig=1,6),(adjgfl(jx,ig),ig=1,4)
402        format (1x,f6.2,f8.2,i5,1x,1p,10e13.5)
        enddo
c
        return
        end
END-GETWIN



cat >gbainput <<'END-GBAINPUT'
gbanisn: 1-d buckled slab adjoint model of hb3 water tube & collimator, etc.
/
/*********************************
/
/ see description of revised input in section 6 of
/ charles slater's memo to dist, dated 4/7/88
/
/*********************************
/
15$$  /  15$$ = integer parameters
  1   /  id  = problem id number;  if .gt. 1000000, disadvantage factors will be computed by group for each material in calc
  1   /   0   /  ith = 0/1 = forward/adjoint calc
  3   /  isct = maximum order of scatter found in any zone
 32   /  isn = order of angular quadrature
  1   /  ige = 1/2/3 = slab/cyl/spherical geometry
  0   /  ibl = 0/1/2/3 = vacuum/reflection/periodic/white(albedo) = left boundary condition
  0   /  ibr = 0/1/2/3 = vacuum/reflection/periodic/white(albedo) = right boundary condition
 22   /  izm = number of zones or regions (same material)
719   /  im  = number of mesh intervals
  0   /  ievt = 0/1/2/3/4/5/6 = fixed src / k-calc / alpha / conc search / zone width search / outer radius search / buckling search
      /  ------- 10 -------
 84   /  igm = number of energy groups
  3   /  iht = position of sigt in xsect table
  4   /  ihs = position of g-g (self-scatter) in xsect table
 87   /  ihm =length of xsect table
```

```
  0   /  ms = mixing table length (10$$, 11$$, 12** arrays)
  0   /  mcr = number of xsect sets read from cards (14** array)
 32   /  mtp = number of xsect sets to be read from tape (13$$ array)
 32   /  mt  = total number of xsect sets (number entered + any mixtures created)
  1   /   0   /  idfm = 0/1 = density factors not used / density factors used (if used, enter 21** array)
  0   /  ipvt = 0/1/2 = no effect / enter initial keff (as pv in 16**) / enter initial alpha (as pv in 16**);  see page 25 for more notes
      /  ------- 20 -------
  1   /   0   /  iqm  = 0/1 = no effect / enter distributed source (in 17** array)
  0   /   1   /  ipm  = 0/1/im = no effect / enter shell src by grp and angle (18**) / enter shell src by interval, grp, and angle
  0   / 116   /  ipp  = interval number which contains shell src if ipm=1;  otherwise, set ipp=0
200   /  iim  = inner (spatial) iteration maximum
  0   /  id1  = -1/0/1/2/3 = no scalar flux or dist src print/ no effect / print angular flux / punch scalar flux / print angular flx and punch scalar flx
  1   /  id2  = 0/1/2 = no effect / read mtp xsect sets from tape in gip format / use xsects and fixed src from previous problem
  0   /  id3  = 0/N = no effect / compute N activities by zone, where N is any positive integer
  0   /  id4  = 0/1 = no effect / compute N activities by interval (where N=id3)
  1   /  icm  = outer (energy) iteration maximum
      /         icm note: if there is no fission, one may set icm=1 in "gbanisn" and it will cycle thru each of the thermal
      /         groups once and then repeat that cycle up to iim times (where iim is the "inner" iteration max) to converge
      /         the upscatter terms -- i.e., with group-banded anisn (and the bands properly defined in the 1$$ array)
      /         icm.gt.1 is not needed to converge upscatter, although icm.gt.1 would be needed if one allows fission.
  1   /  idat1= 0/1/2 = all data in core/ xsects & fixed sources stored on tape / fluxes & currents on tape also
      /         ****  must set idat1=1 if xsects come from a gip tape  ****
      /  ------- 30 -------
  0   /  idat2= 0 for no effect; idat2.gt.0, enter 24$$ array to select Sn, or diff theory, or inf hom media option by group for first "idat2" outers
  0   /  ifg = 0/1/2/3/4 = no effect/ do xsect weighting / read wtg xsects from prev calc / write wtd xsects (fort.10) / read & write
  3   /  iflu= 0/1/2/3/4 = (wtd diff model) = sometimes step/ linear only/ step only/ wtd diff / wtg with neg flx fixup
  1   /  ifn = 0/1/2 = enter fission guess (2**) / enter flux guess (3**) / use flux from prev case
  1   /  iprt= 0/1 = print xsects / don't print xsects
  2   /  ixtr= 0/1/2/3 as noted below:
      /     ixtr=0 no effect; start problem from scratch (requires 3** flux guess array in data block f)
      /     ixtr=1 read flux guess (on unit nt14); set ifn=1 and do not enter 3** array; do not include data block f at all
      /     ixtr=2 write flux soln (on unit nt15)
      /     ixtr=3 read flux guess on one unit (nt14), write flux solution on another unit (nt15)
  e   /  note: ixtr is now last parameter in 15$$ (not nbuf or nsav)
/
16**        /   16** = floating point parameters
    0       /   ev   = first guess for keff (usually 0.0)
    0       /   evm  = eigenvalue modifier
  1e-4      /   eps  = epsilon (accuracy desired)
 1.420892   /   0       /   bf   = buckling factor (normally 1.420892 if buckling is used; otherwise 0)
   27.2     /   0       /   dy   = cylinder or plane height for buckling correction
   27.2     /   0       /   dz   = plane depth for buckling correction
    0       /   dfm1 = transverse dimension for void streaming
    0       /   xnf  = source normalization factor (typ: 1 for keff, 0 for fixed src);  n/cm3 for sphere; n/cm2 for slab; n/cm(of height) for cyl
    0       /   pv   = enter:  0 / keff0 / alpha0, depending on value of ipvt (param 20 in 15$$ array)
   0.5      /   xyf  = lamda2 relaxation factor (normally 0.5)
            /  ------- 10 -------
  1e-4      /   xla1 = point flux convergence criteria if .gt. 0
    0       /   xlah = upper limit for abs(1.0-lamda1) used in linear search
    0       /   eql  = eigenvalue change epsilon
    0       /   xnpm = new parameter modifier
    e
59$$     /  59$$ = array of unit numbers to be used (may skip entire array and take defaults)
    8    /  nt1  = 1st flux and current scratch unit if idat1=2 (default: fort.8)
    9    /  nt2  = 2nd flux and current scratch unit if idat1=2 (default: fort.9)
    1    /  nt3  = 1st xsect and source scratch unit if idat1.gt.0  (default: fort.1)
    2    /  nt4  = 2nd xsect and source scratch unit if idat1.gt.0  (default: fort.2)
    3    /  nt5  = angular flux output unit (default: fort.3)
```

```
    4   /  nt6  = anisn-formatted (nuclide oriented) binary xsect library (default: fort.4) if idat1.ne.1
    4   /  nt7  = gip-formatted    (group  oriented) binary xsect library (default: fort.4) if idat1=1
    2   /  nt8  = few-group xsect library output unit if ifg=3 or ifg=4 (default: fort.2)
    2   /  nt9  = few-group xsect library input  unit if ifg=2 or ifg=4 (default: fort.2)
   14   /  nt14 = flux guess input unit if ixtr=1 or ixtr=3 (default: fort.14)
   15   /  nt15 = flux output unit if ixtr=2 or ixtr=3 (default: fort.15)
    6   /  nt99 = unit number for fido edit of input (default: fort.6)
   e
60$$    /   60$$ new array required for canisn, janisn, and gbanisn (but not regualr anisn); only has one entry (kwrd)
  2400  /   kwrd = thousands of real*4 words to be alocated for storage;  typ:  400 req'd for s4;  500 for s8;  900 for s16
   e
 t      / end of data block b;  t is always required   (there is no data block a; that's the title card)
/
/
/
1$$     /  number of groups in each band; if nbands.lt.igm (as usually the case) fill with zeros; igm entries required anyway
   f1   /  use this for VELM 61n/23g
/  14r1  25  44r1  f0  / use this for ANSLV 39n/44g; yields 1 grp per band in 1st 14 bands, and 25 groups in band 15; and 1 grp per band in the 44 gamma ban
ds
/
/ these 2$$ and 3** arrays here were only needed in a very special burnup-dependent version of the group-banded anisn code
/ that bob childs wrote especially for jim bucholz on the mhtgr project in 1988;  these two arrays are not part of the
/ regular group-banded anisn code and should not be entered (they're listed here only as a reminder to me)
/ 2$$  24  e  /  2$$ number of burnup intervals (used only in bob child's version)    ..... this 2$$ not standard
/ 3**  2.  e  /  3** length of burnup intervals in years (used only in bob's version) ..... this 3** not standard
 t      / end of data block c;  t is always required   (this data block has only the 1$$ array and is reqd by std gb-anisn)
/
/
/ 13$$ id numbers for nuclides or macroscopic materials in 'premixed' xsect library
/      but "only if" supplied in anisn-formatted (nuclide oriented) binary library;
/      this array allows the code to strip off just the nuclides it needs from tape;
/      not needed should not be entered if idat1=1 and input xsects are from gip tape
/ 13$$ / mtp entries; not needed when input xsects are from gip tape
/ 14** cross sections entered off cards if mcr.gt.0
/  t      / end of data block d;  t is required if 13$$ or 14** are entered; otherwise this t should be skipped
/
/
/
/ 17** fixed source specifications (im*igm entries reqd if iqm=1)
/   source in each mesh interval for group 1
/   source in each mesh interval for group 2
/   source in each mesh interval for group 3
/     :     :  :    :       :       :    :   :
/   source in each mesh interval for group 27
/   ... these may all be renormalized using xnf
/ 17**  /  values are n/s/cc;  remember to use "lower case" e's for exponents, not upper case e's
/      144r0  18r7.02795e+12   36r6.55051e+12  18r8.15472e+12  183r0   /  group  1  (halfway up top sect of ans core)   1.9097700e-02
/      144r0  18r7.22984e+13   36r6.73868e+13  18r8.38897e+13  183r0   /  group  2  (halfway up top sect of ans core)   2.1556070e-01
/      144r0  18r8.24511e+13   36r7.68498e+13  18r9.56702e+13  183r0   /  group  3  (halfway up top sect of ans core)   4.3961270e-01
/      144r0  18r4.65807e+13   36r4.34163e+13  18r5.40488e+13  183r0   /  group  4  (halfway up top sect of ans core)   5.6619070e-01
/      144r0  18r6.05776e+13   36r5.64623e+13  18r7.02897e+13  183r0   /  group  5  (halfway up top sect of ans core)   7.3080370e-01
/      144r0  18r6.35937e+13   36r5.92735e+13  18r7.37895e+13  183r0   /  group  6  (halfway up top sect of ans core)   9.0361270e-01
/      144r0  18r3.04993e+13   36r2.84274e+13  18r3.53892e+13  183r0   /  group  7  (halfway up top sect of ans core)   9.8649130e-01
/      144r0  18r4.61450e+12   36r4.30101e+12  18r5.35432e+12  183r0   /  group  8  (halfway up top sect of ans core)   9.9903070e-01
/      144r0  18r3.33162e+11   36r3.10529e+11  18r3.86576e+11  183r0   /  group  9  (halfway up top sect of ans core)   9.9993600e-01
/      144r0  18r2.47229e+10   36r2.30433e+10  18r2.86866e+10  183r0   /  group 10  (halfway up top sect of ans core)   1.0000030e+00
/       f0
/ 17** fixed source specifications (im*igm entries reqd if iqm=1)
```

```
/ volumetric source:  (src(i,g),i=1,im=719),g=1,84)
/
/
/ the following flux-to-dose-rate factors are now being treated as an adjoint source: (note: must use adjoint dort-ready xsects)
17**   / volumetric source:  (src(i,g),i=1,im=719),g=1,84)
    718z 1.9465e-1  718z 1.5977e-1  718z 1.4706e-1  / flux-to-dose-rate conv factors for neutron groups 1, 2, 3
    718z 1.4723e-1  718z 1.5118e-1  718z 1.5411e-1  / flux-to-dose-rate conv factors for neutron groups 4, 5, 6
    718z 1.4596e-1  718z 1.3694e-1  718z 1.2849e-1
    718z 1.2527e-1  718z 1.2562e-1  718z 1.2615e-1
    718z 1.2721e-1  718z 1.2864e-1  718z 1.3008e-1
    718z 1.2975e-1  718z 1.1804e-1  718z 1.0554e-1
    718z 9.5577e-2  718z 9.0488e-2  718z 8.3046e-2
    718z 6.6330e-2  718z 5.8498e-2  718z 5.8080e-2
    718z 5.7731e-2  718z 5.5626e-2  718z 4.9373e-2
    718z 4.1241e-2  718z 3.4447e-2  718z 2.8773e-2
    718z 2.2781e-2  718z 1.6688e-2  718z 1.3503e-2
    718z 1.1148e-2  718z 8.7422e-3  718z 7.9520e-3
    718z 7.6770e-3  718z 7.4241e-3  718z 7.1386e-3
    718z 5.8975e-3  718z 4.0874e-3  718z 3.5585e-3
    718z 3.5825e-3  718z 3.6062e-3  718z 3.6229e-3
    718z 3.6387e-3  718z 3.6528e-3  718z 3.6908e-3
    718z 3.7629e-3  718z 3.8453e-3  718z 3.9356e-3
    718z 4.0311e-3  718z 4.1289e-3  718z 4.2492e-3
    718z 4.3820e-3  718z 4.4897e-3  718z 4.5583e-3
    718z 4.5742e-3  718z 4.5250e-3  718z 4.3706e-3  / flux-to-dose-rate conv factors for neutron groups 58,59,60
    718z 3.7090e-3                                  / f-to-d conv factors for neut-group 61
    a1 f0  a43860                                   / zero-out above neutron data, then continue with gammas
                    718z 1.1020e-2  718z 8.7716e-3  / f-to-d conv factors for gamma-grps 1 & 2
    718z 7.8468e-3  718z 7.4783e-3  718z 6.9265e-3  / flux-to-dose-rate conv factors for gamma groups 3, 4, 5
    718z 6.1909e-3  718z 5.4136e-3  718z 4.6221e-3
    718z 3.9596e-3  718z 3.4686e-3  718z 2.9270e-3
    718z 2.3156e-3  718z 1.7563e-3  718z 1.4417e-3
    718z 1.2797e-3  718z 1.0852e-3  718z 8.7594e-4
    718z 5.6676e-4  718z 3.2767e-4  718z 2.6644e-4
    718z 2.7466e-4  718z 5.7761e-4  718z 2.1439e-3  / flux-to-dose-rate conv factors for gamma groups 21,22,23
/ 17**  a43860  f0  / use this to zero-out the adjoint source for gammas if we only care about the direct neutron dose rate
/
/
/ 18** shell source specifications (not reqd if ipm=0,  mm*igm entries reqd if ipm.eq.1,  mm*im*igm entries reqd if ipm.gt.1)
/   note: for adjoint calcs, the angular dependent adjoint source must
/   be supplied as if it were reflected thru the origin)
/   Below:  Source(33)=ScalarFlux(monodirectional)/Weight(33)
/   18**  / based on full 100 MW power n/g from core, including decay fission gammas from core.
/           The following angular fluxes for quadrature direction 33 = (scalar flux)/(weight 33).
/
/   1-D slab GBANISN sources impingent on the old 1960 water tube and/or the new 1998 water
/   tube in the HFIR HB3 beam tube, based on the equivalent point sources in SRC-DESC.SUM;
/   these forward-directed shell sources in direction 33 (of an S32 1-D slab quad set) were
/   computed using the utility program SRC1D.FOR as:
/   SRC(grp ig, direction 33)= (PtSrc(ig)/[4*pi*(X-X0)^2])/weight(33)
/   where the multigroup PtSrc for HB3 is given in ref dataset SRC-DESC.SUM,
/   where X0(ig), the effective center of emmission for group (ig) in HB3, is
/   given in SRC-DESC.SUM (X0=dist in cm from the plane perpendicular to the tube),
/   where x = x1=116.7841 cm = the point where the old 1960 water tube began
/   and   x = x2=174.27   cm = the point where the new 1998 water tube begins
/
/   impingent [illegible]on src on old 1960 water tube (at X=116.7841 cm), for neut[illegible]in HB3 (velm grp=1,61),  fast=grp 01
/    32z 1.130[illegible]08 32z 1.10592e+10 32z 4.38227e+10 32z 6.55516e+10
```

```
/    32z 2.61608e+11 32z 5.44950e+11 32z 5.09834e+11 32z 5.29409e+11
/    32z 1.06623e+12 32z 2.95410e+11 32z 3.36529e+11 32z 8.76827e+11
/    32z 2.26008e+12 32z 2.90345e+12 32z 1.69825e+12 32z 2.90497e+12
/    32z 1.47587e+12 32z 1.74368e+12 32z 9.58689e+11 32z 4.29052e+11
/    32z 2.04155e+12 32z 1.63431e+12 32z 7.72646e+10 32z 2.26409e+10
/    32z 5.78337e+10 32z 4.50956e+11 32z 1.26373e+12 32z 1.10214e+12
/    32z 7.71693e+11 32z 9.92951e+11 32z 1.29692e+12 32z 2.16579e+12
/    32z 4.21110e+11 32z 1.42750e+12 32z 2.60124e+12 32z 5.88214e+11
/    32z 2.09517e+11 32z 2.69366e+11 32z 3.43813e+11 32z 2.20686e+12
/    32z 2.64203e+12 32z 2.50082e+12 32z 2.19740e+12 32z 1.47693e+12
/    32z 7.83043e+11 32z 7.16313e+11 32z 4.41240e+11 32z 3.28332e+12
/    32z 3.23922e+12 32z 2.48747e+12 32z 2.80919e+12 32z 2.63519e+12
/    32z 2.86782e+12 32z 4.53851e+12 32z 4.99220e+12 32z 3.96223e+12
/    32z 4.69230e+12 32z 9.22237e+12 32z 6.73971e+12 32z 7.47705e+12
/    32z 5.52139e+14
/  impingent gamma src on old 1960 water tube (at X=116.7841 cm), for gammas in HB3 (velm grp=61,84), fast=grp 63
/    32z 3.84536e+09 32z 2.54725e+12 32z 3.55596e+13 32z 4.34705e+12
/    32z 2.76192e+13 32z 1.90569e+13 32z 4.18079e+13 32z 4.70888e+13
/    32z 4.10847e+13 32z 1.01212e+14 32z 1.25714e+14 32z 1.15144e+14
/    32z 9.54013e+13 32z 4.19883e+13 32z 7.18706e+13 32z 8.17303e+13
/    32z 9.83029e+13 32z 2.88737e+14 32z 1.98233e+14 32z 1.63428e+14
/    32z 8.16257e+13 32z 1.10727e+13 32z 8.97349e+09
/  impingent neutron src on new 1998 water tube (at X=174.27 cm), for neutrons in HB3 (velm grp=1,61),  fast=grp 01
/    32z 5.82455e+06 32z 3.96115e+09 32z 9.09120e+09 32z 2.07345e+10
/    32z 6.51723e+10 32z 1.28300e+11 32z 1.51488e+11 32z 1.37816e+11
/    32z 2.38004e+11 32z 9.27745e+10 32z 1.18026e+11 32z 2.45799e+11
/    32z 6.50926e+11 32z 7.20780e+11 32z 5.11900e+11 32z 5.83437e+11
/    32z 4.60156e+11 32z 4.54658e+11 32z 2.75728e+11 32z 1.18870e+11
/    32z 5.14801e+11 32z 4.74618e+11 32z 2.46126e+10 32z 6.19803e+09
/    32z 1.33040e+10 32z 1.43484e+11 32z 4.39295e+11 32z 3.23138e+11
/    32z 2.45247e+11 32z 3.03906e+11 32z 3.96441e+11 32z 6.47767e+11
/    32z 1.09982e+11 32z 3.95492e+11 32z 3.98678e+11 32z 1.25329e+11
/    32z 4.93277e+10 32z 8.12988e+10 32z 7.08402e+10 32z 6.01394e+11
/    32z 7.55624e+11 32z 6.94913e+11 32z 6.05180e+11 32z 3.31031e+11
/    32z 2.10124e+11 32z 2.08309e+11 32z 1.39402e+11 32z 8.03580e+11
/    32z 7.82793e+11 32z 6.92223e+11 32z 7.67867e+11 32z 7.49416e+11
/    32z 7.57499e+11 32z 1.21027e+12 32z 1.30806e+12 32z 1.17264e+12
/    32z 1.26895e+12 32z 1.58393e+12 32z 1.50752e+12 32z 1.93367e+12
/    32z 8.35086e+13
/  impingent gamma src on new 1998 water tube (at X=174.27 cm), for gammas in HB3 (velm grp=61,84), fast=grp 63
/    32z 2.44520e+08 32z 1.31290e+11 32z 2.79299e+12 32z 3.06526e+11
/    32z 2.23919e+12 32z 1.30586e+12 32z 3.53816e+12 32z 4.12907e+12
/    32z 2.77455e+12 32z 5.55316e+12 32z 8.30330e+12 32z 9.51037e+12
/    32z 1.12103e+13 32z 5.71012e+12 32z 7.70454e+12 32z 1.04867e+13
/    32z 1.41704e+13 32z 3.73438e+13 32z 2.62482e+13 32z 2.31424e+13
/    32z 1.71632e+13 32z 2.64146e+12 32z 3.79191e+09
/
/  end of source specifications
/  18**  2013z e  / zero-out all neutron sources to run gamma-only calc
/
 t  / end of data block e;  t is required if 17** or 18** are entered; otherwise this t should be skipped
/
/
/
/ 2**  fission density; im entries required; enter only if ifn=0 (34th param in 15$$) and ixtr=0 (36th param in 15$$ array)
/ 3**  flux guess ((flx(i,g),i=1,im),g=1,igm); enter only if ifn=1 (34th param in 15$$) and ixtr=0 (36th param in 15$$ array)
3** f0              / setting ifn=1 and filling 3** with f0 is recommended for shielding work
 t  / end of data block f;  t is required if 2** or 3** are entered; otherwise this t should be skipped
```

```
/
/
/
1**  / chi(g) fission spectrum; igm entries; not needed if no fissionable material present (if not needed, manual says enter f0)
       f0
/
5**  / avg velocity for each energy group; usually not needed (if not needed, manual says enter f0)
       f0
/
6**   / 1-D xsdrnpm quadrature weights (ige=1 isn=32  mm=  33)
    0.00000e+00  6.78811e-03  1.55634e-02  2.37896e-02  3.11572e-02
    3.73990e-02  4.22891e-02  4.56509e-02  4.73627e-02  4.73627e-02
    4.56509e-02  4.22891e-02  3.73990e-02  3.11572e-02  2.37896e-02
    1.55634e-02  6.78811e-03  6.78811e-03  1.55634e-02  2.37896e-02
    3.11572e-02  3.73990e-02  4.22891e-02  4.56509e-02  4.73627e-02
    4.73627e-02  4.56509e-02  4.22891e-02  3.73990e-02  3.11572e-02
    2.37896e-02  1.55634e-02  6.78811e-03
7**   / 1-D xsdrnpm direction cosines  (ige=1 isn=32  mm=  33)
   -1.00000e+00 -9.94700e-01 -9.72288e-01 -9.32816e-01 -8.77702e-01
   -8.08938e-01 -7.29008e-01 -6.40802e-01 -5.47506e-01 -4.52494e-01
   -3.59198e-01 -2.70992e-01 -1.91062e-01 -1.22298e-01 -6.71844e-02
   -2.77125e-02 -5.29953e-03  5.29953e-03  2.77125e-02  6.71844e-02
    1.22298e-01  1.91062e-01  2.70992e-01  3.59198e-01  4.52494e-01
    5.47506e-01  6.40802e-01  7.29008e-01  8.08938e-01  8.77702e-01
    9.32816e-01  9.72288e-01  9.94700e-01
/
/ 4**  / location of each interval boundary; im+1 entries required
/ 4**  0.0  241i0.01  35.56  35.57   / mesh boundaries
/ 4**  0.0  241i0.01  19.06  19.07   / mesh boundaries
/ 4**  0.0  241i0.01  27.95  27.96   / mesh boundaries
/ 4**  8.0 3i9.0 3i10.0 151i12.54 3i109.06 2i111.6 31i112.6 143.08  / mesh boundaries
4**  / 720 mesh boundaries required here (for these 719 mesh intervals):
     115.0  2i116.7841  1111i117.7366  2i174.27  7i174.95125  7i179.05
     7i183.15  7i187.25  7i191.35  7i195.45  7i199.55  7i203.65
     189i207.75  2i302.1868  15i302.5043  49i310.58  2i334.7709
     127i335.4756  2i399.48  14i401.9445  124i415.44875
     2i477.36125  478.79
/
8$$  / zone numbers by mesh interval (im entries required)
     1  3r2  112r3  3r4  8r5  8r6  8r7  8r8  8r9  8r10  8r11  8r12
     190r13  3r14  16r15  50r16  3r17  128r18  3r19  15r20  125r21
     3r22
/
9$$    /  material numbers by zone (izm entries required); material numbers should correspond to p0 components only
   9   /  1st zone always void; 1.7841 cm thick (thickness doesn't matter in slab geometry)
   9   /  2nd zone void here;  1st aluminum window in 1960 design would go here
   9   /  3rd zone void here;  use water if looking at 1960 design
   5   /  4th zone aluminum = 1st window in 1998 design;  would be water for 1960 design
   1   /  5th zone water (first 4.1 cm in 1998 design)
   1   /  6th zone water (next 4.1 cm in 1998 design)
   1   /  7th zone water (next 4.1 cm in 1998 design)
   1   /  8th zone water (next 4.1 cm in 1998 design)
   1   /  9th zone water (next 4.1 cm in 1998 design)
   1   / 10th zone water (next 4.1 cm in 1998 design)
   1   / 11th zone water (next 4.1 cm in 1998 design)
   1   / 12th zone water (next 4.1 cm in 1998 design)
   1   / 13th zone water (remainder of water in 1998 water tube design)
   5   / 14th zone aluminum = 2nd window in 1998 design;  would be water for 1960 design
```

```
   1   / 15th zone water
/  ---------------------------- may wish to make next 3 zones: all water (1), all stainless steel (13), or all carbon steel (17)
   1   / 16th zone water here; may later try stainless steel or carbon steel;
   1   / 17th zone water here; may later try stainless steel or carbon steel; use aluminum iff modeling 1960 water tube design
   1   / 18th zone water here; may later try stainless steel or carbon steel;
/  ---------------------------- previous 3 zones represent the collimator section
   9   / 19th zone thin void at end of collimator (need incoming flux here)
   9   / 20th zone void upstream of carbon steel shutter drum
  17   / 21th zone carbon steel shutter drum
   9   / 22th zone thin void
/
/  end of 9$$ array (although user may use the "plugdef" file to redefine the entire 9$$ array
/
/  list of possible materials (with this HB3 water tube xsect lib) includes the following:
/
/   mix  1  (ANISN/DORT MATL  1) = Water at 1.00 g/cc
/   mix  2  (ANISN/DORT MATL  5) = Aluminum 6061 (2.7 g/cc)
/   mix  3  (ANISN/DORT MATL  9) = Void (He @ 1.0e-20 atoms/barn*cm)
/   mix  4  (ANISN/DORT MATL 13) = SS304 (7.92 g/cc;  see page 50 of ORNL/TM-11989)
/   mix  5  (ANISN/DORT MATL 17) = Carbon Steel (7.8212 g/cc, 99 wt% Fe, 1 wt% C)
/   mix  6  (ANISN/DORT MATL 21) = Barytes Concrete at 3.09725 g/cc
/   mix  7  (ANISN/DORT MATL 25) = Regular Concrete
/   mix  8  (ANISN/DORT MATL 29) = response functions
/
/
/ note: anisn reads macroscopic cross sections for materials that
/ have been premixed elsewhere (in this case materials 1 to 52).
/ it also allows us to use these to create some secondary materials
/ (like materials 53, 57, 61, 65, 69, and 73), as described below:
/ ================================================================
/
/10$$ / mixture numbers in mixing table:
/       4r-53 4r-57 4r-61 4r-65 4r-69 4r-73   / irrelevant here, but shown as an example
/
/11$$ / component numbers (like nuclid numbers) in mixing table:
/       0 41 45 49 5q4                        / irrelevant here, but shown as an example
/
/12** / number densities (atoms/barn*cm):
/       reset   ss      b-10        b-11      / irrelevant here, but shown as an example
/         0    1.0   6.79702e-3   1.67426e-3  / densities for 1st row of pins (mix 53):
/         0    1.0   6.79702e-3   1.67426e-3  / densities for 2nd row of pins (mix 57):
/         0    1.0   6.79702e-3   1.67426e-3  / densities for 3rd row of pins (mix 61):
/         0    1.0   6.79702e-3   1.67426e-3  / densities for 4th row of pins (mix 65):
/         0    1.0   6.79702e-3   1.67426e-3  / densities for 5th row of pins (mix 69):
/         0    1.0   6.79702e-3   1.67426e-3  / densities for 6th row of pins (mix 73):
/ ================================================================
/
/
/ 16$$ is peculiar to gb-anisn;  always use f1 to specify that all
/ angular fluxes should always be continuous across media boundaries
16$$ f1
/
/ 19$$ order of scatter by zone
  19$$ f3
/
/ 20** radius modifiers by zone (required iff ievt=4)
/
/ 21** density factors by interval (required iff idfm=1)
```

```
!1**  f1  a592  f0.47  a717  f1  / "rarify" carb stl in rotary shutter so at 8 Mev, 25 Rem/hr reduces to 100 mrem/hr (as measured at HFIR)
'
' 22$$ material numbers used for activities; refers to p0 components; use minus sign; id3 entries required (iff id3.gt.0)
' 22$$ -49  / material number for b-10
'
' 23$$ xsect table position for activities; id3 entries required (iff id3.gt.0)
' 23$$ 1    / absorption in b-10
'
' 24$$ calculation type markers; igm entries required, but iff idat2=1;  0/1/2 = sn / diff-th / inf-hom-media
'
' 25**  right boundary albedo by group; igm entries required, if ibr=3 (otherwise not required)
'
' 26**  left  boundary albedo by group; igm entries required, if ibl=3 (otherwise not required)
'
' 27$$  few group parameters; 5 entries required, but only if ifg=1 (otherwise array not needed)
'       /  icon = 0/1/2 = no effect / micro xsects desired / macro xsects desired;   (minus implies cell weighting)
'       /  ihtf = position of sigma total in weighted xsects
'       /  ihsf = position of g-to-g scatter in weighted xsects;  (minus implies upscatter removal)
'       /  ihmf = table length of weighted xsects
'       /  ipun = -1/0/1 = write nuclide tape on fort.10 / no effect / punch wtd xsects (free-form on fort.7)
'   e   /  end of 27$$
'
' 28$$ broad-group number for each fine group; igm entries required, if ifg=1 (otherwise not required)
'
 t  / end of data block g;  this t is always required
!ND-GBAINPUT


 ln -s  /u/mnt4/jab/hfir/water-tube.hb3/dort.xsects/xsects.dort-ready.bin.hfir.hb3.watertube.01may98  fort.4  # link dort-ready xsects to fort.4 for use i
 GBANISN
.n -s  /u/mnt4/jab/hfir/water-tube.hb3/dort.xsects/adjoint.xsects.dort-ready.bin.hfir.hb3.watertube.14may98  fort.4  # link dort-ready xsects to fort.4 for
se in GBANISN

 ln -s  /work1/jab/dort.xsects/adjoint.xsects.dort-ready.bin.hfir.hb3.watertube.14may98  fort.4  # link dort-ready xsects to fort.4 for use in GBANISN

  For this particular library:

  mix  1  (ANISN/DORT MATL  1) = Water at 1.00 g/cc
  mix  2  (ANISN/DORT MATL  5) = Aluminum 6061 (2.7 g/cc)
  mix  3  (ANISN/DORT MATL  9) = Void (He @ 1.0e-20 atoms/barn*cm)
  mix  4  (ANISN/DORT MATL 13) = SS304 (7.92 g/cc;  see page 50 of ORNL/TM-11989)
  mix  5  (ANISN/DORT MATL 17) = Carbon Steel (7.8212 g/cc, 99 wt% Fe, 1 wt% C)
  mix  6  (ANISN/DORT MATL 21) = Barytes Concrete at 3.09725 g/cc
  mix  7  (ANISN/DORT MATL 25) = Regular Concrete
  mix  8  (ANISN/DORT MATL 29) = response functions

banisn  <gbainput  >gbaoutput
lf getwin.f -o getwin
etwin

 cp -p gbaoutput $RTNDIR/gbaoutput.175-300cm.buck
 cp -p fort.15 $RTNDIR/gbadjnt.fort.15.175-300cm.buck
 cp -p getadj.out $RTNDIR/getadj.out.175-300cm.buck

p -p gbaoutput $RTNDIR/gbaoutput
p -p fort.15 $RTNDIR/gbadjnt.fort.15
p -p getadj.out $RTNDIR/getadj.out
```

```
cp -p wwinp $RTNDIR/wwinp

rm *            # dangerous !!! be careful what subdirectory you are in
cd $RTNDIR
rmdir $TMPDIR

#  !!!
#  echo  "Job will be run in "  $TMPDIR
```

Appendix D.2

Listing of the 3-D broad-group weight window generator code (WW308G.F), described in Sect 6, that was actually used to create and write the weight window file used in MCNP Run HB308G for the gamma-only shielding analysis of the HB-3 beam tube and rotary shutter when the 1998 water tube and collimator sections are both flooded, the shutter is closed, and the HFIR is operating at 100 MW.

Note that the parameters used in this stand-alone program are based on information derived from the 1-D adjoint analysis described in Sect 6.1, the normalization guidelines set forth in Sects 6.2 and 6.3, the three-dimensional characteristics of this particular problem as described in Sect 6.4, and the use of magnet points for on-the-fly position-dependent directional biasing as described in Sect 6.5.

```
c     ******************************************************************
c     ******************************************************************
c
c     WW308G.F  (full HB3 problem; 1 dummy neut grp, 4 real gamma grps -- JAB, 6-20-98)
c
c     A utility program to write out a (wwinp) weight-window file that can be used by MCNP4B
c
c     In this case, for the gamma-only version of the full (complete) HB3 beam tube with
c     the 1998 water tube and collimator both "flooded", we want to get the primary
c     gamma dose rate (not neutron dose rate or secondary gamma dose rate) downstream
c     of the rotary shutter in the closed position
c
c     earlier case --> In an earlier case for the simple idealized academic problem we had a narrowly
c     earlier case --> collimated beam on neutrons impingent on the bottom of a 130-cm-diam x 125-cm-thick
c     earlier case --> tank of water (Z=175 cm to Z=300 cm) and we wanted to get the total neutron+gamma dose
c     earlier case --> rate across a 20-cm-diam disk at the top, assuming due to the 61-neutron-group source
c     earlier case --> at the bottom (similar to the 1998 HB3 beam tube when flooded).
c
c     Required input supplied by calling routine:
c
c     imi = number of coarse mesh importance zones (based on fine mesh 1-D GBANISN calc, as processed by Subroutine GETADJ)
c     dimension xmini(3000),xmaxi(0:3000)  ! xmin & xmax for each importance zone (X used in GBANISN & GETADJ.F;  now called Z)
c     dimension emaxi(10)       ! Emax(MeV) for each of the 6 broad neutron groups & each of the 4 broad gamma groups
c     dimension wtlo(3000,10)  ! wtlo(mesh,ig) for a given importance mesh, and broad group (calculated in Subroutine SRCJST)
c
c     ******************************************************************
c
c     Note:  This particular version, used with HB308G.I, has been modified from earlier forms in order to
c     use Subroutine GETWT which is unique to Run HB308G which: (1) has four broad gamma groups and (2) makes
c     extensive use of position-dependent directional biasing (ie, local "magnet points"). -- JAB, 6-18-98
c
c     ******************************************************************
c     ******************************************************************
c
      dimension zmini(3000),zmaxi(0:3000)  ! zmin & zmax for each importance zone (Z used in this subroutine in place of X)
c
      dimension emaxi(10)       ! Emax(MeV) for each of the 6 broad neutron groups & each of the 4 broad gamma groups
      dimension wtlo(3000,10)  ! wtlo(mesh,ig) for a given importance mesh, and broad group (calculated in Subroutine SRCJST)
c
c     For this particular problem, the following 4 arrays don't have to be this big, but that's ok:
c     (u,v,w) = unit vector going from detector point to mesh point; needed iff one wants "in flight" angular biasing
      dimension u(33,33,172)       ! x-direction cosine for above unit vector; used for "on the fly" directional biasing
      dimension v(33,33,172)       ! y-direction cosine for above unit vector; used for "on the fly" directional biasing
      dimension w(33,33,172)       ! z-direction cosine for above unit vector; used for "on the fly" directional biasing
      dimension imindx(33,33,172)  ! importance mesh index (tells what 1-D importance mesh values to use in each 3-D XYZ mesh)
      dimension wtijk(33,33,172)   ! added by jab, 6-15-98, for use with Subroutine GETWT
c
      dimension mhead(4),ia(3),ra(10),geomx(4),geomy(4),geomz(4)  ! wwinp header info & phantom mesh geometry specs
c
ccc   data for a different (earlier) case:
ccc   data mhead/ 2, 0, 2, 10 /  ! see explanation below
ccc   data ia/    6, 4, 0 /      ! number of energy-dependent weight window set to be entered for neutrons, gammas, electrons
ccc   data ra/ 27.0, 27.0, 65.0, -67.5, -67.5, 0.0, 4*1.0 /
ccc   data geomx/ -67.5, 27.0,  67.5, 1.0 /
ccc   data geomy/ -67.5, 27.0,  67.5, 1.0 /
ccc   data geomz/   0.0, 65.0, 325.0, 1.0 /
c
c     data for the gamma-only version of the full (complete) HB3 beam tube
```

```
c         Here, the importance mesh measures 27 x 27 x 142 and goes from:
c         X= -67.5 cm to X=  +67.5  cm  in  27 increments of 5.0 cm each,
c         Y= -67.5 cm to Y=  +67.5  cm  in  27 increments of 5.0 cm each,
c         Z= -5.73 cm to X= +704.27 cm  in 142 increments of 5.0 cm each
        data mhead/ 2, 0, 2, 10 /     ! write some dummy neutron data, then the real 4-group gamma data
        data ia/    1, 4, 0 /         ! write some dummy 1-grp neutron data, then the real 4-group gamma data
        data ra/ 27.0, 27.0, 142.0, -67.5, -67.5, -5.73, 4*1.0 /
        data geomx/ -67.5, 27.0,  67.5, 1.0 /
        data geomy/ -67.5, 27.0,  67.5, 1.0 /
        data geomz/ -5.73, 142.0, 704.27, 1.0 /
c
c       data xd,yd,zd/ 0.0, 0.0, 300.0  /  ! location of detector (or local "magnet point") towards which we want to bias particles
c       data xd,yd,zd/ 0.0, 0.0, 700.0  /  ! location of detector (or local "magnet point") towards which we want to bias particles
c       data xd,yd,zd/ 0.0, 0.0, 478.79 /  ! location of detector (or local "magnet point") towards which we want to bias particles
c       -->  In Subroutine GETWT, we now use position-dependent directional biasing, where "the direction" keeps changing,
c       -->  depending where you are in the problem (ie, XD,YD,ZD keep changing as well as the direction cosines) -- JAB, 6-15-98
c
        data emaxi / 6*20.0, 0.3, 1.0, 3.0, 100.0 / ! for ww308g (6-18-98), use 1 neut grp & 4 gamma groups (emaxg=100 instead of 14)
c       ----------------------------------
c
        open (7,file='wwinp',status='unknown')      !  <-- 7 = ascii file ("wwinp") needed by MCNP
        open (6,file='wwinp.dbg',status='unknown')  !  <-- 6 = debug print file
c
        mhead(1)=1   ! write and use "weights only" for each mesh
        mhead(1)=2   ! write and use "weights & directional info" for each mesh
        mhead(1)=3   ! write "weights & directional info" for each mesh, but only use weights
c
        mhead(1)=2   ! write and use "weights & directional info" for each mesh
        mhead(2)=0   ! dummy version number; always enter 0
        mhead(3)=2   ! number of different particle types for which energy-dependent weight windows will be read (2 for coupled n/g problem)
        mhead(4)=10  ! number of parameters to be read in RA array;  10 for cartesian XYZ specs, 15 for RZth specs
c
        nptype=mhead(3)
c
c       ------------------------------
c       The values of "wtlo" given by GETWING3.SCR must all be multiplied by the same wgt=1.7332472e-2
c       that appears on my MCNP "sdef" card to account for the fact that I am only going to spray particles
c       isotropically across a very narrow cone of directions (ie, only the central void of HB-3 beam tube,
c       where  MIN cos = cos(theta max) = cos(15.13023 deg) = 0.965335056
c       If there were no other biasing, this spec on the sdef card would be:
c       wgt = [mu(max)-mu(min)]/[(+1)-(-1)] = [1.0000000000-0.965335056]/2 = 1.7332472e-2
c       and would cause this to be the starting weight for all particles emitted by my point source(s).
c       ------------------------------
c       In reality, presence of the SB (source-energy biasing) data in my MCNP input deck (as calculated by Subroutine GETADJ
c       in my GETWING3.SCR script file) will cause the starting weights (automatically recalculated internally by MCNP) to be
c       different in each broad energy group, and would make those weights compatible with the "wtlo" weight window data found
c       in the GETADJ.OUT file produced by that routine.  The narrow-cone cosine-effect, however, must still be accounted for
c       separately, and that's what the wtcone parameter does (later in Subroutine GETWT).
c       ------------------------------
ccc         wtcone=1.7332472e-2
ccc         do 11 ie=1,10
ccc         do 11 iz=1,imi
ccc11       wtlo(iz,ie)=wtcone*wtlo(iz,ie)
c       --> Do-loop 11 not necessary with Subroutine GETWT, since wtcone is "built-in" with that subroutine.
c
c       ----------------------------------
c
c       Following info needed iff mhead(1)=2 or mhead(1)=3 such that one wants to write "in flight"
```

```
c       directional biasing info (ie, direction cosines from detector or "magnet points" to each mesh).
c       For simplistic situations involving bulk shielding, this very simplistic definition is good enough.
c       For more complex situations with multiple streaming paths, one would really want to enter the
c       adjoint currents (aJx,aJy,aJz) instead.  See DO-LOOP 20 below.
c
c       The following (at least "imindx") is also needed if I want to assign weight window info to cartesian mesh
c       intervals "automatically" using my simplistic "spherical shell" assignment algorithm. See DO-LOOP 20 below.
c       ----------------------------------
        anx=ra(1)  ! total number of fine mesh in x-direction
        any=ra(2)  ! total number of fine mesh in y-direction
        anz=ra(3)  ! total number of fine mesh in z-direction
c
        nx=nint(anx)
        ny=nint(any)
        nz=nint(anz)
c
        xminn=ra(4)
        yminn=ra(5)
        zminn=ra(6)
c
        xmaxx=geomx(3)
        ymaxx=geomy(3)
        zmaxx=geomz(3)
c
        dx=(xmaxx-xminn)/anx
        dy=(ymaxx-yminn)/any
        dz=(zmaxx-zminn)/anz
c
c       Begin writing the wwinp file:
c       ----------------------------------
        write (7,'(4i10)')      (mhead(i),i=1,4)
        write (7,'(7i10)')      (ia(i),i=1,3)
        write (7,'(1p,6e13.5)') (ra(i),i=1,10)
        write (7,'(1p,6e13.5)') (geomx(i),i=1,4)
        write (7,'(1p,6e13.5)') (geomy(i),i=1,4)
        write (7,'(1p,6e13.5)') (geomz(i),i=1,4)
c       ----------------------------------
c
        do 20 k=1,nz
        z=zminn+dz*(0.5+float(k-1))
c
        do 20 j=1,ny
        y=yminn+dy*(0.5+float(j-1))
c
        do 20 i=1,nx
        x=xminn+dx*(0.5+float(i-1))
c
c       -->  if you want XD=F1(x,y,z), do it here in Subroutine GETWT
c       -->  if you want YD=F2(x,y,z), do it here in Subroutine GETWT
c       -->  if you want ZD=F3(x,y,z), do it here in Subroutine GETWT
c
        ibgg=1  ! added 6-18-98 (ad hoc); set flag for lowest energy gamma group
        call getwt (ibgg,x,y,z,wt,xd,yd,zd)  ! added 6-18-98; this subroutine is unique to problem HB308G
c       ----------------------------------
c         Note that (xd,yd,zd), defined in Subroutine GETWT, are the local "magnet points"
c         toward which particles in an importance cell at (x,y,z) should be (will be) biased,
c         and the value returned as "wt" after each call is the lower weight window limit for
c         this energy group (ibgg) in this particular importance cell (i,j,k) at (x,y,z).
```

```
c       ----------------------------------
        wtijk(i,j,k)=wt                        ! added 6-15-98; wt defined directly in this subroutine; no need to mess with index junk
c
        dist2=(x-xd)*(x-xd)+(y-yd)*(y-yd)+(z-zd)*(z-zd)
        dist=sqrt(dist2)       ! distance from detector (or local "magnet point") location to center of each importance mesh
c
c       Set up importance region "index numbers" for each importance mesh interval;  When we get around to assigning actual
c       energy-dependent weight windows, we'll use these index numbers.  Here, I am simply going to assign weight window index
c       numbers to each 3-D XYZ mesh based on each mesh's distance from the detector of interest -- ie, basically assign the
c       same weight window values to all mesh intervals within a given "spherical shell" (distance) from the detector location.
c       Note, however, that we must distinguish between those mesh that are between the detector and the source, and those mesh
c       that are downstream of the detector.
c       ----------------------------------
ccc        indx=0
ccc        if (z.le.zd) zloc=zd-dist  ! for mesh between the detector and the source
ccc        if (z.gt.zd) zloc=zd+dist  ! for mesh that are downstream of the detector
ccc        do iz=1,imi                ! imi=number of coarse mesh importance zones;  check each one
ccc           if (zloc.ge.zmini(iz) .and. zloc.le.zmaxi(iz)) indx=iz  ! select importance region index number
ccc        enddo
ccc        if (indx.eq.0 .and. z.le.zd) indx=1
ccc        if (indx.eq.0 .and. z.ge.zd) indx=imi
ccc        imindx(i,j,k)=indx     ! used to assign weight window values to cartesian mesh using my simplified spherical shell algorithm
c       --> above deleted on 6-15-98;  "wt" now defined directly in Subroutine GETWT; no need to mess with index junk;
c       --> also note that the "magnet points" (xd,yd,zd) are now also defined in Subroutine GETWT.
c
c       The following unit vectors will be used in place of rigorous
c       directional adjoint currents (aJx, aJy, aJz) for "on the fly"
c       directional biasing in MCNP4B:
c       ----------------------------------
        u(i,j,k)=(x-xd)/dist   ! (u,v,w) is a unit vector pointing from the detector (or local "magnet point") to the center of each mesh
        v(i,j,k)=(y-yd)/dist   ! (u,v,w) is a unit vector pointing from the detector (or local "magnet point") to the center of each mesh
        w(i,j,k)=(z-zd)/dist   ! (u,v,w) is a unit vector pointing from the detector (or local "magnet point") to the center of each mesh
20      continue
c       ----------------------------------
c
c
ccc        write (7,'(1p,6e13.5)') (emaxi(i),i=1,6)  ! for the 6 broad neutron groups
cccc
ccc        do ie=1,6  ! write weight window info for each of the 6 broad neutron groups
ccc           write (7,'(1p,6e13.5)')
ccc     *       (((wtlo(imindx(i,j,k),ie),
ccc     *         u(i,j,k),v(i,j,k),w(i,j,k),
ccc     *         i=1,nx),j=1,ny),k=1,nz)
ccc        enddo
c
c       ----------------------------------
c
ccc        write (7,'(1p,6e13.5)') (emaxi(i),i=7,10)     ! for the 4 broad gamma groups
cccc
ccc        do ie=7,10  ! write weight window info for each of the 4 broad gamma groups
ccc           write (7,'(1p,6e13.5)')
ccc     *       (((wtlo(imindx(i,j,k),ie),
ccc     *         u(i,j,k),v(i,j,k),w(i,j,k),
ccc     *         i=1,nx),j=1,ny),k=1,nz)
ccc        enddo
c       ----------------------------------
c
c       6-18-98:  Even for the case with just four broad gamma groups, one MUST enter some dummy neutron data first:
```

```
c       (in this case, I'll just use the data for the first broad gamma group as the "dummy" neutron data):
        write (7,'(1p,6e13.5)') emaxi(1)  ! for one dummy neutron group
        write (7,'(1p,6e13.5)')
     *       (((wtijk(i,j,k),
     *         u(i,j,k),v(i,j,k),w(i,j,k),
     *         i=1,nx),j=1,ny),k=1,nz)
c       ---------------------------------
c
c       6-18-98:  For the case with four broad gamma groups using Subroutine GETWT:
c
        write (7,'(1p,6e13.5)')  (emaxi(ig),ig=7,10)  ! for the 4 broad gamma groups
c
           write (7,'(1p,6e13.5)')  ! write weights & direction data for 1st (lowest energy) broad gamma group
     *       (((wtijk(i,j,k),
     *         u(i,j,k),v(i,j,k),w(i,j,k),
     *         i=1,nx),j=1,ny),k=1,nz)
c
           write (6,690) (ibgg,k,wtijk(14,14,k),k=1,nz)       ! make a debug printout of wtlow along centerline for QA purposes
690        format (' ibgg=',i1,'  k=',i3,'   wtlow=',1pe13.5) ! make a debug printout of wtlow along centerline for QA purposes
c
           do ibgg=2,4  ! now do rest of gamma groups; update weights; don't bother updating direction data (it stays constant)
              do k=1,nz
                 z=zminn+dz*(0.5+float(k-1))
              do j=1,ny
                 y=yminn+dy*(0.5+float(j-1))
              do i=1,nx
                 x=xminn+dx*(0.5+float(i-1))
                 call getwt (ibgg,x,y,z,wt,xd,yd,zd)  ! added 6-18-98; this subroutine is unique to problem HB308G
c                ---------------------------------
c                  Note that (xd,yd,zd), defined in Subroutine GETWT, are the local "magnet points"
c                  towards which particles in an importance cell at (x,y,z) should be (will be) biased,
c                  and the value returned as "wt" after each call is the lower weight window limit for
c                  this broad group (ibgg) in this particular importance cell (i,j,k) at (x,y,z).
c                ---------------------------------
                 wtijk(i,j,k)=wt                       ! added 6-18-98; wt defined directly in this subroutine; no need to mess with index junk
              enddo
              enddo
              enddo
c
           write (7,'(1p,6e13.5)')  ! write weights & direction data for broad gamma group "ibgg"
     *       (((wtijk(i,j,k),
     *         u(i,j,k),v(i,j,k),w(i,j,k),
     *         i=1,nx),j=1,ny),k=1,nz)
c
           write (6,690) (ibgg,k,wtijk(14,14,k),k=1,nz)     ! make a debug printout of wtlow along centerline for QA purposes
        enddo
c       ---------------------------------
c
        return
        end
        subroutine getwt (ibgg,x,y,z,wt,xd,yd,zd)
c
c       ********************************************************************************************************
c       ********************************************************************************************************
c
c       Input coordinates (x,y,z)
c
c             = integer broad group gamma flag (this is a "ad hoc" param      6-18-98)
```

```
c
c       Output wt=WTLOW to be used for all gamma groups in 3-D importance mesh at this location
c              (xd,yd,zd) = coordinates of fake detector (or local "magnet point") to be used in computing adjoint current vector
c
c       ***************************************************************************************************
c
c       1) This subroutine has been used in the generation of the
c          weight-window file for Run HB308G.I (and some subsequent calcs)
c
c       2) Rate of change for wtlow in water, steel, and concrete closely approximates the
c          rate of change from GBANISN calc in adjoint mode;  values here are based on:
c            velm gamma groups 18-23 (for ibgg=1, the lowest energy gammas)
c            velm gamma groups 13-17 (for ibgg=2)
c            velm gamma groups  9-12 (for ibgg=3)
c            velm gamma groups  1- 8 (for ibgg=4, the highest energy gammas)
c
c       3) The preferred directions in which to bias particles as defined by (XD,YD,ZD)
c          are highly position-dependent, especially once one gets into the concrete block
c          holding the rotary shutter shield plug with its hole.
c
c       ***************************************************************************************************
c       ***************************************************************************************************
c
        wtcone=0.017332472 ! initial starting weight assigned to all gammas on MCNP "sdef" card (if starting only in narrow cone)
c
c       Good values for rw,rc,rs (based on adjoint) that I'll use for velm gamma groups 18-23:
        if (ibgg.eq.1) then
            rw=0.50  ! factor by which wtlow for these gammas should decrease every 5.0 cm in water (based on gbanisn in adjoint mode)
            rc=0.18  ! factor by which wtlow for these gammas should decrease every 5.0 cm in barytes concrete (guess based on rw & rs)
            rs=0.13  ! factor by which wtlow for these gammas should decrease every 5.0 cm in half-density steel (based on gbanisn in adjoint mode)
            wtlow1=2.58980e+15  ! wtlow from GETWING3.SRC (GETADJ.OUT) for imp mesh 1 (Z=174.27 to 179.27 cm) in VELM g-groups 18-23 (below 0.3 MeV)
            w0=wtcone*wtlow1    ! w0 = wtlow to be used in MCNP for this broad group in the source region (see notes on wtcone, above)
        endif
c
c       Good values for rw,rc,rs (based on adjoint) that I'll use for velm gamma groups 13-17:
        if (ibgg.eq.2) then
            rw=0.57  ! factor by which wtlow for these gammas should decrease every 5.0 cm in water (based on gbanisn in adjoint mode)
            rc=0.33  ! factor by which wtlow for these gammas should decrease every 5.0 cm in barytes concrete (guess based on rw & rs)
            rs=0.28  ! factor by which wtlow for these gammas should decrease every 5.0 cm in half-density steel (based on gbanisn in adjoint mode)
            wtlow1=4.94748e+07  ! wtlow from GETWING3.SRC (GETADJ.OUT) for imp mesh 1 (Z=174.27 to 179.27 cm) in VELM g-groups 13-17 (0.3 to 1.0 MeV)
            w0=wtcone*wtlow1    ! w0 = wtlow to be used in MCNP for this broad group in the source region (see notes on wtcone, above)
        endif
c
c       Good values for rw,rc,rs (based on adjoint) that I'll use for velm gamma groups 9-12:
        if (ibgg.eq.3) then
            rw=0.65  ! factor by which wtlow for these gammas should decrease every 5.0 cm in water (based on gbanisn in adjoint mode)
            rc=0.45  ! factor by which wtlow for these gammas should decrease every 5.0 cm in barytes concrete (guess based on rw & rs)
            rs=0.40  ! factor by which wtlow for these gammas should decrease every 5.0 cm in half-density steel (based on gbanisn in adjoint mode)
            wtlow1=4.12119e+02  ! wtlow from GETWING3.SRC (GETADJ.OUT) for imp mesh 1 (Z=174.27 to 179.27 cm) in VELM g-groups 9-12 (1.0 to 3.0 MeV)
            w0=wtcone*wtlow1    ! w0 = wtlow to be used in MCNP for this broad group in the source region (see notes on wtcone, above)
        endif
c
c       Good values for rw,rc,rs (based on adjoint) that I'll use for velm gamma groups 1-8:
        if (ibgg.eq.4) then
            rw=0.73  ! factor by which wtlow for these gammas should decrease every 5.0 cm in water (based on gbanisn in adjoint mode)
            rc=0.51  ! factor by which wtlow for these gammas should decrease every 5.0 cm in barytes concrete (guess based on rw & rs)
            rs=0.46  ! factor by which wtlow for these gammas should decrease every 5.0 cm in half-density steel (based on gbanisn in adjoint mode)
            wtlow1=1.00000e-01  ! wtlow from GETWING3.SRC (GETADJ.OUT) for imp mesh 1 (Z=174.27 to 179.27 cm) in VELM g-groups 1-8 (3.0 to 14.0 MeV)
```

```
      w0=wtcone*wtlow1     ! w0 = wtlow to be used in MCNP for this broad group in the source region (see notes on wtcone, above)
      endif
c
c
      r=sqrt(x*x+y*y)    ! distance from HB-3 centerline
c
      xd=0.0
      yd=0.0
      zd=1000.0
      n=1+int((z-174.27)/5.0)  ! number of imp mesh intervals (in water) between point of impact and present axial location
      m=1+int((r-10.61)/5.0)   ! number of imp mesh intervals (in water, steel, or concrete) between central axis & present radial location
c
c
      if (z.lt.174.27) then          ! if upstream of water tube
          if (r.lt.10.61) then
              wt=w0                  ! ... and inside central void
              return
          else
              wt=w0/(rw**m)          ! ... but outside central region
              zd=200.0               ! ... point to location just past start of water tube
              return
          endif
      endif
c
c
      if (z.lt.274.27) then          ! if axially near water tube, upstream of where concrete begins
          if (r.lt.10.61) then
              wt=w0*(rw**n)          ! ... and inside central water tube
              return
          else
              wt=w0*(rw**(n-m))      ! ... but in pool water (radially outside water tube), upstream of concrete
              zd=320.0               ! ... point just beyond entrance to collimator hole
              return
          endif
      endif
c
c
      if (z.lt.309.27) then          ! if in water tube, just upstream of collimator
          if (r.lt.10.61) then
              wt=w0*(rw**n)          ! ... and inside central water tube
              zd=330.0
              return
          else
              wt=w0*(rw**n)/(rc**m)  ! ... but radially outside central region, probably in concrete
              zd=z                   ! ... point radially inward (shortest path back to path of least resistance in water)
              return
          endif
      endif
c
c
      if (z.lt.404.27) then          ! if somewhere in collimator section
          if (r.lt.10.61) then
              wt=w0*(rw**n)          ! ... and inside flooded rectangular hole
              zd=405.0               ! ... point just beyond exit of water tube (but not too far; need some off-normal scatters)
              return
          endif
          if (r.lt.23.0) then
              wt=w0*(rw**n)/(rs**m)  ! ... but radially outside central reg in steel
```

```
            zd=z                    ! ... point radially inward (shortest path back to path of least resistance in water)
            return
        else
            wt=w0*((rw**n)/(rs**4))/(rc**(m-4))  ! ... radially outside further, in the concrete
            xd=x                                 ! ... point straight ahead axially thru concrete (not back toward steel)
            yd=y                                 ! ... point straight ahead axially thru concrete (not back toward steel)
            zd=1000.0                            ! ... point straight ahead axially thru concrete (not back toward steel)
            return
        endif
    endif
c
    nr=1+int((404.27-2.5-174.27)/5.0)  ! number of imp mesh intervals (in water) upstream of shield plug region
    wr=w0*(rw**nr)/2.0                 ! reference wtlow just upstream of shield plug region
    n2=1+int((z-404.27)/5.0)           ! number of axial imp mesh intervals downstream of where shield plug region begins
    m2=1+int((r-50.0)/5.0)             ! number of radial imp mesh intervals beyond R=50 cm, downstream of where shield plug region begins
c
    if (z.lt.479.27) then              ! if axially somewhere near rotary shutter shield plug or surrounding concrete block
        wt=wr*(rc**(n2-m2))                ! ... far out radially in unimportant regions
        if (r.lt.50.0)  wt=wr*(rc**n2)     ! ... a little closer in radially, where axial transmission is still important
c981    if (r.lt.30.0)  wt=wr*(rs**n2)     ! ... in central region by steel shield plug; see 9-24-98 UPDATE (below)
c
c       preferred directions in this axial region vary tremendously, depending on exact location, as described below:
c       ------------------------------------------------------------------------------------------------------------
        if (x.gt.12.5 .or. x.lt.-12.5) then  ! in top 3/8 or bottom 3/8 of block containing rotart shield plug (x=vertical)
            xd=x
            if (z.lt.444.27) then
                zd=444.27
                zd=447.27
                if (y.lt.0.0) then
                    yd=-42.0
                    return
                else
                    yd=42.0
                    return
                endif
            else
                zd=479.27
                zd=482.27
                if (y.lt.-32.5) then
                    yd=-42.0
                    return
                endif
                if (y.lt.32.5) then
                    yd=0.0
                    return
                else
                    yd=42.0
                    return
                endif
            endif
        else                                 ! else, if in middle 2/8 of block (by hole thru rotary shutter), then:
            xd=0.0
            if (z.lt.429.27) then
                zd=429.27
                zd=432.27
                if (y.lt.0.0) then
                    yd=-42.0
                    return
```

```
                else
                    yd=42.0
                    return
                endif
            endif
            if ((y.ge.-32.5 .and. y.lt.42.0) .and.
     *          (z.ge.429.27 .and. z.lt.454.27)) then
                 yd=-32.5
                 zd=449.27   ! do not return yet; still need to overwrite some of these locations
c982             zd=460.27   ! do not return yet; still need to overwrite some of these locations; see 9-24-98 UPDATE (below)
            endif
            if ((y.ge.-67.5 .and. y.lt.-32.5) .and.
     *          (z.ge.429.27 .and. z.lt.479.27)) then
                 yd=-42.0
                 zd=479.27   ! do not return yet; still need to overwrite some of these locations
                 zd=482.27   ! do not return yet; still need to overwrite some of these locations
            endif
            if ((y.ge.-37.5 .and. y.lt.42.0) .and.
     *          (z.ge.454.27 .and. z.lt.479.27)) then
                 yd=0.0
                 zd=479.27   ! do not return yet; still need to overwrite some of these locations
                 zd=482.27   ! do not return yet; still need to overwrite some of these locations
            endif
            if ((y.ge.42.0 .and. y.le.67.5) .and.
     *          (z.ge.429.27 .and. z.lt.479.27)) then
                 yd=42.0
                 zd=479.27   ! do not return yet; still need to overwrite some of these locations
                 zd=482.27   ! do not return yet; still need to overwrite some of these locations
            endif
            if ((y.ge.-37.5 .and. y.lt.-32.5) .and.
     *          (z.ge.444.27 .and. z.lt.479.27)) then
                 yd=0.0
                 zd=479.27
                 zd=482.27
            endif
            if ((y.ge.32.5 .and. y.lt.37.5) .and.
     *          (z.ge.444.27 .and. z.lt.479.27)) then
                 yd=0.0
                 zd=479.27
                 zd=482.27
            endif
            if ((y.ge.37.5 .and. y.le.42.0) .and.
     *          (z.ge.444.27 .and. z.lt.479.27)) then
                 yd=42.0
                 zd=479.27
                 zd=482.27
            endif
            return
        endif
c       ------------------------------------------------------------------------------------------------------------
    endif
c
c
    n3=1+int((479.27-404.27)/5.0)    ! last imp mesh interval in shield plug
    if (z.ge.479.27) wt=wr*(rc**n3)  ! if axially downstream of rotary shutter shield plug use constant wtlow
c983if (z.ge.479.27) wt=wr*(rs**n3)  ! if axially downstream of rotary shutter shield plug use constant wtlow; see 9-24-98 UPDATE (below)
c
c
```

```
c     ************************************************************************
c     ************************************************************************
c
c     UPDATE (9-24-98): The following minor discrepancy was noted just
c     prior to publication, long after the work had been completed.
c
c     As described elsewhere in this report, the original intent was for
c     statement numbers 981, 982, and 983 in Subroutine GETWT to be active.
c
c     While preparing the final documentation, however, it was noted that
c     these three statements had been commented out (as shown here) at
c     the time (6-20-98) the weight window file was actually prepared for
c     use in MCNP Run HB308G.  With these three statements commented out
c     (as shown here) this routine will reproduce byte-for-byte, the actual
c     weight window file really used by MCNP Run HB308G.
c
c     ------------------------------------------------------------------
c
c     Subsequent to this discovery, I went back (on 9-24-98) and created
c     a version (ww308h) of this routine where these three statements were
c     made active (as originally intended) by uncommenting these lines and
c     generating a new weight window file.  Then took a copy of the original
c     HB308G input, renamed it HB308H, and ran it for 1 million histories
c     just to verify that the results obtained would be the same.
c
c     As indicated below, the results were the statistically identical, but
c     the new version (H) caused a lot more splitting and took longer to run.
c
c     For comparison purposes, this new run HB308H with 1 million histories
c     should be compared with run HB308G2 (where we stopped after 1 million
c     histories).  Comparisons are as follows:
c     ------------------------------------------------------------------
c
c                                       HB308G2          HB308H
c                                       using            using
c                                       ww308g           ww308h
c                                       ----------       ----------
c
c     Number of particles started:      1,000,000        1,000,000
c
c     Number of particles crossing
c     internal boundary surface:        1,411,263        1,413,992
c
c
c     Number of collisions:             212,701,257      577,113,560
c
c     CPU time (wallclock hours):
c     on each of 8 nodes, ORNL SP2      39.26 hrs        37.83 hrs
c
c
c     Tally 45 after 1 M histories:     0.8097 mr/hr     0.8112 mr/hr
c     Point detector on centerline, at
c     Z=479.29 cm (0.5 cm past shield)  +/- 5.7%         +/-5.7%
c
c
c     Tally 65 after 1 M histories:     0.2985 mr/hr     0.2992 mr/hr
c     Point detector on centerline, at
c     Z=524.51 cm (1.5 ft past shield)  +/- 2.0%         +/- 2.1%
```

```
c
c
c       Tally 85 after 1 M histories:          0.2075 mr/hr      0.2074 mr/hr
c       Point detector on centerline, at
c       Z=570.23 cm (3.0 ft past shield)       +/- 1.6%          +/- 1.9%
c
c       ---------------------------------------------------------------------
c
c       Given that the results after 1 million histories were within 0.12 fsd's
c       of each other, that HB308G5 (based on 4 million histories) was still much
c       better converged and took over 6.5 wallclock days on each of 8 nodes on
c       the ORNL SP2 (spread over several weekends), that HB308H would take about
c       as long, and that there was no longer sufficient disk space left to save
c       the boundary fluxes for HB308H anyway, a decision was made to kill HB308H
c       (using the orignally intended weight windows) and simply report the highly
c       converged results from Run HB308G5 where the weight windows based on the
c       above routine were slightly different than intended because these three
c       statements had been accidently commented out when ww308g was originally
c       run.  In other words, while the originally intended biasing scheme did
c       lead to more splitting, the differences in the final results of interest
c       (after 1 million histories) were "so" slight, that running the calculation
c       out to 4 million histories over several more weekends did not seem useful.
c
c       ***************************************************************************
c       ***************************************************************************
c
        return
        end
```

Appendix D.3

Low-Order Justification for the Assumed Mesh-to-Mesh Weight Reduction Factor in Barytes Concrete

Appendix D.3

Low-Order Justification for the Assumed Mesh-to-Mesh Weight Reduction Factor in Barytes Concrete

As shown in Sect 6, a 1-D adjoint analysis was used to calculate the importance (ie, adjoint gamma flux) throughout the water tube, the water-filled collimator, and the "less than full density steel" used to represent the rotary shutter shield plug in the adjoint calculation. (For reasons described in Sect 6.2, the density of the steel was intentionally assumed to be 3.6760 g/cc, while a standard value of 1.0 g/cc was used for the water.) Table 6.3 shows the ratio of the lower weight window limits (ratio of "wtlow") from one 5-cm-thick importance zone to the next for each of the four broad gamma groups in the water and the steel (rw and rs) along the centerline of the system. These are certainly key parameters in constructing the 3-D weight-window file, especially along the centerline of the system. These ratios for water (rw) can also be used to increase the lower weight-window cutoff (ie, decrease the importance) as one gets further from the centerline in the region where the water tube is passing through the reactor pool. As it enters the concrete, however, one needs to know, at least approximately, how fast the lower weight-window cutoff should be increased (ie, how fast the importance should be reduced) as one moves further out radially into the concrete. Basically, one needs to know what mesh-to-mesh weight ratio to use in the concrete. Since virtually all of the important high-energy gammas stream up through the water tube and very very few ever get through the concrete, one does not need to know this particular parameter very accurately. Nevertheless, some approximate value is needed if one is going to use weight windows to kill off the low-importance gammas that might venture into this area and otherwise slow down the calculation. If "rw" and "rs" are the appropriate ratios for the water and the steel in any given broad gamma weight-window group, then it was suggested in Sect 6, that the corresponding ratio for the barytes concrete (rc) might be:

rc=sqrt(rs*sqrt(rs*rw)) .

This was based on an intuitive instinct that this ratio must be somewhere between the ratio for the steel and the ratio for the water, and probably much closer to that for the steel (ie, the half-density steel used in the adjoint calculation). Actually, the formula given above was based on a little more than basic instinct, but not much more. The following few paragraphs explain the underlying logic.

While mass attenuation coefficients (cm2/g) do vary markedly with energy, at a given energy they are surprisingly constant from one element to the next. The mass attenuation coefficients for 8 MeV gammas in water, steel, and regular concrete are, for example: 0.0243, 0.0299, and 0.0245 cm2/g, respectively (see pages 138-139 of Ref 28).

Intuitively, the mesh-to-mesh weight reduction factors (ratios of wtlow from one 5-cm importance mesh to the next) for high-energy gammas in our present application must exhibit "approximately" the same characteristic behavior. Across a typical 5-cm mesh, the ratios "rw" and "rs" for VELM groups 1-8 (above 3 MeV) may be expressed as:

rw = exp(-u0*rho*t) = exp[-u0*(1.0000 g/cc)*(5 cm)] = 0.73 ==> u0=0.06294 cm2/g for groups 1-8 in water

rs = exp(-u0*rho*t) = exp[-u0*(3.6760 g/cc)*(5 cm)] = 0.46 ==> u0=0.04225 cm2/g for groups 1-8 in steel

While not "constant" between materials, they are not drastically different. Across a typical 5-cm mesh, the ratios "rw" and "rs" for VELM groups 18-23 (below 0.3 MeV) may be expressed as:

rw = exp(-u0*rho*t) = exp[-u0*(1.0000 g/cc)*(5 cm)] = 0.50 ==> u0=0.13863 cm2/g for groups 18-23 in water

rs = exp(-u0*rho*t) = exp[-u0*(3.6760 g/cc)*(5 cm)] = 0.13 ==> u0=0.11100 cm2/g for groups 18-23 in steel

Again, while not "constant" between materials, they are not drastically different.

To examine the validity of the simple approximation given in Sect 6 [rc=sqrt(rs*sqrt(rs*rw))], let us assume that, for a given energy, u0 is constant between materials and see where this leads. (Note that while u0, as used here, has the units cm2/g, it is NOT really the gamma mass attenuation coefficient; in this hypothetical argument, it is simply assumed to be a constant parameter that governs the exponential attenuation of the lower weight window cutoff "wtlow" for a given broad group. It will be assumed to be constant between materials, but different for different broad energy groups.) To examine the questionable validity of the above expression, let us start with the expression for rc in terms of rs and rw, plug in

the exponential equivalents (involving the real mass densities for these materials), and see how different the two sides of the equation are for values of u0 that might be of interest:

rc =(?)= sqrt(rs*sqrt(rs*rw))

rc =(?)= rs^0.5 * rs^0.25 * rw^0.25

rc^1.0 =(?)= rs^0.75 * rw^0.25

[exp(-u0*rho(conc)*t)]^1.0

=(?)= [exp(-u0*rho(half-den-steel)*t)]^0.75 * [exp(-u0*rho(water)*t)]^0.25

[exp(-u0*(3.090725 g/cc)*(5 cm))]^1.0

=(?)= [exp(-u0*(3.6760 g/cc)*(5 cm))]^0.75 * [exp(-u0*(1.0 g/cc)*(5 cm))]^0.25

[exp(-u0*15.4536)]^1.0 =(?)= [exp(-u0*18.3800)]^0.75 * [exp(-u0*5.0)]^0.25

[exp(-1.0*15.4536)]^u0 =(?)= [exp(-0.75*18.3800)]^u0 * [exp(-0.25*5.0)]^u0

[exp(-1.0*15.4536)]^u0 =(?)= [exp(-0.75*18.3800)*exp(-0.25*5.0)]^u0

[exp(-15.4536)]^u0 =(?)= [exp(-(13.7850+1.25))]^u0

[exp(-15.4536)]^u0 =(?)= [exp(-15.0350)]^u0 <-- "test equation"

L.H.S. =(?)= R.H.S.

Obviously the two are not "equal", but the question really is "how bad is this approximation for the values of u0 that might be of interest?". For the broad gamma weight window group corresponding to VELM gamma groups 1-8 (above 3 MeV), the approximate formula in its original form [rc=sqrt(rs*sqrt(rs*rw))] would yield rc=0.51630, which would imply that u0=0.042778; plugging this into our test equation we get:

[exp(-15.4536)]^(0.042778) =(?)= [exp(-15.0350)]^(0.042778)

0.51630 =(?)= 0.52563

which shows that the approximate expression for rc in this hardest gamma group (above 3 MeV) is only off by about 2% which is quite acceptable for the intended purpose. Likewise, for the broad gamma weight-window group corresponding to VELM gamma groups 18-23 (below 0.3 MeV), the approximate formula in its original form [rc=sqrt(rs*sqrt(rs*rw))] would yield rc=0.18205, which would imply that u0=0.11023; plugging this into our test equation we get:

[exp(-15.4536)]^(0.11023) =(?)= [exp(-15.0350)]^(0.11023)

0.18205 =(?)= 0.19065

which shows that the approximate expression for rc in the softest gamma group (below 0.3 MeV) is only off by about 5% which again is quite acceptable for the intended purpose of setting weight window lower limits and playing Russian Roulette in the concrete regions far from the centerline which ultimately do not contribute much to the final solution anyway.

Appendix D.4

Listing of the input file for MCNP Run HB308G, used in the gamma-only shielding analysis of the HB-3 beam tube and rotary shutter when the 1998 water tube and collimator sections are both flooded, the shutter is closed, and the HFIR is operating at 100 MW.

Note that solution of this problem requires the use of the WWINP 3-D broad-group weight window file created by the WW308G.F code which is listed in Appendix D.2. Many other aspects of this calculation are described in Sects 6.7 and 6.8.

```
message:  outp=hb308.o  runtpe=hb308.r  wssa=hb308.s  wwinp=wwinp

Isolated model of HB-3 using equivalent point sources (G-only calc)
c
c     ------------------------------------------------------------------------------------------------------------
c
c       HB308 is a series of gamma-only calcs with the 1998 water tube & collimator flooded (using wwinp files)
c
c             Purpose of the early runs in this series is similar to the HB307 runs:  to get a good gamma boundary
c             source on Surf 4197, just 2.4845 cm downstream of the collimator exit, that can then be used in later
c             calcs in this series for the analysis of the radiation transport thru and around the rotary shield plug,
c             to a point just downstream of the rotary shutter (shield plug).  Earlier calcs (see APPROACH.ALT subdir)
c             have already shown the contribution to the dose rate downstream of the flooded collimator due to secondary
c             gammas and directly due to neutrons are both negligible.  The purpose here, therefore, is to focus on the
c             dose rate upstream and downstream of the rotary shutter due to "primary gammas" streaming down the beam tube
c             and entering the flooded water tube.  Unlike the HB307 series, however, we want to start with (and keep)
c             the full (more complex) geometry already developed in the dosimetry calcs (cf Run HF304M4.I) with no
c             approximations.  Likewise, unlike in the HB307 series, we want to keep the 3-D model of the rotary
c             shutter since it will be the focus of later shielding calcs in this series, after we have an adequate
c             boundary source.  (The boundary source developed in the HB307 series is not considered adequate for
c             further MCNP analyses thru & around the rotary shutter, even though it may be suitable for some QAD
c             analyses.)  To aid in these analyses, we hope to make extensive use of wwinp files.
c
c             HB308A.I was created from HB304M4.I (described below), but with many of the features reset.  For example,
c             we changed back from the 1960 design to the 1998 design (wrt location of the aluminum windows), the water
c             tube is now flooded, and rotary shutter is now closed.  Nevertheless, we retained the dosimeter holder ring,
c             the 2-plate collar, and all the other improvements that were made in or prior to Run HB304M4.I.
c
c             Modifications needed to get HB308 from HB304M4.I are as follows:
c             ================================================================
c
c     ok      1) Use "mode p";  start with nps=5000000;  will later use nps=100,000,000 or higher.
c
c     ok      2) Delete the "cut:n" card, previously used to avoid tracking neutrons below 27 keV;
c                will not track any neutrons, but will track ALL primary gammas.
c
c     ok      3) Uncomment the original 61-grp si53, sp53, and ds63 data for neutrons (will be ignored anyway), and to
c                be conservative in the water-tube calcs (unlike dosimetry calcs), put all sources back on centerline;
c                BUT ... on the SDEF card ... tell MCNP to really "use" the si73, sp73, and ds83 data for gammas;
c                sdef specs for this gamma-only calc should include:
c                ---------------------------------------------------
c     ok              sdef  erg=d73  pos ferg d83  $ source def for gammas in HB-3 (total p/s = 1.35399E+17)
c     ok                    par=2            $ par=1 for neut, par=2 for photons
c     ok                    wgt=1.7332472-2  $ use this with d3;  wgt = [mu(max)-mu(min)]/[(+1)-(-1)] = [1.0000000000-0.965335056]/2 = 1.7332472-2
c     ok              si3   h  0.965335056   1.0  $ angular distribution;  mu boundaries (i.e, cosine boundaries wrt vec)
c                ---------------------------------------------------
c
c     ok      4) Comment out whatever neutron tallies & detectors there may have been and add the following gamma detectors:
c                ---------------------------------------------------
c     ok              fc15   G-Flux (p/s/cm2) midway between collimator & shutter at 100 MW
c     ok              fc25   G-Dose (mrem/hr) midway between collimator & shutter at 100 MW
c     ok              fc35   G-Flux (p/s/cm2) 0.5 cm past conc box containing shutter, at 100 MW
c     ok              fc45   G-Dose (mrem/hr) 0.5 cm past conc box containing shutter, at 100 MW
c     ok              fc55   G-Flux (p/s/cm2) 1.5 feet past conc box containing shutter, at 100 MW
c     ok              fc65   G-Dose (mrem/hr) 1.5 feet past conc box containing shutter, at 100 MW
c     ok              fc75   G-Flux (p/s/cm2) 3 feet past conc box containing shutter, at 100 MW
c     ok              fc85   G-Dose (mrem/hr) 3 feet past conc box containing shutter, at 100 MW
c
```

```
c     ok              fc184   Appx G-Dose (mrem/hr) axially, up thru the water tube,  at 100 MW;  30 equal segments, with dz=4.24119 cm
c     ok              fc194   Appx G-Dose (mrem/hr) axially, up thru collimator hole, at 100 MW;  20 equal segments, with dz=4.44500 cm
c
c     ok              fc201   Primary G-Leakage (p/s) at upstream entrance of collimator hole, L(z-) and L(z+) only; 5 spatial regions
c     ok              fc211   Primary G-Leakage (p/s) 2.4945 cm downstream of collimator hole exit, L(z-) and L(z+) only, see segment 5
c     ok              fc221   Primary G-Leakage (p/s) 2.4945 cm downstream of collimator hole exit, lots of angular bins, see segment 5
c     ok              fc231   Primary G-Leakage (p/s) on downstrem surf of box holding shutter, L(z-) and L(z+) only, 10 spatial regions
c
c     ok              fc212  Pri G-Dose (mrem/hr) 2.4945 cm downstream of collimator hole exit (seg 5)  <-- 1st used in HB308G
c     ok              fc232  Primary G-Dose (mrem/hr) on downstrem surf of box holding shutter; seg 10  <-- 1st used in HB308G
c
c                Note 1:  Tallies 184 & 194 were added so one can monitor how well one is tracking photons up thru the flooded
c                water tube & flooded collimator.  If statistics here are not good to excellent, then all else is hopeless.
c
c                Note 2:  Despite potentially good statistics, for any of the above point detectors to be at all "trustworthy",
c                Tally 184 (segment 5) and Tally 194 (segment 5) would have to be well converged in all the higher energy groups;
c                likewise, for those point detectors "past the concrete box" to be very trustworthy, one or more of segments 5-10
c                in Tally 231 would have to be at least fairly well converged also.  If these conditions are not met, then the
c                point detector values may (?) be rubbish, even though they may appear to have good statistics
c
c           -->  Note 3:  Only if the F212 boundary crossing estimate of the primary gamma dose rate downstream of the
c                collimator hole has good statistics, is it possible to have a high degree of confidence in the
c                point detector estimates.  If F2 Tally 212 is well converged, F5 Tally 25 will be more accurate;
c                if F2 Tally 212 is not well converged, F5 Tally 25 may or may not be any good (even if stats are good).
c
c           -->  Note 4:  Only if the F232 boundary crossing estimate of the primary gamma dose rate downstream of the
c                central 6.5-inch-diam disk directly in front of the shutter (seg 10) [and perhaps segments 5-9 also]
c                has good statistics, is it possible to have a high degree of confidence in the point detector estimates.
c                If F2 Tally 232 is well converged in segments 5-10, then F5 Tallies 45, 65 and 85 will be very accurate;
c                if F2 Tally 232 is not well converged, F5 Tallies 45, 65 and 85 may or may not be any good (even if stats are good).
c
c                ------------------------------------------------
c
c                Since this calc is for "primary gammas", not neutrons or secondary gammas, make sure fm cards use proper multiplier:
c     ok         fmXX   1.35399e+17  $ sum of equivalent point sources (p/s) in HB-3 for HFIR at 100 MW (Sn=7.5573e18 n/s in global calc);  will yield fluxe
s in p/s/cm2
c
c     ok       5) For segmented Tally 184 (G-Dose, axially up the water tube)  add Surfs 5100-5130
c     ok          For segmented Tally 194 (G-Dose, axially up collimator hole) add Surfs 5140-5160
c
c     ok       6) Return location of "importance cutoff plane" (Surf 1007) to Z=118.6879 cm to increase efficiency
c                 of the water-tube calcs.  [Surf 1007 is used in Cell 10110 (inner Al wall of beam tube) to kill
c                 all neutrons & photons below this location, ie: all those not within most forward-directed cone.]
c
c              7) On the sdef card and the si3 card, return to the more restrictive angular distribution defined by:
c     ok          wgt=1.7332472-2  $ use this with d3;  wgt = [mu(max)-mu(min)]/[(+1)-(-1)] = [1.0000000000-0.965335056]/2 = 1.7332472-2
c     ok          si3   h  0.965335056   1.0  $ angular distribution;  mu boundaries (i.e, cosine boundaries wrt vec)
c
c              8) Forget about those items (7-10) listed below under the description of HB304;
c                 they were obsolete before we ever got to Run HB304F4.I or Run HB304M4.I
c
c              9) In terms of the basic model, we now want to:
c
c     ok          a) Have aluminum windows 1 and 2 placed in their 1998 axail locations (see Cells 2140, 2141, 4305, 4380)
c     ok          b) Close the rotary shutter (see Surfs 3131 & 3132)
c     ok          c) Flood the water tube (Cells 2145 & 2146 should use matl 8, den=-1.0)
c     ok          d) Flood region downstream of water tube but just upstream of collimator (Cell 4375 should use matl 8, den=-1.0)
c     ok          e) Flood the rect hole in collimator (Cells 4300 & 4305 should use matl 8, den=-1.0)
```

```
c     ok        f) Comment out pt det 15 (B&T measurement point) since tube is now flooded and shutter is closed
c
c           10) Note the following change in the central collimator material (in spite of Pete's Feb'98 dwgs); change to carbon steel based on talks with f
olks on 5-15-98
c               ------------------------------------------------------------------------------------------------
c               c     4310  40  -7.92     4130  -4190 -4230  #(4210 -4211 4212 -4213)  imp:n=1  $ ss body of central collimator with rectangular hole
c               c     Mike Farrar thought the central collimator might be / should be / carbon steel (to get less activation)
c               c     Dan Pinkston confirmed that it was Type 1020 carbon steel (here, I just used pressure vessel carbon steel here; close enough)
c               c     Ron Poor (the draftsman) indicated that existing one had a thin black oxide coating for corrosion protection
c     ok        4310  50  -7.8212  4130  -4190 -4230  #(4210 -4211 4212 -4213)   imp:n=1  $ carbon steel (Type 1020) body of central collimator with rectan
gular hole;
c               ------------------------------------------------------------------------------------------------
c
c           11) Add the following artificial surfs used to facilitate writing & later using an internal boundary source (wssa) file:
c               ------------------------------------------------------------------------------------------------
c     ok        4196  pz  401.9545  $ artificial surf used to create three infintesimal void cells downstream side of pool seal (B); 0.01 cm upstream of bo
undary source
c     ok        4197  pz  401.9645  $ artificial surf used to create three infintesimal void cells downstream side of pool seal (B); boundary source writte
n/inserted here
c     ok        4198  pz  401.9745  $ artificial surf used to create three infintesimal void cells downstream side of pool seal (B); now used for F1 tallie
s
c               ------------------------------------------------------------------------------------------------
c               In the early global calc where we write the boundary source:
c                  (1) Cells 9981, 9982 and 9983, between Surfs 4195-4196, 4196-4197, and 4197-4198 are all regular void cells
c                  (2) the boundary source will be written on Surf 4197
c                  (3) the F1 surface crossing tallies will be written on Surf 4198 (just 0.01 cm downstream of the boundary source)
c
c               In later shielding calcs for just the rotary shutter (shield plug), we'll keep the same (complete) basic model, BUT:
c                  (1) Cell 9981 between Surfs 4195-4196 will be a black void with imp:n=0 to de-couple everything upstream of Surf 4196
c                  (2) Cell 9982 between Surfs 4196-4197 will be a regular void
c                  (3) the boundary source will be read & applied on Surf 4197
c                  (4) Cell 9983 between Surfs 4197-4198 will be a regular void
c                  (5) the F1 surface crossing tallies will be written on Surf 4198 (just 0.01 cm downstream of the boundary source)
c                      so that we have a printed cross-check that our boundary source reproduces the previous result
c               ------------------------------------------------------------------------------------------------
c
c
c           12) Add the following cells to facilitate writing (and later reading & using) the internal boundary source
c               ------------------------------------------------------------------------------------------------
c     ok        9981  61  -1.0e-20  4195  -4196  -9999   imp:n=1   $  in early global calc where we're writing the boundary source
c     ok        c     9981  61  -1.0e-20  4195  -4196  -9999   imp:n=0   $  in later shielding calcs where we're reading & using the boundary source
c     ok        9982  61  -1.0e-20  4196  -4197  -9999   imp:n=1   $  in all cases
c     ok        9983  61  -1.0e-20  4197  -4198  -9999   imp:n=1   $  in all cases
c               ------------------------------------------------------------------------------------------------
c
c           13) In Cells 3001, 3020 and 3050, add the following exclusion spec:
c     ok        #(4195 -4198)  $ to exclude the 3 infinitesimal void slab slices near the boundary source we're writing or using
c
c
c           14) Use the "ssw" card below to write a boundary source file for gammas travelling downstream (ie, moving in the +Z direction)
c               across Surf 4197 from Cell 9982 to Cell 9983, where Surf 4197 is at Z=401.9645 cm, just 2.4845 cm downstream of collimator.
c               [Note that the three infinitesimally thin (0.01-cm-thick) void cells (Cells 9981, 9982, and 9983 defined by Surfaces 4195,
c               4196, 4197, and 4198) cut thru the entire problem geometry in the region between the collimator exit and the rotary shutter
c               shield plug.]  With this boundary source, we can later come back and set imp:n=0 and imp:n=0 in Cell 9981 and use this
c               boundary source in detailed shielding analyses of the rotary shield plug, which may (or may not) need to be redesigned,
c               without having to waste time tracking gammas upstream of Surf 4197, even though we'll retain the complete HB-3 geometry
c               in our model.  This problem should run much faster.
c               ------------------
```

```
c     ok        ssw   +4197 (9983)
c
c
c          15) In the course of performing a long series of dosimetry calcs, a large number of improvements were
c              made to the geometric model in the region(s) around the dosimeters.  While the more restrictive
c              angular distributions associated with items 5 & 6 above (for the present water-tube calcs) preclude
c              any meaningful tallies at the dosimeter locations (ergo, we have commented out detectors 25 & 35),
c              we would still like to keep (for completeness) the more elaborate geometric models associated with
c              dosimetry Run HB304M4.I (described below), upon which Run HB308 is based.  For a complete description
c              of these refinements in chronological order, see items 12-23 under the notes associated with dosimetry
c              Run HB304M4.I (as listed below);  A brief summary description of each is as follows:  -- JAB, 6-10-98
c
c                 (12) Much more realistic description of the dosimeters & dosimeter holder ring;
c                      keep items 12a-12c, but comment out 12d & 12e which were obsolete anyway
c                 (13) Include the 2-plate collar assembly ("coolant collector")
c                 (14) Keep special materials m71 & m72 for dosimetry activation rates
c                 (15) Keep "chamfer" on hole thru vessel nozzel
c                 (16) Keep more realistic model of old (1960) water tube (but comment out in new 1998 water-tube calcs)
c                 (17) Model bulk of dosimeters as carbon steel (see discussion below)
c                 (18) Keep ss square pegs just upstream of dosimeters
c                 (19) Keep this improved description of dosimeter holder ring
c                 (20) Keep efficiency improvements described in item 20 below (although they're moot in our
c                      water-tube calcs since neutrons cannot get to these regions anyway, due to items 5 & 6 above)
c                 (21) Keep geometry correction for the elliptical cone chamfer on hole at nozzel/vessel interface
c                 (22) For the present water-tube calcs, forget about the offset described under item 21 below (needed
c                      for the dosimetry calcs);  for the present water-tube calcs, keep sources on centerline
c                 (23) Keep better description of dosimeter holder cover plate
c
c          16) Running History of HB308 series:
c
c              HB308A.I -- initial run with all the above modifications, but NO BIASING;
c                          did not get any particles crossing the internal boundary surface;
c                          did monitor gamma flux up thru the water tube & water-filled rect hole in collimator;
c                          a diminishing number for particles did get thru most of the water tube, but then
c                          fizzled out rapidly as they started thru the flooded hole in the collimator;
c                          essentially none ever got to the exit end of the collimator hole
c                          (ie, maybe 3 or 5 individual photons out of 5,000,000)!!!
c
c              HB308B.I -- this file (6-13-98); used weight window file based on GETWING.SCR;  note that
c                          GETWING.SCR actually runs the the full HB-3 problem as a buckled slab, with the
c                          VELM 23-group gamma-only flux-to-dose-rate factors serving as the adjoint source
c                          at XD=0.0, YD=0.0, ZD=478.79 cm;  in this case, the directional biasing parameters
c                          (aJx,aJy,aJz) are based on this particular (XD,YD,ZD).  Changes needed to the MCNP
c                          input (to go from HB308A.I to HB308B.I) are as follows:
c
c     ok                   a) must put wwinp=wwinp in header record at top of input
c
c     ok                   b) just after the prdmp card and before the ssw card, must add the following:
c
c                             imp:p  $ obtained from MCNP output table when I ran a fake MCNP run with neutrons; here imp:p=imp:n in all 86 cells
c                                    $ note that non-zero values will be ignored as soon as the wwinp file is read, but it must be entered anyway
c                                    1 0 1 1 1 1 1 1 0 1 1 1 1 1 1 1 1 1 1
c                                    1 1 1 1 1 1 1 1 1 1 1 1 1 1 1 1 1 1 1
c                                    1 1 1 1 1 1 1 1 1 1 1 1 1 1 1 1 1 1 1
c                                    1 1 1 1 1 1 1 1 1 1 1 1 1 1 1 1 1 1 1
c                                    1 1 1 1 1 0
c                               c
c                               c      ------------------------------------------------------------------------------------------
```

```
c                       c       To be consistent with the wwinp file & the biased source dist
c                       c       (see GETADJ.OUT, as printed by the GATWING.SCR), make sure you have
c                       c       WUPN=WTHI= 100*WTLOW  and  WTSURV=WTAVG= 10*WTLOW  on the WWP:p card, and no WWP:n (in this case)
c                       c       ------------------------------------------------------------------------------------
c                       c       WWP:n  wupn  wsurvn  mxspln  mwhere  switchn
c                       c       wwp:n  100  10  100  0  -1       $ 5th parameter is negative to make MCNP4B read the weight window importance file (
wwinp)
c                       c       wwp:p  100  10  100  0  -1       $ 5th parameter is negative to make MCNP4B read the weight window importance file (
wwinp)
c                       c       wwp:n  100  10  50  0  -1        $ 5th parameter is negative to make MCNP4B read the weight window importance file (
wwinp)
c                      wwp:p  100  10  50  0  -1                 $ 5th parameter is negative to make MCNP4B read the weight window importance file (
wwinp)
c                       c       wwp:n  100  10  10  0  -1       $ 5th parameter is negative to make MCNP4B read the weight window importance file (
wwinp)
c                       c       wwp:p  100  10  10  0  -1       $ 5th parameter is negative to make MCNP4B read the weight window importance file (
wwinp)
c                       c      ------------------------------------------------------------------------------------
c
c
c     ok                c) just after the sp73 card, must add the following:
c
c                          sb73  d     0.0  $ dummy 0, followed by "biased" gamma src terms (p/s) for HB-3:
c                          c        ------------------------------------------------------------------------------
c                          c        Biased gamma sources in MCNP order (grp 1=low E, grp 23=high E);
c                          c        Calculated using GETWING.SCR and GBANISN in adjoint mode, where the
c                          c        adjoint sources at Z=478.49 cm were just the gamma flux-to-dose-rate factors;
c                          c        Use these values for the gamma-only mcnp calc with a gamma-only source.
c                          c        (For a coupled n/g calc with a neutron-only source, or for a neutron-only
c                          c        calc with a neutron-only source, these values would be different).
c                          c        Note that this can/should only be used with the corresponding weight
c                          c        window file prepared by GETWING.SCR where the space/energy weights for
c                          c        the gamma groups were calculated using the data in GETADJ.OUT.
c                          c        ------------------------------------------------------------------------------
c                          c        To work well (or even to work "at all") everything MUST be self-consistent !!!!!
c                          c        ------------------------------------------------------------------------------
c                          6.39635E-03  2.08498E+00  1.20937E+01  1.22898E+01  1.34000E+01  $ VELM g-groups 23, 22, 21, 20, 19,
c                          1.88122E+01  3.98199E+08  2.75298E+08  1.84168E+08  1.54966E+08  $ VELM g-groups 18, 17, 16, 15, 14,
c                          2.80658E+08  1.61658E+14  1.29829E+14  8.17425E+13  4.37194E+13  $ VELM g-groups 13, 12, 11, 10,  9,
c                          7.19371E+13  3.75947E+16  1.28016E+16  2.33834E+16  3.03589E+15  $ VELM g-groups  8,  7,  6,  5,  4,
c                          2.88048E+16  1.17397E+15  2.33592E+12                           $ VELM g-groups  3,  2,  1
c
c     update 1:         d) While HB308B.I was submitted and was in execution for 36 hours (on each of 8 nodes),
c                          I had to kill the job.  At the end of this time, it had still not completed even the
c                          first 10,000 histories.  Believe this was due to the terrible quantum leaps in the
c                          source-energy biasing between gamma groups -- ie, the corresponding big changes in
c                          the weight windows simply caused far too much splitting as particles crossed from
c                          one broad group to another, thus flooding the photon bank.  Because the job never
c                          progressed vry far and I had to kill it, no output was ever produced.
c
c     update 2:         e) When running HB308C (later), it was found that we had to modify the weight window generator so as
c                          to write out a set of dummy weight windows for one dummy neutron group (as well as the one real
c                          gamma group) even though we plan to run the gamma-only problem.  Very likely, this is the reason
c                          HB308B didn't run.  Have still not modified GETWING.SCR, and have still not tried HB308B again.
c
c
c                 HB308C.I -- (6-15-98); used weight window file based on WW30
c
```

```
c     ok                  a) WW308C.F -- A stand-alone Fortran program to write out the (wwinp)
c                            weight-window file to be used in Run HB308C.I  (6-15-98)
c
c                            Note 1:  This particular stand-alone program is similar to subroutine WTWIN in GETWING.SCR, except that
c                            it has been modified from the original form in order to use use Subroutine GETWT which is peculiar to
c                            Run HB308C.  WW308C.F has only one broad gamma group [ie: spatially-dependent weight windows only,
c                         --> with no energy biasing], BUT makes extensive use of "position-dependent" directional biasing in a new
c                            sense -- when calculating (aJx,aJy,aJz) for any given importance mesh, the "location of (XD,YD,ZD) itself"
c                            can/will depend on the location of the importance mesh.  Thus, as we navigate thru complicated geometries
c                            involving multiple streaming paths (like the holes theu the rotary shutter of the fairly wide gaps around
c                            the concrete block holding the rotary shutter), the directional biasing parameters (aJx,aJy,aJz) can
c                            actually point in the direction of the local streaming paths of importance, rather to some universal
c                            detector location which might well cause particle to be diverted away from local streaming paths that
c                            are important and should be accounted for.
c
c                            Note 2:  The mesh-to-mesh weight window attenuation factors in the water, concrete, and steel
c                         --> (rw, rc, rs) used here are based on those values produced by GETWING.SCR (using the GBANISN
c                            adjoint calc) for the broad group corresponding to VELM groups 1-7.  While admittedly simplified
c                            (using the same factors everywhere for a given material), they are still based roughly on a
c                            rigorous adjoint solution.
c
c     ok                     Update:  To make the problem run, it was found that we had to modify WW308C.F so as to write out
c                            a set of dummy weight windows for one dummy neutron group (as well as the one real gamma group)
c                            even though we plan to run the gamma-only problem.  Here, I just wrote out the gamma data twice
c                            and told it the first set was neutron data.  Very likely, this is the reason HB308B didn't run.
c
c     ok                  b) This HB308C.I input deck is identical to HB308B.I described above, except that
c                            the biased source data on the sb73 card was commented out since our new wt-window
c                            file only has one broad gamma group (for spatial biasing purposes) and DOES NOT
c                            use any form of source-energy biasing.
c
c                         c) Even though we're going to run the gamma-only calc (mode "p"), I have found by trial-and-error
c                            that BOTH the wwp:n and wwp:p cards are required.  Those used are as follows:
c
c     ok                     wwp:n  100  10  50  0  -1   $ 5th parameter is negative to make MCNP4B read the weight window importance file (wwinp)
c     ok                     wwp:p  100  10  50  0  -1   $ 5th parameter is negative to make MCNP4B read the weight window importance file (wwinp)
c
c
c               HB308D.I -- (6-16-98); used weight window file based on WW308C.F;
c
c                         The adjoint calc described above as part of GETWING.SCR (associated with Run HB308B.I) had been
c                         indicating that many of the gamma groups (especially the high-intensity, low-energy gamma groups)
c                         might be almost negligible.  (This is why, when I included all 23 gamma groups and used 4-group
c                         biasing, there were large quantum changes in the source-energy biasing function and the
c                         corresponding weight windows.)  After running HB308C.I and realizing that it worked better but
c                         was still very inefficient, I decided to write and use the QADD2.FOR program (found in subdirectory
c                         "E:\HFIR\Btubes\Feb98.wrk\APPROACH.ALT") to help me gain some insight to the HB308 series of calcs.
c                         Those interesting findings are noted below:
c
c                         QADD2.FOR Uses simple QAD-like mass attenuation coefficients (for each energy group) to calc the
c                         gamma dose rate downstream of the collimator for both the long and short water tube models, and
c                         tabulates the resulting dose rates due to several gamma sources.
c
c                         Note:  Basically, QADD2.FOR is identical to QADD.FOR, except that we now tally the contributions
c                         to the dose rate by source ENERGY as well as by source LOCATION, and later reorder that list in
c                         order of final importance.  From the original QADD.FOR, for example, we know that most of the dose
c                         rate at x=400 cm down the beam tube (ie, at the end of the flooded water tube & flooded collimator)
c                         comes from the primary gammas streaming down the beam tube and impinging on the water tube.  Before
```

```
c                we spend a whole lot of time in MCNP tracking a lot of gammas that might not be important in the end,
c                we'de like to know which groups are the most important so that we can focus more on them.
c
c                Results for the 1960 water tube:
c                --------------------------------
c                Group 1- 7 sources (of the primary gammas) contribute  96.627%  of the final gamma dose
c                Group 1- 8 sources (of the primary gammas) contribute  99.147%  of the final gamma dose
c                Group 1-11 sources (of the primary gammas) contribute  99.910%  of the final gamma dose
c                Group 1-12 sources (of the primary gammas) contribute  99.963%  of the final gamma dose
c                All other sources can be neglected
c                Also note:  While in our MCNP calc we might tend to undersample VELM Group 1, QADD2 shows
c                that the Group 1 sources only contribute  0.020%  of the final gamma dose
c
c                Results for the 1960 water tube:
c                --------------------------------
c                Group 1- 8 sources (of the primary gammas) contribute  98.051%  of the final gamma dose
c                Group 1-11 sources (of the primary gammas) contribute  99.842%  of the final gamma dose
c                Group 1-12 sources (of the primary gammas) contribute  99.914%  of the final gamma dose
c                All other sources can be neglected
c                Also note:  While in our MCNP calc we might tend to undersample VELM Group 1, QADD2 shows
c                that the Group 1 sources only contribute  0.014%  of the final gamma dose
c
c                Other comments:
c                ---------------
c
c                Sources in VELM groups 1- 8 = 7.984211e15 p/s
c                Sources in VELM groups 1-12 = 2.160073e16 p/s
c                Therefore, if we include groups 9-12 (not recommended), the calc will
c                take 3 times longer and change the results for the 1960 water tube by
c                only 1% (2% in the case of the 1998 water tube).  CPU time would be
c                much better spent running asitional histories on groups 1-8.
c
c                Sources in VELM groups 1-23 = 1.35399e17 p/s
c                -------------------------------------------  ==> Ratio = 16.96
c                Sources in VELM groups 1- 8 = 7.984211e15 p/s
c
c                Thus, by running only VELM source groups 1-8 (which account for 98-99% of
c                the final dose just downstream of the flooded collimator, we should be
c                able to run about 17 times faster than if we tried to accomodate all of
c                the 23 source groups.
c
c                ---------------------------------------------------------------
c                Changes needed to go from HB308C.I to HB308D.I are as follows:
c                ---------------------------------------------------------------
c
a) c                ------------------------------------
   c                QADD2.FOR analysis has shown that if the water tube & collimator are BOTH FLOODED, VELM source groups 1-8 account fo
r 98-99%
   c                of the dose rate downstream of the collimator.  (By the time they get there, of course, the photons may have less en
ergy.)
   c             * Thus, "for this particular FLOODED case", it is sufficient to include source photons from these first 8 VELM groups
only.
   c             * The photon source in VELM grps 1-8 (above 3.0 MeV) = 7.984211E+15 p/s (subtotal for these groups).  For this particu
lar
   c             * FLOODED case, this value may be used, but the SI73, SP73, DS83, any SB73 card, and "all" FM tally cards must be cons
istent.
   c
c     ok         si73  h  3.0000e+0   $ this one Emin(MeV), fo     d by Emax(MeV) for VELM gamma grps 1-8 (lowest to highest e     for MCNP)
```

```
:
c                                4.0000e+0    5.0000e+0    6.0000e+0    7.0000e+0    7.5000e+0    $ VELM g-groups  8,  7,  6,  5,  4,
c                                8.0000e+0    1.0000e+1    1.4000e+1                              $ VELM g-groups  3,  2,  1
c     ok                    sp73  d     0.0  $ dummy 0, followed by gamma src terms (p/s) for HB-3:
c                                2.34929e+15  1.98361e+15  6.75453e+14  1.23378e+15  1.60183e+14  $ VELM g-groups  8,  7,  6,  5,  4,
c                                1.51983e+15  6.19421e+13  1.23250e+11                           $ VELM g-groups  3,  2,  1
c     ok                    ds83  1     $ gamma starting positions (x,y,z) in HB-3:
c                                0 0  92.6    0 0  93.2    0 0  96.4    0 0  93.9    0 0  96.0    $ VELM g-groups  8,  7,  6,  5,  4,
c                                0 0  94.4    0 0  99.9    0 0  97.4                              $ VELM g-groups  3,  2,  1
c                               c       ------------------------------------
c
c
c                               Note:  Even if we used weight windows based on a rigorous "multigroup" gamma adjoint (which would
c                               tend to have the same effect of killing off low-energy gammas close to the real source that don't
c                               contribute much to the final dose rate at the location of interest downstream of the water-filled
c                               collimator), it would not make much sense to "start off" a bunch of low-energy gammas that are
c                               going to be killed almost immediately by the weight window anyway.  Thus, even then, it would save
c                               some time to skip them entirely and simply adjust the fm multipliers (below) accordingly.
c
c
c                           b) Make the following change:
c
c     ok                        c      fm15   1.35399e+17  $ based on VELM gamma groups 1-23; sum of equivalent point sources (p/s) in HB-3 for HFIR at 100
MW (Sn=7.5573e18 n/s in global calc);  will yield fluxes in p/s/cm2
c                               fm15   7.984211E+15  $ based on VELM gamma groups 1-8 only; for FLOODED case only; must be used consistently with SI73, SP73
, SB73 & DS83 data
c
c     ok                        on each of the tally multiplier cards (fm15, fm25, fm35, fm45, fm55, fm65, fm75, fm85),
c                               (fm184,fm194), and (fm201,fm211,fm221,fm231).
c
c
c                           c) To encourage a little more splitting and getting more reliable answers (at the expense of some
c                              efficiency loss), it would be helpful if WTHI could be pulled down a little closer to WTAVG.
c                              Thus, while I'll leave WTAVG=10*WTLO, let me change from WTHI=100*WTLO to WTHI=30*WTLO;
c                              this will require the following two changes:
c
c     ok                       wwp:n  30  10  50  0  -1  $ 5th parameter is negative to make MCNP4B read the weight window importance file (wwinp)
c     ok                       wwp:p  30  10  50  0  -1  $ 5th parameter is negative to make MCNP4B read the weight window importance file (wwinp)
c
c                              If this really does improve the accuracy, I can do some other things later to recoup the
c                              efficiency (and maybe even do better that before).  First, however, Lets see if this helps
c                              the accuracy.
c
c                           ---------------------------------------------------------------
c                           Updated theory notes (after HB308D.I had been run):
c                           ---------------------------------------------------------------
c
c                           1)  Tallies 184 & 194 were added so one can monitor how well one is tracking photons up thru the flooded
c                               water tube & flooded collimator.  If statistics here are not good to excellent, then all else is hopeless.
c                               (still true)
c
c                           2)  Despite potentially good statistics, for any of the above point detectors to be at all "trustworthy",
c                               Tally 184 (segment 5) and Tally 194 (segment 5) would have to be well converged in all the higher
c                               energy groups;  likewise, for those point detectors "past the concrete box" to be very trustworthy,
c                               one or more of segments 5-10 in Tally 231 would have to be at least fairly well converged also.
c                               If these conditions are not met, then the point detector values may (?) be rubbish, even though
c                               they may appear to have good statistics.
c                               (still true)
```

c
c
c

```
c                              | on adjoint info that ready to go;  will kill HB308D2 so I can get on with new tests).
c                              |
c                              | Based on this LATER UPDATE, the "Updated Theory Notes" above should be DISREGARDED.
c                              |
c                        -->   | Based on this LATER UPDATE, Run HB308E and most of the modifications shown there
c                              | should also be DISREGARDED.
c                              |
c                              | (HB308E was originally set up and run prior to the "later update" described above.)
c                              |
c                        -->   | Starting point for HB308F.I will be HB308D.I;  will then include "only a few" of the
c                              | HB308E modifications, as specifically called out in the description of HB308F.I
c
c
c                HB308E.I -- (6-18-98);  used weight window file based on WW308C.F;
c
c                              | Based on the LATER UPDATE mentioned above, Run HB308E and most of the modifications shown
c                              | here should also be DISREGARDED.  Because WW308C.F was messed up, HB308E was a failure anyway.
c                              | Moreover, because of all the new (now unnecessary) geometry cells that were introduced to fix
c                              | the perceived problem, the calc time "per source particle" as 7 times longer than in HB308D1.O.
c                              |
c                              | (HB308E was originally set up and run prior to the "later update" described above.)
c                              |
c                              | Starting point for HB308F.I will be HB308D.I;  will then include "only a few" of the
c                              | HB308E modifications, as specifically called out in the description of HB308F.I
c
c                           Original notes associated with HB308E.I are as follows:
c
c                           Based on the "updated theory notes (after HB308D1.O had been run)", a number of existing cells
c                           were subdivided in a dovetailed fashion (as shown below) so that no photons could stream thru
c                           (axially) without crossing a "real" geometry surface, as needed in order to force the code to
c                           access the weight window file and update the particle's weight (if/when there are few collisions).
c
c     ok                    a) Modifications to Cell 2145, for example, are as follows:
c
c                              c       ------------------------
c                              c       2145   8   -1.0000   -2134  2154 -4110         imp:n=1  $ water inside main cavity of expanded beam tube outside ves
sel (if flooded for maintenance)
c                              c       Here, what was Cell 2145 has been divided into alternating (dovetailed) sections described by Cells 21451 and 21452.
c                              c       This was done so that, when streaming thru the water, photons would have to cross a number of real geometry surfaces
.
c                              c       Only then (or at a collision site which is rare in water) is the code forced to go out and update the particle weigh
t
c                              c       using the information in the weight window file (wwinp).
c                              c       ------------------------
c                              21451   8   -1.0000   -2134  2154 -4110  (-5101              $ water inside main cavity of expanded beam tube outside vessel
 (if flooded for maintenance)
c                                     :(5102 -5103):(5104 -5105):(5106 -5107):(5108 -5109)  $ water inside main cavity of expanded beam tube outside vessel
 (if flooded for maintenance)
c                                     :(5110 -5111):(5112 -5113):(5114 -5115):(5116 -5117)  $ water inside main cavity of expanded beam tube outside vessel
 (if flooded for maintenance)
c                                     :(5118 -5119):(5120 -5121):(5122 -5123):(5124 -5125)  $ water inside main cavity of expanded beam tube outside vessel
 (if flooded for maintenance)
c                                     :(5126 -5127):(5128 -5129))   imp:n=1                 $ water inside main cavity of expanded beam tube outside vessel
 (if flooded for maintenance)
c                              21452   8   -1.0000   -2134  2154 -4110                      $ water inside main cavity of expanded beam tube outside vessel
 (if flooded for maintenance)
c                                     ((5101 -5102):(5103 -5104):(5105 -5106):(5107 -5108)  $ water inside main cavity of expanded beam tube outside vessel
 (if flooded for maintenance)
```

```
c                                    :(5109 -5110):(5111 -5112):(5113 -5114):(5115 -5116)  $ water inside main cavity of expanded beam tube outside vessel
 (if flooded for maintenance)
c                                    :(5117 -5118):(5119 -5120):(5121 -5122):(5123 -5124)  $ water inside main cavity of expanded beam tube outside vessel
 (if flooded for maintenance)
c                                    :(5125 -5126):(5127 -5128):5129)   imp:n=1            $ water inside main cavity of expanded beam tube outside vessel
 (if flooded for maintenance)
c                                 c       ----------------------
c
c
c                              b) Likewise, other key cells were also subdivided in a similar dovetailed fashion, as noted here:
c
c      ok                         Old Cell 4300 now = Cells 43001 and 43002 = rectangular hole up thru collimator (when flooded)
c      ok                         Old Cell 4310 now = Cells 43101 and 43102 = carbon steel (Type 1020) body of central collimator with rectangular hole;
c      ok                         Old Cell 4345 now = Cells 43451 and 43452 = ss removable shield, radially outside beam tube, next to collimator
c      ok                         Old Cell 3002 now = Cells 30021 and 30022 = barytes concrete bioshield (from pool liner to shutter assembly cavity)
c      ok                         Old Cell 3090 now = Cells 30901 and 30902 = carbon steel forming the shield plug (ie, the rotary shutter)
c      ok                         Old Cell 3060 now = Cells 30601 and 30602 = barytes concrete forming bulk of the removable concrete block containing shield
plug
c      ok                         Old Cell 3001 now = Cells 30011 and 30012 = barytes concrete bioshield (outermost part)
c      ok                         Old Cell 2170 now = Cells 2170/1/2/3/4(*) = water pool between pressure vessel and concrete bioshield
c      ok                         Old Cell 4385 now = Cells 43851 and 43852 = water between beam tube & ss sleeve extending from concrete bioshield into pool
c      ok                         Old Cell 4370 now = Cells 43701 and 43702 = ss pool seal (A1) upstream of collimator
c      ok                         Old Cell 4330 now = Cells 43301 and 43302 = ss pool seal (B) downstream of collimator
c      ok                         Old Cell 4335 now = Cells 43351 and 43352 = ss flange around pool seal (B) downstream of collimator
c
c                                 (*) Old Cell 2170 now = Cells 21701 and 21702 in the region above Z=174.95125 cm (Surf 5100), and
c                                     Old Cell 2170 now = Cells 21703 and 21704 in the region below Z=174.95125 cm (Surf 5100).
c
c      ok                      c) Tally 184 should now be for cells 21451 & 21452 (Appx G-Dose (mrem/hr) axially, up thru the water tube
c                                 Results for cells 43001 & 43002 will be complimentary, and mutually exclusive (ie, each will have zeros)
c                                 Also note that the sd184 must now be modified as follows:
c      ok                         sd184    493.55788  29r  $ volume (cc) for each of the 30 segments in Cell 21451
c                                          493.55788  29r  $ volume (cc) for each of the 30 segments in Cell 21452
c
c      ok                      d) Tally 194 should now be for cells 43001 & 43002 (Appx G-Dose (mrem/hr) axially, up thru rectangular collimator hole
c                                 Results for cells 21451 & 21452 will be complimentary, and mutually exclusive (ie, each will have zeros)
c                                 Also note that the sd194 must now be modified as follows:
c                                 sd194    433.74510  19r  $ volume (cc) for each of the 20 segments in Cell 43001
c                                          433.74510  19r  $ volume (cc) for each of the 20 segments in Cell 43002
c
c                              e) Since I expect that these actions will produce a lot more splitting (thus taking longer to run),
c                                 and since I'de really like to compare the accuracy of this run with that of Run HB307C.I which
c      ok                         only had 2,000,000 histories, set nps=2,000,000 in this run. (Will worry about improving efficiency later.)
c
c      ok                      f) To make it easier to look at the flooded 1960 water tube later, I added Cells 1008 and 1009,
c                                 and modified Cell 1010 so that the region inside the 1960 water tube is explicitly represented
c                                 by Cells 1008 (hemispherical tip) and 1009 (cylindrical portion) upstream of the start of the
c                                 1998 water tube.  In present case (flooded 1998 water tube), Cells 1008 & 1009 are both void.
c
c      ok                      g) Also subdivided Cell 1009 into two dovetailed pieces (Cells 10091 and 10092)
c                                 so we won't be hassled if we ever look at the flooded 1960 water tube again.
c
c      ok                      h) Just after the prdmp card and before the ssw card, must update the imp:p data as follows
c                                 (because of all the new cells that have been added):
c
c                                 imp:p  $ obtained from MCNP output table when I ran a fake MCNP run with neutrons; here imp:p=imp:n in all 104 cells;
c                                        $ note that non-zero values will be ig    d as soon as the wwinp file is read, but it must be entered    ay
c                                        1 0 1 1 1 1 1 1 1 1 1 0 1 1 1 1 1 1 1
```

```
c                    2 2 2 2 2 1 1 1 1 1 1 1 1 2 2 1 1 1 1 2
c                    2 2 2 2 2 2 2 2 2 2 2 2 2 1 1 1 1 1 1 1
c                    1 1 1 1 1 1 1 1 1 1 1 1 1 1 1 1 1 1 1 1
c                    1 1 1 1 1 1 1 1 1 1 1 1 1 1 1 1 1 1 1 1
c                    1 1 1 0
c
c
c          HB308F.I -- (6-18-98);  used weight window file based on WW308F.F which included wt windows
c                      for 1 dummy neutron group and 4 real gamma groups, even though all the gammas are started
c                      in wt window broad group 4 (corresponding to VELM groups 1-8);  hopefully this will cause
c                      the gammas that slowed down to low-energy close to the source to be killed off (making the
c                      problem much more efficient) while permitting those that slow down closer to the collimator
c                      to continue on (giving us a good boundary source that still accurately represents both the
c                      high and low-energy gammas near the exit of the flooded collimator).
c
c                      Notes and modifications associated with HB308E should be ignored, except the few noted below.
c
c                      The starting point for HB308F.I will be HB308D.I;  the ONLY modifications are as follows:
c
c     ok               a) To make it easier to look at the flooded 1960 water tube later, I added Cells 1008 and 1009,
c                         and modified Cell 1010 so that the region inside the 1960 water tube is explicitly represented
c                         by Cells 1008 (hemispherical tip) and 1009 (cylindrical portion) upstream of the start of the
c                         1998 water tube.  In present case (flooded 1998 water tube), Cells 1008 & 1009 are both void.
c
c                      b) Just after the prdmp card and before the ssw card, must update the imp:p data as follows
c                         (because of the new cells that have been added):
c
c                         imp:p  $ obtained from MCNP output table when I ran a fake MCNP run with neutrons; here imp:p=imp:n in all 88 cells;
c                                $ note that non-zero values will be ignored as soon as the wwinp file is read, but it must be entered anyway
c                                1 0 1 1 1 1 1 1 1 0 1 1 1 1 1 1 1 1 2
c                                2 2 2 2 1 1 1 1 1 1 1 2 2 1 2 2 2 2 2 2
c                                2 2 2 2 2 2 2 2 1 1 1 1 1 1 1 1 1 1 1 1
c                                1 1 1 1 1 1 1 1 1 1 1 1 1 1 1 1 1 1 1 1
c                                1 1 1 1 1 1 1 1 0
c
c                      c) Since I now know that there will be a lot of splitting going on, lets go back to using
c                         WTHI=100*WTLO  (since WTHI=30*WTLO seemed to give too much splitting).  This will require
c                         the following two changes:
c
c     ok                  wwp:n  100  10  50  0  -1   $ 5th parameter is negative to make MCNP4B read the weight window importance file (wwinp)
c     ok                  wwp:p  100  10  50  0  -1   $ 5th parameter is negative to make MCNP4B read the weight window importance file (wwinp)
c
c
c                      d) While I'de eventually like to compare the accuracy of this run with that of Run HB307C.I which
c     ok                  had 2,000,000 histories, lets start off with a much smaller value, say nps=40,000 & prdmp=8,000
c
c
c                         UPDATE: Experimentation (HB308F1,F2,F3);  June 18-20'98
c                         ------------------------------------------------------
c                         format of wwp card:  wthi2lo wtav2lo mxspln iwhen iflag
c
c                         Calc runs, but seems to start and stop frequently.  Watch the wxxa file
c                         (boundary source file being built) and hb308.msg file for progress.
c                         wxxa starts to bild up iver 1st 30-45 min (to 12,000 bytes), then pauses
c                         for about 6 hrs, then builds up rapidly to abt 435,000 bytes (after
c                         16,000 histories), then pauses again, sometimes for 12-18 hrs and calc
c                         does not seem to progress to next dump.  Splitting is occuring, but maybe
c                         too much, or too erratic.  Calcs generally all terminated manually by me.
```

```
c                Too slow to be very useful in any event.  (HB307C, while it never got
c                any real highenergy particles past the collimator, did get a lot of low
c                energy particles past the collimator and only took 6.25 her on 8 nodes.)
c                Did try several things:
c
c                As particles slow from important fast groups (low wtavg) to less important
c                slow groups (hi wtavg), ratio of wtavg1/wtavg2 may be >1000; fastest to
c                slowest may be >10**8;  generally such photons will be killed by Russian
c                roulette;  normally would be killed by this ratio;  however, MXSPLN
c                controls the max roulette ratio (as well as max split ratio); setting it
c                to 50 will not allow particles to be killed as fast as desired (even
c                though wt ratios are adjusted by mcnp to maintain fair game); tried
c                setting MXSPLN=390625=25**4 in mcnp and max wt ratios in any given imp
c                mesh (as set in a variant of ww308f) to: 25 (broad grp 1 to broad grp 2),
c                25**2 (braod grp 1 to broad grp 3), and 25**3 (broad grp 1 to broad grp 4)
c                in hopes that this would allow particles to be rouletted more often and
c                reduce running time.  Didn't work.  Performed as before. Went back to 50.
c
c                IWHEN controls where/when the particle wts are adjusted; 0 means at
c                collisions and surfaces, 1 means at surfaces, -1 means only at
c                collisions.  Since we have 27*27*142=103518 imp mesh, and since photons
c                travel far in water with no collision, I thought perhaps the extra
c                overhead of adjusting particle wts at each imp mesh boundary crossing
c                was driving up the run time.  (If so, we could go with simpler mesh.)
c                Tried setting IWHEN= -1 to do this at collisions only (hoping this would
c                cut the overhead.  Didn't work.  Performed as before.  Went back to
c                using IWHEN=0.
c
c                Decided I'de better take another look at adjoint into and how I adjusted
c                the wtlow curves for each broad group.
c
c                UPDATE:  This was indeed the problem!!  In WW308F.F, I had tried to artificially rescale the
c                "wtlow" curves individually so that along the axis at about Z=400 cm (just downstream of the
c                water-filled collimator) they would all have about the same value as that for broad weight-
c                window group corresponding to VELM groups 1-8.  I realize now in retrospect that this was a
c                critical mistake.  The broad-group weight window curves may indeed be scaled (if necessary),
c                but they MUST ALL be scaled by the SAME factor. [Even then, one must be careful to make sure
c                they are compatible with the starting weights in the source region.]  This critical flaw was
c                remedied later in WW308G which was then used in HB308G.
c
c                For more details, see my "index.308" file in Subdirectory of "E:\HFIR\BTUBES\FEB98.WRK\H2O-TUBE.308".
c                In particular, see the extensive discussions in "index.308" under the headings:  GETWING2.SCR, GETADJ2.OUT,
c                Critical Comment 1, GETWING3.F, GETWING3.OUT, Critical Comment 2, WW308G.F, and HB308G.
c
c
c           HB308G.I -- This file (6-20-98);  used weight window file based on WW308G.F (described below)
c     ok    6-20-98      Relative to HB308F.I, no substantial changes were made to the MCNP input file;
c     ok                 I simply added diagnostic Tallies 212 & 232 as noted below.
c
c                        THIS RUN WAS HIGHLY SUCCESSFUL
c
c                        The KEY difference in not in the MCNP input file, but in the geometry-independent weight window file (wwinp);
c                        here in HB308G we use the wwinp file generated by WW308G.F described above;  this wwinp file, unlike its
c                        predecessor, allows us to discard with much higher probability those once high-energy photons that slow down
c                        to lower energies too early (ie, back closer to the entrance of the water tube) which will not contribute
c                        significantly to the dose at the endo of the collimator or downstream of the rotary shutter, thus allowing
c                        the calculation to be much more efficient and sp[illegible]much more of its time focusing on those higher-energy
c                        photons that do contribute more.  At the same ti[illegible]he compounded mesh-to-mesh weight window attenuations
```

```
c  factors in the various broad groups are such that wtlow decreases more rapidly for the more energetic photons
c  (causing more splitting where we need it) and less rapidly for the lower energetic ones so that by the time
c  the higher eenrgy one do slow down to lower energies further downstream (near the end of the collimator and
c  beyond), they will no longer be discarded as often and will be tracked with increasing probability so that
c  their contributions in the downstream regions will no longer be ignored.  (See values of WTLOW for mesh along
c  centerline in previous table produced by GETADJ3.OUT if you want to see what I mean.)  This new weight window
c  file (wwinp) produced by WW308G.F was skillfully and thoughtfully crafted, and WORKED LIKE A CHARM !!! (see below)
c
c  +-------------------------------------------------------------------------------------------------------------
c  |  A few notes on WW308G.F:
c  |
c  |  WW308G.F -- generated wwinp file for 1 dummy neut grp & 4 real gamma groups;
c  |              used with HB308G.I (and all continuation runs)
c  |
c  |  Like earlier versions, uses Subroutine GETWT to define XD=F1(x,y,z), YD=F2(x,y,z), ZD=F3(x,y,z)
c  |  which are then used to determine the highly position-dependent directional biasing information used
c  |  in this complex 3-D MCNP model.  [Brief summary:  Given a coordinate location (x,y,z) in the true 3-D
c  |  MCNP model of the HB3 beam tube, the surrounding water, or concrete, and a full 3-D representation of
c  |  the rotary shutter in the concrete box, with surrounding gaps and the big hole thru the shutter, etc,
c  |  Subroutine GETWT will return XD=F1(x,y,z), YD=F2(x,y,z), ZD=F3(x,y,z) corresponding to the coordinates
c  |  of a fake detector towards which photons at (x,y,z) should be biased to maximize the probability of
c  |  transmission thru the entire configuration.]
c  |
c  |  Unlike some earlier versions which wrote a weight window file with information for 1 dummy neut grp and just
c  |  just 1 real gamma group, WW308G.F writes a weight window file that includes information for 1 dummy neut grp
c  |  and FOUR broad gamma groups.  In this case, the energy-dependent values of (rw, rc, rs, wtsrc, and w0),
c  |  ie: the mesh-to-mesh weight window attenuation factors, from one 5-cm importance mesh to the next, which
c  |  determine the 3-D shape of the weight-window function(s), are based on the above considerations.
c  |
c  |  The final values to be used in Subroutine GETWT of our final 3-D weight window generator (WW308G.F) are:
c  |  +-----------------------------------------------------------------------------------------------------
c  |  |  velm gamma groups in this broad-gamma-group:        1-8          9-12         13-17         18-23
c  |  |  wt attenuation factors for water (rigourous):     rw=0.73      rw=0.65      rw=0.57       rw=0.50
c  |  |  wt attenuation factors for concrete (guess):      rc=0.51      rc=0.45      rc=0.33       rc=0.18
c  |  |  wt attenuation factors for half-density steel:    rs=0.46      rs=0.40      rs=0.28       rs=0.13
c  |  |
c  |  |  ini starting wt (wtsrc) assigned to gammas:    1.7332472e-2      ---          ---           ---
c  |  |  wtlow in source region (w0):                   1.7332472e-3   7.14304    8.57521e+5    4.48876e+13
c  |  +-----------------------------------------------------------------------------------------------------
c  |
c  |  Note:  The earlier version (WW308F) also used four broad weight window groups with similar wt attenuation
c  |  factors, but unfortunately I had tried to artificially rescale the "wtlow" curves individually so that
c  |  along the axis at about Z=400 cm (just downstream of the water-filled collimator) they would all have
c  |  about the same value as that for broad weight-window group corresponding to VELM groups 1-8.  I later
c  |  realized that this "individual rescaling" was a critical mistake. That mistake was not repeated in WW308G.
c  |
c  +-------------------------------------------------------------------------------------------------------------
c
c  The only two new additions to the MCNP Run HB308G input file itself were Tallies 212 and 232:
c
c      fc212  Pri G-Dose (mrem/hr) 2.4945 cm downstream of collimator hole exit (seg 5)
c      c      --------------------------
c      c      Note:  Only if this boundary crossing estimate of the primary gamma dose rate downstream of the
c      c      collimator hole has good statistics, is it possible to have a high degree of confidence in the
c      c      point detector estimates.  If F2 Tally 212 is well converged, F5 Tally 25 will be more accurate;
c      c      if F2 Tally 212 is not well converged, F5 Tally 25 may or may not be any good (even if stats are good).
c      c      --------------------------
c
```

```
c
c       fc232  Primary G-Dose (mrem/hr) on downstrem surf of box holding shutter; seg 10
c       c      --------------------------
c       c      Note:  Only if this boundary crossing estimate of the primary gamma dose rate downstream of the
c       c      central 6.5-inch-diam disk directly in front of the shutter (seg 10) [and perhaps segments 5-9 also]
c       c      has good statistics, is it possible to have a high degree of confidence in the point detector estimates.
c       c      If F2 Tally 232 is well converged in segments 5-10, then F5 Tallies 45, 65 and 85 will be very accurate;
c       c      if F2 Tally 232 is not well converged, F5 Tallies 45, 65 and 85 may or may not be any good (even if stats are good).
c       c      --------------------------
c       c      1) Rotary shutter is centered at Z=446.405 cm;  downstream edge of shutter is at Z=477.36125 cm;
c       c         Downstream surf of SS liner on concrete box containing shutter is at Surf 3001 (Z=478.79 cm);
c       c         That is the surface where this F2 tally is made.
c       c      2) Purpose of this tally is simply to see IF any real particles are getting here, and to see WHERE they are coming f
rom.
c       c      --------------------------
c
c      Neither of these will have any bearing on the ability to run the problem successfully, but both are vital indicators
c      which are needed (along with other tally indicators) if we are ultimately have any confidence in the final solution.
c
c
c      It was clear from the first trail calc with 240,000 histories that HB308G (using WW308G) was going to be a success.
c      Unlike HB308D (where HB308D1 and HB308D2 represented different unsuccessful attempts to run the problem slightly
c      differently) or HB308F (where HB308F1, HB308F2, and HB308F3 represented different uncessfull attempts to run the
c      problem slightly differently), HB308G.I & HB308G.O and HB309G2.O, HB308G3.O, HB308G4.O and HB308G5.O are simply
c      continuations of the same initial problem with more histories.  The following little file, HB308G.CON:
c      ------------------------------------------------------------------------------------------------------------
c      message:  c  outp=hb308.o  runtpe=hb308.r  wssa=hb308.s  wwinp=wwinp
c
c      continue
c      nps  4000000
c
c
c      ------------------------------------------------------------------------------------------------------------
c      represents the only input needed for each of the continuation steps (once HB309G.I had been run with 240,000
c      histories).  In each continuation run, we simply "bumped up" the number of histories (nps) desired.
c      A brief history follows (all calcs used 8 nodes ont eh SP2):
c
c
c      HB308G.I  ran NPS up to 240,000 histories between 06/21/98 16:21:40 and 06/21/98 21:50:35 (dump 31=last);
c                these experienced a total of 58,312,798 collisions (used in pt detector estimates) and,
c                more importantly, actually allowed 374,828 real particle tracks to cross surface 4197
c                (just downstram of the flooded collimator and upstream of the rotary shutter); this is where we are
c                saving results for the internal boundary source that we are trying to develop for future use if necessary.
c                While we only ran 240,000 histories in this initial pilot calc, indications are that every 1,000,000
c                histories would take appx 22.84 wall-clock hours on each of 8 nodes on the SP2.  This is not bad;
c                in fact, its very good given the complexity of the problem & the fact that we're getting good results.
c
c      HB308G2   ran NPS up to 1,000,000 histories (starting with above & finishing with dump 126 at 06/23/98 02:08:24);
c                these experienced a total of 212,701,257 collisions (used in pt detector estimates) and,
c                more importantly, actually allowed 1,411,263 real particle tracks to cross surface 4197
c
c      HB308G3   ran NPS up to 2,000,000 histories (starting with above & finishing with dump 251 at 06/24/98 06:19:21);
c                these experienced a total of 415,638,456 collisions (used in pt detector estimates) and,
c                more importantly, actually allowed 2,769,376 real particle tracks to cross surface 4197
c
c                I then "gave it a rest" for a week or two while I went off and ran some activation analyses and
c                activation dose rate analyses for the      y shutter (see HB309 & HB310) so that I could get
c                that done before the 4th of July;  aft     e 4th of July, I came back, and ran a few more histories
```

c on HB308G as follows (beginning on 7-7-98).
c
c Since HB308G was working so well and giving us such good results even downstream of the rotary shutter
c shield plug, the additional histories represented by the following two continuation runs probably weren't
c really necessary, and that the boundary source file that we were generating would probably never be needed.
c (Originally, we never expected such good success and thought the boundary source file would later have to
c used to analyse the daylights out of teh rotary shutter, especially if it had to be redesigned. Thus,
c initially, our focus was on getting a good boundary source. Only with the remarkable success of HB308G,
c and the relatively small dose rates that it was giving us downstream of the rotary shutter, was I slowly
c beginning to realize that we could probably dispose of the whole problem right here in HB308G, with no
c further analyses required.) Still, if it ever is needed, THIS was the time to run up the histories as
c high as reasonably possible before I'm forced to move the boundary source file (HB308G.S) off-line to
c tape storage for archival purposes. Therefore, I went ahead and ran a couple more continuation runs.
c
c HB308G4 ran NPS up to 3,000,000 histories (starting with above & finishing with dump 376 at 07/08/98 11:24:20);
c these experienced a total of 635,895,583 collisions (used in pt detector estimates) and,
c more importantly, actually allowed 4,244,571 real particle tracks to cross surface 4197
c
c HB308G5 ran NPS up to 4,000,000 histories (starting with above & finishing with dump 501 at 07/09/98 06:29:49);
c these experienced a total of 855,219,125 collisions (used in pt detector estimates) and,
c more importantly, actually allowed 5,688,819 real particle tracks to cross surface 4197;
c Objective here was to drive the key fsd's for both the pt detectors and the boundary crossing
c tallies down to the 3-4% range before calling it quits. Moreover, the final internal boundary
c source file that I was generating (HB308G.S with 5,688,819 real tracks) had grown to about 542 MB,
c and that's about all the disk space we could afford to dedicate to this task. It subsequently
c had to be archived to tape so that other calculations would have space to run.
c
c Final results are documented thoroughly and extensively in my on-line technical notebook ("index.308")
c but are too voluminous to reproduce here.
c
c
c ---
c
c HB304 is a "special" variant of HB301 used only to get fast fluxes at the two dosimeter locations.
c
c Would like to have this info so as to compare with values published in Tables E.12 and E.23 (on
c pp 208 & 221) of ORNL/TM-10444, "Evaluation of HFIR Pressure-Vessel Integrity Considering Radiation
c Embrittlement" (1988). Note that fluxes on pp 208 (E>1 MeV and E>0.1 MeV) are those calculated
c by Bob Child's DORT/TORT runs; the "real" fluxes there should either (a) be inferred from
c the Ni58(n,p)Co58 and Fe54(n,p)Mn54 decay data, OR (b) be inferred by dividing his published
c fluxes by the C/E ratios for the decay data, to get the real fluxes. Moreover, in Table E.23
c they applied method (b). Dwgs M-10070-0E-510-E, Rev 2 (1986) and Dwg E-49961, Rev C (1988)
c show the positions of the various "coupons" in the ring around HB-3 corresponding to Key 3.
c
c Cell 2134 (just slightly on HB-4 side of HB-3) corresponds to Key 3 Position 8 where the "real"
c fluxes using Method B are: Flux(E>1 MeV)=1.78+9 n/s/cm2 and Flux(E>0.1 MeV)=3.84+9 n/s/cm2
c
c Cell 2135 (just slightly on HB-2 side of HB-3) corresponds to Key 3 Position 3 where the "real"
c fluxes using Method B are: Flux(E>1 MeV)=0.913+9 n/s/cm2 and Flux(E>0.1 MeV)=1.93+9 n/s/cm2
c
c It will be interesting to see how well (or how poorly) our MCNP results compare with these values!
c
c
c Modifications needed to get HB304 from HB301 are as follows:
c
c 1) To save time, run as "mode n" rather than "mode n p"
c
c 2) Use the following "cut:n" card to avoid tracking neutrons below 27 keV: (ie, keep only neutron grps 1-36)

```
c     cut:n  time(shakes) energy(MeV)  WC1   WC2   SWTM
c     cut:n     1.0e20       0.027     -0.5  -0.25   0.0  $ cutoff:  don't track any neutrons below 27 keV
c
c  3) On the si53, sp53, and ds63 cards describing the source, comment out all info pertaining to neutron
c     groups 37-61 since everything in these groups is below 27 keV; keep only info for grps 1-36 (above 27 keV)
c
c  4) On the fm14 & fm15 multiplier cards, use fm14=fm15=1.20830e16 n/s = sum of equivalent point
c     sources (n/s) over grps 1-36 only (ie, E>27 keV; use for dosimetry calc only) in HB-3 for HFIR at 100 MW
c
c  5) Change location of "importance cutoff plane" (Surf 1007) from Z=118.6879 cm (used to increase efficiency
c     of the water tube calcs, but is downstream of the dosimeters) to Z=75.473 cm which is more like 31.6546 cm
c     upstream of first dosimeter.  Belief is that most of the fast neutrons reaching the dosimeters are those
c     that strike the inner wall of the beam tube in the viscinity of the dosimeters, and that all others can,
c     for all practical purposes, be ignored.  [Surf 1007 is used in Cell 10110 (inner Al wall of beam tube)
c     to kill all neutrons below this location, ie: all those not within most forward-directed cone.]
c
c  6) On the sdef card, we need to "open up" the allowed angular distribution a little wider for the
c     dosimetry calc;  setting mu(min)=0.8 will allow neutrons from even the most forward equiv pt source
c     (at Z=68.7 cm) to hit the beam tube at Z=75.473 cm, which is well (31.654 cm) upstream of the first
c     dosimeter which is located at Z=107.1276 cm.  To accomplish this we need to do 2 things associated
c     with the sdef card:  (a) on the si3 (ang dist) card, set mu(min)=0.8, and (b) on the sdef card
c     itself, set wgt=0.1 =(mumax-mumin)/2
c
c     wgt=0.1  $ use this with mu(min)=0.8 in d3 for dosimetry calc only;  wgt = [mu(max)-mu(min)]/[(+1)-(-1)] = [1.0-0.8]/2 = 0.1
c     si3   h  0.8  1.0  $ open up angular distribution for dosimetry run;  mu boundaries (i.e, cosine boundaries wrt vec)
c
c  7) Change dosimeter specimens from carbon steel to water;  specimens (including foils) are really much smaller
c     than the big chunks of metal originally envisioned. To do this, change Cells 2134 & 2135 to mat1=7, den=-1.0 g/cc
c
c  8) Set up volume-averaged flux detectors for the two dosimeter cells (Cells 2134 & 2135); get N-fluxes by energy;
c     Cell 2134 = just slightly on HB-4 side of HB-3,  Cell 2135 = just slightly on HB-2 side of HB-3
c     May(?) later want to calculate activation rates here directly, or refine desc of dosimeter package inside dxtran sphere.
c
c  9) May(?) want to run as many as nps=5,000,000 histories to get good statistics;
c     will try 2,000,000 first; should go fast because of energy cutoff card above;
c     2,000,000 was subsequently found to be ok with dxtran spheres
c
c 10) May(?) want to have 3.2 cm radius dxtran spheres around each dosimeter so as to get better statistics
c     without having to run as many histories; found to work well with 2,000,000 histories
c
c 11) All the modifications previously used to create HB302 from HB301 should also be incorporated in HB304.
c     HB302 was a "special" varient of HB301;  HB302 was intented to get comparisons with the June 1968
c     Blosser & Thomas measurements. HB302 thus differed from HB301 insofar as:
c
c     a) Aluminum windows 1 and 2 were placed in their 1960 axail locations (see Cells 2140, 2141, 4305, 4380)
c     b) We used the small hole in the rotary shutter since that's what they used on HB-3 (see Surfs 3131 & 3132)
c     c) The was no water in the water tubes; they were void in this calc (see Cells 2145 & 2146)
c     d) Use pt det 15 to get results at B&T measurement point, 655.6626 from tip of HB-3 (ie, at Z=678.1673 cm)
c
c     While HB302 has been already run, and our results compared quite well with measurements (C/E=1.45 generally),
c     the main purpose of including it again here in Run HB304 is simply to verify that I haven't screwed up the
c     source normalization by only looking at the fast groups.  I am pretty sure there is no problem with above
c     appraoch, but want to keep this B&T comparison in the calc as a reference point to verify there is no problem.
c
c 12) Delete the oversimplified spherical representation of the 2 dosimeters (Key 3 Positions 3 & 8)
c     and model then more precisely as particular rectangular regions on the ss304 dosimeter specimen
c     holder ring [see Dwg M-10070-0E-510-E Rev 2 (1987), as well as Dwg E-49961 Rev C (1988), and
c     Dwg M-115-11-0H-001-E, Rev 1 (1992)].  To affect this change
```

```
c       a) Delete the oversimplified dosimeter cells (2134 & 2135) described by surfaces 2121 & 2126,
c          as well as the corresponding exclusion zones in the pool water (Cell 2130).
c       b) Include (instead):  Surfs 2510-2562, Transformation 40, and Cells 2581-2593 (all below).
c       c) Include the following new exclusion regions in the pool water (Cells 2130 & 2133):
c          #(-2530  2531  -2532)  #(-2520  2521  -2522)  #(-2510  2511  -2521)
c          to exclude from the water: the dosimeter holder ring, and the thick and thin inner sleeves
c       d) Use separate volume-averaged tallies (as shown below) for Key 3 Posn 3 and Key 3 Posn 8
c          so that each can be clearly labeled.
c       e) Revise the dxtran spheres around these two dosimeters as shown below.
c          (Update: dxtran spheres later had to be discarded; went with pt detectors embedded within dosimeters)
c          (Update: to get good statistics, we then needed 40,000,000 histories; these take 4 hrs, 35 min wallclock)
c
c   13) It recently became apparent (3-27-98) that there is a rather large 2-plate collar assembly holding a cooling
c       tube on the ss sleeve outside the beam tube, close to dosimeter ring.  Moreover, this collar assembly may
c       shield some of the dosimeters (Key 3, Positions 3 and 8 in particular) from some of the neutrons coming down
c       the HB-3 beam tube. To model this, we had to add Cells 2761-2781 (below) as well as Surfs 2701-2748 (below).
c       In addition, the following two new exclusions requirements had to be included in the description of
c       the water (Cell 2130) between the aluminum reflector container and the pressure vessel:
c       #(-2701  2742  -2748)                    $ exclude bulk of this 2-plate collar assembly
c       #(-2702 2701 2744 -2746 2711 -2710 2720)  $ exclude horz spacer plate extension (Cell 2727)
c       Also need the following new exclusion region added to the description of the water (Cell 2133)
c       just outside the ss sleeve around the beam tube:
c       #( 2742  -2748)  $ water outside ss sleeve, excluding bulk of 2-plate collar assembly
c       -----------------------------------
c       Update on "2-plate collar" assembly:  This is really called a "coolant collector". A very small insert sketch
c       of one is shown up near HB-4 on Dwg E-42027, Sheet 1, while the ref dwg no. for this part in Dwg E-49400.
c       I was unaware of these sketches/drawings when I created the above model.  Note however, that the approximate
c       model that I did create and use was really not too bad and, since it (as a whole) was found to have very little
c       impact on the fluxes at the dosimeter locations, any further refinements are probably unwarrented.  JAB 4-4-98
c
c   14) Material m71 was added to get the Ni58(n,p)Co58 reaction rate [(n,p)=103] in the dosimeters
c       Material m72 was added to get the Fe54(n,p)Mn54 reaction rate [(n,p)=103] in the dosimeters
c       Tallies f25:n and f35:n were modified to calculate fluxes as well as these reaction rates in dosimeters.
c
c   15) In reality, the inner edge of the HB3 vessel hole (where it penetrates the inner surface of the
c       pressure vessel) is slightly rounded and has a curvature of 1.0625 inches (all the way around
c       this elliptically shaped hole).  Because this is rounded, the steel that would otherwise be there
c       in this little corner element is really gone and replaced by water.  Because of its very close
c       proximity to the dosimeter at Key 3 Position 3, the erroneous use of steel instead of water will
c       likely cause one to slightly overestimate the fast flux at this dosimeter location.  I believe
c       (4-2-98) that it is important to model this with water to correctly moderate those neutrons which
c       hit the beam tube downstream of this location and then backscatter toward the dosimeter and pass
c       thru this region.  While I cannot "round the edge", I can certainly replace the rounded edge by a
c       chamfer (ie knock off the sharp steel corner around this ring and replace it by water) by using an
c       elliptically shaped cone whose size and position are carefully calculated to preserve the correct
c       amount of water (ie, so that the amount of water in this chamfer ring is the same as what would be
c       in this ring if the corners were actually rounded with the correct radius).  To model this, we
c       will need:  three new surfaces (Surfs 2110, 2111, and 2112, shown below), one new transformation
c       (*tr42, shown below), and one new water-filled cell (Cell 2134, shown below).  In addition, the
c       main pressure vessel cell (Cell 2150) must now exclude everything inside (ie, include stuff only
c       outside) the elliptically shaped cone defined by Surf 2110.  These changes were first incorporated
c       in Run HB304G on 2 Apr 98. -- J.A. Bucholz (update: this made a small difference, but very little)
c
c   16) If/when doing dosimetry calcs for the old 1960 design, it was decided that one should probably use
c       a better (more realistic) model of the old (1960) water tube since this may have a small effect on
c       backscatter toward the dosimeters.  To do this, we added surfaces 2161-2165 below;  must also:
c       Replace Cell 2140 with one of the following, depending whether you're modeling the old (1960) water tube or not:
c       2140  23  -2.7       (2161 -2162 2163 -2153):(2164 -2165 -2163)  imp:n=1  $ aluminum: part-length model of old (1960) water tube: 1st sph w
```

```
indow & cyl section
c                2140  61  -3.2325-4  (2161 -2162 2163 -2153):(2164 -2165 -2163)  imp:n=1  $ int void: part-length model of old (1960) water tube: 1st sph w
indow & cyl section
c                Delete the old exclusion spec for Cell 1010:
c                #(2151  -2152)  imp:n=1    $ tube void region (above) excluding 1st aluminum window in 1960 design (see cell 2140)
c                and replace it with the following new exclusion spec for Cell 1010:
c                #((2161 -2162 2163 -2153):(2164 -2165 -2163)) imp:n=1    $ tube void region (above) excluding part-length model of old (1960) water tube
c
c            17) While the dosimeter strips are really SS302, they are very tiny (typically 0.417 grams).  The bulk of
c                the 1.16"x2.1" dosimeter package is comprised of three carbon steel Charpy V-notch specimens, with the
c                tiny dosimeter strips laying perpendicularly across these specimens in the V-notches.  Since the bulk
c                of each dosimeter package is carbon steel, Cells 2581 & 2582 were changed to matl m50 at 7.8212 g/cc.
c
c            18) Just upstream of the dosimeters located at Key 3, Positions 3 and 8, are what appear to be two stainless
c                steel pegs.  The one in front of Position 3 is of particular concern since it directly shields the
c                dosimeter from neutrons scattering in the nearby beam tube.  The one in front of Position 8 is of
c                less concern since it is more "off to the side".  Nevertheless, both should be modeled.  While I'll
c                refer to these as "square pegs", each is really a large bolt going thru two thick tabs that stick out
c                from the top and bottom halves of the dosimeter holder assembly front plate (see Dwg E49953, Rev A,
c                dated 30 Jun 1965).  To model these, we will need 7 new surfaces (2533,2543,2544,2553,2554,2563,2564),
c                and 2 new cells (2583 & 2584).  In addition, Cell 2130 (and perhaps Cell 2133) will need the following
c                two exclusion statements:
c                #(2533  -2531  2553  -2554  2543  -2544) $ large water region (above), excluding ss square peg just upstream of dosimeter at Key 3, Positio
ns 3
c                #(2533  -2531  2564  -2563  2543  -2544) $ large water region (above), excluding ss square peg just upstream of dosimeter at Key 3, Positio
ns 8
c
c            19) On 3 Apr 98, Pete Hambaugh gave me a full size dwg of the "Pressure Vessel Surveillance Specimen Mount
c                Assembly for HB-1, 3, and 4", Dwg E-49953, Rev A, dated 6-30-98.  This is a very good drawing of the
c                assembly;  it is much better than the little sketches I was using, and clarifies a number of questions.
c                Thus: For Run HB304H (3 Apr 98) and all subsequent runs, Surfaces 2510-2564 (associated with the dosimeters
c                and the dosimeter specimen holder at Key 3 around HB-3) were all revised based on newly available data shown
c                on this drawing.  In particular, we can now model (with confidence) the large bolts and ss tabs (collectively
c                referred to above and below as the "ss square pegs" which sit very close to the dosimeters in Positions 3 & 8
c                of Key 3.  Transformation tr40 was also revised as shown below, based on that newly available.  Lastly,
c                point detectors 25 and 35 (below) were repositioned so as to correspond to what are the newly revised
c                midpoints of the dosimeter locations, based on this newly available data.
c
c            20) On 4 Apr 98, I made a number of small modeling improvements to improve the overall calculational
c                efficiency and reliability.  While a number of geometry cells were redefined, the actual physical
c                distribution of materials was not changed at all.  (1) The way the water outside the ss sleeve
c                (radially beyond the beam tube) was broken up into cells was changed in order to (a) reduce the
c                number of exclusion regions required (especially in cell 2130) and to (b) allow for a new importance
c                region in the water outside the ss sleeve but inside the vessel in the vicinity of the dosimeters.
c                To accomplish this, one new water cell (Cell 2135) was added while Cells 2130 & 2133 were modified.
c                (2) To allow the nozzel and that portion of the vessel near the dosimeters to have a higher importance,
c                the cell corresponding to the nozzel was extended thru the vessel wall, while the region now called
c                the vessel was pushed back (radially) the same offsetting amount.  This required the modification
c                of Cells 2150 & 2151.  (3) To allow better statistical sampling in those regions close to the
c                dosimeters, I decided to use  imp:n=2  for a number of cells including:
c                ------------------------------------
c                Cells 2131                                      <-- for the water outside the beam tube but inside the ss sleeve surrounding it, near the v
essel nozzel
c                Cells 2132                                      <-- for the ss sleeve surrounding the beam tube near the vessel nozzel
c                Cells 2133, 2134 & 2135                         <-- for the water outside the ss sleeve that is within about 20 cm of the dosimeters
c                Cells 2151 & 2152                               <-- for the newly defined vessel nozzle region and flange
c                Cells 2581, 2582, 2583, 2584, 2591, 2592 & 2593 <-- for the dosimeters & those cells comprising the dosimeter holder ring
c                Cells 2761, 2762, 2771, 2772, 2773, 2774 & 2781 <-- for cells associated with the 2-plate collar holding the cooling tube
```

```
c                ------------------------------------
c                Hopefully these improvements will lead to better fsd's without adding too much to the calculational overhead.
c
c
c            21) The following error was corrected by JAB on 6 Apr, just prior to submitting Run HB304K:
c                ------------------------------------------------------------------------------
c                bad surf:   2110   42  sq  0.9262159  0.9880902  -1.0  0  0  0  0  0  0  0  $ elliptical cone used to define chamfer between HB3 vessel hol
e and inner surf of pressure vessel
c                bad tranf:  *tr42  $ use tr42 to locate and position the elliptical cone used to define chamfer between HB3 vessel hole and inner surf of p
ressure vessel
c                bad tranf:         0.0  -2.14265  128.18364   $ location of local origin (center of elliptical cone), relative to the global origin (cm) in
 HB-3 model
c                bad tranf:           0    90.0000    90.0000  $ degrees from global x,y,z axes to local x axis
c                bad tranf:          90    12.6575   -77.3425  $ degrees from global x,y,z axes to local y axis
c                bad tranf:          90   102.6575    12.6575  $ degrees from global x,y,z axes to local z axis
c
c                The above specification was used in Runs HB304G & HB304H. Subsequent graphical analysis of the flare at the midplane (x=0)
c                showed that this elliptical cone chamfer was NOT a good representation of the rounded corners, and (in fact) cut off too
c                much steel from the vessel and substituted too much water.  The graphical analysis was reworked, using some CAD work
c                and some equations this time, and the following was found to be a much more accurate representation.  -- JAB, 5 Apr 98
c
c                Input files for HB304I & HB304J were also no good. These were failed attempts to fix the problem.  Those two cases
c                (I&J) were never run since similar problems were noticed during the graphical checkout step before final submission.
c
c                Run HB304K (whose correct input is shown below) was the firt run which had this correct. TR42 also changed. -- JAB 6 Apr 98
c                The following corrections to Surf 2110 and Trans *tr42 were made by JAB on 6 Apr 98, just prior to submitting Run HB304K:
c
c                2110   42  sq  0.928252  1.0  -1.0  0  0  0  0  0  0  0  $ elliptical cone used to define chamfer between HB3 vessel hole and inner surf of
 pressure vessel
c                *tr42  $ use tr42 to locate and position the elliptical cone used to define chamfer between HB3 vessel hole and inner surf of pressure vess
el
c                      0.0  -2.02265  127.62367   $ location of local origin (center of elliptical cone), relative to the global origin (cm) in HB-3 model
c                        0    90.0000    90.0000  $ degrees from global x,y,z axes to local x axis
c                       90    12.6929   -77.3071  $ degrees from global x,y,z axes to local y axis
c                       90   102.6929    12.6929  $ degrees from global x,y,z axes to local z axis
c
c
c            22) Numerical experiment in Run HB304M:
c
c                Shift sources 0.54 cm to right of beam tube centerline to account for the anisotropic effect
c                of more neutrons entering the one side of the beam tube than the other -- JAB, 4-7-98  3 am
c
c                In Run HB304M2:  Shift sources 1.05 cm to right of beam tube centerline to account for the anisotropic
c                effect of more neutrons entering the one side of the beam tube than the other;  also need to increase
c                nps by 50% (from 40M to 60M) to preserve statistics at Posn 3, since shifting the source this much will
c                cause fewer neutrons to impact the Key 3 Posn 3 (HB-2 side) of the HB-3 beam tube due to the shift in
c                direction cosines relative to the outward normal of the circular beam tube.  -- JAB, 4-7-98  6 pm
c
c                In Run HB304M3:  Shift sources 1.5 cm to right of beam tube centerline to account for the anisotropic
c                effect of more neutrons entering the one side of the beam tube than the other;  also need to increase
c                nps by from 60M to 80M) to preserve statistics at Posn 3, since shifting the source this much will
c                cause fewer neutrons to impact the Key 3 Posn 3 (HB-2 side) of the HB-3 beam tube due to the shift in
c                direction cosines relative to the outward normal of the circular beam tube.  -- JAB, 4-7-98  6 pm
c
c                In Run HB304M4:  Shift sources 1.6986 cm to right of beam tube centerline to account for the anisotropic
c                effect of more neutrons entering the one side of the beam tube than the other;  also need to increase
c                nps by from 60M to 80M) to preserve statistics at Posn 3, since shifting the source this much will
c                cause fewer neutrons to impact the Key 3 Posn 3 (HB-2 side) of the HB-3 beam tube due to the shift in
```

```
c               direction cosines relative to the outward normal of the circular beam tube.
c               ----------------------------------------
c               Important note:  Rather than trying to find an offset that might match the known dosimetry results better,
c               this particular offset (of 1.6986 cm) was based on a theoretical model which considered the RATIO of
c               ("the radial outward component of the current (from HB3, in direction of HB4) at Z=101.5 cm" to the
c               "the radial outward component of the current (from HB3, in direction of HB2) at Z=107.0 cm") based on
c               80400 source points on a hemispherical shell (R=7.76 cm) 1.0 cm into the Be (just past the hot end of the
c               beam tube) and Cheverton's known fast flux distribution as a function of radial distance from the core
c               centerline (see HFIR Nuclear Design document) in this region, which changes by a factor of 4 from one side
c               of the hemisphere to the other.  See FADIST7.FOR for more details about the methodology used to determine
c               this offset.  -- JAB, 4-15-98  11 am
c               ----------------------------------------
c               On the sdef card, we now need to "open up" the allowed angular distribution a little wider for the
c               dosimetry calc;  setting mu(min)=0.71 will allow neutrons from even the most forward equiv pt source
c               (at Z=68.7 cm) to hit the beam tube at Z=75.473 cm, which is well (31.654 cm) upstream of the first
c               dosimeter which is located at Z=107.1276 cm.  To accomplish this we need to do 2 things associated
c               with the sdef card:  (a) on the si3 (ang dist) card, set mu(min)=0.71, and (b) on the sdef card
c               itself, set wgt=0.145 =(mumax-mumin)/2
c
c               wgt=0.145  $ use this with mu(min)=0.71 in d3 for dosimetry calc only;  wgt = [mu(max)-mu(min)]/[(+1)-(-1)] = [1.0-0.8]/2 = 0.145
c               si3   h  0.71  1.0  $ open up angular distribution for dosimetry run;  mu boundaries (i.e, cosine boundaries wrt vec)
c               ----------------------------------------
c               In Run HB304M4, will also increase nps to 120,000,000 to preserve statistics after mu is opened up from 0.8 to 0.71
c               ----------------------------------------
c
c          23) Added 4-7-98:  Use of Surf 2534 (instead of Surf 2531) in the definition of Cells 2581 & 2582 allows the
c               portion "of the ss304 cover plate of dosimeter holder ring directly upstream of the dosimeters" to be modeled
c               separate from the carbon steel Charpy specimens in the 1-cm-thk dosimeter capsules (Cells 2581 & 2582).
c               To do this also requires that the exclusion specs for Cell 2591 (the holder ring) be modified as follows:
c               #(2534   2551   -2552   2541   -2542)   $ Key 3 dosimetry specimen holder ring (ss304), excluding dosimeter at Key 3, Position 3
c               #(2534   2562   -2561   2541   -2542)   $ Key 3 dosimetry specimen holder ring (ss304), excluding dosimeter at Key 3, Position 8
c
c     ------------------------------------------------------------------------------------------------------------------------
c
c     Used to study shielding effectiveness of water tube (work performed by Jim Bucholz for Mike Farrah, Mar/Apr 1998):
c
c       Ref 1:  Dwg of HB-1 (e:\ham\ustn\allbeam1197.dgn Jan 29, 1998 12:55:09), where HB-3 is said to be the same.
c       Ref 2:  Dwg M-11537-OH-001-E, Feb 13, 1998, 10:30:22, dwg of HB-1 (essentially the same as Ref 1, but smaller)
c       Ref 3:  Dwg E-42027, Sheet 1, Apr 11, 1995, showing location on HB-3 & 1st aluminum window in vessel, as built
c       Ref 4:  Dwg E-42027, Sheet 2, Apr 11, 1995, showing typical beam tube collimator & rotary shutter, as built
c       Ref 5:  Dwg 1546-01-M-5022, Rev Sep 18, 1961, showing concrete around HB-3 beam tube collimator & rotary shutter
c
c       Distance from outside of vessel nozzel boss to radial plane
c       perpendicular to beam tube (as specifically stated in Ref 3):
c         HB-1:  52.0 inches = 132.08 cm
c         HB-2:  54.5 inches = 138.43 cm
c         HB-3:  54.0 inches = 137.16 cm
c         HB-4:  52.0 inches = 132.08 cm
c
c       Notes regarding length of the 1998 water tube:
c
c       The location of the 1st aluminum window relative to the vessel nozzel boss (cf Ref 1 & 2) is believed to be
c       correctly modeled here.  Likewise, the 2nd aluminum window relative to the beam tube collimator assembly
c       (cf Ref 1 & 2) is believed to be correctly modeled here.  Given the location of the beam tube collimator
c       assembly (Ref 1 & 2) relative to the concrete biological shield specifically around HB-3 as shown in Ref 5,
c       however, the length of the new HB-3 water tube [from Surf 2154 at Z=174.95125 cm, to Surf 4110 at Z=302.1868 cm
c       (total length of water when flooded = 127.23555 cm)] is about 2.03 in. shorter than shown for HB-1 on Refs
c       1 & 2, or about 89.8 cm shorter than the water tube originally in HB-3.  Note, however, that this 2" difference
```

```
c       in water tube length between HB-1 and HB-3 is wholly consistent with the data in Ref 3 above if the vessel
c       flange hardware and collimator hardware are the same for HB-1 and HB-3 -- J. A. Bucholz, 3-21-98
c
c
c     BEGIN CELLS:
c
c     HB-3 (Tangential tube); sign on some surfs changed to accomodate this local model
c
1000  61  -3.2325-4  -1000        -1006        imp:n=1    $ endcap void region replaced with He at 2 atm (3.2325-4 g/cc)
1001  24  -2.7       -1001  1000  -1006        imp:n=0    $ endcap inner Al wall (imp=0 to kill all inward-directed neutrons)
1002  5   -0.98465   -1002  1001  -1006        imp:n=1    $ endcap water
1003  24  -2.7       -1003  1002  -1006        imp:n=1    $ endcap outer Al wall
1004  5   -0.98465   -1004  1003  -1006        imp:n=1    $ endcap water jacket
1005  24  -2.7       -1005  1004  -1006        imp:n=1    $ endcap Al Be liner
c     ----------------------
c     Cells 1008 & 1009 should be VOID (61  -3.2325-4) if looking at the 1998 water tube (normal condx or flooded) or the 1960 water tube under normal (dry)
 conditions.
c     Cells 1008 & 1009 should contain WATER (8   -1.0000) ONLY if looking at 1960 water tube when flooded.
1008  61  -3.2325-4  -2164  -2163        imp:n=1  $ hemispherical VOID inside tip of "dry" 1960 water tube
1009  61  -3.2325-4  -2161   2163 -2153  imp:n=1  $ cylindrical   VOID inside 1960 water tube, upstream of where 1998 water tube begins
c     1008  8   -1.0000    -2164  -2163        imp:n=1  $ hemispherical WATER region inside tip of "flooded" 1960 water tube
c     1009  8   -1.0000    -2161   2163 -2153  imp:n=1  $ cylindrical   WATER region inside 1960 water tube, upstream of where 1998 water tube begins
c     ----------------------
1010  61  -3.2325-4  -2153  -1010  1006                    $ tube void region replaced with He at 2 atm (3.2325-4 g/cc)
c     obsolete 1st: #(2151  -2152)   $ obsolete (too approximate)   $ tube void region (above) excluding 1st aluminum window in 1960 design (see cell 2140)
c     obsolete 2nd: #((2161 -2162 2163 -2153):(2164 -2165 -2163))   $ tube void region (above) excluding part-length model of old (1960) water tube: 1st sph
 window & cyl section
      2165  #(-2162 2163)         imp:n=1                 $ tube void region (above), excluding old aluminum 1960 water tube & everything in it
1011  24  -2.7       -2153  -1011  1010  1007  imp:n=1    $ tube inner Al wall (surf 1007 is the "importance cutoff plane")
10110 24  -2.7       -2153  -1011  1010  1006 -1007  imp:n=0    $ tube inner Al wall (used to kill all neutrons not within most forward-directed cone
1012  5   -0.98465   -2153  -1012  1011  1006  imp:n=1    $ tube water
1013  24  -2.7       -2153  -1013  1012  1006  imp:n=1    $ tube outer Al wall
1014  5   -0.98465   -2012  -1014  1013  1006  imp:n=1    $ tube water jacket [now cut off at cage (2012) as it should be]
1015  24  -2.7       -2012  -1015  1014  1006  imp:n=1    $ tube Al Be liner  [now cut off at cage (2012) as it should be]
c
c
c     Main cylindrical components outside HB-3:
c
2024 108  1.23156-1  -9999 9997 -2010  1005  #(-1015 1006) imp:n=1  $ permanent Be refl (0.123156 atoms/b*cm; typical comp, center ring); exclude HB-3
2110  5   -0.98465   -9999 9997  2010 -2011  1015  imp:n=1 $ water between Be refl and aluminum reflector container
2120  23  -2.7       -9999 9997  2011 -2012  1015  imp:n=1 $ aluminum refl container
c
c
2130  7   -0.9899  -9999 9997  2012 -2013   $ large water region between aluminum refl container and the pressure vessel
                    1013  #(-2101 2150)     $ large water region (above); excluding beam tube & regions around beam tube near vessel
c                   2121   2126             $ large water region (above); excluding the two small dosimeter locations (obsolete model)
c                 #(-2530  2531  -2532)     $ large water region (above); excluding the dosimeter holder ring (and dosimeters)
c                 #(-2520  2521  -2522)     $ large water region (above); excluding thick inner hub   of the holder ring
c                 #(-2510  2511  -2521)     $ large water region (above); excluding thin inner sleeve of the holder ring
c                 #(-2702 2701 2744 -2746 2711 -2710 2720)  $ large water region (above); excluding horz spacer plate extension (Cell 2727) on 2-plate collar
 assembly
c                 #(-2701  2742  -2748)     $ large water region (above); excluding bulk of 2-plate collar assy on ss sleeve outside beam tube close to dosi
meter ring
c                 #(2533  -2531  2553  -2554  2543  -2544) $ large water region (above), excluding ss square peg just upstream of dosimeter at Key 3, Positio
ns 3
c                 #(2533  -2531  2564  -2563  2543  -2544) $ large water region (above), excluding ss square peg just upstream of dosimeter at Key 3, Positio
ns 8
                    imp:n=1                 $ large water region (above)
```

```
2131  7   -0.9899   1013  -2130  2150  -2153  imp:n=2 $ water between beam tube and ss sleeve near vessel
2132  40  -7.92     2130  -2131  2150  -2153  imp:n=2 $ ss sleeve around beam tube, near vessel
2133  7   -0.9899   2131  -2101  2150  -2013  $ water just outside ss sleeve but inside main pressure vessel, in vicinity of dosimeters
c                   2121   2126               $ water just outside ss sleeve (above), excluding dosimeter locations
                  #(-2530  2531  -2532)        $ water just outside ss sleeve (above); excluding the dosimeter holder ring (and dosimeters)
                  #(-2520  2521  -2522)        $ water just outside ss sleeve (above), excluding thick inner hub   of the holder ring
                  #(-2510  2511  -2521)        $ water just outside ss sleeve (above), excluding thin inner sleeve of the holder ring
c                 #( 2742  -2748)              $ water just outside ss sleeve (above), large water region (above); excluding bulk of 2-plate collar assy on s
s sleeve outside beam tube close to dosimeter ring
                  #(-2702 2701 2744 -2746 2711 -2710 2720)  $ large water region (above); excluding horz spacer plate extension (Cell 2727) on 2-plate collar
 assembly
                  #(-2701  2742  -2748)      $ large water region (above); excluding bulk of 2-plate collar assy on ss sleeve outside beam tube close to dosi
meter ring
                  #(2533  -2531  2553  -2554  2543  -2544) $ water just outside ss sleeve (above), excluding ss square peg just upstream of dosimeter at Key
3, Positions 3
                  #(2533  -2531  2564  -2563  2543  -2544) $ water just outside ss sleeve (above), excluding ss square peg just upstream of dosimeter at Key
3, Positions 8
                     imp:n=2                  $ water just outside ss sleeve (above)
2134  7   -0.9899   2013 -2016  2100  -2110  2112  imp:n=2  $ water in elliptical cone chamfer ring where hb3 vessel hole penetrates inner wall of vessel
2135  7   -0.9899   2131 -2100 -2105   2013        imp:n=2  $ water outside ss sleeve but inside vessel nozzel
c
c
c     Note regarding dosimeters: the two cards shown below clearly define the location of the actual dosimeters presently
c     in use around HB-3.  Nevertheless, without further (questionable) changes to the model, the results here are probably
c     not even worth tabulating.  Reason:  The equivalent point sources used in this HB-3 analysis (of the voided & flooded
c     water tube) were based on global model point detectors at Z=120.6879, 185.9844, 251.2809 & 316.5774 cm from the radial
c     plane perpendicular to the HB-3 beam tube.  Moreover, for the analysis of the HB-3 water tube (the primary purpose of
c     this study), we spray neutron isotropically only over a very narrow forward-directed cone [cos(theta).gt. 0.965335056]
c     that includes this region of interest, and assign the inner wall of the beam tube an importance of 0.0 for all locations
c     below plane 1007 at Z=118.6879 cm (see cell 10110).  This is done primarily in the name of efficiency in this water tube
c     analysis, but also because points below this would be outside the axial range where we know our equivalent point sources
c     give good results.  Unfortunately, these two dosimeters are located at Z=107.1276 cm and 112.9905 cm respectively (see
c     surfaces 2121 and 2126).  Thus, with the present model, these two dosimeters probably won't see any neutrons except for
c     a few stray ones that might backscatter into this region.  If one really wants to check fluxes at these dosimeters, one
c     would have to lower plane 1007 in cell 10110, and open up the angular range on the sdef card to the point where our
c     equivalent point sources may or may not still be valid.  At any rate, doing so would greatly decrease the efficiency
c     of the water tube analysis that we originally wanted to focus on.  --  J.A. Bucholz, 3-20-98(a)
c
c     Updated thoughts:  Neutron group 16 in the VELM library goes from 0.907 Mev to 1.108 Mev.  Virtually all of the
c     equivalent point neutron sources for these first 16 energy groups lie between Z=31 and Z=70 cm (indeed, most lie
c     between Z=45 cm and Z=60 cm).  Thus, if we use an energy cutoff card set at 1 MeV (as typically done for dosimetry
c     calcs), we could probably make the modifications described above without seriously impacting the quality of the
c     results at the dosimeter locations.  [Efficiency of the water tube calc would go to pot, but if we use this ECUT
c     card for the dosimetry, we would (by definition) not be interested in the water tube results in this calc anyway].
c     Thus, we can probably do the dosimetry study -- at least for fast neutrons above 1 MeV.  Nevertheless, a better
c     course of action might be to take this geometry model, then apply the approach I took last fall with HB-2 (involving
c     a finite line source with all neutrons in a prescribed direction wrt the axis). It gave absolutely excellent results,
c     very quickly.  --  J.A. Bucholz, 3-20-98(b)
c
c       $ obsolete $ 2134  50  -7.8212  -2121   imp:n=1   $ dosimeter (modeled as carbon steel; really Charpy V-notch specimens) just slightly on HB-4 side
of HB-3
c       $ obsolete $ 2135  50  -7.8212  -2126   imp:n=1   $ dosimeter (modeled as carbon steel; really Charpy V-notch specimens) just slightly on HB-2 side
of HB-3
c       $ obsolete $ 2134  7  -1.0000  -2121   imp:n=1   $ dosimeter (now modeled as water; specimens are quite small) just slightly on HB-4 side of HB-3
c       $ obsolete $ 2135  7  -1.0000  -2126   imp:n=1   $ dosimeter (now modeled as water; specimens are quite small) just slightly on HB-2 side of HB-3
c       The above (oversimplified) dosimeter cells have been replaced by Cells 2581 and 2582, along with Cells 2591-2593 for the dosimeter holder assembly (
ring)
c
```

```
c     ---------------------------------
c     Use the following two if looking at the old 1960 HB-3 design:   (must also set options on Cells 4305 & 4380 below)
c     $ obsolete $ 2140  23  -2.7       -1010  2151  -2152  imp:n=1  $ aluminum: 1st window at start of water tube (old 1960 location)
c     2140  23  -2.7       (2161 -2162 2163 -2153):(2164 -2165 -2163)  imp:n=1  $ aluminum: part-length model of old (1960) water tube: 1st spherical window
 & cylindrical section
c     2141  61  -3.2325-4  -1010  2153  -2154  imp:n=1  $ int void: 1st window at start of water tube (new 1998 location)
c
c     Use the following two if looking at the new 1998 HB-3 design:   (must also set options on Cells 4305 & 4380 below)
c       $ obsolete $ 2140  61  -3.2325-4  -1010  2151  -2152  imp:n=1  $ int void: 1st window at start of water tube (old 1960 location)
2140  61  -3.2325-4  (2161 -2162 2163 -2153):(2164 -2165 -2163)  imp:n=1  $ int void: part-length model of old (1960) water tube: 1st spherical window & cyl
indrical section
2141  23  -2.7       -1010  2153  -2154  imp:n=1  $ aluminum: 1st window at start of water tube (new 1998 location)
c     ---------------------------------
c
2144  24  -2.7  -2136  1010  2153 -2154  imp:n=1  $ aluminum ring joining regular section of beam tube to expanded section
c
c     ---------------------------------
c     Use the following two if beam tube is void, as in normal operation:
c       2145  61  -1.0e-20   -2134  2154 -4110         imp:n=1  $ void inside main cavity of expanded beam tube outside vessel (if void, as in normal operat
ion)
c       2146  61  -1.0e-20   -2135  2134  2154  -4110  imp:n=1  $ void in pneumatic tube coils located just inside outer wall of expanded beam tube outside
vessel
c
c     Use the following two if beam tube is flooded for maintenance work:
2145   8   -1.0000   -2134  2154 -4110         imp:n=1  $ water inside main cavity of expanded beam tube outside vessel (if flooded for maintenance)
2146   8   -1.0000   -2135  2134  2154  -4110  imp:n=1  $ water in pneumatic tube coils located just inside outer wall of expanded beam tube outside vessel
c     ---------------------------------
c
2147  24  -2.7  -2136  2135  2154  -4125  imp:n=1  $ aluminum body of expanded section of the new HB-3 beam tube outside vessel
c
c     ---------------------------------
c       In the name of simplification, lets combine the inner & outer SS liners with the main vessel, and treat all as carbon steel
c       2140  40  8.62373-2  -9999 9997  2013 -2014  2100  imp:n=1  $ pressure vessel's inner liner
c       2150  50  8.74142-2  -9999 9997  2014 -2015  2100  imp:n=1  $ main pressure vessel (thick carbon steel)
c       2160  40  8.62373-2  -9999 9997  2015 -2016  2100  imp:n=1  $ pressure vessel's outer liner
c       2150  50  -7.8212    -9999 9997  2013 -2016  2100  imp:n=1  $ main pressure vessel (thick carbon steel + inner & outer liners)
2150  50  -7.8212     -9999  9997  2013 -2016  2101         imp:n=1  $ main pressure vessel (thick carbon steel + inner & outer liners)
2151  50  -7.8212      2100 -2101 -2105  2013  9997                  $ vessel nozzel boss around HB-3
                    #(-2110 -2111)                          imp:n=2  $ vessel nozzel boss around HB-3 (above); excluding HB3 chamfer (surf 2110)
2152  50  -7.8212     -2101  2131  2105 -2106               imp:n=2  $ carbon steel flange on vessel nozzel boss by HB-3
c     ---------------------------------
2170  8   -1.0000     -9999 9997  2016 -2017          $ water pool between pressure vessel and concrete bioshield
                      #(-2136  2153)  #(-2131 -2153)   $ water pool (above) excluding expanded section of HB-3 beam tube
                      #(4100  -4225)                   $ water pool (above) excluding everything inside ss sleeve (water & beam tube) where beam tube enters
concrete bioshield
                      #(-2101 -2106)  imp:n=1          $ water pool (above) excluding vessel boss (and flange) around HB-3
c
c
c     Cells associated with dosimeters & dosimeter specimen holder at Key 3 around HB-3 (see Dwg E-49953, Rev A, 6-30-65):
c     ---------------------------------------------------------------------------------------------------------
c     $ obsolete $ 2581  40 -7.92   2531  -2532  2551  -2552  2541  -2542  imp:n=1  $ dosimeter at Key 3, Position 3, just slightly on HB-2 side of HB-3 (mo
deled as ss304)
c     $ obsolete $ 2582  40 -7.92   2531  -2532  2562  -2561  2541  -2542  imp:n=1  $ dosimeter at Key 3, Position 8, just slightly on HB-4 side of HB-3 (mo
deled as ss304)
c
c     $ obsolete $ 2581  50  -7.8212  2531  -2532  2551  -2552  2541  -2542  imp:n=2  $ dosimeter at Key 3, Position 3, just slightly on HB-2 side of HB-3 (
modeled as carbon steel)
c     $ obsolete $ 2582  50  -7.8212  2531  -2532  2562  -2561  2541  -2542  imp:n=2  $ dosimeter at Key 3, Position 8, just slightly on HB-4 side of HB-3 (
```

```
modeled as carbon steel)
c
c     $ added 4-7-98:  Use of surf 2534 (instead of 2531) allows the ss304 cover plate of dosimeter holder ring to
c     $ added 4-7-98:  be modeled be separate from the carbon steel Charpy specimens in 1-cm-thk dosimeter capsules
2581  50  -7.8212  2534  -2532  2551  -2552  2541  -2542  imp:n=2  $ dosimeter at Key 3, Position 3, just slightly on HB-2 side of HB-3 (modeled as carbon s
teel)
2582  50  -7.8212  2534  -2532  2562  -2561  2541  -2542  imp:n=2  $ dosimeter at Key 3, Position 8, just slightly on HB-4 side of HB-3 (modeled as carbon s
teel)
c
2583  40  -7.92  2533  -2531  2553  -2554  2543  -2544  imp:n=2  $ ss square peg just upstream of dosimeter at Key 3, Position 3
2584  40  -7.92  2533  -2531  2564  -2563  2543  -2544  imp:n=2  $ ss square peg just upstream of dosimeter at Key 3, Position 8
c
2591  40 -7.92   2520  -2530  2531  -2532          $ Key 3 dosimetry specimen holder ring (ss304)
               #(2534  2551  -2552  2541  -2542)   $ Key 3 dosimetry specimen holder ring (ss304), excluding dosimeter at Key 3, Position 3
               #(2534  2562  -2561  2541  -2542)   $ Key 3 dosimetry specimen holder ring (ss304), excluding dosimeter at Key 3, Position 8
               imp:n=2                            $ Key 3 dosimetry specimen holder ring (ss304)
2592  40 -7.92  -2520  2521  -2522  2131  imp:n=2  $ short thick ss304 cylindrical sleeve on Key 3 dosimetry specimen holder
2593  40 -7.92  -2510  2131  -2521  2511  imp:n=2  $ long  thin  ss304 cylindrical sleeve on Key 3 dosimetry specimen holder
c     ------------------------------------------------------------------------------------------------------------------
c
c
c     Cells associated with the 2-plate collar holding cooling tube on ss sleeve outside beam tube close to dosimeter ring
c     ------------------------------------------------------------------------------------------------------------------
2761  40 -7.92  -2701 2131 2742 -2744  imp:n=2  $ 1st (upstream)   ss plate of 2-plate collar assembly
2762  40 -7.92  -2701 2131 2746 -2748  imp:n=2  $ 2nd (downstream) ss plate of 2-plate collar assembly
c
2771  40 -7.92  -2701 2131 2744 -2746 2711 -2712              imp:n=2  $ horizontal ss spacer plates (right & left, top & bottom, treated as one cell)
2772  40 -7.92  -2702 2701 2744 -2746 2711 -2710 2720         imp:n=2  $ horizontal ss spacer plate extension (on one side only); must exclude this from ve
ssel water (Cell 2130)
2773  40 -7.92  -2701 2131 2744 -2746 2724 -2728 #(2722 -2726) imp:n=2  $ vertical   ss spacer plates (right & left, top & bottom, treated as one cell)
2774   7 -0.9899  -2701 2131 2744 -2746 2722 -2726             imp:n=2  $ water between vertical spacer plates
c
2781   7 -0.9899  -2701  2131  2744  -2746          $ water between main upstream & downstream plates of 2-plate collar assembly
                  #(2711  -2712)  #(2724  -2728)    $ water (above), excluding horizontal & vertical spacers
                  imp:n=2                           $ water between main upstream & downstream plates of 2-plate collar assembly
c     ------------------------------------------------------------------------------------------------------------------
c
c
c
c       Intermediate notes using COMJOM-like notation to describe the cells in and around the HB-3 shield plug:
c
c       box1 = (3083 -3073 3023 -3033 3006 -3001)
c       box2 = (3082 -3072 3022 -3032 3005 -3001)
c       box3 = (3103 -3093 3043 -3053 3010 -3002)
c       box4 = (3102 -3092 3042 -3052 3009 -3002)
c       box5 = (3081 -3071 3021 -3031 3004 -3001)
c       box6 = (3080 -3070 3020 -3030 3003 -3002)
c       box7 = (3101 -3091 3041 -3051 3008 -3002)
c       box8 = (3100 -3090 3040 -3050 3007 -3002)
c
c       cyl9  = (-3120 3061 -3062)
c       cyl10 = (-3121 3061 -3063)
c       cyl11 = (-3122 3060 -3064)
c       cyl12 = (-3110)
c
c       Cell 3001 = bconc den  (former cell 3001)  #box3  #box1   imp:n=1  $ revised model of barytes concrete forming bioshield
c       Cell 30[illegible] = ss  den  box1  #box2  #box3   imp:n=1  $ ss liner on bioshield near big (downstream) side of removable block containing shield plug
c       Cell 3[illegible] = ss  den  box3  #box4  #box2   imp:n=1  $ ss liner on bios[illegible] near small (upstream) side of removable block containing sh[illegible] plug
c       Cell 3[illegible] = ss  den  box5  #box6  #box7  #cyl12   imp:n=1  $ ss liner [illegible]ig (downstream) side of removable concrete block containing [illegible]ld plug
```

424

```
c       Cell 3040 = ss  den  box7  #box8  #box6  #cyl12   imp:n=1  $ ss liner on small (upstream) side of removable concrete block containing shield plug
c       Cell 3050 = void den  (box4 OR box2)  #box7  #box5   imp:n=1  $ void immediately upstream of (and around) the removable concrete block containing sh
ield plug
c       Cell 3060 = bconc den  (box8 OR box6)  #cyl11  #cyl12   imp:n=1  $ barytes concrete forming bulk of the removable concrete block containing shield p
lug
c       Cell 3070 = ss  den  cyl11  #cyl10  #cyl12   imp:n=1  $ ss liner inside the removable concrete block containing shield plug
c       cccc    Cell 3080 = void den  (box7 OR box5) inside cyl12  #cyl10   imp:n=1  $ void near centerline, upstream and downstream of shield plug, inside
removable concrete block
c       Cell 3080 = void den  (box7 OR box5) inside cyl12  #cyl9   imp:n=1  $ void near centerline, upstream and downstream of shield plug, inside removable
 concrete block
c       Cell 3090 = cstl den  cyl9   imp:n=1  $ carbon steel forming the actual shield plug
c       Cell 3100 = void den  cly10  #cyl9   imp:n=1  $ void gap around the cylindrical shield plug
c
c       Final MCNP description of the cells in and around the HB-3 shield plug:
c     ---------------------------------------------------------------------------------------------------------------------------------------
c
3000  61  -1.0e-20   -9999 3001 -9998  9990  imp:n=1       $ void downstream of the HB-3 shield plug (shutter); excl small sph around pt where Blosser & Tho
mas made measurements
c
c     Barytes concrete bioshield from the upstream edge of the cavity containing the removable concrete block containing
c     the HB-3 shield plug (really surf 3010), out to the downstream edge of the removable block containing the shield plug:
3001  62  -3.09725   -9999 3010 -3001                        $ barytes concrete bioshield (outermost part)
                    #(3103 -3093 3043 -3053 3010 -3002)    $ barytes concrete bioshield (outermost part)
                    #(3083 -3073 3023 -3033 3006 -3001)    $ barytes concrete bioshield (outermost part)
                    #(4195 -4198)                          $ barytes concrete (above) excluding the 3 infinitesimal void slab slices by boundary source
                    imp:n=1                                $ barytes concrete bioshield (outermost part)
c
c     Barytes concrete bioshield from beyond pool liner (liner not modeled) out to upstream edge of removable block containing shield plug (really surf 3010
)
3002  62  -3.09725   -9999 9997 -3010  2017  2136  $ barytes concrete bioshield (from pool liner to shutter assembly cavity)
                    #(4155  -3010  -4265)   4225  $ barytes concrete (above) excluding everything inside ss bioshield liner around collimator assembly
                    imp:n=1                      $ barytes concrete bioshield (from pool liner to shutter assembly cavity)
c
c     ------------------------
c
3010  40  -7.92  (3083 -3073 3023 -3033 3006 -3001)   $ ss liner on bioshield near big (downstream) side of removable block containing shield plug
                #(3082 -3072 3022 -3032 3005 -3001)  $ ss liner on bioshield near big (downstream) side of removable block containing shield plug
                #(3103 -3093 3043 -3053 3010 -3002)  $ ss liner on bioshield near big (downstream) side of removable block containing shield plug
                imp:n=1                              $ ss liner on bioshield near big (downstream) side of removable block containing shield plug
c
3020  40  -7.92  (3103 -3093 3043 -3053 3010 -3002)   $ ss liner on bioshield near small (upstream) side of removable block containing shield plug
                #(3102 -3092 3042 -3052 3009 -3002)  $ ss liner on bioshield near small (upstream) side of removable block containing shield plug
                #(3082 -3072 3022 -3032 3005 -3001)  $ ss liner on bioshield near small (upstream) side of removable block containing shield plug
                #(4195 -4198)                        $ ss liner (above) excluding the 3 infinitesimal void slab slices by boundary source
                4240  imp:n=1                       $ ss liner on bioshield near small (upstream) side of removable block containing shield plug (excl end
 of collimator assy)
c
3030  40  -7.92  (3081 -3071 3021 -3031 3004 -3001)   $ ss liner on big (downstream) side of removable concrete block containing shield plug
                #(3080 -3070 3020 -3030 3003 -3002)  $ ss liner on big (downstream) side of removable concrete block containing shield plug
                #(3101 -3091 3041 -3051 3008 -3002)  $ ss liner on big (downstream) side of removable concrete block containing shield plug
                3110  imp:n=1                        $ ss liner on big (downstream) side of removable concrete block containing shield plug
c
3040  40  -7.92  (3101 -3091 3041 -3051 3008 -3002)   $ ss liner on small (upstream) side of removable concrete block containing shield plug
                #(3100 -3090 3040 -3050 3007 -3002)  $ ss liner on small (upstream) side of removable concrete block containing shield plug
                #(3080 -3070 3020 -3030 3003 -3002)  $ ss liner on small (upstream) side of removable concrete block containing shield plug
                3110  imp:n=1                        $ ss liner on small (upstream) side of removable concrete block containing shield plug
c
3050  61  -1.0e-20  ((3102 -3092 3042 -3052 3009 -3002): $ void immediately upstream of (and around) the removable concrete block containing shield plug
```

```
                  (3082 -3072 3022 -3032 3005 -3001)) $ void immediately upstream of (and around) the removable concrete block containing shield plug
                 #(3101 -3091 3041 -3051 3008 -3002)  $ void immediately upstream of (and around) the removable concrete block containing shield plug
                 #(3081 -3071 3021 -3031 3004 -3001)  $ void immediately upstream of (and around) the removable concrete block containing shield plug
                 #(-4195  -4245)                      $ void (above) excluding downstream end of collimator assembly and flange
                 #(4195   -4198)                      $ void (above) excluding the 3 infinitesimal void slab slices by boundary source
                 imp:n=1                              $ void immediately upstream of (and around) the removable concrete block containing shield plug
c
3060  62  -3.09725  ((3100 -3090 3040 -3050 3007 -3002): $ barytes concrete forming bulk of the removable concrete block containing shield plug
                  (3080 -3070 3020 -3030 3003 -3002)) $ barytes concrete forming bulk of the removable concrete block containing shield plug
                 #(-3122 3060 -3064)  3110   imp:n=1  $ barytes concrete forming bulk of the removable concrete block containing shield plug
c
3070  40  -7.92   -3122  3060  -3064  3110  3007  -3002  $ ss liner inside the removable concrete block containing shield plug
                #(-3121 3061 -3063)          imp:n=1  $ ss liner inside the removable concrete block containing shield plug
c
c       3080  61  -1.0e-20  -3110  3008  -3001  3121    imp:n=1  $ void near centerline, upstream and downstream of shield plug, inside removable concrete b
lock
3080  61  -1.0e-20  -3110  3008  -3001  3120    imp:n=1  $ void near centerline, upstream and downstream of shield plug, inside removable concrete block
c
3090  50   -7.8212   -3120  3061  -3062  3131  3132     imp:n=1  $ carbon steel forming the shield plug (ie, the rotary shutter)
3091  61  -1.0e-20   -3120  (-3131:-3132)  imp:n=1  $ beam holes thru the rotary shutter); for orientation, see surfs 3131 & 3132
c
3100  61  -1.0e-20  -3121  3061  -3063  3007  -3002      $ void gap around the cylindrical shield plug
                    3110  #(-3120 3061 -3062)  imp:n=1  $ void gap around the cylindrical shield plug
c     ------------------------------------------------------------------------------------------------------------------------------------------------
c
c
c     Cells used for the description of the collimator assembly (etc) inside the concrete:
c     ------------------------------------------------------------------------------------------------------------------------------------------------
c
c     4300  61  -1.0e-20  4130 -4190 4210 -4211 4212 -4213                $ rectangular hole up thru collimator (when void)
4300  8  -1.0000  4130 -4190 4210 -4211 4212 -4213                        $ rectangular hole up thru collimator (when flooded)
                  #(4140 -4145)                                  imp:n=1  $ exclusion used to allow simulating 2nd aluminum window in 1960 design (see cells
 4305 & 4380)
c     -------------------------
c       4305  23  -2.7      4140 -4145 4210 -4211 4212 -4213     imp:n=1  $ aluminum here IFF simulating 2nd aluminum window in 1960 design (downstream end
of water tube)
c       4305  61  -1.0e-20  4140 -4145 4210 -4211 4212 -4213     imp:n=1  $ void here IF modeling 2nd aluminum window in 1998 design (downstream end of wate
r tube not here)
4305  8  -1.0000  4140 -4145 4210 -4211 4212 -4213               imp:n=1  $ water here IF modeling flooded 1998 design (downstream end of water tube not her
e)
c     -------------------------
c     4310  40  -7.92     4130  -4190 -4230  #(4210 -4211 4212 -4213)  imp:n=1  $ ss body of central collimator with rectangular hole
c     Mike Farrar thought the central collimator might be carbon steel (to get less activation)
c     Dan Pinkston confirmed that it was Type 1020 carbon steel (here, I just used pressure vessel carbon steel here; close enough)
c     Ron Poor (the draftsman) indicated that existing one had a thin black oxide coating for corrosion protection
4310  50  -7.8212  4130  -4190 -4230  #(4210 -4211 4212 -4213)   imp:n=1  $ carbon steel (Type 1020) body of central collimator with rectangular hole;
4315  61  -1.0e-20  4190  -4195  4210   -4211 4212 -4213         imp:n=1  $ thin rect void reg (5.5"x2.75") immediately downstream of colimator <-- get axia
l leakage here
4316  61  -1.0e-20  4190  -4195 -4230  #(4210 -4211 4212 -4213)  imp:n=1  $ thin void immediately downstream of steel body of collimator (excl rect hole)
4320  24   -2.7     4125  -4195  4230  -4235                    imp:n=1  $ aluminum: expanded section of beam tube along side the collimator
4321  24   -2.7     4125  -4126  2135  -4230                    imp:n=1  $ aluminum step where beam tube expands again, just upstream of collimator
4330  40  -7.92     4180  -4195  4235  -4240                    imp:n=1  $ ss pool seal (B) downstream of collimator
4335  40  -7.92     3009  -4195  4240  -4245                    imp:n=1  $ ss flange around pool seal (B) downstream of collimator
4340  61  -1.0e-20  4170  -3010  4235  -4260  #(4180 -4240)     imp:n=1  $ void downstream of removable shield and eccentric shield
c       4345  41  -7.92     4150  -4170  4235  -4255  #(4250 -4160)      imp:n=1  $ ss removable shield, radially outside beam tube, next to collimator
4345  40  -7.92     4150  -4170  4235  -4255  #(4250 -4160)      imp:n=1  $ ss removable shield, radially outside beam tube, next to collimator
4350  40  -7.[illegible]  4160  -4170  4255  -4260              imp:n=1  $ s[illegible]centric shield, radially outside removable shield
4355  40  -7.[illegible]  4160  -3010  4260  -4265              imp:n=1  $ s[illegible]shield liner, between eccentric shield and concrete bioshie
```

```
4356  40  -7.92      4155  -4160  4220  -4265                    imp:n=1  $ ss liner on step expansion of bioshield, just upstream of removable shiled
4360  61  -1.0e-20   4135  -4150  4235  -4250                    imp:n=1  $ void just upstream of removable shield around collimator
4365  40  -7.92      4120  -4160  4250  -4220                    imp:n=1  $ ss pool seal (A2) upstream of collimator
4370  40  -7.92      4105  -4135  2136  -4250  #(4125 -4235)     imp:n=1  $ ss pool seal (A1) upstream of collimator
c     4375  61  -1.0e-20  4115  -4130 -4230   #(2135 -4126)     imp:n=1  $ void just upstream of collimator (before 2nd aluminum window in 1998 design)
4375  8  -1.0000    4115  -4130 -4230         #(2135 -4126)     imp:n=1  $ water just upstream of collimator if flooded (before 2nd aluminum window in 1998
 design)
c     -------------------------
c       4380  61  -1.0e-20  4110  -4115  -2135                  imp:n=1  $ void here IFF simulating 2nd aluminum window in 1960 design (downstream end of w
ater tube not here)
4380  23   -2.7     4110  -4115  -2135                          imp:n=1  $ aluminum here IF one wants to model 2nd aluminum window in 1998 design (downstre
am end of water tube)
c     -------------------------
4385  8  -1.0000  4100  -4120  2136  -4220  #(4105 -4250)        imp:n=1  $ water between beam tube & ss sleeve extending from concrete bioshield into pool
4390  40   -7.92  4100  -4155  4220  -4225                      imp:n=1  $ ss sleeve / bioshield liner extending from bioshield into the pool
c     ------------------------------------------------------------------------------------------------------------------------------------------
c
c
c     Cells to facilitate writing (and later reading & using) the internal boundary source;  see explanation above in header info
9981  61  -1.0e-20  4195  -4196  -9999   imp:n=1   $  in early global calc where we're writing the boundary source
c     9981  61  -1.0e-20  4195  -4196  -9999   imp:n=0   $  in later shielding calcs where we're reading & using the boundary source
9982  61  -1.0e-20  4196  -4197  -9999   imp:n=1   $  in all cases
9983  61  -1.0e-20  4197  -4198  -9999   imp:n=1   $  in all cases
c
c
9990  61  -1.0e-20    -9990   imp:n=1   $ small sph around pt where Blosser & Thomas made measurements;  for illustrative purposes only;  may put pt det ins
ide
9999  0  #(-9999 9997 -9998)  imp:n=0   $ external void; everything not inside the (1.3 m diam x 7.0 m long) cylinder modeled here
c
c     END CELLS (next line must be blank)

c     BEGIN SURFACES:
c
c      HB-3 (Tangential tube); described here as if the Z axis now corresponds to HB-3 axis
c
c      The following correspond to the real "physical" location of the spherical tip of the HB-3 beam tube:
c      1000   sz   28.5369   5.08         $ Spherical void OD
c      1001   sz   28.5369   6.03250      $ Spherical inner Al wall OD
c      1002   sz   28.5369   6.15250      $ Spherical water OD
c      1003   sz   28.5369   6.3896875    $ Spherical outer Al wall OD
c      1004   sz   28.5369   6.5497075    $ Spherical water jacket OD
c      1005   sz   28.5369   6.7605275    $ Spherical Al Be liner OD
c      1006   pz   28.5369                $ Plane at end of Cylindrical tube
c
c      Here, the hot tip has been artificially extended inward 18.5369 cm to accomodate innermost equiv point src at Z=10 cm:
1000   sz   10.0   5.08         $ Spherical void OD
1001   sz   10.0   6.03250      $ Spherical inner Al wall OD
1002   sz   10.0   6.15250      $ Spherical water OD
1003   sz   10.0   6.3896875    $ Spherical outer Al wall OD
1004   sz   10.0   6.5497075    $ Spherical water jacket OD
1005   sz   10.0   6.7605275    $ Spherical Al Be liner OD
1006   pz   10.0                $ Plane at end of Cylindrical tube
1007   pz   118.6879            $ Plane below which all importances are zero; located 2 cm upstream of first pt det used to get pt srcs
c      1007   pz   75.473       $ Plane below which all importances are zero; use this for dosimetry only; located 31.6546 cm upstream of first dosimeter
c
c      Cylindrical part of HB-3; described here as if the Z axis now corresponds to HB-3 axis
1010   cz   5.08                  $ Cylindrical void OD
1011   cz   6.03250               $ Cylindrical inner Al wall OD
```

```
1012   cz   6.1515625              $ Cylindrical water OD
1013   cz   6.3896875              $ Cylindrical outer Al wall OD
1014   cz   6.5497075              $ Cylindrical water jacket OD
1015   cz   6.7605275              $ Cylindrical Al Be liner OD
c
c
c      If the Z axis now corresponds to HB-3, then the main cylinders for core, vessel, etc, are described as:
c      Sidewall thicknesses from per comm. with Dick Rothrock (01-11-95); Sidewall dimensions from 1971 report
2010   c/x  26.67  0.0     54.61      $ outer radius--permanent Be refl. reg.
2011   c/x  26.67  0.0     55.245     $ outer radius--water gap
2012   c/x  26.67  0.0     56.8325    $ outer radius--aluminum reflector cage
2013   c/x  26.67  0.0    119.38      $ outer radius--water
2014   c/x  26.67  0.0    119.6975    $ outer radius--inner pressure vessel clad
2015   c/x  26.67  0.0    127.0       $ outer radius--pressure vessel
2016   c/x  26.67  0.0    127.254     $ outer radius--outer pressure vessel clad
2017   c/x  26.67  0.0    274.32      $ outer radius--H2O pool (pool/pool-liner interface at r=274.32 cm; pool diam=18 ft)
c
c      Note: for now, will model boss & flange on HB-3, but will ignore some of the finer details.  Will assume, for example,
c      that the vessel is tight against HB-3, thus ignoring the slightly larger hole actually present in vessel for HB-3, and
c      the sleeve (hydraulic seal) around HB-3 near vessel.  These may be added later (?).
2100   cz    10.0680    $ inner radius of vessel nozzel (boss) around HB-3 beam tube (see dwg E-42027)
2101   cz    21.45      $ outer radius of vessel nozzel (boss) around HB-3 beam tube (see dwg E-42027)
2105   pz   137.16      $ plane defining end of boss on pressure vessel around HB-3 (see dwg E-42027); in model, use 2106 instead
2106   pz   143.9443    $ plane defining end of thick flange mounted on boss on pressure vessel around HB-3 (see dwg E-42027)
c
c      wrong:  2110   42  sq  0.9262159  0.9880902  -1.0  0  0  0  0  0  0  0  $ elliptical cone used to define chamfer between HB3 vessel hole and inner su
rf of pressure vessel
c      The above specification was used in Runs HB304G & HB304H. Subsequent graphical analysis of the flare at the midplane (x=0)
c      showed that this elliptical cone chamfer was NOT a good representation of the rounded corners, and (in fact) cut off too
c      much steel from the vessel and substituted too much water.  The graphical analysis was reworked, using some CAD work
c      and some equations this time, and the following was found to be a much more accurate representation.  -- JAB, 5 Apr 98
c      Input files for HB304I & HB304J were also no good. These were failed attempts to fix the problem.  Those two cases
c      (I&J) were never run since similar problems were noticed during the graphical checkout step before final submission.
c      Run HB304K (whose correct input is shown below) was the firt run which had this correct. TR42 also changed. -- JAB 6 Apr 98
2110   42  sq  0.928252  1.0  -1.0  0  0  0  0  0  0  0  $ elliptical cone used to define chamfer between HB3 vessel hole and inner surf of pressure vessel
2111   42  pz  -0.001  $ plane used to help define which side of the double elliptical cone we want (cone reduces to a point at z=0, but use z=-0.001 to avo
id roundoff)
2112   42  pz  -15.0   $ plane used to define the upstream axial extent of the elliptical cone we want to consider (must be somewhere beyond z=-12.78829; z=
-15 is arbitrary)
c
c      Note regarding dosimeters:  these are really Charpy V-notch specimens, measuring 0.75"x0.75"x1.5";  locations were taken from dwg E-42027
2121   s  0.0  -13.480  107.1276  1.48893  $ sphere simulating dosimeter just slightly on HB-4 side of HB-3   (see above note)
2126   s  0.0   12.284  112.9905  1.48893  $ sphere simulating dosimeter just slightly on HB-2 side of HB-3   (see above note)
c
2130   cz  7.16174    $ inner radius of ss sleeve around HB-3 beam tube, near vessel
2131   cz  7.9338     $ outer radius of ss sleeve around HB-3 beam tube, near vessel
c
2134   cz  6.08626    $ inner radius of pneumatic tubes/coils inside expanded section of the HB-3 beam tube outside the vessel
2135   cz  7.03453    $ pneumatic tube / beam tube interface for the expanded section of the HB-3 beam tube outside the vessel
2136   cz  7.74573    $ outer radius of the expanded section of the HB-3 beam tube outside the vessel
c
2150   pz   96.8375   $ plane defining end of ss sleeve around beam tube, near vessel
2151   pz  116.7841   $ upstream   side of aluminum window forming start of water tube in original HB-3 design (as built)
2152   pz  117.7366   $ downstream side of aluminum window forming start of water tube in original HB-3 design (as built)
2153   pz  174.27     $ upstream   side of aluminum window forming start of water tube in proposed HB-3 design
2154   pz  174.95125  $ downstream side of aluminum window forming start of water tube in proposed HB-3 design
c
c      The following surfaces are used for a part-length model of the old (19  ater tube.
```

```
c       In this part-length model, the downstream end is defined by surf 2153 which is the
c       upstream surface of the 1-st aluminum window defining the start of the 1998 water tube.
2161    cz  3.65125             $ inner radius of cylindrical portion of old (1960) water tube
2162    cz  4.60375             $ outer radius of cylindrical portion of old (1960) water tube
2163    pz  120.30375           $ plane between cylindrical & spherical portion of old (1960) water tube, near upstream end
2164    sz  120.30375  3.65125 $ inner radius of spherical portion of old (1960) water tube, near upstream end
2165    sz  120.30375  4.60375 $ outer radius of spherical portion of old (1960) water tube, near upstream end
c
c
c       Surfaces associated with dosimeters & dosimeter specimen holder at Key 3 around HB-3
c       ------------------------------------------------------------------------------
c       2510    cz  8.41005  $ outer radius of thin cylindrical sleeve on Key 3 dosimetry specimen holder
c       2511    pz  107.056  $ upstream extent of thin cylindrical sleeve on Key 3 dosimetry specimen holder
c       c
c       2520    40  cz  9.36625   $ outer radius      of thick cylindrical sleeve on Key 3 dosimetry specimen holder
c       2521    40  pz  -1.5875   $ upstream   extent of thick cylindrical sleeve on Key 3 dosimetry specimen holder
c       2522    40  pz   1.5875   $ downstream extent of thick cylindrical sleeve on Key 3 dosimetry specimen holder
c       c
c       2530    40  cz  18.57375  $ outer radius      of Key 3 dosimetry specimen holder (ring)
c       2531    40  pz  -0.635    $ upstream   extent of Key 3 dosimetry specimen holder = upstream   surf of all capsule positions in Key 3
c       2532    40  pz   0.635    $ downstream extent of Key 3 dosimetry specimen holder = downstream surf of all capsule positions in Key 3
c       2533    40  pz   -2.54    $ upstream face of small square pegs directly upstream of dosimeters in Key 3, Positions 3 & 8 (downstream face=surf 2531)
c       c
c       2541    px  -1.4732       $ bottom (-X) surf of capsules in Key 3, positions 3 & 8 (specifically); no transformation req'd
c       2542    px   1.4732       $ top    (+X) surf of capsules in Key 3, positions 3 & 8 (specifically); no transformation req'd
c       2543    px  -1.905        $ bottom (-X) surf of small square pegs directly upstream of dosimeters in Key 3, Positions 3 & 8; no transformation req'd;
-X location only a guess
c       2544    px   1.905        $ top    (+X) surf of small square pegs directly upstream of dosimeters in Key 3, Positions 3 & 8; no transformation req'd;
+X location only a guess
c       c
c       2551    40  py   10.993   $ innermost (-Y) surf of capsule in Key 3, Position 3 (specifically); ie, capsule on HB-2 side of HB-3
c       2552    40  py   16.327   $ outermost (+Y) surf of capsule in Key 3, Position 3 (specifically); ie, capsule on HB-2 side of HB-3
c       2553    40  py   10.7675  $ innermost (-Y) surf of square peg just upstream of dosimeter at Key 3, Position 3 (specifically)
c       2554    40  py   12.6725  $ outermost (+Y) surf of square peg just upstream of dosimeter at Key 3, Position 3 (specifically)
c       c
c       2561    40  py  -10.993   $ innermost (+Y) surf of capsule in Key 3, Position 8 (specifically); ie, capsule on HB-4 side of HB-3
c       2562    40  py  -16.327   $ outermost (-Y) surf of capsule in Key 3, Position 8 (specifically); ie, capsule on HB-4 side of HB-3
c       2563    40  py  -13.9075  $ innermost (+Y) surf of square peg just upstream of dosimeter at Key 3, Position 8 (specifically)
c       2564    40  py  -15.8125  $ outermost (-Y) surf of square peg just upstream of dosimeter at Key 3, Position 8 (specifically)
c       ------------------------------------------------------------------------------
c
c
c       Surfaces associated with dosimeters & dosimeter specimen holder at Key 3 around HB-3. (Note: These were all revised
c       as follows by JAB on 3 Apr 98 for Run HB304H, based on newly available data shown on Dwg E-49953, Rev A, 6-30-65):
c       ------------------------------------------------------------------------------------------------------------------
2510    cz  8.17193  $ outer radius of thin cylindrical sleeve on Key 3 dosimetry specimen holder
2511    pz  109.17   $ upstream extent of thin cylindrical sleeve on Key 3 dosimetry specimen holder
c
2520    40  cz   9.5       $ outer radius      of thick cylindrical sleeve on Key 3 dosimetry specimen holder
2521    40  pz  -2.3       $ upstream   extent of thick cylindrical sleeve on Key 3 dosimetry specimen holder
2522    40  pz   0.8       $ downstream extent of thick cylindrical sleeve on Key 3 dosimetry specimen holder
c
2530    40  cz  18.16      $ outer radius      of Key 3 dosimetry specimen holder (ring)
2531    40  pz  -0.8175    $ upstream   extent of Key 3 dosimetry specimen holder ring (ie, just upstream on the 0.3175 cm cover plate, but no water)
2532    40  pz   0.50      $ downstream extent of Key 3 dosimetry specimen holder ring = downstream surf of all capsule positions in Key 3 (capsules are 0.394
"=1.00075 cm thk)
2533    40  pz  -3.25      $ upstream face of small square pegs directly upstream of dosimeters in Key 3, Positions 3 & 8 (downstream face=surf 2531)
2534    40  pz  -0.50      $ upstream face of 1-cm-thk dosimeter capsules (Key 3, Positions 3 & 8) inside dosimeter holder ring
```

```
c
2541   px  -1.50622      $ bottom (-X) surf of capsules in Key 3, positions 3 & 8 (specifically); no transformation req'd
2542   px   1.50622      $ top    (+X) surf of capsules in Key 3, positions 3 & 8 (specifically); no transformation req'd
2543   px  -1.50         $ bottom (-X) surf of small square pegs directly upstream of dosimeters in Key 3, Positions 3 & 8; no transformation req'd; -X loca
tion only a guess
2544   px   3.37         $ top    (+X) surf of small square pegs directly upstream of dosimeters in Key 3, Positions 3 & 8; no transformation req'd; +X loca
tion only a guess
c
2551   40  py   10.10045 $ innermost (-Y) surf of capsule in Key 3, Position 3 (specifically); ie, capsule on HB-2 side of HB-3
2552   40  py   15.59955 $ outermost (+Y) surf of capsule in Key 3, Position 3 (specifically); ie, capsule on HB-2 side of HB-3
2553   40  py   11.0475  $ innermost (-Y) surf of square peg just upstream of dosimeter at Key 3, Position 3 (specifically)
2554   40  py   12.9525  $ outermost (+Y) surf of square peg just upstream of dosimeter at Key 3, Position 3 (specifically)
c
2561   40  py  -10.10045 $ innermost (+Y) surf of capsule in Key 3, Position 8 (specifically); ie, capsule on HB-4 side of HB-3
2562   40  py  -15.59955 $ outermost (-Y) surf of capsule in Key 3, Position 8 (specifically); ie, capsule on HB-4 side of HB-3
2563   40  py  -14.1475  $ innermost (+Y) surf of square peg just upstream of dosimeter at Key 3, Position 8 (specifically)
2564   40  py  -16.0525  $ outermost (-Y) surf of square peg just upstream of dosimeter at Key 3, Position 8 (specifically)
c      ------------------------------------------------------------------------------------------------------------------------
c
c
c     Surfaces associated with the 2-plate collar holding cooling tube on ss sleeve outside beam tube close to dosimeter ring
c     ------------------------------------------------------------------------------------------------------------------------
2701   cz  11.40      $ outer radius of 2-plate collar (surf 2131 defines inner radius)
2702   cz  14.88      $ outer radius of the one spacer plate extension
c
2710   px   0.0       $ horizontal midplane = top surface of the one spacer plate extension
2711   px  -1.11125   $ bottom surface of the horizontal spacer plates
2712   px   1.11125   $ top surface of the horizontal spacer plates
c
2720   py   0.0       $ vertical plane up middle (needed to uniquely define spacer plate extension)
2722   py  -1.80      $ right surface of vertical spacer plates on left
2724   py  -3.22      $ left  surface of vertical spacer plates on left
2726   py   1.80      $ left  surface of vertical spacer plates on right
2728   py   3.22      $ right surface of vertical spacer plates on right
c
2742   pz  100.3275   $ upstream   surface of 1st (upstream)   plate
2744   pz  101.43875  $ downstream surface of 1st (upstream)   plate
2746   pz  105.24875  $ upstream   surface of 2nd (downstream) plate
2748   pz  106.36     $ downstream surface of 2nd (downstream) plate
c      ------------------------------------------------------------------------------------------------------------------------
c
c
c      Surfaces describing the cells in and around the HB-3 shield plug (ie, the rotary shutter):
c      ------------------------------------------------------------------------------------------------------------------------
3001   pz  478.79     $ plane defining end of concrete just past downstream edge of removable concrete block containing HB-3 shield plug (see dwgs 1546-01-M
-5022 and E-42027)
3002   pz  477.8375   $ upstream surf of ss block liner downstream of shutter
3003   pz  447.3575   $ downstream side of ss liner on removable block near midsection of removable concrete block containing shield plug
3004   pz  446.405    $ upstream   side of ss liner on removable block near midsection of removable concrete block containing shield plug
3005   pz  446.0875   $ downstream side of ss liner on bioshield near midsection of removable concrete block containing shield plug
3006   pz  445.4525   $ upstream   side of ss liner on bioshield near midsection of removable concrete block containing shield plug
3007   pz  414.9725   $ downstream side of ss liner on upstream side of removable concrete block containing shield plug
3008   pz  414.02     $ upstream   side of ss liner on upstream side of removable concrete block containing shield plug
3009   pz  392.7475   $ downstream side of ss liner on bioshield (upstream of removable concrete block containing shield plug)
3010   pz  392.1125   $ upstream   side of ss liner on bioshield (upstream of removable concrete block containing shield plug)
c
3020   py  -40[illegible]75  $ inner surf (-Y) of ss liner on big (downstream) side [illegible]movable concrete block containing shield plug
3021   py  -41[illegible]25  $ outer surf (-Y) of ss liner on big (downstream) side [illegible]movable concrete block containing shield plug
```

```
3022   py  -43.4975   $ inner surf (-Y) of ss liner on bioshield near big (downstream) side of removable concrete block containing shield plug
3023   py  -44.1325   $ outer surf (-Y) of ss liner on bioshield near big (downstream) side of removable concrete block containing shield plug
c
3030   py   40.79875  $ inner surf (+Y) of ss liner on big (downstream) side of removable concrete block containing shield plug
3031   py   41.75125  $ outer surf (+Y) of ss liner on big (downstream) side of removable concrete block containing shield plug
3032   py   43.4975   $ inner surf (+Y) of ss liner on bioshield near big (downstream) side of removable concrete block containing shield plug
3033   py   44.1325   $ outer surf (+Y) of ss liner on bioshield near big (downstream) side of removable concrete block containing shield plug
c
3040   py  -36.195    $ inner surf (-Y) of ss liner on small (upstream) side of removable concrete block containing shield plug
3041   py  -37.30625  $ outer surf (-Y) of ss liner on small (upstream) side of removable concrete block containing shield plug
3042   py  -39.6875   $ inner surf (-Y) of ss liner on bioshield near small (upstream) side of removable concrete block containing shield plug
3043   py  -40.3225   $ outer surf (-Y) of ss liner on bioshield near small (upstream) side of removable concrete block containing shield plug
c
3050   py   36.195    $ inner surf (+Y) of ss liner on small (upstream) side of removable concrete block containing shield plug
3051   py   37.30625  $ outer surf (+Y) of ss liner on small (upstream) side of removable concrete block containing shield plug
3052   py   39.6875   $ inner surf (+Y) of ss liner on bioshield near small (upstream) side of removable concrete block containing shield plug
3053   py   40.3225   $ outer surf (+Y) of ss liner on bioshield near small (upstream) side of removable concrete block containing shield plug
c
3060   px  -31.27375  $ bot surf of lower ss liner for cylindrical cavity containing shield plug
3061   px  -30.48     $ top surf of lower ss liner for cylindrical cavity containing shield plug = bottom surf of shield plug
3062   px   30.48     $ top surf of shield plug
3063   px   31.27375  $ bot surf of upper ss liner for cylindrical cavity containing shield plug
3064   px   32.0675   $ top surf of upper ss liner for cylindrical cavity containing shield plug
c
3070   px   40.79875  $ inner surf (+X) of ss liner on big (downstream) side of removable concrete block containing shield plug
3071   px   41.75125  $ outer surf (+X) of ss liner on big (downstream) side of removable concrete block containing shield plug
3072   px   43.4975   $ inner surf (+X) of ss liner on bioshield near big (downstream) side of removable concrete block containing shield plug
3073   px   44.1325   $ outer surf (+X) of ss liner on bioshield near big (downstream) side of removable concrete block containing shield plug
c
3080   px  -40.79875  $ inner surf (-X) of ss liner on big (downstream) side of removable concrete block containing shield plug
3081   px  -41.75125  $ outer surf (-X) of ss liner on big (downstream) side of removable concrete block containing shield plug
3082   px  -43.4975   $ inner surf (-X) of ss liner on bioshield near big (downstream) side of removable concrete block containing shield plug
3083   px  -44.1325   $ outer surf (-X) of ss liner on bioshield near big (downstream) side of removable concrete block containing shield plug
c
3090   px   36.195    $ inner surf (+X) of ss liner on small (upstream) side of removable concrete block containing shield plug
3091   px   37.30625  $ outer surf (+X) of ss liner on small (upstream) side of removable concrete block containing shield plug
3092   px   39.6875   $ inner surf (+X) of ss liner on bioshield near small (upstream) side of removable concrete block containing shield plug
3093   px   40.3225   $ outer surf (+X) of ss liner on bioshield near small (upstream) side of removable concrete block containing shield plug
c
3100   px  -36.195    $ inner surf (-X) of ss liner on small (upstream) side of removable concrete block containing shield plug
3101   px  -37.30625  $ outer surf (-X) of ss liner on small (upstream) side of removable concrete block containing shield plug
3102   px  -39.6875   $ inner surf (-X) of ss liner on bioshield near small (upstream) side of removable concrete block containing shield plug
3103   px  -40.3225   $ outer surf (-X) of ss liner on bioshield near small (upstream) side of removable concrete block containing shield plug
c
3110   cz   8.255     $ cyl (along z axis) defining void in removable concrete block, upstream and downstream of the shield plug
c
3120   c/x  0.0  446.405  30.95625  $ outer radius of carbon steel shield plug (ie, rotary shutter); also see surfs 3131 & 3132
3121   c/x  0.0  446.405  31.75     $ outer radius of void around shield plug = inner radius of ss liner in removable concrete block
3122   c/x  0.0  446.405  32.54375  $ outer radius of ss liner in removable concrete block containing shield plug
c
c      ------------------------------------------------------------------------------------------------------------------------------
c
c       3131  11  cz  4.445    $ the big 3.5"diam beam hole in the rotary shutter;  use this when big hole is turned to "open" position
c       3132  21  cz  1.11125  $ small 0.875"diam beam hole in the rotary shutter;  use this when big hole is turned to "open" position
c
c       3131  12  cz  4.445    $ the big 3.5"diam beam hole in the rotary shutter;  use this when small hole is turned to "open" position
c       3132  22  cz  1.11125  $ small 0.875"diam beam hole in the rotary shutter;  use this when small hole is turned to "open" position
c
```

```
3131  13  cz  4.445    $ the big 3.5"diam beam hole in the rotary shutter;  use this when shutter is turned to "closed" position
3132  23  cz  1.11125  $ small 0.875"diam beam hole in the rotary shutter;  use this when shutter is turned to "closed" position
c
c     ------------------------------------------------------------------------------------------------------------------------------------
c
c
c
c     Axial surfaces used for the description of the collimator assembly (etc) inside the concrete:
c     ------------------------------------------------------------------------------------------
4100  pz  261.9474  $ max upstream axial location of narrow ss sleeve extending thru concrete into pool
4105  pz  286.385   $ upstream axial surf of pool seal (A1)
4110  pz  302.1868  $ upstream   surf of 2nd aluminum window defining end of water tube in 1998 design
4115  pz  302.5043  $ downstream surf of 2nd aluminum window defining end of water tube in 1998 design
4120  pz  304.0467  $ upstream axial surf of pool seal (A2)
4125  pz  304.1     $ step A for 2nd expansion of beam tube just upstream of collimator
4126  pz  304.735   $ step B for 2nd expansion of beam tube just upstream of collimator
4130  pz  310.58    $ upstream surface of collimator
4135  pz  311.785   $ downstream surf of pool seal (A1)
4140  pz  334.7709  $ upstream   surf of 2nd aluminum window defining end of water tube in 1960 design
4145  pz  335.4756  $ downstream surf of 2nd aluminum window defining end of water tube in 1960 design
4150  pz  335.7967  $ upstream surf of removable shield
4155  pz  341.8292  $ upstream   side of ss liner in bioshield near step
4160  pz  342.7817  $ downstream side of ss liner in bioshield near step = upstream surf of eccentric shield
4170  pz  381.5167  $ downstream surf of removable shield and eccentric shield
4180  pz  384.1645  $ upstream   side of pool seal (B)
4190  pz  399.48    $ downstream side of collimator
4195  pz  401.9445  $ downstream side of pool seal (B) = downstream side of flange around pool seal (B)
c
c
c     Artificial surfaces used to facilitate writing & later using an internal boundary source (wssa) file:
c     ------------------------------------------------------------------------------------------------------
c     In the early global calc where we write the boundary source:
c        (1) Cells 9981, 9982 and 9983, between Surfs 4195-4196, 4196-4197, and 4197-4198 are all regular void cells
c        (2) the boundary source will be written on Surf 4197
c        (3) the F1 surface crossing tallies will be written on Surf 4198 (just upstream of the boundary source)
c
c     In later shielding calcs for just the rotary shutter (shield plug), we'll keep the same (complete) basic model, BUT:
c        (1) Cell 9981 between Surfs 4195-4196 will be a black void with imp:n=0 to de-couple everything upstream of Surf 4196
c        (2) Cell 9982 between Surfs 4196-4197 will be a regular void
c        (3) the boundary source will be read & applied on Surf 4197
c        (4) Cell 9983 between Surfs 4197-4198 will be a regular void
c        (5) the F1 surface crossing tallies will be written on Surf 4198 (just upstream of the boundary source)
c            so that we have a printed cross-check that our boundary source reproduces the previous result
c     ------------------------------------------------------------------------------------------------------
4196  pz  401.9545  $ artificial surf used to create three infintesimal void cells downstream side of pool seal (B); 0.01 cm upstream of boundary source
4197  pz  401.9645  $ artificial surf used to create three infintesimal void cells downstream side of pool seal (B); boundary source written/inserted here
4198  pz  401.9745  $ artificial surf used to create three infintesimal void cells downstream side of pool seal (B); now used for F1 tallies
c
c
c     Box surfaces corresponding to rectangular-shaped hole in collimator:
c     --------------------------------------------------------------------
c     Here (like everywhere in this MCNP model of HB-3),
c     Z=central axis; Y is really horizontal; X is really vertical
4210  py  -3.4925   $ ymin
4211  py   3.4925   $ ymax
4212  px  -6.98[illegible]  $ xmin
4213  px   6.[illegible]    $ xmax
c
```

```
c
c     Radial surfaces used for the description of the collimator assembly (etc) inside the concrete:
c     ------------------------------------------------------------------------------------
4220  cz  17.2099    $ inner radius of narrow ss sleeve extending thru concrete into pool
4225  cz  17.4742    $ outer radius of narrow ss sleeve extending thru concrete into pool
4230  cz   9.21131   $ outer radius of collimator = inner radius of (again) expanded aluminum beam tube
4235  cz   9.84631   $ outer radius of (again) expanded aluminum beam tube = inner radius of removable shield
4240  cz  13.97      $ outer radius of pool seal (B)
4245  cz  33.655     $ outer radius of flange holding pool seal (B)
4250  cz  14.0339    $ outer radius of pool seal (A1) = inner radius of pool seal (A2)
4255  cz  19.7564    $ outer radius of removable shield = inner radius of eccentric shield
4260  cz  22.2003    $ outer radius of eccentric shield = inner radius of ss bioshield liner (in this axail section)
4265  cz  22.9315    $ outer radius of ss bioshield liner (in this axail section)
c
c
c     Surfaces 5100-5130 are used only in (segmented cell) Tally 184 which is used to monitor the
c     appx gamma dose rate in each of 30 equal axial segments (dz=4.24119 cm, dVol=493.55788 cc)
c     up thru the water tube (Cell 2145) from Z=174.95125 to 302.1868 cm.  These surfaces are used
c     only in Tally 184, and are not used in any cell descriptions.
c     5100  pz  174.95125
5101  pz  179.19240
5102  pz  183.43360
5103  pz  187.67480
5104  pz  191.91600
5105  pz  196.15720
5106  pz  200.39840
5107  pz  204.63950
5108  pz  208.88070
5109  pz  213.12190
5110  pz  217.36310
5111  pz  221.60430
5112  pz  225.84550
5113  pz  230.08670
5114  pz  234.32780
5115  pz  238.56900
5116  pz  242.81020
5117  pz  247.05140
5118  pz  251.29260
5119  pz  255.53380
5120  pz  259.77500
5121  pz  264.01610
5122  pz  268.25730
5123  pz  272.49850
5124  pz  276.73970
5125  pz  280.98090
5126  pz  285.22210
5127  pz  289.46330
5128  pz  293.70440
5129  pz  297.94560
c     5130  pz  302.18680
c
c     Surfaces 5140-5160 are used only in (segmented cell) Tally 194 which is used to monitor the
c     appx gamma dose rate in each of 20 equal axial segments (dz=4.44500 cm, dVol=433.74510 cc)
c     up thru the rectangular hole in the collimator (Cell 4300) from Z=310.58 to 399.48 cm.
c     These surfaces are used only in Tally 194, and are not used in any cell descriptions.
c     5140  pz  310.58000
5141  pz  315.02500
5142  pz  319.47000
```

```
5143  pz  323.91500
5144  pz  328.36000
5145  pz  332.80500
5146  pz  337.25000
5147  pz  341.69500
5148  pz  346.14000
5149  pz  350.58500
5150  pz  355.03000
5151  pz  359.47500
5152  pz  363.92000
5153  pz  368.36500
5154  pz  372.81000
5155  pz  377.25500
5156  pz  381.70000
5157  pz  386.14500
5158  pz  390.59000
5159  pz  395.03500
c     5160  pz  399.48000
c
c
9990   s  0.0  0.0  678.1673  1.11125 $ small sph (R=radius of small shutter hole), located at pt where Blosser & Thomas made measurements in June 1968 (cf
ORNL-TM-2221)
c
9997   pz    0.0   $ External void boundary (location corresponds to the real radial plane perpendicular to the real beam tube)
9998   pz  700.0   $ External void boundary (far enough out to emcompass point where Blosser & Thomas made measurements in 1968)
9999   cz   65.0   $ External void boundary (radial extent of this model)
c
c
c     END SURFACES (next line must be blank)

c     PROBLEM PARAMETERS:
mode   p
c       mode   n p
c       mode   n
c       nps    40000
c       nps    240000
nps    1000000
c       nps    2000000
c       nps    5000000
c       nps    40000000
c       nps    60000000
c       nps    80000000
c       nps    120000000
c       cut:n  time(shakes) energy(MeV)   WC1   WC2   SWTM
c       cut:n         1.0e20          0.027     -0.5  -0.25   0.0  $ cutoff:  don't track any neutrons below 27 keV
print  60      $ Table 60 shows vol, mass, n-imp by cell; see pp 3-117 of manual for description of other useful tables you may want
c     prdmp  0   80000  0  4  0   $ make restart file after every 80000 histories in fixed src calc; save only the 4 most recent restart files
prdmp  0   8000  0  4  0   $ make restart file after every 80000 histories in fixed src calc; save only the 4 most recent restart files
c
imp:p  $ obtained from MCNP output table when I ran a fake MCNP run with neutrons; here imp:p=imp:n in all 88 cells
       $ note that non-zero values will be ignored as soon as the wwinp file is read, but it must be entered anyway
       1 0 1 1 1 1 1 1 1 1 0 1 1 1 1 1 1 1 1 2
       2 2 2 2 1 1 1 1 1 1 1 2 2 1 2 2 2 2 2 2
       2 2 2 2 2 2 2 2 1 1 1 1 1 1 1 1 1 1 1 1
       1 1 1 1 1 1 1 1 1 1 1 1 1 1 1 1 1 1 1 1
       1 1 1 1 1 1 1 1 0
c
c      ------------------------------------------------------------
```

```
c       To be consistent with the wwinp file & the biased source dist
c       (see GETADJ.OUT, as printed by the GATWING.SCR), make sure you have
c       WUPN=WTHI= 100*WTLOW  and  WTSURV=WTAVG= 10*WTLOW  on the WWP:p card, and no WWP:n (in this case)
c       ------------------------------------------------------------------------------------
c       WWP:n  wupn  wsurvn  mxspln  mwhere  switchn
c       wwp:n  100  10  100  0  -1        $ 5th parameter is negative to make MCNP4B read the weight window importance file (wwinp)
c       wwp:p  100  10  100  0  -1        $ 5th parameter is negative to make MCNP4B read the weight window importance file (wwinp)
cwp:n  100  10  50  0  -1                 $ 5th parameter is negative to make MCNP4B read the weight window importance file (wwinp)
cwp:p  100  10  50  0  -1                 $ 5th parameter is negative to make MCNP4B read the weight window importance file (wwinp)
c       wwp:n  100  10  390625  0  -1              $ 5th parameter is negative to make MCNP4B read the weight window importance file (wwinp)
c       wwp:p  100  10  390625  0  -1              $ 5th parameter is negative to make MCNP4B read the weight window importance file (wwinp)
c       wwp:n  100  10  50  -1  -1              $ 5th parameter is negative to make MCNP4B read the weight window importance file (wwinp)
c       wwp:p  100  10  50  -1  -1              $ 5th parameter is negative to make MCNP4B read the weight window importance file (wwinp)
c       wwp:n  100  10  10  0  -1         $ 5th parameter is negative to make MCNP4B read the weight window importance file (wwinp)
c       wwp:p  100  10  10  0  -1         $ 5th parameter is negative to make MCNP4B read the weight window importance file (wwinp)
c      ------------------------------------------------------------------------------------
c
c       Use the "ssw" card below to write a boundary source file for gammas travelling downstream (ie, moving in the +Z direction)
c       across Surf 4197 from Cell 9982 to Cell 9983, where Surf 4197 is at Z=401.9645 cm, just 2.4845 cm downstream of collimator.
c       [Note that the three infinitesimally thin (0.01-cm-thick) void cells (Cells 9981, 9982, and 9983 defined by Surfaces 4195,
c       4196, 4197, and 4198) cut thru the entire problem geometry in the region between the collimator exit and the rotary shutter
c       shield plug.]  With this boundary source, we can later come back and set imp:n=0 and imp:n=0 in Cell 9981 and use this
c       boundary source in detailed shielding analyses of the rotary shield plug, which may (or may not) need to be redesigned,
c       without having to waste time tracking gammas upstream of Surf 4197, even though we'll retain the complete HB-3 geometry
c       in our model.  This problem should run much faster.
c
csw    +4197 (9983)      $ use this to write the boundary source file
c
c
c      EQUIVALENT POINT SOURCES:
c
cdef   erg=d73  pos ferg d83  $ source def for gammas in HB-3 (total p/s = 1.35399E+17;  source in VELM grps 1-8 = 7.984211E+15 p/s)
       par=2            $ par=1 for neut, par=2 for photons
c      sdef  erg=d53  pos ferg d63  $ source def for neutrons in HB-3 (total n/s = 9.64595E+16);  total n/s above 27 keV = 1.20830e16
c      par=1            $ par=1 for neut, par=2 for photons
       vec  0  0  1     $ reference vector if directional-dependent source is used
       dir=d3           $ angular distribution wrt vec (Caution: choice of angular distribution sampled will dictate choice of wgt)
       wgt=1.7332472-2  $ use this with d3;  wgt = [mu(max)-mu(min)]/[(+1)-(-1)] = [1.0000000000-0.965335056]/2 = 1.7332472-2
c      wgt=0.1    $ use this with mu(min)=0.8 in d3 for dosimetry calc only;  wgt = [mu(max)-mu(min)]/[(+1)-(-1)] = [1.0-0.8]/2 = 0.1
c      wgt=0.145  $ use this with mu(min)=0.71 in d3 for HB304M4 dosimetry calc only;  wgt = [mu(max)-mu(min)]/[(+1)-(-1)] = [1.0-0.8]/2 = 0.145
c      -------------------
c      Ang Dist: to spray isotropically across central void of HB-3 beam tube
ci3    h  0.965335056   1.0  $ angular distribution;  mu boundaries (i.e, cosine boundaries wrt vec)
c      si3   h  0.8  1.0  $ open up angular distribution for dosimetry run;  mu boundaries (i.e, cosine boundaries wrt vec)
c      si3   h  0.71  1.0  $ open up angular distribution for HB304M4 dosimetry run;  mu boundaries (i.e, cosine boundaries wrt vec)
cp3    d  0  1  $ angular distribution; particle emmission probabilities by bin; first value (below lowest bin bound) must be zero
c      -------------------
c
c        ------------------------------------------------------------------------
c        Begin distributions needed to describe the neutron sources in the HB-3 beam tube
c        ------------------------------------------------------------------------
ci53   h  1.0000e-11  $ this one Emin(MeV), followed by Emax(MeV) for the 61 VELM neut grps (lowest to highest energy for MCNP):
          4.1399e-7    1.1253e-6    2.3824e-6    5.0435e-6    1.0677e-5    $ VELM n-groups 61, 60, 59, 58, 57,
          2.2603e-5    4.7851e-5    1.0130e-4    1.6702e-4    2.7536e-4    $ VELM n-groups 56, 55, 54, 53, 52,
          4.5400e-4    7.4852e-4    1.2341e-3    2.0347e-3    2.2487e-3    $ VELM n-groups 51, 50, 49, 48, 47,
          2.6126e-3    3.0354e-3    3.7074e-3    5.5308e-3    9.1188e-3    $ VELM n-groups 46, 45, 44, 43, 42,
          1.5034e-2    2.3579e-2    2.4788e-2    2.6058e-2    2.7000e-2    $ VELM n-groups 41, 40, 39, 38, 37,
          2.8501e-2    3.4307e-2    5.2475e-2    5.6562e-2    8.6517e-2    $ VELM n-groups 36, 35, 34, 33, 32,
```

```
        1.2277e-1    1.4996e-1    1.8316e-1    2.2371e-1    2.7324e-1    $ VELM n-groups 31, 30, 29, 28, 27,
        2.9452e-1    2.9721e-1    2.9849e-1    3.0197e-1    3.8774e-1    $ VELM n-groups 26, 25, 24, 23, 22,
        4.9787e-1    5.2340e-1    6.0810e-1    7.4274e-1    9.0718e-1    $ VELM n-groups 21, 20, 19, 18, 17,
        1.1080e+0    1.3534e+0    1.6530e+0    2.0190e+0    2.2313e+0    $ VELM n-groups 16, 15, 14, 13, 12,
        2.3457e+0    2.4660e+0    3.0119e+0    3.6788e+0    4.4933e+0    $ VELM n-groups 11, 10,  9,  8,  7,
        5.4881e+0    6.7032e+0    8.1873e+0    1.0000e+1    1.2214e+1    $ VELM n-groups  6,  5,  4,  3,  2,
        1.4918e+1                                                      $ VELM n-group   1
sp53  d     0.0  $ dummy 0, followed by neut src terms (n/s) for HB-3:
        6.30365e+16  2.25679e+15  1.52979e+15  1.30212e+15  1.55274e+15  $ VELM n-groups 61, 60, 59, 58, 57,
        1.58981e+15  1.54759e+15  1.45876e+15  9.03837e+14  9.69821e+14  $ VELM n-groups 56, 55, 54, 53, 52,
        9.50610e+14  8.74122e+14  8.53691e+14  8.87245e+14  2.04908e+14  $ VELM n-groups 51, 50, 49, 48, 47,
        2.76622e+14  2.54975e+14  3.36538e+14  7.55438e+14  8.76077e+14  $ VELM n-groups 46, 45, 44, 43, 42,
        9.84217e+14  7.42049e+14  6.69650e+13  1.12860e+14  5.24714e+13  $ VELM n-groups 41, 40, 39, 38, 37,
        1.21873e+14  3.03507e+14  4.96958e+14  1.29680e+14  8.89397e+14  $ VELM n-groups 36, 35, 34, 33, 32,
        5.59006e+14  4.29193e+14  3.63241e+14  4.33245e+14  7.35199e+14  $ VELM n-groups 31, 30, 29, 28, 27,
        2.12840e+14  1.38494e+13  7.68584e+12  3.65651e+13  6.29256e+14  $ VELM n-groups 26, 25, 24, 23, 22,
        5.85513e+14  1.49367e+14  3.61470e+14  5.35177e+14  6.65098e+14  $ VELM n-groups 21, 20, 19, 18, 17,
        5.40055e+14  7.09512e+14  8.07055e+14  8.54720e+14  3.12945e+14  $ VELM n-groups 16, 15, 14, 13, 12,
        2.00073e+14  1.35333e+14  2.41078e+14  1.61947e+14  2.06360e+14  $ VELM n-groups 11, 10,  9,  8,  7,
        1.36477e+14  7.32282e+13  3.05242e+13  8.64293e+12  6.92602e+12  $ VELM n-groups  6,  5,  4,  3,  2,
        2.74800e+09                                                    $ VELM n-group   1
ds63  1     $ neutron starting positions (x,y,z) in HB-3:
        0 0  80.2    0 0  57.3    0 0  65.2    0 0  76.1    0 0  54.5    $ VELM n-groups 61, 60, 59, 58, 57,
        0 0  48.2    0 0  56.5    0 0  55.4    0 0  56.0    0 0  51.1    $ VELM n-groups 56, 55, 54, 53, 52,
        0 0  53.8    0 0  52.6    0 0  61.2    0 0  60.5    0 0  43.0    $ VELM n-groups 51, 50, 49, 48, 47,
        0 0  49.5    0 0  55.0    0 0  65.1    0 0  53.3    0 0  52.7    $ VELM n-groups 46, 45, 44, 43, 42,
        0 0  50.7    0 0  54.0    0 0  69.0    0 0  46.7    0 0  62.6    $ VELM n-groups 41, 40, 39, 38, 37,
        0 0  67.5    0 0  79.8    0 0  52.9    0 0  56.7    0 0  47.4    $ VELM n-groups 36, 35, 34, 33, 32,
        0 0  45.7    0 0  45.6    0 0  42.5    0 0  48.9    0 0  34.2    $ VELM n-groups 31, 30, 29, 28, 27,
        0 0  42.4    0 0  63.8    0 0  53.7    0 0  42.3    0 0  49.6    $ VELM n-groups 26, 25, 24, 23, 22,
        0 0  58.8    0 0  52.9    0 0  50.3    0 0  56.8    0 0  44.1    $ VELM n-groups 21, 20, 19, 18, 17,
        0 0  70.1    0 0  46.8    0 0  59.7    0 0  50.2    0 0  52.1    $ VELM n-groups 16, 15, 14, 13, 12,
        0 0  33.3    0 0  43.5    0 0  65.3    0 0  56.9    0 0  47.9    $ VELM n-groups 11, 10,  9,  8,  7,
        0 0  62.6    0 0  59.5    0 0  42.9    0 0  68.7    0 0  31.1    $ VELM n-groups  6,  5,  4,  3,  2,
        0 0  99.9                                                        $ VELM n-group   1
c       Shift sources 1.6986 cm to right of beam tube centerline to account for the anisotropic effect
c       of more neutrons entering the one side of the beam tube than the other:   -- JAB, 4-7-98
c     0 1.6986 67.5  0 1.6986 79.8  0 1.6986 52.9  0 1.6986 56.7  0 1.6986 47.4    $ VELM n-groups 36, 35, 34, 33, 32,
c     0 1.6986 45.7  0 1.6986 45.6  0 1.6986 42.5  0 1.6986 48.9  0 1.6986 34.2    $ VELM n-groups 31, 30, 29, 28, 27,
c     0 1.6986 42.4  0 1.6986 63.8  0 1.6986 53.7  0 1.6986 42.3  0 1.6986 49.6    $ VELM n-groups 26, 25, 24, 23, 22,
c     0 1.6986 58.8  0 1.6986 52.9  0 1.6986 50.3  0 1.6986 56.8  0 1.6986 44.1    $ VELM n-groups 21, 20, 19, 18, 17,
c     0 1.6986 70.1  0 1.6986 46.8  0 1.6986 59.7  0 1.6986 50.2  0 1.6986 52.1    $ VELM n-groups 16, 15, 14, 13, 12,
c     0 1.6986 33.3  0 1.6986 43.5  0 1.6986 65.3  0 1.6986 56.9  0 1.6986 47.9    $ VELM n-groups 11, 10,  9,  8,  7,
c     0 1.6986 62.6  0 1.6986 59.5  0 1.6986 42.9  0 1.6986 68.7  0 1.6986 31.1    $ VELM n-groups  6,  5,  4,  3,  2,
c     0 1.6986 99.9                                                    $ VELM n-group   1
c      ------------------------------------------------------------------------------
c      Begin distributions needed to describe the gamma sources in the HB-3 beam tube
c      ------------------------------------------------------------------------------
c      si73  h  1.0000e-2   $ this one Emin(MeV), followed by Emax(MeV) for the 23 VELM gamma grps (lowest to highest energy for MCNP):
c               2.0000e-2    4.5000e-2    7.0000e-2    1.0000e-1    1.5000e-1    $ VELM g-groups 23, 22, 21, 20, 19,
c               3.0000e-1    4.0000e-1    5.1000e-1    6.0000e-1    7.0000e-1    $ VELM g-groups 18, 17, 16, 15, 14,
c               1.0000e+0    1.5000e+0    2.0000e+0    2.5000e+0    3.0000e+0    $ VELM g-groups 13, 12, 11, 10,  9,
c               4.0000e+0    5.0000e+0    6.0000e+0    7.0000e+0    7.5000e+0    $ VELM g-groups  8,  7,  6,  5,  4,
c               8.0000e+0    1.0000e+1    1.4000e+1                              $ VELM g-groups  3,  2,  1
c      sp73  d     0.0  $ dummy 0, followed by gamma src terms (p/s) for HB-3:
c               8.72837e+12  2.84514e+15  1.65029e+16  1.67705e+16  1.82855e+16  $ VELM g-groups 23, 22, 21, 20, 19,
c               .56708e+16  1.03805e+16  7.17665e+15  4.80101e+15  4.03975e+    $ VELM g-groups 18, 17, 16, 15, 14,
c               .31636e+15  5.27935e+15  4.23989e+15  2.66951e+15  1.42777e+    $ VELM g-groups 13, 12, 11, 10,  9,
```

```
c                2.34929e+15  1.98361e+15  6.75453e+14  1.23378e+15  1.60183e+14  $ VELM g-groups  8,  7,  6,  5,  4,
c                1.51983e+15  6.19421e+13  1.23250e+11                            $ VELM g-groups  3,  2,  1
c       sb73  d     0.0  $ dummy 0, followed by "biased" gamma src terms (p/s) for HB-3:
c       c        ------------------------------------------------------------------------
c       c        Biased gamma sources in MCNP order (grp 1=low E, grp 23=high E);
c       c        Calculated using GETWING.SCR and GBANISN in adjoint mode, where the
c       c        adjoint sources at Z=478.49 cm were just the gamma flux-to-dose-rate factors;
c       c        Use these values for the gamma-only mcnp calc with a gamma-only source.
c       c        (For a coupled n/g calc with a neutron-only source, or for a neutron-only
c       c        calc with a neutron-only source, these values would be different).
c       c        Note that this can/should only be used with the corresponding weight
c       c        window file prepared by GETWING.SCR where the space/energy weights for
c       c        the gamma groups were calculated using the data in GETADJ.OUT.
c       c        ------------------------------------------------------------------------
c       c        To work well (or even to work "at all") everything MUST be self-consistent !!!!!
c       c        ------------------------------------------------------------------------
c            .   6.39635E-03  2.08498E+00  1.20937E+01  1.22898E+01  1.34000E+01  $ VELM g-groups 23, 22, 21, 20, 19,
c                1.88122E+01  3.98199E+08  2.75298E+08  1.84168E+08  1.54966E+08  $ VELM g-groups 18, 17, 16, 15, 14,
c                2.80658E+08  1.61658E+14  1.29829E+14  8.17425E+13  4.37194E+13  $ VELM g-groups 13, 12, 11, 10,  9,
c                7.19371E+13  3.75947E+16  1.28016E+16  2.33834E+16  3.03589E+15  $ VELM g-groups  8,  7,  6,  5,  4,
c                2.88048E+16  1.17397E+15  2.33592E+12                            $ VELM g-groups  3,  2,  1
c       ds83  1     $ gamma starting positions (x,y,z) in HB-3:
c                0 0  10.01   0 0  61.9    0 0  68.1    0 0  82.1    0 0  83.9    $ VELM g-groups 23, 22, 21, 20, 19,
c                0 0  84.5    0 0  81.6    0 0  84.7    0 0  88.8    0 0  83.2    $ VELM g-groups 18, 17, 16, 15, 14,
c                0 0  86.8    0 0  93.6    0 0  96.9    0 0  99.2    0 0  96.6    $ VELM g-groups 13, 12, 11, 10,  9,
c                0 0  92.6    0 0  93.2    0 0  96.4    0 0  93.9    0 0  96.0    $ VELM g-groups  8,  7,  6,  5,  4,
c                0 0  94.4    0 0  99.9    0 0  97.4                            $ VELM g-groups  3,  2,  1
c
c       ------------------------------------
c       QADD2.FOR analysis has shown that if the water tube & collimator are BOTH FLOODED, VELM source groups 1-8 account for 98-99%
c       of the dose rate downstream of the collimator.  (By the time they get there, of course, the photons may have less energy.)
c     * Thus, "for this particular FLOODED case", it is sufficient to include source photons from these first 8 VELM groups only.
c     * The photon source in VELM grps 1-8 (above 3.0 MeV) = 7.984211E+15 p/s (subtotal for these groups).  For this particular
c     * FLOODED case, this value may be used, but the SI73, SP73, DS83, any SB73 card, and "all" FM tally cards must be consistent.
c
si73  h  3.0000e+0   $ this one Emin(MeV), followed by Emax(MeV) for VELM gamma grps 1-8 (lowest to highest energy for MCNP):
         4.0000e+0    5.0000e+0    6.0000e+0    7.0000e+0    7.5000e+0    $ VELM g-groups  8,  7,  6,  5,  4,
         8.0000e+0    1.0000e+1    1.4000e+1                              $ VELM g-groups  3,  2,  1
sp73  d     0.0  $ dummy 0, followed by gamma src terms (p/s) for HB-3:
         2.34929e+15  1.98361e+15  6.75453e+14  1.23378e+15  1.60183e+14  $ VELM g-groups  8,  7,  6,  5,  4,
         1.51983e+15  6.19421e+13  1.23250e+11                            $ VELM g-groups  3,  2,  1
ds83  1     $ gamma starting positions (x,y,z) in HB-3:
         0 0  92.6    0 0  93.2    0 0  96.4    0 0  93.9    0 0  96.0    $ VELM g-groups  8,  7,  6,  5,  4,
         0 0  94.4    0 0  99.9    0 0  97.4                              $ VELM g-groups  3,  2,  1
c       ------------------------------------
c
c
c       BEGIN-TRANSFORMATIONS:
c
c       Transformations that can/should be used for the holes in the beam tube shield plug (ie, the rotary shutter):
c          When big   hole is turned to "open" position:  use tr11 for big hole in shutter, and tr21 for small hole
c          When small hole is turned to "open" position:  use tr12 for big hole in shutter, and tr22 for small hole
c          When shutter    is turned to "off"  position:  use tr13 for big hole in shutter, and tr23 for small hole
c       ------------------------------------------------------------------------------------------------------------
*tr11  $ use tr11 for big hole in shutter, when big hole is turned to "open" position
       0.0  0.0  446.405  $ location of local origin (center of shutter), relative to the global origin (cm) in HB-3 model
         0    90   90     $ degrees from global x,y,z axes to local x axis
        90     0   90     $ degrees from global x,y,z axes to local y axis
```

```
        90    90    0     $ degrees from global x,y,z axes to local z axis
c
*tr12  $ use tr12 for big hole in shutter, when small hole is turned to "open" position
       0.0  0.0  446.405  $ location of local origin (center of shutter), relative to the global origin (cm) in HB-3 model
         0    90    90    $ degrees from global x,y,z axes to local x axis
        90  -46.5  -136.5 $ degrees from global x,y,z axes to local y axis
        90   43.5  -46.5  $ degrees from global x,y,z axes to local z axis
c
*tr13  $ use tr13 for big hole in shutter, when shutter is turned to "off" position
       0.0  0.0  446.405    $ location of local origin (center of shutter), relative to the global origin (cm) in HB-3 model
         0    90      90    $ degrees from global x,y,z axes to local x axis
        90  -113.25 -203.25 $ degrees from global x,y,z axes to local y axis
        90  -23.25  -113.25 $ degrees from global x,y,z axes to local z axis
c
*tr21  $ use tr21 for small hole in shutter, when big hole is turned to "open" position
       0.0  0.0  446.405    $ location of local origin (center of shutter), relative to the global origin (cm) in HB-3 model
         0    90    90      $ degrees from global x,y,z axes to local x axis
        90   46.5 -43.5     $ degrees from global x,y,z axes to local y axis
        90  136.5  46.5     $ degrees from global x,y,z axes to local z axis
c
*tr22  $ use tr22 for small hole in shutter, when small hole is turned to "open" position
       0.0  0.0  446.405    $ location of local origin (center of shutter), relative to the global origin (cm) in HB-3 model
         0    90   90       $ degrees from global x,y,z axes to local x axis
        90     0   90       $ degrees from global x,y,z axes to local y axis
        90    90    0       $ degrees from global x,y,z axes to local z axis
c
*tr23  $ use tr23 for small hole in shutter, when shutter is turned to "off" position
       0.0  0.0  446.405    $ location of local origin (center of shutter), relative to the global origin (cm) in HB-3 model
         0    90     90     $ degrees from global x,y,z axes to local x axis
        90  -66.75 -156.75  $ degrees from global x,y,z axes to local y axis
        90   23.25  -66.75  $ degrees from global x,y,z axes to local z axis
c
c       *tr40  $ use tr40 to locate and position the Key 3 dosimetry specimen holder relative to HB-3 beam tube
c              0.0  0.0  113.64     $ location of local origin (center of shutter), relative to the global origin (cm) in HB-3 model
c                0    90   90       $ degrees from global x,y,z axes to local x axis
c               90    14  -76       $ degrees from global x,y,z axes to local y axis
c               90   104   14       $ degrees from global x,y,z axes to local z axis
c
c       *tr40 was revised as follows by JAB on 3 Apr 98 for Run HB304H, based on newly available data shown on Dwg E-49953, Rev A, 6-30-65:
*tr40  $ use tr40 to locate and position the Key 3 dosimetry specimen holder relative to HB-3 beam tube
       0.0  0.0  114.22     $ location of local origin (center of shutter), relative to the global origin (cm) in HB-3 model
         0    90   90       $ degrees from global x,y,z axes to local x axis
        90    13  -77       $ degrees from global x,y,z axes to local y axis
        90   103   13       $ degrees from global x,y,z axes to local z axis
c
c       $ incorrect & obsolete:   *tr42  $ use tr42 to locate and position the elliptical cone used to define chamfer between HB3 vessel hole and inner surf
 of pressure vessel
c       $ incorrect & obsolete:          0.0  -2.14265  128.18364   $ location of local origin (center of elliptical cone), relative to the global origin (c
m) in HB-3 model
c       $ incorrect & obsolete:            0    90.0000    90.0000  $ degrees from global x,y,z axes to local x axis
c       $ incorrect & obsolete:           90    12.6575   -77.3425  $ degrees from global x,y,z axes to local y axis
c       $ incorrect & obsolete:           90   102.6575    12.6575  $ degrees from global x,y,z axes to local z axis
c
c       The following correction to *tr42 was made by JAB on 6 Apr 98, just prior to submitting Run HB304K:
c
*tr42  $ use tr42 to locate and position the elliptical cone used to define chamfer between HB3 vessel hole and inner surf of pressure vessel
       0.0  -2.14265  127.62367   $ location of local origin (center of elliptical cone), relative to the global origin (cm) in HB-3 model
         0    90.0000    90.0000  $ degrees from global x,y,z axes to local x axis
```

```
        90    12.6929   -77.3071  $ degrees from global x,y,z axes to local y axis
        90   102.6929    12.6929  $ degrees from global x,y,z axes to local z axis
c       ------------------------------------------------------------------------------------------------------------
c       END-TRANSFORMATIONS
c
c
c       BEGIN MATERIAL DESCRIPTIONS:
c
c       Water gaps in removable reflector region     --Avg. Density= 0.98465 g/cm^3
m5      1001.50c     6.63485-02    8016.50c    3.31742-02
mt5     lwtr.01t
c
c       Water Reflector --Density= 0.9899 g/cm^3
m7      1001.50c     6.67022-02    8016.50c    3.33511-02
mt7     lwtr.01t
c
c       H2O Pool  --Density= 1.0000 g/cm^3
m8      1001.50c     6.73828-02    8016.50c    3.36914-02
mt8     lwtr.01t
c
c       Aluminum reflector container (outside Be reflector; 2.7 g/cc)
m23     13027.52c    5.85482-02   1001.50c  3.45716-04  12000.50c  6.68986-04
        14000.50c    3.47363-04  22000.50c  2.54704-05  24000.50c  6.09789-05
        25055.50c    2.21974-05  26000.55c  1.01905-04  29000.50c  8.74557-05
c
c       Aluminum liners in Be reflectors (2.7 g/cc)
m24     13027.52c    5.85482-02   1001.50c  3.45716-04  12000.50c  6.68986-04
        14000.50c    3.47363-04  22000.50c  2.54704-05  24000.50c  6.09789-05
        25055.50c    2.21974-05  26000.55c  1.01905-04  29000.50c  8.74557-05
c
c       ss liner of pressure vessel, bioshield liner, and other components -- SCALE SS304 (7.92 g/cc;  69.5 w/o Fe, 19.0 w/o Cr, 9.5 w/o Ni,  2.0 w/o Mn)
m40     26000.55c  5.93541-02   24000.50c  1.74281-02
        28000.50c  7.71883-03   25055.50c  1.73629-03
c
c       ss (same as above, but diff color on plot) used for removable shield around collimator -- SCALE SS304 (7.92 g/cc; 69.5 w/o Fe, 19.0 w/o Cr, 9.5 w/o
Ni, 2.0 w/o Mn)
m41     26000.55c  5.93541-02   24000.50c  1.74281-02
        28000.50c  7.71883-03   25055.50c  1.73629-03
c
c       carbon steel in main body of pressure vessel -- SCALE Carbon Steel (7.8212 g/cc;  99.0 w/o Fe, 1.0 w/o C)
m50     26000.55c  8.34929-02    6012.50c  3.92134-03
c
c       Void in reflector components
m60     1001.50c   1.00000-15   8016.50c   1.00000-15
c
c       Void regions in the HB-1,2,and 3 beam tubes (m60 @ 2.0e-15 atoms/b-cm) have been replaced with helium-filled regions
c       where m61 = He (void) at T=300 deg.K and P=2 atm, where rho=3.2325e-4 g/cc, N(He)=4.86816e-5 atoms/(barn*cm)
c       Note: cold source vacuum vessel in HB-4 now has a true void (see m610) as of July 1996.
c       ------------------------
c       Helium void inside beam tubes HB-1,2,3 (He at T=300 deg.K, P=2 atm); cold source vacuum vessel in HB-4 now has a true void (see m610)
m61     2004.50c  4.86816e-5  $  add-jab122395:  For He at T=300 deg.K and P=2 atm, rho=3.2325e-4 g/cc, N(He)=4.86816e-5 atoms/(barn*cm)
c
c       Barytes concrete at 3.09725 g/cc (used for biological shield); shown below are atoms/(barn*cm) by nuclide
m62      1001.50c  1.681e-2   5010.50c  3.378e-4   5011.56c  1.368e-3
         8016.50c  4.195e-2  11023.50c  3.193e-4  12000.50c  1.549e-4
        13027.52c  7.534e-4  14000.50c  1.260e-3  16032.50c  5.401e-3
        20000.50c  3.273e-3  22000.50c  1.336e-4  25055.50c  1.713e-4
        26000.55c  6.875e-4  56138.50c  5.394e-3
```

```
c       real concentration for ba-138 = 3.8787e-3 atoms/(barn*cm); it is available;
c       other nuclide concentrations for which there is no mcnp xsect data:
c       ba-134=1.3037e-4;  ba-135=3.5557e-4;  ba-136=4.2364e-4;  ba-137=6.0575e-4
c       total number density for all barium nuclides in barytes concrete: 5.394030e-3
c       total number density for all nuclides in barytes concrete:  7.801382e-2
c       while this barytes concrete (for ANS project) was 3.09725 g/cc, it can
c       sometimes be made as dense as 3.5 g/cc; see book by Schaffer
c
c
m71     28058.24y  1.0  $ Ni58;  this material (m71) is used only to get the Ni58(n,p)Co58 reaction rate [(n,p)=103] in the dosimeters
m72     26054.24y  1.0  $ Fe54;  this material (m72) is used only to get the Fe54(n,p)Mn54 reaction rate [(n,p)=103] in the dosimeters
c
c
c       Typical beryllium used in permanent reflector (with he-3 and li-6, based in center ring, cell 9024)
m108    4009.50c   1.21135-01   1001.50c   1.34766-03   8016.50c   6.73828-04
        3006.50c   4.80664-8    2003.50c   1.39911-9
mt108   be.01t
c
c
c       ------------------------------------------------------------------------------------------------------------------
c       *** start detectors used to get fluxes at different points down HB-3 beam tube; for HFIR at 100 MW
c       ------------------------------------------------------------------------------------------------------------------
c
c
c       fc15   N-Flux (n/s/cm2) at 655.6626 from tip of HB-3 at 100 MW
c       f15:n  0.0  0.0  678.1673  0.5   $ neut flux at pt 655.6629 cm from real tip of HB-3 beam tube, where Blosser & Thomas made measurements in June 1968
 (cf ORNL-TM-2221)
c       c       fm15   9.64595e16  $ sum of equivalent point sources (n/s) in HB-3 for HFIR at 100 MW (Sn=7.5573e18 n/s in global calc);  will yield fluxes i
n n/s/cm2
c       fm15   1.20830e16  $ sum of equivalent point sources (n/s) for grps 1-36 (E>27 keV; use for dosimetry calc only) in HB-3 for HFIR at 100 MW (Sn=7.557
3e18 n/s in global calc);  will yield fluxes in n/s/cm2
c       e15    $ Emax(ig) in MeV; corresponds to no particular group structure; chosen to facilitate comparison with Blosser & Thomas measurements
c              0.4e-6  1.0e-6  1.9e-6  4.0e-6  6.0e-6  25.0e-6  100.0e-6  170.0e-6
c              640.0e-6  2.4e-3  3.8e-3  2.0e-2  0.1  1.0  2.9  6.3  8.1  20.0
c       Note 1:  Comparisons with B&T are fair only if we use aluminum windows 1 & 2 for 1960 design AND use small hole in rotary shutter.
c       Note 2:  B&T tabulated their results with HFIR power normalized to 1.0 MW;  here we have it at 100.0 MW;  must renormalize later.
c       Note 3:  Many of B&T's results are n/s/cm2/eV, therefore must divide some of our results by delta-E later, where appropriate.
c       Note 4:  The energy ranges above were selected after consulting the B&T report, as well as the barn book to check width of certain resonances.
c
c       Note use of dxtran spheres with tallies 24 & 34 seemed to be a problem for the code;
c       kept getting messages saying "bank is full"; therefore try using point detectors instead,
c       and get rid of all the dxtran cards above.
c
c       fc25   N-Flux (n/s/cm2) for dosimeter at Key 3, Position 3 (100 MW)
c       c      f25:n  0.0   13.25424  116.94465  0.5  $ midpoint of dosimeter (in Cell 2581) at Key 3, Position 3, just slightly on HB-4 side of HB-3
c       c      f25:n  0.0   14.54813  117.26726  0.5  $ dosimeter (in Cell 2581) at Key 3, Position 3, just slightly on HB-4 side of HB-3
c       c      f25:n  0.0   15.84202  117.58986  0.5  $ outer edge of dosimeter (in Cell 2581) at Key 3, Position 3, just slightly on HB-4 side of HB-3
c       c      fm25   9.64595e16  $ sum of equivalent point sources (n/s) in HB-3 for HFIR at 100 MW (Sn=7.5573e18 n/s in global calc);  will yield fluxes in
 n/s/cm2
c       c      Midpoint location was revised as follows on 3 Apr 98 (for Runs HB304H & later) based on the very detailed, newly available, information on Dwg
 E-49953, Rev A (6-30-1965):
c       f25:n  0.0   12.52066  117.11062  0.45  $ midpoint of dosimeter (in Cell 2581) at Key 3, Position 3, just slightly on HB-4 side of HB-3
c       c      f25:n  0.75311  12.52066  117.11062  0.45  $ 0.75311 cm above midpoint of dosimeter (in Cell 2581) at Key 3, Position 3, just slightly on HB-4
 side of HB-3
c       c      f25:n -0.75311  12.52066  117.11062  0.45  $ 0.75311 cm below midpoint of dosimeter (in Cell 2581) at Key 3, Position 3, just slightly on HB-4
 side of HB-3
c       fm25   (  0830e16)  $ sum of equivalent point sources (n/s) for grps  (E>27 keV; use for dosimetry calc only) in HB-3 for HFIR at  MW (Sn=7.5
573e18 n/s in  al calc);  will yield fluxes in n/s/cm2
```

```
c             (1.20830e-8  71  103)  $ to get number of (n,p) "reactions/sec" in Ni58;  note that src had to be multiplied by 1e-24 to convert (n,p) xsect 1
03 from barns to cm2
c             (1.20830e-8  72  103)  $ to get number of (n,p) "reactions/sec" in Fe54;  note that src had to be multiplied by 1e-24 to convert (n,p) xsect 1
03 from barns to cm2
c      e25    $ Emax(ig) in MeV; corresponds to no particular group structure; chosen for dosimetry calcs
c             0.027  0.1  1.0  20.0  t
c      c
c      c
c      fc35   N-Flux (n/s/cm2) for dosimeter at Key 3, Position 8 (100 MW)
c      c      f35:n  0.0  -13.25424  110.33535  0.5  $ midpoint of dosimeter (in Cell 2582) at Key 3, Position 8, just slightly on HB-2 side of HB-3
c      c      f35:n  0.0  -14.54813  110.01274  0.5  $ dosimeter (in Cell 2582) at Key 3, Position 8, just slightly on HB-2 side of HB-3
c      c      f35:n  0.0  -15.84202  109.69014  0.5  $ outer edge of dosimeter (in Cell 2582) at Key 3, Position 8, just slightly on HB-2 side of HB-3
c      c      fm35   9.64595e16  $ sum of equivalent point sources (n/s) in HB-3 for HFIR at 100 MW (Sn=7.5573e18 n/s in global calc);  will yield fluxes in
 n/s/cm2
c      c      Midpoint location was revised as follows on 3 Apr 98 (for Runs HB304H & later) based on the very detailed, newly available, information on Dwg
 E-49953, Rev A (6-30-1965):
c      f35:n  0.0  -12.52066  111.32938  0.45  $ midpoint of dosimeter (in Cell 2582) at Key 3, Position 8, just slightly on HB-2 side of HB-3
c      c      f35:n  0.75311  -12.52066  111.32938  0.45  $ 0.75311 cm above midpoint of dosimeter (in Cell 2582) at Key 3, Position 8, just slightly on HB-
2 side of HB-3
c      c      f35:n -0.75311  -12.52066  111.32938  0.45  $ 0.75311 cm below midpoint of dosimeter (in Cell 2582) at Key 3, Position 8, just slightly on HB-
2 side of HB-3
c      fm35   (1.20830e16)  $ sum of equivalent point sources (n/s) for grps 1-36 (E>27 keV; use for dosimetry calc only) in HB-3 for HFIR at 100 MW (Sn=7.5
573e18 n/s in global calc);  will yield fluxes in n/s/cm2
c             (1.20830e-8  71  103)  $ to get number of (n,p) "reactions/sec" in Ni58;  note that src had to be multiplied by 1e-24 to convert (n,p) xsect 1
03 from barns to cm2
c             (1.20830e-8  72  103)  $ to get number of (n,p) "reactions/sec" in Fe54;  note that src had to be multiplied by 1e-24 to convert (n,p) xsect 1
03 from barns to cm2
c      e35    $ Emax(ig) in MeV; corresponds to no particular group structure; chosen for dosimetry calcs
c             0.027  0.1  1.0  20.0  t
c
c
c      ------------------------------------------------------------------------------------------------------------------------
c      *** start detectors used to get primary gamma fluxes at different points down HB-3 beam tube; for HFIR at 100 MW
c      ------------------------------------------------------------------------------------------------------------------------
c
c      Generally applicable note of great importance:
c      ----------------------------------------------
c      QADD2.FOR analysis has shown that if the water tube & collimator are BOTH FLOODED, VELM source groups 1-8 account for 98-99%
c      of the dose rate downstream of the collimator.  (By the time they get there, of course, the photons may have less energy.)
c      Thus, "for this particular FLOODED case", it is sufficient to include source photons from these first 8 VELM groups only.
c      The photon source in VELM grps 1-8 (above 3.0 MeV) = 7.984211E+15 p/s (subtotal for these groups).  For this particular
c      FLOODED case, this value may be used, but the SI73, SP73, DS83, any SB73 card, and "all" FM tally cards MUST all be consistent.
c      ----------------------------------------------
c
fc15   G-Flux (p/s/cm2) midway between collimator & shutter at 100 MW
f15:p  0.0  0.0  407.46438  0.5   $ G-Flux (p/s/cm2) midway between collimator & shutter at 100 MW
c      fm15   1.35399e+17  $ based on VELM gamma groups 1-23; sum of equivalent point sources (p/s) in HB-3 for HFIR at 100 MW (Sn=7.5573e18 n/s in global c
alc);  will yield fluxes in p/s/cm2
fm15   7.984211E+15  $ based on VELM gamma groups 1-8 only; for FLOODED case only; must be used consistently with SI73, SP73, SB73 & DS83 data
e15    $  Emax(MeV) for the 23 VELM gamma grps (lowest to highest energy for MCNP):
       2.0000e-2    4.5000e-2    7.0000e-2    1.0000e-1    1.5000e-1    $ VELM g-groups 23, 22, 21, 20, 19,
       3.0000e-1    4.0000e-1    5.1000e-1    6.0000e-1    7.0000e-1    $ VELM g-groups 18, 17, 16, 15, 14,
       1.0000e+0    1.5000e+0    2.0000e+0    2.5000e+0    3.0000e+0    $ VELM g-groups 13, 12, 11, 10,  9,
       4.0000e+0    5.0000e+0    6.0000e+0    7.0000e+0    7.5000e+0    $ VELM g-groups  8,  7,  6,  5,  4,
       8.0000e+0    1.0000e+1    1.4000e+1                              $ VELM g-groups  3,  2,  1
c
fc25   G-Dose (mrem/hr) midway between collimator & shutter at 100 MW
f25:p  0.0  0.0  407.46438  0.5   $ G-Dose (mrem/hr) midway between collimator & shutter at 100 MW
```

```
c       fm25   1.35399e+17  $ based on VELM gamma groups 1-23; sum of equivalent point sources (p/s) in HB-3 for HFIR at 100 MW (Sn=7.5573e18 n/s in global c
alc);  will yield fluxes in p/s/cm2
fm25   7.984211E+15  $ based on VELM gamma groups 1-8 only; for FLOODED case only; must be used consistently with SI73, SP73, SB73 & DS83 data
c      ---------------------------------------------------
e25    $ Gamma energy boundaries (Emax, in MeV) from VELM 61n/23g structure:
       1.00000e-02  2.00000e-02  4.50000e-02  7.00000e-02  1.00000e-01
       1.50000e-01  3.00000e-01  4.00000e-01  5.10000e-01  6.00000e-01
       7.00000e-01  1.00000e+00  1.50000e+00  2.00000e+00  2.50000e+00
       3.00000e+00  4.00000e+00  5.00000e+00  6.00000e+00  7.00000e+00
       7.50000e+00  8.00000e+00  1.00000e+01  1.40000e+01
em25   $ Gamma flux-to-dose-rate conversion factors [(mrem/hr)/(p/s/cm2)] for the VELM 61n/23g xsect library,
c      calculated as prescribed in ANSI/ANS-6.1.1-1977, with groups arranged here in order of "increasing"
c      energy for use in MCNP;  first value here corresponds to non-existant group below 1.0e-2 MeV:
       0.00000e+00  2.14390e-03  5.77610e-04  2.74660e-04  2.66440e-04
       3.27670e-04  5.66760e-04  8.75940e-04  1.08520e-03  1.27970e-03
       1.44170e-03  1.75630e-03  2.31560e-03  2.92700e-03  3.46860e-03
       3.95960e-03  4.62210e-03  5.41360e-03  6.19090e-03  6.92650e-03
       7.47830e-03  7.84680e-03  8.77160e-03  1.10200e-02
c
c
fc35   G-Flux (p/s/cm2) 0.5 cm past conc box containing shutter, at 100 MW
c      Rotary shutter centered at Z=446.405 cm; downstream edge of shutter at Z=477.36125 cm;
c      Downstream surf of SS liner on concrete box containing shutter is at Surf 3001 (Z=478.79 cm);
c      This detector is located 0.5 cm downstream of Surf 3001
f35:p  0.0  0.0  479.29  0.49  $ G-Flux (p/s/cm2) midway between collimator & shutter at 100 MW
c      fm35   1.35399e+17  $ based on VELM gamma groups 1-23; sum of equivalent point sources (p/s) in HB-3 for HFIR at 100 MW (Sn=7.5573e18 n/s in global c
alc);  will yield fluxes in p/s/cm2
fm35   7.984211E+15  $ based on VELM gamma groups 1-8 only; for FLOODED case only; must be used consistently with SI73, SP73, SB73 & DS83 data
e35    $  Emax(MeV) for the 23 VELM gamma grps (lowest to highest energy for MCNP):
       2.0000e-2    4.5000e-2    7.0000e-2    1.0000e-1    1.5000e-1    $ VELM g-groups 23, 22, 21, 20, 19,
       3.0000e-1    4.0000e-1    5.1000e-1    6.0000e-1    7.0000e-1    $ VELM g-groups 18, 17, 16, 15, 14,
       1.0000e+0    1.5000e+0    2.0000e+0    2.5000e+0    3.0000e+0    $ VELM g-groups 13, 12, 11, 10,  9,
       4.0000e+0    5.0000e+0    6.0000e+0    7.0000e+0    7.5000e+0    $ VELM g-groups  8,  7,  6,  5,  4,
       8.0000e+0    1.0000e+1    1.4000e+1                              $ VELM g-groups  3,  2,  1
c
fc45   G-Dose (mrem/hr) 0.5 cm past conc box containing shutter, at 100 MW
c      Rotary shutter centered at Z=446.405 cm; downstream edge of shutter at Z=477.36125 cm;
c      Downstream surf of SS liner on concrete box containing shutter is at Surf 3001 (Z=478.79 cm);
c      This detector is located 0.5 cm downstream of Surf 3001
f45:p  0.0  0.0  479.29  0.49  $ G-Dose (mrem/hr) midway between collimator & shutter at 100 MW
c      fm45   1.35399e+17  $ based on VELM gamma groups 1-23; sum of equivalent point sources (p/s) in HB-3 for HFIR at 100 MW (Sn=7.5573e18 n/s in global c
alc);  will yield fluxes in p/s/cm2
fm45   7.984211E+15  $ based on VELM gamma groups 1-8 only; for FLOODED case only; must be used consistently with SI73, SP73, SB73 & DS83 data
e45    $ Gamma energy boundaries (Emax, in MeV) from VELM 61n/23g structure:
       1.00000e-02  2.00000e-02  4.50000e-02  7.00000e-02  1.00000e-01
       1.50000e-01  3.00000e-01  4.00000e-01  5.10000e-01  6.00000e-01
       7.00000e-01  1.00000e+00  1.50000e+00  2.00000e+00  2.50000e+00
       3.00000e+00  4.00000e+00  5.00000e+00  6.00000e+00  7.00000e+00
       7.50000e+00  8.00000e+00  1.00000e+01  1.40000e+01
em45   $ Gamma flux-to-dose-rate conversion factors [(mrem/hr)/(p/s/cm2)] for the VELM 61n/23g xsect library,
c      calculated as prescribed in ANSI/ANS-6.1.1-1977, with groups arranged here in order of "increasing"
c      energy for use in MCNP;  first value here corresponds to non-existant group below 1.0e-2 MeV:
       0.00000e+00  2.14390e-03  5.77610e-04  2.74660e-04  2.66440e-04
       3.27670e-04  5.66760e-04  8.75940e-04  1.08520e-03  1.27970e-03
       1.44170e-03  1.75630e-03  2.31560e-03  2.92700e-03  3.46860e-03
       3.95960e-03  4.62210e-03  5.41360e-03  6.19090e-03  6.92650e-03
       7.47830e-03  7.84680e-03  8.77160e-03  1.10200e-02
c
```

```
c
fc55   G-Flux (p/s/cm2) 1.5 feet past conc box containing shutter, at 100 MW
c      Rotary shutter centered at Z=446.405 cm; downstream edge of shutter at Z=477.36125 cm;
c      Downstream surf of SS liner on concrete box containing shutter is at Surf 3001 (Z=478.79 cm);
c      This detector is located 1.5 feet downstream of Surf 3001
f55:p  0.0  0.0  524.51  5.0   $ G-Flux (p/s/cm2) midway between collimator & shutter at 100 MW
c      fm55   1.35399e+17  $ based on VELM gamma groups 1-23; sum of equivalent point sources (p/s) in HB-3 for HFIR at 100 MW (Sn=7.5573e18 n/s in global c
alc);  will yield fluxes in p/s/cm2
fm55   7.984211E+15  $ based on VELM gamma groups 1-8 only; for FLOODED case only; must be used consistently with SI73, SP73, SB73 & DS83 data
e55    $  Emax(MeV) for the 23 VELM gamma grps (lowest to highest energy for MCNP):
       2.0000e-2    4.5000e-2    7.0000e-2    1.0000e-1    1.5000e-1    $ VELM g-groups 23, 22, 21, 20, 19,
       3.0000e-1    4.0000e-1    5.1000e-1    6.0000e-1    7.0000e-1    $ VELM g-groups 18, 17, 16, 15, 14,
       1.0000e+0    1.5000e+0    2.0000e+0    2.5000e+0    3.0000e+0    $ VELM g-groups 13, 12, 11, 10,  9,
       4.0000e+0    5.0000e+0    6.0000e+0    7.0000e+0    7.5000e+0    $ VELM g-groups  8,  7,  6,  5,  4,
       8.0000e+0    1.0000e+1    1.4000e+1                              $ VELM g-groups  3,  2,  1
c
fc65   G-Dose (mrem/hr) 1.5 feet past conc box containing shutter, at 100 MW
c      Rotary shutter centered at Z=446.405 cm; downstream edge of shutter at Z=477.36125 cm;
c      Downstream surf of SS liner on concrete box containing shutter is at Surf 3001 (Z=478.79 cm);
c      This detector is located 1.5 feet downstream of Surf 3001
f65:p  0.0  0.0  524.51  5.0   $ G-Dose (mrem/hr) midway between collimator & shutter at 100 MW
c      fm65   1.35399e+17  $ based on VELM gamma groups 1-23; sum of equivalent point sources (p/s) in HB-3 for HFIR at 100 MW (Sn=7.5573e18 n/s in global c
alc);  will yield fluxes in p/s/cm2
fm65   7.984211E+15  $ based on VELM gamma groups 1-8 only; for FLOODED case only; must be used consistently with SI73, SP73, SB73 & DS83 data
e65    $ Gamma energy boundaries (Emax, in MeV) from VELM 61n/23g structure:
       1.00000e-02  2.00000e-02  4.50000e-02  7.00000e-02  1.00000e-01
       1.50000e-01  3.00000e-01  4.00000e-01  5.10000e-01  6.00000e-01
       7.00000e-01  1.00000e+00  1.50000e+00  2.00000e+00  2.50000e+00
       3.00000e+00  4.00000e+00  5.00000e+00  6.00000e+00  7.00000e+00
       7.50000e+00  8.00000e+00  1.00000e+01  1.40000e+01
em65   $ Gamma flux-to-dose-rate conversion factors [(mrem/hr)/(p/s/cm2)] for the VELM 61n/23g xsect library,
c      calculated as prescribed in ANSI/ANS-6.1.1-1977, with groups arranged here in order of "increasing"
c      energy for use in MCNP;  first value here corresponds to non-existant group below 1.0e-2 MeV:
       0.00000e+00  2.14390e-03  5.77610e-04  2.74660e-04  2.66440e-04
       3.27670e-04  5.66760e-04  8.75940e-04  1.08520e-03  1.27970e-03
       1.44170e-03  1.75630e-03  2.31560e-03  2.92700e-03  3.46860e-03
       3.95960e-03  4.62210e-03  5.41360e-03  6.19090e-03  6.92650e-03
       7.47830e-03  7.84680e-03  8.77160e-03  1.10200e-02
c
c
fc75   G-Flux (p/s/cm2) 3 feet past conc box containing shutter, at 100 MW
c      Rotary shutter centered at Z=446.405 cm; downstream edge of shutter at Z=477.36125 cm;
c      Downstream surf of SS liner on concrete box containing shutter is at Surf 3001 (Z=478.79 cm);
c      This detector is located 3 feet downstream of Surf 3001
f75:p  0.0  0.0  570.23  5.0   $ G-Flux (p/s/cm2) midway between collimator & shutter at 100 MW
c      fm75   1.35399e+17  $ based on VELM gamma groups 1-23; sum of equivalent point sources (p/s) in HB-3 for HFIR at 100 MW (Sn=7.5573e18 n/s in global c
alc);  will yield fluxes in p/s/cm2
fm75   7.984211E+15  $ based on VELM gamma groups 1-8 only; for FLOODED case only; must be used consistently with SI73, SP73, SB73 & DS83 data
e75    $  Emax(MeV) for the 23 VELM gamma grps (lowest to highest energy for MCNP):
       2.0000e-2    4.5000e-2    7.0000e-2    1.0000e-1    1.5000e-1    $ VELM g-groups 23, 22, 21, 20, 19,
       3.0000e-1    4.0000e-1    5.1000e-1    6.0000e-1    7.0000e-1    $ VELM g-groups 18, 17, 16, 15, 14,
       1.0000e+0    1.5000e+0    2.0000e+0    2.5000e+0    3.0000e+0    $ VELM g-groups 13, 12, 11, 10,  9,
       4.0000e+0    5.0000e+0    6.0000e+0    7.0000e+0    7.5000e+0    $ VELM g-groups  8,  7,  6,  5,  4,
       8.0000e+0    1.0000e+1    1.4000e+1                              $ VELM g-groups  3,  2,  1
c
fc85   G-Dose (mrem/hr) 3 feet past conc box containing shutter, at 100 MW
c      Rotary shutter centered at Z=446.405 cm; downstream edge of shutter at Z=477.36125 cm;
c      Downstream surf of SS liner on concrete box containing shutter is at Surf 3001 (Z=478.79 cm);
```

```
c       This detector is located 3 feet downstream of Surf 3001
f85:p  0.0  0.0  570.23  5.0   $ G-Dose (mrem/hr) midway between collimator & shutter at 100 MW
c       fm85   1.35399e+17  $ based on VELM gamma groups 1-23; sum of equivalent point sources (p/s) in HB-3 for HFIR at 100 MW (Sn=7.5573e18 n/s in global c
alc);  will yield fluxes in p/s/cm2
fm85    7.984211E+15  $ based on VELM gamma groups 1-8 only; for FLOODED case only; must be used consistently with SI73, SP73, SB73 & DS83 data
e85     $ Gamma energy boundaries (Emax, in MeV) from VELM 61n/23g structure:
        1.00000e-02  2.00000e-02  4.50000e-02  7.00000e-02  1.00000e-01
        1.50000e-01  3.00000e-01  4.00000e-01  5.10000e-01  6.00000e-01
        7.00000e-01  1.00000e+00  1.50000e+00  2.00000e+00  2.50000e+00
        3.00000e+00  4.00000e+00  5.00000e+00  6.00000e+00  7.00000e+00
        7.50000e+00  8.00000e+00  1.00000e+01  1.40000e+01
em85    $ Gamma flux-to-dose-rate conversion factors [(mrem/hr)/(p/s/cm2)] for the VELM 61n/23g xsect library,
c       calculated as prescribed in ANSI/ANS-6.1.1-1977, with groups arranged here in order of "increasing"
c       energy for use in MCNP;  first value here corresponds to non-existant group below 1.0e-2 MeV:
        0.00000e+00  2.14390e-03  5.77610e-04  2.74660e-04  2.66440e-04
        3.27670e-04  5.66760e-04  8.75940e-04  1.08520e-03  1.27970e-03
        1.44170e-03  1.75630e-03  2.31560e-03  2.92700e-03  3.46860e-03
        3.95960e-03  4.62210e-03  5.41360e-03  6.19090e-03  6.92650e-03
        7.47830e-03  7.84680e-03  8.77160e-03  1.10200e-02
c
c
fc184   Appx G-Dose (mrem/hr) axially, up thru the water tube, at 100 MW
f184:p  2145   $ Appx G-Dose (mrem/hr) axially, up thru the water tube (Cell 2145), at 100 MW
c       fm184   1.35399e+17  $ based on VELM gamma groups 1-23; sum of equivalent point sources (p/s) in HB-3 for HFIR at 100 MW (Sn=7.5573e18 n/s in global
 calc);  will yield fluxes in p/s/cm2
fm184   7.984211E+15  $ based on VELM gamma groups 1-8 only; for FLOODED case only; must be used consistently with SI73, SP73, SB73 & DS83 data
c       ---------------------------------------------------------------------
c       Note:  Dose rates obtained using (e,em) are correct;  those obtained using (de,df) are approximate;  here I chose
c       to use (de,df) because I only wanted ONE "appx" number for the total gamma dose rate in each tally segment.
c       ---------------------------------------------------------------------
c       e184   $ Gamma energy boundaries (Emax, in MeV) from VELM 61n/23g structure:
c              1.00000e-02  2.00000e-02  4.50000e-02  7.00000e-02  1.00000e-01
c              1.50000e-01  3.00000e-01  4.00000e-01  5.10000e-01  6.00000e-01
c              7.00000e-01  1.00000e+00  1.50000e+00  2.00000e+00  2.50000e+00
c              3.00000e+00  4.00000e+00  5.00000e+00  6.00000e+00  7.00000e+00
c              7.50000e+00  8.00000e+00  1.00000e+01  1.40000e+01
c       em184   $ Gamma flux-to-dose-rate conversion factors [(mrem/hr)/(p/s/cm2)] for the VELM 61n/23g xsect library,
c       c       calculated as prescribed in ANSI/ANS-6.1.1-1977, with groups arranged here in order of "increasing"
c       c       energy for use in MCNP;  first value here corresponds to non-existant group below 1.0e-2 MeV:
c              0.00000e+00  2.14390e-03  5.77610e-04  2.74660e-04  2.66440e-04
c              3.27670e-04  5.66760e-04  8.75940e-04  1.08520e-03  1.27970e-03
c              1.44170e-03  1.75630e-03  2.31560e-03  2.92700e-03  3.46860e-03
c              3.95960e-03  4.62210e-03  5.41360e-03  6.19090e-03  6.92650e-03
c              7.47830e-03  7.84680e-03  8.77160e-03  1.10200e-02
c       ---------------------------------------------------------------------
de184   $ Gamma energy points (MeV) supposedly corresponding to the flux-to-dose-rate factors below
        1.00000e-02  2.00000e-02  4.50000e-02  7.00000e-02  1.00000e-01
        1.50000e-01  3.00000e-01  4.00000e-01  5.10000e-01  6.00000e-01
        7.00000e-01  1.00000e+00  1.50000e+00  2.00000e+00  2.50000e+00
        3.00000e+00  4.00000e+00  5.00000e+00  6.00000e+00  7.00000e+00
        7.50000e+00  8.00000e+00  1.00000e+01  1.40000e+01
df184   $ Gamma flux-to-dose-rate conversion factors [(mrem/hr)/(p/s/cm2)] "near" above energy points (based on VELM 61n/23g xsect library)
        2.14390e-03  2.14390e-03  5.77610e-04  2.74660e-04  2.66440e-04
        3.27670e-04  5.66760e-04  8.75940e-04  1.08520e-03  1.27970e-03
        1.44170e-03  1.75630e-03  2.31560e-03  2.92700e-03  3.46860e-03
        3.95960e-03  4.62210e-03  5.41360e-03  6.19090e-03  6.92650e-03
        7.47830e-03  7.84680e-03  8.77160e-03  1.10200e-02
fs184   $ 29 segment divider planes (for 30 equal segments with dz=4.24119 cm  vol=493.55788 cc):
```

```
        -5101  -5102  -5103  -5104  -5105  -5106  -5107  -5108  -5109  -5110
        -5111  -5112  -5113  -5114  -5115  -5116  -5117  -5118  -5119  -5120
        -5121  -5122  -5123  -5124  -5125  -5126  -5127  -5128  -5129
sd184   493.55788  29r  $ volume (cc) for each of the 30 segments
c
c
fc194   Appx G-Dose (mrem/hr) axially, up thru collimator hole, at 100 MW
f194:p  4300   $ Appx G-Dose (mrem/hr) axially, up thru rectangular collimator hole (Cell 4300), at 100 MW
c       fm194   1.35399e+17  $ based on VELM gamma groups 1-23; sum of equivalent point sources (p/s) in HB-3 for HFIR at 100 MW (Sn=7.5573e18 n/s in global
 calc);  will yield fluxes in p/s/cm2
fm194   7.984211E+15  $ based on VELM gamma groups 1-8 only; for FLOODED case only; must be used consistently with SI73, SP73, SB73 & DS83 data
c       ------------------------------------------------------------------------
c       Note:  Dose rates obtained using (e,em) are correct;  those obtained using (de,df) are approximate;  here I chose
c       to use (de,df) because I only wanted ONE "appx" number for the total gamma dose rate in each tally segment.
c       ------------------------------------------------------------------------
c       e194   $ Gamma energy boundaries (Emax, in MeV) from VELM 61n/23g structure:
c              1.00000e-02  2.00000e-02  4.50000e-02  7.00000e-02  1.00000e-01
c              1.50000e-01  3.00000e-01  4.00000e-01  5.10000e-01  6.00000e-01
c              7.00000e-01  1.00000e+00  1.50000e+00  2.00000e+00  2.50000e+00
c              3.00000e+00  4.00000e+00  5.00000e+00  6.00000e+00  7.00000e+00
c              7.50000e+00  8.00000e+00  1.00000e+01  1.40000e+01
c       em194   $ Gamma flux-to-dose-rate conversion factors [(mrem/hr)/(p/s/cm2)] for the VELM 61n/23g xsect library,
c       c      calculated as prescribed in ANSI/ANS-6.1.1-1977, with groups arranged here in order of "increasing"
c       c      energy for use in MCNP;  first value here corresponds to non-existant group below 1.0e-2 MeV:
c              0.00000e+00  2.14390e-03  5.77610e-04  2.74660e-04  2.66440e-04
c              3.27670e-04  5.66760e-04  8.75940e-04  1.08520e-03  1.27970e-03
c              1.44170e-03  1.75630e-03  2.31560e-03  2.92700e-03  3.46860e-03
c              3.95960e-03  4.62210e-03  5.41360e-03  6.19090e-03  6.92650e-03
c              7.47830e-03  7.84680e-03  8.77160e-03  1.10200e-02
c       ------------------------------------------------------------------------
de194   $ Gamma energy points (MeV) supposedly corresponding to the flux-to-dose-rate factors below
        1.00000e-02  2.00000e-02  4.50000e-02  7.00000e-02  1.00000e-01
        1.50000e-01  3.00000e-01  4.00000e-01  5.10000e-01  6.00000e-01
        7.00000e-01  1.00000e+00  1.50000e+00  2.00000e+00  2.50000e+00
        3.00000e+00  4.00000e+00  5.00000e+00  6.00000e+00  7.00000e+00
        7.50000e+00  8.00000e+00  1.00000e+01  1.40000e+01
df194   $ Gamma flux-to-dose-rate conversion factors [(mrem/hr)/(p/s/cm2)] "near" above energy points (based on VELM 61n/23g xsect library)
        2.14390e-03  2.14390e-03  5.77610e-04  2.74660e-04  2.66440e-04
        3.27670e-04  5.66760e-04  8.75940e-04  1.08520e-03  1.27970e-03
        1.44170e-03  1.75630e-03  2.31560e-03  2.92700e-03  3.46860e-03
        3.95960e-03  4.62210e-03  5.41360e-03  6.19090e-03  6.92650e-03
        7.47830e-03  7.84680e-03  8.77160e-03  1.10200e-02
fs194   $ 19 segment divider planes (for 20 equal segments with dz=4.44500 cm & dVol=433.74510 cc):
        -5141  -5142  -5143  -5144  -5145  -5146  -5147  -5148  -5149  -5150
        -5151  -5152  -5153  -5154  -5155  -5156  -5157  -5158  -5159
sd194   433.74510  19r  $ volume (cc) for each of the 20 segments
c
c
fc201   Primary G-Leakage (p/s) at upstream entrance of collimator hole
c       fm201   1.35399e17  $ based on VELM gamma groups 1-23; use for g-only calc; = sum of equivalent point sources (p/s) in HB-3 for HFIR at 100 MW (Sn=7
.5573e18 n/s in global calc);  will yield fluxes in n/s/cm2
fm201   7.984211E+15  $ based on VELM gamma groups 1-8 only; for FLOODED case only; must be used consistently with SI73, SP73, SB73 & DS83 data
c         fc201   Secondary G-Leakage (p/s) at upstream entrance of collimator hole
c         fm201   9.64595e16  $ use for n/g calc; = sum of equivalent point sources (n/s) in HB-3 for HFIR at 100 MW (Sn=7.5573e18 n/s in global calc);  wil
l yield fluxes in n/s/cm2
f201:p  4130   $ surf at upstream entrance of collimator hole
fs201  -4210  4211  -4212  4213  $ the fifth edit ("the remainder") is the leakage (p/s) thru the central rectangular hole in the collimator at downstream e
xit
```

```
sd201   1  1  1  1  1            $ enter area of 1.0 cm2 for all segments (including "remainder") to get "leakage (p/s)" instead of "current (p/s/cm2)"
c201    0.0  1.0    $ only L(z-) and L(z+)
e201    $  Emax(MeV) for the 23 VELM gamma grps (lowest to highest energy for MCNP):
      2.0000e-2    4.5000e-2    7.0000e-2    1.0000e-1    1.5000e-1    $ VELM g-groups 23, 22, 21, 20, 19,
      3.0000e-1    4.0000e-1    5.1000e-1    6.0000e-1    7.0000e-1    $ VELM g-groups 18, 17, 16, 15, 14,
      1.0000e+0    1.5000e+0    2.0000e+0    2.5000e+0    3.0000e+0    $ VELM g-groups 13, 12, 11, 10,  9,
      4.0000e+0    5.0000e+0    6.0000e+0    7.0000e+0    7.5000e+0    $ VELM g-groups  8,  7,  6,  5,  4,
      8.0000e+0    1.0000e+1    1.4000e+1                              $ VELM g-groups  3,  2,  1
fq201  c e s   $ each cosine = new table;  energy grp down vertically;  spatial segments across horizontally
c
c
fc211   Primary G-Leakage (p/s) 2.4945 cm downstream of collimator hole exit
c       fc211   Primary G-Leakage (p/s) at downstream exit of collimator hole
c       fm211   1.35399e17  $ based on VELM gamma groups 1-23; use for g-only calc; = sum of equivalent point sources (p/s) in HB-3 for HFIR at 100 MW (Sn=7
.5573e18 n/s in global calc);  will yield fluxes in n/s/cm2
fm211   7.984211E+15  $ based on VELM gamma groups 1-8 only; for FLOODED case only; must be used consistently with SI73, SP73, SB73 & DS83 data
c         fc211   Secondary G-Leakage (p/s) at downstream exit of collimator hole
c         fm211   9.64595e16  $ use for n/g calc; = sum of equivalent point sources (n/s) in HB-3 for HFIR at 100 MW (Sn=7.5573e18 n/s in global calc);  wil
l yield fluxes in n/s/cm2
f211:p  4198   $ surf 2.4945 cm downstream of collimator hole exit
c         f211:p  4190   $ surf at downstream exit of collimator hole
fs211  -4210  4211  -4212  4213  $ the fifth edit ("the remainder") is the leakage (p/s) thru the central rectangular hole in the collimator at downstream e
xit
sd211   1  1  1  1  1            $ enter area of 1.0 cm2 for all segments (including "remainder") to get "leakage (p/s)" instead of "current (p/s/cm2)"
c211    0.0  1.0    $ only L(z-) and L(z+)
e211    $  Emax(MeV) for the 23 VELM gamma grps (lowest to highest energy for MCNP):
      2.0000e-2    4.5000e-2    7.0000e-2    1.0000e-1    1.5000e-1    $ VELM g-groups 23, 22, 21, 20, 19,
      3.0000e-1    4.0000e-1    5.1000e-1    6.0000e-1    7.0000e-1    $ VELM g-groups 18, 17, 16, 15, 14,
      1.0000e+0    1.5000e+0    2.0000e+0    2.5000e+0    3.0000e+0    $ VELM g-groups 13, 12, 11, 10,  9,
      4.0000e+0    5.0000e+0    6.0000e+0    7.0000e+0    7.5000e+0    $ VELM g-groups  8,  7,  6,  5,  4,
      8.0000e+0    1.0000e+1    1.4000e+1                              $ VELM g-groups  3,  2,  1
fq211  c e s   $ each cosine = new table;  energy grp down vertically;  spatial segments across horizontally
c
c
fc212  Pri G-Dose (mrem/hr) 2.4945 cm downstream of collimator hole exit (seg 5)
c       --------------------------
c       Note:  Only if this boundary crossing estimate of the primary gamma dose rate downstream of the
c       collimator hole has good statistics, is it possible to have a high degree of confidence in the
c       point detector estimates.  If F2 Tally 212 is well converged, F5 Tally 25 will be more accurate;
c       if F2 Tally 212 is not well converged, F5 Tally 25 may or may not be any good (even if stats are good).
c       --------------------------
c       fm212   1.35399e17  $ based on Pri g-source in VELM gamma groups 1-23; use for VOID g-only calc; = sum of equivalent point sources (p/s) in HB-3 for
HFIR at 100 MW (Sn=7.5573e18 n/s in global calc);  will yield fluxes in n/s/cm2
fm212  7.984211E+15  $ based on Pri g-source in VELM gamma groups 1-8 only; use 1-8 for FLOODED case only; must be used consistently with SI73, SP73, SB73 &
 DS83 data
c       fc212  Sec G-Dose (mrem/hr) 2.4945 cm downstream of collimator hole exit (seg 5)
c       fm212  9.64595e16  $ use for n/g calc; = sum of equivalent point sources (n/s) in HB-3 for HFIR at 100 MW (Sn=7.5573e18 n/s in global calc);  will yi
eld fluxes in n/s/cm2
f212:p 4198   $ Surf 4198 is located 2.4945 cm downstream of collimator hole exit
c       f212:p  4190   $ surf at downstream exit of collimator hole
fs212  -4210  4211  -4212  4213  $ the fifth edit ("the remainder") is the leakage (p/s) thru the central rectangular hole in the collimator at downstream e
xit
sd212  $ enter area of all surface segments (including "the remainder") to get flux in "p/s/cm2"
       $ area (cm2) for each of the 5 surface segments at this axial location (segment 5 = "remainder" = central rectangular hole)
       6182.808036  6182.808036   405.016219   405.016219   97.580450  $ calculated analytically
e212   $ Gamma energy boundaries (Emax, in MeV) from VELM 61n/23g structure:
       1.00000e-02  2.00000e-02  4.50000e-02  7.00000e-02  1.00000e-01
       1.50000e-01  3.00000e-01  4.00000e-01  5.10000e-01  6.00000e-01
```

```
      7.00000e-01  1.00000e+00  1.50000e+00  2.00000e+00  2.50000e+00
      3.00000e+00  4.00000e+00  5.00000e+00  6.00000e+00  7.00000e+00
      7.50000e+00  8.00000e+00  1.00000e+01  1.40000e+01
em212  $ Gamma flux-to-dose-rate conversion factors [(mrem/hr)/(p/s/cm2)] for the VELM 61n/23g xsect library,
c      calculated as prescribed in ANSI/ANS-6.1.1-1977, with groups arranged here in order of "increasing"
c      energy for use in MCNP;  first value here corresponds to non-existant group below 1.0e-2 MeV:
      0.00000e+00  2.14390e-03  5.77610e-04  2.74660e-04  2.66440e-04
      3.27670e-04  5.66760e-04  8.75940e-04  1.08520e-03  1.27970e-03
      1.44170e-03  1.75630e-03  2.31560e-03  2.92700e-03  3.46860e-03
      3.95960e-03  4.62210e-03  5.41360e-03  6.19090e-03  6.92650e-03
      7.47830e-03  7.84680e-03  8.77160e-03  1.10200e-02
fq212  e s   $ print control:  energy grp down vertically;  spatial segments across horizontally
c
c
fc221   Primary G-Leakage (p/s) 2.4945 cm downstream of collimator hole exit
c       fc221   Primary G-Leakage (p/s) at downstream exit of collimator hole
c       fm221   1.35399e17  $ based on VELM gamma groups 1-23; use for g-only calc; = sum of equivalent point sources (p/s) in HB-3 for HFIR at 100 MW (Sn=7
.5573e18 n/s in global calc);  will yield fluxes in n/s/cm2
fm221   7.984211E+15  $ based on VELM gamma groups 1-8 only; for FLOODED case only; must be used consistently with SI73, SP73, SB73 & DS83 data
c         fc221   Secondary G-Leakage (p/s) at downstream exit of collimator hole
c         fm221   9.64595e16  $ use for n/g calc; = sum of equivalent point sources (n/s) in HB-3 for HFIR at 100 MW (Sn=7.5573e18 n/s in global calc);  wil
l yield fluxes in n/s/cm2
f221:p  4198   $ surf 2.4945 cm downstream of collimator hole exit
c         f221:p  4190   $ surf at downstream exit of collimator hole
fs221  -4210  4211  -4212  4213  $ the fifth edit ("the remainder") is the leakage (p/s) thru the central rectangular hole in the collimator at downstream e
xit
sd221   1  1  1  1  1            $ enter area of 1.0 cm2 for all segments (including "remainder") to get "leakage (p/s)" instead of "current (p/s/cm2)"
c221 -0.99939083  $  0 -  2 deg wrt -Z axis
     -0.99619470  $  2 -  5 deg wrt -Z axis
     -0.98480775  $  5 - 10 deg wrt -Z axis
     -0.93969262  $ 10 - 20 deg wrt -Z axis
     -0.86602540  $ 20 - 30 deg wrt -Z axis
     -0.5         $ 30 - 60 deg wrt -Z axis
      0.0         $ 60 - 90 deg wrt -Z axis
      0.5         $ 60 - 90 deg wrt +Z axis
      0.86602540  $ 30 - 60 deg wrt +Z axis
      0.93969262  $ 20 - 30 deg wrt +Z axis
      0.98480775  $ 10 - 20 deg wrt +Z axis
      0.99619470  $  5 - 10 deg wrt +Z axis
      0.99939083  $  2 -  5 deg wrt +Z axis
      1.0         $  0 -  2 deg wrt +Z axis
e221   $  Emax(MeV) for the 23 VELM gamma grps (lowest to highest energy for MCNP):
     2.0000e-2    4.5000e-2    7.0000e-2    1.0000e-1    1.5000e-1    $ VELM g-groups 23, 22, 21, 20, 19,
     3.0000e-1    4.0000e-1    5.1000e-1    6.0000e-1    7.0000e-1    $ VELM g-groups 18, 17, 16, 15, 14,
     1.0000e+0    1.5000e+0    2.0000e+0    2.5000e+0    3.0000e+0    $ VELM g-groups 13, 12, 11, 10,  9,
     4.0000e+0    5.0000e+0    6.0000e+0    7.0000e+0    7.5000e+0    $ VELM g-groups  8,  7,  6,  5,  4,
     8.0000e+0    1.0000e+1    1.4000e+1                              $ VELM g-groups  3,  2,  1
fq221  c e s   $ each cosine = new table;  energy grp down vertically;  spatial segments across horizontally
c
c
fc231   Primary G-Leakage (p/s) on downstrem surf of box holding shutter, 100 MW
c         1) Rotary shutter is centered at Z=446.405 cm;  downstream edge of shutter is at Z=477.36125 cm;
c            Downstream surf of SS liner on concrete box containing shutter is at Surf 3001 (Z=478.79 cm);
c            That is the surface where this F1 tally is made.
c         2) Purpose of this tally is simply to see IF any real particles are getting here, and to see WHERE they are coming from.
c       fm231   1.35399e17  $ based on VELM gamma groups 1-23; use for g-only calc; = sum of equivalent point sources (p/s) in HB-3 for HFIR at 100 MW (Sn=7
.5573e18 n/s in global calc);  will yield fluxes in n/s/cm2
fm231   7.984211E+15  $ based on VELM gamma groups 1-8 only; for FLOODED case only; must be used consistently with SI73, SP73, SB73 & DS83 data
```

```
c         fc231   Secondary G-Leakage (p/s) at downstream exit of collimator hole
c         fm231   9.64595e16  $ use for n/g calc; = sum of equivalent point sources (n/s) in HB-3 for HFIR at 100 MW (Sn=7.5573e18 n/s in global calc);  wil
l yield fluxes in n/s/cm2
f231:p  3001   $  downstrem surf of SS liner on concrete box containing shutter
fs231   3032  -3022  3072  -3082  3031  -3021  3071  -3081  3110  $ the 10th edit ("the remainder") is the leakage (p/s) thru the central 6.5-inch-diam disk
c       Meaning of surface segments (assuming you're outside where monochrometer drum usually is, looking back towards the shutter):
c       ------------------------------------------------------------
c         1) everything to left  of concrete box holding the shutter
c         2) everything to right of concrete box holding the shutter
c         3) what remains above the concrete box holding the shutter
c         4) what remains below the concrete box holding the shutter
c         5) void gap just to left  of concrete box holding the shutter
c         6) void gap just to right of concrete box holding the shutter
c         7) void gap just above the concrete box holding the shutter
c         8) void gap just below the concrete box holding the shutter
c         9) face of concrete box holding the shutter, except the central 6.5-inch-diam disk directly in front of shutter
c        10) central 6.5-inch-diam disk directly in front of shutter
c       ------------------------------------------------------------
sd231   1  1  1  1  1  1  1  1  1  1  $ enter area of 1.0 cm2 for all segments (including "remainder") to get "leakage (p/s)" instead of "current (p/s/cm2)"
c231    0.0  1.0    $ only L(z-) and L(z+)
e231    $  Emax(MeV) for the 23 VELM gamma grps (lowest to highest energy for MCNP):
      2.0000e-2    4.5000e-2    7.0000e-2    1.0000e-1    1.5000e-1    $ VELM g-groups 23, 22, 21, 20, 19,
      3.0000e-1    4.0000e-1    5.1000e-1    6.0000e-1    7.0000e-1    $ VELM g-groups 18, 17, 16, 15, 14,
      1.0000e+0    1.5000e+0    2.0000e+0    2.5000e+0    3.0000e+0    $ VELM g-groups 13, 12, 11, 10,  9,
      4.0000e+0    5.0000e+0    6.0000e+0    7.0000e+0    7.5000e+0    $ VELM g-groups  8,  7,  6,  5,  4,
      8.0000e+0    1.0000e+1    1.4000e+1                              $ VELM g-groups  3,  2,  1
fq231  c e s   $ each cosine = new table;  energy grp down vertically;  spatial segments across horizontally
c
c
fc232  Primary G-Dose (mrem/hr) on downstrem surf of box holding shutter; seg 10
c       --------------------------
c       Note:  Only if this boundary crossing estimate of the primary gamma dose rate downstream of the
c       central 6.5-inch-diam disk directly in front of the shutter (seg 10) [and perhaps segments 5-9 also]
c       has good statistics, is it possible to have a high degree of confidence in the point detector estimates.
c       If F2 Tally 232 is well converged in segments 5-10, then F5 Tallies 45, 65 and 85 will be very accurate;
c       if F2 Tally 232 is not well converged, F5 Tallies 45, 65 and 85 may or may not be any good (even if stats are good).
c       --------------------------
c       1) Rotary shutter is centered at Z=446.405 cm;  downstream edge of shutter is at Z=477.36125 cm;
c          Downstream surf of SS liner on concrete box containing shutter is at Surf 3001 (Z=478.79 cm);
c          That is the surface where this F2 tally is made.
c       2) Purpose of this tally is simply to see IF any real particles are getting here, and to see WHERE they are coming from.
c       --------------------------
c        fm232   1.35399e17  $ based on Pri g-source in VELM gamma groups 1-23; use for VOID g-only calc; = sum of equivalent point sources (p/s) in HB-3 for
 HFIR at 100 MW (Sn=7.5573e18 n/s in global calc);  will yield fluxes in n/s/cm2
fm232   7.984211E+15  $ based on Pri g-source in VELM gamma groups 1-8 only; use 1-8 for FLOODED case only; must be used consistently with SI73, SP73, SB73
& DS83 data
c         fc232   Secndry G-Dose (mrem/hr) on downstrem surf of box holding shutter; seg 10
c         fm232   9.64595e16  $ use for n/g calc; = sum of equivalent point sources (n/s) in HB-3 for HFIR at 100 MW (Sn=7.5573e18 n/s in global calc);  wil
l yield fluxes in n/s/cm2
f232:p  3001   $  downstream surf of SS liner on concrete box containing shutter
fs232   3032  -3022  3072  -3082  3031  -3021  3071  -3081  3110  $ the 10th edit ("the remainder") is the leakage (p/s) thru the central 6.5-inch-diam disk
c       Meaning of surface segments (assuming you're outside where monochrometer drum usually is, looking back towards the shutter):
c       ------------------------------------------------------------
c         1) everything to left  of concrete box holding the shutter,    area = 1438.212778 cm2
c         2) everything to right of concrete box holding the shutter,    area = 1438.212778 cm2
c         3) what remains above the concrete box holding the shutter,    area = 1414.336692 cm2
c         4) what remains below the concrete box holding the shutter,    area = 1414.336692 cm2
c         5) void gap just to left  of concrete box holding the shutter, area =   51.915019 cm2
```

```
c         6) void gap just to right of concrete box holding the shutter, area =  151.915019 cm2
c         7) void gap just above the concrete box holding the shutter,   area =  145.816241 cm2
c         8) void gap just below the concrete box holding the shutter,   area =  145.816241 cm2
c         9) face of concrete box holding the shutter, except the central 6.5-inch-diam disk;  area = 6758.583596 cm2
c        10) central 6.5-inch-diam disk directly in front of shutter,    area =  214.083910 cm2  <-- region of greatest interest
c        Total area of all 10 segments=pi*(65.0**2)
c       ------------------------------------------------------------
sd232   $ enter area of all surface segments (including "the remainder") to get flux in "p/s/cm2"
        $ area (cm2) for each of the 10 surface segments at this axial location (seg 10, the "remainder", is of greatest interest)
        1438.212778  1438.212778  1414.336692  1414.336692  151.915019
         151.915019   145.816241   145.816241  6758.583596  214.083910
e232    $ Gamma energy boundaries (Emax, in MeV) from VELM 61n/23g structure:
        1.00000e-02  2.00000e-02  4.50000e-02  7.00000e-02  1.00000e-01
        1.50000e-01  3.00000e-01  4.00000e-01  5.10000e-01  6.00000e-01
        7.00000e-01  1.00000e+00  1.50000e+00  2.00000e+00  2.50000e+00
        3.00000e+00  4.00000e+00  5.00000e+00  6.00000e+00  7.00000e+00
        7.50000e+00  8.00000e+00  1.00000e+01  1.40000e+01
em232   $ Gamma flux-to-dose-rate conversion factors [(mrem/hr)/(p/s/cm2)] for the VELM 61n/23g xsect library,
c       calculated as prescribed in ANSI/ANS-6.1.1-1977, with groups arranged here in order of "increasing"
c       energy for use in MCNP;  first value here corresponds to non-existant group below 1.0e-2 MeV:
        0.00000e+00  2.14390e-03  5.77610e-04  2.74660e-04  2.66440e-04
        3.27670e-04  5.66760e-04  8.75940e-04  1.08520e-03  1.27970e-03
        1.44170e-03  1.75630e-03  2.31560e-03  2.92700e-03  3.46860e-03
        3.95960e-03  4.62210e-03  5.41360e-03  6.19090e-03  6.92650e-03
        7.47830e-03  7.84680e-03  8.77160e-03  1.10200e-02
fq232   e s   $ print control:  energy grp down vertically;  spatial segments across horizontally
c
c       ------------------------------------------------------------------------------------------------------------------------
c       ********** end of model **********
c       ------------------------------------------------------------------------------------------------------------------------
```

Appendix D.5

Additional Supplemental Results from the Final Gamma-Only Shielding Analysis, Run HB308G

Appendix D.5

Additional Supplemental Results from the Final Gamma-Only Shielding Analysis, Run HB308G

D.5.1 Results 2.4945 cm Downstream of Collimator Exit

The internal boundary source file created and saved during this analysis contains detailed information on 5,688,819 particles that crossed Surface 4197 at Z=401.9645 cm. This surface is located 2.4845 cm downstream of the collimator exit as shown in Fig. 6.5. The file is a binary MCNP "wssa" file containing information on each particle as it crossed this surface. Information includes each particle's coordinates, direction cosines, energy, weight, etc. This file can then be used as an "rssa" binary source file in subsequent MCNP shielding analyses for this rotary shutter assembly or any similar redesigned shutter assembly, as explained in Sect. 6.8.2.

Immediately downstream of that, on Surface 4198 at Z=401.9745 cm (2.4945 cm downstream of the collimator exit), some selected detailed information was tallied and saved for future reference. [For the purposes of this discussion, this will also be referred to as the internal boundary source location, even though it is actually 0.01 cm away.] Because that information was not of any immediate programmatic interest, and because some of it requires additional explanation and careful interpretation, that information was relocated to this appendix.

Figure D5.1 shows a sketch of the 130-cm-diam boundary surface looking back towards the collimator from the rotary shutter. The five small numbers (1,2,3,4,5) indicate the five "segmented areas" used in Tallies 211 and 212. Segment 5 corresponds to the 2.75-inch x 5.5-inch rectangular area directly in front of the water-filled hole in the collimator, while segments 3 and 4 correspond to the two 2.75-inch-wide strips above and below it, and segments 1 and 2 correspond to the two large D-shaped regions to either side. Note that Surface 4198 is located in the void space between the collimator and the rotary shutter (cf Fig 6.5). The region inside the large dotted square in Fig. D5.1 is indeed located in this void region of the cavity holding the rotary shutter assembly, while the region outside the dotted square in Fig. D5.1 actually lies in the barytes concrete forming the biological shield.

Table D5.1 shows the gamma leakage (p/s) across the various segments of the boundary source plane shown in Fig. D5.1. Note that this is the gross leakage in the forward hemisphere integrated over direction cosines 0 to +1, not the net leakage, and that portions of Segments 1 and 2 are actually inside the biological shield. The key thing to note here is that most of the leakage (p/s) comes from Segment 5, the small area directly in front of the water-filled hole in the collimator. Likewise, Table D5.2 shows the area-averaged gamma dose rate corresponding to each of the five segmented areas. The values for segments 1-4 are by-products of the calculation and appear low because of the large areas over which they were averaged. Obviously the only one of any real interest is the average gamma dose rate for the area directly in front of the water-filled hole in the collimator (Segment 5). The value here is 110.861 Rem/hr (+/- 2.7%). This is of special interest for two reasons: (1) It is to be regarded as highly reliable since it is based on a boundary crossing tally (Tally 212) which senses only real particles. Basically this means that the broad-group weight window biasing technique used here was successful in transporting large numbers of important high-energy particles to and through this region. This is imperative if the calculations further downstream are to be meaningful. [The "apparent" poor quality of the low energy fluxes and dose rates is by design, not by accident, and will be discussed momentarily. It is nothing to be concerned about.] (2) This dose rate of 110.861 Rem/hr (+/- 2.7%) is also significant because it is in excellent agreement with the point detector response (103.99 Rem/hr, +/- 0.5%) just a few centimeters further downstream in the void (at Z=407.464 cm), and because it is also in excellent agreement with other results shown in Table 6.8 based on totally independent methods such as 3-group hand calculations, a 23-group point kernel analysis, and an earlier (preliminary, highly simplified) MCNP analysis which used only geometric splitting and no weight windows. Collectively, this body of information provides strong verification that the broad-group weight window approach used here is working properly and that everything is properly normalized.

Why do the results below 1 MeV appear to be so poor, and results below 0.3 MeV non-existant? The answer lies in Sect. 6.6, and in particular with the discussion associated with Figs. 6.3 and 6.4. This final gamma-only analysis (Run HB308G) was optimized, using 3-D broad-group weight windows based on a 1-D adjoint analysis, to obtain the best possible determination of the gamma dose rates downstream of the rotary shutter with the least amount of calculational effort. To realize the efficiencies needed, certain unimportant things get ignored or treated lightly. Near the downstream side of the rotary shutter, all gammas are tracked and treated rigorously because all are important (some more so than others). As one moves back through the steel shutter, and through the water in the collimator section, and then the water in the water tube, the low energy gammas become less and less important, to the point where most are not worth tracking. (Back at the source for example, all gammas below 3 Mev are ignored completely!). As we move forward again, from the source to the shutter, faster gammas begin to slow down, and the code will (because of this highly efficient broad-group weight window biasing scheme) begin to track more and more of these lower energy gammas only when they get close enough to the detector (downstream of the shutter) that they stand a

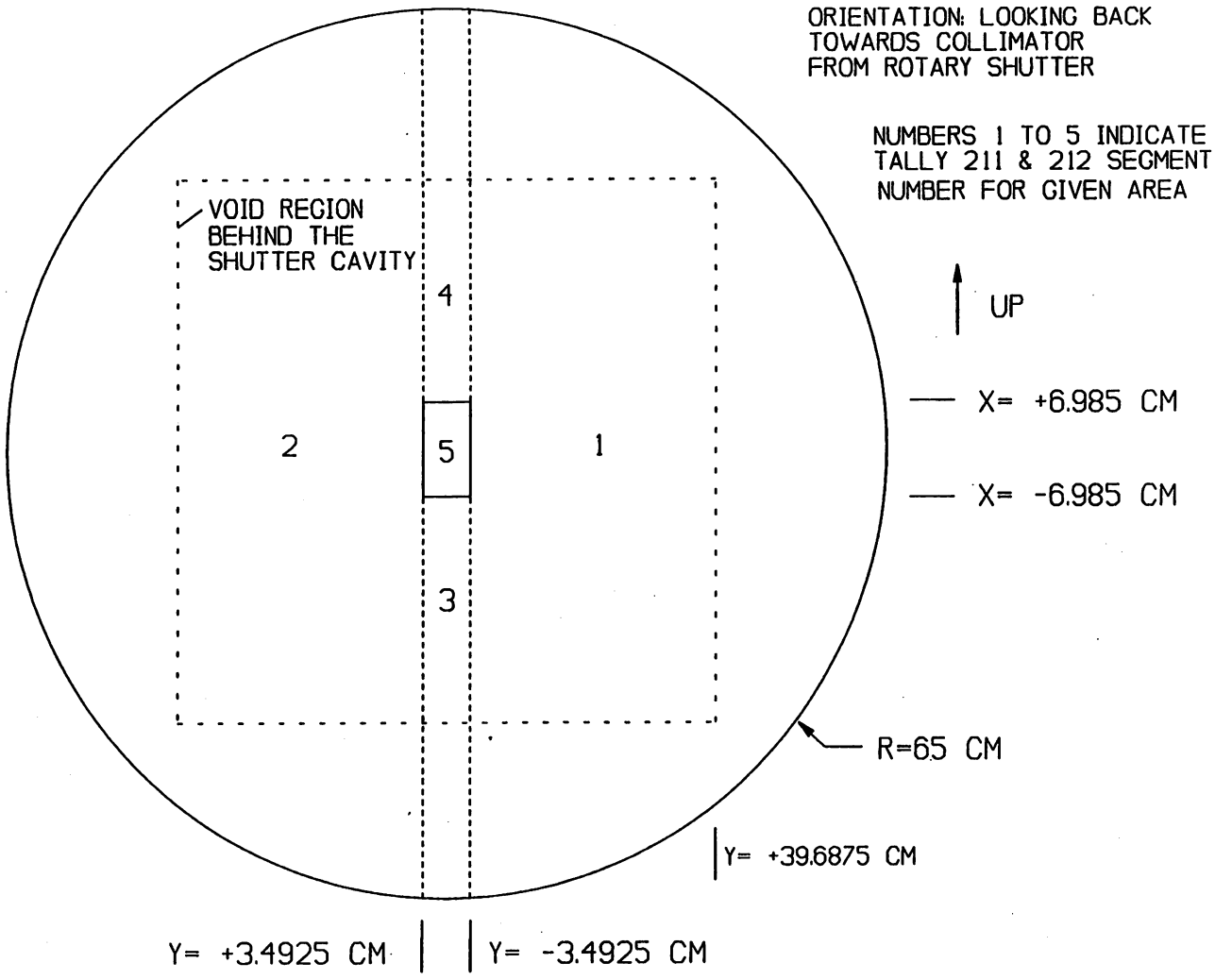


Fig. D5.1. Sketch of the 130-cm-diam internal boundary surface at Z=401.9645 cm, looking back towards the collimator from the rotary shutter.

Table D5.1. Gamma leakage (p/s) across the various segments of a plane surface at Z=401.9745 cm, located 2.4945 cm downstream of the collimator exit. The locations of the various area segments are illustrated in Fig. D5.1, where segment 5 corresponds to the 2.75-inch x 5.5-inch area just downstream of the water-filled hole in the collimator. Also note that: (1) this is the gross leakage in the forward hemisphere, integrated over direction cosines 0 to +1, as calculated by Tally 211 in HB308G, and that (2) because of the weight window biasing scheme used, the less important values below 1 MeV are not terribly accurately. The key thing to note here is that most of the gamma leakage (p/s) comes through the water-filled hole (segment 5).

		Segment 1		Segment 2		Segment 3		Segment 4		Segment 5	
		Area: 6182.81 cm2		Area: 6182.81 cm2		Area: 405.016 cm2		Area: 405.016 cm2		Area: 97.5804 cm2	
Emin (MeV)	Emax (MeV)	photons/sec	fsd	photons/sec	fsd	photons/sec	fsd	photons/sec	fsd	photons/sec	fsd
0.010	- 0.020	0.00000E+00	.0000	0.00000E+00	.0000	0.00000E+00	.0000	0.00000E+00	.0000	0.00000E+00	.0000
0.020	- 0.045	0.00000E+00	.0000	0.00000E+00	.0000	0.00000E+00	.0000	0.00000E+00	.0000	0.00000E+00	.0000
0.045	- 0.070	0.00000E+00	.0000	0.00000E+00	.0000	0.00000E+00	.0000	0.00000E+00	.0000	0.00000E+00	.0000
0.070	- 0.10	0.00000E+00	.0000	0.00000E+00	.0000	0.00000E+00	.0000	0.00000E+00	.0000	0.00000E+00	.0000
0.10	- 0.15	0.00000E+00	.0000	0.00000E+00	.0000	0.00000E+00	.0000	0.00000E+00	.0000	0.00000E+00	.0000
0.15	- 0.30	0.00000E+00	.0000	0.00000E+00	.0000	0.00000E+00	.0000	0.00000E+00	.0000	0.00000E+00	.0000
0.30	- 0.40	7.97578E+06	.3188	5.44666E+06	.2220	2.43470E+06	.3828	2.61066E+06	.5157	1.48976E+07	.1326
0.40	- 0.51	8.50939E+06	.2932	6.58861E+06	.4154	3.74595E+06	.2784	2.60924E+06	.3379	1.68622E+07	.1301
0.51	- 0.60	9.66200E+06	.2587	1.56355E+07	.3237	3.38586E+06	.3350	1.57550E+06	.2936	2.71278E+07	.1875
0.60	- 0.70	2.04353E+06	.2255	2.05637E+06	.2634	1.91463E+06	.4718	1.03452E+06	.4107	9.78026E+06	.2580
0.70	- 1.0	1.04109E+07	.2233	7.80320E+06	.2092	2.89671E+06	.4590	2.02376E+06	.3855	2.24788E+07	.1037
1.0	- 1.5	1.40186E+07	.0835	1.19131E+07	.0281	4.30468E+06	.0412	4.38344E+06	.0372	3.23917E+07	.0293
1.5	- 2.0	9.54427E+06	.0334	9.72564E+06	.0288	3.72337E+06	.0418	3.38778E+06	.0374	2.80892E+07	.0291
2.0	- 2.5	8.96687E+06	.0775	9.59711E+06	.1580	3.06571E+06	.0360	3.12256E+06	.0380	2.82619E+07	.0373
2.5	- 3.0	7.30094E+06	.0384	7.15538E+06	.0304	2.98058E+06	.0455	2.97780E+06	.0487	2.84044E+07	.0296
3.0	- 4.0	1.34884E+07	.0588	1.34270E+07	.0478	6.09097E+06	.0730	5.58397E+06	.0441	1.23560E+08	.0309
4.0	- 5.0	1.06768E+07	.0702	1.08685E+07	.0718	4.86116E+06	.0831	5.63482E+06	.1169	1.89752E+08	.0389
5.0	- 6.0	8.67949E+06	.0737	1.00445E+07	.1365	4.48112E+06	.1305	3.95583E+06	.1383	1.52381E+08	.0498
6.0	- 7.0	9.87543E+06	.1528	9.41383E+06	.1743	7.24625E+06	.2254	5.41813E+06	.1694	3.52357E+08	.0478
7.0	- 7.5	3.11441E+06	.3744	2.17994E+06	.2028	3.01287E+06	.6284	1.17428E+06	.1985	9.75156E+07	.0856
7.5	- 8.0	7.48601E+06	.2555	3.74042E+06	.2612	5.89233E+06	.3209	9.76350E+06	.3276	5.31670E+08	.0475
8.0	- 10.0	6.23397E+05	.6130	1.70587E+06	.9045	1.70174E+05	.3873	2.80719E+05	.5239	3.72511E+07	.1933
10.0	- 14.0	0.00000E+00	.0000	0.00000E+00	.0000	0.00000E+00	.0000	0.00000E+00	.0000	0.00000E+00	.0000
	Total:	1.32376E+08	.0500	1.27302E+08	.0589	6.02071E+07	.0732	5.55365E+07	.0818	1.69278E+09	.0254

Table D5.2. Gamma dose rates (mrem/hr) averaged across the various segments of a plane surface at Z=401.9745 cm, located 2.4945 cm downstream of the collimator exit. The locations of the various area segments are illustrated in Fig. D5.1, where segment 5 corresponds to the 2.75-inch x 5.5-inch area just downstream of the water-filled hole in the collimator. These values were calculated by Tally 212 in HB308G. While the dose rate directly in front of the water-filled hole in the collimator (segment 5) is clearly dominent, average values for the other areas are low because of the large areas over which they were averaged. To see real relative contributions, see integrated leakage terms in Table D5.1 (above). Also note that because of the weight window biasing scheme used, the less important values below 1 MeV are not terribly accurately. The key things to note here are: (1) these estimates are based on real boundary crossing tallies, not point detectors, and (2) that this dose rate in front of the water-filled hole (segment 5) is consistent with the point detector value in Tally 15, as well as with values obtained by other calculational techniques described in Sect 5.

		Segment 1		Segment 2		Segment 3		Segment 4		Segment 5	
		Area: 6182.81 cm2		Area: 6182.81 cm2		Area: 405.016 cm2		Area: 405.016 cm2		Area: 97.5804 cm2	
Emin (MeV)	Emax (MeV)	mrem/hr	fsd	mrem/hr	fsd	mrem/hr	fsd	mrem/hr	fsd	mrem/hr	fsd
0.010	0.020	0.00000E+00	.0000	0.00000E+00	.0000	0.00000E+00	.0000	0.00000E+00	.0000	0.00000E+00	.0000
0.020	0.045	2.35525E-04	.9999	0.00000E+00	.0000	0.00000E+00	.0000	0.00000E+00	.0000	0.00000E+00	.0000
0.045	0.070	0.00000E+00	.0000	0.00000E+00	.0000	0.00000E+00	.0000	0.00000E+00	.0000	0.00000E+00	.0000
0.070	0.10	0.00000E+00	.0000	0.00000E+00	.0000	0.00000E+00	.0000	0.00000E+00	.0000	0.00000E+00	.0000
0.10	0.15	7.16542E-03	.9999	6.15731E+00	.9999	0.00000E+00	.0000	0.00000E+00	.0000	0.00000E+00	.0000
0.15	0.30	9.53401E-01	.6612	1.59188E+01	.6882	4.31463E+00	.9999	0.00000E+00	.0000	5.41496E+01	.5624
0.30	0.40	5.94558E+00	.0946	5.39663E+00	.0594	1.49870E+01	.1947	1.75944E+01	.2831	1.89525E+02	.1141
0.40	0.51	5.48183E+00	.1388	5.46665E+00	.2395	1.94087E+01	.2041	1.49104E+01	.2478	2.49564E+02	.1198
0.51	0.60	1.27932E+01	.0767	1.48217E+01	.1147	3.48919E+01	.1506	2.67742E+01	.1056	5.73758E+02	.1467
0.60	0.70	9.53427E-01	.2323	6.64057E-01	.2460	1.08433E+01	.3934	6.07173E+00	.4671	1.58955E+02	.2553
0.70	1.0	4.46146E+00	.1981	3.97891E+00	.2708	1.57449E+01	.3980	1.66586E+01	.4458	4.86298E+02	.1021
1.0	1.5	7.15299E+00	.0740	6.14073E+00	.0273	3.28587E+01	.0380	3.33746E+01	.0352	9.13195E+02	.0277
1.5	2.0	5.54267E+00	.0330	5.68139E+00	.0287	3.25135E+01	.0395	2.96970E+01	.0365	9.57418E+02	.0280
2.0	2.5	5.74494E+00	.0718	6.42164E+00	.1890	3.00269E+01	.0356	3.06309E+01	.0374	1.10011E+03	.0353
2.5	3.0	5.14400E+00	.0376	5.06071E+00	.0305	3.19434E+01	.0444	3.19602E+01	.0478	1.23092E+03	.0288
3.0	4.0	1.06753E+01	.0570	1.06123E+01	.0461	7.32253E+01	.0699	6.73951E+01	.0431	5.97442E+03	.0304
4.0	5.0	9.65087E+00	.0686	9.80506E+00	.0702	6.69225E+01	.0811	7.72500E+01	.1143	1.06088E+04	.0386
5.0	6.0	8.85268E+00	.0735	1.02105E+01	.1347	6.95966E+01	.1287	6.14632E+01	.1363	9.72342E+03	.0496
6.0	7.0	1.11235E+01	.1521	1.06180E+01	.1734	1.24456E+02	.2246	9.31384E+01	.1686	2.50468E+04	.0477
7.0	7.5	3.77690E+00	.3738	2.64654E+00	.2024	5.57277E+01	.6275	2.17689E+01	.1981	7.48309E+03	.0855
7.5	8.0	9.51124E+00	.2553	4.75079E+00	.2611	1.14210E+02	.3209	1.89246E+02	.3275	4.27606E+04	.0475
8.0	10.0	8.86056E-01	.6123	2.42188E+00	.9042	3.69836E+00	.3870	6.09530E+00	.5235	3.34971E+03	.1933
10.0	14.0	0.00000E+00	.0000	0.00000E+00	.0000	0.00000E+00	.0000	0.00000E+00	.0000	0.00000E+00	.0000
	Total:	1.08657E+02	.0434	1.26774E+02	.1098	7.35369E+02	.0873	7.24029E+02	.0993	1.10861E+05	.0270

reasonable chance of making some contribution to the dose rate at that location (downstream of the shutter). At the present location, just downstream of the collimator, most of the low-energy gammas simply weren't worth tracking yet; here, for example, none of the very low-energy gammas below 0.3 MeV had yet survived Russian Roulette, and only some of those below 1.0 Mev had survived Russian Roulette. Thus, these results at this particular location are poorly calculated by design. Had one really wanted to calculate them with great accuracy "at this particular location," one should have run the adjoint calculation with the adjoint source "at this location" and developed the 3-D broad-group weight windows around that set of working assumptions instead. That, however, was not the objective of this particular analysis. (Be careful what you wish for, you just might get it!). Moreover, for the intended purpose of this analysis, the broad-group weight windows used are functioning exactly as intended. Particularly for biased calculations, the expression "caveat emptor" applies, and users are strongly encouraged to not take results indiscriminately from arbitrary locations and/or energy ranges and automatically assume they are good. For this particular analysis (Run HB308G), the only results that are trustworthy everywhere are those in the first broad weight window group above 3 Mev. Unlike unbiased calculations, the results in the lower energy groups get better and better (here in this biased calculation) as one gets deeper into the shield, closer to the downstream side of the rotary shutter. Having made this point, let us continue.

As shown in Table D5.1, most of the gammas impingent on the rotary shutter come from the water-filled rectangular hole in the collimator. Table D5.3 gives a much more detailed description of that leakage in 23 different energy bins and 7 different directional bins between 0 and 90 degrees with respect to the beam tube centerline. If one were preparing a boundary source for some other code (like DORT or TORT), such information might be useful. Moreover, if one is using MCNP, one would likely be better advised to the MCNP binary surface source file already prepared for that purpose, as outlined in Sect 6.8.2. Even then, however, there would remain a need to verify that the calculation was set up properly and that the boundary source used was the appropriate one. By using the same F1 leakage tally at surface 4198 as in the present calculation (Tally 221), one could and should use the information in Table D5.1 for verification purposes in any such follow-up shielding analyses. Moreover, that is the main/only purpose for including Table D5.3 in this appendix. As long as the follow-up bootstrapped MCNP4B analysis (with the MCNP binary surface source file) uses the same set of 3-D broad-group weight windows used in this analysis (Run HB308G), the quality of the results of interest downstream of the rotary shutter will remain good to excellent.

Nevertheless, the data in Table D5.3 is understandably disquieting to the purists who might wish to use it for some other purpose. Inspection of the data in Table D5.3 quickly shows that the data below 3.0 MeV is questionable, that the data below 1.0 MeV is poor, and that the data below 0.3 MeV is completely missing -- all for the same reason described two paragraphs back. In absolute terms, the only data that is rigorously correct as shown, is the data in the first broad weight-window group above 3.0 MeV. [The zeros in the lower right hand corner will be explained momentarily. Indeed, these particular values are correctly given as zero for a good physical reason.] To supplement this data with something more correct in the lower energy ranges, one can and probably should turn to the results given by the preliminary, highly-simplified MCNP analysis (Run HB307C) described in Table C6.6 of Appendix C.6. That particular analysis did not use broad group weight windows, but relied instead on the use of simple geometric splitting. While that energy-independent biasing technique did not permit the high-energy gammas downstream of the flooded collimator to be calculated as accurately as the present technique, it did calculate the less important low-energy gammas more accurately. (While geometric splitting also entails the use of Russian Roulette, it does not preferentially discriminate against the less important low-energy gammas. To understand the differences between geometric splitting and the use of weight windows, see Appendix C.2.1.) Thus, if one wanted to construct the most physically correct description of the gamma leakage at the downstream exit of the water-filled collimator, one could and should combine the results above 3 MeV from Table D5.3 with the results below 3 MeV from Table C6.6, as shown in Table D5.4. This is undoubtedly the best description of the gamma leakage over the full energy range, even though the low-energy leakage here will not contribute in any significant fashion to the final dose rate downstream of the shutter. In Table D5.4, a few selected values in the 1-3 MeV range were also taken from Table D5.3 for those directional bins 20-60 degrees off the centerline. The reason for that selection was that gammas that have scattered through such large angles and still have this amount of energy (1-3 MeV) left, could only have come from the higher energy range (E > 3 MeV) prior to the scattering event, and these are better calculated in Run HB308G whose results are shown in Table D5.3. This also bears on why the lower right triangular regions of Tables C6.6, D5.3, and Table D5.4 are all filled with zeros. It is not that the calculations are poor or lack enough histories to give meaningful results, but quite the contrary -- physically, these results must be zero. High-energy gammas that reach the end of the water-filled collimator do so by streaming uncollided through most of the collimator, and are therefore very forward-directed. By virtue of the scattering laws, any high-energy gamma that subsequently experiences a scattering event near the end of the collimator and scatters through such a large angle will necessarily be greatly reduced in energy. Thus, the zeros in the lower right hand corner of these two tables are physically correct and should be there as shown.

D.5.2 Dose Rates and Leakage Rates Downstream of the Entire Configuration

Figure D5.2 shows a sketch of the end of the entire shield configuration at Z=478.79 cm, as would be seen if one were standing outside the system, where the monochrometer drum would normally be located, looking back

Table D5.3. Gamma leakage (p/s) and corresponding fsd's, in various energy and angular ranges(*), on the downstream (exit) side of the 2.75-inch x 5.5-inch rectangular hole through the collimator when the 1998 water tube and collimator sections are both flooded and the HFIR is operating at 100 MW. More precisely, these results are for a corresponding 2.75-inch x 5.5-inch area on Surface 4198 at Z=401.9745 cm, which is 2.4945 cm downstream of the collimator exit. Results are shown here for Run HB308G, which used 4 million histories and was based on the new (shorter) 1998 water tube design. (See recommended values in Table D5.4)

Emin (MeV)	Emax (MeV)	Range: 0-90 deg (p/s)	fsd	Range: 0-2 deg (p/s)	fsd	Range: 2-5 deg (p/s)	fsd	Range: 5-10 deg (p/s)	fsd	Range: 10-20 deg (p/s)	fsd	Range: 20-30 deg (p/s)	fsd	Range: 30-60 deg (p/s)	fsd	Range: 60-90 deg (p/s)	fsd
0.010	- 0.020	0.00000e+0	.0000	0.00000e+0	.0000	0.00000e+0	.0000	0.00000e+0	.0000	0.00000e+0	.0000	0.00000e+0	.0000	0.00000e+0	.0000	0.00000e+0	.0000
0.020	- 0.045	0.00000e+0	.0000	0.00000e+0	.0000	0.00000e+0	.0000	0.00000e+0	.0000	0.00000e+0	.0000	0.00000e+0	.0000	0.00000e+0	.0000	0.00000e+0	.0000
0.045	- 0.070	0.00000e+0	.0000	0.00000e+0	.0000	0.00000e+0	.0000	0.00000e+0	.0000	0.00000e+0	.0000	0.00000e+0	.0000	0.00000e+0	.0000	0.00000e+0	.0000
0.070	- 0.10	0.00000e+0	.0000	0.00000e+0	.0000	0.00000e+0	.0000	0.00000e+0	.0000	0.00000e+0	.0000	0.00000e+0	.0000	0.00000e+0	.0000	0.00000e+0	.0000
0.10	- 0.15	0.00000e+0	.0000	0.00000e+0	.0000	0.00000e+0	.0000	0.00000e+0	.0000	0.00000e+0	.0000	0.00000e+0	.0000	0.00000e+0	.0000	0.00000e+0	.0000
0.15	- 0.30	0.00000e+0	.0000	0.00000e+0	.0000	0.00000e+0	.0000	0.00000e+0	.0000	0.00000e+0	.0000	0.00000e+0	.0000	0.00000e+0	.0000	0.00000e+0	.0000
0.30	- 0.40	1.48976e+7	.1326	2.60212e+6	.5315	1.42209e+6	.2526	1.89978e+6	.2095	1.50928e+6	.2234	2.78183e+6	.2672	4.07405e+6	.2231	6.08418e+5	.6289
0.40	- 0.51	1.68622e+7	.1301	6.45530e+5	.3531	2.19592e+6	.2003	2.21741e+6	.3127	3.69025e+6	.2066	2.56250e+6	.4658	5.35002e+6	.2451	2.00575e+5	.5147
0.51	- 0.60	2.71278e+7	.1875	5.84064e+5	.6535	2.05893e+6	.4526	2.66293e+6	.4295	2.92437e+6	.1954	3.70662e+6	.1665	1.47839e+7	.3223	4.06923e+5	.3044
0.60	- 0.70	9.78026e+6	.2580	2.11789e+5	.6543	3.74788e+6	.5615	1.63307e+6	.3566	1.42257e+6	.2676	3.34950e+5	.6436	2.40772e+6	.4893	2.22870e+4	.9999
0.70	- 1.0	2.24788e+7	.1037	2.47652e+6	.3722	3.77853e+6	.2804	3.34796e+6	.3058	4.48964e+6	.2098	1.96937e+6	.2208	5.75657e+6	.1783	6.60207e+5	.3594
1.0	- 1.5	3.23917e+7	.0293	1.24424e+6	.0800	4.55225e+6	.1089	4.17864e+6	.0446	4.97394e+6	.0424	3.97222e+6	.0407	1.33735e+7	.0243	9.68956e+4	.1092
1.5	- 2.0	2.80892e+7	.0291	9.18898e+5	.1340	3.16834e+6	.1100	2.93045e+6	.0517	4.53585e+6	.0755	4.27673e+6	.0306	1.22567e+7	.0254	2.28423e+3	.7336
2.0	- 2.5	2.82619e+7	.0373	1.51561e+6	.3094	2.81103e+6	.2340	2.81453e+6	.0697	4.62852e+6	.0379	8.73551e+6	.0251	7.75675e+6	.0310	0.00000e+0	.0000
2.5	- 3.0	2.84044e+7	.0296	6.74417e+5	.1345	2.64162e+6	.1707	3.42951e+6	.1192	7.41195e+6	.0292	1.33825e+7	.0260	8.64406e+5	.0478	0.00000e+0	.0000
3.0	- 4.0	1.23560e+8	.0309	5.81029e+7	.0546	1.11217e+7	.0603	1.20854e+7	.0316	2.50477e+7	.0243	1.70067e+7	.0304	1.95286e+5	.0726	0.00000e+0	.0000
4.0	- 5.0	1.89752e+8	.0389	1.23224e+8	.0536	1.67702e+7	.0748	1.52703e+7	.0344	3.33276e+7	.0262	1.15851e+6	.0525	1.19444e+3	.7543	0.00000e+0	.0000
5.0	- 6.0	1.52381e+8	.0498	8.71144e+7	.0784	1.76835e+7	.0966	2.19698e+7	.0365	2.55977e+7	.0327	1.51824e+4	.2322	0.00000e+0	.0000	0.00000e+0	.0000
6.0	- 7.0	3.52357e+8	.0478	2.76994e+8	.0565	3.53124e+7	.1009	3.45845e+7	.0338	5.46640e+6	.0527	0.00000e+0	.0000	0.00000e+0	.0000	0.00000e+0	.0000
7.0	- 7.5	9.75156e+7	.0856	5.63270e+7	.1328	3.05521e+7	.1089	1.04385e+7	.0493	1.98043e+5	.2639	0.00000e+0	.0000	0.00000e+0	.0000	0.00000e+0	.0000
7.5	- 8.0	5.31670e+8	.0475	5.16566e+8	.0480	1.39714e+7	.1157	1.07823e+6	.1713	5.41122e+4	.4579	0.00000e+0	.0000	0.00000e+0	.0000	0.00000e+0	.0000
8.0	- 10.0	3.72511e+7	.1933	3.46680e+7	.1975	1.64225e+6	.2234	9.39587e+5	.2139	1.20127e+3	.9999	0.00000e+0	.0000	0.00000e+0	.0000	0.00000e+0	.0000
10.0	- 14.0	0.00000e+0	.0000	0.00000e+0	.0000	0.00000e+0	.0000	0.00000e+0	.0000	0.00000e+0	.0000	0.00000e+0	.0000	0.00000e+0	.0000	0.00000e+0	.0000
	Total:	1.69278e+9	.0254	1.16387e+9	.0283	1.53430e+8	.0431	1.21481e+8	.0268	1.25279e+8	.0249	5.99026e+7	.0351	6.68201e+7	.0815	1.99759e+6	.2399

* Results in the first column are based on Tally 211 and show the total leakage (p/s) for all gammas integrated over the entire forward hemisphere (0 to 90 degrees). Results in the other columns are based on Tally 221 and show the total leakage (p/s) within discrete angular ranges (0-2 degrees of the centerline, 2-5 degrees of the centerline, etc). These results from Tallies 211 and 221 are based on "real" boundary crossing counters, not point detectors. Also note that these are "leakage" rates (p/s) by energy group, not fluxes or currents. One can divide by the area of the hole to get currents, but the fluxes are not immediately available from this data since the effect of individual particle direction cosines with respect to the exit surface have already been applied to get the leakage rates.

Table D5.4. Gamma leakage (p/s) and corresponding fsd's, in various energy and angular ranges(**), on the downstream (exit) side of the 2.75-inch x 5.5-inch rectangular hole through the collimator when the 1998 water tube and collimator sections are both flooded and the HFIR is operating at 100 MW. These results for the new (shorter) 1998 water tube design are based on a combination of data from Table C6.6 (below 3 MeV) and Table D5.3 (above 3 MeV).

Emin (MeV)	Emax (MeV)	Range: 0-90 deg (p/s)	fsd	Range: 0-2 deg (p/s)	fsd	Range: 2-5 deg (p/s)	fsd	Range: 5-10 deg (p/s)	fsd	Range: 10-20 deg (p/s)	fsd	Range: 20-30 deg (p/s)	fsd	Range: 30-60 deg (p/s)	fsd	Range: 60-90 deg (p/s)	fsd
0.010	- 0.020	1.90358e+6	.0710	1.90358e+5	.1424	3.94921e+5	.1035	4.94362e+5	.0972	4.31857e+5	.0967	1.78993e+5	.1280	1.78993e+5	.1375	3.40939e+4	.2887
0.020	- 0.045	1.08476e+7	.0612	6.79038e+5	.1005	1.94051e+6	.0780	2.53432e+6	.0703	2.24452e+6	.0645	1.11089e+6	.0732	1.82687e+6	.0685	5.11409e+5	.0926
0.045	- 0.070	1.34898e+7	.0579	7.24496e+5	.0910	1.96608e+6	.0779	2.44056e+6	.0680	2.61955e+6	.0609	1.61662e+6	.0670	3.21335e+6	.0609	9.09172e+5	.0789
0.070	- 0.10	1.65498e+7	.0544	6.84720e+5	.1004	1.83539e+6	.0704	2.31555e+6	.0650	2.95481e+6	.0611	2.23315e+6	.0582	4.89248e+6	.0582	1.63367e+6	.0700
0.10	- 0.15	2.86673e+7	.0539	7.69955e+5	.0924	2.45476e+6	.0692	3.36678e+6	.0625	4.75610e+6	.0579	4.07991e+6	.0561	9.90997e+6	.0557	3.32984e+6	.0620
0.15	- 0.30	5.46128e+7	.0533	1.64219e+6	.0812	4.53449e+6	.0695	6.07156e+6	.0585	8.44393e+6	.0535	7.28474e+6	.0547	1.91892e+7	.0548	7.44668e+6	.0545
0.30	- 0.40	2.30162e+7	.0536	7.01767e+5	.0901	2.05984e+6	.0723	2.82127e+6	.0633	3.60259e+6	.0594	3.12244e+6	.0584	8.10867e+6	.0559	2.59966e+6	.0596
0.40	- 0.51	2.17889e+7	.0533	6.08009e+5	.0973	1.97177e+6	.0708	2.62807e+6	.0612	3.52304e+6	.0582	3.26449e+6	.0597	7.11427e+6	.0564	2.67922e+6	.0597
0.51	- 0.60	3.37558e+7	.0569	5.39821e+5	.1091	1.62230e+6	.0756	2.44624e+6	.0650	4.48904e+6	.0587	5.11693e+6	.0590	1.33961e+7	.0618	6.14543e+6	.0586
0.60	- 0.70	1.27881e+7	.0494	4.20492e+5	.1089	1.29273e+6	.0731	1.65071e+6	.0713	1.84960e+6	.0626	1.45467e+6	.0599	3.44065e+6	.0514	2.67922e+6	.0560
0.70	- 1.0	3.39917e+7	.0467	1.09953e+6	.0832	3.18210e+6	.0664	3.90376e+6	.0572	4.49472e+6	.0540	3.56282e+6	.0510	1.27852e+7	.0433	4.96351e+6	.0561
1.0	- 1.5	3.70887e+7	.0282	1.81266e+6	.0692	4.25038e+6	.0606	5.11409e+6	.0540	6.35000e+6	.0463	5.73631e+6	.0421	*1.33735e+7	.0243	4.51745e+5	.1012
1.5	- 2.0	3.73697e+7	.0259	3.60259e+6	.0756	3.90944e+6	.0590	4.34129e+6	.0476	6.42387e+6	.0410	6.82447e+6	.0380	*1.22567e+7	.0254	1.13646e+4	.5000
2.0	- 2.5	4.34265e+7	.0355	1.10294e+7	.0909	4.06570e+6	.0589	4.63393e+6	.0443	7.20519e+6	.0389	*8.73551e+6	.0251	*7.75675e+6	.0310	0.00000e+0	.0000
2.5	- 3.0	4.47979e+7	.0431	1.06458e+7	.1333	4.38959e+6	.0645	5.12261e+6	.0461	1.03930e+7	.0441	*1.33825e+7	.0260	*8.64406e+5	.0478	0.00000e+0	.0000
3.0	- 4.0	1.23560e+8	.0309	5.81029e+7	.0546	1.11217e+7	.0603	1.20854e+7	.0316	2.50477e+7	.0243	1.70067e+7	.0304	1.95286e+5	.0726	0.00000e+0	.0000
4.0	- 5.0	1.89752e+8	.0389	1.23224e+8	.0536	1.67702e+7	.0748	1.52703e+7	.0344	3.33276e+7	.0262	1.15851e+6	.0525	1.19444e+3	.7543	0.00000e+0	.0000
5.0	- 6.0	1.52381e+8	.0498	8.71144e+7	.0784	1.76835e+7	.0966	2.19698e+7	.0365	2.55977e+7	.0327	1.51824e+4	.2322	0.00000e+0	.0000	0.00000e+0	.0000
6.0	- 7.0	3.52357e+8	.0478	2.76994e+8	.0565	3.53124e+7	.1009	3.45845e+7	.0338	5.46640e+6	.0527	0.00000e+0	.0000	0.00000e+0	.0000	0.00000e+0	.0000
7.0	- 7.5	9.75156e+7	.0856	5.63270e+7	.1328	3.05521e+7	.1089	1.04385e+7	.0493	1.98043e+5	.2639	0.00000e+0	.0000	0.00000e+0	.0000	0.00000e+0	.0000
7.5	- 8.0	5.31670e+8	.0475	5.16566e+8	.0480	1.39714e+7	.1157	1.07823e+6	.1713	5.41122e+4	.4579	0.00000e+0	.0000	0.00000e+0	.0000	0.00000e+0	.0000
8.0	- 10.0	3.72511e+7	.1933	3.46680e+7	.1975	1.64225e+6	.2234	9.39587e+5	.2139	1.20127e+3	.9999	0.00000e+0	.0000	0.00000e+0	.0000	0.00000e+0	.0000
10.0	- 14.0	0.00000e+0	.0000	0.00000e+0	.0000	0.00000e+0	.0000	0.00000e+0	.0000	0.00000e+0	.0000	0.00000e+0	.0000	0.00000e+0	.0000	0.00000e+0	.0000
	Total:	1.89858e+9	.0248	1.18815e+9	.0277	1.66924e+8	.0360	1.46251e+8	.0180	1.59475e+8	.0196	8.58848e+7	.0232	1.18504e+8	.0430	3.33950e+7	.0515

** Results in the first column show the total leakage (p/s) for all gammas integrated over the entire forward hemisphere (0 to 90 degrees), while results in the other columns show the total leakage (p/s) within discrete angular ranges (0-2 degrees of the centerline, 2-5 degrees of the centerline, etc). These results are based on "real" boundary crossing counters, not point detectors. Also note that these are "leakage" rates (p/s) by energy group, not fluxes or currents. One can divide by the area of the hole to get currents, but the fluxes are not immediately available from this data since the effect of individual particle direction cosines with respect to the exit surface have already been applied to get the leakage rates.

---

* These six values also taken from Table D5.3.

towards the steel-lined concrete block assembly holding the rotary shutter. The small numbers, 1 through 10, indicate the surface segment numbers corresponding to Tallies 231 and 232, described below. Segment 10 in the center is the 6.5-inch-diameter hole in the concrete block assembly coming out from the rotary shutter, while segment 9 is the remainder of the 83.5025 cm x 83.5025 cm face of the steel-lined concrete block assembly holding the rotary shutter, segments 5 to 8 are the 1.74625 cm clearance gaps between the concrete block assembly and the biological shield, and segments 1 to 4 represent portions of the steel-clad biological shield beyond that, out to a radius of 65 cm.

D.5.2.1 Clear Right-to-Left Asymmetry in External Dose and Leakage Rates Due to Steaming in Shutter

Gammas streaming through the large 3.5-inch-diam hole in the rotary shutter as shown in Fig. 6.1 would tend to increase the radiation levels in segments 2 and 6 of Fig. D5.2 above those for segments 1 and 5, once one accounts for the proper spatial orientation of two figures. While the statistics for these regions are not particularly good, the integrated total gamma leakage rates in Table D5.5 do tend to confirm these expectations. Note that the leakage rate for the clearance gap on the right of Fig D5.2 (segment 6) is 2.06 times larger than that for the clearance gap (segment 5) on the left, while the leakage rate for that portion of biological shield on the right (segment 2) is 2.84 times larger than that for the corresponding portion on the left (segment 1). Moreover, the total average dose rates by segment as shown in Table D5.6 indicate the same trend, with the dose rate for segment 6 being 2.20 times larger than that for segment 5, and the dose rate for segment 2 being 3.10 times larger than that for segment 1. While the statistics are poor (because the fluxes and dose rates are relatively low), the trends are undeniable. Had the streaming effects been much more pronounced to the point of being truly significant from a radiological viewpoint, the fluxes and dose rates would have been much larger and the statistics would have automatically been much better.

Asymmetric streaming through the large beam hole in the closed shutter is causing a small but calculationally observable skewness in the fluxes and dose rates on the external surface. Moreover, the skewness in the right-to-left variations (2.2:1 and 3.1:1) is statistically significant beyond any shadow of a doubt, and suggests that while the magnitude of the actual leakages and dose rates were found to be small, the code and technique used here have the sensitivity needed to detect and predict any asymmetric streaming that might be significant. This is most reassuring.

D.5.2.2 Slight Top-to-Bottom Asymmetry in External Dose and Leakage Rates Due to Steaming Around Shutter

Likewise, to a lesser but still observable extent, there is a similar skewness in the external leakages and dose rates in the vertical direction caused by the position of the rotary shield plug inside the cavity. Fig. 3.13 shows the MCNP model of the carbon steel rotary shield plug sitting atop the stainless steel liner inside the concrete block housing assembly. While a 5/16-inch clearance gap was assumed circumferentially around the carbon steel shield plug, and a similar 5/16-inch clearance gap was assumed atop the carbon steel shield plug, no such clearance gap was assumed on the bottom since the carbon steel shield plug was assumed to be sitting flush against the bottom liner. While no attempt was made to bias the gamma flux up or down vertically in the MCNP calculation, the effect of that clearance gap near the top, while small, is still calculationally observable in Tables D5.5 and D5.6. The net leakage from the external clearance gap corresponding to segment 7 at the top in Fig D5.2, is 1.38 times larger than that for segment 8 at the bottom, while the leakage from the biological shield in segment 3 at the top is 1.27 times larger than that for segment 4 at the bottom. Likewise the average dose rate for the external clearance gap at the top (segment 7) is 1.48 times larger than that at the bottom (segment 8), while the average dose rate for that portion of the biological shield in segment 3 at the top is 1.31 times bigger than for segment 4 at the bottom. While these ratios are smaller than those seen from right-to-left, and arguably within the uncertainty of the calculation, the consistency with which these trends appear in a physically correct fashion would suggest that 3-D broad-group weight window approach has endowed the MCNP analysis with sufficient accuracy that it can pick up and sense even these small asymmetric effects, the resolution of which would become more and more precise if magnitude of the fluxes and dose rates were large enough to be radiologically significant.

D.5.2.3 Boundary Crossing Confirmation of Point Detector Dose Rate Downstream of Shield

From Table D5.5, it is clear that the vast majority of gammas getting through the shield come from two areas: the main face of the 83.5 cm x 83.5 cm concrete block holding the shutter (Segment 9, area= 6758.58 cm2, excluding the hole), and the small 6.5-inch-diameter hole (Segment 10, area=214.084 cm2) leading to the rotary shutter. Moreover, almost half of the gammas leaking from the system (p/s) come through the latter. For that reason, point detectors were placed at various locations along the centerline, downstream of the system, as shown in Fig. 6.5. Due to the importance of having an accurate dose rate assessment downstream of the system, it is also highly desirable to have a second confirmation of the centerline dose rates based on a more reliable boundary crossing tally.

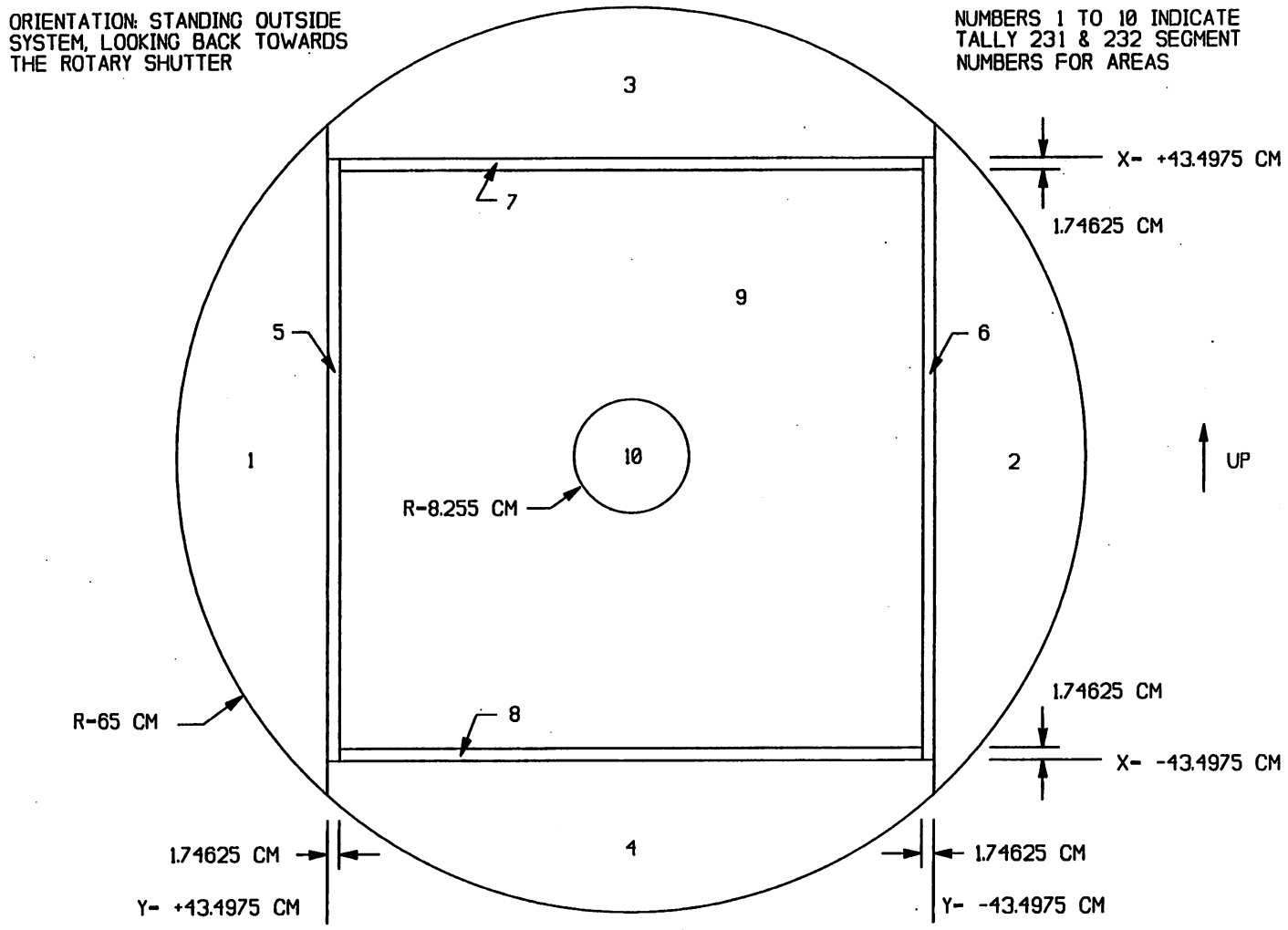


Fig. D5.2. Sketch of the 130-cm-diam external downstream surface of the entire shield configuration at Z=478.79 cm, looking back from outside the system (ie, from where the monochrometer drum would normally be located).

Table D5.5. Gamma leakage (p/s) across the various segments of a plane surface at Z=478.79 cm, corresponding to the downstream surface of the stainless steel liner on the concrete block assembly holding the rotary shutter. The locations of the various area segments are illustrated in Fig. D5.2, where segment 10 corresponds to the 6.5-inch-diam hole in the middle, directly downstream of the shutter, and segment 9 corresponds to the remainder of the central block. These values were calculated by Tally 231 in Run HB308G. The key thing to note here is the large amount of the gamma leakage (p/s) that comes through the 6.5-inch-diam hole in the middle (segment 10), and that this leakage, as well as that through the main face (segment 9), are both well converged.

		Segment 1		Segment 2		Segment 3		Segment 4		Segment 5	
Emin (MeV)	Emax (MeV)	Area: 1438.21 cm2 photons/sec	fsd	Area: 1438.21 cm2 photons/sec	fsd	Area: 1414.34 cm2 photons/sec	fsd	Area: 1414.34 cm2 photons/sec	fsd	Area: 151.915 cm2 photons/sec	fsd
0.010	0.020	4.33683e-1	.6120	9.95054e-1	.4351	3.46030e-1	.3719	7.61389e-1	.6552	0.00000e+0	.0000
0.020	0.045	7.88554e+0	.4410	1.06024e+1	.4325	4.70354e+0	.3640	4.14987e+0	.4031	1.06758e-1	.8280
0.045	0.070	9.38195e-1	.3240	3.71418e+0	.5149	3.11880e+0	.7346	7.78792e-1	.3090	7.39991e-1	.6833
0.070	0.10	3.45151e+0	.3537	9.21514e+0	.5037	2.15051e+0	.4235	3.91844e+0	.3608	9.72587e-1	.3369
0.10	0.15	1.17249e+1	.2526	5.23952e+1	.4438	2.58452e+1	.4983	1.54042e+1	.3888	1.24829e+1	.3634
0.15	0.30	1.72984e+2	.2479	5.46143e+2	.4051	1.79798e+2	.2591	1.38956e+2	.2516	6.04532e+1	.3529
0.30	0.40	1.35250e+2	.2209	3.60723e+2	.3928	1.45431e+2	.2380	1.11955e+2	.2207	4.73037e+1	.2925
0.40	0.51	1.33392e+2	.2347	4.24229e+2	.3706	1.65004e+2	.2300	1.46383e+2	.2102	6.77787e+1	.4542
0.51	0.60	1.63282e+2	.2479	4.92535e+2	.4119	1.95129e+2	.2387	1.51687e+2	.2272	3.47501e+1	.2483
0.60	0.70	1.00414e+2	.2200	2.53398e+2	.3567	1.17014e+2	.2207	8.97897e+1	.2097	1.48802e+1	.2310
0.70	1.0	2.50755e+2	.2039	6.53632e+2	.3328	2.94478e+2	.2260	2.42975e+2	.2173	8.62312e+1	.2127
1.0	1.5	3.51904e+2	.2031	8.55401e+2	.3315	4.00309e+2	.2200	3.26378e+2	.2186	1.08821e+2	.3028
1.5	2.0	2.86583e+2	.2096	6.53274e+2	.3217	3.11184e+2	.2179	2.88515e+2	.2321	7.47920e+1	.2781
2.0	2.5	2.32679e+2	.2123	5.14903e+2	.3355	2.67135e+2	.2238	2.80855e+2	.3510	9.66821e+1	.3346
2.5	3.0	2.06230e+2	.2334	5.10737e+2	.3252	2.46630e+2	.2285	1.85831e+2	.2555	1.39029e+2	.3943
3.0	4.0	3.63945e+2	.2695	7.68513e+2	.3640	3.76245e+2	.2661	2.80202e+2	.2598	1.54533e+2	.3084
4.0	5.0	2.93776e+2	.3799	5.50947e+2	.4091	4.60619e+2	.3428	2.41721e+2	.3288	9.09511e+1	.5046
5.0	6.0	2.81020e+2	.4367	1.07683e+3	.5462	3.13429e+2	.4533	1.58549e+2	.3842	1.00800e+1	.4811
6.0	7.0	1.73862e+2	.6202	2.21017e+2	.5387	7.76778e+1	.6638	2.32817e+2	.4502	8.52340e-1	.9999
7.0	7.5	0.00000e+0	.0000	7.41302e+1	.6613	1.56924e+1	.7819	7.96565e-1	.9999	0.00000e+0	.0000
7.5	8.0	0.00000e+0	.0000	9.78600e+2	.7662	7.83605e+1	.9928	0.00000e+0	.0000	0.00000e+0	.0000
8.0	10.0	0.00000e+0	.0000	0.00000e+0	.0000	0.00000e+0	.0000	0.00000e+0	.0000	0.00000e+0	.0000
10.0	14.0	0.00000e+0	.0000	0.00000e+0	.0000	0.00000e+0	.0000	0.00000e+0	.0000	0.00000e+0	.0000
	Total:	3.17051e+3	.2392	9.01193e+3	.3904	3.68030e+3	.2432	2.90242e+3	.2266	1.00144e+3	.2389

		Segment 6		Segment 7		Segment 8		Segment 9		Segment 10	
Emin (MeV)	Emax (MeV)	Area: 151.915 cm2 photons/sec	fsd	Area: 145.816 cm2 photons/sec	fsd	Area: 145.816 cm2 photons/sec	fsd	Area: 6758.58 cm2 photons/sec	fsd	Area: 214.084 cm2 photons/sec	fsd
0.010	0.020	8.59025e-2	.9999	0.00000e+0	.0000	1.09979e-2	.9999	2.80732e+0	.2651	2.33257e+0	.1428
0.020	0.045	4.93390e-2	.7728	7.32659e-2	.7411	1.45535e-1	.6825	9.49487e+0	.0880	1.47449e+1	.0794
0.045	0.070	9.82748e+0	.9588	3.67787e+1	.9815	2.76332e-1	.5113	2.79090e+1	.0783	3.76023e+1	.0549
0.070	0.10	1.97609e+1	.7451	2.89664e+0	.5360	1.23147e+0	.4865	1.04838e+2	.0597	1.42192e+2	.0431
0.10	0.15	3.46056e+1	.5674	1.42893e+1	.3654	1.25536e+1	.3127	5.48003e+2	.0529	6.59894e+2	.0384
0.15	0.30	1.45676e+2	.5315	3.47514e+1	.2962	3.28326e+1	.2558	2.46285e+3	.0510	2.50157e+3	.0372
0.30	0.40	1.07858e+2	.3641	4.63258e+1	.3681	2.94998e+1	.2727	1.55019e+3	.0520	1.32099e+3	.0370
0.40	0.51	1.20732e+2	.3937	5.08631e+1	.3333	2.30083e+1	.2534	1.53628e+3	.0538	1.24438e+3	.0370
0.51	0.60	1.43379e+2	.4965	3.97639e+1	.2728	4.17505e+1	.3694	1.45508e+3	.0590	1.36578e+3	.0374
0.60	0.70	7.64083e+1	.3858	2.70329e+1	.3679	1.46617e+1	.2943	9.75231e+2	.0502	6.64158e+2	.0362
0.70	1.0	1.94314e+2	.3455	5.30037e+1	.2353	9.01696e+1	.3095	2.51209e+3	.0512	1.68859e+3	.0357
1.0	1.5	2.23132e+2	.3192	1.18111e+2	.2467	1.09089e+2	.2894	3.31417e+3	.0517	2.16100e+3	.0354
1.5	2.0	1.54274e+2	.3146	1.02201e+2	.4156	8.70570e+1	.3520	2.61635e+3	.0534	1.67111e+3	.0349
2.0	2.5	9.53868e+1	.3509	1.08334e+2	.3128	9.07350e+1	.3781	2.21142e+3	.0779	1.38697e+3	.0346
2.5	3.0	1.07533e+2	.3635	6.67464e+1	.2989	2.84201e+1	.3478	1.67637e+3	.0455	1.19483e+3	.0342
3.0	4.0	1.79579e+2	.3517	1.18102e+2	.3509	6.39443e+1	.4379	2.49730e+3	.0470	2.02812e+3	.0332
4.0	5.0	1.49373e+2	.4693	4.47651e+1	.3794	3.86637e+1	.3400	1.58123e+3	.0547	1.79384e+3	.0331
5.0	6.0	7.59244e+1	.5281	3.64006e+1	.5196	2.77237e+1	.5495	1.07907e+3	.0941	1.61421e+3	.0360
6.0	7.0	3.53018e+1	.7640	4.96006e+1	.9328	2.67721e+0	.9999	5.13961e+2	.1100	1.84814e+3	.0444
7.0	7.5	1.74693e+1	.7111	1.15541e+1	.9749	1.51614e+0	.9999	1.06657e+2	.1807	7.02803e+2	.0627
7.5	8.0	1.76436e+2	.9645	0.00000e+0	.0000	0.00000e+0	.0000	2.71564e+2	.7262	1.60594e+3	.0603
8.0	10.0	0.00000e+0	.0000	0.00000e+0	.0000	0.00000e+0	.0000	1.12521e+1	.3630	1.42562e+2	.2340
10.0	14.0	0.00000e+0	.0000	0.00000e+0	.0000	0.00000e+0	.0000	0.00000e+0	.0000	0.00000e+0	.0000
	Total:	2.06711e+3	.3601	9.61594e+2	.2933	6.95966e+2	.2372	2.70641e+4	.0546	2.57918e+4	.0365

Table D5.6. Gamma dose rates (mrem/hr) averaged across the various segments of a plane surface at Z=478.79 cm, corresponding to the downstream surface of the stainless steel liner on the concrete block assembly holding the rotary shutter. The locations of the various area segments are illustrated in Fig. D5.2, where segment 10 corresponds to the 6.5-inch-diam hole in the middle, directly downstream of the shutter, and segment 9 corresponds to the remainder of the central block. These values were calculated by Tally 232 in Run HB308G. While the dose rate directly in front of the central hole (segment 10) is dominent, average values for the other areas are low because of the large areas over which they were averaged. To see real relative contributions, see integrated leakage terms in Table D5.5 (above). The key things to note here are that (1) these estimates are based on real boundary crossing tallies, and that (2) the "average" value here over the central 6.5-inch-diam hole is only 1.944 times lower than the "peak" value at the centerline given by point detector Tally 45. The fact that the two are in such excellent agreement is "positive confirmation" that the point detector values are trustworthy.

		Segment 1		Segment 2		Segment 3		Segment 4		Segment 5	
Emin (MeV)	Emax (MeV)	Area: 1438.21 cm2 mrem/hr	fsd	Area: 1438.21 cm2 mrem/hr	fsd	Area: 1414.34 cm2 mrem/hr	fsd	Area: 1414.34 cm2 mrem/hr	fsd	Area: 151.915 cm2 mrem/hr	fsd
0.010	0.020	6.70053e-7	.6191	1.14777e-6	.4427	4.06067e-7	.4620	3.61796e-7	.7277	0.00000e+0	.0000
0.020	0.045	4.32938e-6	.4502	6.60011e-6	.4117	2.97822e-6	.3583	2.22215e-6	.3961	4.29756e-7	.8180
0.045	0.070	2.08308e-7	.3295	7.71456e-7	.5105	6.56155e-7	.7407	1.82830e-7	.3124	1.48094e-6	.6601
0.070	0.10	7.59168e-7	.3394	2.08195e-6	.4977	4.70405e-7	.4096	9.25882e-7	.3707	2.32742e-6	.3635
0.10	0.15	3.57831e-6	.2624	1.82536e-5	.4230	7.91752e-6	.4549	7.58237e-6	.4464	4.82005e-5	.2922
0.15	0.30	1.17084e-4	.2577	3.00981e-4	.3871	2.24707e-4	.5475	9.35688e-5	.2534	4.07648e-4	.3404
0.30	0.40	1.43372e-4	.2190	3.75211e-4	.3864	1.62716e-4	.2318	1.22031e-4	.2203	3.83539e-4	.2575
0.40	0.51	1.76137e-4	.2379	5.24269e-4	.3626	2.19608e-4	.2279	1.94820e-4	.2044	6.91560e-4	.4197
0.51	0.60	2.59256e-4	.2495	7.66559e-4	.4066	3.10504e-4	.2403	2.42168e-4	.2298	4.78415e-4	.2600
0.60	0.70	1.60092e-4	.2208	4.02963e-4	.3535	1.92365e-4	.2235	1.47680e-4	.2127	2.07565e-4	.2259
0.70	1.0	4.47404e-4	.2071	1.18034e-3	.3236	5.37299e-4	.2252	4.42298e-4	.2172	1.21971e-3	.2024
1.0	1.5	7.31636e-4	.2022	1.79327e-3	.3237	8.42041e-4	.2189	6.87981e-4	.2167	1.94920e-3	.2932
1.5	2.0	6.94597e-4	.2051	1.59216e-3	.3172	7.60416e-4	.2176	6.91422e-4	.2273	1.61405e-3	.2723
2.0	2.5	6.40776e-4	.2082	1.41506e-3	.3332	7.37309e-4	.2241	7.55938e-4	.3340	2.34333e-3	.3252
2.5	3.0	6.26750e-4	.2303	1.54350e-3	.3246	7.55184e-4	.2291	5.78004e-4	.2544	3.76474e-3	.3915
3.0	4.0	1.24055e-3	.2656	2.63225e-3	.3632	1.31442e-3	.2655	9.86158e-4	.2578	4.83640e-3	.3061
4.0	5.0	1.14927e-3	.3777	2.16685e-3	.4083	1.83909e-3	.3426	9.69276e-4	.3256	3.29734e-3	.5021
5.0	6.0	1.24474e-3	.4369	4.72810e-3	.5437	1.40653e-3	.4521	7.19275e-4	.3834	4.19366e-4	.4801
6.0	7.0	8.59747e-4	.6218	1.09079e-3	.5390	3.89021e-4	.6630	1.17091e-3	.4501	3.96144e-5	.9999
7.0	7.5	0.00000e+0	.0000	3.92469e-4	.6613	8.44854e-5	.7807	4.31629e-6	.9999	0.00000e+0	.0000
7.5	8.0	0.00000e+0	.0000	5.39123e-3	.7658	4.38280e-4	.9927	0.00000e+0	.0000	0.00000e+0	.0000
8.0	10.0	0.00000e+0	.0000	0.00000e+0	.0000	0.00000e+0	.0000	0.00000e+0	.0000	0.00000e+0	.0000
10.0	14.0	0.00000e+0	.0000	0.00000e+0	.0000	0.00000e+0	.0000	0.00000e+0	.0000	0.00000e+0	.0000
	Total:	8.50096e-3	.2559	2.63248e-2	.4254	1.02264e-2	.2589	7.81712e-3	.2387	2.17049e-2	.2638

		Segment 6		Segment 7		Segment 8		Segment 9		Segment 10	
Emin (MeV)	Emax (MeV)	Area: 151.915 cm2 mrem/hr	fsd	Area: 145.816 cm2 mrem/hr	fsd	Area: 145.816 cm2 mrem/hr	fsd	Area: 6758.58 cm2 mrem/hr	fsd	Area: 214.084 cm2 mrem/hr	fsd
0.010	0.020	1.38716e-6	.9999	0.00000e+0	.0000	0.00000e+0	.0000	8.22639e-7	.3894	9.63548e-6	.2006
0.020	0.045	2.12474e-7	.7718	3.61231e-7	.7631	6.71678e-7	.7073	9.82171e-7	.0851	4.37461e-5	.0794
0.045	0.070	1.88409e-5	.9565	7.08125e-5	.9802	6.20786e-7	.5194	1.44273e-6	.0753	5.65988e-5	.0583
0.070	0.10	4.12383e-5	.6863	6.51336e-6	.4762	3.50324e-6	.5344	6.74252e-6	.0583	2.50063e-4	.0436
0.10	0.15	1.15200e-4	.5620	8.95831e-5	.4177	4.03445e-5	.2826	4.71959e-5	.0551	1.59958e-3	.0405
0.15	0.30	8.79601e-4	.5107	2.38319e-4	.2791	2.22338e-4	.2604	3.78841e-4	.0507	1.03948e-2	.0368
0.30	0.40	8.89613e-4	.3664	4.07034e-4	.3166	2.85410e-4	.2660	3.59998e-4	.0515	8.11035e-3	.0366
0.40	0.51	1.18849e-3	.3861	5.37017e-4	.2799	2.72010e-4	.2406	4.38628e-4	.0536	9.31381e-3	.0366
0.51	0.60	1.84262e-3	.4833	5.07082e-4	.2647	5.52862e-4	.3441	4.90946e-4	.0586	1.23883e-2	.0369
0.60	0.70	9.41781e-4	.3583	3.45203e-4	.3351	2.26939e-4	.2655	3.46807e-4	.0509	6.26229e-3	.0358
0.70	1.0	2.82895e-3	.3271	8.73417e-4	.2362	1.33234e-3	.2965	1.00310e-3	.0502	1.83411e-2	.0355
1.0	1.5	4.06423e-3	.3073	2.12592e-3	.2418	1.97837e-3	.2778	1.52432e-3	.0495	2.84631e-2	.0353
1.5	2.0	3.45668e-3	.3056	2.20441e-3	.3999	1.97834e-3	.3458	1.37897e-3	.0509	2.60992e-2	.0350
2.0	2.5	2.41958e-3	.3453	2.78778e-3	.3134	2.26931e-3	.3679	1.30285e-3	.0721	2.47421e-2	.0347
2.5	3.0	3.02058e-3	.3606	1.92416e-3	.2994	8.26779e-4	.3406	1.09610e-3	.0447	2.37765e-2	.0343
3.0	4.0	5.67326e-3	.3528	3.84662e-3	.3470	2.10725e-3	.4303	1.84037e-3	.0464	4.60422e-2	.0334
4.0	5.0	5.44136e-3	.4686	1.70163e-3	.3794	1.47673e-3	.3376	1.32412e-3	.0540	4.67043e-2	.0332
5.0	6.0	3.12857e-3	.5293	1.57117e-3	.5195	1.19246e-3	.5474	1.01366e-3	.0938	4.74763e-2	.0360
6.0	7.0	1.62193e-3	.7646	2.37099e-3	.9327	1.31658e-4	.9999	5.33744e-4	.1100	6.01868e-2	.0444
7.0	7.5	8.64589e-4	.7106	5.93144e-4	.9746	7.96595e-5	.9999	1.18871e-4	.1812	2.46268e-2	.0626
7.5	8.0	9.29514e-3	.9651	0.00000e+0	.0000	0.00000e+0	.0000	3.17169e-4	.7272	5.88834e-2	.0603
8.0	10.0	0.00000e+0	.0000	0.00000e+0	.0000	0.00000e+0	.0000	1.47016e-5	.3629	5.85047e-3	.2340
10.0	14.0	0.00000e+0	.0000	0.00000e+0	.0000	0.00000e+0	.0000	0.00000e+0	.0000	0.00000e+0	.0000
	Total:	4.77339e-2	.3710	2.22012e-2	.3380	1.49776e-2	.2425	1.35404e-2	.0597	4.59621e-1	.0374

Note that point detectors count uncollided contributions from each source point, as well as estimated contributions from each collision site in the system (of which there were over 855.2 million in this calculation). Nevertheless, if regions close to the detector point of interest were undersampled, as might happen if no real particles were ever successfully tracked that far into the shield, then the point detector response may or may not be correct and there is no way to tell for sure. In the most unfortunate of circumstances, the point detector response may be well converged because of the millions of small contributions from scattering events closer to the source but, if there are real scattering events or real particles in regions close to the detector that are not being adequately sampled in the calculation for whatever reason (no biasing, being killed by Russian Roulette prematurely, small solid angle as seen from the source, etc), then the point detector response may still differ from reality by a considerable margin -- ie, it may or may not be correct, there is simply no way to tell for sure. Conversely, if it can be verified that all regions are being adequately sampled, including those close to the detector, then the point detector response will likely be the most reliable response because it is based on a much larger number of events. It is critical, however, that one somehow first verify that regions close to the detector are being adequately sampled. That is the role of the boundary crossing detector corresponding to Segment 10 in Fig. D5.2 and Table D5.6. It will count only real particles that have actually been tracked through the entire configuration. If it sees a sufficiently large number of particles in all the key energy groups such that the dose rate associated with the boundary crossing tally has good statistics, one can rest assured that the region of interest downstream of the shield is being adequately sampled and that the point detector response is quite accurate.

In this particular calculation, unlike most of its unbiased predecessors, the response of the boundary crossing tally (Tally 232) for Segment 10 is incredibly excellent beyond any of our prior expectations. Generally, responses from boundary crossing estimators are considered "good to excellent" if the fractional standard deviation of the final response is below 10%. Table D5.6 shows that the total average dose rate for the 6.5-inch-diam disk corresponding to segment 10 is 0.4596 mrem/hr (+/- 3.74%), and that the fsd's for the dose rates in most of the important energy groups are in this same range, except for a couple that are in the 6% range. [Here at this particular location, the groups above 8 MeV are far less important than they were upstream of the steel shutter because most of them have been attenuated or slowed down to lower energies in the process of transporting through the carbon steel shutter.] For the most part, these excellent fsd's are uniformly characteristic of all energy groups. This highly-desirable behavior at this particular location is due to the fact that the 3-D broad-group weight windows were based on a fine-group adjoint analysis in which the adjoint source was intentionally placed at this same location. The fact that large numbers of real particles in all energy groups had actually survived the tracking process and "made it" this far, is a strong indication that the region near the downstream surface of the rotary shutter, and nearby regions that may contribute to the flux streaming through this hole, are indeed being adequately sampled. This, in turn, would suggest that the point detector response at the nearby location (on the centerline, in the void beyond the shield) is even more reliable. That, in fact, is the case, and the two are highly consistent. While the 0.4596 mrem/hr (+/- 3.74%) cited above corresponds to the "average" dose rate over the 6.5-inch-diam disk over the hole in the center at Z=478.79 cm, the point detector tally for the dose rate at Z=479.29 cm (cf Fig. 6.5 and/or Tally 45 in Table 6.6) shows the "peak" dose rate along the centerline to be 0.8934 mrem/hr +/- 3.4%. The two are highly consistent, and because the former confirms adequate sampling in the local region, the latter is deemed to be the best estimate of the local peak dose rate.

The other far less important results in Tables D5.5 and D5.6 are by-products of the calculation and have only been included here for the sake of completeness. The only key results of interest are those noted above.

Appendix E.1

Description of the input for MCNP Run HB309, a neutron-only beam tube calculation to determine the fluxes, and 12 different nuclear reaction rates, in each of 39 1-cm-thick cylindrical shells around the large beam hole in the rotary shutter when the water tube and collimator sections are both void and the shutter is in the open position.

HB309 was an MCNP neutron-only calculation for the HB-3 beam tube under normal conditions with the water tube and collimator sections both void and the rotary shutter wide open. The purpose was to determine the total neutron flux, the thermal neutron flux, and the following 12 reaction rates

Fe54(n,g)Fe55	Fe56(n,g)Fe57	Co59(n,g)Co60
Fe54(n,p)Mn54	Fe57(n,g)Fe58	Co60(n,g)Co61
Fe55(n,a)Cr52	Fe58(n,g)Fe59	
	Fe59(n,g)Fe60	
Mn54(n,g)Mn55	Fe59(n,a)Cr56	
Mn55(n,g)Mn56		

in each of 39 1-cm-thick concentric cylindrical shells around the large hole thru the rotary shutter. These reaction rates were later used in an ad hoc activation program (ACTSRC.FOR) to determine the radionulcide concentrations and gamma emission rates after 30 years of irradiation, followed by decay times ranging from 0 to 60 days. The resulting gamma sources 7 days after shutdown were then used in a subsequent gamma-only shielding calculation (MCNP Run HB310) to determine the gamma dose rate downstream of the "then closed" rotary shield plug, due to these activated gamma sources distributed in the 39 regions around the central hole in the rotary shutter shield plug.

The MCNP input for Run HB309 was created from Run HB308G, but with many of the features reset. For example, we still used the 1998 design (wrt location of the aluminum windows), but the water tube is now void, the large rotary shutter beam hole is now open, and HB309 is a neutron-only calculation which includes all neutrons down to and including thermal.

Because HB309 was built upon HB308G which was built upon HB304M4, the model found here is essentially a "generalized superset" of all the best improvements that have ever been made to date for the HB3 beam tube, dosimeters, water tube, collimator, and rotary shield plug. For the purpose of this calculation (Run HB309) a number of the basic features have been reset as described below:

Modifications needed to get HB309 from HB308G.I are as follows:
==========

1) Eliminate the "wssa=" and "wwinp=" specs from header (message) record;
   not writing any boundary source file & not using any weight-window file.

2) In the PROBLEM PARAMETER section:

   a) Use "mode n"; set nps=20000000 to run 20 million histories

   b) Comment ou the "cut:n" card, previously used in some runs to avoid tracking neutrons below 27 keV;
      will now track all neutrons, but will not track any gammas.

   c) Set prdmp to dump every 80,000 histories

   d) Comment out all the "imp:p" data previously used in HB308G

   e) Comment out the wwp:n & wwp:p cards; will not need weight window file(s) for this calc

   f) Eliminate the SSW card; not writing any boundary source

3) Use the original 61-grp si53, sp53, and ds63 data for neutrons (with all sources back on centerline to be conservative)
   Can leave the si73, sp73, and ds83 data for gammas where they are (this data will just be ignored)
   SDEF specs for this neutron-only calc should include:

```
sdef  erg=d53  pos ferg d63  $ source def for neutrons in HB-3 (total n/s = 9.64595E+16);  total n/s above 27 keV = 1.20830e16
      par=1                  $ par=1 for neut, par=2 for photons
      vec  0  0  1           $ reference vector if directional-dependent source is used
```

```
      dir=d3          $ angular distribution wrt vec (Caution: choice of angular distribution sampled will dictate choice of wgt)
      wgt=1.7332472-2 $ use this with d3;  wgt = [mu(max)-mu(min)]/[(+1)-(-1)] = [1.0000000000-0.965335056]/2 = 1.7332472-2
c     ------------------
c     Ang Dist: to spray isotropically across central void of HB-3 beam tube
si3   h  0.965335056   1.0  $ angular distribution;  mu boundaries (i.e, cosine boundaries wrt vec)
sp3   d  0  1  $ angular distribution; particle emmission probabilities by bin; first value (below lowest bin bound) must be zero
-------------------------------------------------
```

4) In terms of the basic model, we now want to:

a) Verify that aluminum windows 1 and 2 placed in their 1998 axail locations (see Cells 2140, 2141, 4305, 4380)
b) Turn big hole in rotary shutter to "open" position (Surfs 3131 & 3132 should use transformations 11 & 21, respectively)
c) Void the water tube (Cells 2145 & 2146 should use matl 61, den=-1.0e-20)
d) Void the region downstream of water tube but just upstream of collimator (Cell 4375 should use matl 61, den=-1.0e-20)
e) Void the rect hole in collimator (Cells 4300 & 4305 should use matl 61, den=-1.0e-20)
f) Keep pt det 15 (B&T measurement point) just as a touchpoint to make sure things are normalized properly

g) Verify that location of "importance cutoff plane" (Surf 1007) is at to Z=118.6879 cm to increase efficiency of these shutter activation calcs. [Surf 1007 is used in Cell 10110 (inner Al wall of beam tube) to kill all neutrons & photons below this location, ie: all those not within most forward-directed cone.]

5) Note the following change in the central collimator material (in spite of Pete's Feb'98 dwgs); change to carbon steel based on talks with folks on 5-15-98

```
c     4310  40  -7.92     4130  -4190 -4230  #(4210 -4211 4212 -4213)  imp:n=1  $ ss body of central collimator with rectangular hole
c     Mike Farrar thought the central collimator might be / should be / carbon steel (to get less activation)
c     Dan Pinkston confirmed that it was Type 1020 carbon steel (here, I just used pressure vessel carbon steel here; close enough)
c     Ron Poor (the draftsman) indicated that existing one had a thin black oxide coating for corrosion protection
4310  50  -7.8212  4130  -4190 -4230  #(4210 -4211 4212 -4213)  $   carbon steel (Type 1020) body of central collimator with rectangular hole;
      vol=15022.15  imp:n=1  $ vol needed to get flux in Tally 14;  carbon steel (Type 1020) body of central collimator with rectangular hole;
```

6) To facilitate the determination of fluxes and the 12 necessary reaction rates (cf Tallies f24:n thru f144:n) in each of 39 concentric 1-cm-thick cylinders around the large beam hole in the rotary shutter, the following surfaces were added to the model. These particular surfaces will not be used to define any new cells. They will only be used in the segmented volume detectors, f24:n through f144:n described below.

```
c     5170  cz    4.445  $ big hole is defined by surf 3131 which has a radius of 4.445 cm
5171  cz    5.445
5172  cz    6.445
5173  cz    7.445
  :    :      :    <-- series of concentric cylinders, 1-cm apart
5206  cz   40.445
5207  cz   41.445
5208  cz   42.445  $ consider everything past surf 5208 as "the remainder"
c     5209  cz   43.445  $ last point in shutter should be at 43.4433014 cm from its center
```

7) To get the necessary reaction rates in various regions of the rotary shutter, the following materials were added to the model. Note that the material description of the carbon steel used in the rotary shutter was not altered at all, and tracking remains unaffected; these materials specifications were simply added so that the necessary cross section data would be available for use in the various tallies, f34:n through f144:n described below.

```
m71  28058.24y  1.0  $ Ni58;  this material (m71) is used only to get the Ni58(n,P)Co58 reaction rate [(n,P)=103] in the dosimeters
m72  26054.24y  1.0  $ Fe54;  this material (m72) is used only to get the Fe54(n,P)Mn54 reaction rate [(n,P)=103] in the rotary shutter & dosimeters
m73  26058.26y  1.0  $ Fe58;  this material (m73) is used only to get the Fe58(n,g)Fe59 reaction rate [(n,g)=102] in the rotary shutter
m74  27059.50c  1.0  $ Co59;  this material (m74) is used only to get the Co59(n,g)Co60 reaction rate [(n,g)=102] in the rotary shutter
m75  26057.60c  1.0  $ Fe57;  this material (m75) is used only to get the Fe57(n,g)Fe58 reaction rate [(n,g)=102] in the rotary shutter
m76  26056.60c  1.0  $ Fe56;  this material (m76) is used only to get the Fe56(n,g)Fe57 reaction rate [(n,g)=102] in the rotary shutter
```

```
m77  25055.50c  1.0  $ Mn55;  this material (m77) is used only to get the Mn55(n,g)Mn56 reaction rate [(n,g)=102] in the rotary shutter
c
m78  25054.30y  1.0  $ Mn54;  this material (m78) is used only to get the Mn54(n,g)Mn55 reaction rate [(n,g)=102] in the rotary shutter
m79  26055.30y  1.0  $ Fe55;  this material (m79) is used only to get the Fe55(n,A)Cr52 reaction rate [(n,A)=107] in the rotary shutter
m80  26059.30y  1.0  $ Fe59;  this material (m80) is used 1-st to get the Fe59(n,g)Fe60 reaction rate [(n,g)=102] in the rotary shutter
c    26059.30y  1.0  $ Fe59;  this material (m80) is used 2-nd to get the Fe59(n,A)Cr56 reaction rate [(n,A)=107] in the rotary shutter
m81  27060.30y  1.0  $ Co60;  this material (m81) is used only to get the Co60(n,g)Co61 reaction rate [(n,g)=102] in the rotary shutter
m82  26054.26y  1.0  $ Fe54;  this material (m82) is used only to get the Fe54(n,g)Fe55 reaction rate [(n,g)=102] in the rotary shutter
---------------------------------
Tallies f24:n, f34:n, f44:n, f54:n, f64:n, f74:n, f84:n, f94:n, f104:n, f114:n, f124:n, f134:n and f144:n
were added to calculate fluxes & these last 12 reaction rates in the rotary shutter (see specifications below)
```

8) Regarding tallies used here:

a) Comment out HB304 detectors used to get neutron activation rates in dosimeters in HB-3 beam tube;
b) Comment out HB308 detectors used to get primary gamma fluxes at different points down HB-3 beam tube;
c) Keep the original point detector 15 (B&T measurement point) just as a touchpoint to make sure things are normalized properly;

d) Since this calc is for "neutrons-only", make sure that all "fm" multiplier cards use proper multiplier:
fmXX = 9.64595e16 = sum of equivalent point sources (n/s) in HB-3, velm grps 1-61, for HFIR at 100 MW (Sn=7.5573e18 n/s in global calc);
this will yield fluxes in n/s/cm2

e) Add the necessary segmented volume detectors (f24:n through f144:n) shown below. The full list of tallies used is as follows:

```
c     ------------------------------------------------------------------------------------------------------------------
c     *** start detectors used to get fluxes and reaction rates with HFIR at 100 MW
c     ------------------------------------------------------------------------------------------------------------------
c
fc15   N-Flux (n/s/cm2) at 655.6626 from tip of HB-3 at 100 MW
f15:n  0.0  0.0  678.1673  0.5   $ neut flux at pt 655.6629 cm from real tip of HB-3 beam tube, where Blosser & Thomas made measurements in June 1968 (cf ORNL-TM-2221)
fm15   9.64595e16  $ sum of equivalent point sources (n/s) in HB-3, velm grps 1-61, for HFIR at 100 MW (Sn=7.5573e18 n/s in global calc);  will yield fluxes in n/s/cm2
c      fm15   1.20830e16  $ sum of equivalent point sources (n/s) for velm grps 1-36 (E>27 keV; use for dosimetry calc only) in HB-3 for HFIR at 100 MW (Sn=7.5573e18 n/s
e15    $ Emax(ig) in MeV; corresponds to no particular group structure; chosen to facilitate comparison with Blosser & Thomas measurements
       0.4e-6  1.0e-6  1.9e-6  4.0e-6  6.0e-6  25.0e-6  100.0e-6  170.0e-6
       640.0e-6  2.4e-3  3.8e-3  2.0e-2  0.1  1.0  2.9  6.3  8.1  20.0
c
c      Note 1:  Comparisons with B&T are fair only if we use aluminum windows 1 & 2 for 1960 design AND use small hole in rotary shutter.
c      Note 2:  B&T tabulated their results with HFIR power normalized to 1.0 MW;  here we have it at 100.0 MW;  must renormalize later.
c      Note 3:  Many of B&T's results are n/s/cm2/eV, therefore must divide some of our results by delta-E later, where appropriate.
c      Note 4:  The energy ranges above were selected after consulting the B&T report, as well as the barn book to check width of certain resonances.
c
c
fc14   Average N-Flux (n/s/cm2) in metal part of central collimator (@ 100 MW)
c      $ used to get broad group neutron fluxes for ORIGEN analysis (which is later run offline to get activation sources)
fm14   9.64595e16  $ sum of equivalent point sources (n/s) in HB-3, velm grps 1-61, for HFIR at 100 MW (Sn=7.5573e18 n/s in global calc);  will yield fluxes in n/s/cm2
f14:n  4310   $ metal part of central collimator with rectangular hole
e14    $  Emax(MeV) for the 61 VELM neut grps (lowest to highest energy for MCNP):
       4.1399e-7    0.1   20.0  t  $ to get thermal flux below 0.414 eV, resonance-range flux, and fast flux above 0.1 MeV
c
c
fc24   Average N-Flux (n/s/cm2) in cyl shells forming rotary shutter (@ 100 MW)
c      $ used to get broad group neutron fluxes for ORIGEN analysis (which can be run offline later to get activation sources)
fm24   9.64595e16  $ sum of equivalent point sources (n/s) in HB-3, velm grps 1-61, for HFIR at 100 MW (Sn=7.5573e18 n/s in global calc);  will yield fluxes in n/s/cm2
f24:n  3090  $ carbon steel forming the shield plug (ie, the rotary shutter)
fs24   $ surfaces used to divide the rotary shutter shield plug into 1-cm-thick cylindrical shells starting at edge of big hole thru shutter
       -5171  -5172  -5173  -5174  -5175
       -5176  -5177  -5178  -5179  -5180
       -5181  -5182  -5183  -5184  -5185
```

```
      -5186  -5187  -5188  -5189  -5190
      -5191  -5192  -5193  -5194  -5195
      -5196  -5197  -5198  -5199  -5200
      -5201  -5202  -5203  -5204  -5205
      -5206  -5207  -5208
sd24  $ enter volume (cc) for each segment (including "remainder") to get vol-averaged neutron flux (n/s/cm2):
      $ volumes shown here were calculated by mcnp Run VV309;  based on 40,000,000 histories;  most volumes have fsd's of 0.0002
      1.89858E+03  2.27981E+03  2.65511E+03  3.02744E+03  3.39342E+03  $ vol (cc) for each of the 5 cyl shells between r= 4.445 & r= 9.445 cm from big hole centerline
      3.75537E+03  4.11116E+03  4.45690E+03  4.79709E+03  5.12661E+03  $ vol (cc) for each of the 5 cyl shells between r= 9.445 & r=14.445 cm from big hole centerline
      5.44592E+03  5.75543E+03  6.05497E+03  6.33840E+03  6.60982E+03  $ vol (cc) for each of the 5 cyl shells between r=14.445 & r=19.445 cm from big hole centerline
      6.86725E+03  7.10540E+03  7.32554E+03  7.53004E+03  7.70707E+03  $ vol (cc) for each of the 5 cyl shells between r=19.445 & r=24.445 cm from big hole centerline
      7.85115E+03  7.96738E+03  8.04809E+03  8.08235E+03  8.05935E+03  $ vol (cc) for each of the 5 cyl shells between r=24.445 & r=29.445 cm from big hole centerline
      7.95535E+03  6.44147E+03  4.99352E+03  4.08671E+03  3.36986E+03  $ vol (cc) for each of the 5 cyl shells between r=29.445 & r=34.445 cm from big hole centerline
      2.76096E+03  2.23160E+03  1.76511E+03  1.35264E+03  9.88281E+02  $ vol (cc) for each of the 5 cyl shells between r=34.445 & r=39.445 cm from big hole centerline
      6.71165E+02  4.01009E+02  1.86544E+02  3.97575E+01               $ vol (cc) for each of the 4 cyl shells between r=39.445 & r=43.4433014 cm from big hole centerli
e24   $  Emax(MeV) for the 61 VELM neut grps (lowest to highest energy for MCNP):
      4.1399e-7    0.1   20.0  t  $ to get thermal flux below 0.414 eV, resonance-range flux, and fast flux above 0.1 MeV
fq24  s e  $ spatial segments down vertically;  energy groups across horizontally
c
c
fc34  Fe58(n,g)Fe59 "reactions/sec/cc" in shutter seg if N(Fe58)= 1 atom/(b*cm)
fm34  $  Here, 9.64595e16 = sum of equivalent point sources (n/s) in HB-3, velm grps 1-61, for HFIR at 100 MW (Sn=7.5573e18 n/s in global calc);  will yield fluxes in n
      (9.64595e16  73  102)  $ to get number of (n,g) "reactions/sec/cc" in Fe58 if density of Fe58 = 1.0 atoms/(barn*cm)
f34:n 3090  $ carbon steel forming the shield plug (ie, the rotary shutter)
fs34  --> "SAME 38 VALUES AS IN TALLY 24" <--
sd34  --> "SAME 38 VALUES AS IN TALLY 24" <--
e34   --> "SAME AS IN TALLY 24" <--
fq34  --> "SAME AS IN TALLY 24" <--
c
c
fc44  Fe54(n,p)Mn54 "reactions/sec/cc" in shutter seg if N(Fe54)= 1 atom/(b*cm)
fm44  $  Here, 9.64595e16 = sum of equivalent point sources (n/s) in HB-3, velm grps 1-61, for HFIR at 100 MW (Sn=7.5573e18 n/s in global calc);  will yield fluxes in n
      (9.64595e16  72  103)  $ to get number of (n,p) "reactions/sec/cc" in Fe54 if density of Fe54 = 1.0 atoms/(barn*cm)
f44:n 3090  $ carbon steel forming the shield plug (ie, the rotary shutter)
fs44  --> "SAME 38 VALUES AS IN TALLY 24" <--
sd44  --> "SAME 38 VALUES AS IN TALLY 24" <--
e44   --> "SAME AS IN TALLY 24" <--
fq44  --> "SAME AS IN TALLY 24" <--
c
c
fc54  Co59(n,g)Co60 "reactions/sec/cc" in shutter seg if N(Co59)= 1 atom/(b*cm)
fm54  $  Here, 9.64595e16 = sum of equivalent point sources (n/s) in HB-3, velm grps 1-61, for HFIR at 100 MW (Sn=7.5573e18 n/s in global calc);  will yield fluxes in n
      (9.64595e16  74  102)  $ to get number of (n,g) "reactions/sec/cc" in Co59 if density of Co59 = 1.0 atoms/(barn*cm)
f54:n 3090  $ carbon steel forming the shield plug (ie, the rotary shutter)
fs54  --> "SAME 38 VALUES AS IN TALLY 24" <--
sd54  --> "SAME 38 VALUES AS IN TALLY 24" <--
e54   --> "SAME AS IN TALLY 24" <--
fq54  --> "SAME AS IN TALLY 24" <--
c
c
fc64  Fe57(n,g)Fe58 "reactions/sec/cc" in shutter seg if N(Fe57)= 1 atom/(b*cm)
fm64  $  Here, 9.64595e16 = sum of equivalent point sources (n/s) in HB-3, velm grps 1-61, for HFIR at 100 MW (Sn=7.5573e18 n/s in global calc);  will yield fluxes in n
      (9.64595e16  75  102)  $ to get number of (n,g) "reactions/sec/cc" in Fe57 if density of Fe57 = 1.0 atoms/(barn*cm)
f64:n 3090  $ carbon steel forming the shield plug (ie, the rotary shutter)
fs64  --> "SAME 38 VALUES AS IN TALLY 24" <--
sd64  --> "SAME 38 VALUES AS IN TALLY 24" <--
e64   --> "SAME AS IN TALLY 24" <--
fq64  --> "SAME AS IN TALLY 24" <--
```

```
c
c
fc74   Fe56(n,g)Fe57 "reactions/sec/cc" in shutter seg if N(Fe56)= 1 atom/(b*cm)
fm74   $  Here, 9.64595e16 = sum of equivalent point sources (n/s) in HB-3, velm grps 1-61, for HFIR at 100 MW (Sn=7.5573e18 n/s in global calc);  will yield fluxes in n
       (9.64595e16  76  102)  $ to get number of (n,g) "reactions/sec/cc" in Fe56 if density of Fe56 = 1.0 atoms/(barn*cm)
f74:n  3090  $ carbon steel forming the shield plug (ie, the rotary shutter)
fs74   --> "SAME 38 VALUES AS IN TALLY 24" <--
sd74   --> "SAME 38 VALUES AS IN TALLY 24" <--
e74    --> "SAME AS IN TALLY 24" <--
fq74   --> "SAME AS IN TALLY 24" <--
c
c
fc84   Mn55(n,g)Mn56 "reactions/sec/cc" in shutter seg if N(Mn55)= 1 atom/(b*cm)
fm84   $  Here, 9.64595e16 = sum of equivalent point sources (n/s) in HB-3, velm grps 1-61, for HFIR at 100 MW (Sn=7.5573e18 n/s in global calc);  will yield fluxes in n
       (9.64595e16  77  102)  $ to get number of (n,g) "reactions/sec/cc" in Mn55 if density of Mn55 = 1.0 atoms/(barn*cm)
f84:n  3090  $ carbon steel forming the shield plug (ie, the rotary shutter)
fs84   --> "SAME 38 VALUES AS IN TALLY 24" <--
sd84   --> "SAME 38 VALUES AS IN TALLY 24" <--
e84    --> "SAME AS IN TALLY 24" <--
fq84   --> "SAME AS IN TALLY 24" <--
c
c
fc94   Mn54(n,g)Mn55 "reactions/sec/cc" in shutter seg if N(Mn54)= 1 atom/(b*cm)
fm94   $  Here, 9.64595e16 = sum of equivalent point sources (n/s) in HB-3, velm grps 1-61, for HFIR at 100 MW (Sn=7.5573e18 n/s in global calc);  will yield fluxes in n
       (9.64595e16  78  102)  $ to get number of (n,g) "reactions/sec/cc" in Mn54 if density of Mn54 = 1.0 atoms/(barn*cm)
f94:n  3090  $ carbon steel forming the shield plug (ie, the rotary shutter)
fs94   --> "SAME 38 VALUES AS IN TALLY 24" <--
sd94   --> "SAME 38 VALUES AS IN TALLY 24" <--
e94    --> "SAME AS IN TALLY 24" <--
fq94   --> "SAME AS IN TALLY 24" <--
c
c
fc104   Fe54(n,g)Fe55 "reactions/sec/cc" in shutter seg if N(Fe54)=1 atom/(b*cm)
fm104   $  Here, 9.64595e16 = sum of equivalent point sources (n/s) in HB-3, velm grps 1-61, for HFIR at 100 MW (Sn=7.5573e18 n/s in global calc);  will yield fluxes in
       (9.64595e16  82  102)  $ to get number of (n,g) "reactions/sec/cc" in Fe54 if density of Fe54 = 1.0 atoms/(barn*cm)
f104:n  3090  $ carbon steel forming the shield plug (ie, the rotary shutter)
fs104   --> "SAME 38 VALUES AS IN TALLY 24" <--
sd104   --> "SAME 38 VALUES AS IN TALLY 24" <--
e104    --> "SAME AS IN TALLY 24" <--
fq104   --> "SAME AS IN TALLY 24" <--
c
c
fc114   Fe55(n,A)Cr52 "reactions/sec/cc" in shutter seg if N(Fe55)=1 atom/(b*cm)
fm114   $  Here, 9.64595e16 = sum of equivalent point sources (n/s) in HB-3, velm grps 1-61, for HFIR at 100 MW (Sn=7.5573e18 n/s in global calc);  will yield fluxes in
       (9.64595e16  79  107)  $ to get number of (n,A) "reactions/sec/cc" in Fe55 if density of Fe55 = 1.0 atoms/(barn*cm)
f114:n  3090  $ carbon steel forming the shield plug (ie, the rotary shutter)
fs114   --> "SAME 38 VALUES AS IN TALLY 24" <--
sd114   --> "SAME 38 VALUES AS IN TALLY 24" <--
e114    --> "SAME AS IN TALLY 24" <--
fq114   --> "SAME AS IN TALLY 24" <--
c
c
fc124   Fe59(n,g)Fe60 "reactions/sec/cc" in shutter seg if N(Fe59)=1 atom/(b*cm)
fm124   $  Here, 9.64595e16 = sum of equivalent point sources (n/s) in HB-3, velm grps 1-61, for HFIR at 100 MW (Sn=7.5573e18 n/s in global calc);  will yield fluxes in
       (9.64595e16  80  102)  $ to get number of (n,g) "reactions/sec/cc" in Fe59 if density of Fe59 = 1.0 atoms/(barn*cm)
f124:n  3090  $ carbon steel forming the shield plug (ie, the rotary shutter)
fs124   --> "SAME 38 VALUES AS IN TALLY 24" <--
sd124   --> "SAME 38 VALUES AS IN TALLY 24" <--
```

```
e124    --> "SAME AS IN TALLY 24" <--
fq124   --> "SAME AS IN TALLY 24" <--
c
c
fc134   Fe59(n,A)Cr56 "reactions/sec/cc" in shutter seg if N(Fe59)=1 atom/(b*cm)
fm134   $  Here, 9.64595e16 = sum of equivalent point sources (n/s) in HB-3, velm grps 1-61, for HFIR at 100 MW (Sn=7.5573e18 n/s in global calc);  will yield fluxes in
       (9.64595e16  80  107)  $ to get number of (n,A) "reactions/sec/cc" in Fe59 if density of Fe59 = 1.0 atoms/(barn*cm)
f134:n  3090  $ carbon steel forming the shield plug (ie, the rotary shutter)
fs134   --> "SAME 38 VALUES AS IN TALLY 24" <--
sd134   --> "SAME 38 VALUES AS IN TALLY 24" <--
e134    --> "SAME AS IN TALLY 24" <--
fq134   --> "SAME AS IN TALLY 24" <--
c
c
fc144   Co60(n,g)Co61 "reactions/sec/cc" in shutter seg if N(Co60)=1 atom/(b*cm)
fm144   $  Here, 9.64595e16 = sum of equivalent point sources (n/s) in HB-3, velm grps 1-61, for HFIR at 100 MW (Sn=7.5573e18 n/s in global calc);  will yield fluxes in
       (9.64595e16  81  102)  $ to get number of (n,g) "reactions/sec/cc" in Co60 if density of Co60 = 1.0 atoms/(barn*cm)
f144:n  3090  $ carbon steel forming the shield plug (ie, the rotary shutter)
fs144   --> "SAME 38 VALUES AS IN TALLY 24" <--
sd144   --> "SAME 38 VALUES AS IN TALLY 24" <--
e144    --> "SAME AS IN TALLY 24" <--
fq144   --> "SAME AS IN TALLY 24" <--
c
c
c      ------------------------------------------------------------------------------------------------------------------------
c      ********** end of model **********
c      ------------------------------------------------------------------------------------------------------------------------
```

Table E1.1. Key reaction rates (per unit atom density), and associated fsd's, in each segment of the rotary shutter under nominal conditions. This table gives the "reactions/sec/cc" that would exist in the steel portion of each 1-cm-thick cylindrical shell segment of the shutter (going outward from the 3.5-inch-diam beam hole) if the density of the nuclide was 1.0 atoms/(barn*cm). Because the outermost shell segments just "clip the outside corners" of the steel shutter, their volumes are very small. Also note that the most important segments for activation purposes are the first few closest to the beam hole, where the flux has not been attenuated much. These results are based on Run HB309 where the water tube and collimator sections were both void, the shutter was wide open, and the HFIR was operating at 100 MW.

Segment Number	Dist (cm) from centerline of big beam hole		Rot.Shutter Cell 3090 Segment Vol	Tally 84 (total)		Tally 44 (total)		Tally 74 (total)		Tally 64 (total)		Tally 34 (total)		Tally 54 (total)	
seg	rmin	rmax	volume (cc)	Mn55(n,g)Mn56	fsd	Fe54(n,p)Mn54	fsd	Fe56(n,g)Fe57	fsd	Fe57(n,g)Fe58	fsd	Fe58(n,g)Fe59	fsd	Co59(n,g)Co60	fsd
1	4.445	5.445	1.89858E+03	1.84169E+10	.0091	1.20292E+07	.0883	3.36721E+09	.0088	3.19633E+09	.0089	1.57216E+09	.0145	5.78845E+10	.0137
2	5.445	6.445	2.27981E+03	1.25220E+10	.0088	6.67175E+06	.0923	2.25370E+09	.0084	2.14003E+09	.0083	1.14615E+09	.0381	4.06547E+10	.0141
3	6.445	7.445	2.65511E+03	9.38180E+09	.0091	5.25048E+06	.0879	1.67026E+09	.0086	1.58950E+09	.0087	8.48714E+08	.0382	3.06994E+10	.0151
4	7.445	8.445	3.02744E+03	5.16367E+09	.0119	2.58757E+06	.1029	8.73702E+08	.0102	8.45299E+08	.0106	4.32341E+08	.0248	1.76769E+10	.0195
5	8.445	9.445	3.39342E+03	2.77038E+09	.0148	1.10414E+06	.1060	4.41938E+08	.0119	4.33831E+08	.0125	2.31799E+08	.0490	1.04784E+10	.0300
6	9.445	10.445	3.75537E+03	1.82913E+09	.0187	8.03867E+05	.1161	2.69553E+08	.0148	2.63626E+08	.0145	1.50153E+08	.0527	7.29654E+09	.0345
7	10.445	11.445	4.11116E+03	1.23859E+09	.0229	6.54756E+05	.1360	1.68245E+08	.0167	1.69071E+08	.0179	8.94690E+07	.0424	5.34792E+09	.0400
8	11.445	12.445	4.45690E+03	8.55010E+08	.0249	4.41701E+05	.1467	1.15170E+08	.0236	1.16809E+08	.0227	6.46687E+07	.0527	4.09892E+09	.0513
9	12.445	13.445	4.79709E+03	6.40729E+08	.0308	3.78326E+05	.1912	7.62715E+07	.0265	7.88794E+07	.0237	5.18197E+07	.1123	3.11880E+09	.0510
10	13.445	14.445	5.12661E+03	5.04035E+08	.0354	2.53326E+05	.1683	5.46814E+07	.0287	5.81192E+07	.0290	3.51538E+07	.0922	2.74753E+09	.0597
11	14.445	15.445	5.44592E+03	3.92140E+08	.0371	2.03298E+05	.1940	4.23195E+07	.0421	4.55823E+07	.0414	2.67623E+07	.0882	2.22914E+09	.0620
12	15.445	16.445	5.75543E+03	3.35307E+08	.0439	1.62342E+05	.2430	3.23935E+07	.0338	3.51442E+07	.0442	3.00751E+07	.1999	1.70038E+09	.0651
13	16.445	17.445	6.05497E+03	2.73264E+08	.0461	9.57636E+04	.2050	2.76522E+07	.0523	2.91652E+07	.0428	3.66566E+07	.2372	1.43644E+09	.0775
14	17.445	18.445	6.33840E+03	2.27944E+08	.0475	7.33266E+04	.2096	2.20551E+07	.0360	2.46814E+07	.0426	2.40311E+07	.1861	1.15434E+09	.0727
15	18.445	19.445	6.60982E+03	1.92078E+08	.0497	8.56045E+04	.2967	1.76561E+07	.0377	2.06657E+07	.0416	1.43074E+07	.1336	1.03716E+09	.0815
16	19.445	20.445	6.86725E+03	1.72462E+08	.0541	5.96741E+04	.2593	1.46348E+07	.0361	1.77527E+07	.0472	1.27613E+07	.1670	8.20952E+08	.0855
17	20.445	21.445	7.10540E+03	1.58814E+08	.0573	4.36338E+04	.2540	1.27331E+07	.0490	1.46638E+07	.0462	2.23069E+07	.3047	7.84838E+08	.0866
18	21.445	22.445	7.32554E+03	1.38011E+08	.0627	3.66938E+04	.2626	1.07375E+07	.0423	1.31289E+07	.0514	1.09186E+07	.2040	6.02624E+08	.0881
19	22.445	23.445	7.53004E+03	1.10222E+08	.0598	3.31433E+04	.2912	9.74353E+06	.0748	1.16829E+07	.0554	6.67290E+06	.0958	5.61004E+08	.0907
20	23.445	24.445	7.70707E+03	9.73559E+07	.0670	2.71341E+04	.3215	9.28538E+06	.0908	1.13470E+07	.0766	1.23014E+07	.3123	5.46825E+08	.1045
21	24.445	25.445	7.85115E+03	8.52599E+07	.0655	1.70733E+04	.3357	8.09216E+06	.0546	1.08416E+07	.0863	5.22684E+06	.1065	4.63993E+08	.1107
22	25.445	26.445	7.96738E+03	7.89212E+07	.0731	1.25406E+04	.4044	6.72191E+06	.0550	8.76487E+06	.0794	5.80662E+06	.1644	3.46108E+08	.1162
23	26.445	27.445	8.04809E+03	7.39348E+07	.0849	1.37422E+04	.4058	5.83975E+06	.0625	7.26148E+06	.0592	6.27061E+06	.2132	4.29789E+08	.1420
24	27.445	28.445	8.08235E+03	6.10265E+07	.0807	6.98949E+03	.3426	5.30684E+06	.0543	6.93971E+06	.0726	6.00283E+06	.2449	3.42289E+08	.1288
25	28.445	29.445	8.05935E+03	6.61182E+07	.0916	6.42573E+03	.3846	4.89180E+06	.0601	6.17780E+06	.0673	5.91870E+06	.2466	2.56266E+08	.1380
26	29.445	30.445	7.95535E+03	5.89068E+07	.0869	9.50111E+03	.5646	4.45160E+06	.0613	5.27628E+06	.0720	4.47121E+06	.2185	2.45520E+08	.1258
27	30.445	31.445	6.44147E+03	5.39730E+07	.1029	2.73547E+03	.4541	3.90635E+06	.0676	4.86002E+06	.0683	2.85362E+06	.1233	2.86070E+08	.2008
28	31.445	32.445	4.99352E+03	3.89956E+07	.1459	1.59773E+03	.3977	3.36825E+06	.1242	5.20521E+06	.1843	1.96904E+06	.0968	2.64852E+08	.2170
29	32.445	33.445	4.08671E+03	3.61343E+07	.1658	6.43392E+02	.5962	2.54684E+06	.1116	5.25065E+06	.2030	2.53224E+06	.3466	1.72396E+08	.2266
30	33.445	34.445	3.36986E+03	2.99655E+07	.1641	1.59097E+02	.4057	1.98251E+06	.1164	3.97629E+06	.1772	4.48026E+06	.6274	1.17480E+08	.2624
31	34.445	35.445	2.76096E+03	3.16423E+07	.2139	1.51799E+02	.5255	2.16223E+06	.4136	2.23946E+06	.1760	1.98723E+06	.3296	1.87061E+08	.2879
32	35.445	36.445	2.23160E+03	2.99357E+07	.2587	1.80963E+02	.5485	1.60233E+06	.3233	3.02018E+06	.2622	1.74243E+06	.4104	2.08958E+08	.3084
33	36.445	37.445	1.76511E+03	1.87112E+07	.2298	2.74708E+02	.5738	1.60190E+06	.2898	3.40241E+06	.3999	7.31046E+05	.1843	2.95190E+08	.3661
34	37.445	38.445	1.35264E+03	1.51089E+07	.3350	3.34009E+02	.6007	2.55469E+06	.6223	1.84750E+06	.4014	5.80676E+06	.8681	1.55585E+08	.4308
35	38.445	39.445	9.88281E+02	1.29813E+07	.4032	6.53157E+01	.8595	1.23464E+06	.2520	2.21092E+06	.4437	6.43253E+05	.2049	3.65217E+08	.7534
36	39.445	40.445	6.71165E+02	9.25437E+06	.2696	2.51263E+01	.9904	8.49530E+05	.2948	2.70400E+06	.5240	4.54047E+05	.2457	1.77113E+08	.8273
37	40.445	41.445	4.01009E+02	4.44866E+06	.3348	7.91661E+00	.9862	5.14348E+05	.3658	3.18876E+06	.7137	3.32985E+05	.3037	1.06684E+07	.3165
38	41.445	42.445	1.86544E+02	2.29941E+06	.4291	1.51097E-01	.4376	2.57386E+05	.5780	3.15490E+06	.4800	1.66274E+05	.4020	5.70826E+06	.4472
39	42.445	43.4433	3.97575E+01	2.80385E+05	.4664	2.08653E-01	.5825	3.11991E+04	.4251	1.33737E+06	.8622	5.19141E+04	.3602	1.72262E+06	.8887

Table E1.1 (cont)

Segment Number	Dist (cm) from centerline of big beam hole		Rot.Shutter Cell 3090 Segment Vol	Tally 94 (total)		Tally 104 (total)		Tally 114 (total)		Tally 124 (total)		Tally 134 (total)		Tally 144 (total)	
seg	rmin	rmax	volume (cc)	Mn54(n,g)Mn55	fsd	Fe54(n,g)Fe55	fsd	Fe55(n,A)Cr52	fsd	Fe59(n,g)Fe60	fsd	Fe59(n,A)Cr56	fsd	Co60(n,g)Co61	fsd
1	4.445	5.445	1.89858E+03	1.26622E+10	.0086	5.99198E+09	.0082	2.02828E+05	.2832	2.14995E+09	.0086	3.32113E+03	.6430	3.16042E+09	.0094
2	5.445	6.445	2.27981E+03	8.62084E+09	.0082	4.14389E+09	.0079	1.35130E+05	.3302	1.44126E+09	.0081	1.34551E+03	.8074	2.20321E+09	.0093
3	6.445	7.445	2.65511E+03	6.51046E+09	.0086	3.13285E+09	.0082	1.22644E+05	.3433	1.07228E+09	.0085	2.51155E+03	.9021	1.69199E+09	.0098
4	7.445	8.445	3.02744E+03	3.56730E+09	.0101	1.72564E+09	.0098	5.63003E+04	.3929	5.62506E+08	.0100	3.30643E+02	.7197	9.72573E+08	.0121
5	8.445	9.445	3.39342E+03	1.96939E+09	.0124	9.50033E+08	.0119	7.41870E+03	.5560	2.86986E+08	.0117	1.71738E+00	.9999	5.77529E+08	.0158
6	9.445	10.445	3.75537E+03	1.30528E+09	.0147	6.12330E+08	.0141	4.30735E+03	.5923	1.74651E+08	.0137	0.00000E+00	.0000	4.08203E+08	.0190
7	10.445	11.445	4.11116E+03	9.02419E+08	.0173	4.13005E+08	.0164	1.09205E+03	.6387	1.10666E+08	.0158	0.00000E+00	.0000	2.97571E+08	.0221
8	11.445	12.445	4.45690E+03	6.61735E+08	.0196	2.95404E+08	.0193	5.56648E+02	.8312	7.44673E+07	.0178	0.00000E+00	.0000	2.27118E+08	.0245
9	12.445	13.445	4.79709E+03	4.94689E+08	.0226	2.08192E+08	.0210	2.73019E+02	.6480	5.04288E+07	.0203	0.00000E+00	.0000	1.79749E+08	.0278
10	13.445	14.445	5.12661E+03	3.86573E+08	.0247	1.58984E+08	.0231	1.62800E+02	.6590	3.64339E+07	.0221	0.00000E+00	.0000	1.45030E+08	.0298
11	14.445	15.445	5.44592E+03	3.14478E+08	.0276	1.27956E+08	.0254	1.51162E+02	.8926	2.78752E+07	.0242	0.00000E+00	.0000	1.22003E+08	.0331
12	15.445	16.445	5.75543E+03	2.59155E+08	.0299	1.04389E+08	.0275	5.13810E+01	.9188	2.18257E+07	.0253	0.00000E+00	.0000	1.01511E+08	.0353
13	16.445	17.445	6.05497E+03	2.16017E+08	.0319	8.83181E+07	.0294	8.32803E-01	.9999	1.78110E+07	.0276	0.00000E+00	.0000	8.67970E+07	.0374
14	17.445	18.445	6.33840E+03	1.84598E+08	.0336	7.62692E+07	.0320	0.00000E+00	.0000	1.49781E+07	.0294	0.00000E+00	.0000	7.54545E+07	.0394
15	18.445	19.445	6.60982E+03	1.55570E+08	.0358	6.45517E+07	.0344	0.00000E+00	.0000	1.23244E+07	.0312	0.00000E+00	.0000	6.46226E+07	.0412
16	19.445	20.445	6.86725E+03	1.34916E+08	.0373	5.46605E+07	.0353	0.00000E+00	.0000	1.05036E+07	.0322	0.00000E+00	.0000	5.65885E+07	.0434
17	20.445	21.445	7.10540E+03	1.16707E+08	.0387	4.79391E+07	.0492	0.00000E+00	.0000	8.87970E+06	.0333	0.00000E+00	.0000	4.90034E+07	.0440
18	21.445	22.445	7.32554E+03	1.04449E+08	.0409	4.19608E+07	.0676	0.00000E+00	.0000	7.65916E+06	.0358	0.00000E+00	.0000	4.47282E+07	.0466
19	22.445	23.445	7.53004E+03	9.18358E+07	.0423	3.36966E+07	.0414	0.00000E+00	.0000	6.63824E+06	.0377	0.00000E+00	.0000	3.87558E+07	.0473
20	23.445	24.445	7.70707E+03	8.01191E+07	.0439	2.94455E+07	.0433	0.00000E+00	.0000	5.85553E+06	.0407	0.00000E+00	.0000	3.40701E+07	.0491
21	24.445	25.445	7.85115E+03	7.10371E+07	.0459	2.71815E+07	.0457	0.00000E+00	.0000	5.42374E+06	.0424	0.00000E+00	.0000	3.05252E+07	.0517
22	25.445	26.445	7.96738E+03	6.24565E+07	.0486	2.36507E+07	.0469	0.00000E+00	.0000	4.71597E+06	.0430	0.00000E+00	.0000	2.70076E+07	.0543
23	26.445	27.445	8.04809E+03	5.80331E+07	.0507	2.09731E+07	.0514	0.00000E+00	.0000	4.13551E+06	.0443	0.00000E+00	.0000	2.48438E+07	.0561
24	27.445	28.445	8.08235E+03	5.33454E+07	.0525	1.87989E+07	.0522	0.00000E+00	.0000	3.84405E+06	.0470	0.00000E+00	.0000	2.26819E+07	.0569
25	28.445	29.445	8.05935E+03	4.80855E+07	.0554	1.86951E+07	.0732	0.00000E+00	.0000	3.52275E+06	.0520	0.00000E+00	.0000	2.15119E+07	.0615
26	29.445	30.445	7.95535E+03	4.57404E+07	.0574	1.58571E+07	.0602	0.00000E+00	.0000	3.19568E+06	.0520	0.00000E+00	.0000	2.10725E+07	.0629
27	30.445	31.445	6.44147E+03	4.29561E+07	.0624	1.38394E+07	.0661	0.00000E+00	.0000	2.88050E+06	.0585	0.00000E+00	.0000	2.05226E+07	.0692
28	31.445	32.445	4.99352E+03	3.69811E+07	.0811	1.19015E+07	.0872	0.00000E+00	.0000	2.25836E+06	.0722	0.00000E+00	.0000	1.67992E+07	.0851
29	32.445	33.445	4.08671E+03	3.02216E+07	.0886	9.08576E+06	.0992	0.00000E+00	.0000	1.89263E+06	.0876	0.00000E+00	.0000	1.38844E+07	.0949
30	33.445	34.445	3.36986E+03	2.74636E+07	.1042	8.42691E+06	.1374	0.00000E+00	.0000	1.52881E+06	.0991	0.00000E+00	.0000	1.38453E+07	.1134
31	34.445	35.445	2.76096E+03	2.49245E+07	.1301	5.61515E+06	.1367	0.00000E+00	.0000	1.09491E+06	.0961	0.00000E+00	.0000	1.34534E+07	.1408
32	35.445	36.445	2.23160E+03	2.55141E+07	.1563	5.37685E+06	.1587	0.00000E+00	.0000	1.03533E+06	.1168	0.00000E+00	.0000	1.26163E+07	.1583
33	36.445	37.445	1.76511E+03	2.15737E+07	.1802	5.13309E+06	.2009	0.00000E+00	.0000	1.02367E+06	.1584	0.00000E+00	.0000	1.00471E+07	.1740
34	37.445	38.445	1.35264E+03	1.41898E+07	.1794	4.02939E+06	.2865	0.00000E+00	.0000	7.86281E+05	.1892	0.00000E+00	.0000	6.81065E+06	.1906
35	38.445	39.445	9.88281E+02	1.35236E+07	.2207	4.37901E+06	.2695	0.00000E+00	.0000	9.12764E+05	.2023	0.00000E+00	.0000	5.00097E+06	.1827
36	39.445	40.445	6.71165E+02	1.13716E+07	.2647	3.45857E+06	.3010	0.00000E+00	.0000	7.76966E+05	.2421	0.00000E+00	.0000	5.05343E+06	.2388
37	40.445	41.445	4.01009E+02	7.43682E+06	.3631	2.60602E+06	.3672	0.00000E+00	.0000	4.84942E+05	.2841	0.00000E+00	.0000	4.13671E+06	.3567
38	41.445	42.445	1.86544E+02	5.15752E+06	.5030	1.78521E+06	.5332	0.00000E+00	.0000	2.77516E+05	.3638	0.00000E+00	.0000	3.52430E+06	.3689
39	42.445	43.4433	3.97575E+01	1.19179E+06	.5172	3.94089E+05	.6875	0.00000E+00	.0000	9.67132E+04	.3551	0.00000E+00	.0000	1.43811E+06	.5618

Appendix E.2

ACTSRC.FOR: An ad hoc activation program to obtain the (activation) decay gamma source terms (p/s/cc) and (p/s) in each of the 39 1-cm-thick cylindrical shells concentrically centered around the 3.5-inch-diam beam hole through the HB-3 rotary shutter.

Sources obtained represent the "equivalent" gamma source at 1.25 MeV due to the decay of Mn-54, Mn-56, Fe-59, and Co-60, all at 7 days after shutdown following 30 years of exposure under normal conditions (at 100 MW).

More detailed information is also available, by nuclide, for each of the first 60 days after shutdown, if one runs the program and then examines the detailed results in the auxiliary output file (actsrc.aux).

Reaction rates (in each of the 39 zones, during normal operation) upon which this program is based, are listed in the various "data statements" below, and are taken directly from volume-averaged estimates for each of the 12 relevant nuclear reaction rates in each cylindrical shell, as determined by a rigorous MCNP analysis (Run HB309).

Two key assumptions are that the Type 1020 carbon steel rotary shutter initially contained:

0.45 wt% Mn-55 (Type 1020 carbon steel typically contains 0.30-0.60 wt% Mn-55; see page 6.30 of Ref 31)

0.015 wt% Co-59 (HFIR vessel has this amount [see page 106 of Ref 6], while the HB-1 and HB-4 nozzles have 0.005 wt%, and the HB-2 and HB-3 nozzles have 0.03 wt%)

```
c     ************************************************************************************************************
c     ************************************************************************************************************
c
c     ACTSRC.FOR -- a utility program to obtain the (activation) decay gamma source terms (p/s/cc) and (p/s)
c                   in each of the 39 1-cm-thick cylindrical shells concentrically centered around the big
c                   beam hole thru the HB-3 rotary shutter;  sources obtained represent the "equivalent"
c                   gamma source at 1.25 MeV due to the decay of Mn-54, Mn-56, Fe-59, and Co-60, all at 7 days
c                   after shutdown (although more detailed info is also available, by nuclide, for each of
c                   the first 60 days after shutdown, if one digs thru the detailed print statements);
c                   reaction rates (during normal operation) upon which this is based, are taken directly
c                   from volume-averaged estimates of each relevant reaction rate in each cylindrical shell,
c                   as determined by a rigorous MCNP analysis.
c
c                   Two key assumptions are that the Type 1020 carbon steel rotary shutter initially contained:
c
c                   0.45  wt% Mn-55 (Type 1020 carbon steel typically contains 0.30-0.60 wt% Mn-55;
c                                    see pp 6.30 of "Marks' Standard Handbook for Mechanical Engineers")
c
c                   0.015 wt% Co-59 (HFIR vessel has this amount [see pp 106 of ORNL/TM-10444];
c                                    while HB1/4 nozzels have 0.005 wt%, and HB2/3 nozzels have 0.03 wt%)
c
c     ************************************************************************************************************
c     ************************************************************************************************************
c
      implicit double precision (a-h,o-z)
c
      dimension rmin(39),rmax(39),vol(39)
      dimension flxth(39),flxres(39),flxfst(39),flxtot(39)
      dimension xf58ng(39),xf54np(39),xc59ng(39),xf57ng(39)
      dimension xf56ng(39),xm55ng(39),xm54ng(39),xf54ng(39)
      dimension xf55na(39),xf59ng(39),xf59na(39),xc60ng(39)
c
      dimension gsrc7(39) ! (act) decay gamma source terms (p/s/cc) in each of the 39 1-cm-thick cyl shells; calculated here
      dimension greg7(39) ! (act) decay gamma source terms (p/s)    in each of the 39 1-cm-thick cyl shells; calculated here
c
      data rmin/ ! dist (cm) from centerline of big hole thru rotary shutter
     *   4.445d0,  5.445d0,  6.445d0,  7.445d0,  8.445d0,
     *   9.445d0, 10.445d0, 11.445d0, 12.445d0, 13.445d0,
     *  14.445d0, 15.445d0, 16.445d0, 17.445d0, 18.445d0,
     *  19.445d0, 20.445d0, 21.445d0, 22.445d0, 23.445d0,
     *  24.445d0, 25.445d0, 26.445d0, 27.445d0, 28.445d0,
     *  29.445d0, 30.445d0, 31.445d0, 32.445d0, 33.445d0,
     *  34.445d0, 35.445d0, 36.445d0, 37.445d0, 38.445d0,
     *  39.445d0, 40.445d0, 41.445d0, 42.445d0/
c
      data rmax/ ! dist (cm) from centerline of big hole thru rotary shutter
     *   5.445d0,  6.445d0,  7.445d0,  8.445d0,  9.445d0,
     *  10.445d0, 11.445d0, 12.445d0, 13.445d0, 14.445d0,
     *  15.445d0, 16.445d0, 17.445d0, 18.445d0, 19.445d0,
     *  20.445d0, 21.445d0, 22.445d0, 23.445d0, 24.445d0,
     *  25.445d0, 26.445d0, 27.445d0, 28.445d0, 29.445d0,
     *  30.445d0, 31.445d0, 32.445d0, 33.445d0, 34.445d0,
     *  35.445d0, 36.445d0, 37.445d0, 38.445d0, 39.445d0,
     *  40.445d0, 41.445d0, 42.445d0, 43.4433d0/
c
      data vol/ ! volume (cc) of cyl shell "i"; cannot be computed from rmin & rmax; cannot be computed analytically; calculated statistically
     *  1.89858d+03, 2.27981d+03, 2.65511d+03, 3.02744d+03, 3.39342d+03,
     *  3.7553[illegible], 4.11116d+03, 4.45690d+03, 4.79709d+03, 5.12661d+03,
```

```
     *  5.44592d+03, 5.75543d+03, 6.05497d+03, 6.33840d+03, 6.60982d+03,
     *  6.86725d+03, 7.10540d+03, 7.32554d+03, 7.53004d+03, 7.70707d+03,
     *  7.85115d+03, 7.96738d+03, 8.04809d+03, 8.08235d+03, 8.05935d+03,
     *  7.95535d+03, 6.44147d+03, 4.99352d+03, 4.08671d+03, 3.36986d+03,
     *  2.76096d+03, 2.23160d+03, 1.76511d+03, 1.35264d+03, 9.88281d+02,
     *  6.71165d+02, 4.01009d+02, 1.86544d+02, 3.97575d+01/
c
        data flxth/ ! avg thermal flux (n/s/cm2) below 0.41399 eV for shell "i" from HB309A, Tally 24
     *  2.74732d+09, 1.84566d+09, 1.36593d+09, 6.96965d+08, 3.37267d+08,
     *  1.90977d+08, 1.10171d+08, 6.72172d+07, 4.03766d+07, 2.62801d+07,
     *  1.81081d+07, 1.22659d+07, 9.25039d+06, 6.90746d+06, 5.33066d+06,
     *  4.35552d+06, 3.50262d+06, 2.71110d+06, 2.31448d+06, 2.15837d+06,
     *  1.97678d+06, 1.63389d+06, 1.38260d+06, 1.44871d+06, 1.41795d+06,
     *  1.22925d+06, 1.13551d+06, 6.93888d+05, 4.54804d+05, 3.69736d+05,
     *  1.26607d+05, 3.85593d+04, 1.04516d+05, 3.01327d+04, 5.47862d+04,
     *  2.42782d+04, 0.00000d+00, 0.00000d+00, 0.00000d+00/
c
        data flxres/ ! avg resonance-range flux (n/s/cm2) for (0.41399 eV < E < 1.0 MeV) for shell "i" from HB309A, Tally 24
     *  2.02708d+09, 1.66341d+09, 1.42750d+09, 1.05363d+09, 8.08969d+08,
     *  6.74424d+08, 5.60476d+08, 4.76992d+08, 4.02304d+08, 3.49902d+08,
     *  3.05466d+08, 2.65727d+08, 2.35619d+08, 2.08903d+08, 1.82957d+08,
     *  1.63203d+08, 1.45159d+08, 1.32135d+08, 1.18128d+08, 1.06460d+08,
     *  9.47021d+07, 8.52979d+07, 7.89053d+07, 7.24254d+07, 6.51446d+07,
     *  6.18837d+07, 5.78272d+07, 5.26223d+07, 4.75744d+07, 4.22995d+07,
     *  3.80259d+07, 3.51092d+07, 3.16187d+07, 2.50538d+07, 2.44744d+07,
     *  2.20308d+07, 2.09847d+07, 1.97000d+07, 9.80637d+06/
c
        data flxfst/ ! avg fast flux (n/s/cm2) for (1 MeV < E < 20 MeV) for shell "i" from HB309A, Tally 24
     *  7.73721d+08, 5.90820d+08, 5.11630d+08, 3.67896d+08, 2.60845d+08,
     *  2.19476d+08, 1.90583d+08, 1.66833d+08, 1.48498d+08, 1.30761d+08,
     *  1.19669d+08, 1.05416d+08, 9.65105d+07, 8.79522d+07, 7.82697d+07,
     *  7.13853d+07, 6.48972d+07, 6.13374d+07, 5.43873d+07, 4.84026d+07,
     *  4.57820d+07, 4.08429d+07, 3.83933d+07, 3.30346d+07, 3.08990d+07,
     *  2.74878d+07, 2.49149d+07, 2.38801d+07, 2.19426d+07, 1.88337d+07,
     *  1.69396d+07, 1.65887d+07, 1.39530d+07, 1.15256d+07, 1.16599d+07,
     *  1.23392d+07, 7.56120d+06, 7.22905d+06, 1.15976d+07/
c
        data flxtot/ ! total flux (n/s/cm2) for (summed over all energies) for shell "i" from HB309A, Tally 24
     *  5.54812d+09, 4.09989d+09, 3.30506d+09, 2.11850d+09, 1.40708d+09,
     *  1.08488d+09, 8.61231d+08, 7.11041d+08, 5.91178d+08, 5.06943d+08,
     *  4.43243d+08, 3.83409d+08, 3.41380d+08, 3.03762d+08, 2.66558d+08,
     *  2.38944d+08, 2.13559d+08, 1.96184d+08, 1.74829d+08, 1.57021d+08,
     *  1.42461d+08, 1.27775d+08, 1.18681d+08, 1.06909d+08, 9.74616d+07,
     *  9.06007d+07, 8.38777d+07, 7.71962d+07, 6.99718d+07, 6.15029d+07,
     *  5.50922d+07, 5.17364d+07, 4.56763d+07, 3.66095d+07, 3.61891d+07,
     *  3.43942d+07, 2.85459d+07, 2.69290d+07, 2.14040d+07/
c
        data xf58ng/ ! Tally 34  Fe58(n,g)Fe59 "reactions/sec/cc" in shutter seg if N(Fe58)= 1 atom/(b*cm); values shown below are "totals" over all energie
s
     *  1.57216d+09, 1.14615d+09, 8.48714d+08, 4.32341d+08, 2.31799d+08,
     *  1.50153d+08, 8.94690d+07, 6.46687d+07, 5.18197d+07, 3.51538d+07,
     *  2.67623d+07, 3.00751d+07, 3.66566d+07, 2.40311d+07, 1.43074d+07,
     *  1.27613d+07, 2.23069d+07, 1.09186d+07, 6.67290d+06, 1.23014d+07,
     *  5.22684d+06, 5.80662d+06, 6.27061d+06, 6.00283d+06, 5.91870d+06,
     *  4.47121d+06, 2.85362d+06, 1.96904d+06, 2.53224d+06, 4.48026d+06,
     *  1.98723d+06, 1.74243d+06, 7.31046d+05, 5.80676d+06, 6.43253d+05,
     *  4.54047d+05, 3.32985d+05, 1.66274d+05, 5.19141d+04/
c
```

```
      data xf54np/ ! Tally 44  Fe54(n,p)Mn54 "reactions/sec/cc" in shutter seg if N(Fe54)= 1 atom/(b*cm); values shown below are "totals" over all energie
s
     *  1.20292d+07, 6.67175d+06, 5.25048d+06, 2.58757d+06, 1.10414d+06,
     *  8.03867d+05, 6.54756d+05, 4.41701d+05, 3.78326d+05, 2.53326d+05,
     *  2.03298d+05, 1.62342d+05, 9.57636d+04, 7.33266d+04, 8.56045d+04,
     *  5.96741d+04, 4.36338d+04, 3.66938d+04, 3.31433d+04, 2.71341d+04,
     *  1.70733d+04, 1.25406d+04, 1.37422d+04, 6.98949d+03, 6.42573d+03,
     *  9.50111d+03, 2.73547d+03, 1.59773d+03, 6.43392d+02, 1.59097d+02,
     *  1.51799d+02, 1.80963d+02, 2.74708d+02, 3.34009d+02, 6.53157d+01,
     *  2.51263d+01, 7.91661d+00, 1.51097d-01, 2.08653d-01/
c
      data xc59ng/ ! Tally 54  Co59(n,g)Co60 "reactions/sec/cc" in shutter seg if N(Co59)= 1 atom/(b*cm); values shown below are "totals" over all energie
s
     *  5.78845d+10, 4.06547d+10, 3.06994d+10, 1.76769d+10, 1.04784d+10,
     *  7.29654d+09, 5.34792d+09, 4.09892d+09, 3.11880d+09, 2.74753d+09,
     *  2.22914d+09, 1.70038d+09, 1.43644d+09, 1.15434d+09, 1.03716d+09,
     *  8.20952d+08, 7.84838d+08, 6.02624d+08, 5.61004d+08, 5.46825d+08,
     *  4.63993d+08, 3.46108d+08, 4.29789d+08, 3.42289d+08, 2.56266d+08,
     *  2.45520d+08, 2.86070d+08, 2.64852d+08, 1.72396d+08, 1.17480d+08,
     *  1.87061d+08, 2.08958d+08, 2.95190d+08, 1.55585d+08, 3.65217d+08,
     *  1.77113d+08, 1.06684d+07, 5.70826d+06, 1.72262d+06/
c
      data xf57ng/ ! Tally 64  Fe57(n,g)Fe58 "reactions/sec/cc" in shutter seg if N(Fe57)= 1 atom/(b*cm); values shown below are "totals" over all energie
s
     *  3.19633d+09, 2.14003d+09, 1.58950d+09, 8.45299d+08, 4.33831d+08,
     *  2.63626d+08, 1.69071d+08, 1.16809d+08, 7.88794d+07, 5.81192d+07,
     *  4.55823d+07, 3.51442d+07, 2.91652d+07, 2.46814d+07, 2.06657d+07,
     *  1.77527d+07, 1.46638d+07, 1.31289d+07, 1.16829d+07, 1.13470d+07,
     *  1.08416d+07, 8.76487d+06, 7.26148d+06, 6.93971d+06, 6.17780d+06,
     *  5.27628d+06, 4.86002d+06, 5.20521d+06, 5.25065d+06, 3.97629d+06,
     *  2.23946d+06, 3.02018d+06, 3.40241d+06, 1.84750d+06, 2.21092d+06,
     *  2.70400d+06, 3.18876d+06, 3.15490d+06, 1.33737d+06/
c
      data xf56ng/ ! Tally 74  Fe56(n,g)Fe57 "reactions/sec/cc" in shutter seg if N(Fe56)= 1 atom/(b*cm); values shown below are "totals" over all energie
s
     *  3.36721d+09, 2.25370d+09, 1.67026d+09, 8.73702d+08, 4.41938d+08,
     *  2.69553d+08, 1.68245d+08, 1.15170d+08, 7.62715d+07, 5.46814d+07,
     *  4.23195d+07, 3.23935d+07, 2.76522d+07, 2.20551d+07, 1.76561d+07,
     *  1.46348d+07, 1.27331d+07, 1.07375d+07, 9.74353d+06, 9.28538d+06,
     *  8.09216d+06, 6.72191d+06, 5.83975d+06, 5.30684d+06, 4.89180d+06,
     *  4.45160d+06, 3.90635d+06, 3.36825d+06, 2.54684d+06, 1.98251d+06,
     *  2.16223d+06, 1.60233d+06, 1.60190d+06, 2.55469d+06, 1.23464d+06,
     *  8.49530d+05, 5.14348d+05, 2.57386d+05, 3.11991d+04/
c
      data xm55ng/ ! Tally 84  Mn55(n,g)Mn56 "reactions/sec/cc" in shutter seg if N(Mn55)= 1 atom/(b*cm); values shown below are "totals" over all energie
s
     *  1.84169d+10, 1.25220d+10, 9.38180d+09, 5.16367d+09, 2.77038d+09,
     *  1.82913d+09, 1.23859d+09, 8.55010d+08, 6.40729d+08, 5.04035d+08,
     *  3.92140d+08, 3.35307d+08, 2.73264d+08, 2.27944d+08, 1.92078d+08,
     *  1.72462d+08, 1.58814d+08, 1.38011d+08, 1.10222d+08, 9.73559d+07,
     *  8.52599d+07, 7.89212d+07, 7.39348d+07, 6.10265d+07, 6.61182d+07,
     *  5.89068d+07, 5.39730d+07, 3.89956d+07, 3.61343d+07, 2.99655d+07,
     *  3.16423d+07, 2.99357d+07, 1.87112d+07, 1.51089d+07, 1.29813d+07,
     *  9.25437d+06, 4.44866d+06, 2.29941d+06, 2.80385d+05/
c
      data xm54ng/ ! Tally  94  Mn54(n,g)Mn55 "reactions/sec/cc" in shutter seg if N(Mn54)=1 atom/(b*cm); values shown below are "totals" over all energie
s
     *  1.2662[illegible]0, 8.62084d+09, 6.51046d+09, 3.56730d+09, 1.96939d+09,
```

```
     *  1.30528d+09, 9.02419d+08, 6.61735d+08, 4.94689d+08, 3.86573d+08,
     *  3.14478d+08, 2.59155d+08, 2.16017d+08, 1.84598d+08, 1.55570d+08,
     *  1.34916d+08, 1.16707d+08, 1.04449d+08, 9.18358d+07, 8.01191d+07,
     *  7.10371d+07, 6.24565d+07, 5.80331d+07, 5.33454d+07, 4.80855d+07,
     *  4.57404d+07, 4.29561d+07, 3.69811d+07, 3.02216d+07, 2.74636d+07,
     *  2.49245d+07, 2.55141d+07, 2.15737d+07, 1.41898d+07, 1.35236d+07,
     *  1.13716d+07, 7.43682d+06, 5.15752d+06, 1.19179d+06/
c
      data xf54ng/ ! Tally 104  Fe54(n,g)Fe55 "reactions/sec/cc" in shutter seg if N(Fe54)=1 atom/(b*cm); values shown below are "totals" over all energie
s
     *  5.99198d+09, 4.14389d+09, 3.13285d+09, 1.72564d+09, 9.50033d+08,
     *  6.12330d+08, 4.13005d+08, 2.95404d+08, 2.08192d+08, 1.58984d+08,
     *  1.27956d+08, 1.04389d+08, 8.83181d+07, 7.62692d+07, 6.45517d+07,
     *  5.46605d+07, 4.79391d+07, 4.19608d+07, 3.36966d+07, 2.94455d+07,
     *  2.71815d+07, 2.36507d+07, 2.09731d+07, 1.87989d+07, 1.86951d+07,
     *  1.58571d+07, 1.38394d+07, 1.19015d+07, 9.08576d+06, 8.42691d+06,
     *  5.61515d+06, 5.37685d+06, 5.13309d+06, 4.02939d+06, 4.37901d+06,
     *  3.45857d+06, 2.60602d+06, 1.78521d+06, 3.94089d+05/
c
      data xf55na/ ! Tally 114  Fe55(n,A)Cr52 "reactions/sec/cc" in shutter seg if N(Fe55)=1 atom/(b*cm); values shown below are "totals" over all energie
s
     *  2.02828d+05, 1.35130d+05, 1.22644d+05, 5.63003d+04, 7.41870d+03,
     *  4.30735d+03, 1.09205d+03, 5.56648d+02, 2.73019d+02, 1.62800d+02,
     *  1.51162d+02, 5.13810d+01, 8.32803d-01, 0.00000d+00, 0.00000d+00,
     *  0.00000d+00, 0.00000d+00, 0.00000d+00, 0.00000d+00, 0.00000d+00,
     *  0.00000d+00, 0.00000d+00, 0.00000d+00, 0.00000d+00, 0.00000d+00,
     *  0.00000d+00, 0.00000d+00, 0.00000d+00, 0.00000d+00, 0.00000d+00,
     *  0.00000d+00, 0.00000d+00, 0.00000d+00, 0.00000d+00, 0.00000d+00,
     *  0.00000d+00, 0.00000d+00, 0.00000d+00, 0.00000d+00/
c
      data xf59ng/ ! Tally 124  Fe59(n,g)Fe60 "reactions/sec/cc" in shutter seg if N(Fe59)=1 atom/(b*cm); values shown below are "totals" over all energie
s
     *  2.14995d+09, 1.44126d+09, 1.07228d+09, 5.62506d+08, 2.86986d+08,
     *  1.74651d+08, 1.10666d+08, 7.44673d+07, 5.04288d+07, 3.64339d+07,
     *  2.78752d+07, 2.18257d+07, 1.78110d+07, 1.49781d+07, 1.23244d+07,
     *  1.05036d+07, 8.87970d+06, 7.65916d+06, 6.63824d+06, 5.85553d+06,
     *  5.42374d+06, 4.71597d+06, 4.13551d+06, 3.84405d+06, 3.52275d+06,
     *  3.19568d+06, 2.88050d+06, 2.25836d+06, 1.89263d+06, 1.52881d+06,
     *  1.09491d+06, 1.03533d+06, 1.02367d+06, 7.86281d+05, 9.12764d+05,
     *  7.76966d+05, 4.84942d+05, 2.77516d+05, 9.67132d+04/
c
      data xf59na/ ! Tally 134  Fe59(n,A)Cr56 "reactions/sec/cc" in shutter seg if N(Fe59)=1 atom/(b*cm); values shown below are "totals" over all energie
s
     *  3.32113d+03, 1.34551d+03, 2.51155d+03, 3.30643d+02, 1.71738d+00,
     *  0.00000d+00, 0.00000d+00, 0.00000d+00, 0.00000d+00, 0.00000d+00,
     *  0.00000d+00, 0.00000d+00, 0.00000d+00, 0.00000d+00, 0.00000d+00,
     *  0.00000d+00, 0.00000d+00, 0.00000d+00, 0.00000d+00, 0.00000d+00,
     *  0.00000d+00, 0.00000d+00, 0.00000d+00, 0.00000d+00, 0.00000d+00,
     *  0.00000d+00, 0.00000d+00, 0.00000d+00, 0.00000d+00, 0.00000d+00,
     *  0.00000d+00, 0.00000d+00, 0.00000d+00, 0.00000d+00, 0.00000d+00,
     *  0.00000d+00, 0.00000d+00, 0.00000d+00, 0.00000d+00/
c
      data xc60ng/ ! Tally 144  Co60(n,g)Co61 "reactions/sec/cc" in shutter seg if N(Co60)=1 atom/(b*cm); values shown below are "totals" over all energie
s
     *  3.16042d+09, 2.20321d+09, 1.69199d+09, 9.72573d+08, 5.77529d+08,
     *  4.08203d+08, 2.97571d+08, 2.27118d+08, 1.79749d+08, 1.45030d+08,
     *  1.22003d+08, 1.01511d+08, 8.67970d+07, 7.54545d+07, 6.46226d+07,
     *  5.65885d+07, 4.90034d+07, 4.47282d+07, 3.87558d+07, 3.40701d+07,
```

```
     *  3.05252d+07, 2.70076d+07, 2.48438d+07, 2.26819d+07, 2.15119d+07,
     *  2.10725d+07, 2.05226d+07, 1.67992d+07, 1.38844d+07, 1.38453d+07,
     *  1.34534d+07, 1.26163d+07, 1.00471d+07, 6.81065d+06, 5.00097d+06,
     *  5.05343d+06, 4.13671d+06, 3.52430d+06, 1.43811d+06/
c
        open (7,file='actsrc.aux',status='unknown')
        open (8,file='actsrc.out',status='unknown')
c
        greg77=0.0d0
        write (8,21)
21      format (/,' Equivalent gamma sources (at 1.25 MeV, 7 days',
     *   ' after shutdown) for each of 39',/,' cylindrical shells,',
     *   ' concentric about large beam hole in HB-3 rotary shutter:',
     *   //,' Cyl',38x,'GSRC den      GSRC total',/,
     *   ' Shell    Rmin     Rmax    Volume (cc)   ',
     *   ' (p/s/cc)      (p/s)',/)
c
        do i=1,39   ! loop over each of the 39 cyl shells:
        call getsrc (i,vol(i),
     *     xm55ng(i),xf54np(i),xf56ng(i),xf57ng(i),xf58ng(i),
     *     xc59ng(i),xm54ng(i),xf54ng(i),xf55na(i),xf59ng(i),
     *     xf59na(i),xc60ng(i),gsrc7(i),greg7(i))
        greg77=greg77+greg7(i)
        write (8,22) i,rmin(i),rmax(i),vol(i),gsrc7(i),greg7(i)
22      format (i4,f11.4,f9.4,1p,3e14.5)
        enddo
c
        write (8,23) greg77
23      format (55x,'-----------',/,17x,'Total activation gamma',
     *   ' source (p/s)=',1pe13.5)
c
        stop
        end
        subroutine getsrc (ishell,vol,
     *     xm55ng,xf54np,xf56ng,xf57ng,xf58ng,xc59ng,xm54ng,
     *     xf54ng,xf55na,xf59ng,xf59na,xc60ng,gsrc7,greg7)
c
c       ***************************************************************************************************************
c       ***************************************************************************************************************
c
c       Required input:   (all values "double precision")
c       ---------------
c          ishell =  shell number (1=closest to big hole in celter of rotary shutter; 39=furthest away)
c          vol    =  volume of cylindrical shell (cc)
c
c          xm55ng =  Mn55(n,g)Mn56  "reactions/sec/cc" if Mn55 had a density of 1 atom/(barn*cm)
c          xf54np =  Fe54(n,P)Mn54  "reactions/sec/cc" if Fe54 had a density of 1 atom/(barn*cm)
c          xf56ng =  Fe56(n,g)Fe57  "reactions/sec/cc" if Fe56 had a density of 1 atom/(barn*cm)
c          xf57ng =  Fe57(n,g)Fe58  "reactions/sec/cc" if Fe57 had a density of 1 atom/(barn*cm)
c          xf58ng =  Fe58(n,g)Fe59  "reactions/sec/cc" if Fe58 had a density of 1 atom/(barn*cm)
c          xc59ng =  Co59(n,g)Co60  "reactions/sec/cc" if Co59 had a density of 1 atom/(barn*cm)
c
c          xm54ng =  Mn54(n,g)Mn55  "reactions/sec/cc" if Mn54 had a density of 1 atom/(barn*cm)
c          xf54ng =  Fe54(n,g)Fe55  "reactions/sec/cc" if Fe54 had a density of 1 atom/(barn*cm)
c          xf55na =  Fe55(n,A)Cr52  "reactions/sec/cc" if Fe55 had a density of 1 atom/(barn*cm)
c          xf59ng =  Fe59(n,g)Fe60  "reactions/sec/cc" if Fe59 had a density of 1 atom/(barn*cm)
c          xf5[illegible]  Fe59(n,A)Cr56  "reactions/sec/cc" if Fe59 had a density [illegible]atom/(barn*cm)
c          xc6[illegible]  Co60(n,g)Co61  "reactions/sec/cc" if Co60 had a density [illegible]atom/(barn*cm)
```

```
c
c       Returned values:   (all values "double precision")
c       ----------------
c          gsrc7  =  equivalent gamma source density in this shell (p/s/cm2) at 1.25 MeV, 7 days after shutdown
c          greg7  =  equivalent total gamma source  for this shell (p/s)     at 1.25 MeV, 7 days after shutdown
c
c       ************************************************************************************************************
c       ************************************************************************************************************
c
        implicit double precision (a-h,o-z)
        character*3 qa
c
        c=1.0d-24  ! c=1.0d-24 cm2/barn
c
        xm55ng=c*xm55ng
        xf54np=c*xf54np
        xf56ng=c*xf56ng
        xf57ng=c*xf57ng
        xf58ng=c*xf58ng
        xc59ng=c*xc59ng
c
        xm54ng=c*xm54ng
        xf54ng=c*xf54ng
        xf55na=c*xf55na
        xf59ng=c*xf59ng
        xf59na=c*xf59na
        xc60ng=c*xc60ng
c
        dt=7.0d0             ! delta-t = 1 week = 7 days
        dt=dt*8.64d4         ! delta-t in seconds
c
        tburn=30.0d0         ! tburn= 30 years (appx)
        tburn=tburn*52.0d0   ! tburn in weeks
        tburn=tburn*7.0d0    ! tburn in days
        tburn=tburn*8.64d4   ! tburn in seconds
c
        nburn=nint(tburn/dt) ! irradiate for this many timesteps
c
c       From here on, all densities will be in "atoms/cc" and all times will be in "sec"
c
        dcf59=1.80241d-7   ! decay constant ("per sec") for Fe-59  (T-half=44.51 days)
        dcc60=4.16705d-9   ! decay constant ("per sec") for Co-60  (T-half=5.271 years); each decay = 1 gamma at 1.173 MeV + 1 gamma at 1.332 MeV
        dcm56=7.46861d-5   ! decay constant ("per sec") for Mn-56  (T-half=2.578 hours)
        dcm54=2.56968d-8   ! decay constant ("per sec") for Mn-54  (T-half=312.2 days)
c
c       for Mn-54, each decay = 1 gamma at 0.8348 MeV
c       for Mn-56, each decay = 1 or 2 gammas between 0.8468 MeV and 3.370 MeV; avg=1.69 MeV; basically gone after 2-4 days
c       for Fe-59, each decay = 1 gamma at 1.099 MeV "OR"  1 gamma at 1.292 MeV, plus some low energy gammas;  avg=1.19 MeV
c       for Co-60, each decay = 1 gamma at 1.173 MeV "AND" 1 gamma at 1.332 MeV  (always 2 gammas per disintegration)
c
c       Assumed density of Type 1020 carbon steel = 7.8212 g/cc  (99 wt% Fe, 1 wt% C):
c       ------------------------------------------------------------------------
        amn54=0.0d0        ! initial amt of Mn-54, atoms/cc
        amn55=3.85801d20   ! initial amt of Mn-55, atoms/cc  (assuming: 0.45 wt% Mn-55 in Type 1020 carbon steel; typ 0.30-0.60 wt%)
        amn56=0.0d0        ! initial amt of Mn-56, atoms/cc
c
        afe54=4.92617d21   ! initial amt of Fe-54, atoms/cc  ( 5.9  at% Fe-54 in Fe)
        afe55=0.0d0        ! initial amt of Fe-55, atoms/cc
```

```
      afe56=7.65810d22  ! initial amt of Fe-56, atoms/cc  (91.72 at% Fe-56 in Fe)
      afe57=1.75338d21  ! initial amt of Fe-57, atoms/cc  ( 2.1  at% Fe-54 in Fe)
      afe58=2.33784d20  ! initial amt of Fe-58, atoms/cc  ( 0.28 at% Fe-54 in Fe)
      afe59=0.0d0       ! initial amt of Fe-59, atoms/cc
c
      aco59=1.19882d19  ! initial amt of Co-59, atoms/cc  (assuming: 0.015 wt% Co-59 in Type 1020 carbon steel)
      aco60=0.0d0       ! initial amt of Co-60, atoms/cc
c     ------------------------------------------------------------------------
c
      qa='on '  ! <-- control flag;  needed to see small changes in naturally existing isotopes
      qa='off'  ! <-- control flag;  use this to get normal printout
c
      if (qa.eq.'on ')write (7,'(//,a20,//,6x,11a21,/)')   ! <-- used to see small changes in naturally existing isotopes
     *   ' DURING IRRADIATION:',
     *   'amn54','amn55','amn56','afe54',
     *   'afe55','afe56','afe57','afe58',
     *   'afe59','aco59','aco60'
c
      if (qa.eq.'off') write (7,'(//,a20,//,12x,11a10,/)')  ! <-- used for normal printout
     *   ' DURING IRRADIATION:',
     *   'amn54','amn55','amn56','afe54',
     *   'afe55','afe56','afe57','afe58',
     *   'afe59','aco59','aco60'
c
      do i=1,nburn
      iyr=i/52
      iwk=i-52*iyr
c     ------------------------------------------------------------------------
      delm54=  afe54*xf54np - amn54*xm54ng - dcm54*amn54
c
      nmicro=200
      dtsm=dt/dfloat(nmicro)  ! small timestep required for these 2 nuclides because of small half-life of Mn-56
      do j=1,nmicro
         delm55= amn54*xm54ng - amn55*xm55ng
         delm56= amn55*xm55ng - dcm56*amn56
         call adder(j,amn55,'amn55',delm55,dtsm)
         call adder(j,amn56,'amn56',delm56,dtsm)
      enddo
c
      delf54= -afe54*xf54np - afe54*xf54ng
      delf55=  afe54*xf54ng - afe55*xf55na
      delf56= -afe56*xf56ng
      delf57=  afe56*xf56ng - afe57*xf57ng
      delf58=  afe57*xf57ng - afe58*xf58ng
      delf59=  afe58*xf58ng - afe59*xf59ng - afe59*xf59na -dcf59*afe59
c
      delc59=  dcf59*afe59  - aco59*xc59ng
      delc60=  aco59*xc59ng - aco60*xc60ng - dcc60*aco60
c     ------------------------------------------------------------------------
      call adder(i,amn54,'amn54',delm54,dt)

c     call adder(i,amn55,'amn55',delm55,dt)  ! now done inside short-time loop above instead
c     call adder(i,amn56,'amn56',delm56,dt)  ! now done inside short-time loop above instead
c
      call adder(i,afe54,'afe54',delf54,dt)
      call adder(i,afe55,'afe55',delf55,dt)
      call adder(i,afe56,'afe56',delf56,dt)
      call adder(i,afe57,'afe57',delf57,dt)
```

```
      call adder(i,afe58,'afe58',delf58,dt)
      call adder(i,afe59,'afe59',delf59,dt)
c
      call adder(i,aco59,'aco59',delc59,dt)
      call adder(i,aco60,'aco60',delc60,dt)
c     ------------------------------------------------------------------------
      if (qa.eq.'on ') write (7,12) iyr,iwk,                ! <-- used to see small changes in naturally existing isotopes
     *  amn54,amn55,amn56,
     *  afe54,afe55,afe56,afe57,afe58,afe59,
     *  aco59,aco60
c
      if (qa.eq.'off' .and. iwk.eq.0) write (7,11) iyr,iwk,  ! <-- used for normal printout
     *  amn54,amn55,amn56,
     *  afe54,afe55,afe56,afe57,afe58,afe59,
     *  aco59,aco60
c
11    format (' yr=',i2,' week=',i2,1p,11d10.3)     ! <-- used for normal printout
12    format (' yr=',i2,' week=',i2,1p,11d21.14)    ! <-- used to see small changes in naturally existing isotopes
c     ------------------------------------------------------------------------
      enddo
c
c
c     ========================================================================
c
c     save shutdown values for future reference:
c
      amn54z=amn54
      amn55z=amn55
      amn56z=amn56
      afe54z=afe54
      afe55z=afe55
      afe56z=afe56
      afe57z=afe57
      afe58z=afe58
      afe59z=afe59
      aco59z=aco59
      aco60z=aco60
c
c     ========================================================================
c
c     BEGIN DECAY ANALYSIS (to get & print concentrations):
c
c     restore shutdown concentrations:
c
      amn54=amn54z
      amn55=amn55z
      amn56=amn56z
      afe54=afe54z
      afe55=afe55z
      afe56=afe56z
      afe57=afe57z
      afe58=afe58z
      afe59=afe59z
      aco59=aco59z
      aco60=aco60z
c
      c=0.0d0
c
```

```
      xm55ng=c*xm55ng
      xf54np=c*xf54np
      xf56ng=c*xf56ng
      xf57ng=c*xf57ng
      xf58ng=c*xf58ng
      xc59ng=c*xc59ng
c
      xm54ng=c*xm54ng
      xf54ng=c*xf54ng
      xf55na=c*xf55na
      xf59ng=c*xf59ng
      xf59na=c*xf59na
      xc60ng=c*xc60ng
c
      dt=1.0d0              ! delta-t = 1 day
      dt=dt*8.64d4          ! delta-t in seconds
c
      tdecay=60.0d0           ! tdecay= 60 days
      tdecay=tdecay*8.64d4  ! tdecay in seconds
c
      ndecay=nint(tdecay/dt) ! decay for this many timesteps
c
c
      if (qa.eq.'on ')write (7,'(a1,//,a16,//,6x,11a21,/)')     ! <-- used to see small changes in naturally existing isotopes
     *   char(12),
     *   ' AFTER SHUTDOWN:',
     *   'amn54','amn55','amn56','afe54',
     *   'afe55','afe56','afe57','afe58',
     *   'afe59','aco59','aco60'
c
      if (qa.eq.'off') write (7,'(a1,//,a16,//,12x,11a10,/)')  ! <-- used for normal printout
     *   char(12),
     *   ' AFTER SHUTDOWN:',
     *   'amn54','amn55','amn56','afe54',
     *   'afe55','afe56','afe57','afe58',
     *   'afe59','aco59','aco60'
c
      do i=1,ndecay
      iday=i
c     ------------------------------------------------------------------------
c     Note: following block is the same as above, with all reaction rates set to zero
c
      delm54=  afe54*xf54np - amn54*xm54ng - dcm54*amn54
c
      nmicro=30
      dtsm=dt/dfloat(nmicro)  ! small timestep required for these 2 nuclides because of small half-life of Mn-56
      do j=1,nmicro
         delm55= amn54*xm54ng - amn55*xm55ng
         delm56= amn55*xm55ng - dcm56*amn56
         call adder(k,amn55,'amn55',delm55,dtsm)
         call adder(k,amn56,'amn56',delm56,dtsm)
      enddo
c
      delf54= -afe54*xf54np - afe54*xf54ng
      delf55=  afe54*xf54ng - afe55*xf55na
      delf56=  afe56*xf56ng
      delf57=  afe56*xf56ng - afe57*xf57ng
      delf58=  afe57*xf57ng - afe58*xf58ng
```

```
      delf59=  afe58*xf58ng - afe59*xf59ng - afe59*xf59na -dcf59*afe59
c
      delc59=  dcf59*afe59  - aco59*xc59ng
      delc60=  aco59*xc59ng - aco60*xc60ng - dcc60*aco60
c     ------------------------------------------------------------------------
c     Note: following block is the same as above, with all reaction rates set to zero
c
      call adder(k,amn54,'amn54',delm54,dt)

c     call adder(k,amn55,'amn55',delm55,dt)  ! now done inside short-time loop above instead
c     call adder(k,amn56,'amn56',delm56,dt)  ! now done inside short-time loop above instead
c
      call adder(k,afe54,'afe54',delf54,dt)
      call adder(k,afe55,'afe55',delf55,dt)
      call adder(k,afe56,'afe56',delf56,dt)
      call adder(k,afe57,'afe57',delf57,dt)
      call adder(k,afe58,'afe58',delf58,dt)
      call adder(k,afe59,'afe59',delf59,dt)
c
      call adder(k,aco59,'aco59',delc59,dt)
      call adder(k,aco60,'aco60',delc60,dt)
c     ------------------------------------------------------------------------
      if (qa.eq.'on ') write (7,14) iday,                ! <-- used to see small changes in naturally existing isotopes
     *  amn54,amn55,amn56,
     *  afe54,afe55,afe56,afe57,afe58,afe59,
     *  aco59,aco60
c
      if (qa.eq.'off' .and. iwk.eq.0) write (7,13) iday,  ! <-- used for normal printout
     *  amn54,amn55,amn56,
     *  afe54,afe55,afe56,afe57,afe58,afe59,
     *  aco59,aco60
c
13    format (' day=',i2,7x,1p,11d10.3)      ! <-- used for normal printout
14    format (' day=',i2,7x,1p,11d21.14)     ! <-- used to see small changes in naturally existing isotopes
c     ------------------------------------------------------------------------
      enddo
c
c
c     ========================================================================
c
c     BEGIN DECAY ANALYSIS (to get & print disintegrations/sec/cc by nuclide)
c
c     restore shutdown concentrations:
c
      amn54=amn54z
      amn55=amn55z
      amn56=amn56z
      afe54=afe54z
      afe55=afe55z
      afe56=afe56z
      afe57=afe57z
      afe58=afe58z
      afe59=afe59z
      aco59=aco59z
      aco60=aco60z
c
      c=0.0d0
c
```

```
      xm55ng=c*xm55ng
      xf54np=c*xf54np
      xf56ng=c*xf56ng
      xf57ng=c*xf57ng
      xf58ng=c*xf58ng
      xc59ng=c*xc59ng
c
      xm54ng=c*xm54ng
      xf54ng=c*xf54ng
      xf55na=c*xf55na
      xf59ng=c*xf59ng
      xf59na=c*xf59na
      xc60ng=c*xc60ng
c
      dt=1.0d0            ! delta-t = 1 day
      dt=dt*8.64d4        ! delta-t in seconds
c
      tdecay=60.0d0         ! tdecay= 60 days
      tdecay=tdecay*8.64d4  ! tdecay in seconds
c
      ndecay=nint(tdecay/dt) ! decay for this many timesteps
c
c
      write (7,'(a1,//,a41,//,12x,4a10,/)')
     *  char(12),
     *  ' AFTER SHUTDOWN:   disintegretions/sec/cc',
     *  'delm54','delm56','delf59','delc60'
c
      do i=1,ndecay
      iday=i
      k=0
c     ------------------------------------------------------------------------
c     Note: following block is the same as above, with all reaction rates set to zero
c
      delm54=  afe54*xf54np - amn54*xm54ng - dcm54*amn54
c
      nmicro=30
      dtsm=dt/dfloat(nmicro)  ! small timestep required for these 2 nuclides because of small half-life of Mn-56
      do j=1,nmicro
         delm55= amn54*xm54ng - amn55*xm55ng
         delm56= amn55*xm55ng - dcm56*amn56
         call adder(k,amn55,'amn55',delm55,dtsm)
         call adder(k,amn56,'amn56',delm56,dtsm)
      enddo
c
      delf54= -afe54*xf54np - afe54*xf54ng
      delf55=  afe54*xf54ng - afe55*xf55na
      delf56= -afe56*xf56ng
      delf57=  afe56*xf56ng - afe57*xf57ng
      delf58=  afe57*xf57ng - afe58*xf58ng
      delf59=  afe58*xf58ng - afe59*xf59ng - afe59*xf59na -dcf59*afe59
c
      delc59=  dcf59*afe59  - aco59*xc59ng
      delc60=  aco59*xc59ng - aco60*xc60ng - dcc60*aco60
c     ------------------------------------------------------------------------
c     Note: following block is the same as above, with all reaction rates set to zero
c
      call adder(k,amn54,'amn54',delm54,dt)
```

```
c       call adder(k,amn55,'amn55',delm55,dt)  ! now done inside short-time loop above instead
c       call adder(k,amn56,'amn56',delm56,dt)  ! now done inside short-time loop above instead
c
        call adder(k,afe54,'afe54',delf54,dt)
        call adder(k,afe55,'afe55',delf55,dt)
        call adder(k,afe56,'afe56',delf56,dt)
        call adder(k,afe57,'afe57',delf57,dt)
        call adder(k,afe58,'afe58',delf58,dt)
        call adder(k,afe59,'afe59',delf59,dt)
c
        call adder(k,aco59,'aco59',delc59,dt)
        call adder(k,aco60,'aco60',delc60,dt)
c       ------------------------------------------------------------------------
c
        delm54= -delm54
        delm56= -delm56
        delf59= -delf59
        delc60= -delc60
c
        if (delm56.lt.0.001) delm56=0.0
c
        write (7,15) iday,delm54,delm56,delf59,delc60
15      format (' day=',i2,7x,1p,11d10.3)      ! <-- used for normal printout
c       ------------------------------------------------------------------------
        enddo
c
c       ========================================================================
c
c       BEGIN DECAY ANALYSIS (to get & print equivalent gamma source at 1.3 MeV):
c
c       restore shutdown concentrations:
c
        amn54=amn54z
        amn55=amn55z
        amn56=amn56z
        afe54=afe54z
        afe55=afe55z
        afe56=afe56z
        afe57=afe57z
        afe58=afe58z
        afe59=afe59z
        aco59=aco59z
        aco60=aco60z
c
        c=0.0d0
c
        xm55ng=c*xm55ng
        xf54np=c*xf54np
        xf56ng=c*xf56ng
        xf57ng=c*xf57ng
        xf58ng=c*xf58ng
        xc59ng=c*xc59ng
c
        xm54ng=c*xm54ng
        xf54ng=c*xf54ng
        xf55na=c*xf55na
        xf59ng=c*xf59ng
```

```
      xf59na=c*xf59na
      xc60ng=c*xc60ng
c
      dt=1.0d0             ! delta-t = 1 day
      dt=dt*8.64d4         ! delta-t in seconds
c
      tdecay=60.0d0          ! tdecay= 60 days
      tdecay=tdecay*8.64d4   ! tdecay in seconds
c
      ndecay=nint(tdecay/dt) ! decay for this many timesteps
c
c
      write (7,'(a1,//,a19,//,a47,/,a47,//,13x,a10,a9,/)')
     *  char(12),
     *  ' AFTER SHUTDOWN:   ',
     *  '   Equivalent Gamma Source (p/s/cc) at 1.25 MeV',
     *  '   and  Total Gamma Source (p/s) for this shell',
     *  '(p/s/cc)','(p/s)'
c
      do i=1,ndecay
      iday=i
      k=0
c     ------------------------------------------------------------------------
c     Note: following block is the same as above, with all reaction rates set to zero
c
      delm54=  afe54*xf54np - amn54*xm54ng - dcm54*amn54
c
      nmicro=30
      dtsm=dt/dfloat(nmicro)  ! small timestep required for these 2 nuclides because of small half-life of Mn-56
      do j=1,nmicro
         delm55= amn54*xm54ng - amn55*xm55ng
         delm56= amn55*xm55ng - dcm56*amn56
         call adder(k,amn55,'amn55',delm55,dtsm)
         call adder(k,amn56,'amn56',delm56,dtsm)
      enddo
c
      delf54= -afe54*xf54np - afe54*xf54ng
      delf55=  afe54*xf54ng - afe55*xf55na
      delf56= -afe56*xf56ng
      delf57=  afe56*xf56ng - afe57*xf57ng
      delf58=  afe57*xf57ng - afe58*xf58ng
      delf59=  afe58*xf58ng - afe59*xf59ng - afe59*xf59na -dcf59*afe59
c
      delc59=  dcf59*afe59  - aco59*xc59ng
      delc60=  aco59*xc59ng - aco60*xc60ng - dcc60*aco60
c     ------------------------------------------------------------------------
c     Note: following block is the same as above, with all reaction rates set to zero
c
      call adder(k,amn54,'amn54',delm54,dt)

c     call adder(k,amn55,'amn55',delm55,dt)  ! now done inside short-time loop above instead
c     call adder(k,amn56,'amn56',delm56,dt)  ! now done inside short-time loop above instead
c
      call adder(k,afe54,'afe54',delf54,dt)
      call adder(k,afe55,'afe55',delf55,dt)
      call adder(k,afe56,'afe56',delf56,dt)
      call a(k,afe57,'afe57',delf57,dt)
      call a(k,afe58,'afe58',delf58,dt)
```

```
      call adder(k,afe59,'afe59',delf59,dt)
c
      call adder(k,aco59,'aco59',delc59,dt)
      call adder(k,aco60,'aco60',delc60,dt)
c     ------------------------------------------------------------------------
c
      delm54= -delm54
      delm56= -delm56
      delf59= -delf59
      delc60= -delc60
c
c     for Mn-54, each decay = 1 gamma at 0.8348 MeV
c     for Mn-56, each decay = 1 or 2 gammas between 0.8468 MeV and 3.370 MeV; avg=1.69 MeV; basically gone after 2-4 days
c     for Fe-59, each decay = 1 gamma at 1.099 MeV "OR"  1 gamma at 1.292 MeV, plus some low energy gammas;  avg=1.19 MeV
c     for Co-60, each decay = 1 gamma at 1.173 MeV "AND" 1 gamma at 1.332 MeV  (always 2 gammas per disintegration)
c
      egam=1.25d0 ! arbitrary energy; midway between two gamma lines
      gamsrc=0.0d0
      gamsrc=gamsrc + delc60*1.173d0 + delc60*1.332d0
      gamsrc=gamsrc + delf59*1.19d0
      gamsrc=gamsrc + delm54*0.8348d0 + delm56*1.69d0
      gamsrc=gamsrc/egam  ! equivalent number of (p/s/cc) at egam=1.25 MeV
      gamreg=gamsrc*vol
c
      if (i.eq.7) gsrc7=gamsrc  ! save (and report back) values 7 days after shutdown
      if (i.eq.7) greg7=gamreg  ! save (and report back) values 7 days after shutdown
c
      write (7,16) iday,gamsrc,gamreg
16    format (' day=',i2,7x,1p,2d10.3)
c     ------------------------------------------------------------------------
      enddo
c
      return
      end
      subroutine adder(i,amt,name,diff,dt)
      implicit double precision (a-h,o-z)
      character*5 name
c
      delta=diff*dt
c
      if (i.le.5) go to 13
      del=dabs(delta)
c
      if (amt.gt.0.0 .and. del.gt.amt*0.2) then
          write (*,11) name,amt,delta
11        format (' dt too big for ',a5,
     *      '   amt=',1pe13.5,'   delta=',1pe13.5)
          stop
      endif
c
ccc      if (del.lt.amt*(1.0e-14)) then
ccc          write (*,12) name,amt,delta
ccc12        format (' dt too small for ',a5,
ccc     *      '   amt=',1pe13.5,'   delta=',1pe13.5)
ccc      stop
ccc      endif
c
13    amt=amt+delta
```

```
      return
      end
```

Appendix E.3

SI.FOR: A utility program to take the "spatially-dependent (activation) decay gamma source terms per unit volume (p/s/cc) in each of the 39 1-cm-thick cylindrical shells concentrically centered around the 3.5-inch-diam beam hole through the HB-3 rotary shutter, 7 days after shutdown (as calculated by the ACTSRC.FOR program)" and produce the si2 and sp2 (source information and source probability) distributions needed for use with the SDEF card in the subsequent MCNP gamma-only shielding analysis (Run HB310) based on these activation source terms.

```
c     ************************************************************************************************************************
c     ************************************************************************************************************************
c
c     SI.FOR -- a utility program to take the "spatially-dependent (activation) decay gamma source terms per unit volume (p/s/cc)
c               in each of the 39 1-cm-thick cylindrical shells concentrically centered around the big beam hole thru the HB-3
c               rotary shutter 7 days after shutdown (see the GSRC7 array)" and produce the si2 and sp2 (source information and
c               source probability) distributions needed for use with the SDEF card in the next MCNP run (Run HB310).
c
c               Sources (p/s/cc) in the (GSRC7(i),i=1,39) array below, from the ACTSRC.OUT file produced by ACTSRC.FOR,
c               represent the "equivalent" gamma source at 1.25 MeV due to the decay of Mn-54, Mn-56, Fe-59, and Co-60,
c               all at 7 days after shutdown.
c
c
c     Description of activation sources within the Type 1020 carbon steel rotary shutter shield plug represented by Cell 3090.
c     ========================================================================================================================
c
c     Role played by ACTSRC.FOR:
c     --------------------------
c
c     How obtained:  Run HB309A was used to obtain about a dozen key reaction rates for the various isotopes in this material
c     (which initially included 0.45 wt% Mn-55 and 0.015 wt% Co-59), in each of 39 1-cm-thick cylindrical shells concentrically
c     located about the big beam hole in the rotary shutter shield plug when the shutter was wide open and operating under
c     normal conditions.  ACTSRC.FOR is an ad hoc burnup/depletion program that uses those various reaction rates.  Material
c     was assumed to be irradiated for 30 years at full power (although almost everything except Co-59 reaches saturation in
c     just 1 or 2 years);  while the detailed ACTSRC.FOR output shows decay gamma sources (from Mn-54, Mn-56, Fe-59, and Co-60)
c     for each of the first 60 days after shutdown, the results at 7 days after shutdown were selected as typical.  (In reality,
c     things don't change much after day 3 or 4.)  ACTSRC.FOR also shows the corresponding gamma sources (p/s/cc) for each of
c     the 39 cyl shells described above (based on actual amount [cc's] of material in the rotary shutter [Cell 3090] that lie
c     in each of the 39 shells), as well as the total (real)volume-integrated source (p/s) in each piece of Cell 3090 in each
c     shell, 7 days after shutdown.  Most activity comes from Fe-59 and Co-60, both of which have gammas at 1.1 MeV and 1.3 MeV.
c     The equivalent gamma source used here (below) is based on an everage 1.25 MeV per disintegration (i.e., those at 1.1 MeV
c     count for slightly less, and those at 1.3 MeV count for slightly more).
c
c
c     How data is transferred:
c     ------------------------
c
c     This data (p/s/cc of "real" material in each shell) is printed in the ACRSRC.OUT file by ACTSRC.FOR, and fed manually to
c     the SI.FOR program in the form of the GSRC7 array (gsrc7(i),i=1,39).  This program, SI.FOR, creates the radial sampling
c     distribution (si2,sp2) to be used with the SDEF card in the next MCNP run (Run HB310).
c
c
c     What SI.FOR does with it to get MCNP source sampling distributions:
c     --------------------------------------------------------------------
c
c     When creating the sampling distribution within the sampling volume (which must fully enclose Cell 3090), it is necessary to
c     assume that the source density (p/s/cc of "real" material in each shell) is characteristic of the "entire" volume of each shell
c     in the sampling volume.  That source density (in each radial bin) is therefore multiplied by the "entire" volume of the radial
c     shell in each segment of the sampling volume.  The fact that it may really only be characteristic of a tiny piece of real
c     material in each shell of the sampling volume is accounted for by rejecting any sampled points that are not really inside
c     Cell 3090.  Moreover, in SI.FOR, we also subdivide each of the 39 shells of the sampling volume into 3 pieces of equal volume
c     and assume that the inner piece has a source density that is 6% higher than the average, and that the outer piece has a source
c     density that is 6% lower than the average.  (While not necessary, this was done simply to help "smooth out" some of the
c     discontinuities between shells.)  Anyway, that's why the sampling volume below has 117 (=3*39) radial regions instead of 39.
c     Lastly, it must be recognized that the final dose rate determination calc for activation sources will be performed with the
c     shutter closed.  For that reason, the axs vector for the sampling volume on the MCNP SDEF card must be coincident with the
c     axis of the big beam hole of the shutter when closed (i.e., 66.75 degr  off the centerline of the beam tube). -- JAB, 6-30-98
c
```

```
c     ******************************************************************************************************************************
c     ******************************************************************************************************************************
c
      implicit double precision (a-h,o-z)
c
      dimension rmin(39),rmax(39),vol(39)
      dimension gsrc7(39) ! (act) decay gamma source terms (p/s/cc) in each of the 39 1-cm-thick cyl shells; calculated here
c
      data rmin/ ! dist (cm) from centerline of big hole thru rotary shutter
     *  4.445d0,  5.445d0,  6.445d0,  7.445d0,  8.445d0,
     *  9.445d0, 10.445d0, 11.445d0, 12.445d0, 13.445d0,
     * 14.445d0, 15.445d0, 16.445d0, 17.445d0, 18.445d0,
     * 19.445d0, 20.445d0, 21.445d0, 22.445d0, 23.445d0,
     * 24.445d0, 25.445d0, 26.445d0, 27.445d0, 28.445d0,
     * 29.445d0, 30.445d0, 31.445d0, 32.445d0, 33.445d0,
     * 34.445d0, 35.445d0, 36.445d0, 37.445d0, 38.445d0,
     * 39.445d0, 40.445d0, 41.445d0, 42.445d0/
c
      data rmax/ ! dist (cm) from centerline of big hole thru rotary shutter
     *  5.445d0,  6.445d0,  7.445d0,  8.445d0,  9.445d0,
     * 10.445d0, 11.445d0, 12.445d0, 13.445d0, 14.445d0,
     * 15.445d0, 16.445d0, 17.445d0, 18.445d0, 19.445d0,
     * 20.445d0, 21.445d0, 22.445d0, 23.445d0, 24.445d0,
     * 25.445d0, 26.445d0, 27.445d0, 28.445d0, 29.445d0,
     * 30.445d0, 31.445d0, 32.445d0, 33.445d0, 34.445d0,
     * 35.445d0, 36.445d0, 37.445d0, 38.445d0, 39.445d0,
     * 40.445d0, 41.445d0, 42.445d0, 43.4433d0/
c
      data vol/ ! volume (cc) of cyl shell "i"; cannot be computed from rmin & rmax; cannot be computed analytically; calculated statistically
     * 1.89858d+03, 2.27981d+03, 2.65511d+03, 3.02744d+03, 3.39342d+03,
     * 3.75537d+03, 4.11116d+03, 4.45690d+03, 4.79709d+03, 5.12661d+03,
     * 5.44592d+03, 5.75543d+03, 6.05497d+03, 6.33840d+03, 6.60982d+03,
     * 6.86725d+03, 7.10540d+03, 7.32554d+03, 7.53004d+03, 7.70707d+03,
     * 7.85115d+03, 7.96738d+03, 8.04809d+03, 8.08235d+03, 8.05935d+03,
     * 7.95535d+03, 6.44147d+03, 4.99352d+03, 4.08671d+03, 3.36986d+03,
     * 2.76096d+03, 2.23160d+03, 1.76511d+03, 1.35264d+03, 9.88281d+02,
     * 6.71165d+02, 4.01009d+02, 1.86544d+02, 3.97575d+01/
c
      data gsrc7/
     * 1.71804E+06, 1.20939E+06, 9.10533E+05, 5.11462E+05, 2.96828E+05,
     * 2.04527E+05, 1.45949E+05, 1.10877E+05, 8.50310E+04, 7.25228E+04,
     * 5.84760E+04, 4.65858E+04, 4.14990E+04, 3.22381E+04, 2.75541E+04,
     * 2.20748E+04, 2.31075E+04, 1.64953E+04, 1.46455E+04, 1.54328E+04,
     * 1.20202E+04, 9.35205E+03, 1.14168E+04, 9.28401E+03, 7.24319E+03,
     * 6.70739E+03, 7.31088E+03, 6.62929E+03, 4.56713E+03, 3.66936E+03,
     * 4.79983E+03, 5.26502E+03, 7.08731E+03, 4.83427E+03, 8.71481E+03,
     * 4.25503E+03, 3.18232E+02, 1.67852E+02, 5.10060E+01/
c
c     In the MCNP model of the rotary shield plug, the sampling volume is a
c     62-cm-long cylinder, with rmax0=rmax(39), centered about X=Y=0, Z=446.405 cm,
c     and rotated so as to be aligned with the big beam hole the rotary shutter shield plug.
c
      open (8,file='si.out',status='unknown')
c
      dz=62.0
      pi=dacos(-1.0d0)
      tilt=0.12d0
      tilt=0.08d0
```

```
      tilt=0.00d0
      tilt=0.05d0
      tilt=0.06d0
      zero=0.0d0
      ra=rmin(1)
      write (8,11) ra,zero
c
      do i=1,39
c
c     define ra,rb,rc,rd such that Vol(rb-ra)=Vol(rc-rb)=Vol(rd-rc)
      ra=rmin(i)
      rd=rmax(i)
      rb=sqrt(ra*ra+((rd*rd-ra*ra)/3.0d0))
      rc=sqrt(ra*ra+((rd*rd-ra*ra)*2.0d0/3.0d0))
      volsam=dz*pi*(rd*rd-ra*ra)/3.0d0
      srcb=gsrc7(i)*volsam*(1.0d0+tilt)          ! put 6% more source in innermost one-third of cyl shell
      srcc=gsrc7(i)*volsam*(1.0d0)
      srcd=gsrc7(i)*volsam*(1.0d0-tilt) ! put 6% less source in outermost one-third of cyl shell
c
      write (8,'(1x)')
      write (8,11) rb,srcb
      write (8,11) rc,srcc
      write (8,11) rd,srcd
11    format (1x,f11.5,1pe14.5)
c
      enddo
c
      stop
      end
```

Appendix E.4

Input listing for MCNP Run HB310, a gamma-only shielding calculation used to determine the dose rate downstream of the closed rotary shutter, seven days after shutdown, due to prior activation of the carbon steel rotary shutter itself. Source terms used here were determined as noted in Sect 7.

```
message:  outp=hb310.o  runtpe=hb310.r

Isolated model of HB-3 using only activation sources in rotary shutter
c     ------------------------------------------------------------------------------------------------------------
c
c       HB310 is a series of gamma-only calcs to determine the gamma dose rate downstream of the rotary shutter
c             shield plug "due to activation sources in the rotary shutter shield plug itself, 7 days after shutdown"
c
c             1) The starting point for HB310A is Run HB308G.I
c
c     ok      2) Don't use the wwinp file developed for HB308G.I; in fact don't use any wwinp file at all;
c                (If I here start gammas with a wt of 1.0 in a region in which the wt windows in HB308G had
c                an avg wt of 1.0e-9 (for example), each history would split into a billion pieces right at
c                the start, and we definitely don't want to do that.
c     ok         Thus, the WWP:N & WWP:P cards should be commented out completely for this run.
c
c     ok      3) Comment out the SSW card previously used in Run HB308G to write the boundary source file;
c             here we don't need to write any such file, nor do we need to read any such file
c
c     ok      4) Comment out whatever tallies & detectors there may have been, and add the following to get the
c                gamma fluxes & dose rates "due to activation gammas in the rotary shutter, 7 days after shutdown"
c                ---------------------------------------------------
c     ok              fc35   G-Flux (p/s/cm2) 0.5 cm past conc box containing shutter, at 100 MW
c     ok           --> fc45  G-Dose (mrem/hr) 0.5 cm past conc box containing shutter, at 100 MW
c     ok              fc55   G-Flux (p/s/cm2) 1.5 feet past conc box containing shutter, at 100 MW
c     ok           --> fc65  G-Dose (mrem/hr) 1.5 feet past conc box containing shutter, at 100 MW
c     ok              fc75   G-Flux (p/s/cm2) 3 feet past conc box containing shutter, at 100 MW
c     ok           --> fc85  G-Dose (mrem/hr) 3 feet past conc box containing shutter, at 100 MW
c
c     ok              fc231  Primary G-Leakage (p/s) on downstrem surf of box holding shutter, L(z-) and L(z+) only, 10 spatial regions
c     ok           --> fc232  Primary G-Dose (mrem/hr) on downstrem surf of box holding shutter; seg 10  <-- 1st used in HB308G
c
c     ok              In each case, set the value on the FM card = Total activation gamma source (p/s)=  1.61388E+10
c
c     ok      5) Use imp:p=0.0 for the infintisimally thin region just upstream of where the boundary source was calculated
c             in HB308G.I, i.e., upstream of the rotary shutter; at least this will keep me from tracking gammas throughout
c             the entire model where they are not important in this activation dose assessment.  To be more precise:
c             Make Cell 9981 (between Surfs 4195 & 4196) a "black void" with imp:n=0 & imp:p=0 to de-couple everything
c             upstream of Surf 4196.  To do this, set imp:n=0 on Cell 9981 below, then run a dummy MCNP calc, go to the
c             printed output, strip out the neutron inportances from Table 60, and enter those values as gamma importances
c             below, as:
c
c     ok        imp:p  $ obtained from MCNP output table when I ran a fake MCNP run with neutrons; here imp:p=imp:n in all 88 cells;
c                      $ in this case I set imp:p=imp:n=0 in Cell 9981 (position 84 in this table), just upstream of the rotary shutter
c                      1 0 1 1 1 1 1 1 1 1 0 1 1 1 1 1 1 1 1 2
c                      2 2 2 2 1 1 1 1 1 1 1 1 2 2 1 2 2 2 2 2 2
c                      2 2 2 2 2 2 2 2 1 1 1 1 1 1 1 1 1 1 1 1
c                      1 1 1 1 1 1 1 1 1 1 1 1 1 1 1 1 1 1 1 1
c                      1 1 1 0 1 1 1 0
c
c     ok      6) On prdmp card, make restart file after every 800000 histories in fixed src calc;
c             save only the 4 most recent restart files
c
c             7) Be prepared to "run the fool out of it";  if I want fsd's on the order of 0.01, I'll need to get 10,000
c             histories out of the system;  since last 31 cm of rotary shutter may attenuate gammas by 1.0e-4, I may need
c             as many as 100,000,000 histories (maybe considerably less if streaming kicks in, but "a lot" in any event)
c     ok        lets start out by trying nps=40,000,000 and see what we get;    uld take about 10 hours wallclock on each of 8 nodes)
c
```

c ok 8) On the SDEF card below (for the activation sources), don't mess with the starting weights; leave them as 1.0
c
c 9) On SDEF card for Run HB310, include only the activation sources in the rotary shutter, seven days after
c shutdown, as described below; need new sdef paramaters, and (si1,sp1) & (si2,sp2) distributions:
c
c c ----------
c c Description of activation sources within the Type 1020 carbon steel rotary shutter shield plug represented by Cell 3090.
c c How obtained: Run HB309A was used to obtain about a dozen key reaction rates for the various isotopes in this material
c c (which initially included 0.45 wt% Mn-55 and 0.015 wt% Co-59), in each of 39 1-cm-thick cylindrical shells concentrically
c c located about the big beam hole in the rotary shutter shield plug when the shutter was wide open and operating under
c c normal conditions. ACTSRC.FOR is an ad hoc burnup/depletion program that uses those various reaction rates. Material
c c was assumed to be irradiated for 30 years at full power (although almost everything except Co-59 reaches saturation in
c c just 1 or 2 years); while the detailed ACTSRC.FOR output shows decay gamma sources (from Mn-54, Mn-56, Fe-59, and Co-60)
c c for each of the first 60 days after shutdown, the results at 7 days after shutdown were selected as typical. (In reality,
c c things don't change much after day 3 or 4.) ACTSRC.FOR also shows the corresponding gamma sources (p/s/cc) for each of
c c the 39 cyl shells described above (based on actual amount [cc's] of material in the rotary shutter [Cell 3090] that lie
c c in each of the 39 shells), as well as the total (real)volume-integrated source (p/s) in each piece of Cell 3090 in each
c c shell, 7 days after shutdown. Most activity comes from Fe-59 and Co-60, both of which have gammas at 1.1 MeV and 1.3 MeV.
c c The equivalent gamma source used here (below) is based on an everage 1.25 MeV per disintegration (i.e., those at 1.1 MeV
c c count for slightly less, and those at 1.3 MeV count for slightly more). This data (p/s/cc of "real" material in each
c c +----------
c c | Results from ACTSRC.FOR are as follows:
c c |
c c | Equivalent gamma sources (at 1.25 MeV, 7 days after shutdown) for each of 39
c c | cylindrical shells, concentric about large beam hole in HB-3 rotary shutter:
c c |

Cyl Shell	Rmin	Rmax	Volume (cc)	GSRC den (p/s/cc)	GSRC total (p/s)
1	4.4450	5.4450	1.89858E+03	1.71804E+06	3.26184E+09
2	5.4450	6.4450	2.27981E+03	1.20939E+06	2.75717E+09
3	6.4450	7.4450	2.65511E+03	9.10533E+05	2.41757E+09
4	7.4450	8.4450	3.02744E+03	5.11462E+05	1.54842E+09
5	8.4450	9.4450	3.39342E+03	2.96828E+05	1.00726E+09
6	9.4450	10.4450	3.75537E+03	2.04527E+05	7.68074E+08
7	10.4450	11.4450	4.11116E+03	1.45949E+05	6.00020E+08
8	11.4450	12.4450	4.45690E+03	1.10877E+05	4.94166E+08
9	12.4450	13.4450	4.79709E+03	8.50310E+04	4.07901E+08
10	13.4450	14.4450	5.12661E+03	7.25228E+04	3.71796E+08
11	14.4450	15.4450	5.44592E+03	5.84760E+04	3.18456E+08
12	15.4450	16.4450	5.75543E+03	4.65858E+04	2.68122E+08
13	16.4450	17.4450	6.05497E+03	4.14990E+04	2.51275E+08
14	17.4450	18.4450	6.33840E+03	3.22381E+04	2.04338E+08
15	18.4450	19.4450	6.60982E+03	2.75541E+04	1.82128E+08
16	19.4450	20.4450	6.86725E+03	2.20748E+04	1.51593E+08
17	20.4450	21.4450	7.10540E+03	2.31075E+04	1.64188E+08
18	21.4450	22.4450	7.32554E+03	1.64953E+04	1.20837E+08
19	22.4450	23.4450	7.53004E+03	1.46455E+04	1.10281E+08
20	23.4450	24.4450	7.70707E+03	1.54328E+04	1.18942E+08
21	24.4450	25.4450	7.85115E+03	1.20202E+04	9.43721E+07
22	25.4450	26.4450	7.96738E+03	9.35205E+03	7.45113E+07
23	26.4450	27.4450	8.04809E+03	1.14168E+04	9.18836E+07
24	27.4450	28.4450	8.08235E+03	9.28401E+03	7.50366E+07
25	28.4450	29.4450	8.05935E+03	7.24319E+03	5.83754E+07
26	29.4450	30.4450	7.95535E+03	6.70739E+03	5.33597E+07
27	30.4450	31.4450	6.44147E+03	7.31088E+03	4.70928E+07
28	31.4450	32.4450	4.99352E+03	6.62929E+03	3.31035E+07
29	32.4450	33.4450	4.08671E+03	4.56713E+03	1.86645E+07

```
c      c     |  30    33.4450  34.4450   3.36986E+03   3.66936E+03   1.23652E+07
c      c     |  31    34.4450  35.4450   2.76096E+03   4.79983E+03   1.32521E+07
c      c     |  32    35.4450  36.4450   2.23160E+03   5.26502E+03   1.17494E+07
c      c     |  33    36.4450  37.4450   1.76511E+03   7.08731E+03   1.25099E+07
c      c     |  34    37.4450  38.4450   1.35264E+03   4.83427E+03   6.53903E+06
c      c     |  35    38.4450  39.4450   9.88281E+02   8.71481E+03   8.61268E+06
c      c     |  36    39.4450  40.4450   6.71165E+02   4.25503E+03   2.85583E+06
c      c     |  37    40.4450  41.4450   4.01009E+02   3.18232E+02   1.27614E+05
c      c     |  38    41.4450  42.4450   1.86544E+02   1.67852E+02   3.13117E+04
c      c     |  39    42.4450  43.4433   3.97575E+01   5.10060E+01   2.02787E+03
c      c     |                                                      -----------
c      c     |                    Total activation gamma source (p/s)=  1.61388E+10
c      c     |
c      c     |  (*) Volumes shown/used here are the actual volume(s) corresponding
c      c     |      to the rotary shutter (Cell 3090) inside each of these radial
c      c     |      shells.  Because these shells have a horizontal axis while the
c      c     |      shutter has a vertical axis, and also because of the small hole
c      c     |      thru the shutter which cuts thru all/most of these at an angle,
c      c     |      these "real" volumes had to be calculated stoichastically, as
c      c     |      shown in Run VV309.
c      c     +-------------------------------------------------------------------
c      c     shell) is fed to the SI.FOR program which creates the radial sampling distribution (si2,sp2) shown below.  When creating
c      c     the sampling distribution within the sampling volume (which must fully enclose Cell 3090), it is necessary to assume that
c      c     the source density (p/s/cc of "real" material in each shell) is characteristic of the "entire" volume of each shell in the
c      c     sampling volume.  That source density (in each radial bin) is therefore multiplied by the "entire" volume of the radial
c      c     shell in each segment of the sampling volume.  The fact that it may really only be characteristic of a tiny piece of real
c      c     material in each shell of the sampling volume is accounted for by rejecting any sampled points that are not really inside
c      c     Cell 3090.  Moreover, in SI.FOR, we also subdivide each of the 39 shells of the sampling volume into 3 pieces of equal volume
c      c     and assume that the inner piece has a source density that is 6% higher than the average, and that the outer piece has a source
c      c     density that is 6% lower than the average.  (While not necessary, this was done simply to help "smooth out" some of the
c      c     discontinuities between shells.)  Anyway, that's why the sampling volume below has 117 (=3*39) radial regions instead of 39.
c      c     Lastly, it must be recognized that the final dose rate determination calc for activation sources will be performed with the
c      c     shutter closed.  For that reason, the axs vector for the sampling volume shown below must be coincident with the axis of the
c      c     big beam hole of the shutter when closed (i.e., 66.75 degrees off the centerline of the beam tube).  -- JAB, 6-30-98
c      c     ----------------------------
c      sdef  $ activation sources in the rotary shutter, 7 days after shutdown;  total activation gamma source (p/s)=  1.61388E+10
c            par=2                          $ gamma source
c            erg=1.25                       $ will use an "equivalent" activation source at 1.25 MeV (see ACTSRC.FOR program)
c            cel=3090                       $ exclude any points from sampling distribution that are not in rotary shutter shield plug (Cell 3090)
c            pos= 0  0  446.405             $ reference position here is the midpoint of the rotary shutter shield plug
c            axs= 0  -0.9187912  0.3947439  $ ref vector for sampling vol points along centerline of big hole (66.75 degrees off beam tube centerl
ine
c            ext=d1                         $ use d1 to sample uniformly over +/- 31 cm of sampling volume centerline
c            rad=d2                         $ use d2 to sample radial distribution within the sampling volume
c      si1  -31.0  31.0    $ axial bins; used for axial sampling probability within sampling volume;
c      sp1    0.0   1.0    $ sampling probability for each axial bin within sampling volume; uniform
c      si2  $ radial bins; used for radial sampling probability within sampling volume; see SI.FOR program; pts outside Cell 3090 will still be re
jected
c             4.44500   4.80153   5.13336   5.44500   5.79753
c             6.12982   6.44500   6.79471   7.12727   7.44500
c             7.79260   8.12535   8.44500   8.79098   9.12385
c             9.44500   9.78969  10.12265  10.44500  10.78864
c            11.12166  11.44500  11.78776  12.12084  12.44500
c            12.78703  13.12014  13.44500  13.78640  14.11954
c            14.44500  14.78585  15.11902  15.44500  15.78537
c            16.11856  16.44500  16.78495  17.11816  17.44500
c            17.78458  18.11780  18.44500  18.78425  19.11748
c            19.44500  19.78395  20.11719  20.44500  20.78368
```

```
c                 21.11693  21.44500  21.78343  22.11669  22.44500
c                 22.78321  23.11647  23.44500  23.78301  24.11627
c                 24.44500  24.78282  25.11609  25.44500  25.78264
c                 26.11592  26.44500  26.78248  27.11576  27.44500
c                 27.78233  28.11562  28.44500  28.78219  29.11548
c                 29.44500  29.78206  30.11536  30.44500  30.78194
c                 31.11524  31.44500  31.78183  32.11513  32.44500
c                 32.78172  33.11502  33.44500  33.78162  34.11492
c                 34.44500  34.78153  35.11483  35.44500  35.78144
c                 36.11474  36.44500  36.78135  37.11466  37.44500
c                 37.78127  38.11458  38.44500  38.78120  39.11451
c                 39.44500  39.78113  40.11444  40.44500  40.78106
c                 41.11437  41.44500  41.78099  42.11431  42.44500
c                 42.78036  43.11310  43.44330
c            sp2  $ sampling probability for each radial bin within sampling volume; see SI.FOR program; pts outside Cell 3090 will still be rejected
c                 0.00000e+0  1.16938e+9  1.10319e+9  1.03700e+9  9.89634e+8  $ first 4.445 cm represents the big beam hole (void) where sources are ze
ro
c                 9.33617e+8  8.77600e+8  8.70410e+8  8.21142e+8  7.71873e+8
c                 5.59324e+8  5.27664e+8  4.96004e+8  3.65461e+8  3.44775e+8
c                 3.24088e+8  2.79970e+8  2.64123e+8  2.48275e+8  2.19874e+8
c                 2.07428e+8  1.94982e+8  1.82299e+8  1.71980e+8  1.61661e+8
c                 1.51508e+8  1.42932e+8  1.34356e+8  1.39203e+8  1.31324e+8
c                 1.23444e+8  1.20290e+8  1.13481e+8  1.06672e+8  1.02243e+8
c                 9.64558e+7  9.06685e+7  9.67911e+7  9.13123e+7  8.58336e+7
c                 7.96286e+7  7.51213e+7  7.06140e+7  7.18517e+7  6.77846e+7
c                 6.37175e+7  6.06020e+7  5.71717e+7  5.37414e+7  6.66177e+7
c                 6.28469e+7  5.90761e+7  4.98255e+7  4.70052e+7  4.41849e+7
c                 4.62539e+7  4.36358e+7  4.10176e+7  5.08646e+7  4.79855e+7
c                 4.51064e+7  4.12716e+7  3.89355e+7  3.65993e+7  3.33977e+7
c                 3.15073e+7  2.96168e+7  4.23427e+7  3.99460e+7  3.75492e+7
c                 3.57105e+7  3.36891e+7  3.16678e+7  2.88576e+7  2.72241e+7
c                 2.55907e+7  2.76461e+7  2.60812e+7  2.45164e+7  3.11398e+7
c                 2.93772e+7  2.76146e+7  2.91492e+7  2.74992e+7  2.58493e+7
c                 2.07104e+7  1.95381e+7  1.83658e+7  1.71444e+7  1.61740e+7
c                 1.52035e+7  2.30870e+7  2.17802e+7  2.04734e+7  2.60492e+7
c                 2.45747e+7  2.31002e+7  3.60407e+7  3.40007e+7  3.19606e+7
c                 2.52489e+7  2.38197e+7  2.23905e+7  4.67160e+7  4.40717e+7
c                 4.14274e+7  2.33949e+7  2.20707e+7  2.07464e+7  1.79350e+6
c                 1.69198e+6  1.59046e+6  9.69087e+5  9.14233e+5  8.59379e+5
c                 3.00983e+5  2.83947e+5  2.66910e+5
c            c    ------------------------------------------------------------------------------------------------------------------------
c            c    end description of activation sources
c
c    ------------------------------------------------------------------------------------------------------------------------
c
c    HB309 was a neutron-only calc under normal conditions, with shutter open, to get about a dozen nuclear
c          reaction rates in 39 1-cm-thick shells concentric about the big beam hole thru the shutter, so that I
c          could go off and do an activation analysis of the shutter and calculate (offline in ACTSRC.FOR and SI.FOR)
c          the activation sources to be used in Run HB310. HB309 was created by making a number of small modifications
c          to HB308G.  For details on Run HB309, see Sect 7 and/or Appendix E.1.
c
c    ------------------------------------------------------------------------------------------------------------------------
c
c    HB308G  was the final (reference) gamma-only shielding analysis for the HB-3 beam tube with the 1998 water tube
c            and collimator sections both flooded and the rotary shutter in the closed position.  HB308G was created
c            by making a number of small modifications to HB304M4.  Run HB308G is described extensively in Sect 6.
c            The complete input listing for Run HB308G may be seen in Appendix D.4.
c
```

```
c     ------------------------------------------------------------------------------------------------------------
c
c     HB304M4 was the final reference case for the neutron dosimetry analysis described in Sect 4.
c             For a complete listing of this input file, see Appendix B.1.
c
c     ------------------------------------------------------------------------------------------------------------
c
c     Earlier notes on the HB301, HB302, and HB303 series:
c
c     Used to study shielding effectiveness of water tube (work performed by Jim Bucholz for Mike Farrah, Mar/Apr 1998):
c
c       Ref 1:  Dwg of HB-1 (e:\ham\ustn\allbeam1197.dgn Jan 29, 1998 12:55:09), where HB-3 is said to be the same.
c       Ref 2:  Dwg M-11537-OH-001-E, Feb 13, 1998, 10:30:22, dwg of HB-1 (essentially the same as Ref 1, but smaller)
c       Ref 3:  Dwg E-42027, Sheet 1, Apr 11, 1995, showing location on HB-3 & 1st aluminum window in vessel, as built
c       Ref 4:  Dwg E-42027, Sheet 2, Apr 11, 1995, showing typical beam tube collimator & rotary shutter, as built
c       Ref 5:  Dwg 1546-01-M-5022, Rev Sep 18, 1961, showing concrete around HB-3 beam tube collimator & rotary shutter
c
c       Distance from outside of vessel nozzel boss to radial plane
c       perpendicular to beam tube (as specifically stated in Ref 3):
c         HB-1:  52.0 inches = 132.08 cm
c         HB-2:  54.5 inches = 138.43 cm
c         HB-3:  54.0 inches = 137.16 cm
c         HB-4:  52.0 inches = 132.08 cm
c
c       Notes regarding length of the 1998 water tube:
c
c       The location of the 1st aluminum window relative to the vessel nozzel boss (cf Ref 1 & 2) is believed to be
c       correctly modeled here.  Likewise, the 2nd aluminum window relative to the beam tube collimator assembly
c       (cf Ref 1 & 2) is believed to be correctly modeled here.  Given the location of the beam tube collimator
c       assembly (Ref 1 & 2) relative to the concrete biological shield specifically around HB-3 as shown in Ref 5,
c       however, the length of the new HB-3 water tube [from Surf 2154 at Z=174.95125 cm, to Surf 4110 at Z=302.1868 cm
c       (total length of water when flooded = 127.23555 cm)] is about 2.03 inches shorter than shown for HB-1 on Refs
c       1 & 2, and about 89.8 cm shorter than the water tube originally in HB-3. Note, however, that this 2" difference
c       in water tube length between HB-1 and HB-3 is wholly consistent with the data in Ref 3 above if the vessel
c       flange hardware and collimator hardware are the same for HB-1 and HB-3 -- J. A. Bucholz, 3-21-98
c
c     ------------------------------------------------------------------------------------------------------------
c
c     BEGIN CELLS:
c
c     HB-3 (Tangential tube); sign on some surfs changed to accomodate this local model
c
1000  61  -3.2325-4  -1000        -1006        imp:n=1    $ endcap void region replaced with He at 2 atm (3.2325-4 g/cc)
1001  24  -2.7       -1001  1000  -1006        imp:n=0    $ endcap inner Al wall (imp=0 to kill all inward-directed neutrons)
1002  5   -0.98465   -1002  1001  -1006        imp:n=1    $ endcap water
1003  24  -2.7       -1003  1002  -1006        imp:n=1    $ endcap outer Al wall
1004  5   -0.98465   -1004  1003  -1006        imp:n=1    $ endcap water jacket
1005  24  -2.7       -1005  1004  -1006        imp:n=1    $ endcap Al Be liner
c     ----------------------
c     Cells 1008 & 1009 should be VOID (61  -3.2325-4) if looking at the 1998 water tube (normal condx or flooded) or the 1960 water tube under normal (dry)
 conditions.
c     Cells 1008 & 1009 should contain WATER (8   -1.0000) ONLY if looking at 1960 water tube when flooded.
1008  61  -3.2325-4  -2164  -2163        imp:n=1  $ hemispherical VOID inside tip of "dry" 1960 water tube
1009  61  -3.2325-4  -2161   2163 -2153  imp:n=1  $ cylindrical   VOID inside 1960 water tube, upstream of where 1998 water tube begins
c     1008  8   -1.0000    -2164  -2163        imp:n=1  $ hemispherical WATER region inside tip of "flooded" 1960 water tube
c     1009  8   -1.0000    -2161   2163 -2153  imp:n=1  $ cylindrical   WATER region inside 1960 water tube, upstream of where 1998 water tube begins
c     ----------------------
1010  61  -3.2325-4  -2153  -1010  1006                 $ tube void region replaced with He at 2 atm (3.2325-4 g/cc)
```

```
c     obsolete 1st: #(2151  -2152)   $ obsolete (too approximate)   $ tube void region (above) excluding 1st aluminum window in 1960 design (see cell 2140)
c     obsolete 2nd: #((2161 -2162 2163 -2153):(2164 -2165 -2163))   $ tube void region (above) excluding part-length model of old (1960) water tube: 1st sph
 window & cyl section
      2165  #(-2162 2163)          imp:n=1                $ tube void region (above), excluding old aluminum 1960 water tube & everything in it
1011  24  -2.7        -2153  -1011  1010  1007  imp:n=1    $ tube inner Al wall (surf 1007 is the "importance cutoff plane")
10110 24  -2.7        -2153  -1011  1010  1006 -1007  imp:n=0    $ tube inner Al wall (used to kill all neutrons not within most forward-directed cone
1012  5   -0.98465    -2153  -1012  1011  1006  imp:n=1    $ tube water
1013  24  -2.7        -2153  -1013  1012  1006  imp:n=1    $ tube outer Al wall
1014  5   -0.98465    -2012  -1014  1013  1006  imp:n=1    $ tube water jacket [now cut off at cage (2012) as it should be]
1015  24  -2.7        -2012  -1015  1014  1006  imp:n=1    $ tube Al Be liner  [now cut off at cage (2012) as it should be]
c
c
c     Main cylindrical components outside HB-3:
c
2024 108  1.23156-1  -9999 9997 -2010  1005  #(-1015 1006) imp:n=1  $ permanent Be refl (0.123156 atoms/b*cm; typical comp, center ring); exclude HB-3
2110  5   -0.98465   -9999 9997  2010 -2011  1015  imp:n=1 $ water between Be refl and aluminum reflector container
2120  23  -2.7        -9999 9997  2011 -2012  1015  imp:n=1 $ aluminum refl container
c
c
2130  7   -0.9899  -9999 9997  2012 -2013   $ large water region between aluminum refl container and the pressure vessel
                    1013  #(-2101 2150)     $ large water region (above); excluding beam tube & regions around beam tube near vessel
c                   2121   2126             $ large water region (above); excluding the two small dosimeter locations (obsolete model)
c                 #(-2530  2531  -2532)      $ large water region (above); excluding the dosimeter holder ring (and dosimeters)
c                 #(-2520  2521  -2522)      $ large water region (above); excluding thick inner hub   of the holder ring
c                 #(-2510  2511  -2521)      $ large water region (above); excluding thin inner sleeve of the holder ring
c                 #(-2702 2701 2744 -2746 2711 -2710 2720)  $ large water region (above); excluding horz spacer plate extension (Cell 2727) on 2-plate collar
 assembly
c                 #(-2701  2742  -2748)      $ large water region (above); excluding bulk of 2-plate collar assy on ss sleeve outside beam tube close to dosi
meter ring
c                 #(2533  -2531  2553  -2554  2543  -2544) $ large water region (above), excluding ss square peg just upstream of dosimeter at Key 3, Positio
ns 3
c                 #(2533  -2531  2564  -2563  2543  -2544) $ large water region (above), excluding ss square peg just upstream of dosimeter at Key 3, Positio
ns 8
                    imp:n=1                $ large water region (above)
2131  7   -0.9899   1013  -2130  2150  -2153  imp:n=2 $ water between beam tube and ss sleeve near vessel
2132  40  -7.92     2130  -2131  2150  -2153  imp:n=2 $ ss sleeve around beam tube, near vessel
2133  7   -0.9899   2131  -2101  2150  -2013  $ water just outside ss sleeve but inside main pressure vessel, in vicinity of dosimeters
c                   2121   2126              $ water just outside ss sleeve (above), excluding dosimeter locations
                  #(-2530  2531  -2532)       $ water just outside ss sleeve (above); excluding the dosimeter holder ring (and dosimeters)
                  #(-2520  2521  -2522)       $ water just outside ss sleeve (above), excluding thick inner hub   of the holder ring
                  #(-2510  2511  -2521)       $ water just outside ss sleeve (above), excluding thin inner sleeve of the holder ring
c                 #( 2742  -2748)             $ water just outside ss sleeve (above), large water region (above); excluding bulk of 2-plate collar assy on s
s sleeve outside beam tube close to dosimeter ring
                  #(-2702 2701 2744 -2746 2711 -2710 2720)  $ large water region (above); excluding horz spacer plate extension (Cell 2727) on 2-plate collar
 assembly
                  #(-2701  2742  -2748)      $ large water region (above); excluding bulk of 2-plate collar assy on ss sleeve outside beam tube close to dosi
meter ring
                  #(2533  -2531  2553  -2554  2543  -2544) $ water just outside ss sleeve (above), excluding ss square peg just upstream of dosimeter at Key
3, Positions 3
                  #(2533  -2531  2564  -2563  2543  -2544) $ water just outside ss sleeve (above), excluding ss square peg just upstream of dosimeter at Key
3, Positions 8
                    imp:n=2                  $ water just outside ss sleeve (above)
2134  7   -0.9899   2013 -2016  2100  -2110  2112  imp:n=2  $ water in elliptical cone chamfer ring where hb3 vessel hole penetrates inner wall of vessel
2135  7   -0.9899   2131 -2100 -2105   2013        imp:n=2  $ water outside ss sleeve but inside vessel nozzel
c
c
c     Note regarding dosimeters: the two cards shown below clearly define the location of the actual dosimeters presently
c     in use around HB-3.  Nevertheless, without further (questionable) changes to the model, the results here are probably
```

```
c      not even worth tabulating.  Reason:  The equivalent point sources used in this HB-3 analysis (of the voided & flooded
c      water tube) were based on global model point detectors at Z=120.6879, 185.9844, 251.2809 & 316.5774 cm from the radial
c      plane perpendicular to the HB-3 beam tube.  Moreover, for the analysis of the HB-3 water tube (the primary purpose of
c      this study), we spray neutron isotropically only over a very narrow forward-directed cone [cos(theta).gt. 0.965335056]
c      that includes this region of interest, and assign the inner wall of the beam tube an importance of 0.0 for all locations
c      below plane 1007 at Z=118.6879 cm (see cell 10110).  This is done primarily in the name of efficiency in this water tube
c      analysis, but also because points below this would be outside the axial range where we know our equivalent point sources
c      give good results.  Unfortunately, these two dosimeters are located at Z=107.1276 cm and 112.9905 cm respectively (see
c      surfaces 2121 and 2126).  Thus, with the present model, these two dosimeters probably won't see any neutrons except for
c      a few stray ones that might backscatter into this region.  If one really wants to check fluxes at these dosimeters, one
c      would have to lower plane 1007 in cell 10110, and open up the angular range on the sdef card to the point where our
c      equivalent point sources may or may not still be valid.  At any rate, doing so would greatly decrease the efficiency
c      of the water tube analysis that we originally wanted to focus on.  --  J.A. Bucholz, 3-20-98(a)
c
c      Updated thoughts:  Neutron group 16 in the VELM library goes from 0.907 Mev to 1.108 Mev.  Virtually all of the
c      equivalent point neutron sources for these first 16 energy groups lie between Z=31 and Z=70 cm (indeed, most lie
c      between Z=45 cm and Z=60 cm).  Thus, if we use an energy cutoff card set at 1 MeV (as typically done for dosimetry
c      calcs), we could probably make the modifications described above without seriously impacting the quality of the
c      results at the dosimeter locations.  [Efficiency of the water tube calc would go to pot, but if we use this ECUT
c      card for the dosimetry, we would (by definition) not be interested in the water tube results in this calc anyway].
c      Thus, we can probably do the dosimetry study -- at least for fast neutrons above 1 MeV.  Nevertheless, a better
c      course of action might be to take this geometry model, then apply the approach I took last fall with HB-2 (involving
c      a finite line source with all neutrons in a prescribed direction wrt the axis). It gave absolutely excellent results,
c      very quickly.  --  J.A. Bucholz, 3-20-98(b)
c
c       $ obsolete $ 2134  50  -7.8212  -2121   imp:n=1   $ dosimeter (modeled as carbon steel; really Charpy V-notch specimens) just slightly on HB-4 side
of HB-3
c       $ obsolete $ 2135  50  -7.8212  -2126   imp:n=1   $ dosimeter (modeled as carbon steel; really Charpy V-notch specimens) just slightly on HB-2 side
of HB-3
c       $ obsolete $ 2134  7  -1.0000  -2121   imp:n=1   $ dosimeter (now modeled as water; specimens are quite small) just slightly on HB-4 side of HB-3
c       $ obsolete $ 2135  7  -1.0000  -2126   imp:n=1   $ dosimeter (now modeled as water; specimens are quite small) just slightly on HB-2 side of HB-3
c       The above (oversimplified) dosimeter cells have been replaced by Cells 2581 and 2582, along with Cells 2591-2593 for the dosimeter holder assembly (
ring)
c
c      ---------------------------------
c      Use the following two if looking at the old 1960 HB-3 design:   (must also set options on Cells 4305 & 4380 below)
c      $ obsolete $ 2140  23  -2.7       -1010  2151  -2152  imp:n=1  $ aluminum: 1st window at start of water tube (old 1960 location)
c      2140  23  -2.7       (2161 -2162 2163 -2153):(2164 -2165 -2163)  imp:n=1  $ aluminum: part-length model of old (1960) water tube: 1st spherical window
 & cylindrical section
c      2141  61  -3.2325-4  -1010  2153  -2154  imp:n=1  $ int void: 1st window at start of water tube (new 1998 location)
c
c      Use the following two if looking at the new 1998 HB-3 design:   (must also set options on Cells 4305 & 4380 below)
c       $ obsolete $ 2140  61  -3.2325-4  -1010  2151  -2152  imp:n=1  $ int void: 1st window at start of water tube (old 1960 location)
2140  61  -3.2325-4  (2161 -2162 2163 -2153):(2164 -2165 -2163)  imp:n=1  $ int void: part-length model of old (1960) water tube: 1st spherical window & cyl
indrical section
2141  23  -2.7       -1010  2153  -2154  imp:n=1  $ aluminum: 1st window at start of water tube (new 1998 location)
c      ---------------------------------
c
2144  24  -2.7  -2136  1010  2153 -2154  imp:n=1  $ aluminum ring joining regular section of beam tube to expanded section
c
c      ---------------------------------
c      Use the following two if beam tube is void, as in normal operation:
c       2145  61  -1.0e-20   -2134  2154 -4110          imp:n=1  $ void inside main cavity of expanded beam tube outside vessel (if void, as in normal operat
ion)
c       2146  61  -1.0e-20   -2135  2134  2154  -4110  imp:n=1  $ void in pneumatic tube coils located just inside outer wall of expanded beam tube outside
vessel
c
c      Use the following two if beam tube is flooded for maintenance work:
```

```
2145   8   -1.0000   -2134  2154 -4110         imp:n=1  $ water inside main cavity of expanded beam tube outside vessel (if flooded for maintenance)
2146   8   -1.0000   -2135  2134  2154  -4110  imp:n=1  $ water in pneumatic tube coils located just inside outer wall of expanded beam tube outside vessel
c     --------------------------------
c
2147  24  -2.7  -2136  2135  2154  -4125  imp:n=1  $ aluminum body of expanded section of the new HB-3 beam tube outside vessel
c
c     ------------------------------
c       In the name of simplification, lets combine the inner & outer SS liners with the main vessel, and treat all as carbon steel
c       2140  40  8.62373-2  -9999 9997  2013 -2014  2100  imp:n=1  $ pressure vessel's inner liner
c       2150  50  8.74142-2  -9999 9997  2014 -2015  2100  imp:n=1  $ main pressure vessel (thick carbon steel)
c       2160  40  8.62373-2  -9999 9997  2015 -2016  2100  imp:n=1  $ pressure vessel's outer liner
c       2150  50  -7.8212    -9999 9997  2013 -2016  2100  imp:n=1  $ main pressure vessel (thick carbon steel + inner & outer liners)
2150  50  -7.8212     -9999  9997  2013 -2016  2101        imp:n=1  $ main pressure vessel (thick carbon steel + inner & outer liners)
2151  50  -7.8212      2100 -2101 -2105  2013  9997                 $ vessel nozzel boss around HB-3
                  #(-2110 -2111)                             imp:n=2  $ vessel nozzel boss around HB-3 (above); excluding HB3 chamfer (surf 2110)
2152  50  -7.8212     -2101  2131  2105 -2106                imp:n=2  $ carbon steel flange on vessel nozzel boss by HB-3
c     ------------------------------
2170  8   -1.0000     -9999 9997  2016 -2017          $ water pool between pressure vessel and concrete bioshield
                      #(-2136  2153)  #(-2131 -2153)   $ water pool (above) excluding expanded section of HB-3 beam tube
                      #(4100  -4225)                   $ water pool (above) excluding everything inside ss sleeve (water & beam tube) where beam tube enters
concrete bioshield
                      #(-2101 -2106)  imp:n=1          $ water pool (above) excluding vessel boss (and flange) around HB-3
c
c
c     Cells associated with dosimeters & dosimeter specimen holder at Key 3 around HB-3 (see Dwg E-49953, Rev A, 6-30-65):
c     ---------------------------------------------------------------------------------------------------------------
c     $ obsolete $ 2581  40 -7.92   2531  -2532  2551  -2552  2541  -2542  imp:n=1  $ dosimeter at Key 3, Position 3, just slightly on HB-2 side of HB-3 (mo
deled as ss304)
c     $ obsolete $ 2582  40 -7.92   2531  -2532  2562  -2561  2541  -2542  imp:n=1  $ dosimeter at Key 3, Position 8, just slightly on HB-4 side of HB-3 (mo
deled as ss304)
c
c     $ obsolete $ 2581  50  -7.8212  2531  -2532  2551  -2552  2541  -2542  imp:n=2  $ dosimeter at Key 3, Position 3, just slightly on HB-2 side of HB-3 (
modeled as carbon steel)
c     $ obsolete $ 2582  50  -7.8212  2531  -2532  2562  -2561  2541  -2542  imp:n=2  $ dosimeter at Key 3, Position 8, just slightly on HB-4 side of HB-3 (
modeled as carbon steel)
c
c     $ added 4-7-98:  Use of surf 2534 (instead of 2531) allows the ss304 cover plate of dosimeter holder ring to
c     $ added 4-7-98:  be modeled be separate from the carbon steel Charpy specimens in 1-cm-thk dosimeter capsules
2581  50  -7.8212  2534  -2532  2551  -2552  2541  -2542  imp:n=2  $ dosimeter at Key 3, Position 3, just slightly on HB-2 side of HB-3 (modeled as carbon s
teel)
2582  50  -7.8212  2534  -2532  2562  -2561  2541  -2542  imp:n=2  $ dosimeter at Key 3, Position 8, just slightly on HB-4 side of HB-3 (modeled as carbon s
teel)
c
2583  40  -7.92  2533  -2531  2553  -2554  2543  -2544  imp:n=2  $ ss square peg just upstream of dosimeter at Key 3, Position 3
2584  40  -7.92  2533  -2531  2564  -2563  2543  -2544  imp:n=2  $ ss square peg just upstream of dosimeter at Key 3, Position 8
c
2591  40 -7.92   2520  -2530  2531  -2532          $ Key 3 dosimetry specimen holder ring (ss304)
              #(2534  2551  -2552  2541  -2542)   $ Key 3 dosimetry specimen holder ring (ss304), excluding dosimeter at Key 3, Position 3
              #(2534  2562  -2561  2541  -2542)   $ Key 3 dosimetry specimen holder ring (ss304), excluding dosimeter at Key 3, Position 8
              imp:n=2                            $ Key 3 dosimetry specimen holder ring (ss304)
2592  40 -7.92  -2520  2521  -2522  2131  imp:n=2  $ short thick ss304 cylindrical sleeve on Key 3 dosimetry specimen holder
2593  40 -7.92  -2510  2131  -2521  2511  imp:n=2  $ long  thin  ss304 cylindrical sleeve on Key 3 dosimetry specimen holder
c     ---------------------------------------------------------------------------------------------------------------
c
c
c     Cells associated with the 2-plate collar holding cooling tube on ss sleeve outside beam tube close to dosimeter ring
c     ---------------------------------------------------------------------------------------------------------------
2761  40 -7.92  -2701 2131 2742 -2744  imp:n=2  $ 1st (upstream)   ss plate of 2-plate collar assembly
```

```
2762  40 -7.92  -2701 2131 2746 -2748  imp:n=2  $ 2nd (downstream) ss plate of 2-plate collar assembly
c
2771  40 -7.92  -2701 2131 2744 -2746 2711 -2712              imp:n=2  $ horizontal ss spacer plates (right & left, top & bottom, treated as one cell)
2772  40 -7.92  -2702 2701 2744 -2746 2711 -2710 2720        imp:n=2  $ horizontal ss spacer plate extension (on one side only); must exclude this from ve
ssel water (Cell 2130)
2773  40 -7.92  -2701 2131 2744 -2746 2724 -2728 #(2722 -2726) imp:n=2  $ vertical   ss spacer plates (right & left, top & bottom, treated as one cell)
2774   7 -0.9899  -2701 2131 2744 -2746 2722 -2726            imp:n=2  $ water between vertical spacer plates
c
2781   7 -0.9899  -2701  2131  2744  -2746          $ water between main upstream & downstream plates of 2-plate collar assembly
                   #(2711  -2712)  #(2724  -2728)   $ water (above), excluding horizontal & vertical spacers
                   imp:n=2                          $ water between main upstream & downstream plates of 2-plate collar assembly
c     ------------------------------------------------------------------------------------------------------------------------
c
c
c       Intermediate notes using COMJOM-like notation to describe the cells in and around the HB-3 shield plug:
c
c       box1 = (3083 -3073 3023 -3033 3006 -3001)
c       box2 = (3082 -3072 3022 -3032 3005 -3001)
c       box3 = (3103 -3093 3043 -3053 3010 -3002)
c       box4 = (3102 -3092 3042 -3052 3009 -3002)
c       box5 = (3081 -3071 3021 -3031 3004 -3001)
c       box6 = (3080 -3070 3020 -3030 3003 -3002)
c       box7 = (3101 -3091 3041 -3051 3008 -3002)
c       box8 = (3100 -3090 3040 -3050 3007 -3002)
c
c       cyl9  = (-3120 3061 -3062)
c       cyl10 = (-3121 3061 -3063)
c       cyl11 = (-3122 3060 -3064)
c       cyl12 = (-3110)
c
c       Cell 3001 = bconc den  (former cell 3001)  #box3  #box1   imp:n=1  $ revised model of barytes concrete forming bioshield
c       Cell 3010 = ss  den  box1  #box2  #box3   imp:n=1  $ ss liner on bioshield near big (downstream) side of removable block containing shield plug
c       Cell 3020 = ss  den  box3  #box4  #box2   imp:n=1  $ ss liner on bioshield near small (upstream) side of removable block containing shield plug
c       Cell 3030 = ss  den  box5  #box6  #box7  #cyl12   imp:n=1  $ ss liner on big (downstream) side of removable concrete block containing shield plug
c       Cell 3040 = ss  den  box7  #box8  #box6  #cyl12   imp:n=1  $ ss liner on small (upstream) side of removable concrete block containing shield plug
c       Cell 3050 = void den  (box4 OR box2)  #box7  #box5   imp:n=1  $ void immediately upstream of (and around) the removable concrete block containing sh
ield plug
c       Cell 3060 = bconc den  (box8 OR box6)  #cyl11  #cyl12   imp:n=1  $ barytes concrete forming bulk of the removable concrete block containing shield p
lug
c       Cell 3070 = ss  den  cyl11  #cyl10  #cyl12   imp:n=1  $ ss liner inside the removable concrete block containing shield plug
c       cccc    Cell 3080 = void den  (box7 OR box5) inside cyl12  #cyl10   imp:n=1  $ void near centerline, upstream and downstream of shield plug, inside
removable concrete block
c       Cell 3080 = void den  (box7 OR box5) inside cyl12  #cyl9   imp:n=1  $ void near centerline, upstream and downstream of shield plug, inside removable
 concrete block
c       Cell 3090 = cstl den  cyl9   imp:n=1  $ carbon steel forming the actual shield plug
c       Cell 3100 = void den  cly10  #cyl9   imp:n=1  $ void gap around the cylindrical shield plug
c
c       Final MCNP description of the cells in and around the HB-3 shield plug:
c     ------------------------------------------------------------------------------------------------------------------------
c
3000  61  -1.0e-20   -9999 3001 -9998  9990  imp:n=1       $ void downstream of the HB-3 shield plug (shutter); excl small sph around pt where Blosser & Tho
mas made measurements
c
c     Barytes concrete bioshield from the upstream edge of the cavity containing the removable concrete block containing
c     the HB-3 shield plug (really surf 3010), out to the downstream edge of the removable block containing the shield plug:
3001  62  -3.0[illegible]5   -9999 3010 -3001                    $ barytes concrete bioshield (outermost part)
                   #(3103 -3093 3043 -3053 3010 -3002)   $ barytes concrete bioshield (outermost part)
                   #(3083 -3073 3023 -3033 3006 -3001)   $ barytes concrete bioshield (outermost part)
```

```
                    #(4195 -4198)                          $ barytes concrete (above) excluding the 3 infinitesimal void slab slices by boundary source
                    imp:n=1                                $ barytes concrete bioshield (outermost part)
c
c     Barytes concrete bioshield from beyond pool liner (liner not modeled) out to upstream edge of removable block containing shield plug (really surf 3010
)
3002  62  -3.09725   -9999 9997 -3010  2017  2136  $ barytes concrete bioshield (from pool liner to shutter assembly cavity)
                    #(4155  -3010  -4265)   4225  $ barytes concrete (above) excluding everything inside ss bioshield liner around collimator assembly
                    imp:n=1                        $ barytes concrete bioshield (from pool liner to shutter assembly cavity)
c
c     -------------------------
c
3010  40  -7.92  (3083 -3073 3023 -3033 3006 -3001)   $ ss liner on bioshield near big (downstream) side of removable block containing shield plug
                #(3082 -3072 3022 -3032 3005 -3001)  $ ss liner on bioshield near big (downstream) side of removable block containing shield plug
                #(3103 -3093 3043 -3053 3010 -3002)  $ ss liner on bioshield near big (downstream) side of removable block containing shield plug
                imp:n=1                              $ ss liner on bioshield near big (downstream) side of removable block containing shield plug
c
3020  40  -7.92  (3103 -3093 3043 -3053 3010 -3002)   $ ss liner on bioshield near small (upstream) side of removable block containing shield plug
                #(3102 -3092 3042 -3052 3009 -3002)  $ ss liner on bioshield near small (upstream) side of removable block containing shield plug
                #(3082 -3072 3022 -3032 3005 -3001)  $ ss liner on bioshield near small (upstream) side of removable block containing shield plug
                #(4195 -4198)                        $ ss liner (above) excluding the 3 infinitesimal void slab slices by boundary source
                4240  imp:n=1                       $ ss liner on bioshield near small (upstream) side of removable block containing shield plug (excl end
 of collimator assy)
c
3030  40  -7.92  (3081 -3071 3021 -3031 3004 -3001)   $ ss liner on big (downstream) side of removable concrete block containing shield plug
                #(3080 -3070 3020 -3030 3003 -3002)  $ ss liner on big (downstream) side of removable concrete block containing shield plug
                #(3101 -3091 3041 -3051 3008 -3002)  $ ss liner on big (downstream) side of removable concrete block containing shield plug
                3110  imp:n=1                        $ ss liner on big (downstream) side of removable concrete block containing shield plug
c
3040  40  -7.92  (3101 -3091 3041 -3051 3008 -3002)   $ ss liner on small (upstream) side of removable concrete block containing shield plug
                #(3100 -3090 3040 -3050 3007 -3002)  $ ss liner on small (upstream) side of removable concrete block containing shield plug
                #(3080 -3070 3020 -3030 3003 -3002)  $ ss liner on small (upstream) side of removable concrete block containing shield plug
                3110  imp:n=1                        $ ss liner on small (upstream) side of removable concrete block containing shield plug
c
3050  61  -1.0e-20  ((3102 -3092 3042 -3052 3009 -3002): $ void immediately upstream of (and around) the removable concrete block containing shield plug
                     (3082 -3072 3022 -3032 3005 -3001)) $ void immediately upstream of (and around) the removable concrete block containing shield plug
                    #(3101 -3091 3041 -3051 3008 -3002)  $ void immediately upstream of (and around) the removable concrete block containing shield plug
                    #(3081 -3071 3021 -3031 3004 -3001)  $ void immediately upstream of (and around) the removable concrete block containing shield plug
                    #(-4195  -4245)                      $ void (above) excluding downstream end of collimator assembly and flange
                    #(4195   -4198)                      $ void (above) excluding the 3 infinitesimal void slab slices by boundary source
                    imp:n=1                              $ void immediately upstream of (and around) the removable concrete block containing shield plug
c
3060  62  -3.09725  ((3100 -3090 3040 -3050 3007 -3002): $ barytes concrete forming bulk of the removable concrete block containing shield plug
                     (3080 -3070 3020 -3030 3003 -3002)) $ barytes concrete forming bulk of the removable concrete block containing shield plug
                    #(-3122 3060 -3064)  3110   imp:n=1  $ barytes concrete forming bulk of the removable concrete block containing shield plug
c
3070  40  -7.92   -3122  3060  -3064  3110  3007  -3002  $ ss liner inside the removable concrete block containing shield plug
                 #(-3121 3061 -3063)           imp:n=1  $ ss liner inside the removable concrete block containing shield plug
c
c       3080  61  -1.0e-20  -3110  3008  -3001  3121    imp:n=1  $ void near centerline, upstream and downstream of shield plug, inside removable concrete b
lock
3080  61  -1.0e-20  -3110  3008  -3001  3120    imp:n=1  $ void near centerline, upstream and downstream of shield plug, inside removable concrete block
c
3090  50   -7.8212   -3120  3061  -3062  3131  3132     imp:n=1  $ carbon steel forming the shield plug (ie, the rotary shutter)
3091  61  -1.0e-20   -3120  (-3131:-3132)  imp:n=1  $ beam holes thru the rotary shutter); for orientation, see surfs 3131 & 3132
c
3100  61  -1.0e-20  -3121  3061  -3063  3007  -3002      $ void gap around the cylindrical shield plug
                    3110  #(-3120 3061 -3062)  imp:n=1  $ void gap around the cylindrical shield plug
c     ------------------------------------------------------------------------------------------------------------------------------------------------
```

```
c
c
c     Cells used for the description of the collimator assembly (etc) inside the concrete:
c     ------------------------------------------------------------------------------------------------------------------------------
c
c     4300  61  -1.0e-20  4130 -4190 4210 -4211 4212 -4213                  $ rectangular hole up thru collimator (when void)
4300  8  -1.0000  4130 -4190 4210 -4211 4212 -4213                          $ rectangular hole up thru collimator (when flooded)
                  #(4140 -4145)                                    imp:n=1  $ exclusion used to allow simulating 2nd aluminum window in 1960 design (see cells
 4305 & 4380)
c     --------------------------
c       4305  23  -2.7       4140 -4145 4210 -4211 4212 -4213     imp:n=1  $ aluminum here IFF simulating 2nd aluminum window in 1960 design (downstream end
of water tube)
c       4305  61  -1.0e-20  4140 -4145 4210 -4211 4212 -4213     imp:n=1  $ void here IF modeling 2nd aluminum window in 1998 design (downstream end of wate
r tube not here)
4305  8  -1.0000  4140 -4145 4210 -4211 4212 -4213                 imp:n=1  $ water here IF modeling flooded 1998 design (downstream end of water tube not her
e)
c     --------------------------
c     4310  40  -7.92     4130  -4190 -4230  #(4210 -4211 4212 -4213)  imp:n=1  $ ss body of central collimator with rectangular hole
c     Mike Farrar thought the central collimator might be carbon steel (to get less activation)
c     Dan Pinkston confirmed that it was Type 1020 carbon steel (here, I just used pressure vessel carbon steel here; close enough)
c     Ron Poor (the draftsman) indicated that existing one had a thin black oxide coating for corrosion protection
4310  50  -7.8212. 4130  -4190 -4230  #(4210 -4211 4212 -4213)   imp:n=1  $ carbon steel (Type 1020) body of central collimator with rectangular hole;
4315  61  -1.0e-20  4190  -4195  4210   -4211 4212 -4213          imp:n=1  $ thin rect void reg (5.5"x2.75") immediately downstream of colimator <-- get axia
l leakage here
4316  61  -1.0e-20  4190  -4195 -4230  #(4210 -4211 4212 -4213)  imp:n=1  $ thin void immediately downstream of steel body of collimator (excl rect hole)
4320  24   -2.7     4125  -4195  4230  -4235                     imp:n=1  $ aluminum: expanded section of beam tube along side the collimator
4321  24   -2.7     4125  -4126  2135  -4230                     imp:n=1  $ aluminum step where beam tube expands again, just upstream of collimator
4330  40  -7.92     4180  -4195  4235  -4240                     imp:n=1  $ ss pool seal (B) downstream of collimator
4335  40  -7.92     3009  -4195  4240  -4245                     imp:n=1  $ ss flange around pool seal (B) downstream of collimator
4340  61  -1.0e-20  4170  -3010  4235  -4260  #(4180 -4240)      imp:n=1  $ void downstream of removable shield and eccentric shield
c       4345  41  -7.92     4150  -4170  4235  -4255  #(4250 -4160)      imp:n=1  $ ss removable shield, radially outside beam tube, next to collimator
4345  40  -7.92     4150  -4170  4235  -4255  #(4250 -4160)      imp:n=1  $ ss removable shield, radially outside beam tube, next to collimator
4350  40  -7.92     4160  -4170  4255  -4260                     imp:n=1  $ ss eccentric shield, radially outside removable shield
4355  40  -7.92     4160  -3010  4260  -4265                     imp:n=1  $ ss bioshield liner, between eccentric shield and concrete bioshield
4356  40  -7.92     4155  -4160  4220  -4265                     imp:n=1  $ ss liner on step expansion of bioshield, just upstream of removable shiled
4360  61  -1.0e-20  4135  -4150  4235  -4250                     imp:n=1  $ void just upstream of removable shield around collimator
4365  40  -7.92     4120  -4160  4250  -4220                     imp:n=1  $ ss pool seal (A2) upstream of collimator
4370  40  -7.92     4105  -4135  2136  -4250  #(4125 -4235)      imp:n=1  $ ss pool seal (A1) upstream of collimator
c     4375  61  -1.0e-20  4115  -4130 -4230   #(2135 -4126)      imp:n=1  $ void just upstream of collimator (before 2nd aluminum window in 1998 design)
4375  8  -1.0000    4115  -4130 -4230         #(2135 -4126)      imp:n=1  $ water just upstream of collimator if flooded (before 2nd aluminum window in 1998
 design)
c     --------------------------
c       4380  61  -1.0e-20  4110  -4115  -2135                    imp:n=1  $ void here IFF simulating 2nd aluminum window in 1960 design (downstream end of w
ater tube not here)
4380  23   -2.7     4110  -4115  -2135                            imp:n=1  $ aluminum here IF one wants to model 2nd aluminum window in 1998 design (downstre
am end of water tube)
c     --------------------------
4385  8  -1.0000  4100  -4120  2136  -4220  #(4105 -4250)         imp:n=1  $ water between beam tube & ss sleeve extending from concrete bioshield into pool
4390  40   -7.92  4100  -4155  4220  -4225                       imp:n=1  $ ss sleeve / bioshield liner extending from bioshield into the pool
c     ------------------------------------------------------------------------------------------------------------------------------
c
c
c     Cells to facilitate writing (and later reading & using) the internal boundary source;  see explanation above in header info
c     9981  61  -1.0e-20  4195  -4196  -9999   imp:n=1   $  in early global calc where we're writing the boundary source
9981  61  -1.0e-20  4195  -4196  -9999   imp:n=0   $  in later shielding calcs where we're reading & using the boundary source
9982  61  -1.0e-20  4196  -4197  -9999   imp:n=1   $  in all cases
9983  61  -1.0e-20  4197  -4198  -9999   imp:n=1   $  in all cases
c
```

```
c
9990  61  -1.0e-20    -9990   imp:n=1   $ small sph around pt where Blosser & Thomas made measurements;  for illustrative purposes only;  may put pt det ins
ide
9999  0  #(-9999 9997 -9998)  imp:n=0   $ external void; everything not inside the (1.3 m diam x 7.0 m long) cylinder modeled here
c
c     END CELLS (next line must be blank)

c     BEGIN SURFACES:
c
c      HB-3 (Tangential tube); described here as if the Z axis now corresponds to HB-3 axis
c
c      The following correspond to the real "physical" location of the spherical tip of the HB-3 beam tube:
c      1000    sz    28.5369    5.08          $ Spherical void OD
c      1001    sz    28.5369    6.03250       $ Spherical inner Al wall OD
c      1002    sz    28.5369    6.15250       $ Spherical water OD
c      1003    sz    28.5369    6.3896875     $ Spherical outer Al wall OD
c      1004    sz    28.5369    6.5497075     $ Spherical water jacket OD
c      1005    sz    28.5369    6.7605275     $ Spherical Al Be liner OD
c      1006    pz    28.5369                  $ Plane at end of Cylindrical tube
c
c      Here, the hot tip has been artificially extended inward 18.5369 cm to accomodate innermost equiv point src at Z=10 cm:
1000    sz    10.0    5.08          $ Spherical void OD
1001    sz    10.0    6.03250       $ Spherical inner Al wall OD
1002    sz    10.0    6.15250       $ Spherical water OD
1003    sz    10.0    6.3896875     $ Spherical outer Al wall OD
1004    sz    10.0    6.5497075     $ Spherical water jacket OD
1005    sz    10.0    6.7605275     $ Spherical Al Be liner OD
1006    pz    10.0                  $ Plane at end of Cylindrical tube
1007    pz    118.6879              $ Plane below which all importances are zero; located 2 cm upstream of first pt det used to get pt srcs
c       1007    pz    75.473        $ Plane below which all importances are zero; use this for dosimetry only; located 31.6546 cm upstream of first dosimeter
c
c      Cylindrical part of HB-3; described here as if the Z axis now corresponds to HB-3 axis
1010    cz    5.08                    $ Cylindrical void OD
1011    cz    6.03250                 $ Cylindrical inner Al wall OD
1012    cz    6.1515625               $ Cylindrical water OD
1013    cz    6.3896875               $ Cylindrical outer Al wall OD
1014    cz    6.5497075               $ Cylindrical water jacket OD
1015    cz    6.7605275               $ Cylindrical Al Be liner OD
c
c
c      If the Z axis now corresponds to HB-3, then the main cylinders for core, vessel, etc, are described as:
c      Sidewall thicknesses from per comm. with Dick Rothrock (01-11-95); Sidewall dimensions from 1971 report
2010    c/x  26.67  0.0      54.61       $ outer radius--permanent Be refl. reg.
2011    c/x  26.67  0.0      55.245      $ outer radius--water gap
2012    c/x  26.67  0.0      56.8325     $ outer radius--aluminum reflector cage
2013    c/x  26.67  0.0     119.38       $ outer radius--water
2014    c/x  26.67  0.0     119.6975     $ outer radius--inner pressure vessel clad
2015    c/x  26.67  0.0     127.0        $ outer radius--pressure vessel
2016    c/x  26.67  0.0     127.254      $ outer radius--outer pressure vessel clad
2017    c/x  26.67  0.0     274.32       $ outer radius--H2O pool (pool/pool-liner interface at r=274.32 cm; pool diam=18 ft)
c
c      Note: for now, will model boss & flange on HB-3, but will ignore some of the finer details.  Will assume, for example,
c      that the vessel is tight against HB-3, thus ignoring the slightly larger hole actually present in vessel for HB-3, and
c      the sleeve (hydraulic seal) around HB-3 near vessel.  These may be added later (?).
2100    cz    10.0680    $ inner radius of vessel nozzel (boss) around HB-3 beam tube (see dwg E-42027)
2101    cz    21.45      $ outer radius of vessel nozzel (boss) around HB-3 beam tube (see dwg E-42027)
2105    pz   137.16      $ plane defining end of boss on pressure vessel around HB-3 (see dwg E-42027); in model, use 2106 instead
2106    pz   143.9443    $ plane defining end of thick flange mounted on boss on pressure vessel around HB-3 (see dwg E-42027)
```

```
c
c      wrong:  2110   42  sq  0.9262159  0.9880902  -1.0  0  0  0  0  0  0  0 $ elliptical cone used to define chamfer between HB3 vessel hole and inner su
rf of pressure vessel
c      The above specification was used in Runs HB304G & HB304H. Subsequent graphical analysis of the flare at the midplane (x=0)
c      showed that this elliptical cone chamfer was NOT a good representation of the rounded corners, and (in fact) cut off too
c      much steel from the vessel and substituted too much water.  The graphical analysis was reworked, using some CAD work
c      and some equations this time, and the following was found to be a much more accurate representation.  -- JAB, 5 Apr 98
c      Input files for HB304I & HB304J were also no good. These were failed attempts to fix the problem.  Those two cases
c      (I&J) were never run since similar problems were noticed during the graphical checkout step before final submission.
c      Run HB304K (whose correct input is shown below) was the firt run which had this correct. TR42 also changed. -- JAB 6 Apr 98
2110   42  sq  0.928252  1.0  -1.0  0  0  0  0  0  0  0  $ elliptical cone used to define chamfer between HB3 vessel hole and inner surf of pressure vessel
2111   42  pz  -0.001  $ plane used to help define which side of the double elliptical cone we want (cone reduces to a point at z=0, but use z=-0.001 to avo
id roundoff)
2112   42  pz  -15.0   $ plane used to define the upstream axial extent of the elliptical cone we want to consider (must be somewhere beyond z=-12.78829; z=
-15 is arbitrary)
c
c      Note regarding dosimeters:  these are really Charpy V-notch specimens, measuring 0.75"x0.75"x1.5";  locations were taken from dwg E-42027
2121   s  0.0  -13.480  107.1276  1.48893  $ sphere simulating dosimeter just slightly on HB-4 side of HB-3   (see above note)
2126   s  0.0   12.284  112.9905  1.48893  $ sphere simulating dosimeter just slightly on HB-2 side of HB-3   (see above note)
c
2130   cz  7.16174    $ inner radius of ss sleeve around HB-3 beam tube, near vessel
2131   cz  7.9338     $ outer radius of ss sleeve around HB-3 beam tube, near vessel
c
2134   cz  6.08626    $ inner radius of pneumatic tubes/coils inside expanded section of the HB-3 beam tube outside the vessel
2135   cz  7.03453    $ pneumatic tube / beam tube interface for the expanded section of the HB-3 beam tube outside the vessel
2136   cz  7.74573    $ outer radius of the expanded section of the HB-3 beam tube outside the vessel
c
2150   pz   96.8375   $ plane defining end of ss sleeve around beam tube, near vessel
2151   pz  116.7841   $ upstream   side of aluminum window forming start of water tube in original HB-3 design (as built)
2152   pz  117.7366   $ downstream side of aluminum window forming start of water tube in original HB-3 design (as built)
2153   pz  174.27     $ upstream   side of aluminum window forming start of water tube in proposed HB-3 design
2154   pz  174.95125  $ downstream side of aluminum window forming start of water tube in proposed HB-3 design
c
c      The following surfaces are used for a part-length model of the old (1960) water tube.
c      In this part-length model, the downstream end is defined by surf 2153 which is the
c      upstream surface of the 1-st aluminum window defining the start of the 1998 water tube.
2161   cz  3.65125            $ inner radius of cylindrical portion of old (1960) water tube
2162   cz  4.60375            $ outer radius of cylindrical portion of old (1960) water tube
2163   pz  120.30375          $ plane between cylindrical & spherical portion of old (1960) water tube, near upstream end
2164   sz  120.30375  3.65125 $ inner radius of spherical portion of old (1960) water tube, near upstream end
2165   sz  120.30375  4.60375 $ outer radius of spherical portion of old (1960) water tube, near upstream end
c
c
c      Surfaces associated with dosimeters & dosimeter specimen holder at Key 3 around HB-3
c      ------------------------------------------------------------------------------
c      2510   cz  8.41005  $ outer radius of thin cylindrical sleeve on Key 3 dosimetry specimen holder
c      2511   pz  107.056  $ upstream extent of thin cylindrical sleeve on Key 3 dosimetry specimen holder
c      c
c      2520   40  cz  9.36625   $ outer radius      of thick cylindrical sleeve on Key 3 dosimetry specimen holder
c      2521   40  pz  -1.5875   $ upstream   extent of thick cylindrical sleeve on Key 3 dosimetry specimen holder
c      2522   40  pz   1.5875   $ downstream extent of thick cylindrical sleeve on Key 3 dosimetry specimen holder
c      c
c      2530   40  cz  18.57375  $ outer radius      of Key 3 dosimetry specimen holder (ring)
c      2531   40  pz  -0.635    $ upstream   extent of Key 3 dosimetry specimen holder = upstream   surf of all capsule positions in Key 3
c      2532   40  pz   0.635    $ downstream extent of Key 3 dosimetry specimen holder = downstream surf of all capsule positions in Key 3
c      2533   40  pz  -2.54     $ upstream face of small square pegs directly upstream of dosimeters in Key 3, Positions 3 & 8 (downstream face=surf 2531)
c      c
c      2541   px  -1.4732       $ bottom (-X) surf of capsules in Key 3, posi   3 & 8 (specifically); no transformation req'd
```

```
c      2542   px   1.4732       $ top    (+X) surf of capsules in Key 3, positions 3 & 8 (specifically); no transformation req'd
c      2543   px  -1.905        $ bottom (-X) surf of small square pegs directly upstream of dosimeters in Key 3, Positions 3 & 8; no transformation req'd;
-X location only a guess
c      2544   px   1.905        $ top    (+X) surf of small square pegs directly upstream of dosimeters in Key 3, Positions 3 & 8; no transformation req'd;
+X location only a guess
c      c
c      2551   40  py   10.993   $ innermost (-Y) surf of capsule in Key 3, Position 3 (specifically); ie, capsule on HB-2 side of HB-3
c      2552   40  py   16.327   $ outermost (+Y) surf of capsule in Key 3, Position 3 (specifically); ie, capsule on HB-2 side of HB-3
c      2553   40  py   10.7675  $ innermost (-Y) surf of square peg just upstream of dosimeter at Key 3, Position 3 (specifically)
c      2554   40  py   12.6725  $ outermost (+Y) surf of square peg just upstream of dosimeter at Key 3, Position 3 (specifically)
c      c
c      2561   40  py  -10.993   $ innermost (+Y) surf of capsule in Key 3, Position 8 (specifically); ie, capsule on HB-4 side of HB-3
c      2562   40  py  -16.327   $ outermost (-Y) surf of capsule in Key 3, Position 8 (specifically); ie, capsule on HB-4 side of HB-3
c      2563   40  py  -13.9075  $ innermost (+Y) surf of square peg just upstream of dosimeter at Key 3, Position 8 (specifically)
c      2564   40  py  -15.8125  $ outermost (-Y) surf of square peg just upstream of dosimeter at Key 3, Position 8 (specifically)
c      ---------------------------------------------------------------------------
c
c
c      Surfaces associated with dosimeters & dosimeter specimen holder at Key 3 around HB-3. (Note: These were all revised
c      as follows by JAB on 3 Apr 98 for Run HB304H, based on newly available data shown on Dwg E-49953, Rev A, 6-30-65):
c      ---------------------------------------------------------------------------------------------------------------------
2510   cz  8.17193  $ outer radius of thin cylindrical sleeve on Key 3 dosimetry specimen holder
2511   pz  109.17   $ upstream extent of thin cylindrical sleeve on Key 3 dosimetry specimen holder
c
2520   40  cz   9.5      $ outer radius      of thick cylindrical sleeve on Key 3 dosimetry specimen holder
2521   40  pz  -2.3      $ upstream   extent of thick cylindrical sleeve on Key 3 dosimetry specimen holder
2522   40  pz   0.8      $ downstream extent of thick cylindrical sleeve on Key 3 dosimetry specimen holder
c
2530   40  cz  18.16     $ outer radius      of Key 3 dosimetry specimen holder (ring)
2531   40  pz -0.8175   $ upstream   extent of Key 3 dosimetry specimen holder ring (ie, just upstream on the 0.3175 cm cover plate, but no water)
2532   40  pz   0.50     $ downstream extent of Key 3 dosimetry specimen holder ring = downstream surf of all capsule positions in Key 3 (capsules are 0.394
"=1.00075 cm thk)
2533   40  pz  -3.25     $ upstream face of small square pegs directly upstream of dosimeters in Key 3, Positions 3 & 8 (downstream face=surf 2531)
2534   40  pz  -0.50     $ upstream face of 1-cm-thk dosimeter capsules (Key 3, Positions 3 & 8) inside dosimeter holder ring
c
2541   px  -1.50622      $ bottom (-X) surf of capsules in Key 3, positions 3 & 8 (specifically); no transformation req'd
2542   px   1.50622      $ top    (+X) surf of capsules in Key 3, positions 3 & 8 (specifically); no transformation req'd
2543   px  -1.50         $ bottom (-X) surf of small square pegs directly upstream of dosimeters in Key 3, Positions 3 & 8; no transformation req'd; -X loca
tion only a guess
2544   px   3.37         $ top    (+X) surf of small square pegs directly upstream of dosimeters in Key 3, Positions 3 & 8; no transformation req'd; +X loca
tion only a guess
c
2551   40  py   10.10045 $ innermost (-Y) surf of capsule in Key 3, Position 3 (specifically); ie, capsule on HB-2 side of HB-3
2552   40  py   15.59955 $ outermost (+Y) surf of capsule in Key 3, Position 3 (specifically); ie, capsule on HB-2 side of HB-3
2553   40  py   11.0475  $ innermost (-Y) surf of square peg just upstream of dosimeter at Key 3, Position 3 (specifically)
2554   40  py   12.9525  $ outermost (+Y) surf of square peg just upstream of dosimeter at Key 3, Position 3 (specifically)
c
2561   40  py  -10.10045 $ innermost (+Y) surf of capsule in Key 3, Position 8 (specifically); ie, capsule on HB-4 side of HB-3
2562   40  py  -15.59955 $ outermost (-Y) surf of capsule in Key 3, Position 8 (specifically); ie, capsule on HB-4 side of HB-3
2563   40  py  -14.1475  $ innermost (+Y) surf of square peg just upstream of dosimeter at Key 3, Position 8 (specifically)
2564   40  py  -16.0525  $ outermost (-Y) surf of square peg just upstream of dosimeter at Key 3, Position 8 (specifically)
c      ---------------------------------------------------------------------------------------------------------------------
c
c
c     Surfaces associated with the 2-plate collar holding cooling tube on ss sleeve outside beam tube close to dosimeter ring
c     ---------------------------------------------------------------------------------------------------------------------
2701  cz  11.40     $ outer radius of 2-plate collar (surf 2131 defines inner radius)
2702  cz  14.88     $ outer radius of the one spacer plate extension
```

```
c
2710  px   0.0       $ horizontal midplane = top surface of the one spacer plate extension
2711  px  -1.11125   $ bottom surface of the horizontal spacer plates
2712  px   1.11125   $ top surface of the horizontal spacer plates
c
2720  py   0.0       $ vertical plane up middle (needed to uniquely define spacer plate extension)
2722  py  -1.80      $ right surface of vertical spacer plates on left
2724  py  -3.22      $ left  surface of vertical spacer plates on left
2726  py   1.80      $ left  surface of vertical spacer plates on right
2728  py   3.22      $ right surface of vertical spacer plates on right
c
2742  pz  100.3275   $ upstream   surface of 1st (upstream)   plate
2744  pz  101.43875  $ downstream surface of 1st (upstream)   plate
2746  pz  105.24875  $ upstream   surface of 2nd (downstream) plate
2748  pz  106.36     $ downstream surface of 2nd (downstream) plate
c     ------------------------------------------------------------------------------------------------------------------
c
c
c      Surfaces describing the cells in and around the HB-3 shield plug (ie, the rotary shutter):
c      ------------------------------------------------------------------------------------------------------------------------
3001   pz  478.79     $ plane defining end of concrete just past downstream edge of removable concrete block containing HB-3 shield plug (see dwgs 1546-01-M
-5022 and E-42027)
3002   pz  477.8375   $ upstream surf of ss block liner downstream of shutter
3003   pz  447.3575   $ downstream side of ss liner on removable block near midsection of removable concrete block containing shield plug
3004   pz  446.405    $ upstream   side of ss liner on removable block near midsection of removable concrete block containing shield plug
3005   pz  446.0875   $ downstream side of ss liner on bioshield near midsection of removable concrete block containing shield plug
3006   pz  445.4525   $ upstream   side of ss liner on bioshield near midsection of removable concrete block containing shield plug
3007   pz  414.9725   $ downstream side of ss liner on upstream side of removable concrete block containing shield plug
3008   pz  414.02     $ upstream   side of ss liner on upstream side of removable concrete block containing shield plug
3009   pz  392.7475   $ downstream side of ss liner on bioshield (upstream of removable concrete block containing shield plug)
3010   pz  392.1125   $ upstream   side of ss liner on bioshield (upstream of removable concrete block containing shield plug)
c
3020   py  -40.79875  $ inner surf (-Y) of ss liner on big (downstream) side of removable concrete block containing shield plug
3021   py  -41.75125  $ outer surf (-Y) of ss liner on big (downstream) side of removable concrete block containing shield plug
3022   py  -43.4975   $ inner surf (-Y) of ss liner on bioshield near big (downstream) side of removable concrete block containing shield plug
3023   py  -44.1325   $ outer surf (-Y) of ss liner on bioshield near big (downstream) side of removable concrete block containing shield plug
c
3030   py   40.79875  $ inner surf (+Y) of ss liner on big (downstream) side of removable concrete block containing shield plug
3031   py   41.75125  $ outer surf (+Y) of ss liner on big (downstream) side of removable concrete block containing shield plug
3032   py   43.4975   $ inner surf (+Y) of ss liner on bioshield near big (downstream) side of removable concrete block containing shield plug
3033   py   44.1325   $ outer surf (+Y) of ss liner on bioshield near big (downstream) side of removable concrete block containing shield plug
c
3040   py  -36.195    $ inner surf (-Y) of ss liner on small (upstream) side of removable concrete block containing shield plug
3041   py  -37.30625  $ outer surf (-Y) of ss liner on small (upstream) side of removable concrete block containing shield plug
3042   py  -39.6875   $ inner surf (-Y) of ss liner on bioshield near small (upstream) side of removable concrete block containing shield plug
3043   py  -40.3225   $ outer surf (-Y) of ss liner on bioshield near small (upstream) side of removable concrete block containing shield plug
c
3050   py   36.195    $ inner surf (+Y) of ss liner on small (upstream) side of removable concrete block containing shield plug
3051   py   37.30625  $ outer surf (+Y) of ss liner on small (upstream) side of removable concrete block containing shield plug
3052   py   39.6875   $ inner surf (+Y) of ss liner on bioshield near small (upstream) side of removable concrete block containing shield plug
3053   py   40.3225   $ outer surf (+Y) of ss liner on bioshield near small (upstream) side of removable concrete block containing shield plug
c
3060   px  -31.27375  $ bot surf of lower ss liner for cylindrical cavity containing shield plug
3061   px  -30.48     $ top surf of lower ss liner for cylindrical cavity containing shield plug = bottom surf of shield plug
3062   px   30.48     $ top surf of shield plug
3063   px   31.27375  $ bot surf of upper ss liner for cylindrical cavity containing shield plug
3064   px   3[illegible]  $ top surf of upper ss liner for cylindrical cavity con[illegible]ng shield plug
c
```

```
3070   px    40.79875  $ inner surf (+X) of ss liner on big (downstream) side of removable concrete block containing shield plug
3071   px    41.75125  $ outer surf (+X) of ss liner on big (downstream) side of removable concrete block containing shield plug
3072   px    43.4975   $ inner surf (+X) of ss liner on bioshield near big (downstream) side of removable concrete block containing shield plug
3073   px    44.1325   $ outer surf (+X) of ss liner on bioshield near big (downstream) side of removable concrete block containing shield plug
c
3080   px   -40.79875  $ inner surf (-X) of ss liner on big (downstream) side of removable concrete block containing shield plug
3081   px   -41.75125  $ outer surf (-X) of ss liner on big (downstream) side of removable concrete block containing shield plug
3082   px   -43.4975   $ inner surf (-X) of ss liner on bioshield near big (downstream) side of removable concrete block containing shield plug
3083   px   -44.1325   $ outer surf (-X) of ss liner on bioshield near big (downstream) side of removable concrete block containing shield plug
c
3090   px    36.195    $ inner surf (+X) of ss liner on small (upstream) side of removable concrete block containing shield plug
3091   px    37.30625  $ outer surf (+X) of ss liner on small (upstream) side of removable concrete block containing shield plug
3092   px    39.6875   $ inner surf (+X) of ss liner on bioshield near small (upstream) side of removable concrete block containing shield plug
3093   px    40.3225   $ outer surf (+X) of ss liner on bioshield near small (upstream) side of removable concrete block containing shield plug
c
3100   px   -36.195    $ inner surf (-X) of ss liner on small (upstream) side of removable concrete block containing shield plug
3101   px   -37.30625  $ outer surf (-X) of ss liner on small (upstream) side of removable concrete block containing shield plug
3102   px   -39.6875   $ inner surf (-X) of ss liner on bioshield near small (upstream) side of removable concrete block containing shield plug
3103   px   -40.3225   $ outer surf (-X) of ss liner on bioshield near small (upstream) side of removable concrete block containing shield plug
c
3110   cz    8.255     $ cyl (along z axis) defining void in removable concrete block, upstream and downstream of the shield plug
c
3120   c/x  0.0  446.405  30.95625  $ outer radius of carbon steel shield plug (ie, rotary shutter); also see surfs 3131 & 3132
3121   c/x  0.0  446.405  31.75     $ outer radius of void around shield plug = inner radius of ss liner in removable concrete block
3122   c/x  0.0  446.405  32.54375  $ outer radius of ss liner in removable concrete block containing shield plug
c
c      ------------------------------------------------------------------------------------------------------------------------------------------
c
c       3131  11  cz  4.445    $ the big 3.5"diam beam hole in the rotary shutter;  use this when big hole is turned to "open" position
c       3132  21  cz  1.11125  $ small 0.875"diam beam hole in the rotary shutter;  use this when big hole is turned to "open" position
c
c       3131  12  cz  4.445    $ the big 3.5"diam beam hole in the rotary shutter;  use this when small hole is turned to "open" position
c       3132  22  cz  1.11125  $ small 0.875"diam beam hole in the rotary shutter;  use this when small hole is turned to "open" position
c
3131  13  cz  4.445    $ the big 3.5"diam beam hole in the rotary shutter;  use this when shutter is turned to "closed" position
3132  23  cz  1.11125  $ small 0.875"diam beam hole in the rotary shutter;  use this when shutter is turned to "closed" position
c
c      ------------------------------------------------------------------------------------------------------------------------------------------
c
c
c
c     Axial surfaces used for the description of the collimator assembly (etc) inside the concrete:
c     ---------------------------------------------------------------------------------
4100  pz  261.9474  $ max upstream axial location of narrow ss sleeve extending thru concrete into pool
4105  pz  286.385   $ upstream axial surf of pool seal (A1)
4110  pz  302.1868  $ upstream   surf of 2nd aluminum window defining end of water tube in 1998 design
4115  pz  302.5043  $ downstream surf of 2nd aluminum window defining end of water tube in 1998 design
4120  pz  304.0467  $ upstream axial surf of pool seal (A2)
4125  pz  304.1     $ step A for 2nd expansion of beam tube just upstream of collimator
4126  pz  304.735   $ step B for 2nd expansion of beam tube just upstream of collimator
4130  pz  310.58    $ upstream surface of collimator
4135  pz  311.785   $ downstream surf of pool seal (A1)
4140  pz  334.7709  $ upstream   surf of 2nd aluminum window defining end of water tube in 1960 design
4145  pz  335.4756  $ downstream surf of 2nd aluminum window defining end of water tube in 1960 design
4150  pz  335.7967  $ upstream surf of removable shield
4155  pz  341.8292  $ upstream   side of ss liner in bioshield near step
4160  pz  342.7817  $ downstream side of ss liner in bioshield near step = upstream surf of eccentric shield
4170  pz  381.5167  $ downstream surf of removable shield and eccentric shield
```

```
4180  pz  384.1645  $ upstream   side of pool seal (B)
4190  pz  399.48    $ downstream side of collimator
4195  pz  401.9445  $ downstream side of pool seal (B) = downstream side of flange around pool seal (B)
c
c
c     Artificial surfaces used to facilitate writing & later using an internal boundary source (wssa) file:
c     ------------------------------------------------------------------------------------------------
c     In the early global calc where we write the boundary source:
c        (1) Cells 9981, 9982 and 9983, between Surfs 4195-4196, 4196-4197, and 4197-4198 are all regular void cells
c        (2) the boundary source will be written on Surf 4197
c        (3) the F1 surface crossing tallies will be written on Surf 4198 (just upstream of the boundary source)
c
c     In later shielding calcs for just the rotary shutter (shield plug), we'll keep the same (complete) basic model, BUT:
c        (1) Cell 9981 between Surfs 4195-4196 will be a black void with imp:n=0 to de-couple everything upstream of Surf 4196
c        (2) Cell 9982 between Surfs 4196-4197 will be a regular void
c        (3) the boundary source will be read & applied on Surf 4197
c        (4) Cell 9983 between Surfs 4197-4198 will be a regular void
c        (5) the F1 surface crossing tallies will be written on Surf 4198 (just upstream of the boundary source)
c            so that we have a printed cross-check that our boundary source reproduces the previous result
c     ------------------------------------------------------------------------------------------------
4196  pz  401.9545  $ artificial surf used to create three infintesimal void cells downstream side of pool seal (B); 0.01 cm upstream of boundary source
4197  pz  401.9645  $ artificial surf used to create three infintesimal void cells downstream side of pool seal (B); boundary source written/inserted here
4198  pz  401.9745  $ artificial surf used to create three infintesimal void cells downstream side of pool seal (B); now used for F1 tallies
c
c
c     Box surfaces corresponding to rectangular-shaped hole in collimator:
c     --------------------------------------------------------------------
c     Here (like everywhere in this MCNP model of HB-3),
c     Z=central axis; Y is really horizontal; X is really vertical
4210  py  -3.4925   $ ymin
4211  py   3.4925   $ ymax
4212  px  -6.9850   $ xmin
4213  px   6.9850   $ xmax
c
c
c     Radial surfaces used for the description of the collimator assembly (etc) inside the concrete:
c     ----------------------------------------------------------------------------------------------
4220  cz  17.2099   $ inner radius of narrow ss sleeve extending thru concrete into pool
4225  cz  17.4742   $ outer radius of narrow ss sleeve extending thru concrete into pool
4230  cz   9.21131  $ outer radius of collimator = inner radius of (again) expanded aluminum beam tube
4235  cz   9.84631  $ outer radius of (again) expanded aluminum beam tube = inner radius of removable shield
4240  cz  13.97     $ outer radius of pool seal (B)
4245  cz  33.655    $ outer radius of flange holding pool seal (B)
4250  cz  14.0339   $ outer radius of pool seal (A1) = inner radius of pool seal (A2)
4255  cz  19.7564   $ outer radius of removable shield = inner radius of eccentric shield
4260  cz  22.2003   $ outer radius of eccentric shield = inner radius of ss bioshield liner (in this axail section)
4265  cz  22.9315   $ outer radius of ss bioshield liner (in this axail section)
c
c
c     Surfaces 5100-5130 are used only in (segmented cell) Tally 184 which is used to monitor the
c     appx gamma dose rate in each of 30 equal axial segments (dz=4.24119 cm, dVol=493.55788 cc)
c     up thru the water tube (Cell 2145) from Z=174.95125 to 302.1868 cm.  These surfaces are used
c     only in Tally 184, and are not used in any cell descriptions.
c     5100  pz  174.95125
5101  pz  179.19240
5102  pz  183.43360
5103  pz  187.67480
5104  pz  191.91600
```

```
5105  pz  196.15720
5106  pz  200.39840
5107  pz  204.63950
5108  pz  208.88070
5109  pz  213.12190
5110  pz  217.36310
5111  pz  221.60430
5112  pz  225.84550
5113  pz  230.08670
5114  pz  234.32780
5115  pz  238.56900
5116  pz  242.81020
5117  pz  247.05140
5118  pz  251.29260
5119  pz  255.53380
5120  pz  259.77500
5121  pz  264.01610
5122  pz  268.25730
5123  pz  272.49850
5124  pz  276.73970
5125  pz  280.98090
5126  pz  285.22210
5127  pz  289.46330
5128  pz  293.70440
5129  pz  297.94560
c     5130  pz  302.18680
c
c     Surfaces 5140-5160 are used only in (segmented cell) Tally 194 which is used to monitor the
c     appx gamma dose rate in each of 20 equal axial segments (dz=4.44500 cm, dVol=433.74510 cc)
c     up thru the rectangular hole in the collimator (Cell 4300) from Z=310.58 to 399.48 cm.
c     These surfaces are used only in Tally 194, and are not used in any cell descriptions.
c     5140  pz  310.58000
5141  pz  315.02500
5142  pz  319.47000
5143  pz  323.91500
5144  pz  328.36000
5145  pz  332.80500
5146  pz  337.25000
5147  pz  341.69500
5148  pz  346.14000
5149  pz  350.58500
5150  pz  355.03000
5151  pz  359.47500
5152  pz  363.92000
5153  pz  368.36500
5154  pz  372.81000
5155  pz  377.25500
5156  pz  381.70000
5157  pz  386.14500
5158  pz  390.59000
5159  pz  395.03500
c     5160  pz  399.48000
c
c
9990   s  0.0  0.0  678.1673  1.11125 $ small sph (R=radius of small shutter hole), located at pt where Blosser & Thomas made measurements in June 1968 (cf
ORNL-TM-2221)
c
9997   pz    0.0   $ External void boundary (location corresponds to the real radial plane perpendicular to the real beam tube)
```

```
9998   pz  700.0   $ External void boundary (far enough out to emcompass point where Blosser & Thomas made measurements in 1968)
9999   cz   65.0   $ External void boundary (radial extent of this model)
c
c
c     END SURFACES (next line must be blank)

c     PROBLEM PARAMETERS:
mode   p
c       mode   n p
c       mode   n
c       nps    16000
c       nps    40000
c       nps    240000
c       nps    2000000
c       nps    5000000
nps    40000000
c       nps    60000000
c       nps    80000000
c       nps    120000000
c       cut:n  time(shakes) energy(MeV)   WC1   WC2   SWTM
c       cut:n         1.0e20          0.027     -0.5  -0.25   0.0  $ cutoff:  don't track any neutrons below 27 keV
print  60      $ Table 60 shows vol, mass, n-imp by cell; see pp 3-117 of manual for description of other useful tables you may want
prdmp  0   800000  0  4  0   $ make restart file after every 80000 histories in fixed src calc; save only the 4 most recent restart files
c      prdmp  0   80000  0  4  0   $ make restart file after every 80000 histories in fixed src calc; save only the 4 most recent restart files
c      prdmp  0   16000  0  4  0   $ make restart file after every 16000 histories in fixed src calc; save only the 4 most recent restart files
c
imp:p  $ obtained from MCNP output table when I ran a fake MCNP run with neutrons; here imp:p=imp:n in all 88 cells;
       $ in this case I set imp:p=imp:n=0 in Cell 9981 (position 84 in this table), just upstream of the rotary shutter
       1 0 1 1 1 1 1 1 1 1 0 1 1 1 1 1 1 1 1 2
       2 2 2 2 1 1 1 1 1 1 1 2 2 1 2 2 2 2 2 2
       2 2 2 2 2 2 2 2 1 1 1 1 1 1 1 1 1 1 1 1
       1 1 1 1 1 1 1 1 1 1 1 1 1 1 1 1 1 1 1 1
       1 1 1 0 1 1 1 0
c
c       ------------------------------------------------------------------------------------------
c       To be consistent with the wwinp file & the biased source dist
c       (see GETADJ.OUT, as printed by the GATWING.SCR), make sure you have
c       WUPN=WTHI= 100*WTLOW  and  WTSURV=WTAVG= 10*WTLOW  on the WWP:p card, and no WWP:n (in this case)
c       ------------------------------------------------------------------------------------------
c       WWP:n  wupn  wsurvn  mxspln  mwhere  switchn
c       wwp:n  100  10  100  0  -1       $ 5th parameter is negative to make MCNP4B read the weight window importance file (wwinp)
c       wwp:p  100  10  100  0  -1       $ 5th parameter is negative to make MCNP4B read the weight window importance file (wwinp)
c         wwp:n  100  10  50  0  -1              $ 5th parameter is negative to make MCNP4B read the weight window importance file (wwinp)
c         wwp:p  100  10  50  0  -1              $ 5th parameter is negative to make MCNP4B read the weight window importance file (wwinp)
c       wwp:n  5  3  5  0  0  $ just use default values for now
c       wwp:p  5  3  5  0  0  $ just use default values for now
c       wwp:n  100  10  390625  0  -1              $ 5th parameter is negative to make MCNP4B read the weight window importance file (wwinp)
c       wwp:p  100  10  390625  0  -1              $ 5th parameter is negative to make MCNP4B read the weight window importance file (wwinp)
c       wwp:n  100  10  50  -1  -1              $ 5th parameter is negative to make MCNP4B read the weight window importance file (wwinp)
c       wwp:p  100  10  50  -1  -1              $ 5th parameter is negative to make MCNP4B read the weight window importance file (wwinp)
c       wwp:n  100  10  10  0  -1       $ 5th parameter is negative to make MCNP4B read the weight window importance file (wwinp)
c       wwp:p  100  10  10  0  -1       $ 5th parameter is negative to make MCNP4B read the weight window importance file (wwinp)
c      ------------------------------------------------------------------------------------------
c
c       Use the "ssw" card below to write a boundary source file for gammas travelling downstream (ie, moving in the +Z direction)
c       across Surf 4197 from Cell 9982 to Cell 9983, where Surf 4197 is at Z=401.9645 cm, just 2.4845 cm downstream of collimator.
c       [Note: the three infinitesimally thin (0.01-cm-thick) void cells (Cells 9981, 9982, and 9983 defined by Surfaces 4195,
c       4196, and 4198) cut thru the entire problem geometry in the region between the collimator exit and the rotary shutter
```

c shield plug.] With this boundary source, we can later come back and set imp:n=0 and imp:n=0 in Cell 9981 and use this
c boundary source in detailed shielding analyses of the rotary shield plug, which may (or may not) need to be redesigned,
c without having to waste time tracking gammas upstream of Surf 4197, even though we'll retain the complete HB-3 geometry
c in our model. This problem should run much faster.
c
c ssw +4197 (9983) $ use this to write the boundary source file
c
c
c ACTIVATION SOURCES IN ROTARY SHUTTER, 7 DAYS AFTER SHUTDOWN:
c ---
c Description of activation sources within the Type 1020 carbon steel rotary shutter shield plug represented by Cell 3090.
c How obtained: Run HB309A was used to obtain about a dozen key reaction rates for the various isotopes in this material
c (which initially included 0.45 wt% Mn-55 and 0.015 wt% Co-59), in each of 39 1-cm-thick cylindrical shells concentrically
c located about the big beam hole in the rotary shutter shield plug when the shutter was wide open and operating under
c normal conditions. ACTSRC.FOR is an ad hoc burnup/depletion program that uses those various reaction rates. Material
c was assumed to be irradiated for 30 years at full power (although almost everything except Co-59 reaches saturation in
c just 1 or 2 years); while the detailed ACTSRC.FOR output shows decay gamma sources (from Mn-54, Mn-56, Fe-59, and Co-60)
c for each of the first 60 days after shutdown, the results at 7 days after shutdown were selected as typical. (In reality,
c things don't change much after day 3 or 4.) ACTSRC.FOR also shows the corresponding gamma sources (p/s/cc) for each of
c the 39 cyl shells described above (based on actual amount [cc's] of material in the rotary shutter [Cell 3090] that lie
c in each of the 39 shells), as well as the total (real)volume-integrated source (p/s) in each piece of Cell 3090 in each
c shell, 7 days after shutdown. Most activity comes from Fe-59 and Co-60, both of which have gammas at 1.1 MeV and 1.3 MeV.
c The equivalent gamma source used here (below) is based on an everage 1.25 MeV per disintegration (i.e., those at 1.1 MeV
c count for slightly less, and those at 1.3 MeV count for slightly more). This data (p/s/cc of "real" material in each
c +---
c | Results from ACTSRC.FOR are as follows:
c |
c | Equivalent gamma sources (at 1.25 MeV, 7 days after shutdown) for each of 39
c | cylindrical shells, concentric about large beam hole in HB-3 rotary shutter:
c |

Cyl Shell	Rmin	Rmax	Volume (cc)	GSRC den (p/s/cc)	GSRC total (p/s)
1	4.4450	5.4450	1.89858E+03	1.71804E+06	3.26184E+09
2	5.4450	6.4450	2.27981E+03	1.20939E+06	2.75717E+09
3	6.4450	7.4450	2.65511E+03	9.10533E+05	2.41757E+09
4	7.4450	8.4450	3.02744E+03	5.11462E+05	1.54842E+09
5	8.4450	9.4450	3.39342E+03	2.96828E+05	1.00726E+09
6	9.4450	10.4450	3.75537E+03	2.04527E+05	7.68074E+08
7	10.4450	11.4450	4.11116E+03	1.45949E+05	6.00020E+08
8	11.4450	12.4450	4.45690E+03	1.10877E+05	4.94166E+08
9	12.4450	13.4450	4.79709E+03	8.50310E+04	4.07901E+08
10	13.4450	14.4450	5.12661E+03	7.25228E+04	3.71796E+08
11	14.4450	15.4450	5.44592E+03	5.84760E+04	3.18456E+08
12	15.4450	16.4450	5.75543E+03	4.65858E+04	2.68122E+08
13	16.4450	17.4450	6.05497E+03	4.14990E+04	2.51275E+08
14	17.4450	18.4450	6.33840E+03	3.22381E+04	2.04338E+08
15	18.4450	19.4450	6.60982E+03	2.75541E+04	1.82128E+08
16	19.4450	20.4450	6.86725E+03	2.20748E+04	1.51593E+08
17	20.4450	21.4450	7.10540E+03	2.31075E+04	1.64188E+08
18	21.4450	22.4450	7.32554E+03	1.64953E+04	1.20837E+08
19	22.4450	23.4450	7.53004E+03	1.46455E+04	1.10281E+08
20	23.4450	24.4450	7.70707E+03	1.54328E+04	1.18942E+08
21	24.4450	25.4450	7.85115E+03	1.20202E+04	9.43721E+07
22	25.4450	26.4450	7.96738E+03	9.35205E+03	7.45113E+07
23	26.4450	27.4450	8.04809E+03	1.14168E+04	9.18836E+07
24	27.4450	28.4450	8.08235E+03	9.28401E+03	7.50366E+07
25	28.4450	29.4450	8.05935E+03	7.24319E+03	5.83754E+07

```
c      |  26    29.4450  30.4450   7.95535E+03   6.70739E+03   5.33597E+07
c      |  27    30.4450  31.4450   6.44147E+03   7.31088E+03   4.70928E+07
c      |  28    31.4450  32.4450   4.99352E+03   6.62929E+03   3.31035E+07
c      |  29    32.4450  33.4450   4.08671E+03   4.56713E+03   1.86645E+07
c      |  30    33.4450  34.4450   3.36986E+03   3.66936E+03   1.23652E+07
c      |  31    34.4450  35.4450   2.76096E+03   4.79983E+03   1.32521E+07
c      |  32    35.4450  36.4450   2.23160E+03   5.26502E+03   1.17494E+07
c      |  33    36.4450  37.4450   1.76511E+03   7.08731E+03   1.25099E+07
c      |  34    37.4450  38.4450   1.35264E+03   4.83427E+03   6.53903E+06
c      |  35    38.4450  39.4450   9.88281E+02   8.71481E+03   8.61268E+06
c      |  36    39.4450  40.4450   6.71165E+02   4.25503E+03   2.85583E+06
c      |  37    40.4450  41.4450   4.01009E+02   3.18232E+02   1.27614E+05
c      |  38    41.4450  42.4450   1.86544E+02   1.67852E+02   3.13117E+04
c      |  39    42.4450  43.4433   3.97575E+01   5.10060E+01   2.02787E+03
c      |                                                       -----------
c      |                  Total activation gamma source (p/s)=  1.61388E+10
c      |
c      |  (*) Volumes shown/used here are the actual volume(s) corresponding
c      |      to the rotary shutter (Cell 3090) inside each of these radial
c      |      shells.  Because these shells have a horizontal axis while the
c      |      shutter has a vertical axis, and also because of the small hole
c      |      thru the shutter which cuts thru all/most of these at an angle,
c      |      these "real" volumes had to be calculated stoichastically, as
c      |      shown in Run VV309.
c      +-------------------------------------------------------------------
c     shell) is fed to the SI.FOR program which creates the radial sampling distribution (si2,sp2) shown below.  When creating
c     the sampling distribution within the sampling volume (which must fully enclose Cell 3090), it is necessary to assume that
c     the source density (p/s/cc of "real" material in each shell) is characteristic of the "entire" volume of each shell in the
c     sampling volume.  That source density (in each radial bin) is therefore multiplied by the "entire" volume of the radial
c     shell in each segment of the sampling volume.  The fact that it may really only be characteristic of a tiny piece of real
c     material in each shell of the sampling volume is accounted for by rejecting any sampled points that are not really inside
c     Cell 3090.  Moreover, in SI.FOR, we also subdivide each of the 39 shells of the sampling volume into 3 pieces of equal volume
c     and assume that the inner piece has a source density that is 6% higher than the average, and that the outer piece has a source
c     density that is 6% lower than the average.  (While not necessary, this was done simply to help "smooth out" some of the
c     discontinuities between shells.)  Anyway, that's why the sampling volume below has 117 (=3*39) radial regions instead of 39.
c     Lastly, it must be recognized that the final dose rate determination calc for activation sources will be performed with the
c     shutter closed.  For that reason, the axs vector for the sampling volume shown below must be coincident with the axis of the
c     big beam hole of the shutter when closed (i.e., 66.75 degrees off the centerline of the beam tube).  -- JAB, 6-30-98
c     ---------------------------
sdef  $ activation sources in the rotary shutter, 7 days after shutdown;  total activation gamma source (p/s)=  1.61388E+10
      par=2                          $ gamma source
      erg=1.25                       $ will use an "equivalent" activation source at 1.25 MeV (see ACTSRC.FOR program)
      cel=3090                       $ exclude any points from sampling distribution that are not in rotary shutter shield plug (Cell 3090)
      pos= 0  0  446.405             $ reference position here is the midpoint of the rotary shutter shield plug
      axs= 0  -0.9187912  0.3947439  $ ref vector for sampling vol points along centerline of big hole (66.75 degrees off beam tube centerline
      ext=d1                         $ use d1 to sample uniformly over +/- 31 cm of sampling volume centerline
      rad=d2                         $ use d2 to sample radial distribution within the sampling volume
si1  -31.0  31.0    $ axial bins; used for axial sampling probability within sampling volume;
sp1    0.0   1.0    $ sampling probability for each axial bin within sampling volume; uniform
si2  $ radial bins; used for radial sampling probability within sampling volume; see SI.FOR program; pts outside Cell 3090 will still be rejected
       4.44500   4.80153   5.13336   5.44500   5.79753
       6.12982   6.44500   6.79471   7.12727   7.44500
       7.79260   8.12535   8.44500   8.79098   9.12385
       9.44500   9.78969  10.12265  10.44500  10.78864
      11.12166  11.44500  11.78776  12.12084  12.44500
      12.78703  13.12014  13.44500  13.78640  14.11954
      14.44500  14.78585  15.11902  15.44500  15.78537
      16.11856  16.44500  16.78495  17.11816  17.44500
```

```
      17.78458  18.11780  18.44500  18.78425  19.11748
      19.44500  19.78395  20.11719  20.44500  20.78368
      21.11693  21.44500  21.78343  22.11669  22.44500
      22.78321  23.11647  23.44500  23.78301  24.11627
      24.44500  24.78282  25.11609  25.44500  25.78264
      26.11592  26.44500  26.78248  27.11576  27.44500
      27.78233  28.11562  28.44500  28.78219  29.11548
      29.44500  29.78206  30.11536  30.44500  30.78194
      31.11524  31.44500  31.78183  32.11513  32.44500
      32.78172  33.11502  33.44500  33.78162  34.11492
      34.44500  34.78153  35.11483  35.44500  35.78144
      36.11474  36.44500  36.78135  37.11466  37.44500
      37.78127  38.11458  38.44500  38.78120  39.11451
      39.44500  39.78113  40.11444  40.44500  40.78106
      41.11437  41.44500  41.78099  42.11431  42.44500
      42.78036  43.11310  43.44330
sp2  $ sampling probability for each radial bin within sampling volume; see SI.FOR program; pts outside Cell 3090 will still be rejected
      0.00000e+0  1.16938e+9  1.10319e+9  1.03700e+9  9.89634e+8  $ first 4.445 cm represents the big beam hole (void) where sources are zero
      9.33617e+8  8.77600e+8  8.70410e+8  8.21142e+8  7.71873e+8
      5.59324e+8  5.27664e+8  4.96004e+8  3.65461e+8  3.44775e+8
      3.24088e+8  2.79970e+8  2.64123e+8  2.48275e+8  2.19874e+8
      2.07428e+8  1.94982e+8  1.82299e+8  1.71980e+8  1.61661e+8
      1.51508e+8  1.42932e+8  1.34356e+8  1.39203e+8  1.31324e+8
      1.23444e+8  1.20290e+8  1.13481e+8  1.06672e+8  1.02243e+8
      9.64558e+7  9.06685e+7  9.67911e+7  9.13123e+7  8.58336e+7
      7.96286e+7  7.51213e+7  7.06140e+7  7.18517e+7  6.77846e+7
      6.37175e+7  6.06020e+7  5.71717e+7  5.37414e+7  6.66177e+7
      6.28469e+7  5.90761e+7  4.98255e+7  4.70052e+7  4.41849e+7
      4.62539e+7  4.36358e+7  4.10176e+7  5.08646e+7  4.79855e+7
      4.51064e+7  4.12716e+7  3.89355e+7  3.65993e+7  3.33977e+7
      3.15073e+7  2.96168e+7  4.23427e+7  3.99460e+7  3.75492e+7
      3.57105e+7  3.36891e+7  3.16678e+7  2.88576e+7  2.72241e+7
      2.55907e+7  2.76461e+7  2.60812e+7  2.45164e+7  3.11398e+7
      2.93772e+7  2.76146e+7  2.91492e+7  2.74992e+7  2.58493e+7
      2.07104e+7  1.95381e+7  1.83658e+7  1.71444e+7  1.61740e+7
      1.52035e+7  2.30870e+7  2.17802e+7  2.04734e+7  2.60492e+7
      2.45747e+7  2.31002e+7  3.60407e+7  3.40007e+7  3.19606e+7
      2.52489e+7  2.38197e+7  2.23905e+7  4.67160e+7  4.40717e+7
      4.14274e+7  2.33949e+7  2.20707e+7  2.07464e+7  1.79350e+6
      1.69198e+6  1.59046e+6  9.69087e+5  9.14233e+5  8.59379e+5
      3.00983e+5  2.83947e+5  2.66910e+5
c     ------------------------------------------------------------------------------------------------------------------------
c
c     -------------------
c     del for activ calc, 6-30-98:  c     EQUIVALENT POINT SOURCES:
c     del for activ calc, 6-30-98:  c
c     del for activ calc, 6-30-98:  sdef  erg=d73  pos ferg d83  $ source def for gammas in HB-3 (total p/s = 1.35399E+17;  source in VELM grps 1-8 = 7.9842
11E+15 p/s)
c     del for activ calc, 6-30-98:        par=2            $ par=1 for neut, par=2 for photons
c     del for activ calc, 6-30-98:  c     sdef  erg=d53  pos ferg d63  $ source def for neutrons in HB-3 (total n/s = 9.64595E+16);  total n/s above 27 keV
= 1.20830e16
c     del for activ calc, 6-30-98:  c     par=1            $ par=1 for neut, par=2 for photons
c     del for activ calc, 6-30-98:        vec  0  0  1     $ reference vector if directional-dependent source is used
c     del for activ calc, 6-30-98:        dir=d3           $ angular distribution wrt vec (Caution: choice of angular distribution sampled will dictate choi
ce of wgt)
c     del for activ calc, 6-30-98:        wgt=1.7332472-2  $ use this with d3;  wgt = [mu(max)-mu(min)]/[(+1)-(-1)] = [1.0000000000-0.965335056]/2 = 1.73324
72-2
c     del for activ calc, 6-30-98:  c     wgt=0.1    $ use this with mu(min)=0.8 in d3 for dosimetry calc only;  wgt = [mu(max)-mu(min)]/[(+1)-(-1)] = [1.0-
```

```
0.8]/2 = 0.1
c     del for activ calc, 6-30-98:  c     wgt=0.145  $ use this with mu(min)=0.71 in d3 for HB304M4 dosimetry calc only;  wgt = [mu(max)-mu(min)]/[(+1)-(-1)
] = [1.0-0.8]/2 = 0.145
c     del for activ calc, 6-30-98:  c     ------------------
c     del for activ calc, 6-30-98:  c     Ang Dist: to spray isotropically across central void of HB-3 beam tube
c     del for activ calc, 6-30-98:  si3   h  0.965335056   1.0  $ angular distribution;  mu boundaries (i.e, cosine boundaries wrt vec)
c     del for activ calc, 6-30-98:  c     si3   h  0.8  1.0  $ open up angular distribution for dosimetry run;  mu boundaries (i.e, cosine boundaries wrt ve
c)
c     del for activ calc, 6-30-98:  c     si3   h  0.71  1.0  $ open up angular distribution for HB304M4 dosimetry run;  mu boundaries (i.e, cosine boundari
es wrt vec)
c     del for activ calc, 6-30-98:  sp3   d  0  1  $ angular distribution; particle emmission probabilities by bin; first value (below lowest bin bound) mus
t be zero
c     ------------------
c
c       ------------------------------------------------------------------------
c       Begin distributions needed to describe the neutron sources in the HB-3 beam tube
c       ------------------------------------------------------------------------
si53  h  1.0000e-11  $ this one Emin(MeV), followed by Emax(MeV) for the 61 VELM neut grps (lowest to highest energy for MCNP):
         4.1399e-7    1.1253e-6    2.3824e-6    5.0435e-6    1.0677e-5    $ VELM n-groups 61, 60, 59, 58, 57,
         2.2603e-5    4.7851e-5    1.0130e-4    1.6702e-4    2.7536e-4    $ VELM n-groups 56, 55, 54, 53, 52,
         4.5400e-4    7.4852e-4    1.2341e-3    2.0347e-3    2.2487e-3    $ VELM n-groups 51, 50, 49, 48, 47,
         2.6126e-3    3.0354e-3    3.7074e-3    5.5308e-3    9.1188e-3    $ VELM n-groups 46, 45, 44, 43, 42,
         1.5034e-2    2.3579e-2    2.4788e-2    2.6058e-2    2.7000e-2    $ VELM n-groups 41, 40, 39, 38, 37,
         2.8501e-2    3.4307e-2    5.2475e-2    5.6562e-2    8.6517e-2    $ VELM n-groups 36, 35, 34, 33, 32,
         1.2277e-1    1.4996e-1    1.8316e-1    2.2371e-1    2.7324e-1    $ VELM n-groups 31, 30, 29, 28, 27,
         2.9452e-1    2.9721e-1    2.9849e-1    3.0197e-1    3.8774e-1    $ VELM n-groups 26, 25, 24, 23, 22,
         4.9787e-1    5.2340e-1    6.0810e-1    7.4274e-1    9.0718e-1    $ VELM n-groups 21, 20, 19, 18, 17,
         1.1080e+0    1.3534e+0    1.6530e+0    2.0190e+0    2.2313e+0    $ VELM n-groups 16, 15, 14, 13, 12,
         2.3457e+0    2.4660e+0    3.0119e+0    3.6788e+0    4.4933e+0    $ VELM n-groups 11, 10,  9,  8,  7,
         5.4881e+0    6.7032e+0    8.1873e+0    1.0000e+1    1.2214e+1    $ VELM n-groups  6,  5,  4,  3,  2,
         1.4918e+1                                                      $ VELM n-group   1
sp53  d     0.0  $ dummy 0, followed by neut src terms (n/s) for HB-3:
         6.30365e+16  2.25679e+15  1.52979e+15  1.30212e+15  1.55274e+15  $ VELM n-groups 61, 60, 59, 58, 57,
         1.58981e+15  1.54759e+15  1.45876e+15  9.03837e+14  9.69821e+14  $ VELM n-groups 56, 55, 54, 53, 52,
         9.50610e+14  8.74122e+14  8.53691e+14  8.87245e+14  2.04908e+14  $ VELM n-groups 51, 50, 49, 48, 47,
         2.76622e+14  2.54975e+14  3.36538e+14  7.55438e+14  8.76077e+14  $ VELM n-groups 46, 45, 44, 43, 42,
         9.84217e+14  7.42049e+14  6.69650e+13  1.12860e+14  5.24714e+13  $ VELM n-groups 41, 40, 39, 38, 37,
         1.21873e+14  3.03507e+14  4.96958e+14  1.29680e+14  8.89397e+14  $ VELM n-groups 36, 35, 34, 33, 32,
         5.59006e+14  4.29193e+14  3.63241e+14  4.33245e+14  7.35199e+14  $ VELM n-groups 31, 30, 29, 28, 27,
         2.12840e+14  1.38494e+13  7.68584e+12  3.65651e+13  6.29256e+14  $ VELM n-groups 26, 25, 24, 23, 22,
         5.85513e+14  1.49367e+14  3.61470e+14  5.35177e+14  6.65098e+14  $ VELM n-groups 21, 20, 19, 18, 17,
         5.40055e+14  7.09512e+14  8.07055e+14  8.54720e+14  3.12945e+14  $ VELM n-groups 16, 15, 14, 13, 12,
         2.00073e+14  1.35333e+14  2.41078e+14  1.61947e+14  2.06360e+14  $ VELM n-groups 11, 10,  9,  8,  7,
         1.36477e+14  7.32282e+13  3.05242e+13  8.64293e+12  6.92602e+12  $ VELM n-groups  6,  5,  4,  3,  2,
         2.74800e+09                                                    $ VELM n-group   1
ds63  1     $ neutron starting positions (x,y,z) in HB-3:
         0 0  80.2    0 0  57.3    0 0  65.2    0 0  76.1    0 0  54.5    $ VELM n-groups 61, 60, 59, 58, 57,
         0 0  48.2    0 0  56.5    0 0  55.4    0 0  56.0    0 0  51.1    $ VELM n-groups 56, 55, 54, 53, 52,
         0 0  53.8    0 0  52.6    0 0  61.2    0 0  60.5    0 0  43.0    $ VELM n-groups 51, 50, 49, 48, 47,
         0 0  49.5    0 0  55.0    0 0  65.1    0 0  53.3    0 0  52.7    $ VELM n-groups 46, 45, 44, 43, 42,
         0 0  50.7    0 0  54.0    0 0  69.0    0 0  46.7    0 0  62.6    $ VELM n-groups 41, 40, 39, 38, 37,
         0 0  67.5    0 0  79.8    0 0  52.9    0 0  56.7    0 0  47.4    $ VELM n-groups 36, 35, 34, 33, 32,
         0 0  45.7    0 0  45.6    0 0  42.5    0 0  48.9    0 0  34.2    $ VELM n-groups 31, 30, 29, 28, 27,
         0 0  42.4    0 0  63.8    0 0  53.7    0 0  42.3    0 0  49.6    $ VELM n-groups 26, 25, 24, 23, 22,
         0 0  58.8    0 0  52.9    0 0  50.3    0 0  56.8    0 0  44.1    $ VELM n-groups 21, 20, 19, 18, 17,
         0 0  70.1    0 0  46.8    0 0  59.7    0 0  50.2    0 0  52.1    $ VELM n-groups 16, 15, 14, 13, 12,
         0 0          0 0  43.5    0 0  65.3    0 0  56.9    0 0  47.9    $ VE   n-groups 11, 10,  9,  8,  7,
         0 0          0 0  59.5    0 0  42.9    0 0  68.7    0 0  31.1    $ V.   -groups  6,  5,  4,  3,  2,
```

```
      0 0  99.9                                                    $ VELM n-group   1
c     Shift sources 1.6986 cm to right of beam tube centerline to account for the anisotropic effect
c     of more neutrons entering the one side of the beam tube than the other:   -- JAB, 4-7-98
c    0 1.6986 67.5  0 1.6986 79.8  0 1.6986 52.9  0 1.6986 56.7  0 1.6986 47.4    $ VELM n-groups 36, 35, 34, 33, 32,
c    0 1.6986 45.7  0 1.6986 45.6  0 1.6986 42.5  0 1.6986 48.9  0 1.6986 34.2    $ VELM n-groups 31, 30, 29, 28, 27,
c    0 1.6986 42.4  0 1.6986 63.8  0 1.6986 53.7  0 1.6986 42.3  0 1.6986 49.6    $ VELM n-groups 26, 25, 24, 23, 22,
c    0 1.6986 58.8  0 1.6986 52.9  0 1.6986 50.3  0 1.6986 56.8  0 1.6986 44.1    $ VELM n-groups 21, 20, 19, 18, 17,
c    0 1.6986 70.1  0 1.6986 46.8  0 1.6986 59.7  0 1.6986 50.2  0 1.6986 52.1    $ VELM n-groups 16, 15, 14, 13, 12,
c    0 1.6986 33.3  0 1.6986 43.5  0 1.6986 65.3  0 1.6986 56.9  0 1.6986 47.9    $ VELM n-groups 11, 10,  9,  8,  7,
c    0 1.6986 62.6  0 1.6986 59.5  0 1.6986 42.9  0 1.6986 68.7  0 1.6986 31.1    $ VELM n-groups  6,  5,  4,  3,  2,
c    0 1.6986 99.9                                                $ VELM n-group   1
c     ------------------------------------------------------------------------------
c     Begin distributions needed to describe the gamma sources in the HB-3 beam tube
c     ------------------------------------------------------------------------------
c     si73  h  1.0000e-2   $ this one Emin(MeV), followed by Emax(MeV) for the 23 VELM gamma grps (lowest to highest energy for MCNP):
c              2.0000e-2    4.5000e-2    7.0000e-2    1.0000e-1    1.5000e-1    $ VELM g-groups 23, 22, 21, 20, 19,
c              3.0000e-1    4.0000e-1    5.1000e-1    6.0000e-1    7.0000e-1    $ VELM g-groups 18, 17, 16, 15, 14,
c              1.0000e+0    1.5000e+0    2.0000e+0    2.5000e+0    3.0000e+0    $ VELM g-groups 13, 12, 11, 10,  9,
c              4.0000e+0    5.0000e+0    6.0000e+0    7.0000e+0    7.5000e+0    $ VELM g-groups  8,  7,  6,  5,  4,
c              8.0000e+0    1.0000e+1    1.4000e+1                              $ VELM g-groups  3,  2,  1
c     sp73  d     0.0  $ dummy 0, followed by gamma src terms (p/s) for HB-3:
c              8.72837e+12  2.84514e+15  1.65029e+16  1.67705e+16  1.82855e+16  $ VELM g-groups 23, 22, 21, 20, 19,
c              2.56708e+16  1.03805e+16  7.17665e+15  4.80101e+15  4.03975e+15  $ VELM g-groups 18, 17, 16, 15, 14,
c              7.31636e+15  5.27935e+15  4.23989e+15  2.66951e+15  1.42777e+15  $ VELM g-groups 13, 12, 11, 10,  9,
c              2.34929e+15  1.98361e+15  6.75453e+14  1.23378e+15  1.60183e+14  $ VELM g-groups  8,  7,  6,  5,  4,
c              1.51983e+15  6.19421e+13  1.23250e+11                           $ VELM g-groups  3,  2,  1
c     sb73  d     0.0  $ dummy 0, followed by "biased" gamma src terms (p/s) for HB-3:
c     c        ------------------------------------------------------------------------
c     c        Biased gamma sources in MCNP order (grp 1=low E, grp 23=high E);
c     c        Calculated using GETWING.SCR and GBANISN in adjoint mode, where the
c     c        adjoint sources at Z=478.49 cm were just the gamma flux-to-dose-rate factors;
c     c        Use these values for the gamma-only mcnp calc with a gamma-only source.
c     c        (For a coupled n/g calc with a neutron-only source, or for a neutron-only
c     c        calc with a neutron-only source, these values would be different).
c     c        Note that this can/should only be used with the corresponding weight
c     c        window file prepared by GETWING.SCR where the space/energy weights for
c     c        the gamma groups were calculated using the data in GETADJ.OUT.
c     c        ------------------------------------------------------------------------
c     c        To work well (or even to work "at all") everything MUST be self-consistent !!!!!
c     c        ------------------------------------------------------------------------
c              6.39635E-03  2.08498E+00  1.20937E+01  1.22898E+01  1.34000E+01  $ VELM g-groups 23, 22, 21, 20, 19,
c              1.88122E+01  3.98199E+08  2.75298E+08  1.84168E+08  1.54966E+08  $ VELM g-groups 18, 17, 16, 15, 14,
c              2.80658E+08  1.61658E+14  1.29829E+14  8.17425E+13  4.37194E+13  $ VELM g-groups 13, 12, 11, 10,  9,
c              7.19371E+13  3.75947E+16  1.28016E+16  2.33834E+16  3.03589E+15  $ VELM g-groups  8,  7,  6,  5,  4,
c              2.88048E+16  1.17397E+15  2.33592E+12                           $ VELM g-groups  3,  2,  1
c     ds83  1     $ gamma starting positions (x,y,z) in HB-3:
c             0 0  10.01   0 0  61.9    0 0  68.1    0 0  82.1    0 0  83.9    $ VELM g-groups 23, 22, 21, 20, 19,
c             0 0  84.5    0 0  81.6    0 0  84.7    0 0  88.8    0 0  83.2    $ VELM g-groups 18, 17, 16, 15, 14,
c             0 0  86.8    0 0  93.6    0 0  96.9    0 0  99.2    0 0  96.6    $ VELM g-groups 13, 12, 11, 10,  9,
c             0 0  92.6    0 0  93.2    0 0  96.4    0 0  93.9    0 0  96.0    $ VELM g-groups  8,  7,  6,  5,  4,
c             0 0  94.4    0 0  99.9    0 0  97.4                              $ VELM g-groups  3,  2,  1
c
c     ------------------------------------
c     QADD2.FOR analysis has shown that if the water tube & collimator are BOTH FLOODED, VELM source groups 1-8 account for 98-99%
c     of the dose rate downstream of the collimator.  (By the time they get there, of course, the photons may have less energy.)
c    * Thus, "for this particular FLOODED case", it is sufficient to include source photons from these first 8 VELM groups only.
c    * The photon source in VELM grps 1-8 (above 3.0 MeV) = 7.984211E+15 p/s (subtotal for these groups).  For this particular
c    * FLOODED case, this value may be used, but the SI73, SP73, DS83, any SB73 card, and "all" FM tally cards must be consistent.
```

```
c
si73  h  3.0000e+0   $ this one Emin(MeV), followed by Emax(MeV) for VELM gamma grps 1-8 (lowest to highest energy for MCNP):
         4.0000e+0    5.0000e+0    6.0000e+0    7.0000e+0    7.5000e+0    $ VELM g-groups  8,  7,  6,  5,  4,
         8.0000e+0    1.0000e+1    1.4000e+1                              $ VELM g-groups  3,  2,  1
sp73  d     0.0  $ dummy 0, followed by gamma src terms (p/s) for HB-3:
         2.34929e+15  1.98361e+15  6.75453e+14  1.23378e+15  1.60183e+14  $ VELM g-groups  8,  7,  6,  5,  4,
         1.51983e+15  6.19421e+13  1.23250e+11                           $ VELM g-groups  3,  2,  1
ds83  l     $ gamma starting positions (x,y,z) in HB-3:
         0 0  92.6    0 0  93.2    0 0  96.4    0 0  93.9    0 0  96.0    $ VELM g-groups  8,  7,  6,  5,  4,
         0 0  94.4    0 0  99.9    0 0  97.4                              $ VELM g-groups  3,  2,  1
c       ---------------------------------------
c
c
c       BEGIN-TRANSFORMATIONS:
c
c       Transformations that can/should be used for the holes in the beam tube shield plug (ie, the rotary shutter):
c          When big   hole is turned to "open" position:  use tr11 for big hole in shutter, and tr21 for small hole
c          When small hole is turned to "open" position:  use tr12 for big hole in shutter, and tr22 for small hole
c          When shutter    is turned to "off"  position:  use tr13 for big hole in shutter, and tr23 for small hole
c       ------------------------------------------------------------------------------------------------------------
*tr11  $ use tr11 for big hole in shutter, when big hole is turned to "open" position
       0.0  0.0  446.405  $ location of local origin (center of shutter), relative to the global origin (cm) in HB-3 model
         0    90   90     $ degrees from global x,y,z axes to local x axis
        90     0   90     $ degrees from global x,y,z axes to local y axis
        90    90    0     $ degrees from global x,y,z axes to local z axis
c
*tr12  $ use tr12 for big hole in shutter, when small hole is turned to "open" position
       0.0  0.0  446.405  $ location of local origin (center of shutter), relative to the global origin (cm) in HB-3 model
         0    90    90    $ degrees from global x,y,z axes to local x axis
        90  -46.5  -136.5 $ degrees from global x,y,z axes to local y axis
        90   43.5  -46.5  $ degrees from global x,y,z axes to local z axis
c
*tr13  $ use tr13 for big hole in shutter, when shutter is turned to "off" position
       0.0  0.0  446.405    $ location of local origin (center of shutter), relative to the global origin (cm) in HB-3 model
         0    90      90    $ degrees from global x,y,z axes to local x axis
        90  -113.25 -203.25 $ degrees from global x,y,z axes to local y axis
        90  -23.25  -113.25 $ degrees from global x,y,z axes to local z axis
c
*tr21  $ use tr21 for small hole in shutter, when big hole is turned to "open" position
       0.0  0.0  446.405    $ location of local origin (center of shutter), relative to the global origin (cm) in HB-3 model
         0    90    90      $ degrees from global x,y,z axes to local x axis
        90   46.5 -43.5     $ degrees from global x,y,z axes to local y axis
        90  136.5  46.5     $ degrees from global x,y,z axes to local z axis
c
*tr22  $ use tr22 for small hole in shutter, when small hole is turned to "open" position
       0.0  0.0  446.405    $ location of local origin (center of shutter), relative to the global origin (cm) in HB-3 model
         0    90   90       $ degrees from global x,y,z axes to local x axis
        90     0   90       $ degrees from global x,y,z axes to local y axis
        90    90    0       $ degrees from global x,y,z axes to local z axis
c
*tr23  $ use tr23 for small hole in shutter, when shutter is turned to "off" position
       0.0  0.0  446.405    $ location of local origin (center of shutter), relative to the global origin (cm) in HB-3 model
         0    90     90     $ degrees from global x,y,z axes to local x axis
        90  -66.75 -156.75  $ degrees from global x,y,z axes to local y axis
        90   23.25  -66.75  $ degrees from global x,y,z axes to local z axis
c
c       *tr40  use tr40 to locate and position the Key 3 dosimetry specimen holder relative to HB-3 beam tube
c                0.0  113.64     $ location of local origin (center of shu  ), relative to the global origin (cm) in HB-3 model
```

520

```
c                0    90   90       $ degrees from global x,y,z axes to local x axis
c               90    14  -76       $ degrees from global x,y,z axes to local y axis
c               90   104   14       $ degrees from global x,y,z axes to local z axis
c
c       *tr40 was revised as follows by JAB on 3 Apr 98 for Run HB304H, based on newly available data shown on Dwg E-49953, Rev A, 6-30-65:
*tr40  $ use tr40 to locate and position the Key 3 dosimetry specimen holder relative to HB-3 beam tube
       0.0  0.0  114.22     $ location of local origin (center of shutter), relative to the global origin (cm) in HB-3 model
         0    90   90       $ degrees from global x,y,z axes to local x axis
        90    13  -77       $ degrees from global x,y,z axes to local y axis
        90   103   13       $ degrees from global x,y,z axes to local z axis
c
c       $ incorrect & obsolete:   *tr42  $ use tr42 to locate and position the elliptical cone used to define chamfer between HB3 vessel hole and inner surf
 of pressure vessel
c       $ incorrect & obsolete:          0.0  -2.14265  128.18364   $ location of local origin (center of elliptical cone), relative to the global origin (c
m) in HB-3 model
c       $ incorrect & obsolete:            0    90.0000    90.0000  $ degrees from global x,y,z axes to local x axis
c       $ incorrect & obsolete:           90    12.6575   -77.3425  $ degrees from global x,y,z axes to local y axis
c       $ incorrect & obsolete:           90   102.6575    12.6575  $ degrees from global x,y,z axes to local z axis
c
c       The following correction to *tr42 was made by JAB on 6 Apr 98, just prior to submitting Run HB304K:
c
*tr42  $ use tr42 to locate and position the elliptical cone used to define chamfer between HB3 vessel hole and inner surf of pressure vessel
       0.0  -2.02265  127.62367   $ location of local origin (center of elliptical cone), relative to the global origin (cm) in HB-3 model
         0    90.0000    90.0000  $ degrees from global x,y,z axes to local x axis
        90    12.6929   -77.3071  $ degrees from global x,y,z axes to local y axis
        90   102.6929    12.6929  $ degrees from global x,y,z axes to local z axis
c      ------------------------------------------------------------------------------------------------------------------------
c      END-TRANSFORMATIONS
c
c
c      BEGIN MATERIAL DESCRIPTIONS:
c
c       Water gaps in removable reflector region    --Avg. Density= 0.98465 g/cm^3
m5      1001.50c     6.63485-02    8016.50c    3.31742-02
mt5     lwtr.01t
c
c       Water Reflector --Density= 0.9899 g/cm^3
m7      1001.50c     6.67022-02    8016.50c    3.33511-02
mt7     lwtr.01t
c
c       H2O Pool  --Density= 1.0000 g/cm^3
m8      1001.50c     6.73828-02    8016.50c    3.36914-02
mt8     lwtr.01t
c
c       Aluminum reflector container (outside Be reflector; 2.7 g/cc)
m23     13027.52c   5.85482-02   1001.50c  3.45716-04  12000.50c  6.68986-04
        14000.50c   3.47363-04  22000.50c  2.54704-05  24000.50c  6.09789-05
        25055.50c   2.21974-05  26000.55c  1.01905-04  29000.50c  8.74557-05
c
c       Aluminum liners in Be reflectors (2.7 g/cc)
m24     13027.52c   5.85482-02   1001.50c  3.45716-04  12000.50c  6.68986-04
        14000.50c   3.47363-04  22000.50c  2.54704-05  24000.50c  6.09789-05
        25055.50c   2.21974-05  26000.55c  1.01905-04  29000.50c  8.74557-05
c
c       ss liner of pressure vessel, bioshield liner, and other components -- SCALE SS304 (7.92 g/cc;  69.5 w/o Fe, 19.0 w/o Cr, 9.5 w/o Ni,  2.0 w/o Mn)
m40     26000.55c  5.93541-02   24000.50c  1.74281-02
        28000.50c  7.71883-03   25055.50c  1.73629-03
c
```

```
c       ss (same as above, but diff color on plot) used for removable shield around collimator -- SCALE SS304 (7.92 g/cc; 69.5 w/o Fe, 19.0 w/o Cr, 9.5 w/o
Ni, 2.0 w/o Mn)
m41     26000.55c  5.93541-02   24000.50c  1.74281-02
        28000.50c  7.71883-03   25055.50c  1.73629-03
c
c       carbon steel in main body of pressure vessel -- SCALE Carbon Steel (7.8212 g/cc;  99.0 w/o Fe, 1.0 w/o C)
m50     26000.55c  8.34929-02    6012.50c  3.92134-03
c
c       Void in reflector components
m60     1001.50c   1.00000-15   8016.50c   1.00000-15
c
c       Void regions in the HB-1,2,and 3 beam tubes (m60 @ 2.0e-15 atoms/b-cm) have been replaced with helium-filled regions
c       where m61 = He (void) at T=300 deg.K and P=2 atm, where rho=3.2325e-4 g/cc, N(He)=4.86816e-5 atoms/(barn*cm)
c       Note: cold source vacuum vessel in HB-4 now has a true void (see m610) as of July 1996.
c       ------------------------
c       Helium void inside beam tubes HB-1,2,3 (He at T=300 deg.K, P=2 atm); cold source vacuum vessel in HB-4 now has a true void (see m610)
m61     2004.50c  4.86816e-5  $  add-jab122395:  For He at T=300 deg.K and P=2 atm, rho=3.2325e-4 g/cc, N(He)=4.86816e-5 atoms/(barn*cm)
c
c       Barytes concrete at 3.09725 g/cc (used for biological shield); shown below are atoms/(barn*cm) by nuclide
m62      1001.50c  1.681e-2   5010.50c  3.378e-4   5011.56c  1.368e-3
         8016.50c  4.195e-2  11023.50c  3.193e-4  12000.50c  1.549e-4
        13027.52c  7.534e-4  14000.50c  1.260e-3  16032.50c  5.401e-3
        20000.50c  3.273e-3  22000.50c  1.336e-4  25055.50c  1.713e-4
        26000.55c  6.875e-4  56138.50c  5.394e-3
c       real concentration for ba-138 = 3.8787e-3 atoms/(barn*cm); it is available;
c       other nuclide concentrations for which there is no mcnp xsect data:
c       ba-134=1.3037e-4;  ba-135=3.5557e-4;  ba-136=4.2364e-4;  ba-137=6.0575e-4
c       total number density for all barium nuclides in barytes concrete: 5.394030e-3
c       total number density for all nuclides in barytes concrete:  7.801382e-2
c       while this barytes concrete (for ANS project) was 3.09725 g/cc, it can
c       sometimes be made as dense as 3.5 g/cc; see book by Schaffer
c
c
m71     28058.24y  1.0  $ Ni58;  this material (m71) is used only to get the Ni58(n,p)Co58 reaction rate [(n,p)=103] in the dosimeters
m72     26054.24y  1.0  $ Fe54;  this material (m72) is used only to get the Fe54(n,p)Mn54 reaction rate [(n,p)=103] in the dosimeters
c
c
c       Typical beryllium used in permanent reflector (with he-3 and li-6, based in center ring, cell 9024)
m108    4009.50c   1.21135-01   1001.50c   1.34766-03   8016.50c   6.73828-04
        3006.50c   4.80664-8    2003.50c   1.39911-9
mt108   be.01t
c
c
c       --------------------------------
c       Note:  At this point, the actual HB310 input file has 487 lines of old (legacy) detector tally specifications
c       left over from Run HB308G "in place" but "commented out" because they were replaced with the following.  For
c       the sake of shortening this appendix by about 8 pages, the old legacy detector tally specs that were commented
c       out are not shown here.  Instead, only the new detector tally specs actually used in Run HB310 are shown below.
c
c       For the most part, these are very much the same as before, and only the values on the "fm" multiplier cards
c       were changed to reflect the fact that the new source now corresponds to the "total activation gamma source
c       in the rotary shutter, 7 days after shutdown".  Indeed, the "fm" multiplier cards were changed, but I didn't
c       bother to change all the tally title cards or comments.  Thus, any comments you see about it being "at 100 MW"
c       should be disregarded in this case.
c       --------------------------------
c
c       ------------------------------------------------------------------------------------------------------------
c       *** st[illegible]etectors used to get gamma fluxes & dose rates due to activ[illegible] sources in shutter, 7 days after shutdown
```

```
c      ------------------------------------------------------------------------------------------------------------------------
c
fc35   G-Flux (p/s/cm2) 0.5 cm past conc box containing shutter, at 100 MW
c      Rotary shutter centered at Z=446.405 cm; downstream edge of shutter at Z=477.36125 cm;
c      Downstream surf of SS liner on concrete box containing shutter is at Surf 3001 (Z=478.79 cm);
c      This detector is located 0.5 cm downstream of Surf 3001
f35:p  0.0  0.0  479.29  0.49  $ G-Flux (p/s/cm2) midway between collimator & shutter at 100 MW
c      fm35   1.35399e+17   $ based on VELM gamma groups 1-23; sum of equivalent point sources (p/s) in HB-3 for HFIR at 100 MW (Sn=7.5573e18 n/s in global
calc);  will yield fluxes in p/s/cm2
c      fm35   7.984211E+15  $ based on VELM gamma groups 1-8 only; for FLOODED case only; must be used consistently with SI73, SP73, SB73 & DS83 data
fm35   1.61388E+10  $ Total activation gamma source in rotary shutter =  1.61388E+10 (p/s), 7 days after shutdown; all at 1.25 MeV
e35    $  Emax(MeV) for the 23 VELM gamma grps (lowest to highest energy for MCNP):
       2.0000e-2    4.5000e-2    7.0000e-2    1.0000e-1    1.5000e-1    $ VELM g-groups 23, 22, 21, 20, 19,
       3.0000e-1    4.0000e-1    5.1000e-1    6.0000e-1    7.0000e-1    $ VELM g-groups 18, 17, 16, 15, 14,
       1.0000e+0    1.5000e+0    2.0000e+0    2.5000e+0    3.0000e+0    $ VELM g-groups 13, 12, 11, 10,  9,
       4.0000e+0    5.0000e+0    6.0000e+0    7.0000e+0    7.5000e+0    $ VELM g-groups  8,  7,  6,  5,  4,
       8.0000e+0    1.0000e+1    1.4000e+1                              $ VELM g-groups  3,  2,  1
c
fc45   G-Dose (mrem/hr) 0.5 cm past conc box containing shutter, at 100 MW
c      Rotary shutter centered at Z=446.405 cm; downstream edge of shutter at Z=477.36125 cm;
c      Downstream surf of SS liner on concrete box containing shutter is at Surf 3001 (Z=478.79 cm);
c      This detector is located 0.5 cm downstream of Surf 3001
f45:p  0.0  0.0  479.29  0.49  $ G-Dose (mrem/hr) midway between collimator & shutter at 100 MW
c      fm45   1.35399e+17   $ based on VELM gamma groups 1-23; sum of equivalent point sources (p/s) in HB-3 for HFIR at 100 MW (Sn=7.5573e18 n/s in global
calc);  will yield fluxes in p/s/cm2
c      fm45   7.984211E+15  $ based on VELM gamma groups 1-8 only; for FLOODED case only; must be used consistently with SI73, SP73, SB73 & DS83 data
fm45   1.61388E+10  $ Total activation gamma source in rotary shutter =  1.61388E+10 (p/s), 7 days after shutdown; all at 1.25 MeV
e45    $ Gamma energy boundaries (Emax, in MeV) from VELM 61n/23g structure:
       1.00000e-02  2.00000e-02  4.50000e-02  7.00000e-02  1.00000e-01
       1.50000e-01  3.00000e-01  4.00000e-01  5.10000e-01  6.00000e-01
       7.00000e-01  1.00000e+00  1.50000e+00  2.00000e+00  2.50000e+00
       3.00000e+00  4.00000e+00  5.00000e+00  6.00000e+00  7.00000e+00
       7.50000e+00  8.00000e+00  1.00000e+01  1.40000e+01
em45   $ Gamma flux-to-dose-rate conversion factors [(mrem/hr)/(p/s/cm2)] for the VELM 61n/23g xsect library,
c      calculated as prescribed in ANSI/ANS-6.1.1-1977, with groups arranged here in order of "increasing"
c      energy for use in MCNP;  first value here corresponds to non-existant group below 1.0e-2 MeV:
       0.00000e+00  2.14390e-03  5.77610e-04  2.74660e-04  2.66440e-04
       3.27670e-04  5.66760e-04  8.75940e-04  1.08520e-03  1.27970e-03
       1.44170e-03  1.75630e-03  2.31560e-03  2.92700e-03  3.46860e-03
       3.95960e-03  4.62210e-03  5.41360e-03  6.19090e-03  6.92650e-03
       7.47830e-03  7.84680e-03  8.77160e-03  1.10200e-02
c
c
fc55   G-Flux (p/s/cm2) 1.5 feet past conc box containing shutter, at 100 MW
c      Rotary shutter centered at Z=446.405 cm; downstream edge of shutter at Z=477.36125 cm;
c      Downstream surf of SS liner on concrete box containing shutter is at Surf 3001 (Z=478.79 cm);
c      This detector is located 1.5 feet downstream of Surf 3001
f55:p  0.0  0.0  524.51  5.0   $ G-Flux (p/s/cm2) midway between collimator & shutter at 100 MW
c      fm55   1.35399e+17   $ based on VELM gamma groups 1-23; sum of equivalent point sources (p/s) in HB-3 for HFIR at 100 MW (Sn=7.5573e18 n/s in global
calc);  will yield fluxes in p/s/cm2
c      fm55   7.984211E+15  $ based on VELM gamma groups 1-8 only; for FLOODED case only; must be used consistently with SI73, SP73, SB73 & DS83 data
fm55   1.61388E+10  $ Total activation gamma source in rotary shutter =  1.61388E+10 (p/s), 7 days after shutdown; all at 1.25 MeV
e55    $  Emax(MeV) for the 23 VELM gamma grps (lowest to highest energy for MCNP):
       2.0000e-2    4.5000e-2    7.0000e-2    1.0000e-1    1.5000e-1    $ VELM g-groups 23, 22, 21, 20, 19,
       3.0000e-1    4.0000e-1    5.1000e-1    6.0000e-1    7.0000e-1    $ VELM g-groups 18, 17, 16, 15, 14,
       1.0000e+0    1.5000e+0    2.0000e+0    2.5000e+0    3.0000e+0    $ VELM g-groups 13, 12, 11, 10,  9,
       4.0000e+0    5.0000e+0    6.0000e+0    7.0000e+0    7.5000e+0    $ VELM g-groups  8,  7,  6,  5,  4,
       8.0000e+0    1.0000e+1    1.4000e+1                              $ VELM g-groups  3,  2,  1
```

```
c
fc65   G-Dose (mrem/hr) 1.5 feet past conc box containing shutter, at 100 MW
c      Rotary shutter centered at Z=446.405 cm; downstream edge of shutter at Z=477.36125 cm;
c      Downstream surf of SS liner on concrete box containing shutter is at Surf 3001 (Z=478.79 cm);
c      This detector is located 1.5 feet downstream of Surf 3001
f65:p  0.0  0.0  524.51  5.0   $ G-Dose (mrem/hr) midway between collimator & shutter at 100 MW
c      fm65   1.35399e+17   $ based on VELM gamma groups 1-23; sum of equivalent point sources (p/s) in HB-3 for HFIR at 100 MW (Sn=7.5573e18 n/s in global
calc); will yield fluxes in p/s/cm2
c      fm65   7.984211E+15  $ based on VELM gamma groups 1-8 only; for FLOODED case only; must be used consistently with SI73, SP73, SB73 & DS83 data
fm65   1.61388E+10  $ Total activation gamma source in rotary shutter =  1.61388E+10 (p/s), 7 days after shutdown; all at 1.25 MeV
e65    $ Gamma energy boundaries (Emax, in MeV) from VELM 61n/23g structure:
       1.00000e-02  2.00000e-02  4.50000e-02  7.00000e-02  1.00000e-01
       1.50000e-01  3.00000e-01  4.00000e-01  5.10000e-01  6.00000e-01
       7.00000e-01  1.00000e+00  1.50000e+00  2.00000e+00  2.50000e+00
       3.00000e+00  4.00000e+00  5.00000e+00  6.00000e+00  7.00000e+00
       7.50000e+00  8.00000e+00  1.00000e+01  1.40000e+01
em65   $ Gamma flux-to-dose-rate conversion factors [(mrem/hr)/(p/s/cm2)] for the VELM 61n/23g xsect library,
c      calculated as prescribed in ANSI/ANS-6.1.1-1977, with groups arranged here in order of "increasing"
c      energy for use in MCNP;  first value here corresponds to non-existant group below 1.0e-2 MeV:
       0.00000e+00  2.14390e-03  5.77610e-04  2.74660e-04  2.66440e-04
       3.27670e-04  5.66760e-04  8.75940e-04  1.08520e-03  1.27970e-03
       1.44170e-03  1.75630e-03  2.31560e-03  2.92700e-03  3.46860e-03
       3.95960e-03  4.62210e-03  5.41360e-03  6.19090e-03  6.92650e-03
       7.47830e-03  7.84680e-03  8.77160e-03  1.10200e-02
c
c
fc75   G-Flux (p/s/cm2) 3 feet past conc box containing shutter, at 100 MW
c      Rotary shutter centered at Z=446.405 cm; downstream edge of shutter at Z=477.36125 cm;
c      Downstream surf of SS liner on concrete box containing shutter is at Surf 3001 (Z=478.79 cm);
c      This detector is located 3 feet downstream of Surf 3001
f75:p  0.0  0.0  570.23  5.0   $ G-Flux (p/s/cm2) midway between collimator & shutter at 100 MW
c      fm75   1.35399e+17   $ based on VELM gamma groups 1-23; sum of equivalent point sources (p/s) in HB-3 for HFIR at 100 MW (Sn=7.5573e18 n/s in global
calc); will yield fluxes in p/s/cm2
c      fm75   7.984211E+15  $ based on VELM gamma groups 1-8 only; for FLOODED case only; must be used consistently with SI73, SP73, SB73 & DS83 data
fm75   1.61388E+10  $ Total activation gamma source in rotary shutter =  1.61388E+10 (p/s), 7 days after shutdown; all at 1.25 MeV
e75    $  Emax(MeV) for the 23 VELM gamma grps (lowest to highest energy for MCNP):
       2.0000e-2    4.5000e-2    7.0000e-2    1.0000e-1    1.5000e-1    $ VELM g-groups 23, 22, 21, 20, 19,
       3.0000e-1    4.0000e-1    5.1000e-1    6.0000e-1    7.0000e-1    $ VELM g-groups 18, 17, 16, 15, 14,
       1.0000e+0    1.5000e+0    2.0000e+0    2.5000e+0    3.0000e+0    $ VELM g-groups 13, 12, 11, 10,  9,
       4.0000e+0    5.0000e+0    6.0000e+0    7.0000e+0    7.5000e+0    $ VELM g-groups  8,  7,  6,  5,  4,
       8.0000e+0    1.0000e+1    1.4000e+1                              $ VELM g-groups  3,  2,  1
c
fc85   G-Dose (mrem/hr) 3 feet past conc box containing shutter, at 100 MW
c      Rotary shutter centered at Z=446.405 cm; downstream edge of shutter at Z=477.36125 cm;
c      Downstream surf of SS liner on concrete box containing shutter is at Surf 3001 (Z=478.79 cm);
c      This detector is located 3 feet downstream of Surf 3001
f85:p  0.0  0.0  570.23  5.0   $ G-Dose (mrem/hr) midway between collimator & shutter at 100 MW
c      fm85   1.35399e+17   $ based on VELM gamma groups 1-23; sum of equivalent point sources (p/s) in HB-3 for HFIR at 100 MW (Sn=7.5573e18 n/s in global
calc); will yield fluxes in p/s/cm2
c      fm85   7.984211E+15  $ based on VELM gamma groups 1-8 only; for FLOODED case only; must be used consistently with SI73, SP73, SB73 & DS83 data
fm85   1.61388E+10  $ Total activation gamma source in rotary shutter =  1.61388E+10 (p/s), 7 days after shutdown; all at 1.25 MeV
e85    $ Gamma energy boundaries (Emax, in MeV) from VELM 61n/23g structure:
       1.00000e-02  2.00000e-02  4.50000e-02  7.00000e-02  1.00000e-01
       1.50000e-01  3.00000e-01  4.00000e-01  5.10000e-01  6.00000e-01
       7.00000e-01  1.00000e+00  1.50000e+00  2.00000e+00  2.50000e+00
       3.00000e+00  4.00000e+00  5.00000e+00  6.00000e+00  7.00000e+00
       7.50000e+00  8.00000e+00  1.00000e+01  1.40000e+01
em85   $ Gamma flux-to-dose-rate conversion factors [(mrem/hr)/(p/s/cm2)] for VELM 61n/23g xsect library,
```

524

```
c      calculated as prescribed in ANSI/ANS-6.1.1-1977, with groups arranged here in order of "increasing"
c      energy for use in MCNP;  first value here corresponds to non-existant group below 1.0e-2 MeV:
       0.00000e+00  2.14390e-03  5.77610e-04  2.74660e-04  2.66440e-04
       3.27670e-04  5.66760e-04  8.75940e-04  1.08520e-03  1.27970e-03
       1.44170e-03  1.75630e-03  2.31560e-03  2.92700e-03  3.46860e-03
       3.95960e-03  4.62210e-03  5.41360e-03  6.19090e-03  6.92650e-03
       7.47830e-03  7.84680e-03  8.77160e-03  1.10200e-02
c
c
fc231   Primary G-Leakage (p/s) on downstrem surf of box holding shutter, 100 MW
c        1) Rotary shutter is centered at Z=446.405 cm;  downstream edge of shutter is at Z=477.36125 cm;
c           Downstream surf of SS liner on concrete box containing shutter is at Surf 3001 (Z=478.79 cm);
c           That is the surface where this F1 tally is made.
c        2) Purpose of this tally is simply to see IF any real particles are getting here, and to see WHERE they are coming from.
c       fm231   1.35399e17    $ based on VELM gamma groups 1-23; use for g-only calc; = sum of equivalent point sources (p/s) in HB-3 for HFIR at 100 MW (Sn
=7.5573e18 n/s in global calc);  will yield fluxes in n/s/cm2
c       fm231   7.984211E+15  $ based on VELM gamma groups 1-8 only; for FLOODED case only; must be used consistently with SI73, SP73, SB73 & DS83 data
c        fc231   Secondary G-Leakage (p/s) at downstream exit of collimator hole
c        fm231   9.64595e16  $ use for n/g calc; = sum of equivalent point sources (n/s) in HB-3 for HFIR at 100 MW (Sn=7.5573e18 n/s in global calc);  wil
l yield fluxes in n/s/cm2
fm231   1.61388E+10  $ Total activation gamma source in rotary shutter =  1.61388E+10 (p/s), 7 days after shutdown; all at 1.25 MeV
f231:p  3001   $  downstrem surf of SS liner on concrete box containing shutter
fs231   3032  -3022  3072  -3082  3031  -3021  3071  -3081  3110  $ the 10th edit ("the remainder") is the leakage (p/s) thru the central 6.5-inch-diam disk
c      Meaning of surface segments (assuming you're outside where monochrometer drum usually is, looking back towards the shutter):
c      ------------------------------------------------------------
c        1) everything to left  of concrete box holding the shutter
c        2) everything to right of concrete box holding the shutter
c        3) what remains above the concrete box holding the shutter
c        4) what remains below the concrete box holding the shutter
c        5) void gap just to left  of concrete box holding the shutter
c        6) void gap just to right of concrete box holding the shutter
c        7) void gap just above the concrete box holding the shutter
c        8) void gap just below the concrete box holding the shutter
c        9) face of concrete box holding the shutter, except the central 6.5-inch-diam disk directly in front of shutter
c       10) central 6.5-inch-diam disk directly in front of shutter
c      ------------------------------------------------------------
sd231   1  1  1  1  1  1  1  1  1  1  $ enter area of 1.0 cm2 for all segments (including "remainder") to get "leakage (p/s)" instead of "current (p/s/cm2)"
c231    0.0  1.0    $ only L(z-) and L(z+)
e231    $  Emax(MeV) for the 23 VELM gamma grps (lowest to highest energy for MCNP):
     2.0000e-2    4.5000e-2    7.0000e-2    1.0000e-1    1.5000e-1    $ VELM g-groups 23, 22, 21, 20, 19,
     3.0000e-1    4.0000e-1    5.1000e-1    6.0000e-1    7.0000e-1    $ VELM g-groups 18, 17, 16, 15, 14,
     1.0000e+0    1.5000e+0    2.0000e+0    2.5000e+0    3.0000e+0    $ VELM g-groups 13, 12, 11, 10,  9,
     4.0000e+0    5.0000e+0    6.0000e+0    7.0000e+0    7.5000e+0    $ VELM g-groups  8,  7,  6,  5,  4,
     8.0000e+0    1.0000e+1    1.4000e+1                              $ VELM g-groups  3,  2,  1
fq231  c e s   $ each cosine = new table;  energy grp down vertically;  spatial segments across horizontally
c
c
fc232  Primary G-Dose (mrem/hr) on downstrem surf of box holding shutter; seg 10
c      -------------------------
c      Note:  Only if this boundary crossing estimate of the primary gamma dose rate downstream of the
c      central 6.5-inch-diam disk directly in front of the shutter (seg 10) [and perhaps segments 5-9 also]
c      has good statistics, is it possible to have a high degree of confidence in the point detector estimates.
c      If F2 Tally 232 is well converged in segments 5-10, then F5 Tallies 45, 65 and 85 will be very accurate;
c      if F2 Tally 232 is not well converged, F5 Tallies 45, 65 and 85 may or may not be any good (even if stats are good).
c      -------------------------
c      1) Rotary shutter is centered at Z=446.405 cm;  downstream edge of shutter is at Z=477.36125 cm;
c         Downstream surf of SS liner on concrete box containing shutter is at Surf 3001 (Z=478.79 cm);
c         That is the surface where this F2 tally is made.
```

```
c       2) Purpose of this tally is simply to see IF any real particles are getting here, and to see WHERE they are coming from.
c       --------------------------
c        fm232   1.35399e17    $ based on Pri g-source in VELM gamma groups 1-23; use for VOID g-only calc; = sum of equivalent point sources (p/s) in HB-3 f
or HFIR at 100 MW (Sn=7.5573e18 n/s in global calc);  will yield fluxes in n/s/cm2
c        fm232   7.984211E+15  $ based on Pri g-source in VELM gamma groups 1-8 only; use 1-8 for FLOODED case only; must be used consistently with SI73, SP7
3, SB73 & DS83 data
c          fc232   Secndry G-Dose (mrem/hr) on downstrem surf of box holding shutter; seg 10
c          fm232   9.64595e16  $ use for n/g calc; = sum of equivalent point sources (n/s) in HB-3 for HFIR at 100 MW (Sn=7.5573e18 n/s in global calc);  wil
l yield fluxes in n/s/cm2
fm232   1.61388E+10  $ Total activation gamma source in rotary shutter =  1.61388E+10 (p/s), 7 days after shutdown; all at 1.25 MeV
f232:p  3001   $  downstream surf of SS liner on concrete box containing shutter
fs232   3032  -3022  3072  -3082  3031  -3021  3071  -3081  3110  $ the 10th edit ("the remainder") is the leakage (p/s) thru the central 6.5-inch-diam disk
c       Meaning of surface segments (assuming you're outside where monochrometer drum usually is, looking back towards the shutter):
c       ------------------------------------------------------------
c         1) everything to left  of concrete box holding the shutter,    area = 1438.212778 cm2
c         2) everything to right of concrete box holding the shutter,    area = 1438.212778 cm2
c         3) what remains above the concrete box holding the shutter,    area = 1414.336692 cm2
c         4) what remains below the concrete box holding the shutter,    area = 1414.336692 cm2
c         5) void gap just to left  of concrete box holding the shutter, area =  151.915019 cm2
c         6) void gap just to right of concrete box holding the shutter, area =  151.915019 cm2
c         7) void gap just above the concrete box holding the shutter,   area =  145.816241 cm2
c         8) void gap just below the concrete box holding the shutter,   area =  145.816241 cm2
c         9) face of concrete box holding the shutter, except the central 6.5-inch-diam disk;  area = 6758.583596 cm2
c        10) central 6.5-inch-diam disk directly in front of shutter,    area =  214.083910 cm2  <-- region of greatest interest
c        Total area of all 10 segments=pi*(65.0**2)
c       ------------------------------------------------------------
sd232   $ enter area of all surface segments (including "the remainder") to get flux in "p/s/cm2"
        $ area (cm2) for each of the 10 surface segments at this axial location (seg 10, the "remainder", is of greatest interest)
        1438.212778  1438.212778  1414.336692  1414.336692  151.915019
         151.915019   145.816241   145.816241  6758.583596  214.083910
e232    $ Gamma energy boundaries (Emax, in MeV) from VELM 61n/23g structure:
        1.00000e-02  2.00000e-02  4.50000e-02  7.00000e-02  1.00000e-01
        1.50000e-01  3.00000e-01  4.00000e-01  5.10000e-01  6.00000e-01
        7.00000e-01  1.00000e+00  1.50000e+00  2.00000e+00  2.50000e+00
        3.00000e+00  4.00000e+00  5.00000e+00  6.00000e+00  7.00000e+00
        7.50000e+00  8.00000e+00  1.00000e+01  1.40000e+01
em232   $ Gamma flux-to-dose-rate conversion factors [(mrem/hr)/(p/s/cm2)] for the VELM 61n/23g xsect library,
c       calculated as prescribed in ANSI/ANS-6.1.1-1977, with groups arranged here in order of "increasing"
c       energy for use in MCNP;  first value here corresponds to non-existant group below 1.0e-2 MeV:
        0.00000e+00  2.14390e-03  5.77610e-04  2.74660e-04  2.66440e-04
        3.27670e-04  5.66760e-04  8.75940e-04  1.08520e-03  1.27970e-03
        1.44170e-03  1.75630e-03  2.31560e-03  2.92700e-03  3.46860e-03
        3.95960e-03  4.62210e-03  5.41360e-03  6.19090e-03  6.92650e-03
        7.47830e-03  7.84680e-03  8.77160e-03  1.10200e-02
fq232   e s   $ print control:  energy grp down vertically;  spatial segments across horizontally
c
c       ------------------------------------------------------------------------------------------------------------------------
c       ********** end of model **********
c       ------------------------------------------------------------------------------------------------------------------------
```

INTERNAL DISTRIBUTION

1-4. J. A. Bucholz
5. D. H. Cook
6. M. B. Farrar
7. F. Z. Gallmeier
8. R. A. Lillie
9. L. M. Petrie
10. D. L. Pinkston
11. I. I. Popova
12. L. D. Proctor
13. I. Remec
14. J. P. Renier
15. R. B. Rothrock
16. J. C. Ryman
17. C. O. Slater
18. J. C. Wagner
19-20. HFIR Upgrade Files (c/o Don Hogue)
21. RRD Document Control Center (c/o Beverly Large)
22. Central Research Library
23. Laboratory Records-RC
24. Laboratory Records (for submission to OSTI)

EXTERNAL DISTRIBUTION

25. J. S. Tang, Framatome Cogema Fuels, 1180 Town Center Drive, MS-423, Las Vegas, NV 89134